12 11 92
U OM

# AJR

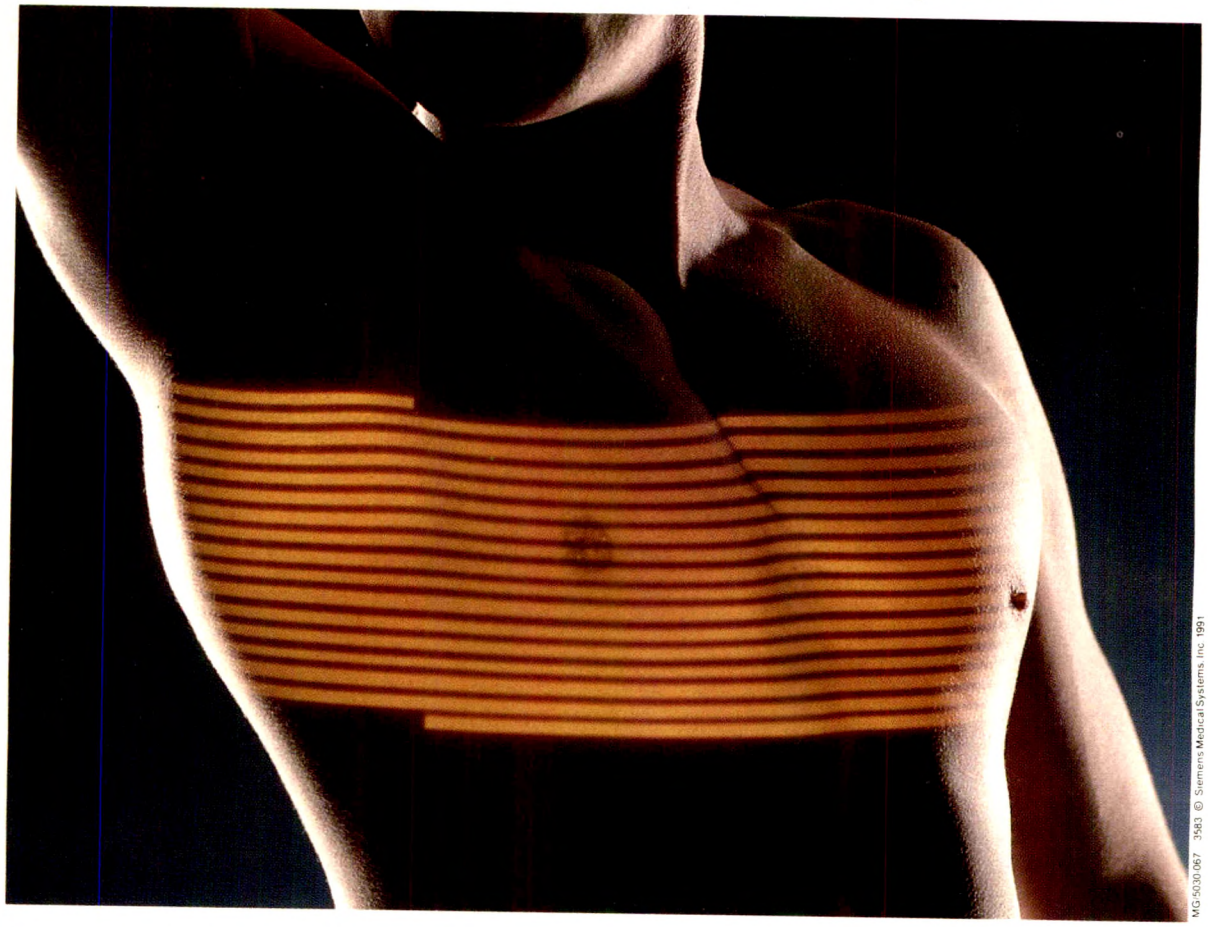
OUK-H03509-33-P02447
33

American
Journal of
Roentgenology

March 1991

SIEMENS

# Drawing circles around the competition.




Now you can scan an entire anatomical region-up to 32cm — in a single breathhold — only 32 seconds* with Spiral CT. The new, fast-volume scanning method for the SOMATOM® Plus-S CT System. It's the clinical advance that's ***drawing circles around the competition.***

Spiral CT software combines the benefits of Dynamic Multiscan...continuous data acquisition...with controlled table movement to capture true contiguous anatomy.

You select the table speed and the exam duration to acquire a complete scan volume with zero interscan delay. The results: anatomical studies with no gaps where lesions or nodules may be hidden...shorter exams that require less contrast material...fewer demands on patients' breath-holding capacity...better patient management...and more economical CT operations.

Once again, Siemens revolutionizes CT perfomance with innovative technology and concern for improved patient care. For more information about our exclusive Spiral CT package, contact your local Siemens representative or call us directly.

*24cm/24 sec. for the SOMATOM Plus

**Siemens Medical Systems, Inc.**
CT Marketing Division
186 Wood Avenue South
Iselin, NJ 08830 (908) 321-4500

***Siemens...***
***technology in caring hands.***

Official Journal of the American Roentgen Ray Society

# AJR

**American Journal of Roentgenology**
Diagnostic Imaging and Related Sciences

**Editor-In-Chief** Robert N. Berk, *La Jolla, California*
*University of California, San Diego*
*School of Medicine and Medical Center*

**Editor Emeritus** Melvin M. Figley, *Seattle, Washington*

**Associate Editor** Saskia von Waldenburg Hilton, *San Diego, California*

**Consulting Editor** Michael S. Huckman, *Chicago, Illinois*

**Statistician** Charles C. Berry, *San Diego, California*

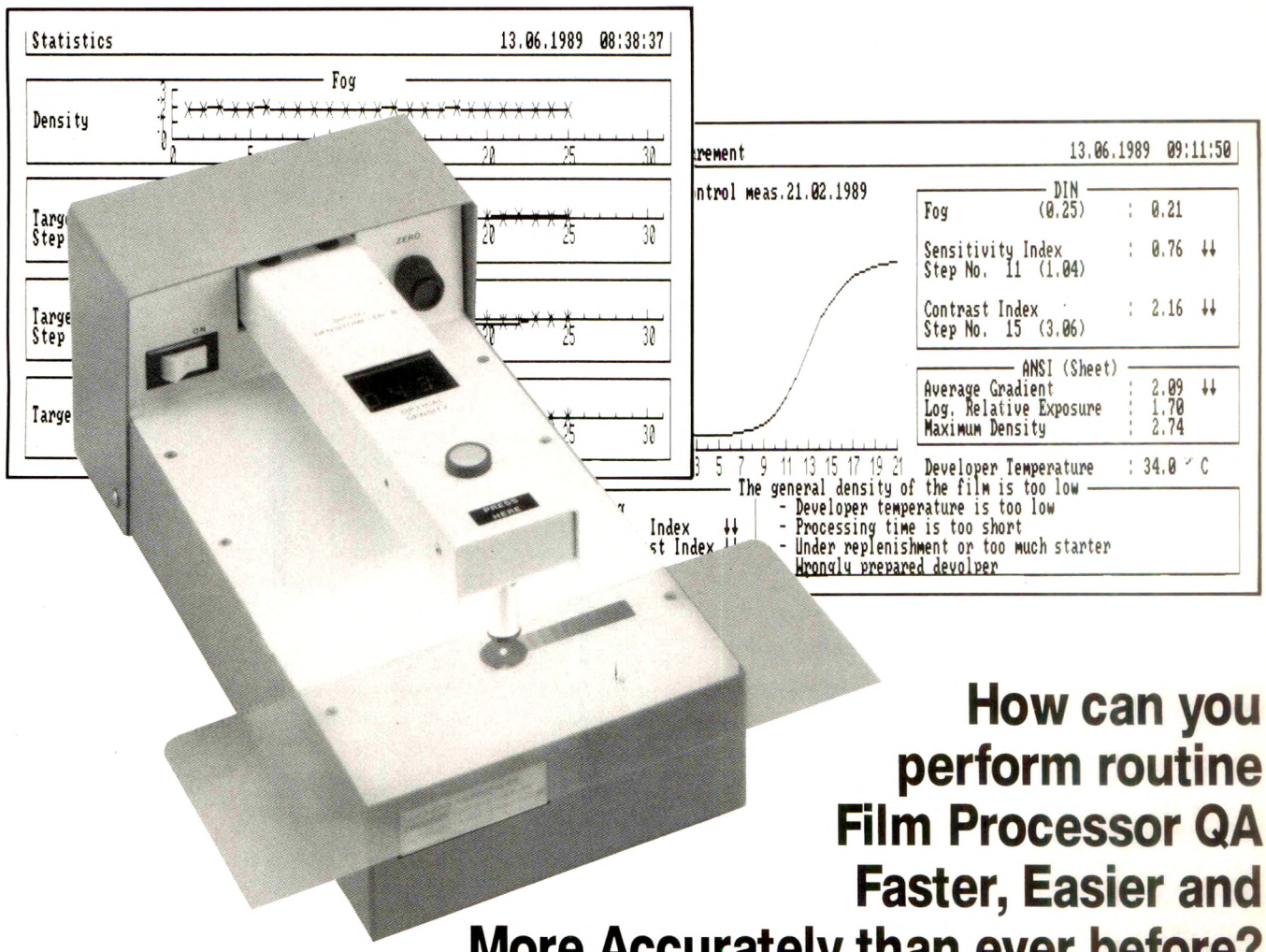
**Editorial Board**

John R. Amberg
Itamar Aviad
Mark E. Baker
Lawrence W. Bassett
Michael A. Bettmann
Felix S. Chew
N. Reed Dunnick
David K. Edwards
Ronald G. Evens
David S. Feigin
Sandra K. Fernbach
Richard H. Gold
William R. Hendee
John R. Hesselink
Charles B. Higgins
Melvyn T. Korobkin
Faye C. Laing
Thomas L. Lawson
Robert G. Levitt
Bruce L. McClennan
Richard P. Moser
Albert A. Moss
Jeffrey H. Newhouse
Donald L. Resnick
Stewart R. Reuter
Charles A. Rohrmann, Jr.
Peter M. Ronai
Sjef H. J. Ruijs
Stuart S. Sagel
David J. Sartoris
Stefan C. Schatzki
William P. Shuman
Edward A. Sickles
Barry A. Siegel
David D. Stark
Edward T. Stewart
Murali Sundaram
Eric vanSonnenberg
Robert K. Zeman

**Editorial Staff:** Margaret Levene, *managing editor*; Katie L. Spiller, Barbara Rose, Barbara L. Halliburton, and Janine Anderson, *manuscript editors*; Nancy Rydbeck, *office manager*; Sheri Smith, *administrative assistant*; Linda J. Waggoner, *administrative secretary*.

AJR, AMERICAN JOURNAL OF ROENTGENOLOGY (ISSN 0361 803X) is the official journal of the American Roentgen Ray Society and is published monthly by Williams & Wilkins, 428 E. Preston St., Baltimore, MD 21202. Annual dues include $50 for journal subscription. Second-class postage paid at Baltimore, MD, and at additional mailing offices. Postmaster, send address changes (Form 3579) to AJR, 428 E. Preston St., Baltimore, MD 21202. Subscription rates $125 ($180 foreign); institutions $135 ($190 foreign); in training $25 ($80 foreign); single copy $18 ($22 foreign). Airmail rates furnished on request. Indexed by *Current Contents* and *Index Medicus*. Copyright © 1991 by American Roentgen Ray Society. 0361–803X/90$3.00


FROM MAL
1981
4d55s2
6S2 1/2
98
97
99
53
Iodine
4d105s2p5
-1
7
5
126.9045
127
75




# How can you perform routine Film Processor QA Faster, Easier and More Accurately than ever before?

# THE FILMCHECK X-Ray Film Processor QA System

- When teamed with an IBM™-compatible computer, it tracks performance and stores data for an unlimited number of x-ray film processors.
- More information, faster! User-friendly!
- Complete processor condition at a glance!
- Stores data for retrieval and comparison!
- Tracks down the source of processor problems!
- Analyzes sheet, spot, cine films from any sensitometer!

TM, International Business Machines, Inc.

**07-442** FILMCHECK Processor QA System includes Digital Densitometer with RS-232C Interface, Interface Cable, and Film Processor QA Software Package . . . . . **ONLY $1695.00**

## ORDER NOW . . .

**phone 516-741-6360, FAX 516-741-5414, or for more details, request Bulletin 4352-44**


**NUCLEAR ASSOCIATES**

VICTOREEN

Division of VICTOREEN, INC.
100 VOICE ROAD • P.O. BOX 349
CARLE PLACE, NY 11514-0349 U.S.A.
(516) 741-6360
FAX (516) 741-5414


**IT HAS ALL THE FEATURES YOU WANT AT A BUDGET-PLEASING PRICE!**

# *AJR* Guidelines for Authors

Address new and revised manuscripts, correspondence, and classified ads to the Editor:

AJR Editorial Office
2223 Avenida de la Playa, Suite 103
La Jolla, CA 92037-3218
Telephone: (619) 459-2229; FAX: (619) 459-8814

Inquiries regarding subscriptions, display advertising, reprints, or permission to republish *AJR* material should be addressed to the publisher:

The Williams & Wilkins Co.
428 E. Preston St.
Baltimore, MD 21202 Telephone: 1-800-638-6423

The *AJR* publishes original contributions to the advancement of medical diagnosis and treatment. Submitted manuscripts should not contain previously published material and should not be under consideration for publication elsewhere. Papers dealing with neuroradiology should be addressed to: American Journal of Neuroradiology, Dept. of Radiology, Massachusetts General Hospital, Boston, MA 02114. At the discretion of the *AJR* Editor, *AJNR* articles that are of interest to the general reader may be republished in the *AJR*. Neuroradiologic papers sent to the *AJR* will be forwarded to the Editorial Office of the *AJNR*.

Manuscript decisions are based on peer review. Reviewers receive manuscripts without title pages to ensure an unbiased review. Statements made in the article, including changes made by the Editor or manuscript editor, are the responsibility of the author and not of the *AJR* or its publisher. Authors will be sent the edited manuscript, galley proof, and proofs of illustrations. If the corresponding author will be unavailable to review galleys, arrangements should be made for a coauthor or colleague to read and return the proof.

The following guidelines are based on instructions set forth in the **Uniform Requirements for Manuscripts Submitted to Biomedical Journals** (*Ann Intern Med* **1988;**108:258–265). Articles will be edited, however, to conform to the individual style of AJR.

### General Guidelines for Major Papers

*Abstract.* Clearly state (in 200 words or less) the purpose, methods, results, and conclusions of the study. Include actual data.

*Introduction.* Briefly describe the purpose of the investigation and explain why it is important.

*Methods.* Describe the research plan, the materials (or subjects), and the methods used, in that order. Explain in detail how disease was confirmed and how subjectivity in observations was controlled.

*Results.* Present results in a clear, logical sequence. If tables are used, do not duplicate tabular data in text, but do describe important trends and points.

*Discussion.* Describe the limitations of the research plan, materials (or subjects), and methods, considering both the purpose and the outcome of the study. When results differ from those of previous investigators, explain the discrepancy.

## AUTHOR'S CHECKLIST

**For priority handling, complete the following checklist, sign the copyright form on the reverse side of this page, and include both with the manuscript.**

_____ Two copies of the manuscript (the original and a photocopy) and two complete sets of figures are submitted. One copy has been retained by the author.

_____ If appropriate, *AJR* Guidelines for case reports, technical notes, pictorial essays, or letters to the Editor have been followed. (See page A8.)

_____ The manuscript, including references, figure legends, and tables, is typed double-spaced on 8½ × 11 in. (21.6 × 27.9 cm) *nonerasable* paper. Right-hand margins are not justified.

_____ All manuscript pages are numbered consecutively beginning with the abstract. Authors' names do not appear on the manuscript pages.

_____ The manuscript is organized as follows: title page, blind title page (title only), abstract, introduction, methods, results, discussion, acknowledgments, references, tables, figure legends, and figures.

_____ Informed consent has been obtained from patients who participated in clinical investigations. If experiments were performed on animals, authors complied with NIH guidelines for use of laboratory animals.

_____ Use of unfamiliar acronyms and abbrevations is kept to a minimum. When abbreviations are used they are defined at first mention, followed by the abbreviation in parentheses.

_____ Metric measurements are used throughout, or the metric equivalent is given in parentheses.

_____ Names and locations (city and state only) of manufacturers are given for equipment and nongeneric drugs.

#### Title Page

_____ The following information is given: title of article; names and complete addresses (including zip code) of all authors; current addresses of authors who have moved since study; acknowledgment of grant or other assistance. The corresponding author is clearly identified, and a current address, phone number, and FAX number are given.

_____ Two copies of a blind title page are included giving only the title (without the authors' names) for use in the review process.

#### Abstract

_____ An abstract of approximately 200 words concisely states the purpose, methods, and results of the study in one paragraph. Actual data are included. Conclusions are stated in a second, summary paragraph.

_____ No abbreviations or reference citations are used.

## References

_____ References (not to exceed 35) are typed double-spaced starting on a separate page and are **numbered consecutively in the order in which they appear in the text**.

_____ All references are cited in the text and are enclosed in brackets and typed on line with the text (not superscript).

_____ Unpublished data are not cited in the reference list, but are cited parenthetically in the text, for example, (Smith DJ, personal communication), (Smith DJ, unpublished data). This includes papers submitted, but not yet accepted, for publication.

_____ Inclusive page numbers (e.g., 333–335) are given for all references.

_____ Journal names are abbreviated according to *Index Medicus*.

_____ Style and punctuation of references follow the format illustrated in the following examples (all authors are listed when six or fewer; when seven or more authors, the first three are listed, followed by "et al."):

*Journal article*

1. Long RS, Roe EW, Wu EU, et al. Membrane oxygenation: radiographic appearance. *AJR* **1986**;146:1257–1260

*Book*

2. Smith LW, Cohen AR. *Pathology of tumors*, 6th ed. Baltimore: Williams & Wilkins, **1977**:100–109

*Chapter in a book*

3. Breon AJ. Serum monitors of bone metastasis. In: Clark SA, ed. *Bone metastases*. Baltimore: Williams & Wilkins, **1983**:165–180

*Paper presented at a meeting*

4. Lau FS, Kirk AN. MR imaging of the spine. Presented at the annual meeting of the American Roentgen Ray Society, Washington, DC, April **1986**

## Tables

_____ Each table is typed double-spaced on a separate page without vertical or horizontal rules; each has a short, descriptive title. Tables do not exceed two pages in length and contain at least four lines of data.

_____ Tables are numbered in the order in which they are cited in the text.

_____ Abbreviations are defined in an explanatory note below each table.

_____ Tables are self-explanatory and do not duplicate data given in the text or figures.

_____ All arithmetic (percentages, totals, differences) has been double checked for accuracy, and tabular data agree with data given in the text.

## Figures and Legends

_____ Two complete sets of original figures are submitted unmounted in labeled envelopes.

_____ Figures are clean, unscratched, 5 × 7 in. (13 × 18 cm) glossy prints with **white borders.** A separate print is submitted for each figure *part*.

_____ All figure parts relating to one patient have the same figure number.

_____ Each figure is labeled on the back with the figure number and an arrow indicating "top." For black-and-white figures, labeling is done on a gummed label, which is then affixed to the back of the print. **Never** use labels on **color** *figures, but write figure number on the back lightly in pencil. Never* use ink on front or back of any figures.

_____ Author's names are *not* written on the backs of figures.

_____ Only removable (rub-on) arrows and letters are used on the figures. Symbols are uniform in size and style and are not broken or cracked.

_____ Images are uniform in size and magnification.

_____ Line drawings are done in black ink on a white background. They are professional in quality, and all use the same size type. (Only glossy prints are acceptable.)

_____ Written permission has been obtained for use of all previously published illustrations (and copies of permission letters are included), and an appropriate credit line is given in the legends.

_____ Legends are typed double-spaced, and figure numbers correspond with the order in which the figures are cited in the text.

## Transfer of Copyright Agreement, Conflict of Interest Acknowledgment, Certification of Coauthors, and Exclusive Publication Statement

Complete copyright to the article entitled: _____

_____

is hereby transferred to the American Roentgen Ray Society (for United States government employees to the extent transferable), effective if and when the article is accepted for publication in the *American Journal of Roentgenology*. In the case of the authors who are officers or employees of the United States government, the American Roentgen Ray Society recognizes that works prepared by officers or employees of the United States government as part of their official government duties are in the public domain.

Authors reserve all proprietary rights other than copyright, such as patent rights and the right to use all or part of this article in future works of their own. The authors retain the right of replication, subject only to crediting the original source of publication and receiving written permission from the publisher.

Authors guarantee that this manuscript contains no matter that is libelous or otherwise unlawful, invades individual privacy, or infringes any proprietary rights.

Authors understand that they will receive no royalty or other compensation from the American Roentgen Ray Society or the publisher.

Authors guarantee that the editor has been or will be informed of any proprietary or commercial interest or conflicts of interest the authors may have that relate directly or indirectly to the subject of this article.

All authors certify that they have made substantive and specific intellectual contributions to the article and assume public responsibility for its content.

Finally, the authors certify that none of the material in this manuscript has been published previously or is currently under consideration for publication elsewhere.

| | | |
|---|---|---|
| First author/date | Second author | Third author |
| Fourth author | Fifth author | Sixth author |

**This agreement must be signed by all authors in order for the manuscript to be published.**

### Case Reports

A case report is a brief description of a special case that provides a message that transcends the individual patient.

*Format.* There is no abstract. The introduction should be a short paragraph giving the general background and the specific interest of the case. No more than one case should be described in detail (similar ones can be mentioned briefly in the discussion). Emphasis should be on the radiologic aspects; clinical information must be limited to that necessary to provide a background for the radiology. The discussion should be succinct and should focus on the specific message and relevance of radiologic methods. A review of the literature is not appropriate.

*Length.* Maximum of five double-spaced, typewritten pages, including the references but not the title page or figure legends.

*References.* Maximum of eight.

*Figures.* Maximum of three or four, unless the text is shortened accordingly. Legends must not repeat the text.

*Tables and Acknowledgments.* Not appropriate in case reports.

### Technical Notes

A technical note is a brief description of a specific technique or procedure, modification of a technique, or equipment of interest to radiologists.

*Format.* No abstract, headings, or subheadings are required. If headings are used, they should be a combination of "Case Report," "Materials and Methods," "Results," and "Discussion." A brief one-paragraph introduction should be included to give the general background. Discussion should be limited to the specific message, including the uses of the technique or equipment. Literature reviews and lengthy case reports are not appropriate.

*Length.* Maximum of five double-spaced, typewritten pages, including the references but not the title page or figure legends.

*References.* Maximum of eight.

*Figures.* Maximum of two, unless the text is shortened accordingly.

*Tables and Acknowledgments.* Not appropriate in technical notes.

### Pictorial Essays

A pictorial essay is an article that conveys its message through illustrations and their legends. Unlike other *AJR* articles, which are based on original research, pictorial essays serve primarily as teaching tools, like exhibits at a scientific meeting. They are not encyclopedic book chapters. The abstract should be a short, introductory paragraph.

*Length.* Maximum of four double-spaced, typewritten pages, including the references but not the title page or figure legends.

*References.* Maximum of four.

*Figures.* Maximum of 30 figure *parts*. Number should be as few as necessary to convey the message of the paper.

*Tables and Acknowledgments.* Not appropriate in pictorial essays.

### Letters to the Editor and Replies

Letters to the Editor and Replies should offer objective and constructive criticism of published articles. Letters may also discuss matters of general interest to radiologists. Do not end a letter with a hand-written signature.

*Format.* All letters should be typed double-spaced on nonletterhead paper, with no greeting or salutation. Name and affiliation should appear at the end of the letter. Titles for letters should be short and pertinent. The title for a reply is simply "Reply."

*Length.* Maximum of two double-spaced, typewritten pages, including references.

*References.* Maximum of four.

*Figures.* Maximum of two.

*Tables and Acknowledgments.* Not appropriate in Letters to the Editor and Replies.

### Opinions, Commentaries, and Perspectives

Opinions, commentaries, and perspectives are special articles dealing with controversial topics or issues of special concern to radiologists.

*Format*. Include a title page but no abstract. Headings may be used to break up the text.

*Length*. Maximum of five double-spaced, typewritten pages.

*References*. Maximum of five.

*Tables and Figures*. Maximum of four.

### Computer Page Articles

Articles published on the computer page deal with practical computer applications to radiology.

*Format*. Include a title page but no abstract.

*Length*. Maximum of eight double-spaced, typewritten pages.

*References*. Maximum of five.

*Figures and Tables*. Maximum of five. Computer printouts are not acceptable. Figures must be submitted as 5 × 7 in. glossy prints.

**All submissions to the *AJR* must be accompanied by a completed copy of the Author's Checklist and the signed Copyright Agreement.**

# RADIOLOGISTS

## MRI FELLOWSHIP/GENERAL DIAGNOSTIC

The Saudi Arabian Oil Company's (SAUDI ARAMCO) Medical Services Organization in Saudi Arabia requires a Radiologist, with MRI and neuroradiology experience, and also a general diagnostic Radiologist. American Board Certification and 2 years' experience after residency required.

Saudi Aramco's 483 bed Dhahran Health Center has all major specialties and most subspecialties. The company also operates out-patient and emergency care clinics in its 3 surrounding communities. Saudi Aramco employees and their dependents comprise the 200,000 patient population. Our Blood Bank is accredited by the American Association of Blood Banks. Consulting liaisons exist with the WHO in Geneva and the Centers for Disease Control in Atlanta.

As a Saudi Aramco employee, you will receive a competitive base compensation package, as well as an expatriate premium. Additional benefits include noncontributory group life insurance, company-matched savings, free medical care at Saudi Aramco's hospital and clinics, housing inside a company community, and extensive recreation facilities and activities. Your eligible children will be enrolled in companyschools, comparable to U.S. private schools. There are up to 13 company holidays annually, and you will be eligible for 36 calendar days of vacation, with round trip airfares to the U.S. or Canada for you and your family.

For consideration, send your resume/salary history indicating area of interest to: **ASC, Employment Dept. 06G-019-1, P.O. Box 4530, Houston, Texas 77210-4530** or call **Velma Guy at 1-800-827-5700 Ext. 8060 or 713-432-8060.**

SAUDI ARAMCO

# *AJR* Business and Subscriber Information

### The American Roentgen Ray Society

*AJR, American Journal of Roentgenology*, is published monthly to disseminate research on current developments in the radiologic sciences and commentary on topics related to radiology. It is published by the American Roentgen Ray Society, 1891 Preston White Dr., Reston, VA 22091; (703) 648-8992. Inquiries regarding society business, the annual ARRS meeting, and membership should be addressed to the Society at the above address.

### Correspondence Concerning the *AJR*

Correspondence regarding display (not classified) advertising, subscriptions, address changes, reprints, and permission requests should be addressed to Williams & Wilkins, 428 E. Preston St., Baltimore, MD 21202; (301) 528–4000.

Correspondence regarding editorial matters and classified advertising should be addressed to Editorial Office, AJR, 2223 Avenida de la Playa, Ste. 103, La Jolla, CA 92037-3218; telephone (619) 459-2229; FAX (619) 459-8814. For information on manuscript submission, see Guidelines for Authors, pages A3–A5.

### Subscriber Information

Subscription requests and inquiries should be sent to Williams & Wilkins, 428 E. Preston St., Baltimore, MD 21202. ARRS annual dues include $50 for journal subscription. Subscription rates are as follows: nonmembers, $125/year ($180 foreign); institutions, $135 ($190 foreign); nonmember in-training, $25 ($80 foreign). Single copies of the Journal may be purchased for $18 ($22 foreign). Airmail rates will be furnished on request.

Call toll-free, 1-800-638-6423 (in Maryland call 1-800-638-4007), with subscription questions or problems. Please have the mailing label from your latest issue available when you call.

If a subscriber receives a damaged copy of the *AJR* or fails to receive an issue, the subscriber should notify Williams & Wilkins (428 E. Preston St., Baltimore, MD 21202) within 60 days of publication (90 days for foreign subscribers) and that issue will be replaced.

Change of address information should be sent to Williams & Wilkins, 428 E. Preston St., Baltimore, MD 21202. Allow 90 days for address changes.

### Copyrights, Permissions, and Reprints

The American Roentgen Ray Society holds the copyright for all material published in the *AJR*. No part of this publication may be reproduced without permission from the ARRS. Requests for such permission should be addressed to Williams & Wilkins, 428 E. Preston St., Baltimore, MD 21202.

For reprints of a particular article, please contact the author designated in the footnotes for that article.

### Indexes

The *AJR* provides volume and yearly indexes (subject and author) in the June and December issues each year. *AJR* articles are also indexed in *Current Contents*, *Index Medicus*, and the cumulative index published by *Radiology*.

# Chief Of Radiology
## Veteran's Administration Hospital

The Chief of Radiology has direct responsibility for all aspects of the Radiology service at the Veteran's Administration Hospital. In consultation with the Department Chair, the candidate works with the Chief of Staff of the VA Hospital to whom he or she reports for all aspects of VA service function which include planning, administration and implementation, including Quality Assurance.

The Chief is a member of the Clinical Executive Board and the Dean's Committee. The Chief of Radiology at the VA serves as Vice Chairman of the Department of Radiology for VA Affairs. Under the direction of the Chair, the candidate is charged with the development and integration of academic programs for the VA Radiology. The Chief will be expected to participate in all activities of the Department at a level appropriate to his or her interests and Department needs. These include clinical activities, housestaff and student educational programs and the development of a research program in Radiology based at the VA.

**Please forward resume to: Dr. Peter Spiegel, Dartmouth-Hitchcock Medical Center, Department of Radiology, 2 Maynard Street, Hanover, NH 03756.**
**An equal opportunity employer.**

**Dartmouth-Hitchcock Medical Center**

The Hitchcock Clinic
Hanover, New Hampshire

---

**National Institutes of Health**
**Public Health Service**
**Department of Health and Human Services**

# Radiologist

The National Institutes of Health (NIH) is seeking an experienced Board-certified radiologist to direct its new Diagnostic Radiology Research Program (DRRP). The Director will organize and conduct a research training program in diagnostic imaging for radiologists and provide a coordinating focus for the many ongoing research initiatives in diagnostic imaging at the NIH. The Diagnostic Radiology Research Program will train between 4-6 radiologists a year, and will have access to extensive research facilities, including an NMR dedicated exclusively to the research program and supported by the NIH Nuclear Medicine Research Center. In addition, the Director will be provided with laboratory facilities, personnel and operating budget to pursue independent research in diagnostic imaging. Applicants should have an ongoing radiology research program and relevant experience in clinical imaging and in teaching of diagnostic radiology. Interested individuals should submit a curriculum vitae and bibliography to:

**Dr. Dinah Singer**
**Office of Intramural Affairs**
**National Institutes of Health**
**Building 1, Room 140**
**9000 Rockville Pike**
**Bethesda, MD 20892**

NATIONAL INSTITUTES OF HEALTH

*NIH is an Equal Opportunity Employer*

---

# RADIOLOGIST

BC/BE radiologist with subspecialty in MRI wanted to join us for an immediate opening of an outpatient MRI imaging center, and also hospital practice in northeastern region.

Situated in a beautiful summer/winter recreational area, in close proximity to several major cities.

This is an excellent professional opportunity in a rapidly growing community.

Fir year, excellent salary with high incentive, giving you an extraordinary financial package with many fringe benefits lead to partnership.

Please reply to:

AJR Box 1
Williams & Wilkins
428 E. Preston Street
Baltimore, MD 21202-3993.

---

# Duke University

## Staff Radiologists

DUKE UNIVERSITY MEDICAL CENTER is seeking qualified candidates for staff positions in the Department of Diagnostic Radiology. Currently there are a limited number of staff positions available in the following sections: General Diagnostic Radiology, Pediatric Radiology, Chest Radiology, Musculoskeletal Radiology, Vascular - Interventional.

We offer an excellent salary and benefits package. The Radiology department is state-of-the-art in diagnostic imaging with diverse resources available for clinical, teaching, and academic pursuits. Staff members have guaranteed academic time and research support. Interested Board Certified Radiologists with appropriate experience should submit letters of inquiry to Office of the Chairman, Department of Radiology, Box 3808, Duke University Medical Center, Erwin Road, Durham, North Carolina 27710.

# You learn from your experience with

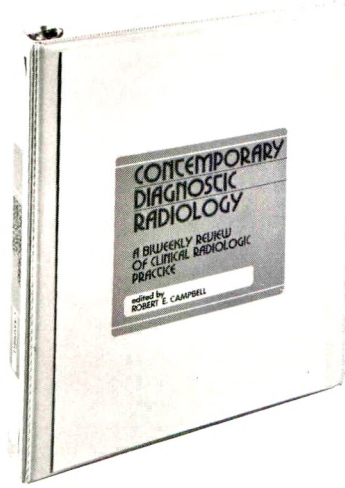
# CONTEMPORARY DIAGNOSTIC RADIOLOGY

Editor: **Robert E. Campbell, M.D.**

*A Biweekly Review of Clinical Radiologic Practice—26 issues a year!*

One of your toughest jobs is keeping up with the many new developments that affect radiology. That's why you want **Contemporary Diagnostic Radiology**... an effective and convenient way to perfect your skills and maintain your professional status.

**Contemporary Diagnostic Radiology** is designed as a continuing education program that lets you work at your own pace. Every two weeks you'll receive an issue that covers a single topic or procedure in detail. Read the information and study the clearly reproduced radiographs—and then, if you choose, respond to a comprehensive examination in the strictest confidence. You set the pace.
Each biweekly lesson brings you pertinent review of the basics in bone radiology... gastrointestinal radiology... pediatric radiology... genitourinary radiology... MR imaging... and all of the topics you want to know more about.




**Contemporary Diagnostic Radiology** works *two ways*. You may choose to subscribe to the non-scoring version, receiving every issue as an important element of your professional reading. The scoring version, however, supplements your reading and computer-coded examinations with confidential result responses, making you eligible for Continuing Medical Education credits co-sponsored by the University of Pennsylvania School of Medicine.

*"As an organization for continuing medical education, the University of Pennsylvania School of Medicine designates this continuing medical education activity as meeting the criteria for 1 credit hour per bi-weekly issue in Category I for Educational Materials for the Physician's Recognition Award of the American Medical Association provided it has been completed according to instructions."*

You can begin this ongoing program **today**. **Contemporary Diagnostic Radiology** is a year-round program, so you can join at any time. To begin your lessons, just fill out the enclosed card and return it to us. Or call **FREE** 1-800-638-6423 from anywhere in the U.S. or Canada. You'll find that **Contemporary Diagnostic Radiology** is the most efficient and inexpensive way to keep up with your dynamic field.

**Williams & Wilkins**

P.O. Box 23291
Baltimore, Maryland 21203-9990

Broadway House
2-6 Fulham Broadway
London SW6 1AA England

clip & mail

## CONTEMPORARY DIAGNOSTIC RADIOLOGY

☐ **Yes!** I want to keep pace in my field! Begin my 26-issue subscription:
☐ Send me the scoring version ($240)
☐ Send me the non-scoring version ($197)
☐ Send me the resident non-scoring version* ($120)
(add $57 for optional airmail delivery outside the U.S.; in Canada, also add 7% GST.)
☐ new subscription ☐ renewal

name

address

city/state/zip

payment options
☐ payment enclosed ☐ bill me
☐ American Express ☐ MasterCard ☐ VISA

printed in USA

card # expiration date

signature/P.O. #

Maryland residents add 5% sales tax. Subscriptions outside the U.S. must be prepaid in U.S. dollars only. Rates valid through October 31, 1991. Please allow 8 weeks for delivery of your first issue, up to 16 weeks for surface delivery outside the U.S. Optional airmail rates add $57 per subscription.

*Residents are eligible for the special in-training rate for up to three years. When requesting this rate, please include training status and institution.

Don't forget: you can order with a **TOLL-FREE** call to 1-800-638-6423 from anywhere in the U.S. or Canada.

**Williams & Wilkins**

P.O. Box 23291
Baltimore, Maryland 21203-9990

Broadway House
2-6 Fulham Broadway
London SW6 1AA England

CDR 52740 J1091S01

*George W. Holmes Lecture*

# Whose Turf Is Imaging? Independent Practice, Academics, and Research

Bruce J. Hillman[1]

Dr. George W. Holmes would be amazed by the technological innovations that have occurred in diagnostic imaging during the past two decades. Just as extraordinary, however, are the changes that have occurred in the politics, economics, and social structure of radiology and medicine in general. My lecture concerns these latter events. Specifically, I will address what I perceive to be the increasing trend of nonradiologist physicians performing diagnostic imaging as part of their practices—what is commonly termed self-referral.

***AJR* 156:443–447, March 1991**

This presentation will address five aspects of self-referral: (1) What do we know about the extent of self-referral? (2) What are the motivations for self-referral? (3) What are known about the ethics, quality, and costs associated with self-referred imaging? (4) I will present the results of a recent assessment of self-referral performed jointly by myself and researchers at the American College of Radiology (ACR) and Abt Associates (Cambridge, MA). (5) What strategies might be used to combat self-referral?

## The Extent of Self-referral

No firm data exist to support the belief that self-referral for diagnostic imaging is on the increase; however, this is the perception of many observers. An evaluation of physicians' claims for imaging services provided to Medicare patients in 1984 (ACR, unpublished communication) indicates that radiologists provide nearly all imaging services for hospital inpatients and in the hospital outpatient setting. However, radiologists submitted only one third of claims for imaging procedures performed in physicians' offices, accounting for 39% of physicians' imaging charges in this setting. This does not take into account claims referable to chiropractors, podiatrists, and other nonphysicians. My own research substantiates this estimate. My evaluation of the private insurance claims for chest radiographs, obstetric sonograms, lumbar spine radiographs, excretory urograms, cystograms, and sonograms of the pelvis or retroperitoneum of over 400,000 patients tracked from January 1986 to June 1988 indicates that radiologists performed 83–98% of these procedures on hospital outpatients, depending on the type of examination. Radiologists performed 26–53% of these examinations when they were performed in physicians' offices.

Levin and Matteucci [1] surveyed academic radiology programs in the United States to determine who controlled various selected procedures in university hospitals. They found that radiologists primarily performed all musculoskeletal, breast, and neuroimaging procedures as well as pulmonary and genitourinary angiography and interventional procedures, percutaneous biliary procedures, ab-

Received July 13, 1990; accepted after revision October 12, 1990

Presented at the annual meeting of the New England Roentgen Ray Society, Cambridge, MA, May 1990.

[1] Department of Radiology, University of Arizona College of Medicine and the University Medical Center, Tucson, AZ 85724.

0361–803X/91/1563–0443
© American Roentgen Ray Society

scess drainages, and cross-sectional imaging. Radiologists shared with other physicians obstetric and vascular sonography, hysterosalpingography, and urethrography. Nonradiologist physicians most often performed renal and biliary extracorporeal lithotripsy; imaging and interventional procedures related to the heart; endoscopic retrograde cholangiopancreatography; and some interventional techniques, such as percutaneous gastrostomy. The growing belief that radiologists' control of peripheral angiography and interventional procedures is threatened is supported by the marketing projections of the Medrad Corporation (Pittsburgh, PA), which believes that sales of catheters and interventional devices to cardiologists are expected to grow far more quickly between now and 1996 than sales to radiologists will grow (Wholey M, personal communication). While, to some extent, this reflects expected growth in cardiac procedures, there is also the assumption that cardiologists will increasingly perform peripheral examinations and interventions.

### Motivations for Self-referral

Changes in the regulation, reimbursement, and social fabric of medicine during the past decade have had a profound effect on the motivations for self-referral.

Although the glut of physicians projected for many specialties has not materialized, the average number of patients treated by each physician is expected to be over 20% fewer in 1990 than it was in 1975 [2]. Despite this, physicians' incomes have escalated at a rate significantly higher than inflation during this period, largely related to their providing "more intense" care—providing more and more complex services to patients than was provided previously [3]. Holohan and Zuckerman [4] recently indicated that much of this was attributable to physicians' increasingly incorporating medical technologies into their office practices. Although no firm evidence exists, my presumption is that prime options for technologies to be incorporated into office practice are imaging devices. This likely phenomenon is encouraged by the increasing ease of operation and safety of imaging innovations of the past 20 years.

Governmental initiatives have also affected motivations for self-referral. The simultaneous implementation of certificate-of-need regulations—now defunct in most states—and the diagnosis-related-groups method of reimbursing hospitals for inpatient stays resulted in the financial instability of many hospitals while encouraging expansion in the outpatient sector, which was encouraged to pursue free-market competition. This opened the way for a new spirit of entrepreneurism in medical imaging while simultaneously disabling the traditional purchasers of expensive imaging equipment, the hospitals. New entities that had not been significant forces in medical imaging—venture capitalists and corporations—as well as physicians became more involved in order to supply the capital for increasingly expensive imaging technology and reap its expected rewards. Monetary goals gained increasing prominence as a result. The emphasis on financial rewards of many of these new ventures required some assurance of a sufficient patient base; self-referral by nonradiologist physicians continues to provide a foundation for ensuring the success of many such ventures.

The real and potential harm to radiologists of the increasing frequency of self-referral is self-evident: decreasing scope and number of referrals for imaging, exclusion from multiphysician and hospital-physician ventures because we cannot refer patients, and strong-arm tactics by referring physician groups to receive payments from radiologists for their referrals [5]. In addition, society should have its own concerns about the practice of self-referral, specifically with respect to its ethics, the resultant quality of imaging, radiation, and its related financial costs.

### Ethics, Quality, and Costs

Proponents of self-referral argue that performing imaging in their own facilities is quicker and easier for the patient, that imaging diagnoses can more rapidly affect patient care when performed in physicians' offices, and that integration of imaging information with other aspects of the patient's care is best performed by the physician primarily responsible for care of the patient. The counterarguments are that self-referral is likely to result in poorer quality imaging, lesser expertise in physician interpretation, and ethical conflicts for physicians who have a financial incentive to refer patients to their own facilities. The position of the American Medical Association (AMA) is that self-referral for medical imaging is an acceptable practice, so long as patients are apprised of the physician's ownership interest in the technology [6]. The rationale of the AMA for this policy is that overuse of imaging attributable to self-referral has not been measurable, that there is insufficient information concerning what constitute appropriate imaging practices, and that the benefits of self-referral outweigh the possible harm [6].

Some of the AMA's argument seems to be valid; we have been negligent in developing standards for appropriate imaging and in defining overuse. However, it is difficult to see how a patient can be said to have a meaningful choice to decline undergoing the imaging his or her physician recommends or seek imaging elsewhere when apprised of a potential conflict of interest. Moreover, there is nothing to indicate that large differences in the use of imaging are attended by differences in health benefits to patients.

What we know about differences in the quality of imaging between radiologists and self-referring physicians is extremely scant. In 1985, Blue Shield of Pennsylvania reported a pilot study involving blind assessments of image quality of chest and bone radiographs obtained by radiologists and other physicians (Blue Shield of Pennsylvania, unpublished communication). Technically nondiagnostic images were attributable to radiologists and orthopedists in 12% and 13% of cases, respectively. Internists, general and family practitioners, and pulmonologists exposed nondiagnostic images in 41–55% of examinations. No direct evaluation of the relative interpretive abilities of different specialties has been performed. However, in a study published in 1983, Rockoff et al. [7] found that more than 90% of hospital-based physicians believe that radiologists perform a unique or important service

or are useful or indispensable. In contrast, only about two thirds of physicians with office practices regard radiologists this way.

Only a little more is known about the costs of self-referral than is known about its quality. In 1978, Schroeder and Showstack [8] published a model demonstrating the potential financial incentives for nonradiologist physicians to incorporate chest imaging in their office practices. Childs and Hunter [9] assessed a relatively small group of physicians caring for an elderly population of patients in Northern California, finding that the capacity to bill for imaging was associated with significantly higher rates of imaging studies. Perhaps the most compelling study was performed in 1978 by Radecki and Steele [10], but not published until 1990. These investigators, working with a number of specialty societies, had 5447 representative physicians keep a diary of all patients encountered and what services were rendered during a several-day period. They found that physicians with imaging facilities "on site" more frequently performed imaging than those whose patients had to go "off site." A similar result was found with regard to a study focusing on family practitioners [11]. Finally, in 1990, Hemenway et al. [12] studied a group of ambulatory centers in the Boston area that had traditionally paid their physicians by salary. The authors assessed physicians' imaging practices before and 6 months after the institution of an incentive-based system that paid physicians partially on the basis of how many patients they saw and what services they performed. In this 6-month period, use of imaging increased 16%.

### The Cost of Self-referral

These studies have been criticized for the lack of generalizability of their patient populations; their small sample sizes; and their lack of controls for differences in patient mix, physician practices, and imaging procedures performed. In an effort to transcend these problems, the ACR recently funded a study intended to focus on the costs associated with self-referral for diagnostic imaging. The research involved a collaboration of ACR researchers; researchers at Abt Associates, a Boston think tank; and me. The goal of the research was to employ a large insurance claims data base to assess differences in imaging use and costs associated with self-referral vs radiologist-referred imaging in physicians' office practices [13].

To address this issue, we developed a method that permitted us to ask two primary questions: (1) Given a patient with a specific set of symptoms, is the patient more likely to receive an imaging examination during an illness if he or she seeks care from a physician who self-refers or from one who refers patients to a radiologist? (2) For all such patients, depending on their choice of physician, what will be the average imaging costs for their episodes of illness?

We purchased access to a private insurance claims data base (Medstat Systems, Inc., Ann Arbor, MI) that summarized all physicians' claims submitted on behalf of 405,000 employees and dependents of large American corporations during the period January 1986 through June 1988. Coverage for imaging was comprehensive, with no copayments required of insured patients. We developed a computer algorithm that segregated appropriate claims for each patient into episodes of medical care related to their presentation to a physician for four types of symptoms: (1) upper respiratory infection, possibly pneumonia; (2) pregnancy; (3) low back pain; and (4) males with trouble urinating.

Episodes were initiated by the computer encountering a diagnostic (ICD-9) code that might represent one of these clinical presentations and terminated after a predesignated period after the initial presentation. We developed a second algorithm to determine whether the physician responsible for the care of the patient during each episode was a self- or radiologist-referring physician, whether an imaging claim with an imaging procedure (CPT-4) code appropriate to the clinical presentation was present during the episode, and if so, whether a radiologist or a nonradiologist physician performed the imaging. The mean frequency of imaging for self- and radiologist-referring physicians, for each of the four clinical presentations, was estimated as

$$\frac{\text{Number of episodes with imaging}}{\text{Total number of episodes}}.$$

The average cost of imaging per episode of medical care was

$$\text{Mean imaging frequency} \times \text{Mean imaging charge}.$$

Adjustments were made in the results to account for possible miscategorization of physicians, and hence episodes, and the assignment of the episodes of physicians who we could not definitely categorize as self- or radiologist-referring.

The algorithm generated 65,988 episodes involving 6419 physicians. Seventy-nine percent of the episodes related to upper respiratory infection. For episodes involving only one nonradiologist physician (92% of all episodes), self-referral resulted in 4.0–4.5 times more imaging than did radiologist referral, depending on the clinical presentation. Because self-referral physicians generally charged more for imaging examinations than radiologists, their episodes generated 4.4–7.5 times the charges per episode of care than the episodes attributed to radiologists. All of these differences are statistically significant. The data on episodes involving two physicians (7% of all episodes) supported these findings. The results were uniformly sustained in a separate analysis that compared self- and radiologist-referring physicians of the same specialty for all specialties represented. There were no significant differences in the complexity of examinations performed by radiologists and self-referring physicians.

Thus, we concluded that self-referral results in much greater use of imaging and promotes much higher imaging charges during episodes of illness; the methodology and analysis ensure that the differences between self- and radiologist-referring physicians cannot be explained on the basis of differences in patient mix, physician specialization, or complexity of imaging examinations. Although this study cannot address imaging use and costs associated with other clinical presentations, the consistency of the results regarding widely disparate organ systems, clinical presentations, and imaging

technologies suggests that differences in physicians' imaging practices based on their ownership of imaging devices may be widespread. This study also does not address to what extent the differences in use associated with self-referral are attributable to financial incentives or whether self-referring physicians' or radiologist-referring physicians' imaging practices might be more appropriate. However, unless one believes that four or more times the use and up to seven times the cost are associated with comparable levels of improvement in patients' health, radiologist referral would appear to represent the more cost-effective technology.

### Combating Self-referral

At the 1989 Radiology Summit meeting, proposals were set forth for combating self-referral [14]. The following are my own views concerning these proposals, which I believe serve as a reasonable framework for suggesting practical approaches to the problem:

1. Generate data that radiologists are cost-effective. This, of course, is the issue that we addressed in the research project that I have just described. The intent of these activities is to generate information that can be presented to legislators, regulatory agencies, and third-party payors who may have a special interest in improving the cost-effectiveness of diagnostic imaging. The results of this research already have found interested ears in the United States Congress and the Physician Payment Review Commission and at the offices of the health and retirement funds of a major union. The data should help to refuel the Ethics in Patient Referrals Act, from which consideration of diagnostic imaging was excluded in the last congressional session, and may also affect the Bureau of Health and Human Services' consideration of "safe harbors" for self-referral. The United Mineworkers Health and Retirement Funds has undertaken, with the ACR and me, a study of its own beneficiaries, using the same methods that we used in our previous study of self-referral. Representatives of the Funds have indicated that they may take some action to limit self-referral if the study reveals similar results. I believe that, given the success of its recent venture, the ACR should continue to fund research into the costs and quality of self-referred imaging and promulgate the results of this research to appropriate agencies.

2. Improve access to expert imaging. More critical reviews of what ought to constitute core radiology training ought to be undertaken. Subspecialization by organ system orientation—specifically not technology orientation—should be encouraged to ensure our unique role as referral specialists who can truly be of service to referring physicians. We should more accurately assess the demand for radiology services and in what areas the demands are most pronounced, then increase the numbers of our trainees accordingly. Radiologic practice should be uniformly of higher quality; although this may occasionally mean sacrificing some revenue, state-of-the-art practice is the underpinning of our future success.

3. Develop standards of practice. As noted by the AMA, little is known about what is appropriate imaging use and what constitutes high quality. This is our own fault. No one will generate this information other than us. Recent initiatives by the ACR to develop standards of practice and conduct research into radiologic appropriateness are steps in the right direction. An important recent development is the recommendation by the Physician Payment Review Commission to Congress [15] that Medicare payment for mammography be based on standards of quality. The ACR and appropriate subspecialty societies should work together to generate the data needed to support expansion of this concept to other imaging indications and further its acceptance by regulatory and reimbursement agencies.

4. Increase radiologists' awareness of the importance of patient interactions. This speaks for itself, as does its corollary of making patients and their physicians more aware of the importance of expert imaging and image interpretation. It is becoming obvious that opportunities for patient-referred imaging may be limited. To the extent possible, however, these situations should be maximized by friendly, efficient, and expert interactions.

5. Improve radiology research and technology assessment. It has become apparent that the specialties responsible for developing new medical technology and assessing it generally gain ascendancy in medical practice. During the past 20 years, the physician researcher has become an "endangered species" [16, 17] in all medical specialties. Radiology is affected more severely than many other specialties. My own research [18–20] in this area indicates that only 1% of academic radiologists spend 50% or more of their time conducting research—the definition of a physician researcher generally accepted among other medical specialties. Indeed, only 22% of academic radiologists have any designated research time at all. In light of my findings that research productivity is linearly related to the amount of time available to do research and that faculty overwhelmingly perceive the lack of research time as the greatest impediment to their performing research, this would seem to be an important root of the radiology research problem. We also seem to be doing little to provide research training to our residents and fellows. My research found that having a radiology research fellowship, publishing research during training, and attending regular research seminars were important predictors of residents and fellows choosing and being successful in research careers, yet only a minority of training programs offer these experiences in an organized fashion. The dearth of research training contributes to radiologists' relative lack of sophistication in research, which is reflected in the predominance of descriptive, rather than investigative, research papers in our journals. This reflects poorly on our specialty and perpetuates the perception among other specialists that we are a "service" and not a scientific specialty, further harming our claims to imaging turf. Academic radiology programs must determine if research, including scientific technology assessment, will be a priority to the extent that they will devote significant resources to faculty and trainees with the talents and interests to pursue research careers.

### Conclusions

In retrospect, the situation I have described may appear unduly bleak. Other physicians have the patients; we depend

on their referrals. However, I believe that any number of circumstances—not the least of which is our ardent attention to combating self-referral by the means I have described and innumerable others that may occur to you—might reverse the situation. As I have detailed, some interventions already are under consideration or underway. Indeed, I am rather optimistic about the future well-being of radiology, assuming that we do not squander our opportunities. Assuming that we do not, and that we continue to attract the very best medical school graduates to our specialty, "Our future's so bright, we gotta wear shades" (Timbuk 3).

## REFERENCES

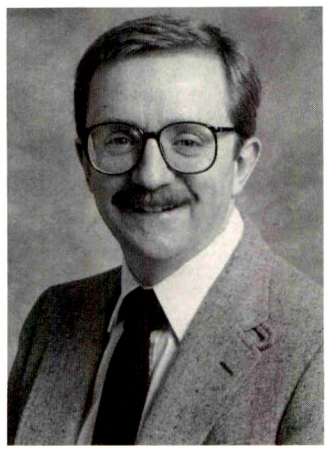

1. Levin DC, Matteucci T. Do radiologists control imaging studies? Survey results from 198 academic institutions. *Radiology* **1989**;170:879–881
2. Starr P. *The social transformation of American medicine.* New York: Basic Books, **1982**:420–425
3. Physician Payment Review Commission. *Annual report to congress.* Washington, DC: Physician Payment Review Commission, **1988**
4. Holohan J, Zuckerman S. Understanding the recent growth in Medicare physician expenditures. *JAMA* **1990**;263:1658–1661
5. Waldholz M, Bogdanich W. Warm bodies. Doctor-owned labs earn lavish profits in a captive market. *Wall Street Journal* **1989** Mar 1:A1, A6
6. Todd JS, Horan JK. Physician referral—the AMA view. *JAMA* **1989**;262:395–396
7. Rockoff SD, Davis DO, Gaskill JW. Physician attitudes towards the competence of general diagnostic radiologists: survey and implications. *AJR* **1983**;140:639–648
8. Schroeder SA, Showstack JA. Financial incentives to perform medical procedures and laboratory tests. *J Health Econ* **1988**;7:337–367
9. Childs AW, Hunter ED. Non-medical factors influencing use of diagnostic x-ray by physicians. *Med Care* **1972**;10:323–335
10. Radecki SE, Steele JP. Effect of on-site facilities on use of diagnostic radiology by non-radiologists. *Invest Radiol* **1990**;25:190–193
11. Strasser RP, Bass MJ, Brennan M. The effect of an on-site radiology facility on radiologic utilization in family practice. *J Fam Prac* **1987**;24:619–623
12. Hemenway D, Killen A, Cashman SB, Parks CL, Bicknell WJ. Physicians' responses to financial incentives. *N Engl J Med* **1990**;322:1059–1063
13. Hillman BJ, Joseph CA, Mabrey MR, Sunshine JH, Kennedy DS, Noether M. The frequency and costs of diagnostic imaging in office practice: a comparison of self-referring and radiologist-referring physicians. *N Engl J Med* (in press)
14. ACR backed on referral. *ACR Bull* **1989**;45:1, 4–6
15. Goldfield J. *The costs of providing screening mammography.* Washington, DC: Physician Payment Review Commission. Report to Congress, **1988**
16. Wyngaarden JB. The clinical investigator as an endangered species. *N Engl J Med* **1979**;301:1254–1259
17. Hillman BJ. The inadequacy in the number and quality of physician researchers. A perspective and approach to the problem. *Invest Radiol* **1985**;20:767–771
18. Hillman BJ, Fajardo LL, Witzke DB, Irion M, Cardenas D, Fulginiti JV. Factors influencing the success of radiologists in publishing research. *Invest Radiol* **1989**;24:849–854
19. Hillman BJ, Fajardo LL, Witzke DB, Irion M, Cardenas D, Fulginiti JV. Factors influencing radiologists to choose research careers. *Invest Radiol* **1989**;23:842–848
20. Hillman BJ, Witzke DB, Fajardo LL, Fulginiti JV. Research and research training in academic radiology departments: a survey of department chairmen. *Invest Radiol* **1990**;25:587–590




# ARRS Announces Appointment of Drs. Chezmar and Gurney as 1991 Figley Fellows in Radiology Journalism



Judith L. Chezmar



Jud W. Gurney

Judith L. Chezmar, of Emory University, and Jud W. Gurney, of the University of Nebraska, have been selected from more than 30 highly qualified applicants to serve as the American Roentgen Ray Society's Melvin M. Figley fellows in radiology journalism for 1991.

The goals of the fellowships include encouraging bright young radiologists to continue with an academic career, accelerating their progress, and stimulating their interest in good radiology journalism, as well as improving the quality of radiology journals by teaching the fundamentals of medical journalism to academicians, training manuscript reviewers and future editors, and providing core teachers of medical journalism in radiology departments around the country.

Drs. Chezmar and Gurney will each spend 1 month in the *AJR* editorial office in La Jolla, CA, to learn the fundamentals of medical writing, manuscript preparation and editing, peer review, the ethics of medical journalism, and journal publication and printing in personal tutorials given by the *AJR* editors and editorial staff.

Dr. Chezmar is an assistant professor of radiology at Emory University School of Medicine in Atlanta, GA. She received an A.B. from Princeton University and an M.D. from the University of Cincinnati. She had her radiology residency at Johns Hopkins and Stanford University Hospitals. Author of over 20 articles and book chapters, mostly in the field of gastrointestinal radiology, she is the coordinator of radiology resident research at Emory.

Dr. Gurney took his undergraduate and graduate education at the University of Nebraska and had his radiology residency at that institution. After serving a year as the Scanlon fellow in pulmonary imaging at the Medical College of Wisconsin, he joined the faculty of the radiology department at his alma mater as an assistant professor in 1989. He has already published nearly 30 articles and book chapters, mostly in the area of his subspecialty, pulmonary radiology.

Review Article

# Breast Sonography

Lawrence W. Bassett[1] and Carolyn Kimme-Smith

**Sonographic equipment for breast imaging has continued to improve, and the role of breast sonography has evolved to that of an indispensable adjunct to mammography. Breast sonography is not useful for screening for breast cancer in any age group. Its main use is for the differentiation of cystic vs solid palpable and mammographically visible masses. If strict sonographic criteria are used for a simple cyst, the diagnostic accuracy approaches 100%. Sonographic diagnosis of a simple cyst precludes the need for further workup, including aspiration, biopsy, or follow-up. This article emphasizes the technical aspects of breast sonography, especially those factors that alter the diagnostic information on the images. These factors can be especially problematic in differentiating cysts and solid masses, the most common diagnostic use of breast sonography. Selection of equipment depends largely on the requirements of a specific practice. Optimally, the sonographic equipment is located close to where mammography is performed, and the sonographic and mammographic findings are interpreted together.**

The breast was one of the first organs examined with sonography when in 1952 Wild and Neal [1] investigated the potential usefulness of A-mode techniques for defining the texture of normal breast tissue and breast lumps. Breast sonography came into wider use after the introduction in the 1970s of equipment specially designed for breast imaging [2–6]. In the late 1970s, because of nationwide concerns over the possibility of radiation-induced breast carcinoma from screening mammography, clinical research on breast sonography emphasized its potential use as a breast cancer screening tool [7–9]. Equipment for breast sonography has continued to improve; but rather than supplanting mammography, the role of sonography has evolved to that of an indispensable adjunct to mammography [10].

## Current Role of Breast Sonography

Early clinical investigations of the value of sonography for breast cancer detection showed results approaching those of mammography [6, 9]. However, these clinical studies included many patients who were symptomatic, and the carcinomas generally were larger than those found in a screening population [11]. In addition, while the sonograms were usually of high technical quality and were obtained by the same technologist, the mammograms came from many different facilities and varied in quality. Later investigators reported poor results for sonography when compared with state-of-the-art mammography in the screening of asymptomatic women [10, 12, 13]. For example, in 1983 Sickles et al. [12] reported that in a prospective study of 1000 women, sonography detected only 58% of 64 pathologically proved cancers, compared with 97% detected by mammography. In that study, sonography detected only 48% of the cancers that had not yet spread to the axillary lymph nodes (mammography detected over 90%), 30% of the nonpalpable malignant lesions (mammography

Received May 15, 1990; accepted after revision September 12, 1990.
Presented at the American College of Radiology Breast Conference, New Orleans, LA, March 1990.
[1] Both authors: Iris Cantor Center for Breast Imaging, Department of Radiological Sciences, University of California, Los Angeles, School of Medicine, and the Jonsson Comprehensive Cancer Center at UCLA, Los Angeles, CA 90024. Address reprint requests to L. W. Bassett, Department of Radiological Sciences, UCLA Medical Center, 10833 Le Conte Ave., Los Angeles, CA 90024-1721.

*AJR* **156:449–455, March 1991** 0361–803X/91/1563–0449 © American Roentgen Ray Society

detected over 90%), and only 8% of the cancers smaller than 1 cm (mammography detected over 90%). Although anecdotal reports of sonographic detection of nonpalpable, mammographically normal cancers have continued to surface [14], the yield of sonography for breast cancer screening has been found to be too low to be of any practical value [10, 12, 13]. The limitations of sonography in screening for breast cancer include inability to depict microcalcifications, difficulty in imaging fatty breasts, inability to differentiate benign from malignant solid masses, and unreliable depiction of solid masses smaller than 1 cm.

Many breast carcinomas are infiltrating, and the sonographic appearance of these cancers is typically that of an irregular, hypoechoic (relative to surrounding parenchymal tissue) mass with inhomogeneous low-level echoes and a poorly visualized posterior wall (Fig. 1) [15]. The echoes distal to an infiltrating carcinoma are frequently diminished, and this "shadowing" had been identified as an important sign of malignancy [6]. However, many cancers have no effect on distal echoes, and some even show enhancement of posterior echoes [10, 16]. A review of 33 pathologically proved cancers depicted with a hand-held sonographic unit found that 19 produced no effect on posterior echoes, eight resulted in distal echo enhancement, and only six caused distal shadowing [10]. Diminished echoes may also be seen posterior to some fibroadenomas [17, 18]. Diagnosis of carcinoma by sonography is further complicated by the fact that some carcinomas, probably fewer than 10–15%, have sonographic features similar to those usually associated with benign solid masses such as fibroadenomas (Fig. 2) [10, 19]. Therefore, it is important that biopsy of a palpable or mammographically detected solid mass not be deferred solely on the basis of "benign" sonographic features.

Another problem that has received less attention is overdiagnosis resulting from the depiction of large numbers of benign solid masses detected incidentally by sonography, leading to "unnecessary" biopsies [20]. As a result of the nonspecificity of sonography in the evaluation of solid breast masses, in many clinical practices biopsies are performed on all masses that are shown to be solid. However, the rate of cancer detection (number of cancers detected over total biopsies performed) resulting from the biopsy of nonpalpable well-circumscribed mammographically undetected masses by using sonography is unacceptably low [10, 11, 21].

Although sonography has been shown to have no role in screening, it is occasionally useful in the evaluation of selected patients with suspected carcinoma. For example, it may help in localizing a suspicious mass detected in only one mammographic projection [22]. However, this is usually accomplished more effectively with additional mammographic positioning [23]. Some radiologists use sonography for the evaluation of an asymmetric density identified by mammography; however, there is no evidence, other than anecdotal, to prove the efficacy of the use of sonography for this purpose and it is not currently recommended [24]. Not only is sonography ineffective in identifying nonpalpable carcinoma in these cases, but a normal-appearing sonogram does not exclude the possibility of carcinoma.

Sonography has been recommended as the primary imaging technique for women younger than 30 with breast problems [11, 25]. The rationale for this approach in younger women includes the lower prevalence of breast cancer, the greater likelihood that the breasts will be dense and poorly suited to mammography, and greater susceptibility to radiation-induced malignant tumors [26, 27]. When a simple cyst is identified at the site of a palpable abnormality, mammograms are not necessary. When sonography does not show a cyst, the mammographic workup in the woman under 30 is tailored to the clinical findings and usually begins with an oblique view of one breast [11]. In a review of 389 women under 35 who had undergone sonographic examinations, sonography, although useful in preventing excisional biopsies of simple cysts, was not reliable in differentiating benign from malignant solid masses [27].

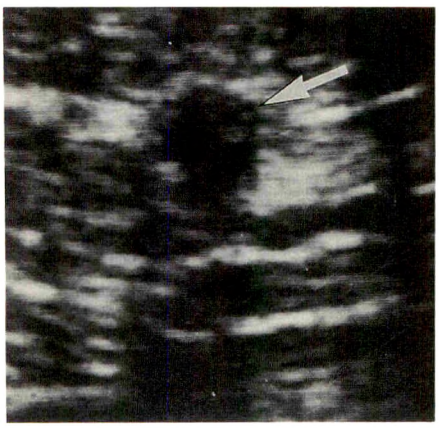


Fig. 1.—Sonogram of infiltrating ductal carcinoma. Mass (*arrow*) has an irregular border, inhomogeneous low-level interior echoes, and poorly defined posterior wall. Note attenuation of echoes posterior to tumor (shadowing).



Fig. 2.—Sonogram of well-circumscribed ductal carcinoma. Mass (*arrow*) has a relatively smooth border, homogeneous internal echoes, and well-defined posterior wall. Note accentuation of echoes posterior to tumor (enhancement).

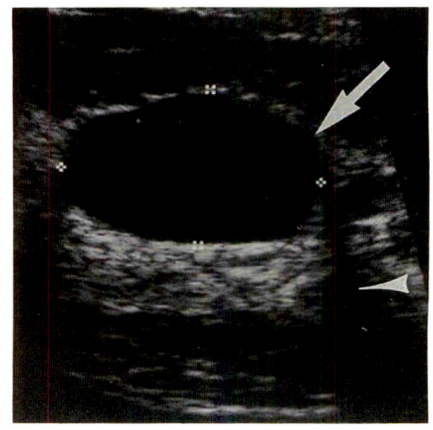


Fig. 3.—Sonogram of typical cyst. Oval mass (*arrow*) has well-defined anterior and posterior borders, anechoic interior, and enhanced through-transmission of sound distally. *Arrowhead* indicates refractive shadows distal to lateral wall of cyst.

Today, the primary role of sonography is in the cyst vs solid differentiation of palpable and mammographically detected masses. In the diagnosis of a simple cyst, sonography has a reported accuracy of 98–100% [21, 28, 29]. Typical features of cysts include round to oval shape, well-circumscribed margins, anechoic interior, and increased through-transmission of sound (Fig. 3). Additional features that may be seen include refractive shadowing posterior to the lateral margins of the cyst, compressibility, and the presence of septa within multiloculated cysts. Although the detection of solid masses smaller than 1 cm is unreliable, because the mass may have an echo intensity similar to that of surrounding breast tissues, cysts as small as 2 mm can be detected easily because the anechoic interior of a cyst provides high contrast with adjacent breast parenchyma [10]. In addition, the increased intensity of echoes distal to a cyst enhances its identification.

The sonographic demonstration that a mammographically detected mass is a simple cyst eliminates the need for any further workup, including aspiration, biopsy, or follow-up [29]. A simple cyst is defined as one with smooth margins, a well-defined posterior wall, enhanced sound transmission distally, and, most importantly, an echo-free interior when imaged with appropriate technical parameters (Fig. 3). By showing that a mammographically detected mass is a simple cyst, sonography can decrease the number of needle localizations and biopsies that need to be performed by 25% [29]. However, it is important to be certain that a mass demonstrated by sonography is the same mass as the mammographically detected one. This can be accomplished by placing a radiopaque marker over the location of the mass with sonographic guidance, and then repeating the mammogram with the marker in place [11].

### Technical Factors and Equipment

In order to use sonography effectively it is important to understand the technical factors that affect the images, and breast sonography presents several technical challenges. For example, breast tissue is heterogeneous, resulting in rapid diminution of the beam owing to reflection and scattering from the many impedance mismatches of tissue interfaces. Extensive refraction from curved breast tissue interfaces adds to beam defocusing [30]. These problems have resulted in the development of tightly focused, large-aperture, high-frequency transducers capable of depicting the smaller breast structures. Additional technical factors to be considered in breast sonography include imaging lesions in the focal zone of the transducer and selecting proper power, time-gain compensation, and gray-scale mapping.

Masses located in the superficial breast tissues may be distorted or missed because they are in the near field of the transducer [31–33]. The heterogeneous intensity pattern of the beam in the near field may cause echoes from surrounding tissues to appear within a cyst, suggesting that it is a solid mass (Fig. 4). For this reason, a satisfactory breast examination with a hand-held transducer requires either the use of a fluid offset (a degassed water-filled bag placed between the transducer and the breast or a commercially produced offset device) or a transducer with a built-in fluid offset [32, 33]. Transducers of automated whole-breast sonographic units are positioned within a water bath and separated from the surface of the breast, and imaging of the superficial tissues with these whole-breast units is less problematic than with a hand-held sonographic probe.

Masses deep in the breast may also be distorted owing to the diverging beam that degrades lateral resolution. This distortion may take the form of blurring of the margins of masses, filling-in of shadows behind small masses, and failure to resolve smaller masses. With a hand-held transducer, the focal zone can be repositioned for deeper breast tissues by moving the transducer to a closer breast surface, moving the patient, or by applying greater compression with the transducer. Transducers of automated scanners are moved closer to or farther from the breast within the water bath to position the focal zone.

Power, sometimes referred to as sonic intensity, output power, percent power, or dB, is the amount of voltage applied to the transducer to produce the ultrasound wave that enters the breast [34]. The amount of power determines the distance

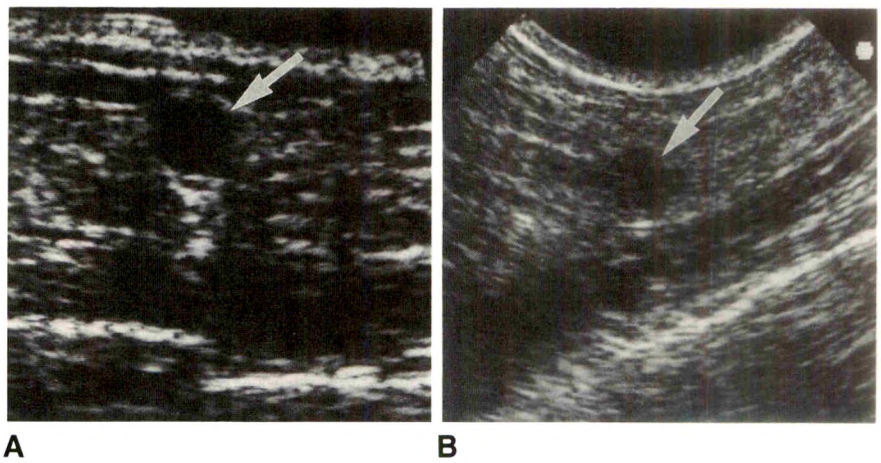



Fig. 4.—Sonograms of 0.5-cm superficial cyst (*arrows*) imaged with 7.5-MHz transducers with and without built-in fluid offsets.

*A*, Transducer with fluid offset shows anechoic interior of cyst.

*B*, Transducer without fluid offset shows artifactual echoes throughout cyst.

the wave travels before it is completely attenuated. A power setting that is too high results in (1) saturation of the amplifier, giving an excessively bright image without texture or variations in gray scale, and (2) amplification of all the dampened cycles in the short pulse of ultrasound emitted by the transducer so that resolution perpendicular to the transducer face (axial resolution) will be degraded. Thus, the operator should keep the power as low as possible, consistent with penetration to the chest wall.

Time-gain compensation, or depth-gain compensation, is an increase in amplification of waves returning from the deeper tissues to compensate for their greater attenuation. For breast imaging, the time-gain compensation is adjusted by the operator of hand-held units according to breast density and size; denser breasts require a time-gain compensation curve that is steeper than less dense breasts. The use of higher-frequency transducers results in greater beam attenuation and also requires a steeper time-gain compensation slope. When the time-gain compensation curve is too steep, the amplification capacity may be exhausted, resulting in inadequate depiction of the deep tissue. Furthermore, shadowing or enhancement behind masses may not be depicted.

Gray-scale mapping circuitry in the sonographic instrument converts received voltages into discrete shades of gray based on their amplitude. The relationship of the voltage to the assigned shade is the gray scale. Linear gray-scale maps assign the same relative number of gray levels to low- and high-amplitude reflections. Logarithmic, sometimes referred to as root, exponential, or quadratic gray-scale, maps assign more gray-level values to low-amplitude reflections, thus increasing image contrast. However, nonlinear gray-scale maps may fill in anechoic masses with artifactual echoes not seen when a linear map is used.

### Selection of Equipment

Selection of equipment for breast sonography depends on many factors, including the number of examinations performed, financial limitations, space constraints, and personal preferences. Automated units produce whole-breast images in overlapping sequential slices that allow easy localization of abnormalities. However, an automated unit is likely to be more expensive and requires more space, a specially trained technologist, and more time for setup, performance, and review of the examination. It also may be more difficult to ensure that a palpable mass matches a sonographically depicted cyst. Currently, the only available automated instru-

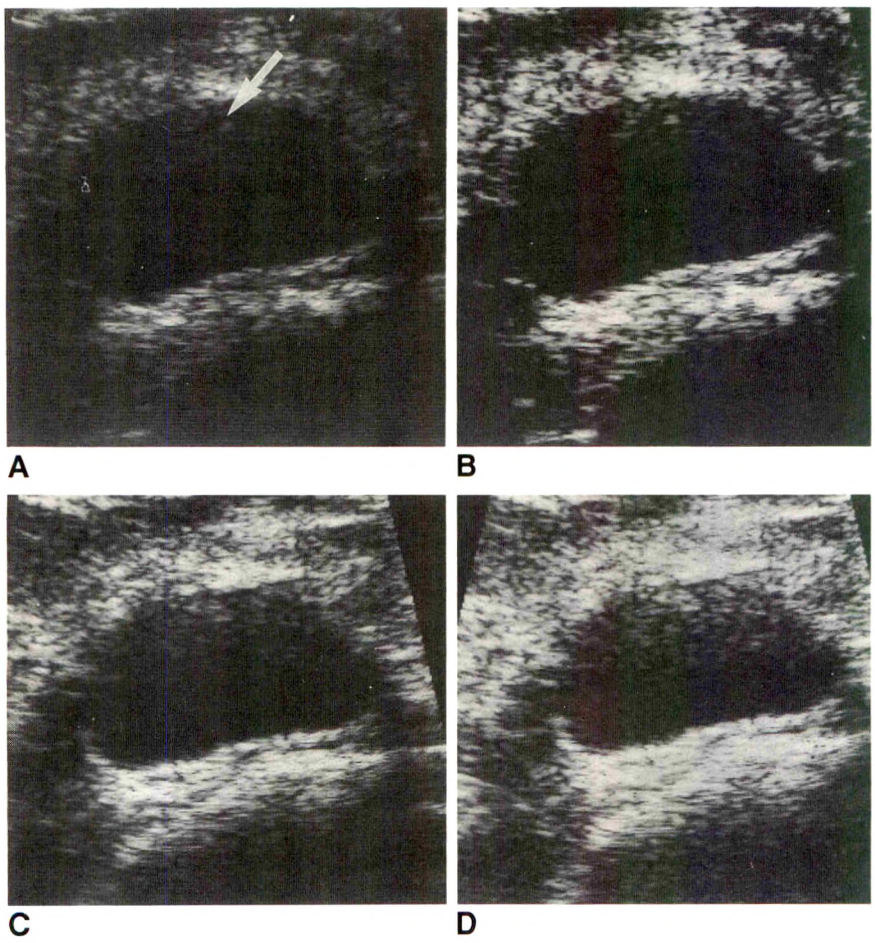



Fig. 5.—Sonograms of cyst. Effects of changing sonographic power and gray scale.

*A*, Cyst has an anechoic interior, except for reverberation echoes (*arrow*) in anterior portion.

*B*, Same power setting as *A*, gray-scale map changed from linear to logarithmic. Echoes in anterior portion of cyst are more obvious. Overall brightness of image is increased.

*C*, High-power setting, linear gray-scale map. Echoes fill in anterior half of cyst interior.

*D*, Same power setting as in *C*, gray-scale map changed from linear to logarithmic. Echoes are visible throughout cyst, although they are brighter anteriorly.

ment is the Labsonics dedicated water-path breast unit (Labsonics Inc, Mooresville, IN). With this automated scanner, examinations can be limited to a localized area of the breast.

Because the major indication for sonography is cyst vs solid differentiation of a palpable or mammographically detected lesion, most breast sonography is performed currently with hand-held units applied directly over the area of interest [35]. The advantages of hand-held units are that they are usually less expensive, smaller, portable, faster, and adaptable for sonographically guided needle aspiration or prebiopsy hookwire localization. The radiologist may elect either to have a small inexpensive hand-held unit permanently located near or in the mammography room or to transport the patient to an area where general sonographic examinations are performed. In either case, the instrument used for breast examinations should be a small-parts (high-frequency) unit with adequate power and time-gain compensation to penetrate 5 cm of breast tissue. Sonographic examinations can be performed by the radiologist or a technologist under the radiologist's direct supervision. If mammography technologists perform the examination, they should receive special training, including correct scanning techniques and basic understanding of the physics of sonography and how it affects breast imaging. Although multipurpose sonographic equipment can cost more than $100,000, small units appropriate for breast imaging are available for $30,000 to $40,000. A multiformat camera, rather than a Polaroid camera, which has limited gray-scale range, is also needed. Several linear- and phased-array units are suitable for breast sonography, as long as they are equipped with a 5.0- or 7.5-MHz transducer, and a 1-cm offset is available for imaging superficial tissues. Mechanical transducers for breast imaging should have a 7.5- to 10.0-MHz transducer, a fluid offset, and a soft membrane separating the standoff fluid and the patient to avoid reverberations in the near field. Annular arrays are excellent for breast imaging, but should be 5 MHz or higher. The annular array is a hybrid transducer, combining the variable focusing property of a phased-array with the mechanical sweep and fluid offset of a mechanical transducer.

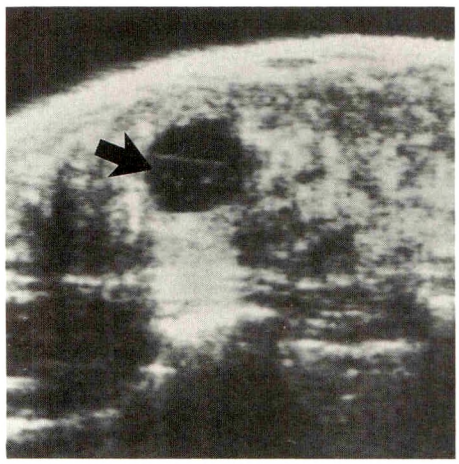


**Fig. 6.—Section from automated whole-breast sonographic examination shows a cyst 2 weeks after several unsuccessful attempts at needle aspiration. Gravity-dependent debris (*arrow*), believed to be due to trauma of attempted aspirations, is layered at bottom of cyst.**

### Problems in Cyst/Solid Differentiation

The presence of artifactual or real echoes within cysts is one of the most frequent dilemmas encountered when performing breast sonography. Frequently this dilemma can be resolved by adjusting technical factors affecting the image, patient positioning maneuvers, or correlation of the sonographic results with mammographic findings and clinical data.

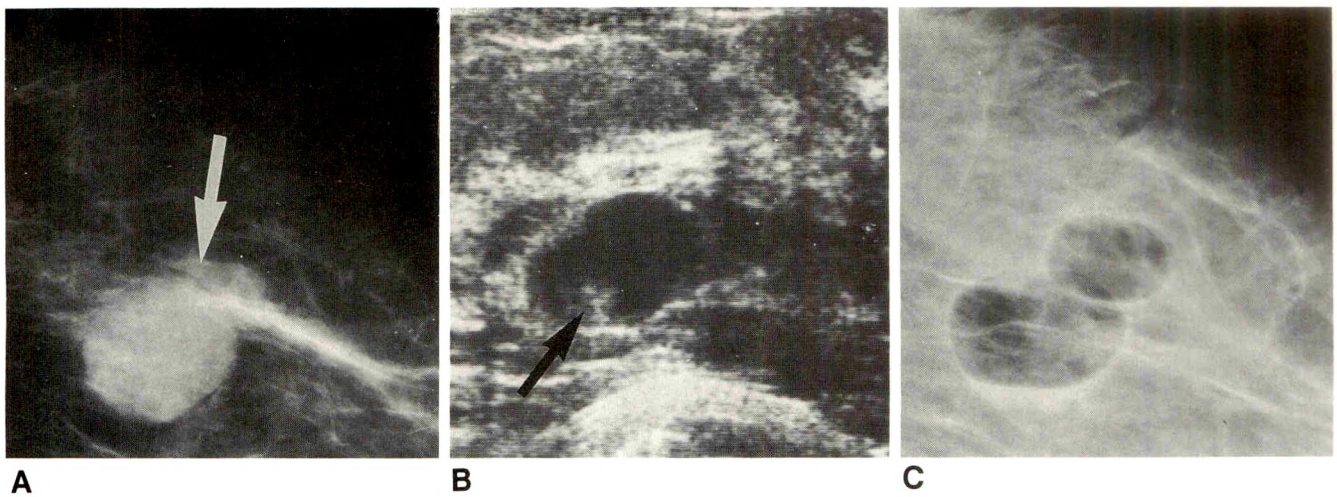



**Fig. 7.—Loculated cyst.**
***A*, Lateral mammogram shows lobulated mass (*arrow*).**
***B*, Sonogram reveals anechoic center and a small nodule (*arrow*) projecting from wall, suggesting intracystic tumor.**
***C*, Pneumocystogram, cyst aspiration followed by insufflation with air, shows a multiloculated cyst containing septa, responsible for apparent nodule seen in *B*.**

In the near field of the transducer, irregularity of the ultrasound wavelets may cause apparent echoes within a cyst (Fig. 4). In addition, because the beam is wider than in the focal zone, the edge of the beam may strike a random scatterer outside of the cyst, and these echoes may be displayed as coming from within the interior of the cyst. Phased-array transducer elements are rectangular, with the long dimension parallel to the slice thickness; the thickness of the slice of the image plane contributes information to the image. Unlike lateral resolution, which can be varied electronically in a phased array, slice thickness resolution is controlled by a fixed-focus lens. Phased-array probes almost always image superficial masses improperly unless a transducer offset device is used to bring the mass into the slice thickness focus. When using mechanical-sector transducers, near-field reverberations may be severe if hard plastic is used to separate a built-in fluid offset from the breast. Thus, a soft membrane should be used to separate the transducer from the breast surface. For similar reasons, artifactual echoes can also be seen when a cyst is imaged in the far field of the transducer.

One of the most common causes of artifactual echoes is the use of an inappropriately high power or time-gain compensation (Fig. 5). In general, increased power or time-gain compensation will fill in the anterior portion of a cyst first, and the posterior boundary of the cyst will continue to be well defined. Changing the gray scale or gray-scale dynamic range in order to increase contrast will also cause the center or all of the interior of a cyst to be filled in with fine textured noise.

A faulty electrical board can also result in artifactual echoes in a cyst, and equipment failure should be suspected when several consecutive masses expected to be cysts show an internal echo structure.

Echoes in a cyst can represent debris. The diagnosis of a cyst is still tenable if these echoes can be seen to move within the cyst fluid during continuous hand-held real-time scanning while the patient's breast is moved. Gravity-dependent debris may be observed layered at the bottom of the cyst.

Patients may be referred for sonography after unsuccessful attempts at needle aspiration. Unfortunately, repeated attempts at aspiration can result in considerable distortion in the breast parenchyma and may cause echoes to appear within a cyst [31]. It may be necessary to repeat the sonography 2–3 weeks later to show resolution of traumatically induced echoes in a cyst, or layering of blood or debris (Fig. 6). Preferably, mammography and sonography should be performed before attempted aspiration of masses that are not readily palpable.

Septa within multiloculated cysts are usually recognized as thin linear bands crossing the cyst interior. Occasionally, a septum will appear to be a nodule in the cyst wall (Fig. 7). Again, repeated real-time scanning while repositioning the transducer in the planes of the cyst may resolve this problem by showing the septum in a plane that makes it recognizable.

The sonographic demonstration of an echogenic mass projecting from the wall of a cyst should raise the possibility of intracystic carcinoma (Fig. 8). Breast carcinoma arising in the wall of a cyst is rare, representing only about 0.5% of all breast cancers [36, 37], but cystic degeneration of previously noncystic carcinoma can have a similar appearance. Because they are freely movable on physical examination, well circumscribed on mammography, and contain fluid on sonography, they may be dismissed as benign masses. Intracystic carcinomas are usually larger than 3 cm when biopsy is performed. To avoid delaying the biopsy of an intracystic carcinoma, or a well-circumscribed carcinoma with only a few visible internal echoes, it is important that strict criteria be used to make the diagnosis of a simple cyst. If a benign cause, such as technical factors, debris, or a septum, cannot be determined to explain echoes in a cystic mass, aspiration [38], pneumocystography (Fig. 7C) [39], or excisional biopsy should be performed.

Posterior enhancement, considered to be a hallmark of cysts, may not be visible on all scans. Hilton et al. [29] showed posterior enhancement to be present to a variable degree in 78 of 80 cysts. However, in 25% of these cases posterior enhancement was not seen on all images. Slight changes in

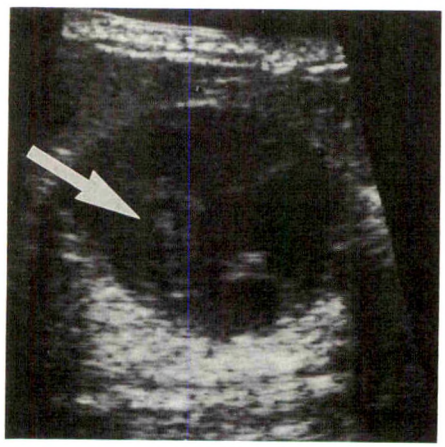


Fig. 8.—Sonogram of intracystic carcinoma. Echogenic tumor (*arrow*) is growing in wall of cyst.

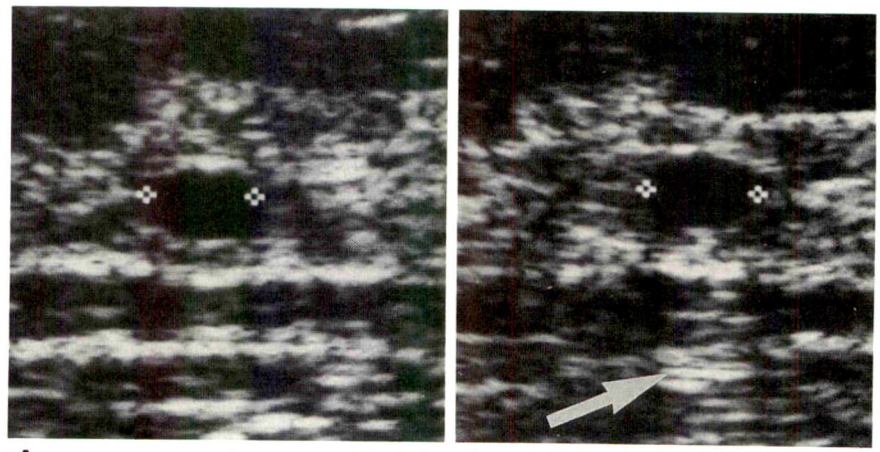


Fig. 9.—Sonograms of 0.5-cm cyst showing variable distal echo enhancement.
*A*, Cyst (*between cursors*) interior is clearly anechoic, but distal echo enhancement is not seen.
*B*, Same cyst, imaged with slightly less transducer compression and a slight change in direction of ultrasound beam. Distal echo enhancement (*arrow*) is demonstrated.

transducer positioning may affect the depiction of enhancement of echoes distal to a cyst (Fig. 9).

### The Future of Breast Sonography

Although sonography is limited to cyst/solid differentiation in most radiologic practices today, improvements in equipment and greater experience in the evaluation of combined mammographic-sonographic examinations may eventually expand the specificity of sonography for the evaluation of solid masses, further reducing the need for excisional biopsies (Fig. 4) [40, 41]. The use of breast sonography to guide cyst aspiration, prebiopsy needle localization, and fine-needle aspiration biopsy is increasing [42, 43]. For these procedures, a hand-held 7.5-MHz or higher-frequency transducer should be used, preferably with a biopsy guide [38]. However, at this time, mammographic localization techniques are more reliable and sonographically guided procedures are usually limited to cases in which the lesion is not visible mammographically [44].

REFERENCES


1. Wild JJ, Neal D. The use of high frequency ultrasonic waves for detecting changes of texture in the living tissue. *Lancet* **1951**;1:655–657
2. Deland FH. A modified technique of ultrasonography for the detection and differential diagnosis of breast lesions. *AJR* **1969**;105:446–452
3. Jellins J, Kossoff G, Buddee FW, Reeve TS. Ultrasonic visualization of the breast. *Med J Aust* **1971**;1:305–307
4. Kobayashi T, Kobayashi T, Takatani O, Hattori N, Kimura K. Differential diagnosis of breast tumors: the sensitivity graded method of ultrasonography. *Cancer* **1974**;33:940–951
5. Kelly-Fry E. Breast imaging. In: Sabbagha RE, ed. *Diagnostic ultrasound applied to obstetrics and gynecology*. New York: Harper & Row, **1980**:327–350
6. Cole-Beuglet C, Goldberg BB, Kurtz AB, Patchefsky AS, Shaber GS, Rubin CS. Clinical experience with a prototype real-time dedicated breast scanner. *AJR* **1982**;139:905–911
7. Kobayashi T. Diagnostic ultrasound in breast cancer: analysis of retrotumorous echo patterns correlated with sonic attenuation by cancerous connective tissue. *JCU* **1979**;7:471–479
8. Jellins J, Kossoff G, Reeve TS, Barraclough BH. Ultrasonic grey scale visualization of breast disease. *Ultrasound Med Biol* **1975**;1:393–404
9. Cole-Beuglet C, Goldberg BB, Kurtz AB, Patchefsky AS, Shaber GS, Rubin CS. Ultrasound mammography: a comparison with radiographic mammography. *Radiology* **1981**;139:693–698
10. Bassett LW, Kimme-Smith C, Sutherland LK, Gold RH, Sarti D, King W. Automated and hand-held breast ultrasound: effect on patient management. *Radiology* **1987**;165:103–108
11. Feig SA. The role of ultrasound in a breast imaging center. *Semin Ultrasound CT MR* **1989**;10:90–105
12. Sickles EA, Filly RA, Callen PW. Breast cancer detection with sonography and mammography: comparison using state-of-the-art equipment. *AJR* **1983**;140:843–845
13. Kopans DB, Meyer JE, Lindfors KK. Whole-breast ultrasound imaging: four-year follow-up. *Radiology* **1985**;157:505–507
14. Egan RL, Egan KL. Detection of breast carcinoma: comparison of automated water-path whole breast sonography, mammography, and physical examination. *AJR* **1984**;143:493–497
15. Cole-Beuglet C, Soriano RZ, Kurtz B, et al. Ultrasound analysis of 104 primary breast carcinomas classified according to histopathologic type. *Radiology* **1983**;147:191–196
16. Calderon C, Vilkomerson D, Mezrich R, Etzold FK, Kingsley B, Haskin M. Differences in the attenuation of ultrasound by normal, benign, and malignant breast tissue. *JCU* **1976**;4:249–254
17. Cole-Beuglet C, Soriano RZ, Kurtz AB, Goldberg BB. Fibroadenoma of the breast: sonomammography correlated with pathology in 122 patients. *AJR* **1983**;140:369–375
18. Jackson VP, Rothschild PA, Kreipke DL, Mail JT, Holden RW. The spectrum of sonographic findings of fibroadenoma of the breast. *Invest Radiol* **1986**;21:34–40
19. Kasumi F, Fukami A, Kuno K, Kajitani T. Characteristic echographic features of circumscribed cancer. *Ultrasound Med Biol* **1982**;8:369–375
20. Kopans DB. What is a useful adjunct to mammography? *Radiology* **1986**;161:560–561
21. Sickles EA, Filly RA, Callen PW. Benign breast lesions: ultrasound detection and diagnosis. *Radiology* **1984**;151:467–486
22. Jackson VP. Sonography of malignant breast disease. *Semin Ultrasound CT MR* **1989**;10:119–131
23. Sickles EA. Practical solutions to common mammographic problems: tailoring the examination. *AJR* **1988**;151:31–39
24. Kopans DB, Swann CA, White G, et al. Asymmetric breast tissue. *Radiology* **1989**;171:639–643
25. Harper AP, Kelly-Fry E, Noe S. Ultrasound breast imaging—the method of choice for examining the young patient. *Ultrasound Med Biol* **1981**;7:231–237
26. Harris VJ, Jackson VP. Indications for breast imaging in women under age 35 years. *Radiology* **1989**;172:445–448
27. Ysrael M, Bassett LW, Gold RH, Ysrael C. Effect of mammography and breast sonography in women under age 35 years. *Radiology* **1989**;173(P):231
28. Jellins J, Kossoff G, Reeve TS. Detection and classification of liquid-filled masses in the breast by gray scale echography. *Radiology* **1977**;125:205–212
29. Hilton SvW, Leopold GR, Olson LK, Wilson SA. Real-time breast sonography: application in 300 consecutive patients. *AJR* **1986**;147:479–486
30. Kossoff G, Jellins J. The physics of breast echography. *Semin Ultrasound* **1982**;3:5–12
31. Rubin E, Miller VE, Berland LL, Han SY, Koehler RE, Stanley RJ. Hand-held real-time breast sonography. *AJR* **1985**;14:623–629
32. Kimme-Smith C, Hansen M, Bassett LW, et al. Ultrasound mammography: effects of focal zone placement. *RadioGraphics* **1985**;5:955–970
33. Kimme-Smith C, Rothschild PA, Bassett LW, Gold RH, Westbrook D. Ultrasound artifacts affects the diagnosis of breast masses. *Ultrasound Med Biol* **1988**;14[suppl 1]:103–210
34. Bassett LW, Gold RH, Kimme-Smith C. Physics. In: Bassett LW, Gold RH, Kimme-Smith C, eds. *Hand-held and automated breast ultrasound*. Thorofare, NJ: Slack, **1986**:11–32
35. Bassett LW, Diamond JJ, Gold RH, McLelland R. Survey of mammography practices. *AJR* **1987**;149:1149–1152
36. Gatchell FG, Dockerty MB, Clagett OT. Intracystic carcinoma of the breast. *Surg Gynecol Obstet* **1958**;106:347–352
37. Czernobilsky B. Intracystic carcinoma of the female breast. *Surg Gynecol Obstet* **1967**;124:93–98
38. D'Orsi CJ, Mendelson EB. Interventional breast ultrasonography. *Semin Ultrasound CT MR* **1989**;10:132–138
39. Tabár L, Pentek Z, Dean PB. The diagnostic and therapeutic value of breast cyst puncture and pneumocystography. *Radiology* **1981**;141:659–663
40. Adler DD. Ultrasound of benign breast conditions. *Semin Ultrasound CT MR* **1989**;10:106–118
41. Fornage BD, Lorigan JG, Andry E. Fibroadenoma of the breast. Sonographic appearance. *Radiology* **1989**;172:671–675
42. Kopans DB, Meyer JE, Lindfors KK, Buchianeri SS. Breast sonography to guide cyst aspiration and wire localization of occult solid lesions. *AJR* **1984**;143:489–492
43. Fornage BD, Faroux MJ, Simatos A. Breast masses: US-guided fine-needle aspiration biopsy. *Radiology* **1987**;162:409–414
44. Weber WN, Sickles EA, Callen PW, Filly RA. Nonpalpable breast lesion localization: limited efficacy of sonography. *Radiology* **1985**;155:783–784


P 24,470

# Book Review

**MRI of the Musculoskeletal System.** A Teaching File. Edited by Jerrold H. Mink and Andrew L. Deutsch. New York: Raven, 640 pp., 1990. $120

Good books on musculoskeletal MR imaging abound, including textbooks (Stoller et al., *Magnetic Resonance Imaging in Orthopaedics and Rheumatology*; Modic, *Magnetic Resonance Imaging of the Spine*), atlases (DeSchepper and Degryse, *Magnetic Resonance Imaging of Bone and Soft Tissue Tumors and their Mimics: A Multi-Planar Atlas*), and some soon to appear (Kang and Resnick, *Magnetic Resonance Imaging Atlas of the Extremities*; Beltran, *Magnetic Resonance Imaging of the Musculoskeletal System*; and Berquist, *MRI of the Musculoskeletal System*, 2nd ed.). The section on musculoskeletal MR in Edelman and Hesselink's *Clinical Magnetic Resonance Imaging* (clearly the magnum opus at this point) is certainly noteworthy.

The work under consideration offers still another learning approach: a teaching file. The book continues the tradition of the American College of Radiology syllabus-style programmed instruction. The material is region-oriented into 207 individual case studies that cover all major musculoskeletal lesions, including the temporomandibular joint and the vertebral column. The book has a section on tumors and a series of cases dealing with the exciting new concept of kinematic MR. Not surprisingly, the case load is heavily knee-weighted! The first chapter, "Technical Considerations in MRI," is simply wonderful and wonderfully simple. It is also fair to caution the reader that although the introductory chapter is manageable, the authors assume a basic knowledge of anatomy and MRI physics.

The format is simple: a short history and physical findings; MR findings, with appropriate images and detailed descriptions thereof; diagnosis; and discussion. Each chapter is prefaced by a short "how-to" outline. Most chapters conclude with a brief summary of teaching points. The book is "show and tell" in print, and it is most effective. Its specialness is the impressively readable material that is presented with welcome clarity, startling revelations and occasional verbosity aside. The book has a durable binding, multiple illustrations of excellent quality that scrupulously follow the text, and a fairly comprehensive index. The recommended readings that follow each section are abundant and timely. Pulsing sequences and timing parameters are supplied with all but one illustration.

In order to determine whether the authors faithfully fulfilled their goals as set forth in the preface, that is, the "text is designed primarily for the practicing radiologist who desires a reference that he can keep next to the view-box," I did an unselected five-case test during an evening MR review session. The book provided more than ample assistance in most categories, including MR findings and discussions on differential diagnosis. (Incidentally, I recommend this simple evaluation, which can be accomplished easily during the 30-day trial period offered by most publishers.)

Many new areas of diagnosis and applications have become available with the advent of musculoskeletal MR imaging. These include bone bruise (edema, hemorrhage, and trabecular microfracture), bone marrow edema, the early detection of avascular necrosis, transient osteoporosis and differentiation of benign from malignant vertebral body collapse, carpal tunnel syndrome and the possible causes of treatment failure, and stress fractures and bone infarction in juvenile rheumatoid arthritis. The book also covers such promising techniques as kinematic MR of the joints, patella tracking, and the effectiveness of gadolinium. The section on tumors I found particularly helpful. For example, in the discussion on desmoid tumors, the book states that the MR signal characteristic reflects the degree of cellularity of the lesion.

In the making of books, there is an old maxim that the best ideas are simple ideas (*New York Times*). Mission accomplished. And simply speaking, inasmuch as musculoskeletal MR now represents about 35% of the case load in any active facility, I intend to keep my copy on the view box.

Murray A. Rosenberg
*Easton, CT 06612*

Review Article

# Gadopentetate Dimeglumine–Enhanced MR Imaging of the Musculoskeletal System

Javier Beltran,[1] Vijay Chandnani,[2] Robert A. McGhee, Jr.,[1] and Sevil Kursunoglu-Brahme[2]

**Contrast-enhanced MR imaging with gadopentetate dimeglumine has been used in the evaluation of musculoskeletal disorders only in recent years, and for the most part it is still under investigation. Review of the literature identified potential uses for this technique: (1) in the spine, for differentiation between scar tissue and recurrent disk herniation and for evaluation of epidural tumors; (2) in musculoskeletal tumors, for differentiation between tumor necrosis and peritumoral edema and for characterization and evaluation of tumors before and after treatment; (3) in the joints for delineation of cartilage and tendon tears, with intraarticular injection, and for differentiation between pannus and joint effusion, with IV injection; and (4) for delineation of infectious processes.**

**Further studies are needed to confirm most of these potential indications. It is unlikely that gadopentetate dimeglumine–enhanced MR imaging will become a routine part of musculoskeletal MR imaging, and its use will be reserved for specific circumstances.**

Contrast-enhanced MR imaging with gadopentetate dimeglumine was approved in the United States for neuroradiologic applications in 1988. Since then much has been written about the information gained with the use of IV MR contrast materials for evaluation of lesions involving the CNS [1–4]. Ongoing research indicates that contrast-enhanced MR imaging also has potential value in imaging of the breast, mediastinum, liver, adrenal glands, and pelvis [5–7]. However, limited information is available regarding the use of contrast-enhanced MR imaging in the musculoskeletal system. We reviewed the potential value of gadopentetate-dimeglumine–enhanced MR imaging in the spine, bone and soft-tissue tumors, joints, and inflammatory and infectious conditions of the musculoskeletal system.

## MR Contrast Agents

Contrast agents can be broadly divided into paramagnetic and superparamagnetic. Paramagnetic materials can be subdivided into metal ions with unpaired electrons (gadolinium, manganese, copper, chromium) and nonmetallic materials (oxygen, nitroxyl radicals) [8]. The paramagnetic metal ion gadolinium, with seven unpaired electrons, is used most frequently because of its efficient T1 shortening effect.

Metal ions are highly reactive species. The body has many binding sites with natural affinity for metals (membranes, transport proteins, enzymes, osseous matrix). When metals are injected as free ions, they can be retained for prolonged periods, causing intolerable side effects. In order to prevent this, they have to be partially chelated to an organic compound. In the case of gadolinium, two chelates have been used: gadopentetate dimeglumine and tetra-azacyclododecane tetraacetic acid (DOTA). Gd-DOTA has been shown to produce fewer adverse reactions than gadopentetate dimeglumine, but its relaxivity is 17% less, therefore requiring a higher dose [8, 9]. Gd-DOTA has higher paramagnetic efficacy at low magnetic fields [9]. Gd-DTPA bismethylamide (Gd-

Received August 6, 1990; accepted after revision October 8, 1990.
[1] Department of Radiology, The Ohio State University Hospitals, 410 W. 10th Ave., Columbus, OH 43210. Address reprint requests to J. Beltran.
[2] Department of Radiology, Veterans Affairs Medical Center, University of California, San Diego, San Diego, CA 92161.

*AJR* 156:457–466, March 1991 0361–803X/91/1563–0457 © American Roentgen Ray Society

DTPA-BMA, S-041) is a new, nonionic gadolinium compound currently under investigation, which offers the potential advantages of similar relaxivity, decreased osmolality, and significantly lower toxicity than gadopentetate dimeglumine (Hayne LA et al., presented at the annual meeting of the Radiological Society of North America, November 1989).

Gadopentetate dimeglumine attached to macromolecules (albumin, dextran) stays longer within the intravascular space (Li KC et al., presented at the annual meeting of the Society for Magnetic Resonance Imaging, May 1990). This property has been used experimentally to study organ perfusion (brain, myocardium). Its role in musculoskeletal ischemia is yet to be investigated. Additional general information on the principles of contrast media can be found in published monographs and textbooks [10–12].

After IV injection, a gadolinium compound disperses rapidly into the extracellular fluid, and 97% can be recovered in the urine and feces [13]. The initial distribution of gadopentetate dimeglumine is relative to blood flow. In the brain, the blood-brain barrier prevents communication between the vascular and the extracellular fluid spaces. When this barrier is broken (tumor, infarction, inflammation), gadopentetate dimeglumine accumulates freely in the extracellular space. In the musculoskeletal system, where there is no barrier to extracellular distribution, gadopentetate dimeglumine enters tissues with increased vascularity (tumor, inflammation) a few minutes after IV injection and is cleared less rapidly than the surrounding normal tissue (muscle, fat). This provides sufficient contrast enhancement to be detected on T1-weighted images.

The optimal dose of gadopentetate dimeglumine depends on the disease and organ to be imaged. With increasing dose there is progressive T1 shortening (higher signal intensity), to a level at which the T2 effects take place. At this point the signal intensity decreases [11]. For musculoskeletal applications, 0.1 mmol/kg of body weight is adequate.

### *Toxicity*

Adverse reactions to gadopentetate dimeglumine described in clinical trials are minimal, and in order of frequency include headaches (10%); nausea (4%); vomiting (2%); and hypotension, gastrointestinal upset, and rash (less than 1%) [14].

### *Imaging Techniques*

Because the effect of gadopentetate dimeglumine is T1 shortening, an imaging protocol including unenhanced T1- and T2-weighted images, followed by a series of enhanced T1-weighted images, frequently is used. In order to optimize techniques, a short TE of around 12 msec is recommended [11]. Another technical factor to consider when using gadopentetate dimeglumine–enhanced MR imaging is field strength. Higher magnetic fields produce increased contrast enhancement on T1- and also on T2-weighted images [11]. Fast imaging techniques with short TEs (about 10 msec) and flip angles of 40–90° are ideal for enhanced MR imaging because tissue enhancement compensates for inherent loss of contrast in fast imaging [11].

If the suspected lesion is surrounded by normal hyperintense fat signal on T1-weighted images (bone marrow, retroperitoneum, and subcutaneous fat), enhanced MR imaging actually may decrease visualization of the lesion. In these cases, fat-suppression imaging techniques such as chemical-shift imaging or selective presaturation may be helpful [15]. Short-tau inversion recovery is less likely to discriminate between fat and paramagnetically relaxed water of the lesion, since both are suppressed [15].

Erleman et al. [16] and Sze et al. [17] recently proposed the use of dynamic enhanced 1.5-T MR imaging with gradient-echo sequences, 40/10/90° (TR/TE/flip angle), for the evaluation of musculoskeletal tumors. With this technique, an unenhanced image followed by a series of three enhanced images/min for about 3 min are obtained in one predetermined slice that depicts the lesion better. Graph curves of signal intensity plotted against time allow determination of rates and slopes in percent increase of signal intensity per minute, providing additional information, such as tumor activity, response to chemotherapy, and tumor recurrence.

## Enhanced MR Imaging in the Evaluation of the Spine

Gadopentetate dimeglumine–enhanced imaging has greatly expanded the role of MR in the evaluation of the spine. Intramedullary processes including neoplasms (astrocytoma, ependymoma) and intradural extramedullary processes such as primary neoplasms (meningioma, neurofibroma) and metastatic neoplasms (including CNS drop metastases) are better and more fully evaluated by MR with the addition of contrast-enhanced images [17–21]. This discussion focuses primarily on the role of gadopentetate dimeglumine–enhanced MR imaging in the evaluation of extradural disease processes involving the spine.

### *Normal Enhancement in the Spine*

Recognition of normal enhancement patterns in the spine is important so that normally enhancing structures are not confused with disease. Enhancement normally is seen in slow-flowing vascular structures (the epidural venous plexus and basivertebral venous plexus) and the dorsal root ganglion, which lacks a blood-nerve barrier [22, 23]. The spinal cord and nerve roots within the thecal sac normally do not enhance, although variable minimal enhancement of nerve roots has been reported [24]. Enhancement of paraspinal muscle, bone marrow, fat, disk material, and ligamenta flava has been demonstrated by quantitative measurement, but this enhancement usually is not detectable by qualitative evaluation [23].

### *Postoperative Spine*

One of the most frequent indications for gadopentetate dimeglumine–enhanced MR imaging in the spine is to help differentiate persistent or recurrent disk protrusion from epidural fibrosis in patients with failed back surgery syndrome. This syndrome of recurrent pain in a patient who has had

back surgery has been reported in 10–40% of back surgery patients and may occur for several reasons, including recurrent or persistent disk herniation (12–16%), epidural fibrosis (6–8%), arachnoiditis (6–16%), and lateral (58%) or central (7–14%) spinal stenosis [24]. The differentiation between epidural fibrosis and disk protrusion is important because the clinical management is different. Surgery is often indicated for recurrent disk protrusion, but repeated surgery when only epidural fibrosis is present may actually exacerbate symptoms.

Criteria for differentiating recurrent disk protrusion from epidural fibrosis have been well described elsewhere [25]. Although unenhanced MR has been shown to be quite accurate in differentiating fibrosis from herniated disk (83–89% accuracy), it is clear that enhanced MR imaging is more accurate and provides a higher level of confidence in making this distinction [24–30]. Disk material normally does not enhance in adults because it is relatively avascular. In contradistinction, epidural fibrosis, which has been shown to be highly vascular, shows rapid enhancement [26]. This difference in enhancement forms the basis for the use of enhanced MR imaging to differentiate recurrent disk protrusion from epidural fibrosis (Figs. 1 and 2). Epidural fibrosis enhances maximally 5–6 min after injection of contrast material [26]. The enhancement of fibrosis initially may be somewhat inhomogeneous, becoming more homogeneous with time [27]. Less intense enhancement may be seen on delayed images (more than 30 min after injection of contrast material) in herniated disks [27]. Therefore, imaging usually is performed immediately after injection of contrast material when evaluating the postoperative spine. A peripheral rim of enhancement related to peridiskal scar may be seen adjacent to a recurrent disk protrusion. This appearance has been termed a "wrapped disk" [26, 27]. Enhancement in various patterns may also be seen within an interspace that was previously operated on, both at and removed from the site of previous surgical curettage [26]. This enhancement may be related to ingrowth of vessels from adjacent bone into the degenerated disk, ingrowth of vascular scar tissue at the site of curettage, or diffusion of contrast material into the disk from adjacent vascular tissues [26, 28]. Disks that have not been operated on occasionally may enhance for reasons elaborated below.

There are possibilities for misinterpretation in differentiating epidural fibrosis from disk protrusion on enhanced MR imaging [27]. If a small disk protrusion is present together with epidural fibrosis, the protrusion may be missed because of partial-volume averaging. Also, a disk protrusion may go undetected if it is fragmented and incorporated into a mass of epidural fibrosis. However, enhanced MR imaging is clearly the best single imaging technique for evaluating the postoperative back.

### *Unoperated Spine*

Enhancement of various structures may be related to degenerative changes in the unoperated spine [21, 24, 27, 30]. The role of enhanced MR imaging in the evaluation of degenerative changes in the unoperated spine seems limited, although abnormalities occasionally may be delineated better, particularly in the cervical spine. The normal enhancement of the epidural/foraminal venous plexus adjacent to a disk protrusion may make it more conspicuous (Simon JH et al., RSNA, November 1989). The venous plexus adjacent to a herniated disk may become distended and congested and can be seen on sagittal enhanced images as triangular areas of hyperintensity above and below the protrusion [31].

Enhancement at the periphery of a disk protrusion related to adjacent epidural fibrosis (long known to be associated with disk protrusions) also may be present [30]. Enhancement may occur within unoperated disks. Focal linear or globular enhancement within the anulus fibrosus related to anular tears has been reported [32]. This is apparently caused by ingrowth of vascular granulation tissue into the anular tear. Linear enhancement may also be seen in the peripheral portion of the intervertebral disk in the region of peripheral anulus fibrosus/posterior longitudinal ligament complex. This type of enhancement has been reported only in disks that have shown other evidence of degeneration, and may be related to scar formation or inflammatory changes within the ligament [33].

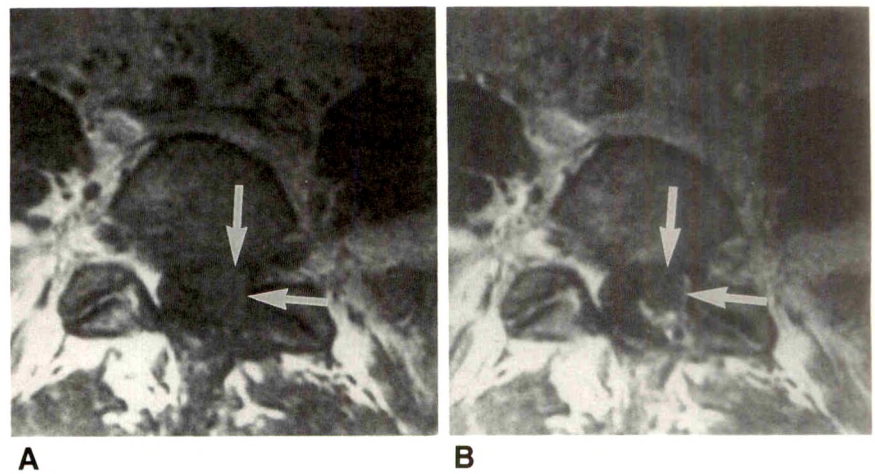



**Fig. 1.—Postoperative recurrent disk protrusion.**

***A*, Axial unenhanced T1-weighted MR image (SE 800/30) at level of recurrent disk protrusion shows a mass (*arrows*) in left side of spinal canal that is displacing and is difficult to separate from adjacent thecal sac.**

***B*, Enhanced T1-weighted MR image (SE 800/30). Recurrent disk protrusion (*arrows*) is partially surrounded by peridiskal fibrosis, making it easier to separate from thecal sac.**

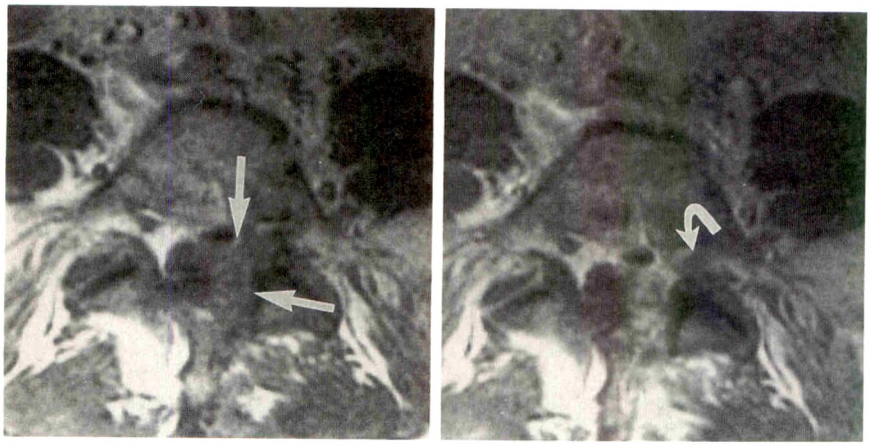


Fig. 2.—Postoperative epidural fibrosis.
*A*, Axial unenhanced T1-weighted MR image (SE 800/30) at level of epidural fibrosis shows a mass (*arrows*) distorting epidural fat within left neural exit foramen and left side of spinal canal. Thecal sac is displaced to the right.
*B*, Enhanced T1-weighted MR image (SE 800/30) shows diffuse, inhomogeneous enhancement of epidural fibrosis, making it easier to identify nerve root in exit foramen (*arrow*).

Enhancement also may be seen in the vertebral body marrow adjacent to a degenerating disk [24, 27]. Hypointensity on unenhanced T1-weighted images within endplates adjacent to a degenerating disk has been shown to be related to replacement of normal hematopoietic marrow with vascular fibrous tissue [33]. Enhancement frequently is seen in these vertebral bodies and may be caused by the ingrowth of this vascular fibrous tissue. Endplates that are adjacent to degenerating disks and are hyperintense on unenhanced T1-weighted images (related to yellow marrow replacement) have not shown enhancement.

*Extradural Neoplasms*

Unenhanced MR imaging has been shown to be excellent in the detection and delineation of neoplasms within the spine [34]. Enhanced MR imaging probably is not necessary in the evaluation of most cases of neoplastic disease of the spine, although some investigators have suggested its use routinely [35]. There are certain situations, however, in which enhanced MR imaging may add important information or more clearly delineate some lesions.

The characteristics of various primary musculoskeletal neoplasms that may involve the spine are discussed elsewhere in this article. The soft-tissue components of these neoplasms frequently enhance and are hyperintense on enhanced MR imaging [21]. This may be useful in evaluating tumor margins (particularly paraspinal extension) or in determining what portion of a lesion is likely to yield diagnostic tissue on biopsy [21].

Vertebral metastases are usually seen on unenhanced T1-weighted MR images as areas of relatively low signal intensity as compared with the adjacent normal bone marrow. With the administration of gadopentetate dimeglumine, these vertebral metastases show variable enhancement and, because they increase in signal intensity (becoming closer to the normal marrow in signal intensity), may be more difficult to detect than on unenhanced MR images (Fig. 3). [21, 24, 35, 36]. This possible masking effect coupled with the high accuracy of unenhanced MR imaging suggests a limited role for gadolinium-enhanced MR imaging in the evaluation of spinal metastases. As with primary spine neoplasms, gadolinium-enhanced MR imaging may be useful in defining tumor margins and paraspinal extension [34]. Regions of more active tumor may be delineated for biopsy after IV injection of gadopentetate dimeglumine [24]. It has been suggested that this technique may play a role in evaluating the response of spinal metastases to treatment, although mild enhancement may be seen in quiescent tumors [24, 35, 36]. Finally, enhanced MR imaging may be useful in assessing the presence and extent of epidural tumor, especially when there is little or no bony involvement [24, 36].

## Enhanced MR Imaging in the Evaluation of Bone and Soft-Tissue Tumors

IV injection of gadopentetate dimeglumine produces increased signal intensity of neoplastic tissue on T1-weighted images within approximately 5 min [37, 38]. This property has been used to evaluate musculoskeletal tumors before and after treatment.

*Preoperative Assessment*

The value of preoperative imaging of musculoskeletal tumors is to provide an accurate staging of the lesion in order to plan for biopsy, surgery, and/or radiation therapy. Routine unenhanced MR techniques offer excellent depiction of the tumor in most circumstances [39, 40]. However, in some cases, additional information may be gained with enhanced MR imaging. Six specific parameters have been evaluated by different researchers using gadopentetate dimeglumine: tumor/muscle contrast, tumor/fat or bone-marrow contrast, tumor vs edema, viable vs nonviable tumor, tumor vascularity, and malignant vs benign tumor.

*Tumor/muscle contrast.*—The contrast-to-noise ratio between tumor and muscle is increased on enhanced T1-weighted spin-echo (SE) sequences when compared with unenhanced T1-weighted images (Fig. 4) [37–41]. This is of particular value when staging bone tumors extending into the surrounding soft tissues or tumors arising primarily in the soft tissues. However, Erleman et al. [37] reported that tumor/

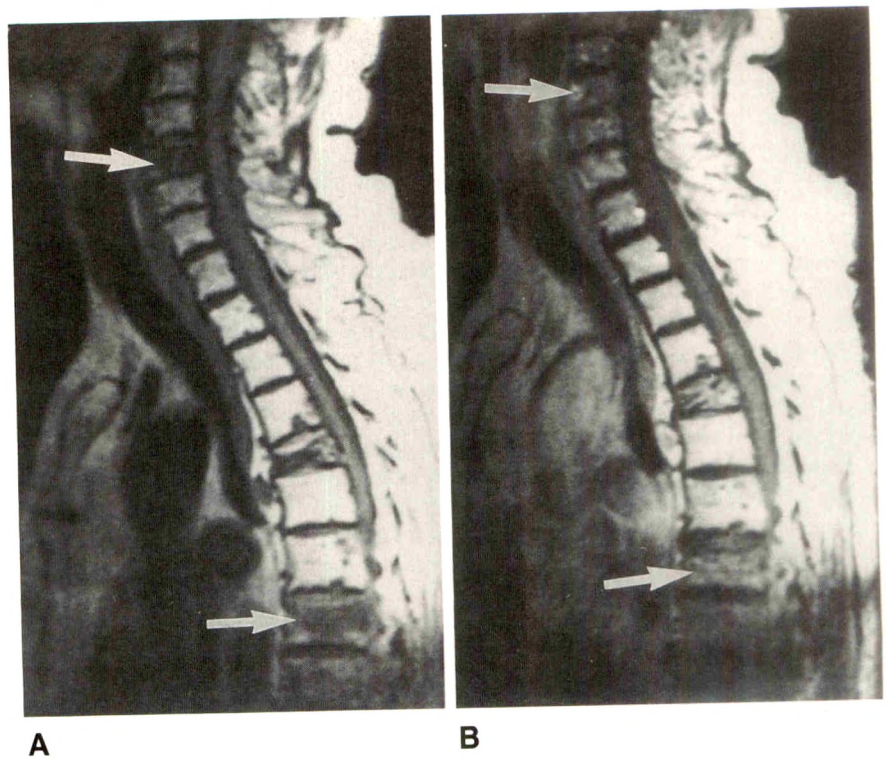



Fig. 3.—Vertebral metastases.
*A*, Sagittal unenhanced T1-weighted MR image (SE 800/20) of cervicothoracic spine shows decreased signal intensity in several vertebral bodies due to metastases (*arrows*).
*B*, Enhanced T1-weighted MR image (SE 800/30). Many of the metastases have enhanced and are now more difficult to identify (*arrows*).

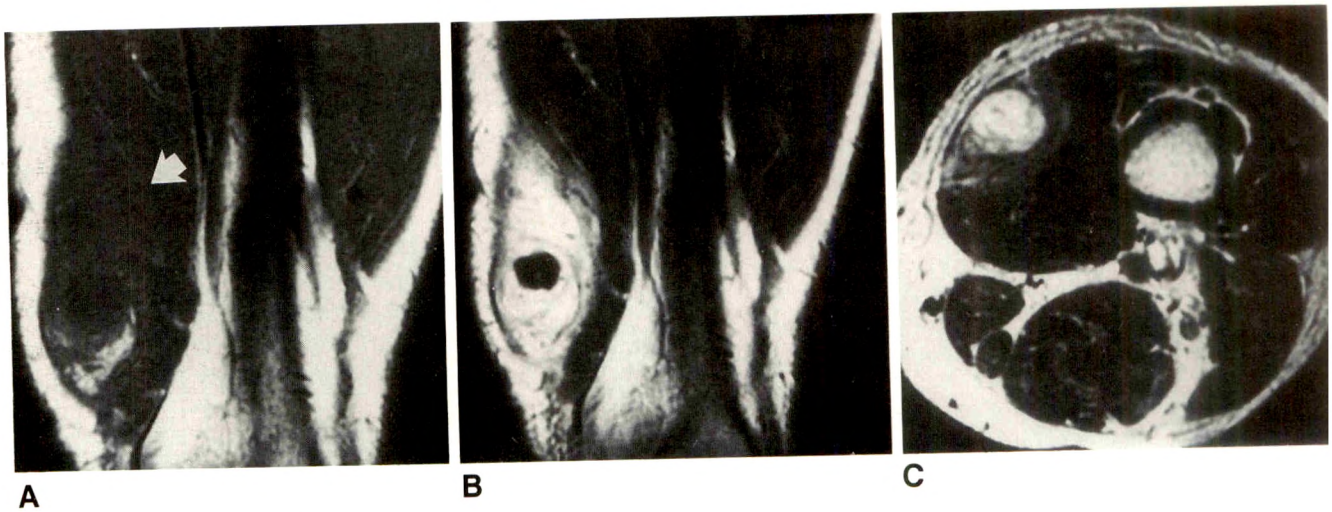



Fig. 4.—Lyposarcoma of the right thigh.
*A*, Coronal unenhanced T1-weighted MR image (SE 600/20) shows tumor is isointense relative to surrounding muscle tissue (*arrow*).
*B*, After contrast administration, T1-weighted MR image (SE 600/20) shows marked tumor enhancement. Central area of nonenhancing tissue represents myxoid degeneration.
*C*, Axial unenhanced T2-weighted MR image (SE 2000/80) shows good contrast between hyperintense tumor and surrounding muscle. Area of myxoid degeneration is not seen.

muscle contrast was 44% lower on enhanced T1-weighted SE images than on unenhanced T2-weighted SE images, especially in benign tumors with cystic components and in chondrogenic and highly necrotic malignant tumors. Similar results were obtained by the same authors (Erleman R et al., RSNA, November 1988), with an enhanced, fast low-angle shot (FLASH) technique. Pettersson et al. [38] found no differences in tumor/muscle contrast between T2-weighted SE images obtained before and after administration of gadopentetate dimeglumine, and von Schulthess et al. (RSNA November 1988) reported that tumor/muscle contrast on enhanced T1-weighted SE images was somewhat better than on unenhanced T1- and T2-weighted SE images. With dynamic enhanced studies, Erleman et al. [37] described rapid enhancement of tumor tissue and no or moderate enhancement of normal muscle tissue.

*Tumor/fat or bone-marrow contrast.*—On enhanced T1-weighted images, tumor tissue may become isointense rela

tive to the normally high-signal-intensity fatty tissue of the subcutaneous fat, fat planes, and fatty bone marrow (Fig. 3). In most cases, however, T2-weighted SE images can depict good contrast between tumor and fatty tissue. Tumor/fat and tumor/bone-marrow contrast was found to be 37–43% lower when enhanced T1-weighted SE images were used than when unenhanced T1-weighted SE images were used [37]. Yousry et al. (RSNA, November 1989) reported improved tumor/bone-marrow contrast when enhanced gradient-echo sequences were used. Dynamic enhanced studies showed practically no enhancement of fat and fatty marrow [37].

*Tumor vs edema.*—Many malignant tumors will have a halo of high signal intensity on T2-weighted images that can represent reactive edema or tumor infiltration [42]. This distinction can be difficult on unenhanced MR images. Bloem et al. (RSNA, November 1988) reported strong enhancement of viable tumor relative to edema, when enhanced T1-weighted SE images were used to study a group of 36 bone tumors. Erleman et al. (RSNA, November 1989) described enhancement of edema in muscle tissue with an enhanced fast imaging technique (90° FLASH) in a group of 132 patients with musculoskeletal neoplasms, and the same researchers [37] reported more rapid enhancement of tumor tissue than of peritumorous edema on dynamic enhanced studies.

*Viable vs nonviable tumor.*—Distinction between viable and necrotic or cystic components of a tumor may be helpful for preoperative selection of a biopsy site. Necrotic and cystic areas can have high signal intensity on unenhanced T2-weighted SE images, making this distinction impossible. Enhanced T1-weighted SE images, enhanced gradient-echo images, and dynamic enhanced studies show enhancement of viable tumor and no enhancement of necrotic tissue or cystic areas (Fig. 4) [37, 41].

*Tumor vascularity.*—Determination of the degree of vascularity of a tumor may be necessary in order to plan surgery or presurgical embolization. Reported series indicate that the degree of tumor enhancement on enhanced T1-weighted SE images correlates with the degree of vascularity [41] (Bloem JL et al., RSNA, November 1988).

*Malignant vs benign tumor.*—Erleman et al. [37], in a series of 69 patients, reported the value of dynamic enhanced studies in determining whether a tumor was benign or malignant. On graph curves of signal intensity plotted against time, slopes with higher than 30% increases in signal intensity per minute were seen in 84% of malignant tumors and slopes lower than 30% per minute were seen in 72% of benign tumors. Fibrotic, cystic, and fatty tumors showed practically no enhancement in a series of 32 patients with primary bone tumors reported by Imhof et al. (RSNA, November 1988). Bloem et al. (RSNA, November 1988) found peripheral enhancement in 10 cases of low-grade chondrosarcomas in a series of 36 bone tumors.

### *Posttreatment Assessment*

Low signal intensity in the region of previous surgery and/or radiation therapy on unenhanced T1- and T2-weighted images is a good indicator of absence of recurrent tumor [43]. On the other hand, a region of high signal intensity on T2-weighted images may represent postsurgical scar or granulation tissue or recurrent tumor [44]. Static T1-weighted SE images obtained after injection of gadopentetate dimeglumine are sensitive but nonspecific in detecting recurrent or residual bone-marrow and soft-tissue neoplasms on follow-up. Poorly defined areas of enhancement can be seen in the region of previous radiation therapy for up to 62 weeks, when enhanced T1-weighted SE images are used (Hanna SL et al., SMRI, May 1990). No enhancement is a good indicator that tumor has not recurred (Kim EE et al., SMRI, May 1989).

Dynamic enhanced studies can improve the low specificity of MR in treated tumors. On graph curves of signal intensity vs time, slopes with more than 30% increases in signal intensity per minute were observed by Hanna et al. (SMRI, May 1990) in patients treated with radiation/chemotherapy. Slopes of less than 30% indicated tumor inactivity. Tumors responding to induction chemotherapy showed slopes equal to or lower than 30%, whereas nonresponding tumors demonstrated slopes over 30% in the same series. Erleman et al. [43] found dynamic enhanced studies more accurate than static enhanced T1-weighted SE studies and scintigraphy in assessing response to chemotherapy.

## Enhanced MR Imaging in the Evaluation of Joints

Recent studies have addressed the biologic distribution of IV and intraarticular injection of gadopentetate dimeglumine in human and experimental models [13, 45], and found these to be safe procedures in the doses studied. Other authors have studied the role of intraarticular injection of gadopentetate dimeglumine in the evaluation of shoulder disorders [46] and of IV injection in the evaluation of knees of patients with rheumatoid arthritis [47].

Hajek et al. [45] studied the effects of intraarticular injections of 500-$\mu$mol concentrations of gadopentetate dimeglumine on the synovial membranes and joint cartilage of rabbits by using macroscopic, microscopic, and X-ray fluorescent spectroscopic techniques. They concluded that there were no significant gross or histologic alterations in the synovial membranes after intraarticular injection of gadopentetate dimeglumine, and that there was no evidence for accumulation of contrast material in articular cartilage or synovium in their study. However, intraarticular injection of gadopentetate dimeglumine is not yet approved by the Food and Drug Administration, and its use requires institutional approval and the patient's informed consent.

### *MR Arthrography*

The role of MR in the imaging of the normal structures and pathologic alterations in the bones and soft tissues about joints is well established. The visualization of these articular structures is improved with the presence of intraarticular fluid [48]. In the absence of native effusion, MR imaging can be performed after intraarticular injection of saline or gadopentetate dimeglumine. This procedure is termed MR arthrography. After intraarticular injection of 500 $\mu$mol of gadopentetate

dimeglumine, MR imaging can be performed by using short TR/TE pulse sequences with excellent contrast between the fluid and articular structures. After intraarticular injection of saline, MR imaging can be performed by using long TR/TE pulse sequences to allow sufficient contrast between the iatrogenically introduced saline and the surrounding articular structures. Advocates of intraarticular injection of gadopentetate dimeglumine argue that postinjection images can be acquired more quickly with gadopentetate dimeglumine than with saline, and that these pulse sequences are less sensitive to motion artifacts because of the short TRs [46]. Disadvantages of MR arthrography include a longer examination time, the use of fluoroscopy, and the conversion of a noninvasive examination into an invasive one.

Flannigan et al. [46] compared MR arthrography of the shoulder with conventional MR imaging and found that intraarticular injection of gadopentetate dimeglumine yielded superior visualization of the fibrocartilage glenoid labrum, glenohumeral ligaments, subscapularis bursa, and type of capsular insertion. Furthermore, they claim that MR arthrography enabled detection of labral tears and capsular striping (Fig. 5) and of full-thickness tears of the articular surface of the supraspinatus tendon (Fig. 6) when these were occult on conventional MR imaging. However, these results are still preliminary, and further testing of this technique is necessary.

Flannigan et al. [46] also reported that partial tears of the bursal surface of the supraspinatus muscle were not recognized when only short TR/TE images were used for gadopentetate-dimeglumine arthrography. These tears were diagnosed preoperatively on the basis of the long TR/TE sequences of conventional MR imaging. Therefore, they recommend MR arthrography of the shoulder as an adjunct to conventional MR imaging when the latter is negative or equivocal and there is strong clinical suspicion of a rotator cuff tear or labral or capsular pathologic changes. No complications were identified in 74 patients who underwent MR arthrography in their series.

### *IV Enhanced MR Imaging of the Knee in Rheumatoid Arthritis*

Differentiation between chronic effusion and inflamed synovium of joints in patients with rheumatoid arthritis is difficult on physical examination. This differentiation is clinically important as the drugs used to treat rheumatoid arthritis (high-dose aspirin, steroids, antimetabolites, immunosuppressants) are relatively toxic. Recent studies have shown the superiority

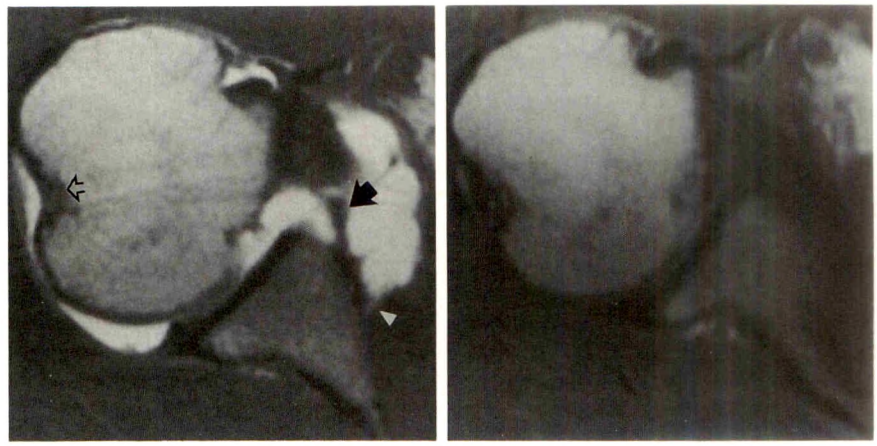



**Fig. 5.—Labral tear.**
***A*, Axial T1-weighted MR image (SE 600/20) of inferior glenohumeral joint after intraarticular injection of gadopentetate dimeglumine shows capsular stripping (*arrowhead*), Bankhart lesion of labrum (*solid arrow*), and Hill-Sachs lesion (*open arrow*).**
***B*, Labral and capsular lesions are not well seen on corresponding unenhanced balanced MR image (SE 2000/20).**

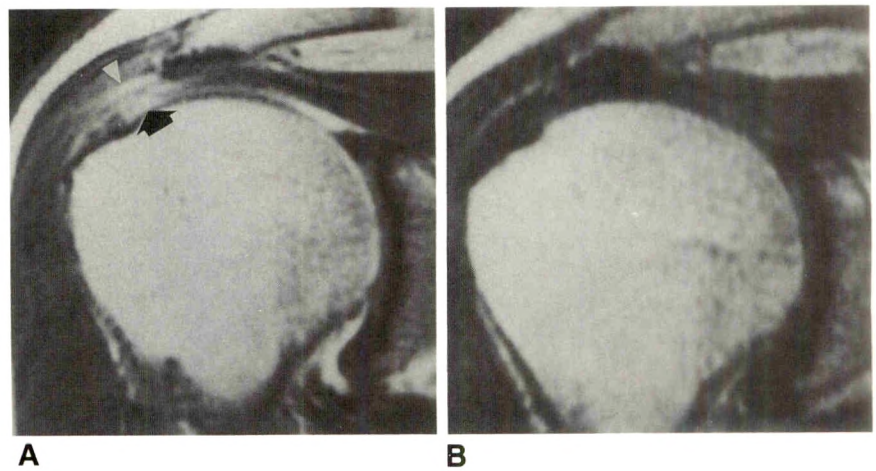



**Fig. 6.—Rotator cuff tear.**
***A*, Coronal oblique T1-weighted MR image of mid shoulder (SE 600/20) after intraarticular injection of gadopentetate dimeglumine shows a full-thickness tear of supraspinatus tendon (*arrow*) and fluid in subdeltoid bursa (*arrowhead*).**
***B*, These findings are occult on corresponding preinjection T2-weighted MR image (SE 2000/80).**

of MR imaging over other radiologic techniques in detecting early erosions, cartilage abnormalities, and lesions of other tissues, such as tendons and ligaments in patients with rheumatoid arthritis [49–52]. These studies have confirmed the difficulty in distinguishing pannus from effusion on conventional short and long TR/TE pulse sequences. Both pannus and effusion are imaged as homogeneous collections of low signal intensity on short TR/TE pulse sequences and of high signal intensity on long TR/TE pulse sequences.

Kursunoglu-Brahme et al. [47] have described the results of their prospective study of MR imaging of the knees after IV injection of gadopentetate dimeglumine in patients with long-standing rheumatoid arthritis of various severities. They claim to be able to distinguish pannus from effusion routinely and reliably on short TR/TE pulse sequences after IV injection of gadopentetate dimeglumine. These images, obtained immediately after injection of gadopentetate dimeglumine, showed diffuse homogeneous brightening of lobulated, frond-like masses in a peripheral, periarticular distribution, having the classically described appearance of inflammatory pannus. The images also showed nonenhancing collections of homogeneous low signal intensity characteristically produced by effusions on short TR/TE images (Fig. 7). They claim that MR imaging after IV injection of gadopentetate dimeglumine is the most sensitive imaging technique for showing the pathologic processes about the knee in patients with rheumatoid arthritis.

### Enhanced MR Imaging in the Evaluation of Infection and Inflammation of the Musculoskeletal System

Little has been written regarding the role of gadopentetate dimeglumine–enhanced MR imaging in the evaluation of infectious and inflammatory diseases of the musculoskeletal system. Hyperemia and edema induced by inflammation are theoretically a good setting for enhancement. This has been shown in experimentally induced cellulitis [53] and abscesses in animal models [54], which show a peripheral rim of enhancement corresponding to the inflammatory and cellular region of the abscess (Fig. 8). The clinical usefulness of this

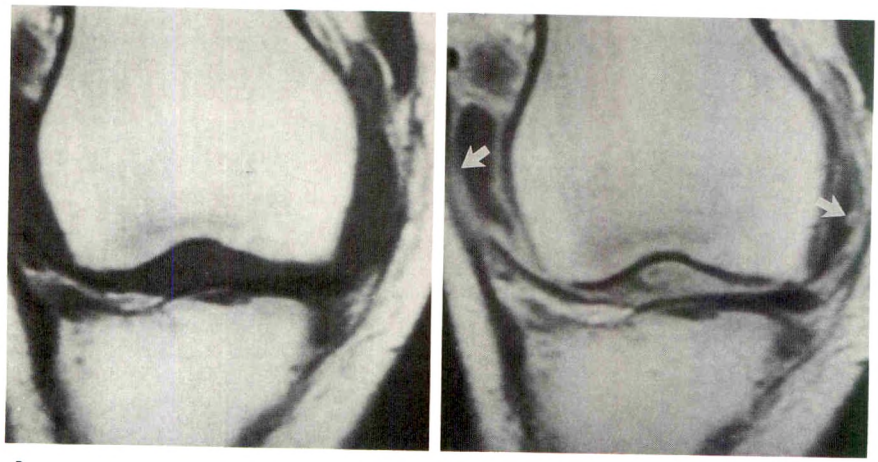


Fig. 7.—Rheumatoid arthritis.
*A*, Coronal unenhanced T1-weighted MR image (SE 800/20) of knee shows fluid and pannus, both with homogeneous low signal intensity.
*B*, Contrast-enhanced coronal T1-weighted MR image (SE 600/20) shows pannus as a high-signal-intensity mass at periphery of knee joint (*arrows*) and effusion as a low-signal-intensity mass located medial to it.



Fig. 8.—Soft-tissue abscesses. Enhanced gradient-refocused MR image with T1 weighting (40/10/90°) shows ring enhancement of two small abscesses (*arrows*).

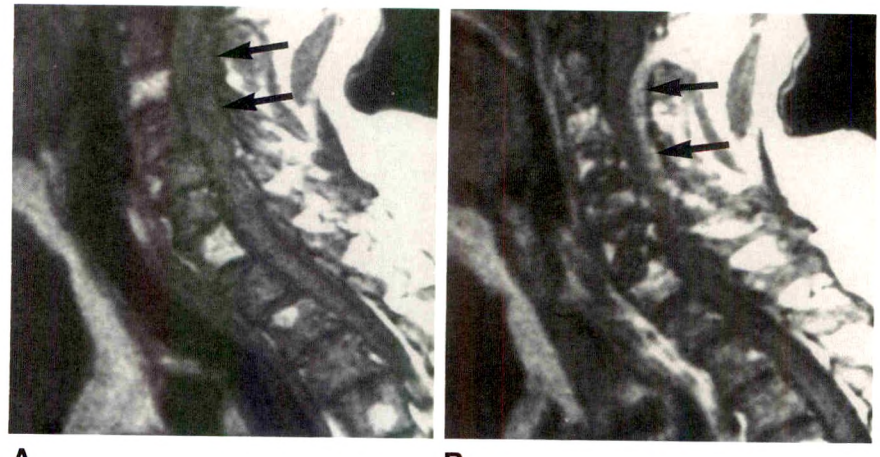


Fig. 9.—Epidural abscess.
*A*, Sagittal unenhanced T1-weighted MR image (SE 600/20) shows poorly defined epidural mass in posterior aspect of cervical spinal canal (*arrows*).
*B*, Enhanced T1-weighted MR image (SE 800/20) shows ringlike enhancement of posterior epidural abscess (*arrows*) with cord compression.

finding is yet to be investigated. Early reports indicate that enhancement can be seen in areas adjacent to musculoskeletal infection [10].

De Roos et al. [55] indicated that enhanced T1-weighted images may be better than T2-weighted images for demonstration of the exact extent of an infectious process and small fistulas.

Unenhanced MR is quite sensitive in the evaluation of vertebral osteomyelitis and epidural abscess [56, 57]. However, it has been reported that enhanced MR imaging is a useful adjunct to unenhanced MR in the evaluation of spinal infections in certain situations. Enhanced MR imaging may be more sensitive in detecting and evaluating the extent of drainable epidural abscesses (Sandhu J et al., RSNA, November 1989). An epidural abscess is seen on enhanced MR imaging as an area of enhancement in the epidural space, sometimes with a nonenhancing central portion representing liquid abscess (Fig. 9). The differentiation of the abscess from the adjacent thecal sac may be seen better with enhanced than with unenhanced MR [58]. Epidural tumors also may enhance after IV injection of gadopentetate dimeglumine. Many epidural abscesses extend contiguously over several vertebral segments. This distribution, which is less common in epidural tumors, can help in differentiating these two entities.

In osteomyelitis, marked enhancement may occur of the marrow and granulation tissue surrounding the infection [24]. It has been suggested that enhanced MR imaging is a useful addition to unenhanced MR to differentiate active infection from one that has responded adequately to antibiotics and to determine the most active area of infection when biopsy is being considered [58]. In patients with diskitis, vertebral osteomyelitis, and associated paravertebral inflammatory changes, progressive decrease and eventual resolution of enhancement has been demonstrated in patients that show clinical improvement after antibiotic therapy [58].

## Conclusions

Although most published data are based on preliminary results in relatively small series, a group of potential indications for the use of enhanced MR imaging in the musculoskeletal system seems to be emerging. In the spine, gadopentetate dimeglumine helps in differentiating between scar tissue and recurrent disk herniation, and in the evaluation of epidural tumors. In musculoskeletal tumors, differentiation between tumor necrosis, peritumoral edema, and viable tumor, and evaluation of activity of the tumor before and after treatment, may be easier with gadopentetate dimeglumine–enhanced MR imaging. Dynamic enhanced MR is a promising technique, but needs to be tested in different institutions, using different equipment. In the joints, intraarticular injection of gadopentetate dimeglumine can better depict cartilage and tendon tears, and IV injection helps in differentiating between pannus and intraarticular fluid. Finally, delineation of an infectious process may be improved with enhanced MR imaging. Further research is necessary to justify the added cost of enhanced MR imaging to unenhanced studies in the musculoskeletal system.

## REFERENCES


1. Bydder GM, Kingsley DP, Brown J, Niendorf HP, Young IR. MR imaging of meningiomas including studies with and without gadolinium-DTPA. *J Comput Assist Tomogr* **1985**;9:690–697
2. Graif M, Byder GM, Steiner RE, Niendorf P, Thomas DG, Young IR. Contrast-enhanced MR imaging of malignant brain tumors. *AJNR* **1985**; 6:855–862
3. Felix R, Schorner W, Laniado M, et al. Brain tumors: MR imaging with gadolinium-DTPA. *Radiology* **1985**;156:681–688
4. Haughton VM, Rimm AA, Czevionke LF, et al. Sensitivity of Gd-DTPA-enhanced MR imaging of benign extraaxial tumors. *Radiology* **1988**; 166:828–833
5. Nyman RS, Rehn SM, Glimelius BLG, Hagberg HE, Hemmingsson AL, Sundstrom CJ. Residual mediastinal masses in Hodgkin disease: prediction of size with MR imaging. *Radiology* **1989**;170:435–440
6. Heywang SH, Wolf A, Pruss E, Hibertz T, Eierman W, Permanette W. MR imaging of the breast with Gd-DTPA: use and limitations. *Radiology* **1989**;170:95–103
7. Stark DD, Weisslender A, Elizondo G, et al. Superparamagnetic iron oxide: clinical application as a contrast agent for MR imaging of the liver. *Radiology* **1988**;168:297–301
8. Gibby WA. MR contrast agents: an overview. *Radiol Clin North Am* **1988**;26:1047–1058
9. Meyer D, Schaefer M, Bonnemain B. Gd-DOTA, a potential MRI contrast agent: current status of physicochemical knowledge. *Invest Radiol* **1988**;23 [suppl]:232–235
10. Traill MR, Sartoris DV. Musculoskeletal system. In: Runge VM, ed. *Enhanced magnetic resonance imaging.* St Louis: Mosby, **1989**:290–300
11. Runge VM, Wood ML, Kaufman D, Price AC. Gd-DTPA: future applications with advanced imaging techniques. *RadioGraphics* **1988**;8:161–179
12. Runge VM, Schaible TF, Goldstein HA, et al. Gd-DTPA: clinical efficacy. *RadioGraphics* **1988**;8:147–159
13. Weinmann HJ, Brash RC, Press WR, Wesbey GE. Characteristics of gadolinium-DTPA complex: a potential NMR contrast agent. *AJR* **1984**; 142:619–624
14. Goldstein H. Product insert. Cedar Knolls, NJ: Berlex Labs., June **1988**
15. Simon JH, Szumowski J. Chemical shift imaging with paramagnetic contrast material enhancement for improved lesion depiction. *Radiology* **1989**;171:539–543
16. Erleman R, Reiser M, Peters PE, Wuisman P, Niedorf HP, Kunze V. Time-dependent changes in signal intensity in neoplastic and inflammatory lesions of the musculoskeletal system following intravenous administration of Gd-DTPA. *Radiologe* **1988**;28:269–276
17. Sze G, Abramson A, Krol G, et al. Gadolinium-DTPA in the evaluation of intradural extramedullary spinal disease. *AJNR* **1988**;9:153–163
18. Valk J. Gd-DTPA in MR of spinal lesions. *AJNR* **1988**;9:345–350
19. Sze G, Krol G, Zimmerman RD, Deck MDF. Intramedullary disease of the spine: diagnosis using gadolinium-DTPA-enhanced MR imaging. *AJNR* **1988**;9:847–858
20. Dillon WP, Norman D, Newton TH, et al. Intradural spinal cord lesions: Gd-DTPA-enhanced MR imaging. *Radiology* **1989**;170:229–237
21. Nelson KL, Modic MT. Spine. In: Runge VM, ed. *Enhanced magnetic resonance imaging.* St. Louis: Mosby, **1989**:193–210
22. Czervionke LF, Daniels DL, Ho PSP, et al. Cervical neural foramina: correlative anatomic and MR imaging study. *Radiology* **1988**;169: 753–759
23. Breger RK, Williams AL, Daniels DL, et al. Contrast enhancement in spinal MR imaging. *AJNR* **1989**;10:633–637
24. Sze G. Gadolinium-DTPA in spinal disease. *Radiol Clin North Am* **1988**;26(5):1009–1024
25. Bundschuh CV, Modic MT, Ross JS, et al. Epidural fibrosis and recurrent disk herniation in the lumbar spine: MR imaging assessment. *AJNR* **1988**;9:169–178
26. Ross JS, Delamarter R, Hueftle MG, et al. Gadolinium-DTPA-enhanced MR imaging of the postoperative lumbar spine: time course and mechanism of enhancement. *AJNR* **1989**;10:37–46
27. Hueftle MG, Modic MT, Ross JS, et al. Lumbar spine: postoperative MR imaging with Gd-DTPA. *Radiology* **1988**;167:817–824
28. Nguyen CM, Ho K-C, Yu S, Haughton VM, Strandt JA. An experimental model to study contrast enhancement in MR imaging of the intervertebral disk. *AJNR* **1989**;10:811–814
29. Ross JS, Blaser S, Masaryk TJ, et al. Gd-DTPA enhancement of posterior

epidural scar: an experimental model. *AJNR* **1989**;10:1083–1088
30. Ross JS, Modic MT, Masaryk TJ, Carter J, Marcus RE, Bohlman H. Assessment of extradural degenerative disease with Gd-DTPA-enhanced MR imaging: correlation with surgical and pathologic findings. *AJNR* **1989**;10:1243–1249
31. Parizel PM, Rodesch G, Baleriaux D, et al. Gd-DTPA–enhanced MR in thoracic disc herniations. *Neuroradiology* **1989**;31:75–79
32. Ross JS, Modic MT, Masaryk TJ. Tears of the anulus fibrosus: assessment with Gd-DTPA–enhanced MR imaging. *AJNR* **1989**;10:1251–1254
33. Modic MT, Steinberg PM, Ross JS, et al. Degenerative disk disease: assessment of changes in vertebral body marrow with MR imaging. *Radiology* **1988**;166:193–199
34. Daffner RH, Lupetin AR, Dash N, et al. MRI in the detection of malignant infiltration of bone marrow. *AJR* **1986**;146:353–358
35. Stimac GK, Porter BA, Olson DA, et al. Gadolinium-DTPA–enhanced MR imaging of spinal neoplasms: preliminary investigation and comparison with unenhanced spin-echo and STIR sequences. *AJNR* **1988**;9:839–846
36. Sze G, Krol G, Zimmerman RD, Deck MDF. Malignant extradural spinal tumors: MR imaging with Gd-DTPA. *Radiology* **1988**;167:217–223
37. Erleman R, Reiser MF, Peters PE, et al. Musculoskeletal neoplasms: static and dynamic Gd-DTPA–enhanced MR imaging. *Radiology* **1989**;171:767–773
38. Pettersson H, Ackerman N, Kaude J, et al. Gadolinium-DTPA enhancement of experimental soft tissue carcinoma and hemorrhage in magnetic resonance imaging. *Acta Radiol* **1987**;28:75–78
39. Petasnick JP, Turner DA, Charters JR, Gitelis S, Zacharias CE. Soft-tissue masses of the locomotor system: a comparison of MR imaging with CT. *Radiology* **1986**;160:125–133
40. Petterson H, Gillespy T, Hamlin DJ, et al. Primary musculoskeletal tumors: examination with MR imaging compared with conventional modalities. *Radiology* **1987**;164:237–241
41. Petterson H, Eliasson J, Egund N, et al. Gadolinium-DTPA enhancement of soft tissue tumors in magnetic resonance imaging: preliminary clinical experience in five patients. *Skeletal Radiol* **1988**;17:319–323
42. Beltran J, Simon DC, Katz W, Weis LD. Increased MR signal intensity in skeletal muscle adjacent to malignant tumors: pathologic correlation and clinical relevance. *Radiology* **1987**;162:251–255
43. Erleman R, Sciuk J, Bosse A, et al. Response of osteosarcoma and Ewing sarcoma to preoperative chemotherapy: assessment with dynamic and static MR imaging and skeletal scintigraphy. *Radiology* **1990**;175:791–796
44. Vanel D, Lacombe MJ, Couanet D, Kalifa C, Spielmann M, Genin J. Musculoskeletal tumors: follow-up MR imaging after treatment with surgery and radiation therapy. *Radiology* **1987**;164:243–245
45. Hajek PC, Sartoris DJ, Glys-Morin V, et al. The effect of intraarticular gadolinium-DTPA on synovial membrane and cartilage. *Invest Radiol* **1990**;25:179–182
46. Flannigan B, Kursunoglu-Brahme S, Snyder S, Karzel R, Del Pizzo W, Resnick D. MR arthrography of the shoulder: comparison with conventional MR imaging. *AJR* **1990**;155:829–832
47. Kursunoglu-Brahme S, Riccio T, Weisman MH, et al. Rheumatoid knee: role of gadopentetate-enhanced MR imaging. *Radiology* **1990**;176:831–835
48. Hajeck PC, Baker LL, Sartoris DJ, Neumann C, Resnick D. MR arthrography: anatomic-pathologic investigation. *Radiology* **1987**;163:141–147
49. Gilkeson G, Polisson R, Sinclair H, et al. Early detection of carpal erosions in patients with rheumatoid arthritis: a pilot study of magnetic resonance imaging. *J Rheumatol* **1988**;15:1361–1366
50. Adams ME, Li DK. Magnetic resonance imaging in rheumatology. *J Rheumatol* **1985**;12:1038–1040
51. Beltran J, Caudill JL, Herman LA, et al. Rheumatoid arthritis: MR imaging manifestations. *Radiology* **1987**;165:153–157
52. Yulish BS, Lieberman JM, Newman AJ, et al. Juvenile rheumatoid arthritis: assessment with MR imaging. *Radiology* **1987**;165:149–152
53. Paajanen H, Brasch RC, Schmiedl U, Ogan M. Magnetic resonance imaging of local soft tissue inflammation using gadolinium-DTPA. *Acta Radiol* **1987**;28:79–83
54. Paajanen H, Grood W, Revel D, Engelstad B, Brasch RC. Gadolinium-DTPA enhanced MR imaging of intramuscular abscesses. *Magn Reson Imaging* **1987**;5:109–115
55. De Roos A, van Meerten ELvP, Bloem JL, Bluemm RG. MRI of tuberculous spondylitis. *AJR* **1986**;147:79–82
56. Modic MT, Feiglin DH, Piraino DW, et al. Vertebral osteomyelitis: assessment using MR. *Radiology* **1985**;157:157–166
57. Angtuaco EJC, McConnell JR, Chadduck WM, Flanigan S. MR imaging of spinal epidural sepsis. *AJR* **1987**;149:1249–1253
58. Post MJD, Sze G, Quencer RM, Eismont FJ, Green BA, Gehbauer H. Gadolinium enhanced MR in spinal infection. *J Comput Assist Tomogr* **1990**;14:721–729

# Detection of Bullous Lung Disease: Conventional Radiography vs Digital Storage Phosphor Radiography

Kathleen M. Buckley[1]
Cornelia M. Schaefer[1,2]
Reginald Greene[1]
Steve Agatston[1]
Jane Fay[1]
Henry J. Llewellyn[1]
Helen E. Mrose[1]
Jami R. Rubens[1]

**The detection of fine linear contours and altered aeration are requirements for the radiologic diagnosis of bullous lung disease and are severe measures of the spatial and contrast resolution of chest imaging systems. We compared plain film radiography with five postprocessing algorithms of storage phosphor digital radiography (2144 × 1744 × 10 bit matrix with 0.2-mm pixel size) in the detection of CT-proved bullous lung disease (35 patients and 25 normal control subjects). Receiver-operating-characteristic analysis of 2160 observations by six interpreters was done to evaluate the observers' performance. By analysis of variance ($p < .05$), we found that the default digital algorithm and the three edge-enhancing algorithms of high and medium frequencies performed less well than plain films did, but the differences fell short of statistical significance. Gray-scale reversal was the only digital algorithm that performed significantly less well than plain films did.**

**We conclude that any differences between digital algorithms and plain films in the detection of bullous lung disease were too small to be detected in this study. Any difference between the two methods in providing clinically important, diagnostic information is likely to be insignificant.**

***AJR* 156:467–470, March 1991**

Storage phosphor digital radiography has a number of technical advantages (e.g., high dynamic range, flexible adjustment of contrast and density scale, and other postprocessing capabilities) that may offset its lower spatial resolution relative to plain film radiography [1–6]. The detection of fine linear contours and altered aeration that is necessary for the diagnosis of bullous lung disease provides a unique test of the spatial and contrast resolution of an imaging system. Previous experimental and clinical studies have reported discordant results in the detection of fine linear structures with digital radiography and have suggested the important role of edge-enhancement postprocessing [2–4, 7, 8]. We compared plain film radiography with five postprocessing algorithms of storage phosphor radiography in the detection of bullous lung disease.

## Materials and Methods

We studied a total of 60 patients who had undergone CT of the chest for clinical indications. Thirty-five patients had a diagnosis of bullous lung disease. Twenty-five persons served as control subjects. There were 40 men and 20 women from 25 to 88 years of age (mean ± standard error = 60 ± 1.5 years). Each patient in the study group had posteroanterior radiographs of the chest obtained with storage phosphor and conventional technique within 1 week of the CT examination of the thorax. The CT examinations (GE 9800, General Electric Medical Systems, Milwaukee, WI) consisted of multislice scans (10 mm thick at 10-mm intervals) through the chest with selected thin sections (1.5 mm thick with high-resolution algorithm) as warranted by clinical circumstances. The official interpretation of the CT findings served as the basis for the expected findings on the radiographs. Criteria for the diagnosis of bullous lung disease included the identification of discrete, localized areas of low attenuation

Received March 29, 1990; accepted after revision October 10, 1990.

[1] Department of Radiology, Massachusetts General Hospital and Harvard Medical School, 32 Fruit St., Boston, MA 02114. Address reprint requests to R. Greene.

[2] Present address: Department of Radiology, Medizinische Hochschule Hannover, Hannover, Germany.

0361–803X/91/1563–0467
© American Roentgen Ray Society

surrounded by well-defined, paper-thin margins consisting of inverted pleura or compressed lung parenchyma or both. In some cases the bullae were surrounded by diffuse emphysema, but in most cases they were located within otherwise normal parenchyma. Other causes of localized hyperinflation (e.g., honeycomb lung, bronchiectasis, or oligemia) were specifically excluded. The bullae were divided into three classes according to size: (1) small, less than 2 cm in short axis diameter ($n = 6$); (2) intermediate, 2–4 cm in diameter ($n = 22$); and (3) large, greater than 4 cm in diameter ($n = 7$). Seven patients with large bullae and eight control subjects had a CT diagnosis of diffuse emphysema.

The conventional and digital radiographs were obtained with the same exposure factors: 140 kVp, 3-mm aluminum filter, 1.2-mm nominal focus, 12:1 oscillating grid, 183-cm source-to-image distance, and phototimed exposure (Tridoros 712 MP, Siemens Medical Systems, Erlangen, Germany). According to previous measurements, the average skin entrance exposure was 20 mR ($5.16 \times 10^{-6}$ C/kg) with both techniques [9]. The conventional images were obtained with Lanex medium screens, OC film, and automatic film processing with standard chemicals (Kodak M7B processor, Rochester, NY) at 36°C. The digital images (1744 × 2144 × 10 bit matrix size) were acquired with storage phosphor plates (ST, Fuji, Kanagawa, Japan) and digitized with a helium-neon laser readout unit (TCR 201, Toshiba America, Tustin, CA). A laser printer produced 17 × 21 cm hardcopies (Fugi, Kanagawa, Japan) of the storage phosphor radiographs with standard chemicals at 36.5°C. The digital images were processed according to five algorithms. Edges were enhanced with an unsharp mask subtraction technique according to the following formula:

$$A^* = A + f(A - B)$$

with $A^*$ = edge-enhanced image, A = original image, f = enhancement factor, and B = unsharp mask. The unsharp mask (B) was produced by locally averaging pixel values across a certain area. The size of this area determined the spatial frequency (cycles/mm) that was enhanced in the final image ($A^*$). This edge-enhanced image was produced by weighted addition of the edge image (A − B) to the original image. The degree of edge enhancement was determined by the flexible weighting factor (f), which could be chosen on a scale of 0 to 16. We tested the effect of gray-scale reversal (mode 2) and subtle, moderate, and pronounced enhancement of high (modes 1, 3, and 4) and medium (mode 5) frequencies.

The five digital algorithms were as follows:

Mode 1: The default algorithm (SR-1) approximated the appearance of an optimal conventional radiograph. It used a sigmoid, long-contrast Hurter and Driffield (H&D) curve with slight nonlinear edge enhancement of high spatial frequencies (enhancement factor, 0.5; enhanced frequency range centered at 1.4 cycles/mm).

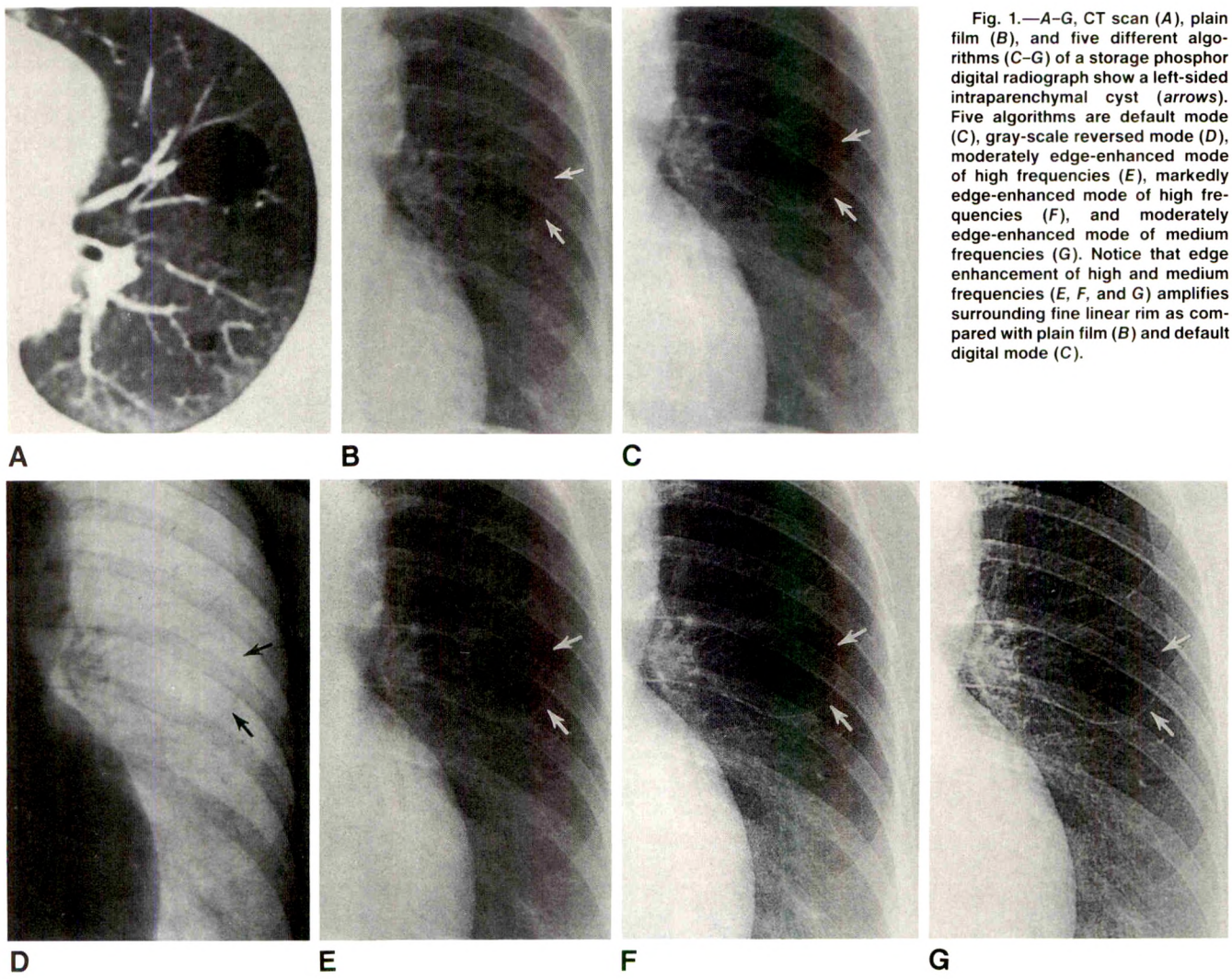



**Fig. 1.—*A–G*, CT scan (*A*), plain film (*B*), and five different algorithms (*C–G*) of a storage phosphor digital radiograph show a left-sided intraparenchymal cyst (*arrows*). Five algorithms are default mode (*C*), gray-scale reversed mode (*D*), moderately edge-enhanced mode of high frequencies (*E*), markedly edge-enhanced mode of high frequencies (*F*), and moderately edge-enhanced mode of medium frequencies (*G*). Notice that edge enhancement of high and medium frequencies (*E, F,* and *G*) amplifies surrounding fine linear rim as compared with plain film (*B*) and default digital mode (*C*).**

Mode 2: The gray-scale reversed algorithm (SR-2) used an identical H&D curve as the default algorithm except for reversal of gray-scale polarity.

Mode 3: The edge-enhanced algorithm (SR-3) performed a moderate enhancement of high spatial frequencies and was identical to the default algorithm except for a larger enhancement factor of 3.

Mode 4: The edge-enhanced algorithm (SR-4) performed a marked enhancement of high spatial frequencies and was identical to the default mode 1 except for a larger enhancement factor of 5.

Mode 5: The edge-enhanced algorithm (SR-5) performed a moderate enhancement of medium spatial frequencies and was identical to mode 3 except for the enhanced frequency range (enhancement factor 3, enhanced frequency range centered at 0.71 cycles/mm, Figs. 1A–1G).

The conventional and digital images were intermingled in random order and divided into three subsets. Six board-certified radiologists interpreted the subsets in differing order to avoid interpreter bias. Three separate sessions per interpreter extended over a 4-week period. The definitions and exclusions of bullous lung disease used in this study were reviewed before each session. The interpreters did not know the proportion of normal to abnormal cases. They were asked to indicate the presence of bullae according to a five-level scale of confidence (1 = definitely negative, 2 = probably negative, 3 = indeterminate, 4 = probably positive, 5 = definitely positive). Interpretation time was not limited.

Observer performance was tested according to receiver-operating-characteristic (ROC) analysis of pooled, averaged, and individual interpreter data for a total of 2160 observations. ROC curves were obtained by a maximum-likelihood curve-fitting algorithm, and perceptual accuracy was measured by the area under the ROC curve [10–13].

ROC curves were produced by fitting the pooled interpreter data from all observers and were used to demonstrate performance graphically [10]. Averaged ROC areas ($A_z \pm$ standard error) were produced by individually fitting the confidence ratings for each observer and averaging the estimated areas across the observers. These areas were used to measure performance of each imaging mode [11–13]. The significance of differences between the $A_z$ of the six imaging modes was tested with a one-factor analysis of variance for repeated measures. Paired $A_z$ values were compared with Scheffé's F-test at a two-tailed $p$ less than .05 [14]. A preliminary arc-sine transformation was performed to stabilize the data and to meet the assumptions of homogeneity and normal distribution of variances needed for analysis of variance [14]. The arc-sine transformation was considered the appropriate procedure because it applies to variables that express proportions.

Performance with respect to the three subclasses of bullae (small, intermediate, and large) was tested with pooled and individual data for plain film and for the digital algorithms with the best and worst performance. Significance of differences for the pooled data was tested by calculating the critical ratio ($p < .05$) [15].

In addition, the interpretation data of each observer with plain film and the best digital algorithm were subjected to a maximum-likelihood algorithm that incorporated estimations of variances and covariances of the ROC parameters into a univariate z-score test ($p < .05$) for the true-positive fraction at a constant false-positive fraction of 0.2 [16–18].

## Results

Performance with all digital algorithms (averaged ROC area ± standard error) was lower than that with plain films. However, no statistically significant difference was found between plain films and four of the five digital algorithms at a $p$ level of .05. The gray-scale reversed algorithm was the only digital algorithm that performed significantly worse than plain films did (Fig. 2 and Table 1). The algorithm with moderate enhancement of high spatial frequencies (mode 3) performed best among the digital modes. Five of the six interpreters had higher ROC areas with the plain films than with the best digital algorithm. However, the differences were not statistically significant (Table 2).

Analysis of performance according to the size of bullae indicated that the gray-scale reversed mode was inferior to plain films in the detection of small and intermediate-sized bullae. Plain films and the best digital algorithm with moderate enhancement of high spatial frequencies (mode 3) were equivalent in the detection of bullae of all sizes (Table 3).

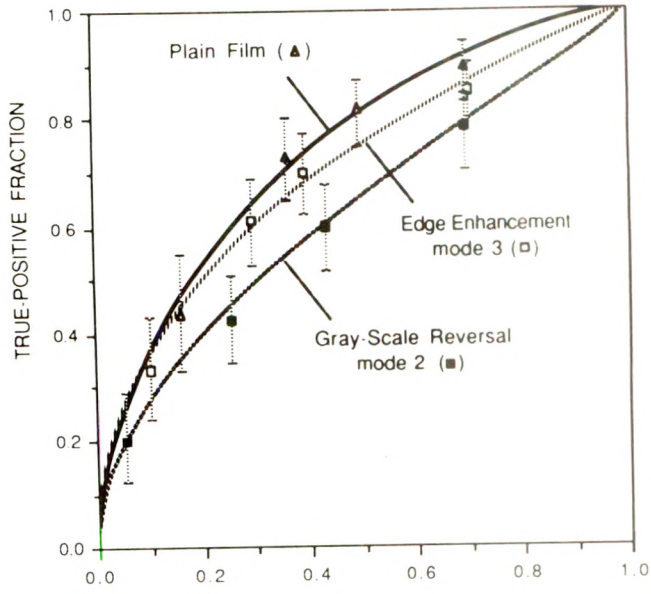



**Fig. 2.—Receiver-operating-characteristic curves derived from pooled data by six observers for plain film and the two digital storage phosphor modes with the lowest and highest performance, that is, gray-scale reversed mode and edge-enhanced mode 3 with moderate enhancement of high spatial frequencies.**

**TABLE 1: Average Performance and Range of Receiver-Operating-Characteristic (ROC) Areas by Six Readers**

| Technique/ Postprocessing Algorithm | ROC Area | | Significance: SR vs Plain Film |
|---|---|---|---|
| | Mean ± SEM | Range | |
| Plain film | 0.76 ± 0.04 | 0.64–0.87 | — |
| SR-1, Default: slight edge enhancement (high freq.) | 0.70 ± 0.02 | 0.67–0.75 | $p < .19$ |
| SR-2, Gray-scale reversal | 0.60 ± 0.05 | 0.37–0.72 | $p < .05$ |
| SR-3, Moderate edge enhancement (high freq.) | 0.72 ± 0.02 | 0.67–0.80 | $p < .31$ |
| SR-4, Marked edge enhancement (high freq.) | 0.71 ± 0.02 | 0.60–0.80 | $p < .20$ |
| SR-5, Moderate edge enhancement (medium freq.) | 0.71 ± 0.05 | 0.60–0.75 | $p < .10$ |

Note.—The gray-scale reversed algorithm (SR-2) is the only mode that performed significantly ($p < .05$) less well than plain film performed.

**TABLE 2: Individual and Average Performance with Plain Film and the Best Digital Mode**

| Reader | Plain Film (mean ± SEM) | SR-3 (mean ± SEM) |
|---|---|---|
| 1 | 0.87 | 0.81 |
| 2 | 0.79 | 0.68 |
| 3 | 0.69 | 0.68 |
| 4 | 0.84 | 0.75 |
| 5 | 0.72 | 0.70 |
| 6 | 0.64 | 0.69 |
| Average | 0.76 ± 0.04 | 0.72 ± 0.02 |

Note.—There are no significant differences between plain film and the best digital mode with moderate enhancement of high frequencies.

**TABLE 3: Average Performance According to the Size of the Bullae**

| Technique[a] | Large Bullae | Intermediate Bullae | Small Bullae |
|---|---|---|---|
| Plain film | 0.88 ± 0.03 | 0.72 ± 0.03 | 0.58 ± 0.11 |
| SR-2 | 0.78 ± 0.05 | 0.62 ± 0.03[b] | 0.41 ± 0.06[b] |
| SR-3 | 0.84 ± 0.04 | 0.71 ± 0.03 | 0.48 ± 0.06 |

[a] SR-2 = storage phosphor radiography with gray-scale reversal, SR-3 = storage phosphor radiography with moderate enhancement of high frequencies.
[b] Significantly lower than plain film at $p < .05$.

## Discussion

Although the averaged ROC areas for the detection of bullous lung disease were lower for all digital modes than for plain films, the differences were not sufficiently high or consistent enough to approach statistical significance ($p < .05$). The absence of a measurable significant difference in the performance of the various modes suggests that any differences in the performance of digital algorithms and plain films in the detection of bullous lung disease were too small to be measured in this study. The lack of a significant difference does not prove that no clinically significant information would be lost with digital storage phosphor radiography, but it does indicate that such loss, if any, would probably be small. Alternatively, the relative low performance for all techniques including plain films may indicate that our test was too severe to detect minor differences.

The diagnosis of bullae requires both low contrast discrimination because of slight alterations of aeration and high spatial resolution for the detection of fine linear contours. We did not test the extent to which the interpreter actually relied on each of these factors. Although in previous studies edge enhancement of high spatial frequencies was found to improve the detection of fine linear structures, in this study digital performance was not significantly improved by edge enhancement of medium or high frequencies [4, 7, 8]. This may be due to the opposing effects of this particular type of edge enhancement (i.e., enhancement of high spatial frequencies) on the visibility of linear structures and contrast. It amplifies the conspicuity of sharp, well-defined lines, but decreases the conspicuity of low-contrast differences. The inferior performance of the gray-scale reversed mode in the detection of bullae reconfirms the finding in other studies that this algorithm tends to degrade performance [19, 20].

ACKNOWLEDGMENTS

We thank Nancy Speroni, Sandra Laquidara, Laurie Lizotte, and Nancy Williams for technical assistance; Joyce Buchanan for manuscript preparation; and Toshiba America Medical Systems for general support.

REFERENCES

1. Sonoda M, Takano M, Miyahara J, Kato H. Computed radiography utilizing scanning laser stimulated luminescence. *Radiology* **1983**;148:833–838
2. Goodman LR, Foley WD, Wilson CR, Tikovsky RS, Hoffman RG. Pneumothorax and other lung diseases: effect of altered resolution and edge enhancement on diagnosis with digitized radiographs. *Radiology* **1988**;167:83–88
3. Farjado LL, Hillman BJ, Pond GD, Carmody RF, Johnson JE, Ferrell WR. Detection of pneumothorax: comparison of digital and conventional chest imaging. *AJR* **1989**;152:475–480
4. Oestmann JW, Greene RE, Rubens J, et al. High frequency edge-enhancement in the detection of fine pulmonary lines: parity between storage phosphor digital images and conventional chest images. *Invest Radiol* **1989**;24:643–646
5. Seeley GW, Fisher HD, Stempski MO, Borgstrom M, Bjelland J, Capp MP. Total digital radiology department: spatial resolution requirements. *AJR* **1987**;148:421–426
6. MacMahon H, Vyborny CJ, Metz CE, Doi K, Sabeti V, Solomon SL. Digital radiography of subtle pulmonary abnormalities: an ROC study of the effect of pixel size on the observer performance. *Radiology* **1986**;158:21–26
7. Schaefer CM, Greene RE, Oestmann JW, et al. Digital storage phosphor imaging versus conventional film radiography in CT-documented chest disease. *Radiology* **1990**;174:207–210
8. Schaefer CM, Greene RE, Llewellyn HJ, et al. Digital storage phosphor imaging of interstitial lung disease: impact of postprocessing. *Radiology* (in press)
9. Oestmann JW, Greene R, Rhea J, et al. "Single-exposure" dual energy digital radiography in the detection of pulmonary nodules and calcifications. *Invest Radiol* **1989**;24:517–521
10. Berbaum KS, Dorfman DD, Franken EA. Measuring observer performance by ROC analysis: indications and complications. *Invest Radiol* **1989**;24:1–9
11. Metz CE. Basic principles of ROC analysis. *Semin Nucl Med* **1978**;8:283–298
12. Dorfman DD, Alf E. Maximum likelihood estimation of parameters of signal detection theory and determination of confidence intervals: rating-method data. *J Math Psychol* **1969**;6:487–496
13. Swets JA, Pickett RM. Evaluation of diagnostic systems: methods from signal detection theory. New York: Academic Press, **1982**
14. Armitage P, Berry G. *Statistical methods in medical research*, 2nd ed. Oxford: Blackwell Scientific, **1987**
15. Hill AB. *Principles of medical statistics*, 9th ed. New York: Oxford University Press, **1971**
16. Metz CE. Statistical analysis of ROC data in evaluating diagnostic performance. In: Herbert D, Myers R, eds. *Multiple regression analysis: applications in the health sciences*. New York: American Institute of Physics, **1986**:365–384
17. Metz CE, Wang PL, Kronman HB. A new approach for testing the significance of differences between ROC curves measured from correlated data. In: Deconinck F, ed. *Information processing in medical imaging*. The Hague: Nijoff, **1984**:432–445
18. Metz CE. ROC methodology in radiologic imaging. *Invest Radiol* **1986**;21:720–733
19. Oestmann JW, Kushner DC, Bourgouin PM, Llewellyn HJ, Mockbee BW, Greene R. Subtle lung cancers: impact of edge-enhancement and gray scale reversal on detection with digitized chest radiographs. *Radiology* **1988**;167:657–658
20. MacMahon H, Metz CE, Doi K, Kim T, Giger ML, Chan HP. Digital chest radiography: effect on diagnostic accuracy of hard copy conventional video, and reversed gray scale video display formats. *Radiology* **1988**;168:669–673

Technical Note

# Percutaneous Removal of Transvenous Pacing Lead Perforating the Heart, Pericardium, and Pleura

Larry-Stuart Deutsch,[1] Hong Dang,[2] Jeffrey C. Brandon,[1] Richard Ott,[3] Byron Allen,[4] and Cheryl Futerman[1]

Removal of nonfunctioning cardiac pacemaker leads is sometimes difficult because of fibrous fixation [1, 2], and most cases are treated by simply placing a new lead adjacent to the retained nonfunctioning lead. Detachment of the retained lead with subsequent migration [1, 2] and right atrial [3] or right ventricular [4] perforation is relatively uncommon, but it does occur, and all of these cases have been treated by conventional open surgical techniques. This report describes successful percutaneous treatment of a unique case of a fractured, migrating pacemaker lead that caused right atrial perforation and the previously unreported complication of pericardial and pleural perforation accompanied by pneumothorax.

## Case Report

The patient, a 36-year-old interventional radiologist, had successful implantation of a permanent pacemaker in July 1988 for sick sinus syndrome (Pacesetter Inc., Silmar, CA; Generator Model 251-6 and Pacing Lead Model 1015M). A chest radiograph obtained 16 months later to investigate a suspected pacemaker malfunction showed a fractured electrode lead at the left subclavian insertion site. Accordingly, a new right ventricular endocardial pacing lead was implanted; the old lead was left in situ after being sutured in place at the venous entry site. Approximately 5 months later, the patient complained of mild episodic chest pain. A chest radiograph at that time showed migration of the fractured end of the original pacemaker lead, which now was looped in the right atrium with part of the loop traversing the orifice of the tricuspid valve. The distal tip of the lead had not changed position and remained fixed at the right ventricular apex. Four days later, while in the process of deciding among various treatment options, the patient experienced the sudden onset of severe right-sided chest pain. A chest radiograph showed that the fractured tip of the pacing lead had migrated farther and had perforated not only the right atrial wall but also the pericardium and pleura by approximately 1 cm (Fig. 1), resulting in a small pneumothorax. Echocardiography showed only a minimal amount of pericardial fluid.

After a discussion of the surgical and nonsurgical alternatives, the patient opted for an attempt at percutaneous removal with ready-to-go surgical backup. Accordingly, he was transferred to the operating room, where he was prepared and draped in the usual manner for cardiac surgery. The cardiac surgery team was scrubbed, the anesthesiologist in attendance, the bypass pump primed, and the cardiac instrument set opened and ready for use. Under fluoroscopic guidance, a 9-French vascular access sheath was placed percutaneously into the right internal jugular vein and the right atrium was catheterized by using an 8-French multipurpose (MPA) catheter (Cook Inc., Bloomington, IN) introduced over a soft-tip Benson guidewire. A Cook Inc. 0.038-in. (0.965 mm) alligator jaw retrieval guidewire was placed through the MPA catheter, and the segment of the pacemaker lead protruding through the atrial wall was grasped and easily freed from the atrial wall. Multiple unsuccessful attempts were made then to grasp the distal right ventricular end of the pacemaker lead by using this retrieval set and by using a standard right ventricular cardiac bioptome. The free end of the lead was grasped successfully with a loop snare fashioned from a reversed 0.018-in. (0.457 mm) guidewire

Received August 6, 1990; accepted after revision September 12, 1990.
[1] Cardiac/Vascular/Interventional Radiology Section, University of California Irvine Medical Center, 101 City Dr., Orange, CA 92668. Address reprint requests to L.-S. Deutsch.
[2] University of Southern California Medical School, USC-LA County Hospital, 1200 N. State St., Los Angeles, CA 90033.
[3] Cardiothoracic Surgery Section, University of California Irvine Medical Center, 101 City Dr., Orange, CA 92668.
[4] Cardiology Division, University of California Irvine Medical Center, 101 City Dr., Orange, CA 92668.

*AJR* 156:471–473, March 1991 0361–803X/91/1563–0471 © American Roentgen Ray Society

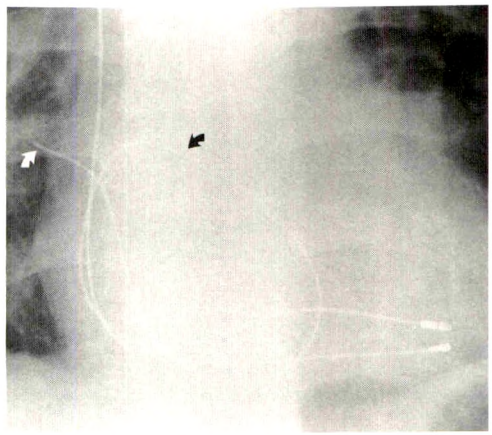


**Fig. 1.—Posteroanterior chest radiograph shows proximal segment of fractured pacing lead coiled in right atrium (*black arrow*) with its right ventricular electrode tip situated caudad to replacement electrode tip. Proximal end of fractured lead extends through right atrial free wall into pleural space (*white arrow*), and leftmost segment of its loop projects through tricuspid valve into right ventricle.**

and an 8-French MPA catheter and was removed through the 9-French vascular access sheath. Moderate traction for approximately 90 sec dislodged the distal tip from the right ventricle, enabling the entire pacer lead to be pulled out intact.

The patient was carefully monitored during the entire procedure, which took approximately 35 min. He showed no significant change in vital signs during the procedure or during an ensuing 30 min on the operating table. Arrhythmias that occurred were of short duration and easily treated by simply repositioning the retrieval instruments. Indeed, traction on the pacing lead sufficient to invaginate the right ventricular apex to a level close to the plane of the tricuspid valve did not result in significant ECG or hemodynamic changes. Echocardiography performed shortly after the procedure and again 12 hr later showed no significant accumulation of fluid within the pericardium. A chest radiograph obtained 12 hr later did, however, show an increase in the size of the pneumothorax sufficient to require drainage via a small-caliber chest tube for 24 hr. The patient was discharged the following day without incident and returned to work 2 days later.

## Discussion

Although atrial perforation by cardiac pacing electrodes does not occur as often as ventricular perforation does, cases of right atrial perforation have been reported [3, 4]. Because the wall of the right atrium, unlike that of the right ventricle, is relatively thin and nonmuscular, it generally is assumed that nonsurgical withdrawal of a lead from a perforation site in the atrium would be far more likely to result in significant and uncontrollable bleeding than in the case of a ventricular perforation. Accordingly, such cases are treated by open surgical removal of the lead and suture repair of the perforation site, which often can be performed without the need for cardiopulmonary bypass [3, 4]. The situation is analogous to the problem of cardiac perforation during right-sided catheterization of the heart with preformed 7- to 9-French catheters (e.g., Cournand, NIH, Lehman) before the general acceptance of the soft flow-directed Swan-Ganz type catheters. Withdrawal of the catheter from a perforation of the right ventricle rarely resulted in significant clinical sequelae. However, withdrawal of such catheters from right atrial perforations often was associated with significant and potentially life-threatening bleeding. For that reason, the standard practice in such cases has been to leave the catheter in place across the atrial wall and perform urgent open surgical repair.

The shaft of a cardiac pacing electrode is constructed of a 3-French radiopaque braided wire lead sheathed in a 7-French nonradiopaque plastic insulating sleeve. As it was impossible to determine on the radiograph whether the perforating segment of the catheter was sheathed or bare, the analogy between perforation of the right atrium by a catheter or a pacing electrode was unclear in this case, and the real risk of significant bleeding therefore difficult to assess. Although it seemed likely that the perforating segment consisted of only a small-caliber unsheathed wire braid, we elected to minimize the risks by performing the procedure with "ready-to-go" cardiac surgery standby, thereby greatly increasing the monetary cost while minimizing the physiologic cost.

The Cook 0.038-in. (0.965 mm) alligator jaw retrieval guide was chosen for the initial retraction of the proximal tip because of its sidebiting grasping capability. The absence of a free end in this patient prevented the use of either a loop snare or helical basket. Withdrawal of the segment that had perforated the atrial wall was accomplished first to prolong the amount of time between "unsealing" the perforation and concluding intensive monitoring to detect delayed bleeding problems that might require urgent surgical intervention. Once the proximal tip was freed, the removal of the distal tip from the right ventricular apex by traction on the exteriorized free end proved straightforward. Although complications of forceful and prolonged traction on right ventricular pacing leads have been reported, including refractory arrhythmias with shock after invagination of the right ventricular wall [5], ventricular tachycardia [6], lead fracture and ventricular rupture [7], successful removal of a chronically implanted transvenous lead by traction also has been reported [5–8]. Although interventional radiologists generally prefer femoral approach techniques, we opted for a right internal jugular approach because it provided a relatively straight-line force vector unlikely to compromise the tricuspid valve.

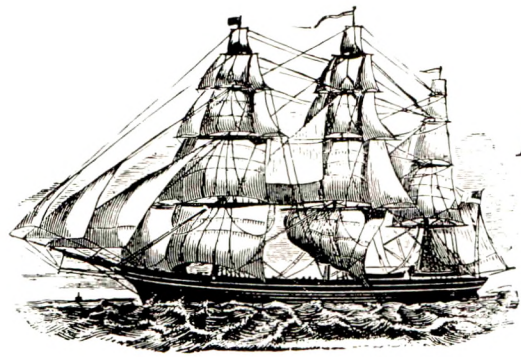
In this particular case, the choice of therapy as well as the discussion of risks and alternatives was certainly influenced by the fact that the patient was himself an experienced interventional radiologist with a strong desire to avoid thoracotomy. He was able to understand the risks and uncertainties of percutaneous treatment far better than most patients and thus able to give truly informed consent.

Complications of cardiac pacemaker implantation, including lead fracture, lead migration, and perforation of the cardiac chamber, are uncommon but well documented, although the progressive perforation of the pericardium and pleura seen in our case have not been reported before. However, the current practice of leaving functionless noninfected electrodes in situ [1, 2] suggests that this complication may be seen again. On the basis of this case, we think it is likely that such a complication can be treated percutaneously, but until more cases are reported, we think it would be premature to do so without a high level of surgical backup.

REFERENCES


1. Rettig G, Doenecke P, Sen S, Volkmer I, Bette L. Complications with retained transvenous pacemaker electrodes. *Am Heart J* **1979**;98: 587–594
2. Zerbe F, Ponizynski A, Dyszkiewicz W, Ziemianski A, Dziegielewski T, Krug H. Functionless retained pacing leads in the cardiovascular system: complication of pacemaker treatment. *Br Heart J* **1985**;54:76–79
3. Pappas G, Shoultz CA, Blount SG. Fractured intracardiac transvenous pacemaker catheter. *Am Heart J* **1969**;78:807–810
4. Irwin JM, Greer GS, Lowe JE, German LD, Gilbert MR. Atrial lead perforation: case report. *PACE* **1987**;10:1378–1381
5. Imparato AM, Kim GE. The trapped endocardial electrode: removal by prolonged graded skin traction. *Ann Thorac Surg* **1972**;4:605–608
6. Bilgutay AM, Jensen NK, Schmidt WR, Garamella JJ, Lynch MF. Incarceration of transvenous pacemaker electrode: removal by traction. *Am Heart J* **1969**;77:377–379
7. Furman S. Removal of myocardial fragment containing a pacemaker electrode. *Ann Thorac Surg* **1975**;19:716–718
8. Wallace HW, Sherafat M, Blakemore WS. The stubborn pacemaker catheter. *Surgery* **1970**;68:914–915





Scientific Program (200 papers)
Instructional Courses (60 hours)
Categorical Course on
Body MR Imaging
The Caldwell Lecture
Award Papers
Scientific Exhibits
Social, Golf, and Tennis Programs
Guest Programs



Come to the
American Roentgen
Ray Society
91st
ANNUAL MEETING
Boston, MA
Sheraton Boston Hotel
May 5-10, 1991

## Radiologic-Pathologic Conferences of the Massachusetts General Hospital

# Candidal Splenic Abscesses

Felix S. Chew,[1] Peter L. Smith, Daniel Barboriak

A 56-year-old man receiving chemotherapy for acute myelogenous leukemia presented with persistent fevers. Sonography and CT of the abdomen showed multiple round focal lesions in the spleen, some with central areas of increased echogenicity or high attenuation (Fig. 1). A single lesion was found in the liver. Chest radiographs showed multifocal patchy opacities, some with cavitation. The differential diagnosis included pyogenic or fungal abscesses, leukemic infiltrates, and metastatic tumor. The patient underwent exploratory laparotomy and splenectomy. The spleen was enlarged (480 g) and contained multiple small round abscesses. Microscopy showed unicellular yeast and branching hyphae. The final pathologic diagnosis was disseminated candidiasis with candidal splenic abscesses.

Candidal and other fungal splenic abscesses consist of pus, necrotic tissue, and fungus surrounded by layers of histiocytes, chronic inflammatory cells, and fibrosis [1–2]. On sonograms, one may see a "wheel-within-a-wheel" appearance with a peripheral hypoechoic zone (fibrosis), an enclosed hyperechoic zone (inflammatory cells), and a hyperechoic center (pus, necrotic debris, and fungal elements) [1]; one may also see hypoechoic lesions with a hyperechoic center (fibrosis surrounding inflammatory cells without central necrosis). With healing, lesions become uniformly hyperechoic (fibrosis without central inflammatory mass) and eventually small and hyperechoic (scar, often calcified). On CT scans, the abscesses are well-defined, nonenhancing lesions of relatively low attenuation, occasionally with a central focus of higher attenuation. Typical lesions are smaller than 2 cm. Splenomegaly is common. Involvement of liver, spleen, or both may be demonstrated, but fungal abscesses in neutropenic patients are not always detectable, even in the presence of disseminated infection. The lesions become apparent with the return of neutrophil function [2].

Fungal splenic abscesses occur almost exclusively in immunosuppressed patients receiving multidrug chemotherapy [3]. The diagnosis has become much more common in recent years as the population at risk has increased in size and as more sensitive imaging techniques have been applied [3]. The presentation is nonspecific: persistent fevers, malaise, and weight loss. The most frequent pathogens are *Candida*, *Aspergillus*, and *Cryptococcus*. A histologic diagnosis is often necessary because blood and tissue cultures may be falsely negative, particularly with candidal infections [2–3]. The treatment is usually splenectomy; antifungal therapy with close radiologic follow-up may be sufficient in some cases [2]. Without prompt treatment the infection is often fatal.

REFERENCES

1. Pastakia B, Shawker TH, Thaler M, O'Leary T, Pisso PA. Hepatosplenic candidiasis: wheels within wheels. *Radiology* **1988**;166:417–421
2. von Eiff M, Essink M, Roos N, Hiddemann W, Buchner T, van de Loo J. Hepatosplenic candidiasis, a late manifestation of *Candida septicaemia* in neutropenic patients with haematologic malignancies. *Blut* **1990**;60:242–248
3. Nelken N, Ignatius J, Skinner M, Christensen N. Changing clinical spectrum of splenic abscess: a multicenter study and review of the literature. *Am J Surg* **1987**;154:27–34

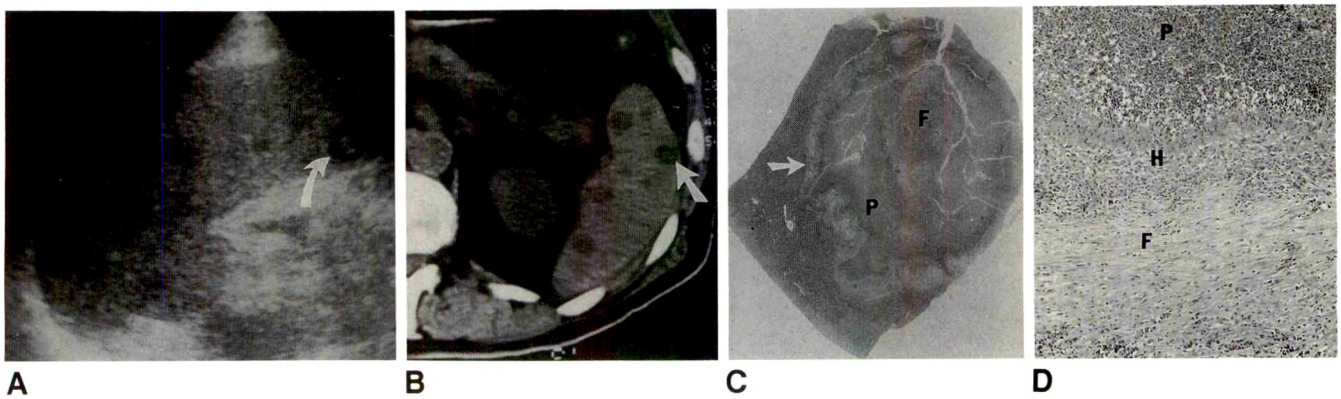



**Fig. 1.—*A*, Sonogram shows hypoechoic splenic lesions, one with a "wheel-within-a-wheel" appearance (*arrow*).**
***B*, Unenhanced CT scan shows multiple low-attenuation round splenic lesions, some with central high attenuation (*arrow*).**
***C*, Low-power (× 2.5) micrograph of abscess shows serpiginous fibrotic layer (*arrow*) surrounding pus (P) and fungus ball (F).**
***D*, Higher-power (× 125) micrograph of abscess wall shows normal spleen at bottom and layers of fibrosis (F), chronic inflammatory cells, and histiocytes (H). Pus (P) is at top.**

**From the weekly radiologic-pathologic correlation conference conducted by Jack Wittenberg. Pathology editor: Andrew E. Rosenberg. Radiology editors: Felix S. Chew, William E. Palmer, Daniel I. Rosenthal.**

[1] All authors: Department of Radiology, Massachusetts General Hospital and Harvard Medical School, 32 Fruit St., Boston, MA 02114. Address reprint requests to F. S. Chew.

Commentary

# Mammography and Malpractice

E. James Potchen,[1] Mark A. Bisesi,[1] Arlene E. Sierra,[1] and Joseph E. Potchen[2]

Despite intensive investigation into diagnosis and treatment, mortality from breast cancer has decreased relatively little since the 1940s [1]. Today, breast cancer will develop in approximately one in 10 women. Nearly one third of these women ultimately will die of their disease [2]. Screening mammography is an effective way to reduce mortality from breast cancer [3–5]. As a result of the ability to improve survival, the medical and legal professions are paying greater attention to issues of malpractice in the care of patients with breast cancer.

This paper seeks to clarify some important concerns of radiologists regarding mammography and malpractice. We begin with an example of a malpractice case and then address the elements of malpractice as they pertain to the diagnosis and management of breast cancer. The radiologist's responsibilities in the evaluation of symptomatic and asymptomatic women also are discussed. Finally, we derive some conclusions based on these observations.

## An Example

*Borgren v. United States* is an example of a case in which a plaintiff was awarded damages for a radiologist's failure to diagnose breast cancer [6]. In 1980, a 52-year-old multiparous woman was referred for screening mammography by an Army physician. Her initial mammogram revealed a "slight asymmetry" but was otherwise unremarkable. The radiologist recommended a second examination in 6 months. The patient did not return for the follow-up examination.

Three years later, an area of induration in the left upper breast was noted on physical examination. Mammography revealed a "benign calcification" in the left breast, but no other abnormalities were noted. Two years later, in 1985, another mammogram was reportedly unchanged. In 1986, the patient discovered a lump in her left breast. A mammogram reportedly showed an area of architectural distortion in the left upper quadrant that retrospectively was visible on the mammograms obtained in 1983 and 1985. A modified radical mastectomy was performed that revealed a stage II infiltrating ductal and lobular carcinoma with 16 of 26 axillary lymph nodes positive for tumor.

At issue in this case was whether the interpretation of the mammograms obtained in 1983 and 1985 constituted malpractice. The mere fact that a lesion is retrospectively visible does not mean that negligence has occurred. However, the defense admitted that the 1985 interpretation was negligent, and an expert witness convinced the court that the 1983 interpretation was negligent as well.

On the basis of the assumption that the doubling time of an average tumor was between 80 and 210 days, the court determined that the number of cancerous lymph nodes increased significantly between 1983 and 1986. As nodal status is the main prognostic indicator of disease-free survival, the court also determined that the 3-year delay in diagnosis led to a diminished chance of effective treatment and a decreased chance of survival. The plaintiff ultimately was awarded $1 million in damages, which was reduced 10% for failure to obtain an initial follow-up mammogram as instructed.

Received August 20, 1990; accepted after revision October 1, 1990.
[1] Department of Radiology, Michigan State University, B 220 Clinical Center, 138 Service Rd., East Lansing, MI 48824. Address reprint requests to E. J. Potchen.
[2] Nisen and Elliott, Ste. 2500, 200 W. Adams St., Chicago, IL 60606.

*AJR* 156:475–480, March 1991 0361–803X/91/1563–0475 © American Roentgen Ray Society

### The Elements of Malpractice

Although decisions about malpractice often seem capricious to physicians, in reality clearly defined criteria must be met for a plaintiff's malpractice action to be successful. Malpractice, a claim in tort law, is based on the concept of negligence of a practicing professional person. There must be a *breach* of the *standard of care* that is the *proximate cause* of *substantial injury*.

A physician who provides care for a patient accepts a duty to adhere to a standard of care expected of a reasonably prudent and responsible physician practicing under the same, or similar, conditions. Physicians who fail to practice to this standard are said to have breached this duty. The court relies on expert testimony to determine what the standard of care should be. No single standard applies to every case. Rather, the standard is determined for each case on the basis of the testimony of experts. As discussed elsewhere [7], expert radiologists may volunteer their services or, occasionally, are approached by attorneys. It has been said that the determination of the standard ultimately depends on a contest of experts. Once a breach of duty has been established, the plaintiff also must show that it was the proximate cause of substantial injury to the patient. If a breach of duty does not harm a patient or is not the cause of substantial injury, malpractice has not occurred.

In the past, the standard of care for physicians in most jurisdictions was based on the "reasonable skill" that a physician in good practice would ordinarily exhibit in a similar case in the same locality [8]. Under this "locality rule," a defendant physician was bound to exercise "such care and diligence as a good practitioner practicing in a same or similar community or hospital" [9]. The locality rule arose at a time when a significant difference existed between the opportunities for continued medical education available to a rural physician and those available to an urban one.

Recently, the uniform standards of medical schools and increasing opportunities for postgraduate education have led the courts to adopt a national standard of care. The national standard incorporates the rule that a physician is under a duty to use that degree of care and skill that is expected of a reasonably competent practitioner of the same specialty, acting in the same or similar circumstances. In *Darling v. Charleston Community Memorial Hospital* [10], regarding the weight to be given to evidence concerning the community standard of care for hospitals, the court stated:

> Custom is relevant in determining the standard of care because it illustrates what is feasible, it suggests a body of knowledge of which the defendant should be aware, and it warns of the possibility of far-reaching consequences if a higher standard is required. . . . But custom should never be conclusive. . . . Courts must in the end say what is required; there are precautions so imperative that even their universal disregard will not excuse their omission.

Although evidence that a defendant's conduct conformed to local usage may reflect due care, it is not conclusive. It may be overcome by contrary expert testimony that the prevailing custom or usage itself constitutes negligence [11].

This issue is especially important in the diagnosis of breast cancer because national standards are established by various organizations, such as the American College of Radiology (ACR). The legal implications of a failure to obtain ACR accreditation remain to be established. However, we think that the standards established by the process of ACR accreditation may be accepted by a court as an expectation of a reasonably prudent and responsible radiologist.

Similarly, radiologists and referring physicians who fail to abide by the recommendations of their national organizations in the use of screening mammography may be found to have breached a standard of care. Physicians who disagree with these national recommendations should be prepared to defend their position with well-reasoned arguments. The authors have had personal experience with cases in which a primary physician's failure to recommend appropriate screening mammography has been the basis of successful malpractice litigation.

In addition to failure to adhere to screening recommendations, three major aspects of the diagnosis of breast cancer may be the basis for malpractice litigation. They are the failure to diagnose, the false-positive overcall, and the failure to communicate. Missed diagnoses have always provided the basis for the majority of malpractice claims against radiologists [12, 13]. Although missed fractures were the most common cause of litigation in the past, a recent analysis has shown that failure to diagnose malignancy, particularly lung cancer and colonic cancer, has become the major basis for malpractice suits [14].

In relation to breast cancer, the most successful malpractice cases are due to a failure to diagnose. These usually are directed against physicians who fail to obtain a surgical consultation when a patient has a palpable mass [15, 16]. Less attention has been paid to overcall. However, any surgical procedure can lead to complications, and a radiologist conceivably could be found liable if a positive mammographic interpretation subsequently is found to be unwarranted. Finally, radiologists may be sued for failure to adequately communicate information to primary care clinicians, especially when it leads to delayed treatment.

### The Failure to Diagnose

A failure to diagnose may be due to one of two types of interpretive errors, a "miss" or an error in judgment [17]. A miss occurs when an abnormal finding is not detected. An error in judgment occurs when an abnormality is observed but is interpreted incorrectly. Either type of error can be the basis for malpractice litigation. Unfortunately, it is difficult to sort out simple errors from a negligent breach in the standard of care.

No diagnostic test is completely accurate. All tests have limitations. The mere fact that a mammographic lesion is visible retrospectively does not mean that malpractice has occurred. The nature and magnitude of the missed abnormality are important considerations in determining negligence.

In our opinion, masses, clusters of calcifications, asymmetry, and architectural distortions should not go unobserved. However, the court should be made aware that calcifications are more difficult to see in young women who have dense breasts.

Unfortunately, no large-scale clinical studies have been performed to provide an estimate of how many breast cancers are visible retrospectively when the diagnosis of cancer ultimately is established. This information is available for chest radiographs from lung cancer screening studies [7], but these data are not directly applicable to the problems of breast cancer screening. With lung cancer, we know that 90% of peripheral lesions can be found on radiographs obtained from 4 to 53 months before the examination in which the tumor finally was found [18]. Similarly, some breast cancers undoubtedly will be evident in retrospect, even when the initial examination was interpreted to an optimal standard of care. Simply, some opacities may initially be considered normal even in the best hands only to turn out on subsequent studies to be due to malignancy. Every effort is made to minimize that number. However, the technique of mammography is by its nature imperfect. These imperfections should not be the basis for malpractice litigation. Indeed, by insisting that the radiologist find every breast cancer on the mammogram, society may place a burden on the radiologist whose only defense would be to increase the number of false-positive diagnoses in an effort to avoid missing anything that eventually could turn up as a malignant tumor on a subsequent examination. This may lead to a tremendous number of false-positive diagnoses, which would induce "dis-ease" in patients and become an overwhelming economic burden for society.

An effective quality control system is the best defense against a claim of failure to diagnose breast cancer when a lesion is found in retrospect. Quality control measures to accredit mammography systems are being adopted in many states. In addition to periodic testing of mammographic equipment and frequent evaluation of mammographic technologists, we recommend that radiologists audit their own performance annually. If radiologists can establish that their standards of practice are consistent with what is known to be the best possible practice of physicians faced with similar judgments, then the radiologists' practice in a specific case can be defended better.

Spring and Kimbrell-Wilmot [19] have outlined the essential features of a mammographic audit. As they point out, the starting point is to determine the population under consideration. For mammography, it is essential to know the age of the patient and whether the examination was performed for screening or symptomatic purposes. In addition, an effective way to determine follow-up, such as surgical or pathologic reports, must be established. Sickles et al. [20] recently published an audit of the University of California San Francisco (UCSF) Mobile Mammography Screening Program that can be a model for radiologists. Their study provides an excellent example of the amount of information that can be obtained when the appropriate feedback mechanisms are in place.

An information system must be monitored to provide accurate, up-to-date awareness of individual false-negative and false-positive rates. If a radiologist's interpretive process results in excessive false-positive or false-negative observations, the criteria for recommending surgical consultation can be adjusted. Under ideal circumstances, receiver-operating-characteristic (ROC) curves should be generated annually for each radiologist [21]. Unfortunately, it is virtually impossible to acquire all of the information necessary to determine sensitivity because the number of false-negative interpretations is difficult to assess. A local cancer registry can be helpful, but in practical terms some estimate must be made of the number of false-negative diagnoses.

Sickles et al. [20] estimated the number of false-negatives on the basis of biopsy records of UCSF. They considered an interpretation false-negative when a biopsy showed the presence of a tumor after a mammogram was normal. They estimate that half of their screening patients are referred by UCSF physicians, so doubling the number of identifiable false-negative diagnoses provides a rough estimate of the overall rate. This method can be adopted by other radiologists if pathology records are available and referral patterns are known.

Although determination of sensitivity and specificity is optimal, practicing radiologists can assess their performance more easily by determining positive predictive value. Although the use of positive predictive value has theoretical and practical limitations, it is the easiest statistic to generate because it requires only abnormal interpretations to be followed up. In general, radiologists will recommend six to eight biopsies per cancer detected. In other words, of every 100 interpretations when surgical consultation is recommended, 13 to 17 patients actually will have breast cancer. Radiologists who recommend fewer than three biopsies per cancer detected will have a positive predictive value greater than 33%. However, their false-negative rate will be very high (undercall). In contrast, radiologists who recommend more than 12 biopsies per cancer detected will have a positive predictive value of less than 8% (overcall). Although this often is thought to be a safe strategy from the standpoint of defensive medicine, it is detrimental to patients' welfare and the cost of medical care. It also may incur a liability risk for complications of surgery that later appears to be unwarranted. Most people agree that a positive predictive value between 10% and 20% is appropriate for screening mammography.

In assessing information obtained in a medical audit, it is important to recognize that the results are most valuable for serial evaluation rather than comparison with a national standard. Differences in population alone can account for some variation in sensitivity and specificity between locations. Statistics can be used for general comparison, but close comparisons to hold local results to specific published studies are not necessary.

Finally, a point should be made about quality assurance programs and medical malpractice. State laws vary as to how information in the medical audit can be used [22]. In some states, such as California, this information cannot be used in court if it is obtained as part of a formal quality assurance program. In other states, where no specific laws have been passed, the discoverability of quality assurance information is determined by the judge in each case. However, as Southwick and Slee [23] have pointed out with respect to peer review committees, the legal risks of inaction are much greater than

the legal risks of a medical audit. Assessment of performance shows the court that a radiologist is committed to achieving optimal practice standards. In addition, continued emphasis on the acquisition of this information for accreditation purposes is likely. When a radiologist is sued for failure to identify a cancer, the best recourse is to have clearly established quality control measures in place. These may include annual assessment of performance and accreditation of technologists and equipment. Any specific case can be reduced to the question of whether the radiologist's performance represents the best possible practice of diagnostic radiology. It also is necessary to be aware that diagnostic decisions require a trade-off between the problem of excessive false-negative judgments (undercall) and excessive false-positive diagnoses (overcall). Although individual ROC curves represent an optimal form of performance awareness, knowledge of positive predictive value is obtained more easily and should be available to the court.

In court, the most common contest of expert testimony in failure to diagnose cases is whether the lesion should have been detected or recognized when the mammogram first was interpreted. Usually the two sides of the argument are heard, and the jury must decide which expert is most convincing. All radiologists who provide testimony must be impartial and prudent in their assessment of contested radiographs and should resist the temptation to declare boastfully to the court, "I never would have missed an obvious lesion like that!"

### The False-Positive Overcall

Although most attention has been directed toward the false-negative error, false-positive errors are receiving increased legal scrutiny. When defensive radiologists become too concerned about missing a lesion, they may recommend an excessive number of surgical consultations, resulting in a large number of biopsies per cancer found [24]. Failure to diagnose breast cancer may cause obvious injury. The patient may die. False-positive error may cause more subtle injury. Excessive false-positive examinations can lead to excessive and unnecessary surgical biopsies, which have been the subject of litigation. When a women is told that her screening mammogram is suspicious for cancer and, therefore, a surgical biopsy is needed, her state of health changes.

Disease, as defined by the world health organization, is a perceived inability to cope with one's physical, psychological, or social environment. Radiologists may induce disease ("disease") by suggesting that a woman has cancer where there is none. This is a necessary component of an imperfect diagnostic test. However, when excessive, false-positive overcall may become a subject for litigation. A false-positive mammogram may lead to emotional stress, which could become incapacitating. Radiologists should recognize that overuse of recommendations to return for repeated mammographic examination ahead of the standard reexamination time (e.g., reevaluation in 4–6 months) also can cause high anxiety.

Although overcall often is motivated by a desire to avoid malpractice litigation, it actually may cause litigation if the patient becomes aware that unnecessary surgery was due to the radiologist's overcall. This is especially true if a radiologist is known to have a tendency to overread mammograms. Referring physicians often become aware of a radiologist's practice of excessive false-positive interpretations, and they may occasionally share that insight with their patients. Thus, unnecessary false-positive interpretations are as important to avoid as false-negative interpretations. Just as in the case of false-negative interpretation, the best protection against a claim of causing disease by recommending an unwarranted surgical biopsy is to know individual performance statistics.

Radiologists should be aware of the positive predictive value of their performance. Many studies proclaim the need to do biopsies of suspicious lesions at a rate of six to eight biopsies per cancer found to maximize the potential for the cure of nonpalpable breast cancer. Hall et al. [25] has shown that strict adherence to interpretation criteria can improve on that statistic. The Karolinska group in Stockholm have demonstrated a remarkable reversal of the biopsy-to-cancer ratio by using the Svane system [26, 27] of breast cancer diagnosis. This system entails the rigorous use of fine-needle aspiration for suspected nonpalpable breast cancer. The standard biopsy-to-cancer ratio may be decreased without increasing the interval cancer rate. As the accuracy of mammography interpretation improves, radiologists may well be held to new standards.

Achieving a balance between undercall, which results in an increase in interval cancers (cancers that are found between scheduled screening examinations), and overcall is the core of the diagnostic dilemma. Experts who testify on either side of this issue should be prepared to explain these facts to a judge and a jury who are charged with determining the facts of an individual case.

### The Failure to Communicate

Communication of findings is crucial to the use of radiologic information. Detection of an abnormality does a patient little good if action is not taken in a timely manner. In a recent study, Robertson and Kopans [28] found that no action was taken within 2.5 months on 63% of abnormal mammograms despite communication by a written report and a telephone call. By 4.5 months, this had decreased to 6%. This study points out that even under optimal conditions, delays in follow-up evaluation and treatment are inevitable. Under usual conditions, probably more delays occur than radiologists would like to acknowledge.

In addition to having dedicated mammographic units, trained technologists, and high standards of interpretation, radiologists must establish standard business procedures for the communication of mammographic results. Radiologists can be found negligent if their standard procedures fail to notify a clinician in a timely manner. In our opinion, radiologists should attempt to establish a standard practice of verbal communication whenever a surgical consultation is recommended. This verbal communication can be as simple as having a secretary call the referring physician or the physician's office and reading the report. A notation of this verbal communication should be included on the written report. Our

experience suggests that some courts also think that radiologists share the responsibility to remind patients when a follow-up examination is due.

Anyone who interprets a mammogram may be uncertain as to whether a significant abnormality is present. Different radiologists may have different levels of confidence in their interpretation of the film. A lack of confidence often is conveyed in the report to such a degree that no substantial communication is effected. The confusion as to what was meant by such a report also has formed the basis of malpractice litigation. In order to eliminate ambiguity, a definitive recommendation should be present in the conclusion of the report. Any uncertainty should be acknowledged clearly.

A standard hedge, which becomes the customary practice of some radiologists, will not protect them from malpractice litigation. In fact, a hedge may cause confusion about the findings and recommendations and, consequently, increase the likelihood of litigation. Although a radiologist may be uncertain about the significance of a mammographic finding, a specific recommendation for subsequent care or evaluation still should be provided.

A practice standard that establishes a limited number of customary conclusions on the report may be useful to correlate the mammographic interpretation with what ultimately happens to the patient. How can the number of biopsies recommended per cancer found be determined if it is not a standard practice to recommend surgical consultation in the mammography report? Incidentally, it is usually preferable to recommend a surgical consultation rather than a biopsy. This practice provides the surgeon with the latitude to avoid biopsy if extenuating circumstances are present that are not known by the radiologist. The use of standard conclusions enhances communication and also facilitates the medical audit.

A New Jersey case demonstrates the importance of effective communication. A radiologist identified a lung cancer on a routine preoperative radiograph of a patient admitted for minor orthopedic surgery [29]. Although the radiologist noted the lesion in the report, he did not contact the attending physician. The written report did not reach the patient's chart until after her discharge and was not noted until several months later. The plaintiff's complaint against the radiologist was dismissed initially, but later the dismissal was reversed by an appellate court. This case illustrates that radiologists increasingly are expected to take an active role in communicating abnormalities affecting patients' care.

Finally, the widespread dissemination of medical information has resulted in an increased number of women who refer themselves for screening mammography. This complicates the role of the radiologist. As Brenner [30] has indicated, "The duty to ensure follow-up examination and communication of results, which has been imposed on the primary-care clinician in the past, now may be imposed on the radiologist engaged in a self-referred mammographic practice." In our opinion, a radiologist who accepts self-referred patients should see that a breast examination is performed at the time of mammography. However, legal obligations of the radiologist to self-referred patients are in a state of flux. It is unclear to what extent the radiologist must assume responsibility for follow-up care.

## Mammography in the Symptomatic Patient

Mammography has two distinct categories, screening and symptomatic, that merit separate discussion in relation to issues of medical malpractice. A review of the legal literature reveals that the most successful malpractice cases are against physicians who fail to obtain a surgical consultation when a palpable mass is present. Mammography in a woman with a palpable mass is used to provide additional information, such as the presence of multiple lesions or fibrocystic change. Physicians must be made aware that a normal mammogram can occur in the presence of a palpable breast cancer, particularly in women with dense breasts. Edeiken [31] found that 22% of women with a palpable cancer had a normal mammogram. Thus, a persistent palpable mass requires surgical evaluation, regardless of mammographic findings. The liability in these cases falls on the physician who chooses to rely on the normal mammogram despite clinical evidence of a suspicious mass. Some radiologists have addressed this problem by establishing a standard disclaimer on their reports that a normal mammogram does not exclude cancer if the woman has a suspicious mass.

## Screening Mammography

Screening mammography is an effective way to improve breast cancer survival in asymptomatic women [3, 4]. Although some argument exists about the benefit of screening mammography for younger women, virtually all of the studies show an improved survival for women more than 50 years old [5, 32]. Thus far, screening mammography is the only effective means of improving survival for women with breast cancer. The current ACR recommendations for mammographic screening [33] include a baseline mammogram before the woman is 40 years old, annual or biennial mammograms between the ages of 40 and 49 (depending on the presence of risk factors), and annual mammograms for women 50 years or older.

Facilities performing screening mammography are coming under increasing legal scrutiny. Many states require that screening mammography centers meet accreditation requirements. In Michigan, for example, a law recently was passed that requires ACR accreditation, or its equivalent. Accreditation involves the use of approved, dedicated radiographic devices and specially trained technologists as well as competent radiologists [34]. The expectations of the radiologist's performance have been discussed. As we have indicated, malpractice cases usually center on missed diagnoses, the failure to communicate abnormal findings effectively and, increasingly, the false-positive interpretations.

The use of fine-needle biopsy may affect the standard of care of screening mammography in the future. If this technique becomes widely available, all radiologists will be expected to provide rapid assessment of suspicious mammographic findings. Under these conditions, radiologists who recommend repeated examinations or surgical consultation may be liable for causing "dis-ease" in patients who ultimately do not have breast cancer. In such instances, a plaintiff may

argue that an earlier diagnosis based on the results of fine-needle biopsy would have prevented psychological distress.

## Conclusions and Recommendations

As malpractice litigation continues to increase, physicians should be aware of the criteria that constitute medical malpractice. The increasing use of mammography for breast cancer screening accentuates the radiologist's role in reducing mortality from this disease. Most cases of malpractice against radiologists center on the failure to diagnose, false-positive diagnoses, and problems of communication. We recommend that radiologists consider adopting the following measures to diminish the risk of litigation and increase the rate of successful defense if litigation does occur: (1) Obtain ACR accreditation, or its equivalent. (2) Establish standard business practices that are designed to ensure use of proper equipment and proper performance by technologists. (3) Develop a standard set of conclusions for the mammographic report that clearly state recommendations for follow-up (e.g., routine reevaluation, reevaluation in 4–6 months, obtain surgical consultation). (4) Add a disclaimer on your reports that a normal mammogram does not exclude cancer when a palpable mass is present. (5) Audit your performance periodically, and modify your criteria for recommendation as your performance indicates. (6) Establish a reliable communication network for transmission of reports to physicians and follow-up of positive studies. This may well include a standard practice of verbal communication to the referring physician. (7) Be prepared to present your performance statistics to the court if malpractice litigation occurs.

REFERENCES


1. Silverberg E, Boring CC, Squire TS. Cancer statistics. *CA* **1990**;40:9–26
2. Spratt JS, Donegan WL, Greenberg RA. Epidemiology and etiology. In: Donegan WL, Spratt JS, eds. *Cancer of the breast*. Philadelphia: Saunders, **1988**:46–73
3. Shapiro S, Venet W, Strax P, Venet L. *Periodic screening for breast cancer*. Baltimore, MD: Johns Hopkins University Press, **1988**
4. Seidman H, Gelb SK, Silverberg E, La Verda N, Lubera JA. Survival experience in the Breast Cancer Detection Demonstration Project. *CA* **1987**;37:258–290
5. Eddy DM. Screening for breast cancer. *Ann Intern Med* **1989**;111: 389–399
6. *Borgren v. United States* 716 F. Supp 1378 (D. Kan. **1989**)
7. Potchen EJ, Bisesi MA. When is it malpractice to miss lung cancer on chest radiographs? *Radiology* **1990**;175:29–32
8. *Taber v. Riordan* 403 N.E.2d 1349 (Ill. **1980**)
9. *Borowski v. Von Solbrig* 328 N.E.2d 301 (Ill. **1975**)
10. *Darling v. Charleston Community Memorial Hospital* 211 N.E.2d 253 (Ill. **1965**)
11. *Chiero v. Chicago Osteopathic Hospital* 392 N.E.2d 203 (Ill. **1979**)
12. Berlin L. Malpractice and radiologists. *AJR* **1980**;135:587–591
13. Berlin L. Malpractice and radiologists, update 1986: an 11.5 year perspective. *AJR* **1986**;147:1291–1298
14. Hamer MM, Morlock F, Foley HT, Ros PR. Medical malpractice in diagnostic radiology: claims, compensation and patient injury. *Radiology* **1987**;164:263–266
15. *Glickich v. Spievack* 452 N.E.2d 287 (Mass. **1983**)
16. *DeBurkarte v. Louvar* 393 N.W.2d 131 (Iowa **1986**)
17. Berlin L, Does the "missed" radiographic diagnosis constitute malpractice? *Radiology* **1977**;123:523–527
18. Muhm JR, Miller WE, Fontana RS, Sanderson DR, Uhlenhopp MA. Lung cancer detected during a screening program using four-month chest radiographs. *Radiology* **1983**;148:609–615
19. Spring DB, Kimbrell-Wilmot K. Evaluating the success of mammography at the local level: how to conduct an audit of your practice. *Radiol Clin North Am* **1987**;25:983–992
20. Sickles EA, Ominksy SH, Sullilto RA, Galvin HB, Monticciolo DL. Medical audit of a rapid-throughput mammography screening practice: methodology and results of 27,114 examinations. *Radiology* **1990**;175:323–327
21. Swets JA, Pickett RM. *Evaluation of diagnostic systems: methods from signal detection theory*. New York: Academic Press, **1982**
22. Woodruff WA. The confidentiality of medical quality assurance records. *Army Lawyer* May **1987**:5–12
23. Southwick AF, Slee DA. Quality assurance in health care: confidentiality of information and immunity for participants. *J Leg Med* **1984**;5:343–397
24. *Francisco v Parchment Medical Clinic* 232 N.W.2d 736 (Mich. App. **1978**)
25. Hall FM, Storella JM, Silverstone DZ, Wyshak G. Nonpalpable breast lesions; recommendations for biopsy based on suspicion of carcinoma at mammography. *Radiology* **1988**;167:353–358
26. Svane G. Sterotaxic needle biopsy of non-palpable breast lesions: a clinical and radiologic follow up. *Acta Radiol* **1983**;24:385–390
27. Azaveado E, Svane G, Auer G. Stereotaxic fine-needle biopsy in 2594 mammographically detected non-palpable lesions. *Lancet* **1989**;1:1033–1066
28. Robertson CL, Kopans DB. Communication problems after mammographic screening. *Radiology* **1989**;172:443–444
29. *Jenoff v. Gleason* 521 A.2d 1323 (NJ Super. Ct. App. Div. **1987**).
30. Brenner RJ. Medicolegal aspects of screening mammography. *AJR* **1989**;153:53–56
31. Edeiken S. Mammography and palpable cancer of the breast. *Cancer* **1988**;61:263–265
32. Eddy DM, Hasselblad V, McGivney W. The value of mammography screening in women under age 50 years. *JAMA* **1988**;259:1512–1519
33. American College of Radiology. *Policy statement breast cancer screening center*. Reston, VA: American College of Radiology, **1985**
34. Michigan Department of Public Health. *Breast cancer screening and detection in Michigan: recommendations to reduce mortality*. Lansing: Michigan Department of Public Health, February **1990**

Pictorial Essay

# Extracolonic Manifestations of the Familial Adenomatous Polyposis Syndromes

R. K. Harned,[1] J. L. Buck,[2] W. W. Olmsted,[3] R. P. Moser,[2, 4] and P. R. Ros[5]

**The classic prototypes of the gastrointestinal polyposis syndromes are familial polyposis coli and Gardner syndrome. Extracolonic manifestations have been described in both diseases, and the distinction between them has become less clear. In fact, some authorities have suggested that familial polyposis coli and Gardner syndrome may represent a spectrum of the same disease. In both conditions, extracolonic expressions are the rule rather than the exception, and familiarity with them is essential for accurate diagnosis and correct patient management. In this pictorial essay, we discuss familial polyposis coli and Gardner syndrome together under the heading familial adenomatous polyposis syndromes. The colonic characteristics of these syndromes will be reviewed briefly, followed by examples of the most common extracolonic manifestations.**

## Colonic Manifestations

The familial adenomatous polyposis syndromes are inherited diseases (autosomal dominant) with a high degree of penetrance. Approximately two thirds of all cases are inherited, with one third occurring spontaneously. Polyps of the colon usually arise in the first or second decade, and generally 100 or more polyps should be identified to establish the diagnosis (Fig. 1). Histologically, the polyps are tubular or tubulovillous adenomas. Colonic cancer develops in almost 100% of untreated patients (Fig. 2). Total colectomy with rectal mucosectomy and construction of an ileoanal pouch is the currently accepted therapy.

## Gastric Involvement

Studies from Japan and the United States indicate that gastric polyps are present in approximately 20–60% of patients with familial adenomatous polyposis syndromes [1, 2]. The fundic gland polyp (or hamartoma) is most common, particularly in Western populations, and differs histologically from the hyperplastic polyp [1, 2]. Fundic gland polyps are multiple, small, and involve the gastric fundus and body, sparing the antrum (Fig. 3). There is no potential for malignancy. Fundic gland polyps may occur also in patients without polyposis. They have the same distribution, but tend to occur in middle-aged women. Gastric adenomas can also occur and appear to be more prevalent in the Japanese population [1]. These polyps are slightly larger than the hamartomas, may be solitary or multiple, and preferentially involve the antrum. They are premalignant, and a few cases of gastric adenocarcinoma have been reported [1]. In some patients, adenomas and fundic gland polyps may coexist. In general, gastric polyps in patients with familial adenomatous polyposis syndromes should be followed closely, but prophylactic gastrectomy is not recommended.

Received June 19, 1990; accepted after revision September 12, 1990.

The opinions or assertions contained herein are the private views of the authors and are not to be construed as official or as reflecting the views of the Department of the Navy, Army, or Defense.

Presented at the annual meeting of the American Roentgen Ray Society, San Francisco, May 1988.

[1] Department of Radiology, University of Nebraska Medical Center, 600 S. 42nd St., Omaha, NE 68198-1045. Address reprint requests to R. K. Harned.
[2] Department of Radiologic Pathology, Armed Forces Institute of Pathology, Washington, DC 20306-6000.
[3] Department of Radiology, George Washington University, 901 23rd St., N.W., Washington, DC 20037.
[4] Present address: Department of Radiology, Pennsylvania State University, The Milton S. Hershey Medical Center, Hershey, PA 17033.
[5] Department of Radiology, University of Florida College of Medicine, Box J-374, JHMC, Gainesville, FL 32610.

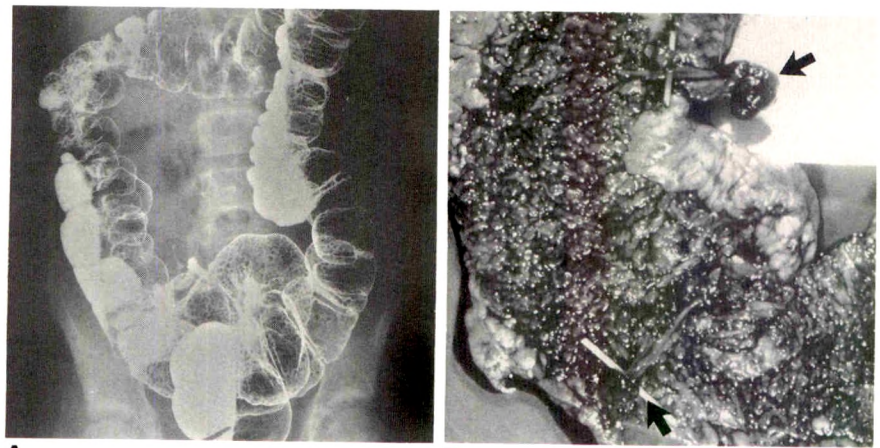


Fig. 1.—Colonic manifestations of familial adenomatous polyposis syndromes (familial polyposis coli and Gardner syndrome).

*A*, Double-contrast colonic examination shows diffuse distribution of multiple small sessile polyps.

*B*, Accompanying gross specimen with sessile adenomas carpeting colon and two larger pedunculated adenomas (*arrows*).

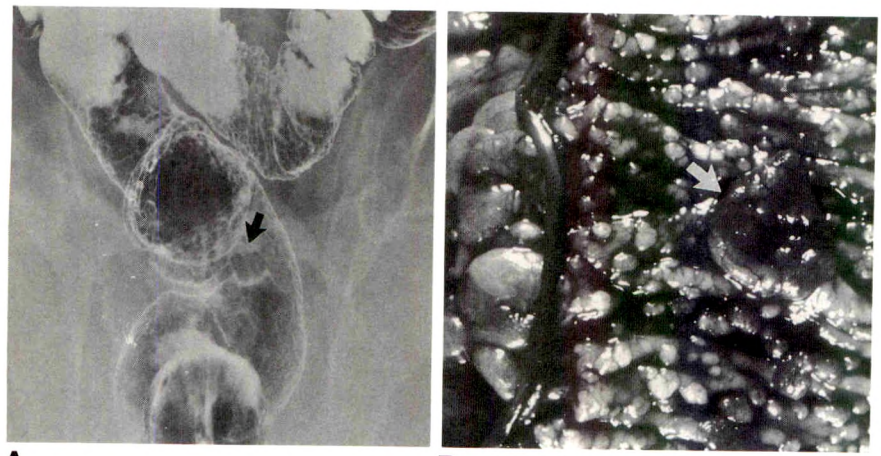


Fig. 2.—Rectal adenocarcinoma in a patient with familial polyposis coli.

*A*, Double-contrast colonic examination shows multiple polyps and rectal adenocarcinoma (*arrow*).

*B*, Accompanying gross specimen of rectum shows adenocarcinoma (*arrow*) and sessile adenomas.

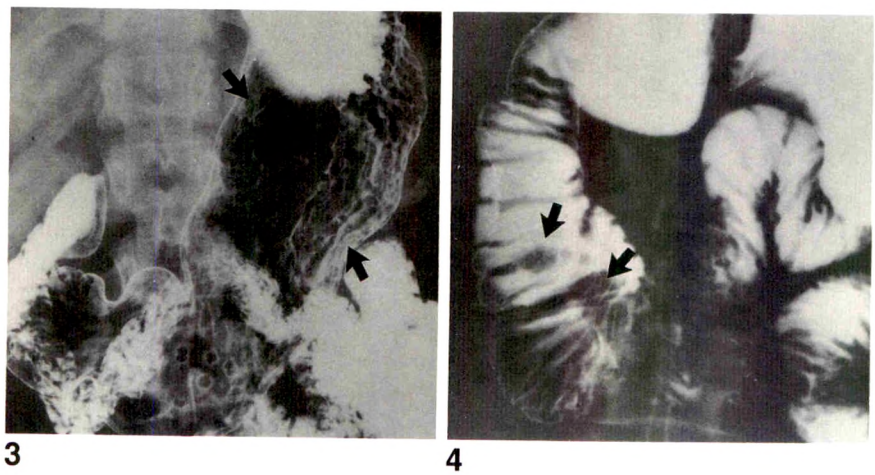


Fig. 3.—Fundic gland polyps in a 25-year-old woman with familial polyposis coli. Upper gastrointestinal series shows multiple small polyps involving fundus and body (*arrows*) with sparing of antrum.

Fig. 4.—57-year-old woman presenting with dyspepsia 30 years after colon resection for familial polyposis coli. Upper gastrointestinal study shows multiple small duodenal polyps (*arrows*).

### Duodenal Involvement

Sixty to one hundred percent of these patients have duodenal polyps, making this site the second most common location for polyps in the familial adenomatous polyposis syndromes (Fig. 4) [1, 2]. Histologically, the polyps are adenomas [2]. They tend to be multiple, very small, and difficult to detect radiologically. These premalignant adenomas lead to an increased prevalence of duodenal carcinoma. The polyps are prone to occur after the colon disease has been cured by colectomy. Patients should be carefully monitored and larger adenomas endoscopically removed.

### Periampullary and Biliary Involvement

It has been estimated that up to 12% of patients with the familial adenomatous polyposis syndromes will develop periampullary carcinoma (Fig. 5) [2, 3]. This prevalence is second only to that of colonic cancer. Most of the malignant lesions are duodenal adenocarcinomas involving the papilla [1, 2]. These periampullary neoplasms also tend to occur after colectomy. Much less common in these syndromes are carcinomas of the pancreas, gallbladder, and bile ducts (Fig. 6).

### Jejunal and Ileal Involvement

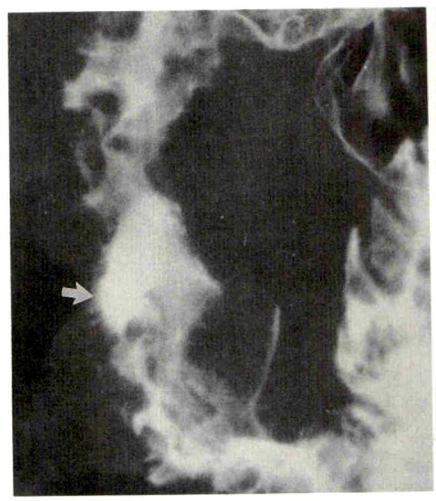
In the Japanese literature, jejunal and ileal polyps have been reported in approximately 60% of patients with familial adenomatous polyposis syndromes. The prevalence in Western populations is unknown. Adenomas are dominant in the jejunum, whereas lymphoid hyperplasia is more common in the ileum. Several cases of carcinoma have been reported. These malignant lesions may also occur after colectomy (Fig. 7).

### Mesenteric Fibromatosis

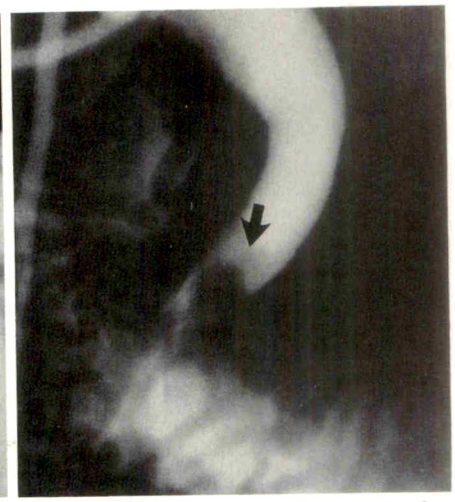
Mesenteric fibromatosis is an aggressive fibrous tumor, locally invasive but without evidence of metastases. There is a high rate of occurrence after colectomy as well as recurrence after excision of the fibrous tumor [2]. Histologically, mesenteric fibromatosis comprises proliferating fibroblasts, either packed tightly together or in a myxomatous matrix (Ros et al., presented at the annual meeting of the Society of Gastrointestinal Radiologists, January 1987). The lesions are vascular, and necrosis is rare. On radiographs, a noncalcified soft-tissue mass may displace bowel loops (Fig. 8). Mucosal irregularities, caused by local invasion, may be evident on barium studies. Sonographic examinations may show either a hyper- or hypoechoic mass (Ros et al., SGR, January 1987). Fibromatosis classically appears as a homogeneous muscle density on CT without evidence of necrosis (Fig. 9) (Ros et al., SGR, January 1987).

### Skeletal and Dental Manifestations

At least 50% of patients with the familial adenomatous polyposis syndromes have osseous involvement [1, 2]. Mul-



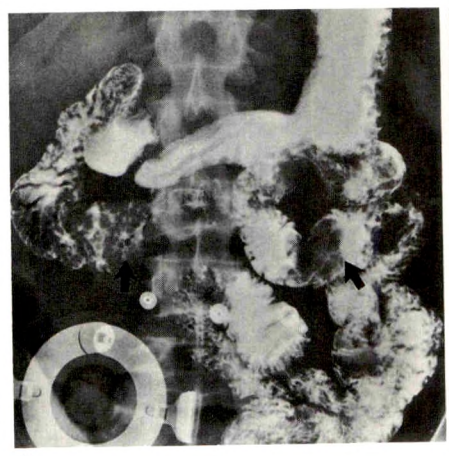
5



6

Fig. 5.—58-year-old man with jaundice and weight loss 20 years after colectomy for Gardner syndrome. Upper gastrointestinal series shows an ulcerating mass in mid descending duodenum (*arrow*).

Fig. 6.—49-year-old woman with "acute cholecystitis" was found to have cholangiocarcinoma of the common bile duct at surgery (*arrow*). Further studies revealed polyposis of colon and a family history of familial polyposis coli. (Reprinted with permission from Harned and Williams [3].)



A



B

Fig. 7.—55-year-old man had a colectomy for familial polyposis coli 31 years before anemia was discovered on a routine physical examination.

*A*, Upper gastrointestinal study shows multiple polypoid lesions in second and third portions of duodenum and proximal jejunum (*arrows*).

*B*, Multiple adenomas involving duodenum and jejunum (*arrows*) were found in gross specimen, and a deeply invasive adenocarcinoma was also discovered in proximal jejunum (*arrowhead*).

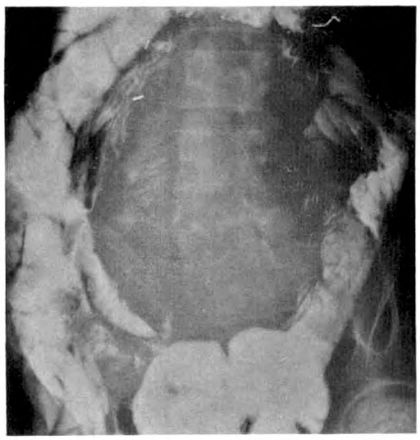
tiple osteomas are the most common lesions, and the outer table of the skull, angle of the mandible, and frontal sinuses are the most common locations (Fig. 10). Radiologically, they appear as smoothly marginated blastic lesions. Osteomas may precede both clinical and radiologic evidence of colonic polyposis. In the pelvis, the osteomas appear as punctate densities (Fig. 11). Long bone involvement is manifested by cortical hyperostosis (Fig. 11). Rare cases of osteosarcoma have been reported. A spectrum of dental abnormalities has also been described, including hypercementomas, odontomas, dentigerous cysts, supernumerary teeth, and multiple caries [1].

### Skin and Eye

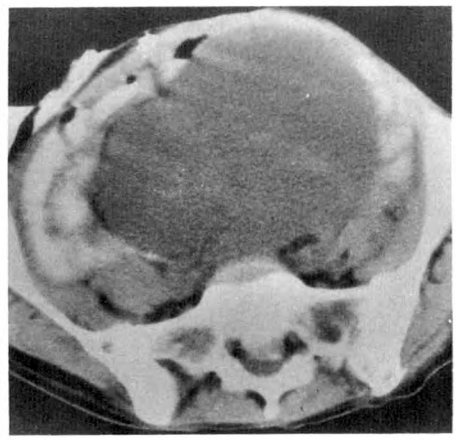
Multiple epidermal cysts are present in approximately 65% of patients with familial adenomatous polyposis syndromes and are typically located on the legs, face, scalp, and arms (Fig. 12) [2]. Pigmented lesions of the ocular fundus have been found in 90% of patients with Gardner syndrome who also had other extracolonic manifestations [4]. These lesions may serve as a marker when present bilaterally in people at risk for familial adenomatous polyposis syndromes [4].

### Thyroid Carcinoma

There is an increased prevalence of thyroid carcinoma in these syndromes, with a suggested prevalence in one series of 0.6% [1, 2, 5]. Women dominate four to one in the age range of 15–35 years. Papillary adenocarcinoma is most common and tends to be multicentric. Thyroid carcinoma may precede recognition of colonic polyps and may also occur after colectomy [5].



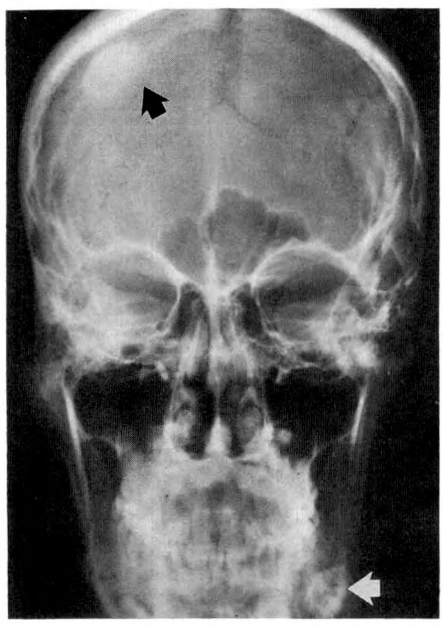
8



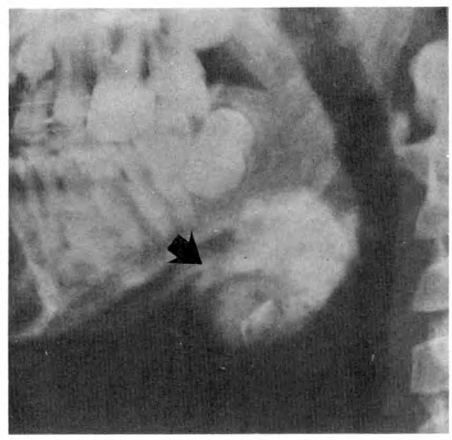
9

**Fig. 8.—Mesenteric fibromatosis presenting as a noncalcified, midabdominal soft-tissue mass displacing loops of small intestine peripherally.**

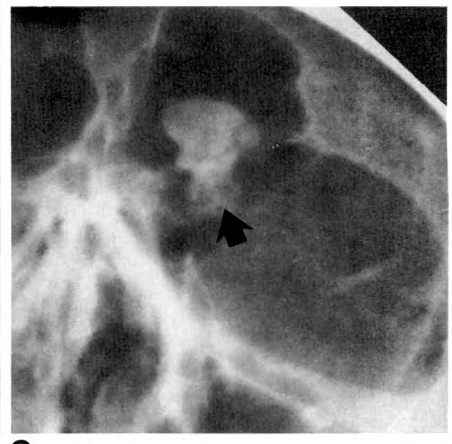
**Fig. 9.—Mesenteric fibromatosis most often appears as a large, homogeneous, musclelike density on CT scans. Absence of areas of decreased density may be of help in differentiating mesenteric fibromatosis from lymphoma and leiomyosarcoma, which frequently have large areas of necrosis.**



A



B



C

**Fig. 10.—Radiographs of osteomas in the most common locations in patients with familial adenomatous polyposis syndromes.**
*A*, Osteoma, outer table of skull (*black arrow*) and angle of mandible (*white arrow*).
*B*, Osteoma, angle of mandible (*arrow*).
*C*, Osteoma, frontal sinus (*arrow*).

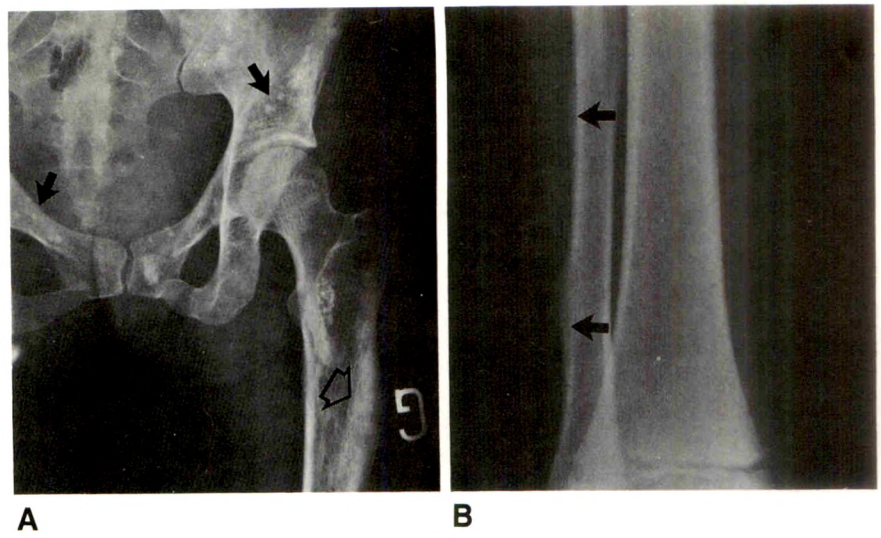


Fig. 11.—Less common locations of bone lesions in patients with familial adenomatous polyposis syndromes.

*A*, Osteomas appear on radiograph as punctate densities of pelvis (*solid arrows*). Note cortical hyperostosis of proximal femur (*open arrow*).

*B*, Radiograph shows cortical hyperostosis of fibula (*arrows*).

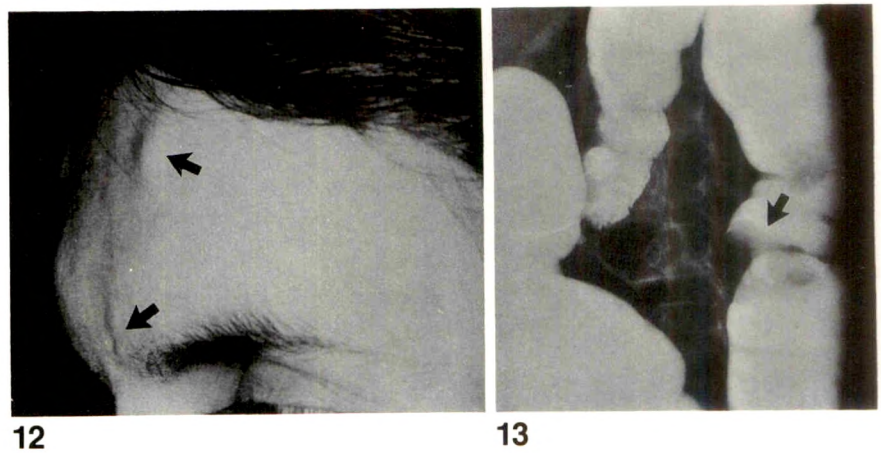


Fig. 12.—Epidermal cysts of forehead (*arrows*) in a patient with Gardner syndrome.



Fig. 13.—13-year-old girl with Turcot syndrome. Barium enema shows adenocarcinoma in descending colon (*arrow*) and at least two adjacent polyps. She also had a medullary glioblastoma of the spinal cord. (Reprinted with permission from Radin et al. [6].)

## CNS Neoplasms (Turcot Syndrome)

Turcot syndrome is rare, presents in the second decade, and is characterized by colonic adenomas and CNS tumors such as glioblastomas and medulloblastomas (Fig. 13) [6]. Colonic malignant tumors are common, but patients most often die from the accompanying CNS tumors. Jagelman [2] found 10 cases of brain tumors in 161 patients with Gardner syndrome and familial polyposis coli. The findings of that study are not conclusive but suggest that Turcot syndrome, or at least CNS neoplasms, may be a legitimate expression of the familial adenomatous polyposis syndromes.

## Conclusions

Extracolonic manifestations of the familial adenomatous polyposis syndromes (familial polyposis coli and Gardner syndrome) are common, often life-threatening, and should be considered an integral part of these syndromes. Patients with these syndromes are at particular risk from the extracolonic expressions of duodenal/periampullary carcinoma, jejunal and ileal carcinoma, thyroid carcinoma, CNS neoplasms, and mesenteric fibromatosis. Before and after colectomy, radiologists should encourage periodic systemic surveillance of patients with familial adenomatous polyposis syndromes, including examination of the thyroid and entire gastrointestinal tract.

## REFERENCES

1. Ushio K, Sasagawa M, Doi H, et al. Lesions associated with familial polyposis coli: studies of lesions of the stomach, duodenum, bones and teeth. *Gastrointest Radiol* **1976**;1:67–80
2. Jagelman DG. Extracolonic manifestations of familial polyposis coli. *Cancer Genet Cytogenet* **1987**;27:319–325
3. Harned RK, Williams SM. Familial polyposis coli and periampullary malignancy. *Dis Colon Rectum* **1982**;25:227–229
4. Traboulsi EI, Krush AJ, Gardner EJ, et al. Prevalence and importance of pigmented ocular fundus lesions in Gardner's syndrome. *N Engl J Med* **1987**;316:661–667
5. Thompson JS, Harned RK, Anderson JC, Hodson PE. Papillary carcinoma of the thyroid and familial polyposis coli. *Dis Colon Rectum* **1983**;26:583–585
6. Radin DR, Fortgang FC, Zee CS, Mikity VG, Halls JM. Turcot syndrome: a case with spinal cord and colonic neoplasms. *AJR* **1984**;142:475–476

# Book Review

**CT Review.** Edited by Janet E. S. Husband. New York: Churchill Livingstone, 266 pp., 1989. $50

This excellent book, carefully edited, comfortable to hold, and chock-full of the current status of CT, is a delight to read and a must-have for every radiology department library. The text is based on a series of lectures given at the International London Course of Whole Body Computed Tomography held in Scotland in 1989. The faculty consisted of recognized authorities in all aspects of CT from the United States, United Kingdom, and Holland. Their lectures have been thoughtfully collated and edited by Janet Husband of the Royal Marsden Hospital, Surrey.

The chapters include an up-to-date status summary of the application of body CT from thyroid imaging to the staging of gynecologic malignancy, and even a chapter on the pitfalls in CT diagnosis. Other subjects covered are CT of atelectasis, inflammatory disease of the pancreas, cystic renal disease, and blunt trauma and interventional CT, just to name a few. Each chapter contains an overview of the subject, details of the CT examination of the area involved, description of findings, a differential diagnosis, and lavish references for those who may wish to delve into the subject in more detail. MR is referred to, with some MR images, and its role vis a vis CT is mentioned, but a detailed comparison is not made.

The chapter on blunt abdominal trauma is particularly well written, referenced, and illustrated. The indications for CT in patients with nonpenetrating trauma are given, and the technique of preparing the patients and performing the examination is described in sufficient detail for the physician to use the technique as a standard for this type of examination. The CT findings that might be seen in injury to each abdominal organ are described and discussed and include pertinent statistical information. Those who sometimes see patients in emergent situations will find this chapter most useful.

The chapter on staging of bladder and prostatic cancer is another example of the usefulness of this book. Staging classifications are discussed and illustrated. Patterns of tumor spread, recommendations on the use of CT, and the CT findings of various stages of cancer spread are described in detail. Finally, a discussion of the accuracy of CT and its limitations is presented. Some comparison of CT vs MR in staging these cancers would be useful, but this does not detract from an excellent presentation of this subject.

The text is well printed, the type is easy to read, and the articles are well illustrated. The book would be better if the images were printed on a higher grade of paper, but this is merely a personal observation that in no way detracts from the overall value of the book.

Every resident should purchase a copy of this book as a ready review of CT in its current state of the art. The practicing radiologist also will find it an excellent overview of CT and a reference that can be used over and over. I heartily recommend it to every radiologist and radiology resident.

Gerald A. L. Irwin
*Winthrop University Hospital*
*Mineola, NY 11501*

# Intraabdominal *Mycobacterium tuberculosis* vs *Mycobacterium avium-intracellulare* Infections in Patients with AIDS: Distinction Based on CT Findings

D. Randall Radin[1]

**Abdominal CT scans of 71 patients with AIDS who had proved disseminated infection due to *Mycobacterium tuberculosis* (27 patients) or *Mycobacterium avium-intracellulare* (44 patients) were reviewed retrospectively to identify radiologic features that can be used to distinguish the two infections. CT findings in patients with disseminated *M. tuberculosis* included focal lesions in the liver (11%), spleen (30%), kidneys (19%), pancreas (7%), and gastrointestinal tract (15%) and lymph nodes with central or diffuse low attenuation (93%). CT findings in patients with disseminated *M. avium-intracellulare* included marked hepatomegaly (20%); marked splenomegaly (14%); focal lesions in the liver (9%), spleen (7%), and kidneys (2%); diffuse jejunal wall thickening (18%); lymph nodes with central low attenuation (14%); and enlarged lymph nodes exclusively of homogeneous soft-tissue density (55%).**

**The presence of focal visceral lesions and low-attenuation lymph nodes suggests disseminated *M. tuberculosis*, whereas marked hepatic and splenic enlargement, diffuse jejunal wall thickening, and enlarged soft-tissue-density lymph nodes suggest disseminated *M. avium-intracellulare*. Recognition of these CT features can lead to a tentative diagnosis so that appropriate therapy can be instituted before the results of mycobacterial cultures become available.**

***AJR* 156:487–491, March 1991**

Disseminated infections due to *Mycobacterium avium-intracellulare* (MAI) [1] and *Mycobacterium tuberculosis* (MTB) [2] in patients with AIDS were first reported in 1982 and 1983, respectively. In 1987, the Centers for Disease Control included disseminated extrapulmonary infection by both MAI and MTB in a list of diseases that indicate a diagnosis of AIDS in patients with laboratory evidence of infection with human immunodeficiency virus (HIV) [3]. Distinction between MTB and MAI infection is important because of the therapeutic implications [1, 4]. Standard antimycobacterial therapy is far more effective in AIDS patients with MTB infection than in those with MAI infection. Findings in one large series suggest that clinical features and findings on chest radiographs may help to distinguish between MTB and MAI infection in HIV-infected patients [4]. Abdominal CT findings in AIDS patients with disseminated mycobacterial infection have been described in several studies and review articles [5–10]. However, a comparative study of abdominal CT findings in MTB and MAI infection has not yet been reported.

Received July 25, 1990; accepted after revision September 13, 1990.

[1] Department of Radiology, University of Southern California School of Medicine, L. A. County-USC Medical Center, 1200 N. State St., Los Angeles, CA 90033-1084. Address reprint requests to D. R. Radin.

0361–803X/91/1563–0487
© American Roentgen Ray Society

## Materials and Methods

According to mycobacteriology laboratory records at our hospital, cultures of specimens from lymph node biopsies, bone marrow biopsies, or blood yielded MTB in 173 patients and MAI in 373 patients between February 1985 and February 1990. An abdominal CT examination done during the same hospital admission during which the biopsy with positive mycobacterial results was performed was available for 33 patients with MTB infection and 45 patients with MAI infection. Medical records of these 78 patients were reviewed. Six

**TABLE 1: Clinical Features of 71 Patients with AIDS and Disseminated Mycobacterial Infection**

| Feature | Number (%) of Patients with MTB ($n$ = 27) | Number (%) of Patients with MAI ($n$ = 44) |
|---|---|---|
| HIV risk factor | | |
| Homosexuality | 18 (67) | 35 (80) |
| IV drug use | 4 (15) | 4 (9) |
| Homosexuality and IV drug use | 2 (7) | 5 (11) |
| Other | 2 (7) | 0 (0) |
| Unknown | 1 (4) | 0 (0) |
| Previous AIDS-defining illness | 2 (7) | 31 (70) |
| Concurrent AIDS-defining illness | 2 (7) | 5 (11) |
| Disseminated mycobacterial infection as only AIDS-defining illness | 23 (85) | 8 (18) |

Note.—MTB = *Mycobacterium tuberculosis*; MAI = *Mycobacterium avium-intracellulare*; HIV = human immunodeficiency virus.

patients with MTB infection and one patient with MAI infection were excluded because of a lack of serologic proof of HIV infection.

All but one of the 71 patients with AIDS who had disseminated mycobacterial infection were men. The 27 patients with MTB ranged in age from 21 to 54 years (average, 35 years). The 44 patients with MAI ranged in age from 25 to 53 years (average, 35 years). HIV risk factors and the temporal relationship of mycobacterial infection to nonmycobacterial AIDS-defining illness are indicated in Table 1. Kaposi sarcoma was the only previous or concurrent disease in the four MTB patients with nonmycobacterial AIDS-defining illness. Extracutaneous Kaposi sarcoma was documented in only one of these four patients. Previous and concurrent diseases in the 36 MAI patients with nonmycobacterial AIDS-defining illness were Kaposi sarcoma in 11 patients (with known extracutaneous involvement in only one patient); lymphoma (three patients); *Pneumocystis carinii* pneumonia (24 patients); cytomegalovirus infection (nine patients); esophageal candidiasis (four patients); cryptococcosis (two patients); and histoplasmosis, toxoplasmosis, and cryptosporidiosis (one patient each).

CT examinations of the 71 patients were performed on a Picker 1200 SX scanner. Slices 10 mm thick were obtained at 10-mm or 15-mm intervals. IV contrast medium was administered in all but seven cases. The studies were reviewed retrospectively and evaluated for liver and spleen size; the presence of hepatic, splenic, renal, pancreatic, adrenal, and gastrointestinal lesions and ascites; and the location, size, and density of abdominal lymph nodes.

Of the 27 patients with MTB infection, involvement of abdominal lymph nodes was proved by percutaneous fine-needle aspiration in nine patients and autopsy in three patients. Follow-up CT examination after antituberculous therapy showed resolution of abdominal adenopathy in one patient. In seven of the 14 patients without direct evidence of abdominal nodal involvement, MTB was cultured from peripheral lymph node biopsy specimens. Splenic lesions in three patients and renal and pancreatic lesions in one patient each were confirmed to be due to MTB by fine-needle aspiration or autopsy. Of the 44 patients with MAI infection, involvement of abdominal lymph nodes was proved by percutaneous fine-needle aspiration of soft-tissue-density nodes in three patients and necrotic nodes in three patients. Involvement of nodes less than 10 mm in diameter was found at autopsy in one patient. Biopsy specimens of peripheral nodes yielded MAI in two patients. Hepatic lesions were confirmed at autopsy in one patient.

## Results

Abdominal CT findings in the 71 patients with AIDS and disseminated mycobacterial infection are presented in Tables 2 and 3. Although hepatomegaly and splenomegaly were seen in a minority of patients in each group, marked enlargement occurred only in patients with MAI. Because only one third of these MAI patients had other diseases commonly associated with hepatosplenomegaly (lymphoma, cytomegalovirus infection, histoplasmosis), it is likely that MAI infection was responsible for the marked hepatic and splenic enlargement in most instances. CT evidence of focal involvement of solid abdominal viscera was far more frequent in patients with MTB. CT showed one or more round or oval hypodense lesions between several millimeters and 2 cm in diameter in the liver, spleen, kidneys, and/or pancreas in 12 (44%) of the 27 MTB patients (Fig. 1) but in only six (14%) of the 44 MAI patients (Fig. 2). These parenchymal lesions had a similar appearance in both groups of patients but tended to be more numerous in the patients with MTB. A striking finding was the

**TABLE 2: Abdominal CT in 71 Patients with AIDS and Disseminated Mycobacterial Infection: Extranodal Findings**

| CT Finding | Number (%) of Patients with MTB ($n$ = 27) | Number (%) of Patients with MAI ($n$ = 44) |
|---|---|---|
| Hepatomegaly | 5 (19) | 20 (45) |
| Mild (19–20 cm cephalocaudal diameter) | 5 (19) | 11 (25) |
| Marked (21–24 cm cephalocaudal diameter) | 0 (0) | 9 (20) |
| Splenomegaly | 7 (26) | 10 (23) |
| Mild (14–15 cm cephalocaudal diameter) | 7 (26) | 4 (9) |
| Marked (16–21 cm cephalocaudal diameter) | 0 (0) | 6 (14) |
| Focal lesions in solid viscera | 12 (44) | 6 (14) |
| Liver | 3 (11) | 4 (9) |
| Spleen | 8 (30) | 3 (7) |
| Kidney | 5 (19) | 1 (2) |
| Pancreas | 2 (7) | 0 (0) |
| Adrenal abnormalities | 0 (0) | 0 (0) |
| Gastrointestinal tract abnormalities | 4 (15) | 8 (18) |
| Ascites | 5 (19) | 5 (11) |

Note.—MTB = *Mycobacterium tuberculosis*; MAI = *Mycobacterium avium-intracellulare.*

**TABLE 3: Abdominal CT in 71 Patients with AIDS and Disseminated Mycobacterial Infection: Nodal Findings**

| CT Finding | Number (%) of Patients with MTB ($n$ = 27) | Number (%) of Patients with MAI ($n$ = 44) |
|---|---|---|
| Solid nodes only | 2 (7) | 38 (86) |
| Largest node ≥10 mm | 1 (4) | 24 (55) |
| Largest node <10 mm | 1 (4) | 14 (32) |
| Necrotic nodes | 25 (93) | 6 (14) |
| With solid nodes ≥10 mm | 17 (63) | 5 (11) |

Note.—MTB = *Mycobacterium tuberculosis*; MAI = *Mycobacterium avium-intracellulare*.

presence of innumerable small hypodense lesions virtually replacing the entire spleen in three patients with disseminated MTB infection (Fig. 3). No adrenal abnormality was identified in any patient in either group. Autopsy of three patients with MTB who died 4–6 days after CT examination revealed hepatic, splenic, renal, and/or adrenal involvement that was not evident on CT.

CT showed abnormalities of the gastrointestinal tract in less than one of five patients in each group, although some lesions may have been missed because of suboptimal bowel opacification, particularly of the small intestine. In the patients with MAI, the abnormality was diffuse wall thickening of the jejunum (seven patients, Fig. 4) or entire small bowel (one patient). Findings in the four MTB patients were gastric involvement by lesser omental adenopathy (one patient), extraluminal gas in the hepatoduodenal ligament due to a sinus tract from the proximal duodenum (two patients, Fig. 5), circumferential wall thickening of the transverse duodenum (one patient), and circumferential wall thickening of the terminal ileum and cecum (one patient, Fig. 6). A small to moderate volume of ascites was seen in five patients in each group.

Enlargement of abdominal lymph nodes was common in both groups, but some differences were noteworthy. Although widespread nodal involvement was seen in patients in each group, enlarged nodes were seen in the splenic hilum and adjacent to the pancreatic tail in four (15%) of 27 MTB patients but in none of 44 MAI patients. Solid nodes, defined as homogeneous nodes with density greater than that of muscle, were 10 mm or more in diameter in two thirds of the

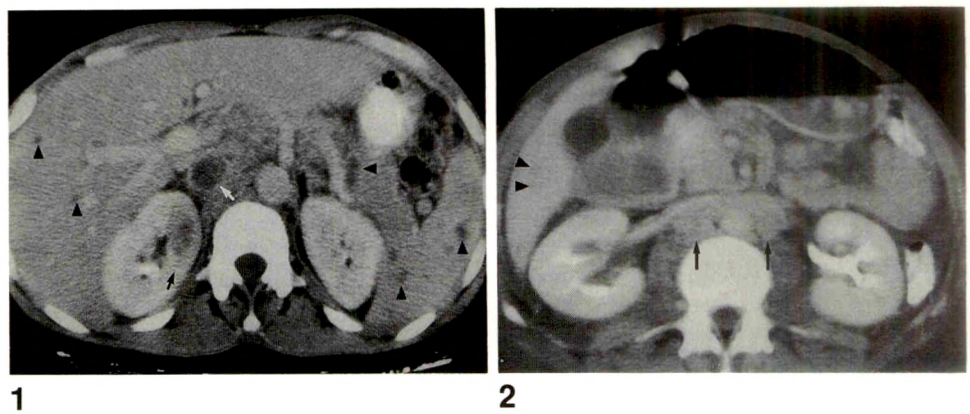


**Fig. 1.—CT scan shows multiple small low-attenuation lesions (*arrowheads*) in liver, spleen, and pancreas; solitary right renal lesion (*black arrow*); and lymph node with central low attenuation (*white arrow*) anterolateral to crus of right hemidiaphragm. Cultures of fine-needle aspirates of splenic lesion and retroperitoneal lymph node grew *Mycobacterium tuberculosis*.**

**Fig. 2.—CT scan shows two small low-attenuation lesions (*arrowheads*) inferiorly in right lobe of liver and homogeneous soft-tissue density paraaortic lymph nodes (*arrows*). Blood culture, bone marrow biopsy, and endoscopic biopsy of duodenum yielded *Mycobacterium avium-intracellulare*.**

1 2

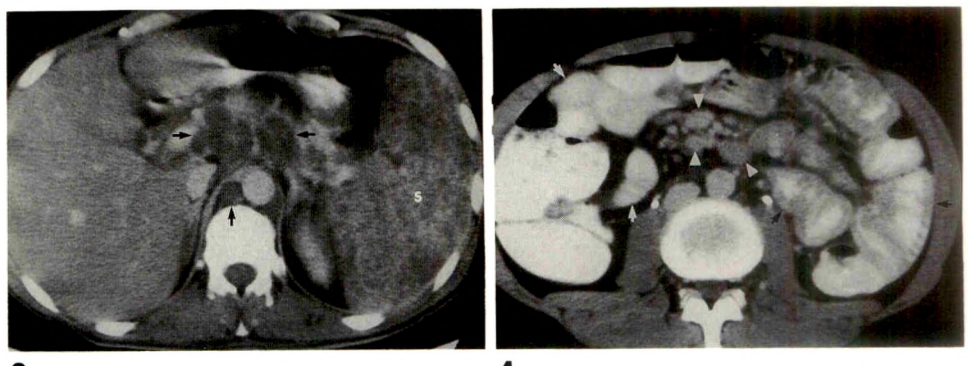
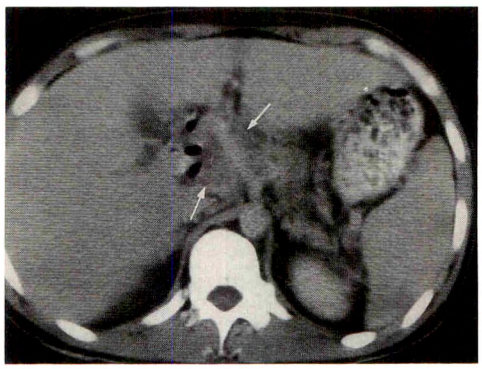


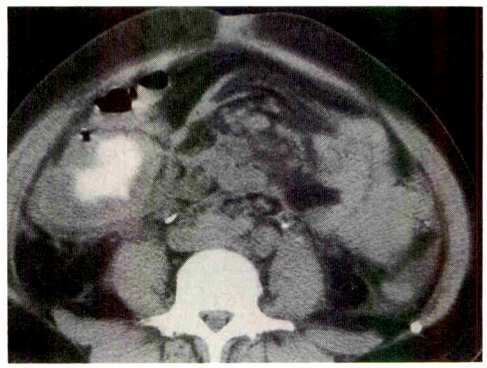
**Fig. 3.—CT scan shows innumerable low-attenuation lesions throughout enlarged spleen (S) and multiple homogeneous water-density retroperitoneal and retrocrural lymph nodes (*arrows*). Culture of fine-needle aspirate of retroperitoneal lymph node grew *Mycobacterium tuberculosis*.**

**Fig. 4.—CT scan shows diffuse thickening of jejunal wall (*black arrows*) in left side of abdomen, normal ileum (*white arrows*) in right side of abdomen, and homogeneous soft-tissue density mesenteric lymph nodes (*arrowheads*). *Mycobacterium avium-intracellulare* was recovered from blood, stool, and bone marrow.**

3 4



5



6

Fig. 5.—CT scan shows extraluminal gas in region of hepatoduodenal ligament, adjacent to lymphadenopathy (*arrows*) surrounding hepatic artery. Upper gastrointestinal series confirmed sinus tract extending superiorly from postbulbar duodenum. Stool culture and fine-needle aspirate of peripancreatic lymph node yielded *Mycobacterium tuberculosis*.

Fig. 6.—CT scan shows marked irregular thickening of cecal wall and mesenteric and retroperitoneal lymphadenopathy. Bone marrow and left inguinal lymph node biopsy specimens grew *Mycobacterium tuberculosis*.

patients in each group (Figs. 2 and 4). However, necrotic nodes, defined as nodes with central or diffuse low density, were present in 93% of MTB patients (Figs. 1 and 3) but in only 14% of MAI patients (Fig. 7). On the other hand, solid nodes 10 mm or larger were present exclusively in 55% of patients with MAI but in only one patient with MTB.

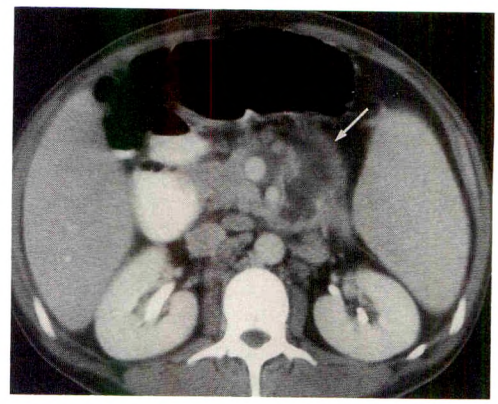


Fig. 7.—CT scan shows splenomegaly, necrotic mesenteric lymphadenopathy (*arrow*), and paraaortic lymphadenopathy of homogeneous soft-tissue density. Fine-needle aspirate of mesenteric mass yielded *Mycobacterium avium-intracellulare*.

## Discussion

A striking difference between patients with AIDS and disseminated MTB infection and those with AIDS and disseminated MAI infection was the temporal relationship between mycobacterial and nonmycobacterial AIDS-defining illnesses. Whereas 82% of the MAI patients had one or more previous or concurrent AIDS-defining illnesses, 85% of the MTB patients had disseminated MTB infection as their only AIDS-defining illness. Similar findings have been noted by others and have been ascribed to the relative virulence of the organisms and progressive impairment of the immune system in the course of HIV infection [4, 11].

Results in this series suggest that a number of abdominal CT findings may help to distinguish disseminated MTB from disseminated MAI infection. Although mild enlargement of the liver and/or spleen was present in a minority of patients in each group, marked hepatomegaly (cephalocaudal diameter ≥21 cm) and marked splenomegaly (cephalocaudal diameter ≥16 cm) were seen only in patients with MAI. The finding of a normal-sized spleen in most patients with MAI in this series differs from an earlier study in which all of 17 patients with disseminated MAI infection had splenomegaly [5].

As has been reported by others [5, 6, 10], CT demonstration of focal visceral lesions in patients with AIDS and disseminated mycobacterial infection is the exception rather than the rule. In this series, small hypodense lesions were seen in spleen, liver, kidneys, and/or pancreas in almost half of the patients with MTB but in only one seventh of the patients with MAI. Furthermore, focal visceral lesions usually were more numerous in affected MTB patients. Interestingly, no patient with MTB or MAI had CT evidence of adrenal involvement.

Although evidence of involvement of the gastrointestinal tract was seen in less than 20% of patients in each group, the CT appearance of bowel lesions, when present, can suggest whether mycobacterial infection is due to MAI or MTB. Whereas MAI infection of bowel typically was manifested as diffuse jejunal wall thickening, MTB infection resulted in segmental duodenal or ileocecal wall thickening or extraluminal gas due to a duodenal fistula. Similar findings have been reported before [6, 7, 10].

In this study, the most useful nodal feature for distinguishing between MTB and MAI infection was the presence or absence of necrosis. Abdominal CT showed lymph nodes with central or diffuse low density in 93% of the patients with MTB but in only 14% of the patients with MAI. Necrotic abdominal nodes have been described previously in both MTB and MAI infection in patients with AIDS [5–10]. In one study [5], the frequency of necrosis in abdominal lymph nodes in disseminated MAI was 12%. The frequency of necrosis in tuberculous abdominal nodes in AIDS has not been reported before. Results in this series cast doubt on a previously published suggestion that fine-needle aspiration of enlarged abdominal nodes may not be necessary if they have "the characteristic low attenuation of MAI lymphadenopathy" [10].

The greater frequency of focal visceral lesions and of necrotic lymph nodes in patients with AIDS and disseminated MTB than in those with AIDS and disseminated MAI may be due to differences in host immunity. Histologic evidence of

limited tissue response with poor formation of granulomas and lack of caseation is typical of MAI infection in AIDS and helps to distinguish it from MTB infection [1, 9]. A relative paucity of findings on chest radiographs in patients with MAI infection has been ascribed to a lesser ability to mount an inflammatory response [4].

The results of this study must be viewed with some caution. Because of its retrospective nature, abdominal CT examinations were available for only a small percentage of all AIDS patients with disseminated mycobacterial infection. As a result, the selection of patients involved unknown biases. More importantly, suspected visceral and nodal involvement was not proved in many cases, particularly in patients with MAI infection. Although most, if not all, of the focal visceral lesions and necrotic nodes probably were due to mycobacterial infection, it is not known what percentage of lymph nodes with homogeneous soft-tissue density, especially those smaller than 15 mm, were involved. Other common causes of solid adenopathy in patients with HIV infection include lymphoma, Kaposi sarcoma, and the lymphadenopathy syndrome [10]. Since this study was completed, we have begun to perform percutaneous fine-needle aspiration of such nodes in HIV-seropositive patients with unexplained symptoms (usually fever) and have recovered MAI from 10-mm-diameter paraaortic nodes in four cases. Despite the limitations of this study, some tentative conclusions can be drawn. Abdominal CT findings suggestive of disseminated MTB infection include multiple necrotic lymph nodes; multiple focal lesions in the spleen, liver, kidneys, and/or pancreas; segmental ileocecal wall thickening; and extraluminal gas due to a duodenal fistula. Findings suggestive of disseminated MAI infection include multiple nodes 10 mm or more in diameter with soft-tissue density, marked hepatomegaly, marked splenomegaly, and diffuse jejunal wall thickening. Although definitive diagnosis requires a positive culture, recognition of typical abdominal CT findings can help to suggest a tentative diagnosis, so that appropriate therapy can be instituted early during the 4- to 6-week period required for results of mycobacterial cultures.

## REFERENCES


1. Greene JB, Sidhu GS, Lewin S, et al. Mycobacterium avium-intracellulare: a cause of disseminated life-threatening infection in homosexuals and drug abusers. *Ann Intern Med* **1982**;97:539–546
2. Pitchenik AE, Fischl MA, Dickinson GM, et al. Opportunistic infections and Kaposi's sarcoma among Haitians: evidence of a new acquired immunodeficiency state. *Ann Intern Med* **1983**;98:277–284
3. Centers for Disease Control. Revision of the CDC surveillance case definition for acquired immunodeficiency syndrome. MMWR **1987**;36[suppl 1S]:3S–15S
4. Modilevsky T, Sattler FR, Barnes PF. Mycobacterial disease in patients with human immunodeficiency virus infection. *Arch Intern Med* **1989**;149:2201–2205
5. Nyberg DA, Federle MP, Jeffrey RB, Bottles K, Wofsy CB. Abdominal CT findings of disseminated *Mycobacterium avium-intracellulare* in AIDS. *AJR* **1985**;145:297–299
6. Hulnick DH, Megibow AJ, Naidich DP, Hilton S, Cho KC, Balthazar EJ. Abdominal tuberculosis: CT evaluation. *Radiology* **1985**;157:199–204
7. Balthazar EJ, Gordon R, Hulnick D. Ileocecal tuberculosis: CT and radiologic evaluation. *AJR* **1990**;154:499–503
8. Jeffrey RB Jr, Nyberg DA, Bottles K, et al. Abdominal CT in acquired immunodeficiency syndrome. *AJR* **1986**;146:7–13
9. Megibow AJ, Balthazar EJ, Hulnick DH. Radiology of nonneoplastic gastrointestinal disorders in acquired immune deficiency syndrome. *Semin Roentgenol* **1987**;22:31–41
10. Federle MP. A radiologist looks at AIDS: imaging evaluation based on symptom complexes. *Radiology* **1988**;166:553–562
11. Pitchenik AE, Cole C, Russell BW, Fischl MA, Spira TJ, Snider DE Jr. Tuberculosis, atypical mycobacteriosis, and the acquired immunodeficiency syndrome among Haitian and non-Haitian patients in south Florida. *Ann Intern Med* **1984**;101:641–645

# Book Review

**CT and MRI of the Liver and Biliary System.** (Vol. 12 in the series Contemporary Issues in Computed Tomography.) Edited by Paul M. Silverman and Robert K. Zeman. New York: Churchill Livingstone, 328 pp., 1990. $75

The purpose of this compact monograph, which joins an expanding number of texts on hepatic and abdominal cross-sectional imaging, is to "provide a practical, state-of-the-art review of CT and MRI in hepatobiliary imaging." The editors and authors are to be congratulated not only for achieving this purpose but also for doing so in a comprehensive yet concise, readable, well-structured, and, overall, excellent product. Edited by two distinguished diagnostic radiologists, with contributions from an outstanding collection of recognized authorities, the book is one of a continuing series (Contemporary Issues in Computed Tomography) with identical format and proved practicality.

The book starts with excellent discussions of relevant hepatic anatomy, as well as technical aspects of CT and MR, stressing strategies for administration of IV contrast material, scanning protocols for CT, and optimization of pulse sequences for MR. Although other contemporary texts have more extensive reviews of these topics, the sections in this monograph are a good blend of scholarly review and practical approach in a manageable volume. Some of this material has been published by the contributing authors in a recent MR review journal, but they have modified their material, where appropriate, for the book.

On casual inspection, the reader may be confused at first by the apparent overlapping and occasionally conflicting coverage of topics in the sequential chapters on MR of the liver, malignant liver disease, benign masses of the liver, and diffuse liver disease. Intentional or not, the ultimate result of this editorial approach is a combination of balance and reinforcement. The different approaches and points of view of the various authors are stated without any editorial effort to impose conformity of opinion; this absence of overt or covert editorial bias is the basis for the value of this book.

The only limitations of this book are likely to be the result of attempting to publish a current review of a technique (MR imaging) during its active evolution. Necessary deadlines in the publication process mean that a document that is current when written may become dated by the time of publication if the field is undergoing the rapid evolution that MR has experienced for the past decade. The considerable experience and insight of the editors and contributing authors clearly have minimized any negative impact that this "time in the publishing pipeline" had on this book, and I think that the book's value is not diminished significantly by this lag from pen to print. However, this is not to say that the book does not have any weaknesses. This lag effect is the probable explanation for the unfortunate paucity of references published more recently than 1988. Similarly, the burgeoning field of MR angiography, with significant applications to imaging in portal hypertension, liver transplantation, and evaluation of mass lesions described or reported in the past 18 months, was not included in this work and undoubtedly would be the basis for a full chapter in any subsequent edition. Also, new and anticipated developments in gradient-echo and echoplanar imaging of the liver eventually will require reevaluation of strategies for MR imaging of the upper abdomen.

What is clear is that MR, and to a lesser extent CT, continues to undergo significant evolutionary advances and that the need for an updated, thorough review for practicing radiologists will persist. This timely text—well organized, readable, and excellently illustrated—fills the current need. I welcome this book, and I recommend it highly to those in training and to anyone who is involved with abdominal imaging. As the field evolves, I will look forward to the second edition.

H. Esterbrook Longmaid III
*New England Deaconess Hospital*
*Boston, MA 02215*

# Gallstone Fragmentation During Biliary Lithotripsy: Effect of Stone Composition and Structure

Robert K. Zeman[1]
Tania Marchand[1,2]
William J. Davros[1]
Brian S. Garra[1]
Mark Glass-Royal[1]
Roger D. Soloway[3]

**In vitro lithotripsy with the Siemens Lithostar was conducted on 36 radiolucent or minimally calcified gallstones housed in an anthropomorphic phantom. The ease and pattern of fragmentation were correlated with global composition for the entire stone, regional or microcomposition (determined by Fourier-transform infrared spectroscopy), and microstructure (determined by scanning electron microscopy). Stones made up of more than 62% cholesterol required 50% more shock waves to pulverize all fragments to 0.3 cm or less than did stones of less than 62% cholesterol ($p < .01$). An inverse relationship was found between the number of shock waves needed for fragmentation and the cholesterol content ($r = .77$). Although a broad range of fragmentation responses occurred, little variation was seen in the ease of fragmentation within stone families. The majority of stones fractured along radially oriented cholesterol plates, but one third of stones treated showed initial chipping or flaking at the periphery before radial fracture. This type of peripheral erosion most often occurred in stones with peripheral pigment rims. These stones required more shock waves and lagged in pulverization compared with more homogeneous cholesterol stones.**

**The efficiency of fragmentation during biliary lithotripsy correlates with the stones' global cholesterol content. A stone's architecture, as reflected by its regional composition and microstructure, partially predicts the mechanism of fragmentation. These in vitro data may be useful in further refining criteria for selecting patients and understanding the fragmentation process.**

*AJR* 156:493–499, March 1991

Prior in vitro studies have suggested that only gallstone size, not composition or morphology, influences the effectiveness of fragmentation during lithotripsy [1, 2]. Although some initial experience supports this concept [3], our early clinical experience suggests that stones with rim or nidus calcification vary more in the degree of fragmentation than do stones without discernible calcium. An in vitro study was performed to clarify this dichotomy and the range of fragmentation response of stones that qualify for lithotripsy under our existing clinical protocol. Our purpose was twofold: (1) to determine the relationship between stone microcomposition (regional composition)/microstructure and effectiveness of fragmentation and (2) to determine if the mechanism of fragmentation is related to the underlying architecture of a gallstone.

## Materials and Methods

Thirty-six stones collected after cholecystectomy from 12 patients were used for this study. Each patient provided three matched stones that appeared to be from a single family and were of comparable size (1.1–1.8 cm in diameter). The stones were selected from a larger group collected from 31 patients. The stones were selected so that they would conform to the characteristics that would allow their treatment under many of the existing lithotripsy protocols in the United States. Both Siemens and Dornier protocols (Siemens Medical Systems, Iselin, NJ; Dornier Medical Systems, Marietta, GA) require stones to be radiolucent

Received August 7, 1990; accepted after revision September 25, 1990.

Presented in part at the Society of Gastrointestinal Radiology 18th annual meeting and postgraduate course, Palm Desert, CA, February 1989.

[1] Department of Radiology, Georgetown University Medical Center, 3800 Reservoir Rd., Washington, DC 20007. Address reprint requests to R. K. Zeman.

[2] Present address: Department of Radiology, Norwalk Hospital, Norwalk, CT 06850.

[3] Department of Internal Medicine, Gastroenterology Division, University of Texas Medical Branch at Galveston, Galveston, TX 77550.

0361–803X/91/1563–0493
© American Roentgen Ray Society

on a plain radiograph or to have a calcific rim or nidus no larger than 3 mm. Specimen radiographs (45 kVp, 2 mAs) and radiographs (65 kVp, phototimed) with the stones submerged in saline in a 50-ml cavity at the center of a 24-cm phantom were obtained as a means of screening stones. The 12 patients had a total of 57 stones, of which only 36 were studied.

After they were stored (from 1 to 5 weeks) in bile (nine) or saline (27), all the stones were weighed and their maximal diameter was measured. Twelve stones (one from each patient) were sent for infrared spectroscopy. Two types of infrared spectroscopy were performed: Fourier-transform infrared spectroscopy (FTIRS), followed by conventional infrared spectroscopy (IRS). FTIRS was performed with the Digilab FTS 60 FTIR spectrometer (Digilab Corp., Boston, MA). This nondestructive analysis was performed on a freshly cleaved cross section taken through the center of the stone. This cleavage plane was created by using the lithotripter and removing the stone as soon as a full thickness fracture was created. Wave numbers were plotted against absorbance to determine regional cholesterol-to-bilirubin ratios and percentage bilirubin within the mucin-bilirubin peak. Subsequently, the stones were dehydrated, reweighed, pulverized, and submitted for conventional infrared spectroscopy to measure global cholesterol and pigment content [4]. Amounts of global cholesterol and bilirubin for the whole stone were determined as a percentage of dry weight. The contralateral half of the stone was studied for microstructural characteristics by using the Hitachi S-570 (Hitachi Ltd, Tokyo, Japan) scanning electron microscope. Magnification ranging from 25 to 400 times was used. The pattern, depth, and orientation of crystal alignment were studied [5]. The presence of pigment bands or rings was recorded. The electron microscopic appearance was correlated with the FTIRS composition data and the appearance of the stones on radiographs. It is generally accepted that stones that are visually similar in size and pigment content have comparable composition [6]. This allows us to extrapolate information regarding stone morphology and composition from a representative stone to others in that family.

The remaining 24 stones (two from each patient) were fragmented with the Siemens Lithostar (Siemens Medical Systems, Iselin, NJ). The stones were housed in a dilute contrast-filled 50-ml mock gallbladder within a previously described anthropomorphic phantom [7]. This phantom is made of an agar graphite gel possessing an attenuation of 0.5 dB/cm and sound transmission speed of approximately 1540 m/sec with backscatter comparable with that of liver parenchyma. This material therefore attenuates shock waves similarly but perhaps more homogeneously than would be expected clinically when using a transhepatic blast path. The mock gallbladder represented a fluid-filled space at the center of the phantom, which was designed to coincide with the focal zone of the lithotripter.

Shock waves were administered at 19 kV at a rate of 1.2/sec. The experiment was ended for each stone when the largest fragment diameter was 0.3 cm. Early fragmentation up to 200 shock waves was observed with a magnifying glass through a polyethylene window covering the mock gallbladder to see the orientation of fracture lines as the stone began to fragment. At 10, 50, and 100 shock waves, the greatest fragment diameters were recorded. Subsequently, fragments were visually inspected and measured at 200-shock-wave intervals (for the first 2000 shock waves) and at 500-shock-wave intervals up to a maximum of 4000 shock waves. The pattern of stone fragmentation and the largest fragment at each inspection interval was recorded. The stone interior was visually inspected before complete pulverization. The patterns and success of fragmentation were correlated with the microcomposition and microstructural data and compared for individual subgroups with the Student t test.

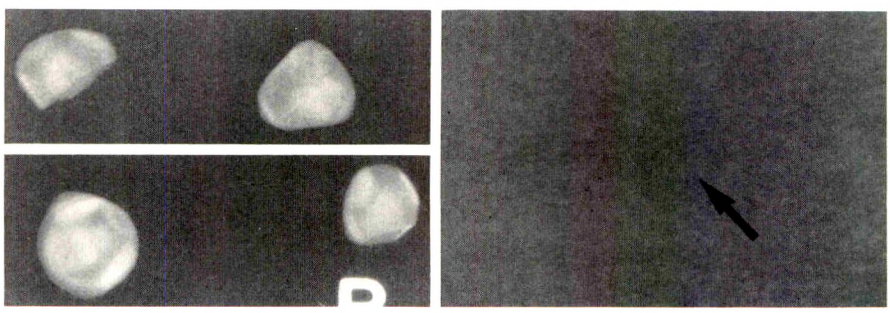
## Results

### *Microcomposition and Microstructure vs Effectiveness of Fragmentation*

Radiographs of the individual stones in saline were found to more closely approximate a plain film of the abdomen than did specimen radiographs. Of those stones ultimately selected for study, specimen radiographs detected the stones in 36/36 cases when surrounded by air. Rim, nidus, or diffuse hyperdensity was present in 24/36 stones. Submerged in saline, 25/36 stones were the same density as saline. Nine showed rim or nidus calcification, and two were radiolucent (Fig. 1). All three stones within a single family showed radiologically identical density for nine families. Two of three stones within a single family were identical for the remaining three families.

The composition and structural data are shown for the 12 stone sets in Table 1. The cholesterol content ranged from 45% to 79% and bilirubin from 1% to 11%. Cholesterol-to-bilirubin ratios in the stone core ranged from 0.2 to 1.1 and in the rim from 0.2 to 1.0

Scanning electron micrographs showed a predominantly radial distribution of cholesterol crystals in 11/12 stones (Fig. 2). In the twelfth stone, random plates of cholesterol crystals were interspersed with amorphous pigment. Pigment was seen interdigitating with cholesterol crystals in the nidus of 11 stones. Nine of these 11 also had pigment identified in the rim. The pigment deposits in the rim appeared more homogeneous and circumferentially arranged than the more central pigment deposition in seven of the nine stones in this category (Fig. 2). Three stones showed a rim consisting of radially oriented cholesterol plates separated from the stone interior



A B

**Fig. 1.—Discordant specimen radiograph and radiograph of stone housed in phantom.**

***A*, Specimen radiograph reveals presence of increased density in stone rim and nidus of all stones in this family.**

***B*, Radiograph of stone (lower right corner in *A*) submerged in saline and housed in an anthropomorphic phantom revealed a stone that is nearly isodense. On original radiograph, barely perceptible nidus (*arrow*) was seen surrounded by slight lucency. Rim is not clearly present.**

by a pigment band or surrounding a more central portion of the stone that contained pigment.

Of the nine stones with pigmented rims, the rim was less than 1 mm thick in five stones and 1–3 mm thick in three stones. One stone had a 5-mm rim. Similarly in stones with cholesterol rims, the thickness of the rim was less than 1 mm for one stone and 1–3 mm for two stones. Despite the high frequency of rim pigment seen on electron microscopy, only two of the 12 stone families showed high-density rims on plain radiographs. Single or multiple internal bands of pigment were seen within six stones. These bands were always less than 1 mm thick. These internal bands did not appear to be related to the rim or nidus characteristics of the stones.

Good agreement was found between the scanning electron microscopic appearance of stones and their regional composition. The rim of a stone always appeared to be more homogeneous on electron microscopy and to have a relatively greater concentration of pigment or cholesterol than the nidus had. Of the four stones with pigmented rims more than 1 mm thick, the cholesterol-to-bilirubin ratio ranged from 0.1 to 0.3. Of the eleven stones containing pigment centrally, the cholesterol-to-bilirubin ratio ranged from 0.1 to 1.1 Although we did not try to correlate the scanning electron microscopic appearance with global composition, the four stones made up of more than 75% cholesterol had only one band or amorphous plate of pigment that was narrower than 1 mm per high power (>100×) field. No relationship was found between a stone's cholesterol content and its appearance on plain radiographs.

**TABLE 1: Correlation of Imaging, Composition, and Fragmentation Data**

| Stone Family | Radiologic Appearance[a] | Mean Global Chol | Mean Global Br | Chol/Br | | Fragmentation Pattern[b] | Shock Waves[c] |
|---|---|---|---|---|---|---|---|
| | | | | Core | Rim | | |
| 1 | N | 0.55 | 0.08 | 0.20 | 1.2 | C, Ra | 1.6, 2.5 |
| 2 | I | 0.61 | 0.09 | 0.80 | 0.2 | C, Ra | 1.0, 1.6 |
| 3 | I | 0.79 | 0.03 | 1.05 | 1.0 | F, Ra | 0.6, 1.0 |
| 4 | R | 0.75 | 0.04 | 0.10 | 0.1 | Ra | 1.4, 1.8 |
| 5 | I | 0.58 | 0.10 | 0.80 | 0.3 | C, Ra | 2.0, 2.5 |
| 6 | R | 0.45 | 0.05 | 0.20 | 0.2 | C, Ra | 4.0, 4.0 |
| 7 | L | 0.77 | 0.08 | 1.10 | 0.6 | Ra | 1.0, 1.0 |
| 8 | I | 0.50 | 0.02 | 0.70 | 0.8 | Ra | 1.0, 1.0 |
| 9 | I | 0.50 | 0.11 | 0.30 | 0.6 | Ra | 1.8, 2.0 |
| 10 | I | 0.60 | 0.07 | 0.60 | 0.3 | F, Ra | 1.0, 1.2 |
| 11 | I | 0.65 | 0.05 | 1.10 | 1.0 | Ra | 1.6, 2.0 |
| 12 | I | 0.77 | 0.01 | 1.00 | 0.3 | Ra | 1.0, 1.0 |

Note.—Chol = cholesterol, Br = bilirubin.

[a] N = nidus, I = isodense, R = rim, L = lucent.

[b] C = chipped, F = flaked, Ra = radial fracture.

[c] Shock waves (×1000) to achieve 0.3-cm fragment for two stones in family.

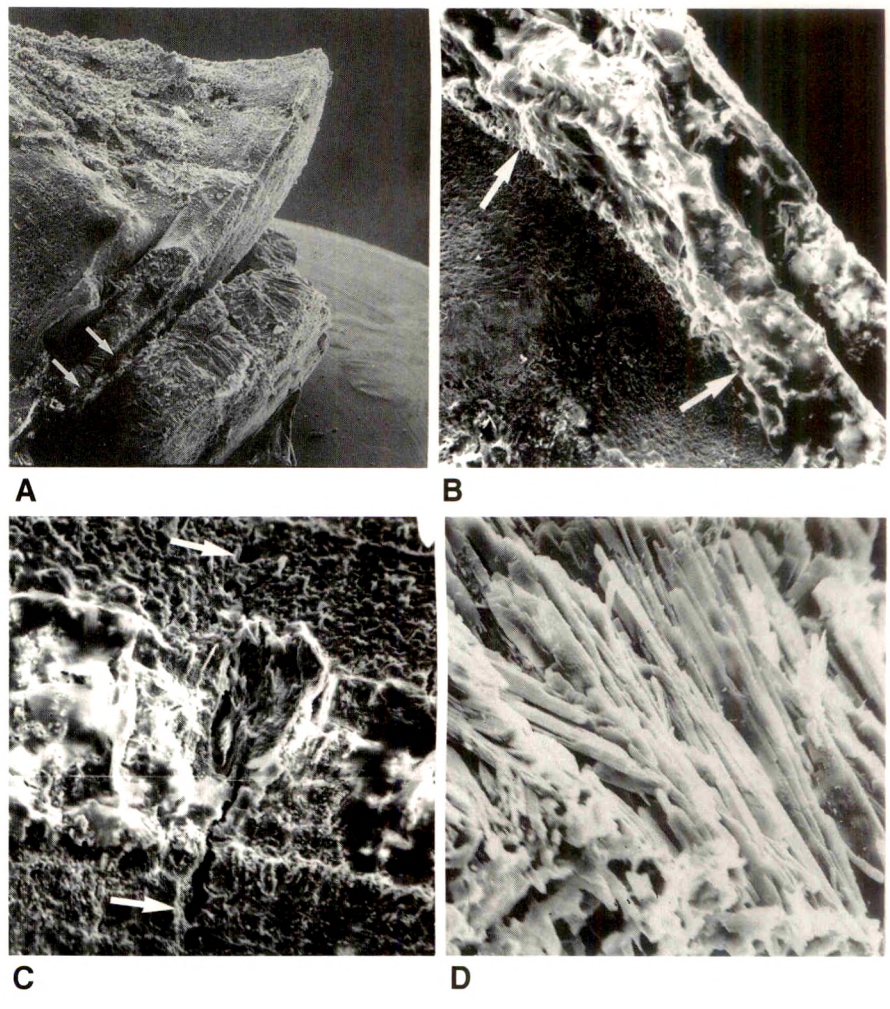



**Fig. 2.—Scanning electron microscopy of stone crystal structure.**

***A*, This stone shows radially oriented plates of cholesterol in its rim and interior. They are separated by a thin 0.15-mm band of pigment (*arrows*). As stone was cleaved for electron microscopy, fracture line developed in an area where rim had been eroded away by initial shock waves (×25).**

***B*, A pigmented 1-mm rim (*arrows*) is identified in this stone. Pigment appears amorphous and more circumferentially arranged than are interior cholesterol plates (×50).**

***C*, As this stone was cleaved, a fracture line (*arrows*) extended from a region of cholesterol plates through a 200-μm pigment band into cholesterol-rich stone interior. These very thin pigment bands did not provide a significant obstacle to development of fracture lines (×200).**

***D*, Cholesterol crystals are repetitive and predictably radially oriented. In this stone, cleavage plane passes from top left to bottom right of image, parallel to long axis of cholesterol plates (×400).**

The number of shock waves required to make all fragments 0.3 cm or smaller varied between 600 and 2500 (Table 1). The mean was 1654. One stone family had multiple large fragments (0.7–0.9 cm) remaining after 4000 shock waves. The mean intrafamily variation in the number of shock waves to reach the 0.3-cm end point was 300 ± 286. Correlation was found between global cholesterol content and the number of shock waves required to reach the end point of fragmentation. The mean number of shock waves required to reach 0.3 cm was 1940 ± 1017 for stones with less than 62% cholesterol content (the midpoint of the cholesterol range of stones in this study). The mean was 1240 ± 440 for stones with greater than 62% cholesterol. The difference is significant at the .01 level ($t = 3.15$). The one stone family that resisted fragmentation had only 45% cholesterol. The ability to produce effective fragmentation showed a moderate correlation with cholesterol content ($r = .77$, Fig. 3). In addition to its relationship to overall global composition, the ability to reach the end point of fragmentation also appeared to be related to microcomposition. The mean number of shock waves for stones possessing a cholesterol-to-bilirubin ratio of less than 0.5 in their core or rim was 1900 ± 950. For those stones with a ratio of greater than 0.5, the mean number of shock waves was 1150 ± 430. The difference was significant at the .05 level ($t = 2.09$).

Within the group of stones studied, plain radiographs did not stratify stones with regard to the number of shock waves required to achieve a 0.3-cm fragment. The one stone pair that resisted fragmentation down to 0.3 cm did have a dense rim on plain films. For those stones with a pigment band more than 1 mm thick on electron microscopy, fragmentation was significantly more difficult (2412 ± 1031 vs 1268 ± 493 shock waves) for 0.3 cm or less pulverization. This difference is significant at the .001 level ($t = 10.8$) and proves that lamination (seen on electron microscopy) reduces the ability to fragment stones even if it is not identifiable on plain films.

*Relationship Between Gallstone Architecture and Fragmentation Mechanism*

The treated gallstones exhibited three patterns of fragmentation. They chipped (1 mm or greater circumferential sections breaking off from the stone periphery), flaked (fragments less than 1 mm thick peeling off from the stone), or fractured radially toward the stone core and perpendicular to the surface (Table 1). All 12 stone families (24 stones) ultimately fractured radially. Six stone pairs initially broke radially. No variation within families was seen in this group. The remaining six families initially exhibited flaking or chipping of the stone periphery as we have defined it. Four stone families showed chipping of the surface before radial cleavage of the stone interior. In seven of eight stones, these chips broke from the stone surface on the side of the incoming shock waves (Fig. 4). Also in seven of eight of these stones, the first radial cleavage plane developed through an area where the surface rim had been eroded. The only intrafamily variation occurred in one stone where chips came from the rim but their precise origin could not be localized. For five stones, the fracture line developed first on the surface of the stone nearest the shock-wave generator. In three stones, it was not evident where the fracture line began. Two stone families (four stones) showed initial peripheral flaking. Radial fracture began in an area where the peripheral coat was eroded in one stone and through an area of intact rim in three stones. This group seemed to have the greatest intrafamily variation in that one stone of each pair showed continued flaking even after radial fragmentation.

The way in which the stones fragmented was partially predicted by stone morphology and architecture. All six stone families that peripherally chipped or flaked had rims (four pigment, two cholesterol) on electron microscopy and confirmed by FTIRS. The four stone families that chipped all had 1- to 3-mm rims (three pigment, one cholesterol), whereas

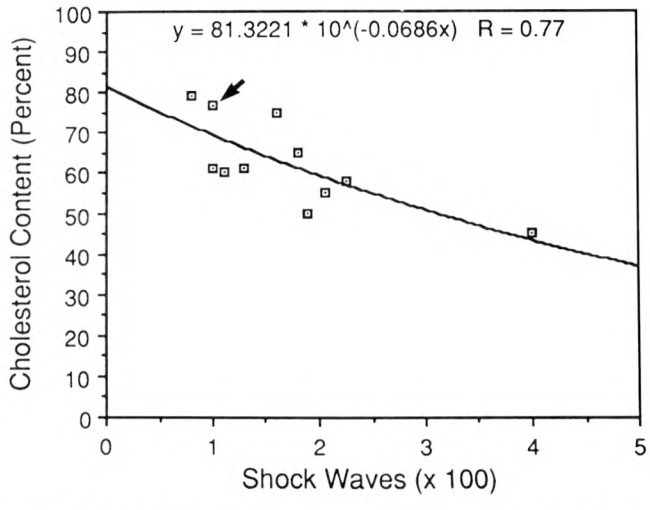



**Fig. 3.—Correlation plot of number of shock waves to produce stone fragments 0.3 cm or less vs global cholesterol content (fragmentation data are averaged for 12 stone pairs). Arrow indicates two overlapping data points.**



**Fig. 4.—Development of a fracture line after peripheral stone erosion. Initially, this stone showed peripheral flaking of its thin cholesterol coat (*small arrows*). In exposed area, a fracture line (*large arrow*) developed. With subsequent application of shock waves, radial cleavage occurred in this plane. (Stone was photographed in situ in phantom but has been rotated to show surface nearest shock-wave generator).**

the stones that flaked had rims thinner than 1 mm (one pigment, one cholesterol). Plain radiographs showed no predictive value in determining the way in which stones fragmented. Even electron microscopy was not specific in predicting the pattern of fragmentation; five families of stones showed peripheral rims but did not show chipping or flaking. Two of these had cholesterol rims, and one of these stone families had a 5-mm-thick pigment rim. The remaining stones that initially fractured radially were all homogeneous with radially oriented internal cholesterol crystals.

After normalizing the stone sizes for each family, the largest fragment size (as a percentage of original stone size) is plotted vs the number of shock waves at each observation interval (Fig. 5). Those stones that initially chipped showed an initial lag in fragmentation and have curves that generally lie to the right of the plot (families, 1, 2, 5, and 6; Fig. 5B). This suggests that an early lag may occur in observing pulverization of stones that initially chip. Once a broad area of the peripheral coat was eroded, significant diminution of the smaller more central portion of the stone took place. One stone pair (family 12) showed an initial lag in fragmentation despite radially fracturing. Regardless of the stone morphology or how it fragmented, all stone families, except Family 6, exhibited exponential decay in fragment size (r range from 0.92 to 1.00). Irrespective of the fragmentation mechanism, there always is a progressively diminishing return in fragment reduction with increasing numbers of shock waves for all stones.

## Discussion

Our work has clarified our understanding of how stones fragment and suggests a broad range of fragmentation responses to lithotripsy for families of stones that appear to meet existing protocol criteria for minimal or no calcification on plain radiographs. Within any single stone family, stones seem to exhibit a similar responsiveness to shock waves. Stone composition as determined by infrared spectroscopy and microstructure as depicted with scanning electron microscopy correlated with the fragmentation mechanism and relative rate of pulverization.

Stones that are predominantly composed of cholesterol break in two ways. They may initially cleave along radial fracture lines or initially chip or flake from their periphery. When stones cleave radially, the fragments resemble slices being cut from a pie. The shock waves appear to propagate parallel to the long axis of the crystal. Subsequently, fragments become smaller, and as they begin to separate they may break perpendicular to their long axis. A minority of stones exhibit chipping or flaking of their peripheral coats before radial fracture. We speculate that peripheral differences in regional composition may shield the stone interior from shock waves and could cause reduced transmission of shock-wave energy. Once the stone periphery has eroded, pulverization is seen to accelerate in these stones. Thus, stone lamination, especially with pigment, influences the mechanism of fragmentation, delays pulverization, and increases the difficulty in achieving fine pulverization. Stones with cholesterol rims or pigment bands less than 1-mm thick may still fracture radially.

Crystal analysis by using electron microscopy revealed the presence of a pigment or cholesterol rim in all six stone families that exhibited chipping or flaking in response to shock waves. In four of these six families, the peripheral rim was composed of interlocking plates of pigment arranged in a circumferential but somewhat disorganized manner. Pigment appears to be more randomly oriented and distinctly less repetitive and radially oriented than are interior cholesterol plates. In the remaining two families exhibiting a rim on electron microscopy, a thin band of radially oriented cholesterol plates was separated from the stone interior by a band of pigment less than 1 mm thick. Although these crystal appearances have been suggested previously on electron microscopy [6, 8, 9], our results are the first linking stone crystal structure to the way in which fragmentation occurs. Contrary to the claims of some vendors, we believe it is the stone and not solely the lithotripter power source or focal volume that determines the course of fragmentation [10].

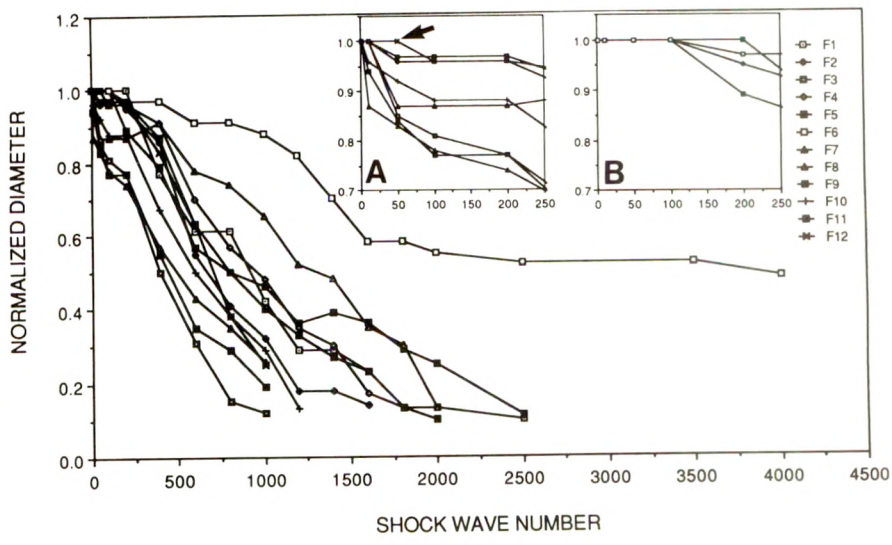



**Fig. 5.—Plot of fragment size vs number of shock waves necessary to achieve fragmentation for each stone family. Inset A represents stone families 3, 4, and 7–12. Inset B represents families 1, 2, 5, 6, or those families that showed initial "chipping" of fragments. Inset B illustrates an initial lag in fragmentation for these families. Only family 12 (*arrow*) showed a comparable lag despite a radial fragmentation pattern.**

It has been suggested that shock waves fragment stones because of their compressive effects and because of the cavitation effects they produce, resulting in surface erosion at the edge of a stone [11,12]. The cavitation effects are thought to act superficially and contribute to fragmentation through the violent expansion and collapse of microbubbles in surrounding bile. The shock wave itself is believed to transmit deep into the stone, with some component of the shock wave actually reflecting internally from the far edge of the stone [11, 13]. The shock wave may then produce mechanical stresses within the stone that exceed the stone's tensile strength. It is theorized that the displacement of fragments from the stone surface opposite the incoming shock wave plays a major role in fragmentation. This latter process is called spallation. Although our work did not determine whether or not shock waves are internally reflected within stones, *visible* spallation from the far stone surface was not seen. In those stones that showed peripheral erosion, this process began on the side of the stone nearest the incoming shock wave in all but one stone. In those stones that fractured radially, it was impossible to tell where the fracture line began but it usually traversed the entire stone diameter. We cannot exclude microscopic spallation in any of our stones, but macroscopic spallation was not evident and should be questioned as a major mechanism of fragmentation.

Even though our data suggest that it is the stone architecture that determines how stones break, it is unclear if the initial peripheral erosion occurring in some stones is due to the direct effects of shock waves, cavitation, or both. In those stones that initially break radially, it seems unlikely that surface cavitation alone could cause deep-seated radial fissures to develop. Stones can be fragmented while embedded in solid media with a high cavitation threshold [12], but they do not pulverize as finely as they do when they are surrounded by a fluid environment. This finding and our current observations suggest that once initial fragmentation has occurred, cavitation probably plays an increasing role as progressively smaller fragments with increasing surface area are produced. The cloud of multiple targets being bombarded with countless microbubbles most likely contributes to the exponential decay in fragment size that was observed. Fragment swirling and movement away from the shock-wave focal zone may further contribute to the diminishing return observed as pulverization proceeds [14].

Our data relating stone composition and fragmentation partially disagree with those of previous investigators [1, 2]. These groups found no relationship between fragmentation outcome and gallstone cholesterol content. The methods used in our study differed markedly from those of Schachler et al. [1]. Our stones represented a subset of stones that were lucent or minimally calcified on plain radiographs. Fragmentation was performed in a gallbladder-mimicking cavity surrounded by a phantom that attenuated shock waves and diffused their focus in a manner similar to liver parenchyma [7, 15]. Schachler and colleagues fragmented stones in water by using an intrinsically more powerful spark-gap device. The lack of an attenuating substance in the "blast path" used by Schachler et al. may have allowed unrealistically powerful shock waves to reach the treated stones. It could be argued that the power we used was too low, but the 380 bar we selected was only 60 bar less than the mean pressure we use for clinical gallstone treatments with our lithotripter. As our attenuating gel is more homogeneous than the multiple layers of subcutaneous and hepatic tissue a shock wave traverses in clinical treatment, we think the power level selection was justified. Although the global characteristics of the stones treated were presented by Schachler, the relative number of stones bearing rim or nidus pigment and calcification was not reported. The latter has an indirect effect on global cholesterol content and on the pattern and effectiveness of fragmentation. Recent clinical data suggest that calcified stones may be treated with lithotripsy but may not be as responsive to shock waves as their noncalcified counterparts are [16]. Our laboratory results agree with this observation in that stones containing pigmented bands often are of high density and harbor coexistent calcium.

Extrapolating the in vitro imaging characteristics of stones to clinical imaging and its relationship to fragmentation is complex. Specimen radiographs were superior to radiographs of the stones submerged in saline in depicting stone features (Fig. 1). The latter probably more closely mimics a plain film of the abdomen. In clinical practice gallstones are usually surrounded by attenuating tissue and fluid (bile). On specimen radiographs, no stones appeared isodense when surrounded by air, yet the majority of the same stones were isodense when surrounded by saline. Brink et al. [17] recognized this phenomenon in their work regarding the imaging characteristics of stones removed at cholecystectomy. They addressed this problem by assuming that only the densest stones would be evident on plain films. On the basis of our in vitro model, this is probably true, but it is also heavily dependent on the regional composition within stones. Caution must be used in extrapolating data from studies with specimen radiographs to clinical abdominal radiographs.

The current study suggests that stones that are lucent or minimally calcified on plain films can usually be fragmented, but variation in their cholesterol content and crystal structure produces a range of responsiveness to shock waves. Stones containing pigment bands or rims may lag in their initial pulverization and require additional shock waves. Stones from the same family are strikingly similar in their pattern and ease of fragmentation. In the laboratory, infrared spectroscopy and electron microscopy partially predict the pattern and effectiveness of gallstone fragmentation. Future investigation to determine whether or not CT can be used to detect features of stones in vivo that result in poor fragmentation may be valuable.

ACKNOWLEDGMENTS

The authors acknowledge Yvonne Carew for assistance in the preparation of this manuscript and David Martini for technical assistance.

REFERENCES


1. Schachler R, Sauerbruch T, Wosiewitz U, et al. Fragmentation of gallstones using extracorporeal shock waves: an in-vitro study. *Hepatology* **1988**;8:925–929
2. Schwab F, Albert M, Shehan C. Radiology of gallstones: in-vitro correlation with efficacy of shockwave lithotripsy. *Radiology* **1989**;173(P):204
3. Sackmann M, Delius M, Sauerbruch T, et al. Shockwave lithotripsy of gallbladder stones: the first 175 patients. *N Engl J Med* **1988**;318: 393–397
4. Trotman BW, Morris TA, Sanchez HM, Soloway RD, Ostrow JD. Pigment versus cholesterol cholelithiasis: identification and quantification by infrared spectroscopy. *Gastroenterology* **1977**;72:495–498
5. Wosiewitz U. Scanning electron microscopy in gallstone research. *Scan Electron Microsc* **1983**;1:419–430
6. Spiro H. Gallbladder and biliary duct disorders. In: *Clinical gastroenterology*. New York: Macmillan, **1983**:1068–1072
7. Davros WJ, Zeman RK, Garra BS. Tissue mimicking phantom for use in studying the effects of lithotripsy on gallstones. *Radiology* **1988**;169(P):380
8. Been JM, Bills PM, Lewis D. Microstructure of gallstones. *Gastroenterology* **1979**;76:548–555
9. Osuga T, Mitamura K, Miyagawa S, Sata N, Kintaka S, Portman OW. A scanning electron microscopic study of gallstone development in man. *Lab Invest* **1974**;31:699–704
10. Ferrucci JT. Biliary lithotripsy: 1989. *AJR* **1989**;153:15–22
11. Delius MK, Brendel W. Mechanisms of action in extracorporeal shockwave lithotripsy. In: Ferrucci JT, Delius MK, Burhenne MJ, eds. *Biliary lithotripsy*. Chicago: Year Book Medical, **1989**:31–42
12. Zeman RK, Davros WJ, Garra BS, Horii SC. Cavitation effects during lithotripsy: I. Results of in-vitro experiments. *Radiology* **1990**;177:157–161
13. Forrsmann B, Hepp W, Chaussy C, et al. Eine methode zur beruehrungsfreien zertruemmerung von nierensteinen durch stosswellen. *Biomed Tech* **1977**;22:164–168
14. Zeman RK, Davros WJ, Garra BS, et al. The relationship between stone motion, targeting, and fragmentation during experimental biliary lithotripsy. *Radiology* **1990**;176:125–128
15. Hall TJ, Cox GG, Insana MF, Soller NM, Rosenthal SJ. A phantom for studying pressure distributions in extracorporeal shockwave lithotripsy. *Radiology* **1989**;173(P):472
16. Rawat B, Burhenne HJ. Extracorporeal shockwave lithotripsy of calcified gallstones: work in progress. *Radiology* **1990**;175:667–670
17. Brink JA, Simeone JF, Mueller PR, Richter JM, Prien EL, Ferrucci JT. Physical characteristics of gallstones removed at cholecystectomy: implications for extracorporeal shock-wave lithotripsy. *AJR* **1988**;151:927–931



Radiology Outreach Foundation

The Radiology Outreach Foundation (ROF) is a nonprofit corporation whose goal is to help disadvantaged countries improve their health care by providing radiology equipment, books, consultation, education, and training to their practitioners. This assistance is on an application basis that is independent of political, ethnic, or religious orientation of the grantee. It depends on the need of the people and the ability of the ROF to meet that need. The ROF is approved by the U.S. Internal Revenue Service as a tax-exempt organization. It is endorsed by the following radiologic societies: American Association of Women Radiologists, American College of Radiology, American Roentgen Ray Society, Association of University Radiologists, Radiological Society of North America, Society of Chairmen of Academic Radiology Departments, Society for Pediatric Radiology, European Society of Pediatric Radiology.

All donations to the ROF are tax deductible. Persons who would like to contribute financially to the ROF, would be interested in being a visiting professor, would like to send books or journals to any of the institutions supported by the ROF, or would like further information about the ROF should write to Charles A. Gooding, M.D., President, Radiology Outreach Foundation, 3415 Sacramento St., San Francisco, CA 94118 USA.

# Book Review

**Radionuclides in Nephro-Urology.** Edited by M. Donald Blaufox, Norman K. Hollenberg, and Claude Raynaud. (Vol. 79 in Contributions to Nephrology. Series editors: G. M. Berlyne and S. Giovannetti.) New York: Karger, 232 pp., 1990. $128.75

This book is the proceedings of the 7th International Symposium on Radionuclides in Nephro-Urology, held during May 1989. This 1-week meeting focused on radiopharmaceuticals, applications of radionuclides in children, and the role of nuclear medicine in the evaluation of renovascular hypertension. Forty-three papers were presented, including a special invited paper on hypertension and three reports on collaborative studies. This compendium of basic and clinical research is targeted to nephrologists, urologists, pediatricians, and nuclear medicine specialists. Content and clinical usefulness are of sufficient merit to recommend it to each of these subspecialists, with the possible exception of nonacademic pediatricians. The number of images is surprisingly small, but they are of good quality, as are the diagrams and tables.

The first section is on radiopharmaceuticals and concentrates primarily on $^{99m}$Tc-mercaptoacetylglycylglycylglycine ($^{99m}$Tc-MAG$_3$). It presents experimental data on the chemistry and physiology of $^{99m}$Tc-MAG$_3$ and compares it with the current most popular renal tubular agent, Hippuran. Unfortunately, most of the papers presume previous knowledge of the mechanisms of action of $^{99m}$Tc-MAG$_3$ and therefore are not aimed at the general radiologist or practicing nephrologist or urologist. Although this section is somewhat specialized, it does expose the reader to what may become a widely used radiopharmaceutical, especially useful for studies of renal function, evaluation of renal transplants, and, perhaps, studies of renovascular hypertension. The final paper in this section discusses an interesting application of thallium for renal evaluation during cardiac studies.

The second section, "Renal Function," is more research than clinically oriented. This does not diminish its value; the data are presented clearly. Important points are made about the importance of adequate hydration before clearance studies and diuretic renography; the potential problem of a single, global measurement of glomerular filtration rate, and diabetic patients. Nuclear medicine specialists with an interest in physiology and basic research will find this section quite valuable.

Section 3, "Renal Imaging," contains excellent information for the clinician. The papers on diuresis renography, renal mobility, and use of $^{99m}$Tc-MAG$_3$ in imaging renal transplants are especially illuminating, relevant, and practical. The data presented in this section, in general, can be applied to clinical practice by most nuclear medicine specialists as well as by radiologists. Images, graphs, and tables are of excellent quality and relevance in this section.

The section on imaging children is of limited scope. Much of the data is academic rather than clinical and focuses heavily on the use of dimercaptosuccinic acid. Although this radiopharmaceutical is extremely valuable in assessing renal volume and renal scarring, it is a relatively unfamiliar agent to most pediatricians. A comparison of conventional Lasix (furosemide) diuresis renography with direct intrapelvic infusion renography appropriately advises caution with diuresis renography.

The final two sections, "Hypertension" and "Special Reports of Collaborative Studies in Captopril Renography," are devoted to the use of inhibitors of angiotensin-converting enzymes in the evaluation of suspected renovascular hypertension. A good review of the subject would be welcome at the beginning of this section. The various authors put the problem of diagnosis of renovascular hypertension into proper perspective and as a group address existing issues: radiopharmaceutical of choice, parameters for evaluation, false positives and false negatives, selection of patients, dose of captopril, protocols, complications, and so forth. Although no consensus exists as yet, multicenter trials are discussed and give the reader some hope that some order will come soon from the current conflicting recommendations.

In summary, this work should be a nice addition to the library of large departments and academic institutions. It clearly is directed at those with sound basis in renal physiology and radiopharmaceutical chemistry. Its cost and significant investigational bent limit widespread potential (e.g., general pediatrics, smaller nuclear medicine departments). Despite this, *Radionuclides in Nephro-Urology* is a concise, well-edited, in-depth delineation of the current, most exciting topics in radionuclide renal imaging.

Michael S. Kipper
*North County Medi-Scan*
*Vista, CA 92083*

# Natural History of Acquired Renal Cystic Disease in Dialysis Patients: A Prospective Longitudinal CT Study

Errol Levine[1]
Sharon L. Slusher[2]
Jared J. Grantham[2]
Louis H. Wetzel[1]

**Patients with end-stage kidney disease, particularly those treated with dialysis, develop proliferative processes in their native kidneys that result in the formation of multiple acquired renal cysts, renal adenomas, and carcinomas. Data about these abnormalities have been acquired mainly from retrospective studies. We undertook a longitudinal prospective study in which the native kidneys of 30 dialysis patients were surveyed by serial CT during a 7-year period to study the natural history of acquired renal cystic disease and the frequency of associated complications. Acquired cysts were seen in 87% of patients at the end of the study compared with 57% at the study's onset, and a significant increase was seen in mean renal volume with time. Five patients (17%) developed large hemorrhagic renal cysts and four (13%) developed large perinephric hematomas. Renal cell carcinomas developed in two patients (7%) without renal symptoms. One carcinoma invaded the renal capsule, but did not cause metastases. The other carcinoma was widely metastatic. Our findings are consistent with those of earlier studies documenting an increased prevalence of renal cell carcinoma in dialysis patients as compared with the general population. However, our conclusions are limited because the study sample is small and no control population was studied.**

**We conclude that acquired renal cystic disease in dialysis patients is a progressive disorder often associated with cyst hemorrhage. Dialysis patients may also have an increased prevalence of renal cell carcinoma.**

***AJR* 156:501–506, March 1991**

As surviving nephrons decrease in number in patients with chronic renal insufficiency, renotropic factors are thought to accumulate, causing nephron and collecting duct hyperplasia [1]. Prolonged renotropic stimulation is believed to cause renal cyst formation and renal neoplasms. This process is most pronounced in dialysis patients. Indeed, acquired renal cystic disease appears to be an almost inevitable accompaniment of prolonged dialysis, occurring in up to 90% of patients treated with dialysis for 10 years or more [2]. By itself, this entity is of limited clinical significance, although some patients develop cyst and perinephric hemorrhage, cyst infection, renal calculi, and renal neoplasms [1–3]. Accordingly, some investigators have recommended periodic imaging of the native kidneys of long-term dialysis patients [2, 4, 5]. However, data about complications of acquired renal cystic disease have been derived mainly from retrospective studies, and it is not clear how significantly the disorder influences the morbidity and mortality of dialysis patients [6]. Therefore, we undertook a longitudinal prospective CT study of the native kidneys of a small group of dialysis patients to study the natural history of acquired renal cystic disease and the frequency of associated complications.

## Subjects and Methods

In January 1983 we started obtaining serial CT scans of the native kidneys of some of our dialysis patients. Criteria for scanning included patients' willingness to undergo CT, no history

Received July 5, 1990; accepted after revision September 27, 1990.

Presented at the annual meeting of the Society of Uroradiology, Vancouver, B.C., September 1990.

[1] Department of Diagnostic Radiology, 2-169 Bell Memorial Hospital, University of Kansas Medical Center, 39th St. and Rainbow Blvd., Kansas City, KS 66103. Address reprint requests to E. Levine.

[2] Department of Medicine, Division of Nephrology, University of Kansas Medical Center, Kansas City, KS 66103.

0361–803X/91/1563–0501
© American Roentgen Ray Society

of underlying renal cystic disease or of previous contrast reactions, and the presence of both native kidneys. By April 1986, initial CT scans had been obtained in 53 patients. We defined our population for the current study as all patients who had at least two CT scans between January 1983 and March 1990. Thirty-eight patients fulfilled this criterion. Of the 15 patients who did not have follow-up CT scans, eight died during the study period and seven were lost to follow-up. Another eight patients who had satisfactorily functioning renal transplants for more than 6 months during the study period also were excluded from the analysis. Consequently, the final study group consisted of 30 patients, in whom 88 abdominal CT scans were obtained (mean, 2.9 scans per patient). Scans were obtained at about 2-year intervals (78 scans) or when patients developed abdominal pain or hematuria during follow-up (10 scans). The total and mean follow-up periods between the first and last CT scans in the 30 patients were 1658 and 55.3 months (SEM, ±4.2), respectively. The endpoint of the study for each patient was defined as the time of the last CT scan, and ages, duration of dialysis, and other data were calculated at this time.

The study group consisted of 18 men and 12 women 29–80 years old (mean, 50 years). Fifteen were black, 13 were white, one was Oriental, and one was American Indian. Twenty-four were treated with hemodialysis, two with peritoneal dialysis, and four with both methods. Renal biopsies in 16 patients revealed chronic glomerulonephritis in eight, tubulointerstitial nephropathy in three, lupus nephritis in two, toxic nephritis in one, amyloid in one, and hereditary nephritis in one. Of 14 patients in whom diagnosis of the original renal disease was made clinically, 11 had presumed hypertensive nephrosclerosis and three had diabetic nephropathy. Eleven patients received renal transplants that underwent acute rejection, so their serum creatinine levels never returned to normal.

All patients underwent CT on a General Electric 8800 or 9800 scanner (General Electric Medical Systems, Milwaukee, WI) or a Siemens DRH scanner (Siemens Medical Systems, Iselin, NJ) after informed consent was obtained. Eight-three of 88 CT scans were obtained with and without IV contrast enhancement by using 150 ml of meglumine diatrizoate (60%) or 150 ml of iohexol (300 mg I/ml) administered by drip infusion. IV contrast medium was not used in five instances when patients had cardiac failure. None of the patients who received IV contrast medium experienced any adverse effects. Contiguous 8- or 10-mm sections of the kidneys were obtained routinely. When necessary, additional 4- or 5-mm sections were obtained. Eight patients in whom CT findings suggested possible renal neoplasms were evaluated with sonography also by using commercially available real-time scanners with 3.5- and 5.0-MHz transducers.

All CT scans were evaluated for the presence of cysts and neoplasms. The progression of acquired renal cystic disease was evaluated by counting the number of cysts per kidney in each patient on the first and last CT scans. Each patient was assigned to one of three groups: (1) those with no cysts, (2) those with occasional cysts (fewer than five per kidney), and (3) those with multiple bilateral renal cysts (i.e., acquired renal cystic disease). The length (l), width (w), and anteroposterior dimension (AP) were recorded for both kidneys in each patient on the first and last CT scans. The volume (V) of each kidney was estimated according to the modified equation for an ellipsoid, namely, $V = 0.49 \times l \times w \times AP$. A mean renal volume was determined for each patient on the first and last CT scans from the estimated values for the two kidneys. Medical records of all patients were analyzed to determine duration of dialysis, and when relevant, data and cause of death. We did not analyze total duration of renal failure before dialysis, because data regarding this aspect usually were unavailable.

## Results

### *Clinical and CT Findings*

By the end of the study in March 1990, 16 patients (53%) were alive and 14 (47%) had died. Causes of death included acute myocardial infarction (three), congestive heart failure (one), pneumonia (two), septicemia (two), cancer (four), bowel infarction (one), and pulmonary thromboembolism (one). Autopsies were performed in six patients. Among the patients who died of cancer, two had pancreatic carcinoma, one had ovarian carcinoma, and one had metastatic renal cell carcinoma.

As evaluated on CT scans at the completion of the study, four patients (13%) showed no renal cysts and were assigned to group 1. Nine (30%) had fewer than five cysts per kidney and were classified under group 2. Seventeen patients (57%) had acquired renal cystic disease and were assigned to group 3. The mean ages of the patients in groups 1–3 were 59.5, 51.1, and 47 years, respectively. These means did not differ significantly ($p > .05$, one-way analysis of variance test). The total and mean durations of dialysis for the 30 patients at the end of the study were 2941 and 98 months (SEM, ±7.2), respectively. The mean durations of dialysis for groups 1–3 were 66.3 months (SEM, ±21.5), 83.0 months (SEM, ±8.0), and 113.5 months (SEM, ±9.5), respectively. Only groups 1 and 3 differed significantly in this regard ($p < .05$, one-way analysis of variance test). The three groups did not differ significantly in duration of CT follow-up.

The mean renal volumes for groups 1–3 as evaluated on the last CT scans were 38.8 $cm^3$ (SEM ± 4.2), 59.7 $cm^3$ (SEM, ±7.7), and 225.1 $cm^3$ (SEM, ±40.0), respectively. The mean renal volume for group 3 was significantly greater than that of either group 1 or 2 ($p < .05$, one-way analysis of variance test). The mean renal volume of normal kidneys is about 330 $cm^3$ (SD, ±84) [7].

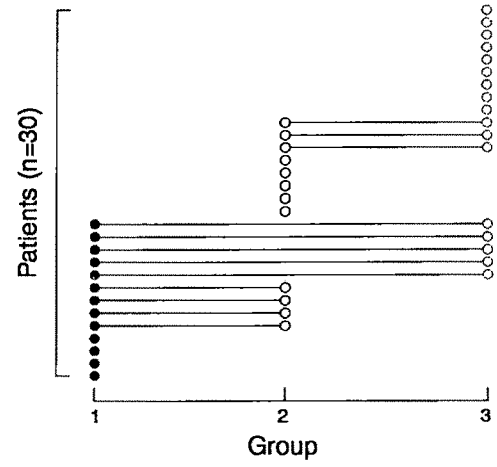



**Fig. 1.—Increase in acquired renal cysts in 30 dialysis patients during study period. Group 1 patients had no cysts, group 2 had occasional cysts (fewer than five per kidney), and group 3 had multiple bilateral renal cysts (acquired renal cystic disease). Status of each patient at beginning and end of study is shown.**

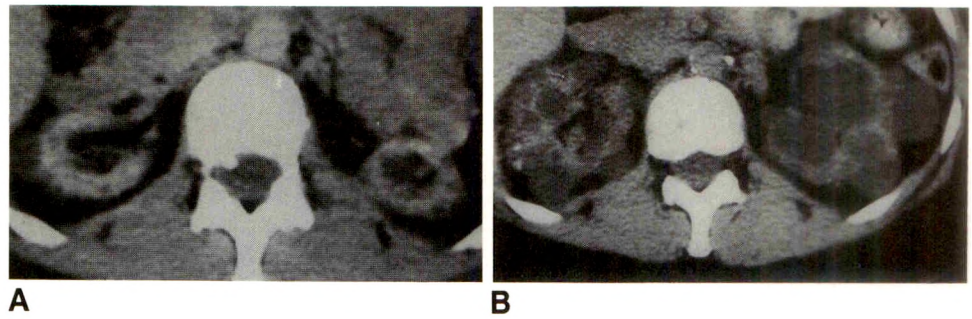



**Fig. 2.—Acquired renal cystic disease in 45-year-old man on hemodialysis.**

***A*, Contrast-enhanced CT scan after 4 years of dialysis shows bilateral small cysts in shrunken kidneys (mean renal volume = 64 $cm^3$).**

***B*, Follow-up CT scan 4 years later shows enlargement of cysts and kidneys (mean renal volume = 412 $cm^3$).**

*Progression of Renal Cystic Disease*

As evaluated on their first CT scans, 13 patients (43%) were assigned to group 1, eight (27%) to group 2, and nine (30%) to group 3. At the time of the last CT scan, progression of renal cystic involvement was seen in many patients, with four patients (13%) assigned to group 1, nine (30%) to group 2, and 17 (57%) to group 3 (Figs. 1 and 2). The mean renal volume for the 30 patients at the beginning of the study was 78.9 $cm^3$ (SEM, ±17.0) and the mean volume at the end of the study was 150.6 $cm^3$ (SEM, ±27.5). This represents a significant increase in mean volume with time ($p < .05$, two-sample t test). Changes in mean renal volume in individual patients are shown in Figure 3.

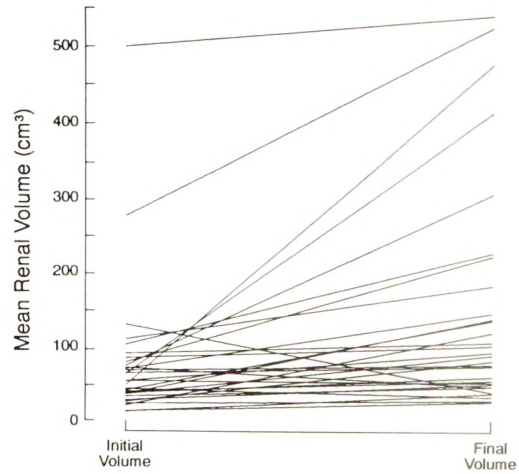



**Fig. 3.—Changes in mean renal volume in 30 dialysis patients during study period with volume measurements obtained from first and last CT scans. Normal renal volume = 330 $cm^3$ (SD, ±84).**

*Cyst Hemorrhage and Perinephric Bleeding*

Hemorrhagic cysts were seen in 15 (50%) of 30 patients. All had acquired cystic disease. In 10 patients (33%), one or more hemorrhagic cysts smaller than 2 cm were seen on CT. Five patients (17%) had larger hemorrhagic cysts ranging in size from 2 to 5 cm (Fig. 4). Differentiation of these lesions from renal neoplasms on CT was suggested by absence of contrast enhancement. Sonography was performed in all five patients. In one, the lesion had disappeared, suggesting rupture of a hemorrhagic cyst into the collecting system; disappearance of the lesion was confirmed by CT. In four patients, the lesions were anechoic on sonography and resolved on follow-up CT. Four patients (13%), all with acquired cystic disease, developed large perinephric hematomas during follow-up (Fig. 5). Two were managed conservatively and the hematomas resolved completely on serial CT, without evidence of underlying renal neoplasms. Two patients underwent nephrectomies because of persistent bleeding. The bleeding was thought to be due to cyst hemorrhage, and neither had an underlying renal neoplasm.

*Renal Neoplasms*

Histologically proved renal cell carcinomas developed in two (7%) of 30 patients. One, a 46-year-old man with renal failure due to chronic glomerulonephritis, had been treated with hemodialysis for 120 months. His first CT scan showed acquired renal cystic disease without evidence of renal neoplasm. A CT scan 24 months later in the absence of renal symptoms showed a left-sided renal cell carcinoma with lymph node metastases (Fig. 6). A left nephrectomy confirmed a poorly differentiated multifocal renal cell carcinoma with nodal metastases. Chest CT showed pulmonary metastases. He died 5 months later owing to pulmonary and cerebral metastases, confirmed at autopsy. Another patient, an 80-year-old man with renal failure due to hypertensive nephrosclerosis, had been treated with hemodialysis for 53 months. His first CT scan showed small kidneys without cysts or neoplasms. A CT scan 25 months later in the absence of renal symptoms showed acquired cystic disease and an enhancing right renal mass (Fig. 7). Sonography confirmed its solid nature. The patient was unfit for surgery because of congestive heart failure that caused his death 6 months later. Autopsy confirmed a papillary renal cell carcinoma with capsular invasion but without metastases. A third patient has a solid 2.5-cm renal mass. Surgery has not been performed because of her poor general medical condition, and she is being followed up with serial CT at 6-month intervals.

## Discussion

Acquired cystic disease is a bilateral disorder that develops in end-stage kidneys [1, 2]. Our study confirms its progressive

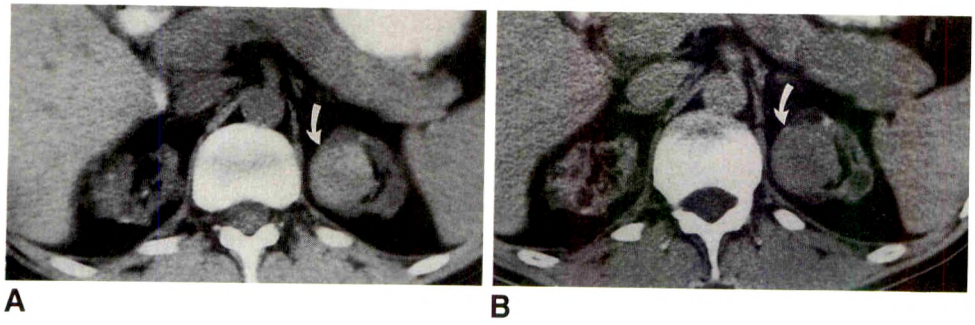



Fig. 4.—Acquired renal cystic disease with cyst hemorrhage in a 41-year-old man with gross hematuria.

*A*, Unenhanced CT scan shows 3.8-cm high-density (44 H) mass (*arrow*) in upper pole of left kidney.

*B*, After contrast enhancement, attenuation value of mass (*arrow*) was 43 H. Note multiple bilateral renal cysts. Mass had resolved completely on follow-up CT.

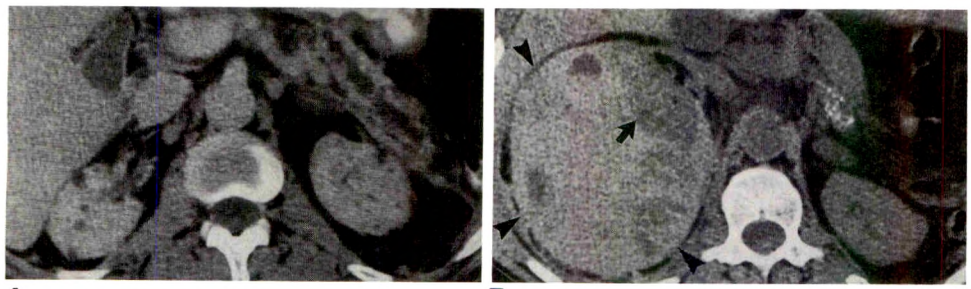



Fig. 5.—Large perinephric hematoma complicating acquired renal cystic disease in a 55-year-old man managed by hemodialysis for 41 months.

*A*, Contrast-enhanced CT scan shows multiple bilateral small renal cysts. Dilated pancreatic duct is associated with chronic pancreatitis.

*B*, Unenhanced CT scan 5 months later during episode of acute flank pain shows perinephric hematoma (*arrowheads*) causing anterior displacement of right kidney (*arrow*).

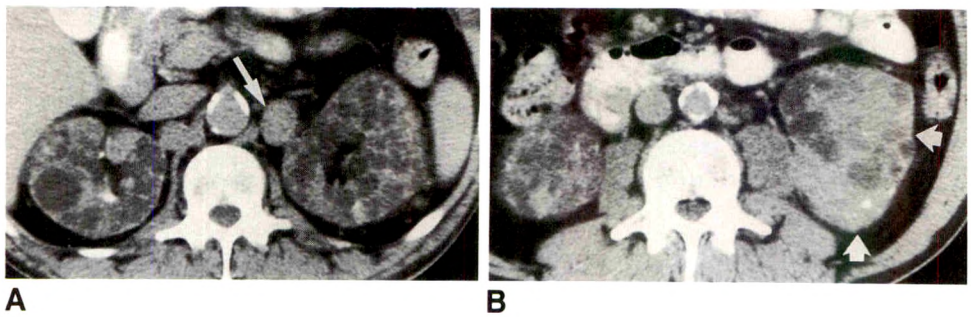



Fig. 6.—Acquired renal cystic disease and metastatic renal cell carcinoma in 46-year-old man managed by hemodialysis for 120 months.

*A*, Contrast-enhanced CT scan shows multiple renal cysts and nephromegaly (mean renal volume = 542 $cm^3$). Enlarged left renal hilar lymph node (*arrow*).

*B*, Caudal CT scan reveals two solid masses (*arrows*) in lower pole of left kidney. Masses enhanced by 30 H.

(Reprinted with permission from Levine and Grantham [8].)

nature. At the completion of the study, 57% of patients were shown to have acquired renal cystic disease, compared with 30% of patients when the study began (Fig. 1). If all patients with cysts are counted, 87% had renal cysts at the completion of the study compared with 57% at the study's onset (Fig. 1). In addition, significant increases in mean renal volume were seen in many patients with time (Figs. 2 and 3). Increases in renal volume with time in dialysis patients usually are due to cyst development and/or enlargement [7]. Our study also confirms a clear relationship between the occurrence of acquired renal cystic disease and increasing duration of dialysis.

Cyst hemorrhage is common in acquired renal cystic disease and may cause gross hematuria, flank pain, and renal colic [2]. In 15 patients (50%), all with acquired renal cystic disease, hemorrhagic cysts were seen on CT. Five of these were large, varying in size from 2 to 5 cm (Fig. 4). Differentiation between cyst hemorrhage and neoplasm was based on absence of contrast enhancement on CT, anechoicity on sonography, and resolution of lesions on serial imaging. Large perinephric hematomas, as occurred in four patients (13%), usually result from rupture of hemorrhagic cysts (Fig. 5) [9]. Heparinization during hemodialysis and bleeding disorders may predispose to this complication [9]. None of the patients with perinephric hematomas had underlying renal neoplasms, as compared with nondialysis patients in whom spontaneous perinephric hemorrhage is associated with renal cell carcinoma in about 56% of cases [10]. Patients with retroperitoneal hemorrhage usually can be treated successfully with bed rest, analgesics, blood transfusions, and correction of coagulation or bleeding abnormalities [9]. If bleeding is not controlled by these means, therapeutic renal artery embolization or nephrectomy may be necessary. Patients managed conservatively should be followed by serial CT until the hematoma has resolved to exclude an underlying neoplasm.

Two histologically proved renal carcinomas were detected in our study during 1658 months of follow-up by CT. This represents an annual incidence of 0.048%. Prolonged duration of dialysis is an important risk factor for the development of renal cell carcinoma [2]. Consequently, the incidence of carcinoma also may be expressed in terms of patient-years of dialysis at risk. In our patients with a total duration of dialysis of 2941 months, the annual incidence of carcinoma

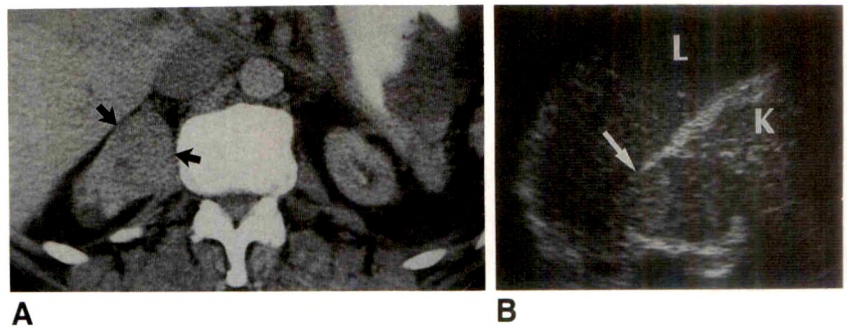



**Fig. 7.—Renal cell carcinoma in 80-year-old man managed by hemodialysis for 53 months.**

***A*, Contrast-enhanced CT scan shows 4.2-cm mass (*arrows*) in upper pole of right kidney. Mass enhanced by 23 H. Note small cysts posteriorly in right kidney and atrophy of left kidney.**

***B*, Longitudinal sonogram of right kidney (K) shows echogenic mass (*arrow*) in upper pole. L = liver.**

was 0.027%. Accordingly, depending on the method of calculation, the annual incidence of renal cell carcinoma among our patients was 0.027–0.048%. The significance of these data is limited because the study sample was small and no control population was studied. However, our findings suggest that the annual incidence of renal carcinoma among dialysis patients is three to six times greater than the age-adjusted annual incidence of 0.008% of renal cell carcinoma among the general population in the United States [11]. This finding is consistent with that of the Michigan Kidney Registry, which recently reported six invasive renal cell carcinomas (0.144%) in 4161 dialysis patients [3]. This represents a fivefold increase in renal cell carcinoma in dialysis patients compared with the general population from the same geographic area [3]. The annual incidence of renal cell carcinoma among Japanese dialysis patients is about 40 times greater than the expected rate [2].

Small renal neoplasms (3 cm or less) are significantly more common than invasive or metastatic carcinomas in dialysis patients [1]. Although these are often considered to be adenomas, they cannot be distinguished from larger neoplasms histologically and some evolve into invasive carcinomas [9]. Few data are available regarding the frequency of metastatic renal cancer in dialysis patients. Our previous review of 14 long-term dialysis series showed that 43 (7%) of 601 patients had renal tumors, but only two patients (0.33%) had metastatic neoplasms [1]. Of 234 renal carcinomas in 80,553 Japanese dialysis patients, about 20% of neoplasms were metastatic, and the frequency of metastatic carcinoma in the entire patient group was about 0.05% [2]. At least 36 reported deaths have been attributed to metastatic renal cell carcinoma among dialysis patients [2].

Various investigators have suggested that periodic imaging should be used to monitor the status of the native kidneys of dialysis patients [2, 4, 5]. However, the value of routine renal screening has been questioned because of lack of data about the effect of screening on patient outcome [6]. We screened our patients with CT at about 2-year intervals. In one patient, no evidence of a renal neoplasm was seen on the first CT scan, but metastatic renal cell carcinoma was found when the patient was reevaluated 24 months later (Fig. 6). Accordingly, it is likely that a program designed to detect neoplasms at a curable stage requires at least annual screening. Screening may be done with either CT or sonography. However, fibrotic shrunken end-stage kidneys are difficult to image with sonography [5], and we prefer CT for screening purposes, supplemented by sonography when necessary. In the absence of contraindications to IV contrast administration, CT scans should always be obtained with and without contrast enhancement. Contrast administration helps greatly in differentiating between hemorrhagic cysts and neoplasms and, in our experience, does not have any harmful effects in patients receiving regular dialysis treatments [4].

The annual costs of the Medicare-funded long-term dialysis program are high. In December 1987, 94,352 patients in the United States were being treated with either hemodialysis or peritoneal dialysis [12]. The 1987 Medicare cost per patient treatment was $26,000 per year [12]; ancillary costs may add another $20,000 per patient per year [6]. Those investigators who have recommended periodic renal imaging in dialysis patients believe that screening should start after completion of 3 years of dialysis [1, 5]. Annual CT screening of all long-term dialysis patients after 3 years would add about $36 million (60,000 patients at $600 per CT examination) to the Medicare budget [6]. Available data do not suggest that such an expense is justified. The small number of patients in our study precludes the derivation of the kind of data necessary to formulate policy. However, the mortality rate of the 30 patients during our survey was 47%. In 1986 the average life expectancy for persons beginning dialysis in the United States was 4 years [12]. For dialysis patients 65 years and older it was shorter, 2.5 years. Because renal cell carcinoma is a relatively rare cause of death among dialysis patients, it therefore seems unlikely that an aggressive renal imaging program will significantly reduce the mortality of dialysis patients.

Although neither of our two patients with renal carcinoma benefited from tumor detection by serial imaging, our study and studies by other investigators [2, 3] suggest an increased prevalence of renal cell carcinoma among dialysis patients. Physicians treating dialysis patients, therefore, need to retain a high awareness of this potential complication. The occurrence of hematuria, flank pain, or any unexplained fever or systemic illness in dialysis patients constitutes an indubitable indication for renal imaging. Also, it is possible that further research may identify a subset of dialysis patients in whom annual renal imaging may be performed in a cost-effective manner. A primary consideration should be the general medical condition of each individual patient. As indicated by one of our patients, the discovery of a renal cell carcinoma in an elderly unfit patient may have no effect on patient management or prognosis. On the other hand, a patient with a good

general medical condition may benefit greatly if imaging shows a renal neoplasm when it is still localized to the kidney and can be resected completely.

Known risk factors for carcinoma may also help identify those patients who may benefit from renal imaging. These include prolonged dialysis, the presence of acquired renal cystic disease, large kidneys, and male sex [2]. In a Japanese survey, 77% of 226 renal carcinomas occurring in dialysis patients affected those with acquired cystic disease, and the mean duration of dialysis in patients with carcinoma was about 83 months [2]. Renal cell carcinoma occurring in dialysis patients is about four times more common in men than in women [2]. The mean age of dialysis patients with renal cell carcinoma is about 50 years, which is about 10 years younger than that of patients with renal carcinoma in the general population [2, 3].

In conclusion, acquired renal cystic disease is a progressive disorder among dialysis patients. Cyst hemorrhage and perinephric hemorrhage are important complications of the disorder. Dialysis patients also may have an increased rate of renal cell carcinoma. However, the available evidence shows no justification for the high cost of an annual renal imaging program in *all* dialysis patients. Our study sample is too small to permit any final conclusions, and further research is needed. However, we believe that with more extensive studies it may be possible ultimately to define a subset of dialysis patients in whom serial renal imaging may be performed in a cost-effective manner. Such a selective screening program may reduce preventable deaths due to renal cell carcinoma in dialysis patients.

REFERENCES

1. Grantham JJ, Levine E. Acquired cystic disease: replacing one kidney disease with another. *Kidney Int* **1985**;28:99–105
2. Ishikawa I. Acquired renal cystic disease. In: Gardner KD, Bernstein J, eds. *The cystic kidney*. Dordrecht, the Netherlands: Kluwer Academic, **1990**:351–377
3. Port FK, Ragheb NE, Schwartz AG, Hawthorne VM. Neoplasms in dialysis patients: a population-based study. *Am J Kidney Dis* **1989**;14:119–123
4. Levine E, Grantham JJ, Slusher SL, Greathouse JL, Krohn BP. CT of acquired cystic kidney disease and renal tumors in long-term dialysis patients. *AJR* **1984**;142:125–131
5. Taylor AJ, Cohen EP, Erickson SJ, Olson DL, Foley WD. Renal imaging in long-term dialysis patients: a comparison of CT and sonography. *AJR* **1989**;153:765–767
6. Mindell HJ. Imaging studies for screening native kidneys in long-term dialysis patients. *AJR* **1989**;153:768–769
7. Ishikawa I, Saito Y, Onouchi Z, et al. Development of acquired cystic disease and adenocarcinoma of the kidney in glomerulonephritic chronic hemodialysis patients. *Clin Nephrol* **1980**;14:1–6
8. Levine E, Grantham JJ. Radiology of cystic kidneys. In: Gardner KD, Bernstein J, eds. *The cystic kidney*. Dordrecht, the Netherlands: Kluwer Academic, **1990**:171–206
9. Levine E, Grantham JJ, MacDougall ML. Spontaneous subcapsular and perinephric hemorrhage in end stage kidney disease: clinical and CT findings. *AJR* **1987**;148:755–758
10. Belville JS, Morgenthaler A, Loughlin KR, Tumeh SS. Spontaneous perinephric and subcapsular renal hemorrhage: evaluation with CT, US and angiography. *Radiology* **1989**;172:733–738
11. Resseguie LJ, Nobrega FT, Farrow GM, Timmons JW, Worobec TG. Epidemiology of renal and ureteral cancer in Rochester, Minnesota, 1950–1974, with special reference to clinical and pathologic features. *Mayo Clin Proc* **1978**;53:503–510
12. *National kidney and urologic diseases advisory board 1990 long-range plan: window on the 21st century*. Washington, DC: U.S. Department of Health and Human Services, **1990**:30–34, 183–186. National Institutes of Health publication 90-583

# Arteriovenous Fistulas Complicating Biopsy of Renal Allografts: Treatment of Bleeding with Superselective Embolization

N. M. deSouza[1]
J. F. Reidy[1]
C. G. Koffman[2]

**The use of superselective embolization was assessed as a treatment for bleeding from postbiopsy arteriovenous fistulas (AVFs) in renal transplants. AVFs commonly occur after biopsy procedures in renal transplants, but severe bleeding is rare. Transcatheter embolization can be used to control bleeding, but unless it is sufficiently selective, the procedure results in loss of significant amounts of renal parenchyma. During a 4-year period, embolization procedures were attempted in seven patients 30–65 years old. All had AVFs shown on arteriography. Five patients underwent embolization; occlusion occurred only in the branch supplying the AVF. In one patient with three large AVFs, two were found to have occluded the day after embolization was attempted. In another, an AVF occluded when superselective catheter position was achieved but before embolization. Catheter manipulation in these cases may have precipitated occlusion. In five cases, coaxial embolization techniques were used. Embolization materials consisted of coils in three cases: 0.038 in. (0.97 mm) in one case, 0.025 in. (0.64 mm) in one case, 0.018 in. (0.46 mm) in one case; 0.038 in. (0.97 mm) coils and gelatin foam particles in one case; and localized contrast extravasation in one case. Serum creatinine level was measured before and after embolization in all patients, and radionuclide studies were undertaken in three cases. In all patients, bleeding was effectively controlled. None of the patients showed an increase in serum creatinine level after embolization, and in four, significant improvement was seen. Nuclear medicine studies showed no loss of renal function and a dramatic improvement in one patient. No complications due to the procedure were seen.**

**Our experience suggests that superselective embolization with coaxial catheter techniques is an effective method of treating bleeding from postbiopsy AVFs in renal transplants with minimal loss of renal parenchyma.**

*AJR* 156:507–510, March 1991

Hemorrhage from arteriovenous fistulas (AVFs) is a well-known complication of renal biopsy that usually requires only conservative treatment. However, when severe bleeding occurs after biopsy, the patient's life and graft survival are threatened. Surgical treatment usually entails nephrectomy. Published reports of superselective renal embolization are largely concerned with native kidneys [1–6]. We report seven cases in which superselective transcatheter embolization in renal allografts was used effectively as a means of controlling bleeding while allowing maximal conservation of renal parenchyma.

## Materials and Methods

Between 1985 and 1989, seven renal transplantation patients (30–53 years old; mean, 40 years) were referred to us for examination. All had hematuria; three required transfusion (largest transfusion required was 7 units), and four had a collecting system filled with thrombus. All had undergone multiple biopsies, the time from the most recent biopsy to embolization varied between 7 and 25 days. The mean time between transplantation and embolization was 2.4 months.

Received August 6, 1990; accepted after revision October 3, 1990.

[1] Department of Radiology, Guys Hospital, St. Thomas' St., London SE1, England. Address reprint requests to N. M. deSouza.

[2] Department of Renal Transplantation, Guys Hospital, St. Thomas' St., London SE1, England.

0361–803X/91/1563–0507
© American Roentgen Ray Society

Nine AVFs were shown on angiography in seven patients: one patient had three AVFs, and the other six patients each had a single fistula. Because of the angle between the main renal transplant artery and the external iliac artery (all transplantations were end-to-side anastomoses), a contralateral femoral approach with a cross-over technique was used in three patients, and an ipsilateral approach was used in the other four (Figs. 1A and 1B). A coaxial technique was used only if a superselective technique with a single catheter was not possible. Initially, a 3-French Teflon catheter (Cook Inc., Bloomington, IN) was used, but later a Tracker-18 catheter (Target Therapeutics, San Jose, CA) was preferred (Figs. 2A and 2B). A single catheter was used in two patients and a coaxial technique in the other five (a 3-French Teflon catheter in three and a Tracker-18 catheter in the other two).

Embolization was done with 0.038-in. (0.97 mm) and 0.025-in. (0.64 mm) steel coils, 0.018-in. platinum coils, small particulate matter in the form of absorbable gelatin material (Gelfoam, Upjohn, Kalamazoo, MI), and localized extravasation of contrast material. Steel coils (0.038 in. [0.97 mm] and 0.025 in. [0.64 mm]) were used in two patients, platinum coils (0.018 in. [0.46 mm]) in one patient, steel coils (0.038 in. [0.97 mm]) and Gelfoam particles in one, and localized contrast extravasation in one.

Serum level of creatinine was measured before and after embolization in all patients. Radionuclide imaging with gadopentate dimeglumine was done in three patients before and after embolization.

## Results

Eight embolizations were attempted in seven patients—the patient with the three fistulas had two attempted single-catheter procedures that resulted in occlusion (Figs. 3A and 3B). Of the other six patients with a single fistula, five had successful embolization with immediate control of bleeding (coaxial technique in four, single catheter in one, Figs. 1A and 1B) and one had the vessel occluded with superselective catheter manipulation (coaxial technique), but continued with diminished hematuria for another 3 weeks, which then resolved spontaneously. Although parenchymal perfusion was not formally assessed during angiography, on the postembolization films only the vessel supplying the fistula was shown to be occluded, and all the grafts appeared well perfused with no demonstrable macroscopic areas of infarction.

Four patients showed a dramatic fall in serum level of

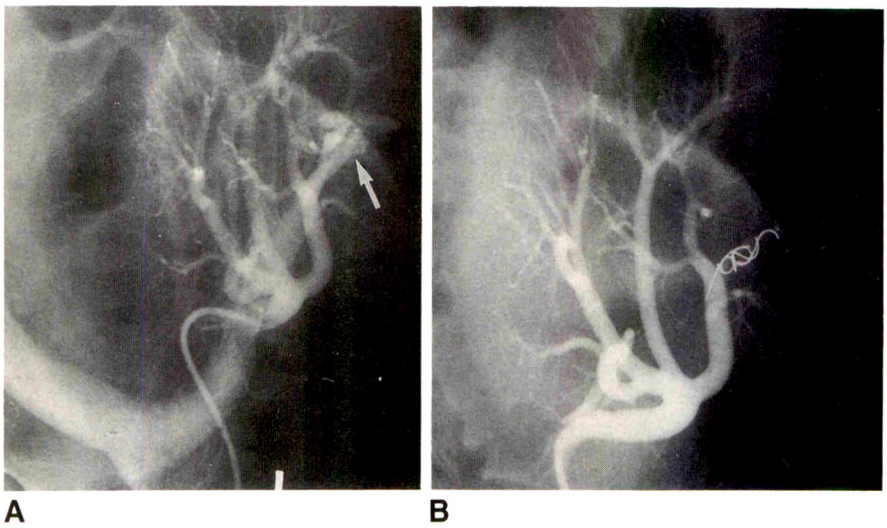



**Fig. 1.—*A*, Angiogram shows large arteriovenous fistula in a lower-pole branch of a renal transplant artery (*arrow*) with considerable arteriovenous shunting.**
***B*, Angiogram obtained after superselective placement of platinum coils shows that fistula is occluded and early venous filling is no longer seen.**

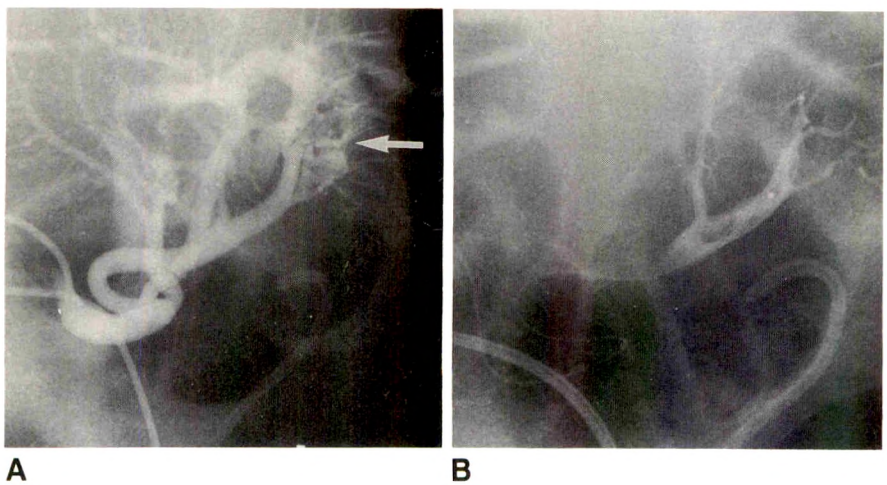



**Fig. 2.—*A*, Angiogram shows an extremely tortuous main renal transplant artery with a peripheral lower-pole fistula (*arrow*).**
***B*, Radiograph shows a Tracker-18 catheter with a radiopaque tip negotiating this tortuous renal transplant artery and achieving a superselective position in branch to be embolized.**

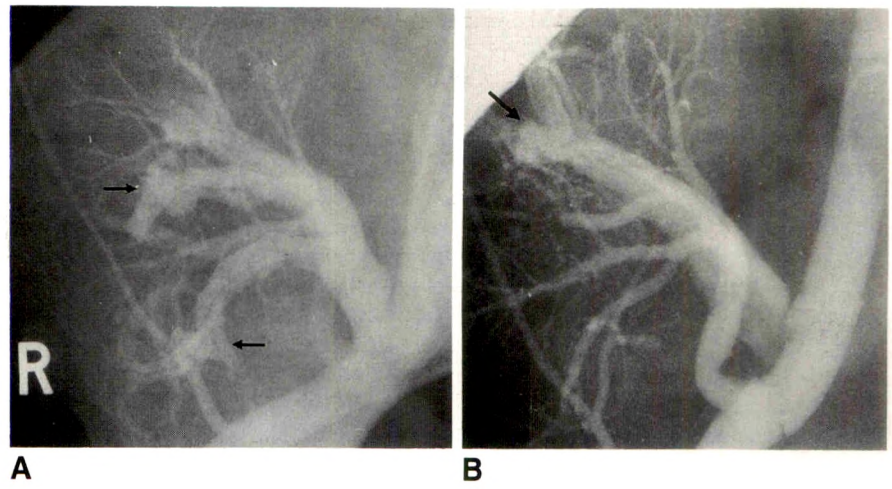



**Fig. 3.—*A*, Angiogram shows two arteriovenous fistulas in mid- and lower-pole branches (*arrows*) with a large arteriovenous shunt.**
***B*, Angiogram obtained a few days later shows occlusion of arteriovenous fistulas, but an upper-pole fistula not previously shown is now visible (*arrow*).**

creatinine (mean change, −527 mmol/l; range, −470 to −600 mmol/l), whereas in the other three, levels remained stable. Radionuclide studies showed a dramatic improvement in one patient and no change in function in the other two patients studied.

The long-term results, however, depend on the underlying graft function, and although five patients continue to have functioning grafts, two grafts were lost 22 days and 1 year after embolization due to graft rejection and acute tubular necrosis.

## Discussion

The prevalence of hemorrhage after renal biopsy has been variably reported to be from 0% to 16% [7, 8]. The prevalence of postbiopsy AVFs in renal allografts is said to be lower than in native kidneys because of the more superficial location of the transplants and, therefore, more accurate biopsy [9]. Treatment is aimed at preserving as much renal function as possible, and a conservative approach is the best first course because 70% of fistulas are reported to close spontaneously [10]. Bleeding is not usually severe, and only two of our patients required substantial transfusion; the largest transfusion required was seven units.

However, other consequences of persistent bleeding can have a serious adverse effect on renal transplant function. Clot retention in the collecting system, which was seen in four of our patients, results in obstruction, which then leads to worsening ischemia and acute tubular necrosis as well as the risk of infection in these immunosuppressed patients. These secondary complications of hemorrhage strengthen the case for early intervention as opposed to waiting for the AVF to occlude. Essential to this consideration is that embolization is safe and results in a minimal loss of renal parenchyma.

Surgery, which may involve nephrectomy or partial nephrectomy or manipulation of the kidney resulting in renal ischemia, is undesirable. Embolization with minimal renal infarction of normal parenchyma is the treatment of choice and is best achieved with a superselective technique.

Selective renal artery embolization was first used to control hemorrhage in 1973 [1]. Since then, several reports of selective renal embolization for bleeding in native kidneys have been published [1–4]. The experience in renal transplants is limited to a few case reports. Sennett et al. [8] describe a single case of intraoperative embolization followed 3 months later by a direct percutaneous procedure. Two other cases of successful transcatheter embolization have been reported in renal transplants [3, 11]. In these cases, single catheters were used, and embolization was achieved with steel coils, Gelfoam, or both. Renal volume loss determined from post-embolization arteriograms was less than 30% in 12 of 15 patients and 30–50% in the three remaining patients [3].

In order to minimize the loss of renal parenchyma, superselective embolization is necessary, with the catheter tip positioned as close as possible to the site of bleeding or the AVF. If the catheter placement is not selective enough, normal renal parenchyma will be injured, resulting in infarction. Sometimes a single catheter can be positioned optimally, but when this is not possible, we think that coaxial embolization techniques are necessary. These were used successfully in five of our seven cases. Initially we used 3-French Teflon catheters, but these have been replaced by Tracker-18 catheters, which are more flexible and have radiopaque tips. Their use with steerable floppy-tipped guidewires during monitoring with digital angiography allows precise superselective placement of these catheters before embolization. A variety of embolization materials have been used to occlude AVFs and other sources of bleeding in the kidney. Gelfoam is easy to use and is not permanent, but the concern that the necessarily small particles might pass through the fistula is always present. We prefer coils, which should be placed precisely in the artery feeding the AVF. Platinum microcoils (0.018 in. [0.46 mm]) placed with a catheter such as the Tracker-18 are ideal when coaxial embolization techniques are necessary.

In our patients, hemorrhage was controlled with minimal loss of renal parenchyma and with no loss of renal function either from the diagnostic angiography or the embolization, although Fisher et al. [3] reported a 30–50% loss in renal volume in three of 15 patients. The final outcome in our

patients, however, was determined largely by the underlying graft function.

In summary, improved methods of embolization, and in particular coaxial techniques, make superselective embolization the preferred method for effectively controlling postbiopsy bleeding in renal allografts. It offers the potential for maximal renal preservation and low risk in immunosuppressed patients who tolerate surgery badly. Between 1985 and 1989, seven patients were referred to us because of postbiopsy hematuria. Superselective embolization was successfully achieved in five patients, of whom four required a coaxial technique. Vessels in two patients occluded after superselective catheter manipulation, which was performed coaxially in one patient. Although we did not angiographically assess any postembolization infarction, the overall improvement in renal function suggests a minimal parenchymal loss due to the procedure. Technological advances with a careful superselective technique and early intervention before complications occur are important for optimal results.

## REFERENCES

1. Bookstein JJ, Goldstein HM. Successful management of post-biopsy arteriovenous fistula with selective arterial embolization. *Radiology* **1973**;109:535–536
2. Goldman ML, Fellner SK, Parrott TS. Transcatheter embolization of renal arteriovenous fistula. *Urology* **1975**;6:386–388
3. Fisher RG, Ben-Menachem Y, Whigham C. Stab wounds of the renal artery and branches: angiographic diagnosis and treatment by embolization. *AJR* **1989**;152:1231–1235
4. Uflacker R, Paolini RM, Lima S. Management of traumatic hematuria by selective renal artery embolization. *J Urol* **1984**;132:662–667
5. Orzel JA, Coldwell DM, Eskridge JM. Superselective embolization for renal hemorrhage with a new coaxial catheter and steerable guidewire. *Cardiovasc Intervent Radiol* **1988**;11:343–345
6. Diesce T, Drouillard J, Joffre F, et al. Advantages of interventional radiology in hemorrhagic complications of percutaneous nephrolithotomy: report of four cases and review of the literature. *J Intervent Radiol* **1988**;3:91–95
7. Diaz-Buxo JA, Kopen DF, Donadino JB. Renal allograft arteriovenous fistula following percutaneous biopsy. *J Urol* **1974**;112:577–580
8. Sennett CA, Messersmith RN, Yousefzadeh DK, Thistlethwaithe JR Jr. Percapsular and percutaneous embolization of renal transplant pseudoaneurysm and AV fistula: case report. *Cardiovasc Intervent Radiol* **1989**;12:270–273
9. Debruyne FMJ, Koene RAP, Moonen WA, Renders GAM, Chafik ML. Intrarenal arteriovenous fistula following renal allograft biospy. *Euro Urol* **1978**;109:535–536
10. Messing E, Kessler R, Kavaney PB. Renal arteriovenous fistulas. *Urology* **1976**;8:101–107
11. Benoit G, Charpentier B, Roche A, Bellamy J, Mohamedi D, Fries D. Arteriocalyceal fistula after grafted kidney biopsy: successful management by selective catheter embolization. *Urology* **1984**;24:487–490

# Carcinoma of the Prostate: MR Images Obtained with Body Coils Do Not Accurately Reflect Tumor Volume

Leslie E. Quint[1]
Jeffrey S. Van Erp[1]
Peyton H. Bland[1]
Steven H. Mandell[2]
Elizabeth A. Del Buono[2]
H. Barton Grossman[3]
Gary M. Glazer[1,4]
Paul W. Gikas[2]

**MR imaging with a body coil is unreliable in directly demonstrating tumor spread through the prostatic capsule. However, the likelihood of extracapsular spread of prostatic cancer rises with increasing tumor volume. The aim of our study was to assess the accuracy of MR with a body coil in diagnosing capsular penetration indirectly via an estimation of prostatic tumor volumes. Twenty-six patients with proved prostatic cancer that was clinically confined to the gland underwent MR imaging before radical prostatectomy and whole-mount pathologic sectioning of the specimen. Twenty of 31 lesions prospectively outlined on the MR images corresponded to cancers outlined on the pathology slides, and tumor volumes were calculated by using a voxel summation technique. On MR, tumor volume was underestimated in 11 of 20 cases and overestimated in nine of 20 cases. Only two of 20 size estimates based on MR findings were within 10% of actual tumor volume. Overlap in MR tumor volumes was significant between lesions with and without capsular penetration at microscopy. Factors contributing to inaccuracies in measurements of tumor volume on MR images included the variable histologic make-up of the tumors.**

**Our results show that, although knowledge of the size of a prostatic lesion is important in predicting the behavior of the tumor, MR imaging with a body coil is not reliable for accurate estimation of tumor volume.**

*AJR* 156:511–516, March 1991

Reports in the pathologic literature have shown that total tumor volume in prostatic carcinoma is directly correlated with histologic grade, extraprostatic tumor extension, seminal vesicle invasion, and metastatic spread to lymph nodes [1–3]. It has been reported that tumors smaller than 1 $cm^3$ are usually confined to the prostate, whereas tumors larger than 3 $cm^3$ are likely to have extraprostatic spread of disease [4–6].

Although there is controversy over the accuracy of MR in staging prostatic cancer [7–16], a recent report [17] indicates that MR imaging using a body coil is unreliable in directly demonstrating tumor spread through the prostatic capsule. Given the direct relationship between tumor size and the likelihood of extracapsular invasion, we assessed the accuracy of MR by using a body coil to detect capsular penetration indirectly via an estimation of prostatic tumor volume. The method used was a comparison of tumor volume measurements on MR images with corresponding measurements on matching pathologic whole-mount sections.

## Subjects and Methods

The MR images used for this study were obtained as part of a multiinstitutional investigation that aimed to assess the efficacies of MR imaging and endorectal sonography in staging patients with prostatic cancer [17]. Patient selection criteria for this national study included the following: biopsy-proved prostatic cancer, clinical stage A or B disease (confined to the gland), lack of contraindications to MR, no history of previous treatment for prostatic cancer,

Received August 1, 1990; accepted after revision September 27, 1990.

L. E. Quint is the recipient of an American Cancer Society Clinical Oncology Career Development Award.

Presented at the annual meeting of the American Roentgen Ray Society, Washington, DC, May 1990.

This work was supported in part by National Cancer Institute grant 5-401-CA45205 (RDOG 1).

[1] Department of Radiology, Box 0030, University of Michigan Medical Center, 1500 E. Medical Center Dr., Ann Arbor, MI 48109–0030. Address reprint requests to L. E. Quint.

[2] Department of Pathology, University of Michigan Medical Center, Ann Arbor, MI 48109.

[3] Department of Surgery, University of Michigan Medical Center, Ann Arbor, MI 48109.

[4] Present address: Department of Diagnostic Radiology and Nuclear Medicine, Stanford University School of Medicine, Stanford, CA 94305.

0361–803X/91/1563–0511
© American Roentgen Ray Society

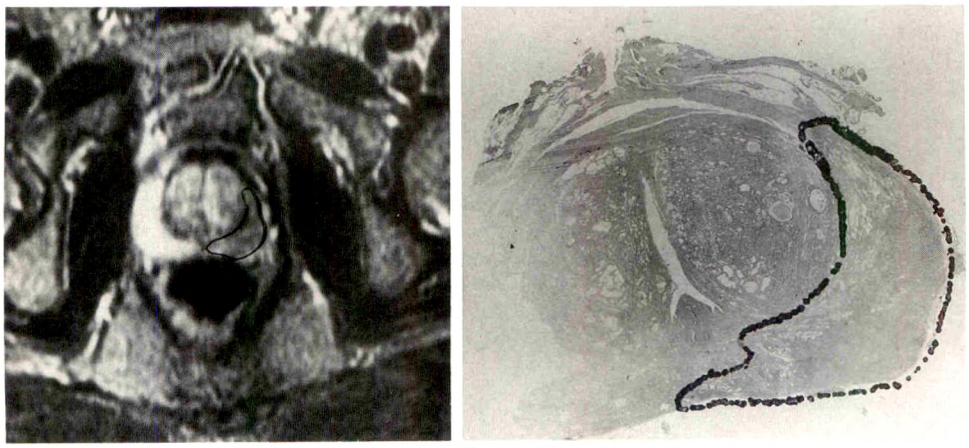



**Fig. 1.—*A* and *B*, Volume of lesion in left posterior peripheral region of prostate was underestimated on MR imaging (*A*) by only 5% of volume determined from pathologic examination of specimen (*B*). Capsular penetration was present at microscopic examination.**

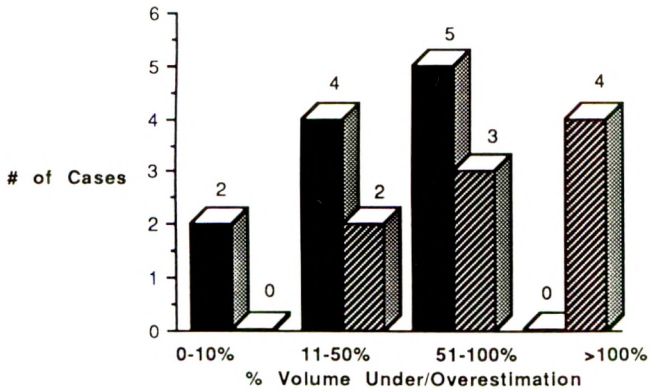



**Fig. 2.—Bar graph shows degree of under- (*solid bar*) or over-estimation (*hatched bar*) of tumor volumes on MR images in 20 cases.**

and agreement to undergo both preoperative MR and radical prostatectomy. Twenty-six consecutive patients fulfilling these criteria were referred from the urology clinic at our institution and entered into the study after giving informed consent. In all patients, radical prostatectomy was performed within 3 weeks of MR scanning. Only patients from our institution were included in the study reported here.

All patients were imaged by using spin-echo pulse sequences and a body coil on a superconducting system operating at 1.5 T (Signa, General Electric, Milwaukee, WI). Both relatively T1-weighted, 600/20 (TR/TE), and relatively T2-weighted (2500/20,80; 2500/40,80; or 2500/60,120) axial images were obtained through the prostate and seminal vesicles by using a 24- or 28-cm field of view. T1-weighted images 5–10 mm thick with 0- to 2-mm interscan gaps were obtained by using a 256 × 256 matrix and two excitations. T2-weighted images were contiguous slices 5 mm thick, obtained in an interleaved fashion by using a 128 × 256 matrix and two excitations. Variations in T2-weighted sequences were mandated by protocol changes from the national study.

All MR studies were interpreted prospectively by an experienced radiologist who was blinded to the results of the clinical evaluation and any other imaging studies. Prostatic lesions were identified as areas of low signal intensity within the normally high-signal-intensity peripheral region on the T2-weighted images. These criteria were used since most cancers detectable on MR images have this appearance. Each lesion was manually outlined on the hard-copy T2-weighted images with a film marking pencil.

After fixation in buffered formalin, the radical prostatectomy specimens were coated with India ink on the left half and a blue dye on the right half. Whole-mount pathologic sections stained with hematoxylin and eosin were prepared at 5-mm intervals in the axial plane to correspond with the MR images. An experienced pathologist reviewed all 26 cases and, after meticulous microscopic evaluation, outlined all malignant lesions on the glass slides with a marking pen. Other information recorded at the time of review included the absence or presence and site of capsular penetration by tumor.

The traced MR images were correlated visually with the outlined whole-mount sections in order to match lesions seen on MR with those seen on microscopy. A lesion was considered a "match" if both imaging and pathologic examinations revealed tumor in the same craniocaudal and axial location, regardless of lesion size. Lesions noted on MR images with no corresponding lesions on pathologic examination were considered false positives; lesions identified at pathologic examination but not detected prospectively on MR images were considered false negatives.

Total volumes for each lesion seen on MR images and on pathologic specimens were calculated by using a voxel summation technique, as follows: the whole-mount glass slide or MR film was placed on a view box in line with a video camera connected to a VICOM 1850 digital image processing system (VICOM Systems, Inc., San Jose, CA). The image of the slide or MR image was displayed on a video monitor and digitized into a 512 × 512 pixel matrix for subsequent analysis. Digitized images from the video camera had a dynamic range of 7 bits. The outlines previously drawn on the slide or film were retraced on the computer screen by using a cursor controlled by a trackball. All computer tracings were performed by one author; he used a consistent method whereby the inner margin of each pen/pencil outline was followed as the border. The spatial conversion factor needed to calculate the traced area was obtained by using a 1-in. (2.54 cm) grid placed on the view box. Each pixel represented an area element of 0.1365 × 0.1365 mm for the pathologic slides and 0.6250 × 0.6250 mm for the MR films. In order to ensure accuracy, the conversion factor was recalculated at the beginning of each session. The areas (in square centimeters) of each lesion were multiplied by 0.5 cm (as all T2-weighted sections were 0.5 cm thick) and summed to obtain the total volume (in cubic centimeters).

Receiver-operating-characteristic (ROC) analysis of the data was performed to determine the effect of varying a single MR volume threshold in predicting capsular penetration. This was accomplished

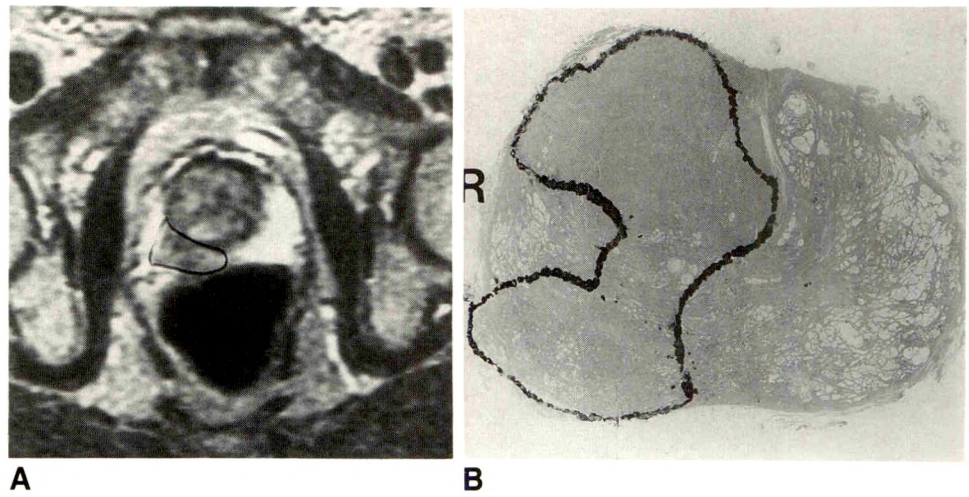



**Fig. 3.—*A*, MR image shows a lesion in right posterior peripheral region of prostate. Central hypointense region was interpreted prospectively as representing benign prostatic hyperplasia.**
***B*, Pathologic whole-mount section shows tumor infiltrating into central region of gland; capsular penetration was also present at microscopic examination. Tumor volume was underestimated by 87% when MR images were used.**

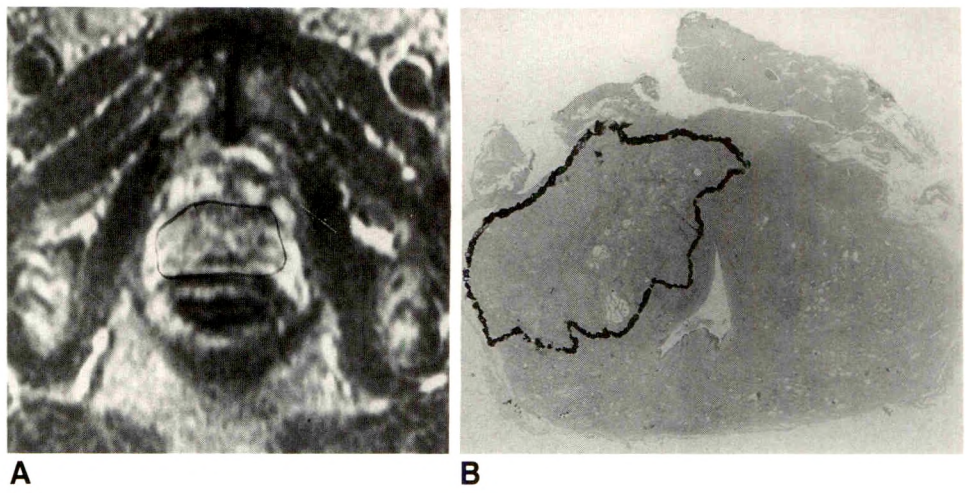



**Fig. 4.—*A*, Diffuse low intensity throughout gland on MR image suggested a large tumor occupying most of gland.**
***B*, Pathologic examination of specimen showed tumor limited to right side of gland, with spread through capsule. Tumor volume was overestimated on MR images by 43%.**

by using the ROCFIT computer program from Metz et al. (Metz CE, Wang P-L, Kronman HB, Shen J-H, personal communication), which is a modified form of the RSCORE II program of Dorfman [18].

In order to check the accuracy and reproducibility of the volume measurement method, manual computer tracings from the previously marked MR films and pathologic slides were repeated in six cases several weeks after the first tracing. Volumes obtained from the second set of tracings were compared with volumes obtained from the original set. Subsequently, pencil marks were erased from the MR films in three of these cases, and this unmarked set of films was presented to the radiologist for lesion reoutlining, followed by retracing on the computer. Again, the measurements of volume obtained in this trial were compared with the original measurements for these three cases. Because of the time required for the histopathologic examinations, the pathologic tracings were not repeated, and no estimate of error was obtained for this portion of the volume calculation.

## Results

Thirty-one lesions were diagnosed prospectively on MR imaging. Twenty of these corresponded to malignant lesions seen on microscopic examination of the whole-mount sections. Eleven showed no matching lesion on pathologic examination. At histologic examination of the corresponding whole-mount sections, four of these 11 false-positive lesions represented areas of benign prostatic hyperplasia and seven represented normal prostatic tissue.

Fifty-four malignant lesions were identified in the 26 radical prostatectomy specimens at microscopic examination; 14 patients had more than one lesion. Seventeen of 54 lesions had a volume less than 0.1 $cm^3$ on the basis of pathologic examination. MR detected none of these tiny cancers. Thirty-seven of 54 tumors were greater than 0.1 $cm^3$ on pathologic examination; 20 of these 37 were detected prospectively on MR images (20/37 = 54% detection rate for lesions >0.1 $cm^3$). The smallest matching lesion (seen on pathologic and MR examinations) had a volume of 0.13 $cm^3$ according to pathologic findings.

Of the 20 matched lesions, 12 were predominantly or entirely within the peripheral zone and eight involved both peripheral and central regions of the gland on pathologic analysis. Six of 20 matched lesions were 0.1–1 $cm^3$ on the basis of pathologic examination, two were 1–3 $cm^3$, nine were 3–10 $cm^3$, and three were greater than 10 $cm^3$. Mea-

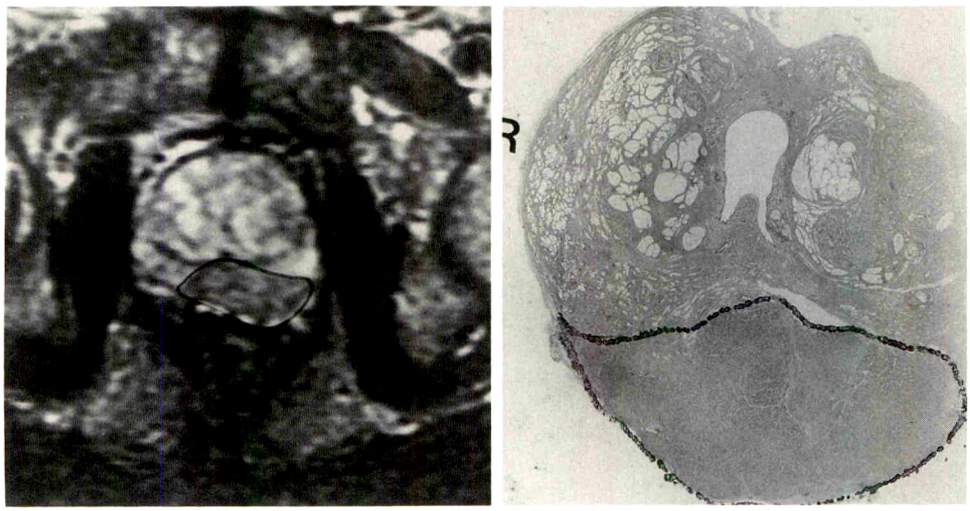



**Fig. 5.—*A* and *B*, Paired MR image (*A*) and pathologic whole-mount section (*B*) show an apparently close size match for outlined lesion. However, tumor volume was overestimated on MR images by 166% because of mistaken inclusion of a large, malignant periprostatic lymph node (present on more cranially located sections). Microscopic examination confirmed capsular penetration by tumor.**

surements based on MR findings underestimated tumor volume in 11 of 20 cases and overestimated volume in nine of 20. None of the 11 underestimated tumors had an actual volume less than <1 $cm^3$, two lesions were 1–3 $cm^3$, six were 3–10 $cm^3$, and three were greater than 10 $cm^3$. Of the nine overestimated cases, six were less than 1 $cm^3$ on pathologic examination, none were 1–3 $cm^3$, and three were 3–10 $cm^3$. Thus, MR tended to overestimate the volume of small tumors and underestimate the large tumors. Only two of 20 MR size estimates were within 10% of actual tumor volume (underestimated cases) (Figs. 1 and 2). Four tumors were underestimated by 11–50% of true volume and five by 51–100% (Fig. 3). Two lesions were overestimated on MR by 11–50%, three by 51–100%, and four by more than 100% of pathologic tumor volume (Figs. 4 and 5). The greatest volume overestimation, 1168%, occurred when a tumor of 0.19 $cm^3$ at pathologic examination was measured as 2.41 $cm^3$ on MR.

If 3 $cm^3$ had been used as the volume threshold on pathologic specimens for diagnosing capsular penetration in the 20 matched lesions, one would have been false negative (pathologic volume, 0.8 $cm^3$) and one false positive (pathologic volume, 5.8 $cm^3$).

The poor correlation between measurements of tumor volume based on MR images and pathologic specimens for each of the 20 matched lesions is depicted in Figure 6. There was significant overlap in MR values between tumors larger than 3 $cm^3$ on pathologic examination and those smaller than 3 $cm^3$ (Fig. 7A) and between lesions with and without capsular penetration by tumor at microscopy (Fig. 7B). All four lesions with volumes less than or equal to 1.1 $cm^3$ on MR images showed no capsular penetration on microscopic examination, and all 10 lesions greater than or equal to 3.2 $cm^3$ did have capsular invasion. However, six of 20 lesions were between 1.2 and 3.1 $cm^3$ on MR images, thus giving rise to an indeterminate category containing 30% of cases.

ROC analysis revealed that 3 $cm^3$ was the optimal MR size threshold for prediction of extracapsular tumor spread, giving an 82% sensitivity and 100% specificity. However, the 95% confidence interval was quite large (Fig. 8).

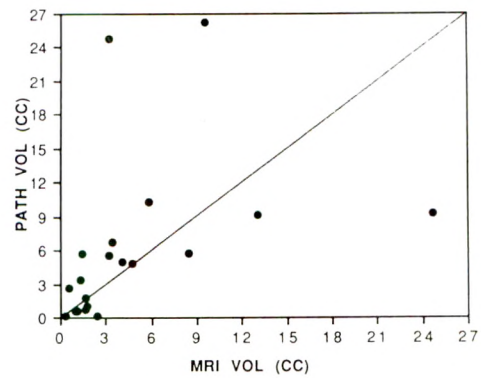



**Fig. 6.—Scatterplot shows volume (VOL) of prostatic tumor determined on basis of MR images vs volume determined from examination of pathologic (PATH) specimens for the 20 matched lesions. Note large degree of scatter away from 45° line, indicating poor correlation between values obtained.**

Retracings performed only on the computer monitor revealed an average volume error of 5.0% (SD, 4.8%). The combined retracings on both the MR films and the computer showed an error of 8.7% (SD, 6.0%).

## Discussion

We found poor correlation between tumor volumes determined from MR images and pathologic specimens for lesions of all sizes. Therefore, it is not surprising that there was extensive overlap in MR values between lesions with histopathologic evidence of capsular invasion and lesions without capsular invasion. Preliminary examination of the data via ROC analysis suggested that 3 $cm^3$ might be a good MR cutoff for diagnosing capsular penetration, yielding perfect specificity and good sensitivity (82%). This result was, at first,

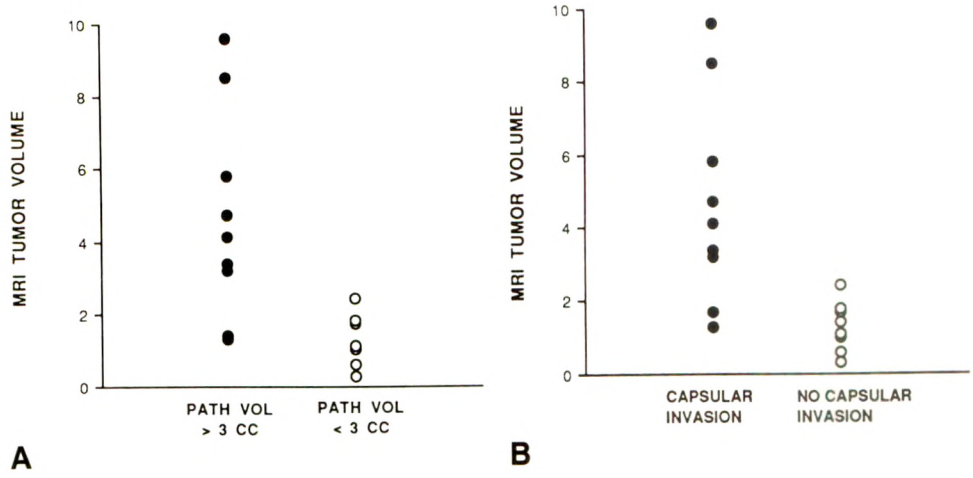



**Fig. 7.—*A* and *B*, Graphs show significant overlap in tumor volumes (VOL) on MR images between lesions found to be larger than 3 $cm^3$ at pathologic (PATH) examination and lesions found to be smaller than 3 $cm^3$ (*A*), as well as between lesions with and without capsular penetration at microscopy (*B*).**

somewhat surprising, given the poor size correlation. However, further statistical analysis of the data showed a wide confidence interval on the ROC curve (Fig. 8), suggesting that these sensitivity and specificity values may be in error. A larger data sample containing more cases would be needed to resolve this issue.

Sources of error in our study included the frequent difficulty we had in determining exact lesion boundaries on MR images. In particular, tumor boundaries that extended into the central zone may have been partially obscured by adjacent benign hyperplastic tissue. Other potential pitfalls included hemorrhage within or near the lesion after biopsy [16] and tissue shrinkage after resection of the gland, because of lack of blood flow, loss of other tissue fluids, or properties of histologic tissue processing [19].

Few other studies have addressed the ability of MR to show volumes of prostatic tumors. In one study [16] of 34 prostatic cancer lesions imaged at 1.5 T, 6 and 2 $cm^3$, respectively, were found to be the MR thresholds for correctly diagnosing or excluding capsular invasion; these values differed somewhat from ours (3.2 and 1.1 $cm^3$, respectively). Similar to our study, a large proportion of lesions (56%) fell between the upper and lower MR thresholds for diagnosing or excluding capsular invasion, leading to a large indeterminate category. Other investigations done at 0.35 T [15] and 1.5 T [14] found that tumor volumes were underestimated on MR in 12 of 20 and five of eight visualized lesions, respectively. In contrast to our findings, volume was not overestimated for any lesion in either of these two studies.

None of the three studies cited above gave details about the methods used to calculate tumor size. Since prostatic cancers are often irregularly shaped, simple mathematical formulas using diameter measurements are frequently inadequate for estimating tumor size. Our study circumvented this problem by tracing tumor outlines and using voxel summation techniques to calculate true areas, rather than estimated areas, on each section. These area measurements were then used to generate volume estimations. One previous study [16] did not use whole-mount or step sectioning of the pathologic specimens. Therefore, correlation could not be made

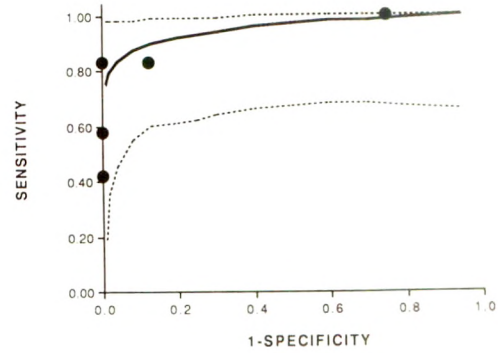



**Fig. 8.—Receiver-operating-characteristic curve shows effect of varying a single MR volume threshold in predicting capsular penetration. A volume cutoff of 3 $cm^3$ yields 82% sensitivity and 100% specificity; however, the 95% confidence limit (*broken lines*) is quite wide.**

between MR and pathologic volume measurements, and, in fact, the abnormalities measured on MR were not proved to correspond to the cancers staged pathologically. Kahn et al. [15] reported the size range measured on MR only for tumors with proved capsular invasion. Since the size range on MR for lesions without capsular invasion was not reported, the amount of overlap between these two groups is unclear. The study of Carrol et al. [14] correlated tumor volume only with lesion detection on MR. These authors did not give the range of tumor size underestimation, and they did not correlate tumor sizes on MR with the presence or absence of capsular penetration at pathologic examination.

Multiple complex factors undoubtedly contribute to the difficulty in determining tumor volumes on MR images. One of these relates to the histologic make-up of the tumors. On microscopic examination, the tumors are often markedly irregular, without well-circumscribed borders. Fingerlike projections of carcinoma often are seen interdigitating with areas of benign tissue, producing tumor islands on cross section (Fig. 9). In a large proportion of cases, the glands contain underlying benign prostatic hyperplasia. Although in the classic case the cancer is peripheral and the hyperplastic tissue is

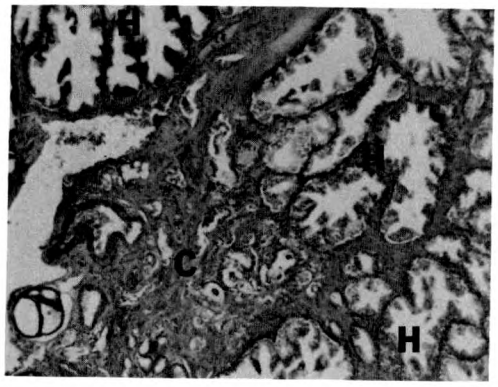



**Fig. 9.—Histopathologic section of prostate shows adenocarcinoma (C), manifested by small acini interdigitated with glandular hyperplasia (H).**

more central, in reality these tissue types are often intermingled. Schiebler et al. [20] have shown that benign hyperplasia has a variable MR appearance, depending on the histologic composition and the glandular morphology, and is sometimes indistinguishable from carcinoma on the basis of relative signal intensities. Thus, if hyperplastic tissue is intermixed with cancerous tissue, or if it interdigitates with the margins of a cancerous lesion, or if it is only adjacent to a cancerous lesion, the volume of the cancer may be dramatically over- or underestimated.

Other possible limitations of our study included the use of a body coil for reception and only a single type of pulse sequence (spin echo). Recent articles [21, 22] have suggested that MR imaging of the prostate can be improved greatly by using endorectal surface coils, leading to higher signal-to-noise ratios and increased spatial resolution. It is likely that extraprostatic tumor extension will be easier to visualize with an endorectal coil, and thus tumor volume calculations will be unnecessary for predicting capsular penetration. However, these coils are still experimental, and are not yet readily available to practicing radiologists. In addition, it is possible that more detailed prostatic imaging may be obtainable with the use of other types of probes, such as phased-array coils, or with the use of other pulse sequences, including fat-suppression techniques.

In conclusion, although knowledge of the size of a prostatic lesion is important in predicting the behavior of the tumor, and MR is capable of detecting some cancerous prostatic lesions, MR is not reliable for accurate estimations of true tumor volume when currently available techniques are used. However, MR accuracy in this setting may improve with the advent of new technology such as endorectal surface coils, better imaging sequences, and the use of contrast agents. Further studies will be needed to assess these technologic improvements when they become available.

ACKNOWLEDGMENT

We thank Dede Remick for her valuable assistance.

REFERENCES

1. Cantrell BB, DeKlerk DP, Eggleston JC, Boitnott JK, Walsh PC. Pathological factors that influence prognosis in stage A prostatic cancer: the influence of extent versus grade. *J Urol* **1981**;125:516–520
2. Guileyardo JM, Sarma DP, Johnson WD, Akazaki K, Correa P. Incidental prostatic carcinoma: tumor extent versus histologic grade. *Urology* **1982**;20:40–42
3. Gleason DF. Histologic grading and clinical staging of prostatic carcinoma. In: Tannenbaum M, ed. *Urologic pathology: the prostate*. Philadelphia: Lea & Febiger, **1977**:171–197
4. McNeal JE, Kindrachuk RA, Freiha FS, Bostwick DG, Redwine EA, Stamey TA. Patterns of progression in prostate cancer. *Lancet* **1986**;1:60–63
5. Stamey TA, McNeal JE, Freiha FS, Redwine E. Morphometric and clinical studies on 68 consecutive radical prostatectomies. *J Urol* **1988**;139:1235–1241
6. McNeal JE. The prostate gland: morphology and pathobiology. In: Stamey TA, ed. *1988 Monographs in urology*. Princeton, NJ: Custom Publishing Services, **1988**:50
7. Biondetti PR, Lee JKT, Ling D, Catalona WJ. Clinical stage B prostate carcinoma: staging with MR imaging. *Radiology* **1987**;162:325–329
8. Phillips ME, Kressel HY, Spritzer CE, et al. Prostatic disorders: MR imaging at 1.5 T. *Radiology* **1987**;164:386–392
9. Friedman AC, Seidmon EJ, Radecki PD, Lev-Toaff A, Caroline DF. Relative merits of MRI, transrectal endosonography and CT in diagnosis and staging of carcinoma of prostate. *Urology* **1988**;31:530–537
10. Houston ST, Jones LW, Waluch V. Nuclear magnetic resonance imaging in detecting and staging prostatic cancer. *Urology* **1988**;31:171–175
11. Buonocore E, Hesemann C, Pavlicek W, Montie JE. Clinical and in vitro magnetic resonance imaging of prostatic carcinoma. *AJR* **1984**;143:1267–1272
12. Poon PY, McCallum RW, Henkelman MM, et al. Magnetic resonance imaging of the prostate. *Radiology* **1985**;154:143–149
13. Hricak H, Dooms GC, Jeffrey RB, et al. Prostatic carcinoma: staging by clinical assessment, CT, and MR imaging. *Radiology* **1987**;162:331–336
14. Carrol CL, Sommer FG, McNeal JE, Stamey TA. The abnormal prostate: MR imaging at 1.5 T with histopathologic correlation. *Radiology* **1987**;163:521–525
15. Kahn T, Bürrig K, Schmitz-Dräger B, Lewin JS, Fürst G, Mödder U. Prostatic carcinoma and benign prostatic hyperplasia: MR imaging with histopathologic correlation. *Radiology* **1989**;173:847–851
16. Bezzi M, Kressel HY, Allen KS, et al. Prostatic carcinoma: staging with MR imaging at 1.5 T. *Radiology* **1988**;169:339–346
17. Rifkin MD, Zerhouni EA, Gatsonis C, et al. Comparison of magnetic resonance imaging and ultrasonography in staging early prostate cancer: results of a multi-institutional cooperative trial. *N Engl J Med* **1990**;323:621–626
18. Dorfman DD. RSCORE II. In: Swets JA, Pickett RM, eds. *Evaluation of diagnostic systems: methods from signal detection theory*. New York: Academic **1982**:212–232
19. Boonstra H, Oosterhuis JW, Oosterhuis AM, Fleuren GJ. Cervical tissue shrinkage by formaldehyde fixation, paraffin wax embedding, section cutting and mounting. *Virchows Arch [A]* **1983**;402:195–201
20. Schiebler ML, Tomaszewski JE, Bezzi M, et al. Prostatic carcinoma and benign prostatic hyperplasia: correlation of high-resolution MR and histopathologic findings. *Radiology* **1989**;172:131–137
21. Schnall MD, Lenkinski RE, Pollack HM, Imai Y, Kressel HY. Prostate: MR imaging with an endorectal surface coil. *Radiology* **1989**;172:570–574
22. Martin JF, Hajek P, Baker L, Gylys-Morin V, Fitzmorris-Glass R, Mattrey R. Inflatable surface coil for MR imaging of the prostate. *Radiology* **1988**;167:268–270

Case Report

# MR Imaging in Sclerosing Mesenteritis

Alan J. Kronthal,[1] Young S. Kang, Elliot K. Fishman, Bronwyn Jones, Janet E. Kuhlman, and Clare M. C. Tempany

Sclerosing mesenteritis is a rare entity that lies within a spectrum of diseases causing fibrofatty thickening of the mesentery. We present a case in which characteristic findings were noted on plain film, small-bowel series, and CT. MR imaging proved helpful in further evaluating the nature of the lesion and delineating vascular involvement. To our knowledge, this is the first description of the MR imaging appearance of sclerosing mesenteritis.

## Case Report

A 64-year-old man presented with a long history of abdominal pain and weight loss. CT (Fig. 1A) showed a mesenteric mass of soft-tissue density that contained calcifications and had a surrounding pattern of radiating spicules. Biopsy of the mass yielded a diagnosis of sclerosing mesenteritis, and the patient was treated conservatively. One year later, CT showed slight enlargement of the mass, and MR imaging (Signa, General Electric, Milwaukee, WI, operating at 1.5 T; Figs. 1B–1E) was performed to evaluate vascular involvement. The mass had intermediate signal intensity on T1-weighted images, with scattered foci of lower signal corresponding to areas of calcification. On T2-weighted images, the mass was of low signal, most compatible with fibrosis. Gradient-echo images revealed that a jejunal branch of the superior mesenteric artery ended abruptly as it entered the mass. Flow within the superior mesenteric vein could not be seen along most of its course, and multiple collateral vessels were seen. Dilated small-bowel loops also were noted, compatible with a partial small-bowel obstruction. Small-bowel series showed angling and kinking of small-bowel loops in the left lower quadrant and luminal narrowing, separation of loops, and irregular fold thickening. Exploratory laparotomy revealed a large hard mass at the mesenteric root with involvement of the superior mesenteric artery and vein and several small-bowel loops. Jejunoileal bypass and biopsy of the mass were performed, confirming a diagnosis of sclerosing mesenteritis. The patient's symptoms improved slightly, and no further treatment is planned at this time.

## Discussion

Sclerosing mesenteritis is one entity within a spectrum of rare diseases that are characterized by fibrofatty thickening of the small-bowel mesentery [1]. The specific diagnosis usually depends on which of the three major pathologic features predominate: fatty degeneration or lipodystrophy, inflammation or panniculitis, or fibrosis or sclerosing (retractile) mesenteritis [2]. The entity has also been called liposclerotic mesenteritis and mesenteric Weber-Christian disease [3]. The specific cause of these changes is unknown, although various theories such as ischemia of the mesentery or an autoimmune response have been proposed [3, 4]. Whatever the cause, the final stage appears to be a series of inflammatory changes affecting the mesentery [5]. Subsequent fat necrosis is thought to occur, resulting in intense reactive fibrosis with progressive scarring and retraction. The disease has been described in patients from ages 8 to 80, but it is most common in middle-aged men [1].

Histologically, the lesions are composed of fibrous tissue, lipophages, lymphocytes, plasma cells, and eosinophils [5]. Calcifications are frequently present, probably as a result of fat necrosis [1]. The lesion involves the mesenteric and submucosal fat of the small bowel, often with extension into the bowel muscle and submucosa. The mucosa, however, re-

Received July 27, 1990; accepted after revision September 10, 1990.

[1] All authors: The Russell H. Morgan Department of Radiology and Radiological Science, The Johns Hopkins Medical Institutions, 600 N. Wolfe St., Baltimore, MD 21205. Address reprint requests to E. K. Fishman.

*AJR* 156:517–519, March 1991 0361–803X/91/1563–0517 © American Roentgen Ray Society

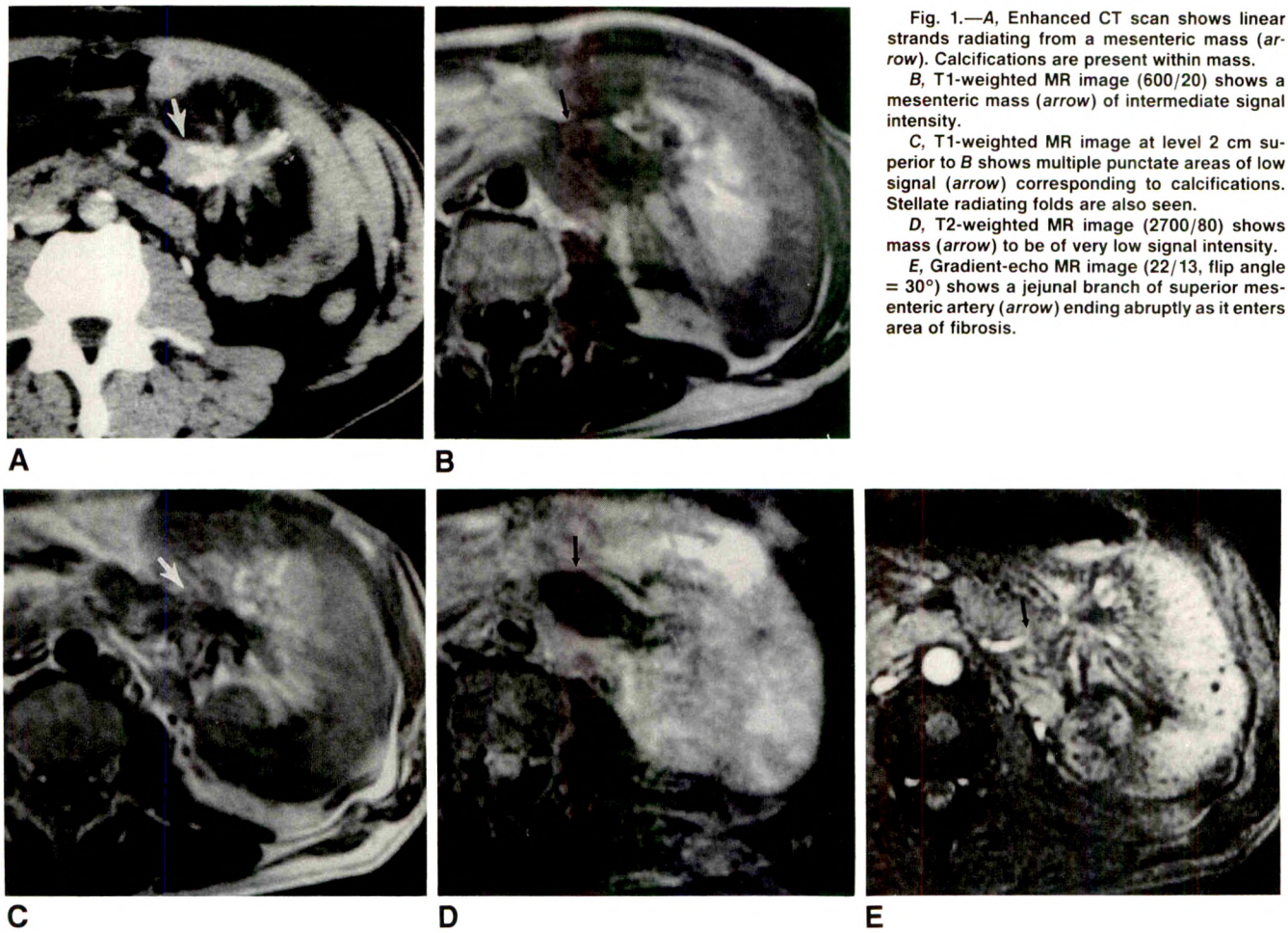



Fig. 1.—*A*, Enhanced CT scan shows linear strands radiating from a mesenteric mass (*arrow*). Calcifications are present within mass.

*B*, T1-weighted MR image (600/20) shows a mesenteric mass (*arrow*) of intermediate signal intensity.

*C*, T1-weighted MR image at level 2 cm superior to *B* shows multiple punctate areas of low signal (*arrow*) corresponding to calcifications. Stellate radiating folds are also seen.

*D*, T2-weighted MR image (2700/80) shows mass (*arrow*) to be of very low signal intensity.

*E*, Gradient-echo MR image (22/13, flip angle = 30°) shows a jejunal branch of superior mesenteric artery (*arrow*) ending abruptly as it enters area of fibrosis.

mains intact [5]. The process can obstruct mesenteric lymphatics, resulting in submucosal edema and lymphangiectasia. Mesenteric arteries and veins often display luminal narrowing [6].

Abdominal pain is the most frequent symptom, often accompanied by nausea, vomiting, malaise, weight loss, low-grade fever, diarrhea, or constipation [1]. An abdominal mass is frequently palpable [5].

Radiologic features of sclerosing mesenteritis on conventional barium studies and CT have been previously described. Small-bowel series often show separation of loops with kinking and angulation of the small bowel, suggesting a serosal process [5]. The folds may be thickened because of either extension of the mesenteric process into the submucosa or edema from lymphatic obstruction. The colon may occasionally be involved, with narrowing and rigidity; thumbprinting also has been reported [4]. CT shows a mesenteric mass containing a variable proportion of fat and soft tissue, with radiating linear strands; calcifications are occasionally present.

Differential diagnosis includes carcinoid, desmoid, and mesenteric lymphoma or carcinomatosis. Carcinoid may evoke a dense fibrotic reaction within the mesentery, simulating retractile mesenteritis. Elevated urinary 5-hydroxyindoleacetic acid levels, liver metastases, or multiplicity of mesenteric masses favors the diagnosis of carcinoid [7]. Desmoid tumors, usually associated with Gardner syndrome, are tumor-like fibromatoses that tend to occur in injured or surgically traumatized sites [6]. Differentiation from retractile mesenteritis can usually be made by studying the clinical history or finding associated colonic polyposis on gastrointestinal studies [8]. Thickened leaves radiating from the mesenteric root have been seen in breast carcinoma [7]. The absence of ascites or tumor elsewhere makes this diagnosis less likely [1]. Similarly, lymphoma may involve the mesentery, but the absence of retroperitoneal involvement or nodal involvement elsewhere is unusual. Except for treated lymphoma, the presence of calcifications, as occasionally seen in sclerosing mesenteritis, would be distinctly unusual in any of these processes.

The MR imaging appearance of sclerosing mesenteritis has not been described before. Two aspects of MR imaging make it a valuable technique for evaluation of this disease. The first is tissue characterization: fibrous tissue containing preponderantly nonmobile protons with very short T2 has low signal on all sequences. Although masses of fibrous origin, depending on their fatty and vascular content, have recently been shown to exhibit a variety of signal characteristics, low signal

should suggest mature fibrotic reaction (Quinn SF et al., presented at the annual meeting of the American Roentgen Ray Society, May 1990). Therefore, T2-weighted or fat-suppressed pulse sequences may help distinguish benign end-stage fibrofatty proliferation from malignant tumors such as lymphoma or metastases. Additional investigation is needed to determine whether the fibrotic response to carcinoid shows similar signal characteristics. Second, noninvasive assessment of large to medium-sized vessels is possible with MR imaging. As in this case, routine gradient-echo images or T1-weighted images with presaturation easily depict absence of flow within major mesenteric vessels and presence of collateral pathways.

In the vast majority of cases, sclerosing mesenteritis has a benign course, and no specific treatment is indicated. Bowel resection is necessary only when complicated by mechanical obstruction. Progressively enlarging lesions and mesenteric venous thrombosis, both of which were encountered in this case, are rare complications [1]. The few reported cases of severe and progressive disease have been successfully treated with chemotherapeutic agents [3].

Sclerosing mesenteritis is a rare entity affecting the small-bowel mesentery. Although small-bowel series and CT are helpful in confirming a mesenteric disease, they are not specific for the tissue characteristics of the lesion. MR imaging appears to be valuable for suggesting the fibrous nature of this disease and evaluating vascular involvement.

## REFERENCES

1. Clemett AR, Tacht DG. The roentgen diagnosis of retractile mesenteritis. *Radiology* **1969**;107:787–790
2. Thompson GT, Fitzgerald EF, Somers SS. Retractile mesenteritis of the sigmoid colon. *Br J Radiol* **1985**;58:266–267
3. Bush RW, Mammar SP Jr, Rudolph RH. Sclerosing mesenteritis: response to cyclophosphamide. *Arch Intern Med* **1986**;146:503–505
4. Han SY, Koehler RE, Keller FS, Ho KJ, Zornes SL. Retractile mesenteritis involving the colon: pathologic and radiologic correlation. *AJR* **1986**; 147:268–270
5. Pérez-Fontán FJ, Soler R, Sanchez J, Iglesias P, Samjurjo P, Ruiz J. Retractile mesenteritis involving the colon: barium enema, sonographic, and CT findings. *AJR* **1986**;147:937–940
6. Kelly JK, Hwang W-S. Idiopathic retractile (sclerosing) mesenteritis and its differential diagnosis. *Am J Surg Pathol* **1989**;13:513–521
7. Seigel RS, Kuhns LR, Borlaza GS, McCormick TL, Simmons JL. Computed tomography and angiography in ileal carcinoid tumor and retractile mesenteritis. *Radiology* **1980**;134:437–440
8. Menuck LS. Abdominal desmoid masses in Gardner's syndrome. *Gastrointest Radiol* **1976**;1:81–84

Case Report

# Retroperitoneal Sarcoidosis

David Bernard Bach[1] and Alexander Dale Vellet

Sarcoidosis, a disease of unknown etiology, primarily affects the mediastinal and hilar lymph nodes, the lungs, the skin, and the eyes. Less often, there is involvement of the liver, spleen, peripheral lymph nodes, salivary glands, bones, heart, and nervous system. The diagnosis is usually suspected on the basis of typical clinical features or chest radiographic findings, which are abnormal in about 90% of patients at the time of presentation [1]. Involvement of intraabdominal or retroperitoneal lymph nodes occurs rarely, but when it does occur, other manifestations of sarcoidosis, such as typical hilar adenopathy, are usually present. We report two patients with normal findings on chest radiographs, in whom periportal and retroperitoneal lymphadenopathy were the presenting radiographic manifestations, and describe the findings on MR imaging. MR was performed after sarcoidosis was diagnosed on the basis of pathologic examination of tissue excised surgically.

## Case Report

The first patient, a 51-year-old white woman, had a 3-year history of arthralgia. She had episodes of erythema nodosum involving both arms and legs, and she had been treated with small doses of steroids with some initial improvement. She also complained of aching pain in her arms, hands, neck, back, hips, and lower legs. She was fatigued and had night sweats.

On admission, she appeared well. The erythrocyte sedimentation rate was elevated (44 mm/hr). Sonography showed a mass behind the inferior vena cava (Fig. 1A). The mass, which was 6 cm in its greatest dimension, contained faint low-level echoes and showed increased through-transmission.

A percutaneous needle aspiration of the retroperitoneal mass was performed under CT guidance (Fig. 1B). This procedure yielded numerous sheets and clusters of lymphocytes that initially were interpreted as consistent with lymphoma. At the time of staging laparotomy, biopsies of the retroperitoneal mass and of the liver revealed noncaseating granulomatous inflammation consistent with sarcoidosis. No evidence for malignancy was found. All cultures of the excised tissues were negative for tuberculosis.

MR was performed 7 months after laparotomy. The retrocaval adenopathy was of homogeneously diminished signal intensity on T1-weighted images (300/20 [TR/TE], Fig. 1C). On the corresponding T2-weighted images (2000/70, Fig. 1D), a bilobed low signal intensity was surrounded by a peripheral high signal. Further MR examinations, performed as follow-up over the next 18 months, showed no change in the signal characteristics.

In the second patient, CT showed splenomegaly, periportal lymphadenopathy, and retroperitoneal adenopathy adjacent to the inferior vena cava and aorta. During IV injection of contrast material (Fig. 2A), multiple areas of relatively decreased attenuation were seen in the spleen. MR was performed 6 weeks after laparotomy. Minimal splenomegaly of diminished signal intensity was seen on T1-weighted images. On T2-weighted images, the spleen had patchy, diminished inhomogeneous signal intensity. On gradient-echo images (25/13) the

Received August 6, 1990; accepted after revision September 13, 1990.

[1] Both authors: Department of Diagnostic Radiology and Nuclear Medicine, University Hospital, University of Western Ontario, P.O. Box 5339, London, Ontario N6A 5A5, Canada. Address reprint requests to D. B. Bach.

*AJR* **156:520–522, March 1991** 0361–803X/91/1563–0520 © American Roentgen Ray Society

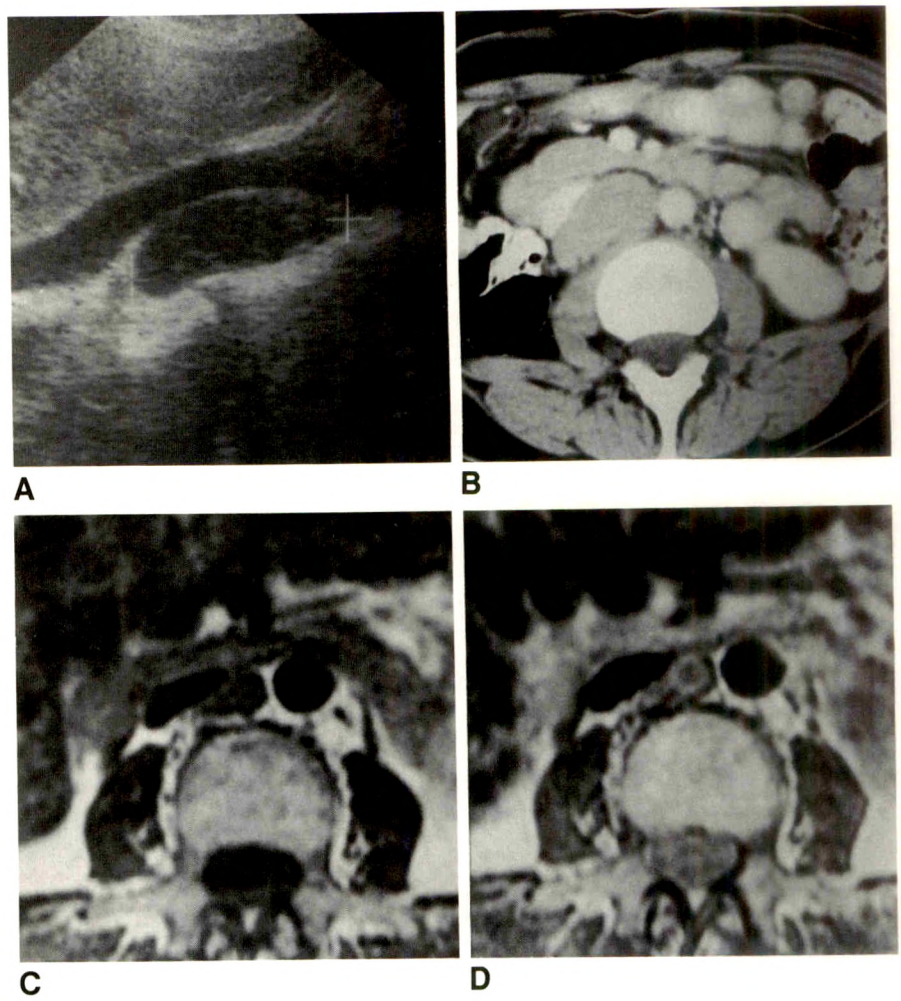



Fig. 1.—51-year-old woman with sarcoidosis.
*A*, Sonogram shows sonolucent mass displacing inferior vena cava anteriorly.
*B*, CT scan obtained before biopsy, with patient prone, shows mass lies between inferior vena cava and aorta.
*C*, Axial T1-weighted MR image (300/20) shows low signal intensity in oblong retrocaval adenopathy, with subtle patchy inhomogeneity.
*D*, Axial T2-weighted MR image (2000/70) shows retrocaval mass with peripheral high signal intensity and a bilobed low-signal-intensity central focus.

spleen had inhomogeneous signal intensity, suggestive of fairly extensive splenic T2 shortening. The signal characteristics within the retroperitoneal lymphadenopathy were nonspecific, although dissimilar from those noted in the first case in that the signal intensity on the T2-weighted images was homogeneous and intermediate.

## Discussion

Reports of intraabdominal and retroperitoneal lymphadenopathy in patients with sarcoidosis have been published in the radiology literature [2, 3], but this is rare; sarcoidosis was present in only one of nine cases of benign intraabdominal lymphadenopathy culled from 2100 CT examinations [4]. Involvement of the kidney, pancreas, and uterus by sarcoid has been described [5–7], with associated lymphadenopathy. The radiologic features in the abdomen are nonspecific, usually suggesting lymphoma or metastatic disease. Some patients have a history of sarcoidosis, but most often the diagnosis is made at biopsy of peripheral nodes or at laparotomy performed to exclude lymphoma, as in our two patients.

The MR findings in abdominal and splenic sarcoidosis have not been described before. Like CT, MR is unable to characterize intraabdominal or retroperitoneal lymphadenopathy associated with sarcoidosis. The central low signal intensity on T2-weighted images of retroperitoneal lymphadenopathy in the first patient is of uncertain significance, but it may be caused by the central nodal fibrosis that is associated with chronic granulomatous disease.

The pattern of splenic enhancement on CT seen in our second patient has been described in sarcoidosis [8]. The degree of splenic T2 shortening noted on both T2-weighted and gradient-echo images in the second case is consistent with chronic splenic fibrosis. Except for nodular sclerosing Hodgkin disease, these features are somewhat atypical for splenic lymphoma. Although not specific, the ability of MR imaging to show suggestive nodal or splenic fibrosis allows the diagnosis of chronic granulomatous disease to be entertained. This is particularly pertinent because both patients had diagnoses of probable lymphoma.

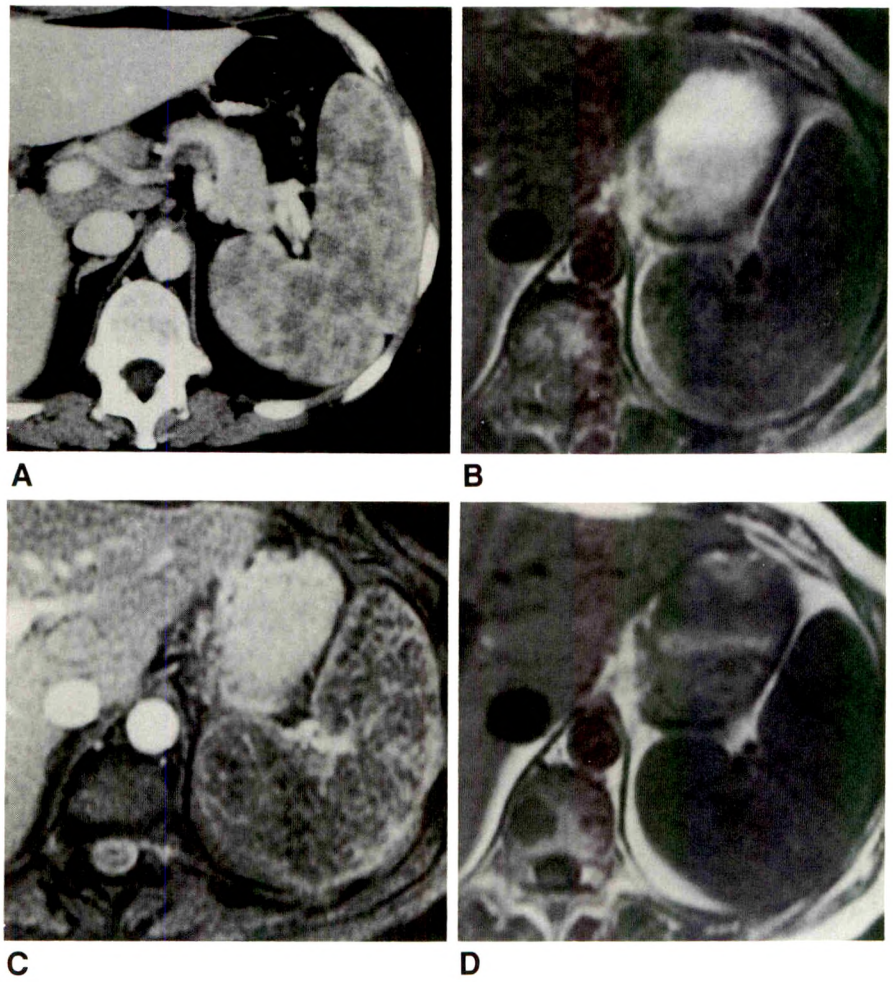



**Fig. 2.—61-year-old woman with sarcoidosis.**
***A*, Enhanced CT scan shows soft-tissue mass between inferior vena cava and portal vein. Note multiple areas of low density in enlarged spleen.**
***B–D*, Patchy inhomogeneity on axial T2-weighted (*B*, 2000/70 [TR/TE]) and gradient-echo (*C*, 25/13) MR images, both of which are of predominantly diminished signal intensity, is consistent with intrasplenic fibrosis. Focal sarcoid deposit within lumbar vertebral body is noted as intermediate-signal-intensity focus on axial T1-weighted (*D*, 300/30) MR image and as increased signal intensity on T2-weighted image (*C*).**

REFERENCES

1. Sharma OP. *Sarcoidosis: clinical management*. London: Butterworths, **1984**
2. Meranze S, Coleman B, Arger P, Mintz M, Markowitz L. Retroperitoneal manifestations of sarcoidosis on computed tomography. *J Comput Assist Tomogr* **1985**;9:50–52
3. Saksouk FA, Haddad MC. Detection of mesenteric involvement in sarcoidosis using computed tomography. *Br J Radiol* **1987**;60:1135–1136
4. Deutch SJ, Sandler MA, Alpern MB. Abdominal lymphadenopathy in benign diseases: CT detection. *Radiology* **1987**;163:335–338
5. Hughes JJ, Wilder WM. Computed tomography of renal sarcoidosis. *J Comput Assist Tomogr* **1988**;12:1057–1058
6. Sagalow BR, Miller CL, Wechsler RJ. Pancreatic sarcoidosis mimicking pancreatic cancer. *JCU* **1988**;16:131–134
7. Duszlak EJ, Costello P, Crosson AW, Clouse ME. Pelvic sarcoidosis. *J Comput Assist Tomogr* **1982**;6:1032–1033
8. Mathieu D, Vanderstigel M, Schaeffer A, Vasile N. Computed tomography of splenic sarcoidosis. *J Comput Assist Tomogr* **1986**;10:679–680

Pictorial Essay

# CT Appearance of the Pelvis After Cesarean Section

Diane M. Twickler,[1,2] Anthony T. Setiawan,[1] Rebecca S. Harrell,[1] and Charles E. L. Brown[2]

**Myometrial defects at the incision site after cesarean section may appear bizarre on CT scans, especially in the case of low transverse incisions, but may not indicate clinically significant dehiscence. These CT findings should be regarded as common in the patient without complications after cesarean section, so that unnecessary surgical intervention and additional treatment can be avoided.**

Postpartum metritis after cesarean section is common, occurring with a frequency of 1–6%, depending on socioeconomic factors and the presence of high-risk factors during labor and delivery [1]. In most cases of postpartum metritis, appropriate antibiotic agents are adequate to prevent serious sequelae; however, parametrial phlegmon, pelvic abscess, uterine incisional necrosis with dehiscence, and septic thrombophlebitis occur in up to 10% of patients [1]. Failure to respond to appropriate antibiotic agents warrants further investigation to delineate the specific complication. CT can be used to evaluate the patient for the serious complications of postpartum metritis [2].

A recent article has described the CT appearance of the pelvis after uncomplicated vaginal delivery [3]. The appearance of the pelvis after uncomplicated cesarean section has not been described. This study was undertaken to learn the common appearances of the uterus after uncomplicated cesarean section.

## Subjects and Methods

Fifteen consecutive women undergoing cesarean section and elective bilateral tubal ligation for sterilization were studied from August 1986 to November 1987. The concomitant bilateral tubal ligation eliminated the genetic risk of gonadal irradiation by CT. After institutional review board approval, informed consent was obtained from the patients before the CT examination.

Contrast-enhanced pelvic CT was performed 1–5 days after surgery. We decided to use IV contrast material because, in our previous experience, surgically proved dehiscence was not seen on unenhanced CT and was seen on enhanced CT (unpublished data). Ten-millimeter contiguous axial images were obtained from the uterine fundus to the symphysis pubis by using a Synerview 1200 SX (Picker, Highland Heights, OH) or CT 8800 (General Electric Medical Systems, Milwaukee, WI) scanner. The IV iodinated contrast medium was administered as a 50-ml bolus injection (Conray 60, Mallinckrodt Medical Inc., St. Louis, MO, or Hypaque 60, Winthrop Pharmaceuticals, New York, NY), followed by a 200-ml drip infusion (Conray 30, Mallinckrodt Medical Inc.).

The indications for cesarean section were repeated ($n$ = 11) and primary ($n$ = 4), including breech presentation ($n$ = 2), fetal distress ($n$ = 1), and unsatisfactory progression of labor ($n$ = 1). Six women had vertical incisions; nine women had low transverse incisions. All women remained afebrile throughout the hospital course, without complications. All women were discharged from the hospital on day 4 or 5.

The parametrium was defined as the loose connective tissue between the broad ligament leaves [1] found along the lateral uterus to the level of the cervix. Radiologic myometrial discontinuity was

Received July 16, 1990; accepted after revision September 12, 1990.

[1] Department of Radiology, The University of Texas Southwestern Medical Center at Dallas, 5323 Harry Hines Blvd., Dallas, TX 75235. Address reprint requests to D. M. Twickler.

[2] Department of Obstetrics and Gynecology, The University of Texas Southwestern Medical Center at Dallas, Dallas, TX 75235.

*AJR* **156:523–526, March 1991** 0361–803X/91/1563–0523 © American Roentgen Ray Society

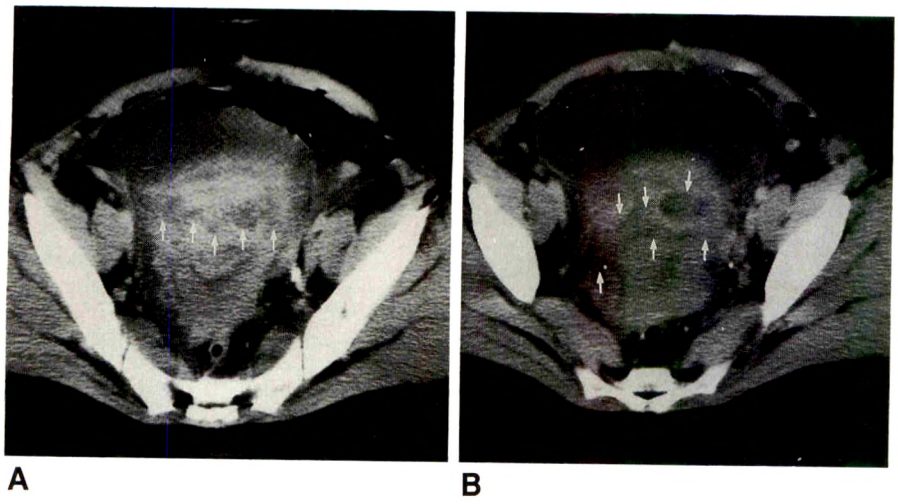



Fig. 1.—*A*, CT scan at level of low transverse incision shows myometrium has high density after contrast administration. Jagged horizontal low-density line running through width of uterus (*arrows*) represents partial voluming of transverse incision.

*B*, CT scan caudal to previous slice again shows multiple areas of discontinuity of lower uterine segment that are markedly irregular and poorly defined (*arrows*). These were believed to represent continued partial voluming of transverse uterine incision.

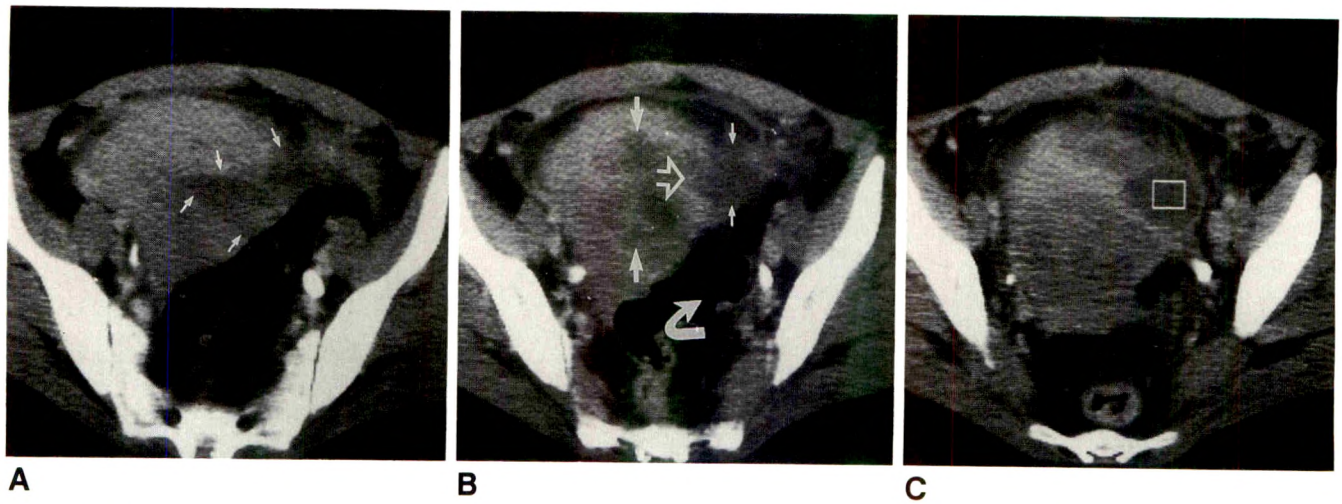



Fig. 2.—*A*, Axial CT scan at level of low transverse incision shows loss of continuity along left lateral margin of myometrium (*arrows*).

*B*, Next 10-mm slice shows left myometrial irregularity (*open arrow*) with low density in endometrial cavity (*large straight arrows*) and left parametrium (*small straight arrows*). Rectum is clearly defined because of normal luminal gas (*curved arrow*).

*C*, More caudal CT slice shows a low-density area (23 H, *box*) with high-density rim along left myometrium.

present when loss of clear margination of the myometrium was found at the site of incision, as represented by low-density irregularities, or gaps were seen in the apposition of the incision site.

## Results

The CT studies were divided into two groups on the basis of the type of uterine incision (vertical uterine incisions or low transverse incisions), and findings were classified according to locations. In the low transverse incisions, areas of myometrial discontinuity were seen in eight of nine patients. Parametrial fluid was present in seven of nine patients. In one patient (Fig. 1), multiple areas of discontinuity were seen in the area of the incision. Another patient had a low-density area with a loculation measuring 23 H along the left myometrial incision site (Fig. 2). In another case, air and fluid were seen in multiple locations (subcutaneous fat, rectus sheath, prevesical space of Retzius, endometrial cavity, and parametrium), in addition to a discontinuity at the lower uterine segment (Fig. 3).

Reviewing the group of women with vertical uterine incisions, four of six had areas of myometrial discontinuity. Parametrial fluid was commonly found in association with myometrial discontinuity (Fig. 4). An area of loculated low density (17 H) along the left lateral uterus was present along the left broad ligament and extended inferiorly to the bladder flap (Fig. 5). The bladder flap is formed by blunt dissection of the loose reflection of peritoneum (serosa) above the upper margin of the bladder and anterior lower uterine segment, near the incision site.

The most significant finding in both groups was the common occurrence of myometrial discontinuity. Vertical incisions all had sharply marginated defects. In the transverse incisions, where the CT plane is parallel to the transverse section,

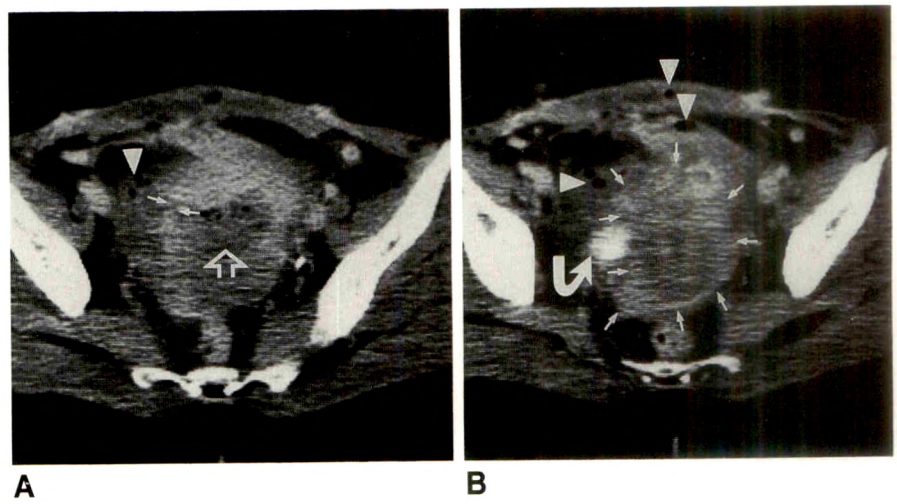



Fig. 3.—*A*, CT scan at level of transverse incision. Loss of myometrial continuity is seen along right side (*solid arrows*) with associated air (*arrowhead*) and fluid in right parametrial space. Air and fluid (*open arrow*) are apparent in endometrial cavity.

*B*, Inhomogeneous uterus (*straight arrows*) probably is due to plane of lower transverse incision and partial-volume effects. Partial voluming of bladder (*curved arrow*) accounts for high density to right of uterus, confirmed on caudal images. Multiple air pockets (*arrowheads*) can be seen in right parametrium, anterior space of Retzius, and anterior abdominal wall.

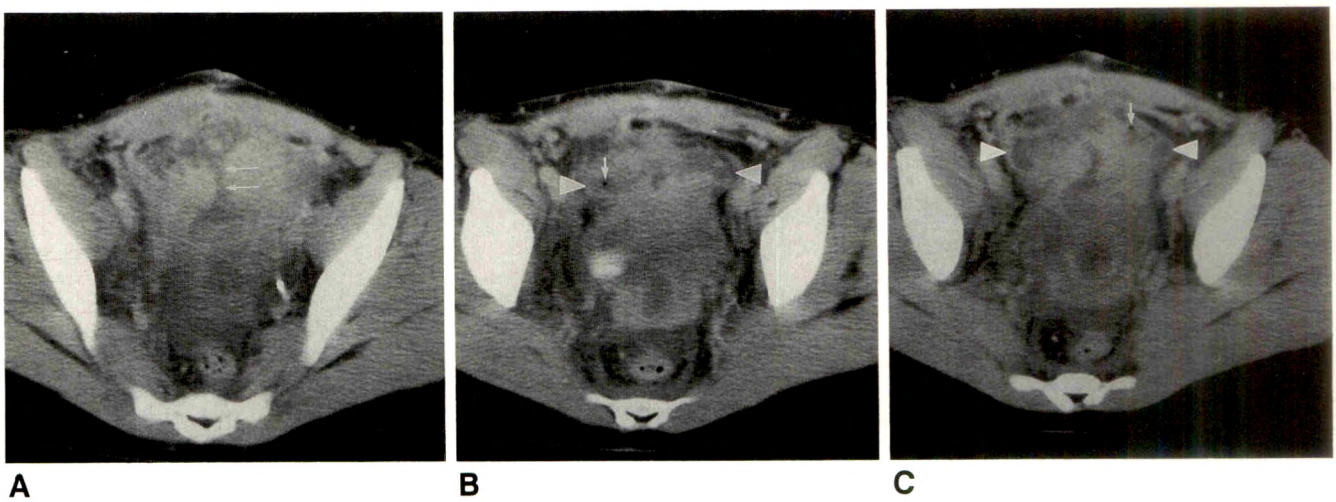



Fig. 4.—*A*, CT scan shows vertical uterine incision and sharply marginated uterine defect (*arrows*). *B* and *C*, Distal CT scans show parametrial fluid (*arrowheads*) with small pockets of air (*arrows*).

poorly defined margins were demonstrated. In all women, regardless of uterine incision type, fluid was apparent in the endometrial cavity; air was present in seven of 15 cases.

## Discussion

When confronted with the clinical findings of postpartum metritis without response to antibiotic agents, parametrial phlegmon, septic thrombophlebitis, uterine incisional necrosis with dehiscence, or pelvic abscess must be considered [1]. CT can be helpful in diagnosing those complications, but evaluation is much more difficult after cesarean section because the findings of abscess, phelgmon, or dehiscence can be mimicked by "normal" postoperative findings. Our study was prompted by a particular case of postpartum fever after cesarean section. A CT scan showed myometrial discontinuity and was interpreted as uterine incisional necrosis with dehiscence. At the time of surgery, the uterus was normal, there was no necrosis, and the incision was intact.

Our data show that uterine discontinuity is commonly seen in the immediate postpartum period. These observations may not represent clinically significant uterine incisional necrosis with dehiscence, even in the presence of endometrial or parametrial air. The findings probably represent edema in the region of the incision, with areas of compromised blood supply. As there is no gold standard, the findings could represent mild dehiscence, which has no clinical significance. This is unlikely because the clinical prevalence of dehiscence of a uterine incision in a subsequent pregnancy is less than 1% [4]. If patients are asymptomatic, this mild edema or dehiscence may resolve. The common parametrial low-density fluid collections and air appear to have no clinical significance after cesarean section. These findings explain why the clinical diagnosis of uterine incisional necrosis with dehiscence

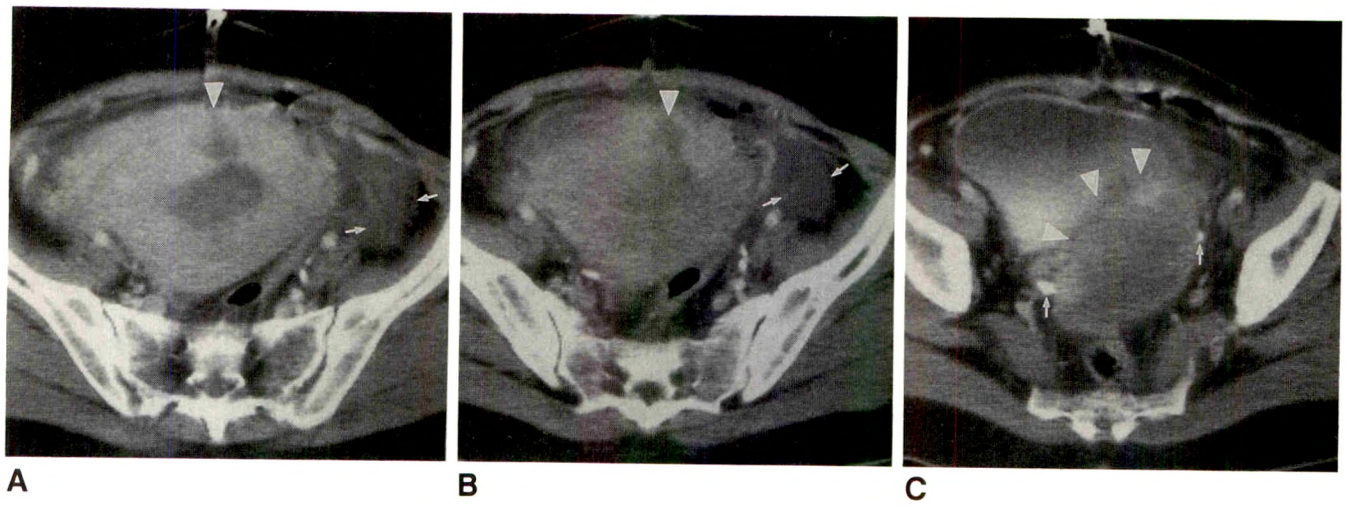



Fig. 5.—*A*, Axial CT scan from a continuous study in a patient with a vertical uterine incision (*arrowhead*) shows low midline low-density area of anterior myometrium. In addition, a low-density region can be seen along left broad ligament (*arrows*).

*B*, Subsequent caudal CT scan shows more clearly defined low-density area on left side, measuring 17 H (*arrows*). Anterior myometrial defect of vertical incision is seen again (*arrowhead*).

*C*, At level of lower uterine segment and bladder, outline of uterus is poorly defined, with mass effect on bladder (*arrowheads*) and ureters (*arrows*). This is the area of the bladder flap, the blunt dissection of the loose serosa at the upper margin of the bladder and anterior uterine segment, at the uterine incision.

after cesarean section correlates poorly with CT findings. This concept is an important one, because it may prevent unnecessary surgery on the basis of CT findings alone.

The unusual appearances of myometrial discontinuity in the case of low transverse incisions as compared with vertical uterine incisions can be explained easily. The incision of the low transverse type is parallel to the plane on contiguous axial images, while the vertical uterine incision is perpendicular, thus accounting for the larger and more poorly defined defect of the low transverse incision. Partial-volume effects of the transverse incision also cause the poorly defined appearance.

## REFERENCES

1. Cunningham FG, MacDonald PC, Gant NF. Puerperal infections. In: Cunningham FG, MacDonald PC, Gant NF, eds. *Williams obstetrics*, 18th ed. Norwalk, CT: Appleton & Lange, **1989**:461–476
2. Brown CEL, Lowe TW, Cunningham FG, Weinreb JC. Puerperal thrombophlebitis: impact and diagnosis and treatment using x-ray computed tomography and magnetic resonance imaging. *Obstet Gynecol* **1986**;68:789–794
3. Garagiola DM, Tarver RD, Gibson L, Rogers RE, Wass JL. Anatomic changes in the pelvis after uncomplicated vaginal delivery: a CT study on 14 women. *AJR* **1989**;153:1239–1241
4. Eden RD, Parker RT, Gall SA. Rupture of the pregnant uterus: a 53 year review. *Obstet Gynecol* **1986**;68:671–673

# CT Pelvimetry: The Foveae Are Not an Accurate Landmark for the Level of the Ischial Spines

Daniel Aronson[1,2]
Ruben Kier[1]

**The most important distance measured during CT pelvimetry is the interspinous diameter of the pelvis as seen on axial scans, because most cases of obstructed labor occur at the level of the ischial spines. As the spines are difficult to identify on the anteroposterior digital scout radiograph, the fovea of the femoral head has been used as a landmark to determine the level of the appropriate axial slice. We assessed the accuracy of this landmark on CT scans in 23 women undergoing CT pelvimetry and in 20 nonpregnant women having pelvic CT scans. In each case the relationship between the level of the foveae and the level of the ischial spines was determined. True interspinous distances were measured and compared with the apparent interspinous distances at the level of the foveae. In none of the women were the ischial spines above the foveae. In 15 (65%) of 23 pregnant women and in seven (35%) of 20 nonpregnant women, the ischial spines were below the foveae. An incorrect scanning level led to an overestimation of interspinous distance by an average of 1.0 cm.**

**We conclude that for CT pelvimetry, the fovea as seen on the anteroposterior digital radiograph is an inaccurate landmark for the level of the ischial spines.**

***AJR* 156:527–530, March 1991**

A small maternal pelvis is a contraindication to attempting vaginal delivery of a fetus in breech presentation because of the potential difficulty in delivering the aftercoming fetal head [1, 2]. A pelvis too small for safe vaginal delivery has been defined as one measuring less than either 12 cm in the widest transverse diameter of the pelvic inlet, 11 cm in the anteroposterior diameter of the pelvic inlet, or 10 cm at the midpelvis between the ischial spines [1] (termed the bispinous, interspinous, or midpelvic diameter). Digital pelvimetry on a CT scanner has been advocated as a replacement for conventional radiographic pelvimetry to obtain these measurements because it reduces the absorbed radiation dose [3].

The bispinous diameter is the most important measurement derived from pelvimetry, because it is the narrowest point of the midpelvis, where most cases of obstructed labor occur [2, 4]. Federle et al. [3] suggested that because the ischial spines were frequently difficult to visualize on an anteroposterior radiograph, an axial CT scan at the level of the ischial spines was the best way to measure the midpelvic diameter. They empirically determined that the ischial spines usually lie at the same level as the foveae of the femoral heads. As the foveae are easily seen on the anteroposterior digital radiograph, they were considered a useful landmark for prescribing the axial image [3]. Using this method, we encountered a few patients in whom the fovea was an unreliable landmark. Thus, we performed a study designed to determine if the fovea of the femoral head is an accurate landmark for the level of the ischial spines.

## Materials and Methods

We reviewed CT scans of 23 consecutive unselected pregnant women referred for pelvimetry between March 1987 and February 1990. We also reviewed the pelvic CT scans

Received June 29, 1990; accepted after revision September 25, 1990.

Presented at the annual meeting of the American Roentgen Ray Society, Washington, DC, May 1990.

[1] Department of Diagnostic Radiology, Yale University School of Medicine, 333 Cedar St., New Haven, CT 06510. Address reprint requests to R. Kier.

[2] Present address: Russell H. Morgan Department of Radiology and Radiological Science, The Johns Hopkins University School of Medicine, 600 N. Wolfe St., Baltimore, MD 21205.

0361–803X/91/1563–0527
© American Roentgen Ray Society

of 20 consecutive unselected nonpregnant women referred for unrelated indications between July and December 1989, because these studies used contiguous axial slices that would be expected to show both the foveae and the ischial spines, even if they were at separate levels.

CT scanning was performed on a GE 9800 scanner (GE Medical Systems, Milwaukee, WI). The pelvimetry protocol followed the technique of Federle et al. [3]. First, an anteroposterior digital radiograph was obtained to determine the level of the inlet, measured as the maximum distance between the ileopectineal lines. Second, a lateral digital radiograph was obtained so that the anteroposterior inlet could be measured (the minimum distance from the midportion of the sacral promontory to the posterior and superior aspect of the symphysis pubis). Third, an axial CT scan was obtained at the level of the fovea, as determined by the anteroposterior scout view, to measure the minimum interspinous distance. In this series, if the radiologist monitoring the study recognized that the ischial spines were not seen well on the initial axial CT scan, one (three cases) or two (two cases) additional axial CT scans were obtained. For the last three pelvimetry cases, the level of the axial CT scan was chosen from a lateral scout view that showed the ischial spines. We obtained the anteroposterior scout view at 70 mA and 120 kVp, the lateral scout view at 120 mA and 140 kVp, and the axial image with 10-mm collimation at 40 mA and 80 kVp.

The relationship of the level of the foveae to the level of the ischial spines was determined by either of two methods. In 32 cases, axial CT scans showing both structures were used. These included all 20 nonpregnant women. In eight cases, the foveae on the anteroposterior scout were identified, and this level was compared with the level of the ischial spines as identified on the lateral scout view. In three pelvimetry cases, only a single axial image was available, the ischial spines were not visible on the axial image showing the foveae, and the spines were not clearly seen on either the lateral or anteroposterior digital radiograph. For these cases, the configuration of the pelvis on the axial image was used to assess whether the spines were above or below this level, although no measurement of this error was possible. To prevent underestimation of average error by excluding these three patients, we assumed that they had the same error as the average of all other cases with the foveae and ischial spines at different levels.

In cases for which the foveae and the ischial spines were at different levels, the true interspinous distance was compared with the apparent interspinous distance at the level of the foveae.

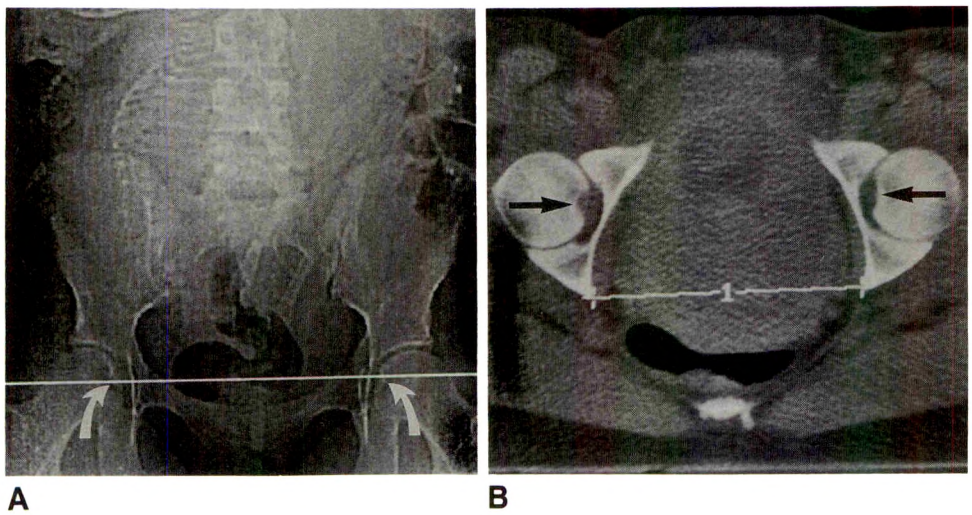
Twelve of the 23 pelvimetry patients were scanned with their hips flexed because they were more comfortable in this position. The relationship of the level of the foveae to the level of the ischial spines in this subgroup was compared with that in the other 11 pregnant patients scanned with their hips normally extended.

## Results

In no cases were the ischial spines above the foveae. Eight (35%) of 23 pelvimetry patients had the ischial spines at the level of the foveae. Fifteen (65%) of 23 had the ischial spines below the level of the foveae, with an average distance of 1.2 cm in the 12 patients for whom this could be measured (Figs. 1 and 2). Thirteen (65%) of 20 control subjects had the ischial spines at the level of the foveae. Seven (35%) of 20 had the ischial spines below the foveae, with an average distance of 0.9 cm.

Among patients who had the foveae and the ischial spines at different levels, axial measurements were available at both levels in 11 cases (seven control, four pregnant). In these patients, an incorrect scanning level at the foveae would have led to an overestimation of interspinous distance averaging 1.0 cm. This measurement could not be made for three pelvimetry patients in whom the axial slice through the spine was prescribed from the lateral scout view, and for eight pelvimetry patients in whom an axial slice through the ischial spines was not obtained.

The presence or absence of hip flexion affected the relationship of the level of the foveae to the level of the ischial spines. In pregnant patients, hip flexion was associated with a higher frequency (75%) and significantly higher (Wilcoxon signed-rank test, $p = .01$) average error ($1.07 \pm 0.76$ cm) compared with pregnant patients without hip flexion (55%



A B

**Fig. 1.—Pregnant patient with foveae 1.5 cm above level of ischial spines.**

***A*, Anteroposterior digital radiograph shows fetus in breech presentation. Level chosen for axial CT scan is indicated by transverse line through level of foveae (*arrows*).**

***B*, Axial CT scan shows foveae (*arrows*) of femoral head, but fails to show ischial spines. Triangular shape of posterior columns of acetabula indicate that axial CT scan is above desired level.**

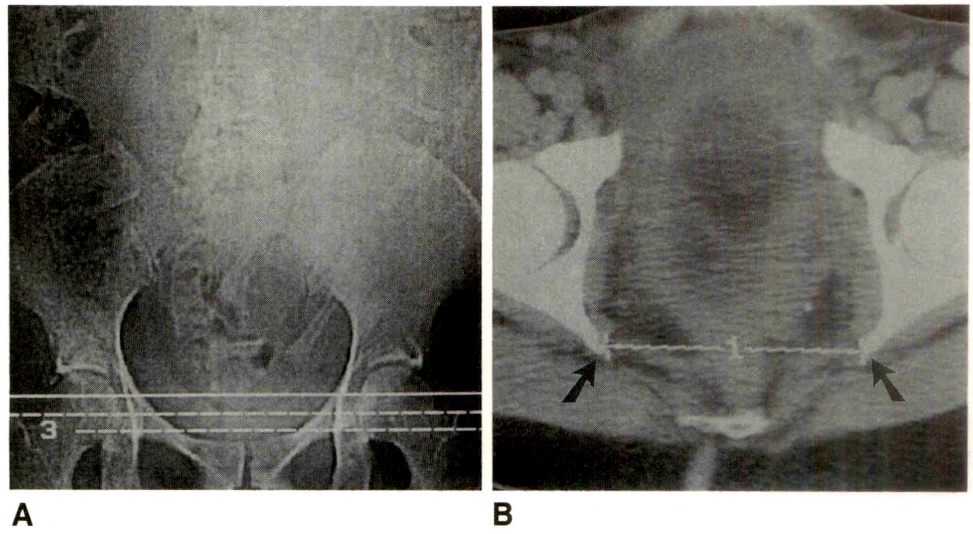



Fig. 2.—Pregnant patient with foveae 2.0 cm above level of ischial spines.

*A*, Anteroposterior digital radiograph of fetus in breech presentation. Three transverse lines indicate levels chosen for axial slices. First slice (*solid line*) was through foveae, with subsequent slices 1.0 cm and 2.0 cm below foveae.

*B*, Axial CT scan obtained 2.0 cm below level of foveae shows ischial spines (*arrows*) projecting posteriorly and medially. Interspinous distance measured 9.9 cm. At level of foveae, apparent interspinous distance was 11.8 cm.

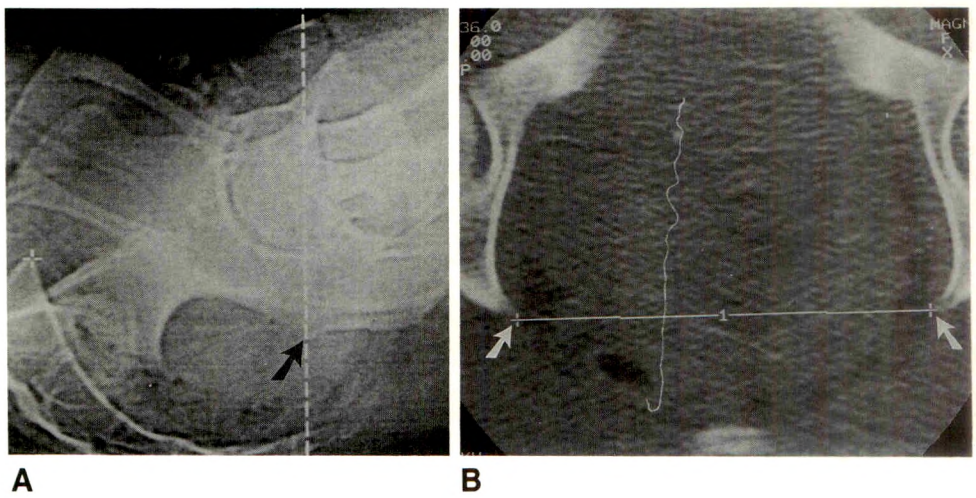



Fig. 3.—Pregnant patient with axial CT image accurately prescribed from lateral digital radiograph.

*A*, Lateral digital radiograph shows fetus in breech presentation. Ischial spines (*arrow*) project posteriorly, and line depicts level chosen for axial CT scan.

*B*, Axial CT scan shows ischial spines (*arrows*).

frequency, 0.51 ± 0.56 cm average error). Compared with pregnant patients without hip flexion, the control patients (also scanned without hip flexion) showed a lower frequency (35%) and significantly lower (Wilcoxon signed-rank test, $p = .03$) average error (0.32 ± 0.49 cm).

## Discussion

Our data indicate that the foveae of the femoral heads are an inaccurate landmark for the level of the ischial spines. The results suggest that three factors contribute to this inaccuracy. First, 35% of the control subjects had the ischial spines below the level of the foveae, indicating that differences in levels are common normal variants. Second, pregnancy, even without hip flexion, increases the likelihood of the ischial spines being below the foveae and also will increase the average distance that the ischial spines are below the foveae. This may reflect changes in posture induced by the ligamentous laxity of pregnancy or by descent of the fetus into the pelvis during labor [5]. Third, hip flexion will increase both the likelihood and severity of error in pregnant patients, presumably by altering the relationship of the femoral heads to the acetabulum.

An incorrect landmark, if unrecognized, can have serious consequences for the patient. In our series, eight of 23 pelvimetry patients never had an accurate axial measurement of interspinous distance, because only one axial image was obtained at the level of the foveae. In other patients, an incorrect scanning level was found to overestimate the interspinous distance by an average of 1 cm. Because an interspinous distance less than 10 cm in a breech presentation is an indication for cesarian section, this error may lead to an inappropriate and potentially dangerous attempt at vaginal delivery [1, 2].

These results indicate the need for an alternative landmark for the level of ischial spines. We observed that in 16 (70%) of the 23 pelvimetry patients, the ischial spines were clearly identified on the lateral digital radiograph (Fig. 3). Thus, when

the ischial spines are seen on the lateral scout view, the axial CT image can be prescribed accurately.

Our current approach for CT pelvimetry begins with an anteroposterior and lateral digital radiograph to measure the transverse and anteroposterior pelvic inlets, respectively. We also assess for fetal presentation. If the fetus is breech, we describe the presence of flexion or extension of the hips and knees. We also try to determine if there is hyperextension of the fetal neck, a contraindication to vaginal delivery because of the potential for cervical spine injury [6]. Whenever possible, we scan the patient without hip flexion. To determine the level of the ischial spines for the axial CT scan, we first check the lateral scout view. If the ischial spines are seen on this image, we use this level to prescribe the axial CT image. If the ischial spines are not seen on the lateral scout view, we look for the ischial spines on the anteroposterior scout view near the inferior margin of the foveae. If the ischial spines are not seen on either scout view, we select the inferior margin of the foveae as the level for the axial image and consider a second axial slice 1.0 cm caudad if the ischial spines are not identified on the first axial image.

ACKNOWLEDGMENT

We appreciate the helpful comments of Richard R. Viscarello, of the Department of Obstetrics and Gynecology, Yale University School of Medicine.

REFERENCES

1. Gimovsky ML, Willard K, Neglio M, Howard T, Zerne S. X-ray pelvimetry in a breech protocol: a comparison of digital radiography and conventional methods. *Am J Obstet Gynecol* **1985**;153:887–888
2. Collea JV, Rabin SC, Weghorst GR, Quilligan EJ. The randomized management of term frank breech presentation: vaginal delivery vs. cesarean section. *Am J Obstet Gynecol* **1978**;131:186–193
3. Federle MP, Cohen HA, Rosenwein MF, Brant-Zawadzki MN, Cann CE. Pelvimetry by digital radiography: a low-dose examination. *Radiology* **1982**;143:733–735
4. Oxorn H. *Human labor and birth*, 5th ed. Norwalk, CT: Appleton-Century-Crofts, **1986**:31
5. Bryant-Greenwood G, Ali S, Mandel M, Greenwood F. Ovarian and decidual relaxins in human pregnancy. *Adv Exp Med Biol* **1987**;219:709–713
6. Watson WJ, Benson WL. Vaginal delivery for the selected frank breech infant at term. *Obstet Gynecol* **1984**;64:638–640

Review Article

# Automated Percutaneous Lumbar Diskectomy

Gary Onik[1] and Clyde A. Helms[2]

**The use of automated percutaneous lumbar diskectomy for the treatment of herniated lumbar disks is increasing. More than 3000 physicians have been trained to perform the procedure, and over 40,000 cases have been completed worldwide. This review describes the development of automated percutaneous lumbar diskectomy, the selection of appropriate patients, how the technique is performed, and its efficacy relative to other methods of treatment.**

Automated percutaneous lumbar diskectomy (APLD) is a relatively new advance in the treatment of herniated lumbar disks. The technique involves the placement, under fluoroscopic guidance and with local anesthesia, of a small automated suction probe into the affected disk. A small portion of the central nuclear material is then aspirated. The concept of the procedure is to decrease the intradiskal pressure and to transmit this decreased pressure through the rent in the anulus to the herniation, thereby relieving the pressure on the affected nerve root and resolving the patient's symptoms. Development of this technique was instigated by the general trend toward less invasive procedures throughout medicine and the perception that the traditional surgical treatment for herniated lumbar disks was associated with variable results and significant morbidity.

Over 3000 physicians have been trained in small group workshops to perform the APLD procedure, and more than 40,000 cases have been completed on a worldwide basis (Allen R, personal communication). In their recent policy statement on herniated disks [1], the American Academy of Orthopedic Surgeons has listed percutaneous diskectomy as an accepted procedure for the treatment of herniated lumbar disks, and the National Blue Cross/Blue Shield Technology Assessment Committee has determined APLD to be safe and efficacious in treating contained herniated lumbar disks, removing it from investigational status. With this extensive experience accumulating, it is appropriate at this point to review the knowledge available about this procedure. In this review we discuss the indications and patient selection for the procedure, as well as provide a description of the technique and review the available results.

## Development of Automated Percutaneous Lumbar Diskectomy

The recent literature dealing with the morbidity of simple open diskectomy has emphasized the potential for possible complications associated with this procedure. Stolke et al. [2], in a prospective study of 481 procedures performed by experienced neurosurgeons, found a complication rate of 13%, including one death, three nerve injuries, and an approximate diskitis rate of 1%. Ramirez and Thisted [3] reviewed 28,000 simple open diskectomies performed in a community setting and found that one in 64 patients had a major complication, one in 335 had a major neurologic complication, one in approximately 500 had a cardiovascular complication, and one in 1700 died from the procedure. It is the concern over these risks associated with open diskectomy that has prompted the search for less morbid procedures.

Chymopapain injection was the first of the less invasive treatments for herniated lumbar disks. Unfortunately, treat-

Received May 14, 1990; accepted after revision September 12, 1990.
[1] Department of Radiology, Presbyterian-University Hospital, DeSoto and O'Hara Sts., Pittsburgh, PA 15213. Address reprint requests to G. Onik.
[2] Department of Radiology, University of California, San Francisco, San Francisco, CA 94143.

 0361–803X/91/1563–0531 © American Roentgen Ray Society

ment with chymopapain had associated problems: anaphylaxis, severe back spasms in a significant number of patients, disk space narrowing, and associated transverse myelitis with paraplegia. It was this last complication, with its possible legal ramifications, that greatly curtailed the use of chymopapain in the United States.

Percutaneous diskectomy, a mechanical decompression of the disk, is an attempt to effect the same results as chymopapain without the associated complications. Percutaneous diskectomy was introduced by Hijikata et al. [4] in 1975 as a form of treatment for herniated lumbar disks. Since that original article, a number of other investigators have used manual disk removal techniques similar to that of Hijikata et al. and have reported success rates of 72–87% [5–11]. All these hand methods of percutaneous diskectomy have the common elements of a relatively large cannula (6 mm or larger) being used to gain access to the disk space with the disk being removed by some form of grasping forceps. Although these recently published articles have shown this technique to be efficacious, the method has not been without significant morbidity. At least two instances of major vascular injuries have been reported with this type of procedure [5–9]. In addition, since the disk is entered multiple times, the diskitis rates reported with this method have been consistent with the 1% diskitis rate reported for open diskectomy [12, 13].

APLD, first reported by Onik et al. [14], takes advantage of a 2-mm reciprocating suction cutter that can cut separate pieces of disk material up to 200 times per minute. The Nucleotome aspiration probe (Surgical Dynamics, Inc., San Leandro, CA) works by aspirating nucleus pulposus into its recessed side port. A flared inner cutter is pneumatically driven across the port, cutting off disk material, which is then suspended in saline and aspirated away (Fig. 1 ). Since anulus fibrosus cannot be sucked into its side port, the Nucleotome cannot cut its way out of the disk, adding to the safety of the procedure. By automating the process, it is possible to decrease the size of the instrumentation, thereby decreasing the chances for nerve injury, vessel damage, and soft-tissue trauma in a large patient population. Because the instrument is placed into the disk and remains there without being removed, the chances of contamination and diskitis are lowered to approximately one fifth that of an open procedure or of percutaneous diskectomy done by hand [15]. Since that first report by Onik et al., a large amount of data has accumulated showing the concept of APLD to be successful. Currently, 19 studies on APLD, comprising over 3600 patients, are either published or in press [15–33]. Twelve of the reports show a success rate of 80% or greater, and six of the studies show a success rate of 70–80%. In all these studies, no major complications were reported; specifically, no death, permanent nerve injury, or vessel damage was reported. A diskitis rate of 0.2%, three to five times lower than that for other diskectomy methods, was reported.

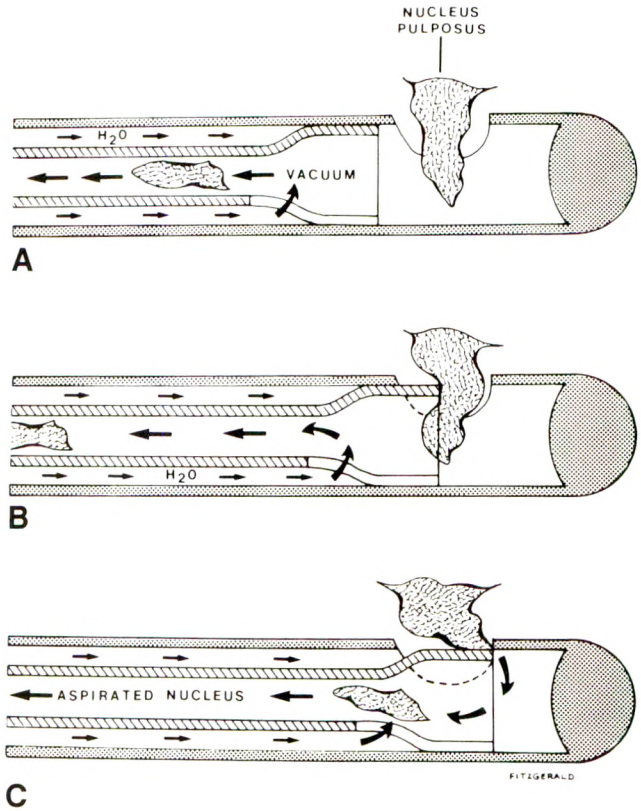



**Fig. 1.—*A*, Drawing of Nucleotome illustrates how suction is applied to central bore, thereby aspirating disk material into side port.**
***B*, An inner cutting sleeve is pneumatically driven across side port, effectively guillotining disk material.**
***C*, Disk material is suspended in saline, which flows between walls of Nucleotome and inner cutting sleeve, and is aspirated away.**
**(Reprinted from Onik et al. [14].)**

## Selection of Patients

As with all back operations, good results depend on proper selection of patients (Table 1). As with any disk operation, the procedure is predominantly for those patients with leg pain secondary to a herniated disk and is *not* for patients with chronic or acute low back pain. Before considering APLD, an adequate course of at least 6 weeks of simple conservative care, including rest, analgesics, and physical therapy, should have been attempted without success. In practice, it is unusual to operate on any patient who has not had 3 months of conservative treatment.

APLD should be performed only on those patients whose disk herniations are contained by the anulus fibrosis or pos-

**TABLE 1: Criteria Used to Select Patients for Automated Percutaneous Lumbar Diskectomy**

| Criteria |
|---|
| Clinical |
| Sciatica (leg pain predominates over back pain) |
| Physical findings that correlate with pain |
| Failure of conservative therapy (6 weeks) |
| Radiologic |
| Herniated nucleus pulposus contained by anulus or posterior longitudinal ligament |
| Exclusion of free fragments, spinal stenosis, calcified disks |

terior longitudinal ligament, that is, a protrusion (Fig. 2). Performing the procedure in patients with extruded or free fragments of disk would lead to a large number of failed procedures. The major burden in selecting patients for APLD falls on radiologic imaging. Preoperative CT or MR scans should be obtained to confirm the presence of a small to moderate focal bulge or herniation that is consistent with the patient's symptoms (Fig. 3) and to exclude a free disk fragment. Myelography alone is not adequate because it does not exclude complicating abnormalities such as lateral recess stenosis, calcified disk herniations, or far lateral disk herniations.

It is extremely important to determine the size of the disk herniation. In one report, 90% of patients with herniated disks comprising 50% or more of the thecal sac had extruded or free fragments (Fig. 4) [34].

In addition, the shape of the herniation can be used as an indication of whether the herniation is extruded or contained. Contained herniations tend to have smooth obtuse margins that blend at its base with the rest of the anulus fibrosus.

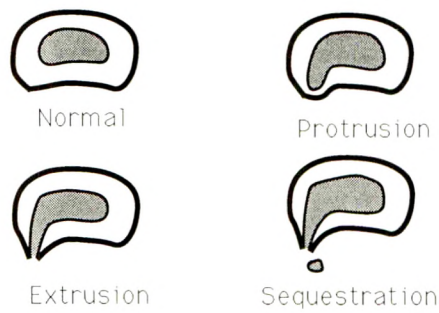



**Fig. 2.—Diagram of stages of herniated nucleus pulposus illustrates various stages of disk herniations. Automated percutaneous lumbar diskectomy should be performed only in a protrusion.**

Irregular herniations, that is, those with sharp angles to the anular margin, probably have extruded fragments (Fig.4 ).

CT or MR demonstration of a piece of disk material above or below the disk space or filling a lateral recess is a contraindication to APLD because a migrated fragment of disk certainly would not be affected by central disk decompression (Fig. 5). When there is any doubt as to whether the herniation is extruded through the posterior longitudinal ligament, diskography can be performed to investigate the integrity of the anulus and posterior longitudinal ligament. Free flow of contrast material into the epidural space indicates a complete tear of the anulus and posterior longitudinal ligament and a high likelihood that the herniation has extruded (Fig. 6). Demonstration of flow of contrast material through the anular tear to cover the disk herniation also indicates that a communication still exists between the center of the disk and the herniation. This confirms the possibility that extraction of disk material or transmission of pressure differences between the disk herniation and the center of the disk can still occur (Fig. 7). When diskography does not demonstrate a herniation that is seen on CT or MR, percutaneous diskectomy should not be undertaken. Edwards et al. [35] showed that when herniations did not stain when contrast material was injected into the center of the disk for CT diskography, chymopapain was successful in only 10% of cases because the anular tear had closed, not allowing communication between the herniated nucleus pulposus and the nucleus. It stands to reason that this criterion is applicable to percutaneous diskectomy as well.

Considering that APLD is a procedure for patients with contained herniations only, what proportion of the disk herniation population might be helped by APLD? In a recent prospective surgical series [36], 20% of patients operated on with an open procedure had contained disk herniations. Considering that over 200,000 disk operations are performed

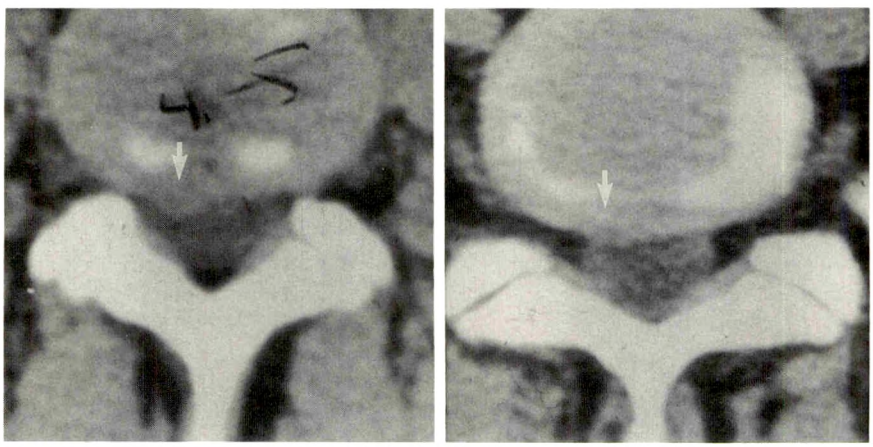



**Fig. 3.—CT scans of focal disk protrusions (*arrows*) that are good candidates radiologically for percutaneous diskectomy.**

***A*, Focal protrusion at L4–L5 level is consistent with leg pain. Automated percutaneous lumbar diskectomy was performed, and the patient did well for 2 years.**

***B*, CT scan 2 years later after recurrence of right leg pain. Contained herniated nucleus pulposus at L5–S1 level was successfully treated with automated percutaneous lumbar diskectomy.**

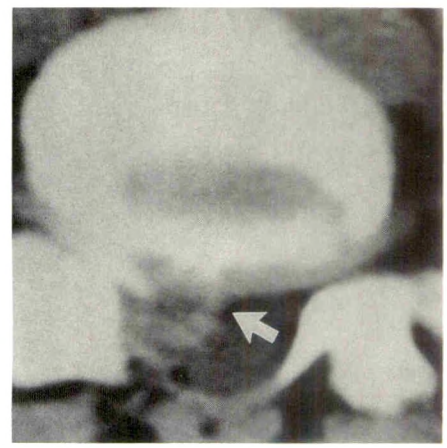


**Fig. 4.—CT scan shows a large disk herniation that is not a candidate for percutaneous diskectomy owing to its large size (50% of thecal sac). Sharp angulation between margin of anulus and herniation (*arrow*) indicates a probable extrusion.**

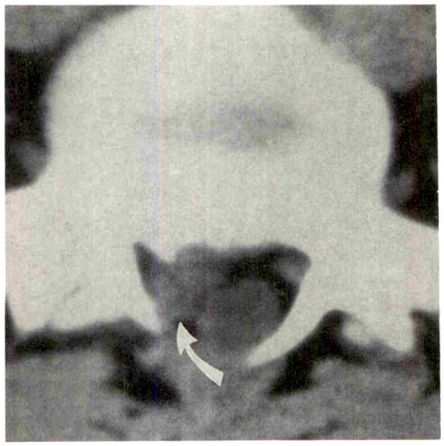


Fig. 5.—CT scan through lateral recess reveals migrated disk material (*arrow*), which suggests a free fragment. This patient is not a candidate for percutaneous diskectomy.

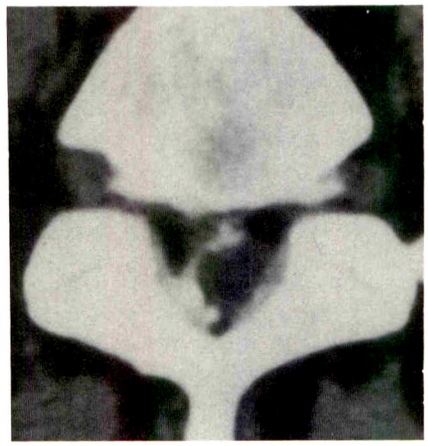


Fig. 6.—CT diskogram shows free flow of contrast material into epidural space, which indicates a noncontained disk. This patient is not a candidate for percutaneous diskectomy.

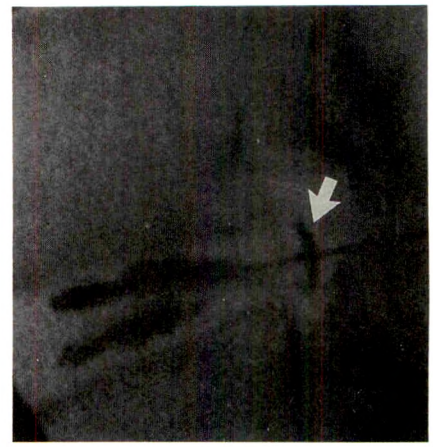


Fig. 7.—Diskogram shows staining of disk protrusion (*arrow*) without free flow of contrast material. This patient is a good candidate for percutaneous diskectomy.

each year in the United States, approximately 40,000 of these patients could be spared a major surgical procedure.

### Technique

A detailed description of the APLD technique is beyond the scope of this review; however, a number of technical points are pertinent because they help explain why APLD has such a low morbidity rate.

APLD reaches the disk via a posterolateral approach. The instruments pass just anterior to the superior articular facet, behind the nerve, in a trajectory toward the center of the disk (Fig. 8). Certain radiologic landmarks prevent injury to vital structures during placement of the instruments. A line that connects the posterior vertebral bodies, anterior to which lie the nerve, bowel, and great vessels, prevents injury to these structures (Fig. 9). When the instruments are against the anulus, they should be at this line but not anterior to it. On the anteroposterior view, an imaginary line connecting the medial border of the pedicles indicates the lateral border of the thecal sac. If the instruments are lateral to this line when they are lying against anulus fibrosus, they will not be impinging on the thecal sac (Fig. 10).

The procedure must be performed with only local anesthesia used, to allow the patient to react to any nerve root impingement. If the patient experiences radicular pain during the procedure, the instruments are redirected, thus preventing a nerve root injury. Localization of the instruments to the center of the disk is first carried out with an 18-gauge trocar. Once this trocar is localized to the center of the disk, the larger 2.8-mm cannula and dilator are brought down over the trocar to the disk. The dilator is removed, and the anulus is incised with a trephine. The trephine and trocar are removed, and the Nucleotome is then placed within the disk (Fig. 11). The procedure is monitored by watching the disk material being aspirated, which is visualized in the aspiration line. When no more disk material is seen, the procedure is concluded and the instruments are removed. The position of the

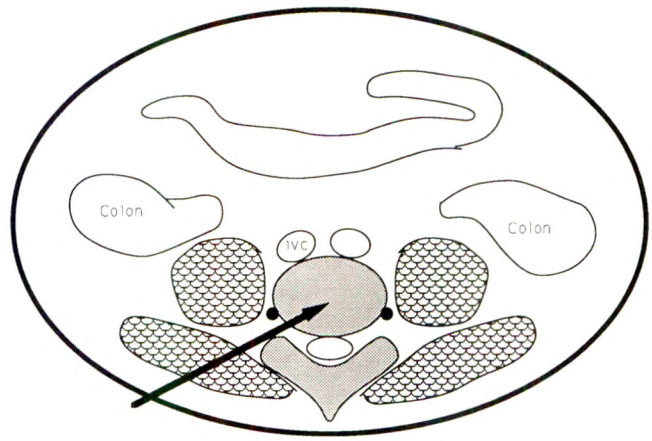



Fig. 8.—Diagram shows path taken during percutaneous diskectomy. ivc = inferior vena cava.

cannula on the anulus prevents the Nucleotome from injuring surrounding soft-tissue structures if it is inadvertently brought out of the disk.

The approach to the L5–S1 disk space is essentially the same as for L4–L5 and has been described in detail elsewhere [37]. The introduction of a curved cannula, through which the straight Nucleotome, which is flexible, can be placed, allows consistent entry into the L5–S1 disk in over 90% of cases [38].

### Results of APLD Compared with Other Techniques

The findings of a prospective multiinstitutional study to evaluate APLD have been reported [15]. Satisfying the inclusion criteria for selection were patients with classic sciatica whose herniated lumbar disks on imaging studies were consistent with their symptoms. Patients were prospectively excluded from this study if they had had previous lumbar surgery or chymopapain injection; if they had worker's compensation

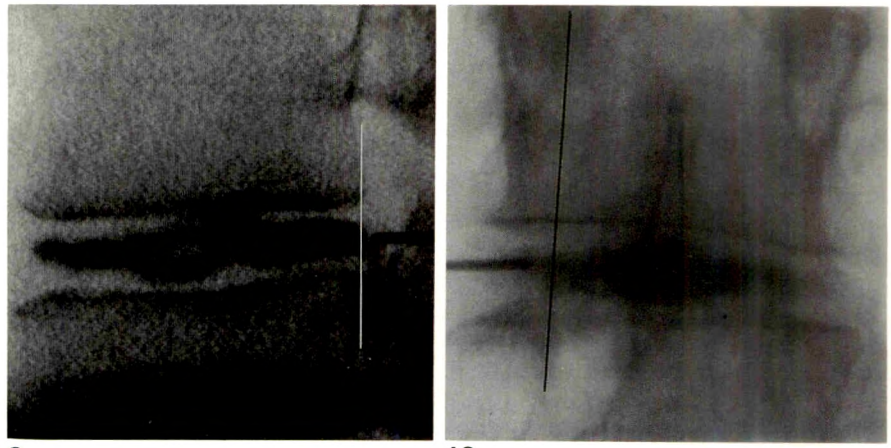


**Fig. 9.—Tip of trocar is lying against an imaginary line (*white line*) that joins posterior vertebral bodies when anulus is felt. This ensures that structures such as nerve, colon, and great vessels, which lie anterior to this line, will not be injured.**



**Fig. 10.—When lying against anulus, tip of trocar is lateral to imaginary line (*black vertical line*) joining medial border of pedicles. Therefore, thecal sac, which lies medial to this line, will not be injured.**

9 10

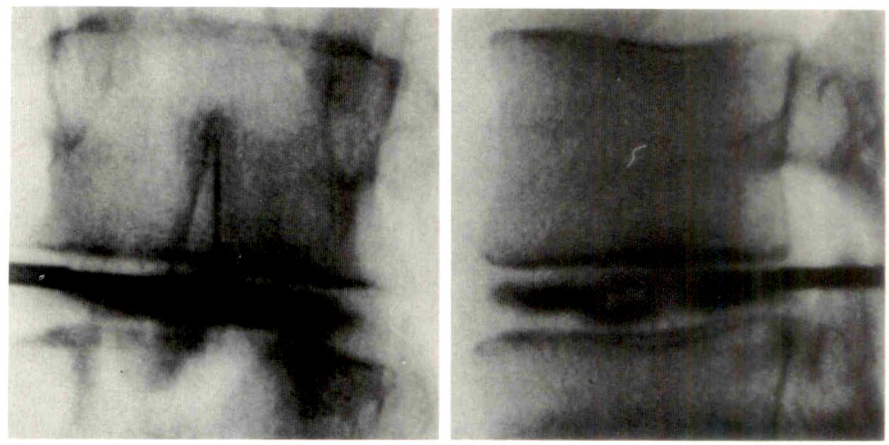


**Fig. 11.—*A* and *B*, Anteroposterior (*A*) and lateral (*B*) views show Nucleotome in a posterocentral position within disk.**

A B

claims; or if imaging studies revealed other causes for pain such as severe degenerative facet disease, spinal stenosis, or evidence of a free disk fragment. The criteria for success were stringent, the most essential being patient satisfaction with the results of the procedure. If a second procedure was required, be it another percutaneous diskectomy or an open procedure, APLD was considered a failure.

From November 1984 through May 1987, 506 APLD procedures were performed by 18 different surgeons. Of the 506 cases, 11 cases were lost to follow-up and 327 cases met the prospective study criteria; 168 cases were knowingly done that did not meet the protocol and were reported as such by the study group. The mean duration of preoperative conservative care for the study group was 11.5 months, making it extremely unlikely that the symptoms in this patient population would have resolved with further conservative care. In the 327 patients who met the protocol and had follow-ups of 1 year or more, the success rate was 75%. In those patients outside the protocol, procedures were successful in 49%. Of the 81 patients within the protocol for whom APLD was considered to have failed, 41 patients underwent either a laminectomy, a microdiskectomy, or a fusion. Nineteen of these patients underwent another percutaneous diskectomy; only three of these required a subsequent open operation. If these 16 patients who were successfully treated by a second percutaneous diskectomy are included, the success rate of the procedure rises to 80%. Of the 44 patients who subsequently underwent an open procedure, 30 (68%) had free fragments of disk unsuspected by preoperative imaging.

The findings in this study have been reproduced by other investigators. In another prospective multiinstitutional study conducted in Italy [16], 650 patients were treated with APLD with a 72% success rate; the selection and success criteria were the same as in the first multiinstitutional study. In a French prospective multiinstitutional study [17], 286 patients were treated with a success rate of 78%, again confirming these results.

Currently, 19 studies comprising over 3600 patients are either published or in press that confirm the results obtained by the initial multiinstitutional study (Table 2). A success rate of 80% or greater was reported in 12 of these and of 70% or greater in 18. Only one retrospective study comprising 17 patients reported a success rate less than 70% [23]. Of note is the small number of patients in this study as well as the fact that patients with back pain only were included in this series.

The efficacy of APLD appears to compare favorably with the results previously reported with chymopapain injection and open diskectomy, although it is difficult to draw conclusions without a comparative randomized study. In a number of studies, the efficacy of treatment with chymopapain has been reported to be from 40% [39] to 85% [40] and that of open diskectomy has been reported as 77% [41] to 99% [42], whereas success rates reported for microdiskectomy (the same approach as a traditional laminectomy or laminotomy performed with an operating microscope) have consistently been as high as 95% [43, 44]. It must be pointed out, however, that success in open diskectomy has always been defined as relief of leg pain, disregarding any new or residual back pain that may have been left over or have been caused by the procedure. In the only prospective study reported for microdiskectomy, 25% of patients had chronic back pain after the procedure [45]. In a recent study by Hanley and Shapiro [42], 14% of patients had new disabling back pain after open diskectomy.

**TABLE 2: Results of Studies Evaluating the Success of Automated Percutaneous Lumbar Diskectomy**

| Researchers | No. of Patients | Success Rate (%) |
|---|---|---|
| Onik et al. [15] | 506 | 75.4[a] |
| Bocchi et al. [16] | 650 | 72.0[a] |
| Benazet and Roy-Camille [17] | 286 | 78.3 |
| Maroon and Allen [18] | 1054 | 82.9[b] |
| Lesoin et al. [19] | 30 | 83.3 |
| Hammon [20] | 49 | 79.0 |
| Flynn et al. [21] | 50 | 80.0 |
| Davis and Onik [22] | 200 | 77.5 |
| Goldstein et al. [23] | 17 | 53.0 |
| Gill and Blumenthal [24] | 62 | 79.0 |
| Russell et al. [25] | 94 | 83.0 |
| Swiecicki [26] | 100 | 83.0 |
| Capanna and Capanna [27] | 10 | 80.0 |
| Cooney [28] | 50 | 82.0 |
| Corkhill et al. [29] | 21 | 88.0 |
| Rezaian and Silver [30] | 27 | 94.0 |
| Cartolari et al. [31] | 24 | 83.0[c] |
| Kaps and Cotta [32] | 67 | 82.0 |
| Davis et al. [33] | 518 | 86.0 |

Note.—Major complications comprised [a]one case of diskitis, [b]two cases of diskitis, and [c]one case of diskitis and one transient nerve root irritation.

In the only comparative study reported to date comparing APLD with open diskectomy and chymopapain injection, APLD, with its reported success rate of 83% in 100 patients treated, was equal to laminectomy and superior to treatment with chymopapain [25].

Even if the most optimistic success rates reported for microdiskectomy are considered, the difference in efficacy between open diskectomy and APLD appears to be only 10–15%. If APLD is to be a viable procedure, the advantages of the procedure have to outweigh this lower success rate, which appears to be due to missed free fragments of disk material. We believe the advantages of APLD outweigh its slightly lower efficacy for several reasons: (1) Its performance under local anesthesia markedly decreases the chance for nerve injury while avoiding the risks associated with general anesthesia. (2) With the posterolateral approach, there is no violation of the spinal canal. Therefore, the procedure is not associated with epidural fibrosis and the chronic pain syndrome that can result. Because of this, a patient in whom percutaneous diskectomy fails can later undergo an open procedure without negative effects. (3) No bone or ligament removal is associated with the procedure; therefore, the chances of postoperative instability are decreased. (4) The disk is entered only once with the automated removal probe. Therefore, APLD is associated with a markedly decreased infection rate compared with open diskectomy. (5) Because of the minimal trauma associated with the procedure, the procedure can be done on an outpatient basis; 70% of patients can return to work within 2 weeks of the procedure [22].

Compared with chymopapain treatment, APLD has a very low prevalence of associated back spasm, with virtually no risk of anaphylaxis or transverse myelitis, which have made chymopapain injection risky. A comparison of the postoperative imaging of APLD with that of laminectomy is interesting. While immediate postoperative resolution of the herniated nucleus pulposus can occur (Fig. 12), it has been shown that in most cases the herniated nucleus pulposus appears unchanged even in patients who have obtained symptomatic

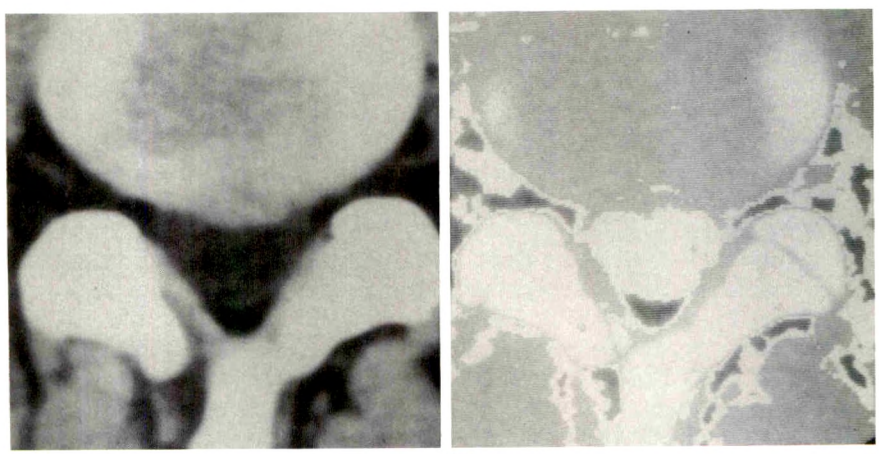



**Fig. 12.—CT scans before and immediately after automated percutaneous lumbar diskectomy.**
***A*, L4–L5 herniated nucleus pulposus is slightly to the left. (Reprinted from Onik et al. [14].)**
***B*, CT blink-mode image immediately after the procedure shows complete resolution of herniated nucleus pulposus.**

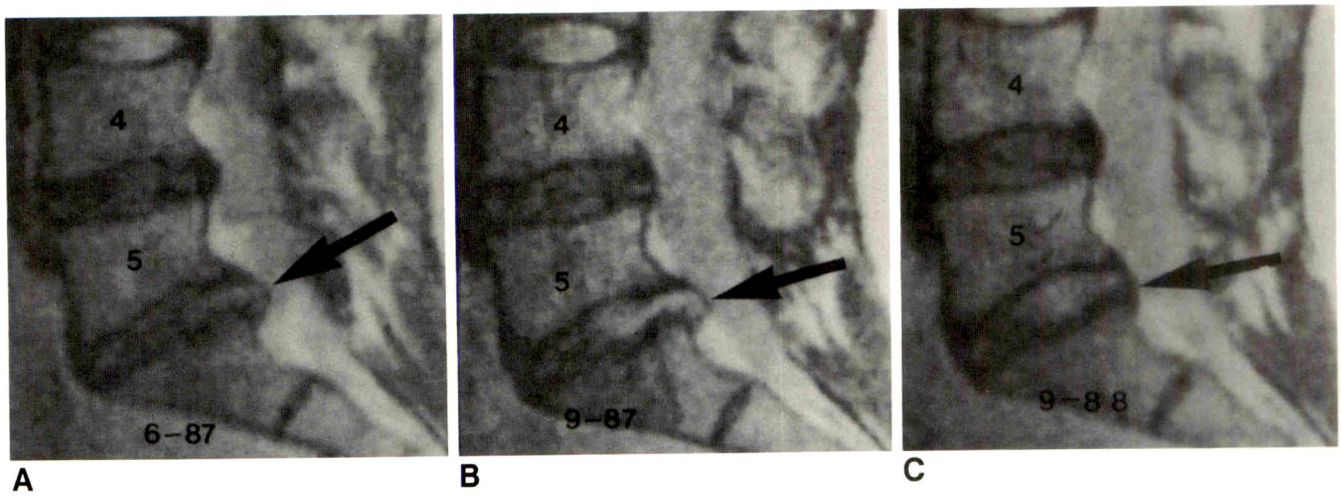



**Fig. 13.—MR scans before and 3 and 15 months after automated percutaneous lumbar diskectomy.**
***A*, Before diskectomy. Protrusion is noted at L5–S1 level (*arrow*).**
***B*, 3 months after procedure, patient is markedly improved and has returned to work; however, herniation (*arrow*) appears unchanged.**
***C*, 15 months after procedure, patient remains asymptomatic. MR shows complete resolution of herniation (*arrow*). Note that there is no evidence of epidural scarring and disk space has not lost any height.**

relief from the procedure [46]. These patients presumably have improved because the herniated nucleus pulposus is softer and exerts less pressure on the nerve. It is possible, however, that it may take longer periods of radiologic follow-up to demonstrate the morphologic changes in the herniated nucleus pulposus associated with APLD (Fig. 13). Long-term radiologic follow-up studies on successfully treated patients are not yet available. What is clear, however, is that APLD is not associated with epidural scarring, which makes postoperative imaging after laminectomy so difficult (Fig. 13).

## Conclusions

APLD has been shown to be both efficacious and extremely safe in treating patients with herniated lumbar disks contained by the anulus and posterior longitudinal ligament. APLD fulfills the most important criteria for an excellent interventional radiologic procedure: a high success rate with minimal associated morbidity. We should not forget that our first goal as physicians is "to do no harm." APLD has the least potential to do harm compared with other available procedures for treating herniated lumbar disks, thereby making it the procedure of first choice. However, caution must be exercised in the careful selection of patients and attention given to radiologic localization to ensure safe and effective results.

## REFERENCES

1. American Academy of Orthopaedic Surgeons (AAOS). Policy statement. *AAOS Bull* October **1989**:13–15
2. Stolke D, Sollman W-P, Seifert V. Intra- and postoperative complications in lumbar disk surgery. *Spine* **1989**;14:56–58
3. Ramirez LF, Thisted R. Complications and demographic characteristics of patients undergoing lumbar diskectomy in community hospitals. *Neurosurgery* **1989**;25:226–231
4. Hijikata S, Yamagishi M, Nakayama T, et al. Percutaneous diskectomy: a new treatment method for lumbar disk herniation. *J TodenHosp* **1975**; 5:5–13
5. Hijikata S. Percutaneous nucleotomy: a new concept technique and 12 years' experience. *Clin Orthop* **1989**;238:9–23
6. Hoppenfeld S. Percutaneous removal of herniated lumbar disks: 50 cases with ten-year follow-up periods. *Clin Orthop* **1989**;238:92–97
7. Kambin P, Schaffer JL. Percutaneous lumbar diskectomy: review of 100 patients and current practice. *Clin Orthop* **1989**;238:24–34
8. Monteiro A, Lefevre R, Pieters G, Wilmet E. Lateral decompression of a pathological disk in the treatment of lumbar pain and sciatica. *Clin Orthop* **1989**;238:56–63
9. Schreiber A, Suezawa MD, Leu H. Does percutaneous nucleotomy with diskography replace conventional diskectomy? Eight years of experience and results in treatment of herniated lumbar disks. *Clin Orthop* **1989**;238:35–42
10. Shepperd JAN, James SE, Leach AB. Percutaneous disk surgery. *Clin Orthop* **1989**;238:43–49
11. Stern MN. Early experience with percutaneous lateral diskectomy. *Clin Orthop* **1989**;238:50–55
12. Wilson DH, Harbaugh R. Lumbar diskectomy: a comparative study of microsurgical and standard technique. In: Hardy R, ed. *Lumbar disk disease*. New York: Raven, **1982**:147–156
13. El-Gindi S, Arefs AJ. Infection of intervertebral disks after operation. *J Bone Joint Surg [Br]* **1976**;58-B:114–116
14. Onik GM, Helms CA, Ginsburg L, Hoaglund FT, Morris J. Percutaneous lumbar diskectomy using a new aspiration probe. *AJNR* **1985**;6:290–293
15. Onik G, Mooney V, Maroon JC, et al. Automated percutaneous diskectomy: a prospective multi-institutional study. *Neurosurgery* **1990**;26(2):228–233
16. Bocchi L, Ferrata P, Passarello F, et al. La neucleoaspirazione secondo Onik nel trattamento dell'ernia discale lombare analisi multicentria del primi risultate su oltre 650 trattamenti. *Riv Neuroradiol* **1989**;2:119–122
17. Benazet JP, Roy-Camille R. Automated percutaneous lumbar diskectomy: results of French multicenter study of 287 cases. *Rachis* (in press)
18. Maroon JC, Allen RC. A retrospective study of 1,054 APLD cases: a twenty-month clinical follow-up at 35 US centers. *J Neurol Orthop Med Surg* **1989**;10(4):335–337
19. Lesoin F, Autricque A, Clarisse J, Villette L, Jomin M. La Nucleotomie percutanee automatisee en pathologie discal lombaire. *J Chir* (Paris) **1989**;126:185–188
20. Hammon W. Percutaneous lumbar nucleotomy. *Neurosurgery* **1989**;24:635
21. Flynn LM, Morrow RE, Brannon J, et al. Arthroscopically assisted lateral percutaneous lumbar diskectomy using the Onik Nucleotome. *J Neurol Orthop Med Surg* **1988**;9:45–47
22. Davis GW, Onik G. Clinical experience with automated percutaneous lumbar diskectomy. *Clin Orthop* **1989**;238:98–102

23. Goldstein TB, Mink JH, Dawson EG. Early experience with automated percutaneous lumbar diskectomy in the treatment of lumbar disk herniations. *Clin Orthop* **1989**;238:77–82
24. Gill K, Blumenthal SL. Clinical experience with automated percutaneous diskectomy—the Nucleotome system. *Orthopedics* (in press)
25. Russell GS, Highland T, Dreisinger T. Percutaneous lumbar diskectomy: one-year follow-up in private practice. *Surg Rounds Orthop* (in press)
26. Swiecicki M. Results of percutaneous lumbar diskectomy compared to laminectomy and chemonucleolysis. In: Mayer HM, Brock M, eds. *Percutaneous lumbar diskectomy*. Berlin: Springer-Verlag, **1989**:133–137
27. Capanna AH, Capanna DM. Correlations of amount of disk removed by percutaneous lumbar diskectomy and clinical results. In: Mayer HM, Brock M, eds. *Percutaneous lumbar diskectomy*. Berlin: Springer-Verlag, **1989**:138–140
28. Cooney FD. Comparison of chemonucleolysis with chymopapain to percutaneous automated diskectomy: a surgeon's first 50 cases of each. In: Mayer HM, Brock M, eds. *Percutaneous lumbar diskectomy*. Berlin: Springer-Verlag, **1989**:163–168
29. Corkhill G, Kimple J, Corkhill R. Automated percutaneous nucleotomy by pain scale. In: Mayer HM, Brock M, eds. *Percutaneous lumbar diskectomy*. Berlin: Springer-Verlag, **1989**:169–172
30. Rezaian SM, Silver ML. Percutaneous diskectomy—personal observations of 27 cases. In: Mayer HM, Brock M, eds. *Percutaneous lumbar diskectomy*. Berlin: Springer-Verlag, **1989**:173–176
31. Cartolari R, Davidovits P, Gagliardelli M. Automated percutaneous lumbar diskectomy. In: Mayer HM, Brock M, eds. *Percutaneous lumbar diskectomy*. Berlin: Springer-Verlag, **1989**:157–162
32. Kaps H, Cotta H. Early results of automated percutaneous lumbar diskectomy. In: Mayer HM, Brock M, eds. *Percutaneous lumbar diskectomy*. Berlin: Springer-Verlag, **1989**:153–156
33. Davis GW, Helms C, Onik G. Automated percutaneous lumbar diskectomy: a prospective study of 518 cases with 1 year follow-up. *Spine* (in press)
34. Fries JW, Abodeely DA, Vijungco JG, Yeager VL, Gaffey WR. Computed tomography of herniated and extruded nucleus pulposus. *J Comput Assist Tomogr* **1982**;6:874–887
35. Edwards W, Orme T, Orr-Edwards B. CT diskography: prognostic value in the selection of patients for chemonucleolysis. *Spine* **1987**;12:792–795
36. Jackson RP, Cain JE, Jacobs RR, Cooper BR, McManus GE. The neuroradiographic diagnosis of lumbar herniated nucleus pulposus: I. A comparison of computed tomography (CT), myelography, CT-myelography, discography, and CT-discography. *Spine* **1989**;14(12):1356–1361
37. Onik G, Maroon J. Percutaneous automated diskectomy—a less invasive alternative for the treatment of herniated lumbar disks. *Perspect Radiol* **1988**;1(2):1–36
38. Onik GM, Maroon J, Davis G. Automated percutaneous diskectomy at the L5–S1 level: use of a curved cannula. *Clin Orthop* **1989**;238:71–76
39. Shields CB, Reiss SJ, Garretson HD. Chemonucleolysis with chymopapain; results in 150 patients. *J Neurosurg* **1987**;67:187–191
40. Javid M. Signs and symptoms after chemonucleolysis. *Spine* **1988**;13:1428–1437
41. Spangfort EV. The lumbar disk herniation: a computer aided analysis of 2,504 operations. *Acta Orthop Scand Suppl* **1972**;142:1
42. Hanley EN, Shapiro DE. The development of low-back pain after excision of a lumbar disk. *J Bone Joint Surg [Am]* **1989**;71-A:719–721
43. Zahrawi F. Microlumbar diskectomy (MLD). *Spine* **1988**;13:358–359
44. Silvers HR. Microsurgical versus standard lumbar laminectomy. *Neurosurgery* **1988**;22:837–844
45. Schutz H, Watson CPN. Microsurgical discectomy: a prospective study of 200 patients. *Can J Neurol Sci* **1987**;14:81–83
46. Bonneville JF, Runge M, et al. Le disque intervertebral lombaire apres Nucleotomie, percutanee par aspiration. Etude tomodensitometrique. Comaraison avec la chimionucleolyse. *Rachis* **1989**;1:113–121

# MR Imaging in Fibromatosis: Results in 26 Patients with Pathologic Correlation

Stephen F. Quinn[1]
Scott J. Erickson[2]
Paul M. Dee[3]
Arthur Walling[4]
Donald A. Hackbarth[5]
Gregory J. Knudson[2,6]
H. Stephens Moseley[7]

**Fibromatoses are a diverse group of soft-tissue lesions that have been inconsistently categorized and treated. The purpose of our study was to establish the range of appearances of fibromatoses on MR images and perform a pathologic correlation to explain the variable signal-intensity patterns. During a 3-year period, 26 patients with deep fibromatoses were examined with MR. The MR images were evaluated for signal-intensity characteristics, and findings were correlated retrospectively with the pathologic diagnoses. The results showed that the MR appearance of fibromatoses is similar to that of other soft-tissue lesions, and the signal intensities vary greatly from lesion to lesion and within lesions themselves. The fibromatoses were either hyperintense, isointense, hypointense, or of mixed signal intensity relative to adjacent skeletal muscle. The hypointense areas appear to be zones of hypocellularity and dense collagen deposition. Microscopically all of the lesions invaded adjacent structures, but the MR appearances of the margins varied and were judged to be well demarcated ($n$ = 14), intermediate ($n$ = 5), or poorly demarcated ($n$ = 6).**

**Our experience shows that fibromatoses have a variable MR appearance no different from that of other soft-tissue lesions, and this variability reflects the composition and cellularity of the lesions.**

***AJR* 156:539–542, March 1991**

Received July 9, 1990; accepted after revision September 12, 1990

[1] Department of Radiology, Good Samaritan Hospital and Medical Center, 1015 N. W. 22nd Ave., Portland, OR 97210 and Department of Radiology, Oregon Health Sciences University, 3181 S. W. Sam Jackson Park Rd., Portland, OR 97201. Address reprint requests to S. F. Quinn at Good Samaritan Hospital.

[2] Department of Radiology, Medical College of Wisconsin, 8700 W. Wisconsin Ave., Milwaukee, WI 53226.

[3] Department of Radiology, University of Virginia Hospital, Charlottesville, VA 22908.

[4] Florida Orthopedic Institute, 4175 E. Fowler Ave., Tampa, FL 33617.

[5] Department of Orthopedics, Medical College of Wisconsin, 8700 W. Wisconsin Ave., Milwaukee, WI 53226.

[6] Present address: Radiology Associates of Appleton, 424 E. Wisconsin Ave., P.O. Box 117, Appleton, WI 54912.

[7] Department of Surgery, Division of Surgical Oncology, Good Samaritan Hospital and Medical Center, 1015 N. W. 22nd Ave., Portland, OR 97210.

0361–803X/91/1563–0539
© American Roentgen Ray Society

Fibromatoses are a diverse group of soft-tissue lesions that have not been consistently classified or treated (Table 1) [1]. Most of the superficial fibromatoses, for example palmar and penile fibromatoses, can be diagnosed by visual inspection. The deep fibromatoses, on the other hand, may need the same evaluation that soft-tissue sarcomas require.

At our institutions, MR has become the primary method of evaluating soft-tissue masses, including the fibromatoses. The majority of radiologic articles addressing fibromatoses deal primarily with CT [2–6]. Reports of MR appearances of fibromatoses have been limited to single cases [7, 8] and brief descriptions within broader discussions [9–15]. In this report, we have attempted to establish a range of appearances of fibromatoses on MR and perform a pathologic correlation in an attempt to explain the variable signal intensity pattern.

## Materials and Methods

During a 3-year period, 26 patients with deep fibromatoses were examined with MR. The majority ($n$ = 22) had wide-margin surgical resections within several weeks of the MR examinations. Four of the lesions were recurrences, as determined by findings on physical examination and MR imaging. There were 17 women and nine men, and the age range was 9–63 years (average, 33 years).

The MR examinations were performed with 0.35-T, 1.0-T, and 1.5-T MR units. No contrast material was used. Surface coils were used in some cases. Matrix sizes varied from 128 × 128 to 256 × 256 with one to four excitations. Slice thickness varied from 3 to 5 mm. T1-weighted images (100–600/16–20 [TR/TE]), proton-density-weighted images (1000–2000/

20–40), and T2-weighted images (2000–2500/60–80) were obtained in all patients. Sagittal, axial, and coronal images were obtained depending on the location of the lesion.

The sites of involvement included the chest wall ($n = 3$), abdominal-pelvic wall ($n = 1$), lower extremity ($n = 12$), upper extremity ($n = 5$), abdominal cavity ($n = 2$), pelvic cavity ($n = 1$), and brachial plexis ($n = 2$). The sites of origin included fascia ($n = 9$), muscle ($n = 10$), and mixed or indeterminate sites of origin ($n = 6$).

The MR images were evaluated for signal-intensity characteristics and correlated retrospectively with the pathologic diagnoses.

## Results

The MR signal intensity of the fibromatoses varied markedly (Table 2). All of the lesions exhibited some heterogeneity with different regions of varied signal intensities, and only one lesion, which had been previously sampled by biopsy, had surrounding edema. One lesion had a central area of cystic necrosis. The majority of cases with increased signal intensity on the T1-weighted images were only marginally hyperintense relative to the adjacent skeletal musculature ($n = 10$). There were three cases, however, in which the signal intensity on T1-weighted images was markedly increased relative to skeletal muscle. Histologically, two of these cases had abundant myxoid material (Fig. 1), and the third contained a large amount of fat, probably related to muscle atrophy (Fig. 2).

The fibromatoses that were hypointense ($n = 3$) or heterogeneous with prominent hypointense foci ($n = 4$) relative to adjacent musculature were found to be relatively hypocellular with dense deposits of collagen. There was no evidence of hemosiderin, calcium, or hypervascularity (Fig. 3).

The lesions of fibromatosis varied from 1 to 11 cm in size, with a mean greatest dimension of 5.6 cm. One case was correctly predicted to be multifocal.

The margins of the fibromatoses were characterized as well demarcated ($n = 14$, Fig. 4), intermediate ($n = 5$), or poorly demarcated ($n = 7$, Fig. 5) on MR images. Microscopically all of the lesions had some regions of invasion into adjacent soft tissues. Three of the fibromatoses had a surrounding hypointense rim. One lesion invaded the posterior femur.

**TABLE 1: Fibromatoses**

| |
|---|
| I. Superficial (fascial) fibromatoses |
| Palmar fibromatosis (Dupuytrens contracture) |
| Plantar fibromatosis (Ledderhose disease) |
| Penile fibromatosis (Peyronie disease) |
| Knuckle pads |
| II. Deep (musculoaponeurotic fibromatoses |
| Extraabdominal fibromatosis (extraabdominal desmoid) |
| Abdominal fibromatosis (abdominal desmoid) |
| Intraabdominal fibromatosis (intraabdominal desmoid) |
| Pelvic fibromatosis |
| Mesenteric fibromatosis |
| Gardner syndrome |

Note.—Reprinted with permission from Enzinger and Weiss [1].

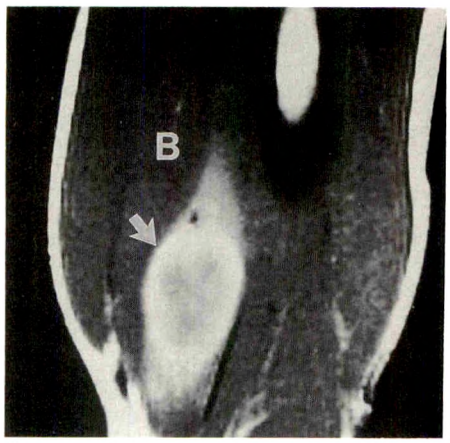
**TABLE 2: MR Signal Intensities of Fibromatoses**

| Image Type | Increased SI | Decreased SI | Equal SI | Mixed SI |
|---|---|---|---|---|
| T1-Weighted | 14 | 3 | 5 | 4 |
| T2-Weighted | 18 | 3 | 1 | 4 |

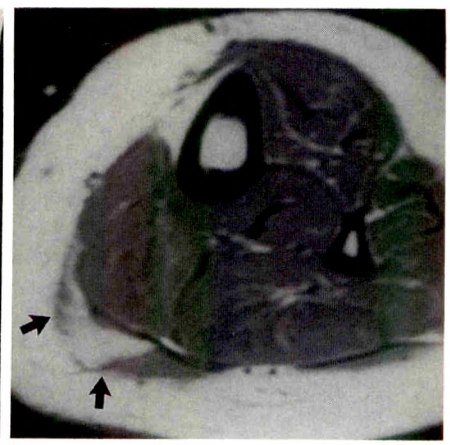
Note.—All signal intensity (SI) measurements are relative to adjacent skeletal muscle. Mixed SI indicates mixed signal intensity relative to adjacent skeletal muscle with prominent hypointense areas.

## Discussion

The fibromatoses are uncommon lesions. Extraabdominal fibromatoses have an incidence of three or four cases per million people [16]. Abdominal fibromatoses were found in 0.03% of 50,346 patients admitted to the hospital for neoplastic disease [17]. The initial evaluation of deep fibromatosis is important because the extent of the lesion needs to be delineated. The surgical margins need to be as wide as reasonably possible to help decrease recurrence [1]. Half of the fibromatoses in our series were judged to be well demar-




1



2

**Fig. 1.—Sagittal T1-weighted MR image shows fibromatosis of upper extremity with hyperintense signal that may be related to proteins within myxoid material. Spindle-shaped mass (*arrow*) is seen within biceps brachialis muscle (B). Fibromatosis has a higher signal intensity than adjacent musculature has. (Image courtesy of Michael Talbot, Oregon Health Sciences University, Portland, OR).**

**Fig. 2.—Axial T1-weighted MR image of calf shows fibromatosis with high signal intensity related to fat. Area of high signal intensity is seen in medial portion of gastrocnemius muscle (*arrows*).**

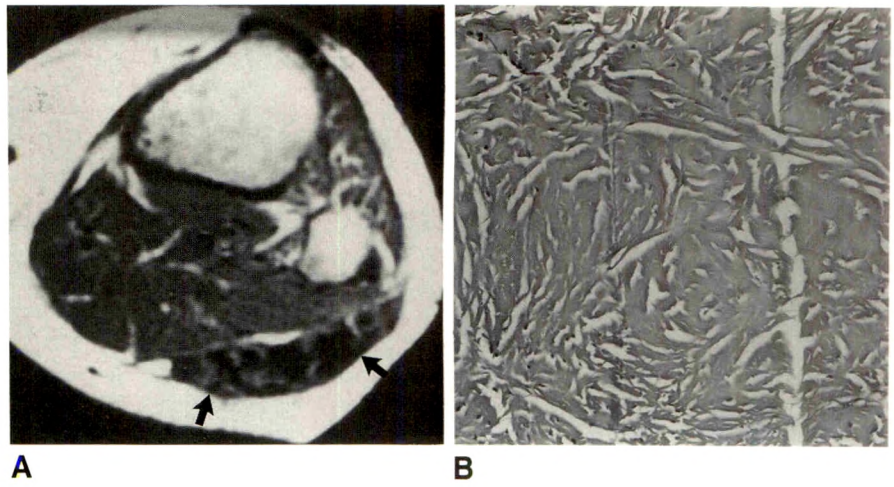



Fig. 3.—*A*, Axial T1-weighted MR image shows fibromatosis with hypointense signal in posterior calf (*arrows*).

*B*, Photomicrograph shows dense deposition of collagen and little cellularity, accounting for decreased signal intensity on T1-weighted image. (H and E, ×10)

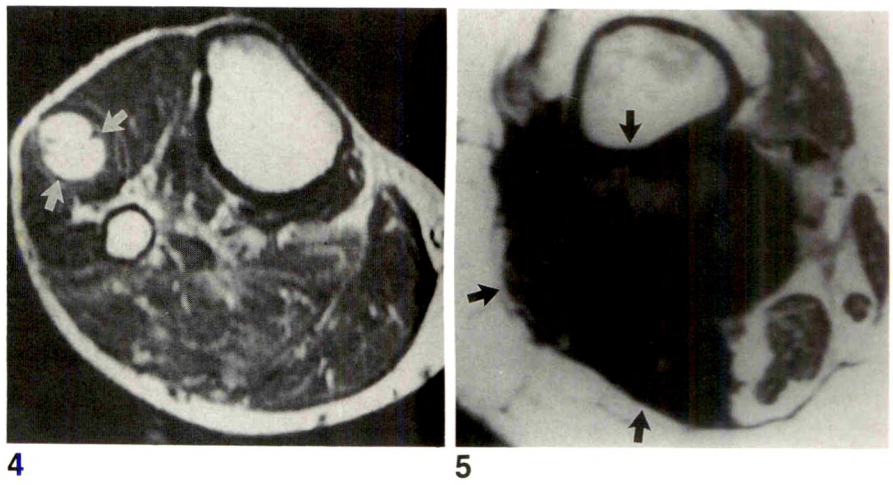



Fig. 4.—Axial T2-weighted MR image shows fibromatosis with well-demarcated margins with cystic necrosis. A focal, well-circumscribed lesion (*arrows*) is seen in lateral aspect of anterior compartment of lower extremity. (Image courtesy of Clark ED and Bidell J, Portland, OR).

Fig. 5.—Axial proton-density-weighted MR image of distal thigh shows fibromatosis with poorly demarcated margins. A poorly demarcated lesion is infiltrating posterior compartment (*arrows*) and is closely applied to femur. At surgery, fibromatosis was found to be invading periosteum.

cated. This appearance is actually misleading, because all of the lesions microscopically invaded adjacent structures.

The fibromatoses display a variety of signal intensities. In some cases with high signal intensity on T1-weighted images this could be attributed to fat within the lesions. This does not explain the high signal intensity on T1-weighted images in the cases with myxoid material, because myxomas, in our experience, have prolonged T1 relaxation values relative to adjacent musculature. We speculate that an unidentified protein within these lesions causes the T1 relaxation value to shorten.

On T2-weighted images, the majority of the fibromatoses had notably increased signal intensity, as do the majority of other soft-tissue tumors [10]. The majority of the fibromatoses have a high signal intensity on T2-weighted images, but approximately one third of the current cases were notably hypointense or had hypointense foci. We believe that these areas of diminished signal intensity are best explained as patches of hypocellularity and dense collagen deposition. Hemosiderin did not appear to be the cause of the areas of decreased signal intensity in our cases [18]. Sundaram et al. [15] described areas of decreased signal intensity on T2-weighted images and attributed this to acellularity and abundant collagen.

Our experience shows that fibromatoses have a variable MR appearance, the same as other soft-tissue lesions do, and this variability reflects the composition and cellularity of the lesions.

ACKNOWLEDGMENTS

Thanks to Mary Alice Payne for preparation of this manuscript and to Anthony D'Agostino and Gonzalo Madiedo for pathologic correlation.

REFERENCES

1. Enzinger FM, Weiss SW. Fibromatoses. In: Enzinger FM, Weiss SW, eds. *Soft tissue tumors*. St. Louis: Mosby, **1988**:136–163
2. Francis IR, Dorovini-Zis K, Glazer G, et al. The fibromatoses: CT-pathologic correlation. *AJR* **1986**;147:1063–1066
3. Hudson TM, Vandergriend RA, Springfield DS, et al. Aggressive fibroma-

tosis: evaluation by computed tomography and angiography. *Radiology* **1984**;150:495–501
4. Young JWR, Aisner SC, Levine AM, Resnik CS, Dorfman HD. Computed tomography of desmoid tumors of bone: desmoplastic fibroma. *Skeletal Radiol* **1988**;17:333–337
5. Black WC, Armstrong P, Daniel TM, Cooper PH. Computed tomography of aggressive fibromatosis in the posterior mediastinum (case report). *J Comput Assist Tomogr* **1987**;11:153–155
6. Magid D, Fishman EK, Witaram M, Siegelman SS. Musculoskeletal desmoid tumors: CT assessment during therapy. *J Comput Assist Tomogr* **1988**;12:222–226
7. Sundaram M, Duffrin H, McGuire MH, Vas W. Synchronous multicentric desmoid tumors (aggressive fibromatosis) of the extremities. *Skeletal Radiol* **1988**;17:16–19
8. Hamlin DJ, Page R, Pettersson H, Bland KI. Magnetic resonance characteristics of an abdominal desmoid tumor. *Comput Radiol* **1986**;10:11–13
9. Kransdorf MJ, Jelinek JS, Moser RP, et al. Soft tissue masses: diagnosis using MR imaging. *AJR* **1989**;153:541–547
10. Totty WG, Murphy WA, Lee JKT. Soft tissue tumors: MR imaging. *Radiology* **1986**;160:135–141
11. Petasnick JP, Turner DA, Charters JR, Gitelis S, Zacharias CE. Soft tissue masses of the locomotor system: comparison of MR imaging with CT *Radiology* **1986**;160:125–133
12. Aisen AM, Martel W, Braunstein EM, et al. MRI and CT evaluation o primary bone and soft tissue tumors. *AJR* **1986**;146:749–756
13. Weekes RG, Berquist TH, McLeod RA, Zimmer WD. Magnetic resonanc imaging of soft tissue tumors: comparison with computed tomography *Magn Reson Imaging* **1985**;3:345–352
14. Pettersson H, Gillespy T, Hamlin DJ, et al. Primary musculoskeletal tumors examination with MR imaging compared with conventional modalities *Radiology* **1987**;164:237–241
15. Sundaram M, McGuire MH, Schajowicz F. Soft tissue masses: histologi basis for decreased signal (short T2) on T2 weighted MR images. *AJ* **1987**;148:1247–1250
16. Reitamo JJ, Haury P, Nykyri E, et al. The desmoid tumor. 1. Incidence sex, age and anatomical distribution in the Finnish population. *Am J Cli Pathol* **1982**;77:665–685
17. Pack GT, Ehrlich HE. Neoplasms of the anterior abdominal wall with specia consideration of desmoid tumors: experience with 391 cases and collectiv review of the literature. *Int Abstr Surg* **1944**;79:177–198
18. Allen PW. The fibromatoses: a clinicopathologic classification based o 140 cases, Part 1. *Am J Surg Pathol* **1977**;1:255–269

Case Report

# CT Appearance of Angiosarcoma Associated with Chronic Lymphedema

Ella Kazerooni[1] and Christian Hessler[1,2]

Angiosarcoma is an uncommon, rapidly progressive neoplasm of the vascular endothelium that may be associated with chronic lymphostatic lymphedema of the extremities. Although it is seen more frequently in lymphedema of the upper extremities after mastectomy for breast carcinoma, it is also associated with idiopathic or congenital lymphedema. This case illustrates the classic clinical course of angiosarcoma associated with idiopathic lymphedema and the previously undescribed CT appearance of lymphedema complicated by diffuse infiltrating angiosarcoma involving the entire right lower extremity. The extreme skin thickening, frequently nodular, with marked fibrous septal thickening and lakes of encapsulated fluid surrounding and directly involving muscle groups differs from the less marked honeycomb pattern typical of lymphedema on CT.

## Case Report

A 26-year-old woman with a 16-year history of idiopathic lymphedema of the right lower extremity was admitted for the evaluation of progressively increased swelling of the right leg associated with mottled discoloration of the skin. One year before, evaluation by the referring physician had revealed lymphedema confined below the knee, which did not respond to conservative therapy. Mottling of the skin below the knee and significant local pain, thought to be cellulitis, developed 6 weeks before admission. However, despite antibiotic and heparin therapy, mottling, erythema, pain, and marked edema rapidly progressed to the right groin. A 9-day course of IV vancomycin, heparin, and steroid therapy on the current admission failed to prevent rapid progression of edema and discoloration to the buttock and lower back. Contrast-enhanced CT showed marked swelling of the leg manifested as increased attenuation of the subcutaneous fat, thickening of the fibrous septa, and a honeycomb pattern with lakes of encapsulated fluid in and around muscles, more severe than that seen in typical lymphedema. Extreme skin thickening below the knee was frequently nodular. An above-the-knee amputation was performed. Pathologic examination showed a diffuse infiltrating neoplasm that extended to the margins of resection. The malignant cells were arranged in solid sheets and surrounded well-defined vascular spaces, with some areas resembling a cavernous hemangioma. Aggressive angiosarcoma was present in the dermis, subcutis, and skeletal muscle of the foot, leg, and thigh, with extensive venous invasion. After surgery, edema and pain persisted in the remaining limb. The patient died 2 weeks after surgery, before chemotherapy could be undertaken.

## Discussion

Angiosarcoma associated with chronic lymphedema of the upper extremity has been recognized as a complication in patients after mastectomy; more than 220 cases have been described in the literature [1]. This uncommon neoplasm occurs in 0.07–0.45% of patients who survive 5 or more years after radical mastectomy and occurs after an average latency of 10.25 years from mastectomy (range, 1–26 years) [2]. This is much shorter than the duration of edema seen with the fewer reported cases of congenital or idiopathic lymphedema, 45.9 and 21.8 years, respectively [3]. Angiosarcoma has been reported only in association with primary

Received August 14, 1990; accepted after revision September 24, 1990.
[1] Department of Radiology, University of Michigan Hospitals, 1500 E. Medical Center Dr., Ann Arbor, MI 48109-0030. Address reprint requests to E. Kazerooni.
[2] Present address: Route du Village 12, 1066 Epalinges, Switzerland.

 0361–803X/91/1563–0543 © American Roentgen Ray Society

and secondary (lymphostatic) chronic edema, be it congenital, idiopathic, posttraumatic, or caused by filariasis, but never in renal, cardiac, or cirrhotic edema (high flow). The clinical course may be insidious, initially manifesting as increased edema or an innocuous skin discoloration, which progresses to confluent areas of ecchymosis, palpable nodules, and ulceration. In addition to local recurrence, pulmonary and pleural metastases are common [3].

Initially, angiosarcoma was thought to represent metastases from primary breast carcinoma [2]. Although it has also been speculated that postmastectomy radiation therapy could contribute to its occurrence, many postmastectomy patients with angiosarcoma have not received radiation therapy [3]. Neither of these causes plays a role in cases of idiopathic or congenital lymphedema.

In all cases, chronic lymphostasis results from the absence or diminished number of normal regional lymph nodes or lack of functional afferent lymphatics, whether it is due to congenital hypoplasia, surgery, trauma, or infection. Proliferation of the lymphatic endothelium to improve collateral circulation has been hypothesized to occur in the setting of chronic lymphostasis, a stimulus that may predispose to the growth of mutant cells and malignancy [4]. Chronic stasis may slow the transport of fluid and protein from the interstitium into lymphatic tissue, altering the local response of the lymphatic system to antigens, as evidenced by the increased susceptibility of the lymphedematous extremity to infection. Just as there is an increased risk of cancer in systematically immunosuppressed visceral organ transplantation patients, localized immunosuppression is known to represent a site of preferential tumor growth, representing an "immunologically privileged site" [4].

Initially, these vascular sarcomas were presumed to arise from chronically dilated lymphatic vessels and were termed lymphangiosarcomas [2]. Histochemical and electron microscopic studies provide equal support for origin from the vascular endothelium, and Enzinger and Weiss [5] have stated that the distinction between lymphangiosarcoma and hemangiosarcoma is difficult and often arbitrary, despite microscopic, histochemical, and ultrastructural evaluation, as both arise from endothelial cells. Lymphangiosarcoma and hemangiosarcoma together have been termed angiosarcoma [5].

Amputation or disarticulation has been successful in most series when performed as the initial primary therapy. Although such surgery is radical, such as interscapulothoracic amputation or hip disarticulation, this appears to offer the best opportunity for long-term survival. Radical surgery at the time of recurrence does little to prevent widespread metastases. Radiation therapy and chemotherapy may have some role when combined with radical surgery or in the treatment of metastatic disease [3].

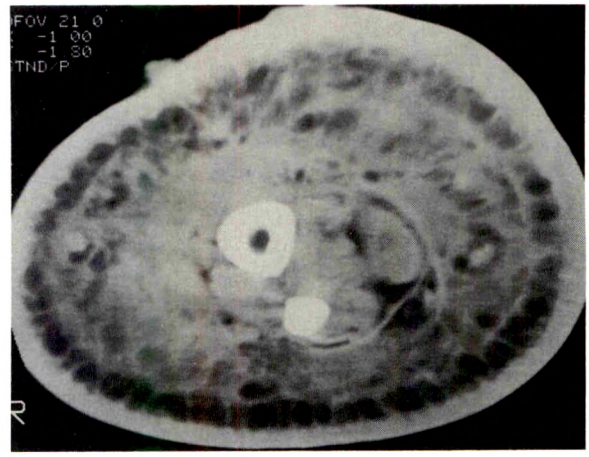



**Fig. 1.—Contrast-enhanced CT scan shows marked skin thickening with raised nodules, thickened fibrous septa, and lakes of encapsulated fluid.**

The CT appearance of angiosarcoma has not been reported before. The increased attenuation of the subcutaneous fat, thickening of the fibrous septa, and a honeycomb pattern with lakes of encapsulated fluid seen in portions of the thigh have been described as the usual appearance of lymphedema [6]. However, the additional findings of extreme skin thickening, multiple cutaneous nodules, marked increased attenuation of the subcutaneous fat, and fluid collections both within and surrounding muscle groups, as seen in the leg, have not been described and correspond to the findings seen at amputation in this case (Fig. 1). Although the indications for CT evaluation in such cases are unlikely to arise frequently, clinically suspected deep venous thrombosis could not be evaluated otherwise, and the CT appearance is striking.

## REFERENCES

1. Martin MB, Kon ND, Kawamoto EH, Myers RT, Sterchi JM. Post-mastectomy angiosarcoma. *Am Surg* **1984**;50:541–545
2. Stewart FW, Treves N. Lymphangiosarcoma in postmastectomy lymphedema: report of six cases in elephantiasis chirurgica. *Cancer* **1948**;1:64–81
3. Sordillo PP, Chapman R, Hajdu SI, Magill GB, Golbey RB. Lymphangiosarcoma. *Cancer* **1981**;48:1674–1679
4. Schreiber H, Barry FM, Russell WC, Macon WL, Ponsky JL, Pories WJ. Stewart-Treves syndrome: lethal complication of postmastectomy lymphedema and regional immune deficiency. *Arch Surg* **1979**;114:82–85
5. Enzinger FM, Weiss SW. Malignant vascular tumors. In: Soft-tissue tumors. St. Louis: Mosby, **1988**:545–557
6. Hadjis NS, Carr DH, Banks L, Pflug JJ. The role of CT in the diagnosis of primary lymphedema of the lower extremity. *AJR* **1985**;144:361–364

Technical Note

# Aspiration of the Hip in Patients Treated with Girdlestone Arthroplasty

J. Shannon Swan,[1] Ethan M. Braunstein,[2] and William Capello[3]

Aspiration of any postoperative hip may be difficult, but in a joint in which infection has occurred and arthroplasty components have been removed, obtaining fluid for culture is particularly challenging. Hips treated with Girdlestone or resection arthroplasty should be reassessed for residual infection before revision, because the results of aspiration will influence the surgeon's approach to the patient. We describe a technique for gaining access to the resection arthroplasty site that has been successful in our patients.

## Technique

If the patient has not had recent plain radiographs, we obtain an anteroposterior scout film to evaluate postoperative anatomy and to search for radiologic evidence of infection. Suspicious findings include periostitis or poorly defined destruction of the resected femoral head or acetabulum. The patient is placed supine on a fluoroscopy table. The resection arthroplasty site is observed under image intensification, and the preferred location for puncture is marked with a suitable marking pen or other method. The area is thoroughly cleansed and draped. A needle is placed just above the approximate midpoint of a line drawn between the greater and lesser trochanters (Fig. 1). This localization is important, because the arthroplasty site is more cranial than one may suspect because of the previous resection of the femoral head and neck. The position of the femoral vessels also should be noted so that they can be avoided along with other possible complicating structures, such as renal transplants and stomas.

Local anesthesia is administered. A 20-gauge spinal needle is then inserted from an anterior approach, essentially perpendicular to the fluoroscopy table, with the needle directed to the area between the acetabulum and the resected femur. Aspiration is attempted after sufficient depth is achieved. Suitable depth may be apparent when the posterior wall of the acetabulum is contacted, but often no intervening osseous or cartilaginous tissue is present. One may detect resistance from scar tissue only when the needle is advanced. In such cases, the proper depth must be estimated and aspiration done with slow withdrawal of the needle. If no fluid is returned, 5–10 ml of nonbacteriostatic sterile saline may be injected and aspiration repeated. Injection of saline should be accomplished with little resistance if needle placement is correct. A small amount of contrast material may be injected also. Contrast material should flow away from the needle easily. The pseudocapsule tends to have a rather linear configuration roughly paralleling the acetabular margins. We obtain a single spot film after a low-volume contrast injection to document intraarticular placement of the needle (Fig. 2).

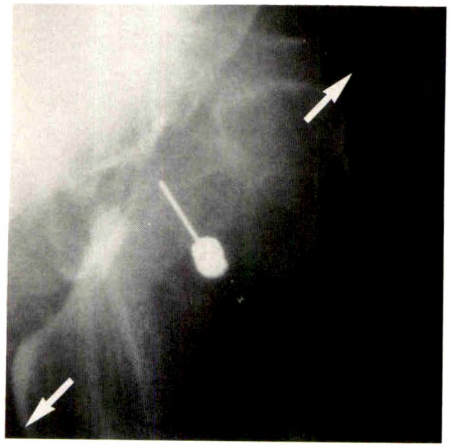
## Discussion

In the past 2 years, eight patients have been referred to us for preoperative evaluation. Seven men and one woman were studied; ages ranged from 38 to 70 years. All had been previously treated for infected total hip prostheses with Girdlestone procedures followed by appropriate antibiotic regimens.

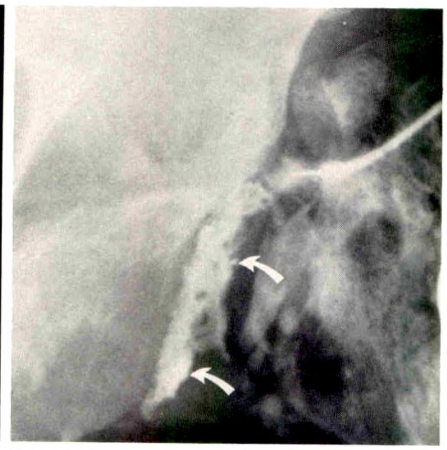
We have aspirated various locations above the intertrochanteric line, because fluid return was difficult to obtain in our first few patients. We found only one location that gave consistent and sufficient fluid return, namely, the midpoint of

Received September 24, 1990; accepted after revision October 30, 1990.
[1] Department of Radiology, University of Wisconsin Health Sciences Center, 600 Highland Ave., Madison, WI 53792. Address reprint requests to J. S. Swan.
[2] Department of Radiology, Indiana University Medical Center, 926 W. Michigan St., Indianapolis, IN 46202.
[3] Department of Orthopedic Surgery, Indiana University Medical Center, Room 600, 541 Clinical Dr., Indianapolis, IN 46202.

*AJR* 156:545–546, March 1991 0361–803X/91/1563–0545 © American Roentgen Ray Society



1



2

**Fig. 1.—Radiograph of patient who underwent a typical modified Girdlestone arthroplasty after removal of total hip prosthesis and antibiotic treatment. Spinal needle has been placed above a point approximately bisecting intertrochanteric line (*arrows*).**

**Fig. 2.—Radiograph shows linear appearance of pseudocapsule after low-volume contrast injection (*arrows*). Flow of contrast material away from needle tip shows placement of needle in pseudocapsule.**

the intertrochanteric line. Adequate fluid for bacteriologic study was obtained in all eight patients. The fluid return was always serosanguinous. Thus far, saline injection and reaspiration have not been necessary. Seven patients had negative cultures at aspiration and underwent revision arthroplasty. One patient has not had a revision arthroplasty yet, but his cultures and aspiration were negative, and he has had no clinical signs of infection.

When total hip arthroplasties fail, the cause is usually related to infection or aseptic loosening. Of greater clinical concern is infection, which can be quite difficult to eradicate. Ultimate control of infection usually requires removal of the prosthetic components [1]. The resection arthroplasty or Girdlestone procedure is often done as a salvage operation in these circumstances [2]. The acetabulum and resected femur are allowed to articulate with one another after being rounded off at the time of component removal. In some patients this is the final treatment, assuming infection is controlled. For optimal hip function, however, a second total hip arthroplasty is necessary. Patients who are possible candidates for revision undergo a modified Girdlestone procedure in which no rounding off of the bones is done when the components are removed [3]. Criteria for revision of the Girdlestone arthroplasty with a second total hip arthroplasty include: freedom from infection for at least 3–6 months, initial infection by a Gram-positive organism of low virulence, and negative Gram stains at surgery [3].

In the patient with an infected total hip prosthesis, the dilemma facing the surgeon is the presence of residual infection. The radiologist plays an important role in patients' treatment by performing an accurate diagnostic aspiration, potentially making a diagnosis of infection without subjecting the patient to unnecessary surgery. We recommend this simple technique as an initial approach to aspiration of the hip in patients who have undergone Girdlestone arthroplasty.

## REFERENCES

1. Anderson LD, Meyer FN. Management of infected implants. In: Chapman MW, ed. *Operative orthopedics*. Philadelphia: Lippincott, **1988**:876–882
2. Grauer JD, Amstutz HC, O'Carroll PF, Dorey FJ. Resection arthroplasty of the hips. *J Bone Joint Surg [Am]* **1989**;71-A:669–678
3. Colandruccio RA. Arthroplasty of hips. In: Crenshaw AH, ed. *Campbell's operative orthopedics*. St. Louis: Mosby, **1987**:1456

Review Article

# Sonography of the Fetal Heart: Findings on the Four-Chamber View

John P. McGahan[1]

**The normal and pathologic sonographic appearances of the fetal heart on four-chamber views are reviewed. Performed correctly, the four-chamber view is the best method of examining the complex cardiac anatomy of the small fetal heart and of detecting major congenital heart disease.**

Congenital heart disease is the most common severe congenital anomaly found in neonates [1]. It has been estimated that more than eight in 1000 live births have structural abnormalities of the heart or great vessels [2]. These anomalies may be associated with serious morbidity and mortality in the fetus and the neonate. While a number of noncardiac fetal malformations have been diagnosed routinely for over a decade, it is only recently with advances in sonographic instrumentation that imaging of the fetal heart has improved [3]. However, because of the complexities of cardiac anatomy and the small size of the fetal heart, optimal examination requires special professional expertise in prenatal sonography combined with detailed knowledge of cardiac anatomy. This sophisticated examination of the fetal heart requires the use of high-resolution real-time equipment, with detailed examination of the heart in several anatomic planes, and the use of M-mode sonography, pulsed Doppler sonography, and color flow mapping. Most persons performing routine fetal obstetric sonography do not have such instrumentation or expertise to examine the fetal heart in great detail. However, many major structural defects of the heart, especially those causing the most serious morbidity and mortality, should be well recognized by obtaining a routine four-chamber view. This article reviews the normal and abnormal appearances of the fetal four-chamber view of the heart.

## Indications

A four-chamber view of the heart has been proposed as a routine portion of the sonographic examination of the fetus to be obtained from 18 weeks to term [1, 4, 5]. It has been proposed that a satisfactory four-chamber view of the heart may be obtained in 95% of pregnancies after 18 weeks [4]. Difficulty in performing a satisfactory examination of the fetal heart may be due to maternal body habitus, fetal position, or markedly increased or decreased amniotic fluid volume.

A number of fetuses are at high risk for congenital heart disease. Risk factors can be divided into fetal risk factors and maternal risk factors (Table 1). For instance, the risk of congenital heart disease has been reported at 0.8% [2], but this risk increases to up to 4% if a sibling has a heart defect and 12% risk if a parent has a heart defect [6]. If a noncardiac structural abnormality is detected on prenatal sonography, there is a very high risk of associated cardiac malformations in these cases, therefore requiring a careful examination of the fetal heart [7, 8]. However, in most cases, congenital heart disease is a spontaneous event without associated high-risk factors. Even in a referral-based practice, the majority of prenatally diagnosed cases of congenital heart disease fall into a low-risk group [9]. Therefore, for routine obstetric sonography, the four-chamber view has been proposed as

Received July 23, 1990; accepted after revision October 8, 1990.
[1] Department of Radiology, University of California Davis Medical Center, 2516 Stockton Blvd., TICON II, Sacramento, CA 95817.

the simplest, and yet a highly accurate, method of detecting significant congenital heart disease [4].

### Importance of Prenatal Diagnosis

It is important to diagnose some of the more severe cases of congenital heart disease because of the high morbidity and mortality rates if untreated [2]. However, in the past 5 years, survival rates for major cardiac anomalies are much improved. Simplification of surgical techniques, improvement of other operations, and development of new operations have allowed the surgical repair of many complex congenital defects. Technical advances in intraoperative and postoperative care such as extracorporeal membrane oxygenation, deep hypothermia, cardioplegia, and intraaortic balloons have helped facilitate performance of complex operations and have improved infant survival [10]. Therefore, it is important to recognize a possible abnormality on a four-chamber view of the heart because it (1) allows time for a second look at fetal echocardiography for a more precise diagnosis, (2) allows prenatal counseling for the parents, (3) allows time for planned delivery, (4) allows time for relocation of family to centers equipped to handle such cases, (5) allows search time when heart transplantation is considered, and (6) eliminates delay in definitive diagnosis and treatment [11].

**TABLE 1: Risk Factors for Congenital Heart Disease[a]**

| Risk Factors |
|---|
| Fetal |
| Extracardiac abnormality |
| Chromosomal abnormality |
| Fetal cardiac arrythmia |
| Nonimmune hydrops |
| Question of cardiac anomaly on prior sonogram |
| Intrauterine growth retardation |
| Maternal |
| Family history of congenital heart disease (parent or sibling) |
| Teratogenic exposure (e.g., alcohol, amphetamines, anticonvulsives, lithium) |
| Maternal disorders (diabetes mellitus, collagen vascular disease, phenylketonuria) |
| Maternal infection (e.g., rubella) |
| Familial syndromes |

[a] Adapted from Copel et al. [4].

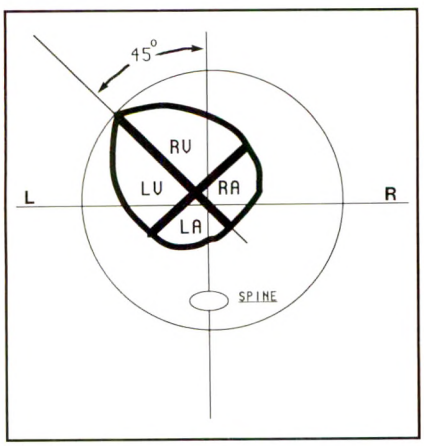
### Technique and Normal Anatomy

When evaluating the fetal heart, the fetal position should be documented. The site of the stomach and the relationship of the suprahepatic portion of the inferior vena cava to the right atrium are noted to determine the situs. The four-chamber view is obtained in a horizontal section, just above the region of the diaphragm. The fetal spine is identified and the chest is scanned in the transverse axis to obtain a four-chamber view. Regardless of the fetal position, the apex of the heart should point at approximately a 45° angle to the left anterior chest wall on the same side as the fetal stomach. A line drawn through the intraventricular septum will traverse a plane approximately 45° with a line drawn between the spine and the sternum (Fig. 1) [12]. It is important to note if the heart is deviated from this position, as this may indicate a situs abnormality or result from fetal cardiac malpositioning or a noncardiac thoracic mass.

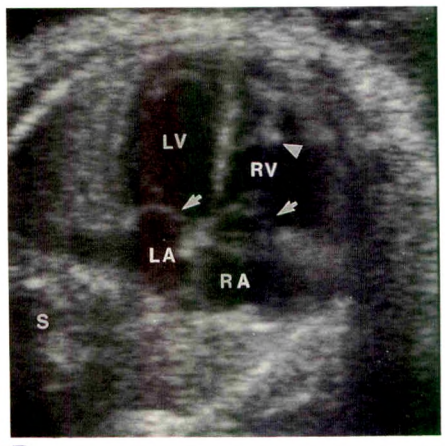
In general, the two ventricles are of approximately equal size when studied on a four-chamber view of the heart. DeVore et al. [13] have made precise measurements of the internal dimensions of the left and right ventricles on M-mode sonograms obtained during diastole at the atrioventricular valve region. Although there is almost a one-to-one ratio, later in pregnancy the right ventricle assumes more of the cardiac output and is slightly larger than the left ventricle [13]. While M mode is much more precise than real-time examination, the use of real-time sonography should enable one to recognize that the right ventricle and the left ventricle are almost the same size (Fig. 1).

The right atrium can be identified sonographically by following the suprahepatic portion of the inferior vena cava into that chamber. The flap of the foramen ovale can be identified opening into the left atrial cavity. This recognition can help separate the right from the left atrium. The left atrium is the most posteriorly situated structure within the thoracic cavity.

Once the atrium is identified, the atrioventricular connections require recognition of certain morphologic features of




A




B

**Fig. 1.—*A*, Schematic drawing through normal fetal thorax shows four cardiac chambers. A line drawn through intraventricular septum will traverse a plane approximately 45° with a line drawn between fetal spine and sternum. (Modified and reprinted with permission from Comstock [12].)**

***B*, Magnified sonogram of fetal heart and thorax shows four chambers. Note trabeculated appearance of muscles of right ventricle (*arrowhead*) and atrioventricular valves (*arrows*).**

**L = left, R = right, LV = left ventricle, RV = right ventricle, RA = right atrium, LA = left atrium, S = spine.**

the right and left ventricles. For instance, the right ventricle appears more trabeculated within the ventricular cavity than the left ventricle does because of the more prominent moderator band near the apex of the right ventricle (Fig. 1). Often within the left ventricle, a very bright reflection from the papillary muscles may be seen within that chamber (Fig. 2) [14]. This should not be misinterpreted as a mass or tumor within the ventricle. The atrioventricular valves are then identified separating the atria from the ventricle. The leaflets of the tricuspid valve are usually inserted slightly lower in the ventricular septum than is the mitral valve.

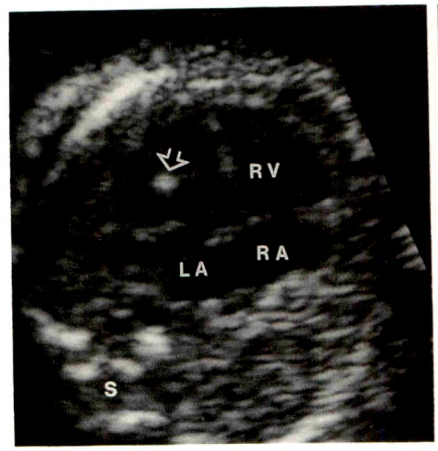
The relationship of the aorta and the pulmonary artery to the ventricular chambers cannot be assessed on this four-chamber view. The relationship of the pulmonary artery and aorta to the ventricular chamber is better assessed by other views. For instance, the relationship of the aorta to the left ventricle is best evaluated by a left ventricular long-axis view of the fetal heart (Fig. 3). This view is obtained by turning the transducer from the transverse plane used for the four-chamber view, so the ultrasound plane is directed between the right shoulder of the fetus and the fetal stomach. However, many anomalies are initially recognized by noting associated septal defects, or ventricular disproportion, on the four-chamber view [4]. In fact, in a recent review of over 1000 pregnancies with 74 structurally abnormal fetal hearts, an abnormality was identified on the four-chamber view in 71 (96%) [4].

### Abnormal Four-Chamber View of the Heart

A systematic approach to the four-chamber view of the heart will allow detection of both intracardiac as well as intrathoracic abnormalities. Six questions should be asked whenever evaluating the four-chamber view of the heart:

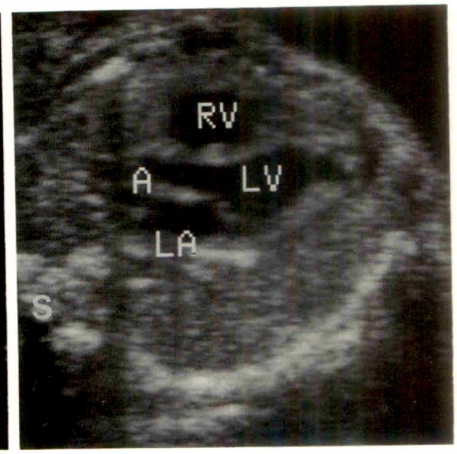
#### *Is the Heart in Its Normal Position?*

When evaluating the four-chamber view of the heart for normal position, cardiac situs should be evaluated. Situs abnormalities may be associated with specific syndromes such as asplenia or polysplenia. These specific abnormalities, including asplenia (bilateral right-sidedness) and polysplenia (bilateral left-sidedness), are also characterized by complex congenital heart disease. These abnormalities initially may be identified prenatally on sonography by recognition of the discordance between the location of the fetal stomach, which is normally located on the left, and the fetal heart, with the



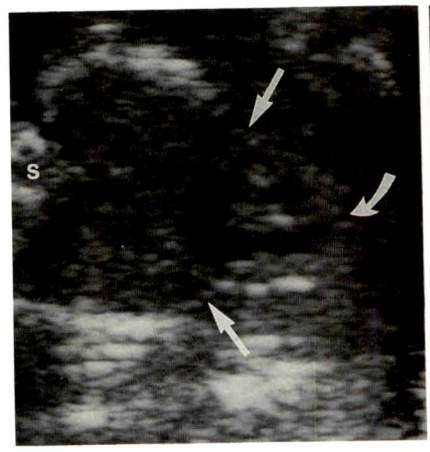

2

Fig. 2.—Normal papillary muscle on four-chamber view of heart. Bright echogenic focus (*arrow*) within left ventricle corresponds to a papillary muscle and is a normal finding. LA = left atrium, RA = right atrium, RV = right ventricle, S = spine. (Courtesy of D. Nyberg, Seattle, WA.)



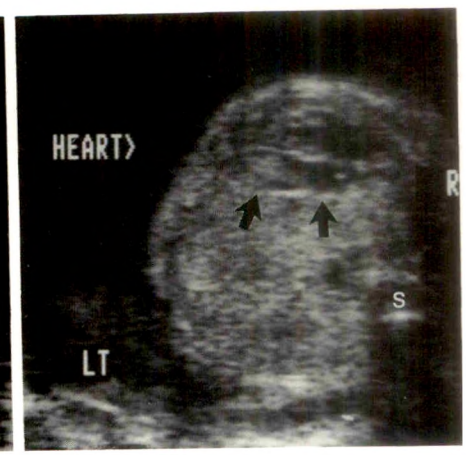

3

Fig. 3.—Long-axis view of heart. Sonogram shows normal left-ventricular long-axis view of heart with aorta (A) originating from left ventricle (LV). LA = left atrium, RV = right ventricle, S = spine.




4

Fig. 4.—Pentalogy of Cantrel. Four-chamber view of heart shows an ectopic thoracic cordis (*curved arrow*), which was associated with an omphalocele. *Straight arrows* indicate margins of anterior thoracic cavity. S = spine.




5

Fig. 5.—Type III cystic adenomatoid malformation. Transverse sonogram through fetal thorax shows large echogenic mass within left thorax displacing heart to right (*arrows*). LT = left, S = spine, R = right.

apex normally to the left [15]. Positional abnormalities of the heart also may occur in such anomalies as pentalogy of Cantrel, that is, thoracic ectopic cordis, which is associated with an abdominal wall defect (Fig. 4).

More commonly, the four-chamber view of the heart may be used as a normal anatomic marker for extracardiac abnormalities of the fetal thorax. For instance, if there is a large mass within one side of the fetal thorax, this mass may first be appreciated by noting the abnormal position and orientation of the four-chamber view of the heart. For instance, in type III cystic adenomatoid malformation, a large pulmonary mass will cause cardiac displacement into the contralateral thoracic cavity (Fig. 5) [16]. By noting the abnormal position of the four-chamber heart, one can better ascertain if there is a mass lesion within the thorax.

*Is the Heart Normal in Size in Comparison with the Fetal Thorax?*

A four-chamber view of the heart can be used to assess cardiothoracic disproportion or a disproportionately small fetal thorax. Such measurements may be obtained from real-time images but are more accurately obtained from M mode. Well-standardized tables are available that compare the chest circumference with other routine measurements, including the biparietal diameter, femoral length, and head circumference. Standardized measurements of the ratio of the cardiac biventricular outer dimensions compared with the chest circumference obtained by real-time and M-mode measurements have been tabulated throughout pregnancy (Fig. 6) [17]. These ratios may be helpful in predicting cardiomegaly or pulmonary hypoplasia. More detailed information concerning M-mode measurements may be obtained from other references [3, 5, 13, 17].

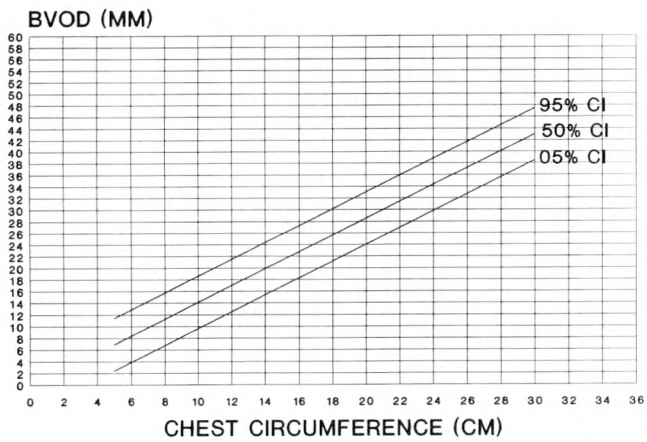


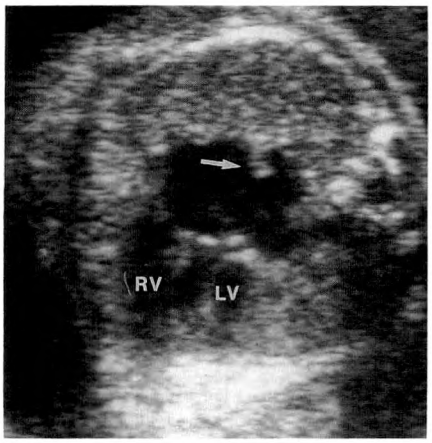

**Fig. 6.—Confidence-limit (CI) graph for M-mode biventricular outer dimension (BVOD). Mean, 95%, and 5% confidence limits for individual predictions of the biventricular outer dimensions regressed against chest circumference. (Reprinted with permission from DeVore et al. [13].)**

*Are the Ventricular Chambers Approximately Equal in Size?*

If ventricles are not the same size, there may be a complex cardiac abnormality. For instance, coarctation of the aorta may be indirectly diagnosed by noting that the left ventricle is smaller than the right ventricle on the four-chamber view [6]. It is unusual to identify the coarctation itself, but noting that the left ventricle appears smaller than the right on the four-chamber view provides indirect evidence of the possibility of a coarctation.

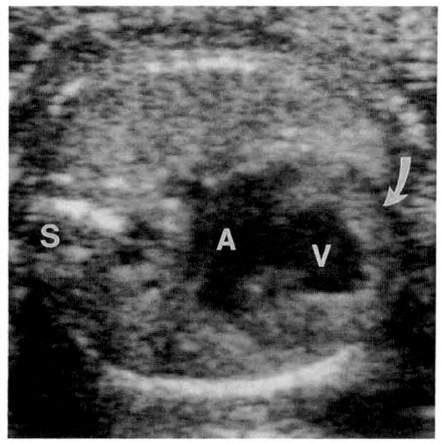
More common abnormalities easily detected by noting discrepancies in the sizes of the ventricles are cardiac abnormalities associated with hypoplasia of either the left or right ventricle. Hypoplasia of the left ventricle is usually termed the hypoplastic left heart syndrome [18]. This is a severe anomaly usually consisting of underdevelopment of the aorta, aortic valve, left ventricle, or mitral valve with an intact ventricular septum. In hypoplastic left ventricle, the left ventricle varies in size from essentially slitlike to smaller than normal, depending on the degree of hypoplasia of the mitral valve (Fig. 7) [19].

There is considerably more confusion concerning hypoplasia of the right ventricle. Most authors do not consider this a separate syndrome. However, this may be considered one of two anomalies, either pulmonary atresia with an intact ventricular septum or a tricuspid atresia with an associated ventricular septal defect (VSD). There is usually severe hy-




7

**Fig. 7.—Hypoplastic left ventricle. Four-chamber view of heart shows a hypoplastic left ventricle (LV) and a small remnant of atrial septum (*arrow*). Note size discrepancy between right ventricle (RV) and small left ventricle.**




8

**Fig. 8.—Two-chamber heart. Four-chamber view of heart shows a single atrium or an atrial septal defect with a common atrium (A) that empties into a single ventricle (V). Note thickening of wall of ventricular chamber (*arrow*). S = spine.**

poplasia of the right ventricle associated with abnormalities of the pulmonary outflow tract in pulmonary atresia with an intact ventricular septum [20]. In tricuspid atresia with a VSD there may be a hypoplastic right ventricle. The amount of hypoplasia of the right ventricle depends on the size of the VSD.

Another anomaly that may be embryologically different from severe hypoplastic right ventricle or severe hypoplastic left ventricle is the anomaly in which there is a single ventricle [21]. This anomaly usually is associated with two atria emptying into a single ventricular cavity, which may have the appearance of a right or left ventricle or may be an intermediate cavity. Such an anomaly should be easily recognized on a four-chamber view of the heart. Figure 8 shows a case of a single ventricle associated with a single atrium (i.e., two-chamber heart) that was detected prenatally.

### *Is There a Septal Defect?*

Other abnormalities that may be detected on the four-chamber view of the heart include defects in the atrial, atrioventricular, or ventricular septum. The most common prenatal cardiac abnormality detected on a four-chamber view of the heart in one series was complete atrioventricular septal defect (endocardial cushion defect). This defect was detected in 16 (100%) of 16 cases on a four-chamber view of the heart [4]. Likewise, large VSDs may be detected by a four-chamber view of the heart. VSDs that are moderate to large in size are often associated with complex cardiac abnormalities. Therefore, initial detection of a VSD will necessitate a more careful search of the fetal heart for a more complex cardiac abnormality.

Small and even moderate-sized VSDs may be overlooked [4, 9]. Even moderate to large VSDs may not be visualized if careful scanning is not performed. When evaluating the atrial or ventricular septum, a careful search of the entire septum is needed to exclude a VSD as illustrated in Figure 9. By obtaining only a single four-chamber view, a septal defect can easily be overlooked. It is possible that use of color flow imaging, in combination with routine scanning, will allow more easy recognition of these small VSDs. In any case, detection of an atrial septal defect, VSD, or endocardial cushion defect on a four-chamber view should prompt a complete fetal cardiac examination (Fig. 10).

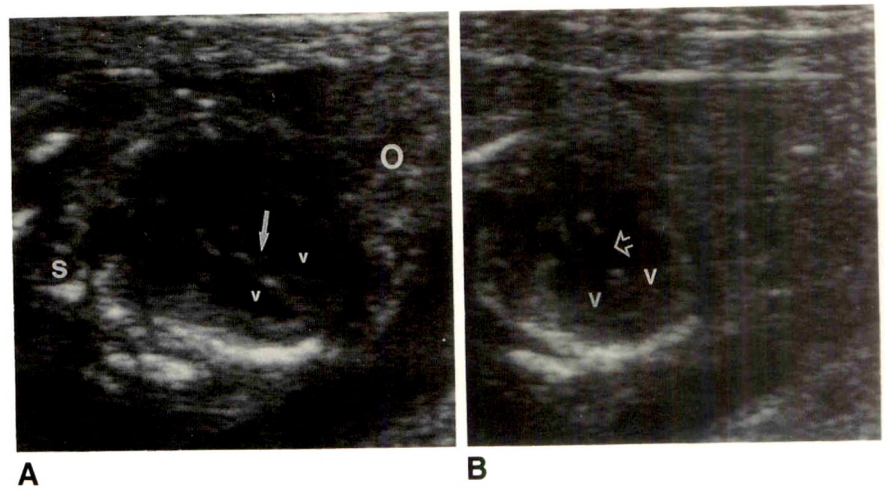



**Fig. 9.—Ventricular septal defect.**
***A*, Complete scanning of ventricular septum is needed to exclude ventricular septal defects. For instance, in this four-chamber view of the heart in a fetus with an omphalocele (O) and transposition of the great vessels, ventricular septum appears intact (*arrow*). S = spine, V = ventricle.**
***B*, By obtaining a different scan plane through intraventricular septum, however, a large ventricular septal defect (*arrow*) is identified between the two ventricles.**

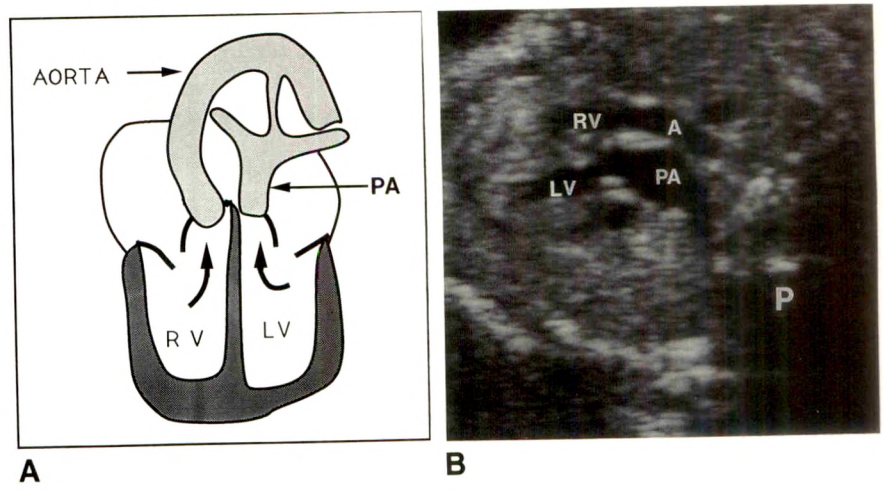



**Fig. 10.—Transposition of great arteries.**
***A*, Diagram shows transposition of great vessels with aorta originating from right ventricle (RV) and pulmonary artery (PA) originating from left ventricle (LV). There may be an accompanying septal defect.**
***B*, Four-chamber view demonstrated a large atrial septal defect. This more cephalic view shows the parallel course of aorta (A) and pulmonary artery rather than normal perpendicular course of these vessels. P = posterior. (Reprinted with permission from Nyberg and Emerson [7].)**

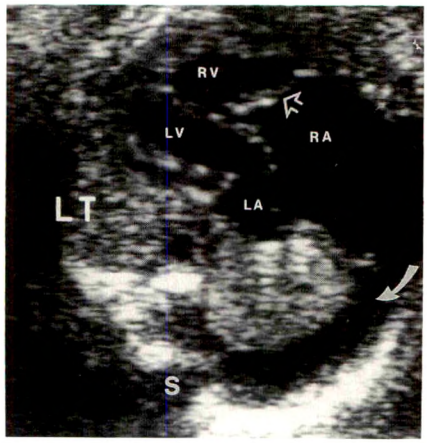



Fig. 11.—Ebstein anomaly. Attempted four-chamber view of heart shows marked dilatation of right atrium (RA) and inferior displacement of tricuspid leaflet (*open arrow*) into right ventricle (RV). There is also pleural effusion (*solid arrow*). LT = left, LV = left ventricle, LA = left atrium, S = spine. (Courtesy of D. Nyberg, Seattle, WA.)

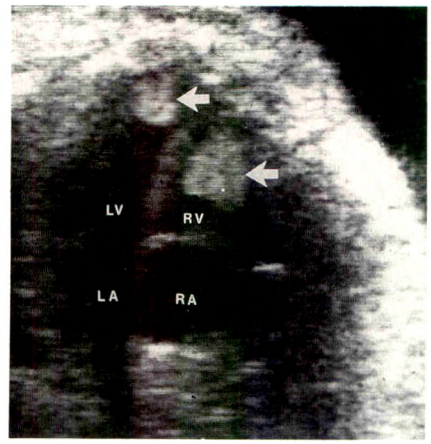



Fig. 12.—Cardiac rhabdomyomas. Four-chamber view of fetal heart shows echogenic masses (*arrows*) corresponding to cardiac rhabdomyomas in a fetus later documented to have tuberous sclerosis. LV = left ventricle, RV = right ventricle, LA = left atrium, RA = right atrium.

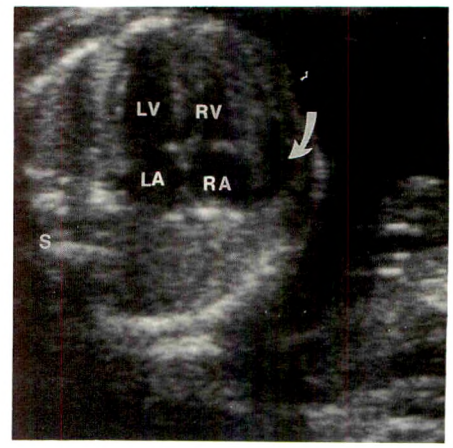



Fig. 13.—Pericardial effusion. In a twin pregnancy, this four-chamber view of heart is associated with a small pericardial effusion (*arrow*) in a fetus with hydrops. LV = left ventricle, RV = right ventricle, LA = left atrium, RA = right atrium, S = spine.

*Are the Atrioventricular Valves in a Normal Position?*

Abnormal position of the atrioventricular valves is easily detected on a four-chamber view [4]. Usually this abnormality is right-sided and is associated with malformations of the tricuspid valve, in which the septal leaflet of this valve is displaced into the cavity of the right ventricle—Ebstein anomaly (Fig. 11). This produces a grossly enlarged dilatation of the right atrium that may be recognized prenatally on the four-chamber view of the heart [4]. Similar enlargement of the right atrium can result from tricuspid dysplasia and regurgitation without inferior displacement of the tricuspid valve [7].

*Is There Any Abnormality of the Endocardium, Myocardium, or Pericardium?*

A four-chamber view of the heart also may be helpful to identify such problems as increased thickness and abnormal echogenicity of the heart muscle, as occurring with cardiomyopathies including endocardial fibroelastosis. This anomaly is characterized by gross thickening of the endocardium. Sonographically, the four-chamber view shows a large heart with poor contractility and a diffusely echogenic endocardium [22].

Focally increased echogenicity may be identified within the ventricles as a mass lesion associated with congenital heart tumors such as rhabdomyomas. Most rhabdomyomas are associated with syndromes such as tuberous sclerosis (Fig. 12) [23].

Normally a small amount of fluid is present within the pericardial sac. The four-chamber view may be helpful in detecting pericardial effusions appreciated as an anechoic region separating the two layers of the pericardium. Recognition of pericardial effusions may be a clue to systemic disorders such as fetal hydrops (Fig. 13).

**Pitfalls of Four-Chamber Views**

Several anomalies may be difficult to diagnose with a four-chamber view of the heart. These include tetralogy of Fallot, transposition of the great arteries, simple VSDs, and coarctation of the aorta. However, there is some discrepancy within the literature concerning the prenatal diagnoses of these abnormalities. For instance, Copel et al. [4] diagnosed all cases of tetralogy of Fallot with a four-chamber view, while DeVore et al. [24] have stressed that the VSD in tetralogy of Fallot usually is not visible on a four-chamber view, and recognition of the aortic dilatation is the key to correct diagnosis (Fig. 14). This abnormality is characterized by a VSD, an overriding aorta, stenosis of the right ventricular outflow tract, and right ventricle hypertrophy (Fig. 14). Therefore, in addition to the four-chamber view of the heart it may be important to assess the relationship of the aorta and the pulmonary arteries to the ventricular cavity. This may be performed easily by obtaining a left-ventricular long-axis view (Fig. 3). This view can assess the aortic root dilatation and the overriding aorta associated with tetralogy of Fallot.

Similarly, transposition of the great vessels without a VSD may be missed with the four-chamber view of the heart [6]. Again, a long-axis view of the heart may be helpful in assessing the abnormal relationship of the aorta and the pulmonary arteries to the ventricular chambers. Normally, the pulmonary artery lies anterior to the aorta. The pulmonary artery bifurcates into the right and left pulmonary arteries. The aorta and the pulmonary artery usually cross perpendicular to each other while in transposition they have a more parallel course (Fig. 10).

Other anomalies such as very small VSDs are typically missed with the four-chamber view of the heart. Similarly, coarctation of the aorta may be missed, but there may be indirect evidence of this anomaly by an enlarged right ventricle as compared with the left ventricle. Encouraging is the fact

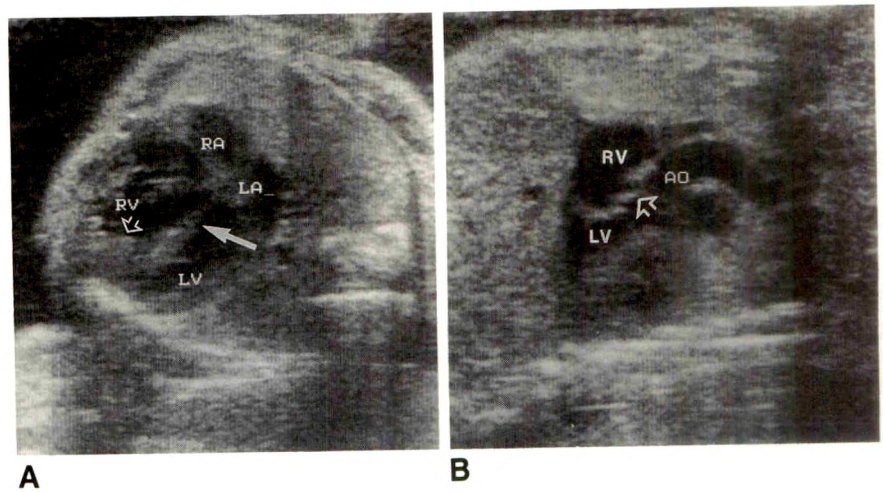



**Fig. 14.—Tetralogy of Fallot.**

***A*, Four-chamber view of heart shows right ventricular hypertrophy (*open arrow*) and slightly increased size of ventricle (RV) as compared with left ventricle (LV). However, ventricular septum appears intact (*solid arrow*). RA = right atrium, LA = left atrium.**

***B*, Long-axis view of heart shows a dilated aortic root (AO) overriding intraventricular septum (*arrow*). Ventricular septal defect was not appreciated.**

that, in one report, 96% of structural abnormalities of the heart were identifiable on a four-chamber view of the heart. In another report, cardiac lesions were not identified in 17 of 74 cases examined by prenatal sonography [25]. However, most of these missed anomalies were VSDs, many of which closed spontaneously and were associated with good neonatal outcomes [25].

A review of the data presented in the literature seems to indicate that a technically adequate four-chamber view of the heart is an important anatomic marker to exclude major structural abnormalities of the fetal heart and thorax. It is important to recognize these abnormalities because of the high associated morbidity and mortality, which affect perinatal management and decisions. Therefore, it is important for those practicing routine obstetric sonography to be familiar with the normal appearance of the four-chamber view of the heart as a marker for both intra- and extracardiac thoracic abnormalities.

## ACKNOWLEDGMENTS

I thank Karen Anderson and Edie Johnson for manuscript preparation.

## REFERENCES

1. Allan LD, Crawford DC, Chita SK, Tynan MJ. Prenatal screening for congenital heart disease. *BMJ* **1986**;292:1717–1719
2. Moller JH, Neal WA. *Heart disease in infancy*. New York: Appleton–Century–Crofts, **1981**
3. DeVore G. Fetal echocardiography: state of the art. *Clin Diagn Ultrasound* **1986**;19:79–106
4. Copel JA, Pilu G, Green J, Hobbins JC, Kleinman CS. Fetal echocardiographic screening for congenital heart disease: the importance of the four-chamber view. *Am J Obstet Gynecol* **1987**;157:648–655
5. DeVore GR. The prenatal diagnosis of congenital heart disease—a practical approach for the fetal sonographer. *JCU* **1985**;13:229–245
6. Benacerraf BR, Sanders SP. Fetal echocardiography. *Radiol Clin North Am* **1990**;28:131–147
7. Nyberg DA, Emerson SD. Cardiac malformations. In: *Diagnostic ultrasound of fetal anomalies. Text and atlas*. In: Nyberg DA, Mahoney BS, Pretorius DH, eds. Chicago: Year Book Medical, **1990**:300–341
8. McGahan JP, Nyberg DA, Mack LA. Sonography of facial features of alobar and semilobar holoprosencephaly. *AJR* **1990**;154:143–148
9. Benacerraf BR, Pober BR, Sanders SP. Accuracy of fetal echocardiography. *Radiology* **1987**;165:847–849
10. Ilbawi MN. Current status of surgery for congenital heart diseases. *Clin Perinatol* **1989**;16:157–176
11. Johnston J, Sakala EP. Neonatal cardiac allotransplantation facilitated by in utero diagnosis of hypoplastic left-sided heart syndrome. The Loma Linda University Heart Transplant Group. *West J Med* **1990**;152:70–72
12. Comstock CH. Normal fetal heart axis and position. *Obstet Gynecol* **1987**;70:255–259
13. DeVore GR, Siassi B, Platt LD. Fetal echocardiography. IV: M-mode assessment of ventricular size and contractility during the second and third trimesters of pregnancy in the normal fetus. *Am J Obstet Gynecol* **1984**;150:981–988
14. Levy DW, Mintz MC. The left ventricular echogenic focus: a normal finding. *AJR* **1988**;150:85–86
15. Chitayat D, Lao A, Wilson RD, Fagerstrom C, Hayden M. Prenatal diagnosis of asplenia/polysplenia syndrome. *Am J Obstet Gynecol* **1988**;158:1085–1087
16. Johnston RJ, McGahan JP, Hanson FW, Lindfors KK. Type III congenital cystic adenomatoid malformation associated with elevated maternal serum alpha-fetoprotein. *J Perinatol* **1988**;8:222–224
17. DeVore GR, Horenstein J, Platt LD. Fetal echocardiography. VI: Assessment of cardiothoracic disproportion—a new technique for the diagnosis of thoracic hypoplasia. *Am J Obstet Gynecol* **1986**;155:1066–1071
18. Yagel S, Mandelberg A, Hurwitz A, Jlaser Y. Prenatal diagnosis of hypoplastic left ventricle. *Am J Perinatol* **1986**;3:6–8
19. Silverman NH, Snider AR. Hypoplastic left or right heart. In: *Two-dimensional echocardiography in congenital heart disease*. New York: Appleton–Century–Crofts, **1982**:189–200
20. Marvin WJ Jr, Mahoney LT. Pulmonary atresia with intact ventricular septum. In: Adams FH, Emmanouilides GC, Riemenschneider TA, eds. *Moss' heart disease in infants, children and adolescents*, 4th ed. Baltimore: Williams & Wilkins, **1989**:338–348
21. Elliott LP, Anderson RH, Bargeron LM Jr, Kirklin JK, White RD. Single ventricle or univentricular heart. In: Adams RH, Emmanouilides GC, Riemenschneider TA, eds. *Moss' heart disease in infants, children and adolescents*, 4th ed. Baltimore: Williams & Wilkins, **1989**:485–503
22. Achiron R, Malinger G, Zaidel L, Zakut H. Prenatal sonographic diagnosis of endocardial fibroelastosis secondary to aortic stenosis. *Prenat Diagn* **1988**;8:73–77
23. Schaffer RM, Cabbad J, Minkoff H, Schiller M, Haller JO, Shapiro AJ. Sonographic diagnosis of fetal cardiac rhabdomyoma. *J Ultrasound Med* **1986**;5:531–533
24. DeVore GR, Siassi B, Platt LD. Fetal echocardiography. VIII: Aortic root dilatation—a marker for tetralogy of Fallot. *Am J Obstet Gynecol* **1988**;159:129–136
25. Crawford DC, Chita SK, Allen LD. Prenatal detection of congenital heart disease: factors affecting obstetric management and survival. *Am J Obstet Gynecol* **1988**;159:352–356

# Art Page

## John Sloan's "X-rays"

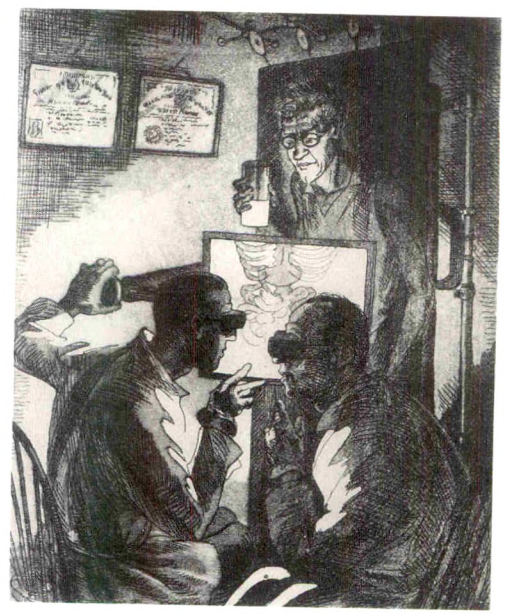
Stefan C. Schatzki[1]

The American painter John Sloan was born in Lock Haven, PA, in 1871. At the age of 20, he began to work for the *Philadelphia Inquirer*. As photography was still very expensive, newspapers in the late nineteenth century often employed artists for pictorial representation of the news, and Sloan thus began his career learning to sketch rapidly the events that he witnessed.

In 1904, Sloan moved to New York to join several other Philadelphia artists (Robert Henri, William Glackens, George Luks, and Everett Shinn), most of whom had worked on the *Inquirer* with him. For the next 10 to 15 years, he and his colleagues recorded the reality of the rapidly growing city, which was responding to the influx of people from many countries. This reality included poverty, with its contrasting color and dirt, and resulted in the group being called the Ashcan School. During this time, Sloan captured the essence of New York and its citizens in a series of paintings that have made him one of the major figures in American twentieth-century art. "Wake of the Ferry," "Hairdresser's Window," "McSorley's Bar," "Dust Storm, Fifth Avenue," and "Window on the Street" are some of the paintings that Sloan's good friend, the Irish painter John Butler Yeats, called his "poems" about the city.

Sloan was also one of America's most accomplished printmakers. His early works recorded the everyday activities of New Yorkers and remain some of the best-known American prints. In 1926, he produced the etching "X-rays." Alternative titles were "Fluoroscope," "Department of the Interior," or "A Consultation on the Interior Arrangements of John Sloan." Sloan sold very few of the 55 copies of this etching, using them to help pay physician's fees as late as 1947. The picture clearly contains a number of factual errors (red goggles, absent lead aprons, no collimation on an oversized screen), most of which can be attributed to Sloan's eyes not being adapted to the dark. However, this self-portrait remains the only observation by a major American artist of radiologic practices of the past.

In his later years, Sloan continued to paint, primarily in the summer in Gloucester and Santa Fe, spending winters teaching at the Art Students' League in New York. He seldom again achieved the spontaneous, unique observations of his early New York paintings. He died in Hanover, NH, in 1971.



**John Sloan (1871–1950). X-rays, 1926. Etching, 25 × 20 cm. Private collection.**

[1] Department of Radiology, Mount Auburn Hospital, 330 Mount Auburn St., Cambridge, MA 02238.

*AJR* **156:554, March 1991** 0361–803X/91/1563–0554 © American Roentgen Ray Society

Pictorial Essay

# Sonographic Diagnosis of the Amniotic Band Syndrome

Doris J. Burton[1,2] and Roy A. Filly[1]

The amniotic band syndrome (ABS), also known as the amniotic band disruption complex or limb–body wall complex, is a common cause of fetal malformations, estimated to occur in one in 1200 live births [1]. The malformations range from mild deformities to severe anomalies that are incompatible with postnatal life. Although a wide range of malformations can occur in this syndrome, characteristic features can often suggest the diagnosis. Sonographers should be familiar with features suggestive of ABS on antenatal sonography and be able to differentiate ABS from developmental anomalies that can mimic ABS.

The pathogenesis of ABS is thought to be disruption of the amnion, allowing the embryo, or fetus, to enter the chorionic cavity and contact the chorionic side of the amnion. Fetal parts may then become entrapped by the fibrous septa that traverse the chorionic space. Entanglement of fetal parts is random and the slash defects so created are nonembryologic in distribution. The fetal head, trunk, and extremities may be involved individually or in combination. If the amnion is disrupted early in gestation, during the period of embryogenesis, the fibrous septa of the chorionic cavity may interfere with normal embryologic development also, so that embryologic malformations such as a classic encephalocele or omphalocele may also be found in a fetus with ABS [2].

When the calvaria is involved in ABS, the resultant destructive lesions include encephaloceles and, with severe involvement, may resemble anencephaly. Whereas "typical" anencephaly is characterized by complete absence of the calvaria, that which occurs in ABS may demonstrate asymmetric preservation of a portion of the calvaria, generally near the skull base (Fig. 1). Classic encephaloceles occur in the midline, whereas those seen with ABS occur away from the midline. Similarly, when facial clefts occur in ABS they tend to occur in nonembryologic distributions (Fig. 2). When one of these asymmetric malformations involving the craniofacial region is observed, the sonographer should suspect ABS and search for other associated malformations.

Truncal deformities seen in ABS include abdominal wall defects. Whereas exteriorization of the liver rarely occurs in isolated gastroschisis, it commonly occurs in fetuses with ABS and an abdominal wall defect, and it therefore should lead the sonographer to suspect ABS when seen. The defects of the torso in ABS may be extensive and involve the chest as well as the abdominal wall (gastropleuroschisis). In this deformity exteriorization of the heart, liver, and bowel may occur (Fig. 3). In addition to wall defects and exteriorization of organs, spinal deformities commonly occur in ABS. The spine may demonstrate kyphosis, lordosis, scoliosis, and/or marked angulation deformities (Fig. 4). With severe spinal involvement, amputation of the distal spine may occur (Fig. 5). The combination of severe spinal deformity and an abdominal wall defect is diagnostic of ABS.

Extremities are frequently involved in ABS, alone or in combination with the malformations previously described. Asymmetric amputations may involve one or more digits or portions of an extremity (Fig. 6). Focal constrictions caused by the amniotic bands may occur with distal lymphedema (Fig. 7). An amputation virtually diagnostic of ABS is one with

Received July 5, 1990; accepted after revision October 8, 1990.

[1] Department of Radiology (L-374), University of California, San Francisco, 505 Parnassus, San Francisco, CA 94143-0628.

[2] Present address: Department of Radiology, Sansum Medical Clinic, 317 W. Pueblo St., P.O. Box 1239, Santa Barbara, CA 93102-1239. Address reprint requests to D. J. Burton.

*AJR* **156:555–558, March 1991** 0361–803X/91/1563–0555 © American Roentgen Ray Society

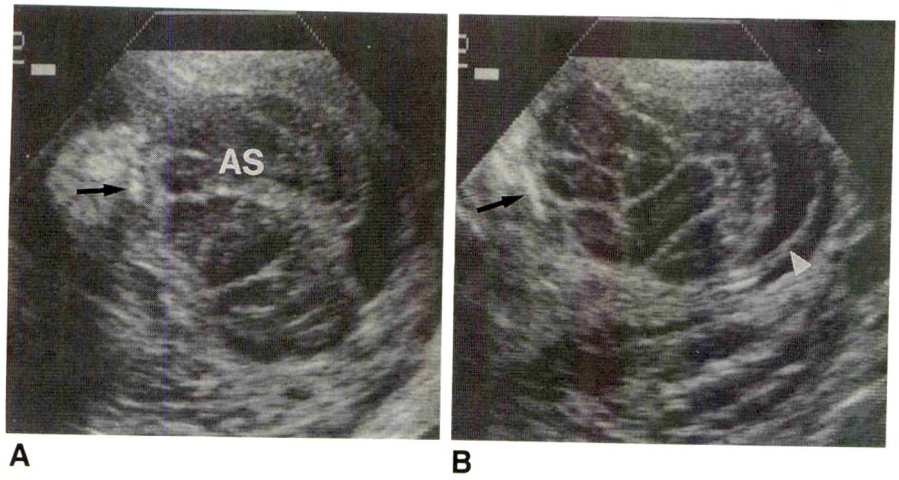



Fig. 1.—*A*, Sonogram of anencephaly with a large amount of angiomatous stroma (AS). Anencephaly occurring with amniotic band syndrome is frequently asymmetric with a portion of calvaria preserved near base of skull (*arrow*).

*B*, An amniotic band is also shown (*arrowhead*).

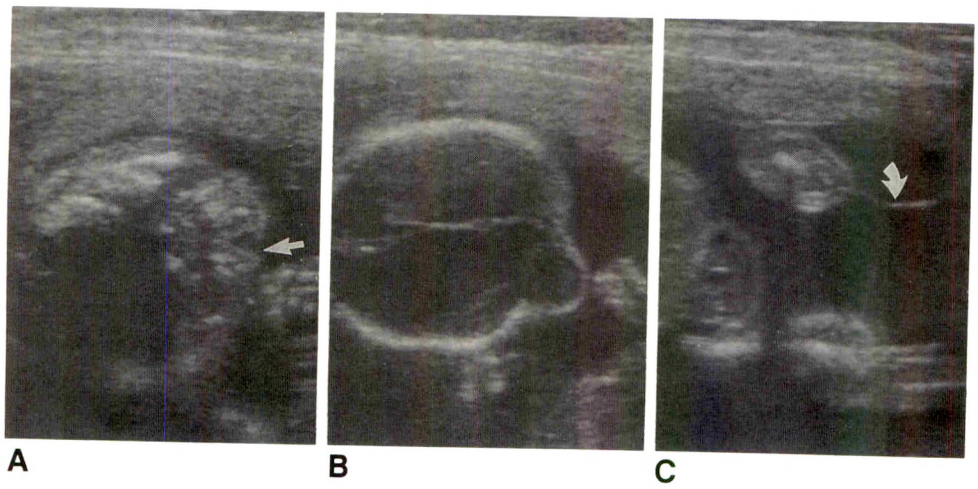



Fig. 2.—Sonograms of craniofacial anomalies in a fetus with amniotic band syndrome (ABS).

*A*, Slash defect in maxillary region produced by an amniotic band (*straight arrow*). Facial clefts seen in ABS tend to be nonembryologic in distribution as contact of an amniotic band with fetus occurs randomly.

*B*, Asymmetric encephalocele.

*C*, Amniotic bands are frequently seen attached to fetal parts. Here an amniotic band is attached to a fetal extremity (*curved arrow*).

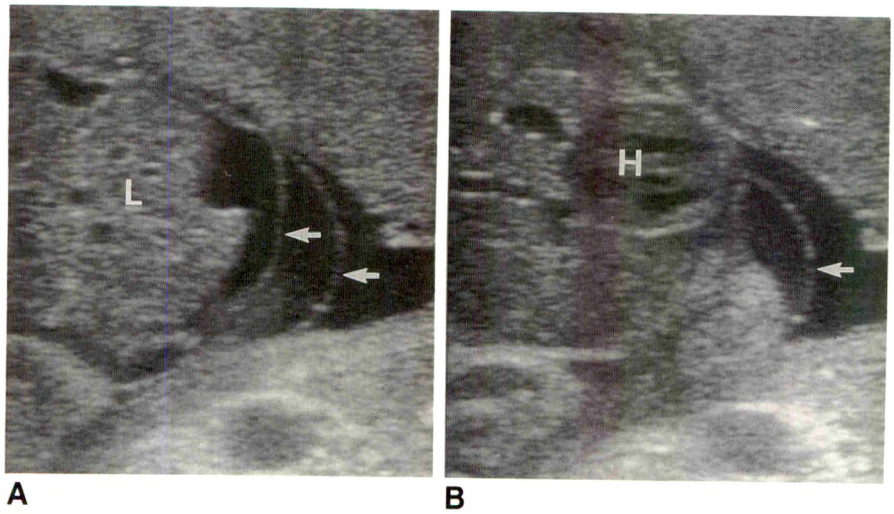



Fig. 3.—Sonograms show abdominal wall defects in fetuses with amniotic band syndrome (ABS). These can be extensive and cause exteriorization of thoracic organs as well as abdominal organs.

*A*, Exteriorized liver (L) in a fetus with ABS and a gastropleuroschisis.

*B*, Heart (H) also is exteriorized. Amniotic bands (*arrows*) are seen in both *A* and *B*.

the distal bone protruding beyond the soft tissue at the site of the amputation [3].

This discussion has thus far centered on the fetal malformations commonly seen in ABS. A search for the amniotic bands themselves also should be made. Observation of such bands is helpful in confirming the diagnosis of ABS; however, identification of such bands is not necessary to make the diagnosis. Indeed, a diagnosis of ABS should never be made on observation of these bands in the absence of fetal deformities. This is a crucial point, as several types of membranes may be seen in normal pregnancies. These include the amnion itself before it fuses to the chorion at approximately 16 weeks

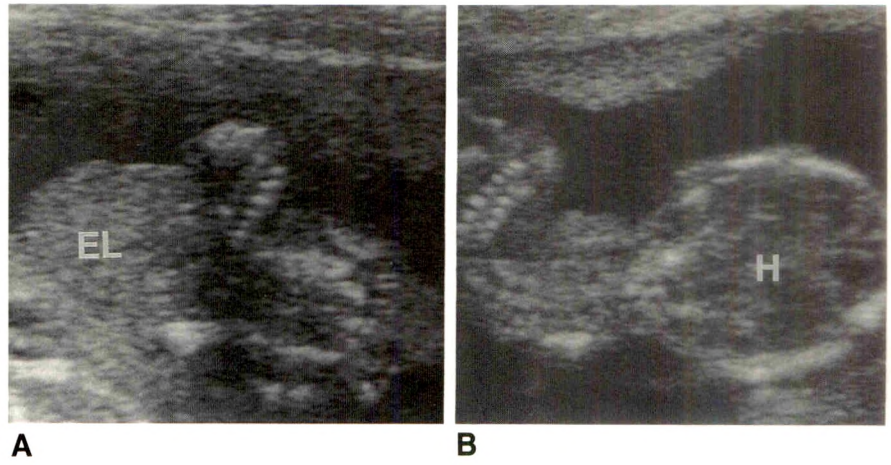



Fig. 4.—*A* and *B*, Sonograms show a sharply angled spinal deformity in a fetus with amniotic band syndrome. EL = exteriorized liver, H = fetal head.

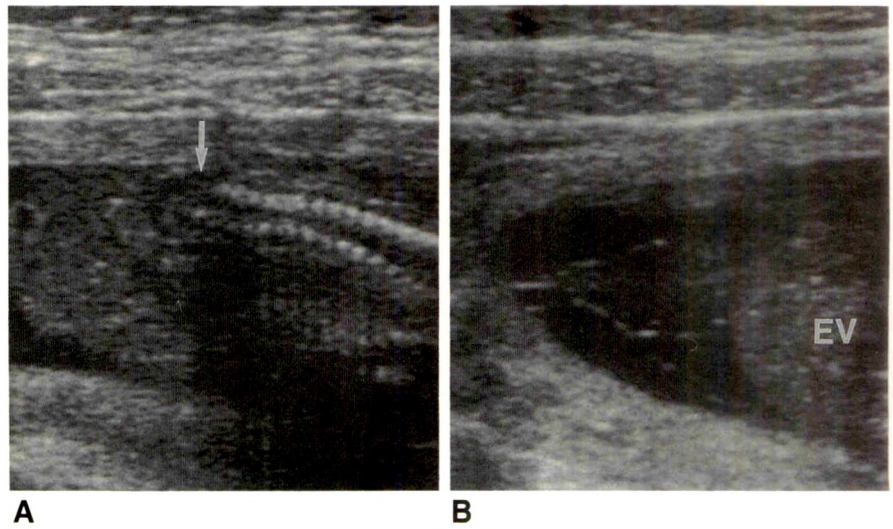



Fig. 5.—*A*, Sonogram shows amputation of spine (*arrow*) due to amniotic band syndrome (ABS).

*B*, Sonogram shows exteriorized viscera (EV) with attached amniotic bands. Severe spinal deformity, such as amputation or angulation, combined with an abdominal wall defect is diagnostic of ABS.

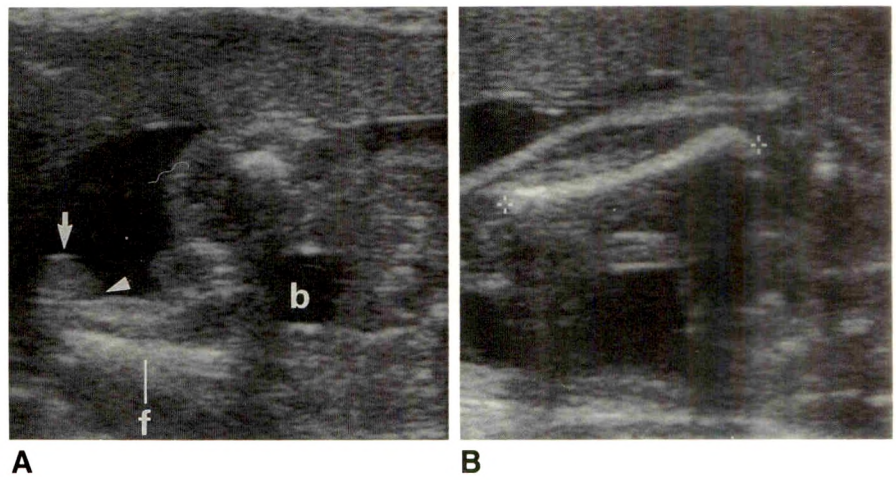



Fig. 6.—*A*, Sonogram shows extremity amputation and deformity, which often occur in amniotic band syndrome (ABS). Amputation of lower extremity immediately above knee in a fetus with ABS. f = femur, b = bladder, *arrow* = soft tissue at amputation site. Constriction (*arrowhead*) caused by amniotic band is also seen.

*B*, Sonogram of normal contralateral femur for comparison.

gestational age, visualization of the amnion after chorioamniotic separation (usually after amniocentesis, Fig. 8), and visualization of the membrane separating diamniotic twin pregnancies. Additionally, amniotic sheets have recently been described [4]. These sheets develop from uterine synechiae and are characterized by having a free edge projecting into the amniotic cavity (Fig. 9). This membrane must be scanned in multiple planes to document the free edge. Proper identification of such sheets is critical, as they have no associated fetal malformations and do not adversely affect the outcome

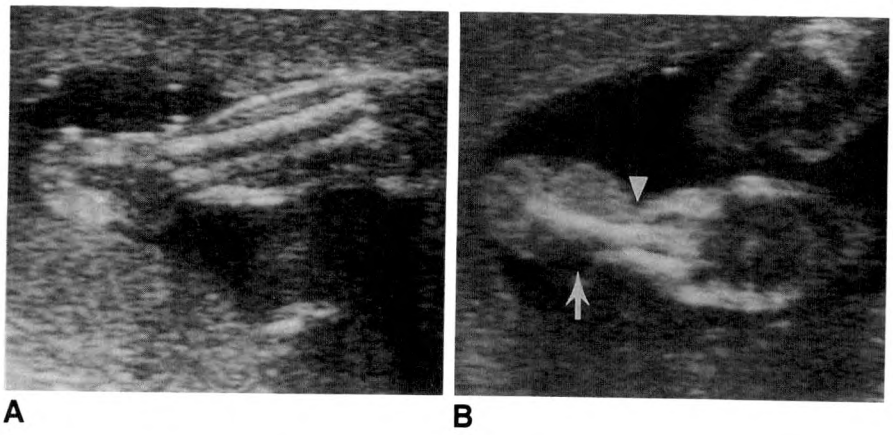



Fig. 7.—*A*, Sonogram of normal lower extremity for comparison.

*B*, Sonogram shows constriction deformity (*arrowhead*) of lower extremity caused by an amniotic band resulting in amputation of fibula (*arrow*) and distal soft-tissue swelling. These features are virtually diagnostic of amniotic band syndrome.

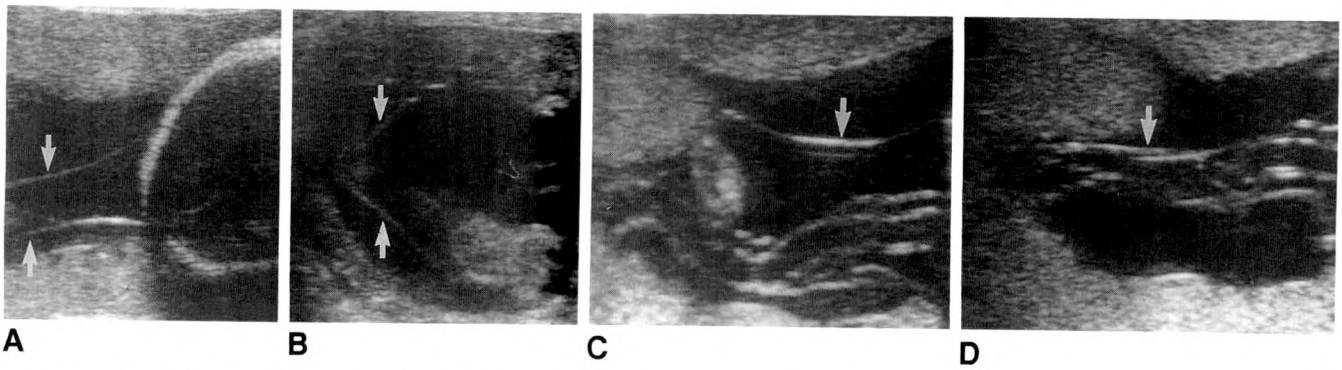



Fig. 8.—*A–D*, Sonograms show chorioamniotic separation after amniocentesis. Fetus is entirely contained within amnion (*arrows*). Amniotic band syndrome should never be diagnosed on basis of presence of intrauterine membranes when no fetal anomalies are present. Other causes for membranes should be considered.

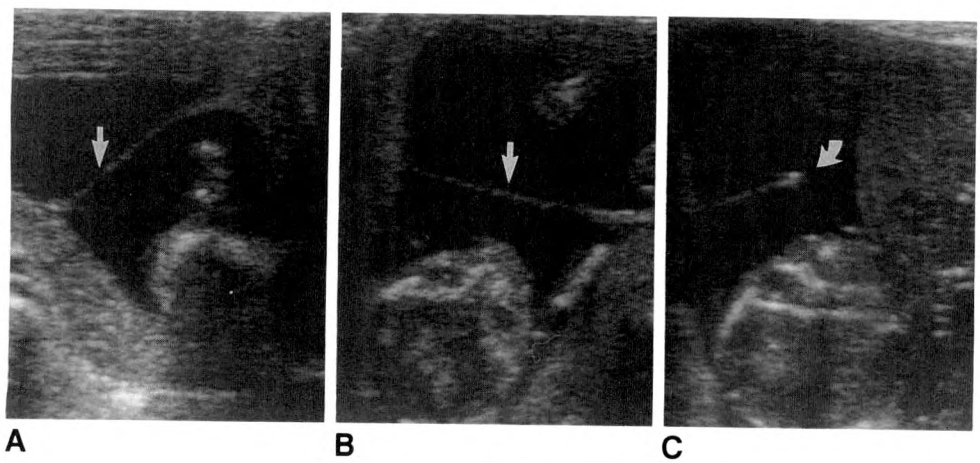



Fig. 9.—*A* and *B*, Sonograms show amniotic sheet (*arrows*) traversing amniotic cavity. Fetal parts were seen to move freely on both sides of sheet.

*C*, Scanning plane altered to reveal free edge (*curved arrow*) of amniotic sheet.

of the pregnancy. By mistakenly diagnosing this membrane as an amniotic band, a potentially normal pregnancy may be terminated.

In conclusion, the amniotic band syndrome can be diagnosed by observing characteristic fetal malformations involving the craniofacial region, trunk, and extremities alone or in combination. Demonstration of the amniotic bands themselves is not necessary for the diagnosis; further, the diagnosis should never be made solely on the basis of a membrane observed in the uterine cavity.

## REFERENCES

1. Seeds JW, Cefalo RC, Herbert WNP. Amniotic band syndrome. *Am J Obstet Gynecol* **1982**;144:243–248
2. Higginbottom MC, Jones KL, Hall BD, Smith DW. The amniotic band disruption complex: timing of amniotic rupture and variable spectra of consequent defects. *J Pediatr* **1979**;95:544–549
3. Mahony BS, Filly RA, Callen PW, Golbus MS. The amniotic band syndrome: antenatal sonographic diagnosis and potential pitfalls. *Am J Obstet Gynecol* **1985**;152:63–68
4. Randel SB, Filly RA, Callen PW, Anderson RL, Golbus MS. Amniotic sheets. *Radiology* **1988**;166:633–636

Case Report

# CT Amniography: Value in Detecting a Monoamniotic Pair in a Triplet Pregnancy

Steven K. Sargent,[1] William Young,[2] Peter Crow,[2] and Wendy Simpson[3]

Monoamniotic twinning is uncommon (1–3%) in twin gestations and is associated with high fetal mortality rates [1, 2]. Although monoamnionicity can be excluded with sonography by demonstrating a membrane separating the fetuses, separate placental sites, different fetal sexes, or a "stuck twin," the absence of these findings does not confirm monoamnionicity [3, 4]. Only the sonographic demonstration of entangled or knotted umbilical cords or conjoined twins is diagnostic of monoamnionicity [5, 6].

Because many obstetricians elect to deliver monoamniotic twins prematurely to avoid the high fetal mortality rate from cord entanglement, a means of confirming monoamnionicity when entangled umbilical cords cannot be shown would be helpful. We describe a case in which CT amniography was used to confirm the presence of monoamniotic pair in a triplet pregnancy before elective cesarean delivery at 34 weeks gestation.

## Case Report

A 20-year-old woman, gravida 2, para 1, premature 0, abortion 0, living 1, was referred for an obstetric sonographic examination at 17 weeks because she was "large for dates." Triplets were diagnosed. One fetus was identified as a male and was clearly in a separate gestational sac with a separate placenta. The other two fetuses were female. No separating membrane could be identified, and they shared a common placenta. There was no evidence of a stuck twin. Because of these findings and extreme proximity of these two fetuses, monoamnionicity was suspected. No entanglement of the umbilical cords could be seen; however, scanning was complicated by the presence of the male triplet whose sac was the most anterior. Serial scans documented adequate fetal growth, and we continued to suspect a monoamniotic pair in a triplet pregnancy.

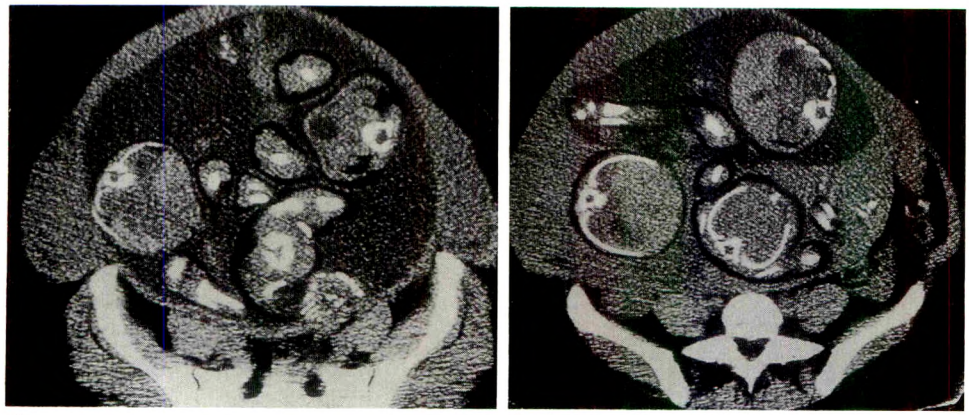
By $33\frac{1}{2}$ weeks the woman had hypertension and proteinuria; therefore, amniocentesis was scheduled to assess fetal lung maturity. To confirm monoamnionicity, we decided to use limited CT scans before and after instillation of iodinated contrast material into the presumed monoamniotic sac. Informed consent was obtained from the patient. The proposed examination was carefully explained and the patient clearly understood that in addition to amniocentesis, the procedure would involve the instillation of nonionic water-soluble contrast material into the amniotic fluid followed by two CT images that involved X-ray exposure to the fetus. The potential risks in each of these steps were discussed.

The patient was placed on the CT table. By using sonography, a transverse plane containing all three fetuses was located and marked. A single CT scan was obtained at this level (Fig. 1A). The presumed monoamniotic sac was then punctured under sonographic guidance. Fluid was removed for determination of the lecithin/sphingomyelin ratio, and 12 ml of nonionic water-soluble contrast material (Isovue 300 [61% iopamidol], Squibb Diagnostics, Princeton, NJ) was instilled. The patient was rolled gently side-to-side to ensure adequate mixing of the contrast material and amniotic fluid. A second CT scan was obtained at the same level (Fig. 1B). The fluid surrounding both female fetuses increased uniformly in density compared with the unenhanced scan, while the fluid surrounding the male fetus did not change. This finding confirmed that the two female fetuses were in the same amniotic sac.

At cesarean delivery, two healthy female infants with knotted umbilical cords were delivered from a single amniotic sac. They weighed 2010 and 1770 g and had Apgar scores of 7/9 and 5/9, respectively, at 1 and 5 min. The male fetus, in a separate sac, weighed 2280 g, with an Apgar score of 7/9 at 1 and 5 min.

Received June 15, 1990; accepted after revision September 10, 1990.
[1] Department of Diagnostic Radiology, Dartmouth-Hitchcock Medical Center, 2 Maynard St., Hanover, NH 03756. Address reprint requests to S. K. Sargent.
[2] Department of Maternal and Child Health, Dartmouth-Hitchcock Medical Center, 2 Maynard St., Hanover, NH 03756.
[3] Department of Pathology, Dartmouth-Hitchcock Medical Center, 2 Maynard St., Hanover, NH 03756.

 0361–803X/91/1563–0559 © American Roentgen Ray Society



A B

Fig. 1.—*A*, CT scan in a plane containing all three fetuses before amniocentesis and contrast instillation.

*B*, CT scan in same plane as *A* after amniocentesis and contrast instillation into monoamniotic gestational sac shows opacification of amniotic fluid around both female fetuses confirming monoamnionicity.

## Discussion

Monoamniotic twins develop when the blastocyst divides late, after the seventh day, and the ectodermal plate and the amniotic sac have developed [7]. Both fetuses are enclosed in a single amniotic cavity and share a single placenta. Although monoamniotic twinning is estimated to occur in only 1–3% of twin gestations [1], these pregnancies are of considerable interest because of the high frequency of associated morbidity and mortality. Benirschke and Kim [1] reported a 50% perinatal mortality rate for monochorionic monoamniotic twins. This fetal mortality rate has been attributed largely to umbilical cord problems, including true knotting. In addition, fetal anomalies have been reported to occur in approximately 10% of monoamniotic twins [7]. Twin transfusion syndrome also may occur [2, 3, 7]. Numerous articles have discussed these problems and the difficulties in identifying monoamniotic pregnancy with sonography [2–5, 8].

Largely because of the fear of late fetal loss related to umbilical cord complications, many obstetricians elect to deliver monoamniotic twins at about 34 weeks. Thus, when a twin pregnancy is discovered, an effort should be made to exclude monoamnionicity. Recognition of a separating membrane between the fetuses excludes monoamnionicity absolutely, but as Townsend and Filly [3] state, "Lack of membrane visualization is not predictive of monoamniotic gestation." If separate placental sites, differing fetal sexes, or a stuck twin can be identified, diamniotic placentation can be inferred and monoamnionicity excluded. When none of these findings are seen, one should suspect a monoamniotic gestation.

At least three reports have shown that demonstrating entanglement of the umbilical cords by sonography can confirm monoamnionicity [3, 5, 6]. Other than entangled or knotted umbilical cords, only the demonstration of conjoined twins is sonographic proof of monoamnionicity. Amniography with iodinated water-soluble contrast material and plain films was the technique of choice before the advent of sonography. In this case, nonionic, low-osmolality, water-soluble contrast material and CT scanning was used to diagnose definitively a monoamniotic pair in a triplet pregnancy. The advantages of CT amniography are that it is fast and easy to perform, and the space around each fetus is clearly delineated anatomically on images that are easily interpreted.

X-ray exposure is limited to a small volume of fetal tissue. Dose rates to the exposed volume for a full 360°-circumference scan and 120-kV, 140-mA technique are estimated to vary between approximately 0.5 and 2.5 rad (5–25 mGy) per slice depending on the location of the fetus within the uterus. The closer the fetus is located to the mother's skin, the higher the fetal dose. Dose rates could be lowered by decreasing kilovoltage and amperage and/or by using a gantry circumference less than the full 360°. This technique should be used only when an exhaustive sonographic attempt to demonstrate diamniotic placentation or knotted umbilical cords has failed and when confirmation of monoamnionicity will significantly alter obstetric management.

Low-osmolality contrast agents are known to be well tolerated by fetuses considerably earlier in gestation than in our case [9]. After the contrast material is instilled in the amniotic fluid, the contrast material will be swallowed by the fetus and, in the absence of obstruction, pass through the fetal gastrointestinal tract. Absorption of these agents from normal bowel is negligible. No harmful shifts of fetal body fluid into the bowel are expected.

In summary, when a monoamniotic pregnancy is suspected on sonographic examination and convincing evidence of cord entanglement cannot be demonstrated, CT amniography, a new technique, can be used to show that two fetuses occupy the same amniotic cavity.

## REFERENCES


1. Benirschke K, Kim CK. Multiple pregnancy (first of two parts). *N Engl J Med* **1973**;288:1276–1329
2. Filly RA, Goldstein RB, Callen PW. Monochorionic twinning: sonographic assessment. *AJR* **1990**;154:459–469
3. Townsend RR, Filly RA. Sonography of nonconjoined monoamniotic twin pregnancies. *J Ultrasound Med* **1988**;7:665–670
4. Mahony BS, Filly RA, Callen PW. Amnionicity and chorionicity in twin pregnancies: prediction using ultrasound. *Radiology* **1985**;155:205–209
5. Nyberg DA, Filly RA, Golbus MS, et al. Entangled umbilical cords: a sign of monoamniotic twins. *J Ultrasound Med* **1984**;3:29–32
6. Bhakthauathsalan AB, Heinz L, Wafalosky J. Ultrasound diagnosis of monoamniotic twins with cord entanglement: case report with double survival. *J Clin Ultrasound* **1985**;13:137–140
7. Colburn DW, Pasquale SA. Monoamniotic twin pregnancy. *J Reprod Med* **1982**;27:165–168
8. Rodis JF, Vintzileos AM, Campbell WA, et al. Antenatal diagnosis and management of monoamniotic twins. *Am J Obstet Gynecol* **1987**; 157:1255–1257
9. Cohen MD. Choosing contrast media for the evaluation of the gastrointestinal tract of neonates and infants. *Radiology* **1987**;162:447–456

# Deferoxamine-Induced Bone Dysplasia in Patients with Thalassemia Major

Paula W. Brill[1]
Patricia Winchester[1]
Patricia J. Giardina[2]
Susanna Cunningham-Rundles[2]

**Metaphyseal irregularity and abnormal vertebral bodies resembling a bone dysplasia were seen in two of five children with thalassemia major who were begun on a regimen of hypertransfusion and chelation with deferoxamine before the age of 3 years. Similar changes were not seen in 22 other children in whom chelation was started after the age of 3. Whether the dysplastic bone growth was related to drug dose or age of onset of chelation could not be determined, as deferoxamine dosages differed in the two groups. Findings on radiographs included flattening of the thoracic and lumbar vertebral bodies, circumferential metaphyseal osseous defects, sharp zones of provisional calcification, and widened growth plates. Healing was noted in one of the patients after the dose of deferoxamine was decreased. Zinc levels in both affected patients did not differ from those in the 25 other chelated patients.**

*AJR* 156:561–565, March 1991

Current treatment of thalassemia major includes the use of blood transfusions to maintain hemoglobin at acceptable levels and chelation to remove excess iron stores resulting from multiple transfusions. In 1988, de Virgiliis et al. [1] reported the occurrence of a growth disturbance associated with radiologic changes in the long bone metaphyses in patients with thalassemia major treated with hypertransfusion and chelation. They related the abnormalities to the early institution of chelation therapy with deferoxamine and postulated that a direct toxic effect of the drug on growing bone or the loss of minerals other than iron, or both factors, could be responsible. They recommended delaying chelation therapy until after the age of 3 years and until the patient had received 20 to 30 blood transfusions and had accumulated a large iron load as evidenced by a serum ferritin level of 800–1000 ng/ml.

In 1989 we instituted a retrospective radiologic study of our population of 27 patients with thalassemia major who have been treated with hypertransfusion and who began chelation therapy with deferoxamine before the age of 7 years. Our aims were to characterize the long bone abnormalities more fully, to determine whether the spine is also affected, to establish the prevalence of bony abnormalities in relation to the patient's age and iron load at the onset of chelation therapy, and to consider the significance of zinc deficiency in the production of bone lesions.

## Materials and Methods

In 1989, 27 patients with thalassemia major in whom deferoxamine treatment had been started before the age of 7 years were treated in the New York Hospital Thalassemia Clinic with a regimen of hypertransfusion and chelation. Hypertransfusion involved the regular administration of RBC transfusions to maintain a pretransfusion hemoglobin level greater

Received July 26, 1990; accepted after revision October 8, 1990.

Presented at the annual meeting of the Society for Pediatric Radiology, Cincinnati, April 1990.

This work was supported in part by National Institutes of Health grants NCI CA29502 and NIH 19898-01, the General Clinical Research Centers Program Office of the Division of Research Resources Foundation (RR-47), and the Children's Blood Foundation.

[1] Department of Radiology, The New York Hospital–Cornell Medical Center, 525 E. 68th St., New York, NY 10021. Address reprint requests to P. W. Brill.

[2] Department of Pediatrics, Division of Pediatric Hematology, The New York Hospital–Cornell Medical Center, New York, NY 10021.

0361–803X/91/1563–0561
© American Roentgen Ray Society

than 11 g/dl. Deferoxamine was administered subcutaneously during an 8-hr period by using a battery-operated syringe pump. The dosage of deferoxamine in these 27 patients was maximized to 60 mg/kg per day in the last 3 years of observation. Before this, the deferoxamine chelation dosage was 20–40 mg/kg per day. Six patients (cases 1–5 and 8) (Table 1) were begun at a dosage of 40–60 mg/kg per day, whereas the remainder were begun at 20–40 mg/kg per day. These dosages are approximate because of differences in patients' compliance with the recommended use of deferoxamine 5–7 days of each week.

We retrospectively reviewed all available radiographs of each patient. Since the onset of deferoxamine therapy, all patients had yearly radiographs of the hands and wrists for bone age and yearly chest radiographs to monitor heart size. Twenty-six patients had one or two examinations of the thoracic and lumbosacral spine in frontal and lateral projections. Nine patients had additional radiographs after trauma. Ten patients had abdominal radiographs for a variety of clinical indications; the femoral heads and necks were included in these films. The chest radiographs included the proximal humeral epiphyses and metaphyses. In cases 1–5, frontal and lateral radiographs of the knees were obtained in addition to the other radiologic studies listed above.

We recorded the appearance of the metaphyses and spine as well as instances of premature epiphyseal fusion and fractures. We made a qualitative assessment of osteopenia as mild, moderate, or severe. The radiologic findings were correlated with growth patterns, age at onset and duration of therapy with deferoxamine, serum ferritin level, number of blood transfusions at the time chelation was started, dose of deferoxamine, and serum zinc levels. Zinc levels were measured by atomic absorption on blood collected without hemolysis into tubes with zinc-free stoppers. Serum levels of zinc were obtained twice.

In patients with bone lesions, the effect of a decrease in the dose of deferoxamine was documented on follow-up radiographs. The results of visual and auditory assessment were recorded.

**TABLE 1: Age, Ferritin Levels, and Transfusion Status in 27 Children with Thalassemia Major Who Started Deferoxamine Chelation Before 7 Years of Age**

| Case No. | Present Age (yr) | Status at Onset of Chelation | | |
|---|---|---|---|---|
| | | Age (yr) | Ferritin (ng/ml) | No. of RBC Units Transfused |
| 1 | 7 | 1.7 | 1302 | 12 |
| 2 | 7 | 1.8 | 2006 | 33 |
| 3 | 6 | 1.8 | 2094 | 18 |
| 4[a] | 7 | 2.1 | 1969 | 26 |
| 5[a] | 5 | 2.8 | 1448 | 28 |
| 6 | 10 | 3.0 | 5564 | 31 |
| 7 | 11 | 3.3 | 4068 | 48 |
| 8 | 6 | 4.0 | 1497 | 9 |
| 9 | 15 | 4.4 | 4340 | 68 |
| 10 | 13 | 4.5 | 4340 | 66 |
| 11 | 14 | 4.5 | 2300 | 42 |
| 12 | 15 | 4.9 | 2400 | 56 |
| 13 | 15 | 4.9 | 2600 | 76 |
| 14 | 14 | 5.0 | 4600 | 74 |
| 15 | 17 | 5.3 | 2703 | 55 |
| 16 | 16 | 5.3 | 1250 | 45 |
| 17 | 18 | 5.4 | 2610 | 97 |
| 18 | 15 | 5.4 | 4000 | 92 |
| 19 | 19 | 5.4 | 2580 | 65 |
| 20 | 15 | 5.6 | 1800 | 65 |
| 21 | 19 | 5.8 | 2880 | 77 |
| 22 | 18 | 5.8 | 4200 | 96 |
| 23 | 14 | 5.9 | 2110 | 160 |
| 24 | 18 | 6.0 | 2855 | 76 |
| 25 | 17 | 6.2 | 5000 | 77 |
| 26 | 19 | 6.3 | 1620 | 69 |
| 27 | 17 | 6.8 | 7000 | 94 |

[a] This patient had metaphyseal and vertebral changes.

## Results

Serum ferritin level, number of transfusions, and age at onset of chelation are listed in Table 1. Five of the 27 thalassemic children began chelation therapy before age 3 years. Radiographs of two of the five (cases 4 and 5) showed changes in the long bones and spine, first noted at 7 and 4 years of age, respectively. At the time of initial chelation both had received over 25 transfusions and had serum ferritin levels greater than 1400 ng/dl. Growth rate decreased within 6 months of chelation therapy in both children. In case 4, growth fell gradually during a 4-year period to below the fifth percentile. In case 5, subsequently found to be hypothyroid, the growth failure was more abrupt, with height below the fifth percentile after 2 years of chelation. Leg pain and prominent knees developed in case 4 at the age of 6 years and prompted radiologic evaluation. The case 5 patient was asymptomatic except for decreased growth rate. All 27 patients were of normal height at birth and in infancy, but most showed a gradual decrease in height percentile during childhood. Four patients who entered puberty (cases 11, 13, 16, and 21) were growing at or above the fifth percentile, with one at the 50th percentile (case 11).

Zinc levels were obtained once in 19 of the patients. Serum zinc levels were low (<74 μg/dl) in seven cases (37%) compared with the normal adult range of 75–142 μg/dl. The patients with low serum levels of zinc were cases 6, 7, 17, 21, 22, 24, and 27. The serum zinc level in these patients was 52–73 μg/dl (mean, 63 μg/dl). With the exception of cases 6 and 7, all were older than 15 years when the serum zinc level was measured. The two children with low serum levels of zinc, who were 9 and 10 years old when the serum level of zinc was assessed (cases 6 and 7), were also noted to have very high serum ferritin levels relative to age and to number of transfusions.

The case 4 patient, who had normal audiometry at the onset of treatment, was found to have a high-frequency hearing deficit when the bone lesions were recognized. The hearing loss did not change with a reduction in dose of deferoxamine. Yearly audiometry in all the other patients has been normal. No visual or neurologic deficits have been found in any of the patients.

### *Radiologic Changes*

Irregular metaphyses and flattening of vertebral bodies were seen in cases 4 and 5 (Figs. 1 and 2). In case 4, at the age of 7 the bone was circumferentially deficient at the periphery of the metaphyses, especially in the distal femur and proximal tibia. The ulnar metaphysis was irregular with a flame-shaped sclerotic area projecting proximally. In the distal radius there was a second line of density just proximal to the




Fig. 1.—Case 4.

*A* and *B*, Anteroposterior (*A*) and lateral (*B*) radiographs of the knee in a 7-year-old boy. Metaphyses of distal femur and proximal tibia are circumferentially deficient. Note irregularity of distal femoral metaphysis with small bony fragments medially and posteriorly. Irregular ossification of patella reflects delayed skeletal development. Fibular growth plate is slightly widened but well defined; metaphysis is flared.

*C*, Radiograph of right hand shows metaphyseal irregularity, most evident in distal ulna and proximal phalanx of thumb. In distal ulna, a flame-shaped area of sclerosis extends proximally from growth plate. In medial portion of distal radius, there is a subtle line of density proximal to normal dense line of primary spongiosa.

*D*, Radiograph of lumbar spine shows flattened vertebral bodies.

*E* and *F*, Radiographs of both knees 9 months after reduction of dose of deferoxamine shows evidence of healing with filling in of bone at periphery of metaphyses. Sclerosis of fibular metaphyses was not evident previously.

dense line of the primary spongiosa. The distal tibial metaphysis was irregularly sclerotic. The proximal humeri and femora had minimal metaphyseal sclerosis. The vertebral bodies in the thoracic and lumbar regions were flattened. In case 4, at the age of 3 the chest, hand, and wrist were normal; at the age of 5, a double line of metaphyseal density was present in the distal ulna and at the base of the first metacarpal. In case 5 the changes were similar but less marked at the age of 4 years; radiographs at age 3 years were normal. No patients developed premature fusion of



Fig. 2.—Case 5. Radiograph of left knee in a 4¾-year-old girl. Changes are similar to but less marked than those noted in case 4 (Fig. 1). This was true of other tubular bones and spine as well. Follow-up 5 months later showed no evidence of healing.

epiphyses. Osteopenia was mild in 25 patients and moderate in two (cases 1 and 22). Four patients had traumatic fractures of long bones. All healed normally.

After the bone changes in cases 4 and 5 were recognized, the dosage of deferoxamine was reduced from 60 to 40 mg/kg per day. After 9 months on this reduced dosage, radiographs of the knees in case 4 showed evidence of healing with filling in of bone in the periphery of the metaphyses (Fig. 1E). The wrist lesions were unchanged. The case 5 patient was found to be hypothyroid at the same time that her bone lesions were recognized; she was treated with levothyroxine. Five months later her bone lesions were unchanged.

## Discussion

Iron chelation therapy prolongs the life span of patients with severe beta thalassemia, but the optimal dose and timing of therapy are still being established. Visual, auditory, and CNS complications [2, 3] as well as growth retardation [1, 4] have been attributed to deferoxamine administration.

In a Sardinian study of thalassemic patients undergoing chelation treatment with the subcutaneous infusion of deferoxamine, growth retardation and metaphyseal abnormalities were noted to occur frequently in patients in whom chelation was started before the age of 3 years. Irregular metaphyses were noted in 16 of 23 patients who began chelation before the age of 3, and in four of 26 patients who began chelation later [1]. The mean dosage of deferoxamine was 70 ± 14 mg/kg per day in the group starting treatment before age 3 and 62 ± 18 mg/kg per day in the second group. The metaphyseal changes were similar to those seen in our patients. The spine was not commented on or illustrated. A third group of 22 patients who started deferoxamine treatment after age 3 and received 20 mg/kg per day by the intramuscular route had no bony changes. In a Canadian observation, decreased growth and bony changes were attributed to deferoxamine treatment in patients who began treatment as late as 6 years of age [4]. That work, published as an abstract, described the bony abnormalities as suggestive of a chondrodysplasia of metabolic origin. Neither the prevalence of the bony changes nor the appearance of the spine was noted.

In our study population, metaphyseal and vertebral changes were noted only in two of five patients who began chelation before the age of 3 years. There were no significant differences in serum ferritin level, number of blood transfusions, or age at onset of treatment with deferoxamine between the two affected children and the three other children who began deferoxamine treatment before the age of 3 years. None of the 22 patients who began deferoxamine therapy after the age of 3 exhibited any bony abnormalities except osteopenia and fractures.

The effect of dose on producing the bony changes has not been established from our data or that of others. The dose of deferoxamine in the 22 patients who started treatment after the age of 3 was lower than that of the five children treated earlier. Consequently, the effect of age cannot be separated from that of dose. The evidence of healing in case 4 after the dose was reduced suggests that the effect on growing bone is at least partially related to dose.

The radiologic findings in the metaphyses and spine resemble but are not identical to those of a spondylometaphyseal dysplasia. A large number of spondylometaphyseal dysplasias have been described [5], but most are not well-defined entities. In the thalassemic patients under discussion, ossification at the periphery of the metaphysis was deficient, so that the lucency in the physeal region was wider peripherally than centrally. This was most marked in the knees. In the spondylometaphyseal dysplasias and metaphyseal chondrodysplasias, the physeal widening is usually uniform across the width of the bone. The physeal widening in the thalassemic patients more closely resembles that seen in pseudochondroplasia [6] and in some severe cases of the Fairbank type of multiple epiphyseal dysplasia. We are not aware of a published case of spondylometaphyseal dysplasia with the combination of the same metaphyseal and vertebral body changes present in our patients. Spondyloenchondrodysplasia is another bone dysplasia with vertebral and metaphyseal abnormalities [7]. The findings in this condition differ from those in our patients in that the vertebral bodies are flatter, and cartilaginous lucencies are seen in the metaphyses and flat bones. Review of previous radiographs of our patients revealed that the changes were acquired and did not represent a congenital bone dysplasia.

It has been suggested that chelation may lead to zinc and copper deficiency, which could affect growing bone [1, 8]. Serum zinc levels in 37% of our patients were below normal but were low in the normal range in the two affected patients. The significance of low normal zinc levels remains a matter of conjecture and may reflect fluctuating levels of zinc that could be deleterious to growth, as in our study, or may indicate that the negative effect of chelation reported by others [1] is affected by other factors including other divalent metals or unknown host factors in the Sardinian population. Although increased age and greater number of lifetime transfusions appear to be related to lower serum levels of zinc, the relationship between trace element pools and iron over-

load are clearly complex. As noted, two patients with low serum zinc levels were also observed to have disproportionately increased serum ferritin levels (cases 6 and 7).

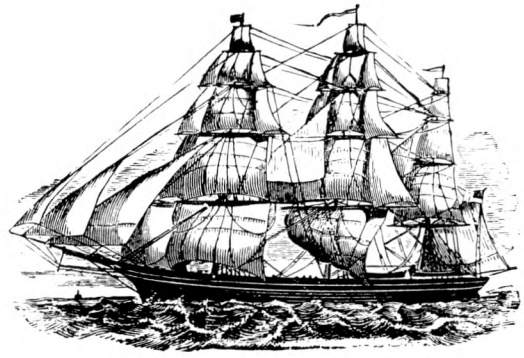
In a study of immune response in patients with thalassemia, we have observed that thalassemic patients as a whole have lower serum zinc levels than do normal subjects and that patients can be subdivided into two statistically distinct groups on the basis of serum zinc levels [9]. Immune response impairment was associated only with the group with low serum levels of zinc. Study of deferoxamine dose, age, and transfusions in the context of serial trace element levels will be required to understand the basis of the potentially intrinsic differences among thalassemia patients. This in turn may elucidate factors causing susceptibility to the bone changes that are the focus of this report.

ACKNOWLEDGMENTS

We thank Leonard O. Langer for helpful discussions. Serum ferritin determinations were performed by Robert W. Grady.

REFERENCES

1. De Virgiliis S, Congia M, Frau F, et al. Deferoxamine-induced growth retardation in patients with thalassemia major. *J Pediatr* **1988**;113: 661–669
2. Olivieri NF, Buncic JR, Chew E, et al. Visual and auditory neurotoxicity in patients receiving subcutaneous deferoxamine infusions. *N Engl J Med* **1986**;314:869–873
3. Dickerhoff R. Acute aphasia and loss of vision with desferrioxamine overdose. *Am J Pediatr Hematol Oncol* **1987**;9:287–288
4. Harris JN, McGee A, Calderbank M, et al. Deferoxamine-induced growth retardation in patients with thalassemia major (abstr). *Blood* **1989; 74[7, suppl 1]:220a**
5. **Taybi H, Lachman RS.** *Radiology of syndromes, metabolic disorders, and skeletal dysplasias,* 3rd ed. Chicago: Year Book Medical, **1990**:801–802
6. Spranger JW, Langer LO, Wiedemann H-R. *Bone dysplasias: an atlas of constitutional disorders of skeletal development.* Philadelphia: Saunders, **1974**:128
7. Schorr S, Legum C, Ochshorn M. Spondyloenchondrodysplasia. *Radiology* **1976**;118:133–139
8. Arcasoy A. Zinc status and zinc therapy in beta thalassemia (letter). *Am J Pediatr Hematol Oncol* **1989**;11:245–246
9. Cunningham-Rundles S, Bockman RS, Lin A, et al. Physiological and pharmacological effects of zinc on immune response. *Ann N Y Acad Sci* **1990**;587:113–122



# Come to the American Roentgen Ray Society 91st ANNUAL MEETING

## Boston, MA

Sheraton Boston Hotel
May 5-10, 1991

Scientific Program (200 papers)
Instructional Courses (60 hours)
Categorical Course on Body MR Imaging
The Caldwell Lecture
Award Papers
Scientific Exhibits
Social, Golf, and Tennis Programs
Guest Programs



# Aortic Thrombosis After Umbilical Artery Catheterization in Neonates: Prevalence of Complications on Long-Term Follow-up

Joanna J. Seibert[1,2]
Francis J. Northington[2]
Jane F. Miers[2]
Bonnie J. Taylor[2,3]

**We previously reported the early natural history of aortic thrombosis occurring after umbilical artery catherization in 21 neonates. Ten of those neonates were reevaluated at 36–42 months of age for evidence of hypertension, renal abnormalities, and leg-growth disturbances. They were compared with an age-matched control group of seven infants. Blood pressures were greater than the 95th percentile in three infants and between the 50th and the 95th percentile in six of the 10 infants. Height was less than the fifth percentile for age in four infants with aortic thrombosis. One child had a 1.0-cm discrepancy in leg-length measurements, and seven of nine patients exhibited a 0.5–2.0 cm discrepancy between legs in either thigh or calf circumference. Sonography showed no evidence of residual clot in the aorta or renal vessels. Doppler flow was normal in all cases. Despite resolution of neonatal aortic thrombosis, complications resulting in renovascular hypertension (three of 10 patients) and leg-growth abnormalities (eight of nine) can occur. Hypertension (one of seven) and leg-growth discrepancy (four of seven) were less frequent in the 3-year follow-up of the seven matched control infants.**

**We suggest that infants with known aortic thrombosis receive long-term follow-up to detect these potential problems.**

*AJR* 156:567–569, March 1991

In 1987 we reported a prospective study of 81 neonates evaluated for aortic thrombosis with abdominal sonography to determine the frequency of symptoms and risk factors associated with aortic thrombosis related to an umbilical artery catheter [1]. In the original study, we found that 21 (26%) of the 81 infants screened had sonographically detectable aortic clots. Of these, six (29%) were asymptomatic, and an additional five (24%) had only hematuria. The remaining 10 had moderate to severe symptoms including cardiovascular collapse. Of the 21 infants with detectable thrombosis, 17 had extensive thrombi defined as 40% or more stenosis of the cross-sectional area of the aorta, propagating to the renal and/or iliac arteries, and/or causing proximal aortic dilatation. It is this group of 21 infants that we followed up for long-term complications of leg growth, renal abnormalities, and blood pressure abnormalities.

## Subjects and Methods

Of the 21 original infants, five died in the neonatal period. One of the deaths was directly attributable to cardiovascular decompensation due to extensive catheter-associated aortic thrombosis. Two other infants were excluded because of unrelated renal abnormalities, and four were lost to follow-up. The study group consisted of 10 infants with aortic thrombosis (patients) and seven matched infants from the original study group who did not have aortic thrombi (control subjects). The clinical evaluation included height, weight, leg length and circumference measurements, blood pressure measurements, and urinalysis for evidence of blood and/or protein. Aortic and renal sonography with Doppler flow, and renal length and right-to-left ratio measurements were performed with an Acuson computed real-time scanner.

Received July 13, 1990; accepted after revision September 10, 1990.

Presented at the annual meeting of the Society of Pediatric Radiology, San Antonio, TX, April 1989, where it received the Bronze Award.

[1] Department of Radiology, University of Arkansas for Medical Sciences and Arkansas Children's Hospital, 800 Marshall St., Little Rock, AR 72202-3591. Address reprint requests to J. J. Seibert.

[2] Department of Pediatrics, University of Arkansas for Medical Sciences and Arkansas Children's Hospital, 800 Marshall St., Little Rock, AR 72202-3591.

[3] Department of Neonatology, University of Arkansas for Medical Sciences and Arkansas Children's Hospital, 800 Marshall St., Little Rock, AR 72202-3591.

0361–803X/91/1563–0567
© American Roentgen Ray Society

This study was approved by the human research and use committee, and informed consent was obtained from all parents.

Birth weights of the 10 patients ranged from 960 to 3500 g; all were between 36 and 42 months of age at follow-up. One of the 10 had a congenital bone dysplasia and was excluded from the leg-length measurements; two of the 10 had severe ventilator-dependent bronchopulmonary dysplasia requiring prolonged hospitalization; eight of the 10 had severe thrombosis in the original study by the criteria previously mentioned; despite being severely affected, seven of the 10 were asymptomatic or had only hematuria in the original study.

All 81 infants' charts were reviewed to select control subjects without clots who matched the 10 patients for birth weight, pulmonary disease, and neonatal complications. Seven control subjects were reevaluated at 47–52 months of age.

Height and weight were measured in nine of the 10 patients and all seven control subjects. Separate leg measurements were performed, including length from the iliac crest to the floor and midthigh and midcalf circumferences.

Blood pressure was measured in all subjects in the study. Systolic and diastolic pressures were compared with age standards from data published by the National Heart, Lung, and Blood Institute [2]. Sonography was performed on nine of the 10 patients and all control subjects to evaluate renal normalcy and length and to exclude residual clot in the aorta. Sonographic evaluation was performed with an Acuson 128 equipment with a sector 328 and linear 382 transducer by using previously described techniques for evaluating the kidneys [3–8] and the aorta [1]. Length measurements were made of each kidney in the longitudinal plane and compared with a graph for age [5], weight [3], and right-to-left renal ratios [8]. Both kidneys also were evaluated with Doppler sonography for patency of the renal arteries and renal veins and for presence of flow throughout the upper, middle, and lower poles of both kidneys and in the interlobar and arcuate vessels as described by Taylor et al. [9].

## Results

### *Height and Weight*

Four of the nine patients who were measured had heights below the fifth percentile for age, but all six of the boys and two of the girls were within normal limits when height vs weight ratios were plotted. The control group all fell within the fifth to 95th percentile for height. Height/weight ratios in the control group were normal also.

### *Leg Measurements*

One patient had a leg-length discrepancy of 1 cm. Seven of the nine patients measured had a discrepancy in circumference measured either at midcalf or midthigh. Six of these were discrepancies of 0.5 cm, one of 1 cm, and one of 2 cm. One of the six patients had a 0.5-cm discrepancy in circumference at both midthigh and midcalf. This patient was one of twins, both of whom had aortic thrombosis in the neonatal period. The twin with no thigh or calf difference had a very small clot at the tip of the catheter. The twin with the discrepancy in circumference had a large clot that blocked greater than 40% of the aorta and predominantly involved the left side. This child was 8 cm shorter than his twin. Only one of the control subjects showed 0.5-cm leg-length discrepancy. Three showed 0.5-cm thigh or calf circumference differences.

### *Urinalysis*

Voided urine samples were obtained in eight of the 10 patients. Trace protein was found in urine from two of the eight. Findings in all other patients were normal. Results of urinalysis in the control subjects were normal.

### *Blood Pressure*

Blood pressure was measured in all subjects. Three of the 10 patients had systolic blood pressure greater or equal to the 95th percentile for age. Six of the remaining seven patients had systolic pressures in the 50th to 90th percentile for age (Fig. 1). Only one control subject had mild systolic hypertension, with a normal diastolic pressure. As a group, the patients exhibited higher systolic and diastolic blood pressures than the control subjects did (Fig. 1).

### *Sonography*

No evidence of residual aortic clot was found in the patients. Flow in both renal arteries and veins was normal. However, abnormalities in renal size were found. Seven of the nine patients examined had below-normal measurements for their age in one or both kidneys. Two of these patients also had abnormal right-to-left renal length ratios. The mean ratio of right kidney length to left kidney length in normal infants is 0.973 ± 2 SD (0.881–1.065) [8]. In the two children with abnormal ratios, the right kidney was disproportionately larger than the left one. In one of these children, the clot had been located specifically in the left wall of the aorta, extending from the iliac artery to the level of the renal arteries. This was also the child with both the left thigh and calf circumferences smaller than those on the right side, and this child was hypertensive. When renal lengths were adjusted for weight, and plotted on curves previously generated by Han and Babcock [3], all fell within the expected range. All control subjects showed normal right-to-left renal ratios and normal renal size for both weight and age.

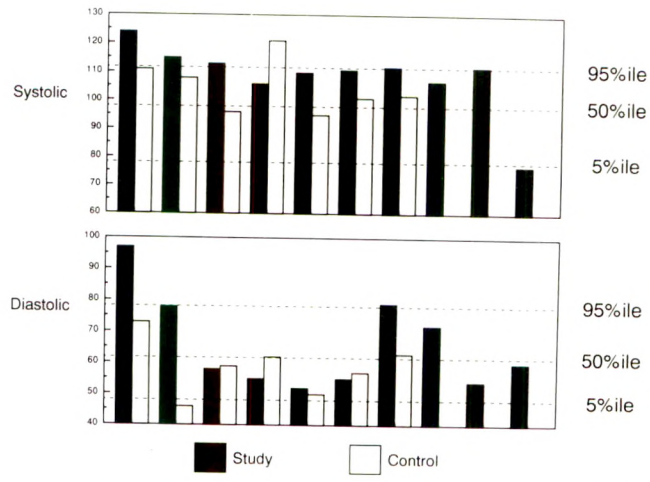



**Fig. 1.—Blood pressure measurements in patients and control subjects.**

## Discussion

Sonography is well established for evaluating renal normalcy and length in the neonatal period and throughout childhood [3–5]. The relationship of renal length, which is important in evaluating children with hypertension, is less clear. Blane et al. [4] reported that in the neonatal period the length of the left kidney should equal the length of the right kidney plus 3.0 mm with a measurement of 4.4 mm as one standard deviation. Rosenbaum et al. [5] found that the left kidney was usually 1.9 mm longer than the right kidney but did not find this significant in individual instances. Klare et al. [8] found that a radiologically measured disparity of the kidneys exceeding 10 mm was found only in 6% of normal children, with the left kidney always being the longer one. They reported a mean ratio of the right kidney to the left kidney as 0.973 ± 2 SD (0.881–1.065). We elected to use this ratio to detect early findings of possible vascular insufficiency in one kidney.

The long-term sequelae of aortic thrombosis have been evaluated by other groups, but our study is the first one with matched control subjects. Boros and colleagues [10] published a 4-year follow-up study of 14 children, 10 of whom had arterial thrombi associated with an umbilical catheter on pull-out aortography; they evaluated the children at approximately 4 years of age for leg length and circumference discrepancy, pulse pressure differences, and gait abnormalities. They found no evidence of long-term sequelae from aortic thrombosis. However, tibial and femoral lengths were discrepant by a mean of 0.1 cm each. Thigh circumferences differed by a mean of 0.5 cm with a maximum difference of 2 cm, as we report. Popliteal pulse pressures obtained by auscultation varied up to 10 mm Hg between extremities but had a mean of 3.4 mm Hg. They were unable to make any positive correlations between their findings and the location of the thrombus that each child had had.

Tooley [11] in 1972 reported follow-up examinations at regular intervals on 693 surviving children out of 827 infants who had had an umbilical artery catheter placed. The catheters were placed low in the aorta. Twenty-three percent of the 123 who died had aortic thrombi. Only one of the clots involved the renal artery, which Tooley attributes to the low placement of the catheters. Of the survivors, the rate of thrombi is unknown. He looked for long-term sequelae of occlusion of the aorta by checking pulses, lower-extremity blood pressures, capillary refill, leg circumferences, and gait. No long-term sequelae were noted. Wesstrom [12] in 1980 examined 49 18-month-old children who had had umbilical artery catheters, evaluating gross motor skills, neurologic examinations, and leg growth. One child with occlusion of an iliac artery had ipsilateral growth disturbance with a calf circumference of 1.5 cm less than the other leg. Another child seen when 1 year old had a 10-mm Hg blood pressure difference in the affected extremity. In 1985 Malin et al. [13] reported renal size abnormalities on renal scan after 1 year in two infants who had developed renal artery occlusion due to umbilical artery catheters in the neonatal period.

In our group of former neonates with clots, usually with a high catheter, we found leg length and thigh and calf circumference discrepancies, which other authors (Boros et al. [10] and Wesstrom [12]) also reported. Renal length abnormalities reported by Malin et al. [13] were present in our patients and were not found in a group of matched control subjects. The patients also tended to have higher systolic blood pressures than the control subjects. Although our numbers are small, we feel that they are suggestive of true sequelae, especially when compared with matched control subjects.

The effects of thrombi associated with umbilical artery catheters are still unknown. Other authors have advocated more vigorous therapy for treatment when thrombi are detected [11–17]. None of the patients in our original study were treated [1]. The results of our study suggest that the validity of treatment needs to be studied, and long-term follow-up of the sequelae of aortic thrombosis is warranted.

## REFERENCES


1. Seibert JJ, Taylor BJ, Williamson SL, Szabo JS, Corbitt SL. Sonographic detection of neonatal umbilical-artery thrombosis: clinical correlation. *AJR* **1987**;148:965–968
2. National Heart, Lung, and Blood Institute. *Report of the second Task Force on Blood Pressure Control in Children—1987. Pediatrics* **1987**;79:1–25.
3. Han BK, Babcock DS. Sonographic measurements and appearance of normal kidneys in children. *AJR* **1985**;145:611–616
4. Blane CE, Bookstein FL, DiPietro MA, Kelsch RC. Sonographic standards for normal infant kidney length. *AJR* **1985**;145:1289–1291
5. Rosenbaum DM, Korngold E, Teele RL. Sonographic assessment of renal length in normal children. *AJR* **1984**;142:467–469
6. Currarino G. Roentgenographic estimation of kidney size in normal individuals with emphasis on children. *AJR* **1965**;93:464–466
7. Ekof O, Ringertz H. Kidney size in children: a method of assessment. *Acta Radiol* **1976**;17:617–625
8. Klare B, Geiselhardt B, Wesch H, Scharer K, Immich H, Willich E. Radiological kidney size in childhood. *Pediatr Radiol* **1985**;9:153–160
9. Taylor KJW, Morse SS, Christopher MR, Bia M, Schiff M. Vascular complications in renal allografts: detection with duplex Doppler US. *Radiology* **1987**;162:31–38
10. Boros SJ, Nystrom JF, Thompson TR, Reynolds JW, Williams HJ. Leg growth following umbilical artery catheter-associated thrombus formation: a 4-year follow-up. *J Pediatr* **1987**;87:973–976
11. Tooley WH. What is the risk of an umbilical artery catheter? *Pediatrics* **1972**;50:1–2
12. Wesstrom G. Umbilical artery catheterization in newborns. *Acta Paediatr Scand* **1980**;69:371–376
13. Malin SW, Baumgart S, Rosenberg HK, Foreman J. Nonsurgical management of obstructive aortic thromboses complicated by renovascular hypertension in the neonate. *J Pediatr* **1980**;106:630–634
14. Vailas GN, Brouillett RT, Scott JP, Shknonik A, Conway J, Wiringa K. Neonatal aortic thrombosis: recent experience. *J Pediatr* **1986**;109:101–108
15. Emami A, Saldanha R, Knupp C, Kodroff M. Failure of systemic thrombolytic and heparin therapy in the treatment of neonatal aortic thrombosis. *Pediatrics* **1987**;79:773–777
16. Schmidt B, Andrew M. Neonatal thrombotic disease: prevention, diagnosis, and treatment. *J Pediatr* **1988**;113:407–410
17. Strife JL, Ball WS, Towbin R, Keller MS, Dillon T. Arterial occlusions in neonates: use of fibrinolytic therapy. *Radiology* **1988**;166:395–400

# Book Review

**Primer of Sectional Anatomy with MRI and CT Correlation.** By Charles P. Barrett, Steven J. Poliakoff, and Lawrence E. Holder. Baltimore: Williams & Wilkins, 108 pp., 1990. $19.95

This 101-page primer, with 16 pages of introduction, purports to "impart first-hand knowledge of the size, shape, and three dimensional relationships of the parts of the body." Overall, this spiral-bound book is a worthy effort and should help first-year anatomy and radiology residents considerably. The list price of $19.95 is not unreasonable.

Sectional anatomy is introduced by photographs of cadaveric cross sections matched in each plate (total of 50) with either a corresponding CT scan or an MR image. The match of photographs with radiologic images is good to excellent. The head and neck are well covered; sagittal, parasagittal, and some coronal sections are included.

Unfortunately, the authors skip from one type of image to the other, as in the abdomen, where the shift is from CT scans to MR images. Thereafter, however, images of the legs and arms are all MR images, whereas in practice, CT scans commonly are used. This mixture of the two imaging procedures in the same body area rather than a duplication of the two at each level may confuse students and give them an erroneous impression of the relative merits of each imaging technique for a given body part or, later in their careers, confuse their choice of a technique in any given clinical situation. The complementary nature of the techniques is described briefly, but the number and choice of images does not support or reinforce this important concept in the student's mind.

In plates of the extremities, which are limited in number, no images at the levels of the elbow, wrist, or knee are provided, an oversight that does not provide anatomic information on areas readily examined and clinically important, such as the knee. No coronal or parasagittal sections of the knee or of the hip and shoulder are included. Such additions would help students achieve a three-dimensional understanding of anatomy, which is the goal expressed by the authors.

Images in the seven sections into which this text is divided are referenced well to *Grant's Atlas of Anatomy*, edited by Anderson, and *Color Atlas of Anatomy*, by Rohen and Yokochi, and this is most useful. Another good feature is the presentation of sequential review images, as in plates 16, 22, and 31, but no review images are given for the abdomen and pelvis. The use of MR images only for the chest, particularly for the mediastinum, and also for the pelvis is a shortcoming.

Theodore A. Tristan
*Camp Hill, PA 17011-2837*

# Posterior Fossa Intracranial Hemorrhage in Infants Treated with Extracorporeal Membrane Oxygenation: Sonographic Findings

Dorothy I. Bulas[1,2]
George A. Taylor[3]
Charles R. Fitz[1,2]
Mary Ellen Revenis[2,4]
Penny Glass[2,4]
J. David Ingram[1,2]

**Posterior fossa hemorrhage was documented by autopsy in five infants who had been treated with extracorporeal membrane oxygenation over a 5-year-period. In all five cases, the diagnosis was made prospectively by cranial sonography. Sonographic findings were compared with those in a control group of 15 infants with normal posterior fossae at autopsy. The following sonographic abnormalities were exhibited in neonates with posterior fossae hemorrhage: loss of definition of the cerebellum and fourth ventricle on midline sagittal images, heterogeneous cerebellar parenchyma, focal hypoechoic lesions, ventricular dilatation, and tentorial abnormalities. Bright foci inferior to the third ventricle were seen in four neonates in the normal control group. These foci measured 5–10 mm in diameter. One cranial sonogram was falsely interpreted as showing a posterior fossa hemorrhage because of prominent echoes in the interpeduncular cistern.**

**Infants treated with extracorporeal membrane oxygenation are at risk for developing posterior fossa hemorrhage. Awareness of sonographic signs and potential pitfalls in the interpretation of posterior fossa hemorrhage is important for early and accurate recognition of these unusual and sometimes treatable hemorrhages.**

*AJR* 156:571–575, March 1991

Infants treated with extracorporeal membrane oxygenation (ECMO) are known to be at high risk for cerebrovascular injury [1–6]. Although the majority of lesions are located in the supratentorial white matter, these infants are also at risk for developing hemorrhage in the posterior fossa [7]. Because of their relatively inaccessible location and unusual appearance, posterior fossa hemorrhages may be difficult to recognize on sonography. In this article, we report our experience with the sonographic diagnosis of parenchymal and subdural posterior fossa hemorrhages in infants treated with ECMO and discuss potential pitfalls that may lead to the erroneous diagnosis of posterior fossa hemorrhage.

## Materials and Methods

Two hundred seventy-five neonates with severe respiratory failure have been treated with ECMO at our institution since 1984. Criteria for placement on ECMO at our institution have been described previously [8]. Excluded from ECMO therapy were infants weighing less than 2 kg and infants with evidence of significant intracranial hemorrhage (greater than grade 1) before ECMO. All patients were treated with venoarterial bypass via the common carotid artery and jugular vein. Reconstruction of these vessels was not performed at our institution once the infants were taken off ECMO.

Cranial sonography was performed before ECMO was started and then daily while the infant was on bypass. A 5-MHz sector transducer (Acuson, Mountain View, CA) was used for all studies. Coronal and sagittal images were routinely obtained via the anterior fontanelle.

Cranial CT scans were obtained while infants were on ECMO whenever it was necessary to clarify sonographic findings and in all survivors within 3 weeks of decannulation. These studies were performed on a GE 9800 scanner (General Electric, Milwaukee, WI) by obtaining

Received April 30, 1990; accepted after revision September 12, 1990.

[1] Department of Diagnostic Imaging and Radiology, Children's National Medicine Center and George Washington University School of Medicine and Health Sciences, 111 Michigan Ave. N.W., Washington, DC 20010-2970. Address reprint requests to D. I. Bulas.

[2] Department of Pediatrics, Children's National Medical Center and George Washington University School of Medicine and Health Sciences, Washington, DC 20010-2970.

[3] Department of Radiology, The Johns Hopkins Medical Institutions, Baltimore, MD 21203.

[4] Department of Neonatology, Children's National Medical Center, Washington, DC 20010-2970.

0361–803X/91/1563–0571
© American Roentgen Ray Society

Bayley scales of infant development were used to assess neurodevelopmental outcome in survivors.

Fifty-four neonates (20%) who had been treated with ECMO died. Autopsies were performed in 26 (48%) of these infants.

In 12 of 275 infants, sonography was prospectively interpreted as showing posterior fossa hemorrhages. Nine of these 12 died. Autopsies were performed in six of these infants, and autopsy findings were compared with cranial sonograms obtained within 24 hr before death.

Autopsy findings in 15 additional neonates with no evidence of posterior fossa hematomas were reviewed and compared with cranial sonograms obtained within 24 hr before death. This control group was used to establish the sonographic appearance of the normal posterior fossa in these neonates by evaluating the size and echogenicity of all structures.

## Results

Sonographically identified posterior fossa hemorrhages were confirmed in five of six autopsy cases. Of these five posterior fossa hemorrhages correctly diagnosed sonographically, four of the lesions were recognized within 72 hr after the initiation of ECMO, and one was identified on the 19th day of ECMO. Two infants had congenital diaphragmatic hernias, two had hyaline membrane disease, and one was septic when placed on ECMO. Four of five infants were premature (gestational ages between 34 and 36 weeks).

Several similarities were noted in the sonographic appearance of the posterior fossa hemorrhages. Loss of definition of the cerebellum and fourth ventricle on the midline sagittal view was present in all five infants (Fig. 1). Poorly defined regions of mixed echogenicity within the cerebellum were present in four infants, and discrete hypoechoic lesions that enlarged on serial examinations were identified in two infants. The tentorium was elevated or shifted in four infants. All five infants eventually developed ventricular dilatation (moderate hydrocephalus in three and mild hydrocephalus in two).

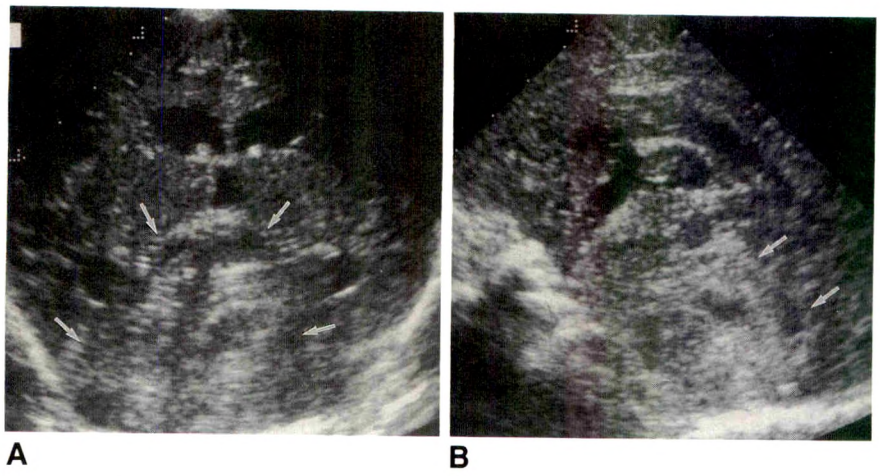
No brain hemorrhage was found at autopsy in the sixth patient believed to have a posterior fossa hemorrhage on the basis of sonographic findings (Fig. 2).

The sonographic findings in the control group of 15 infants who had been placed on ECMO but who had normal posterior fossae at autopsy were evaluated retrospectively. Special attention was focused on the sonographic appearance of the posterior fossa in the coronal plane when the transducer was directly over the third ventricle. Results showed that four of the 15 normal infants had bright foci inferior to the third ventricle on final coronal sonograms. The diameters of these foci ranged from 5 to 10 mm. Posterior fossae were normal at autopsy in all four cases.

## Discussion

The frequency of posterior fossa hemorrhage in the neonate is much lower than hemorrhages in or around the lateral and third ventricles. Before the introduction of CT scanning, posterior fossa hemorrhage was usually identified only at autopsy, with a prevalence of 16–21% in the population of premature neonates [9, 10]. The prevalence in term infants is much lower, but scattered cases can be found in the literature [11, 12]. With the introduction of CT and sonography, the diagnosis has been made more frequently [13–16]. The largest series reported is from Toronto, where 11 term and six preterm infants with posterior fossa hemorrhage were identified over a 4-year period, for a prevalence of 2.5% [16].

Trauma is thought to be the most common cause of posterior fossa hemorrhage. Difficult delivery was identified as a predisposing factor in 70–85% of infants with posterior fossa hemorrhage [16, 17]. Trauma from prolonged or precipitous labor, or forceps or breech delivery, may lead to laceration of the tentorium and dural sinuses, as well as to contusion or



A B

Fig. 1.—41-week-old infant placed on extracorporeal membrane oxygenation for persistent pulmonary hypertension caused by sepsis.

*A*, Coronal cranial sonogram shows a heterogeneous cerebellum, elevation of tentorium (*arrows*), and hydrocephalus.

*B*, Midline sagittal sonogram shows complete obliteration of fourth ventricular and cerebellar contours (*arrows*).

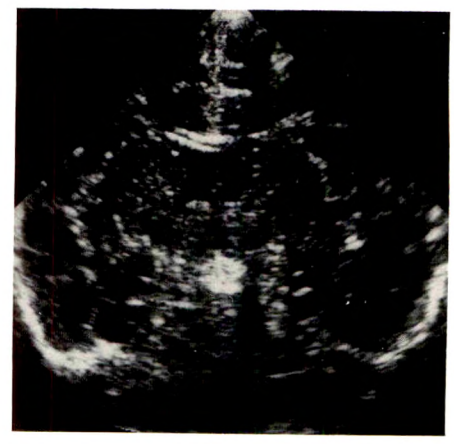


Fig. 2.—5-month-old infant with hypoplastic right ventricle placed on extracorporeal membrane oxygenation after cardiac surgery. Coronal sonogram shows a brightly echogenic focus inferior to third ventricle. No cranial hemorrhages were identified at autopsy the next day.

laceration of the underlying cerebellum. Asphyxia may cause venous congestion with endothelial damage predisposing to venous hemorrhage [18].

In premature infants, asphyxia may cause hemorrhage of the germinal matrix in the roof of the fourth ventricle. This is substantiated by the fact that most premature infants with posterior fossa hemorrhage have supratentorial germinal matrix hemorrhages as well [16, 19].

The pathogenesis of posterior fossa hemorrhage in infants on ECMO remains unclear. Potential risk factors include episodes of significant hypoxia, with subsequent endothelial damage and impaired autoregulation of cerebral blood flow [2, 7, 18, 20]. The use of systemic heparin and increased venous pressure after jugular vein ligation also may increase the risk of these unusual hemorrhages [2, 7, 20].

Early recognition of posterior fossa hemorrhage is important owing to the potential for rapid bleeding while the infant is heparinized. Sonography is thought to be limited in the evaluation of the posterior fossa because of the inaccessibility of the cerebellum and the difficulty in identifying hemorrhage within the normally echogenic tentorium, vermis, and subarachnoid space. Although several authors have successfully identified posterior fossa hemorrhages [19, 21, 22], the sensitivity of sonography in identifying posterior fossa hemorrhage has been poor, with Koch et al. [23] missing five of six, von Gontard et al. [24] two of two, and de Campo [25] three of four.

In addition to the five infants with posterior fossa hemorrhages confirmed by autopsy, we have a series of seven infants diagnosed by CT as having posterior fossa hemorrhages. One infant died and no autopsy was performed; the remaining six are alive. Four of seven posterior fossa hemorrhages were diagnosed prospectively by sonography, while three appeared normal sonographically. Hydrocephalus, heterogeneous cerebellar echogenicity, and obliteration of the fourth ventricle and cerebellar contours were noted on sonograms in all four cases in which large cerebellar hemorrhages were confirmed by CT (Figs. 3 and 4). In the remaining three cases, small subdural or cerebellar hematomas were missed sonographically (Fig. 5). Our improved sensitivity in detecting posterior fossa hemorrhages with sonography may be due to the fact that intracranial hemorrhages in infants with ECMO tend to be hypoechoic from unclotted heparinized blood [1, 3]. These hypoechoic hemorrhages stand out against the normally echogenic vermis and tentorium. The rapid expansion of these hemorrhages with changing echo texture of the cerebellum, increasing mass effect, and ventricular dilatation were additional features that made identification of these hemorrhages possible by sonography. Small hemorrhages were missed despite close and frequent monitoring. Thus,

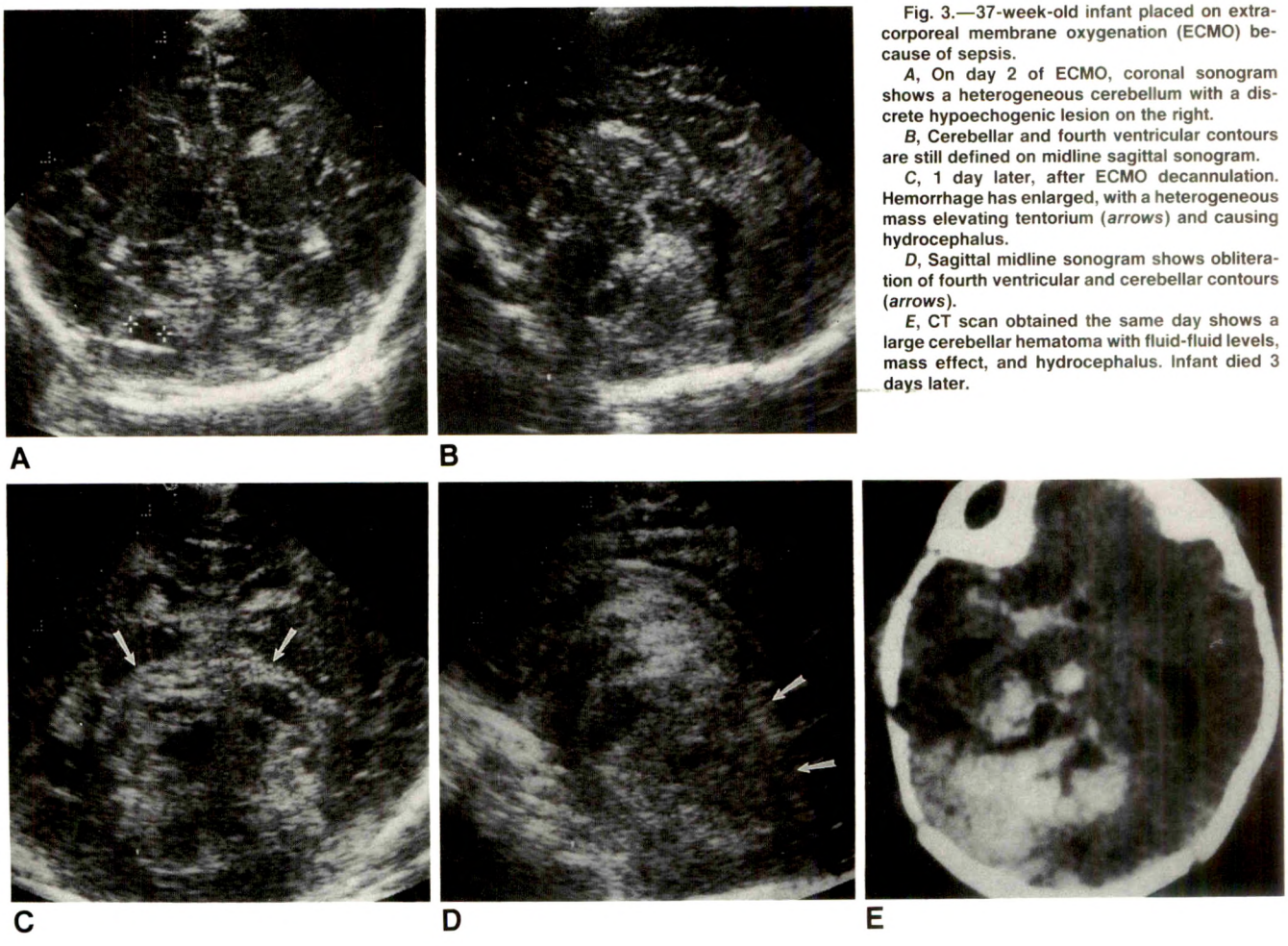



**Fig. 3.—37-week-old infant placed on extracorporeal membrane oxygenation (ECMO) because of sepsis.**

***A*, On day 2 of ECMO, coronal sonogram shows a heterogeneous cerebellum with a discrete hypoechogenic lesion on the right.**

***B*, Cerebellar and fourth ventricular contours are still defined on midline sagittal sonogram.**

***C*, 1 day later, after ECMO decannulation. Hemorrhage has enlarged, with a heterogeneous mass elevating tentorium (*arrows*) and causing hydrocephalus.**

***D*, Sagittal midline sonogram shows obliteration of fourth ventricular and cerebellar contours (*arrows*).**

***E*, CT scan obtained the same day shows a large cerebellar hematoma with fluid-fluid levels, mass effect, and hydrocephalus. Infant died 3 days later.**

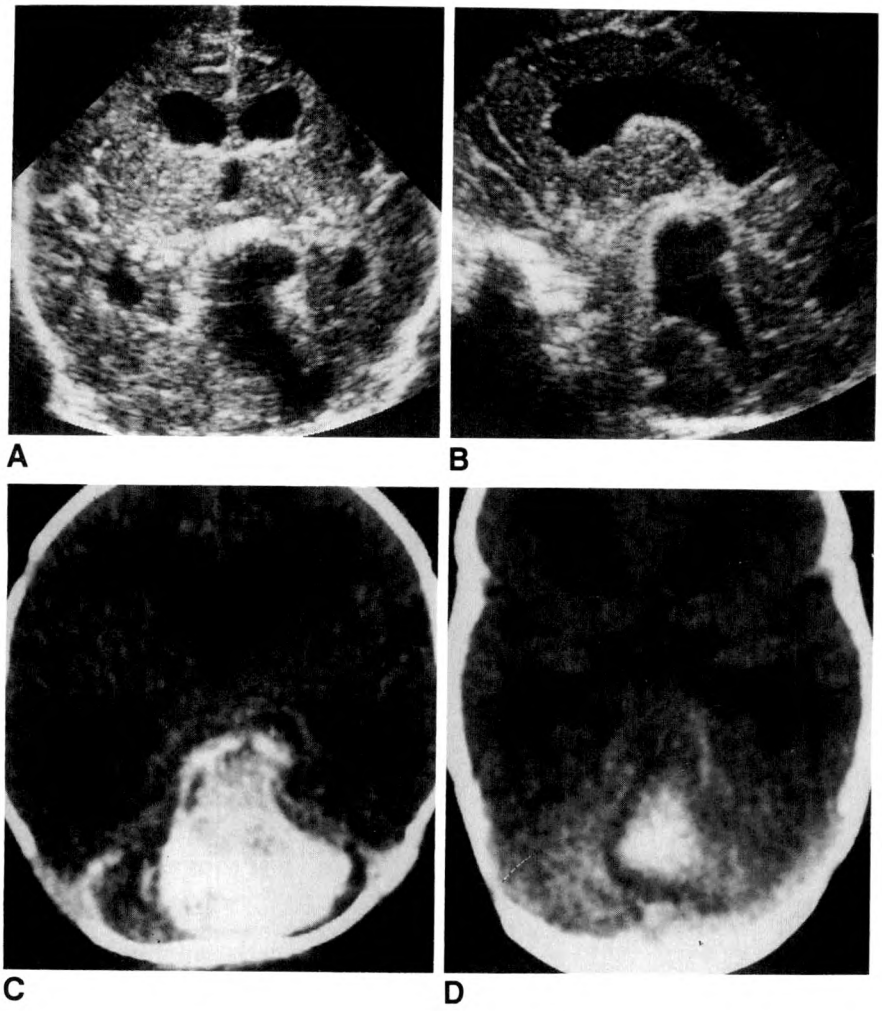



**Fig. 4.—40-week-old infant with meconium aspiration. Initial cranial sonograms were normal.**

***A* and *B*, On day 3 of extracorporeal membrane oxygenation (ECMO), a large hypoechogenic mass is identified on both coronal (*A*) and sagittal (*B*) sonograms. Hydrocephalus has developed.**

***C*, CT scan obtained the same day confirms a large cerebellar hematoma with hydrocephalus.**

***D*, The infant was taken off ECMO and treated conservatively. Follow-up CT scan obtained 1 month later shows partial resolution of hematoma. The infant survived, and at 14 months of age had only mild motor delay.**

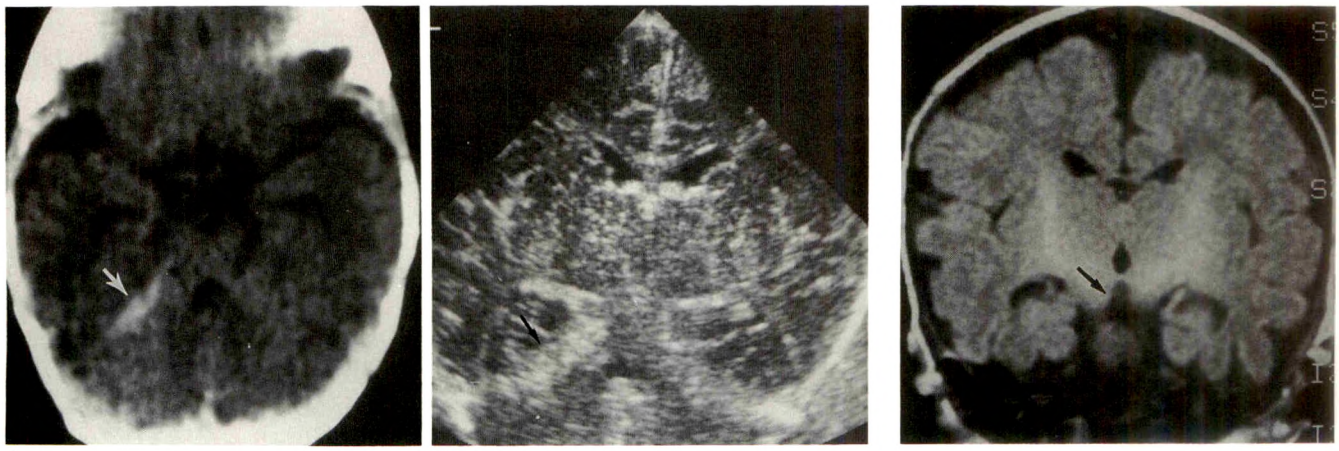
follow-up CT or MR scans are recommended for all infants after treatment with ECMO [26].

One infant with an unusually echogenic region inferior to the third ventricle was incorrectly interpreted as having posterior fossa hemorrhage. This region is in the vicinity of the interpeduncular cistern, a dilatation of the subarachnoid space between the cerebral peduncles (Fig. 6) [27, 28]. Yousefzadeh and Naidich [29] have noted that shallow cisterns filled with blood vessels may appear hyperechoic because of pulsations transmitted from apposing brain surfaces and blood vessels. The interpeduncular cistern contains the end of the basilar artery as the posterior cerebral arteries branch. The floor, known as the posterior perforated substance, is pierced by numerous branches of the posterior cerebral artery. With these arteries crossing through the fluid-filled space, it is not surprising that numerous interfaces may cause echoes to be reflected if the transducer is positioned just perpendicular to this region. The fact that these echoes are not always imaged may be due to the small area that this cistern encompasses and the angle needed for the interfaces to optimally reflect the sound beam. Technical factors also may affect the echogenicity of cisterns. Yousefzadeh and Naidich [29] noted that the persistence mode could create hyperechoic artifacts that could be misinterpreted as hemorrhage. They recommended using both persistence and nonpersistence images when an unusually bright region is encountered.

Before 1981, posterior fossa hemorrhages were managed surgically with evacuation of the hematoma [12, 13, 16, 30]. Survival rates appeared promising, but the majority of the infants had long-term neurologic disabilities. In 1981, Fishman et al. [14] recommended a conservative approach if there were no clinical signs of brainstem compression. Survival has been good, with few patients requiring long-term shunting [17, 23]. Cerebellar hematomas, however, still have a worse prognosis than tentorial subdural hematomas [16].

Our approach has been conservative. Once an intracranial abnormality is identified, systemic heparin is decreased while artificially high bypass rates are maintained. If the hemorrhage extends uncontrollably despite this therapy, the infant is removed from ECMO bypass. Six infants with sonographically identified hemorrhage died while being taken off ECMO. The remaining six hemorrhages resorbed spontaneously.

When sonography was able to identify a posterior fossa hemorrhage, the outcome was poor, with only a 33% (three/nine) survival. However, if the infant survived the first few days off ECMO, the long-term prognosis was favorable; only one of three infants demonstrated significant motor delay at 2 years of age.



A B

**Fig. 5.—40-week-old infant placed on extracorporeal membrane oxygenation for meconium aspiration. Serial cranial sonograms were interpreted as normal.**
***A*, CT scan 3 days after decannulation shows a small right tentorial subdural hematoma (*arrow*).**
***B*, In retrospect, mild thickening of right tentorium (*arrow*) was present on coronal sonogram. The infant had mild hypotonia at 2 years of age.**

**Fig. 6.—Coronal cranial MR image shows interpeduncular cistern (*arrow*). The echogenicity of this region may vary on coronal sonograms.**

If a posterior fossa hemorrhage was missed sonographically, but recognized on CT, the prognosis was favorable. These hemorrhages tended to be small or limited to the subdural space without evidence of hydrocephalus. No significant motor delay has been identified in this group at 2-year follow-ups.

ECMO therapy can be lifesaving for infants with intractable respiratory failure. Yet, because of its association with life-threatening posterior fossa injury, familiarity with sonographic signs of posterior fossa hemorrhage and potential pitfalls in interpretation are important for the successful management of these severely ill infants.

## REFERENCES


1. Bowerman RA, Zwischerberger JB, Andrews AF, Bartlett RH. Cranial sonography of infant treated with ECMO. *AJR* **1985**;145:161–166
2. Cilley RE, Zwischenberger JB, Andrews AF, Bowerman RA, Roloff DW, Bartlett RH. Intracranial hemorrhage during extracorporeal membrane oxygenation in neonates. *Pediatrics* **1986**;78:699–704
3. Taylor GA, Fitz CR, Miller MK, Garin DB, Catena LM, Short BL. Intracranial abnormalities in infants treated with extracorporeal membrane oxygenation: imaging with US and CT. *Radiology* **1987**;165:675–679
4. Luisiri A, Graviss ER, Weber T, et al. Neurosonographic changes in newborns treated with extracorporeal membrane oxygenation. *J Ultrasound Med* **1988**;7:429–438
5. Taylor GA, Fitz CR, Kapur S, Short BL. Cerebrovascular accidents in neonates treated with extracorporeal membrane oxygenation. Sonographic-pathologic correlation. *AJR* **1989**;153:355–361
6. Babcock DS, Han BK, Weiss RG, Ryckman FC. Brain abnormalities in infants on extracorporeal membrane oxygenation: sonographic and CT findings. *AJR* **1989**;153:571–576
7. Ichord R, Short BL, Taylor G. Cerebellar hemorrhage in neonates treated with ECMO. *J Pediatr* (in press)
8. Beck R, Anderson KD, Pearson GD, Garin J, Miller MK, Short BL. Criteria for ECMO in population of infants with PPHN. *J Pediatr Surg* **1986**;21:297–302
9. Martin R, Roessman U, Foronoff A. Massive intracerebellar hemorrhage in low birth weight infants. *J Pediatr* **1976**;80:290–293
10. Grunnett ML, Shields DW. Cerebellar hemorrhage in the premature infant. *J Pediatr* **1976**;88:605–608
11. Coblentz RG. Cerebellar SDH in infant two weeks old with second degree hydrocephalus operations and recovery. *Surgery* **1940**;8:771–776
12. Carter LP, Pittman HW. Posterior fossa subdural hematoma of the newborn. *Neurosurgery* **1971**;34:423–426
13. Serfontein GL, Rom S, Stein S. Posterior fossa subdural hemorrhage in the newborn. *Pediatrics* **1980**;65:40–43
14. Fishman MA, Percy AK, Cheek WR, Speer ME. Successful conservative management of cerebellar hematoma in term neonates. *J Pediatr* **1981**;98:466–468
15. Blank NK, Strand R, Gilles FH, Palakshappa A. Posterior fossa subdural hematomas in neonates. *Arch Neurol* **1978**;35:108–111
16. Scotti G, Flodmark O, Harwood-Nash DC, Humphries RP. Posterior fossa hemorrhages in the newborn. *J Comput Assist Tomogr* **1981**;5:68–72
17. Williamson WD, Percy AK, Fishman MA, et al. Cerebellar hemorrhage in the term neonate: developmental and neurologic outcome. *Pediatr Neurol* **1985**;1:356–360
18. Volpe JJ. Neonatal intracranial hemorrhage pathophysiology, neuropathology, and clinical features. *Clin Perinatol* **1977**;4:77–102
19. Peterson CM, Smith WL, Franken GA. Neonatal intracerebellar hemorrhage detection by real time ultrasound. *Radiology* **1984**;150:391–392
20. Taylor GA, Short BL, Fitz CR. Imaging of cerebrovascular injury in infants treated with ECMO. *J Pediatr* **1989**;114:635–639
21. Foy P, Dubbins PA, Woldroup L, et al. Ultrasound demonstration of cerebellar hemorrhage in a neonate. *JCU* **1982**;10:196–198
22. Bejar R, Coen RW, Ekkpoudia I, James HE, Gluck L. Real time ultrasound diagnosis of hemorrhagic pathological conditions in the posterior fossa of preterm infants. *Neurosurgery* **1985**;16:281–289
23. Koch TK, Jahnke SE, Edwards MSB, Davis SL. Posterior fossa hemorrage in term newborns. *Pediatr Neurol* **1985**;1:96–99
24. Von Gontard A, Arnold D, Adis B. Posterior fossa hemorrhage in the newborn—diagnosis and management. *Pediatr Radiol* **1988**;18:347–348
25. De Campo M. Neonatal posterior fossa haemorrhage: a difficult ultrasound diagnosis. *Australas Radiol* **1989**;33:150–153
26. Lewin JS, Masaryk TJ, Modie MT, Ross JS, Stork EK, Wiznitzer M. Extracorporeal membrane oxygenation in infants: angiographic and parenchymal evaluation of the brain with MR imaging. *Radiology* **1989**;173:361–365
27. Grant EG, Schellinger D, Richardson JD. Real-time ultrasonography of the posterior fossa. *J Ultrasound Med* **1983**;2:73–87
28. Weddington M. *Atlas of human intracranial anatomy*. Rutland, VT: Academy Books, **1984**:220
29. Yousefzadeh DK, Naidich TP. US anatomy of the posterior fossa in children: correlation with brain sections. *Radiology* **1985**;156:353–361
30. Ravenel SD. Posterior fossa hemorrhage in the term newborn: report of two cases. *Pediatrics* **1979**;64:39–42

Case Report

# Schmid-Like Metaphyseal Chondrodysplasia Simulating Child Abuse

Paul K. Kleinman[1]

Schmid metaphyseal chondrodysplasia is characterized by mild to moderate flaring and irregularity of the metaphyses, a normal spine, and frequently short stature [1, 2]. It is rarely diagnosed in patients younger than 2 years old without a reported family history of the condition. This report describes a case of metaphyseal chondrodysplasia radiologically resembling the Schmid type in a 5-month-old patient with an apparent leg-length discrepancy. Child abuse was initially suspected radiologically, until additional radiographs of the patient and his father were obtained. Subsequently, another sibling with similar radiologic features was born.

## Case Report

The 8 lb. 11 oz. (3.97 kg) infant was born after an uncomplicated 40-week pregnancy. The patient was essentially well until 5 months of age, when he underwent radiologic examination of the lower extremities for a suspected leg-length discrepancy. The radiologic findings on this limited examination suggested the diagnosis of child abuse. The patient was admitted for further evaluation.

The height was 71 cm (>95th percentile), weight was 7.5 kg (50th percentile), and the head circumference was 44 cm (75th percentile). Findings on physical examination were within normal limits. The alkaline phosphatase level was 457 units per liter (normal, 40–180 units/l). The other results of the routine laboratory studies, including calcium and phosphorus levels, were normal. "Vitamin D–resistant rickets" had been diagnosed in the father at infancy, and he later underwent corrective osteotomies for bowing of both lower extremities. He is now clinically well at a height of 5 ft. 1 in. (1.54 m) and is not on any vitamin therapy. On the basis of the skeletal survey performed on the child and the father, "Schmid-like" metaphyseal chondrodysplasia was diagnosed. Subsequently a second male infant was born with similar radiologic features. Additional family history was limited, but no other affected persons were identified.

## Radiologic Findings

Skeletal survey of the 5-month-old infant showed irregularity and mild sclerosis involving all of the long-bone metaphyses (Fig. 1). The findings were most pronounced in the femurs, tibiae, and humeri, where the appearance of fragmentation suggested metaphyseal injury associated with abuse. The acromion processes were mildly irregular, and the anterior ribs were cupped; the hands and feet, spine, and skull were normal.

Skeletal survey performed on the patient's father showed mild to moderate rhizomelia and minimal metaphyseal deformity (Fig. 2). A selected image of the subsequent affected sibling is shown in Figure 3.

## Discussion

The clinical and radiologic features of Schmid metaphyseal chondrodysplasia have recently been delineated by Lachman et al. [1]. Distinctive findings include enlarged capital femoral epiphyses, coxa vara, greater involvement of the femurs distally then proximally, and anterior rib changes. The radiologic features of the cases reported here are consistent with Schmid metaphyseal chondrodysplasia. However, the normal

Received July 31, 1990; accepted after revision October 8, 1990.
[1] Department of Radiology, University of Massachusetts Medical Center, 55 Lake Ave., N., Worcester, MA 01655. Address reprint requests to P. K. Kleinman.
*AJR* 156:576–578, March 1991 0361–803X/91/1563–0576 © American Roentgen Ray Society

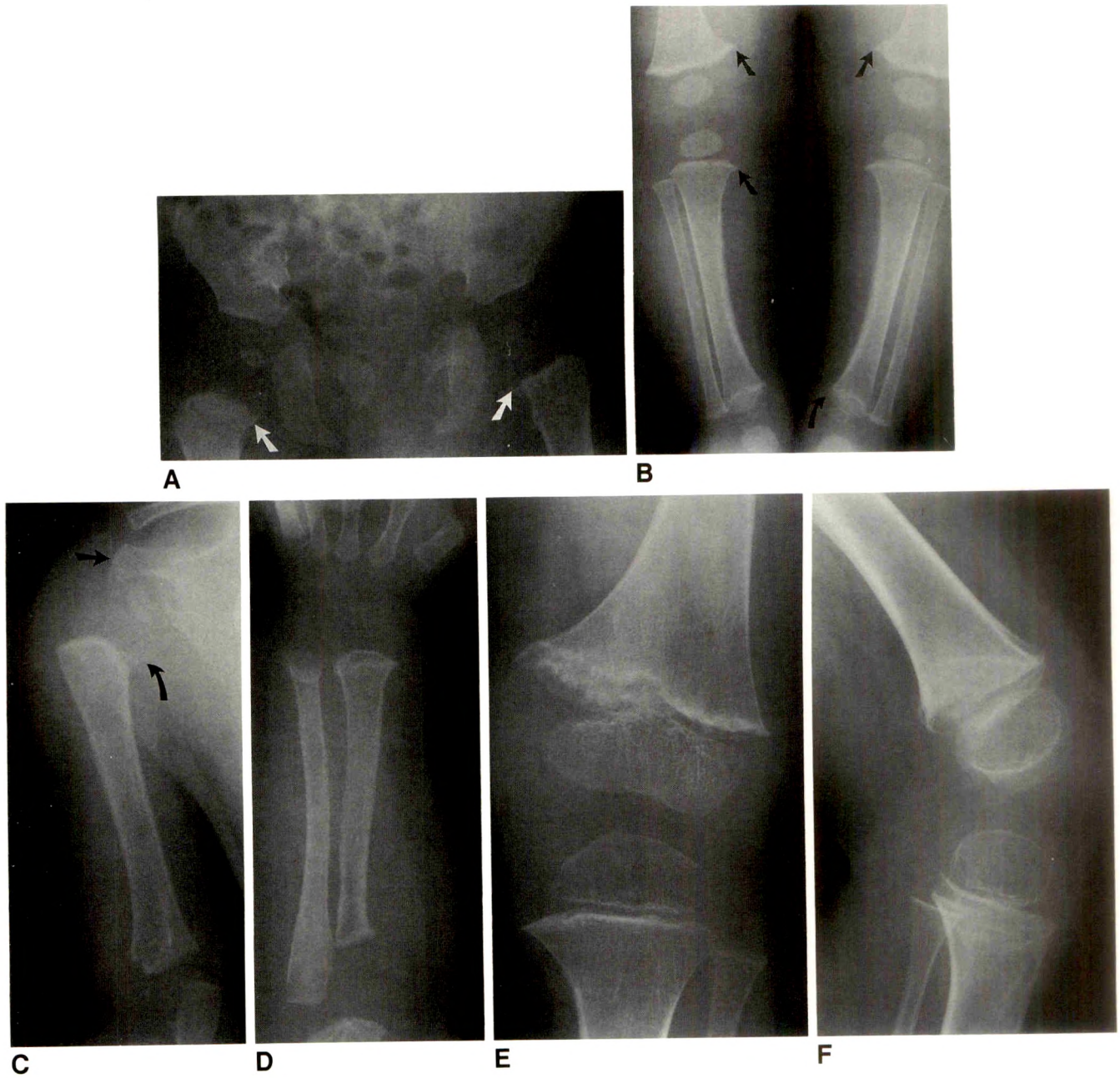



Fig. 1.—5-month-old patient with Schmid-like metaphyseal chondrodysplasia.

*A*, Anteroposterior radiograph of pelvis shows spurlike projections suggesting corner fractures arising from medial aspects of femoral metaphyses (*arrows*). Metaphyseal margins of growth plate are irregular and sclerotic. Distance between ossified capital femoral epiphyses and metaphyses is increased.

*B*, Radiograph of knees and lower legs shows asymmetric spurring involving distal femoral and proximal tibial metaphyses (*straight arrows*). Sclerosis and irregularity is noted in distal tibial and fibular metaphyses. Viewing metaphyses obliquely accentuates appearance of cupping of distal tibial metaphyses with a suggestion of a bucket-handle fracture on left side (*curved arrow*).

*C*, Radiograph of right proximal humerus. An irregular bony spur is noted arising from medial humeral metaphysis (*curved arrow*). Distance between ossified epiphysis and metaphysis is increased with apparent varus angulation. Irregularity and sclerosis is noted involving distal humerus and acromion process (*straight arrow*).

*D*, Radiograph of forearm shows irregularity and sclerosis involving distal radius and apparent cupping of distal ulna.

*E* and *F*, Same patient at 2 years old. Anteroposterior (*E*) and lateral (*F*) radiographs of left knee show persistent irregularity and sclerosis of distal femoral metaphysis. This is most evident medially, where apparent widening of physis is present.

birth length and only mild short stature of the father contrast with the more severe height reduction seen in classic Schmid metaphyseal chondrodysplasia. Until these patients are followed up further and additional family members are studied, it seems prudent to regard this entity as a Schmid-like metaphyseal chondrodysplasia.

The metaphyseal alterations producing the appearance of discrete fragments in these infants are strikingly similar to the

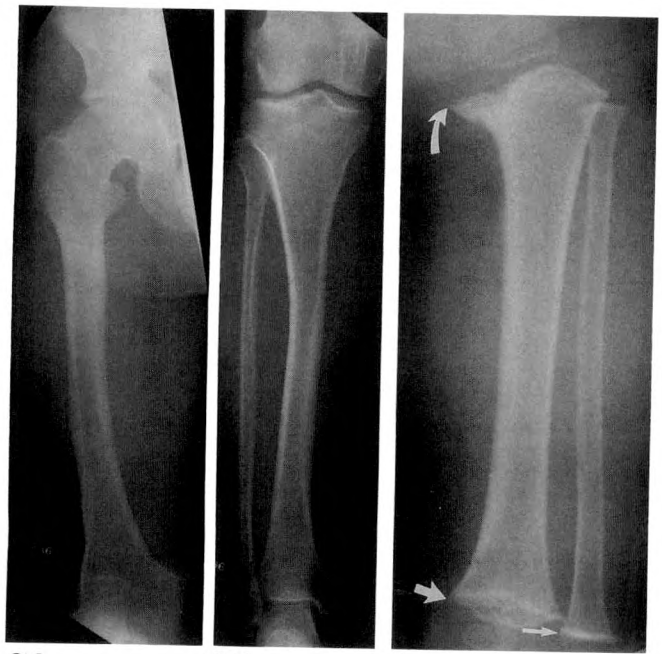



**Fig. 2.—Patient's 24-year-old father.**
***A*, Radiograph of femur shows coxa vara, shortening of femoral neck, and a broad femoral head. Note modeling deformity of distal femur.**
***B*, Radiograph of lower leg shows modeling deformity of proximal tibia, but examination is otherwise unremarkable.**

**Fig. 3.—Patient's 1-year-old brother. Radiograph of lower leg shows sclerosis and irregularity of metaphyses, beaking of medial tibial metaphysis (*curved arrow*), and apparent spurs involving medial aspects of distal tibia and fibula (*straight arrows*). Appearance of focal spurs and beaks is probably spurious, and as with true metaphyseal fractures in abuse, these are more extensive than is evident on a single radiographic projection.**

corner-fracture pattern in young abused infants. As most new cases of Schmid metaphyseal chondrodysplasia are diagnosed after infancy, it is understandable that diagnostic confusion between these two entities is uncommon. Child abuse was considered here because the findings were encountered on a limited radiologic study performed on an otherwise well young infant.

Langer et al. [3] have described a group of patients with metaphyseal fragmentation similar to that seen in our cases, as well as developmental coxa vara and mild spinal changes. The pattern of metaphyseal involvement was reminiscent of child abuse [4], and thus the authors have labeled the condition spondylometaphyseal dysplasia, corner-fracture type. Whether the lesions seen in their patients and those presented here are true fractures or fragmented metaphyses due to abnormal endochondral bone growth is a question requiring further study. Conditions associated with a corner-"fracture" pattern include child abuse; birth injury; Menke syndrome; spondylometaphyseal dysplasia, corner-fracture type; and metaphyseal chondrodysplasia [5].

Despite the similarity between the radiologic findings of this type of metaphyseal chondrodysplasia and child abuse, a misdiagnosis should not occur if a thorough skeletal survey is performed and a family history is obtained carefully. When limited radiologic studies are performed that reveal findings suggestive of child abuse, a definitive diagnosis should be reserved until a thorough radiologic examination has been conducted.

## REFERENCES

1. Lachman RS, Rimoin DL, Spranger J. Metaphyseal chondrodysplasia, Schmid type clinical and radiographic delineation with a review of the literature. *Pediatr Radiol* **1988**;18:93–102
2. Schmid F. Beitrag zur dysostosis enchondralis metaphysaria. *Monatsschr Kinderheilk* **1949**;97:393
3. Langer LO Jr, Brill PW, Ozonoff MB, et al. Spondylometaphyseal dysplasia, corner fracture type: a heritable condition associated with coxa vara. *Radiology* **1990**;175:761–766
4. Kleinman PK, Marks SC Jr, Blackbourne BD. The metaphyseal lesion in abused infants: a radiologic-histopathologic study. *AJR* **1986**;146: 895–905
5. Brill PW, Winchester P. Differential diagnosis of child abuse. In Kleinman PK, ed. *Diagnostic imaging of child abuse*. Baltimore: Williams and Wilkins, **1987**:221–241

Pictorial Essay

# MR Anatomy and Pathology of the Hypothalamus

Daniel J. Loes,[1] Thomas J. Barloon,[1] William T. C. Yuh,[1] Robert L. DeLaPaz,[2] and Yutaka Sato[1]

**The hypothalamus, the ventral-most portion of the diencephalon, surrounds the anterior inferior portion of the third ventricle (Fig. 1). It functions primarily as an integrative mechanism for various autonomic and neuroendocrine activities including temperature regulation, water balance, behavior, and appetite. This pictorial essay illustrates the value of MR in depicting the normal anatomy and abnormalities of the hypothalamic region.**

## Normal Anatomy

At least 12 cell clusters or nuclei are recognized within the hypothalamic region (Fig. 2). In actuality, the usefulness of anatomic subdivisions is limited because dendrites and axons of cell bodies overlap between various nuclei, resulting in overlapping functions. The supraoptic and paraventricular nuclei, which secrete vasopressin and oxytocin, have the most well-defined functions. With the exception of the mamillary nuclei, which are characteristic because of their contour, the individual hypothalamic nuclei cannot be distinctly identified on MR with standard spin-echo pulse sequences. However, the boundaries of the hypothalamus (Fig. 3) and hypothalamic abnormalities are well depicted by MR.

## Pathology

### *Chiasmatic-Hypothalamic Glioma*

Hypothalamic gliomas frequently invade the optic chiasm and vice versa; hence, the primary site of origin may be difficult to determine. Children are affected more than adults. The diencephalic syndrome (emaciation, alertness, hyperactivity, and pallor) is seen in up to 20% of children younger than 3 years. Neurofibromatosis type I is present in 20–50% of these patients. Pathologic findings are usually a low-grade astrocytoma, frequently the juvenile pilocytic variety. MR (Fig. 4) typically shows a suprasellar mass involving the optic chiasm and hypothalamus that is hypointense on T1-weighted

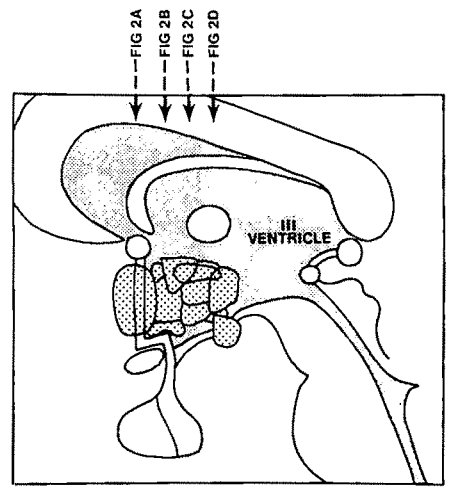



**Fig. 1.—Hypothalamic nuclei (*stippled area*) surround anterior inferior third ventricle. (Adapted from Netter [1].)**

Received July 9, 1990; accepted after revision October 10, 1990.
Presented at the annual meetings of the American Society of Neuroradiology, Los Angeles, March 1990, and the American Roentgen Ray Society, Washington, DC, May 1990.
[1] Department of Radiology, The University of Iowa College of Medicine, Iowa City, IA 52242. Address reprint requests to T. J. Barloon.
[2] Department of Radiology and Nuclear Medicine, Stanford University Medical Center, Stanford, CA 94305.

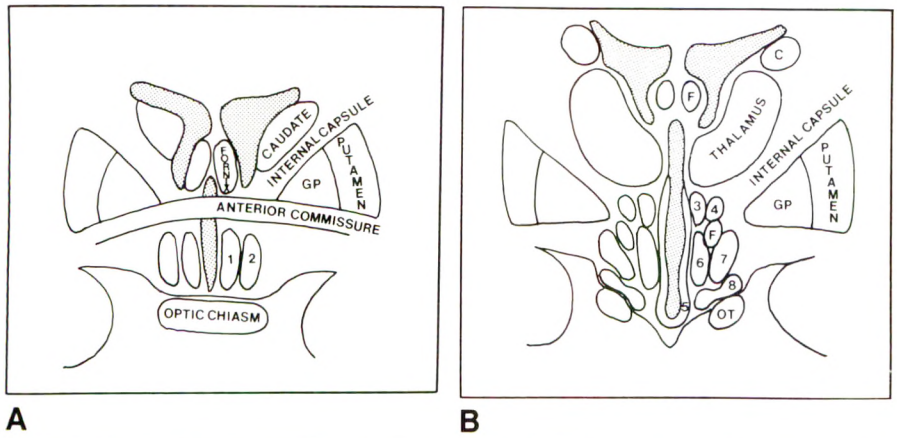



Fig. 2.—*A–D*, Normal coronal anatomy of hypothalamic region viewed from anterior (*A*) to posterior (*D*), as indicated in Fig. 1. Hypothalamic nuclei: 1 = medial preoptic area, 2 = lateral preoptic area, 3 = paraventricular nucleus, 4 = dorsal hypothalamic area, 5 = periventricular arcuate nucleus, 6 = anterior hypothalamic area, 7 = lateral hypothalamic area, 8 = supraoptic nucleus, 9 = dorsal medial nucleus, 10 = ventromedial nucleus, 11 = posterior hypothalamic area, 12 = mamillary nucleus. GP = globus pallidus, F = fornix, C = caudate, OT = optic tract, ST = subthalamic nucleus.

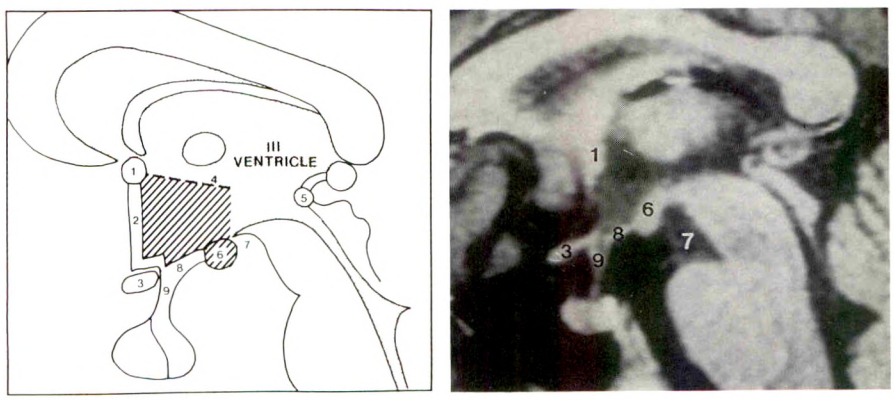



Fig. 3.—*A* and *B*, Normal sagittal anatomy of hypothalamic region shown on a line drawing (*A*) and corresponding T1-weighted MR image (*B*). Anterior: 1 = anterior commissure, 2 = lamina terminalis, 3 = optic chiasm; superior: 4 = hypothalamic sulcus; posterior: 5 = posterior commissure, 6 = mamillary bodies, 7 = interpeduncular fossa; inferior: 8 = tuber cinereum, 9 = infundibulum, 3 = optic chiasm; lateral (*not shown*): optic tracts, capsulopeduncular transition zone. Note.—Position of hypothalamic sulcus (groove between hypothalamus and thalamus) is located along anterior half of a line drawn between anterior (1) and posterior (5) commissures.

images, is hyperintense on T2-weighted images, and enhances inhomogeneously with contrast administration.

### *Germinoma*

Germinomas are most commonly located in the pineal region; their next most frequent site is the hypothalamus, which can be affected without pineal involvement. Hypothalamic germinomas affect males and females equally, unlike pineal region germinomas, which show a strong male predominance. Tumor spread may occur via CSF pathways. Germinomas are low-grade malignant tumors that are radiosensitive. On MR (Fig. 5), germinomas are usually mildly hypointense on T1-weighted images and hyperintense on T2-weighted images, but may be isointense on both pulse sequence. They generally show homogeneous enhancement with administration of contrast material.

### *Primary CNS Lymphoma*

The prevalence of primary CNS lymphoma is higher in AIDS patients and other immunosuppressed individuals. MR (Fig.

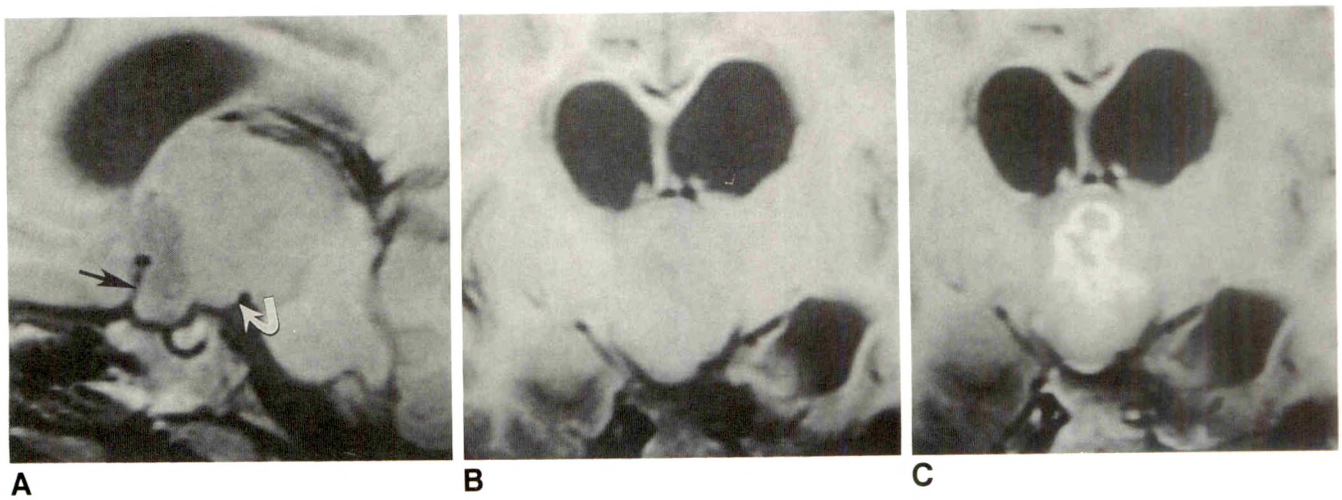



Fig. 4.—Chiasmatic-hypothalamic glioma in a 2-year-old emaciated and hyperactive girl.
*A*, Sagittal T1-weighted MR image shows large midline mass involving optic chiasm (*straight arrow*) and hypothalamus (*curved arrow*).
*B* and *C*, Coronal T1-weighted images before (*B*) and after (*C*) contrast administration show nonuniform enhancement of tumor, which extends superiorly to foramen of Monro causing an obstructive hydrocephalus.

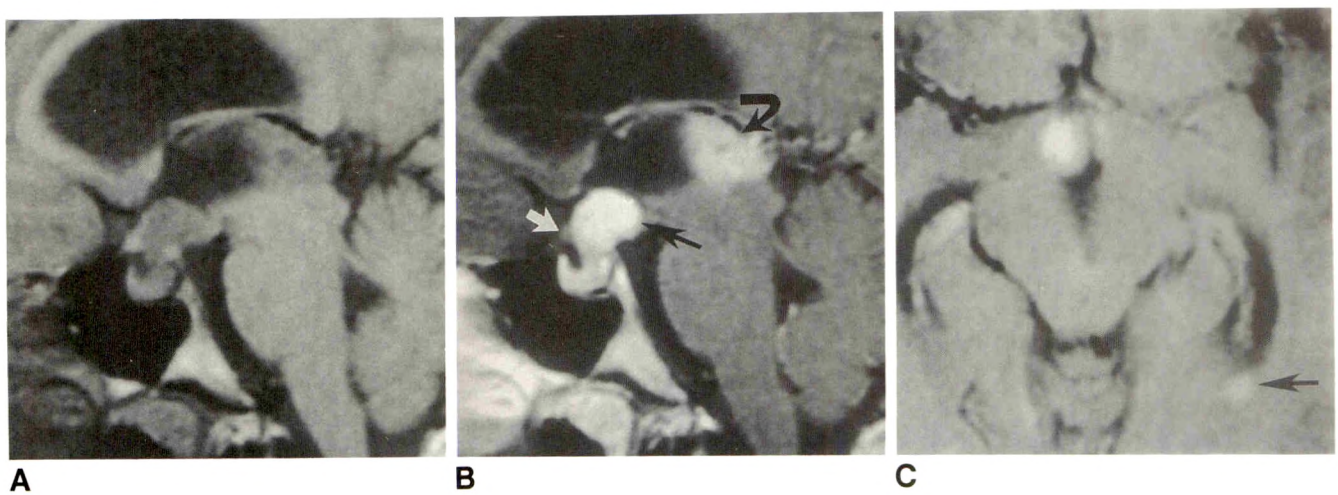



Fig. 5.—Germinoma in an 18-year-old man with diabetes insipidus.
*A* and *B*, Sagittal T1-weighted MR images before (*A*) and after (*B*) contrast administration show enhancing masses in floor of anterior third ventricle (*straight black arrow*) and pineal region (*curved arrow*). Optic chiasm (*white arrow*) is not involved.
*C*, Axial T1-weighted image obtained after contrast administration shows third enhancing mass (*arrow*) in left lateral ventricle.
(Reprinted with permission from Hawes et al. [2].)

6) typically shows solitary or multicentric well-defined mass lesions located in deep gray nuclei, periventricular white matter, or corpus callosum. Primary CNS lymphoma tends to be slightly hypointense on T1-weighted images, but may be hyperintense, isointense, or hypointense with respect to gray matter on T2-weighted images. Primary CNS lymphoma typically shows contrast enhancement, although signs of central necrosis may be seen in AIDS patients.

### *Hypothalamic Hamartoma*

Hypothalamic hamartomas are rare congenital malformations located in the region of the tuber cinereum–mamillary body. They comprise neuronal tissue similar to that of the hypothalamus. Hypothalamic hamartomas are a cause of precocious puberty and laughing seizures in children; boys are affected more often than girls. Hypothalamic hamartomas also may be found incidentally in adults, where they may mimic low-grade gliomas. MR shows a sessile (Fig. 7) or polypoid (Fig. 8) mass in the tuber cinereum region of the hypothalamus that is isointense on T1-weighted images and isointense or mildly hyperintense on T2-weighted images. The lesions are stable in size over time and typically do not show contrast enhancement.

### *Histiocytosis*

The histiocytoses are a diverse group of diseases of unknown cause with a common pathologic feature of being

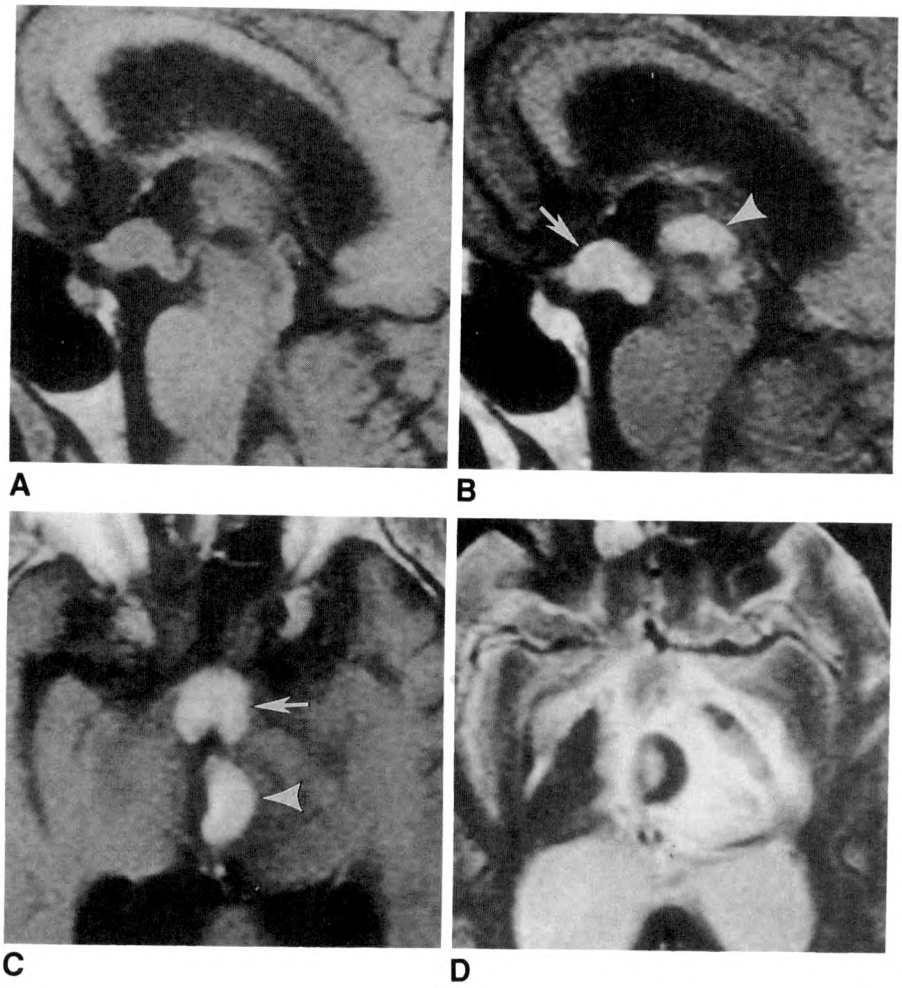



Fig. 6.—Primary CNS lymphoma in a 62-year-old man with increasing confusion over 1 month.
*A–C*, Sagittal T1-weighted MR images obtained before (*A*) and after (*B*) contrast administration and axial T1-weighted image after contrast administration (*C*) show enhancing mass lesions in hypothalamus (*arrows*) and left thalamus (*arrowheads*).
*D*, Axial T2-weighted MR image shows surrounding edema.

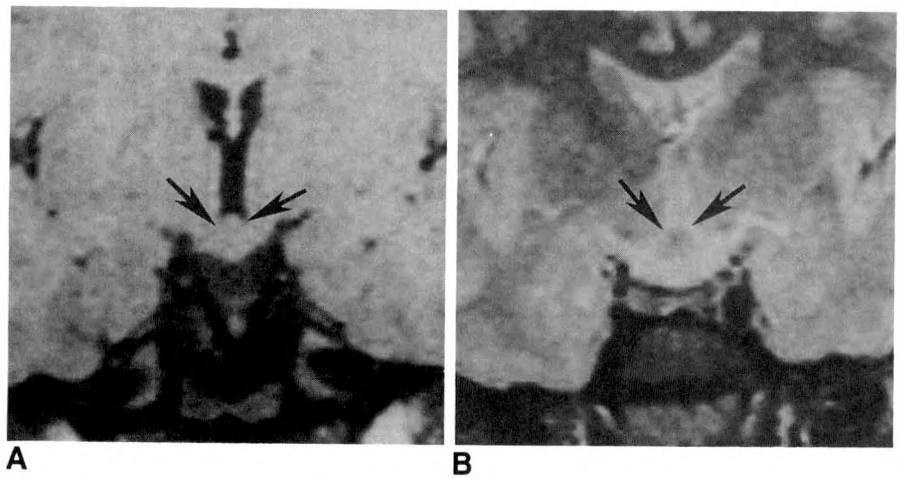



Fig. 7.—Hypothalamic hamartoma in a 5-year-old girl with precocious puberty.
*A* and *B*, Coronal T1-weighted (*A*) and T2-weighted (*B*) MR images show a midline hypothalamic mass (*arrows*) bulging into inferior floor of third ventricle. Lesion is isointense on both T1- and T2 weighted images and is centered in region of tuber cinereum.

proliferations of macrophages. Several organ systems may be involved, including skin, bone, eyes, and CNS. In the CNS, hypothalamic involvement frequently results in diabetes insipidus. MR (Fig. 9) shows a suprasellar mass involving the infundibulum and hypothalamus that is hypointense on T1-weighted images, hyperintense on T2-weighted images, and enhances homogeneously with administration of contrast.

*Sarcoidosis*

Sarcoidosis is a systemic, noncaseating granulomatous disease of unknown cause. It is common in blacks and usually occurs in the third to fourth decades. CNS involvement occurs in 5% of individuals and has two main forms: leptomeningeal

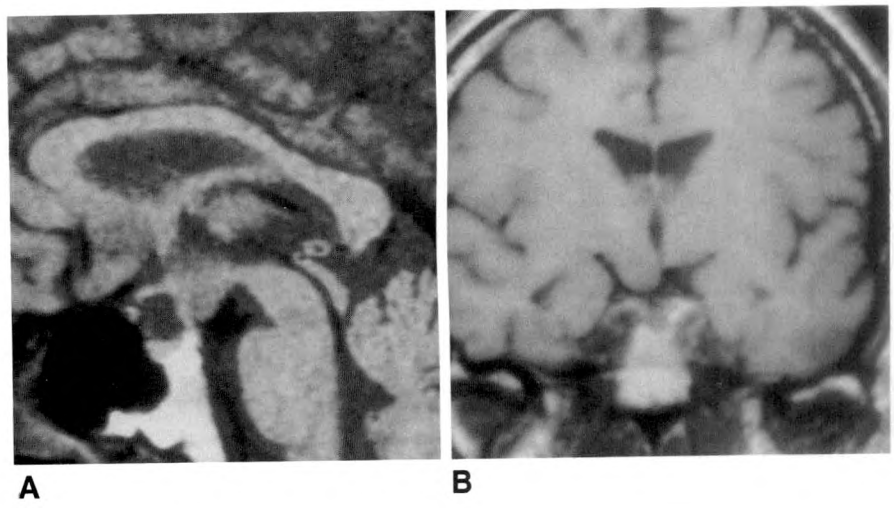



Fig. 8.—Hypothalamic hamartoma in a 66-year-old-man.

*A* and *B*, Sagittal (*A*) and coronal (*B*) T1-weighted MR images show an incidental pedunculated isointense mass off the tuber cinereum.

Hypothalamic hamartomas have a fairly characteristic MR appearance; however, follow-up at 6-month to 1-year intervals is necessary to exclude a low-grade glioma.

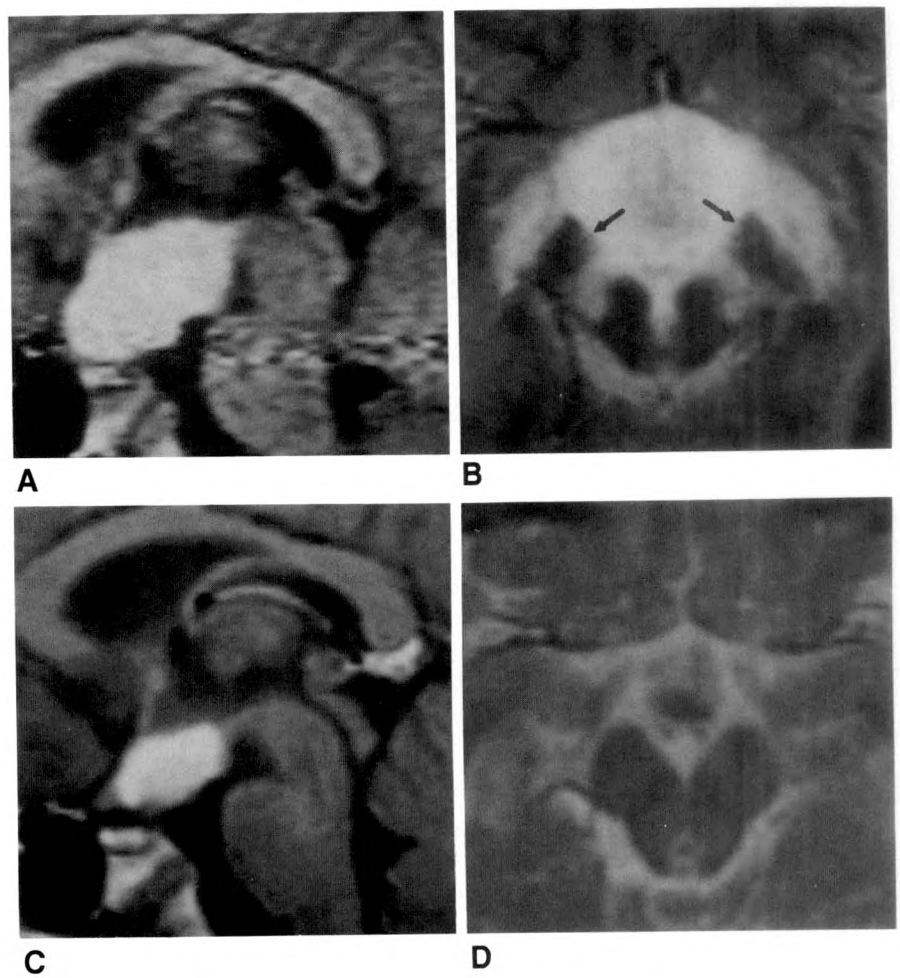



Fig. 9.—Histiocytosis in a 9-year-old boy with diabetes insipidus. Medical history was significant for histiocytosis involving temporal bone.

*A* and *B*, Sagittal T1-weighted MR image obtained after contrast administration (*A*) and axial T2-weighted image (*B*) show large enhancing hypothalamic mass splaying cerebral peduncles (*arrows*).

*C* and *D*, Corresponding images 3 weeks after low-dose radiation treatment show significant decrease in size (*C*) and signal intensity (*D*) of lesion.

Dramatic response to low-dose radiation strongly favors a diagnosis of histiocytosis over hypothalamic glioma.

and parenchymal. Leptomeningeal disease is most common and frequently involves the infundibulum and hypothalamus. The disease usually responds to steroid treatment. The leptomeningeal form of CNS sarcoidosis on MR (Fig. 10) typically is isointense on T1-weighted images, is mildly hyperintense on T2-weighted images, and enhances homogeneously with administration of contrast material.

*Ectopic Posterior Pituitary Gland*

Ectopic posterior pituitary glands may be caused by trauma or the presence of a mass, or may be congenital in origin. Although an ectopic posterior pituitary gland may be associated with dwarfism, many of these patients are asymptomatic. Normally, the supraoptic and paraventricular nuclei secrete

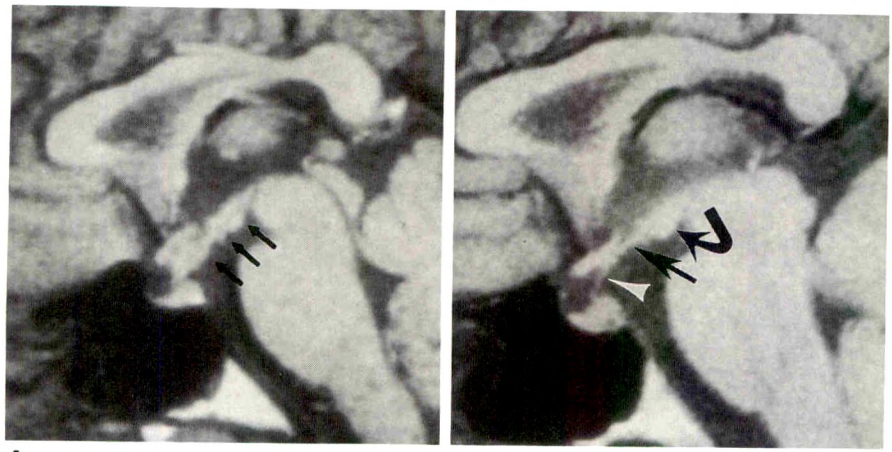


Fig. 10.—Sarcoidosis in a 38-year-old black woman with recent onset of visual difficulties.

*A*, Sagittal T1-weighted MR image shows abnormal thickening in hypothalamic region (*arrows*) involving tuber cinereum, mamillary bodies, and infundibulum.

*B*, After a 3-week course of steroids given because of prior diagnosis of sarcoidosis, a second sagittal T1-weighted MR image shows dramatic resolution of findings with return to normal hypothalamic region anatomy. Note normal mamillary bodies (*curved arrow*), tuber cinereum (*straight arrow*), and infundibulum (*arrowhead*).

Tuberculosis also can produce basilar leptomeningeal disease; hence, when there is no evidence for sarcoidosis outside the CNS, confirmation with CSF studies or biopsy is necessary before steroid therapy is begun.

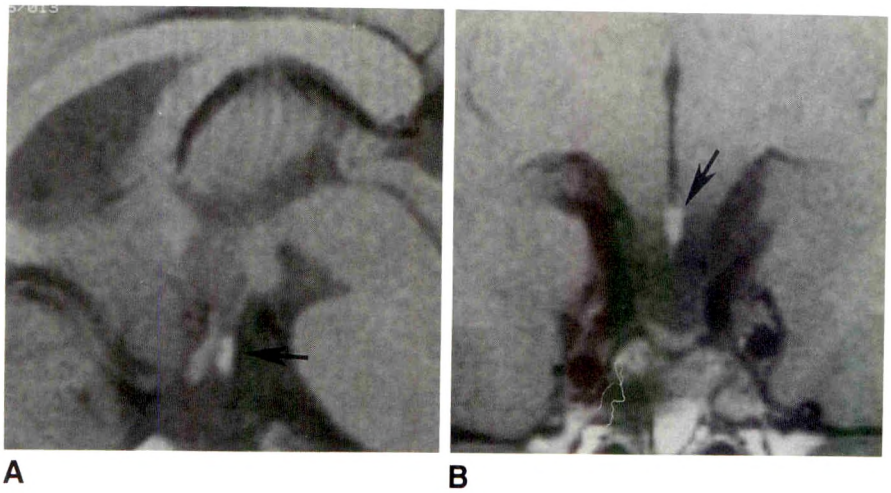


Fig. 11.—Ectopic posterior pituitary gland in a 7-year-old boy with short stature.

*A* and *B*, Sagittal (*A*) and coronal (*B*) T1-weighted MR images show small hyperintense oblong nodule (*arrows*) in inferior portion of tuber cinereum. Pituitary tissue within sella does not show high signal in its posterior portion, and an infundibulum connecting pituitary gland to hypothalamus is not present.

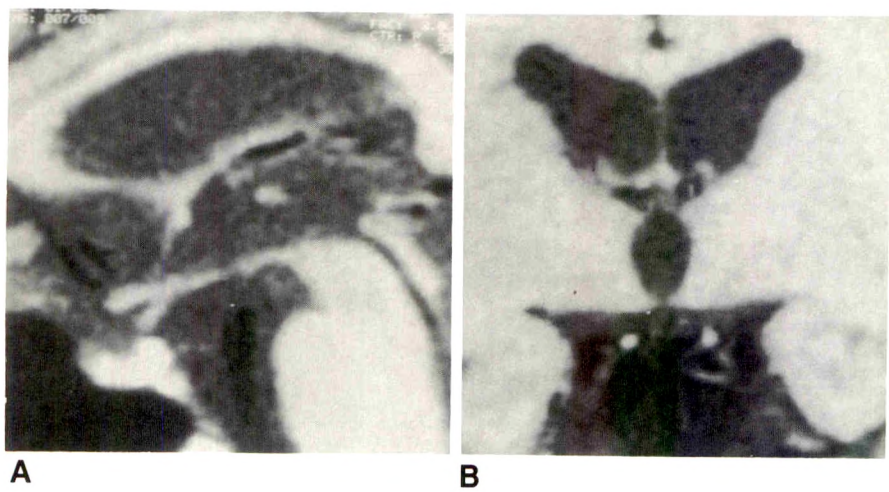


Fig. 12.—Wernicke encephalopathy in a 60-year-old alcoholic man with encephalopathy, ataxia, and oculomotor dysfunction.

*A* and *B*, Sagittal (*A*) and coronal (*B*) T1-weighted MR images show striking atrophy of mamillary bodies.

vasopressin and oxytocin within liposome vesicles that are transported along axons within the neurohypophyseal tract to the posterior lobe of the pituitary. A recent experiment by Kucharczyk et al. [3] showed that the phospholipid membrane component of these hormone-carrying vesicles, rather than the actual hormones, best explains the normal bright signal within the posterior lobe of the pituitary. Transection, compression, or absence of the infundibulum and its neurohypophyseal tract results in the proximal build-up of neurosecretory granules within liposome vesicles before the point of interruption, hence displacement of the normal bright signal of the posterior lobe of the pituitary out of the sella. MR

images (Fig. 11) show a small midline mass within the tuber cinereum–infundibular region that has homogeneous high-signal intensity on T1-weighted images and is isointense on T2-weighted images. The absence of both a normal infundibulum and high-signal-intensity tissue within the posterior sella on T1-weighted images is necessary to confirm the diagnosis.

### *Wernicke Encephalopathy*

Wernicke encephalopathy is caused by thiamine deficiency and is most commonly seen in alcoholics. When the classic triad of oculomotor dysfunction, ataxia, and encephalopathy is not present, diagnosis can be difficult. Atrophy of the mamillary bodies is a relatively specific macroscopic feature of chronic Wernicke encephalopathy. The MR appearance of chronic Wernicke encephalopathy consists of nearly complete absence of the mamillary bodies, which is best shown on T1-weighted images (Fig. 12).

**Summary**

While MR can nicely depict hypothalamic region anatomy and disease, definitive diagnosis of hypothalamic lesions requires correlation with history, clinical findings, and frequently biopsy, as several entities may mimic each other.

REFERENCES

1. Netter FH. *The CIBA collection of medical illustration*, vol. 1. *Nervous system*. Part 1. *Anatomy and physiology*. West Caldwell, NJ: Ciba-Geigy Corp., **1983**
2. Hawes DR, Yuh WTC, Wen BC. Gadolinium-enhanced MR imaging in management of midline cerebral dysgerminoma. *Comput Med Imaging Graph* **1990**;13(6):463–468
3. Kucharczyk W, Lenkinski R, Kucharczyk J, Henkelman RM. The effect of phospholipid vesicles on the NMR relaxation of water: an explanation for the MR appearance of the neurohypophysis? *AJNR* **1990**;11:693–700

# Book Review

**Imaging Anatomy of the Head and Spine.** A Photographic Color Atlas of MRI, CT, Gross, and Microscopic Anatomy in Axial, Coronal, and Sagittal Planes, 2nd ed. By H. N. Schnitzlein and F. Reed Murtagh. Baltimore: Urban & Schwarzenberg, 450 pp., 1990. $195

Though difficult to believe, the second edition of this atlas has been expanded and improved significantly to secure its place as the premier text of its kind. The first edition combined superb gross anatomic sections with excellent correlative CT scans and average intermediate-field-strength MR images. This edition has replaced the older MR images with state-of-the-art 1.5-T images. The coronal and sagittal CT scans of cadaveric heads thankfully have been eliminated. The axial CT scans of the head are now scans of actual patients, not of cadaveric specimens. The layout of the table of contents has been improved and now is broken up into regional sections: imaging anatomy of the brain, special topics of brain imaging, selected regions of the head and neck, and imaging anatomy of the spine. In addition to expanded and improved existing chapters, new subsections include the brainstem in situ, infants and children, cavernous sinus and parasellar region, nasal cavity, paranasal sinuses, pharynx and parapharyngeal region, and intraoperative sonography of the spine.

The page layout has been improved significantly. For example, the design now takes better advantage of white space by using a larger type size and increased leading (spacing between lines). In addition, the labeling conforms better to the illustrations. Labeling also has been expanded, primarily because of the increased resolution now shown on the high-field-strength images. Micrographs now are labeled as to their nature and location (e.g., "Through the Red Nucleus"). Labels of the MR images include the technique used to obtain the images.

Page by page, the book shows significant improvement, though some minor weaknesses are still evident. The section on imaging anatomy of the brain depicts superb gross specimens with MR images, CT scans, and micrographs. The plane-of-section reference has been changed from a lateral skull to a profile drawing of a person, with some bony structures highlighted, allowing for better appreciation of external landmarks. Proton-density images are emphasized for showing superficial anatomy, and T2-weighted images illustrate deep structures. The coronal T2-weighted MR images have a band of hyperintensity across them. Whether this is intentional is uncertain. I found it annoying and thought it might be from a nonhomogeneous magnetic field. Also, the sagittal plane images lack T2 weighting. Although few imagers routinely acquire this sequence, having reference images available would be helpful. Lastly, I was disappointed with the coronal section because it does not emphasize the hippocampal formation.

In the section on special topics of brain imaging, the chapter on the brainstem in situ now contains outstanding MR images. One minor improvement would be the addition of a drawing of the plane-of-section reference that showed a line through the brainstem at the level of interest. The chapter on the ventricles and cisterns has been improved significantly with the addition of MR images and photographs of gross anatomic specimens. The chapter on the vasculature of the brain has been expanded with the addition of a few angiograms. The goal of this chapter is unclear because of the wealth of splendid angiography texts available. I can envision this chapter evolving into one on three-dimensional angiography in the next edition. The chapter on the developing brain is a new and welcome addition. However, T1-weighted axial images are lacking, the variance in the window and center settings is frustrating, and improved reference labeling of the axial images would be nice.

The chapter on the orbit in "Selected Sections of the Head and Neck" has been expanded significantly with MR images and photographs of cadaveric sections. The chapter on the sellar and parasellar regions is new and outstanding, with the exception of one poorly reproduced lateral angiogram. The chapter on the temporal bone has added beautiful images of the cerebellopontine angle and temporomandibular joint. The chapter on the pharynx and the sinuses is probably the most significant improvement in the book. The layout and images are outstanding and blend perfectly with the rest of the text. A small focus on the osteomeatal complex would have been a treat. The chapter on the larynx is the only one to not use high-field-strength images. However, do not be disheartened—the 0.3-T, T1-weighted images are outstanding.

The final section on the imaging anatomy of the spine is broken up into chapters by location: cervical, thoracic, and lumbar. The new high-field-strength MR images and the addition of photographs of sagittal and coronal cadaveric specimens have greatly enhanced this section. The chapter on the cervical spine lacks gradient-echo axial images, which most centers now obtain routinely. The previous edition contained a wonderful table on the location of fiber tracts in the spinal cord that unfortunately has been deleted from this edition. In the chapter on the lumbar spine, the gross specimens and sagittal and coronal images are spectacular. However, the axial images are poorly reproduced and inconsistently mix T1-weighted, T2-weighted, and gradient-echo images at various levels. The final chapter on intraoperative sonography is brief and to the point with excellent images and drawings. This is an important area of neuroradiologic imaging that is underused.

In summary, the second edition of this book has been improved substantially, preserving it as the leading atlas of its type and justifying the purchase of the updated edition. Its flaws and omissions are relatively minor and probably would not be noticed by most readers. This text belongs on the shelf of every neuroradiologist, neurosurgeon, and neurologist and in every radiology department or imaging center where MR images of the brain or spine are interpreted.

Wallace W. Peck
*St. Joseph Hospital*
*Orange, CA 92668*

# Congenital Nasal Masses: CT and MR Imaging Features in 16 Cases

A. James Barkovich[1,2]
Pierre Vandermarck[1]
Michael S. B. Edwards[2]
Philip H. Cogen[2]

**The imaging studies of 16 children with pathologically proved nasal encephaloceles (eight), nasal dermal sinuses/nasal dermoids (seven), and nasal cerebral heterotopias, more commonly known as nasal gliomas (one), were retrospectively reviewed and compared with normal control subjects to define the normal anatomy and analyze deformities caused by these lesions. Nasal encephaloceles were always identified as complex masses of mixed soft tissue and CSF intensity that were contiguous with intracranial structures. The nasal glioma appeared as a mixed-intensity mass that, on the basis of the CT scan, appeared to be continuous with intracranial structures. Nasal dermal sinuses could only be identified as they coursed through the skin and subcutaneous soft tissue. They could not be identified when intraosseous. Moreover, on CT and, particularly, on MR, a number of potential diagnostic pitfalls were encountered. The most important of these was the normal fat deposition that occurs within bone during normal maturation and during aeration of the frontal sinuses and nasal bones. These fatty changes can easily be mistaken for fatty tumors if they are not recognized as normal anatomic changes. Interestingly, the classic plain film findings for congenital nasal masses were present only in the encephaloceles and nasal glioma; dermoids and dermal sinuses showed none of the classic plain film findings. In the six patients who had both CT and MR, the masses were easily identified and characterized by each imaging method.**

**Congenital nasal masses are well characterized by both CT and MR. It is important to understand the normal changes in the anatomy of the nasofrontal region in the pediatric age group to avoid false-positive diagnoses in this region.**

*AJNR* 12:105–116, January/February 1991; *AJR* 156:587–598, March 1991

The congenital midline nasal masses are rare anomalies; their rate of occurrence is approximately one in every 20,000–40,000 live births [1, 2]. The most common of these masses are dermoid/epidermoid tumors (almost always associated with dermal sinus tracts), nasal cerebral heterotopias (nasal gliomas), and nasal encephaloceles [1–6]. Less common masses include simple inclusion cysts, hemangiomas, and aberrant ethmoidal sinuses [2].

When pediatric patients present with a midline nasal mass or a nasal dimple, an imaging study is usually obtained to better characterize and delineate the disease and to plan for appropriate therapeutic intervention. We have found, however, that the complex anatomy and often subtle findings make interpretation of these images difficult. In this report, we define the normal embryology and anatomy of the frontonasal region in infants and children, and then present the CT and MR features of 16 patients who presented with congenital midline nasal masses.

## Materials and Methods

The imaging studies of 16 children with pathologically proved nasal encephaloceles (eight), nasal dermoids/dermal sinuses (seven), and nasal gliomas (one) were retrospectively reviewed

Received February 22, 1990; revision requested June 14, 1990; revision received July 15, 1990; accepted July 24, 1990.

[1] Department of Radiology, Neuroradiology Section, University of California, San Francisco, 505 Parnassus Ave., San Francisco, CA 94143-0628. Address reprint requests to A. J. Barkovich.

[2] Department of Neurological Surgery, Division of Pediatric Neurosurgery, University of California, San Francisco, CA 94143.

0361–803X/91/1563–0587
© American Roentgen Ray Society

**TABLE 1: Patient Data**

| Patient No. | Age | Sex | Imaging Method | Diagnosis | Presentation | FC Size (mm) | Crista | | Mass | | | | IOD (mm) | Associated Anomalies |
|---|---|---|---|---|---|---|---|---|---|---|---|---|---|---|
| | | | | | | | Size (mm) | Bifid | Location | Size (mm) | MR | CT | | |
| 1 | 3 mo | F | CT | DS dermoid | Nasal mass | 5 | 4 | (+) | Glabella & intracranial | 6 × 4<br>4 × 4 | – | Low atten. | 15 | – |
| 2 | 12 mo | M | MR | Dermoid | Nasal mass | 0 (closed) | 7 | (–) | Left lateral nasal bridge | 10 × 10 | Short, T1, T2 | – | 18 | – |
| 3 | 2 yr | F | CT and MR | DS epidermoid | Nasal mass | 3 | 4 | (–) | Glabella | 3 × 4 | Long T1, T2 | Low atten. | 22 | – |
| 4 | 2 yr | F | CT and MR | DS | Nasal dimple | 2 | 4 | (–) | – | – | – | – | 18 | – |
| 5 | 3 yr | M | CT and MR | DS dermoid | Nasal dimple and mass | 6 | 4 | (–) | Glabella & nasal bridge | 3 × 5 | Short T1, T2 | Low atten. | 16 | – |
| 6 | 3 yr | M | MR | DS | Nasal dimple | 0 (closed) | 3 | (–) | – | – | – | – | 13 | – |
| 7 | 12 yr | F | CT and MR | DS | Nasal dimple | 7 | 5 | (–) | – | – | – | – | 23 | Colloid cyst |
| 8 | 9 mo | F | CT | Nasal glioma | Nasal mass | Poorly defined | 7 | (–) | Left glabella | 10 × 13 | – | Soft-tissue Atten. | 12 | – |
| 9 | 1 wk | F | CT and MR | NE | Nasal mass | 15 | Not seen | (–) | Glabella & ethmoids | 30 × 50 | Heterogeneous soft tissue & CSF | – | 16 | L temporal arachnoid cyst |
| 10 | 6 wk | F | MR | NF | Nasal mass | 5 | 2 | (–) | Low frontal | 20 × 20 | Heterogeneous soft tissue & CSF | – | 12 | Subfrontal cyst |
| 11 | 3 mo | F | CT and MR | NF and NE | Nasal mass | 14 | 3 | (–) | Glabella & ethmoids | 20 × 35 | Heterogeneous soft tissue | – | 20 | Bilateral temporal arachnoid cysts |
| 12 | 4 mo | F | MR | NE | Meningitis, nasal mass | 14 | Not seen | – | Glabella & ethmoids | 15 × 30 | Heterogeneous soft tissue & CSF | – | 28 | ACC |
| 13 | 6 mo | M | CT | NE | Nasal mass | 20 | 3 | (–) | Ethmoids & glabella | 25 × 20 | – | Heterogeneous soft tissue | 20 | ACC |
| 14 | 6 mo | M | CT | NO | Proptosis, orbital masses | 8 | 4 | (–) | Bilateral orbits | 10 × 15 mass each orbit | – | Heterogeneous mostly fluid | * | R. parietal schizencephaly |
| 15 | 10 mo | F | MR | NF and NE | Nasal mass | 15 | 3 | (+) | Glabellar & low frontal | 8 × 15 | Mixed short & intermediate T1, T2 | – | 26 | ACC, lipoma |
| 16 | 24 yr | M | MR | NE | Nasal mass | 20 | Not seen | – | Glabellar | 30 × 40 | Heterogeneous soft tissue & CSF | – | 25 | – |

Note.—FC = foramen cecum, DS = dermal sinus, NE = nasoethmoidal encephalocele, NF = nasofrontal encephalocele, NO = nasoorbital encephalocele, IOD = interorbital distance, ACC = agenesis of the corpus callosum.

* We were unable to measure IOD due to poorly defined medial orbital walls.

(Table 1). The eight patients (three males, five females) with encephaloceles all presented with nasal (six patients), low frontal (one), or orbital (one) masses. They ranged in age from 1 week to 24 years old at the time of their imaging study (mean, 3.5 years; median, 4 months). Four patients had MR scans only, two had CT scans only, and two had both MR and CT scans. The three patients (one male, two females) with nasal dermal sinuses presented with nasal dimples; the four patients (two males, two females) with associated dermoids presented with nasal masses. These seven patients ranged in age from 3 months to 12 years at the time of their imaging study (mean, 2.6 years; median, 3 years). Four patients had CT and MR, two had only MR, and one had only CT. The patient with the nasal glioma presented with a nasal mass and was 9 months old at the time of the study; she was studied only by CT.

Eleven of the 12 MR scans were obtained at 1.5 T using a 256 × 256 matrix. Axial 3-mm (1-mm gap) spin-echo (SE) 600/20/2 (TR/TE/excitations) MR images were obtained in all these patients. Axial SE 2500/20,70/2 images with a 3-mm slice thickness were obtained in two patients and a 5-mm slice thickness in nine patients. Sagittal SE 600/20 images with a 3- or 4-mm slice thickness were obtained in 10 patients (one did not have a sagittal imaging sequence) and coronal SE 600/20 images with a 4- or 5-mm slice thickness were obtained in 11 patients. A single patient (case 11) was scanned at 0.35 T. Axial SE 2000/40,80 and coronal SE 500/30 images were obtained by using a 7-mm slice thickness with a 3-mm gap and a 256 × 128 matrix.

CT scans were obtained in 10 patients. Among the eight patients with encephaloceles, four had CT. Of these, axial and coronal 5-mm contiguous images were obtained in three; the other was scanned using 1.5-mm contiguous images in the axial and coronal planes after intrathecal infusion of water-soluble contrast medium. The five patients with dermal sinus tracts and the one with the nasal glioma were scanned using 1.5-mm contiguous images in the axial and coronal planes. Sagittal reconstructions were performed in two patients. Two patients were scanned both before and after the intrathecal introduction of water-soluble contrast material. IV contrast administration was not used in any study.

CT scans of 29 patients (18 males, 11 females) and MR scans of 16 patients (nine males, seven females) without frontonasal disease were then reviewed to establish the normal appearance of the frontonasal structures in this age group (Table 2). The patients ranged from 1 to 25 months old at the time of their scan. These patients all presented with acquired orbital or intracranial disease unrelated to the nose or base of the anterior cranial fossa. The normal CT controls were assessed by axial images of 3-mm slice thickness; six patients had coronal 3- or 5-mm images as well. Both soft tissue and bone detail algorithms were present in all patients. The normal MR controls had sagittal 3-mm (13 patients) or 5-mm (three patients) SE 600/20 images. Axial 5-mm SE 2500–2800/20–30,60–100 images were available in all patients. Coronal 3-mm SE 600/20 images were available in seven patients. Axial 3-mm SE 600/20 images were available in five patients.

All scans were carefully scrutinized for normal landmarks, including the crista galli, nasal bones, frontal bones, nasal septum, foramen cecum, and glabella. The size of the foramen cecum was measured on axial scans as the distance from the most anterior aspect of the base of the crista galli to the most posterior aspect of the frontal bones. The greatest width and any abnormalities in the shape of the crista galli were recorded. The interorbital distance (defined as the narrowest distance between the medial walls of the orbits at the level of the cribiform plate) was measured. Any abnormal soft tissue or bony masses were noted.

Measurements of both the foramen cecum and the crista galli have a large potential for error because the value obtained may, theoretically, vary depending on the orientation of the imaging plane to the skull base. Fortunately, axial CT images at our institution are obtained routinely in a plane parallel to the canthomeatal line, resulting in a (usually) consistent orientation. Further possibility for error exists in the fact that the size of the foramen cecum and the width of the crista vary at different axial levels. Fortunately, the phenomenon of volume averaging results in visualization of the narrowest diameter of a foramen and the largest diameter of any bone structure within a slice; therefore, we feel that the measurements we have recorded are accurate and comparable. Indeed, upon scanning a skull phantom five times at slightly different scan angles, results varied by less than 20%. Moreover, all varied by less than 25% from the measurement obtained directly from the skull.

## Results

### *Normal Patients*

The normal nasofrontal region was found to have a complex but consistent structure on both CT and MR. The relevant structures include the cartilaginous nasal septum, the nasal bones, the external soft tissues of the nose, the nasal processes of the frontal bones, the cribriform plate, the foramen cecum, and the crista galli. In normal patients, the subcutaneous fat of the nose had sharp, discrete separation from the overlying skin anteriorly in all patients (Figs. 1 and 2). Posteriorly, the subcutaneous fat was bordered in the midline by the cartilaginous nasal septum and laterally by the cartilaginous bridges of the nose inferiorly and the nasal bones superiorly. The septum was of higher attenuation than fat on CT and of lower intensity than fat on short TR/TE and long TR/short TE MR images. The cartilage and fat were isointense on long TR/TE images. The nasal septum was always widened anteroinferiorly (Fig. 1). The paired nasal bones were always slightly separated at their most inferior margin (Figs. 1D and 2A).

In young patients, characteristic changes in signal intensity were often seen paracentrally (bilaterally and symmetrically) in the nasal processes of the frontal bone and, sometimes, in the nasal bones. These changes in signal intensity probably

**TABLE 2: Summary of Control Patients**

| Imaging Method | No. of Patients | FC Size (mm) | Crista | | |
|---|---|---|---|---|---|
| | | | Size (mm) | Bifid | IOD (mm) |
| CT | 29 | 4 (SD = 3) | 3 (SD = 2) | 3/29 | 18 (SD = 4) |
| MR | 16 | 3 (SD = 3) | 3 (SD = 2) | 0/16 | 19 (SD = 5) |

Note.—FC = foramen cecum, IOD = interorbital distance.

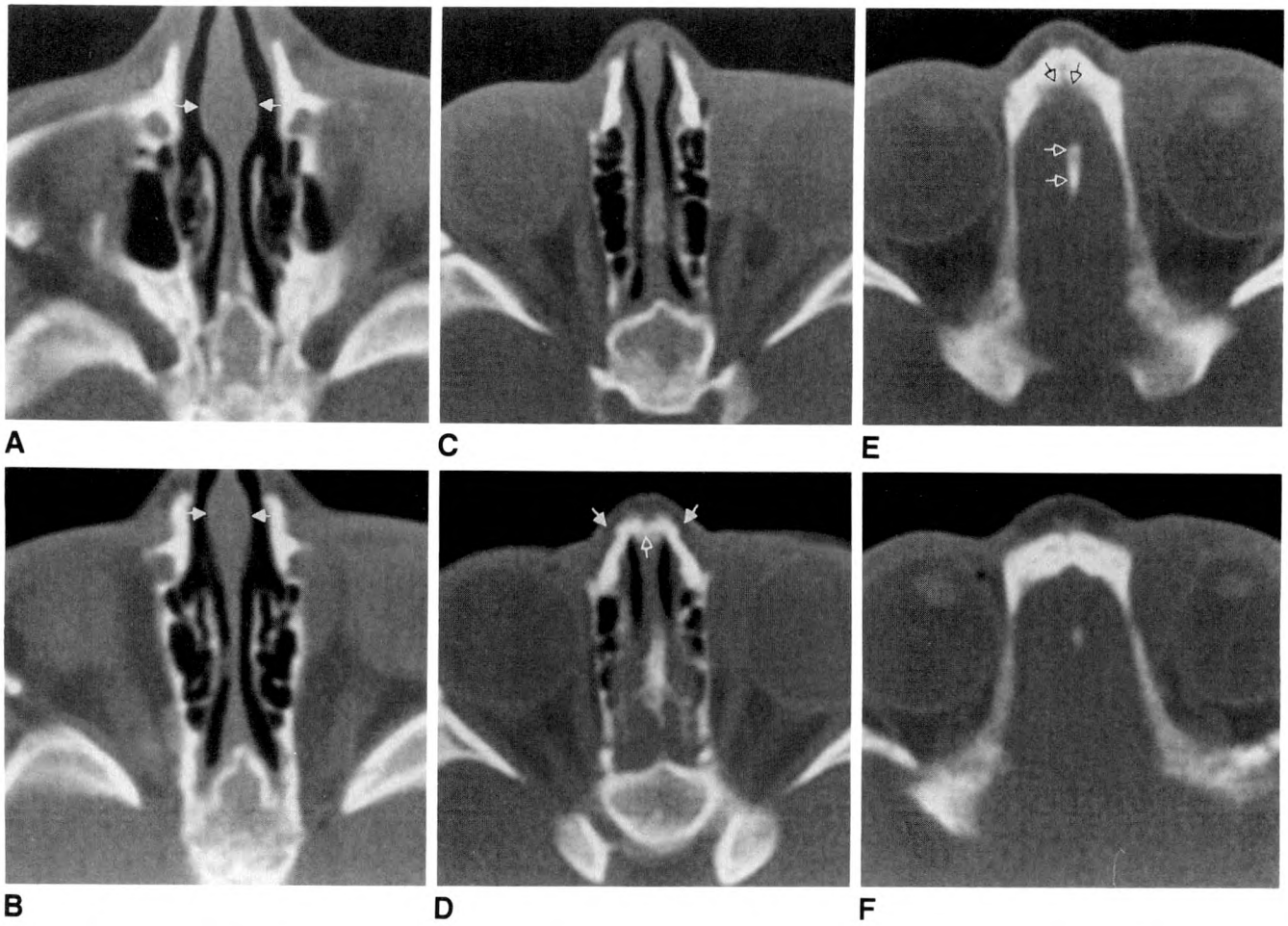



**Fig. 1.—Thin section (3-mm) axial images through nose and base of anterior cranial fossa of a 4-month-old. The patient was scanned for orbital cellulitis.**

***A* and *B*, The anteroinferior portion of the nasal septum is always focally widened (*arrows*) at all ages.**

***C* and *D*, A slight separation between the nasal bones is always present at their most anteroinferior margin (*open arrow*). This does not imply that a sinus tract is coursing through it. The subcutaneous fat under the skin of the nose (*closed arrows*) should be homogeneous and clearly separated from the skin at this age.**

***E* and *F*, These images are slightly superior to the foramen cecum. Crista galli is marked by *open white arrows*, and nasal processes of frontal bones by *open black arrows*. At this age there is very little diploic space within frontal bones or crista galli.**

represent fatty metamorphosis prior to pneumatization [7]. The pneumatizing bone marrow is of low attenuation compared with cortical bone on CT (Fig. 2) and has very short T1 and T2 relaxation times on MR (Figs. 3 and 4). The appearance on MR parallels that of the pneumatizing sphenoid bone [7].

The foramen cecum lies posterosuperior to the pneumatizing nasal processes of the frontal bone, being positioned between the frontal bone and the crista galli (Figs. 1–5). The size of the foramen ranged from 0 to 10 mm (average size, 4 mm; SD = 3 mm). It had the attenuation of fibrous tissue on CT (higher attenuation than brain) when large enough so that beam hardening from adjacent bone did not attenuate all the signal. On MR, the material in the foramen was always of low to medium intensity on all imaging sequences (Figs. 4 and 6), and was difficult to see on T1-weighted images before fatty changes occurred in the crista galli (Fig. 6).

The crista galli was located in the midline dorsal to the foramen cecum. It was bifid in three of the 29 patients imaged by CT. A bifid crista was never seen on MR. The side-to-side diameter of the crista (measured from the outer margin of the cortex on either side) varied from 1 to 8 mm (mean, 3 mm; SD = 2 mm). The signal of the marrow within the center of the crista was identical to that of the diploic space of the skull on CT (Figs. 2 and 5). It has a short T1 relaxation time (comparable to fat) on MR of all patients more than 14 months old (Figs. 3 and 4); it was isointense with brain in all patients 12 months old or younger. (No patients between 12 and 14 months old were scanned.) The signal of the crista on short TR images initially turned bright posteroinferiorly (Fig. 3); the high signal intensity then moved anteriorly and superiorly (Fig. 4).

The interorbital distance ranged from 12 to 26 mm (mean, 18 mm; SD = 4 mm).

*Dermal Sinus Patients*

All studies demonstrated soft-tissue intensity in the subcutaneous fat of the nose, representing the tract itself. In the

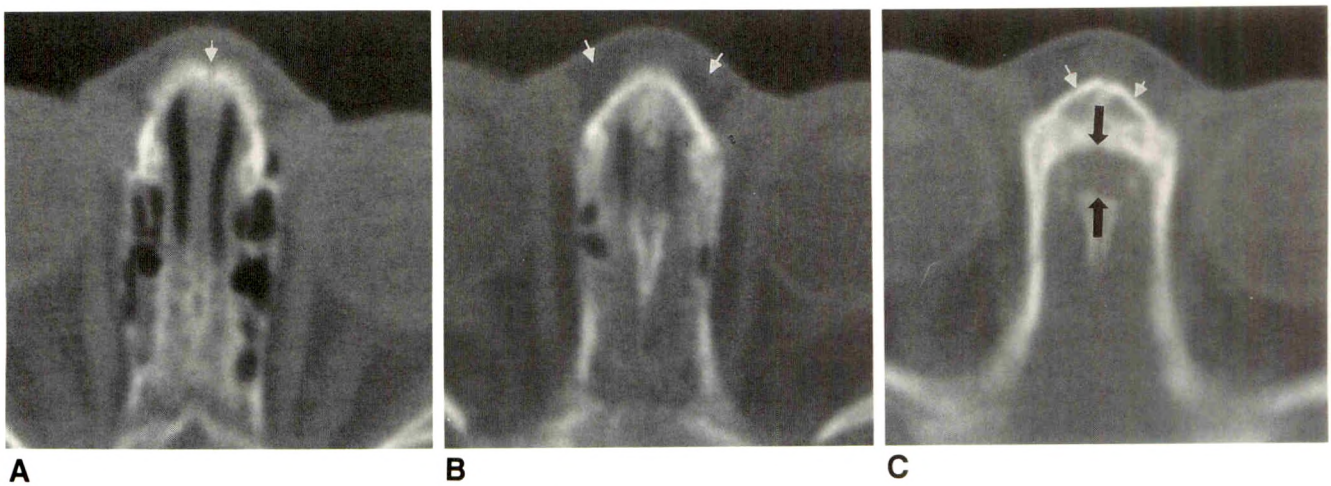



Fig. 2.—Axial CT scans through nose and cribriform plate region in an 11-month-old.
*A*, Note separation of inferior aspects of nasal bones (*arrow*), as seen in Fig. 1D. This is a consistent finding at all ages.
*B*, By the age of 11 months, the marrow within the crista galli is more visible. The anterior cortical rim of the crista is often not visible at this level and does not imply erosion. Subcutaneous fat (*arrows*) is homogeneous.
*C*, Low attenuation is seen in nasal processes of frontal bones (*white arrows*). This is a normal process that may represent the development of bone marrow or perhaps early pneumatization of bone. Foramen cecum is marked by *black arrows*.

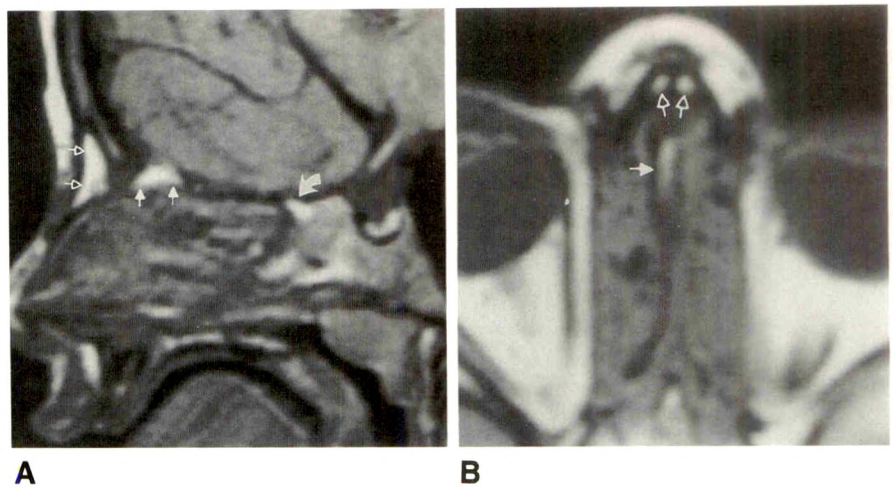



Fig. 3.—MR images through nasal region in a 12-month-old.
*A*, Sagittal T1-weighted image show high signal intensity in nasal processes of frontal bones (*open arrows*) and in posteroinferior crista galli (*closed arrows*). Note that high signal intensity is just beginning to develop in the anterosuperior sphenoid bone (*curved arrow*).
*B*, The high signal intensity representing marrow and/or the process of penumatization is seen in the paired nasal bones (*open arrows*) and inferior crista galli/vertical plate of the ethmoid bone (*closed arrow*).

four patients with associated dermoid (three) or epidermoid (one) tumors, the mass could be seen Figs. 7–9). The associated tumors were extracranial in three patients and both extra- and intracranial in one. The masses were all of low attenuation on CT with the exception of the extracranial component in patient 3 (Fig. 9), which was of soft-tissue density. The three dermoids exhibited short T1 and T2 relaxation times (Fig. 8) and the epidermoid had prolonged T1 and T2 relaxation times compared with brain (Fig. 7) on MR. The masses were all round to oval in shape and ranged from 3 to 10 mm in their largest diameter; the intracranial dermoid seemed to erode the adjacent inner table of the frontal bone (Fig. 9). The foramen cecum was patent in five of the seven patients, ranging in size from 2 to 7 mm (mean, 4 mm; SD = 2 mm) (Table 3). The diameter of the crista galli ranged from 3 to 7 mm (mean, 4 mm; SD = 2 mm); only the patient with the intracranial dermoid had a bifid crista. The interorbital distance ranged from 13 to 23 mm (mean, 18 mm; SD = 3 mm).

*Nasal Glioma Patient*

The single patient with a nasal glioma was studied only with CT. A 13-mm heterogeneous soft-tissue mass was seen extending continuously from the region of the foramen cecum inferiorly and anteriorly into the subcutaneous tissues at the glabella, just to the left of the midline. The mass appeared to extend intracranially on the coronal images (Fig. 10) and, indeed, a pedicle was seen to extend into an enlarged foramen cecum at surgery. The crista galli appeared truncated anteriorly where it bordered the nose (Fig. 10). The interorbital distance was 12 mm. The size of the foramen cecum could not be reliably determined in this patient because images were obtained in an oblique, half-axial plane.

*Cephalocele Patients*

Four cephaloceles extended inferiorly through the foramen cecum into the ethmoidal sinuses and beneath the nasal

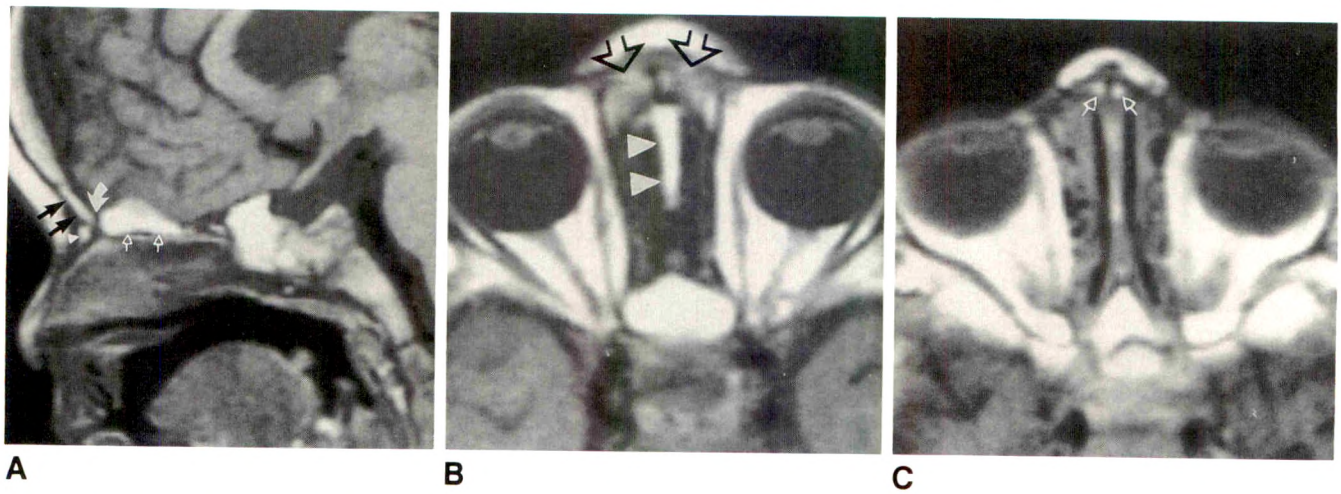



Fig. 4.—MR images through cribriform plate region in a 19-month-old child.

*A*, Sagittal SE 600/20 image shows high signal intensity in nasal processes of frontal bones (*black arrows*), nasal bones (*arrowhead*), and crista galli/vertical plate of the ethmoid bone (*open arrows*). Note that the high signal intensity in the crista galli has markedly increased as compared with the 11-month-old patient shown in Fig. 3. The foramen cecum is within the area of low signal intensity demarcated by the *curved arrow*. Incidentally noted is marked high signal intensity in the presphenoid bone, which will soon begin to undergo cavitation.

*B*, Axial SE 600/20 image shows patchy high signal intensity in nasal processes of frontal bones (*black arrows*) and marked high signal intensity in inferior crista galli/vertical plate of the ethmoid (*white arrowheads*).

*C*, Axial SE 600/20 image, slightly inferior to (*B*). Paired areas of hyperintensity (*arrows*) represent marrow that is probably cavitating in the nasal bones.

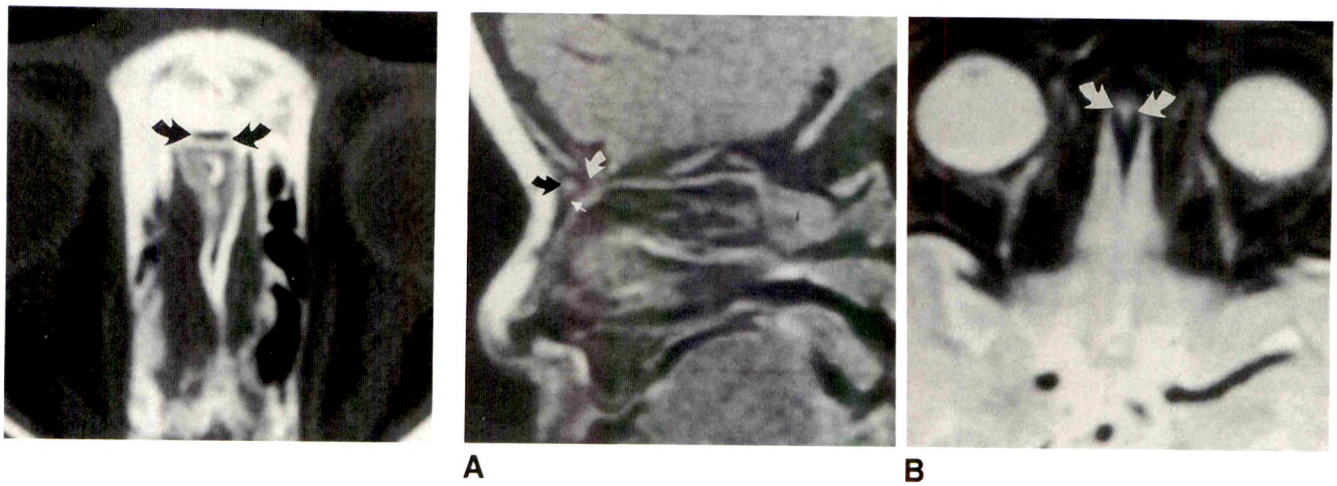



Fig. 5.—CT scan of a small foramen cecum in a 2-year-old. The foramen is seen as an oblong lucency (*arrows*) immediately anterior to inferior aspect of crista galli. This was among the smallest foramina seen in our series.

Fig. 6.—MR images of crista galli/foramen cecum area in a 7-month-old patient.

*A*, Before fat is deposited in the frontal bones, nasal bones, and crista galli, the foramen cecum is difficult to see. On this sagittal SE 600/20 image, the nasal process of the frontal bone is marked by the *curved black arrow*, the nasal bone is marked by the *straight white arrow*, and the probable location of the foramen cecum is shown by the *curved white arrow*.

*B*, At this age, the location of the foramen cecum is identified better on T2-weighted images. Here the foramen (*arrows*) is demarcated by the crista galli posteriorly and the nasal processes of the frontal bones anteriorly. Because both bony structures are very dark on this T2-weighted image, the foramen is more easily seen.

bones into the nasal soft tissues (Fig. 11); these were labeled as nasoethmoidal encephaloceles [8]. One cephalocele extended anteriorly between the frontal bones and above the nasal bones into the soft tissues in the glabellar and inferior frontal region and was labeled a nasofrontal encephalocele (Fig. 12). Two lesions extended both inferiorly through the foramen cecum beneath the nasal bones and anteriorly between the frontal and nasal bones; we considered these to be both nasofrontal and nasoethmoidal encephaloceles (Fig. 13). The final lesion, a nasoorbital encephalocele, extended through the foramen cecum, then inferiorly and laterally behind the frontal processes of the maxillary bones into both orbits, laterally displacing the globes (Fig. 14). All of the extracranial masses were lobulated and had a mixed signal intensity of both soft tissue and water intensities. Fat from an interhemispheric lipoma extended into the cephalocele in patient 15 (Fig. 13). The extracranial masses ranged in size from 8 × 15 mm to 30 × 50 mm.

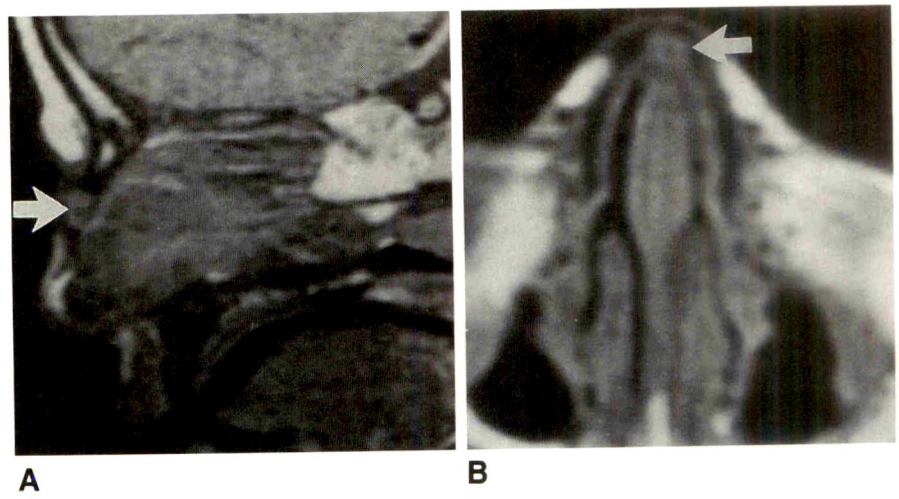



Fig. 7.—Patient 3: 2-year-old girl with dermal sinus and epidermoid.

*A*, Sagittal SE 600/20 image shows a small mass, isointense with nasal cartilage and hypointense compared with brain, adjacent to nasal cartilage in the midline anteriorly (*arrow*). The associated dermal sinus is not visualized. The sinus tracts themselves were not seen on either MR or CT scans in any patient.

*B*, Axial SE 600/20 image shows epidermoid tumor, which actually lies within the nasal cartilage in the midline (*arrow*) immediately inferior to the nasal bones.

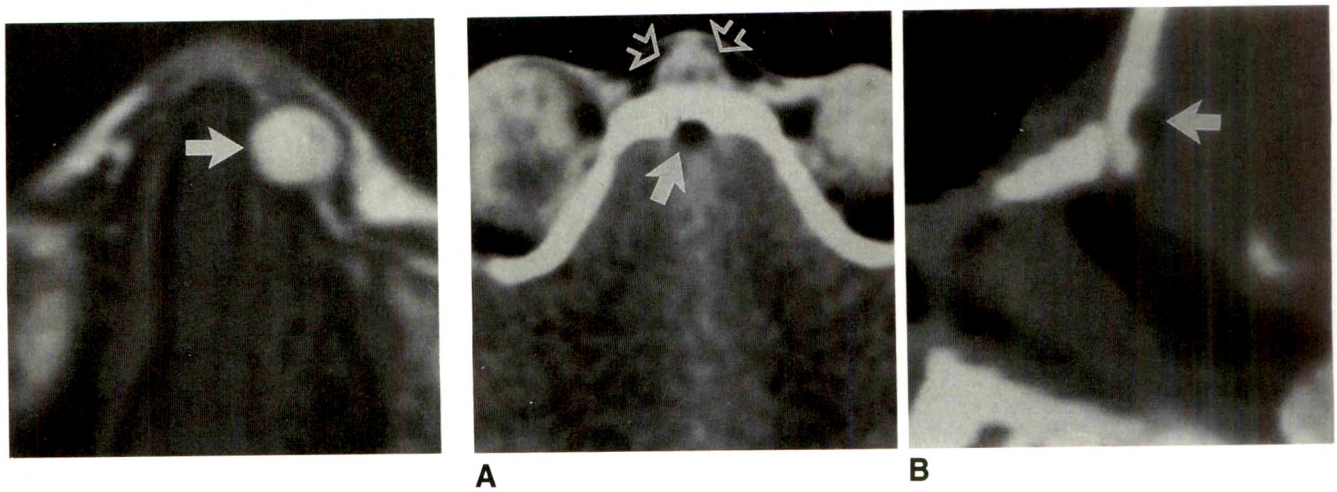



Fig. 8.—Patient 2: 12-month-old boy with nasal dermoid. Axial SE 600/20 image shows a round mass (*arrow*) with short T1 relaxation time sitting within left lateral nasal cartilage. T2-weighted images (not shown) showed a short T2 relaxation time. At surgery, this was found to be a dermoid.

Fig. 9.—Patient 1: 3-month-old girl with dermal sinus and intra- and extracranial dermoid.

*A*, Axial image from a CT scan performed with intrathecal iohexol because an encephalocele was initially suspected. A small, round hypodense mass (*closed arrow*) is seen in the midline immediately above the foramen cecum. The adjacent frontal bones are smoothly eroded. An associated soft-tissue mass is seen in adjacent extracranial soft tissues (*open arrows*).

*B*, Sagittal reformation using bone windows shows mass (*arrow*) sitting in anteroinferior portion of anterior cranial fossa, immediately above the foramen cecum. Identification of intracranial dermoids is important because it suggests the appropriate surgical management of these patients.

**TABLE 3: Summary of Patients with Nasal Masses**

| Diagnosis | No. of Patients | FC Size (mm) | Crista | | |
|---|---|---|---|---|---|
| | | | Size (mm) | Bifid | IOD (mm) |
| Cephalocele | 8 | 12 (SD = 5) | 3 (SD = 2) | 1/8 | 21 (SD = 7) |
| Dermal sinus | 7 | 3 (SD = 2) | 4 (SD = 2) | 1/7 | 18 (SD = 3) |
| Nasal glioma | 1 | Not measurable | 4 | 1/1 | 12 |

Note.—FC = foramen cecum, IOD = interorbital distance.

The foramen cecum was enlarged in all patients with nasoethmoidal encephaloceles and in the patient with the nasoorbital encephalocele, ranging from 8 to 20 mm in diameter (mean, 12 mm; SD = 5 mm). The crista galli was either absent (possibly eroded) or present but small in all patients in this group. In all of the patients with a detectable crista galli, the anterior margin of the crista was smoothly concave, suggesting erosion of bone by the cephalocele (Fig. 14). In patient 15, the remaining crista appeared bifid. The interorbital distance ranged from 12 to 28 mm (mean, 21 mm; SD = 7 mm).

A high rate of associated brain anomalies was present in this group. Three patients with nasoethmoidal encephaloceles had agenesis of the corpus callosum; one of these (patient 15) had an interhemispheric lipoma (Fig. 13) and carried a

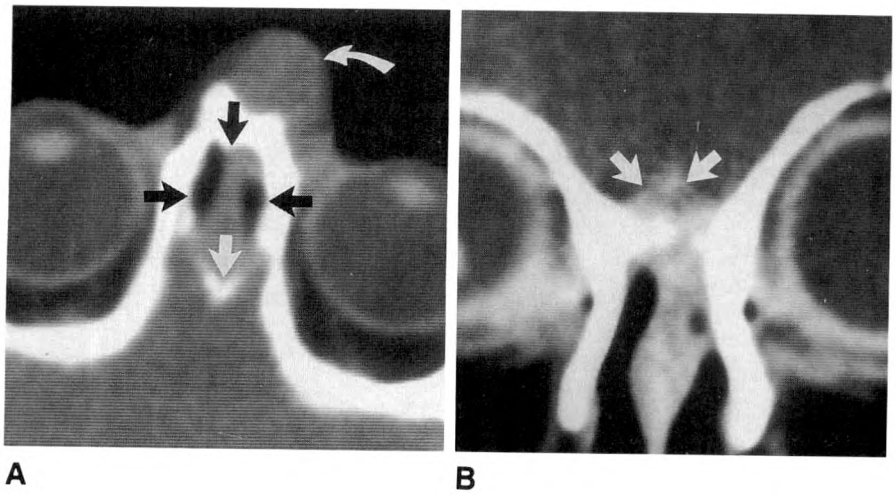



Fig. 10.—Patient 8: 9-month-old girl with nasal glioma.

*A*, Axial CT scan shows a markedly widened foramen cecum (*black arrows*) with an extremely small (possibly eroded) crista galli (*straight white arrow*). *Curved white arrow* points to the mass in the glabellar region.

*B*, Coronal CT image shows apparent extension of the mass (*arrows*) intracranially through the foramen cecum. On CT, this mass could not be differentiated from an encephalocele.

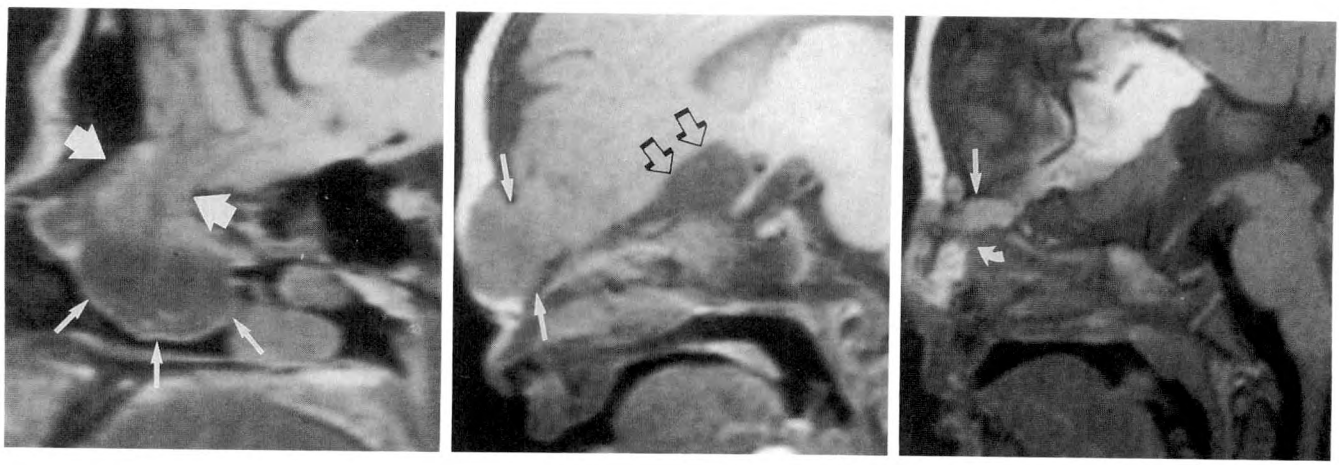


Fig. 11.—Patient 16: 24-year-old man with nasoethmoidal encephalocele. Sagittal SE 600/20 MR image shows that the foramen cecum is markedly widened (*wide arrows*). A heterogeneous mass is seen to extend inferiorly through the foramen cecum into the nasal cavity and ethmoid air cells (*thin arrows*). The brain is stretched as it enters the mass. The nasoethmoidal encephaloceles all seemed to widen the foramen cecum.

Fig. 12.—Patient 10: 6-week-old girl with nasofrontal encephalocele. A soft-tissue mass that is continuous with brain is seen extending anteriorly between the frontal bones into the soft tissues in the subfrontal and glabellar regions. The disruption of the calvaria (*white arrows*) is at the site where the fonticulus frontalis was located and may be a persistence of that primitive fontanelle. A subfrontal cyst (*open black arrows*) is present beneath the gyrus rectus.

Fig. 13.—Patient 15: 10-month-old girl with nasofrontal and nasoethmoidal encephaloceles and midline craniofacial dysraphism. Sagittal SE 600/20 MR image shows absence of corpus callosum. A large interhemispheric lipoma is seen in the frontal region. The lipoma extends out of the calvaria in the interfrontal region at the location of the fonticulus frontalis (*straight arrow*) and inferiorly into the nasal region near the site of the foramen cecum (*curved arrow*). (Reprinted with permission from [26].)

clinical diagnosis of median cleft face syndrome. Two patients had large middle temporal fossa arachnoid cysts, one unilaterally and one bilaterally. One patient had a subfrontal cyst (Fig. 12). Finally, one patient had a unilateral right parietal schizencephaly.

## Discussion

### *Embryology of the Nasofrontal Region*

The membranous neurocranium (the cranial vault) originates as a capsular membrane around the developing brain. In the very early stages of gestation it is composed of two tissue layers, which are of both mesodermal and ectodermal origin. At the sixth or seventh gestational week, the external layer differentiates into an inner membrane of primitive dura and an outer membrane with osteogenic properties. The nasal and frontal bones will develop from intramembranous ossification of the latter during the seventh or eighth week of gestation [3, 9, 10].

Posterior to the nasal and frontal bones lies the anterior wall of the nasal capsule (Fig. 15). This capsule is a part of the chondrocranium (skull base), which forms the floor of the developing brain. During the eighth gestational week, the nasal capsule may be considered a box of cartilage divided by a median cartilaginous septum. As the lateral walls of the capsule ossify later in development to form the lateral masses of the ethmoid and the inferior concha bones, the anterior two-thirds of the midline nasal septum will remain cartilaginous. The posterior portion of the septum, formed by the fusion of the presphenoid cartilages in the midline, will ossify

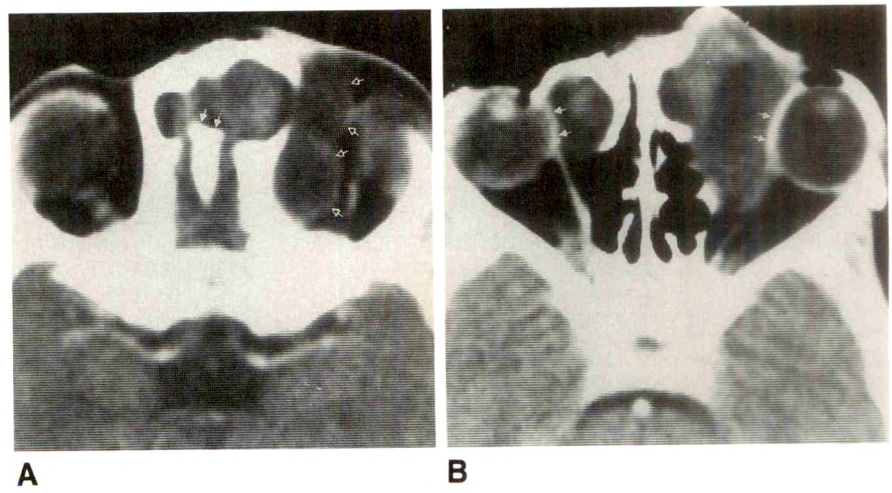



**Fig. 14.—Patient 14: 6-month-old boy with nasoorbital encephalocele.**

***A*, Axial contrast-enhanced CT scan through level of foramen cecum shows erosion of the anterior aspect of the crista galli (*closed arrows*). Soft tissue is seen extending through foramen cecum on the left toward the orbit. Water-density masses are seen within the left orbit (*open arrows*), displacing the globe laterally.**

***B*, At a slightly lower level, heterogeneous masses composed of CSF and dysplastic brain tissue are seen in the medial aspects of the orbits, displacing the globes (*arrows*) bilaterally.**

at birth to become the perpendicular plate of the ethmoid bone. Its upper edge will form the crista galli [3, 9, 11].

Two transient spaces are formed by the developing structures in the nasofrontal region (Fig. 15). The first is a small fontanelle, the fonticulus nasofrontalis, which lies in the midline between the paired frontal and nasal bones [3, 9, 12–14]. The second is the prenasal space, bounded posteriorly by the anterior wall of the nasal capsule and anteriorly by the nasal bones and fonticulus [1–3, 12, 15].

Toward the end of the second gestational month, a diverticulum of dura extends anteroinferiorly through the prenasal space and transiently contacts the superficial ectoderm in the region that will become the nose. As normal development progresses, the nasal processes of the frontal bone grow inferiorly to surround the dural projection and form a canal, the foramen cecum [1–3, 15]. The dural projection eventually involutes into a fibrous structure that fills the obliterated foramen. In normal children, the bony foramen is, therefore, filled by fibrous tissue [1, 3].

Nasal dermoids, nasal encephaloceles, and nasal gliomas result from aberrations of this normal development process [2, 3]. The most widely accepted theory at present is that proposed by Brunner and Harned [16] and elaborated upon by Pratt [1] and Sessions [3]. These authors suggest that nasal dermal sinuses and some nasal gliomas and encephaloceles result from incomplete regression of the projection of dura that transiently traverses the prenasal space. If the dural projection remains adherent to the skin, a small dimple will be present on the external surface of the nose; this dimple is the external orifice of a dermal sinus tract (Fig. 16). The tract can terminate anywhere along the path of the dural projection or can extend upward, through the foramen cecum, into the cranial vault. Dermoid and epidermoid tumors result from desquamation of cells of the dermis and epidermis lining the tract. They may develop anywhere along the tract. If large, the associated dermoid may occasionally extend posteriorly, beneath the crista galli, or anteriorly, through the fonticulus.

Nasal cephaloceles and gliomas are also explained by this concept. Cephaloceles presumably result from herniation of intracranial tissues into the dural projection through the fora-

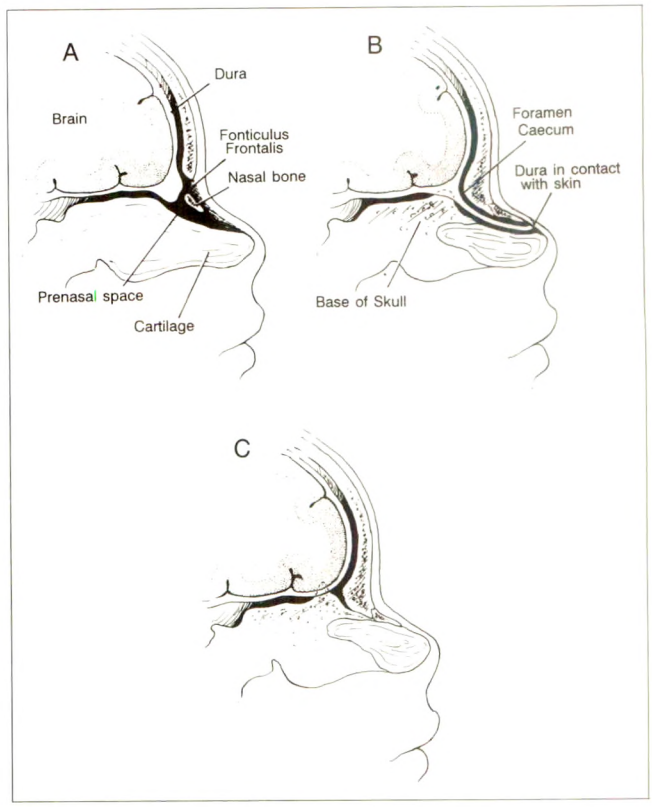



**Fig. 15.—Schematics showing normal development of the base of the skull and prenasal space. (Adpated from [2].)**

***A*, A small fontanelle, the fonticulus frontalis, is transiently present between the developing frontal bones and the developing nasal bones. A second transient space, the prenasal space, is present at the same time, lying between the developing nasal bones and the cartilage of the developing nasal capsule.**

***B*, Slightly later in development, the fonticulus frontalis has closed. The prenasal space has narrowed as a result of growth of the nasal processes of the frontal bones. This space, now completely surrounded by bone, is termed the foramen cecum. A projection of dura extends from the intracranial space through the foramen cecum and comes in contact with the skin in the region that will form the nose.**

***C*, Slightly later in development, the dural projection separates from the skin of the nose and retracts back into the cranium. After this retraction and involution of the dural projection, the foramen cecum partially fuses and the prenasal space is obliterated.**

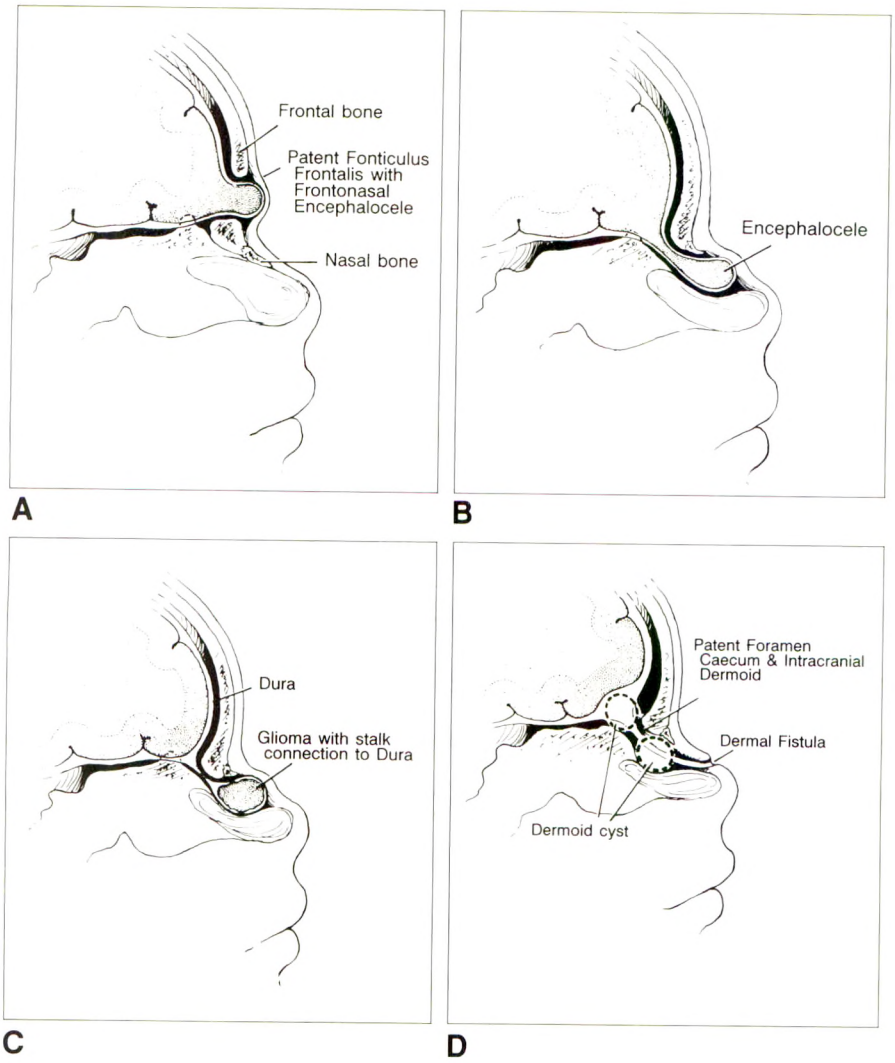



Fig. 16.—Schematics illustrating the results of aberrant development in the anterior skull base.

*A*, If the fonticulus frontalis fails to close, the result is a frontonasal encephalocele.

*B*, A failure of the foramen cecum to close results in a frontoethmoidal encephalocele.

*C*, If the dural projection through the foramen cecum involutes late in development or only involutes proximally, the result is a nasal glioma with a fibrous stalk connecting it to the intracranial contents across the foramen cecum.

*D*, Dermal sinuses result from a lack of involution of the dural projection through the foramen cecum. Any part of the dermal sinus may involute. A dermoid or epidermoid tumor may form anywhere along the tract of the dermal sinus as a result of desquamation of the lining of the tube.

men cecum (nasoethmoidal and nasoorbital cephaloceles) or hernation through the fonticulus (nasofrontal cephalocele) (Fig. 16). Although nasoethmoidal cephaloceles can be explained by a mere lack of regression of the most cranial aspect of the dural projection, the explanation of nasofrontal and nasoorbital cephaloceles requires either an abnormal development of the respective fontanelles or orbital structures or an increase in intracranial pressure resulting in the focal brain herniation.

Nasal gliomas (also known as nasal cerebral heterotopias) are composed of dysplastic brain tissue within the nasal cavity or subcutaneous tissue over the glabellar region, separate from intracranial contents. In about 15% of patients with nasal gliomas, a connection with intracranial structures persists in the region of the foramen cecum [17]. Sessions [3] suggests that these lesions probably result from herniation of the brain through the foramen cecum into the dural projection with subsequent regression (in most patients) of the more craniad portion of the projection. The result is a sequestration of the glial tissue within the nose or nasal soft tissues.

*Present Data*

Congenital midline nasal masses are rare but important anomalies that almost always present in childhood. Patients with nasal encephaloceles and nasal gliomas typically present with nasal (rarely orbital) masses. Patients with dermal sinuses most commonly present because of nasal dimples or masses; occasionally, however, the dermal sinuses and cephaloceles become infected and this infection is the reason for presentation. The infection is usually superficial (localized to the skin or sinus ostia); rarely, the infection extends intracranially [2, 3, 12].

Radiologic evaluation is important in the work-up of midline nasal masses. Classically, plain films were obtained to look for widening of the nasal septum, erosion or separation of contiguous bones, increased interorbital distance, or a bony defect in the cribiform plate [18]. The facial bony defects are useful in the classification of frontoethmoidal cephaloceles into three subtypes [19]. In the nasofrontal group, the defect lies between the frontal and nasal bones with the frontal

bones being displaced superiorly and the nasal bones and nasal cartilage displaced inferiorly. Nasoethmoidal cephaloceles course through a defect that lies between the nasal bones and the nasal cartilage. The nasal and frontal bones (and the frontal processes of the maxillae) are displaced superiorly and anteriorly, whereas the nasal cartilage, nasal septum, and ethmoid bones are displaced posteriorly and inferiorly. In the nasoorbital form, the anterior margin of the bony defect is formed by the frontal process of the maxilla; the posterior margin is formed by the lacrimal bone and the lamina papyracea of the ethmoid bone. Therefore, the location of a bony defect as determined by plain radiographs is valuable both in the detection of frontoethmoidal cephaloceles and in the determination of their subtype. CT and MR scans may show any intra- or extracranial soft-tissue masses, defects in or separation of bones, enlargement of the foramen cecum, or distortion of the crista galli [2, 12].

In the present series, both MR and CT were able to clearly differentiate dermoids and dermal sinuses from the cephaloceles. The cephaloceles had marked widening of the calvarial openings (foramen cecum or fonticulus frontalis) through which the brain herniation occurred. The crista galli was always eroded, the interorbital distance was mildly increased, and a soft-tissue mass was seen to extend into the nasal cavity, nasal or frontal soft tissues, or orbits (Figs. 11–14). It is unfortunate that an accurate measurement of the size of the foramen cecum was not available in the patient with the nasal glioma. We suspect that it would have been enlarged, because the anterior portion of the crista galli was eroded and a stalk was seen to extend upward through the foramen at surgery. However, because 85% of nasal gliomas do not connect with intracranial structures [17], it is unlikely that foramen cecum size is ever useful in differentiating nasal gliomas from dermoids or cephaloceles.

The location of the cephalocele as determined by MR scans seems to verify the theories of Brunner and Harned [16], Pratt [1], and Sessions [3] regarding pathogenesis. All the nasoethmoidal cephaloceles clearly extended into the nasal cavity via the foramen cecum. All the nasofrontal cephaloceles coursed through the site of the fonticulus frontalis. In two patients, the intracranial tissue coursed through both spaces simultaneously. In the nasoorbital cephalocele, brain tissue presumably initially traversed the foramen cecum before deviating laterally into the orbits.

Another interesting feature of these cephaloceles was the high rate of associated brain anomalies. Three patients had large intracranial cysts, two had agenesis of the corpus callosum, one had agenesis of the corpus callosum with an interhemispheric lipoma, and one had right parietal schizencephaly. Both the callosal agenesis and the schizencephaly have been associated with teratogenic effects during the late second gestational month [20, 21], the same time at which the prenasal space and fonticulus frontalis form. This temporal relationship suggests that these associations should be common, and, indeed, a high frequency of agenesis of the corpus callosum in patients with basal encephaloceles has been reported [22]. The high rate of associated brain anomalies observed in this series is in disagreement with some earlier reports [19, 23], which describe a frequent, but significantly lower rate. Previous reports stressed hydrocephalus and ocular anomalies as being the most common. We suspect that the present study is more accurate because of the use of more sensitive modern imaging techniques.

MR is superior to CT in the evaluation of nasal cephaloceles because it more clearly and noninvasively demonstrates the pathway of intracranial herniation and the presence of associated anomalies. Moreover, obtaining high-quality images in multiple planes is valuable in planning surgical approaches to these lesions. For these reasons alone, MR would seem to be the technique of choice for initial screening of patients with midline nasal masses.

With CT, it was only possible to differentiate the nasal glioma from an encephalocele after infusion of intrathecal contrast material; encephaloceles fill with contrast whereas nasal gliomas do not. Although part of the difficulty in the present series may have been caused by poor angling of the CT gantry, a difficulty in differentiation should be expected because, embryologically, nasal gliomas are encephaloceles in which the connection to the brain has partially or completely sealed off. Therefore, the foramen cecum may remain enlarged and the crista galli may be eroded in the presence of a large soft-tissue mass in the nasal cavity. The lack of communication with the subarachnoid space (ruling out a cephalocele) can be demonstrated only by the absence of flow of contrast material into the nasal mass. We suspect that it will be difficult to demonstrate the presence or lack of this communication by MR.

Nasal dermal sinuses and nasal dermoids turned out to be very difficult to evaluate both by CT and MR. The most important information to be obtained in these studies (in fact the major reason the studies are requested) is to assess the extent of the dermal sinus or dermoid and, in particular, to determine whether intracranial extension of the sinus or intracranial tumor is present. In the absence of intracranial disease, the surgical therapy consists of exposing and removing the sinus tract as it courses upward to the skull base. If the tract extends upward through the foramen cecum but there is no intracranial tumor, many surgeons will merely tie off the tract at the skull base [12]. If there is intracranial tumor, however, a combined intracranial-extracranial approach is mandatory in order to adequately treat the patient. Therefore, it is very important to assess the full extent of dermoid or epidermoid tumor but less important to determine whether the sinus tract extends intracranially.

Examination of our data reveals that the classically used criteria of foramen cecum size, abnormality of the shape or bifidity of the crista galli, and interorbital distance were identical in our control group and dermal sinus group. Therefore, we must concur with Pensler et al. [12] that these findings are helpful only when positive. We add, furthermore, that these findings are rarely present.

Both CT and MR were excellent in the detection of dermoid and epidermoid tumors in the nose. The single dermoid that extended intracranially was well visualized by CT in spite of its small (4 × 4 mm) size. Thus, our results substantiate those of others [12, 24] who have found CT to be accurate in the

detection of intracranial tumors in patients with dermal sinus tracts. We expect that MR should be as sensitive as or more sensitive than CT in the detection of these masses.

It is important to note that neither CT nor MR accurately delineated the dermal sinus itself as it coursed through the nose or foramen cecum. Moreover, both imaging methods (particularly MR) were replete with potential pitfalls, most of which were related to the fatty metamorphosis of the marrow [25] and the signal intensity changes accompanying aeration of the frontal sinuses [7]. Unfortunately, these changes occur from approximately 12 months to 5 years of age, the same ages at which most patients with dermal sinuses present [5, 12, 24].

One potential pitfall is the shape of the nasal septum. In normal patients, the nasal septum widens in its inferior portion 5 to 10 mm posterior to the junction with the bridge of the nose (Fig. 1). This normal widening should not be mistaken for expansion resulting from inclusion of a sinus tract within the septum.

A second potential pitfall results from the low density (on CT) and diminution of T1 and T2 relaxation times (on MR) associated with fatty change in the inferior frontal sinuses and, sometimes, nasal bones prior to pneumatization (Figs. 2–4). The best way to differentiate these areas from fatty tumors is to recognize the characteristic location; dermoids will usually pass posterior to these pneumatizing spaces. Furthermore, the pneumatizing spaces are usually paired with a small bony septum between them (Figs. 2–4); such septa are never seen in dermoids.

The final major potential pitfall, which is the most serious because it may result in an unncessary craniotomy, is mistaking the crista galli or subjacent perpendicular plate of the ethmoid bone for a dermoid. The central portion of these bones begins to undergo fatty change at approximately the 12th postnatal month. The fatty change appears initially in the posterior and inferior portion of the perpendicular plate and seems to progress anteriorly and superiorly until fatty signal is seen throughout. It is easy, particularly on coronal MR, to mistake this high signal intensity for a dermoid with intracranial extension because of the proximity to the foramen cecum. It is critical to locate the foramen and crista in the sagittal and axial planes in order to ascertain whether the high signal truly represents a dermoid as opposed to marrow within bone. If necessary, a high-resolution CT scan with thin sections should be obtained to verify whether intracranial tumor is present.

In conclusion, we have reviewed imaging studies performed on 16 patients with congenital midline nasal masses and 45 normal patients. CT and MR seem equally sensitive in the detection of these masses. MR was superior in delineating the extent and morphology of encephaloceles; moreover, a high rate of occurrence of associated anomalies, which are more easily detected by MR, were present in patients with encephaloceles. CT and MR were equally sensitive in the detection of dermoid and epidermoid tumors associated with dermal sinus tracts; however, neither technique was able to resolve the sinus tracts themselves. Care should be taken not to mistake pneumatizing bone or fatty bone marrow for dermoid tumors in these patients.

## REFERENCES


1. Pratt LW. Midline cysts of the nasal dorsum: embryologic origin and treatment. *Laryngoscope* **1965**;75:968–980
2. Hughes GB, Sharpino G, Hunt W, Tucker HM. Management of the congenital midline nasal mass: a review. *Head Neck Surg* **1980**;2:222–233
3. Sessions RB. Nasal dermal sinuses: new concepts and explanations. *Laryngoscope* **1982**;92(Suppl 29):7–28
4. Bradley PJ. Results of surgery for nasal dermoids in children. *J Laryngol Otol* **1982**;96:627–633
5. Bradley PJ, Singh SD. Congenital nasal masses: diagnosis and management. *Clin Otolaryngol* **1982**;7:87–97
6. Bradley PJ. The complex nasal dermoid. *Head Neck Surg* **1983**;5: 469–473
7. Aoki S, Dillon WP, Barkovich AJ, Norman D. Marrow conversion before pneumatization of the sphenoid sinus: assessment with MR imaging. *Radiology* **1989**;172:373–375
8. Diebler C, Dulac O. Cephaloceles: clinical and neuroradiological appearance. *Neuroradiology* **1983**;25:199–216
9. Sperber GH. *Craniofacial embryology*, 3rd ed. Bristol: Wright PSG, **1981**
10. Gasser RF. Early formation of the basicranium in man. In: Bosma JF, ed. *Symposium on development of the basicranium*. Bethesda: U.S. Department of Health, Education and Welfare, **1976**
11. Pansky B. *Review of medical embryology*. New York: McMillan, **1982**
12. Pensler JM, Bauer BS, Naidich TP. Craniofacial dermoids. *Plast Reconstr Surg* **1988**;82(6):953–958
13. Bosma JF. Introduction to the symposium on development of the basicranium. In: Bosma JF, ed. *Symposium on development of the basicranium*. Bethesda: U.S. Department of Health, Education and Welfare, **1976**
14. Bosma JF. Anatomy of the infant head. Baltimore: The Johns Hopkins University Press, **1986**
15. Littlewood AH. Congenital nasal dermoid cysts and fistulas. *Plast Reconstr Surg* **1961**;27:471–488
16. Brunner H, Harned JW. Dermoid cysts of the dorsum of the nose. *Arch Otolaryngol* **1942**;36:86–93
17. Gorenstein A, Kern EB, Facer GW, Lows ER Jr. Nasal gliomas. *Arch Otolaryngol* **1980**;106:536
18. Johnson GF, Weisman PA. Radiological features of dermoid cysts of the nose. *Radiology* **1964**;82:1016–1021
19. Suwanwela C, Suwanwela N. A morphological classification of sincipital encephalomengoceles. *J Neurosurg* **1972**;36:201–211
20. Barkovich AJ, Norman D. MR of schizencephaly. *AJNR* **1988**;9:297–302
21. Barkovich AJ, Norman D. Anomalies of the corpus callosum: correlation with further anomalies of the brain. *AJNR* **1988**;9:493–501
22. Yokota A, Matsukodo Y, Fuwa I, Moroki K, Nagahiro S. Anterior basal encephalocele of the neonatal and infant period. *Neurosurgery* **1986**; 19:468–478
23. Rapport RL, Dunn RC Jr, Alhady F. Anterior encephalocele. *J Neurosurg* **1981**;54:213–219
24. McQuown SA, Smith JD, Gallo AE. Intracranial extension of nasal dermoids. *Neurosurgery* **1983**;12:531–535
25. Okada Y, Aoki S, Barkovich AJ, et al. Cranial bone marrow in children: assessment of normal development with MR imaging. *Radiology* **1989**; 171:161–164
26. Barkovich AJ. *Pediatric neuroimaging*. New York: Raven Press, **1990**:88

# Idiopathic Growth Hormone Deficiency: MR Findings in 35 Patients

James J. Abrahams[1]
Eric Trefelner[1]
Susan D. Boulware[2]

**Idiopathic growth hormone deficiency is a disorder that is not clearly understood. We therefore evaluated the MR scans of 35 patients with idiopathic growth hormone deficiency in an attempt to define more clearly the abnormalities of the hypothalamo-hypophyseal axis, determine the frequency of these abnormalities, and determine whether a relationship exists between the MR findings and the patient's clinical history and endocrine function. Patients with MR abnormalities fell into two groups: those with an ectopic neurohypophysis (15 patients, or 43%), which consisted of a neurohypophysis near the median eminence, absence of the infundibulum, and absence of the normal posterior pituitary bright spot; and those with a small anterior pituitary gland (15 patients, or 43%), which was an isolated finding in five patients and associated with an ectopic neurohypophysis in 10 patients. Examination of endocrine function identified two groups of patients: those with multiple hormone deficiencies and those with isolated growth hormone deficiency. An ectopic neurohypophysis was present in 87% of the first group and 10% of the second group. The anterior pituitary dysfunction in those with an ectopic neurohypophysis was thought to be related to the absent infundibulum, which normally houses the portal system.**

**Our MR findings demonstrated that over 40% of patients with idiopathic growth hormone deficiency have an ectopic neurohypophysis and absence of the infundibulum. We believe that the growth hormone deficiency in these patients is related to the absent infundibulum.**

*AJNR* 12:155–160, January/February 1991; *AJR* 156:599–604, March 1991

Growth hormone deficiency (GHD), defined as a peak serum growth hormone level of less than 10 mcg/l after two standard provocation tests, will produce pituitary dwarfism if untreated [1]. It is considered idiopathic when no obvious cause—such as tumor, surgery, radiation, etc.—is identified. The anterior lobe of the pituitary gland, which secretes growth hormone as well as adrenocorticotropic hormone, prolactin, thyrotropin, follicle-stimulating hormone, and luteinizing hormone, depends on hypothalamic regulation for normal function. Communication exists between the anterior pituitary and hypothalamus via the hypothalamohypophyseal portal system, which travels through the infundibulum. The posterior pituitary, which secretes antidiuretic hormone and oxytocin, communicates with the hypothalamus through direct extension of neurosecretory cells, which also travel in the infundibulum [2]. One can see then how disease of the hypothalamus or disruption of its pathways of communication could result in pituitary dysfunction.

Although the cause of idiopathic growth hormone deficiency (IGHD) is not known, it is believed, most often, to be due to an abnormality of the hypothalamus [3]. Radiographic evidence supporting this theory has been scanty. Recently, however, an ectopic neurohypophysis (ENH) has been described on MR images in a few patients with IGHD [4–6]. The exact role of this finding and how it may relate to the origin of this disease is not known. We therefore examined a larger series of 35 IGHD patients to (1) more clearly define the structural abnormalities of the

Received June 13, 1990; revision requested August 27, 1990; revision received September 7, 1990; accepted September 7, 1990.

Presented at the annual meeting of the American Society of Neuroradiology, Los Angeles, March 1990.

[1] Department of Radiology, Yale University School of Medicine, 333 Cedar St., New Haven, CT 06510. Address reprint requests to J. J. Abrahams.

[2] Department of Endocrinology (Pediatrics), Yale University School of Medicine, New Haven, CT 06510.

0361–803X/91/1563–0599
© American Roentgen Ray Society

hypothalamohypophyseal axis and determine if other abnormalities exist, (2) determine the frequency of these abnormalities, and (3) determine whether a relationship exists between these abnormalities and the patient's clinical history and endocrine function.

## Materials and Methods

Of 78 patients being treated for GHD, 42 were diagnosed as having IGHD. Of these 42, 35 had MR scans. A single attending neuroradiologist, aware of the presence of IGHD, interpreted the scans, but was blinded to the actual laboratory values and to any other clinical history. The scans were evaluated specifically for posterior pituitary ectopia, anterior pituitary size, infundibular discontinuity or abnormalities, and hypothalamic lesions. A patient was considered to have posterior pituitary ectopia when we identified a nodule of bright signal (T1-weighted) in the region of the median eminence that was associated with absence of the normal posterior sella bright spot. Anterior pituitary size was judged, by gross inspection, to be either large, small, or normal, and the signal characteristics of the anterior pituitary gland were compared with gray matter. Scans were performed on a 1.5-T GE Signa unit (General Electric, Milwaukee, WI) using standard pituitary protocols—sagittal 600/20 (TR/TE) and coronal 500/25 sequences with and without gadopentetate

**TABLE 1: MR Findings, Clinical Histories, and Endocrine Function in 35 Patients with Idiopathic Growth Hormone Deficiency**

| Case No. | Sex | Age at MR | Delivery | Infundibulum | Anterior Pituitary | Posterior Pituitary | Level of Growth Hormone |
|---|---|---|---|---|---|---|---|
| Patients with Multiple Hormone Deficiencies | | | | | | | |
| 1 | M | 1 day | SVD | Absent | Normal | Ectopic[a] (2 × 3 mm) | SD |
| 2 | M | 5 yr | SVD | Absent | Small | Ectopic[a] (4 × 5 mm) | SD |
| 3 | M | 8 yr | SVD | Absent | Normal | Ectopic[a] (3 × 3.5 mm) | SD |
| 4 | F | 1.5 yr | SVD | Absent[b] | Small | Ectopic[a] (4 × 5 mm) | SD |
| 5 | F | 3 yr | SVD | Absent | Small | Ectopic[a] (2 × 3 mm) | SD |
| 6 | M | 9 yr | SVD | Absent | Right half small | Ectopic[a] (4.5 × 5 mm) | SD |
| 7 | M | 14 yr | C/S | Absent | Small | Ectopic[a] (4 × 6 mm) | D |
| 8 | F | 1 day | C/S | Absent | Small | Ectopic[a] (3.5 × 4 mm) | SD |
| 9 | M | 1 day | C/S | Absent | Normal | Ectopic[a] (4 × 5 mm) | SD |
| 10 | M | 4 wk | C/S | Absent | Normal | Ectopic[a] (2 × 3 mm) | SD |
| 11 | M | 1 day | C/S | Absent | Small | Ectopic[a] (3.5 × 2 mm) | D |
| 12 | F | 6 yr | SVD | Absent | Small | Ectopic[a] (3 × 5 mm) | SD |
| 13 | M | 4 yr | SVD | Absent[b] | Small | Ectopic[a] (4 × 7 mm) | D |
| 14 | M | 5 yr | SVD | Normal | Normal | Normal | SD |
| 15 | M | 1.5 yr | SVD | Normal | Small | Normal | SD |
| Patients with Isolated Growth Hormone Deficiency | | | | | | | |
| 16 | F | 3 yr | C/S | Absent[b] | Normal | Ectopic[a] (5 × 6 mm) | D |
| 17 | F | 7 yr | C/S[c] | Absent | Small | Ectopic[a] (5 × 5 mm) | SD |
| 18 | M | 14 yr | C/S | Normal | Small | Normal | D |
| 19 | F | 8 yr | SVD | Normal | Normal | Normal | D |
| 20 | M | 16 yr | SVD | Normal | Normal | Normal | D |
| 21 | M | 6 yr | SVD | Normal | Normal | Normal | SD |
| 22 | M | 2 yr | C/S | Hypoplastic | Small | Not seen | SD |
| 23 | M | 16 yr | SVD | Normal | Small | Normal | D |
| 24 | M | 14 yr | SVD | Normal | Normal | Normal | SD |
| 25 | M | 4 yr | SVD | Normal | Normal | Normal | D |
| 26 | M | 12 yr | SVD | Normal | Small | Normal | D |
| 27 | M | 8 yr | SVD | Normal | Normal | Normal | D |
| 28 | M | 14 yr | SVD | Normal | Normal | Normal | D |
| 29 | M | 15 yr | SVD | Normal | Normal | Normal | D |
| 30 | M | 8 yr | SVD | Normal | Normal | Normal | D |
| 31 | M | 4 yr | C/S | Normal | Normal | Normal | D |
| 32 | M | 4 yr | C/S[c] | Normal | Normal | Normal | D |
| 33 | F | 7 yr | SVD | Normal | Normal | Normal | D |
| 34 | F | 8 yr | SVD | Normal | Normal | Normal | D |
| 35 | M | 13 yr | SVD | Normal | Normal | Normal | D |

Note.—The hypothalamus was normal in all patients, and no patient had diabetes insipidus. SVD = spontaneous vaginal delivery, C/S = cesarean section, D = diminished (9–6 mcg/l), SD = severely diminished (6–0 mcg/l).

[a] All ectopic posterior pituitary glands were located near the median eminence.

[b] This patient received gadopentetate dimeglumine and the infundibulum was still not seen.

[c] Breech presentation.

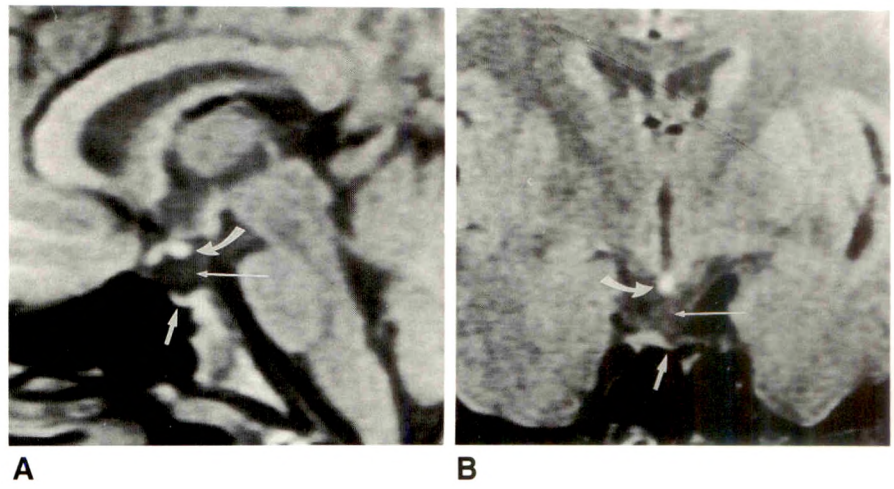



Fig. 1.—Small anterior pituitary gland associated with an ectopic neurohypophysis (ENH).

*A* and *B*, Sagittal (600/20) (*A*) and coronal (2000/20) (*B*) MR images show a small anterior pituitary gland with a shallow sella (*short arrow*). Compare with the normal pituitary seen in Fig. 3. The ENH, which appears as a nodule or bright signal in the median eminence (*curved arrow*), is associated with an absent infundibulum (*long arrow*).

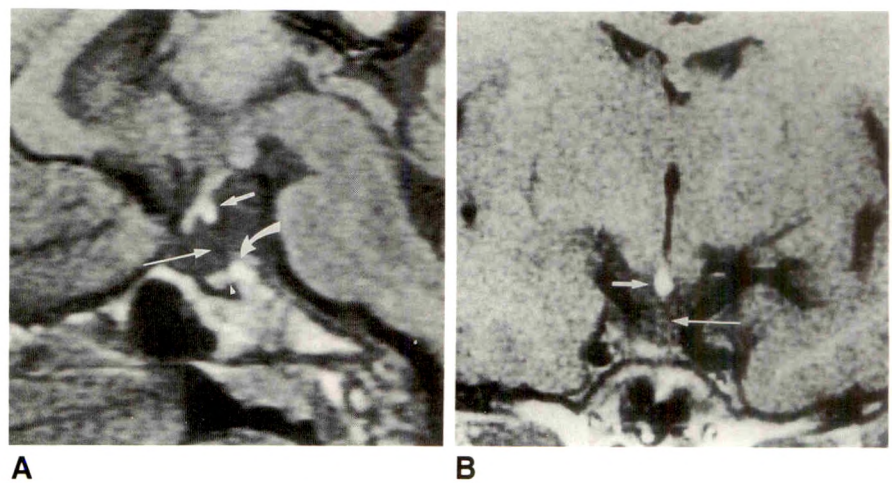



Fig. 2.—Ectopic neurohypophysis (ENH) in a patient with idiopathic growth hormone deficiency.

*A* and *B*, Sagittal (600/20) (*A*) and coronal (600/20) (*B*) MR images show that the ENH is actually a constellation of abnormalities consisting of an ENH near the median eminence (*short arrow*), absence of the infundibulum (*long arrow*), and absence of the normal posterior pituitary bright spot (*arrowhead*). The area of bright signal behind the gland corresponds to fatty marrow in the dorsum sella and posterior clinoids (*curved arrow*).

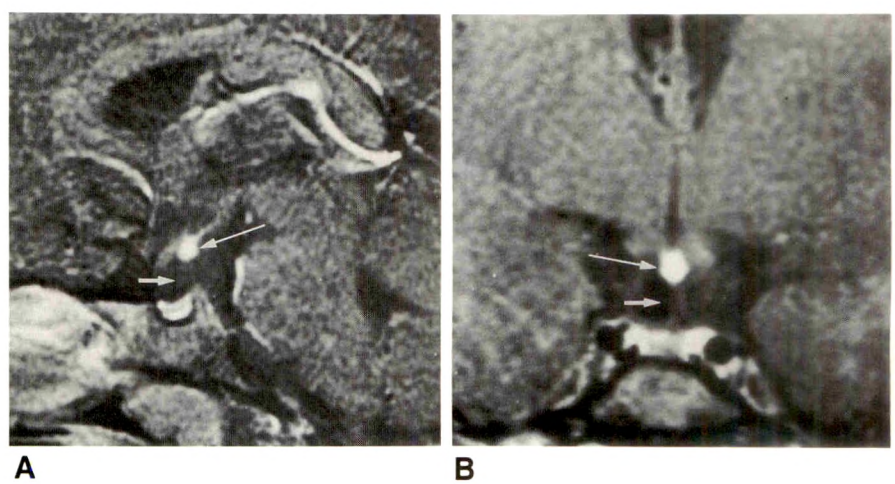



Fig. 3.—*A* and *B*, Contrast-enhanced sagittal (600/20) (*A*) and coronal (500/25) (*B*) MR images of an ectopic neurohypophysis (*long arrow*). Note that even with contrast enhancement the infundibulum cannot be identified (*short arrow*). The enhancing anterior pituitary gland is of normal size in this patient.

dimeglumine; and sagittal 600/20, coronal 600/20, and coronal 2000/20,80 sequences before administration of contrast material. The results from the MR scans were then compared with the clinical histories (gender, delivery, etc.) and with endocrine laboratory values.

## Results

### *MR Findings*

The 35 patients with abnormalities noted on their MR scans fell into two basic groups: those with an ectopic neurohypophysis (15 patients, or 43%) and those with a small anterior pituitary gland (15 patients, or 43%) (see Table 1). The small anterior pituitary gland demonstrated normal signal characteristics relative to gray matter and was an isolated finding in five patients and was associated with an ENH (Fig. 1) in 10 patients. In several cases the anterior pituitary could not be identified at all.

The ENH was actually a constellation of findings consisting of an ENH near the median eminence, absence of the infundibulum, and absence of the normal posterior sella bright spot (Fig. 2). In all cases the ENH was identified near the median eminence in the usual location of the proximal infundibulum. It had the same signal characteristics as a normal neurohypophysis (bright on T1-weighted images, which diminished on T2-weighted images) and did not demonstrate a chemical shift artifact. The size of the ENH varied (see Table 1) and its shape ranged from round to oval. The infundibulum was absent in all patients with an ENH but present in the other patients. It is worth noting that even after enhancement with gadopentetate dimeglumine the infundibulum was not visualized in the patients with an ENH (Fig. 3). The bright signal of the neurohypophysis, which is usually seen in the posterior sella, was absent in all of the patients with an ENH. These patients did not have diabetes insipidus, suggesting that the ENH is a functioning unit.

### *Endocrine Studies*

Analysis of endocrine function in the 35 patients yielded two groups: those with multiple hormone deficiencies (GHD plus abnormality of at least one other anterior pituitary hormone, 15 patients) and those with isolated GHD (20 patients) (see Table 1). An ENH was identified in 87% of patients with multiple hormone deficiencies and in 10% of those with isolated GHD.

Prolactin was elevated (>30 $\mu$g/dl) in three patients, indeterminant (20–30 $\mu$g/dl) in two patients, and normal (<20 $\mu$g/dl) in the remaining 30 patients. An ENH was found in two patients with an elevated prolactin level (both in the indeterminant range) and in 11 patients with a normal prolactin level. No patient had diabetes insipidus. The presence of a small anterior pituitary gland did not clearly relate to the clinical histories or laboratory values.

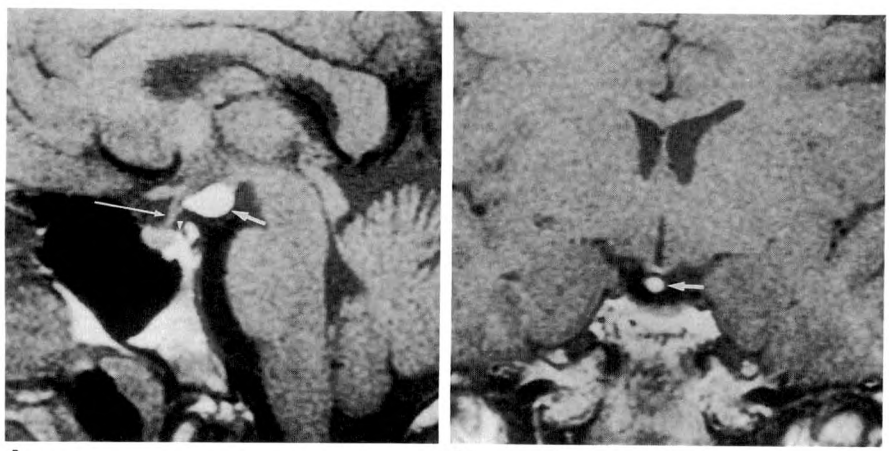
### *Clinical Histories*

Of the 35 patients with IGHD 26 were male and nine were female. Of those with an ENH, there were nine males and six females. A small anterior pituitary gland was found in 10 males and three females.

Eleven patients were delivered by cesarean section and the rest by spontaneous vaginal delivery. Two cesarean sections were associated with a breech presentation. There were no vaginal breech deliveries and there was no patient with birth trauma or known anoxia. Of the 11 cesarean sections, five patients had multiple hormone deficiencies, all associated with an ENH, and six patients had isolated growth hormone deficiency, two associated with an ENH.

## Discussion

Forty-three percent of our patients with IGHD had an ENH. When we divided these patients into a multiple hormone



A B

**Fig. 4.—Lipoma of the tuber cinereum.**
***A* and *B*, Sagittal (600/20) (*A*) and coronal (600/20) (*B*) MR images. A lipoma (*short arrow*), which may appear similar to an ectopic neurohypophysis, can be differentiated by its larger size and more irregular shape and by the presence of a normal infundibulum (*long arrow*) and a posterior pituitary bright spot (*arrowhead*).**

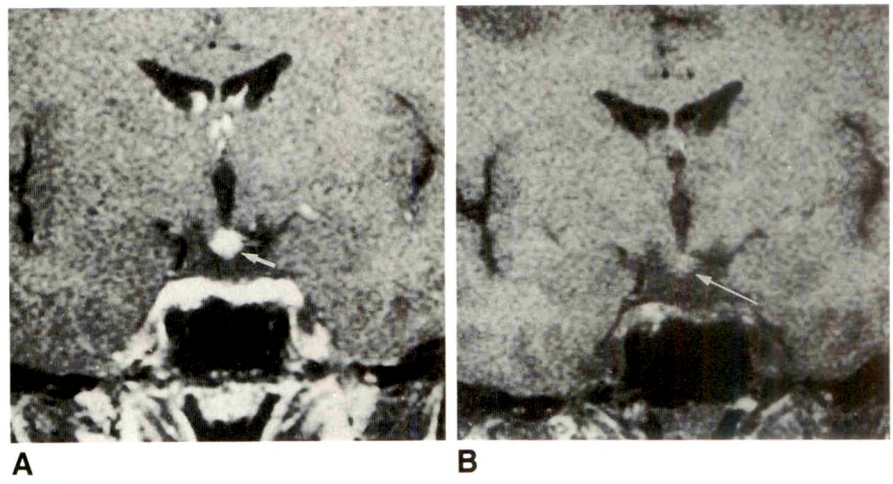



Fig. 5.—Histiocytosis X.
*A* and *B*, Coronal MR images with (500/25) and without (600/20) contrast enhancement. The enhancing histiocytosis X (*short arrow*), which at first glance may appear similar to an ectopic neurohypophysis, can be differentiated by the lack of bright signal on the unenhanced scan (*long arrow*).

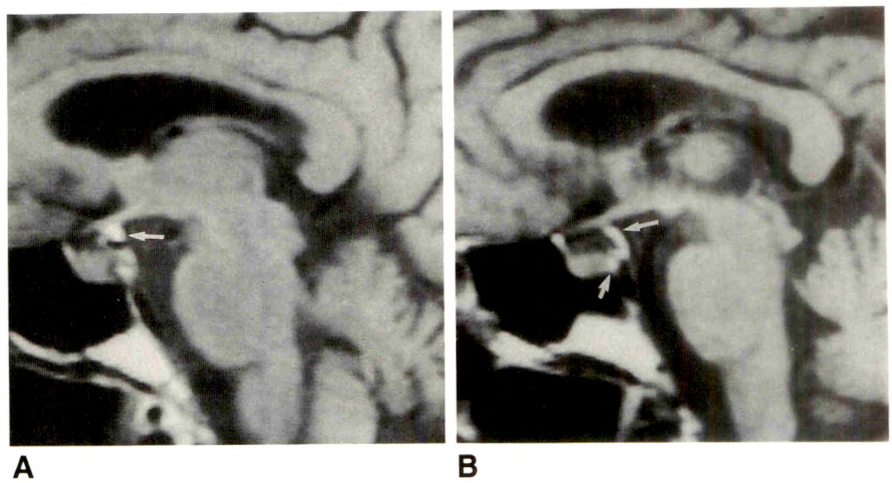



Fig. 6.—Fatty marrow in the dorsum sella and posterior clinoids.
*A*, Sagittal (600/20) MR image left of midline shows an area of bright signal that looks like an ectopic neurohypophysis (*arrow*).
*B*, The midline sagittal (600/20) MR image, however, clearly establishes that this is actually fatty marrow in the dorsum sella and posterior clinoid (*long arrow*). The bright signal of the normal posterior pituitary is also identified (*short arrow*).

deficiency group and an isolated growth hormone deficiency group, then 87% of the former had an ENH compared with only 10% of the latter. This suggests that an ENH is associated with multiple endocrine dysfunction. Also supporting this is the fact that the patients with an ENH tended to have more severely diminished growth hormone levels. It is interesting that the neurohypophysis, which is ectopic, functions relatively normally while the adenohypophysis does not. We believe this is due to the absent infundibulum, which normally contains the hypothalamohypophyseal portal system. Without the portal system, communication with the hypothalamus is disrupted and the anterior pituitary therefore malfunctions. The ENH, on the other hand, is situated proximally near the hypothalamus. Disruption of the infundibulum, which is distal to the ENH, would therefore not be expected to interfere with communication between the neurohypophysis and hypothalamus. This appears to be the reason why the ENH functions in a relatively normal capacity and why these patients do not develop diabetes insipidus.

We also found that 43% of patients with IGHD had a small anterior pituitary gland. This finding appeared to be random and did not clearly correlate with the other MR findings, clinical histories, or laboratory values. It is not known why the anterior pituitary is small in some patients and not others. Perhaps the small size is related to hypoplasia secondary to diminished hypothalamic stimulation or to diminished blood supply from absence of the hypothalamohypophyseal portal system.

The male predominance in our group of patients with IGHD may be a reflection of referral bias; that is, pediatricians and families are more likely to be concerned about short stature in boys than in girls. The more even gender distribution of children with an ENH (more severely affected patients) supports this notion. It is interesting that previous reports have suggested a high rate of breech deliveries in IGHD patients [7, 8]. Our study, however, does not substantiate this finding.

Although the ENH has a characteristic appearance on MR, it still must be differentiated from other entities. A lipoma of the tuber cinereum has similar signal characteristics to the

ENH [9], also appearing bright on the T1-weighted images and dropping in signal on the T2-weighting images (Fig. 4). The lipoma can be differentiated by its chemical shift artifact, presence of an infundibulum, and often larger size and more irregular shape [9]. Histiocytosis X or another granuloma may look like an ENH on the contrast-enhanced scan because of its bright signal, location near the median eminence, and often absent bright signal in the posterior pituitary (Fig. 5). It can be readily differentiated on the unenhanced scan by its lack of bright signal and presence of an infundibulum [10, 11]. Occasionally, fatty marrow in the cephalad tip of the dorsum sella may at first glance look like an ENH on the sagittal T1-weighted image (Fig. 6). The infundibulum is present, however, and it is our observation that the coronal image will demonstrate the fat to be separate from the median eminence.

The cause of IGHD has eluded physicians for years [1]. However, with the use of MR imaging, we have demonstrated that over 40% of patients with IGHD will have an ENH and absence of the infundibulum. We believe that the growth hormone deficiency in these patients is related to the absent infundibulum. IGHD should no longer be used to describe these patients, since they are no longer idiopathic. A better term might be growth hormone deficiency associated with an ENH. The cause of growth hormone deficiency in the IGHD patients without an ENH still remains unknown.

REFERENCES

1. Kaplan SA. Growth and growth hormone. In: Kaplan SA, ed. *Clinic pediatric endocrinology.* Philadelphia: Saunders, **1990**:1–62
2. Sabshin JK. The pituitary gland—anatomy and embryology. In: Goodri I, Lee K-J, eds. *The pituitary.* Amsterdam-New York-Oxford: Elsevi **1987**:19–26
3. Mac Gillivray MH. Disorders of growth and development. In: Felig P, Baxt JD, Broadus AE, Forohman LA, eds. *Endocrinology and metabolism.* Ne York: McGraw-Hill, **1987**:1581–1628
4. Fujisawa I, Kikuchi K, Nishimura K, et al. Transection of the pituitary sta development of an ectopic posterior lobe assessed with MR imagin *Radiology* **1987**;165:487–489
5. Kikuchi K, Fujisawa I, Momoi T, et al. Hypothalamic-pituitary function growth hormone-deficient patients with pituitary stalk transection. *J C Endocrinol Metab* **1988**;67:817–823
6. Kelly WM, Kucharczyk W, Kucharczyk J, et al. Posterior pituitary ectopi an MR feature of pituitary dwarfism. *AJNR* **1988**;9:453–460
7. Shizume K, Harada Y, Ibavashi Y. Survey studies on pituitary diseases Japan. *Endocrinol Jpn* **1977**;24:139–147
8. Inoue Y, Nemoto Y, Fujita K, et al. Pituitary dwarfism: CT evaluation of tl pituitary gland. *Radiology* **1986**;159:171–173
9. Truwit CL, Barkovich AJ. Pathogenesis of intracranial lipoma: an MR stu of 42 patients. *AJNR* **1990**;11:665–674
10. Rosenfield NS, Abrahams JJ. Brain MR in patients with Langerhans c histiocytosis: finding and enhancement with Gd-DTPA. *Pediatr Radi* **1990**;20:433–436
11. Tien RD, Newton TH, McDermott MW, et al. Thickened pituitary stalk MR images in patients with diabetes insipidus and Langerhans cell histi cytosis. *AJNR* **1990**;11:703–708

# MR Imaging in Chronic Partial Epilepsy: Role of Contrast Enhancement

Allen D. Elster[1]
Waqar Mirza[2]

**Gadopentetate dimeglumine was administered prospectively to 150 consecutive patients who had had partial epilepsy for longer than 1 year to determine whether it is routinely indicated for the diagnosis of this disorder. MR abnormalities correlating with clinical or electroencephalographically documented seizure foci were detected in 69 cases (46%). Contrast enhancement was seen in 33 of these lesions, but the presence of enhancement altered the original radiologic diagnosis in only 17 (11%) of 150 cases. In only two cases (1%) did contrast administration reveal lesions that were not definitely apparent on the unenhanced images. The utility of contrast administration could not be predicted on the basis of seizure type (simple or complex) or the presence of secondary generalization.**

**Gadopentetate dimeglumine does not appear to be routinely required in the MR workup of patients with chronic partial epilepsy. It should be used selectively to clarify or better define the nature of abnormalities encountered on unenhanced images.**

*AJNR* 12:165–170, January/February 1991; *AJR* 156:605–610, March 1991

The importance of MR imaging in evaluating patients with partial seizures has been demonstrated convincingly [1–19]. Even when unenhanced MR has been compared with contrast-enhanced CT, the superiority of MR has been well established [1–7, 18]. MR has been shown to be of particular value in epilepsies of temporal lobe origin, since lesions in the inferior temporal lobes may be inapparent on CT because of beam-hardening artifacts.

Recently, the accuracy of cranial MR diagnosis has been improved by the introduction of a paramagnetic contrast agent, gadopentetate dimeglumine [20–29]. The routine use of this agent has been proved to increase the detection rate of certain intracranial lesions, especially those of a vascular nature and those involving the meninges [20, 21, 24]. Moreover, gadopentetate dimeglumine may significantly improve radiologic specificity, particularly with regard to defining the extent or nature of certain neoplasms and the differentiation of aggressive processes from benign ones [20, 25, 28]. Although gadopentetate dimeglumine may be useful for delineating or characterizing a large number of intracranial diseases, its utility for the evaluation of seizure patients remains largely uninvestigated. Therefore, we designed a prospective study to determine the efficacy of routine administration of gadopentetate dimeglumine in a large population of patients with partial seizures referred for routine cranial MR imaging.

## Subjects and Methods

The subjects comprised a group of consecutive patients with partial epilepsy of longer than 1 year in duration who were referred for cranial MR imaging over a 17-month period. The mean age of the subjects was 27.6 years (range, 2–76 years). Forty pediatric patients (under age 18) were studied with Institutional Review Board approval after informed consent was obtained from a parent or guardian. Eight patients who could not complete the exami-

Received May 8, 1990; revision requested August 9, 1990; revision received September 6, 1990; accepted September 6, 1990.

[1] Department of Radiology, Bowman Gray School of Medicine, Wake Forest University, 300 S. Hawthorne Rd., Winston-Salem, NC 27103. Address reprint requests to A. D. Elster.

[2] Department of Neurology, Bowman Gray School of Medicine, Wake Forest University, Winston-Salem, NC 27103.

0361–803X/91/1563–0605
© American Roentgen Ray Society

**TABLE 1: Classification of Partial Epileptic Seizures in Study Population**

| Seizure Type | No. |
|---|---|
| Simple partial seizures, focal or localized, without impairment of consciousness | 10 |
| Complex partial seizures, focal, but with impairment of consciousness | 79 |
| Combined complex and simple partial seizures | 12 |
| Partial seizures evolving to secondarily generalized seizures | 49 |

Note.—Descriptions derived from the international classification of epileptic seizures [30].

nation owing to illness or inadequate sedation were excluded from the study. Because of motion or technical artifacts, the images of nine other patients were judged to be inadequate. These subjects were also excluded from the series until 150 patients with technically satisfactory MR examinations were enrolled.

Before imaging, all patients were evaluated by an experienced epileptologist. All patients also underwent electroencephalographic (EEG) monitoring to document their seizure focus. The specific subtype of partial seizure disorder for each patient was then classified on the basis of criteria [30] developed by the International League Against Epilepsy (Table 1).

MR imaging was performed exclusively at a field strength of 1.5 T (Vista MR unit, Picker, Highland Heights, OH). Unenhanced spin-density and T2-weighted coronal images and T1-weighted sagittal or axial images were obtained routinely. Gadopentetate dimeglumine (Magnevist, Berlex Laboratories, Wayne, NJ) was administered by IV infusion at a dose of 0.1 mmol/kg. T1-weighted coronal and axial images were obtained beginning approximately 5 min after infusion.

Specific imaging parameters varied somewhat with the plane of imaging. T1-weighted sequences obtained before and after contrast administration were exclusively spin-echo, 600/20/2 (TR/TE/excitations). Other imaging parameters included a slice thickness of 5–6 mm, field of view of 20–25 cm, and image acquisition matrix of 256 × 256. Spin-density- and T2-weighted sequences, 2000–2500/20,80/1 (TR/TE/excitations), were used in all patients, with other parameters similar to those of the T1-weighted images. A gradient moment nulling technique (MAST, Picker) was used on all T2-weighted sequences, since it has been shown to be highly effective for reducing phase-shift artifacts intracranially, particularly over the temporal lobes [31, 32].

The unenhanced images alone were first interpreted by an experienced neuroradiologist who was blinded to knowledge of seizure subtype and EEG focus. After his initial principal radiologic diagnosis was recorded, the reader was shown the enhanced images and asked to assess whether contrast enhancement (or lack thereof) altered the principal unenhanced diagnosis. These data were later correlated with surgical pathology (when available) as well as neurologic and EEG assessment.

## Results

Of the 150 cases studied, 69 (46%) demonstrated MR abnormalities that by clinical or EEG assessment were thought to correlate with the patient's seizure focus. The final radiologic diagnoses in the 150 patients are recorded in Table 2. Radiologic rather than pathologic diagnoses are recorded, since most of the 150 patients had either normal scans or clinically benign lesions and were medically manageable. In the 17 patients who underwent surgery, no significant discrepancies were encountered between the radiologic and pathologic diagnoses (Table 3).

The imaging findings with regard to contrast enhancement are presented in Table 4. Contrast enhancement was seen in 33 (48%) of the 69 detected lesions. All but two of these lesions, however, could be definitely seen on the unenhanced study. The two lesions representing false-negative unenhanced diagnoses are shown in Figures 1 and 2.

In 17 cases (11% of the study population), the presence of contrast enhancement was believed to modify in some way the initial unenhanced radiologic diagnosis (Table 5). In seven of these lesions the role of contrast enhancement was to better define the size or nature of suspected neoplasms. In two cases contrast-enhanced images only demonstrated inflammatory foci within areas of edema (Fig. 3). In four cases the presence of contrast enhancement radically changed the unenhanced diagnosis from a nonneoplastic to tumor category (Figs. 4 and 5).

Because relatively few patients derived significant benefit from contrast administration, no good predictors could be established of when gadopentetate dimeglumine would prove useful. The 17 cases in which contrast enhancement proved useful spanned the complete gamut of clinical presentation, seizure subtype, and duration of symptoms. Accordingly,

**TABLE 2: Primary Radiologic Diagnosis in Patients with Partial Seizures**

| Seizure Origin | No. |
|---|---|
| Normal/no causative abnormality | 81 |
| Neoplasm | 19 |
| Trauma/postoperative | 14 |
| Vascular malformation | 12 |
| Congenital/developmental | 9 |
| Mesial temporal sclerosis | 7 |
| Stroke/infarct | 5 |
| Other | 3 |

**TABLE 3: Abnormalities Found in Operated Patients**

| Diagnosis | No. ($n$ = 17) | | |
|---|---|---|---|
| | Total | Seen Before Enhancement | No. Enhancing |
| Astrocytoma | 6 | 6 | 3 |
| Oligodendroglioma | 1 | 1 | 1 |
| Oligoastrocytoma | 1 | 1 | 1 |
| Ganglioglioma | 1 | 1 | 1 |
| Cavernous angioma | 5 | 5 | 5 |
| Sclerosis/gliosis | 2 | 2 | 0 |
| Abscess | 1 | 1 | 1 |

**TABLE 4: Imaging Findings in Patients with Chronic Partial Epilepsy**

| Enhancement of Lesion | Finding Before Enhancement | |
|---|---|---|
| | Normal | Abnormal |
| Yes | 2 | 31 |
| No | 81 | 36 |
| Total | 83 | 67 |

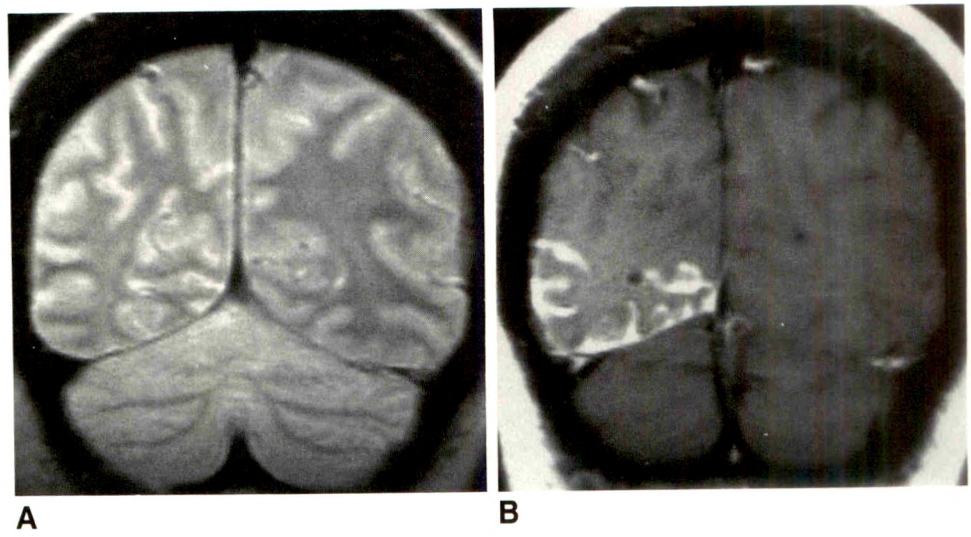



Fig. 1.—37-year-old woman with port-wine nevus on right side of face and 24-year history of complex partial seizures.

*A*, Unenhanced T2-weighted MR image is normal.

*B*, Enhanced T1-weighted image shows extensive leptomeningeal abnormality confirming intracranial component of Sturge-Weber syndrome.

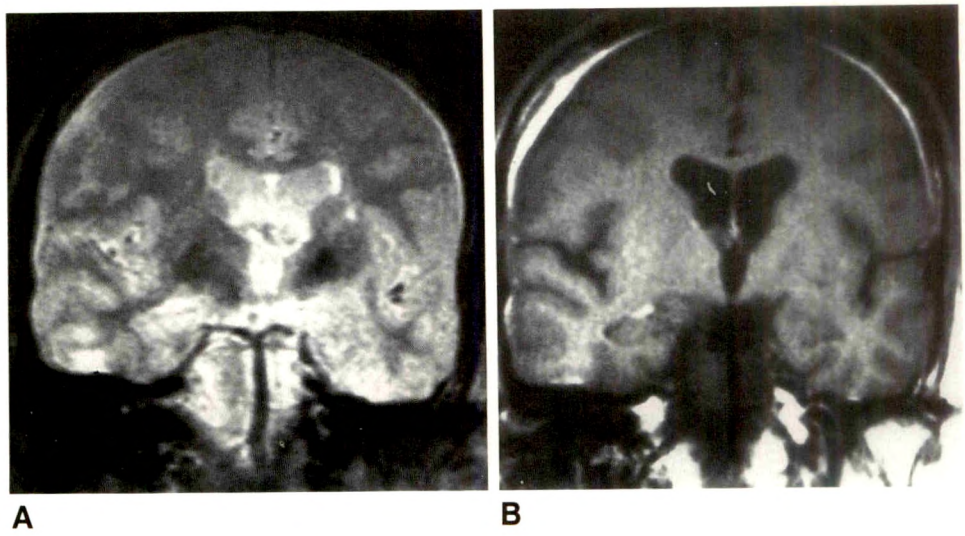



Fig. 2.—29-year-old man with 1-year history of partial seizures with secondary generalization.

*A*, Unenhanced T2-weighted image is essentially normal, degraded somewhat by motion artifact. In retrospect, there may be a subtle abnormality in right calvaria.

*B*, Enhanced T1-weighted image shows definitely abnormal foci in right parietal and left temporal bones with associated dural thickening. Pathologic diagnosis was metastatic cancer from a mediastinal germ cell neoplasm.

**TABLE 5: How Contrast Enhancement Altered the Radiologic Diagnoses in Patients with Partial Epilepsy**

| Type of Assistance | No. ($n$ = 150) |
|---|---|
| Better definition of margins, extent, grade, or nature of suspected neoplasm | 7 |
| Better delineated extent of vascular anomaly | 3 |
| Confirmation of recurrent tumor in operative bed | 2 |
| Delineation of infection or abscess | 2 |
| Other/miscellaneous | 3 |

neither the subtype of seizure (Table 1), the presence of definitive EEG focus, nor the length of time the patient had experienced seizures was helpful for deciding whether to use contrast material.

## Discussion

A number of articles have now documented the superiority of MR imaging over CT for the evaluation of patients with partial epilepsy [1–19]. In 1985, Laster et al. [1] reviewed 34 patients with epilepsy of longer than 5 years in duration who had normal contrast-enhanced CT scans. In four patients, lesions of potential surgical significance were seen only on MR. Two of these underwent surgical resection, revealing a glioma and thrombosed vascular malformation.

In another early study, Ormson et al. [6] compared the sensitivities of contrast-enhanced CT with unenhanced MR in 25 patients with refractory partial epilepsy. MR was found to be superior to CT for the detection of low-grade gliomas in these patients, but neither technique effectively identified most cases of surgically proved hippocampal sclerosis.

Latack et al. [3] first compared CT, MR, and positron emission tomographic (PET) findings in patients with 50 partial seizures. Again, the superiority of MR over CT was demonstrated convincingly. Additionally, the potential contribution of PET scanning in this disorder was first established.

Since these early studies, numerous other articles have appeared that support the general superiority of MR over CT

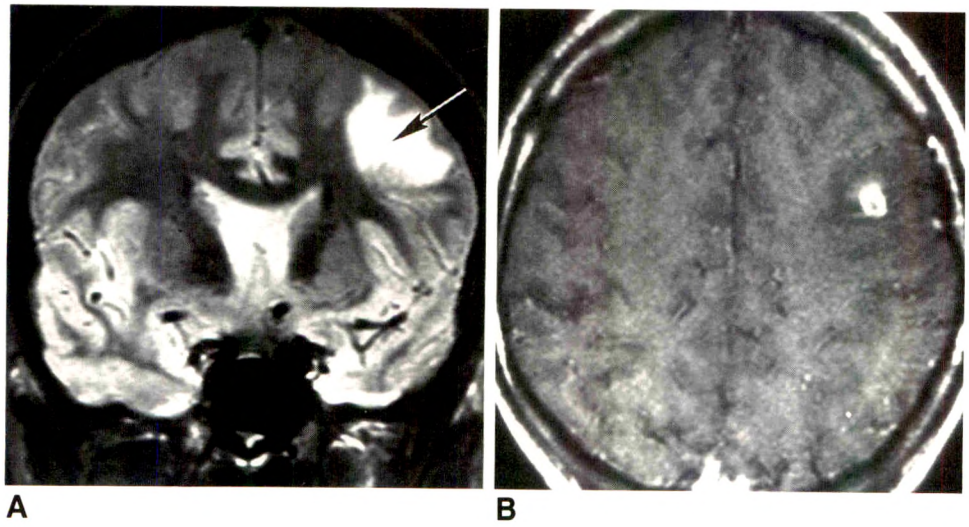



Fig. 3.—23-year-old farm worker with simple partial seizures for 3 years, now increasing in severity.

*A*, Unenhanced T2-weighted image reveals vasogenic edema in left posterior frontal lobe (*arrow*).

*B*, Enhanced image reveals tiny, round, enhancing nodule. A second smaller nodule (*not shown*) was also found in occipital lobe. Pathologic diagnosis: neurocysticercosis.

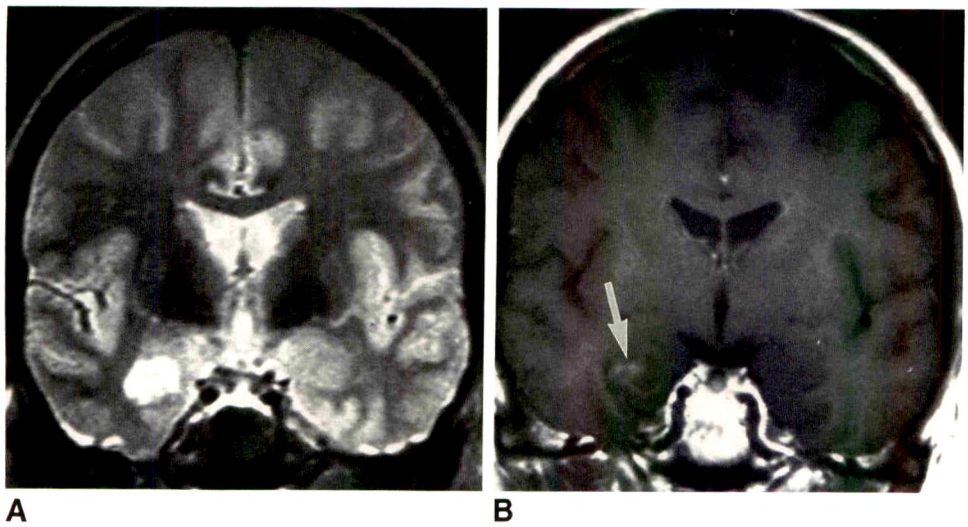



Fig. 4.—37-year-old man with complex partial seizures.

*A*, T2-weighted image shows high-signal lesion in medial right temporal pole. Speculative diagnosis was hippocampal sclerosis.

*B*, Enhanced T1-weighted image reveals subtle enhancement (*arrow*) of lesion, consistent with a low-grade glioma rather than mesial temporal sclerosis.

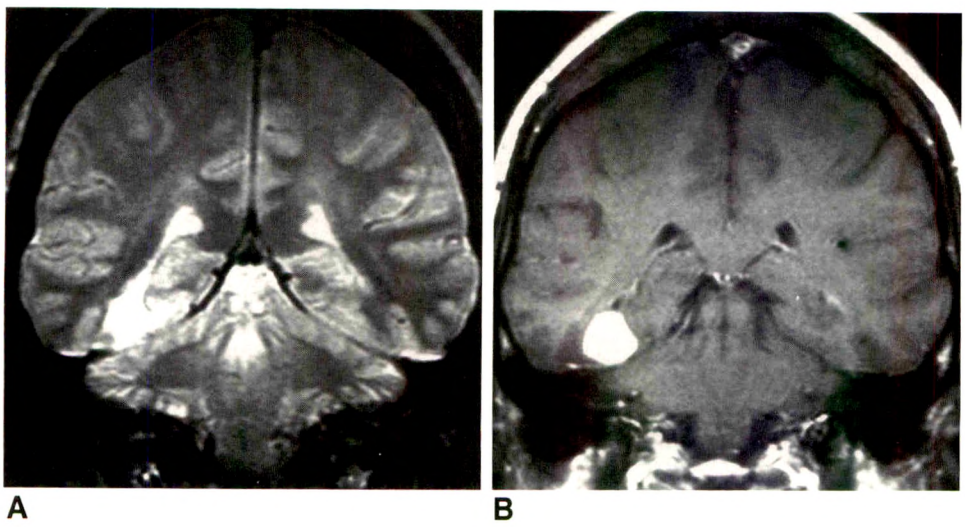



Fig. 5.—18-year-old woman with 3-year history of simple partial seizures with secondary generalization.

*A*, T2-weighted MR image shows peripheral wedge-shaped high-signal abnormality in right occipital lobe. Unenhanced diagnosis: old infarct or scar; neoplasm also to be considered.

*B*, Intense enhancement on T1-weighted image changes radiologic diagnosis strongly in support of a neoplasm. Pathology: ganglioglioma.

for evaluating patients with partial epilepsy. Depending on the series chosen, the increased diagnostic yield of MR over CT varies from about 8% to 20% [2–5, 7–19]. The advantage of MR over CT in these studies stems largely from increased detection of lesions in the temporal lobes and at the vertex. These areas are often visualized poorly on axial CT scans because of partial-volume effects or beam-hardening artifacts. Over the last 3 years, the use of paramagnetic contrast agents has significantly affected cranial MR diagnosis. A number of studies have now documented both an increase in sensitivity [20, 21, 24] and specificity [20, 25, 28] resulting from the adjunctive use of gadopentetate dimeglumine in the MR imaging of a variety of intracranial diseases. Until recently, however, the role of gadopentetate dimeglumine in the evaluation of seizure patients has remained largely uninvestigated.

This topic was first addressed as a side issue in the large prospective series reported by Elster et al. [20], where the utility and cost-effectiveness of routine gadopentetate dimeglumine administration was first analyzed. These investigators administered gadopentetate dimeglumine prospectively to 500 consecutive patients with a variety of neurologic problems, including seizures. A multifactorial analysis of their data revealed the clinical indication of "seizures" to be a relatively poor predictor for when gadopentetate dimeglumine would prove radiologically useful. However, Elster et al. did not analyze their patients with regard to seizure subtype, duration of symptoms, or clinical presentation.

While our large prospective study was underway, Cascino et al. [19] published a preliminary report describing their experience with contrast-enhanced MR imaging in 23 seizure patients. Their study population comprised a select group of surgical candidates with intractable epilepsy. In their series, 26% of patients had enhancing lesions, but contrast enhancement was not reported to increase specificity or diagnostic accuracy in any case.

Conversely, our prospective series was designed to encompass a wide range of seizure patients: both those with intractable seizures slated for surgery and those with seizures that could be managed medically. While surgical proof of diagnosis was obtained in relatively few of our patients, we believe our prospective study better represents the more typical neurology-based population of seizure patients, that is, those with mostly benign disease who can be successfully managed medically.

In this group of patients, the routine administration of gadopentetate dimeglumine is probably not indicated. In only two of 150 patients (Figs. 1 and 2) would significant lesions potentially have been missed without the use of contrast material. Review of appropriate medical history in these two patients would have revealed suspected Sturge-Weber syndrome in one and prior extracranial neoplasm in the other. Both clinical scenarios are now recognized to represent relatively high-yield indications for the routine administration of MR contrast agents [20, 33–35]. Thus, if proper medical history is obtained, the risk of missing a significant intracranial lesion in a patient with chronic partial seizures seems low.

Conversely, when a lesion is identified before enhancement, administration of gadopentetate dimeglumine may provide additional diagnostic benefits. Such benefits include increased diagnostic confidence, improved delineation of lesion margins, and improved ability to differentiate between indolent and aggressive lesions. Representative examples of this utility have been shown in Figures 3–5, and have been amply illustrated previously in works by Elster et al. [20, 29], Runge et al. [28], and others [25, 27, 35].

It should be stressed, however, that the alteration of radiologic diagnoses through the use of MR contrast agents does not necessarily translate into a change in clinical management. Frequently, patient management decisions hinge only indirectly around the results of imaging studies at all, and are difficult to study in an unbiased manner. For example, some aggressive surgeons may biopsy or resect all accessible tumors regardless of their imaging characteristics; others may elect to observe nonenhancing or benign-appearing lesions. If stereotaxic biopsy is considered, contrast enhancement of a focus within the lesion provides a relatively high-yield biopsy site. This information may not be needed if an open biopsy is planned, however. In summary, therefore, the utility of gadopentetate dimeglumine for radiologic diagnosis always exceeds its ultimate clinical impact, and this impact will vary further depending on the sophistication and philosophy of the referring physician.

As a final caveat, it should also be emphasized that the conclusions of our report cannot necessarily be extended to patients with all forms of epilepsy. Our findings relate only to patients with partial seizures of relatively long duration (greater than 1 year). Patients with primary generalized epilepsies and patients with partial seizures of recent onset may benefit more or less from the administration of gadopentetate dimeglumine.

In conclusion, the use of gadopentetate dimeglumine in patients with chronic partial epilepsy does not seem to be warranted routinely. Unenhanced images will affect the initial radiologic diagnosis in only 11% of cases, and the likelihood of missing an important abnormality by performing unenhanced imaging alone is small. Gadopentetate dimeglumine should thus continue to be used selectively in patients with chronic partial epilepsy to clarify or better define the nature of abnormalities encountered on unenhanced scans.

## REFERENCES


1. Laster DW, Perry JK, Moody DM, Ball MR, Witcofski RL, Riela AR. Chronic seizure disorders: contribution of MR imaging when CT is normal. *AJNR* **1985**;6:177–180
2. Schörner W, Meencke HJ, Felix R. Temporal-lobe epilepsy: comparison of CT and MR imaging. *AJR* **1987**;149:1231–1239
3. Latack JT, Abou-Khalil BW, Siegel GJ, et al. Patients with partial seizures: evaluation by MR, CT, and PET imaging. *Radiology* **1986**;159:159–163
4. Jabbari B, Gunderson CH, Frantz W, et al. Magnetic resonance imaging in partial complex epilepsy. *Arch Neurol* **1986**;43:869–872
5. Conlon P, Trimble MR, Rogers D, Callicott C. Magnetic resonance imaging in epilepsy: a controlled study. *Epilepsy Res* **1988**;2:37–43
6. Ormson MJ, Kispert DB, Sharbrough FW, et al. Cryptic structural lesions in refractory partial epilepsy: MR imaging and CT studies. *Radiology* **1986**;160:215–219
7. Theodore WH, Dorwart R, Holmes M, Porter RJ, Di Chiro G. Neuroimaging

in refractory partial seizures: comparison of PET, CT, and MRI. *Neurology* **1986**;36:750–759
8. Sperling MR, Wilson G, Engel J, et al. Magnetic resonance imaging in intractable partial epilepsy: correlative studies. *Ann Neurol* **1986**;20:57–62
9. Kuzniecky R, De La Sayette V, Ethier R, et al. Magnetic resonance imaging in temporal lobe epilepsy: pathologic correlations. *Ann Neurol* **1987**; 22:341–347
10. Aaron J, New PFJ, Strand R, et al. NMR imaging in temporal lobe epilepsy due to gliomas. *J Comput Assist Tomogr* **1984**;8:608–613
11. Smith AS, Weinstein MA, Quencer RM, et al. Association of heterotopic gray matter with seizures: MR imaging. *Radiology* **1988**;168:195–198
12. Maertens PM, Machan BC, Williams JP, et al. Magnetic resonance imaging of mesial temporal sclerosis: case reports. *J Comput Tomogr* **1987**; 11:136–139
13. Kramer RE, Lüders H, Lesser RP, et al. Transient focal abnormalities of neuroimaging studies during focal status epilepticus. *Epilepsia* **1987**;28:528–532
14. Lesser RP, Modic MT, Weinstein MA, et al. Magnetic resonance imaging (1.5 tesla) in patients with intractable focal seizures. *Arch Neurol* **1986**;43:367–371
15. Triulzi F, Franceschi M, Fazio F, DelMaschio A. Nonrefractory temporal lobe epilepsy: 1.5 T MR imaging. *Radiology* **1988**;166:181–185
16. Gerard G, Shabas D, Rossi D. MRI in epilepsy. *Comput Radiol* **1987**; 11:223–227
17. Brooks BS, King DW, El Gammal T, et al. MR imaging in patients with intractable complex partial epileptic seizures. *AJNR* **1990**;11:93–99
18. Heinz ER, Heinz TR, Radtke R, et al. Efficacy of MR vs CT in epilepsy. *AJNR* **1988**;9:1123–1128
19. Cascino GD, Hirschorn KA, Jack CR, Sharbrough FW. Gadolinium-DTPA–enhanced magnetic resonance imaging in intractable partial epilepsy. *Neurology* **1989**;39:1115–1118
20. Elster AD, Moody DM, Ball MR, Laster DW. Is Gd-DTPA required for routine cranial MR imaging? *Radiology* **1989**;173:231–238
21. Breger RK, Papke RA, Pojunas KW, et al. Benign extraaxial tumors: contrast enhancement with Gd-DTPA. *Radiology* **1987**;163:427–429
22. Brant-Zawadzki M, Berry I, Osaki L, et al. Gd-DTPA in clinical MR of the brain. 1. Intraaxial lesions. *AJNR* **1986**;7:781–788, *AJR* **1986**;147: 1223–1230
23. Berry I, Brant-Zawadzki M, Osaki L, et al. Gd-DTPA in clinical MR of the brain. 2. Extraaxial lesions and normal structures. *AJNR* **1986**;7:789–793, *AJR* **1986**;147:1231–1235
24. Haughton VM, Rimm AA, Czervionke LF, et al. Sensitivity of Gd-DTPA–enhanced MR imaging of benign extraaxial tumors. *Radiology* **1988**;166: 829–833
25. Russell EJ, Schaible TF, Dillon W, et al. Multicenter double-blind placebo-controlled study of gadopentate dimeglumine as an MR contrast agent: evaluation in patients with cerebral lesions. *AJNR* **1989**;10:53–63
26. Sze G, Shin J, Krol G, et al. Intraparenchymal brain metastases: MR imaging versus contrast-enhanced CT. *Radiology* **1988**;168:187–194
27. Powers TA, Partain CL, Kessler RM, et al. Central nervous system lesions in pediatric patients: Gd-DTPA–enhanced MR imaging. *Radiology* **1988**;169:723–726
28. Runge VM, Schaible TF, Goldstein HA, et al. Gd-DTPA clinical efficacy. *RadioGraphics* **1988**;8:147–179
29. Elster AD, Rieser GD. Gd-DTPA–enhanced cranial MR imaging in children: initial clinical experience and recommendations for its use. *AJNR* **1989**;10:1027–1030
30. Commission on Classification and Terminology of the International League Against Epilepsy. Proposal for revised clinical and electroencephalographic classification of epileptic seizures. *Epilepsia* **1981**;22:489–501
31. Elster AD. Motion artifact suppression technique (MAST) for cranial MR imaging: superiority over cardiac gating for reducing phase-shift artifacts. *AJNR* **1988**;9:671–674
32. Quencer RM, Hinks RS, Pattany PH, Horen M, Post MJD. Improved MR imaging of the brain by using compensating gradients to suppress motion-induced artifacts. *AJNR* **1988**;9:431–438
33. Elster AD, Chen MYM. MR imaging in Sturge-Weber syndrome: role of gadopentetate dimeglumine and gradient-echo techniques. *AJNR* **1990**;11:685–689
34. Lipski S, Brunelle F, Aicardi J, Hirsch JF, Lallemand D. Gd-DOTA–enhanced MR imaging in two cases of Sturge-Weber syndrome. *AJNR* **1990**;11:690–692
35. Sze G, Milano E, Johnson C, Heier L. Detection of brain metastases: comparison of contrast-enhanced MR with unenhanced MR and enhanced CT. *AJNR* **1990**;11:785–791

# Diagnosis of Carotid Artery Stenosis: Comparison of 2DFT Time-of-Flight MR Angiography with Contrast Angiography in 50 Patients

Andrew W. Litt[1]
Elizabeth M. Eidelman[1]
Richard S. Pinto[1]
Thomas S. Riles[2]
Stuart J. McLachlan[3]
Sicco thoe Schwartzenberg[2]
Jeffrey C. Weinreb[1]
Irvin I. Kricheff[1]

**Fifty patients underwent 2DFT time-of-flight MR angiography and intraarterial contrast angiography for evaluation of possible carotid atherosclerotic disease. The MR angiography technique employed contiguous axial flow-sensitive (short TR/TE) slices that were reformatted and postprocessed by using a maximum-intensity projection algorithm to provide 16 angiographic views of the carotid arteries. Both studies were independently reviewed by two observers in a blinded manner. Carotid arteries were categorized as normal, mildly stenotic, moderately stenotic, severely stenotic, or occluded. For the 94 carotid arteries available for review, one observer reported a 70% agreement between the two techniques and the second observer reported a 56% agreement ($p = .0001$). The best correlation was in the severely stenotic category and the worst was in the occluded category. Agreement between observers was 67% for MR angiography and 72% for contrast angiography, which was similar to that between the two techniques. Although not all carotid atherosclerotic disease was visualized equally well, 2DFT time-of-flight MR angiography had a good overall correlation with the "gold standard" of intraarterial contrast angiography, supporting its use as a screening technique. While further improvements are needed, use of MR angiography as the primary diagnostic tool for many patients with suspected carotid stenosis should continue to increase.**

*AJNR* 12:149–154, January/February 1991; *AJR* 156:611–616, March 1991

Cerebrovascular disease is the third leading cause of death in the United States, and ischemic disease caused by atherosclerotic carotid artery disease is responsible for the vast majority of strokes [1]. Accordingly, much effort has been directed toward developing noninvasive methods for evaluating the carotid bifurcation. For example, several recent reports have described MR techniques that exploit and manipulate either the phase phenomenon [2–5] or the time-of-flight effects [6–9] characteristic of flowing spins in imaging the extracranial carotid arteries.

While initially successful in visualizing the normal carotid bifurcation, phase contrast subtraction techniques could not image stenoses accurately because velocity variation within the imaging voxel caused phase cancellation and thus signal void at and distal to the diseased segment [4]. Using a time-of-flight volumetric (3DFT) gradient-echo technique, Masaryk et al. [7] compared MR angiograms with intraarterial digital subtraction angiography (DSA) in 12 patients with good correlation between the two methods (Masaryk et al. Paper presented at the annual meeting of the Radiological Society of North America, Chicago, November 1989). However, in three-dimensional imaging techniques, because the entire volume is being excited with each TR, signal loss due to saturation occurs as blood flows deeper into the volume being scanned. This may create problems in evaluating the distal internal carotid artery. Moreover, in vessels with very slow flow, such as the carotid dissection, the spins within the vessel will become saturated, reducing their signal and possibly making detection of this condition more difficult.

In two-dimensional (2DFT) time-of-flight sequences the relative contrast between the flowing blood and stationary tissues is increased by the high signal of the

Received May 9, 1990; revision requested July 5, 1990; revision received August 1, 1990; accepted August 1, 1990.

Presented at the annual meeting of the American Society of Neuroradiology, Los Angeles, March 1990.

[1] Department of Radiology, New York University Medical Center, 560 First Ave., New York, NY 10016. Address reprint requests to A. W. Litt.

[2] Department of Vascular Surgery, New York University Medical Center, New York, NY 10016.

[3] Philips Medical Systems North America, Shelton, CT 06484.

0361–803X/91/1563–0611
© American Roentgen Ray Society

maximally magnetized spins as they flow into the slice. These 2DFT sequences have also been used to obtain images of the carotid arteries [6, 8], although the applicability of this technique to depicting the diseased carotid artery has not previously been explored. We used a 2DFT time-of-flight technique to study patients with suspected carotid artery disease and compared the results with those obtained by using intraarterial contrast angiography to evaluate the accuracy of MR angiography in imaging carotid artery stenosis.

## Materials and Methods

Between March 1989 and March 1990, 50 patients were referred for MR angiography of the carotid arteries. All patients were being evaluated for suspected atherosclerotic extracranial carotid artery disease and had previously undergone contrast angiography. The MR was performed within 24 hr of the contrast angiogram in 32 patients, within 7 days in six patients, and within 4 months in 12 patients. The patients (28 men and 22 women) ranged in age from 31 to 87 years (mean, 65.8 years).

All patients were studied on a standard 1.5-T MR system (Philips Gyroscan S15) with 10 mT/m gradients using the routine head/neck coil. MR angiograms of the carotid arteries were acquired by using a 2DFT time-of-flight technique (Groen et al., paper presented at the annual meeting of the Society of Magnetic Resonance in Medicine, San Francisco, August 1988) involving the acquisition of 50–60 thin (2–3 mm), contiguous or overcontiguous, axial slices, using a spoiled gradient-echo sequence that was first-order flow compensated in read- and slice-selection directions. The MR signal from stationary tissue was suppressed owing to the short repetition times, typically 40–60 msec, and the use of large flip angles, 60–90°, while high signal was obtained from unsaturated blood flowing into the slice. Other scan parameters were TE = 14–22, field of view = 250 mm, matrix size = 180 × 256, and two excitations. The axial slices typically required 14 min for acquisition.

To suppress the venous flow, a presaturation slab, 50 mm thick, was applied at a 2.5-mm offset cephalad to the slice being imaged. The presaturation slab tracked with the slice to ensure consistent venous saturation. Relaxation of the slice-refocusing gradient allowed for a small amount of slice dephasing that provided additional suppression of the stationary tissue.

Projection MR angiograms were created from the stack of 2D slices by the use of a maximum-intensity projection algorithm. Sixteen projections were obtained at 8° intervals starting from the straight anteroposterior view. They were then displayed as a cine movie loop or filmed as individual hard-copy images. The projection processing was carried out as a background batch job on the Gyroscan VAX 11/750 (Digital Equipment Corp., Maynard, MA) or in the array processor (AP500, Analogic Corp., Wakefield, MA). Typical processing time in VAX background mode for a full image projection is about 90 sec/projection while the corresponding time in the AP500 is 10 sec. To better visualize the anatomy, a user-defined region-of-interest was drawn around each carotid artery on one of the axial slices and was used to confine the 3D projection to a limited area (Simon et al. Paper presented at the annual meeting of the Radiological Society of North America, Chicago, November 1989). This minimized interference from other anatomy and significantly decreased the processing time.

Contrast arteriography was performed via femoral artery catheterization using either film-screen (37 patients) or digital subtraction (13 patients) technique. In three patients, only the right carotid artery was examined, using retrograde right brachial injections with film-screen technique; in one case, only the left carotid artery was studied for clinical reasons.

Both MR and contrast angiograms were reviewed retrospectively. Each study was independently read by two trained neuroradiologists blinded to the patient's name and clinical history, the results of the other study, and the interpretation of the other observer. A "forced-choice" evaluation of the internal carotid artery at and just above the carotid bifurcation was made on the basis of an estimate of carotid artery narrowing, with the studies reported as normal (0–15% stenosis), mild (16–49% stenosis), moderate (50–79% stenosis), severe

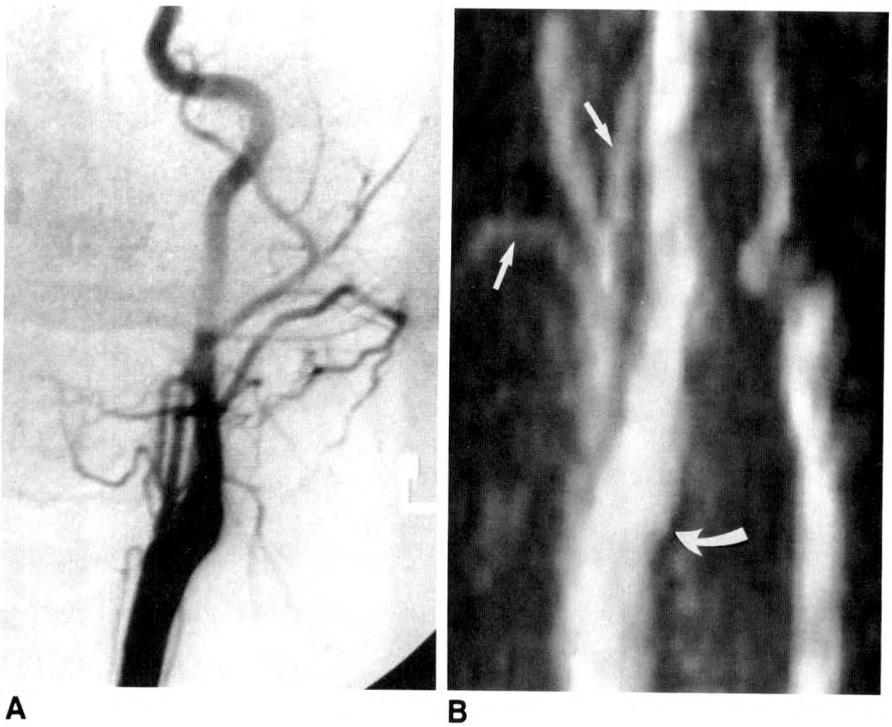



**Fig. 1.—*A* and *B*, Contrast (*A*) and MR (*B*) angiograms of a normal carotid bifurcation in a 38-year-old man. Note the normal carotid bulb (*curved arrow*) and the branches of the external carotid (*straight arrows*) in the MR image.**

(80–99% stenosis), or occluded. The original 2D axial slices were not used in evaluation of the MR angiograms. Correlation of results between techniques and between observers was calculated using the Spearman rank correlation test. This examines the nonrandomness of ranked (nonordinal) data in which no statement about the parameter mean can be made in advance.

## Results

Among the 50 patients studied, three left carotid arteries and one right carotid artery were excluded because they were not studied by contrast angiography. Despite the overall high quality of the MR angiographic images (Figs. 1–6), two other vessels were excluded because the MR angiogram of those vessels were thought to be indeterminate by at least one observer. This left 94 carotid arteries available for review.

Interpretations by the first observer (Table 1) showed MR and contrast angiography in agreement in 66 of 94 vessels for an overall correlation of 70% ($r = .84$, $p = .0001$). The highest level of correlation was in the severe category, with 95% of the vessels correctly diagnosed by MR. The greatest discrepancy between the techniques was in the occluded category, with only 29% correctly interpreted. Of those 28 vessels in which MR angiography did not match contrast angiography, the studies were only one category apart for all but four vessels.

The MR and contrast angiography readings of the second observer (Table 2) were identical in 53 of 94 vessels for a correlation of 56% ($r = .74$, $p = .0001$). Correlation was again best in the severe angiographic category (89%) and worst in the occluded category (25%). Of the 41 cases in which MR and angiography were not in agreement, only 10 were different by more than one category.

Correlation between observers 1 and 2 in interpreting the contrast angiograms was 68 of 94 vessels, or 72% ($r = .87$, $p = .0001$), with the best agreement in the severe category (Table 3). Agreement between observers 1 and 2 in interpreting the MR angiograms was 63 of 94, or 67% ($r = .83$, $p = .0001$), with the highest correlation again in the severe category (Table 4).

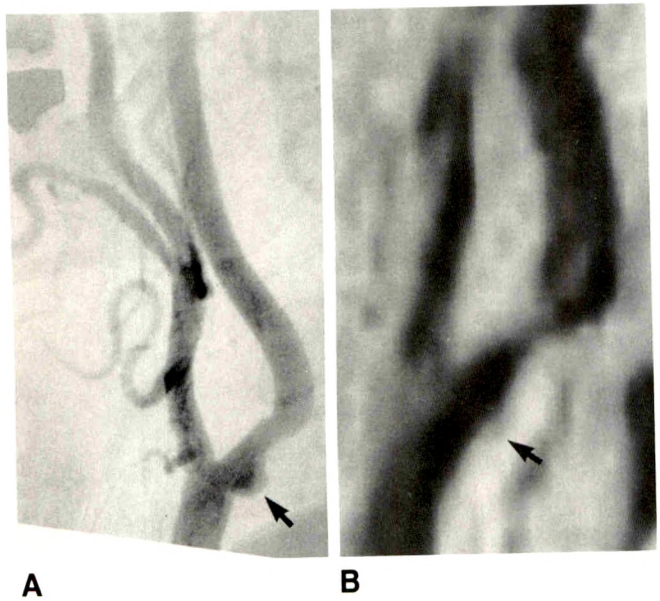



**Fig. 2.—*A* and *B*, Contrast (*A*) and MR (*B*) angiograms show good correlation in a case of mild stenosis. The outpouching or ulceration at the carotid bifurcation (*arrow*) is seen on both studies.**

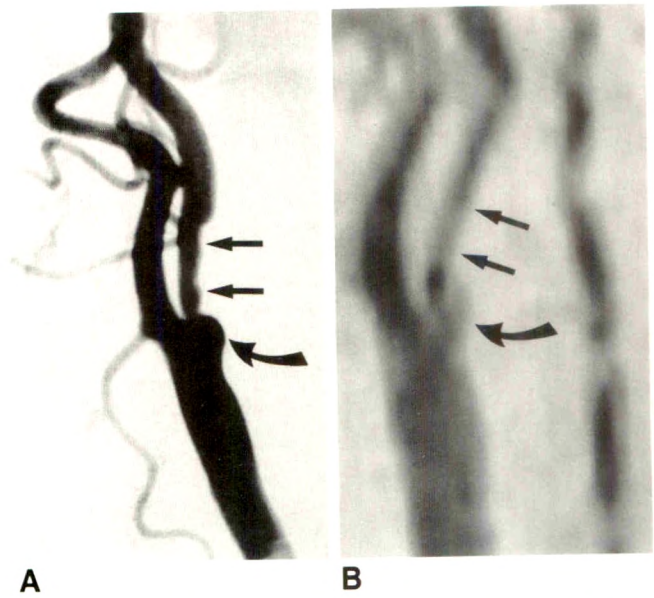



**Fig. 3.—*A* and *B*, Moderate stenosis is seen on both contrast (*A*) and MR (*B*) angiographic studies in a 73-year-old man. The length of the stenosis (*straight arrows*) appears longer on the MR image, possibly because of turbulence distal to the stenosis. The outpouching or ulceration (*curved arrow*) is well seen.**

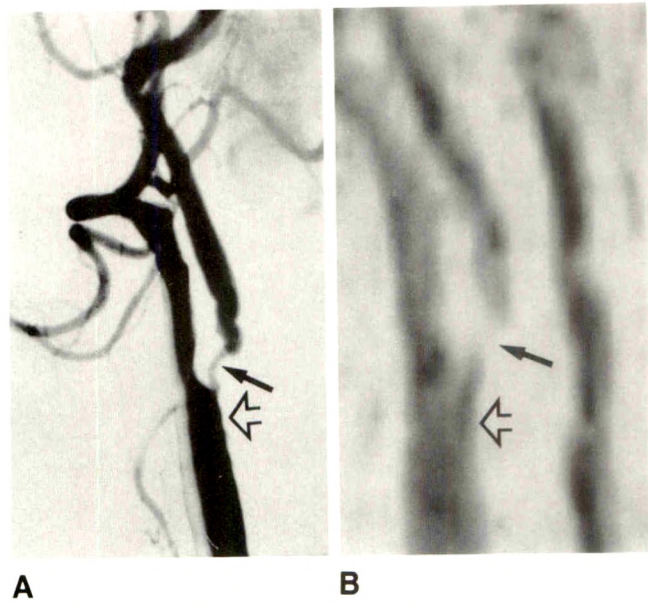



**Fig. 4.—*A* and *B*, Contrast (*A*) and MR (*B*) angiograms show severe carotid stenosis with some flattening of the carotid bulb (*open arrow*) proximal to the bifurcation, and faint visualization of the region of stenosis (*closed arrow*).**

## Discussion

The purpose of this study was to compare intraarterial contrast angiography with MR angiography using a 2D time-

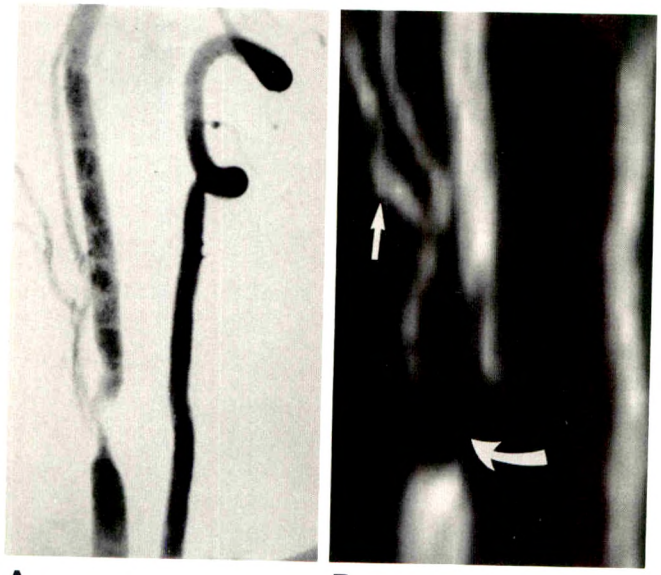



Fig. 5.—*A* and *B*, Contrast (*A*) and MR (*B*) angiograms in a case of severe stenosis. Although a branch of the external carotid is seen on the MR image (*straight arrow*), the area of stenosis is not visualized, presumably because of turbulence (*curved arrow*).

of-flight technique to evaluate the accuracy of the latter in imaging atherosclerotic disease of the extracranial carotid artery. Although numerous papers have described various MR angiographic techniques, the only one that compared MR with contrast angiography in the study of extracranial carotid arteries was reported by Masaryk et al. in 1989 [7]. That study, however, was done using a volumetric (3DFT) technique and examined only 15 patients. In this report, two observers independently interpreted each MR and contrast study in a blinded fashion. Intermethod as well as interobserver correlations were calculated. The two observers reached overall correlations of 70% and 56%, respectively, in comparing MR angiograms and contrast angiograms. These results are statistically significant for a study population of this size. This level of agreement is similar to that between the two observers for each study: they agreed 72% of the time on the intraarterial angiograms and 67% of the time on the MR angiograms. Thus, MR angiography was demonstrated to have a good statistical correlation when compared with the "gold standard" of contrast angiography.

In fact, the correlation on a routine clinical basis might actually be somewhat higher than demonstrated. Because the measurement of exact percentage of stenosis is often problematic, we elected to estimate the degree of stenosis

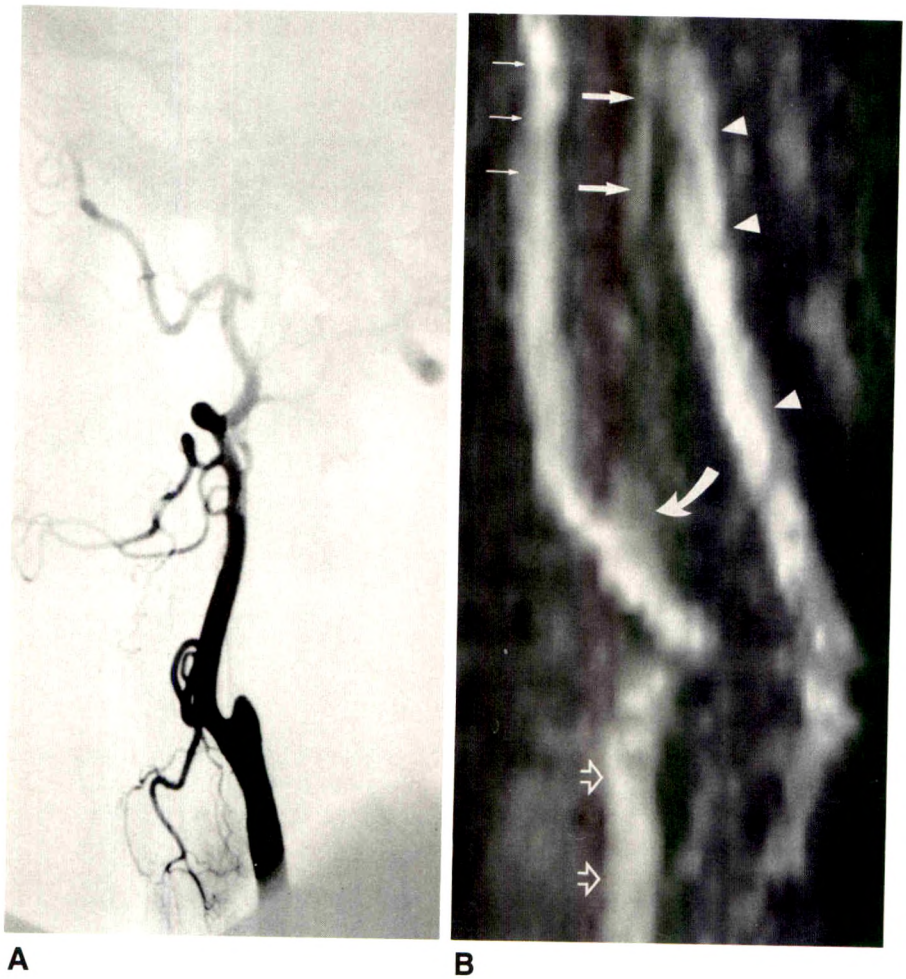



Fig. 6.—*A* and *B*, Views of contrast (*A*) and MR (*B*) angiography in a case of internal carotid occlusion. The common carotid artery (*open arrows*) is seen well, as are the main trunk of the external carotid artery (*small straight arrows*) and the vertebral artery (*arrowheads*). The proximal internal carotid artery (*curved arrow*) is seen just above the bifurcation. Note the faint vascular-appearing structure distal to the area of discontinuity on the MR image (*larger straight arrows*). It is difficult to determine whether this represents continuation of the internal carotid, a branch of the external carotid, or an artifact.

**TABLE 1: MR vs Contrast Angiography: Findings by Observer 1**

| | Contrast Angiography | | | | |
|---|---|---|---|---|---|
| | Normal (%) | Mild (%) | Moderate (%) | Severe (%) | Occluded (%) |
| MR Angiography | | | | | |
| Normal (%) | 5 (63) | 2 (9.5) | 0 | 0 | 0 |
| Mild (%) | 2 (25) | 14 (67) | 0 | 1 (2.5) | 0 |
| Moderate (%) | 1 (12) | 3 (14) | 8 (42) | 1 (2.5) | 0 |
| Severe (%) | 0 | 0 | 11 (58) | 37 (95) | 5 (71) |
| Occluded (%) | 0 | 0 | 0 | 0 | 2 (29) |

Note.—Percentages are relative to total number of cases in each contrast angiography category. Overall agreement for observer 1 was 70%.

**TABLE 2: MR vs Contrast Angiography: Findings by Observer 2**

| | Contrast Angiography | | | | |
|---|---|---|---|---|---|
| | Normal (%) | Mild (%) | Moderate (%) | Severe (%) | Occluded (%) |
| MR Angiography | | | | | |
| Normal (%) | 1 (11) | 1 (4) | 0 | 0 | 0 |
| Mild (%) | 4 (44) | 5 (23) | 0 | 0 | 0 |
| Moderate (%) | 1 (11) | 10 (45) | 3 (37) | 2 (4) | 0 |
| Severe (%) | 3 (33) | 6 (27) | 5 (63) | 42 (89) | 6 (75) |
| Occluded (%) | 0 | 0 | 0 | 3 (6) | 2 (25) |

Note.—Percentages are relative to total number of cases in each contrast angiography category. Overall agreement for observer 2 was 56%.

**TABLE 3: Contrast Angiography: Comparison of Interpretations by Observers 1 and 2**

| | Observer 2 | | | | |
|---|---|---|---|---|---|
| | Normal | Mild | Moderate | Severe | Occluded |
| Observer 1 | | | | | |
| Normal | 6 | 2 | 0 | 0 | 0 |
| Mild | 3 | 15 | 3 | 0 | 0 |
| Moderate | 0 | 3 | 4 | 11 | 1 |
| Severe | 0 | 2 | 1 | 36 | 0 |
| Occluded | 0 | 0 | 0 | 0 | 7 |

Note.—Overall agreement between observers was 72%.

**TABLE 4: MR Angiography: Comparison of Findings by Observers 1 and 2**

| | Observer 2 | | | | |
|---|---|---|---|---|---|
| | Normal | Mild | Moderate | Severe | Occluded |
| Observer 1 | | | | | |
| Normal | 2 | 3 | 1 | 1 | 0 |
| Mild | 0 | 5 | 9 | 3 | 0 |
| Moderate | 0 | 1 | 5 | 7 | 0 |
| Severe | 0 | 0 | 1 | 50 | 4 |
| Occluded | 0 | 0 | 0 | 1 | 1 |

Note.—Overall agreement between observers was 67%.

as is usually done with routine clinical examinations in most institutions. However, the use of a "forced-choice" ranking system caused the observers to have to make difficult decisions when a study, whether an MR or contrast angiogram, was on the borderline between two categories. For example, the difference between 49% stenosis (mild category) and 50% stenosis (moderate category) is difficult to ascertain visually. This problem with the "forced-choice" analysis is demonstrated by the 67% and 72% interobserver correlations for each of the two techniques. If only differences of more than one category are considered, the overall correlation between MR and contrast angiography for each observer is 96% and 89%, respectively, and the interobserver correlation is 97% for contrast angiography and 95% for MR angiography.

The best correlation between techniques and, in fact, between observers in the same technique was in the severe category. Although the severely narrowed vessel lumen was occasionally seen on the MR examination (Fig. 4), MR angiograms in the severely stenotic cases often did not show the region of stenosis well. Conversely, an apparent discontinuity in the vessel on the MR angiogram with a clearly defined proximal and distal portion of adjacent vessel always correlated with a severe stenosis on contrast angiography (Fig. 5). This discontinuity results from intravoxel spin dephasing, which occurs because in laminar flow there is a range of velocities across the vessel diameter. Spins moving at varying velocity acquire different amounts of phase and may appear to cancel each other in the image. In addition, the flow void caused by the rapid acceleration of spins through the area of stenosis will also contribute to the discontinuity. Whereas the dephasing problem may be ameliorated with thinner slices and shorter echo times, the phase changes resulting from acceleration are more difficult to correct. In fact, the use of additional flow-compensating gradients to achieve this cor-

rection may have the deleterious side effect of increasing the echo time and hence the dephasing.

Other potential causes for signal loss in the region of stenosis that could lead to overestimation of the degree of narrowing are calcium or old hemorrhage within the atheroma. These would cause local field inhomogeneities that would result in spin dephasing, but again shorter echo times and thinner slices should reduce this problem.

This apparent discontinuity seen in the severely stenotic vessels is partially responsible for the poor correlation of MR and contrast angiography in the occluded cases. The occluded internal carotid arteries were often misinterpreted on the MR images as patent, because a small external carotid vessel or an artifact seen cephalad to the area of discontinuity was thought to be the continuation of the internal carotid artery (Fig. 6). While some of these cases were correctly interpreted because of the availability of multiple projections, in most it was difficult to correctly diagnose an occluded vessel, and these misdiagnoses were all interpreted as severe stenosis. The other factor in producing this error was the limitation of the study to the extracranial carotid circulation. Presumably, had additional cephalad slices been obtained and the vascular anatomy in the petrous and cavernous portions of the carotid arteries been defined, it would have been easier to distinguish between branches of the external carotid artery and continuation of the internal carotid artery itself. In addition, evaluation of the siphon is important in patients with carotid bifurcation stenosis to exclude tandem lesions prior to surgery.

Flow-related phase effects also caused some problems in the interpretation of normal carotid arteries. Although the carotid bulb was often seen (Fig. 1), in many cases there was some apparent "flattening" of the bulb, probably caused by the reversal of flow known to occur at this location [9]. If interpreted by strict contrast angiographic criteria, this flattening would be considered as evidence of mild stenosis, which could be misleading in some cases.

The most significant overall limitations of the 2DFT technique were an occasional "step-ladder" artifact seen in the projections and rare cases of poor signal to noise in the vessel. The artifact was most likely caused by minimal patient motion between axial slices. The overall poor signal is not as clearly understood but may result from poor cardiac output, which reduces the amount of spin refreshment in the vessel at each TR.

The maximum-intensity projection algorithm is also known to create some artifacts in patients with stenosis [9]. In general, it causes an apparent decrease in vessel diameter as well as an artificial lengthening of the stenotic portion (Fig. 3). This accounts for the tendency of both observers to have overestimated the degree of stenosis on the MR angiograms. The first problem is correctable by adjusting one's interpretation of the stenosis to account for the slightly underestimated diameter on the MR study. Observer 1 had more MR angiographic experience than observer 2, which may account for his better overall rate of correlation. The problem of overestimating the length of stenosis was noted by both observers and is not easily correctable.

Intraarterial contrast angiography remains the "gold standard" for the complete evaluation of atherosclerotic carotid artery disease. However, the small but measurable complication rate related to this procedure as well as its invasive nature argue strongly for the development and implementation of alternative diagnostic methods. The good correlation shown in this study between 2DFT time-of-flight MR angiography and contrast angiography suggests that the MR technique is sufficient as a screening method to separate those patients with a potentially correctable stenosis from those in whom surgery is not indicated. For many of the patients with a nonsurgical stenosis or a normal carotid bifurcation, MR angiography will probably be the only examination performed. Continued improvement of this technique as well as its extension to include visualization of the petrous and cavernous portions of the internal carotid artery should reduce the number of individuals requiring contrast angiography in the future. Finally, correlation of other diagnostic techniques, such as duplex sonography, with MR angiography may provide additional diagnostic certainty and further reduce the indications for contrast angiography.

## ACKNOWLEDGMENTS

We acknowledge Mary Sue Shields for her help in coordinating the patients for this study and the MR Advanced Clinical Development Group of Philips Medical Systems North America for providing and supporting the prototype MR angiographic software used.

## REFERENCES

1. Kricheff II. Arteriosclerotic ischemic cerebrovascular disease. *Radiology* **1987**;162:101–109
2. Dumoulin CL, Hart HR. Magnetic resonance angiography. *Radiology* **1986**;161:717–720
3. Axel L, Morton D. MR flow imaging by velocity-compensated/uncompensated difference images. *J Comput Assist Tomogr* **1987**;11:31–34
4. Masaryk TJ, Ross JS, Modic MT, Lenz GW, Haacke EM. Carotid bifurcation: MR imaging. *Radiology* **1988**;166:461–466
5. Dumoulin CL, Souza SP, Walker MF, Wagle W. Three-dimensional phase contrast angiography. *Magn Reson Med* **1989**;9:139–149
6. Gullberg GT, Wehrli FW, Shimakawa A, Simons MA. MR vascular imaging with a fast gradient refocusing pulse sequence and reformatted images from transaxial sections. *Radiology* **1987**;165:241–246
7. Masaryk TJ, Modic MT, Ruggieri RM, et al. Three-dimensional (volume) gradient-echo imaging of the carotid bifurcation: preliminary clinical experience. *Radiology* **1989**;171:801–806
8. Keller PJ, Drayer BP, Fram EK, Williams KD, Dumoulin CL, Souza SP. MR angiography with two-dimensional acquisition and three-dimensional display. *Radiology* **1989**;173:527–532
9. Anderson CM, Saloner D, Tsuruda JS, Shapeero LG, Lee RE. Artifacts in maximum-intensity-projection display of MR angiograms. *AJR* **1990**; 154:623–629

# Pulsed-Spray Thrombolysis of Arterial and Bypass Graft Occlusions

Karim Valji[1]
Anne C. Roberts
Gary B. Davis
Joseph J. Bookstein

**Pulsed-spray thrombolysis is accomplished through forceful injection of a spray of highly concentrated urokinase into clot by using catheters with multiple side holes. We previously reported the immediate technical efficacy of the method in eight arterial and 10 bypass graft occlusions. We now describe the clinical efficacy of the method in a second, larger series of 23 native artery occlusions and 25 bypass graft occlusions. Transluminal angioplasty was performed after thrombolysis in 21 of the arteries and 24 of the bypass grafts. Initial thrombolysis was observed in all artery occlusions and all but one bypass graft occlusion with an average time for pulsed-spray lysis of 65 ± 28 min in native arteries and 93 ± 38 min in bypass grafts. Recanalization with improvement in symptoms or distal pulses after thrombolysis and angioplasty was achieved in 74% of treated arterial occlusions and 92% of treated graft occlusions. Of the 15 arteries that were recanalized and did not require adjunctive surgery, seven remained patent at 3–28 months follow-up. Nine of 23 recanalized bypass grafts required early adjunctive surgery. Of the nine synthetic and five saphenous vein grafts successfully recanalized and not requiring surgical revision, the mean patency was 4.3 ± 3.1 months and 3.0 ± 2.2 months, respectively. Minor complications were seen in 23% of cases. The two major complications (4%) involved one groin hematoma requiring surgery and one episode of gastrointestinal hemorrhage.**

**We conclude that combined pulsed-spray thrombolysis and angioplasty achieve rapid and consistent arterial and graft recanalization with minimal risk. The method offers a favorable alternative to standard thrombolytic therapy of arterial occlusions. In occluded synthetic and vein bypass grafts, the technique is sometimes beneficial, either alone or combined with surgical revision.**

*AJR* 156:617–621, March 1991

The present standard method for transcatheter treatment of peripheral vascular occlusions involves local infusion of urokinase at the site of thrombosis; as lysis progresses, the infusing catheter is often gradually advanced through a channel in the occlusion created with a guidewire [1–3]. This technique has increased the consistency of fibrinolysis and reduced complications compared with early experience with IV streptokinase [4]. Although methods of regional urokinase infusion are widely accepted in the treatment of occluded arteries and vascular grafts, they remain incompletely effective, costly, and time-consuming.

During the past several years, we have pursued experimental and clinical investigations to develop techniques that combine mechanical clot disruption with rapid dispersal of fibrinolytic agent throughout clot [5, 6]. Other investigators have recently shown similar interest in accelerating thrombolysis through either mechanical means [7] or combined pharmacomechanical techniques [8, 9]. In our current method, termed pulsed-spray thrombolysis (PST), small volumes of highly concentrated urokinase are forcefully injected into clot as a high-pressure spray. We previously reported our technical results with PST, which demonstrated rapid and consistent thrombolysis of occluded hemodialysis grafts, native arteries, and bypass grafts [10]. However, early and long-term clinical outcome was not specifically

Received June 28, 1990; accepted after revision September 27, 1990.

Presented at the 90th annual meeting of the American Roentgen Ray Society, Washington, DC, May 1990.

[1] All authors: Department of Radiology (H-756), University of California, San Diego, Medical Center, 225 Dickinson St., San Diego, CA 92103 and Department of Radiology, Veterans Affairs Medical Center, La Jolla, CA 92161. Address reprint requests to K. Valji at UCSD Medical Center.

0361–803X/91/1563–0617
© American Roentgen Ray Society

addressed in that report. The present study was designed to expand on our earlier work in a larger series of patients to evaluate the speed and consistency of PST in the recanalization of occluded arteries and bypass grafts, the frequency of complications arising from PST, and the immediate and long-term clinical efficacy of the procedure.

## Materials and Methods

Between November 1987 and December 1989, 51 patients with 60 occluded arteries or arterial bypass grafts were referred for transcatheter thrombolytic therapy at the University of California, San Diego, and the La Jolla Veterans Affairs Medical Center. Only the pulsed-spray method was used during the study period. The medical records and angiograms of these patients were reviewed to determine the treated graft or artery site, the dose of urokinase and time of pulsed-spray therapy, procedural results before and after transluminal angioplasty (TLA), immediate clinical results, complications, and long-term follow-up. When recent follow-up was unavailable from medical records, patients were interviewed by telephone to identify any symptoms that might suggest reocclusion of the treated extremity.

### *Pulsed-Spray Method*

The technique of pulsed-spray thrombolysis has been previously described [10–12]. Patients are treated with aspirin (325 mg/day) on the day of and for 4–6 months after therapy. The occluded vessel is usually approached through an ipsilateral femoral puncture; occasionally, the contralateral diagnostic catheter puncture may be used. The occlusion is crossed with a guidewire. A Bentson or LT wire is tried initially; a Glidewire (Terumo Co., Medi-tech, Watertown, MA), beaded wire (Cook, Bloomington, IN), or Rosen wire is often helpful in more resistant occlusions. If a wire will not pass through the entire occlusion, thrombolysis is generally not attempted. Otherwise, the diagnostic catheter is advanced beyond the occlusion, and the runoff vessels are evaluated. Multiple side holes are punched into a 5-French tapered catheter at 8-mm intervals with a 27-gauge needle. The number of holes is determined by the length of clot the catheter will span. In vitro tests demonstrated uneven volumes of injectate when holes spanned a length exceeding 15 cm; therefore, we treat long occlusions in segments. The therapeutic catheter is placed across the occlusion, and the end hole is plugged with a beaded wire.

The patient is given 5000–7000 IU of heparin immediately after the occlusion is crossed and is maintained on 1000–2000 IU/hr until the procedure is completed. Despite the well-recognized variability in anticoagulative response to heparin infusions, we generally do not monitor coagulation or fibrinolytic parameters because recanalization is usually completed before the results could influence the conduct of the procedure. When heparin infusion is continued after treatment, the activated partial thromboplastin time is followed.

Highly concentrated (25,000 IU/ml) urokinase (Abbokinase, Abbott Laboratories, North Chicago, IL) is forcefully injected through the catheter in 0.2-ml pulses by using a tuberculin syringe. The catheter is turned periodically to improve distribution of urokinase. About 150,000 IU of urokinase are initially injected during 15–20 min (about two pulses per minute). In recent cases, we have not injected urokinase into the distal 1 cm of clot until considerable lysis was noted proximally to avoid distal embolization of lysing clot.

Under fluoroscopy, small injections of contrast material are made every 20–30 min through the therapeutic catheter or indwelling arterial sheath to monitor clot lysis and blood flow through the occluded vessel. Additional urokinase is given at a reduced rate (about one pulse per minute) or concentration (5000–10,000 IU/ml) until only scattered, small (2–3 mm) residual thrombi are present and antegrade flow is brisk. Persistent filling defects may represent more organized thrombi or atherosclerotic plaques; a trial of additional urokinase pulse injections at these sites may be useful. After clot dissolution is complete, underlying stenoses that are often responsible for thrombosis are sought and treated with TLA. Heparin therapy is stopped at the end of the procedure unless more than scattered 2- to 3-mm clots remain or residual stenosis after TLA is greater than about 30%. In such cases, heparin infusion is continued overnight.

### *Definitions*

Complete thrombolysis is defined as total or near-total clot dissolution immediately after pulsed-spray therapy, with antegrade flow reestablished through the previously occluded segment. Clinical success requiring adjunctive surgery is defined as vessel patency with antegrade flow at the completion of PST and angioplasty with improvement in symptoms and/or distal pulses, with surgical treatment of residual disease (atherosclerotic plaque or intimal hyperplasia) required before the patient is discharged from the hospital. Clinical success not requiring adjunctive surgery is defined as complete vessel patency after PST and angioplasty, with improvement in symptoms and/or distal pulses and no operative intervention required before discharge.

Major complications are defined as procedure-related events that led to transfusion or surgery for bleeding, an operation not originally planned, or a prolonged hospital stay. Criteria of persistent vessel patency at follow-up are persistent improvement in claudication or rest pain or in distal pulses, or increase in ankle-brachial index of greater than 0.20.

## Results

### *Native Artery Occlusions*

Recanalization was attempted in 31 arterial thromboses; thrombolysis was not performed in eight of these cases (four iliac and four superficial femoral arteries) because the occlusions could not be crossed initially with a guidewire. Seven of these eight patients subsequently underwent bypass procedures. The 23 treated vessels included common and external iliac (four), common iliac (one), external iliac (one), common femoral (one), superficial femoral (10), popliteal (five), and peroneal arteries (one). The age of thromboses, based on symptoms, ranged from minutes (acute thrombosis at an angioplasty site) to about 1 year. The precise clot age was often difficult to define. Clinical indications for PST included chronic pain in the lower extremity at rest (seven), life-style-limiting claudication (three), nonhealing foot ulcers (seven), threatened limb loss (two), and acute ischemic symptoms from postangioplasty thrombosis (three) or prior insertion of an intraaortic balloon pump into a common femoral artery (one).

The initial results of thrombolysis are summarized in Table 1. Complete or near-complete lysis with antegrade flow invariably occurred in the pulsed segment after urokinase treatment. In a recent case, a local infusion of urokinase (60,000 IU/hr) was administered for 12 hr after PST to dissolve residual thrombus within a tibioperoneal artery. This residual

**TABLE 1: Technical Results of Pulsed-Spray Thrombolysis**

| | Native Artery | Bypass Graft |
|---|---|---|
| Cases referred for therapy | 31 | 29 |
| Occlusions crossed with guidewire | 23 | 25 |
| Complete or near-complete lysis | 23 | 24 |
| Average dose of urokinase (units) | 406,000 ± 138,000 | 496,000 ± 160,000 |
| Average time for lysis (min) | 65 ± 28[a] | 93 ± 38[b] |

[a] Time for first 15 cases. More recent cases were not recorded.
[b] Time for first 18 cases. More recent cases were not recorded, including four later cases that received additional urokinase infusions.

material had not been exposed to spray injections, but had only received downstream effluent. No additional lysis was demonstrated after the infusion. Twenty-one of 24 reperfused arteries subsequently underwent angioplasty.

The clinical results of combined PST and angioplasty are summarized in Table 2. In six patients, the procedure failed to provide clinical benefit. In two of these cases, rethrombosis occurred immediately after (and we believe because of) TLA of underlying iliac artery stenoses, and further lysis was not attempted. In a third patient with a successfully lysed popliteal artery occlusion, severe proximal peroneal artery spasm reduced runoff to a single vessel, and the patient could not tolerate further transcatheter therapy. Another popliteal artery occlusion was completely recanalized, but no improvement in ischemic foot symptoms was achieved because runoff below the ankle was absent. In a fifth case, thrombolysis of a peroneal artery occlusion was successful but poor outflow prevented healing of a toe ulcer, and the toe was eventually amputated. In a sixth case, residual unlysable clot in the tibioperoneal trunk extending from an acute popliteal artery embolus required embolectomy.

Two of the 17 clinical successes required adjunctive surgery. Atherosclerotic plaque resistant to TLA (in the distal superficial femoral artery in one patient and in the common femoral artery in another) necessitated endarterectomy in both cases.

The remaining 15 cases (65%) were treated solely with PST and angioplasty. Seven of these arteries remained patent at 3- to 28-month (mean, 14.6 ± 8.8 mo) follow-up. Criteria used to define persistent patency were improved symptoms (three cases), distal pulses (three cases), or ankle-brachial index (one case). Five patients demonstrated evidence of restenosis or reocclusion at 1–12 months; two of these patients eventually required amputation for irreversible ischemic limb changes, and two other patients underwent bypass grafting. The trial of thrombolytic therapy did not alter the intended surgical procedure in any of these cases. Three patients with initial clinical improvement were lost to follow-up soon after treatment.

**TABLE 2: Clinical Results of Pulsed-Spray Thrombolysis and Angioplasty**

| | Native Arteries | Synthetic Grafts | Vein Grafts |
|---|---|---|---|
| Thrombolytic procedures | 23 | 15 | 10 |
| Clinical failures (%) | 6 (26) | 1 (7) | 1 (10) |
| Clinical successes with adjunctive surgery (%) | 2 (9) | 5 (33) | 4 (40) |
| Clinical successes without adjunctive surgery (%) | 15 (65) | 9 (60) | 5 (50) |

### *Bypass Graft Occlusions*

Of 29 bypass grafts considered for therapy, four grafts were not treated because the proximal anastomoses could not be cannulated. A guidewire was passed completely through all of the bypass graft occlusions that were successfully cannulated. The 15 synthetic grafts treated included femoro-femoral (eight), femoropopliteal (five), one limb of an aortofemoral bypass graft (one), and a common femoral artery graft placed after blunt pelvic trauma. The 10 vein grafts treated were in situ or reversed saphenous vein, occasionally with interposed nonsaphenous vein segments.

Immediate and long-term results of thrombolysis and angioplasty are indicated in Tables 1 and 2. Complete or near-complete clot dissolution was achieved in all but one treated case (96%). The single failure of initial thrombolysis occurred in a saphenous vein femoropopliteal graft in which severe, diffuse spasm developed during urokinase treatment; the graft was ultimately replaced. Clinical failure also occurred in one other case, in which residual clot in the proximal portion of one limb of an aortobifemoral graft led to rethrombosis. Local infusions of urokinase (60,000–75,000 IU/hr) were given overnight after PST in one vein and three synthetic grafts to treat minimal residual clot before angioplasty. Minimal additional lysis was demonstrated in two of the four patients. In all of these cases, which occurred late in our series, we administered infusions rather than continuing local pulsed-spray injections, primarily for logistical reasons (e.g., patient unwilling to remain on the angiography table, emergent need for the angiography suite). Angioplasty was performed after thrombolysis in 24 of 25 grafts.

Of the 23 clinical successes, nine grafts (five synthetic and four vein) required adjunctive surgical revision to maintain patency despite attempts at TLA. Four of the synthetic grafts were femorofemoral grafts with persistent anastomotic stenoses (thought to be due to intimal hyperplasia) that were not entirely responsive to TLA. The fifth case was a femoropopliteal graft with residual disease at the distal anastomosis and popliteal artery; the graft reclotted after initial thrombolysis and was reopened with additional urokinase injections. Four vein grafts required early revision of the proximal and/or distal anastomoses.

The mean patency of the nine synthetic grafts successfully treated solely with PST and angioplasty was 4.3 ± 3.1 months. Three of these have remained patent at 6- to 10-month follow-up. The remaining six rethrombosed after 2 weeks to 4 months. Four of these grafts were successfully retreated with PST.

The mean patency of the five saphenous vein grafts successfully treated solely with PST and angioplasty was 3.0 ± 2.2 months at 1- to 6-month follow-up. Anastomotic restenosis was identified in two cases while the grafts were patent, and they were revised. The other three vein grafts reclotted and were revised or replaced.

### *Complications*

Minor complications occurred in 11 cases (23%), including four moderate-sized hematomas at the puncture site, two episodes of transient renal dysfunction that resolved with conservative therapy, and five cases of distal embolization. The emboli in three of these patients were successfully lysed with local urokinase infusions. In a fourth case, clot that migrated to the peroneal artery during an ultimately unsuccessful procedure on a popliteal artery occlusion was removed at the time of bypass surgery. The fifth case of embolization occurred during attempted passage of a guidewire through an iliac artery occlusion; an embolus to the popliteal artery was removed with a Fogarty catheter at the time of aortofemoral bypass grafting.

Two major complications (4%) developed, including one puncture-site hematoma that required surgical evacuation. Another patient had gastrointestinal hemorrhage, which we attributed to excessive anticoagulation; the fibrinogen level was normal at the time of bleeding and the activated partial thromboplastin time was greater than 150 sec. Blood transfusion was not required in this case.

## Discussion

Our results confirm and extend observations we reported previously, namely that PST has several important advantages over conventional transcatheter methods for treating peripheral vascular occlusions. PST is exceedingly rapid. By evaluating the first 33 cases, we found the mean time for complete or near-complete lysis was 65 min for arterial occlusions and 93 min for bypass graft occlusions. With PST alone, lysis time is reduced by a factor of 10 or more compared with other reported series that used local infusions of urokinase [1, 2, 8, 13–16]. The entire procedure is performed in a single therapeutic session. Many of the major disadvantages of prolonged catheter infusions (e.g., the cost of intensive-care monitoring, the need for periodic angiography, patient's discomfort from indwelling catheters) are avoided with PST. Some added time is required from the physician and in the angiography suite. We are currently testing a mechanical pulse injector that may further improve the delivery of urokinase pulses, accelerate lysis, and reduce demands on the angiographer's time.

The consistency of clot dissolution is also remarkably high with PST. In all but one of 48 treated cases, we achieved initial complete or near-complete clot lysis in the pulsed region. We attribute part of this success to selection of patients; only occlusions that could be crossed completely with a guidewire were treated with PST. On this basis, treatment was withheld from 26% of native arterial occlusions considered for therapy. We and others [2] find the guidewire test valuable in excluding cases in which lysis is unlikely.

The frequency of major (4%) and minor (8%) bleeding complications in our series is comparable to or less than that in most large reported series that used regional urokinase infusion techniques [1, 2, 8, 14, 15]. Factors limiting hemorrhage with PST include direct injection of urokinase into clot, reduction in the overall dose of urokinase administered (400,000–500,000 IU with PST vs >1,000,000 IU for most local infusion techniques), and a shorter period of heparin therapy.

The risk of downstream embolization of clot may be increased by mechanical disruption of thrombus and the acceleration of fibrinolysis. We have limited this potential problem with our method by leaving the distal 1 cm of occlusion untreated until some lysis occurs proximally, avoiding higher pulse frequency or larger volumes than indicated in the above protocol, and delaying angioplasty until lysis is complete. In one of the eight untreated arterial occlusions that could not be crossed, guidewire manipulation led to a downstream embolus that was later recovered during bypass surgery. Distal emboli occurred in four (8%) of 48 treated cases. In three of these patients, emboli were successfully lysed by advancing a catheter directly or coaxially to the embolus and infusing urokinase locally. We obtain angiograms of the run-off vessels after every procedure to look for distal emboli. Downstream embolization during regional infusion thrombolysis has been reported with similar frequency in other series [2, 15, 16]. We consider occasional episodes of embolization an acceptable risk of the pulsed-spray method.

PST is of benefit in some clinical situations in which the use of local urokinase infusion therapy may be controversial. Clot age is not a determinant of suitability for PST. We treat chronic occlusions as aggressively as acute thromboses if a guidewire will pass through the obstructed segment. Second, some investigators have suggested that local urokinase infusions used in treating arterial emboli may precipitate further embolization from more central thrombi through systemic fibrinolytic effects [17]. Because urokinase is injected directly into clot with our technique, we believe that systemic effects are minimized; therefore, we are less reluctant to treat embolic occlusions. Finally, blood flow is restored so rapidly with PST that a trial of transcatheter therapy is often appropriate and safe despite severe, acute limb ischemia (excluding patients with profound sensorimotor deficits) when prolonged infusion therapy might not be suitable.

Successful recanalization of occluded vessels depends on a number of important adjuncts to urokinase injections. Vigorous anticoagulation during treatment is mandatory to prevent rethrombosis and pericatheter clot formation. Because of routine use of aspirin in conjunction with angioplasty, and

because of the frequent need for TLA after thrombolysis, we administer aspirin before treatment. Inadequate heparin or aspirin therapy was probably responsible for a number of cases in which clot propagation or rethrombosis occurred during fibrinolysis and angioplasty. Finally, correction of underlying stenoses due to atherosclerotic plaque or intimal hyperplasia is necessary to prevent early rethrombosis. When angioplasty or atherectomy is unsuccessful in restoring luminal caliber, early surgical revision is advised.

Pulsed-spray thrombolysis of occluded bypass grafts rapidly restores blood flow to the acutely ischemic limb supplied by the graft and allows a more rational operative approach to underlying graft abnormalities. New observations from our follow-up of successfully recanalized grafts indicate that when transcatheter therapy is used alone, the results are generally not lasting. In particular, the long-term patency rates after PST and angioplasty of saphenous vein bypass grafts are discouraging, in keeping with the data of others in this regard [13, 18]. Thus, although the pulsed-spray technique is very effective in recanalizing clotted arterial bypass grafts, its overall clinical efficacy is debatable, particularly with venous bypass grafts. Early detection of impending graft failure with serial duplex sonography, which allows surgical revision before thrombosis occurs, may be a more favorable approach in managing these patients.

Only scattered reports have described long-term follow-up of patients treated for arterial thromboses with fibrinolytic therapy. Hess and coworkers [19] noted an 80% 1-year patency rate in a series of 313 clotted native arteries successfully treated with streptokinase or urokinase. McNamara and Bomberger [20] observed 6-month patency rates after thrombolysis of iliac and superficial femoral artery occlusions of 92% and 50%, respectively. In our series, clinically successful recanalization was achieved in 74% of cases. In a small subset of these patients, surgical endarterectomy was required in addition to transcatheter therapy. Our evaluation of the long-term efficacy of PST and angioplasty alone in the treatment of arterial occlusions is limited by the variable criteria used to define persistent patency, the small sample size, and the somewhat short length of follow-up. Given these limitations, however, about half of the 65% of cases that were clinical successes that did not require adjunctive surgery remained patent at long-term follow-up. We consider PST and angioplasty a favorable alternative to conventional thrombolytic therapy in patients with native arterial occlusions. The risks from PST are small, and subsequent bypass procedures are not generally hampered by an attempt at transcatheter treatment.

In summary, our results indicate that PST, usually with supplementary angioplasty, achieves rapid and effective recanalization of thrombosed arteries and bypass grafts. In a significant proportion of native arteries, and in a smaller fraction of treated grafts, there is long-term benefit.

## REFERENCES


1. Motarjeme A. Thrombolytic therapy in arterial occlusion and graft thrombosis. *Semin Vasc Surg* **1989**;2:155–178
2. McNamara TO, Fischer JR. Thrombolysis of peripheral arterial and graft occlusions: improved results using high-dose urokinase. *AJR* **1985**;144:769–775
3. Gardiner GA, Rao AK. Thrombolysis for peripheral arterial occlusions. *Radiology* **1990**;175:34–36
4. Collen D, Stump DC, Gold HK. Thrombolytic therapy. *Ann Rev Med* **1988**;39:405–423
5. Bookstein JJ, Saldinger E. Accelerated thrombolysis: in vitro evaluation of agents and methods of administration. *Invest Radiol* **1985**;20:731–735
6. Valji K, Bookstein JJ. Fibrinolysis with intrathrombic injection of urokinase and tissue-type plasminogen activator: results in a new model of subacute venous thrombosis. *Invest Radiol* **1987**;22:23–27
7. Bildsoe MC, Moradian GP, Hunter DW, Castaneda-Zuniga WR, Amplatz K. Mechanical clot dissolution: new concept. *Radiology* **1989**;171:231–233
8. Sullivan KL, Gardiner GA, Shapiro MJ, Bonn J, Levin DC. Acceleration of thrombolysis with a high-dose transthrombus bolus technique. *Radiology* **1989**;173:805–808
9. Kandarpa K, Drinker PA, Singer SJ, et al. Forceful pulsatile local infusion of enzyme accelerates thrombolysis: in vivo evaluation of a new delivery system. *Radiology* **1988**;168:739–744
10. Bookstein JJ, Fellmeth B, Roberts A, Valji K, Davis G, Machado T. Pulsed-spray pharmacomechanical thrombolysis: preliminary clinical results. *AJR* **1989**;152:1097–1100
11. Valji K, Roberts AC, Davis GB, Bookstein JJ. Pharmacomechanical thrombolysis and angioplasty in the management of clotted hemodialysis grafts: early and late clinical results. *Radiology* **1991**;178:243–247
12. Valji K, Bookstein JJ. Pulsed-spray pharmacomechanical thrombolysis. In: Castaneda-Zuniga WR, Maynar M, eds. *Percutaneous revascularization techniques*. New York: Thieme Medical Publishers (in press)
13. Durham JD, Geller SC, Abbott WM, et al. Regional infusion of urokinase into occluded lower-extremity bypass grafts: long-term clinical results. *Radiology* **1989**;172:83–87
14. Meyerovitz MF, Goldhaber SZ, Reagan K, et al. Recombinant tissue-type plasminogen activator versus urokinase in peripheral arterial and graft occlusions: a randomized trial. *Radiology* **1990**;175:75–78
15. Gardiner GA, Harrington DP, Koltun W, Whittemore A, Mannick JA, Levin DC. Salvage of occluded arterial bypass grafts by mean of thrombolysis. *J Vasc Surg* **1989**;9:426–431
16. Price C, Jacocks MA, Tytle T. Thrombolytic therapy in acute arterial thrombosis. *Am J Surg* **1988**;156:488–491
17. Paulson EK, Miller FJ. Embolization of cardiac mural thrombus: complication of intraarterial fibrinolysis. *Radiology* **1988**;168:95–96
18. Belkin M, Donaldson MC, Whittemore AD, et al. Observations on the use of thrombolytic agents for thrombotic occlusion of infrainguinal vein grafts. *J Vasc Surg* **1990**;11:289–296
19. Hess H, Mietaschk A, Brueckl R. Peripheral arterial occlusions: a six-year experience with local low-dose thrombolytic therapy. *Radiology* **1987**;163:753–758
20. McNamara TO, Bomberger RA. Factors affecting initial and 6 month patency rates after intraarterial thrombolysis with high dose urokinase. *Am J Surg* **1986**;152:709–712

# Memorial

## Charles P. Hyslop, 1924–1990



*It is better to be making the news than taking it; to be an actor rather than a critic.*
Sir Winston Spencer Churchill

Charles Peter Hyslop, retired clinical director of radiology for Sharp Memorial Hospital and a founder of the San Diego Diagnostic Radiology Medical Group, died at the age of 66 on October 10, 1990, from complications of prostatic carcinoma. He was born in New York City on March 22, 1924. His father, George Hall Hyslop, was a neurologist in private practice and a member of the clinical faculty at Columbia University, College of Physicians and Surgeons. His mother, Esther NcNaull Hyslop, was active in New York's cultural community. She both designed and produced jewelry in the later years of her life. His grandfather, James Hervey Hyslop, was professor of logic and ethics at Columbia University. At the turn of the century, he cofounded the American Society for Psychical Research.

Pete, as he was known to his family, had many friends and colleagues. A keen observer and a careful listener, he retained memories of his youth in the east. He could reproduce authentically multiple ethnic dialects of his native city as well as give his own impressions of Metropolitan Opera divas, interurban train conductors, or New England prep school teachers, to the amusement of his audiences. His good-natured humor defused many eruptions, common to any radiology department.

Dr. Hyslop graduated from Phillips Exeter Academy and was in the accelerated physician training program during World War II, with undergraduate education at Yale and medical school at Columbia University. He married Constance Hopkins in 1945. Their families vacationed in the summers at Point O'Woods on Fire Island, off the southern coast of Long Island. A summertime romance there in their teen-age years led to close friendship and then marriage. Pleasant memories of those family holidays remained important to both Pete and Connie.

Pete received his training in radiology at the University of Colorado in Denver from 1950 to 1953. He served in the United States Navy Medical Corps as a radiologist at San Diego's Balboa Naval Hospital before returning to work as a staff radiologist at the Veteran's Administration Hospital in Denver. He returned to San Diego with his family in 1957. They settled in La Jolla. He joined Howard Brown and later Harvey A. Humphrey in practice at Sharp Memorial Hospital. In 1971 he became clinical director of radiology for that institution and served as director until his planned retirement on his 62nd birthday in 1986. He provided 29 years of professional service to Sharp Memorial Hospital and was also a staff radiologist for Children's Hospital of San Diego, Sharp Cabrillo Hospital, and Mesa Vista Hospital.

Dr. Hyslop's avocational interests were varied. He was an avid tennis player, and he enjoyed hiking, skiing, and water sports at Wind and Sea beach, within easy walking distance of his home. He read widely, with emphasis on history and science. He collected coins and American Southwestern art. He assembled an extensive library of the American West and a collection of American jazz records and tapes. Trips to ancestral Scotland, the California Sierras, and the Stanford Camp and return visits to Point O'Woods were among his favorite vacations.

Pete Hyslop was an excellent clinical radiologist and a sensitive, creative leader. He was a member of many professional organizations, including the San Diego County Medical Society. He was a former president of the San Diego Radiological Society, a fellow of the American College of Radiology (ACR), past councilor and alternate councilor of the ACR, and a member of the clinical faculty of the University of California, San Diego.

He is survived by his wife, Connie, who provided great support and love during their 45 years of marriage. Three daughters, Susan, Sallie, and Nina; two sons, Charles, Jr., and Stephen; and one grandchild, Nicole Lee Hyslop, also survive.

Pete led a full and vigorous life, which was cut short too soon. He will be sorely missed by his family and by a legion of friends and admirers.

Richard T. Trackler
*La Jolla, CA 92037*

# The Importance of Preoperative Evaluation of the Subclavian Vein in Dialysis Access Planning

R. Stephen Surratt[1]
Daniel Picus[1]
Marshall E. Hicks[1]
Michael D. Darcy[1]
Michael Kleinhoffer[1]
Martin Jendrisak[2]

**Adequate venous outflow is critical to the proper function of a vascular-access graft (arteriovenous fistula) used for chronic hemodialysis. Stenosis of the subclavian vein can significantly compromise this venous outflow. The development of such subclavian vein stenoses has been associated with the prior placement of temporary subclavian vein dialysis catheters. We evaluated the importance of preoperative detection of these stenoses before placement of a permanent vascular-access graft in the upper extremity. Upper extremity venography was performed before placement of a permanent vascular-access graft in 43 patients. A total of 62 extremities were evaluated. A 40% prevalence of moderate or severe subclavian vein stenosis was found in patients with prior or existing temporary dialysis catheters in the subclavian vein. No stenoses were found in patients without a history of dialysis catheters in the subclavian vein. This difference in the prevalence of subclavian vein stenosis is statistically significant ($p < .001$). In no case was the stenosis suspected clinically.**

**Before placement of a permanent vascular-access graft, the subclavian vein should be evaluated in all patients with a history of a temporary dialysis catheter in the subclavian vein. The use of sites other than the subclavian vein for temporary dialysis is strongly encouraged.**

*AJR* 156:623–625, March 1991

Percutaneous catheters in the subclavian vein have been used for temporary hemodialysis for the past 20 years. The subclavian approach for temporary dialysis access is popular because of its overall low complication rate and the ease of catheter placement. Recent reports, however, have described a high frequency of subclavian vein stenosis in patients with a history of previous temporary subclavian dialysis catheters [1–4]. Subclavian vein stenosis in these patients became apparent only after placement of a permanent vascular-access graft in the ipsilateral extremity and was manifested by arm swelling and inefficient hemodialysis. Long-term sequelae of such subclavian vein stenosis can include reduced vascular access flow, graft thrombosis, and pronounced venous hypertension [1, 2].

As subclavian vein stenosis has been shown to have an adverse impact on the efficiency of dialysis, such stenoses must be identified before the placement of a permanent vascular-access graft. Currently, the gold standard in evaluating subclavian vein abnormalities, particularly in the portion of the vein behind the clavicle, is contrast venography [5]. Therefore, in an effort to identify patients with subclavian vein stenosis, and to define better the role of upper extremity venography in the preoperative evaluation of dialysis patients, we prospectively evaluated a series of patients with upper extremity venography before placement of a permanent vascular-access graft.

## Subjects and Methods

Between January 1989 and February 1990 we obtained 37 bilateral and six unilateral upper extremity venograms before placing a vascular-access graft. Both extremities of each

Received August 30, 1990; accepted after revision October 10, 1990.

[1] Mallinckrodt Institute of Radiology, Washington University School of Medicine, 510 S. Kingshighway Blvd., St. Louis, MO 63110. Address reprint requests to R. S. Surratt.

[2] Department of Surgery, Washington University School of Medicine, Box 8109-3358 CSRB, 4939 Audubon St., St. Louis, MO 63110.

0361–803X/91/1563–0623
© American Roentgen Ray Society

patient were included unless a prior permanent vascular-access graft had been placed in that extremity. Thus, a total of 62 extremities in 43 patients were included. There were 19 men and 24 women whose ages ranged from 11 to 84 years (mean, 55 years). In 35 of the 62 extremities, there was either a history of, or an existing, indwelling subclavian dialysis catheter. The remaining 27 extremities had never had a subclavian catheter placed. No statistically significant differences were seen between the two groups with regard to age ($p = .92$) or sex ($p = .61$).

Upper extremity venography was performed with digital subtraction angiography via a large-bore angiocath placed in either a forearm or antecubital vein. Images were acquired with a 40-cm image intensifier at one or two frames per second. Conray-43 (Mallinckrodt, St. Louis, MO) was used routinely. Usually two or three separate injections of 10–15 ml of contrast material were performed for each extremity, with imaging over the appropriate location. In all studies, we evaluated the venous drainage of the upper arm, the axillary and subclavian veins, and the brachiocephalic vein and superior vena cava.

All pertinent images were reviewed by three experienced vascular radiologists without knowledge of the patient's history of subclavian vein access. The subclavian vein was classified as normal, less than 50% stenotic, greater than 50% stenotic, or occluded. To determine whether a temporary subclavian dialysis catheter had ever been placed, we obtained a thorough history from the patient when venography was performed. Additionally, the infraclavicular regions were inspected for the presence of scars. When necessary, this history of catheter placement was confirmed by review of data from the dialysis center.

All data were subjected to either the chi-square or Fisher's exact test [6]. As both extremities were not included in all patients, significance testing was done by choosing one extremity at random in patients who had both arms studied. This allowed extremities to be treated as independent variables for the determination of statistical significance.

## Results

Of the 35 extremities with prior or existing subclavian catheters, upper extremity venography showed subclavian occlusion with collaterals in four (11%) and greater than 50% stenosis in 10 (29%), giving a 40% overall prevalence of significant stenosis or occlusion. All 27 extremities without prior or existing subclavian catheters had normal venograms. A statistically significant difference ($p < .001$) was found between the two groups. An analysis of one extremity per person (chosen at random from those who had both studied) gave a similar result—43% of patients with prior subclavian catheters had evidence of stenosis and all 20 patients without prior catheters had normal venograms ($p < .001$).

## Discussion

In the past two decades, the subclavian approach for temporary hemodialysis access has become the technique of choice. This approach is popular because of its overall low rate of acute complications and ease of catheter placement [7]. Acute complications of catheter placement occur in up to 7% of patients and can include either catheter malposition, sepsis, hemothorax, or pneumothorax [8, 9].

Chronic complications of subclavian dialysis catheters have not been as well recognized. One important chronic complication is the development of long-term subclavian vein stenosis [5, 10]. Presumably, these stenoses occur slowly, allowing time for adequate venous collateral formation. Thus, the stenoses commonly go undetected until venous flow rates are increased by the placement of a permanent vascular-access graft in the ipsilateral extremity.

As adequate venous drainage is necessary to accommodate the increased venous flow rates that occur after placement of a permanent vascular-access graft, normal venous drainage must be documented before a vascular-access graft is placed. The detection of clinically silent subclavian vein stenoses in these patients allows the surgeon to plan alternative sites for permanent vascular-access grafts and prevents the placement of a vascular-access graft in an upper extremity with compromised venous drainage.

Our study showed a 40% frequency of either greater than 50% subclavian vein stenosis or subclavian vein occlusion in patients who had had subclavian catheters placed for temporary vascular access. In no case was the stenosis suspected clinically. The degree of venous stenosis that is hemodynamically significant with high venous flow rates is unknown. We chose to define a stenosis of greater than 50% as hemodynamically significant. However, all but two patients in our series had stenoses greater than 75%.

Other authors also have reported a high frequency of subclavian vein stenosis related to temporary hemodialysis catheter placement. Fant et al. [1] reported a series of three patients with prior subclavian dialysis catheters who developed arm swelling after placement of a permanent vascular access in the ipsilateral arm. Venography confirmed subclavian vein stenosis in each case. Additionally Cimochowski et al. [4] reported a retrospective series in which they compared a group of patients who had prior subclavian dialysis catheters to a group with prior internal jugular catheters. They found a 50% frequency of subclavian vein stenoses in the subclavian catheter group of patients compared with no stenoses in the group of patients with internal jugular catheters.

Contrast venography is the gold standard for imaging abnormalities of the subclavian and innominate vein. Early reports have shown that color flow Doppler sonography may have a role in the detection of upper extremity venous thrombosis [11]. However, it is not yet clear whether color flow Doppler sonography will accurately be able to detect stenoses of the subclavian vein, particularly behind the clavicle, where no acoustic window is available [11]. In our experience, this is the exact location in which stenoses related to subclavian vein catheters occur. Currently we are using contrast venography as our screening method of choice. It is minimally invasive, and contrast material is not a serious concern in this population of patients who are already on hemodialysis. Additionally, in our practice, the charge for the two examinations is similar.

We conclude that the subclavian vein should be imaged before placement of a vascular-access graft in all patients who have a history of prior or indwelling subclavian catheters. As no stenoses were detected in the group of patients who had never had catheters placed, there appears to be no need to image the subclavian vein in these patients. Whenever

possible, we strongly encourage the use of sites other than the subclavian vein for temporary dialysis catheter placement.

## REFERENCES


1. Fant GF, Dennis VW, Quarles LD. Late vascular complications of the subclavian dialysis catheter. *Am J Kidney Dis* **1986**;7:225–228
2. McNally PG, Brown CB, Moorhead PJ, Raferty AT. Unmasking subclavian vein obstruction following creation of arteriovenous fistulae for haemodialysis: a problem following subclavian line dialysis? *Nephrol Dial Transplant* **1987**;1:258–260
3. Spinowitz BS, Galler M, Golden RA, et al. Subclavian vein stenosis as a complication of subclavian catheterization for hemodialysis. *Arch Intern Med* **1987**;147:305–307
4. Cimochowski GE, Worley E, Rutherford WE, et al. Superiority of the internal jugular over the subclavian access for temporary dialysis. *Nephron* **1990**;54:154–161
5. Benenati JF, Becker GJ, Mail JT, Holden RW. Digital subtraction venography in central venous obstruction. *AJR* **1986**;147:685–688
6. Colton T. Inference on proportions. In: Colton T, ed. *Statistics in medicine*. Boston: Little, Brown, **1974**:151–188
7. Anderson JT, Gammelgaard J, Nielson LM, Clausen E. Subclavian vein catheterization for acute and chronic haemodialysis: a safe temporary vascular access. *Int Urol Nephrol* **1986**;18:327–332
8. Vanherweghem JL, Cabolet P, Goldman M, et al. Complications related to subclavian catheters for hemodialysis. *Am J Nephrol* **1986**;6:339–345
9. Vanholder R, Lameire N, Verbanck J, et al. Complications of subclavian catheter hemodialysis: a five year prospective study in 257 consecutive patients. *Int J Artif Organs* **1982**;5:297–303
10. Schwab SJ, Quarles LD, Middleton JP, et al. Hemodialysis associated subclavian vein stenosis. *Kidney Int* **1988**;33:1156–1159
11. Knudson GJ, Wiedmeyer DA, Erickson SJ, et al. Color Doppler sonographic imaging in the assessment of upper extremity deep venous thrombosis. *AJR* **1990**;154:399–403

# FORTHCOMING ARTICLES

## SPECIAL ARTICLES

**Fleischner Lecture. Developmental abnormalities in the systemic blood supply to the lungs: a review.** *Ellis K*

**Neuhauser Lecture. Bronchopulmonary dysplasia and research in diagnostic radiology.** *Northway WH Jr*

## REVIEW ARTICLE

**Radiation injury of the brain.** *Valk PE, Dillon WP*

## CARDIOPULMONARY RADIOLOGY

**Chest CT combined with artificial pneumothorax: value in determining origin and extent of tumor.** *Watanabe A, Shimokata K, Saka H, Nomura F, Sakai S*

**Lymphoma of the lung: CT findings in 31 patients.** *Lewis ER, Caskey CI, Fishman EK*

**Mediastinal seroma after esophagogastrectomy.** *Kronthal AJ, Heitmiller RF, Fishman EK, Kuhlman JE*

**Case report. Noncompaction of ventricular myocardium: CT appearance.** *Conces DJ, Ryan T, Tarver RD*

## BREAST RADIOLOGY

**Perspective. Medicolegal aspects of breast imaging: variable standards of care relating to different types of practice.** *Brenner RJ*

## GASTROINTESTINAL RADIOLOGY

**Detection of active intraabdominal arterial hemorrhage: value of dynamic contrast enhanced CT.** *Jeffrey RB Jr, Cardoza JD, Olcott EW*

**Diagnosis of pneumoperitoneum on supine abdominal radiographs.** *Levine MS, Scheiner JD, Rubesin SE, Laufer I, Herlinger H*

**Pictorial essay. Imaging the gallbladder: a historical perspective.** *Feld R, Kurtz AB, Zeman RK*

**Pictorial essay. Sonography of focal lesions of the spleen.** *Goerg C, Schwerk WB, Goerg K*

**Amyloidosis of the small intestine: findings on double-contrast radiography.** *Tada S, Iida M, Matsui T, et al.*

**Case report. Visceral calcification in patients with AIDS is not always due to *Pneumocystis carinii*.** *Towers MJ, Withers CE, Hamilton PA, Kolin A, Walmsley S*

**Case report. Pancreatic microcystic adenoma presenting with acute hemoperitoneum: CT diagnosis.** *Rubin GD, Jeffrey RB Jr, Walter JF*

**Case report. Hydatid cyst of the liver: identification of detached lining of the cyst on CT scans made after cyst puncture.** *Acunaş B, Rozanes I, Acunaş G, Çelik L, Alper A, Gökmen E*

## GENITOURINARY RADIOLOGY

**Carcinoma of the cervix: value of MR imaging in detecting parametrial involvement.** *Sironi S, Belloni C, Taccagni GL, DelMaschio A*

**Prostatic urethra dilatation with the Gianturco self-expanding metallic stent: a feasibility study in cadaver specimens and dogs.** *Dobben RL, Wright KC, Dolenz K, Wallace S, Gianturco C*

**Technical note. A simplified method for antegrade ureteral stent placement.** *Krauthamer R*

## MUSCULOSKELETAL RADIOLOGY

**Acute effects of exercise on MR of skeletal muscle: concentric vs eccentric actions.** *Shellock FG, Fukunaga T, Mink J, Edgerton VR*

**Repair of Achilles tendon ruptures with a polylactic acid implant: assessment with MR imaging.** *Liem MD, Zegel HG, Balduini FC, Turner ML, Becker JM, Caballero-Saez A*

## PEDIATRIC RADIOLOGY

**Extension of growth plate cartilage into the metaphysis: a sign of fracture healing in abused infants.** *Kleinman PK, Marks SC Jr, Spevak MR, Belanger PL, Richmond JM*

**Pictorial essay. Normal metaphyseal radiologic variants not to be confused with findings of infant abuse.** *Kleinman PK, Belanger PL, Karellas A, Spevak MR*

**Osteomyelitis of the talus: an unusual cause of limp in childhood.** *Grattan-Smith JD, Wagner ML, Barnes DA*

**Case report. Polysplenia syndrome with congenital short pancreas.** *Herman TE, Siegel MJ*

## NEURORADIOLOGY

**Evaluation of CSF shunt function: value of functional examination using contrast material.** *Benzel EC, Mirfakhraee M, Hadden TA*

**Diagnosis of ruptured intracranial dermoid cyst: value of MR over CT.** *Smith AS, Benson JE, Blaser SI, Mizushima A, Tarr RW, Bellon EM*

**MR evaluation of spinal dermal sinus tracts in children.** *Barkovich AJ, Edwards MSB, Cogen P*

**Pictorial essay. Tubes in the alimentary and respiratory tract: appearances on CT scans of the head and neck.** *Price DB*

## VASCULAR RADIOLOGY

**Review. Inferior vena caval filters: analysis of four currently available devices.** *Grassi CJ*

**Percutaneous transluminal angioplasty of the subclavian arteries: long-term results in 52 patients.** *Hebrang A, Maskovic J, Tomac B*

**Technical note. Kissing balloon technique for angioplasty of the popliteal artery trifurcation.** *Mewissen MW, Beres RA, Bessette JC, Lipchik EO*

## CONTRAST MATERIAL

**The risks of death and of severe nonfatal reactions with high vs low osmolar contrast media: a metaanalysis.** *Caro JJ, Trindade E, McGregor M*

**Case report. Atypical contrast reactions associated with systemic interleukin-2 therapy.** *Fishman JE, Aberle DR, Moldawer NP, Belldegrun A, Figlin RA*

## COMPUTER PAGE

**An ultrafast network for communication of radiologic images.** *Stewart BK, Lou SL, Wong WK, Huang HK*

## MEETING NEWS

**Radiology Summit Meeting 1990: action strategies for the new decade.** *McClennan BL*

## ARRS 1991 MEETING CASE OF THE DAY QUESTIONS

**Introduction.** *John F. O'Connor*

**General diagnosis case of the day.** *Eschelman DJ, Panageas E, Rosen MP, Romo LV, O'Connor JF*

**Chest case of the day.** *Eschelman DJ, Argy N, Fielding JR, et al.*

**Abdominal case of the day.** *Eschelman DJ, Duva-Frissorà AD, Martin LC, et al.*

**Neuroradiology case of the day.** *Parker DR, Eschelman DJ, Gibbens DT, Rabinov JD, O'Connor JF*

**Pediatric case of the day.** *O'Connor JF, Martin LC, Chen HH, Dobkin BL, Sax EJ, Eschelman DJ*

# Fate of Manuscripts Rejected for Publication in the *AJR*

Felix S. Chew[1]

**The fate of rejected manuscripts that were originally submitted to the *American Journal of Roentgenology (AJR)* during the first 5 months of 1986 was investigated to learn whether, when, and where they had been published. *AJR*, a peer-reviewed journal of diagnostic radiology with a circulation of over 21,000, annually publishes about 500 papers and receives over 11,500 citations. MEDLINE searches conducted 45 to 54 months after the dates of rejection by *AJR* located 162 (64%) published papers out of a consecutive series of 254 manuscripts rejected by *AJR*, including 69% of the rejected major papers and 62% of the rejected case reports. The papers had been published in 30 different radiologic and 27 different nonradiologic journals. Most of these journals published fewer papers, had smaller circulations, and had lower impact factors (a ratio of citations received to papers published) than *AJR* does. The mean time lapse between rejection by *AJR* and publication in other journals was 15 months. The delay in publication was greater for papers published in nonradiologic and foreign journals than for papers published in radiologic and American journals.**

**The results of this study indicate that rejection of a manuscript by a peer-reviewed journal such as *AJR* delays but by no means precludes publication. At least 82% of the major papers and 70% of the case reports that are submitted to *AJR* are eventually published, either in *AJR* or elsewhere. Because a scientific paper represents not only many hours of writing and manuscript preparation but also a great investment of research time and resources, authors are reluctant to abandon rejected manuscripts. In the majority of cases, submission to other journals gains acceptance and publication.**

***AJR* 156:627–632, March 1991**

Publication of research in peer-reviewed journals marks the final step in the scientific process. Through the process of peer review and publication, a research study is validated, disseminated, credited, and archived. Once published, a paper and the information it contains can be indexed, retrieved, cited, and incorporated into the knowledge base [1]. When a paper is rejected this process comes to an abrupt halt. Unless the paper can be accepted for publication elsewhere, the work will be lost. I investigated the fate of submissions that were rejected by the *AJR* to learn whether, when, and where these manuscripts had been published. *AJR* is a peer-reviewed journal of diagnostic radiology [2, 3] with a circulation of over 21,000. Its editors choose approximately 500 papers to publish each year from about 1,250 submissions. Papers published in the *AJR* receive in aggregate over 11,500 citations per year [4].

## Materials and Methods

I studied a consecutive series of 254 rejected manuscripts that consisted of all submissions received by the *AJR* editorial office between January 2, 1986, and May 27, 1986, that were ultimately rejected. For each, the title, the corresponding author's name, the dates of receipt and rejection, and the manuscript type were obtained from *AJR* files. *AJR* had classified 141 of them as major papers, 95 as case reports, and 18 as technical notes or computer papers.

Received May 17, 1990; accepted after revision September 12, 1990.

The 1990 Melvin M. Figley Fellow in Radiology Journalism was supported by a grant from the American Roentgen Ray Society and the *AJR*.

[1] Department of Radiology, Massachusetts General Hospital and Harvard Medical School, 32 Fruit St., Boston, MA 02114. Address reprint requests to F. S. Chew.

0361–803X/91/1563–0627
© American Roentgen Ray Society

Manuscripts, institutional affiliations, and names of coauthors were not available. No assessment of manuscript quality or suitability for publication was made. The series included no manuscripts in the field of neuroradiology (neuroradiology papers published by *AJR* pass through the editorial offices of the *American Journal of Neuroradiology* first).

MEDLINE (National Library of Medicine, Bethesda, MD) searches were conducted 45–54 months after the date of rejection. The titles of published papers located by this search were compared with the titles of rejected manuscripts. There were few title changes, and although the rejected and published papers could not be compared directly, the reviewers' comments and the editorial correspondence resolved any questions about the identity of the papers. The MEDLINE provided full bibliographic citations.

The number of papers eventually published may have been underestimated because not all journals are indexed by the National Library of Medicine on MEDLINE. Furthermore, in journals that are indexed, not every item in every issue is included. For example, many journals publish case reports as letters to the editor; some of these letters might not be indexed, even though major papers from the same issue of the same journal would be. Any paper published after the date that the MEDLINE searches were conducted would not be included.

The delay in publication that followed rejection was calculated from the date of rejection to the cover date of the publishing journal. The cover date may not always correspond with the actual publication date because some journals do not adhere to established publication schedules.

Three characteristics of the journals that published manuscripts rejected by the *AJR* were studied; size, circulation, and impact factor. The size of the journals was defined in terms of the number of papers published during 1986; these figures were obtained from the MEDLINE. The circulation of the journals was obtained from standard references [5, 6]. Impact factors were obtained from the *1986 Science Citation Index* [7]. The impact factor is a ratio between the number of citations a journal receives and the number of papers it publishes [8]. A high impact factor is an indication that papers published in the journal are frequently cited (referenced) in the bibliographies of subsequent publications. The impact factor can be used as an index of the quality of a journal [8]. Journals for which the *Science Citation Index* publishes no impact factor are generally journals that receive too few citations to reach the threshold for coverage.

## Results

The MEDLINE searches located 162 (64%) published papers out of 254 previously rejected manuscripts, including 97 major papers, 59 case reports, and six technical notes or computer papers (Table 1). Sixty-nine percent of the rejected major papers, 62% of rejected case reports, and 33% of rejected technical notes or computer papers were published elsewhere.

The delay between rejection by *AJR* and publication elsewhere for all published manuscripts ranged from 2 to 38 months, with a mean of 14.7 months (Figs. 1 and 2). No significant difference was demonstrated in the mean delay in publication among major papers, case reports, and technical notes or computer papers. For papers published in radiologic journals, the mean delay in publication was 13.7 months and for papers published in nonradiologic journals, the mean delay was 17.5 months; this difference was significant (Student's t test, $p < .002$) (Table 2). A similar difference in delay was observed between papers published in United States journals and foreign journals (Table 2).

**TABLE 1: Subsequent Publication of Rejected *AJR* Manuscripts According to Type of Manuscript**

| Type of Manuscript | Number of Papers | | Mean Delay ± SEM[a] (months) |
|---|---|---|---|
| | Rejected by *AJR* | Published Subsequently (%) | |
| Major papers | 141 | 97 (69) | 14.1 ± 0.65 |
| Case reports | 95 | 59 (62) | 15.4 ± 0.92 |
| Technical notes | 18 | 6 (33) | 17.2 ± 3.83 |
| All papers | 254 | 162 (64) | 14.7 ± 0.53 |

[a] SEM = standard error of the mean.

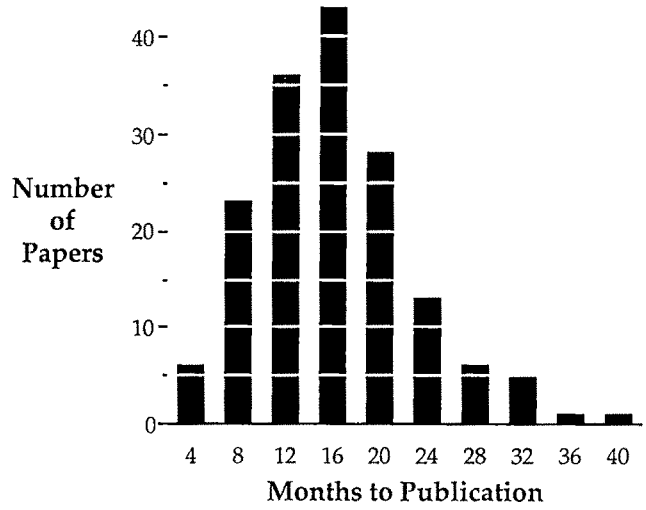



**Fig. 1.—Frequency distribution of publication delay for manuscripts rejected by *AJR* that were ultimately published in other journals.**

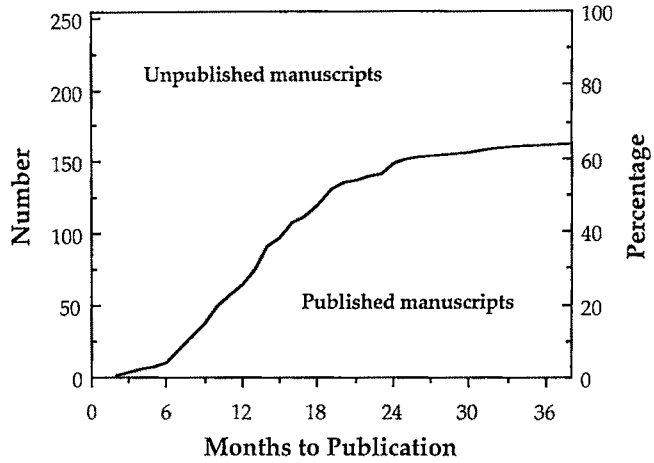



**Fig. 2.—Cumulative number and percentage of manuscripts rejected by *AJR* ($n = 254$) that were ultimately published in other journals ($n = 162$) as a function of time. Rate of publication was slow for the first 6 months, more rapid for the following 20 months, and then slow again. No paper was published after 38 months.**

**TABLE 2: Publication Delay and Number of Rejected *AJR* Manuscripts Published According to Type of Journal**

| Type of Journal | Number of Papers Published | Mean Delay ± SEM[a] (months) |
|---|---|---|
| Radiologic | 120 | 13.7 ± 0.54[b] |
| Nonradiologic | 42 | 17.5 ± 1.28[b] |
| United States | 132 | 14.0 ± 0.57[c] |
| Foreign | 30 | 17.7 ± 1.30[c] |

[a] SEM = standard error of the mean.
[b] Significant difference ($p < .002$).
[c] Significant difference ($p < .007$).

The rejected submissions that were eventually published appeared in 57 different journals (Table 3). Ten of the journals published 81 (50%) of the papers. Twenty-six journals published two or more papers each. The 30 radiologic journals published 120 (74%) of the papers, and the 27 nonradiologic journals published 42 (26%, Table 4). The 43 American journals published 132 (81%) of the papers and the 14 foreign journals published 30 (19%).

The journal that published the greatest number of rejected submissions to *AJR* was *Radiology* (15 major papers). Assuming constant rates of submission, rejection, and eventual publication, the estimated annual publication in *Radiology* of submissions previously rejected by *AJR* was 36 papers, constituting about 5% of the papers published by *Radiology*. The two radiologic subspecialty journals that published the largest numbers of rejected submissions to *AJR* were the *Journal of Computer Assisted Tomography (JCAT)* (seven major papers and seven case reports) and *Skeletal Radiology* (three major papers and five case reports). The estimated annual contributions to these journals by papers previously rejected by *AJR* were 34 and 19 papers, respectively, constituting 13% of the papers in *JCAT* and 15% of the papers in *Skeletal Radiology*. Three major papers published by *AJR* were accepted on the second try; *AJR* does not identify resubmissions of previously rejected manuscripts and treats them as new submissions.

The two general medical journals that published the largest numbers of rejected papers were the *Southern Medical Journal* (two major papers and four case reports) and the *New York State Journal of Medicine* (three case reports). The estimated annual contributions to these journals by papers previously rejected by the *AJR* were 14 and seven papers, respectively, constituting approximately 39% of the radiology papers in the *Southern Medical Journal* and 72% of the radiology papers in the *New York State Journal of Medicine*.

The mean size of journals that published manuscripts rejected by *AJR* was 226 papers published per year (Table 5). Twenty-two (14%) of the manuscripts rejected by *AJR* were published in four journals that were larger than *AJR: Cancer, Journal of Urology, Radiology*, and *Chest*.

Circulation figures were available for 50 of the 57 journals (Table 5). These journals had a mean circulation of 9429, and they published 153 of the manuscripts rejected by *AJR*. Twenty-nine (19%) of the rejected manuscripts were published in seven journals with larger circulations than the *AJR:*

**TABLE 3: Journals That Published Rejected *AJR* Manuscripts**

| Journal Title | No. Published |
|---|---|
| Radiology | 15 |
| Journal of Computer Assisted Tomography (JCAT) | 14 |
| Skeletal Radiology | 8 |
| Acta Radiologica: Diagnosis | 7 |
| Clinical Nuclear Medicine | 7 |
| Pediatric Radiology | 7 |
| Canadian Association of Radiologists Journal | 6 |
| Gastrointestinal Radiology | 6 |
| Southern Medical Journal | 6 |
| British Journal of Radiology | 5 |
| Journal of Clinical Ultrasound (JCU) | 5 |
| Clinical Imaging (formerly Journal of Computer Tomography) | 4 |
| Investigative Radiology | 4 |
| Journal of Urology | 4 |
| AJR | 3 |
| Cardiovascular and Interventional Radiology | 3 |
| Clinical Radiology | 3 |
| Computerized Medical Imaging and Graphics (formerly Computerized Radiology) | 3 |
| Journal of Ultrasound in Medicine | 3 |
| Magnetic Resonance Imaging | 3 |
| New York State Journal of Medicine | 3 |
| Urologic Radiology | 3 |
| Urology | 3 |
| Chest | 2 |
| Journal of Trauma | 2 |
| Orthopedics | 2 |
| Annales de Radiologie, Arzneimittelforschung, Critical Reviews in Diagnostic Imaging, European Journal of Radiology, Journal of Nuclear Medicine, Journal of Thoracic Imaging, RadioGraphics, Radiologia Medica, Rays, RÖFO: Fortschritte auf dem Gebiete der Röntgenstrahlen und der Nuklearmedizin, Ultrasound in Medicine and Biology, Acta Cytologica, Alabama Journal of Medical Sciences, American Journal of Gastroenterology, American Journal of Sports Medicine, American Journal of Surgery, American Review of Respiratory Diseases, Annals of Emergency Medicine, Cancer, Clinical Orthopedics and Related Research, European Journal of Pediatrics, Head and Neck Surgery, Indian Pediatrics, Israel Journal of Medical Sciences, Japanese Journal of Surgery, Journal of the American Medical Women Association, Journal of Clinical Gastroenterology, Journal of the National Medical Association, Journal of Vascular Surgery, Spine, Surgery | 1 each |

**TABLE 4: Type of Journal That Published Rejected *AJR* Manuscripts**

| Type of Journal | Number of Journals | Type of Manuscript | | | Total Manuscripts Published |
|---|---|---|---|---|---|
| | | Major Papers | Case Reports | Technical Notes | |
| United States | | | | | |
| Radiologic | 21 | 60 | 31 | 4 | 95 |
| Nonradiologic | 22 | 20 | 16 | 1 | 37 |
| Foreign | | | | | |
| Radiologic | 9 | 15 | 9 | 1 | 25 |
| Nonradiologic | 5 | 2 | 3 | 0 | 5 |

**TABLE 5: Size, Circulation, and Impact Factor of Journals That Published Rejected *AJR* Manuscripts**

| Type of Journal | Size[a] Mean ± SD | Circulation[b] Mean ± SD | Impact Factor[c] Mean ± SD |
|---|---|---|---|
| Radiologic | 172 ± 158 | 6,139 ± 7,958 | 0.980 ± 0.957 |
| Nonradiologic | 285 ± 211 | 12,848 ± 8,693 | 1.019 ± 0.952 |
| United States | 241 ± 213 | 10,794 ± 9,551 | 1.122 ± 1.035 |
| Foreign | 182 ± 93 | 3,211 ± 1,780 | 0.603 ± 0.344 |
| All journals | 226 ± 192 | 9,429 ± 9,146 | 1.001 ± 0.944 |

[a] Number of papers published in 1986. Source: MEDLINE.

[b] From *Ulrich's International Periodicals Directory 1989–1990* [5] and *Standard Periodical Directory 1989* [6].

[c] From Garfield [7].

*Radiology, Orthopedics, New York State Journal of Medicine, Southern Medical Journal, Journal of the National Medical Association, RadioGraphics*, and *American Journal of Surgery*.

Impact factors were available for 47 of the 57 journals (Table 5). These journals had impact factors that ranged from 0.009 to 4.547 with a mean of 1.001. They published 142 of the manuscripts rejected by *AJR*. The average impact factor, weighted for the number of rejected manuscripts published, was 1.135 (SD 0.947). Eighteen (13%) of the rejected manuscripts were published in journals with impact factors greater than *AJR*'s impact factor of 2.277: *Radiology, American Review of Respiratory Diseases, Cancer*, and *Journal of Nuclear Medicine*.

Case reports were published in journals with impact factors ranging from 0.009 to 1.880. The average impact factor for journals publishing previously rejected case reports, weighted for the number published, was 0.822 (SD 0.574). Major papers were published in journals with impact factors ranging from 0.009 to 4.547. The average impact factor for journals publishing previously rejected major papers, weighted for the number published, was 1.296 (SD 1.057). This difference in impact factor between journals publishing case reports and journals publishing major papers was significant (Student's t test, $p < .004$) and could be accounted for by the 15 major papers published in *Radiology*.

A significant but weak negative correlation was noted between delay in the publication of case reports and the impact factor of the journal in which the case report appeared ($r = .220$). The delay in publication accounted for less than 5% of the variation in impact factor. No such correlation was found for major papers.

## Discussion

Rejection letters are familiar to all who write to publish. Because a scientific paper represents not only many hours of writing and manuscript preparation but also a great investment of research time and resources [9, 10], authors are reluctant to abandon a rejected manuscript. Furthermore, because publication is such a crucial stage in the research process [1], an unpublished study is usually treated as a study never performed. Publication in peer-reviewed scientific journals is highly prized because it is difficult.

### *Decision to Reject*

The editorial decision at the *AJR* to accept or reject a submission is based on peer review. All manuscripts are reviewed by two or more referees selected by the editor from a roster of over 700. When these reviews are in hand, the editor performs his or her own review and makes the decision. If the referees disagree with each other or if they do not fully address a paper, the editor may ask for additional reviews. Although the editor has complete discretion, decisions to reject are usually justified to the author in the editor's letter of rejection, and excerpts of the reviews are usually included to aid the author in revising his paper should he decide to submit it elsewhere. Editors of *AJR* have always been senior academic radiologists. The referees are virtually all academic radiologists, but they may be at earlier stages of their careers. The quality of the referees and of their reviews is not uniform, and both they and the editors are subject to making errors and dubious judgments: the peer review system is not infallible.

Factors other than peer review that may influence the acceptance of a paper are competition for space in the journal, suitability for the journal's audience, and conformity with the journal's goals. A journal with many submissions can be more selective than one with few submissions. *AJR*'s own standard rejection letter states: "Many papers with merit must be rejected because of the intense competition for pages in the journal." If *AJR* accepted more pages than it could publish, a large backlog would be created, resulting in longer and longer delays in publication.

### *Acceptance and Publication*

The *AJR* acceptance rate during 1986 for major papers was 43%; for case reports it was 20%. The proportion of rejected manuscripts published in other journals was similar for both major papers and case reports, but because the initial rejection rate at the *AJR* was higher for case reports, a smaller proportion of case reports was ultimately published. Thus, the fate of manuscripts submitted to *AJR* can be described in the following way: (1) of a hypothetical cohort of 100 major papers submitted to *AJR*, 43 would be accepted and published by *AJR*, 39 would be published elsewhere, and 18 would not be published; (2) of a hypothetical cohort of 100 case reports submitted to *AJR*, 20 would be accepted and published by *AJR*, 50 would be published elsewhere, and 30 would not be published.

### *Lost Research*

Only half of the medical research presented at scientific meetings and published in abstract form is ever published as full-length papers in peer-reviewed journals [11, 12]. By extrapolation, and in light of the results of this study, approximately 28% of the research presented at meetings and published in abstract form is not submitted for publication, and 22% is submitted, rejected, and not published. Results of many randomized clinical trials are never published, more

because papers are not submitted than because papers are rejected [13].

Reasons research work is never submitted may include research projects that are poorly conceived or executed, projects that encounter insoluble problems, or projects that simply never reach completion. A more subtle obstacle may be a presumption on the part of authors that their work is not publishable because the results were neutral or unfavorable to the experimental hypothesis [13]. For example, if a new imaging technique were tested but shown to be inferior to existing techniques, the study would be less likely to be submitted for publication than if the new technique had been shown to be superior.

Reasons submitted papers never get published include failure to pass peer review and procrastination on the part of authors in resubmitting their rejected work to other journals. Although research that is never published represents wasted effort and resources, studies whose results are unreliable should not be published. Ideally, such papers would be identified during the peer review process. An *AJR* survey showed that procrastination on the part of authors was a significant element in the publication lag of papers that had been provisionally accepted pending satisfactory revision (Berk RN, personal communication). The element of procrastination might be more extreme in cases in which the paper had been rejected, because resubmission has no particular guarantee of success.

### *Delay in Publication*

The typical publication lag in *AJR* in 1986 was approximately 4 months from final acceptance to mailing of the journal (Berk RN, personal communication). Thus, if a rejected submission had received final acceptance rather than rejection, it would have appeared in print 4 months later. Most accepted manuscripts require revision, a process that usually adds about a month to the publication lag. Therefore, the 15-month mean interval between rejection by *AJR* and publication elsewhere actually represents a 10-month delay in publication. Most of the manuscripts that are rejected by *AJR* are rejected within 1 month of submission, making the mean interval between submission to *AJR* and publication in another journal about 16 months. In comparison, the publication lag for clinical research papers and case reports in the biomedical literature in general is about 10 months [9].

The slightly longer delay found for papers published in nonradiologic journals may be explained by the possibility that radiology papers are stockpiled by nonradiologic journals and published as space permits. Nonradiologic journals may have longer publication lags than radiologic journals, particularly in view of the fact that the editorial staffs of the two largest radiology journals pride themselves on prompt handling of manuscripts and rapid publication of accepted papers [14, 15].

### *Journals That Publish Rejected Manuscripts*

Journal editors generally do not know whether a submission has been rejected by another journal. This is not altogether undesirable, as an author can obtain another chance at peer review without bias. It is noteworthy that the most frequently cited paper ever published by *AJR* [16] was itself a reject from another journal (Collins VP, personal communication). It is not known how many other submissions to *AJR* have been previously rejected by other journals. In a survey of general medical journals, the proportion of previously rejected published papers ranged from 2% to 32% [17]. Because of differences in submission requirements among journals, particularly in the presentation of the figures and the legends [18, 19], it is clear that some submissions to the *AJR* are prepared in the styles of other journals and represent previously rejected submissions (Berk RN, personal communication). Furthermore, occasionally an *AJR* reviewer will note that a paper he or she reviewed for another journal is now being considered by *AJR*. Because *AJR* and *Radiology*, the two largest radiology journals, are similar in content, audience, and editorial outlook [2, 3], we suspect that manuscripts rejected by one are frequently submitted to the other. At one time *Radiology* and *AJR* considered sharing reviews of rejected manuscripts (Berk RN, personal communication), but decided against it [20].

Authors aim to publish their work in the best journal that reaches their audience. We studied three objective, independently quantified characteristics that might be included in criteria for the worthiness of a journal: size, circulation, and impact factor. The vast majority of manuscripts rejected by the *AJR* were published in journals whose sizes and circulations were smaller and whose impact factors were lower than *AJR*'s.

Suitability for a journal's audience may be a factor in papers published in nonradiologic journals. Radiologic papers are often of interest to nonradiologists, but few subscribe to *AJR* (about 3% of *AJR* subscribers are neither board-certified radiologists nor radiologists-in-training, according to an unpublished 1988 *AJR* readership survey).

The inverse correlation between the delay in appearance of case reports and the impact factor of the journals in which they appeared suggests that some case reports may be submitted to journals of successively lower prestige until accepted. This appeared to be a very small effect. A similar observation has been made in the internal medicine literature [11].

### *Conclusion*

The disappointed author, rejection notice in hand, should not necessarily become discouraged. Rejection by *AJR*, and probably other peer-reviewed journals as well, does not consign a manuscript to oblivion: at least 82% of the major papers and 70% of the case reports that are submitted to *AJR* are eventually published, either in the *AJR* or elsewhere. Rejection necessarily invokes delay, but the majority of papers rejected by the *AJR* are published within 18 months of their original submission to the *AJR*.

Peer review is a professional evaluation of a research manuscript that is performed by experts in the field. This service is offered anonymously and costs the author nothing

but the time required by the editors and referees to evaluate the manuscript (3–4 weeks at the *AJR*). The author truly has nothing to lose, and the paper might even be accepted. In case of rejection, the author should consider the comments from the editors and the referees as specific guides to improving the manuscript. Often a more suitable journal can be found. However, if the science is flawed and the results are unreliable, there is no purpose in pursuing publication.

ACKNOWLEDGMENTS

Access to the files and the data bases of the *AJR* editorial office was provided graciously by Robert N. Berk, Editor-in-Chief. The MEDLINE searches were performed expertly by Patricia Kinnison and Martha Bovee of the Reference Department, The Biomedical Library, University of California, San Diego, La Jolla, CA.

REFERENCES

1. Chew FS, Relyea-Chew A. How research becomes knowledge: an analysis of citations to published papers. *AJR* **1988**;150:31–37
2. Figley MM. Publication in radiology: challenges to tradition. *Radiology* **1985**;157:633–636
3. Chew FS. The scientific literature in diagnostic radiology for American readers: a survey and analysis of journals, papers, and authors. *AJR* **1986**;147:1055–1061
4. Garfield E, ed. *SCI journal citation reports, science citation index 1988 annual*, vol. 19. Philadelphia: ISI Press, **1989**
5. *Ulrich's international periodicals directory 1989–1990, 28th edition*. New York: Bowker, **1989**
6. *Standard periodical directory 1989*, 12th ed. New York: Oxbridge Communications, **1989**
7. Garfield E, ed. *SCI journal citation reports, science citation index 1986 annual*, vol 19. Philadelphia: ISI Press, **1987**
8. Garfield E. Citation analysis as a tool in journal evaluation. *Science* **1972**;178:471–479
9. Roland CG, Kirkpatrick RA. Time lapse between hypothesis and publication in the medical sciences. *N Engl J Med* **1975**;292:1273–1276
10. King DW, McDonald DD, Roderer NK. *Scientific journals in the United States: their production, use, and economics*. Stroudsburg, PA: Hutchinson Ross, **1981**
11. Goldman L, Loscalzo A. Fate of cardiology research originally published in abstract form. *N Engl J Med* **1980**;303:255–259
12. Goldman L, Loscalzo A. Publication rates of research originally presented in abstract form in three subspecialties of internal medicine. *Clin Res* **1982**;30:13–17
13. Dickersin K, Chan S, Chalmers TC, Sacks HS, Smith H Jr. Publication bias and clinical trials. *Controlled Clin Trials* **1987**;8:343–353
14. Siegelman SS. Annual report of the editor of Radiology [for 1989]. In: *Radiologic Society of North America: 1990 Directory of Members*. Oak Brook, IL: RSNA, **1990**:381–382
15. Berk RN. AJR achieves goal to speed publication. *AJR* **1987**;149:312
16. Chew FS. *AJR*: the 50 most frequently cited papers in the past 50 years. *AJR* **1988**;150:227–233
17. Whitman N, Eyre S. The pattern of publishing previously rejected articles in selected journals. *Fam Med* **1985**;17:26–28
18. Publication information for authors. *Radiology* **1990**;175:46A, 52A, 56A
19. *AJR* guidelines to authors. *AJR* **1990**;154:A3–A5
20. Siegelman SS. Editor's page: the rival editors. *Radiology* **1988**;166:784

# Letters

## Prevention of Claustrophobia Induced by MR Imaging: Use of Alprazolam

Patients who have claustrophobia and other anxiety-related disorders may be unable to remain inside an MR imager long enough for an imaging study to be completed. Some centers have studies cancelled for as many as 30% of patients because of this problem. My colleagues and I have used oral Xanax (alprazolam) prophylactically to treat claustrophobia in 100 adults who were scheduled for MR imaging. We were able to complete the MR studies in all 100 patients.

The treatment is as follows: Approximately 30 to 60 min before the MR study, the patient is given 0.5 mg of alprazolam orally. After checking in at the admissions desk, the patient is given an additional 0.5 mg of alprazolam sublingually. The pill is bitter, but patients are encouraged to keep it under the tongue as long as possible before they swallow it.

None of our 100 patients became unconscious or insensible when this regimen was used, and none required any other medication. All were warned not to drive themselves home.

Because of its short onset of action and short duration of effect, alprazolam is particularly well suited for use in outpatients. Ventilatory depression and retention of carbon dioxide do not occur.

David S. Klein
*Shenandoah Valley Pain Clinic*
*Staunton, VA 24401*
*Ohio State University*
*Columbus, OH 43210*

## Prevention of Vomiting Induced by IV Contrast Media

Recent investigations indicate no appreciable differences between older, ionic, high-osmolar and newer, nonionic, low-osmolar IV contrast media with regard to mortality rates [1] and nephrotoxic effects [2, 3]. There is, however, a considerable difference in minor reactions, which are greatly decreased with the use of the newer agents [1]. Nausea and vomiting are among the commonest reactions and the more severe of minor reactions. Control of nausea and elimination of vomiting would make the use of ionic, high-osmolar agents more acceptable and at a savings that could amount to $1 billion each year just for the media alone.

In 1967, on the theory that nausea and vomiting were caused by a sudden drop in blood pressure, raising both the patient's legs was tried to increase blood pressure. "Leg raising" as used here includes raising one (if the medium is being injected into the other arm) or both arms. The Trendelenburg position also could be used.

A total of 4591 excretory urograms have been done with ionic, high-osmolar media, and 387 patients became nauseated. On the basis of previous studies [4], about 83 patients would have been expected to vomit. When the leg-raising maneuver was used, however, only 10 patients vomited, 0.22% of all patients. This compares favorably with the 0.36% who vomit when the nonionic, low-osmolar agents are used [1].

Leg raising must be started immediately after nausea begins; any delay makes this treatment less effective. Patients must understand that they should notify the radiologist or technician, who must remain with them for at least 3 min, about anything they notice.

It is difficult to determine the effect of leg raising on nausea, but the impression is that the duration and severity of the nausea are diminished. Most other minor reactions can be controlled by medication.

Should nausea and vomiting occur before the injection of contrast medium has been completed, the injection can be started again as soon as vomiting stops without a recurrence of symptoms in almost 100% of cases.

There are, however, specific indications for use of the newer, nonionic, low-osmolar agents, especially in patients who have asthma or heart disease or who previously have had significant reactions to contrast medium [5].

M. H. Nathan
*Scottsdale, AZ 85253*

REFERENCES

1. Katayama F, Yamagudi K, Kozuka T, Takashimi T, Seez P, Hutsura K. Adverse reactions to ionic contrast media. *Radiology* **1990**;175:621–631
2. Parfrey PS, Griffiths SM, Brenden J, et al. Contrast material–induced renal failure in patients with diabetes mellitus, renal insufficiency or both. *N Engl J Med* **1989**;320:149–153
3. Schwab SJ, Hlatkey MA, Pieper KS, Davidson CJ. Contrast nephrotoxicity: a randomized controlled trial of a non-ionic and an ionic radiographic contrast agent. *N Engl J Med* **1989**;320:149–153
4. Och SF, Little E, Buchtel B, Giesen A, Morel S. Untoward reactions observed in 10,000 consecutive excretory urographies. *J LA State Med Soc* **1962**;114:150–155
5. Bettmann MA. Ionic versus non-ionic contrast agents in intravenous use: are all the answers in? *Radiology* **1990**;175:616–618

## Stereotactic Breast Biopsy with a 20-Gauge Needle

We read the article by Löfgren et al. [1] on stereotactic fine-needle aspiration biopsy of the breast and the accompanying commentary [2] with great interest. Löfgren et al. failed to obtain representative material in 26% of the lesions. Forty percent of the lesions (see Table 3, benign lesions [1]) showed no atypia, but sonography was not used, and half were simple cysts, so the unique contribution from stereotactic aspiration should be that diagnostic surgery was averted in more than 20% of cases. Furthermore, the article and the commentary emphasize the need to have an experienced staff, and an article by Kopans [3] contains a similar statement. Thus, the usefulness of stereotactic fine-needle aspiration biopsy appears to be rather moderate in comparison with the investment and training necessary.

We have a different opinion. Instead, we think, like the hope expressed in the commentary [2], that stereotaxis will mean a general increase in the specificity of mammographic findings. In our first year of mammographic screening with an attachable Siemens unit, we had a failure rate well below 10%, quite in accordance with results [4, 5] of centers that used older free-standing equipment. Our technique is quite basic, but it differs from the one used by Löfgren et al. [1] in some important respects: The skin is anesthetized. The needle is 20 gauge to avoid deflection, and it has a stylet to avoid contamination. It is rotated at insertion as advocated, and once in correct position, the lesion is stabbed decisively, while suction is applied, in three to six quick strokes, with an amplitude of 1.5–2.0 cm. The large gauge allows aspiration of abundant material, and the swift movement prevents coherent pieces of tissue. Usually a faint vibration is felt in the needle. Profuse bleeding blocks aspiration.

In combination with a ruler graded in millimeters, the stereotactic needle guide becomes a wonderful instrument for "mapping" a lesion in the lesion's orthogonal dimensions. We do at least five different needle passes in rapid succession, and usually a single radiologic check of the needle's position is sufficient. We think that the technical difficulties have been widely overestimated because of the results of earlier approaches that used a smaller gauge needle. We fail to see how mammographers of today can meet their responsibilities without the stereotactic needle guide.

Toomas I. Mathiesen
Ingrid Idvall
*Mammographic Screening & Research Center*
*RTG, Ängelholms Sjukhus, S-26201, Sweden*

REFERENCES

1. Löfgren M, Andersson I, Lindholm K. Stereotactic fine-needle aspiration for cytologic diagnosis of nonpalpable breast lesions. *AJR* **1990**;154:1191–1195
2. Jackson VP, Bassett LW. Stereotactic fine-neelde aspiration biopsy for nonpalpable breast lesions. *AJR* **1990**;154:1196–1197
3. Kopans DB. Fine-needle aspiration of clinically occult breast lesions. *Radiology* **1989**;170:313–314
4. Dowlatshahi K, Gent HJ, Schmidt R, Jokich PM, Bibbo M, Sprenger E. Nonpalpable breast tumors: diagnosis with stereotaxic localization and fine-needle aspiration. *Radiology* **1989**;170:427–433
5. Azavedo E, Svane G, Auer G. Stereotactic fine-needle biopsy in 2594 mammographically detected non-palpable lesions. *Lancet* **1989**;1:1033–1036

## Hepatic Calcifications Presumably Due to Congenital Syphilis

Hepatic calcifications in the newborn are uncommon and have been attributed to several causes, including tumor, vascular thrombosis, and transplacental infection. Congenital syphilis has not been reported before as a cause of neonatal hepatic calcifications.

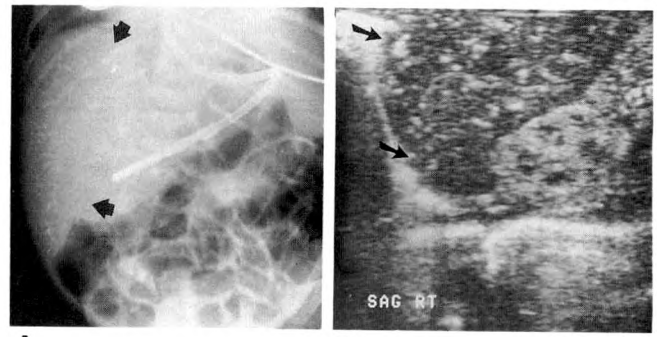



**Fig. 1.—Hepatic calcifications presumably due to congenital syphilis.**
***A*, Radiograph of abdomen shows multiple punctate calcifications (*arrows*) in right upper quadrant.**
***B*, Sonogram of liver shows multiple echogenic foci (*arrows*) representing calcifications. Increased echogenicity of kidney was thought to be nonspecific; no evidence of renal disease was found.**

A 780-g female was born at 28 weeks gestation. The mother had received no prenatal care and had active syphilis at the time of delivery. The infant was seronegative for human immunodeficiency virus, toxoplasma, rubella virus, cytomegalovirus, and herpes simplex virus. Congenital syphilis was diagnosed on the basis of several positive tests: RPR (rapid plasma reagent), ART (automated reagent test), TPHA (*Treponema pallidum* hemagglutination antigen), and VDRL (veneral disease research laboratory). Cultures of blood and respiratory secretions showed no evidence of other infection. Liver function studies were unremarkable. Physical examination showed marked hepatomegaly. A radiograph of the abdomen showed numerous punctate calcifications in the right upper quadrant (Fig. 1A). Sonograms of the liver showed multiple echogenic foci throughout both lobes, indicating hepatic calcifications (Fig. 1B). Radiographs of the long bones and chest were unremarkable. The infant was treated with penicillin for 14 days. No further manifestations of congenital syphilis have occurred.

Vascular causes of liver calcifications include calcified portal vein thromboemboli and ischemic necrosis from shock and vascular insufficiency [1, 2]. Radiologically, the involved areas usually have branching calcifications. Peripheral calcification suggests a portal vein origin; diffuse involvement suggests ischemic infarction [2]. Calcification, either extensive or nodular, may be seen within hepatic tumors such as hemangioma, hamartoma, and hepatoblastoma. Hepatic calcifications associated with transplacental infection may be due to congenital infection with toxoplasma, herpes simplex virus, echovirus 11, or cytomegalovirus. These have been described as dystrophic, probably as a result of long-standing infection [3]. Other causes of neonatal hepatitis, including congenital syphilis, previously have not been related to hepatic calcifications [3]. The absence of tissue confirmation in this patient makes the determination of the cause of the liver calcifications somewhat tentative. However the lack of any other demonstrable disease process and the clinical course of the infant do suggest that congenital syphilis was indeed the causative agent.

The increasing prevalence of congenital syphilis emphasizes the need for familiarity with the imaging findings of this disease. It is a transplacental infection that affects multiple organ systems in both the fetus and the neonate. Although it has been estimated that bony involvement occurs in the majority of untreated cases, early antibiotic therapy may abort both the clinical signs and symptoms and the bony changes [4]. The lack of bony findings in this patient probably is due to prompt treatment with antibiotics. The presence of diffuse, punctate calcifications in both lobes of the liver suggests a widespread

dystrophic process. The lack of demonstrable liver disease may be related to the time of infection during the prenatal period and subsequent completeness of liver regeneration and repair.

Marvin S. Kogutt
*Tulane University Medical Center*
*New Orleans, LA 70112*

REFERENCES

1. Friedman AP, Haller JO, Boyer B, Cooper R. Calcified portal vein thromboemboli in infants: radiography and ultrasonography. *Pediatr Radiol* **1981**;140:381–382
2. Nguyen DL, Leonard JC. Ischemic hepatic necrosis: a cause of fetal liver calcification. *AJR* **1986**;147:596–597
3. Shackelford GD, Kirks DR. Neonatal hepatic calcification secondary to transplacental infection. *Pediatr Radiol* **1977**;122:753–757
4. Swischuk LE. *Imaging of the newborn, infant, and young child*, 3rd ed. Baltimore: Williams & Wilkins, **1989**:745–746

## Differentiation of Child Abuse from Osteogenesis Imperfecta

The article by Ablin et al. [1] on the differentiation of child abuse from osteogenesis imperfecta is an excellent article and reviews the literature on the subject fairly. As the authors point out, the diagnosis of osteogenesis imperfecta is difficult to make and will remain so in mild cases until a definitive laboratory test for identification of the defective collagen is available. Until then, the diagnosis in mild cases is made on the balance of probabilities of the variety of clinical symptoms and changes on radiographs.

In their article, Ablin et al. rely heavily on the presence of blue sclerae as an indication of osteogenesis type 1. Children with osteogenesis type 1 do have blue sclerae, but not all children with blue sclerae have osteogenesis. The quality of blueness of the sclerae is subjective, and the presence of blue sclerae alone is not sufficient to make the diagnosis of osteogenesis imperfecta. Also, children with osteogenesis are not immune from child abuse. Fractures of posterior ribs and metaphyses are not features of the fractures of osteogenesis imperfecta of the mild varieties. If these features are present, then the diagnosis of child abuse must be considered, irrespective of the color of the child's sclerae. The absence of wormian bones in the skull and the fact that no further fractures occur when the child is removed from the environment in which the injury was sustained would further suggest a diagnosis of child abuse and not osteogenesis imperfecta.

Difficulty arises when the courts get conflicting medical advice from experts, and the onus of the diagnosis then frequently is thrust on a judge, who is faced with the unenviable task of deciding which of the conflicting evidence to believe. If the diagnosis is made in favor of osteogenesis imperfecta, then the danger exists that this child will be cited in future scientific publications as evidence, for example, that fractures of the posterior ribs occur in children with mild osteogenesis imperfecta, even though accumulated clinical experience dictates otherwise.

Ablin et al. [1] point out that Paterson is a member of the Department of Biochemical Medicine, Ninewells Hospital and Medical School, University of Dundee; he is neither a pediatrician nor a radiologist. They also question the validity of Paterson's work because much of it is based on questionnaires and does not include objective review of radiographs [2–5]. Some of the patients included in his scientific papers and cited as having osteogenesis imperfecta have had the diagnosis confirmed by the courts, after conflicting medical evidence.

I, like all radiologists, am concerned about making a wrong diagnosis of child abuse, because of the devastating effects on child and family. I also am concerned about making a wrong diagnosis of osteogenesis imperfecta, because of the implications for a life-style and because of genetic implications, should this diagnosis be wrong. It would be nice if we had a definitive test, but until we do, we are left with a diagnosis based on the balance of probabilities, and one that is based on the accumulated experiences of nearly 40 years of clinical practice from across the world.

Helen Carty
*Royal Liverpool Childrens Hospital*
*Liverpool L12 2AP, England*

REFERENCES

1. Ablin DS, Greenspan A, Reinhart M, Grix A. Differentiation of child abuse from osteogenesis imperfecta. *AJR* **1990**;154:1035–1046
2. Paterson C, McAllion S, Shaw J. Clinical and radiological features of osteogenesis imperfecta type IVA. *Acta Paediatr Scand* **1987**;76:548–552
3. Carty H, Shaw D. Osteogenesis imperfecta type IVA (letter). *Acta Paediatr Scand* **1988**;77:752–754
4. Taitz L. Child abuse and osteogenesis imperfecta (letter). *Br Med J* **1988**;296:292
5. Paterson C, McAllion S. Osteogenesis imperfecta in the differential diagnosis of child abuse. *Br Med J* **1989**;299:1451–1452

*Reply*

We thank Helen Carty for her kind comments on our review article, "Differentiation of Child Abuse from Osteogenesis Imperfecta" [1]. We all agree with her comments and astute observations. Mild cases of osteogenesis imperfecta types I and IV may be difficult to diagnose on the basis of radiographs alone. However, they usually can be identified correctly after consultation among pediatrician, geneticist, and radiologist and close correlation of clinical history, family history, physical examination, radiologic examination, and, if necessary, collagen analysis. We agree that blue sclerae may be seen in disorders other than osteogenesis imperfecta and even in normal infants. However, metaphyscal corner fractures and posterior rib fractures are not typical features of *mild* osteogenesis imperfecta type I or IV, and their presence in these patients should be considered highly suggestive of child abuse.

The misdiagnosis of osteogenesis imperfecta in a child who actually is abused will do great harm to an already injured child and may even lead to a fatality. This misdiagnosis also will provide protectors of child abusers or investigators of osteogenesis imperfecta with false or misleading data about features assumed to be associated with the disease. Children with osteogenesis imperfecta indeed can be abused. The radiologist, pediatrician, and geneticist should work together as a team to arrive at the correct diagnosis and to clarify these matters for the judge, jury, or child protective services.

In our article [1], we have called attention to the less than scientific approach of Paterson's work [2, 3], and we shed doubt on its validity. Paterson is neither a pediatrician nor a radiologist. His methods lack a systematic review of radiologic data on the reported patients with osteogenesis imperfecta type IV, as only some of the radiographs were analyzed [2–4]. Also his data collection was based on questionnaires given to patients and parents, which may be subject to errors. His papers do not have photographic and radiologic examples of patients with osteogenesis imperfecta type IV to support his statements. In one of his studies of patients with type IV disease, prevalence of skull and rib fractures has been high [2, 4], suggestive of the misdiagnosis of osteogenesis imperfecta for actual child abuse. Carty states in her letter that some of Paterson's patients were "labeled" as having osteogenesis imperfecta by the courts and not by physicians. Thus, some conclusions on osteogenesis imperfecta may be

unjustified if actual cases of child abuse were included in the original data. The proper diagnosis of child abuse or osteogenesis imperfecta is of utmost importance. The main reason for writing our original article was to help physicians, pediatricians, radiologists, geneticists, and members of the legal system to identify these two entities correctly for the sake of the abused child.

Deborah S. Ablin
Adam Greenspan
Michael Reinhart
Arthur Grix
*University of California, Davis, Medical Center*
*Sacramento, CA 95817*

REFERENCES

1. Ablin DS, Greenspan A, Reinhart M, Grix A. Differentiation of child abuse from osteogenesis imperfecta. *AJR* **1990**;154:1035–1046
2. Paterson CR, McAllion SJ, Shaw JW. Clinical and radiological features of osteogenesis imperfecta type IVA. *Acta Paediatr Scand* **1987**;76:548–552
3. Paterson CR, McAllion S, Miller R. Osteogenesis imperfecta with dominant inheritance and normal sclerae. *J Bone Joint Surg [Br]* **1983**;65–B:35–39
4. Carty H, Shaw DG. Osteogenesis imperfecta type IVA (letter). *Acta Paediatr Scand* **1988**;77:752–754

## Doppler Assessment of Fetal Circulation in a Case of Fetal Death

As far as we know, Doppler assessment of the major vessels in human fetuses with prolonged hypoxemia has not been described before. We used pulsed Doppler sonography to study the velocity waveforms in the middle cerebral artery, descending aorta, renal artery, femoral artery, and umbilical artery in a fetus with severe growth retardation at 26 weeks gestation.

A 34-year-old woman at 26 weeks gestation was referred for pulsed Doppler sonography because of severe growth retardation of the fetus and oligohydramnios shown on real-time sonography. The woman had a history of diabetes mellitus and chronic hypertension. No other fetal anomaly was evident. Pulsed Doppler sonography showed reverse diastolic blood-flow velocities in the descending aorta, renal artery, femoral artery, and umbilical artery. The pulsatility index ([peak velocity − lowest diastolic velocity] ÷ [mean velocity]) of the middle cerebral artery was 1.9 and at a 95% tolerance limit below the mean value for the gestational age (Fig. 1). In utero fetal death was diagnosed at 28 weeks gestation, and delivery was induced. Autopsy showed a macerated 470-g stillborn female with visceral congestion and autolysis. The placenta was immature, weighed 135 g, and had focal infarction.

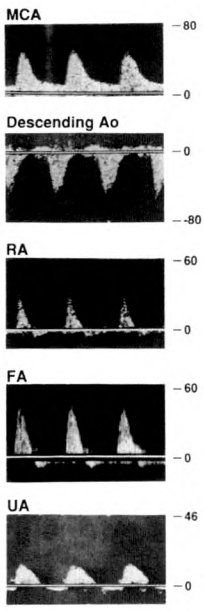



**Fig. 1.—Doppler images of fetus with severe growth retardation at 26 weeks gestation show waveforms of blood-flow velocities in middle cerebral artery (MCA), descending aorta (Ao), renal artery (RA), femoral artery (FA), and umbilical artery (UA). Diastolic component in MCA decreased relatively. Reverse diastolic blood-flow velocities in descending Ao, RA, FA, and UA were evident. All values are in cm/sec.**

In this case, pulsed Doppler sonography showed reversed diastolic blood-flow components in all arteries except the middle cerebral artery. The finding in the middle cerebral artery suggests that the compensatory decrease in the cerebral vascular resistance is not maintained. Richardson et al. [1] reported that an initial increase in cerebral blood flow induced by hypoxemia in fetal lambs was not maintained when associated with progressive acidemia. These results suggest that the animal was not able to maintain a protective circulatory response under the experimental conditions of prolonged hypoxemia with worsening acidemia. The reverse flow of the descending aorta or umbilical artery is an ominous sign for fetal outcome as has been reported previously [2, 3]. The reverse flow in the renal artery has not been described before but suggests prolonged hypoxemia with increased renal vascular resistance. In normal fetuses, the pulsatility index of the femoral artery increases with advancing gestation, and the reverse flow appears only late in the third trimester (Mari G et al., presented at the meeting of the International Perinatal Doppler Society, August 1989). The finding of reverse flow in the femoral artery at 26 weeks gestation suggests compromised hemodynamics. In conclusion, the human fetus also may not be able to maintain a protective circulatory response under prolonged hypoxemia in utero.

Toshiyuki Hata
Giancarlo Mari
Robert J. Carpenter, Jr.
*Baylor College of Medicine*
*Houston, TX 77030*

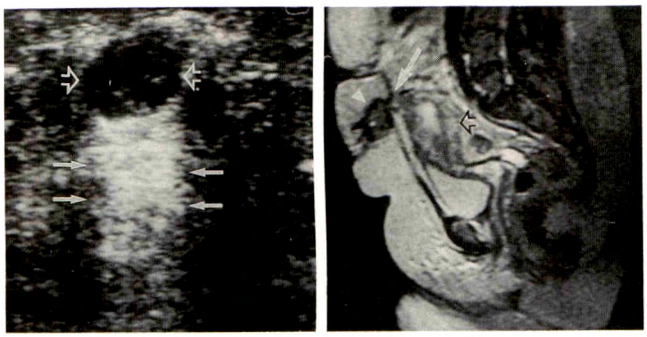
REFERENCES

1. Richardson BS, Rurak D, Patrick JE, Homan J, Carmichael L. Cerebral oxidative metabolism during sustained hypoxemia in fetal sheep. *J Dev Physiol* **1989**;11:37–43
2. Woo JSK, Liang ST, Lo RLS. Significance of an absent or reversed end diastolic flow in Doppler umbilical artery waveforms. *J Ultrasound Med* **1987**;6:291–297
3. Illyes M, Gati I. Reverse flow in the human fetal descending aorta as a sign of severe fetal asphyxia preceding intrauterine death. *JCU* **1988**;16:403–407

## Imaging of Periumbilical Endometriosis

Cutaneous endometriosis has been well described in the gynecologic literature, with few reports in the radiologic literature [1]. We present three cases of endometriosis involving the abdominal wall and the imaging findings.

A 50-year-old woman (gravida 10, para 10) had a 19-year history of a periumbilical mass, which enlarged and became tender during menses. Symptoms began after cesarean delivery of a normal term infant. Physical examination during menses revealed a vertical subumbilical scar and a firm, nodular mass in the abdominal wall. A sonogram obtained during ovulation showed a hypoechoic mass in the periumbilical region (Fig. 1A). MR of the abdomen, performed at 1.5 T with spin-echo sequences of 2000/20, 80 (TR/TE), showed a rim of low signal intensity surrounding a central component with signal intensity similar to that of myometrium. Scattered foci of high signal intensity also were present centrally. A strand of tissue ex-



A B

**Fig. 1.—Periumbilical endometriosis.**

***A*, Sonogram of anterior abdominal wall shows hypoechoic mass (*open arrows*) with prominent posterior enhancement of sound transmission (*solid arrows*).**

***B*, T2-weighted spin-echo sagittal MR image (2000/80) shows mass in subcutaneous tissue (*arrowhead*) with low-intensity rim, central focus of high intensity, and posterior attachment (*solid arrow*) to uterus (*open arrow*).**

tending posteriorly was attached to the uterus (Fig. 1B). Pathologic examination of a specimen obtained via sonographically guided aspiration of the mass revealed hemosiderin-laden macrophages, blood, and benign glandular cells consistent with endometriosis.

In two other pathologically proved cases of endometriosis involving the anterior abdominal wall, sonography showed a subcutaneous hypoechoic mass, and CT showed a midline, solid mass in the lower, anterior abdominal wall.

Development of endometriosis in the umbilicus and anterior abdominal wall occurs primarily through iatrogenic transplantation. Cesarean section is the most common procedure associated with cutaneous endometriosis [1]. The ectopic endometrium may respond to hormonal stimulation, resulting in hemorrhagic cysts. These cysts tend to rupture periodically, causing a fibrotic reaction because of leakage of blood. Adhesions to the peritoneum and adjacent organs may result.

MR findings in pelvic endometriosis have been well described [2]. Our case has similar features: foci of high signal intensity consistent with subacute or chronic hemorrhage; a rim of low signal intensity on T2-weighted images, probably representing a fibrous capsule or deposition of hemosiderin; and adhesions to the uterus. T1-weighted images would be expected to increase the specificity of these findings. A report of endometriosis of the thigh evaluated by MR also noted low signal intensity on T2-weighted images, which suggested deposition of hemosiderin [3]. The sonographic and CT findings of endometriosis are variable and nonspecific [3, 4].

The differential diagnosis of a mass in the anterior abdominal wall is extensive. It includes hematoma, abscess, hernia, suture granuloma, sebaceous cyst, and neoplasms such as sarcoma, lymphoma, dermoid cyst, lipoma, and metastasis. In a female of reproductive age, relationship of the mass to the umbilicus or to a gynecologic surgical scar, imaging evidence of fibrosis or adhesions, and a mass with evidence of subacute hemorrhage on MR images suggest this diagnosis.

Daniel M. Marder
John P. McGahan
William E. Brant
*University of California, Davis, Medical Center*
*Sacramento, CA 95817*
Joseph Leeba
*Sharp Rees-Stealy Clinic*
*San Diego, CA 92101*

REFERENCES

1. Chatterjee SK. Scar endometriosis: a clinicopathologic study of 17 cases. *Obstet Gynecol* **1980**;56(1):81–84
2. Nishimura K, Togashi K, Itoh K, et al. Endometrial cysts of the ovary: MR imaging. *Radiology* **1987**;162:315–318
3. Gitelis S, Petashick JP, Turner DA, et al. Endometriosis simulating a soft tissue tumor of the thigh: CT and MR evaluation. *J Comput Assist Tomogr* **1985**;9(3):573–576
4. Sandler MA, Karo JJ. The spectrum of ultrasonic findings in endometriosis. *Radiology* **1978**;127:229–231

## Oblique Plain Radiographs in the Diagnosis of Ureteral Calculi

In the July 1990 issue of AJR, Gatewood and Berkowitz [1] describe four patients in whom oblique radiographs obtained before excretory urography showed presacral ureteral calculi not seen on the routine scout abdominal radiograph. These authors point out that "because ureteral calculi may be obscured by contrast material during IV urography, the cause of the obstruction may remain obscure, and additional diagnostic workup, such as a retrograde or antegrade ureteropyelography or CT, then is needed. . . . Our experience with these cases suggests that an ipsilateral posterior oblique plain abdominal radiograph of the supine patient may be useful. . . when a calculus is not identified on the anteroposterior view."

The take-home message of this article is not clear to me. Unfortunately, ureteral calculi almost never can be diagnosed definitively or excluded on the basis of the findings on the initial plain abdominal radiograph. Obviously, an oblique view occasionally might be useful, but are the authors recommending that most or all patients undergoing excretory urography for possible ureteral obstruction have an additional scout oblique radiograph? In the proper clinical context, such as no known tumor and young age (three of the four patients described by Gatewood and Berkowitz were <40 years old), would it not be assumed that ureteral obstruction was caused by a nonvisualized calculus even if the area of concern was obscured by contrast medium? Would the addition of a normal preliminary oblique radiograph exclude that possibility?

I am reminded of the recommendation [2], and subsequent rebuttal [3], that before having excretory urography, those patients with any history suggesting calculus disease should have five preliminary tomograms of the kidneys in addition to the scout abdominal radiograph. Using this routine, Schwartz et al. [2] did detect unsuspected nonsymptomatic renal calculi. However, ignoring considerations of cost and exposure to radiation, I doubt that this information, or information obtained from oblique scout radiographs of the pelvis, would affect subsequent diagnostic or therapeutic decisions very often.

Ferris M. Hall
*Beth Israel Hospital*
*Harvard Medical School*
*Boston, MA 02115*

REFERENCES

1. Gatewood OMB, Berkowitz JE. Oblique plain radiographs are useful for detecting opaque presacral ureteral calculi. *AJR* **1990**;155:89–90
2. Schwartz G, Lipschitz S, Becker JA. Detection of renal calculi: the value of tomography. *AJR* **1984**;143:143–145
3. Hall FM. Renal calculi and tomography (letter). *AJR* **1985**;144:217–218

*Reply*

We thank Dr. Hall for his comments. The need to ascertain as precisely as possible the cause of an obstructing ureteral lesion is self-evident and fundamental. The probability of having a radiopaque ureteral calculus is high in patients, especially young ones, who have clinical manifestations of renal or ureteral colic. When a calculus is not seen on the anteroposterior scout abdominal radiograph in such patients, an opaque calculus may be "camouflaged" in the presacral portion of the ureter. An ipsilateral oblique view will bring such a calculus readily into view and permit subsequent matching of the calculus with the ureteral obstruction. If such preliminary identification of the calculus is not made, the cause of the obstruction often remains obscure or, at best, presumptive, particularly if the offending stone continues to elude detection after ureteral opacification. Conversely, the findings on a normal scout oblique radiograph can exclude an opaque calculus as the source of obstruction of the presacral portion of the ureter. Inasmuch as radiolucent calculi are far less prevalent [1], the addition of this view to the preliminary workup of an IV urogram is useful because it affords an immediate definitive diagnosis leading to prompt and more definitive therapeutic decisions.

The take-home message, therefore, is our recommendation to obtain additional preliminary ipsilateral oblique scout radiographs in patients in whom the presence of a ureteral calculus is strongly suspected *if* a calculus is not shown on the initial anteroposterior radiograph [2].

Olga M. B. Gatewood
Joan E. Berkowitz
*The Johns Hopkins Hospital*
*Baltimore, MD 21205*

REFERENCES

1. Spirnak JP, Resnick MI. Urinary stones. In: Smith DR, ed. *General urology*, 11th ed. Los Altos, CA: Lange, **1984**:253–256
2. Gatewood OMB, Berkowitz JE. Oblique plain radiographs are useful for detecting opaque presacral ureteral calculi. *AJR* **1990**;155:89–90

## Radiology of the Cervical Spine in Trauma Patients

Vandemark's review [1] nicely points out the occasional friction between the radiologist who must interpret radiographs of the cervical spine of trauma patients and the surgeons and emergency physicians who request the radiographs. Dr. Vandemark correctly notes that some of the indications cited by requesting clinicians result in an extremely low yield of significant findings.

I think it is only fair to note that many of these clinicians are following guidelines set by the Committee on Trauma, American College of Surgeons (ACS). This committee promulgates standards for trauma care and is responsible for the curriculum of the Advanced Trauma Life Support (ATLS) course, given at many different sites throughout the United States and in several foreign countries each year. The course is intended for all physicians, but the primary target is the physician who does not deal with major trauma on a day-to-day basis.

The ATLS syllabus [2] includes a section on evaluation of the cervical spine in trauma patients. This section lists specific indications that mandate cross-table lateral radiographs of the cervical spine. These include multiple trauma, any injury above the clavicle, any head injury with resultant loss of consciousness, and injury produced by or in a high-speed vehicle. It also provides instruction on interpretation of the lateral radiograph. The intent is more that students be able to distinguish normal from abnormal, than that they be able to reach a specific diagnosis. (None of the cross-table lateral radiographs reproduced in Vandemark's review would be considered normal by ATLS criteria because all show soft-tissue swelling.)

The ATLS syllabus stresses that the cross-table lateral radiograph may be normal in 5–15% of patients who have significant injury of the cervical spine. It states that additional views, tomograms, or CT scans may be required if signs, symptoms, or the mechanism of injury raises clinical suspicion, even though the cross-table radiograph is normal. It makes no recommendation as to which studies should be performed, or in what order, as this is properly the province of the radiologist, orthopedist, and neurosurgeon. Vandemark's scheme for tailored imaging of the cervical spine is extremely useful in this regard. The ATLS syllabus recommends that spinal immobilization be continued until the immobilization device is removed by the neurosurgeon or orthopedist. The radiologist is not considered responsible for "clearing" of the cervical spine.

As a graduate of both the ATLS and the ATLS Instructor courses, I have developed considerable respect for the systematic, orderly approach to the care of the trauma patient that these courses advocate. The ACS has done a great service to all victims of trauma by developing these courses and by establishing national guidelines for trauma care. Vandemark's comments are in substantial agreement with the ATLS guidelines, although he is more restrictive about the indications for imaging the cervical spine. However, as radiologists who rarely, if ever, face the substantial stress and uncertainty that result from primary responsibility for the care of victims of multiple trauma, we have little credibility when it comes to determining whether a cervical spine study is indicated in a specific patient. We must recognize that clinicians are unlikely to deviate from ATLS guidelines on our say-so alone. As Vandemark correctly points out, communication and close cooperation between radiologist and referring physician are essential.

Donald L. Miller
*Warren Grant Magnuson Clinical Center*
*National Institutes of Health*
*Bethesda, MD 20892*

REFERENCES

1. Vandemark RM. Radiology of the cervical spine in trauma patients: practice pitfalls and recommendations for improving efficiency and communication. *AJR* **1990**;155:465–472
2. American College of Surgeons. *Advanced trauma life support instructor manual*. Chicago: American College of Surgeons, **1989**

*Reply*

Dr. Miller rightly points out the value of advanced trauma life support (ATLS) training in the care of patients with suspected injury of the cervical spine. ATLS as a protocol approach to trauma is especially useful when a high-risk patient is involved or when treating physicians are limited in their training or exposure to trauma. Nevertheless, the majority of patients with suspected injury of the cervical spine fall into the categories of medium, low, or no risk. In these patients, I do not support use of rigid protocols for ordering radiographs of the cervical spine for reasons outlined in my article [1]. Without question, use of a tailored approach to ordering radiographs in the emergency department assumes the presence of experienced, appropriately trained and supervised physicians. Under these circumstances, patient risk usually can be assessed accurately so that the ordering of radiographs can be individualized. The approach offered in my article is conservative, in my opinion, and meets the needs of the patient and the ordering physician alike. The risk-tailored ap-

proach to cervical spine radiology, in my experience, allows significant economies in time and effort, precious commodities in any emergency department.

Finally, I am more optimistic than Dr. Miller about our ability as radiologists to educate referring physicians in the most effective methods of imaging emergency department patients. Radiologists who are involved actively in the problems of emergency medicine will develop the credibility needed to be valued consultants and to modify ordering practices when such changes promote improved care for patients.

Robert M. Vandemark
*Duke University Medical Center*
*Durham, NC 27710*

REFERENCE

1. Vandemark RM. Radiology of the cervical spine in trauma patients: practice pitfalls and recommendations for improving efficiency and communication. *AJR* **1990**;155:465–472

## Biopsy Gun and Sheath for CT-Guided Percutaneous Biopsies

We describe a technique for quickly obtaining multiple percutaneous biopsy samples that requires only one CT-directed introduction of a needle. The materials used include an automated Bard Disposable Biopty Gun with a 20-gauge biopsy needle (C. R. Bard, Inc., Covington, GA) and an 18-gauge Lunderquist Special Procedure Sheath/Needle (Meadox Surgimed, Inc., Oakland, NJ). Biopsies were performed successfully in three patients by using this procedure. One (Fig. 1) had a mass in the right adrenal gland, one had a pleural-based mass in the posterior chest wall, and one had an enlarged paraaortic lymph node on the left side.

The technique involves using CT to identify the lesion and then marking the mass with a metallic pellet. The direction of the biopsy approach is selected, and the exact distance from the skin to the lesion is measured. When it is discharged, the automated biopsy gun delivers the indwelling biopsy needle approximately 17 mm beyond the length of the loaded unit. In accordance with this, the sheath portion of the Lunderquist sheath/needle is cut to the proper length, and its end is reflared and fixed to its plastic hub so that when percutaneously introduced under CT guidance, the tip of the sheath will lie approximately 1 cm proximal to the lesion. The Lunderquist sheath then is reaffixed to its needle, and this unit is positioned under CT guidance to leave the sheath tip at the desired location before the needle is removed. The patient is moved out from the CT scanner before biopsy specimens are obtained. The biopsy gun easily is introduced through the indwelling sheath until gentle soft-tissue resistance is encountered, thus indicating that the end of the sheath has been reached. At this point, the cocked biopsy gun is fired and removed while the sheath is left in place. After the biopsy specimen is extracted from the device and given to the cytologist in attendance, the biopsy gun is recocked and placed into the indwelling sheath again. Additional samples are acquired without further CT guidance.

Recent reports [1–3] have discussed the superiority of core tissue specimens obtained from biopsy guns and the ease of using this instrument as compared with conventional manual needle techniques. We think that our technique is a reliable and safe means of quickly acquiring many samples from a particular lesion, especially in patients who have lesions in areas that are considered technically difficult to access.

Louis J. Brisson
Harry G. Zegel
*Presbyterian Medical Center of Philadelphia*
*Philadelphia, PA 19104*

REFERENCES

1. Parker SH, Hopper KD, Yakes WF. Image-directed percutaneous biopsies with a biopsy gun. *Radiology* **1989**;171:663–669
2. Chuang VP, Alspaugh JP. Sheath-needle for liver biopsy in high-risk patients. *Radiology* **1988**;166:261–262
3. Crummy AB, McDermott JC, Wojtowycz M. A technique for embolization of biopsy tracts. *AJR* **1989**;153:67–68

## Membranous Stenosis of the Inferior Vena Cava: Prevention of Placement of a Kimray-Greenfield Filter via the Jugular Vein

In 1962, Kimura et al. [1] reported three cases of obliteration of the hepatic part of the inferior vena cava by a congenital membrane. He treated two of these successfully with transcardiac membranotomy. On the basis of a review of cases of obstruction of the hepatic part of the inferior vena cava reported in Japan, Hirooka and Kimura [2] classified the condition into seven types. We report a case of stenosis of the inferior vena cava at the level of the diaphragm that prevented placement of a Kimray-Greenfield filter via jugular cutdown.

The patient was a 62-year-old man with symptomatic deep-vein thrombosis of the lower extremity who was being treated with heparin. Despite adequate anticoagulation, he had an episode of dyspnea and chest pain. Findings on lung scan suggested pulmonary embolus. A phlebogram showed extensive thrombus in the right iliofemoral system. It was decided that placement of a caval filter was appropriate. An attempt to place a filter via a left femoral approach was unsuccessful because of acute angulation of the left common iliac vein. The patient was taken to the operating room, and the right

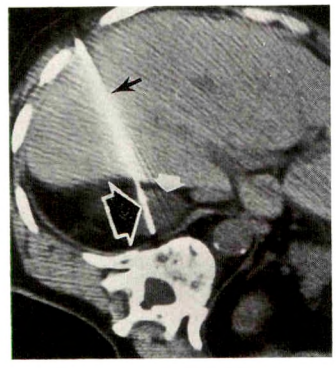


**Fig. 1.—CT scan shows biopsy of mass (*white arrow*) in right adrenal gland. Biopsy gun (*large black arrow*) was inserted through an indwelling sheath (*small black arrow*).**



**Fig. 1.—Digital inferior vena cavagram obtained via a femoral approach shows tight stenosis in suprahepatic part (*arrows*) of inferior vena cava at level of hemidiaphragm. *Arrowhead* = right renal vein.**

internal jugular vein was exposed surgically. With some difficulty, a J-type guidewire was passed through a moderate stenosis at the level of the diaphragm (Fig. 1). Despite numerous attempts, the carrier capsule (24 French) of the Kimray-Greenfield filter could not be passed beyond the stenosis. The stenosis was dilated with a 10-mm balloon, but the filter still could not be passed beyond the stenosis.

The condition encountered in this patient was a type III stenosis of the hepatic part of the inferior vena cava as described by Hirooka and Kimura [2]. It was asymptomatic and had no effect on blood flow in the hepatic vein. However, it did prevent placement of a caval filter via the jugular vein. We speculate that balloon dilatation was unsuccessful because of the muscular composition of the stenosis, which rapidly returned to its former shape after the balloon was deflated. Others [2] have reported successful balloon dilatation of severe caval stenoses associated with obstruction of the hepatic vein.

John C. Holder
Gary W. Barone
John F. Eidt
*University of Arkansas for Medical Sciences*
*Little Rock, AR 72205-7199*

REFERENCES

1. Kimura C, Shirotani T, Kuma M, et al. Transcardiac membranotomy for obliteration of the inferior vena cava in the hepatic portion. *J Cardiovasc Surg* **1962**;3:393–404
2. Hirooka M, Kimura C. Membranous obstruction of the hepatic portion of the inferior vena cava. *Arch Surg* **1970**;100:656–663

## Modified Delivery Catheter for Wallstent Treatment of Renal Artery Stenosis

We have used the Wallstent self-expandable endoprosthesis in the treatment of seven cases of postostial recurrent stenosis of the renal artery and four postangioplasty technical failures of the renal arteries. When placing the stent in the renal artery, we had severe difficulties positioning the proximal end of the stent in continuity with the aortic wall, despite frequent angiographic control via a contralaterally inserted 5-French pigtail catheter. This was due to poor visualization of the unexpanded endoprosthesis during placement and of the proximal end of the stent after release. Indeed, the catheter for delivery of the Wallstent endoprosthesis has three markers. The two distal markers indicate the distal end of the stent before and after release, and the most proximal marker indicates the position of the stent before release. No marker indicates the proximal end of the stent after release. For use in the iliac and femoropopliteal arteries, the two distal markers are sufficient, as they can be used to center the stent on the lesion [1, 2].

In stenting the renal artery, it is important not only to center the stent on the stenotic area but also to have it protrude as little as possible within the aorta. It is well known that it is hard to visualize the Wallstent endoprosthesis, especially in the abdomen, so that during release of the stent, it is difficult to follow the progression of deployment without markers. With the three-marker delivery catheter, exact positioning is difficult, because the proximal marker will be in the aorta during release. Therefore, we asked the manufacturer to add a fourth marker indicating the final proximal end of the stent. The two inner markers indicate approximately the final position of the implanted stent. With this new catheter, we were able to position the stent accurately in three patients with postostial recurrent stenosis (Fig. 1). Undoubtedly, this modification will be useful in the stent treatment of ostial stenosis of the renal artery. One major problem with the use of the Wallstent endoprosthesis in the renal arteries remains to be solved. Because the Wallstent shortens significantly on deployment from the catheter, the length of the stent will depend entirely on the diameter that the prosthesis is allowed to obtain. So, a stent that is not fully expanded will be longer than a less expanded one, and the proximal end of the stent will not correspond to the fourth added marker. Therefore, it would be advisable to determine the length of the stent at various diameters, in order to have an idea about how accurately the additional marker will indicate the final position of the stent.

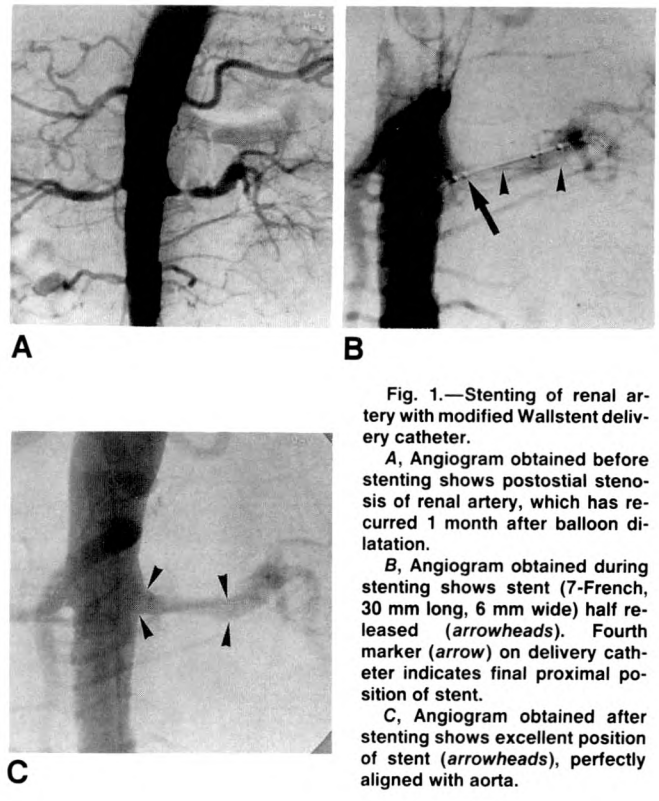



**Fig. 1.—Stenting of renal artery with modified Wallstent delivery catheter.**

***A*, Angiogram obtained before stenting shows postostial stenosis of renal artery, which has recurred 1 month after balloon dilatation.**

***B*, Angiogram obtained during stenting shows stent (7-French, 30 mm long, 6 mm wide) half released (*arrowheads*). Fourth marker (*arrow*) on delivery catheter indicates final proximal position of stent.**

***C*, Angiogram obtained after stenting shows excellent position of stent (*arrowheads*), perfectly aligned with aorta.**

G. Wilms
P. Peene
A. L. Baert
*University Hospitals, K. U. Leuven*
*B-3000 Leuven, Belgium*

REFERENCES

1. Raillat C, Rousseau H, Joffre F, Roux D. Treatment of iliac artery stenoses with the Wallstent endoprosthesis. *AJR* **1990**;154:613–616
2. Rousseau H, Raillat C, Joffre F, Knight C, Ginestet M. Treatment of femoropopliteal stenoses by means of self-expandable endoprosthesis: midterm results. *Radiology* **1989**;172:961–964

Letters are published at the discretion of the Editor and are subject to editing.

Letters to the Editor must not be more than two *double-spaced*, typewritten pages. One or two figures may be included. Abbreviations should not be used. See Author Guidelines, page A5.

Material being submitted or published elsewhere should not be duplicated in letters, and authors of letters must disclose financial associations or other possible conflicts of interest.

Letters concerning a paper published in the *AJR* will be sent to the authors of the paper for a reply to be published in the same issue. Opinions expressed in the Letters to the Editor do not necessarily reflect the opinions of the Editor.

# Review of Current Literature

Initials and addresses of corresponding authors are provided in parentheses for each article so that the reader can obtain reprints directly. Abstracts are printed verbatim from each journal.

## The New England Journal of Medicine

**Regression of coronary artery disease as a result of intensive lipid-lowering therapy in men with high levels of apolipoprotein B.** Brown G, Albers JJ, Fisher LD, et al. (GB, Cardiology Division, RG-22, University of Washington, Seattle, WA 98195). *N Engl J Med* 323(19):1289–1298, Nov. 1990

*Background and Methods.* The effect of intensive lipid-lowering therapy on coronary atherosclerosis among men at high risk for cardiovascular events was assessed by quantitative arteriography. Of 146 men no more than 62 years of age who had apolipoprotein B levels ≥125 mg per deciliter, documented coronary artery disease, and a family history of vascular disease, 120 completed the 2½-year double-blind study, which included arteriography at base line and after treatment. Patients were given dietary counseling and were randomly assigned to one of three treatments: lovastatin (20 mg twice a day) and colestipol (10 g three times a day); niacin (1 g four times a day) and colestipol (10 g three times a day); or conventional therapy with placebo (or colestipol if the low-density lipoprotein [LDL] cholesterol level was elevated).

*Results.* The levels of LDL and high-density lipoprotein (HDL) cholesterol changed only slightly in the conventional-therapy group (mean changes, −7 and +5 percent, respectively), but more substantially among patients treated with lovastatin and colestipol (−46 and +15 percent) or niacin and colestipol (−32 and +43 percent). In the conventional-therapy group, 46 percent of the patients had definite lesion progression (and no regression) in at least one of nine proximal coronary segments; regression was the only change in 11 percent. By comparison, progression (as the only change) was less frequent among patients who received lovastatin and colestipol (21 percent) and those who received niacin and colestipol (25 percent), and regression was more frequent (lovastatin and colestipol, 32 percent; niacin and colestipol, 39 percent; $P<0.005$). Multivariate analysis indicated that a reduction in the level of apolipoprotein B (or LDL cholesterol) and in systolic blood pressure, and an increase in HDL cholesterol correlated independently with regression of coronary lesions. Clinical events (death, myocardial infarction, or revascularization for worsening symptoms) occurred in 10 of 52 patients assigned to conventional therapy, as compared with 3 of 46 assigned to receive lovastatin and colestipol and 2 of 48 assigned to receive niacin and colestipol (relative risk of an event during intensive treatment, 0.27; 95 percent confidence interval, 0.10 to 0.77).

*Conclusions.* In men with coronary artery disease who were at high risk for cardiovascular events, intensive lipid-lowering therapy reduced the frequency of progression of coronary lesions, increased the frequency of regression, and reduced the incidence of cardiovascular events.

**The effect of ursodiol on the efficacy and safety of extracorporeal shock-wave lithotripsy of gallstones: the Dornier National Biliary Lithotripsy Study.** Schoenfield LJ, Berci G, Carnovale RL, et al. (LJS, Division of Gastroenterology, Cedars-Sinai Medical Center, 8700 Beverly Blvd., Ste. 7511, Los Angeles, CA 90048). *N Engl J Med* 323(18):1239–1245, Nov. 1990

*Background.* In the treatment of gallstones with extracorporeal shock-wave lithotripsy, the bile acid ursodiol is administered to dissolve the gallstone fragments. We designed our study to determine the value of administering this agent.

*Methods.* At 10 centers, 600 symptomatic patients with three or fewer radiolucent gallstones 5 to 30 mm in diameter, as visualized by oral cholecystography, were randomly assigned to receive ursodiol or placebo for six months, starting one week before lithotripsy.

*Results.* The stones were fragmented in 97 percent of all patients, and the fragments were ≤5 mm in diameter in 46.8 percent. On the basis of an intention-to-treat analysis of all 600 patients, 21 percent receiving ursodiol and 9 percent receiving placebo ($P<0.0001$) had gallbladders that were free of stones after six months. Among those with completely radiolucent solitary stones <20 mm in diameter, 35 percent of the patients receiving ursodiol and 18 percent of those receiving placebo ($P<0.001$) were free of stones after six months. Biliary pain, usually mild, occurred in 73 percent of all patients but in only 13 percent of those who were free of stones after three and six months ($P<0.01$). There were few adverse events. Only diarrhea occurred with a significantly different frequency in the two groups: 32.6 percent were affected in the ursodiol group, as compared with 24.7 percent in the placebo group ($P<0.04$). Severe biliary pain occurred in 1.5 percent of all patients, acute cholecystitis in 1.0 percent, and acute pancreatitis in 1.5 percent; endoscopic sphincterotomy was performed in 0.5 percent, and cholecystectomy in 2.5 percent.

*Conclusions.* Extracorporeal shock-wave lithotripsy with ursodiol was more effective than lithotripsy alone for the treatment of symptomatic gallstones, and equally safe. Treatment was more effective for solitary than multiple stones, radiolucent than slightly calcified stones, and smaller than larger stones.

**Ulcerative colitis and colorectal cancer: a population-based study.** Ekbom A, Helmick C, Zack M, Adami HO (AE, Dept. of Surgery, University Hospital, S-751 85 Uppsala, Sweden). *N Engl J Med* 323(18):1228–1233, Nov. 1990

*Background.* The risk of colorectal cancer is increased among patients with ulcerative colitis. The magnitude of this increase in risk

and the effects of the length of follow-up, the extent of disease at diagnosis, and age at diagnosis vary substantially in different studies.

*Methods.* To provide accurate estimates of the risk of colorectal cancer among patients with ulcerative colitis, we studied a population-based cohort of 3117 patients given a diagnosis of ulcerative colitis from 1922 through 1983 who were followed up through 1984.

*Results.* Ninety-two cases of colorectal cancer occurred in 91 patients. As compared with the expected incidence, the incidence of colorectal cancer in the cohort was increased (standardized incidence ratio [ratio of observed to expected cases] = 5.7; 95 percent confidence interval, 4.6 to 7.0). Less extensive disease at diagnosis was associated with a lower risk; for patients with ulcerative proctitis, the standardized incidence ratio was 1.7 (95 percent confidence interval, 0.8 to 3.2); for those with left-sided colitis, 2.8 (95 percent confidence interval, 1.6 to 4.4); and for those with pancolitis (extensive colitis, or inflammation of the entire colon), 14.8 (95 percent confidence interval, 11.4 to 18.9). Age at diagnosis and the extent of disease at diagnosis were strong and independent risk factors for colorectal cancer. For each increase in age group at diagnosis (<15 years, 15 to 29 years, 30 to 39 years, 40 to 49 years, 50 to 59 years, and ≥60 years), the relative risk of colorectal cancer, adjusted for the extent of disease at diagnosis, decreased by about half (adjusted standardized incidence ratio = 0.51; 95 percent confidence interval, 0.46 to 0.56). The absolute risk of colorectal cancer 35 years after diagnosis was 30 percent for patients with pancolitis at diagnosis and 40 percent for those given this diagnosis at less than 15 years of age.

*Conclusions.* Close surveillance and perhaps even prophylactic proctocolectomy should be recommended for patients given a diagnosis of pancolitis, especially those who are less than 15 years of age at diagnosis.

**Spinal bone loss and ovulatory disturbances.** Prior JC, Vigna YM, Schechter MT, Burgess AE (JCP, Dept. of Medicine, #3318, 910 W. 10th Ave., Vancouver, B.C. V5Z 1M9, Canada). *N Engl J Med* 323(18):1221–1227, Nov. 1990

*Background.* Osteoporosis develops in women with estrogen deficiency and amenorrhea who lose bone at an accelerated rate. It is not known to what extent bone loss differs between ovulatory women with regular menstrual cycles who are training intensely and those who are sedentary.

*Methods.* We measured the density of cancellous spinal bone from the 12th thoracic vertebra to the 3rd lumbar vertebra by quantitative computed tomography on two occasions one year apart in 66 premenopausal women 21 to 42 years of age. All the women had two consecutive ovulatory cycles immediately before entering the study. Twenty-one women were training for a marathon, 22 ran regularly but less intensively, and 23 had normal levels of activity. The lengths of the women's menstrual cycles and luteal phases, diet, exercise levels, and hormonal levels were also determined. We defined ovulatory disturbances as anovulatory cycles and cycles with short luteal phases.

*Results.* The mean (±SD) spinal bone density in the 66 women decreased 3.0±4.8 mg per cubic centimeter per year (2.0 percent per year) (P<0.001). Amenorrhea did not develop in any woman during the year of observation (only 2.7 percent of the cycles were >36 days long). Ovulatory disturbances occurred in 29 percent of all cycles, however. Bone loss was strongly associated with these disturbances (r = 0.54, 24 percent of the variance). The 13 women who had anovulatory cycles lost bone mineral at a rate of 6.4±3.8 mg per cubic centimeter per year (4.2 percent per year). The women training for a marathon had menstrual cycles similar to those of the women in the other two groups.

*Conclusions.* Decreases in spinal bone density among women with differing exercise habits correlated with asymptomatic disturbances of ovulation (without amenorrhea) and not with physical activity.

**The diagnosis and prognosis of autosomal dominant polycystic kidney disease.** Parfrey PS, Bear JC, Morgan J, et al. (JCB, Faculty of Medicine, Memorial University of Newfoundland, St. John's, Newfoundland, A1B 3V6, Canada). *N Engl J Med* 323(16):1085–1090, Oct. 1990

*Background.* Autosomal dominant polycystic kidney disease is usually caused by a mutant gene at the PKD1 locus on the short arm of chromosome 16, but in about 4 percent of families with the disorder it is caused by unknown mutations elsewhere in the genome. The natural course of the disease in both genetic forms is not well characterized.

*Methods.* We studied 17 families with autosomal dominant polycystic kidney disease to compare presymptomatic diagnosis by ultrasonography with diagnosis by genetic-linkage studies and to relate clinical variation of the disease to whether the PKD1 mutation was implicated.

*Results.* In 10 families the disorder was found to cosegregate with polymorphic DNA markers flanking the PKD1 locus, in 2 families it did not, and in 5 families linkage could not be determined. In the 10 families with the PKD1 mutation, 46 percent of the members less than 30 years old who had a 50 percent risk of inheriting a mutation had renal cysts, as compared with 11 percent of the members of the two families without linkage (P<0.001). In the PKD1 families, all 67 diagnoses made by ultrasonography were confirmed by determination of the genotype as inferred from linkage. Forty of 48 members (83 percent) less than 30 years old who inherited the PKD1 mutation had renal cysts. All 27 members 30 years old or older who inherited the mutation had renal cysts, suggesting that the probability of a false negative diagnosis did not exceed 0.13 in this age group (P<0.05).

The mean (±SE) age at the onset of end-stage renal disease among members of the PKD1 families was 56.7±1.9 years, as compared with 69.4±1.7 years among members with cysts in the families without linkage (P = 0.0025). Hypertension and renal impairment were less frequent and occurred later in the families without the PKD1 mutation.

*Conclusions.* At present, in most persons with a 50 percent risk of autosomal dominant polycystic kidney disease, imaging techniques are the only mode of reaching a diagnosis before symptoms appear. In such persons a negative ultrasonographic study during early adult life indicates that the likelihood of inheriting a PKD1 mutation is small. In the few who inherit a non-PKD1 mutation for polycystic kidney disease, renal failure is likely to occur relatively late in life.

**Predicting the appropriate use of carotid endarterectomy, upper gastrointestinal endoscopy, and coronary angiography.** Brook RH, Park RE, Chassin MR, Solomon DH, Keesey J, Kosecoff J (RHB, Rand Corp., 1700 Main St., Box 2138, Santa Monica, CA 90406). *N Engl J Med* 323(17):1173–1177, Oct. 1990

*Background and Methods.* In a nationally representative population 65 years of age or older, we have demonstrated that about one quarter of coronary angiographies and upper gastrointestinal endoscopies and two thirds of carotid endarterectomies were performed for reasons that were less than medically appropriate. In this paper we examine whether specific characteristics of patients (age, sex, and race), physicians (age, board-certification status, and experience with the procedure), or hospitals (teaching status, profit-making status, and size) predict whether a procedure will be performed appropriately.

*Results.* In general, we found that little of the variability in the appropriateness of care (4 percent or less) could be explained on the basis of standard, easily obtainable data about the patient, the physician, or the hospital. For all three procedures, however, performance in a teaching hospital increased the likelihood that the reasons would be medically appropriate (P = 0.09 for angiography, P = 0.30 for endoscopy, and P<0.01 for endarterectomy). In addition, angiographies were more often performed for appropriate reasons in older or more affluent patients (P<0.01 for both). Being treated by a surgeon who performed a high rather than a low number of procedures decreased the likelihood of an appropriate endarterectomy by one third, from 40 to 28 percent (P<0.01).

*Conclusions.* Appropriateness of care cannot be closely predicted from many easily determined characteristics of patients, physicians, or hospitals. Thus, for the present, if appropriateness is to be im-

proved it will have to be assessed directly at the level of each patient, hospital, and physician.

## Cancer

**Prospective evaluation of radiologically directed fine-needle aspiration biopsy of nonpalpable breast lesions.** Masood S, Frykberg ER, McLellan GL, Scalapino MC, Mitchum DG, Bullard JB (SM, Dept. of Pathology, University Hospital of Jacksonville, 655 W. 8th St., Jacksonville, FL 32209). *Cancer* 66:1480–1487, 1990

The application of fine-needle aspiration biopsy (FNAB) to the diagnosis of nonpalpable breast lesions was evaluated with a new method which uses standard needle localization under mammographic guidance to assure accurate sampling by FNAB. This method was prospectively applied to 100 mammographically detected breast lesions in 100 women (mean age, 53 years). All 100 patients underwent surgical excision of these nonpalpable lesions after cytologic aspiration. Sufficient aspirated material was obtained for cytologic diagnosis from 91 patients (91%). The histologic and cytologic interpretations were then compared. Twenty malignancies were ultimately diagnosed by histology (12 invasive ductal carcinoma, six ductal carcinoma *in situ*, and two lobular carcinoma *in situ*), of which 17 had been cytologically diagnosed. There were no false-positive diagnoses of malignancy by FNAB. False-negative readings (3.3%) included two cases of lobular carcinoma *in situ* and one case of ductal carcinoma *in situ*. This technique thus demonstrated a sensitivity of 85%, specificity of 100%, and overall diagnostic accuracy of 96.7% for the nonsurgical detection of malignancy in nonpalpable breast lesions. These results suggest that the established safety, reliability, and cost-effectiveness of FNAB can be maintained in this clinical setting. This procedure may obviate the need for open surgical biopsy in those patients with an unequivocal diagnosis of malignancy. It can also be done using standard techniques and equipment available in many community hospitals.

Reprinted by permission from the American Cancer Society.

## Chest

**Computed tomography in patients with esophageal perforation.** Backer CL, LoCicero J III, Hartz RS, Donaldson JS, Shields T (CLB, Box 22, Children's Memorial Hospital, 2300 Children's Plaza, Chicago, IL 60614). *Chest* 98(5):1078–1080, Nov. 1990

Contrast esophagram is the diagnostic procedure of choice in patients with clinically suspected perforation of the esophagus. In patients in whom the usual clinical signs or symptoms are unrecognized and in whom the diagnosis is obscure, the diagnosis of a perforated esophagus may be suggested by the finding of mediastinal fluid and air on CT. Three patients are reviewed. The perforations included one spontaneous, one from erosion of an esophageal carcinoma, and one iatrogenic. In two of the three patients, the diagnosis of perforated esophagus had not been made initially and in one patient the initial esophagram was interpreted as normal. Computed tomography of the chest in each patient led to the suspected diagnosis of perforated esophagus. Prompt appropriate surgical intervention followed. The findings of mediastinal fluid and more importantly mediastinal air on CT of the chest are strongly suggestive of esophageal perforation.

## Gastroenterology

**Gallbladder motility in cholesterol gallstone disease: effect of ursodeoxycholic acid administration and gallstone dissolution.** Festi D, Frabboni R, Bazzoli F, et al. (DF, Istituto di Clinica Medica e Gastroenterologia, Università di Bologna, Italy). *Gastroenterology* 99:1779–1785, 1990

Gallbladder motility was evaluated by ultrasonography in 75 cholesterol gallstone patients and in 77 matched control subjects. All 75 gallstone patients were candidates for oral bile acid therapy (radiolucent gallstones, <2 cm in diameter, in well-opacified gallbladder), and 38 of them were also studied during ursodeoxycholic acid administration. An additional 20 gallstone patients were studied 1 year after confirmed gallstone dissolution with oral bile acids. Gallstone patients showed significantly greater fasting and residual volumes, a decreased percent of gallbladder emptying, but a similar absolute emptying and emptying rate compared with the control subjects. Greater fasting volumes and reduced percents of gallbladder emptying were also found in gallstone-free patients who achieved complete dissolution with oral bile acids. After ursodeoxycholic acid administration, fasting gallbladder volumes were greater, and percents of gallbladder emptying were further decreased than in untreated gallstone patients. In conclusion, greater fasting volumes, and not reduced gallbladder contractility, account for the defective gallbladder function in radiolucent (cholesterol-rich) gallstone patients. This condition is likely to precede, and possibly to promote, gallstone formation because it persists after gallstone dissolution. Ursodeoxycholic acid administration worsens the defect observed in gallstone patients. This finding also suggests, although indirectly, that the expected normalization of cholesterol saturation during oral bile acid administration is not paralleled by an improvement in gallbladder function.

Reprinted with permission by the American Gastroenterological Association.

## Digestive Diseases and Sciences

**Improved scintigraphic assessment of severe cholestasis with the hepatic extraction fraction.** Lieberman DA, Brown PH, Krishnamurthy GT (DAL, Portland VA Medical Center, P. O. Box 1034, Portland, OR 97207). *Dig Dis Sci* 35(11):1385–1390, Nov. 1990

In previous studies, we found that biliary scintigraphy with technetium-99m-labeled iminodiacetic acid ([$^{99m}$Tc]IDA) provided excellent discrimination between intrahepatic and extrahepatic cholestasis, except in patients with profound cholestasis who had poor visualization of the biliary tree. In this study, we have used deconvolution analysis to determine the hepatic extraction fraction (HEF) of a hypothetical single circulatory pass of [$^{99m}$Tc]IDA. Our hypothesis was that extraction of radionuclide from the blood would be normal in patients with extrahepatic obstruction alone, but would be impaired in patients with intrahepatic disease (IHD). The purpose of this study was to compare the HEF in patients with profound cholestasis (bilirubin $\geq$ 3.0 mg/dl) due to either IHD or common bile duct obstruction (CBDO). Normal subjects ($N$ = 13) had an HEF of 100%. Patients with CBDO ($N$ = 13) had slightly reduced HEF values (92.8 $\pm$ 3.2%) despite profound hyperbilirubinemia (6.1 $\pm$ 1.0 mg/dl). Patients with IHD ($N$ = 23) had a markedly reduced HEF (43.1 $\pm$ 4.1%) which was significantly lower than patients with CBDO and normal subjects ($P$ < 0.001). We conclude that the determination of the HEF during biliary scintigraphy is helpful in distinguishing between intrahepatic and extrahepatic disease in patients with hyperbilirubinemia (bilirubin $\geq$ 3.0 mg/dl).

**Dynamic CT scanning of pancreatic duct after secretin provocation in pancreas divisum.** Lindström E, Ihse I (EL, Dept. of Surgery, University Hospital, S-581 85 Linköping, Sweden). *Dig Dis Sci* 35(11):1371–1376, Nov. 1990

Variations in pancreatic duct diameter at CT scanning and serum pancreatic amylase response following secretin administration were studied in 29 patients with pancreas divisum and unexplained upper abdominal pain. Eleven healthy individuals were used as controls. At endoscopic retrograde pancreatography (ERP) six patients had signs of marked and six moderate pancreatitis, whereas there were no pancreatitis changes in 17 of the patients. At CT scanning patients with marked pancreatitis (ERP) had significantly increased pancreatic duct diameter as compared to patients without signs of pancreatitis.

The duct was visualized in 52% of all patients before and 71% after secretin stimulation the corresponding figures for healthy controls, being 18% both before and after secretin. In patients without signs of pancreatitis, it was demonstrated in 5/17 (29%) before and 11/17 (65%) after secretin, whereas it was seen in 10/12 (83%) pancreatitis patients both before and after the hormonal provocation. In five of the nonpancreatitis patients in whom the duct was measurable before and at all study intervals (10, 20, and 50 min) after secretin, there was a significant duct dilation response both at 10 min and when comparing the maximal duct diameter after secretin to the initial values. In contrast secretin did not affect the duct caliber in pancreatitis patients. Serum pancreatic amylase increased significantly after secretin administration to healthy controls and nonpancreatitis patients but was uninfluenced in the marked and moderate pancreatitis groups, respectively. However, when all pancreatitis patients were grouped together, the amylase levels were significantly elevated by secretin. In conclusion, secretin provocation caused duct dilation at CT scanning in pancreas divisum patients without signs of pancreatitis at ERP. In this group secretin also increased the number of patients with visualized pancreatic duct. However, in pancreas divisum patients with pancreatitis and in healthy controls no such findings were observed. Secretin stimulation increased s-amylase in a nonspecific way. If secretin at CT scanning causes dilation of the pancreatic duct compared to its initial measurable width or visualization of an initially not demonstrable duct in patients with unexplained upper abdominal pain, the presence of pancreas divisum without morphologically manifest pancreatitis should be considered.

**Measurement of gastric emptying rate in humans: simplified scanning method.** Holt S, Colliver J, Maninder G, Neal C, Verhulst SJ, Taylor TV (SH, Division of Digestive Diseases and Nutrition, Two Richland Medical Park, Ste. 506, Columbia, SC 29203). *Dig Dis Sci* 35(11):1345–1351, Nov. 1990

Simultaneous measurements of the gastric emptying rate of the solid and liquid phase of a dual-isotope-labeled test meal were made using a gamma camera and a simple scintillation detector, similar to that used in a hand-held probe. A simple scanning apparatus, similar to that used in a hand-held scintillation probe, was compared with simultaneous measurements made by a gamma camera in 16 healthy males. A dual-labeled test meal was utilized to measure liquid and solid emptying simultaneously. Anterior and posterior scans were taken at intervals up to 120 min using both a gamma camera and the scintillation probe. Good relative agreement between the methods was obtained both for solid-phase (correlation range 0.92–0.99, mean 0.97) and for liquid-phase data (correlation range 0.93–0.99, mean 0.97). For solid emptying data regression line slopes varied from 0.75 to 1.03 (mean 0.84). Liquid emptying data indicated that slopes ranged from 0.71 to 1.06 (mean 0.87). These results suggested that an estimate of the gamma measurement could be obtained by multiplying the scintillation measurement by a factor of 0.84 for the solid phase and 0.87 for the liquid phase. Correlation between repeat studies was 0.97 and 0.96 for solids and liquids, respectively. The application of a hand-held probe technique provides a noninvasive and inexpensive method for accurately assessing solid- and liquid-phase gastric emptying from the human stomach that correlates well with the use of a gamma camera, within the range of gastric emptying rate in the normal individuals in this study.

## The Journal of Bone and Joint Surgery

**Results of treatment of displaced patellar fractures by partial patellectomy.** Saltzman CL, Goulet JA, McClellan RT, Schneider LA, Matthews LS (CLS, Dept. of Surgery, Section of Orthopaedics, University of Michigan, TC-2912/0328, 1500 E. Medical Center Dr., Ann Arbor, MI 48109-0328). *J Bone Joint Surg [AM]* 72-A(9):1279–1285, Oct. 1990

The results of partial patellectomy as a treatment for displaced patellar fractures were assessed retrospectively with use of clinical, radiographic, and isokinetic strength-testing criteria. Forty patients who had been followed for an average of 8.4 years were studied. In the extremity that had been operated on, the mean active range of motion was 94 per cent, the circumference of the thigh was 100 per cent, and the strength of the quadriceps was 85 per cent of these measurements in the contralateral extremity. The over-all result was rated as excellent in twenty patients, good in eleven, fair in six, and poor in three. There was a significant statistical correlation between the type of fracture and the outcome. The results of this study indicate that partial patellectomy can be an effective treatment for selected patellar fractures.

## Clinical Orthopaedics and Related Research

**The value of indium 111 leukocyte scanning in the evaluation of painful or infected total knee arthroplasties.** Rand JA, Brown ML (JAR, Mayo Clinic, 200 1st St., S.W., Rochester, MN 55905). *Clin Orthop* 259:179–182, Oct. 1990

Evaluation of painful total knee arthroplasties (TKAs) for infection can be difficult. Indium 111 ($^{111}$In) leukocyte bone scanning provides a minimally invasive technique for evaluation of possible infection. Thirty-eight patients with a painful TKA who had surgical exploration after $^{111}$In leukocyte scanning were reviewed. The scan had an accuracy of 84%, a sensitivity of 83%, and a specificity of 85%. The $^{111}$In leukocyte scans must be interpreted in conjunction with the clinical evaluation of the patient because they are less accurate for study of TKAs than of total hip arthroplasties.

## The Journal of Urology

**Preliminary evaluation of color Doppler imaging for investigation of intrascrotal pathology.** Krieger JN, Wang K, Mack L (JNK, Dept. of Urology, University of Washington, School of Medicine, Seattle, WA). *J Urol* 144:904–907, Oct. 1990

Color Doppler ultrasound facilitates investigation of blood flow in addition to imaging parenchymal abnormalities. To assess the clinical use of this technique we evaluated 25 consecutive patients with indications for intrascrotal imaging. Color flow imaging added useful information in all 11 patients evaluated for chronic scrotal pain and in 6 of 7 evaluated for acute scrotal pain. In contrast, color flow ultrasound provided little additional information in 7 patients with intrascrotal masses. Color flow ultrasound imaging is a promising method that may prove to be useful for assessment of selected patients with intrascrotal pathological conditions.

## Pediatrics

**Screening for neuroblastoma at 3 weeks of age: methods and preliminary results from the Quebec Neuroblastoma Screening Project.** Tuchman M, Lemieux B, Auray-Blais C, et al. (MT, Dept. of Pediatrics, University of Minnesota, Box 400, Mayo Bldg., 420 Delaware St., S.E., Minneapolis, MN 55455). *Pediatrics* 86(5):765–773, Nov. 1990

A large neuroblastoma screening study was recently started in the province of Quebec, Canada. This project, a collaboration between the Quebec Network for Genetic Medicine and the University of Minnesota, is studying the impact of screening infants for the preclinical detection of neuroblastoma on the population-based mortality caused by this tumor. All infants born in Quebec during a 5-year period will be screened twice, at 3 weeks and at 6 months. Urinary homovanillic acid and vanillylmandelic acid determination from dried filter paper samples is used for screening. Initial qualitative screening

is done by means of thin-layer chromatography with confirmatory quantitative screening by gas chromatography-mass spectrometry (GC-MS). During the initial 6 months of 3-week screening, 41 673 neonates (92% compliance rate) were screened and 10.6% of them were tested also by GC-MS. Nine of these neonates had positive results on two GC-MS tests and were referred for evaluation to rule out the presence of neuroblastoma. Four had the tumor, 1 had a calcified adrenal gland, and 4 had no tumor detected. Three additional neonates had clinical diagnosis of neuroblastoma before they reached the screening age of 3 weeks. A neuroblastoma that did not secrete homovanillic acid or vanillylmandelic acid was diagnosed clinically in 1 additional patient who tested negative by screening.

Reprinted by permission of PEDIATRICS © 1990.

## The Journal of Pediatrics

**Diagnosis of cerebrovascular disease in sickle cell anemia by magnetic resonance angiography.** Wiznitzer M, Ruggieri PM, Masaryk TJ, Ross JS, Modic MT, Berman B (MW, Rainbow Babies and Childrens Hospital, 2101 Adelbert Rd., Cleveland, OH 44106). *J Pediatr* 117:551–555, Oct. 1990

The study of blood flow by means of magnetic resonance techniques has led to a noninvasive magnetic resonance angiography (MRA) technique for imaging large cerebral vessels. Ten children with sickle cell hemoglobinopathy and a history of acute neurologic syndromes were studied with combined parenchymal magnetic resonance imaging (MRI) and MRA. Six had abnormal MRI findings and MRA-defined luminal lesions in the vascular distribution of these parenchymal infarctions. The three children with previous intraarterial angiography had MRA abnormalities that corresponded with vascular lesions on conventional angiograms. Four had normal MRI and MRA findings. We conclude that a combination of MRI and MRA provides a noninvasive screening test for large-vessel disease in this population.

## The Journal of Nuclear Medicine

**Significance of fill-in after thallium-201 reinjection following delayed imaging: comparison with regional wall motion and angiographic findings.** Tamaki N, Ohtani H, Yonekura Y, et al. (NT, Dept. of Radiology and Nuclear Medicine, Kyoto University Hospital, Shogoin, Sakyo-ku, Kyoto, 606 Japan). *J Nucl Med* 31:1617–1623, 1990

To identify reversible defects, reinjection of a small amount of thallium-201 ($^{201}$Tl) following 3-hr delayed imaging was performed in 60 patients with coronary artery disease who had perfusion abnormalities on their post-exercise $^{201}$Tl images. Thallium-201 uptake was visually scored and judged as normal (Group I), reversible defect (Group II), new fill-in after reinjection (Group IIIa) and no fill-in even after reinjection (Group IIIb). New fill-in after reinjection was observed in 27 segments of the 85 segments (32%), showing persistent defect on the stress and delayed images. The wall motion in Group IIIa was worse than Group II but better than Group IIIb. Group IIIa showed Q-wave on ECG more often (69%) than Group II (27%) ($p<0.01$), but less often than Group IIIb (85%) ($p<0.05$). These data indicate that the reinjection $^{201}$Tl imaging often identifies new fill-in in the areas of no redistribution on the delayed images and it may hold promise for assessing tissue viability which the conventional imaging may underestimate.

## Journal of Thoracic Imaging

**Ultrafast computed tomography in the diagnosis of aortic aneurysms and dissections.** Stanford W, Rooholamini SA, Galvin JR (WS, Dept. of Radiology, The University of Iowa Hospitals and Clinics, Iowa City, IA 52242). *J Thorac Imaging* 5(4):32–39, 1990

UFCT, by virtue of its 50 to 400 millisecond acquisition times, 0.75 to 1.5 mm resolution, and excellent vascular opacification, provides a rapid, minimally invasive method for assessing aortic aneurysms and dissections. During a 3.5-year period, 50 patients with suspected thoracic, thoracoabdominal, and abdominal aortic aneurysms or dissections were evaluated using the Imatron C-100 UFCT scanner. Eighteen patients had thoracic or thoracoabdominal aneurysms, 17 had thoracic or thoracoabdominal dissections, 7 had abdominal aneurysms, and in 8 no aneurysms or dissections were found. In 23 of the 35 patients with thoracic or thoracoabdominal aneurysms or dissections, the UFCT findings accurately reflected the findings at aortography, surgery, or autopsy. There was one false-positive examination. The remaining 11 patients with UFCT findings of aneurysm or dissection were followed clinically. In the 7 patients with abdominal aneurysms, 4 were confirmed by angiography or surgery, and 3 were followed clinically. Of the 8 patients with negative UFCT examinations, 2 had subsequent angiography that failed to show an aneurysm, and 6 were followed from 6 to 30 months without developing findings suggestive of aneurysm. UFCT appears to be a useful, minimally invasive technique for detecting and following aortic aneurysms and dissections.

## Journal of Ultrasound in Medicine

**Takayasu's arteritis: carotid duplex sonographic appearance, including color Doppler imaging.** Bond JR, Charboneau JW, Stanson AW (JRB, Dept. of Diagnostic Radiology, Mayo Clinic, 200 1st St., Rochester, MN 55905). *J Ultrasound Med* 9:625–630, Nov. 1990

Takayasu's arteritis (also known as pulseless disease, aortoarteritis, and aortic arch syndrome) is a chronic inflammatory arteriopathy that affects the aorta and its main branches as well as the pulmonary arteries. We report the carotid duplex sonographic findings of Takayasu's arteritis in three patients. Takayasu's arteritis can be suspected by noting a long segment of diffuse, homogeneous, circumferential vessel wall thickening in the proximal common carotid artery, resulting in narrowing of the lumen. The internal and external carotid arteries are normal.

Reprinted with permission by the American Institute of Ultrasound in Medicine.

## Journal of Computer Assisted Tomography

**Computed tomography of renal lymphoma.** Cohan RH, Dunnick NR, Leder RA, Baker ME (RHC, 928 Salisbury Green, Virginia Beach, VA 23452). *J Comput Assist Tomogr* 14(6):933–938, Nov./Dec. 1990

The CT studies of 29 patients with renal or perirenal lymphoma were retrospectively reviewed. Four patterns of disease were identified. Seventeen of 29 patients (59%) had bilateral renal masses. Only seven of these patients had associated enlarged retroperitoneal lymph nodes. Eight patients (28%) had single renal or perirenal lesions adjacent to or contiguous with bulky retroperitoneal lymphadenopathy. Three patients had infiltration of the perirenal space without significant renal parenchymal involvement, and one patient had a solitary renal mass. No patients in this series had diffuse involvement of the kidney without a focal mass. Renal involvement with lymphoma should be considered in any patient who develops multiple homogeneous solid renal or perirenal masses, even in the absence of other retroperitoneal disease.

**Impending rupture of nonaneurysmal bacterial aortitis: CT diagnosis.** Mantello MT, Panaccione JL, Moriarty PE, Esposito WJ (MTM, Dept. of Radiology, Brigham and Women's Hospital, Harvard Medical School, 75 Francis St., Boston, MA 02115). *J Comput Assist Tomogr* 14(6):950–953, Nov./Dec. 1990

The CT appearance of mycotic abdominal aortic aneurysms leading to eventual rupture has been well described. On the other hand, ruptured nonaneurysmal bacterial aortitis has not been demonstrated in the CT literature. We present two cases with subsequent rupture documented on CT. The characteristic findings of periaortic density and adjacent gas collection should suggest the diagnosis of acute aortic infection. This may herald impending rupture, even in the absence of aneurysmal dilatation, and should direct therapy accordingly.

**Case of anaphylaxis and four cases of allergic reaction following Gd-DTPA administration.** Salonen OLM (OLMS, Dept. of Diagnostic Radiology, Helsinki University Central Hospital, Haartmaninkatu 4, 00290 Helsinki, Finland). *J Comput Assist Tomogr* 14(6):912–913, Nov./Dec. 1990

Although Gd-diethylenetriamine pentaacetic acid (Gd-DTPA) is considered to be safe and well tolerated by patients, we have seen adverse reactions in 5 of 344 cases. This paper reports those five cases of reactions to intravenous Gd-DTPA injection.

## Magnetic Resonance Imaging

**MRI of aggressive fibromatosis: frequent appearance of high signal intensity on $T_2$-weighted images.** Feld R, Burk DL Jr, McCue P, Mitchell DG, Lackman R, Rifkin MD (RF, Thomas Jefferson University Hospital, Dept. of Radiology, 10th and Sansom Sts., Philadelphia, PA 19107). *Magn Reson Imaging* 8:583–588, 1990

Magnetic resonance imaging of seven patients with eight pathologically proven desmoid tumors tumors was performed and retrospectively reviewed. On $T_2$-weighted images, all but one lesion demonstrated increased signal intensity relative to muscle, and had signal intensity similar to that of fat. The signal was heterogenous in six of these seven lesions. In a patient with synchronous multicentric lesions, light microscopy correlation revealed increased cellularity in one lesion with increased signal intensity and dense collagenous elements in a second lesion, with decreased signal intensity. High signal intensity appears to be typical but nonspecific, and in following these patients could indicate recurrent tumor, superimposed inflammatory process or granulation tissue.

# News

## NIH Seeks Director for Diagnostic Radiology Research Program

The National Institutes of Health (NIH) is seeking an experienced board-certified radiologist to direct its new Diagnostic Radiology Research Program (DRRP). The director will organize and conduct a research training program in diagnostic imaging for radiologists and provide a coordinating focus for the many ongoing research initiatives in diagnostic imaging at the NIH. The DRRP will train four to six radiologists a year. Participants will have access to extensive research facilities, including a nuclear magnetic resonance (NMR) facility dedicated exclusively to the research program and supported by the NIH NMR Center. In addition, the director will be provided with laboratory facilities, personnel, and an operating budget to pursue independent research in diagnostic imaging. Applicants should have an ongoing radiology research program and relevant experience in clinical imaging and in teaching of diagnostic radiology. Interested persons should submit a curriculum vitae and bibliography to Dr. Dinah Singer, Office of Intramural Affairs, Bldg. 1, Rm. 140, National Institute of Health, Bethesda, MD 20892.

## NIH Fellowship in Radiologic Research

The newly established Diagnostic Radiology Research Program (DRRP) at the National Institutes of Health (NIH) is offering 2-year fellowships to encourage young men and women to pursue a program of original basic research at the NIH campus. Candidates who recently have completed clinical training in diagnostic radiology or nuclear medicine or, under special circumstances, are currently in residency will be considered for these positions. The fellowships emphasize basic research; fellows will have no clinical responsibilities except as related to their research projects. In addition to the imaging laboratories of the DRRP, facilities in the In Vivo NMR Center, the positron emission tomography program of the Dept. of Nuclear Medicine, Biomedical Engineering and Instrumentation Branch, and other laboratories on the NIH campus will be made available. Fellows will have full-time appointments, with an annual starting salary of $37,000. Initial appointments will be made for July 1991. Candidates should submit a curriculum vitae, at least two letters of reference, and a preliminary statement about their proposed area of research to Dr. John Doppman, Bldg. 10, Rm. 1C-660, National Institutes of Health, Bethesda, MD 20892; fax: (301) 496-9933.

## Prostate Ultrasound

The Division of Diagnostic Ultrasound, Dept. of Radiology, Jefferson Medical College, Thomas Jefferson University Hospital, Philadelphia, is offering Prostate Ultrasound, March 22 and May 3. This 1-day program provides an overview of both established and recently developed approaches to ultrasound of the prostate. Special emphasis is given to endorectal scanning. Each participant will have the opportunity to perform endorectal scanning of the prostate with a variety of commercially available instruments. Program coordinator: Matthew D. Rifkin. Category 1 credit: 9 hr. Fee: $375. Information: Judith C. Kaneff, Education Coordinator, Division of Diagnostic Ultrasound, Thomas Jefferson University Hospital, Rm. 792-B, Main Bldg., Philadelphia, PA 19107; (215) 955-8533.

## MRI Workshop in Hawaii, 1991

MRI Workshop in Hawaii, 1991, will be held March 24–29 at the Ritz-Carlton Mauna Lani, Big Island, HI. Each morning, lecturers will detail their methods, review clinical disorders, and discuss new and future developments in MR imaging. Late afternoon focus sessions will provide time for extended discussions. Participants are invited to bring interesting cases or curiosities for "Stump the Stars." Category 1 credit: 37 hr. Fee: $595. Information: Susan Block, Dept. of Nuclear Medicine, Queen's Medical Center, 1301 Punchbowl St., Honolulu, HI 96813; (808) 547-4544.

## Lithotripsy: Biliary and Renal

The Division of Diagnostic Ultrasound, Dept. of Radiology, Jefferson Medical College, Thomas Jefferson University, Philadelphia, is offering Lithotripsy: Biliary and Renal, March 25–28. The program is designed to provide a comprehensive, practical introduction to sonographically guided lithotripsy. It consists of two concurrently run courses, one on biliary lithotripsy and one on renal lithotripsy. Participants will have the opportunity to become familiar with a variety of equipment, observe actual lithotripsy procedures, and gain hands-on experience in setting up and conducting a sonographically guided lithotripsy procedure. Program coordinators: Susan Gordon, Demetrius Bagley, Jr., and Barry B. Goldberg. Category 1 credits: 27 hr. Fee: $1000 for either the biliary course or the renal course. Information: Judith C. Kaneff, Education Coordinator, Division of Diagnostic Ultrasound, Thomas Jefferson University Hospital, Rm. 792-B, Main Bldg., Philadelphia, PA 19107; (215) 955-8533.

## Mammographic Interpretation: A Practical Approach

The Dept. of Radiology, Tufts University–New England Medical Center Hospitals, is sponsoring Mammographic Interpretation: A Practical Approach, March 25–28, May 20–23, Sept. 23–26, and Oct. 28–31, in Boston. This intensive tutorial course is designed to

teach a practical approach to interpretation of mammograms and localization of needles. Enrollment in each session will be limited to 25 students. Category 1 credit: 28 hr. Fee: $800; Information: Marc J. Homer, M.D., Box 388, Dept. of Radiology, New England Medical Center Hospitals, 750 Washington St., Boston, MA 02111; (617) 956-0045.

## Neonatal Neurosonography

The Division of Diagnostic Ultrasound, Dept. of Radiology, Jefferson Medical College, Thomas Jefferson University Hospital, Philadelphia, is offering Neonatal Neurosonography, April 4–5. The program will be a complete introduction to sonographic evaluation of the neonatal brain. Topics will include physical principles and instrumentation, scanning techniques and infection control procedures, recognition of normal anatomic structures, identification of abnormal echo patterns, natural history and sequelae of intracranial hemorrhage, detection and classification of hemorrhage, and more advanced topics such as color Doppler imaging of the neonatal cerebrovascular circulation. The course will not include hands-on experience scanning infants. Program coordinators: Donald Mitchell and Matthew Pasto. Category 1 credit: 13.5 hr. Fee: $375. Information: Judith C. Kaneff, Education Coordinator, Division of Diagnostic Ultrasound, Thomas Jefferson University Hospital, Rm. 792-B, Main Bldg., Philadelphia, PA 19107; (215) 955-8533.

## Joint American-European Course in Davos

The European Association of Radiology and the Johns Hopkins Radiological Alumni Association are cosponsoring a joint meeting, April 7–12, in Davos, Switzerland. The topic this year will be the abdomen. The faculty will cover the anatomic and physiologic basis for radiologic-pathologic correlation and the diagnostic approach to specific disorders in the abdomen, pelvis, and retroperitoneum. Both classic and newer diagnostic imaging and interventional techniques will be stressed. The program will include small-group seminars, exhibits, quizzes, special lectures, and a classic film reading session. Category 1 credit: 40 hr. Fee: physicians: $500; residents, $400. Information: B. G. Brogdon, M.D., Dept. of Radiology, University of South Alabama Medical Center, 2451 Fillingim St., Mobile, AL 36617; telephone: (205) 471-7868; fax: (205) 471-7882; or Martin W. Donner, M.D., Dept. of Radiology, The Johns Hopkins Hospital, Baltimore, MD 21205; (301) 955-7697.

## General Radiology Review Course

The Dept. of Radiological Sciences, University of California, Los Angeles, will present General Radiology Review Course, April 7–12, at the Miramar Sheraton Hotel, Santa Monica, CA. The course will include the basics of diagnostic radiology and will cover sonography, nuclear medicine, angiography, CT, and MR. Course director: Poonam Batra. Category 1 credit: 40 hr. Fee: $425. Information: Darryl Bailey, Program Coordinator, Dept. of Radiological Sciences, B2-170, UCLA Medical Center, Center for Health Sciences, Los Angeles, CA 90024-1731; telephone: (213) 825-8763; fax: (213) 206-5725.

## Fundamentals of Medical Ultrasonics

The Royal Postgraduate Medical School, University of London, will offer Fundamentals of Medical Ultrasonics, April 17–19. The course will be a combination of lectures, demonstrations, and workshops. It is designed to provide both a theoretical and a practical basis in medical ultrasound. Topics to be covered include ultrasound wave motion and propagation; ultrasound field; transducers; pulse echo techniques; Doppler, duplex, and color Doppler techniques; quality assurance; nondiagnostic techniques; and bioeffects and hazards. Faculty: A. Evans, T. K. Hames, K. McCarty, N. McDicken, R. Skidmore, and J. Woodcock. Course organizer: K. N. Humphries. Information: Wolfson Conference Centre, Royal Postgraduate Medical School, Hammersmith Hospital, Du Cane Rd., London W12 ONN, England; telephone 081 740 3117 or 081 740 3245; fax: 081 740 4950.

## Radiation Oncology Clinical Research Seminar

The Dept. of Radiation Oncology and the Division of Continuing Education, University of Florida, and the American Cancer Society, Florida Division, Inc., are sponsoring the 21st annual Radiation Oncology Clinical Research Seminar, April 25–27, at the University Centre Hotel, Gainesville, FL. The seminar will consist of 1 day of case presentations and 2 days of clinical research papers. Seminar coordinator: William M. McCollough. Guest faculty: Gerald Hanks and Barbara Fowble. Category 1 credit: up to 18 hr. Fee: radiation therapists, $250; residents, $125; radiation therapy technologists, $35 for either Friday or Saturday, $60 for both days. Information: William M. McCollough, M.D., Dept. of Radiation Oncology (J-385), J. Hillis Miller Health Center, Gainesville, FL 32610-0385; (904) 395-0316.

## New Orleans Radiology Society Spring Roentgen Conference

The New Orleans Radiology Society will present its 13th Spring Roentgen Conference, held in conjunction with the New Orleans Jazz and Heritage Festival, April 25–28. Program chairman: Marty Landry. Faculty: B. Drayer, L. Goodman, R. B. Jeffrey, D. Kirks, J. Madewell, M. Manco-Johnson, and A. Motarjeme. Category 1 credit: 18 hr. Fee: $450. Information: Marty Landry, M.D., Program Chairman, New Orleans Radiology Society, P. O. Box 19991, New Orleans, LA 70119; (504) 483-5863.

## Symposium on Diagnostic Ultrasound

The State University of New York, Health Science Center at Brooklyn, is sponsoring the 15th annual Spring Weekend Symposium in Diagnostic Ultrasound, April 26–28, at the Waldorf-Astoria Hotel, New York City. Category 1 credit: 18 hr. Fee: physicians, $450; residents, fellows, and technologists, $325. Information: Ms. Gloria Jorge, Box 1198, SUNY Health Science Center at Brooklyn, 450 Clarkson Ave., Brooklyn, NY 11203; (718) 270-1603.

## Abdominal Ultrasound

The Division of Diagnostic Ultrasound, Dept. of Radiology, Jefferson Medical College, Thomas Jefferson University Hospital, Philadelphia, is offering Abdominal Ultrasound, April 29–May 2. Emphasis in this course is placed on an integrated approach combining recognition of normal sonographic anatomy of the abdomen and typical sonographic patterns of pathologic changes. Topics will include a review of the principles of ultrasound physics; instrumentation and imaging techniques, including Doppler sonography; aspiration and biopsy techniques; and ultrasound evaluation of prevertebral vessels, liver, biliary system, kidneys and retroperitoneum, pancreas, spleen, thyroid and parathyroid glands, and abdominal collections. Hands-on experience with a variety of ultrasound instrumentation will be provided. Program coordinator: Rick Feld. Category 1 credit: 27 hr. Fee: $600. Information: Judith C. Kaneff, Education Coordinator, Division of Diagnostic Ultrasound, Thomas Jefferson University Hospital, Rm. 792-B, Main Bldg., Philadelphia, PA 19107; (215) 955-8533.

## Leading Edge in Diagnostic Ultrasound

The Division of Diagnostic Ultrasound, Dept. of Radiology, Jefferson Medical College, Thomas Jefferson University Hospital, will sponsor the 11th annual Leading Edge in Diagnostic Ultrasound Conference, May 16–17, at the Taj Mahal Casino-Hotel, Atlantic City, NJ. The conference will be preceded by the 1-day Preconference Tutorial in Vascular Ultrasound, May 15. Codirectors: Leading Edge, Barry B. Goldberg and Alfred B. Kurtz; Vascular Tutorial, Peter N. Burns and Laurence A. Needleman. Category 1 credit: Leading Edge, 14 hr; vascular tutorial, 8.5 hr. Fee (physicians/fellows, residents, and sonographers): Leading Edge only, $375/$285; vascular tutorial only, $240/$180; both courses, $475/$370. Information: Judith C. Kaneff, Education Coordinator, Division of Diagnostic Ultrasound, Thomas Jefferson University Hospital, Rm. 792-B, Main Bldg., Philadelphia, PA 19107; (215) 955-8533.

## International Pediatric Radiology '91

International Pediatric Radiology '91, the second conjoint meeting of the European Society of Pediatric Radiology (ESPR) and The Society for Pediatric Radiology (SPR), will be held in Stockholm, Sweden, May 27–31. The meeting will include a symposium, Pediatric Imaging: Update '91; long and short scientific papers; named lectures; scientific posters; and technical exhibits. Information for SPR members: Lynne Tiras, I. M. M., 4550 Post Oak Pl., Ste. 248, Houston, TX 77027 or Carol M. Rumack, M.D., Secretary, The Society for Pediatric Radiology, The Children's Hospital, Dept. of Radiology, Box 125, 1056 E. 19th Ave., Denver, CO 80218-1088; (303) 861-6540. Information for ESPR members: IPR '91 Congress, c/o Stockholm Convention Bureau, Box 6911, S-102 39, Stockholm, Sweden.

## American College of Cryosurgery Annual Meeting

The American College of Cryosurgery will hold its 12th annual meeting, June 6–10, at the Sheraton Grande Torrey Pines Hotel, La Jolla, CA. This multidisciplinary meeting will emphasize new advances in cryosurgery, especially the use of sonography and cryosurgery in all of the major medical specialties represented at the meeting. Information: American College of Cryosurgery, ATTN: Michael Thompson, P. O. Box 3116, Evanston, IL 60204-3116; (708) 869-3954.

## Advanced Techniques in MRI

The Depts. of Radiology, Duke University and Stanford University Medical Centers, will present Advanced Techniques in MRI, June 22–28, at Kiawah Island, SC. The course is intended for physicians, physicists, engineers, and technologists who seek a fundamental understanding of the technology of MR. The course will start with basic principles of MR imaging and progress to descriptions of high-speed imaging techniques, cardiac imaging, and MR spectroscopy. Particular attention will be given to the physical basis of MR and the mechanisms by which it is exploited. Clinical examples will be included as appropriate. The deadline for registration is May 1. Course coordinator: G. Allan Johnson. Information: G. Allan Johnson, Ph.D., Dept. of Radiology, Box 3302, Duke University Medical Center, Durham, NC 27710; (919) 660-2711, ext. 4354.

## Advances in Gastroenterology

The Division of Gastroenterology, Dept. of Medicine, University of California, San Diego, will present Advances in Gastroenterology, July 15–19, at the Hotel Del Coronado, Coronado (San Diego), CA. The course will provide information of direct clinical relevance to practicing internists, gastroenterologists, surgeons, and radiologists. Recent advances in the understanding and management of gastrointestinal disease will be covered. Emphasis will be on an interdisciplinary approach, stressing novel aspects of the clinical assessment and treatment of patients with gastrointestinal diseases, including disorders of the liver and pancreas. Program directors: Jon I. Isenberg and Alan F. Hoffman; program codirectors: Kiertisin Dharmasathaphorn and Stephen J. Pandol. Category 1 credit: 19–22 hr. Fee: practicing physicians, $425; physicians in training and technologists, $275. Information: Dawne Ryals, Ryals & Associates, P. O. Box 1925, Roswell, GA 30077-1925; telephone: (404) 641-9773; fax: (404) 552-9859.

## Radiology for the Non-Radiologist

The Dept. of Radiology, University of California, San Diego, School of Medicine will present Radiology for Non-Radiologists, July 18–21, at the Hotel Del Coronado, Coronado (San Diego), CA. The course will provide nonradiologists with state-of-the-art information on the role of diagnostic imaging and interventional procedures in the evaluation and treatment of patients. A faculty of expert subspecialists will outline the present status of the most important services provided by diagnostic radiologists in both hospital and outpatient settings. Program director: David S. Feigin. Category 1 credit: pending. Fee: physicians in practice, $400; residents, fellows, nurses, and technologists, $250. Information: Dawne Ryals, Ryals & Associates, P. O. Box 1925, Roswell, GA 30077-1925; telephone: (404) 641-9773; fax (404) 552-9859.

## Issues in Musculoskeletal Imaging and Magnetic Resonance Imaging

The Dept. of Radiology, Hoag Memorial Hospital Presbyterian, Newport Beach, CA, will present Issues in Musculoskeletal Imaging, July 22–24, and Magnetic Resonance Imaging, July 25–27, at the Ritz-Carlton Resort Hotel, Laguna Niguel, CA. Program directors: Musculoskeletal, Michael Brant-Zawadzki; MR, Joel K. Lipman. Category 1 credit: up to 31 hr. Fee: physicians, $695. Information: Dawne Ryals, Ryals & Associates, P. O. 1925, Roswell, GA 30077-1925; telephone: (404) 641-9773; fax: (404) 552-9859.

## European Society of Gastrointestinal Radiologists Annual Meeting

The 2nd annual meeting of the European Society of Gastrointestinal Radiologists will take place in Oxford, England, Sept. 8–11. The main topics will be pancreatitis, the esophagus, and inflammatory bowel disease. Information: Dr. D. J. Nolan, ESGR, Dept. of Radiology, John Radcliffe Hospital, Oxford OX3 9DU, England; telephone: (0)865 220813; fax: (0)865 220818.

## The American Board of Radiology Examinations

Written examinations for the American Board of Radiology (ABR) are scheduled for Oct. 3–4. Oral examinations will be held at the Executive West Hotel in Louisville, KY, June 3–7. The ABR will accept applications for admission to the examinations after July 1, but not later than Sept. 30, in the year *preceding* the year in which the examination is to be taken. For application forms and further information: Office of the Secretary, The American Board of Radiology, 300 Park, Ste. 440, Birmingham, MI 48009.

# Meeting and Course Review

For the reader's convenience, a summary of upcoming meetings and courses is provided. Detailed listings are given in the *AJR* issue given in parentheses.

**Cyanoacrylate Embolization Course,** times arranged, Baltimore (July 1990)
**Visiting Fellowships in Ultrasound,** times arranged, Baltimore (Aug 1990)
**Visiting Fellowships in Interventional Radiology,** times arranged, Baltimore (Oct 1990)
**Swallowing Center Preceptorship,** times arranged, Baltimore (Jan)
**Imaging Fellowship,** times arranged, Miami Beach, FL (Jan)
**Sun Valley Imaging Meeting,** Feb. 23–March 2, Sun Valley, ID (Nov 1990)
**Principles and Practice of Clinical MRI,** Feb. 28–March 3, Lake Buena Vista, FL (Nov 1990)
**Advanced Seminars in Diagnostic Imaging,** March 1–3, Laguna Niguel, CA (Nov 1990)
**Winter Congress on Diagnostic Imaging,** March 2–9, Val D'Isere, France (Dec 1990)
**Masters Diagnostic Radiology Conference,** March 3–8, Maui, HI (Dec 1990)
**Practicum in Diagnostic Ultrasound,** March 4–8 and April 22–26 (Oct 1990)
**Course on MR Imaging,** March 4–7, Coronado (San Diego), CA (Nov 1990)
**Musculoskeletal Imaging,** March 4–8, Barbados (Nov 1990)
**Update on Body Imaging and Neuroradiology,** March 4–8, Acapulco, Mexico (Dec 1990)
**MR Imaging Fellowships at LAC/USC Imaging Science Center,** March 4–8, April 1–5, May 6–10, June 3–7, Aug. 5–9, Sept. 16–20, Oct. 7–11, and Nov. 4–8, Los Angeles (Feb)
**Fetal Assessment Practicums,** March 4–8 and April 8–12, Baltimore (Feb)
**Pediatric Radiology Course,** March 11–15, Park City, UT (Dec 1990)
**Obstetrics and Gynecology,** March 11–15 and April 22–26, Philadelphia (Dec 1990)
**Advances in PET and SPECT Imaging,** March 14–16, Baltimore (Jan)
**Breast Imaging Conference,** March 21–24, Lake Buena Vista, FL (Dec 1990)
**Orthopedic Radiology 1991,** March 25–27, Boston (Nov 1990)
**1991 MRI Update at Vail,** March 25–29, Vail, CO (Jan)
**Ultrasound 1991,** April 2–5, Boston (Nov 1990)
**National Council on Radiation Protection and Measurements Annual Meeting,** April 3–4, Washington, DC (Nov 1990)
**CT Symposium,** April 5–6, Madison, WI (Jan)
**Differential Diagnosis in Radiology,** April 6–8, Ann Arbor, MI (Jan)
**MRI Fellowships at Johns Hopkins,** April 8–12 and June 17–21, Baltimore (Oct 1990)
**Ultrasound in Obstetrics and Gynecology,** April 10–12, Ann Arbor, MI (Feb)
**Society for Magnetic Resonance Imaging Annual Meeting,** April 13–17 (Nov 1990)
**Skeletal Radiology Course,** April 13–18, Scottsdale, AZ (Feb)
**Society of Computed Body Tomography Annual Course,** April 15–19, Washington, DC (Feb)
**San Diego Residents' Radiology Review Course,** April 21–26, La Jolla, CA (Dec 1990)
**Clinical Nuclear Medicine 1991,** April 22–25, Boston (Nov 1990)
**Introduction to Interventional Radiology,** April 27, La Jolla, CA (Dec 1990)
**Radiology Review Course,** April 28–May 3, Miami Beach, FL (Feb)
**International Radiopharmaceutical Dosimetry Symposium,** May 7–10, Oak Ridge, TN (Jan)
**Thoracic Imaging 1991,** May 13–17, Toronto (Jan)
**Sonography Symposium,** May 24–25, Nashville, TN (Feb)
**Contemporary Medical Imaging VIII,** June 19–23, Destin, FL (Feb)
**Leeds Gastroenterology Course for Radiologists,** July 1–5, Leeds, England (Dec 1990)
**International Congress of Radiation Research,** July 7–12, Toronto (May 1990)
**Neuroradiology in the Rockies,** July 7–12, Snowmass at Aspen, CO (Feb)
**World Congress in Ultrasound,** Sept. 1–6, Copenhagen (Sept 1990)
**International Workshop on Hypertrophic Osteoarthropathy,** Sept. 8–11, Dubrovnik, Yugoslavik (Jan)
**European Congress of Radiology 1991,** Sept. 15–20, Vienna, Austria (Oct 1990)

*AJR* carries announcements of courses, symposia, and meetings of interest to its readers if received a minimum of 5 months before the event. There is no charge; receipt of items by the *AJR* Editorial Office is not acknowledged. Submit items for publication typed double-spaced. Provide title, date, location, brief description, sponsor, course directors, fees, category I credit, and address and telephone number for additional information. Faculty from the host institution will not be listed. Guest faculty names will appear **only** if initials are provided. Mail news items to *AJR* Editorial Office, 2223 Avenida de la Playa, Suite 103, La Jolla, CA 92037-3218.

# Invitation to the 1991 American Roentgen Ray Society Meeting in Boston, MA, May 5–10, 1991

I am pleased to extend an invitation to all radiologists to attend the 91st annual meeting of the American Roentgen Ray Society in Boston, MA, May 5–10, 1991. In keeping with the ARRS tradition, outstanding scientific and social programs will be provided.

The excitement of a meeting set in Boston, MA, in the spring requires no further description. The opportunity for busy radiologists to attend a major national meeting while enjoying all that Boston, MA, has to offer is ideal.

The scientific program, instructional courses, and categorical course are certain to be interesting and informative (see schedule below).

### Scientific Program

Two hundred scientific papers have been selected from more than 400 abstracts. Scientific sessions will be devoted to all major body systems, angiography, interventional techniques, sonography, and mammography, as well as technologies. Special emphasis has been placed on discussion of new developments.

The innovative and timely Friday morning minisymposium is entitled "Breast Imaging Update 1991." An outstanding faculty has been assembled for what I am sure will be a very stimulating program.

### Instructional Courses

Robert J. Stanley, Chairman, and Bruce McClennan, Associate Chairman of the Instructional Course Committee, have put together 60 instructional courses. Faculty members have been drawn from across the country. A superlative educational experience is anticipated, and advance registration is recommended.

### Categorical Course

An extraordinary categorical course on spine and body MR imaging has been fashioned. The course covers all aspects of the field, including equipment and principles of diagnosis. This course is certain to be popular, and advance registration is advised.

**Summary of 1991 American Roentgen Ray Society Meeting**

| Sunday May 5 | Monday May 6 | Tuesday May 7 | Wednesday May 8 | Thursday May 9 | Friday May 10 |
|---|---|---|---|---|---|
| | 8:00–9:30 Instructional courses | 8:00–9:30 Instructional courses | 8:00–9:30 Instructional courses | 8:00–9:30 Instructional courses | 8:00–10:00 Symposium: breast imaging update |
| 10:00–12:30 Categorical course: spine and body MR imaging | 10:00–10:30 Opening ceremonies | | | | |
| | 10:30–12:30 Scientific programs | 10:00–12:30 Scientific programs | 10:00–12:30 Scientific programs | 10:00–12:30 Scientific programs | 10:30–12:30 Symposium: breast imaging update |
| 2:00–3:00 Categorical course: spine and body MR imaging | 1:30–3:30 Categorical course: spine and body MR imaging | 1:30–3:30 Scientific programs | 1:30–3:30 Caldwell lecture and award session | 1:30–3:30 Scientific programs | |
| 3:30–5:00 Categorical course: spine and body MR imaging | 4:00–5:30 Instructional courses and categorical course: spine and body MR imaging | 4:00–5:30 Instructional courses and categorical course: spine and body MR imaging | 4:00–5:30 Instructional courses and categorical course: spine and body MR imaging | 4:00–5:30 Instructional courses and categorical course: spine and body MR imaging | |

### Scientific Exhibits

The more than 200 scientific exhibits coordinated by N. Reed Dunnick will cover the entire breadth of the field of diagnostic radiology. The technical exhibits will be integrated among the scientific exhibits to enhance the interaction of the attendees with technical exhibitors, a format that has proven to be very satisfactory.

### Caldwell Lecture

N. Thorne Griscom, M.D., has agreed to present the Caldwell Lecture at the 1991 meeting. This promises to be one of the highlights of the meeting and is concerned with pediatric pulmonary disorders encountered in the adult.

### Social Events

Boston, MA, offers an unlimited number of diversions, and Abner M. Landry, Jr., Chairman of the Annual Meeting Committee, has engaged a Boston-based tour consultant to plan a variety of tours. The annual golf and tennis tournaments for attendees and their companions are scheduled for Monday. The traditional cocktail party given by the society in the exhibit area for all registrants will be Sunday evening and will provide a convenient and early meeting place.

This promises to be a truly outstanding event in exceptional surroundings. I hope you will be able to accept our invitation. Plan now to attend.

John A. Kirkpatrick
President-Elect, ARRS

**Forthcoming ARRS Meeting Information**

Details of the American Roentgen Ray Society Meeting in Boston, MA, May 5–10, 1991, will appear in the **February, March,** and **April** 1991 issues of the *AJR*. Information about the scientific program, instructional programs, and social events and hotel and travel forms will be published in the Journal.

See pages 654–660 of this issue for more information concerning the meeting.

## Transportation Discounts

United Airlines is offering special airfares to the 1991 ARRS meeting for travel to and from Boston, MA, between May 1 and 14 inclusive. To obtain a 5% discount from any United available/applicable fare (MaxSavers and first class included) or a 40% discount off standard coach fares, telephone (toll-free) 1-800-521-4041 between the hours of 8:00 a.m. and 11:00 p.m. EST and immediately reference special ARRS account number 429JW. For travel to and from Canada, United will offer published Canadian meeting fares in selected markets. This discount can be as much as 35% off normal coach fares. No discounts are permitted from Mexico, the Bahamas, or the Orient. In addition, ARRS attendees who fly on United as outlined above will be eligible for a special drawing. The prize is one complimentary round-trip ticket good for travel in the continental United States before February 28, 1992 (holiday periods excluded).

Hertz Rent-A-Car service also can be arranged at discounted rates by calling United Airlines reservations at 1-800-521-4041.

# American Roentgen Ray Society:
## Officers, Committees, and Membership Information

### Officers

**President:** M. Paul Capp
**President-elect:** John A. Kirkpatrick, Jr.
**1st Vice-president:** A. Everette James, Jr.
**2nd Vice-president:** Andrew K. Poznanski
**Secretary:** Joseph T. Ferrucci, Jr.
**Treasurer:** Beverly P. Wood

**Executive Council:** R. J. Alfidi, R. N. Berk, M. P. Capp, W. J. Casarella, N. R. Dunnick, R. G. Evens, J. T. Ferrucci, Jr., A. E. James, Jr., J. A. Kirkpatrick, Jr., A. M. Landry, Jr., J. E. Madewell, A. A. Moss, A. K. Poznanski, L. F. Rogers, R. J. Stanley, J. H. Thrall, K. H. Vydareny, N. O. Whitley, B. P. Wood, G. R. Leopold, chairman

### Committees

**Editorial Policy:** R. N. Berk, E. Buonocore, Melvin M. Figley, S. v. W. Hilton, M. S. Huckman, C. A. Rohrmann, Jr., R. J. Stanley, R. I. White, W. J. Casarella, chairman

**Education and Research:** C. B. Higgins, B. J. Hillman, R. A. McLeod, R. J. Stanley, W. M. Thompson, N. O. Whitley, chairman

**Finance and Budget:** R. J. Alfidi, R. K. Gedgaudas-McClees, J. R. Thornbury, K. H. Vydareny, J. H. Thrall, chairman

**Nominating:** G. A. W. Gooding, L. F. Rogers, K. H. Vydareny, chairman

**Publications:** E. Buonocore, C. A. Rohrmann, Jr., R. J. Stanley, R. I. White, W. J. Casarella, chairman

**Membership:** J. E. Madewell, A. A. Moss, K. H. Vydareny, R. J. Alfidi, chairman

### Representatives to Other Organizations

**American Board of Radiology:** J. A. Kirkpatrick, Jr., E. C. Klatte, L. F. Rogers

**American College of Radiology:** J. M. Dennis, R. A. Gagliardi, J. E. Madewell, B. L. McClennan, R. J. Stanley

**American Medical Association:** S. F. Ochsner, delegate; K. L. Krabbenhoft, alternate; K. L. Kidd, CPT Advisory Committee

**American National Standards Institute:** M. E. Haskin

**National Council on Radiation Protection and Measurements:** F. Miraldi, E. L. Saenger

**Armed Forces Institute of Pathology:** J. E. Madewell

### Meeting Arrangements

**Annual Meetings:** May 5–10, 1991, Sheraton Boston, Boston; May 10–15, 1992, Marriott's World Center, Orlando, FL

**Annual Meeting Committee:** H. C. Carlson, J. K. Crowe, N. R. Dunnick, R. R. Lukin, R. J. Stanley, R. D. Steele, Jr., A. M. Landry, Jr., chairman

**Instructional Courses:** Bruce L. McClennan, associate chairman; R. J. Stanley, chairman

**Scientific Program:** P. Arger, E. Buonocore, D. O. Davis, K. B. Hunter, D. Kushner, T. C. McLoud, W. A. Murphy, Jr., L. B. Talner, J. H. Thrall, J. A. Kirkpatrick, chairman

**Scientific Exhibits:** J. R. Haaga, R. G. Ramsey, N. R. Dunnick, chairman

### ARRS Membership

An application form is printed in the February issue of the Journal. For consideration at the 1992 ARRS meeting, send completed forms before February 1, 1992, to American Roentgen Ray Society, 1891 Preston White Dr., Reston, VA 22091. Active members are graduates of an approved medical or osteopathic school or hold an advanced degree in an allied science. They must practice radiology or work in an associated science in the United States or Canada and be certified by the American Board of Radiology, American Osteopathic Board of Radiology, or Royal College of Physicians of Canada or otherwise adequately document training and credentials. Corresponding members are foreign radiologists or scientists who are active in radiology or an allied science. Members-in-training are residents or fellows in radiology or postgraduate students in an allied science. Additional application forms can be obtained from the ARRS offices in Reston, VA.

### Business Office

Paul Fullagar, Executive Director, American Roentgen Ray Society, 1891 Preston White Dr., Reston, VA 22091; (703) 648-8992.

# 1991 ARRS Meeting Summary, May 5–10, 1991 Boston, MA

A comprehensive description of the meeting, including the instructional courses, categorical course, and the Friday symposium, appears in this issue of the *AJR*. Meeting and registration forms also can be found in the February and March issues. These may be photocopied.

## Accreditation

All courses and scientific sessions carry AMA Category 1 credit on an hour-for-hour basis.

## Meeting Format

*Scientific Program.* Sessions will be grouped in parallel sessions so that registrants may choose topics related to their interests. A total of 189 scientific papers will be presented, Monday–Thursday, May 6–9. In addition, on Wednesday, May 8, the afternoon session will feature award papers and the Caldwell Lecture, which will be delivered by N. Thorne Griscom, M.D. On Friday, May 10, there will be a special 4-hr symposium on breast imaging.

*Categorical Course on Spine and Body MR.* This 15.5-hr course will be held Sunday–Thursday.

*Luncheon Sessions.* Registrants may enroll in special luncheon sessions, Monday–Thursday. A box lunch will be provided.

## Exhibits

*Scientific and Technical Exhibits and Case of the Day* will be set up in the Hynes Convention Center, Hall A, adjacent to the Sheraton Boston Hotel, Monday–Thursday, May 5–9. The Case of the Day will be presented by John F. O'Connor of Boston University School of Medicine.

## Local Activities

*General Reception.* Sunday evening, May 5, for all registrants.

*Golf Tournament.* Monday, May 6 at a local country club.

*Men's and Women's Tennis Tournaments.* Monday, May 6, at the Winchester Tennis Club.

*Local Tours.* See February issue of the *AJR* for a description of the activities and registration forms.

## Meeting Registration

Preregistration will be accepted until April 20. There will be on-site registration. Official badges and program books will be available at the registration desk, Sheraton Boston Hotel. No confirmations will be mailed.

## Course Registration

Register early—enrollment is limited. List first, second, and third choices for each period. Also, indicate whether you wish to take the categorical course. Deadline for registration by mail is April 20. All ticket orders will be filled according to postmarked date. Course tickets *will not* be mailed. Tickets will be available beginning at 1:00 p.m. on Saturday, May 4, at the ARRS registration desk in the Sheraton Boston Hotel. There will be on-site registration for courses not already filled.

## Hotel Registration

Reservations are handled by the ARRS Housing Bureau, Sheraton Boston Hotel, Attn: Reservations Office, 39 Dalton St., Boston, MA 02199. These must be received by April 13. Make check payable to Sheraton Boston Hotel. See reservation form in this issue for prices and complete instructions.

## Fees

| | |
|---|---|
| Meeting: | |
| ARRS members and resident members | No fee |
| Nonmembers | $250 |
| Nonmember physicians in training (with verification) | 25 |
| Categorical course | 75 |
| Luncheon sessions/each | 12 |
| Local tours | 20–75 |

## Cancellations and Fee Refunds (Excluding Hotel Fees)

Fees will be refunded only if cancellation is received by April 20, 1991. Send to American Roentgen Ray Society, 1891 Preston White Drive, Reston, VA 22091.

## Transportation Discounts

United Airlines is offering discounts of up to 40% on airfares. Call (800) 521-4041 and reference ARRS account number 429JW.

Hertz Rent-A-Car is offering special rates on car rentals. Reserve a Hertz car at these special rates through United Airlines when you make your plane reservations, or call Hertz directly at (800) 772-3773.

May Be Photocopied

**Deadline: April 20**

# Meeting and Local Activities Registration Form: ARRS 91st Annual Meeting May 5–10, 1991, Boston, MA

If you plan to attend, please complete this form. Official badges and program booklets will be available at the ARRS Registration Desk, Sheraton Boston Hotel. **There will be no confirmations before the meeting.** Preregistration by mail will be accepted until April 20. On-site registration will be available.

**Make all checks payable to: American Roentgen Ray Society**

Mail to: American Roentgen Ray Society
1891 Preston White Drive
Reston, VA 22091

**Please type or print:**

Registrant

Last Name _____ First Name or Initials _____

Street _____

City _____ State _____ ZIP Code _____

Accompanying Guest

Name _____ (Accompanying person's name to be printed on badge)

Street _____

City _____ State _____ ZIP Code _____

| **Check appropriate categories:** | Registration fee: |
|---|---|
| ☐ Member ARRS | None |
| ☐ Nonmember | $250 |
| ☐ Nonmember physician in training (please complete section below) | $25 |
| ☐ Course faculty, presenter of scientific paper, scientific exhibitor, technical exhibitor (circle one) | None |
| ☐ ACR luncheon course, Monday, May 6 | $12 |
| ☐ ACR luncheon course, Tuesday, May 7 | $12 |
| ☐ ACR luncheon course, Wednesday, May 8 | $12 |
| ☐ ACR luncheon course, Thursday, May 9 | $12 |
| ☐ Categorical course | $75 |
| ☐ Social programs (see next page) | ____ |
| **Total enclosed** | ____ |

## Instructional Courses

Please register early for Instructional Courses. Attendance is limited. List first, second, and third choices for each day by course number. Ticket orders are filled according to postmark. ARRS members, nonmembers, and those in radiology training may take all courses without charge except the categorical course, **for which all registrants must pay $75. Nonmembers also must pay the meeting registration fee. All who wish to attend courses must complete this section.**

Course tickets will be available at the ARRS Registration Desk at the Sheraton Boston Hotel beginning Saturday, May 4, at 1 p.m.

Complete section at right for courses other than the categorical course. Be sure to fill out second and third choices for each day.

| Course Choices | Morning | | | Afternoon | | |
|---|---|---|---|---|---|---|
| | 1st | 2nd | 3rd | 1st | 2nd | 3rd |
| Monday | | | | | | |
| Tuesday | | | | | | |
| Wednesday | | | | | | |
| Thursday | | | | | | |

Friday ____ Check if you wish to attend the breast imaging symposium (only course offered this day).

**For Nonmember Physicians in Training:**

_____ is in training in my department.

Training Program Director _____

Institution _____ Date _____

(OVER)

## Local Activities

No refunds after April 20

| | | |
|---|---|---|
| **Sunday, May 5, 1:30–4 p.m., Welcome to Boston** | _____tickets @ $20 | $_____ |
| **Monday, May 6, 7:45–10 a.m., Breast Cancer Screening Program** | _____tickets @ no charge | |
| **Monday, May 6, 2–4:30 p.m., Welcome to Boston** | _____tickets @ $20 | $_____ |
| **Monday, May 6, 2:30–5:30 p.m., Cambridge and Harvard University** | _____tickets @ $25 | $_____ |
| **Tuesday, May 7, 9 a.m.–12:00 noon, In the Footsteps of JFK** | _____tickets @ $25 | $_____ |
| **Tuesday, May 7, 8:30 a.m.–5 p.m., Newport, Rhode Island** | _____tickets @ $63 | $_____ |
| **Wednesday, May 8, 1:30–5:30 p.m., Lexington and Concord** | _____tickets @ $25 | $_____ |
| **Wednesday, May 8, 2–4 p.m., Antiques Through the Centuries** | _____tickets @ $22 | $_____ |
| **Thursday, May 9, 9 a.m.–3 p.m., Salem and Marblehead** | _____tickets @ $45 | $_____ |
| **Thursday, May 9, 1:30–4 p.m., Beacon Hill Tour** | _____tickets @ $28 | $_____ |
| **Friday, May 10, 8 a.m.–12 noon, Filene's Basement** | _____tickets @ $25 | $_____ |

Preregistration is required.

## Annual ARRS Golf Tournament, Monday, May 6

The tournament will be at the Ferncroft Country Club, Danvers, MA. Transportation, luncheon, greens fee, cart, prizes and hors d'oeuvres and drinks after play is completed are included in the $100 fee. Preregistration is important.

Name: _____ Telephone: _____

Address: _____

Handicap (if any): _____

My foursome includes (list handicaps): _____

_____ _____tickets @ $100 $_____

## Men's and Women's Tennis Tournaments, Monday, May 6

The tournaments will be at the Winchester Indoor Tennis Club. Tennis attire is required. Fee of $60 includes transportation, luncheon, court fees, and balls.

Name: _____ Telephone _____

Address: _____

_____tickets @ $60 $_____

May Be Photocopied

**Deadline: April 6**

# Hotel Registration Form: ARRS 91st Annual Meeting May 5–10, 1991, Sheraton Boston Hotel Boston, MA

**Mail to:**

**ARRS Housing Bureau**
Sheraton Boston Hotel
Attention: Reservations Office
39 Dalton St.
Boston, MA 02199

**(PLEASE MAKE CHECKS PAYABLE TO THE SHERATON BOSTON HOTEL—*NOT* TO THE ARRS)**

Individual guest name _____

Address _____

City & State _____ ZIP _____

Arrival date/time _____ Departure date/time _____

Individual requesting reservation _____

Address _____

City & State _____ ZIP _____

**Please forward with your reservation a deposit** of one night's room rate to be applied to the last night of your scheduled stay, or provide credit card information to guarantee your reservation. The hotel accepts American Express, Diners Club, Carte Blanche, Visa, and Master Card credit cards. The deposit will hold your room until 6 a.m. of the morning following your scheduled arrival date. In the event of an early departure, the deposit is nonrefundable unless the hotel is notified prior to or at the time of check-in. Cancellation notice of 14 days is required for a deposit refund.

**Check accommodations desired**

| Room Category | Main House | Towers |
|---|---|---|
| Single | $144, $172 | $200 |
| Double | $160, $188 | $216 |
| Executive suite | $260 | $300 |
| Mini suite | $260 | — |
| 1-bedroom suite | $340 | $400 |
| 2-bedroom suite | $460 | $540 |

Deposit amount (1 night's rate) $_____

☐ Check enclosed

☐ Credit card: _____
Type of card Exp. date

_____
Card number

_____
Signature

**Important Information:**

1. Reservations must be received by the Sheraton Boston Hotel/ ARRS Housing Bureau no later than April 6 to be assured of written confirmed accommodation. Reservations after that time are subject to availability. We urge you to make your reservations promptly.
2. Written confirmation of your reservation will be sent to you by the hotel.
3. To change or cancel reservations, please call the hotel directly at (617) 236-2000.
4. If you plan to share a room, please send in only one housing form. Be sure to list all names of occupants of rooms. Assignment is delayed until complete information is received.
5. Check-in is after 3 p.m., or earlier if the room is available. Check-out time is 1 p.m.
6. Parking is available at the hotel.

## Categorical Course in Spine and Body MR Imaging

## American Roentgen Ray Society 91st Annual Meeting

***May 5–9, 1991, Sheraton Boston Hotel, Boston, MA***

*Course Director, Anton N. Hasso, M.D.*
*Course Codirector, David D. Stark, M.D.*

| | |
|---|---|
| **Sunday, May 5** | **Fundamentals/New Developments** |
| 9:50–10:00 | Welcome/Introduction (*Hasso/Stark*) |
| 10:00–10:30 | Fundamental MRI (*Matwiyoff*) |
| 10:30–11:00 | Fast Scanning (*Hendrick*) |
| 11:00–11:40 | Sedation/Anesthesia/Patient Monitoring (*Hinshaw/Shellock*) |
| 11:40–12:20 | MR Angiography |
| | Body (*Edelman*) |
| | Head and Neck (*Hasso*) |
| 12:20–2:00 | Lunch Break |
| | **Spine/Neck** |
| 2:00–2:30 | Flow/Spine CSF Flow (*Bradley*) |
| 2:30–3:00 | Congenital/Developmental Lesions (*Naidich*) |
| 3:00–3:30 | Mass Lesions/Myelopathy (*Sze*) |
| 3:30–4:00 | Coffee Break |
| 4:00–4:30 | Infective Spondylitis (*Sharif*) |
| 4:30–5:00 | 3D Spine/Degenerative/Postoperative (*Ross*) |
| 5:00–5:30 | Neck Soft Tissues (*Vogl*) |
| **Monday, May 6** | **Contrast Agents/Motion Artifact Suppression** |
| 1:30–2:00 | MR Contrast Agents, Introduction (*Wolf*) |
| 2:00–2:30 | Contrast Agents for Body MR (*Stark*) |
| 2:30–3:00 | Motion Artifact Suppression (*Ehman*) |
| 3:00–3:30 | Coffee Break |
| | **Pediatric** |
| 3:30–4:15 | Pediatric Abdomen/Pelvis (*Dietrich*) |
| 4:15–5:00 | Pediatric Musculoskeletal/Marrow (*Moore*) |
| 5:00–5:45 | Pediatric Cardiovascular (*Higgins*) |
| **Tuesday, May 7** | **Abdomen/Pelvis** |
| 3:45–4:15 | Liver (*Mitchell*) |
| 4:15–5:00 | Male Pelvis |
| | Prostate/Bladder (*Rifkin*) |
| | Testes/Scrotum (*Fritzsche*) |
| 5:00–5:45 | Female Pelvis |
| | Neoplasms (*Hricak*) |
| | Non-neoplastic Disorders (*McCarthy*) |
| **Wednesday, May 8** | **Neck/Musculoskeletal** |
| 3:45–4:25 | Infection and Avascular Necrosis (*Beltran*) |
| 4:25–5:05 | Soft Tissue/Bone Neoplasms (*Seeger*) |
| 5:05–5:45 | Knee (*Reiser*) |
| **Thursday, May 9** | **Musculoskeletal** |
| 3:45–4:15 | Temporomandibular Joints (*Fulmer*) |
| 4:15–4:45 | Wrist (*Kneeland*) |
| 4:45–5:15 | Shoulder (*Crues*) |
| 5:15–5:45 | Foot and Ankle (*Solomon*) |

# 1991 American Roentgen Ray Society Instructional Courses and Symposium

Robert J. Stanley, Director, and Bruce L. McClennan, Associate Director

Sixty Instructional Courses will be presented during the 91st annual meeting of the American Roentgen Ray Society (ARRS) beginning Monday, May 6, and continuing through Thursday, May 9. Each of the Instructional Courses listed on the next page will be 90 min long. In addition, there will be a week-long Categorical Course in Spine and Body MR Imaging and a half-day Symposium, Current Topics in Breast Imaging.

The Categorical Course in Spine and Body MR Imaging will have 15.0 hr of instruction and will begin on Sunday, May 5, and conclude on Thursday, May 9. The Symposium, Current Topics in Breast Imaging, will be on Friday, May 10, from 8 a.m. to 12 noon. All courses carry Category 1 credit on an hour-to-hour basis.

### Registration Information

To register for courses, complete the meeting registration form in this section and mail promptly. Tickets also will be available at the Instruction Course Registration Desk, Sheraton Boston Hotel for courses that have not been sold out. All courses will take place in the headquarters' hotel.

After reviewing the course list, select three for each morning and afternoon session. Write the course number and name of the first instructor on the registration form. Please note that the -01 residents'-masters' tutorials are intended primarily for residents and that attendance will be limited.

All who register for the Categorical Course in Spine and Body MR Imaging (including ARRS members) must pay a fee of $75 and must take the entire series of classes. The Categorical Course totals 15.0 hr of instruction and includes a syllabus.

## Course Schedule

### Sunday, May 5, through Thursday, May 9

The Categorical Course in Spine and Body MR Imaging will have 15.0 hr of instruction over 5 days. Topics and instructors are listed on p. 658.

### Monday, May 6, through Friday, May 10

A total of 60 courses will be offered (see next page) plus a symposium, Current Issues in Breast Imaging.

## ACR Luncheon Presentations on Socioeconomics of Radiology

A series of luncheon presentations on the socioeconomics of radiology will be arranged by the American College of Radiology (ACR). A box lunch will be provided. The presentations will be from 12:30 to 1:30 p.m. and do not conflict with other elements of the program. Advance registration is required. Cost per session is $12.

**Date, Topic, Speaker**

**Monday, May 6:** Governmental Issues for Radiology, Gary Price, ACR Director of Government Relations

**Tuesday, May 7:** Economic Issues of Radiology Practice, Emmett O. Templeton, M.D., Chairman, ACR Commission on Economics

**Wednesday, May 8:** Current Legal Issues in Radiology, Thomas W. Greeson, J.D., ACR Legal Counsel

**Thursday, May 9:** Update on ACR Activities, James M. Moorefield, M.D., Chairman, ACR Board of Chancellors

**Symposium: Current Issues in Breast Imaging**
**Friday, May 10, 1991, 8:00 a.m. to 12:00 noon**

| Time | Topic (*Presenter*) |
|---|---|
| 8:00 a.m. | Introduction and ACR accreditation (*Kopans DB*) |
| 8:30 a.m. | Are the screening guidelines wrong? (*Moskowitz M*) |
| 9:00 a.m. | Proper positioning—not just basic, but required (*Eklund GW*) |
| 9:30 a.m. | Now that I've found it, what should I do about it? (*Kopans DB*) |
| 10:00 a.m. | Questions and break |
| 10:30 a.m. | The therapeutic implications of diagnostic findings—extensive intraductal component and the pre- and postirradiated breast (*Sadowsky NL*) |
| 11:00 a.m. | How can you tell that you are screening at appropriate thresholds? (*Sickles EA*) |
| 11:30 a.m. | Questions and panel discussion |

Note.—There is no fee for this symposium. However, to facilitate planning, please register on the meeting registration form.

**American Roentgen Ray Society Instructional Courses: May 6–May 9, 1991**

| Topic | Monday | Tuesday | Wednesday | Thursday |
|---|---|---|---|---|
| | | Morning (all sessions begin at 8:00 a.m.) | | |
| Residents'-masters' tutorial | 101. Some basic signs of chest X-ray diagnosis including plain film/CT correlation. *Fraser RG, Heitzman ER* | 201. Advances in imaging the brain and spine: impact on diagnosis and treatment of CNS abnormalities. *Quencer RM.* | 301. The role of ultrasound in pediatric gastrointestinal tract disease. *McAlister WH* | 401. Angioplasty—past and present. *Tegtmeyer CJ* |
| Pediatrics | 102. Evaluation of pneumonia in the pediatric patient. *Singleton EB* | 202. A practical approach to pediatric abdominal diagnosis. *Wood BP, Senac MO* | 302. Diagnostic imaging of child abuse. *Kleinman PK* | 402. Musculoskeletal and cranial pediatric ultrasonography. *Teele RL, Share J* |
| Technique and technology | 103. Ultrafast CT scanning—an update. *Sheedy PF* | 203. CT and US guided biopsies: practical approaches, pitfalls and new techniques. *Charboneau JW, Reading CC* | 303. Advances in abdominal CT examination techniques. *Berland LL, Megibow AJ* | 403. Computer assisted 3-D imaging: state of the art. *Fishman EK, Ney D* |
| Chest | 104. CT of the lung parenchyma. *Pugatch RD* | 204. Pulmonary manifestations of the immunocompromised patient. *Vydareny KH, Gross BH* | 304. Plain chest radiograph manifestations of esophageal and diaphragmatic diseases. *Stark P, Tarver RD* | 404. Thoracic infections and their complications. *Choplin RH, Reed JC* |
| Gastrointestinal | 105. Biliary diagnosis: a problem oriented approach. *Koehler RE, Balfe DM* | 205. Inflammatory bowel disease from beginning to end. *Gore RM, Laufer I* | 305. Radiologic screening for colorectal cancer. *Gelfand DW, Ott D* | 405. Radiologic evaluation of the pharynx and esophagus. *Rubesin SE, Levine MS* |
| Genitourinary/retroperitoneum | 106. CT/MRI of the retroperitoneum. *Lee JKT, Heiken JP* | 206. The radiologic evaluation of the adrenal. *Kenney PJ* | 306. Imaging of acute renal inflammatory disease. *McClennan BL* | 406. CT and MRI of the kidney. *Newhouse JH, Amis ES* |
| Body imaging/CT, MR imaging, sonography | 107. Staging of lymphoma. *Gedgaudas-McClees RK, Torres WE* | 207. The peritoneum and mesentery: anatomy, pathology, and technique. *Halvorsen RA, Silverman PM* | 307. Computed tomographic evaluation of the liver. *Moulton JS* | 407. Sonographic evaluation of the adult acute abdomen. *Wilson SR* |
| Neuroradiology | 108. Supratentorial neoplasms—MRI. *Leeds NE* | 208. MRI and CT in the evaluation of head trauma. *Davis KR* | 308. MRI of the sella and parasellar region. *El Gammal T, Brooks BS* | 408. Imaging CNS vascular disease: radiologic-pathologic correlation. *Osborn AG* |
| Radiologic practice | 109. The battle over turf: who has it and how to get it. *Hillman BJ* | 209. Cost containment in radiology departments. *Janower ML* | 309. Pointers on scientific manuscript preparation. *Berk RN, Levene M, Hilton S, Spiller KL* | 409. The future of digital radiology: technical and clinical considerations. *Ovitt TW, Hunter TB* |
| Radiologic-pathologic correlation | 110. Radiographic pathology of the GI mucosa. *Ghahremani GG* | 210. Radiologic-pathologic correlation of GI tract tumors. *Lichtenstein JE, Olmsted WW* | 310. Arthropathies: radiologic-pathologic correlations. *Madewell J* | 410. Imaging and pathologic correlation of bone and soft-tissue neoplasms. *Hudson TM* |
| | | Afternoon (all sessions begin at 4:00 p.m.) | | |
| Musculoskeletal | 111. The analytic approach to the film (an imaging discipline). *Jacobson HG, Edeiken J* | 211. Current practice in musculoskeletal ultrasonography. *Adler RS, Fornage BD* | 311. The pelvis and hip: anatomic-clinical correlations. *Pitt MJ* | 411. Evaluation of bone and marrow in osteoporosis and other metabolic conditions. *Rosenthal DI* |
| Body imaging/sonography | 112. Imaging and biopsy of the prostate. *Papanicolaou N, Tung GA* | 212. Transvaginal sonography in obstetrics and gynecology. *Fleischer AC, Rao BK* | 312. Update on ultrasound in hepatobiliary imaging. *Kane RA* | 412. Peripheral vascular ultrasound imaging. *Carroll BA* |
| Head and neck/nuclear medicine | 113. Imaging of the sinonasal cavities. *Som PM* | 213. Imaging of head and neck cancers. *Curtin HD* | 313. SPECT brain imaging. *Mountz JM* | 413. Nuclear cardiology in clinical practice. *Thrall JH* |
| Body imaging/CT, MR imaging, sonography | 114. Use of diagnostic imaging for the follow-up of treated cancer patients. *Kagan AR, Steckel RJ* | 214. Pitfalls in plain film and CT analysis of the mediastinum. *Glazer HS, Molina P* | 314. Radiologic evaluation of the transplant kidney. *Baumgartner BR, Pozniak MA* | 414. MRI of the thorax with CT correlation. *McLoud TC* |
| Angiography/interventional | 115. New devices in peripheral vascular intervention: diagnosis and therapy. *Becker G, Katzen BT* | 215. Billary calculus disease: interventional management. *Mueller PR, vanSonnenberg E, Teplick SK* | 315. Update on embolotherapy. *Keller FS, Waltman AC* | 415. Plugging vessels and opening ureters: treating kids with catheters. *Fellows KE, Hoffer FA* |

# Classified Advertisements

## Positions Available

**RADIOLOGIST / PULMONARY RADIOLOGY CHIEF**—The Dept. of Radiology at the University of Minnesota has a full-time position available in the pulmonary radiology section at the rank of tenure-track assistant professor, tenured associate professor, or tenured professor beginning April 30, 1991. At the assistant professor level, minimum requirements are board certification in radiology, a minimum of 1 yr postresidency specialty training or experience in pulmonary radiology, and a demonstrated involvement in quality research accepted or published in peer-reviewed journals. Appointment at the rank of associate professor requires a minimum of 4 yr postresidency experience, a professional distinction in research and writing, and demonstrated effectiveness in teaching and advising. Appointment at the rank of professor requires a minimum of 6 yr postresidency experience, a national reputation in research, and evidence of leadership in candidate's professional field. Responsibilities will include all facets of radiology as well as graduate and undergraduate medical instruction. Research performance will be strongly encouraged and evaluated. Salary is negotiable and competitive and is dependent on past scholarly productivity and post-M.D. experience. Applicants must be licensed or able to obtain a license to practice medicine in the state of Minnesota before appointment date. Applications will be accepted through May 16, 1991. Send letters to William M. Thompson, M.D., Professor and Chairman, Dept. of Radiology, Box 292 UMHC, University of Minnesota, 420 Delaware St., S.E., Minneapolis, MN 55455. The University of Minnesota is an equal opportunity educator and employer and specifically invites and encourages applications from women and minorities. 3a

**THE DEPT. OF RADIOLOGY, VIRGINIA COMMONWEALTH UNIVERSITY / MEDICAL COLLEGE OF VIRGINIA AND THE MCGUIRE VA MEDICAL CENTER, RICHMOND, VA**, seek faculty for positions in diagnostic radiology (chest, GI, mammography, CT/ultrasound/MRI, musculoskeletal, pediatrics, ER, angio/interventional, and neuroradiology), nuclear medicine, and radiological physics. MCV is a 1,058-bed facility (205 for pediatric patients) and a Level I Trauma Center. The McGuire VAMC is an 800-bed facility (pediatrics excluded). ABR certification of eligibility required. Individual should have experience working in a culturally diverse environment. Academic rank and salary commensurate with experience. For position description or to submit CV, write or phone A. V. Proto, M.D., Dept. of Radiology, MCV Box 470, Richmond, VA 23298-0470; (804) 786-7212. VCU/MCV is an equal opportunity/affirmative action employer. Women and minorities are encouraged to apply. 3–4a

**HEAD, CROSS-SECTIONAL IMAGING SECTION** The Dept. of Radiology, University of Rochester Medical Center, Strong Memorial Hospital, Rochester, NY, is seeking a board-certified radiologist with subspecialty experience in body imaging for a faculty position as Head of Cross-Sectional Imaging Section, including ultrasound, CT, MRI, and body interventional. Strong Memorial Hospital is a 750-bed, tertiary-care hospital. State-of-the-art MRI, CT, and ultrasound equipment is available. Teaching of medical students, radiology residents, and fellows and the opportunity for developing research projects are afforded. Rank and salary are commensurate with experience. Interested candidates should forward CV to Robert E. O'Mara, M.D., Chair, Dept. of Radiology, Box 648, University of Rochester Medical Center, Rochester, NY 14642; (716) 275-2733. EO/AA/M-F employer. 3ap

**RADIOLOGIST / GENITOURINARY**—The Dept. of Radiology at the University of Minnesota has a full-time position available in the genitourinary section at the rank of tenure-track assistant professor, tenured associate professor, or tenured professor beginning May 16, 1991. At the assistant professor level, minimum requirements are board certification in radiology, a minimum of 1 yr postresidency specialty training or experience in genitourinary radiology, and a demonstrated involvement in quality research accepted or published in peer-reviewed journals. Appointment at the rank of associate professor requires a minimum of 4 yr postresidency experience, a professional distinction in research and writing, and demonstrated effectiveness in teaching and advising. Appointment at the rank of professor requires a minimum of 6 yr postresidency experience, a national reputation in research, and evidence of leadership in candidate's professional field. Responsibilities will include all facets of genitourinary radiology as well as graduate and undergraduate medical instruction. Research performance will be strongly encouraged and evaluated. Salary is negotiable and competitive and is dependent on past scholarly productivity and post-M.D. experience. Applicants must be licensed or able to obtain a license to practice medicine in the state of Minnesota before appointment date. Applications will be accepted through April 30, 1991. Send letters to William M. Thompson, M.D., Professor and Chairman, Dept. of Radiology, Box 292 UMHC, University of Minnesota, 420 Delaware St., S.E., Minneapolis, MN 55455. The University of Minnesota is an equal opportunity educator and employer and specifically invites and encourages applications from women and minorities. 3a

**RADIOLOGIST, CT/ABDOMINAL IMAGING**—An opening exists for a board-certified/eligible radiologist with fellowship training or equivalent experience in CT to serve on the CT service in abdominal imaging with participation in other aspects of the division. Extensive clinical research opportunities exist at the Yale Medical School and the Yale–New Haven Hospital. Academic rank commensurate with experience. Numerous benefits including paid sabbatical. Candidates must be U.S. citizens or must qualify as a permanent resident in the United States. Please send CV and bibliography to Arthur T. Rosenfield, M.D., Yale University School of Medicine, Dept. of Diagnostic Radiology, 333 Cedar St., New Haven, CT 06510. Yale is an equal opportunity/affirmative action employer. Applications from women and members of minority groups are encouraged. Applications should be submitted no later than May 1, 1991. 3–4a

**DIAGNOSTIC RADIOLOGIST**—Yale University School of Medicine seeks a board-certified radiologist, with additional experience or training in ultrasound/CT, for a full-time faculty position. Academic rank is at the level of assistant or associate professor, depending on qualifications. Candidates must be competent in all aspects of ultrasound, including vascular, and must be able to do cross-sectional interventional procedures. Must have credentials to work at the local VA hospital as well as a strong adademic background with research goals. Candidates must be U.S. citizens or must qualify as permanent residents in the United States. Please send CV and bibliography to Lynwood Hammers, D.O., or Kenneth J. W. Taylor, M.D., Diagnostic Radiology, Yale University School of Medicine, 333 Cedar St., New Haven, CT 06510. Yale University is an equal opportunity employer; applications from women and minority group members are encouraged. Application deadline is May 1, 1991. 3–4a

**RADIOLOGIST / MUSCULOSKELETAL**—The Dept. of Radiology at the University of Minnesota has a full-time position available in the musculoskeletal section at the rank of tenure-track assistant professor, tenured associate professor, or tenured professor beginning May 16, 1991. At the assistant professor level, minimum requirements are board certification in radiology, a minimum of 1 yr postresidency specialty training or experience in musculoskeletal radiology, and a demonstrated involvement in quality research accepted or published in peer-reviewed journals. Appointment at the rank of associate professor requires a minimum of 4 yr postresidency experience, a professional distinction in research and writing, and demonstrated effectiveness in teaching and advising. Appointment at the rank of professor requires a minimum of 6 yr postresidency experience, a national reputation in research, and evidence of leadership in candidate's professional field. Responsibilities will include all facets of musculoskeletal radiology as well as graduate and undergraduate medical instruction. Research performance will be strongly encouraged and evaluated. Salary is negotiable and competitive and is dependent on past scholarly productivity and post-M.D. experience. Applicants must be licensed or able to obtain a license to practice medicine in the state of Minnesota before appointment date. Applications will be accepted through April 30, 1991. Send letters to William M. Thompson, M.D., Professor and Chairman, Dept. of Radiology, Box 292 UMHC, University of Minnesota, 420 Delaware St., S.E., Minneapolis, MN 55455. The University of Minnesota is an equal opportunity educator and employer and specifically invites and encourages applications from women and minorities. 3a

**DIAGNOSTIC RADIOLOGIST, IMMEDIATE OPENING AT ROSE MEDICAL CENTER (RMC), DENVER, CO**—A 7-person radiology group is recruiting 2 radiologists with fellowship training, 1 in interventional radiology and 1 in ultrasound, especially high-risk OB/fetal. The practice involves all imaging modalities. Highly competitive first yr salary and generous fringe benefit package. Position leads to offer of equal shares in the professional corporation after 1 yr, if mutually agreed upon. RMC is affiliated with the University of Colorado. Contact David W. Wilder, M.D., or Jeffrey A. Levy, M.D.; (303) 320-2256. 3–4a

**GOOD LIFE, GOOD MONEY**—Radiologist needed for growing practice that covers 2 hospitals as well as 2 free-standing clinics. Modalities include R&F, general, mammography, CT, MRI, nuclear medicine, SPECT, and special procedures. Denton, population 60,000, located 30 mi. north of Dallas/Fort Worth, has 2 recreational lakes within 15 mi. and 2 major universities. Attractive financial and benefit packages with early partnership are offered. Contact Family Radiology with CV at 1614 Scripture, Ste. 2, Denton, TX 76201; (817) 387-6159. 3a

**MUSCULOSKELETAL RADIOLOGIST, MALLINCKRODT INSTITUTE OF RADIOLOGY/WASHINGTON UNIVERSITY**—The musculoskeletal section is enlarging and has need for an additional person at the instructor, assistant professor, or associate professor level. The section performs all aspects of musculoskeletal imaging including CT, MRI, bone biopsy, and arthrography of all joints. The section also performs all diagnostic and screening mammography and breast procedures and directs emergency dept. radiology. The volume of clinical material is large. Teaching, academic, and working conditions are well-supported. Send CV to Louis A. Gilula, M.D., or William A. Murphy, M.D., Mallinckrodt Institute of Radiology, Barnes Hospital, 510 S. Kingshighway Blvd., St. Louis, MO 63110. 3–6a

**RADIOLOGIST / NEURORADIOLOGY**—The Dept. of Radiology at the University of Minnesota has 3 full-time positions available in the neuroradiology section at the rank of tenure-track assistant professor, tenured associate professor, or tenured professor beginning as soon as possible. At the assistant professor level, minimum requirements are board certification in radiology, a minimum of 1 yr postresidency specialty training or experience in neuroradiology, and a demonstrated involvement in quality research accepted or published in peer-reviewed journals. Appointment at the rank of associate professor requires a minimum of 4 yr postresidency experience, a professional distinction in research and writing, and demonstrated effectiveness in teaching and advising. Appointment at the rank of professor requires a minimum of 6 yr postresidency experience, a national reputation in research, and evidence of leadership in candidate's professional field. Responsibilities will include all facets of neuroradiology as well as graduate and undergraduate medical instruction. Research performance will be strongly encouraged and evaluated. Salary is negotiable and competitive and is dependent on past scholarly productivity and post-M.D. experience. Applicants must be licensed or able to obtain a license to practice medicine in the state of Minnesota before appointment date. Applications will be accepted through April 1, 1991. Send letters to William M. Thompson, M.D., Professor and Chairman, Dept. of Radiology, Box 292 UMHC, University of Minnesota, 420 Delaware St., S.E., Minneapolis, MN 55455. The University of Minnesota is an equal opportunity educator and employer and specifically invites and encourages applications from women and minorities. 3a

**RADIOLOGIST / NEURORADIOLOGY CHIEF**—The Dept. of Radiology at the University of Minnesota has a tenured position available for the H. O. Peterson Endowed Professor of Neuroradiology at the rank of professor beginning as soon as possible. The dept. is seeking a neuroradiologist of international renown to fill this most prestigious endowed professorship in research and serve as section head of neuroradiology. At the professor level, minimum requirements are board certification in radiology, a 3-yr accredited radiology residency, a minimum of 6 yr postresidency radiology experience in neuroradiology, a national reputation in research, and evidence of leadership in the candidate's professional field. Radiologist will be responsible for directing the neuroradiology section, requiring expertise in all facets of neuroradiology, digital subtraction angiography, interventional radiology, CT, and MRI. Responsibilities also include graduate and undergraduate medical instruction in clinical neuroradiology, including postresidency trainees. Research performance will be strongly encouraged and evaluated. Salary is negotiable and competitive and is dependent on past scholarly productivity and post-M.D. experience. Applicants must be licensed or able to obtain a license to practice medicine in the state of Minnesota before appointment date. Applications will be accepted through April 1, 1991. Send letters to William M. Thompson, M.D., Professor and Chairman, Dept. of Radiology, Box 292 UMHC, University of Minnesota, 420 Delaware St., S.E., Minneapolis, MN 55455. The University of Minnesota is an equal opportunity educator and employer and specifically invites and encourages applications from women and minorities. 3a

**MICHIGAN**—Opportunity for a BE/BC radiologist to join 1 other in a hospital-based, rural practice. Experience in CT, ultrasound, nuclear medicine, mammography, and general radiology. Competitive salary. Send CV to David L. Carter, M.D., 6796 Garfield St., Cass City, MI 48726. 3–4ap

**RADIOLOGIST, MARYLAND**—BC/BE radiologist needed to join 9-physician radiology dept. Special skills in angio/interventional and MRI desired. Fellowship training preferred. Must be willing to do most aspects of diagnostic radiology. Part of a larger multispecialty group, providing care for BC/BS affiliated HMO as well as growing FFS practice. Excellent benefits and salary. Located in Columbia, MD, near the cultural advantages and medical schools of the Baltimore-Washington, DC, area. Direct CV to Patuxent Medical Group, Inc., 2 Knoll North Dr., Ste. 401, Columbia, MD 21045; Attn: Physician Recruiter. 3ap

**DIAGNOSTIC RADIOLOGIST, PART-TIME, TUCSON, AZ**—Radiologist to join 24-person group on approximately 1/2-time basis with 1-yr renewable contract. No night or weekend call, work every other Saturday a.m. Includes health, life, disability, and malpractice insurance. General diagnosis, mammography, CT, and ultrasound. Contact R. O. Broome, M.D., Radiology, Ltd., 6516 E. Carondelet Dr., Bldg. C, Tucson, AZ 85710. 3–5ap

**CROSS-SECTIONAL IMAGING/MRI, CT, ULTRASOUND**—The Dept. of Radiology, Strong Memorial Hospital, University of Rochester, Rochester, NY, is seeking a board-eligible/certified radiologist for its body imaging section. An appointment as assistant professor or higher is available at a level appropriate to experience. One yr fellowship training or equivalent experience is required. Research and teaching opportunities are afforded in a strong academic dept. with state-of-the-art radiologic equipment. Send letter of inquiry to Robert E. O'Mara, M.D., Chair, Dept. of Radiology, Box 648, University of Rochester Medical Center, Rochester, NY 14642; (716) 275-2733. EO/AA/M-F employer. 3ap

**INTERVENTIONAL RADIOLOGIST**—Board-certified radiologist with fellowship training in vascular/interventional radiology needed for a position starting July 1, 1991. Academic rank is at the assistant or associate professor level depending on qualifications. This active clinical service performs the entire range of diagnostic and interventional procedures including embolization, angioplasty, infusion therapy, IVC filter placement, and atherectomy. The interventional inpatient service admits 100 patients per yr, primarily for embolization and angioplasty. The interventional clinic evaluates referred patients with peripheral and renal vascular disease and vascular malformations. Clinical and fundamental research interests are ongoing in atherectomy, embolization devices, and endourology. Please send applications with CV to Robert I. White, Jr., M.D., Professor and Chairman, Diagnostic Radiology, Yale University School of Medicine, P.O. Box 3333, New Haven, CT 06510. Yale University is an equal opportunity/affirmative action employer. Applications from women and minority group members are encouraged. Application deadline is May 1, 1991. 3–4a

**MAMMOGRAPHY**—Immediate opening for a board-certified or eligible radiologist in the mammography section. Large screening and diagnostic program performs approximately 13,000 exams/yr including needle localization, cyst aspiration, and ultrasound through a mobile unit and an outpatient screening program. Program is very interactive with patients and referring physicians. Academic rank commensurate with experience. Yale University is an equal opportunity/affirmative action employer. Applications from women and minority group members are encouraged. Send current CV or phone Carol Lee, M.D., Yale University School of Medicine, Dept. of Diagnostic Radiology, 333 Cedar St., New Haven, CT 06510; (203) 785-2425. Application deadline is May 1, 1991. 3–4a

**UCLA SCHOOL OF MEDICINE, CARDIOVASCULAR RADIOLOGIST**—The UCLA Dept. o Radiological Sciences is recruiting for a full-time position in academic cardiovascular radiology Title will be determined by level of training and experience. American Board of Radiology certification and eligibility for California licensure is required. Send detailed resume, including references, to Hooshang Kangarloo, M.D., Chair, Dept of Radiological Sciences, UCLA School of Medicine, Los Angeles, CA 90024-1721. An equa opportunity/AA employer. 3–5a

**PEDIATRIC RADIOLOGY STAFF POSITION**—Children's Hospital and Medical Center, University of Washington School of Medicine, Seattle WA, has an opening for an academic radiologis at the junior faculty level. Applicants must have completed a minimum of 1 yr of pediatric radiology fellowship beyond a standard 4-yr radiology residency. Board certification and Washingtor licensure will be required. Preference is given t applicants with special competence in digital and integrated imaging of pediatric disease. CHMC is a modern, 207-bed medical center that is located less than 2 mi. from the University of Washingtor and serves as its main pediatric teaching unit The medical staff is composed of a mixture c attending faculty and community physicians, with fellows and residents in virtually all specialties The Dept. of Radiology performs approximately 37,000 radiography-fluoroscopy, 4000 CT, 360( ultrasound, and 2000 nuclear medicine exams annually. The 4000 newborn studies at University Hospital are also our responsibility. Technica staffing is at a high level, and the imaging equipment is state-of-the-art. High-field MRI will be operational in early 1991. Coverage is provided by 8 full-time radiologists, 2 fellows, and 3 residents. The successful applicant will be appointed and compensated at the level of assistant professor. Income and fringe benefits are competitive with other Pacific Coast academic centers. Fou wk vacation and up to 3 wk education time including meeting travel expenses, are provided CHMC and UW are equal opportunity employers Inquire for additional details to Eric L. Effmann M.D., Professor and Director, CHMC Radiology P.O. Box C5371, Seattle, WA 98105. 3a

**SEATTLE COLLEAGUE WANTED**—Growing radiology group seeks new member. Full-service radiology dept. (50,000 procedures/yr) offers diagnostic, nuclear medicine, ultrasound (including vascular-Doppler), interventional, CT, and MRI. Outpatient imaging dept. (building permits pending) scheduled to open late 1991 that will include high-field GE Signa MR with MRA Extremely favorable track for partnership. Fo further information regarding this opening, please contact Mr. Richard G. Wedig, Highline Community Hospital, 16251 Sylvester Rd., S.W. Seattle, WA 98166; (206) 248-4561. 3–4ap

**IMMEDIATE OPENING**—Fourth BC/BE radiologist needed for 223-bed hospital centrally located between the San Francisco Bay area and the Sierras. All modalities except MRI. Residency programs in OB/GYN, internal medicine, surgery, and family practice. Send CV to William Brock, M.D., San Joaquin General Hospital, P.O. Box 1020, Stockton, CA 95201; (209) 468-6600. AA/EOE. 3ap

**DIAGNOSTIC RADIOLOGIST**—Immediate opening for board-certified/eligible radiologist with expertise in CT, MRI, ultrasound, mammography, nuclear medicine, and angiography. Active ACR-accredited mammography program. 175-bed hospital and private clinic. Join group of 3 board-certified radiologists. Excellent living area on the southern Oregon coast with fishing, crabbing, and boating opportunities. Four-hr drive for superb skiing. Send inquiries and CV to Michael S. Quinn, M.D., or Normal A. Fiet, M.D., South Coast Radiologists, P.C., 2650 N. 17th St., Coos Bay, OR 97420; (503) 267-5411. 3ap

**FACULTY POSITION, MULTISPECIALTY DIAGNOSTIC RADIOLOGIST**—The Dept. of Radiology, at the George Washington University Medical Center, Washington, DC, is seeking a board-certified diagnostic radiologist with formal extra training in abdominal imaging, including MR, ultrasound, CT, and thoracic diagnosis. This is a full-time, non–tenure-track, faculty position at the assistant professor level. Research interest and experience are highly desirable. The George Washington University Medical Center is a 485-bed hospital located in Foggy Bottom, 7 blocks from the White House, with a broad representation in all medical and surgical subspecialties. The Radiology Dept. is equipped with a new 1.5-T Signa MR, 2 GE 9800 CT, and state-of-the-art ultrasound, angiographic, and general radiographic units. Salary and academic rank are commensurate with position. Applications will be accepted through April 3, 1991. Letter of inquiry must be accompanied by CV and should be sent to David O. Davis, M.D., Dept. of Radiology, The George Washington University Medical Center, 901 23rd St., N.W., Washington, DC 20037. The George Washington University is an affirmative action/equal opportunity employer. 3a

**BC/BE RADIOLOGIST**—Full-time staff radiologist needed at active tertiary-care medical center for interpreting general diagnostic films (excluding mammography) and performing radiologic procedures and fluoroscopy. Supervision and training of residents with affiliated medical center required. Additional subspecialty skills, training in ultrasound, CT, and/or angiographic and interventional procedures are beneficial. Candidate should be qualified to hold a faculty position with Yale University School of Medicine and must be a U.S. citizen or must qualify as a permanent resident of the United States. Send CV and letters of reference to Caroline Taylor, M.D., Chief, Radiology, Dept. of Veterans Affairs Medical Center, West Haven, CT 06516. The DVA Medical Center and Yale University are equal opportunity/affirmative action employers. Applications from women and minority group members are encouraged. Application deadline is May 1, 1991. 3–4a

**IMMEDIATE OPENINGS, CHARLOTTE, NC**—Service-oriented, 7-member group seeks 2 new associates in CT/ultrasound/MR and nuclear medicine. Fellowship training and/or staff level experience required. Must be willing to participate in all phases of general diagnostic radiology practice. Interventional experience helpful but not required. We serve 2 hospitals with a total of 260 beds. Equipment includes 3 GE 9800 CT, GE Signa 1.5-T MRI, Acuson and Toshiba ultrasound with color Doppler, 3 Toshiba SPECT, and Siemens 750 ZLC. Competitive salary leading to partnership after 2 yr. Send CV to Carl J. Eisenberg, M.D., Mercy Hospital, 2001 Vail Ave., Charlotte, NC 28105; (704) 379-5860. 3–5ap

**DIAGNOSTIC RADIOLOGIST**—Dept. of Veterans Affairs Medical Center, Dayton, OH, offers a full-time position for a diagnostic radiologist. The Dayton VA consists of a 495-bed general and medical hospital, 284-bed nursing home, and 625-bed domiciliary. A new, state-of-the-art, acute-care hospital will be ready for occupancy by the end of 1991. Excellent cultural activities include theater, museums, symphony, and ballet. Send CV to Berta H. Baumann, M.D., Chief, Radiology Service, VA Medical Center, 4100 W. Third St., Dayton, OH 45428; (513) 268-6511, ext. 2151. An equal opportunity employer. 3xa

**DIAGNOSTIC RADIOLOGIST NEEDED IMMEDIATELY**—Outstanding opportunity. All modalities. Locums considered. Robert L. Dever, M.D., 1901 Sunset Dr., Poplar Bluff, MO 63901; (314) 686-2043, evenings. 3ap

**DIAGNOSTIC RADIOLOGIST** needed to replace a retiring partner in an outpatient practice with Denver's largest multispecialty group. General radiology practice with mammography, ultrasound, and nuclear medicine. Future expansion to include CT and possibly outpatient interventional radiography. Send CV to Kari Miller, Accord Medical Centers, 1555 Clarkson, Denver, CO 80203. 3a

**DIRECTOR, DIAGNOSTIC RADIOLOGY**—Applications accepted for Director, Diagnostic Radiology, OHSU, Portland, OR. Faculty position opens on or about July 1, 1991. Associate or full professor based on experience. Musculoskeletal radiology fellowship, minimum of 5 yr as Vice-Chairman or Director of Diagnostic Radiology required. Send CV to William Weidner, M.D., Diagnostic Radiology, UHN-72, Oregon Health Sciences University, Portland, OR 97201-3098; (503) 494-4498. Equal opportunity, affirmative action employer. 3–6a

**PEDIATRIC RADIOLOGIST**—Division of Pediatric Radiology, OHSU, Portland, OR, invites applications for a faculty position available on or about July 1, 1991. Completion of approved fellowship in pediatric radiology and ABR certification required. Send CV to William Weidner, M.D., Diagnostic Radiology, UHN-72, Oregon Health Sciences University, Portland, OR 97201-3098; (503) 494-4498. Equal opportunity, affirmative action employer. 3–6a

**DIAGNOSTIC RADIOLOGIST**—University of Florida Health Science Center/Jacksonville is seeking a staff radiologist for a full-time faculty position. Special interest, expertise, or fellowship training in CT, ultrasound, MR, interventional, or nuclear radiology is preferable. Salary and fringe benefits are excellent. An academic appointment will be at the instructor, assistant professor, associate professor, or professor academic rank based on training, background, and experience. Application recruiting deadline is May 1, 1991. Send CV and references to Chairman, Search Committee, Dept. of Radiology, University Medical Center, 655 W. Eighth St., Jacksonville, FL 32209. AA/EOE. 3–4a

**DIAGNOSTIC RADIOLOGIST**—BC/BE radiologist wanted to join expanding practice of 12 radiologists in northeastern Pennsylvania. Practice includes 3 hospitals (720 beds) and free-standing MRI. Candidate must have experience in angiography and interventional radiology, and be willing to cover other areas of diagnostic imaging. Contact Paul M. Leiman, M.D., Dept. of Radiology, Moses Taylor Hospital, 700 Quincy Ave., Scranton, PA 18501; (717) 963-2601. 3–4ap

**CHIEF OF RADIOLOGY, VAMC, DENVER, CO** The Dept. of Radiology at the University of Colorado Health Sciences Center, in conjunction with the Denver Veterans Administration Medical Center, invites applications for the Chief of the Imaging Service at the Denver VAMC. Position requires interest in general diagnostic radiology, but those with special experience in nuclear medicine, interventional radiology, or neuroradiology are encouraged to apply. The 401-bed Denver VAMC has a recently renovated 20,000 sq. ft. imaging service and is closely affiliated with the UC Health Sciences Center. All diagnostic modalities are represented. Interested candidates should contact Michael L. Manco-Johnson, M.D., Professor and Chairman, Dept. of Radiology, University of Colorado Health Sciences Center, Campus Box C-277, 4200 E. 9th Ave., Denver, CO 80262; (303) 270-7719. The University of Colorado Health Sciences Center and Veterans Administration are committed to equal opportunity and affirmative action. 3–4a

**COME TO CALIFORNIA WITH A LICENSE FROM ANY STATE**—Loma Linda VA Hospital has a vacancy for a board-certified radiologist. A current license from any state is acceptable. Loma Linda is located 70 mi. east of Los Angeles near beaches, mountain ski resorts, and southland theme parks. This is a 500-bed, full-service hospital with a comprehensive diagnostic facility including ultrasound, CT, and MRI integrated with the Loma Linda University Medical Center residency training program. Opportunities exist to pursue clinical or academic interests. For additional information, contact Peter Dure-Smith, M.D., Chief, Radiology (114), Jerry L. Pettis Memorial Veterans Hospital, 11201 Benton St., Loma Linda, CA 92357; (714) 422-3069, fax (714) 422-4106. Equal opportunity employer. 3–8ap

**PEDIATRIC RADIOLOGIST**—Yale–New Haven Medical Center and Yale University School of Medicine seek a pediatric radiologist for a full-time faculty appointment. Academic rank is at the level of assistant or associate professor, depending on qualifications. A strong interest in patient care, research, and teaching is required. Please send inquiries, along with CV, to Marc Keller, M.D., Diagnostic Radiology, Yale University School of Medicine, 333 Cedar St., New Haven, CT 06510. Yale University is an equal opportunity/affirmative action employer. Applications from women and minority group members are encouraged. Application deadline is May 1, 1991. 3–4a

**SAN ANTONIO, TX**—Group covering multiple hospitals and clinics seeks radiologists with imaging and angiography skills. Send CV to Search Committee, M & S X-Ray Associates, P.O. Box 15920, San Antonio, TX 78212-9510. 3–8ap

**DIAGNOSTIC RADIOLOGIST**—Two young, progressive radiologists seek a third, recently trained, BC/BE, general radiologist to join in a rapidly growing practice in a 100-bed hospital. 31,000 exams/yr, including ultrasound, nuclear medicine, mammography, and CT. No angiography. An MR rotation is available at a free-standing center. Call will be shared equally. 9-wk vacation. The Oneida City Hospital is located in the scenic eastern Finger Lakes, with a 4-season climate, near a medical school. Excellent starting salary, with full partnership following 2 yr; no buy-in. Please send CV with letter to Ralph Stevens, M.D., Dept. of Radiology, Oneida City Hospital, 321 Genesee St., Oneida, NY 13421. 2–4ap

**NEURORADIOLOGIST, BIG SKY COUNTRY**—Group of 5 radiologists seek a BC, fellowship-trained colleague. Hospital and busy clinical practice. Must be a capable, general diagnostic radiologist. One yr to partnership. Send letter/CV to Bruce Pinkerton, M.D., Dept. of Diagnostic Radiology, Deaconess Medical Center. P.O. Box 2547, Billings, MT 59103. 2–7ap

**DUKE UNIVERSITY MEDICAL CENTER/STAFF RADIOLOGISTS**—Duke University Medical Center is seeking qualified candidates for staff positions in the Dept. of Diagnostic Radiology. A limited number of staff positions currently are available in the following sections: general diagnostic, pediatric, chest, vascular/interventional, and musculoskeletal radiology. We offer an excellent salary and benefits package. The radiology dept. is state-of-the-art in diagnostic imaging with diverse resources available for clinical, teaching, and academic pursuits. Staff members have guaranteed academic time and research support. Interested board-certified radiologists with appropriate experience should phone Robert Vandemark, M.D. at (919) 681-2711 ext. 5233, for additional information. Letters of inquiry should be sent to Carl E. Ravin, M.D., Dept. of Radiology, Box 3808, Duke University Medical Center, Erwin Rd., Durham, NC 27710. AA/EOE. 2–7a

**MEMPHIS, TENNESSEE**—Immediate opening for a board-certified, general radiologist to join a 5-person group currently performing 80,000 exam/yr in a diversified practice. MRI experience preferable. Excellent salary, benefits, and full partnership within 3 yr with no buy-in. Practice covers 3 community hospitals (250 beds) and 2 outpatient offices. No angiography duties and minimal interventional radiology. Democratically run, fee-for-service practice made up of young, academically oriented radiologists. Send CV to Robert A. Duke, M.D., Diagnostic Imaging, P.C., 1068 Cresthaven Rd., Ste. 100, Memphis, TN 38119; (901) 682-5053. 2–3ap

**RADIOLOGIST, BRIGHAM AND WOMEN'S HOSPITAL** — The Dept. of Radiology at the Brigham and Women's Hospital/Harvard Medical School wishes to recruit a staff person in ultrasound. This position offers diverse clinical work and extensive opportunities for research in abdominal, obstetric, vascular, and other areas of ultrasound. Rank and salary commensurate with experience. Evidence of interest in academic radiology and certification by the American Board of Radiology are preferred. Please send CV to B. Leonard Holman, M.D., Chairman, Dept. of Radiology, Brigham and Women's Hospital, 75 Francis St., Boston, MA 02115. Brigham and Women's Hospital/Harvard Medical School is an affirmative action/equal opportunity educator and employer. 2–4a

**MINNEAPOLIS, MINNESOTA**—Private practice opportunity for a neuroradiologist with procedural orientation to join an expanding group of 5 radiologists; 2 are ASNR members. Practice is primarily based at growing, free-standing, outpatient imaging centers and includes two 1.5-T Signa MR units, 3 GE 9800 CT scanners, and accompanying fluoroscopic-radiography equipment. A third MR unit is being installed in the Twin Cities and should be operational in early spring 1991. We are heavily oriented toward spine and musculoskeletal imaging and related procedures. Candidates must be interested in spine imaging and related procedures, such as myelography, nerve blocks, facet arthrograms/therapeutic procedures, and diskography. We are also affiliated with a 750-bed, tertiary hospital in Minneapolis. The practice is academically oriented and encourages clinical research and publication, although this is not required. No calls please. Send letters of inquiry and complete CV to Kurt P. Schellhas, M.D., Center for Diagnostic Imaging, 5775 Wayzata Blvd., Ste. 190, St. Louis Park, MN 55416. 2–4ap

**RADIOLOGIST NEEDED** with experience in CT, ultrasound, nuclear medicine, mammography, and general radiology to provide vacation coverage for 2 practices in rural western Montana. One practice requires some traveling. Position would be excellent for person who wishes to semiretire in a pleasant scenic area. Great opportunity for recreational activities. Send inquiries to Tyler H. Gill, M.D., 1200 Westwood Dr., Hamilton, MT 59840; (406) 363-2211. 2–6a

**FACULTY OPENING IN THORACIC IMAGING** The Johns Hopkins University Hospital has an opening at the junior faculty level in the Division of Thoracic Imaging. The division is fully integrated across all modalities including MRI, CT, and interventional procedures. Research opportunities are exceptional with protected research time available to rapidly establish an academic career. Academic rank and salaries will be determined by previous experience. The candidate must be board-certified. Contact Elias A. Zerhouni, M.D., Director, Thoracic Imaging & MRI Divisions, Dept. of Radiology, Johns Hopkins Hospital, Baltimore, MD 21205; (301) 955-4062. 1–6a

**DEPT. OF RADIOLOGICAL SCIENCES, UCLA** Professorships available for qualified candidates who have extensive experience in image processing, picture archiving and communications systems, teleradiology, medical imaging instrumentation, radiographic detector technology, and communication theory. Applicants must have an excellent track record in research, experience in industrial collaboration, teaching, and administration. The successful applicants are expected to provide research guidance to junior faculty members, postdoctoral fellows, and graduate students; develop research programs through extramural funding agencies; and participate in the administration of the dept. teaching program. Please send CV and 3 reference letters to H. K. Huang, M.D., Professor and Chief, Medical Imaging Division, Dept. of Radiological Sciences, University of California, Los Angeles, CA 90024-1721. 2–3a

**RADIOLOGIST, WESTERN MASSACHUSETTS** Large radiology group in western MA is seeking a general diagnostic radiologist with experience and interest in body imaging, and expertise in nonvascular interventional procedures. Primary assignment at 868-bed, tertiary-care hospital with radiology residency program. Practice also includes 3 community hospitals and 6 private offices. Full partnership after 1 yr. Available on or before July 1, 1991. Send CV to Director of Recruiting, Radiology & Imaging, Inc., 130 Maple St., Springfield, MA 01103. 2–4ap

**PENN STATE UNIVERSITY, THE MILTON S. HERSHEY MEDICAL CENTER, FACULTY POSITION IN NUCLEAR MEDICINE**—The Division of Nuclear Medicine of the Dept. of Radiology at the Penn State University's Milton S. Hershey Medical Center is recruiting a physician with board certification in nuclear medicine (ABNM) for a full-time academic position. Board certification in diagnostic radiology (ABR) is desirable but not essential. Penn State University Hospital is a 350-bed, tertiary-care facility (currently expanding to 500 beds) in Hershey, PA, near Harrisburg, the state capitol. Nuclear Medicine is a division of the Dept. of Radiology, which has an academic faculty of 20 physicians and 6 Ph.D.'s. The Nuclear Medicine Division currently performs 5000 exams/yr and is expected to increase as renovations and expansion are completed in subsequent years. There are currently 5 gamma cameras and a Hologic QDR 1000W bone-density unit in place, with 1 additional camera being added in 1991 or 1992. Four or 5 of the 6 will be tomographic. Areas of emphasis currently include cardiac and pediatric nuclear medicine. An interest in neuronuclear medicine and brain tomography is desirable but not essential. An interest in clinical and/or basic research is desirable. Applicants should respond as soon as possible with a letter of interest and current CV. Please direct inquiries to Douglas F. Eggli, M.D., Chief, Division of Nuclear Medicine, Dept. of Radiology, Penn State University/Hershey Medical Center, P.O. Box 850, Hershey, PA 17033. Penn State University is an affirmative action, equal opportunity employer. Women and minorities are encouraged to apply. 2–4a

**TWO DIAGNOSTIC RADIOLOGISTS** with recent training are sought for growing hospital practice of 3 BC radiologists in Elizabethtown, KY. Fellowship training in body imaging and intervention welcome. Modern, well-equipped radiology dept. at 300-bed regional hospital that includes 2 GE 9800 CT, GE 1.5-T MR, GE LU dedicated angiographic suite with DSA, ultrasound, nuclear medicine, and ACR-certified, dedicated mammography. Position available immediately. Send letters of inquiry with CV to Elizabethtown Radiology, P.S.C., P.O. Box 2489, Elizabethtown, KY 42701; (502) 765-4144. 2–4ap

**MAMMOGRAPHY FACULTY POSITION**—Th Dept. of Radiology at Johns Hopkins Universi Hospital has a faculty position available in mar mography. The mammography section is part the thoracic imaging division. The section offe a strong potential for academic growth wi emphasis on original research and teachin Protected academic time is available for canc dates interested in developing a strong academ career. Support, resources, and opportunities a available for creative research. The candidate ca also participate in all other aspects of diagnost imaging as desired. Academic rank and sala will be determined by previous experience. Canc date must be board-certified. Contact Elias Zerhouni, M.D., Director, Thoracic Imaging ar MRI Divisions, Dept. of Radiology, Johns Hopkir Hospital, Baltimore, MD 21205; (301) 955-406 1–6a

**MUSCULOSKELETAL / MRI RADIOLOGIS THOMAS JEFFERSON UNIVERSITY HOSPITA** We are recruiting a faculty musculoskeletal rac ologist (either junior or senior level) for an impc tant and challenging position in our dept. Th position encompasses MRI of the musculoske etal system and other body applications, pla film musculoskeletal radiology, tomography, ar arthrography. Jefferson currently operates 4 G 1.5-T Signa MRI units and 3 CT scanners. Clos relationships are maintained with busy orth pedic, rheumatology, trauma, and spinal cor injury services. A thriving clinical practice, activ teaching program, and well-equipped researc facilities all combine to make this an outstandin career opportunity. Excellent faculty income and many other benefits are provided. Intereste applicants should contact David C. Levin, M.D Chairman, Dept. of Radiology, Thomas Jefferso University Hospital, 11th and Walnut Sts., Phil delphia, PA 19107; (215) 955-7265. Jefferson an equal opportunity/affirmative action employe 1–4a

**NUCLEAR MEDICINE OR INTERVENTIONA RADIOLOGIST** — Progressive, 7-person grou seeks to add an interventional radiology or nuclea medicine (special competency preferred) fellov ship-trained radiologist for spring 1991. This bus expanding practice is hospital- and recently ful service imaging center-based. Both institution use leading edge technology. The proximity Lake Tahoe, the gaming industry, the state capitc and a major university provides many cultura entertainment, and sporting opportunities. Sen CV to Colby Laughlin, M.D., Reno Diagnosti Center, 590 Eureka Ave., Reno, NV 89512. 12–3

**BC RADIOLOGIST, KANSAS CITY, MO**—Seve radiologists currently covering a 600-bed, tertiar medical center seek a radiologist with a specia competency or fellowship in nuclear medicin The position, open immediately, includes con petitive salary and fringe benefits, and leads t full partnership. Send CV and letter of inquiry t J. M. Speckman, M.D., 6400 Prospect, Ste. 31 Kansas City, MO 64132. 1–4ap

**ABDOMINAL IMAGING**—A staff position is avai able at The Cleveland Clinic Foundation in th section of abdominal imaging. The Clevelan Clinic is a 1000-bed, tertiary-care facility with large outpatient population and an internationa referral base. The section of abdominal imagin encompasses body CT, ultrasound, body MF gastrointestinal radiology, and mammography Applicants should be fellowship-trained, or pos sess equivalent experience. Send CV to Davi M. Paushter, M.D., Head, Section of Abdomina Imaging, Hospital Radiology, Cleveland Clini Foundation, One Clinic Center Dr., Cleveland, Ol 44195-5103. The Cleveland Clinic is an equa opportunity employer. (M-F-H-V). 2–3ap

**THE PENN STATE UNIVERSITY, MILTON S. HERSHEY MEDICAL CENTER, CHIEF OF MRI** The Pennsylvania State University Dept. of Radiology is seeking a full-time faculty chief of the section of Magnetic Resonance Imaging (MRI). The MRI section performs over 3000 MRI scans/yr on our 1-T Siemens system. We have just purchased a second magnet (1.5-T Toshiba MRI-150A). Both our in-house and outpatient magnet systems have significant research capacity for clinical and applications projects. A Nuclear Magnetic Resonance (NMR) Imaging/Spectroscopy center, directed by Michael B. Smith, Ph.D., with over 6500 sq. ft., is completed. It is connected to our outpatient MRI system. In this NMR center, we have 3 magnets: a 9.4-T Bruker AM-400 widebore spectrometer with micro imaging; a 1.9-T Oxford 26-cm-bore horizontal magnet interfaced to a Nicolet 1280 computer; and a 3.0-T Bruker 90-cm-bore spectrometer/imager which will be the first of its kind and 100% dedicated to research. The NMR center will also be completely equipped with surgical and animal preparation area, biochemistry laboratory, radiofrequency and electronics laboratory, full machine shop, computer resources, and office space for faculty, staff, postdoctorates, and students. The successful candidate must be experienced in both clinical and research MR, and have publications that confirm his/her experience. The chief of MRI will be responsible for developing further our clinical MRI service and integrating it with our new NMR research center. Clinical responsibility will be in MRI, either in neuroradiology, body imaging, or both, depending on the successful candidate's experience and certification. Independent original research is expected and is amply funded both in time and money. The academic rank will depend upon the candidate's achievement. The salary is dependent on the achieved rank and experience. The position is open to individuals who have completed an accredited residency program in radiology; can obtain a Pennsylvania medical license; can obtain medical staff privileges at University Hospital; and are board certified by the American Board of Radiology or its equivalent. Applicants should respond as soon as possible with a letter of interest and current CV. Please direct inquiries to John E. Madewell, M.D., Professor and Chairman, Dept. of Radiology, The Penn State University, Milton S. Hershey Medical Center, P.O. Box 850, Hershey, PA 17033. Penn State University is an affirmative action, equal opportunity employer. Women and minorities are encouraged to apply. 2–4a

**OREGON**—Group of 13 radiologists in Salem, OR, seeks BC/BE radiologist with general radiology skills. Practice includes 454-bed community hospital, large out-patient office, and multispecialty clinic. Near ideal family community and recreational amenities. Send CV to John Eyre, M.D., Salem Radiology, 919 Oak St., S.E., Salem, OR 97301. 2–5ap

**RADIOLOGIST, HOUSTON, TEXAS** — Large, well-established, multispecialty group is seeking a full-time, BC/BE radiologist due to growth in practice. Our group consists of over 100 physicians, including 5 radiologists. In addition to plain film interpretation, the practice includes fluoroscopy, urography, tomography, ultrasound, and mammography totaling 75,000 studies/yr. We are in the process of acquiring CT capability. Four-and-a-half-day work-wk and no call gives you time to enjoy the variety of activities Houston has to offer. We provide excellent benefits, including malpractice with tail coverage and a very competitive financial package. Interested candidates should send CV to MacGregor Medical Association, 2550 Holly Hall, Houston, TX 77054, Attn: Karen Aszman, Professional Relations Specialist. 2–3ap

**THE UNIVERSITY OF LOUISVILLE, DEPARTMENT OF DIAGNOSTIC RADIOLOGY** is seeking applications from BC/BE diagnostic radiologists to fill full-time faculty positions in the following areas in its 400-bed, teaching hospital: (1) cross-sectional body imaging and (2) general radiology (GI, GU, bone, chest). Candidates must be willing to participate in undergraduate and graduate teaching and in research activities in their respective areas. These are fine opportunities in a growing and busy dept. with excellent equipment. Both tenure and non-tenure track appointments are available, and academic rank will be commensurate with training and experience. Compensation negotiable and competitive. Louisville continues to be ranked one of the top 10 places to live in America by Rand McNally. Send inquiries with CV and 3 references to Hollis A. Thomas, M.D., Professor and Chairman, Dept. of Diagnostic Radiology, Humana Hospital-University of Louisville, 530 S. Jackson St., Louisville, KY 40202. An equal opportunity/affirmative action employer. 2–3a

**FLORIDA, STAFF RADIOLOGIST**—Opportunity for board-certified/eligible diagnostic radiologist with experience in reading plain films, fluoroscopy, ultrasound, CT, nuclear medicine, and some angiography in the radiology service at this progressive, GM&S, Dept. of Veterans Affairs (VA) Medical Center. Potential academic appointment and affiliation in surgery with the University of Florida. Competitive salary plus incentive pay commensurate with qualifications. Excellent employment benefits including 30 days paid vacation and 15 days sick leave per yr; liberal life and health insurance benefits; malpractice insurance; and retirement program. Moving expenses paid. "Florida's new gateway city" is located in northern Florida with a mild climate yr round. Extensive outdoor recreational activities, reasonable cost of living, no state income tax, and fine schools and nearby universities provide opportunity for continuing education and cultural diversion. Florida license not required. Contact or send CV to Richard Parker, M.D., Chief of Radiology, VA Medical Center, Lake City, FL 32055-5898; (904) 755-3016, ext. 2543. An equal opportunity employer. 2–4a

**SEATTLE AND SUBURBS** — BC associate needed immediately for rapidly growing practice dedicated to mammography and breast diagnosis. Four offices; 2 also have general ultrasound. 85% OB-GYN. Mammography or ultrasound fellowship or extensive experience helpful. Association leading to partnership. Send letter and CV to Irwin Schiller, D.O. and Marita Acheson, M.D., c/o Breast Diagnostic Center, 411 Strander Blvd., #303, Seattle, WA 98188; (206) 575-9123. 1–3ap

**FAIRBANKS, AK**—Four diagnostic radiologists seek fifth partner for diversified practice including general radiology, ultrasound, nuclear medicine, MRI (GE 1.5-T), and CT (GE 9800). Hospital and office practice. Desirable life-style advantages in a university town. Unlimited access to the outdoors. Excellent salary, benefits, retirement, and vacation. One yr to full partnership. Contact Douglas Hutchinson, M.D., 1919 Lathrop #5, Fairbanks, AK 99701; (907) 452-5092. 2–4ap

**CONNECTICUT**—Expanding group of 8 radiologists has a position available for an additional angio/interventional, BC/BE radiologist with expertise in general radiology also. Practice includes a 435-bed, fully equipped, university-affiliated, community hospital and a 47-physician, multispecialty clinic. Excellent salary and benefits leading to full partnership after second yr. For information, send CV to Paul C. Lakin, M.D., Dept. of Radiology, New Britain General Hospital, 100 Grand St., New Britain, CT 06050. 1–4ap

**MUSCULOSKELETAL RADIOLOGIST** — The Dept. of Radiology, University of Texas Health Science Center at San Antonio, seeks a musculoskeletal radiologist. Salary and academic rank are commensurate with the candidate's experience. Excellent research opportunities are available in a new 30,000 sq. ft. research imaging center. The Health Science Center lies in the northern suburbs of San Antonio adjacent to excellent living areas and schools. Replies and CVs should be sent to Stewart R. Reuter, M.D., Chairman, Dept. of Radiology, 7703 Floyd Curl Dr., San Antonio, TX 78284-7800. Equal opportunity/affirmative action employer. 1–3a

**VASCULAR/INTERVENTIONAL RADIOLOGIST** Large radiology group in western Massachusetts is seeking a BC vascular/interventional radiologist to join existing 5-person vascular/interventional team. Fellowship or equivalent experience required. Must also have expertise in CT and general diagnostic radiology. Primary assignment at 868-bed, tertiary-care hospital with radiology residency program. Practice also includes 3 community hospitals and 6 private offices. Full partnership after 1 yr. Available July 1991. Send CV to Director of Recruiting, Radiology and Imaging, Inc., 130 Maple St., Springfield, MA 01103. 1–3ap

**DIAGNOSTIC RADIOLOGIST, TEXAS**—Progressive, well-diversified group (15 radiologists) has immediate opening for a BC/BE diagnostic radiologist with competence in a broad range of modalities. Additional consideration for fellowship. Excellent opportunity with excellent salary and benefits. Send CV with letter of inquiry to Will Gray, M.D., 1101 N. 19th St., Abilene, TX 79601. 3–5ap

**DIAGNOSTIC RADIOLOGISTS**—Owing to expansion and retirement, several positions are available with a large, dynamic radiology group in the Central New Jersey/Bucks County, PA, region. Openings for radiologists with expertise in 1 or more of the following: nuclear medicine, general, and angio/interventional. Immediate availability. Send letter and CV to E. Tarasov, M.D., 838 W. State St., Trenton, NJ 08618. 3–4a

**IMMEDIATE OPENING, DIAGNOSTIC RADIOLOGIST**—Excellent opportunity for a young, dynamic, preferably board-certified radiologist to join an active, 9-member group. Growing practice includes a 700-bed hospital system with state-of-the-art equipment and excellent working facilities. Skills in all phases of diagnostic radiology desired. Attractive and competitive benefits package leading to full partnership. Contact Sanford E. Rabushka, M.D., 11133 Dunn Rd., Ste. 1017, St. Louis, MO 63136; (314) 653-4300. 11–4ap

**DIAGNOSTIC RADIOLOGIST**—Eight board-certified radiologists in expanding, hospital-based private practice seek BC/BE general radiologist to associate. Competence in all modalities expected with need for MRI training emphasized for 2 MRI facilities in practice. Opportunity in midwestern city of 72,000 people offers generous compensation/vacation. Full partnership after 2 yr. Reply to Box H89, *AJR* (see address this section). 12–3ap

**DIAGNOSTIC RADIOLOGIST** needed in Conway Hospital, a community hospital located 10 mi. west of the resort/seaside community of Myrtle Beach, SC. The dept. performs 44,000 exams/yr including CT, MRI, nuclear medicine, ultrasound, mammography, and special procedures. All exams are done on state-of-the-art equipment. Our 3-person group offers a very strong financial package with all benefits including 17-wk vacation. Lovely, rapidly growing resort area includes 60 mi. of sandy beaches, 70 golf courses, and beautiful seaside homes. Contact Gary Rike, M.D., P.O. Box 917, Conway, SC 29526; (803) 347-7277. 12–5ap

**RADIOLOGISTS** — New York City, combined private radiology practice, and fee-for-service hospital practice has an immediate opening for a board-certified radiologist with experience in CT, ultrasound, and interventional radiology. In addition, MRI and mammography experience is preferred. This well-established practice has 3 private offices on the upper East Side of Manhattan as well as operations in 2 hospitals in Manhattan. Other studies performed in the practice are diagnostic radiology, nuclear imaging, and vascular duplex imaging. The practice continues to expand in all imaging modalities with its recent opening of a second state-of-the-art MRI unit. Excellent benefit package includes health, life, disability, and malpractice insurance; profit sharing plan; continuing medical education; and a travel and entertainment account for professional use. Send CV to Box F67, *AJR* (see address this section). 1–3ap

**THE DEPT. OF RADIOLOGY AT TRIPLER ARMY MEDICAL CENTER, HONOLULU, HI**, is recruiting academic radiologists for several divisions of the dept. including ultrasound, chest, skeletal, neuro, and general diagnostic radiology. Our dept. offers a fully accredited residency program with 20 residents and 16 attending full-time staff. Numerous consultants from across the country lecture on a continuing and regular basis. The hospital is a modern, tertiary-care center serving Hawaii and the entire Pacific Basin. A strong residency program, diverse and interesting patient population, excellent equipment, and a tropical lifestyle are positive aspects of the practice. Academic credentials and/or experience are necessary. Recently graduated fellows are encouraged to apply. Board certification is mandatory. Candidates should be particularly interested in patient care, teaching, and research. Salary and benefits are competitive and generous. Tripler is an EO/EEO employer. Please contact Mark F. Hansen, M.D., Col., MC, Chief, Dept. of Radiology, TAMC, HI 96859-5000; (808) 433-6393. 8–7a

**VASCULAR/INTERVENTIONAL RADIOLOGIST** Progressive, private-practice group is seeking a second fellowship-trained vascular and interventional radiologist for its expanding interventional radiology service. We are currently performing more than 1000 procedures/yr. We are budgeted for 2 state-of-the-art vascular suites, the first to be installed early in 1991. We will break ground soon on a new imaging center to include 2 MRI and 2 CT (including a cine CT) scanners. We have a noninvasive lab and retain admitting privileges for our interventional service. We are located in Fresno, CA, at Saint Agnes Medical Center. Saint Agnes is a tertiary-referral center for the San Joaquin Valley, and Fresno is one of the fastest growing cities in CA. We are located 90 mi. from Yosemite National Park and less than 2 hr from excellent winter skiing and 2 hr from the coast. We offer 2 yr to full partnership with excellent salary and benefits. Please contact Art Fontaine, M.D., Dept. of Imaging, Saint Agnes Medical Center, 1303 E. Herndon, Fresno, CA 93710; (209) 449-3210. 10–3ap

**TEN-PERSON RADIOLOGY GROUP** located in Corpus Christi is seeking a new associate to start July 1990 or as late as July 1991. Must be board-certified or eligible. Will perform all diagnostic studies, including interventional, CT, MRI, nuclear medicine, and ultrasound. Please send CV to Search Committee, P.O. Box 5608, Corpus Christi, TX 78465-5608. 3xa

**RADIOLOGIST** — Full-time; nice, small, well-located North Carolina town. Join active, hospital-based, service-oriented practice. General diagnostic, nuclear medicine, ultrasound, CT, and mobile MRI. No arteriography. Reply with CV to Box I95, *AJR* (see address this section). 2–4ap

**NORTHERN CALIFORNIA/SAN FRANCISCO BAY AREA**—The Permanente Medical Group is seeking a BC radiologist with multimodality interests and fellowship training in MR or interventional radiology to join a 10-person group serving a 337-bed acute-care hospital and 2 outpatient clinics. Teaching opportunities are available with residents of subspecialty services on rotation from Stanford University Hospital and our own medical residents. We are currently siting a GE 1.5-T MRI system and installing a new LU arm. Competitive salary and excellent benefits. Please send inquiries and CV to Bruce Baker, M.D., Chief, Dept. of Radiology, Kaiser-Permanente Medical Center, 900 Kiely Blvd., Santa Clara, CA 95051; (408) 236-4444. EOE. 2–4a

**DENVER, CO**—Group of 8 diagnostic radiologists engaged in a predominantly hospital-based practice is seeking a new member on or about 10-1-90. The group provides diagnostic imaging services for a 565-bed, tertiary-care teaching hospital. The new member should be trained in diagnostic radiology and have fellowship training, and/or additional experience beyond residency level, in nuclear medicine. The new member will be primarily responsible for nuclear medicine but must be willing to participate in other modalities of diagnostic imaging. Salary, benefits, vacation time, and time to partnership are all competitive for the Rocky Mountain region. Interested parties should send their CV to Steve A. Holt, M.D., Western Radiologists, P.C., 3665 Cherry Creek Dr., N., Ste. 350, Denver, CO 80209. 2–4ap

**SALT LAKE CITY, UT**— Opportunity for board-certified diagnostic radiologist, with recent MRI fellowship training, to join group of 7 board-certified radiologists. Experience in all aspects of general radiology required. Practice includes 2 hospitals, 2 private offices, and a freestanding MRI center. Send letter and CV to Neel E. Bennett, M.D., Medical Director and Chairman, Dept. of Radiology, Holy Cross Hospital, 1050 E. S. Temple, Salt Lake City, UT 84102; (801) 350-4636. 3xa

**DIAGNOSTIC RADIOLOGIST**—A 4-member radiology group located in beautiful southwestern Montana is currently seeking an additional board-certified/eligible radiologist. Expertise in MRI preferred. Hospital-based and office practice. Excellent school system and outstanding, year-round recreational activities. Approximately 35,000 exams last yr. Hospital is acquiring MRI and updating CT services. One yr to full partnership. Contact Dennis L. Rich, M.D., 300 N. Willson, Bozeman, MT 59715; (406) 587-8631. 10–3ap

**ULTRASOUND/CT/MRI** — Opportunity for a board-certified radiologist specializing in ultrasound, body CT, and body MRI to pursue an academic career at the New York Hospital-Cornell Medical Center. Dept. provides state-of-the-art equipment, including Acuson ultrasound, GE 9800 CT, and GE Signa 1.5-T MR. Wide variety of ultrasound exams include abdominal, OB-GYN, color Doppler, small parts, neonatal head, transvaginal, and transrectal. Prefer candidate with prior fellowship in sectional imaging or ultrasound. Responsibilities include clinical practice, teaching, and research. Position available 7/1/91 or earlier. Please send CV to Elias Kazam, M.D., Dept. of Radiology, The New York Hospital-Cornell Medical Center, 525 E. 68th St., New York, NY 10021. 1–4ap

**DIAGNOSTIC RADIOLOGIST** sought to join a fee-for-service group practice at 2 mid-Bronx hospitals. Board-certification with expertise in imaging and in special procedures/interventional radiology preferred. Please send CV to Arthur Avenue Radiology, P.C., P.O. Box 4332, Great Neck, NY 11027. 10–3ap

**DIAGNOSTIC RADIOLOGIST**—Excellent opportunity in well-established, South Carolina hospital-based practice for BC/BE radiologist. Competitive salary. Full partnership in 1 yr. Send CV to Box H87, *AJR* (see address this section). 12–3ap

**BROAD SPECTRUM RADIOLOGIST/UPSTATE NEW YORK** — Radiologist wanted for hospital-based practice 90 mi. northwest of New York City. Excellent recreational activities and easy access to metropolis. All modalities available. Excellent salary and benefits leading to early partnership. Immediate availability, but can wait for right applicant. Call G. Bilick; (914) 794-3300, ext. 2216 or send CV to P.O. Box 144, Harris, NY 12742. 3–6ap

## Positions Desired

**PGY-2 RADIOLOGY RESIDENCY POSITION SOUGHT**—Radiology resident in first yr of training seeks second yr position (to start 7/91) in university-based program. Hardworking. Strong credentials. Reply Box J7, *AJR* (see address this section). 3bp

## Fellowships and Residencies

**FELLOWSHIP IN NEURORADIOLOGY**—A fellowship position in neuroradiology is available July 1, 1991, in the Dept. of Radiology at New England Medical Center Hospitals, Boston, MA. The hospital is the teaching unit of Tufts University School of Medicine. The program is for 1 or 2 yr and includes both adult and pediatric case material. The fellow will be trained in the technique and interpretation of carotid and vertebral angiography as well as myelography. CT and MRI of the head and spine form major components of the Neuroradiology Service, as does interventional neuroradiology. Neuroradiologic services at the New England Medical Center Hospitals are carried out in liaison with the Depts. of Neurology, Neurosurgery, and Pediatric Neurology. Joint radiologic and clinical conferences are held frequently and, within a short time, the applicants will have considerable exposure to an array of neuroradiologic material. The Dept. of Neuropathology also runs conferences, allowing correlation to be made between radiologic interpretation and pathology. Interested applicants should call Samuel M. Wolpert, M.D., Professor of Radiology and Neurology, Director of Fellowship Program, (617) 956-6333. 3–4cp

**UNEXPECTED OPENING FOR A THIRD YR RADIOLOGY RESIDENT** beginning July 1, 1991, in the Radiology Residency Training Program at Jewish Hospital of St. Louis. This fully accredited program in diagnostic radiology is expanding from 2–3 residents per yr. The program is listed as Washington University Program B in the Directory of Graduate Medical Education Programs. Please contact Lawrence M. Kotner, Jr., M.D., Program Director, Radiology Residency Training Program, Jewish Hospital of St. Louis, 216 S. Kingshighway, St. Louis, MO 63110; (314) 454-7230. 3cp

**IMAGING FELLOW IN CARDIOVASCULAR IMAGING**—Yale is offering a unique environment for training in echocardiography, cardiovascular MRI, cineangiogram interpretation, as well as extensive research opportunities. Candidates must be U.S. citizens or must qualify as a permanent resident in the United States. Please send CV and bibliography to Gregory Weltin, M.D., Yale University School of Medicine, Dept. of Diagnostic Radiology, 333 Cedar St., New Haven, CT 06510. Yale is an equal opportunity/affirmative action employer. Applications from women and members of minority groups are encouraged. Applications should be submitted no later than May 1, 1991. 3–4c

**CARDIOVASCULAR AND INTERVENTIONAL RADIOLOGY**—The Harvard Medical School and Brigham and Women's Hospital, Dept. of Radiology, is offering a 2-yr fellowship starting July 1, 1992, in cardiovascular and interventional radiology including peripheral and coronary angiography, cardiac catheterization, digital vascular imaging, all types of interventional procedures, noninvasive vascular techniques, and cardiovascular MRI. Research time available for participation in original or ongoing clinical and/or laboratory projects. Please send CV to B. Leonard Holman, M.D., Chairman, Dept. of Radiology, Brigham and Women's Hospital, 75 Francis St., Boston, MA 02115. Brigham and Women's Hospital/Harvard Medical School is an affirmative action/equal opportunity educator and employer. 3–8c

**UNEXPECTED OPENING FOR VASCULAR AND INTERVENTIONAL FELLOWSHIP BEGINNING JULY 1991** is offered at the University of Maryland. The fellow will participate in all aspects of diagnostic vascular radiology, as well as nonvascular interventional procedures, including percutaneous and laser angioplasty, embolization, biliary and GU intervention, and insertion of IVC filters. Contact Gerald S. Johnston, M.D., 22 S. Greene St., Baltimore, MD 21201; (301) 328-3477. The University of Maryland is an affirmative action/equal opportunity employer and encourages applications from members of minority groups. 3–5cp

**NEURORADIOLOGY FELLOWSHIP**—The Dept. of Radiology at the University of Michigan has an opening for a 1st- or 2nd-yr neuroradiology fellow beginning July 1, 1991. The fellowship provides a diverse adult and pediatric neuroradiologic clinical experience using state-of-the-art imaging equipment at the University of Michigan Hospitals and the affiliated VA Hospital. There are extensive clinical and laboratory research opportunities. Six full-time faculty neuroradiologists and numerous intra- and interdepartmental conferences promote an outstanding training experience. Candidates must be board-certified or eligible in radiology and eligible for a Michigan medical license. Interested applicants should call or write James A. Brunber, M.D., Director, Division of Neuroradiology, University of Michigan Hospitals, B2B 311, Ann Arbor, MI 48109-0030; (313) 936-8868. A nondiscriminatory, affirmative action employer. 3c

**FELLOWSHIP POSITION IN CHEST RADIOLOGY** to begin July 1991 or 1992. Excellent training in radiographic and cross-sectional imaging modalities. Clinical and basic physics research opportunities in chest, MR, and CT. For information and application form, contact Colleen J. Bergin, M.D., Dept. of Radiology, S-058, Stanford University Medical Center, Stanford, CA 94305. 3c

**SECOND YR RADIOLOGY RESIDENT**—Unexpected opening on July 1, 1991, for a radiology resident at the second yr training level. Candidate must have completed 1 yr of radiology residency in an approved training program. Send CV to David Bryk, M.D., Director of Radiology, Maimonides Medical Center, 4802 10th Ave., Brooklyn, NY 11219. 3–4cp

**FELLOWSHIP IN ULTRASOUND / CT / ANGIO / INTERVENTIONAL**—A 1-yr fellowship program available beginning July 1992 at Lehigh Valley Hospital Center in Allentown, PA. LVHC is a 492-bed, acute-care, university-affiliated hospital. The fellowship program offers training in CT (head and body), ultrasound, angiography (neuro and visceral), and interventional radiography. MRI experience is also available. For further information, contact Robert Kricun, M.D., Dept. of Radiology, Lehigh Valley Hospital Center, P.O. Box 689, Allentown, PA 18105. 2–7c

**FELLOWSHIP IN GENERAL RADIOLOGY/MAMMOGRAPHY 1991**—A fellowship is being offered in the Dept. of Radiology of the New England Medical Center Hospitals, Tufts University School of Medicine. This yr, the fellowship will provide experience in general radiology with a special emphasis on breast and GI radiology. The breast imaging portion of the fellowship includes training in all aspects of mammographic interpretation, breast ultrasound, and percutaneous needle localization for nonpalpable breast lesions. The dept. has 2 Senographe Units, an automated breast ultrasound scanner, and a small parts scanner. There will be involvement with the multidisciplinary Breast Health Center, which serves as a regional referral center as well as a resource for second opinions. Weekly conferences with the other disciplines involved in breast care, including surgery, hematology-oncology, radiation therapy, and pathology, guarantee close clinical-radiographic-pathologic correlation. Participation in clinical research will be available. The rotation through GI radiology will provide training in the performance and interpretation of double-contrast upper GI series and barium enema studies. Responsibility will include all areas of GI radiology. Attendance at a weekly GI-Radiology Correlative Conference is an integral part of the program. There will be opportunity for participation in clinical investigative projects. For further information, please contact Marc J. Homer, M.D., at (617) 956-0045. 2–3cp

**FELLOWSHIP POSITIONS**—The Dept. of Radiology and Radiological Sciences of Vanderbilt University School of Medicine has 1-yr fellowship positions for 1991–92 in the following areas: musculoskeletal (2), ultrasound (1), and angiography (1). Research opportunities are available and encouraged. Candidates must be board-certified or board-qualified in diagnostic radiology, and obtain a Tennessee medical license. Address inquiries and CV to Martin P. Sandler, M.D., Director, Fellowship Committee, Dept. of Radiology, Medical Center North, Vanderbilt University, Nashville, TN 37232-2675. An equal opportunity/affirmative action employer. 2–3c

**WINTHROP FELLOWSHIP IN ABDOMINAL IMAGING**—The Cleveland Clinic Foundation is offering 2 fellowship positions, each encompassing 1-yr of advanced training in body CT, ultrasound, and body MR, beginning July 1, 1992. One of these positions is supported by the Winthrop Corporation in order to advance expertise and research in the field of abdominal imaging. The Cleveland Clinic Foundation is a 1000-bed, tertiary-care hospital, with an international referral source, and a large outpatient population. The fellowship positions allow subspecialty training on state-of-the-art equipment, including ultrasound and CT-guided interventional procedures. Please submit CV and 2 letters of reference to David M. Paushter, M.D., Head, Section of Abdominal Imaging, Hospital Radiology, Cleveland Clinic Foundation, One Clinic Center Dr., Cleveland, OH 44195-5103. 2–3cp

**FELLOWSHIP IN ABDOMINAL IMAGING AND INTERVENTIONS** —The Dept. of Radiology, Massachusetts General Hospital and Harvard Medical School, offers a 2-yr fellowship in abdominal imaging and interventions beginning July 1, 1992. Training covers all aspects of abdominal imaging (radiography, fluoroscopy, ultrasound, CT, and MR) and nonvascular interventions in the GI and GU tracts. Research is active and participation is encouraged. Candidates should be ABR-eligible or certified. Address inquiries to Peter R. Mueller, M.D. or Nicholas Papanicolaou, M.D., Dept. of Radiology, Massachusetts General Hospital, Boston, MA 02114. An equal opportunity employer. 1–3cp

**FELLOWSHIPS AT THOMAS JEFFERSON UNIVERSITY HOSPITAL**—The Dept. of Radiology at Thomas Jefferson University Hospital in Philadelphia offers the following fellowship programs each yr. Ultrasound/CT/MRI — Jefferson's ultrasound division is 1 of the largest in the world and performs all currently available exams including obstetric, vascular, lithotripsy, invasive, and endoluminal. We also operate 4 GE 1.5-T MRI units and 3 CT scanners. Contact Barry Goldberg, M.D., regarding this program. Cardiovascular/interventional — this division is housed in a new suite containing Philips angio units with DSA and performs the full range of vascular and nonvascular interventional procedures. Contact Geoffrey Gardiner, Jr., M.D. Neuro/ENT radiology — very active clinical services supply a wealth of material to this division, which is housed in a neurosciences imaging center containing all imaging modalities. Contact Carlos Gonzalez, M.D. Breast imaging — Jefferson's new breast imaging center performs approximately 85 studies/day including ultrasound and needle localizations. Contact Stephen Feig, M.D. Chest — includes biopsies and CT. Contact Robert Steiner, M.D. MRI — a dedicated body MRI program including excellent research opportunities in addition to a large clinical case load. Contact Matthew Rifkin, M.D. Ultrasound — a dedicated ultrasound program. Contact Barry Goldberg, M.D. Musculoskeletal — includes MRI of the musculoskeletal system. Contact David Karasick, M.D. All program directors listed above can be contacted at the Dept. of Radiology, Thomas Jefferson University Hospital, Philadelphia, PA 19107. Jefferson is an equal opportunity/affirmative action employer. 3xc

**FELLOWSHIP IN ULTRASOUND AND BODY CT-MRI**—Unexpected position available July 1, 1991. A 1-yr body imaging fellowship at the Dept. of Radiology, University of Rochester Medical Center, a 750-bed, tertiary-care hospital. State-of-the-art equipment is available, including a free-standing MR center. Applicants must have completed an approved residency in diagnostic radiology and must be board-eligible or certified. For inquiries, please contact Deborah J. Rubens, M.D., Dept. of Radiology, Box 648, University of Rochester Medical Center, Rochester, NY 14642; (716) 275-8365. EO/AA/M-F employer. 2–4c

**FELLOWSHIP IN ULTRASOUND AND BODY CT/MRI** — July 1, 1992, to June 30, 1993, at the New York Hospital-Cornell Medical Center. Dept. provides state-of-the-art equipment including Acuson ultrasound, GE 9800 CT, and GE Signa 1.5-T MR. Wide variety of ultrasound exams include abdominal, OB-GYN, color Doppler, small parts, neonatal head, transvaginal, and transrectal. Applicant should be ABR eligible or certified. Send CV to Elias Kazam, M.D., Dept. of Radiology, The New York Hospital-Cornell Medical Center, 525 E. 68th St., New York, NY 10021. 1–4cp

**FELLOWSHIP POSITIONS**—The University of Texas, M. D. Anderson Cancer Center, Dept. of Diagnostic Radiology, is currently accepting applications for fellowships in different subspecialties in diagnostic imaging, including oncologic radiology, body imaging, and vascular/interventional radiology for the academic yr 1992. The dept. is equipped with state-of-the-art ultrasonography, CT, MRI, PET, angiography, routine fluoroscopy, radiography, and mammography. Candidates interested in these positions should write to Chusilp Charnsangavej, M.D., Professor and Deputy Chairman for Academic Affairs, Dept. of Diagnostic Radiology, Box 57, University of Texas M. D. Anderson Cancer Center, 1515 Holcombe Blvd., Houston, TX 77030. An employer equal opportunity affirmation action. 2–4c

**NEURORADIOLOGY FELLOWSHIP**—The Dept. of Radiology, Strong Memorial Hospital, University of Rochester School of Medicine and Dentistry offers a 1- or 2-yr neuroradiology fellowship to begin July 1, 1991. Training is offered in MRI, CT, and special procedures, with the opportunity to perform both pediatric and carotid ultrasound. Assistance in teaching of medical students and residents is expected. Additional training in maxillofacial, dental, and ENT radiology also is available, as is the opportunity to perform both clinical and laboratory research. A very strong neuroscience community exists. The dept. consists of 25 radiologist faculty, 16 residents, and 3–5 fellows. State-of-the-art equipment is available in all modalities including new single and biplane angiographic systems, 3 third-generation CT, a 1.5-T MRI, and a midfield MR. Strong Memorial Hospital is a 750-bed, tertiary-care hospital with 100 beds dedicated to pediatric diseases. Candidates must have completed an accredited diagnostic radiology residency program, be board-certified or eligible, and have a New York state medical license by July 1, 1991. Send inquiries to Robert E. O'Mara, M.D., Box 648, University of Rochester Medical Center, Rochester, NY 14642; (716) 275-2733. EO/AA/M-F employer. 1–6c

**IMMEDIATE UNEXPECTED OPENING FOR RESIDENCY IN DIAGNOSTIC RADIOLOGY, PRESBYTERIAN MEDICAL CENTER OF PHILADELPHIA**—Sudden resignation from our program at the 2nd-yr level leaves us with an opening starting Feb. 1, 1991. The required start date is between Feb. 1 and July 1, 1991. The program includes intensive exposure to all modalities, a rich conference schedule, opportunities for and encouragement of clinical research and publication. Full approval of the applicant's current program is required. Send CV, and phone David B. Freiman, M.D., Dept. of Medical Imaging, Presbyterian Medical Center of Philadelphia, 39th & Market Sts., Philadelphia, PA 19104; (215) 662-9138. 2–3cp

**ABDOMINAL IMAGING FELLOWSHIP** — The Dept. of Radiology at the University of Florida is offering 1-yr fellowships in abdominal imaging beginning July 1, 1991, and July 1, 1992. Minimum requirements include successful completion of an accredited radiology residency. The fellowship includes training in all aspects of abdominal imaging (gastrointestinal and genitourinary radiology, CT, ultrasound, and MRI) by a 3-person subspecialty faculty. The program offers full clinical experience and research opportunities. Applicants must be eligible to obtain a license in the state of Florida. For additional information, contact Pablo R. Ros, M.D., Professor, Dept. of Radiology, Box J-374, Gainesville, FL 32610-0374; (904) 395-0288. The University of Florida is an equal opportunity/affirmative action employer and encourages applications from women and minorities. 10–6c

**VASCULAR / INTERVENTIONAL RADIOLOGY FELLOWSHIP, ST. LOUIS VASCULAR INSTITUTE AT THE CHRISTIAN HOSPITAL, ST. LOUIS, MO**—A 1- to 2-yr fellowship in vascular and interventional radiology is offered beginning July 1, 1991. Training includes all aspects of diagnostic angiography and vascular and nonvascular interventional techniques. Candidates must have completed a diagnostic radiology residency in an accredited training program, must be certified by or eligible for certification by the ABR, and must be able to obtain a Missouri license. Direct inquiries to Saadoon Kadir, M.D., Dept. of Radiology, Christian Hospital Northeast, 11133 Dunn Rd., Ste. 1017, St. Louis, MO 63136. 11–4cp

**PEDIATRIC RADIOLOGY FELLOWSHIP** — The Dept. of Radiology at Children's Hospital of Philadelphia (CHOP) offers a 1- or 2-yr pediatric radiology fellowship beginning July 1, 1992. A 1-yr pediatric neuroradiology fellowship program is also offered and may be taken separately or in combination with a second yr adult neuroradiology fellowship at Jefferson University Medical Center in Philadelphia. A special (1-yr) cross-sectional imaging (CT, ultrasound, and MRI) fellowship may be arranged. CHOP is a 294-bed pediatric hospital affiliated with the University of Pennsylvania. Radiology has an attending faculty of 11 and performs 90,000 cases/yr (plain films, fluoroscopy, ultrasound, CT, nuclear medicine, neuroradiology, angiography/interventional radiology, and MRI). Our equipment is state-of-the-art and new since 1988 and includes ATL ultrasound equipment with duplex and color flow Doppler; gamma camera with SPECT; a high-resolution fast Siemens Somatom Plus CT scanner; and a 1.5-T Siemens Magnetom MRI installation with spectroscopy. A pediatric outpatient radiology facility has recently opened. We have an active teaching program for radiology residents and fellows. The patient population is large and varied, from routine emergencies to complicated tertiary care problems. The fellowship provides not only a broad clinical experience with subspecialty training, but offers opportunities for clinical and basic research and scholarship. Applicants must have completed a diagnostic radiology residency, be board-certified or eligible, and be able to obtain a Pennsylvania medical license. Salary and fringe benefits are highly competitive. Address inquiries to Sandra S. Kramer, M.D., Dept. of Radiology, The Children's Hospital of Philadelphia, 34th St. and Civic Center Blvd., Philadelphia, PA 19104; (215) 590-2575. The Children's Hospital of Philadelphia and the University of Pennsylvania are equal opportunity/affirmative action employers. 1–3cp

**DUKE UNIVERSITY MEDICAL CENTER FELLOWSHIP POSITIONS** — Duke University Medical Center is seeking qualified candidates for fellowship positions in the Dept. of Diagnostic Radiology. Currently there are positions available in the following areas: chest, musculoskeletal, and vascular/interventional radiology, ultrasound, advanced diagnostic imaging, MRI, neuroradiology, abdominal imaging, mammography, and research fellowships. The radiology dept. is state-of-the-art in diagnostic imaging with diverse resources available for clinical, teaching, and academic pursuits. Fellowship training is generally organized by organ systems, although experience can be individualized to accommodate special interests. Salary and benefits are competitive and academic time is guaranteed. For additional information, please phone Richard Leder, M.D. at (919) 681-2711 ext. 5310. Applications are due Feb. 1 of the preceding yr and can be obtained by writing to N. Reed Dunnick, M.D., Dept. of Radiology, Duke University Medical Center, Erwin Rd., Box 3808, Durham, NC 27710. AA/EOE. 2–7c

**WOMEN'S IMAGING FELLOWSHIP**—A 1- or 2-yr comprehensive experience in women's imaging modalities is offered in Tucson, AZ. Procedures in which we expect the fellow to gain expertise include high-volume, low-cost screening mammography and its associated administrative, financial, and epidemiological aspects; problem-solving diagnostic mammography, including invasive mammographic procedures (e.g., stereotactic guided cytology and galactography); high-volume obstetric and gynecologic sonography. Annual stipend is $50,000. Contact Arizona State Radiology, 7250 E. Ventana Canyon Dr., Tucson, AZ 85715; (602) 620-4911. 10–3cp

**INTEGRATED CHEST RADIOLOGY FELLOWSHIP AT JOHNS HOPKINS UNIVERSITY HOSPITAL**—The Dept. of Radiology, Division of Thoracic Imaging, Johns Hopkins University is offering a 1- to 2-yr academically oriented fellowship in chest radiology. The fellowship offers an integrated experience in cross-sectional imaging, including over 4000 chest CT and 1000 thoracic MRI exams/yr. Strong research interests in high-resolution CT, MRI, digital imaging methods, and interventional thoracic radiology offer the candidate an exciting environment to work in. The fellowship is available starting July 1, 1991. Contact Elias A. Zerhouni, M.D., Director of Thoracic Imaging and MRI, Dept. of Radiology, Johns Hopkins Hospital, Baltimore, MD 21205; (301) 955-4062. 1–6c

## Tutorials/Courses

**ALASKA 1991-CRUISE THE INLAND PASSAGE, BREAST IMAGING AT SEA, JULY 7–14, 1991, AND MRI AT SEA, JULY 14–21, 1991**—Medical Seminars International, Inc., 18981 Ventura Blvd., Ste. 303, Tarzana, CA 91356; (818) 774-9077, fax (818) 774-0244. 3–6d

## Other

**VISITING PROFESSORSHIPS, THOMAS JEFFERSON UNIVERSITY HOSPITAL**—The Dept. of Radiology at Thomas Jefferson University Hospital in Philadelphia is offering visiting professorships over the next several yr, while some of our faculty members are on sabbatical leave. These positions can have either a 6-mo or 1-yr term. In particular, we are seeking candidates with expertise in either ultrasound or general diagnostic radiology, but emphasis in other areas may be acceptable as well. Funding for these positions is appropriate for a senior faculty member from another institution on sabbatical with partial funding of his/her own, or for a junior faculty member. These positions are also open to highly qualified foreign radiologists with current academic appointments at prestigious foreign medical schools. Visiting faculty members will do some clinical work in our dept. and also have access, for research or educational purposes, to state-of-the-art imaging modalities of all types, as well as well-equipped physics and physiology research laboratories. Interested persons should contact David C. Levin, M.D., Chairman, Dept. of Radiology, Thomas Jefferson University Hospital, Philadelphia, PA 19107. Jefferson is an equal opportunity/affirmative action employer. 3xe

**AJR Classified Advertisements Information**

**Box Responses and Address for Ad Placement**

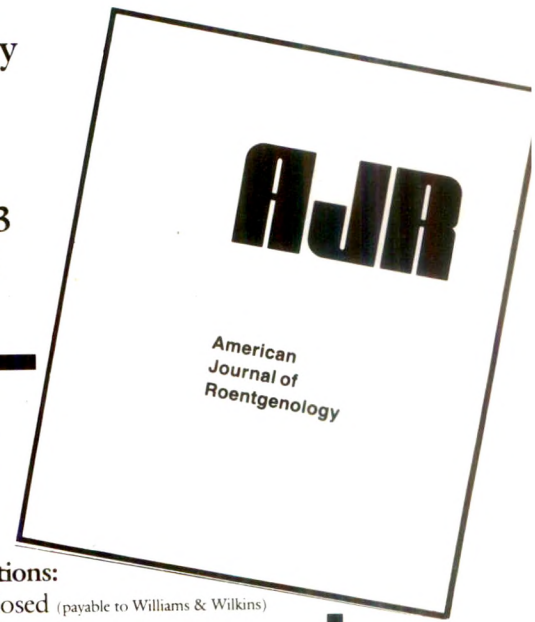
Write Box _____, *AJR*, 2223 Avenida de la Playa, Suite 103, La Jolla, CA 92037-3218; Phone: (619) 459-2229; FAX: (619) 459-8814.

# No one ever said a lot of knowledge is a dangerous thing.

IN FACT, for radiologists, the only danger is not keeping up with what's new. **AJR: American Journal of Roentgenology** is your monthly guide to the latest advances, with articles that are timely, succinct, and relevant to daily practice.

**AJR**
**American Journal of Roentgenology**
Published monthly
Robert N. Berk, M.D., Editor
The University of California, San Diego

Call toll-free to order: **1-800-638-6423**
from anywhere in the U.S. or Canada.
Or clip and mail this coupon.




Subscribe to **AJR** now. (Current rates available for up to three years.)

☐ Individual $125/year
☐ Institutional $135/year
☐ In-training* $25/year
(Add $55/year outside the U.S.; in Canada, also add 7% GST.)
☐ 3 years ☐ 2 years ☐ 1 year

Maryland residents add 5% sales tax. Subscriptions outside the U.S. must be prepaid in U.S. dollars. Rates valid through October 31, 1991.

Name _____

Address _____

City/State/Zip _____

*Please specify institution and training status _____

**Payment Options:**
☐ Check enclosed (payable to Williams & Wilkins)
☐ Bill me ☐ AmEx
☐ MasterCard ☐ VISA

Card # _____ Exp. Date _____

Signature _____

Return coupon to:
**Williams & Wilkins**
P.O. Box 23291, Baltimore, MD 21203-9990

**AJR: AMERICAN JOURNAL OF ROENTGENOLOGY** is the official journal of the American Roentgen Ray Society and is published by Williams & Wilkins.

J1037S01

GEORGE W. HOLMES LECTURE

443 **Whose turf is imaging? Independent practice, academics, and research.** *Hillman BJ*

REVIEW ARTICLES

449 **Breast sonography.** *Bassett LW, Kimme-Smith C*

457 **Gadopentetate dimeglumine–enhanced MR imaging of the musculoskeletal system.** *Beltran J, Chandnani V, McGhee RA Jr, Kursunoglu-Brahme S*

CARDIOPULMONARY RADIOLOGY

467 **Detection of bullous lung disease: conventional radiography vs digital storage phosphor radiography.** *Buckley KM, Schaefer CM, Greene R, et al.*

471 **Technical note. Percutaneous removal of transvenous pacing lead perforating the heart, pericardium, and pleura.** *Deutsch L-S, Dang H, Brandon JC, Ott R, Allen B, Futerman C*

BREAST RADIOLOGY

475 **Commentary. Mammography and malpractice.** *Potchen EJ, Bisesi MA, Sierra AE, Potchen JE*

GASTROINTESTINAL RADIOLOGY

481 **Pictorial essay. Extracolonic manifestations of the familial adenomatous polyposis syndromes.** *Harned RK, Buck JL, Olmsted WW, Moser RP, Ros PR*

487 **Intraabdominal *Mycobacterium tuberculosis* vs *Mycobacterium avium-intracellulare* infections in patients with AIDS: distinction based on CT findings.** *Radin DR*

493 **Gallstone fragmentation during biliary lithotripsy: effect of stone composition and structure.** *Zeman RK, Marchand T, Davros WJ, Garra BS, Glass-Royal M, Soloway RD*

GENITOURINARY RADIOLOGY

501 **Natural history of acquired renal cystic disease in dialysis patients: a prospective longitudinal CT study.** *Levine E, Slusher SL, Grantham JJ, Wetzel LH*

507 **Arteriovenous fistulas complicating biopsy of renal allografts: treatment of bleeding with superselective embolization.** *deSouza NM, Reidy JF, Koffman CG*

511 **Carcinoma of the prostate: MR images obtained with body coils do not accurately reflect tumor volume.** *Quint LE, Van Erp JS, Bland PH, et al.*

517 **Case report. MR imaging in sclerosing mesenteritis.** *Kronthal AJ, Kang YS, Fishman EK, Jones B, Kuhlman JE, Tempany CMC*

520 **Case report. Retroperitoneal sarcoidosis.** *Bach DB, Vellet AD*

523 **Pictorial essay. CT appearance of the pelvis after cesarean section.** *Twickler DM, Setiawan AT, Harrell RS, Brown CEL*

527 **CT pelvimetry: the foveae are not an accurate landmark for the level of the ischial spines.** *Aronson D, Kier R*

MUSCULOSKELETAL RADIOLOGY

531 **Review. Automated percutaneous lumbar diskectomy.** *Onik G, Helms CA*

539 **MR imaging in fibromatosis: results in 26 patients with pathologic correlation.** *Quinn SF, Erickson SJ, Dee PM, et al.*

543 **Case report. CT appearance of angiosarcoma associated with chronic lymphedema.** *Kazerooni E, Hessler C*

545 **Technical note. Aspiration of the hip in patients treated with Girdlestone arthroplasty.** *Swan JS, Braunstein EM, Capello W*

FETAL RADIOLOGY

547 **Review. Sonography of the fetal heart: findings on the four-chamber view.** *McGahan JP*

555 **Pictorial essay. Sonographic diagnosis of the amniotic band syndrome.** *Burton DJ, Filly RA*

559 **Case report. CT amniography: value in detecting a monoamniotic pair in a triplet pregnancy.** *Sargent SK, Young W, Crow P, Simpson W*

PEDIATRIC RADIOLOGY

561 **Deferoxamine-induced bone dysplasia in patients with thalassemia major.** *Brill PW, Winchester P, Giardina PJ, Cunningham-Rundles S*

567 **Aortic thrombosis after umbilical artery catheterization in neonates: prevalence of complications on long-term follow-up.** *Seibert JJ, Northington FJ, Miers JF, Taylor BJ*

571 **Posterior fossa intracranial hemorrhage in infants treated with extracorporeal membrane oxygenation: sonographic findings.** *Bulas DI, Taylor GA, Fitz CR, Revenis ME, Glass P, Ingram JD*

576 **Case report. Schmid-like metaphyseal chondrodysplasia simulating child abuse.** *Kleinman PK*

NEURORADIOLOGY

579 **Pictorial essay. MR anatomy and pathology of the hypothalamus.** *Loes DJ, Barloon TJ, Yuh WTC, DeLaPaz RL, Sato Y*

587 **Congenital nasal masses: CT and MR imaging features in 16 cases.** *Barkovich AJ, Vandermarck P, Edwards MSB, Cogen PH*

599 **Idiopathic growth hormone deficiency: MR findings in 35 patients.** *Abrahams JJ, Trefelner E, Boulware SD*

605 **MR imaging in chronic partial epilepsy: role of contrast enhancement.** *Elster AD, Mirza W*

611 **Diagnosis of carotid artery stenosis: comparison of 2DFT time-of-flight MR angiography with contrast angiography in 50 patients.** *Litt AW, Eidelman EM, Pinto RS, et al.*

VASCULAR RADIOLOGY

617 **Pulsed-spray thrombolysis of arterial and bypass graft occlusions.** *Valji K, Roberts AC, Davis GB, Bookstein JJ*

623 **The importance of preoperative evaluation of the subclavian vein in dialysis access planning.** *Surratt RS, Picus D, Hicks ME, Darcy MD, Kleinhoffer M, Jendrisak M*

SPECIAL ARTICLE

627 **Fate of manuscripts rejected for publication in the *AJR*.** *Chew FS*

OTHER CONTENT

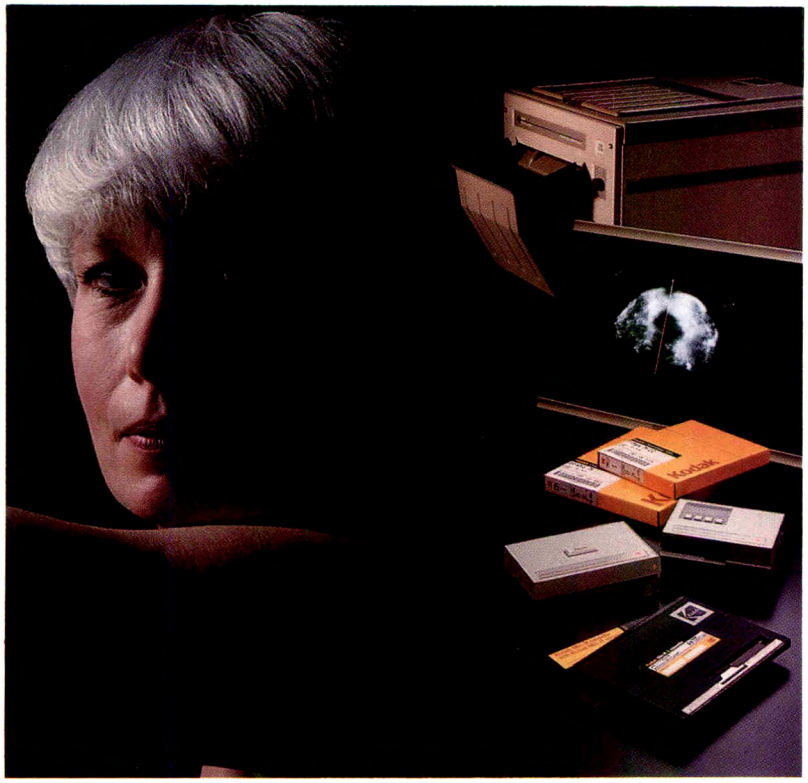
**Book reviews** 456, 486, 492, 500, 570, 586
448 **Melvin M. Figley Fellowship recipients**
474 **Radiologic-Pathologic Conference**
554 **Art page**
622 **Memorial, Charles P. Hyslop**
626 **Forthcoming articles**
633 **Letters**
641 **Review of current literature**
647 **News**
651 **Invitation to the 1991 ARRS meeting**
653 **American Roentgen Ray Society information**
654 **1991 ARRS meeting summary**
655 **1991 ARRS meeting registration forms**
659 **1991 ARRS meeting courses and symposium**
661 **Classified advertisements**
A6 **Guidelines for authors**
A14 ***AJR* business and subscriber information**

# AJR

American
Journal of
Roentgenology

April 1991

© Eastman Kodak Company, 1991.




***Choices: film, screens, cassettes, processors, chemicals...Kodak gives you more, including technical help and quality control...So you can choose the mammography image you prefer.***

*Mammography is the single most effective imaging modality for the diagnosis of breast disease. Whatever your mammographic imaging preference, Kodak can provide optimal image quality. More contrast? Grids? Magnification techniques? Lower dosage? Extended processing? There are Kodak products to match your needs. There's also a complete quality-control system, plus the expertise and assistance of your Kodak representative.*

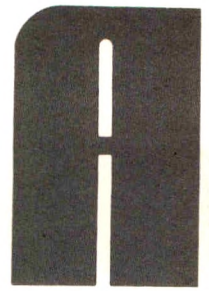
*New breast cancer screening guidelines are likely to increase demand for mammography. For details on the choices, talk to your Kodak representative.*

# MAMMOGRAPHY. THE MOST CHOICES ARE FROM KODAK

***The first choice in quality imaging...worldwide***

Kodak

Official Journal of th



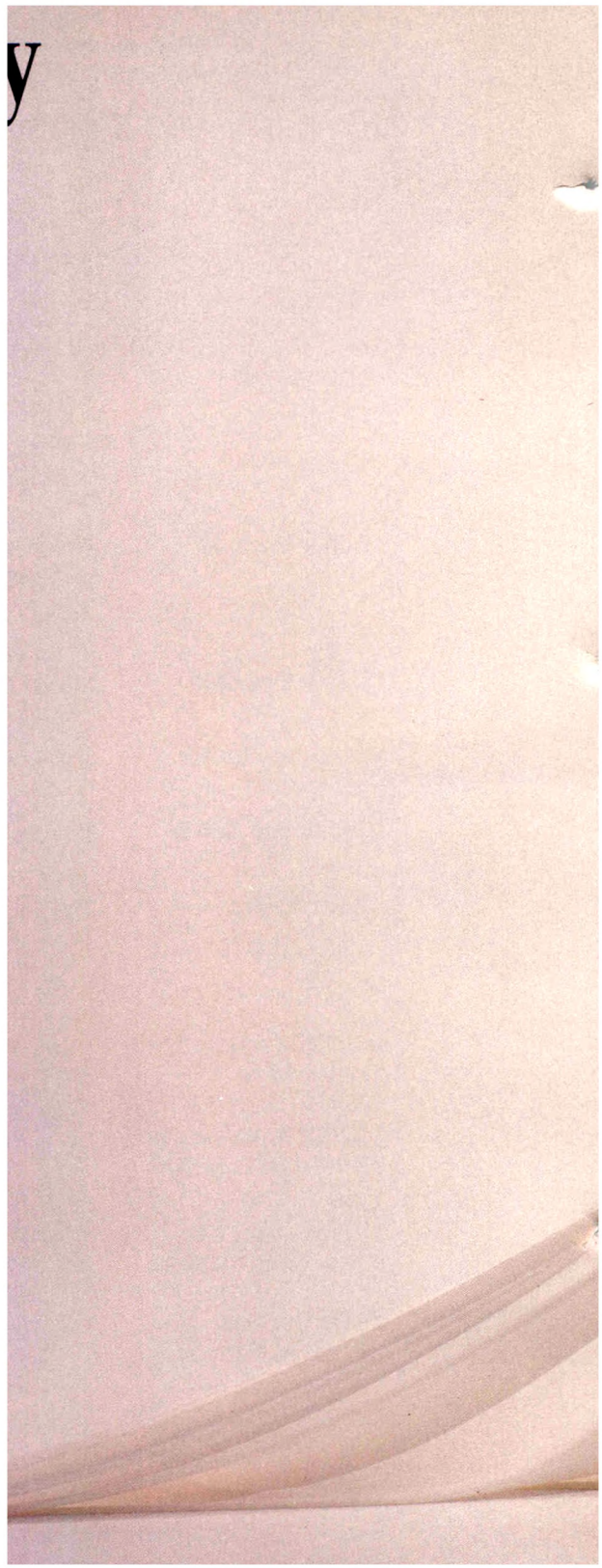
**American Jou**
Diagnostic Ima

| | |
|---|---|
| **Editor-In-Chief** | Robert N. B<br>*University of*<br>*School of M* |
| **Editor Emeritus** | Melvin M. Fi |
| **Associate Editor** | Saskia von \ |
| **Consulting Editor** | Michael S. H |
| **Statistician** | Charles C. E |

| | |
|---|---|
| John R. Amberg | John |
| Itamar Aviad | Charl |
| Mark E. Baker | Melvy |
| Lawrence W. Bassett | Faye |
| Michael A. Bettmann | Thom |
| Felix S. Chew | Rober |
| N. Reed Dunnick | Bruce |
| David K. Edwards | Richa |
| Ronald G. Evens | Albert |
| David S. Feigin | Jeffre |
| Sandra K. Fernbach | Donal |
| Richard H. Gold | Stewa |
| William R. Hendee | Charle |

**Editorial Staff:** Margaret Levene,
Barbara L. Halliburton, and Janine An
*manager*; Sheri Smith, *administrati*
*secretary*.

AJR, AMERICAN JOURNAL OF ROENTGENOLOGY
Society and is published monthly by Williams & Wilkir
journal subscription. Second-class postage paid at B
changes (Form 3579) to AJR, 428 E. Preston St., Balt
($190 foreign); in training $25 ($80 foreign); single cop
*Contents* and *Index Medicus*. Copyright © 1991 by Am



# *IMAGINE...X-RAY FILM PROCESSOR QC IN THE PALM OF YOUR HAND!*




***IMAGINE...**performing daily film processor QC in seconds!*
***IMAGINE...**a compact, lightweight, portable scanning QC system that has more features and capabilities than you ever dreamed were possible!*

# MINISCAN

## You can use it **WITH** or **WITHOUT** a Computer!

### MINISCAN is a...

- Standard high quality transmission densitometer.
- Scanning QC densitometer to measure, analyze and store data for up to 20 independent sensitometric strips in its own built-in memory (no external computer or software needed)!
- Complete film processor QC system (when combined with the Film Processor QC Software Package) to track and monitor the performance of a virtually unlimited number of film processors. PLUS generate comprehensive reports, control charts, and corrective action forms, and more!

## MINISCAN...*More Than You Ever Imagined!*

*For more details, request Bulletin 501-44*

**NUCLEAR ASSOCIATES**
VICTOREEN
Division of VICTOREEN, INC.
100 VOICE ROAD • P.O. BOX 349
CARLE PLACE, NY 11514-0349 U.S.A.
(516) 741-6360
FAX (516) 741-5414

# *AJR* Business and Subscriber Information

### The American Roentgen Ray Society

*AJR, American Journal of Roentgenology*, is published monthly to disseminate research on current developments in the radiologic sciences and commentary on topics related to radiology. It is published by the American Roentgen Ray Society, 1891 Preston White Dr., Reston, VA 22091; (703) 648-8992. Inquiries regarding society business, the annual ARRS meeting, and membership should be addressed to the Society at the above address.

### Correspondence Concerning the *AJR*

Correspondence regarding display (not classified) advertising, subscriptions, address changes, reprints, and permission requests should be addressed to Williams & Wilkins, 428 E. Preston St., Baltimore, MD 21202; (301) 528–4000.

Correspondence regarding editorial matters and classified advertising should be addressed to Editorial Office, AJR, 2223 Avenida de la Playa, Ste. 103, La Jolla, CA 92037-3218; telephone (619) 459-2229; FAX (619) 459-8814. For information on manuscript submission, see Guidelines for Authors, pages A14–A16.

### Subscriber Information

Subscription requests and inquiries should be sent to Williams & Wilkins, 428 E. Preston St., Baltimore, MD 21202. ARRS annual dues include $50 for journal subscription. Subscription rates are as follows: nonmembers, $125/year ($180 foreign); institutions, $135 ($190 foreign); nonmember in-training, $25 ($80 foreign). Single copies of the Journal may be purchased for $18 ($22 foreign). Airmail rates will be furnished on request.

Call toll-free, 1-800-638-6423 (in Maryland call 1-800-638-4007), with subscription questions or problems. Please have the mailing label from your latest issue available when you call.

If a subscriber receives a damaged copy of the *AJR* or fails to receive an issue, the subscriber should notify Williams & Wilkins (428 E. Preston St., Baltimore, MD 21202) within 60 days of publication (90 days for foreign subscribers) and that issue will be replaced.

Change of address information should be sent to Williams & Wilkins, 428 E. Preston St., Baltimore, MD 21202. Allow 90 days for address changes.

### Copyrights, Permissions, and Reprints

The American Roentgen Ray Society holds the copyright for all material published in the *AJR*. No part of this publication may be reproduced without permission from the ARRS. Requests for such permission should be addressed to Williams & Wilkins, 428 E. Preston St., Baltimore, MD 21202.

For reprints of a particular article, please contact the author designated in the footnotes for that article.

### Indexes

The *AJR* provides volume and yearly indexes (subject and author) in the June and December issues each year. *AJR* articles are also indexed in *Current Contents*, *Index Medicus*, and the cumulative index published by *Radiology*.

# FREE DEMONSTRATION DISC

## TELLS YOU HOW TO CONFORM TO JCAHO PATIENT DOSE MEASUREMENTS DR.2.2.10.2

## Call or write today for your FREE RADCOMP™

## X-Ray Entrance Skin Exposure Program Demo Disc!

Phone 516-741-6360, FAX 516-741-5414,
or write and request
FREE RADCOMP disc #4423-44

**NUCLEAR ASSOCIATES**

VICTOREEN

Division of VICTOREEN, INC.
100 VOICE ROAD • P.O. BOX 349
CARLE PLACE, NY 11514-0349 U.S.A.
(516) 741-6360
FAX (516) 741-5414

TM, Victoreen, Inc.

### RADIOLOGIST

BC/BE radiologist with subspecialty in MRI wanted to join us for an immediate opening of an outpatient MRI imaging center, and also hospital practice in northeastern region.

Situated in a beautiful summer/winter recreational area, in close proximity to several major cities.

This is an excellent professional opportunity in a rapidly growing community.

Fir year, excellent salary with high incentive, giving you an extraordinary financial package with many fringe benefits lead to partnership.

Please reply to:

AJR Box 1
Williams & Wilkins
428 E. Preston Street
Baltimore, MD 21202-3993.

**National Institutes of Health**
**Public Health Service**
**Department of Health and Human Services**

### Radiologist

The National Institutes of Health (NIH) is seeking an experienced Board-certified radiologist to direct its new Diagnostic Radiology Research Program (DRRP). The Director will organize and conduct a research training program in diagnostic imaging for radiologists and provide a coordinating focus for the many ongoing research initiatives in diagnostic imaging at the NIH. The Diagnostic Radiology Research Program will train between 4-6 radiologists a year, and will have access to extensive research facilities, including an NMR dedicated exclusively to the research program and supported by the NIH Nuclear Medicine Research Center. In addition, the Director will be provided with laboratory facilities, personnel and operating budget to pursue independent research in diagnostic imaging. Applicants should have an ongoing radiology research program and relevant experience in clinical imaging and in teaching of diagnostic radiology. Interested individuals should submit a curriculum vitae and bibliography to:

**Dr. Dinah Singer**
**Office of Intramural Affairs**
**National Institutes of Health**
**Building 1, Room 140**
**9000 Rockville Pike**
**Bethesda, MD 20892**

NATIONAL INSTITUTES OF HEALTH

*NIH is an Equal Opportunity Employer*

# *AJR* Guidelines for Authors

Address new and revised manuscripts, correspondence, and classified ads to the Editor:

AJR Editorial Office
2223 Avenida de la Playa, Suite 103
La Jolla, CA 92037-3218
Telephone: (619) 459-2229; FAX: (619) 459-8814

Inquiries regarding subscriptions, display advertising, reprints, or permission to republish *AJR* material should be addressed to the publisher:

The Williams & Wilkins Co.
428 E. Preston St.
Baltimore, MD 21202 Telephone: 1-800-638-6423

The *AJR* publishes original contributions to the advancement of medical diagnosis and treatment. Submitted manuscripts should not contain previously published material and should not be under consideration for publication elsewhere. Papers dealing with neuroradiology should be addressed to: American Journal of Neuroradiology, Dept. of Diagnostic Radiology, 1653 W. Congress Pkwy., Chicago, Il 60612. At the discretion of the *AJR* Editor, *AJNR* articles that are of interest to the general reader may be republished in the *AJR*. Neuroradiologic papers sent to the *AJR* will be forwarded to the Editorial Office of the *AJNR*.

Manuscript decisions are based on peer review. Reviewers receive manuscripts without title pages to ensure an unbiased review. Statements made in the article, including changes made by the Editor or manuscript editor, are the responsibility of the author and not of the *AJR* or its publisher. Authors will be sent the edited manuscript, galley proof, and proofs of illustrations. If the corresponding author will be unavailable to review galleys, arrangements should be made for a coauthor or colleague to read and return the proof.

The following guidelines are based on instructions set forth in the **Uniform Requirements for Manuscripts Submitted to Biomedical Journals** (*Ann Intern Med* **1988;**108:258–265). Articles will be edited, however, to conform to the individual style of AJR.

### General Guidelines for Major Papers

*Abstract.* Clearly state (in 200 words or less) the purpose, methods, results, and conclusions of the study. Include actual data.

*Introduction.* Briefly describe the purpose of the investigation and explain why it is important.

*Methods.* Describe the research plan, the materials (or subjects), and the methods used, in that order. Explain in detail how disease was confirmed and how subjectivity in observations was controlled.

*Results.* Present results in a clear, logical sequence. If tables are used, do not duplicate tabular data in text, but do describe important trends and points.

*Discussion.* Describe the limitations of the research plan, materials (or subjects), and methods, considering both the purpose and the outcome of the study. When results differ from those of previous investigators, explain the discrepancy.

## AUTHOR'S CHECKLIST

**For priority handling, complete the following checklist, sign the copyright form on the reverse side of this page, and include both with the manuscript.**

_____ Two copies of the manuscript (the original and a photocopy) and two complete sets of figures are submitted. One copy has been retained by the author.

_____ If appropriate, *AJR* Guidelines for case reports, technical notes, pictorial essays, or letters to the Editor have been followed. (See page A16.)

_____ The manuscript, including references, figure legends, and tables, is typed double-spaced on 8½ × 11 in. (21.6 × 27.9 cm) *nonerasable* paper. Right-hand margins are not justified.

_____ All manuscript pages are numbered consecutively beginning with the abstract. Authors' names do not appear on the manuscript pages.

_____ The manuscript is organized as follows: title page, blind title page (title only), abstract, introduction, methods, results, discussion, acknowledgments, references, tables, figure legends, and figures.

_____ Informed consent has been obtained from patients who participated in clinical investigations. If experiments were performed on animals, authors complied with NIH guidelines for use of laboratory animals.

_____ Use of unfamiliar acronyms and abbrevations is kept to a minimum. When abbreviations are used they are defined at first mention, followed by the abbreviation in parentheses.

_____ Metric measurements are used throughout, or the metric equivalent is given in parentheses.

_____ Names and locations (city and state only) of manufacturers are given for equipment and nongeneric drugs.

### Title Page

_____ The following information is given: title of article; names and complete addresses (including zip code) of all authors; current addresses of authors who have moved since study; acknowledgment of grant or other assistance. The corresponding author is clearly identified, and a current address, phone number, and FAX number are given.

_____ A blind title page is included in each copy of the manuscript, giving only the title (without the authors' names) for use in the review process.

### Abstract

_____ An abstract of approximately 200 words concisely states the purpose, methods, and results of the study in one paragraph. Actual data are included. Conclusions are stated in a second, summary paragraph.

_____ No abbreviations or reference citations are used.

### References

_____ References (not to exceed 35) are typed double-spaced starting on a separate page and are **numbered consecutively in the order in which they appear in the text**.

_____ All references are cited in the text and are enclosed in brackets and typed on line with the text (not superscript).

_____ Unpublished data are not cited in the reference list, but are cited parenthetically in the text, for example, (Smith DJ, personal communication), (Smith DJ, unpublished data). This includes papers submitted, but not yet accepted, for publication.

_____ Papers presented at a meeting are not cited in the reference list, but are cited parenthetically in the text (e.g., Smith DJ et al., presented at the annual meeting of the American Roentgen Ray Society, May 1990). After first mention, use (Smith DJ et al., ARRS meeting, May 1990).

_____ Inclusive page numbers (e.g., 333–335) are given for all references.

_____ Journal names are abbreviated according to *Index Medicus*.

_____ Style and punctuation of references follow the format illustrated in the following examples (all authors are listed when six or fewer; when seven or more authors, the first three are listed, followed by "et al."):

*Journal article*

1. Long RS, Roe EW, Wu EU, et al. Membrane oxygenation: radiographic appearance. *AJR* **1986**;146:1257–1260

*Book*

2. Smith LW, Cohen AR. *Pathology of tumors*, 6th ed. Baltimore: Williams & Wilkins, **1977**:100–109

*Chapter in a book*

3. Breon AJ. Serum monitors of bone metastasis. In: Clark SA, ed. *Bone metastases*. Baltimore: Williams & Wilkins, **1983**:165–180

### Tables

_____ Each table is typed double-spaced on a separate page without vertical or horizontal rules; each has a short, descriptive title. Tables do not exceed two pages in length and contain at least four lines of data.

_____ Tables are numbered in the order in which they are cited in the text.

_____ Abbreviations are defined in an explanatory note below each table.

_____ Tables are self-explanatory and do not duplicate data given in the text or figures.

_____ All arithmetic (percentages, totals, differences) has been double checked for accuracy, and tabular data agree with data given in the text.

### Figures and Legends

_____ Two complete sets of original figures are submitted unmounted in labeled envelopes.

_____ Figures are clean, unscratched, 5 × 7 in. (13 × 18 cm) glossy prints with **white borders.** A separate print is submitted for each figure *part*.

_____ All figure parts relating to one patient have the same figure number.

_____ Each figure is labeled on the back with the figure number and an arrow indicating "top." For black-and-white figures, labeling is done on a gummed label, which is then affixed to the back of the print. **Never** use labels on **color** figures, but write figure number on the back lightly in pencil. *Never* use ink on front or back of any figures.

_____ Author's names are *not* written on the backs of figures.

_____ Only removable (rub-on) arrows and letters are used on the figures. Symbols are uniform in size and style and are not broken or cracked.

_____ Images are uniform in size and magnification.

_____ Line drawings are done in black ink on a white background. They are professional in quality, and all use the same size type. (Only glossy prints are acceptable.)

_____ Written permission has been obtained for use of all previously published illustrations (and copies of permission letters are included), and an appropriate credit line is given in the legends.

_____ Legends are typed double-spaced, and figure numbers correspond with the order in which the figures are cited in the text.

---

### Transfer of Copyright Agreement, Conflict of Interest Acknowledgment, Certification of Coauthors, and Exclusive Publication Statement

Complete copyright to the article entitled: _____

_____

is hereby transferred to the American Roentgen Ray Society (for United States government employees to the extent transferable), effective if and when the article is accepted for publication in the *American Journal of Roentgenology*. In the case of the authors who are officers or employees of the United States government, the American Roentgen Ray Society recognizes that works prepared by officers or employees of the United States government as part of their official government duties are in the public domain.

Authors reserve all proprietary rights other than copyright, such as patent rights and the right to use all or part of this article in future works of their own. The authors retain the right of replication, subject only to crediting the original source of publication and receiving written permission from the publisher.

Authors guarantee that this manuscript contains no matter that is libelous or otherwise unlawful, invades individual privacy, or infringes any proprietary rights.

Authors understand that they will receive no royalty or other compensation from the American Roentgen Ray Society or the publisher.

Authors guarantee that the editor has been or will be informed of any proprietary or commercial interest or conflicts of interest the authors may have that relate directly or indirectly to the subject of this article.

All authors certify that they have made substantive and specific intellectual contributions to the article and assume public responsibility for its content.

Finally, the authors certify that none of the material in this manuscript has been published previously or is currently under consideration for publication elsewhere.

| | | |
|---|---|---|
| First author/date | Second author | Third author |
| Fourth author | Fifth author | Sixth author |

**This agreement must be signed by all authors in order for the manuscript to be published.**

### Case Reports

A case report is a brief description of a special case that provides a message that transcends the individual patient.

*Format.* There is no abstract. The introduction should be a short paragraph giving the general background and the specific interest of the case. No more than one case should be described in detail (similar ones can be mentioned briefly in the discussion). Emphasis should be on the radiologic aspects; clinical information must be limited to that necessary to provide a background for the radiology. The discussion should be succinct and should focus on the specific message and relevance of radiologic methods. A review of the literature is not appropriate.

*Length.* Maximum of five double-spaced, typewritten pages, including the references but not the title page or figure legends.

*References.* Maximum of eight.

*Figures.* Maximum of four, unless the text is shortened accordingly. Legends must not repeat the text.

*Tables and Acknowledgments.* Not appropriate in case reports.

### Technical Notes

A technical note is a brief description of a specific technique or procedure, modification of a technique, or equipment of interest to radiologists.

*Format.* No abstract, headings, or subheadings are required. If headings are used, they should be a combination of "Case Report," "Materials and Methods," "Results," and "Discussion." A brief one-paragraph introduction should be included to give the general background. Discussion should be limited to the specific message, including the uses of the technique or equipment. Literature reviews and lengthy case reports are not appropriate.

*Length.* Maximum of five double-spaced, typewritten pages, including the references but not the title page or figure legends.

*References.* Maximum of eight.

*Figures.* Maximum of two, unless the text is shortened accordingly.

*Tables and Acknowledgments.* Not appropriate in technical notes.

### Pictorial Essays

A pictorial essay is an article that conveys its message through illustrations and their legends. Unlike other *AJR* articles, which are based on original research, pictorial essays serve primarily as teaching tools, like exhibits at a scientific meeting. They are not encyclopedic book chapters. The abstract should be a short, introductory paragraph.

*Length.* Maximum of four double-spaced, typewritten pages, including the references but not the title page or figure legends.

*References.* Maximum of four.

*Figures.* Maximum of 30 figure *parts*. Number should be as few as necessary to convey the message of the paper.

*Tables and Acknowledgments.* Not appropriate in pictorial essays.

### Letters to the Editor and Replies

Letters to the Editor and Replies should offer objective and constructive criticism of published articles. Letters may also discuss matters of general interest to radiologists. Do not end a letter with a hand-written signature.

*Format.* All letters should be typed double-spaced on nonletterhead paper, with no greeting or salutation. Name and affiliation should appear at the end of the letter. Titles for letters should be short and pertinent. The title for a reply is simply "Reply."

*Length.* Maximum of two double-spaced, typewritten pages, including references.

*References.* Maximum of four.

*Figures.* Maximum of two.

*Tables and Acknowledgments.* Not appropriate in Letters to the Editor and Replies.

### Opinions, Commentaries, and Perspectives

Opinions, commentaries, and perspectives are special articles dealing with controversial topics or issues of special concern to radiologists.

*Format.* Include a title page but no abstract. Headings may be used to break up the text.

*Length.* Maximum of five double-spaced, typewritten pages.

*References.* Maximum of five.

*Tables and Figures.* Maximum of four.

### Computer Page Articles

Articles published on the computer page deal with practical computer applications to radiology.

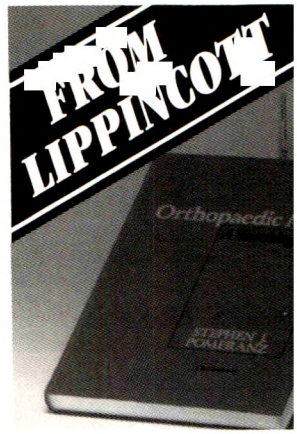
*Format.* Include a title page and an abstract.

*Length.* Maximum of eight double-spaced, typewritten pages.

*References.* Maximum of five.

*Figures and Tables.* Maximum of five. Computer printouts are not acceptable. Figures must be submitted as 5 × 7 in. glossy prints.

**All submissions to the *AJR* must be accompanied by a completed copy of the Author's Checklist and the signed Copyright Agreement.**




# Data for

## Orthopaedic MRI
## A Teaching File

*By Stephen J. Pomeranz, M.*

Here is a comprehensive e
ration of common musculos
injuries and entities—what e
radiologic clinician needs to
to perform orthopedic MR ir
to-day practice. Each case stu
provides:

- images accompanied by li
drawings that illustrate key
features.
- extensive labeling highligl
the pathologic and nonpath
pathology and anatomy.
- a question-and-answer sty
identifying findings and suit
differential diagnoses for the
findings.

*About 450 Pages. 300 MR Images, 200 Line Drawings.*
*0-397-51105-1.* **$89.50**

## Diagnostic Medi
## Sonography: A
## Guide to Clinical
## Practice · Three
## Volume Series

*Edited by Diane M. Kawan*
*M.Ed., R.T.(R), R.D.M.S.; Mi*
*Berman, Ph.D., R.D.M.S.; a*
*Marveen Craig, R.D.M.S.*

### *Volume I: Obstetri*
### *and Gynecology*

*Mimi C. Berman, Ph.D., R.D.M.S., Volume Editor*

Concentrates on obstetric
gynecologic sonographic ex
Covers anatomy, physiology,
ratory values, scanning techr
and normal and abnormal sc
graphic anatomic representa
and pathology. Clinical data
closely correlated to an exte
collection of top-quality son
grams and schematics. Uniqu
chapters cover computer sof



*Fleischner Lecture*

# Developmental Abnormalities in the Systemic Blood Supply to the Lungs

Kent Ellis[1]

**Developmental abnormalities in the systemic blood supply to the lungs occur in association with congenital heart disease, congenital lung disease, and rarely with apparently normal heart and lungs. Although most of these anomalies are rare, in the aggregate they are relatively common and of special interest to students of chest and heart disease.**

*AJR* 156:669–679, April 1991

The various possibilities for normal and abnormal systemic arterial supplies to the lungs comprise (1) the bronchial arteries, the normal systemic arterial supply after birth; (2) a patent ductus arteriosus, a potential intrauterine supply that is considered anomalous after birth; (3) major aortopulmonary collateral arteries (MAPCAs); (4) a direct origin of the right or left pulmonary artery from the ascending aorta; and (5) other systemic arteries including connections between coronary arteries and pulmonary arteries.

The bronchial arteries [1, 2] provide the normal systemic arterial supply to the lungs after birth and comprise generally one to three small arteries from the upper dorsal aorta or right first intercostal artery supplying each lung. Tiny accessory arteries between the aorta and its branches and the lungs are also nearly always present. Numerous actual or potential connections exist between the bronchial arteries and the esophageal, intercostal, phrenic, internal mammary, coronary, and other regional arteries. Many connections between bronchial and pulmonary vessels occur at the capillary and precapillary levels, but the existence, size, and number of the normal direct connections more proximally between the bronchial and pulmonary arteries are controversial. The bronchial arteries arise de novo in the 9th to 12th weeks of fetal life, several weeks after the pulmonary arteries have formed [3].

The bronchial arteries may enlarge greatly after birth to provide collateral flow to the pulmonary arteries when the pulmonary artery supply is obstructed or with growth of inflammatory or neoplastic tissue in the lungs, especially in the presence of systemic oxygen desaturation. Transpleural adhesions may provide a substantial source of collateral flow to both pulmonary and bronchial arteries from chest wall arteries. Bronchial arterial collateral to the lung nearly always appears to be acquired after birth.

Persistent ductus arteriosus is a well-known source of anomalous systemic arterial supply to the lung. A patent ductus arteriosus is much more common in congenital heart disease [4] (3% to >50% prevalence) than in the general population (<0.1%). Patent ductus arteriosi are derived from the sixth aortic arches and are paired in the early embryo. The right ductus arteriosus with the right dorsal aorta normally is resorbed early (by the 45th embryologic day) [5]. Kutsche and Van Mierop [6] point out that the sixth arches account for only the ductus arteriosi and not the proximal right or left pulmonary artery.

Received July 16, 1990; accepted after revision October 18, 1990.

Presented at the annual meeting of the Fleischner Society, Scottsdale, AZ, April 1990.

[1] Department of Radiology, College of Physicians and Surgeons of Columbia University, Columbia-Presbyterian Medical Center, 622 W. 168th St., New York, NY 10032.

0361–803X/91/1564–0669
© American Roentgen Ray Society

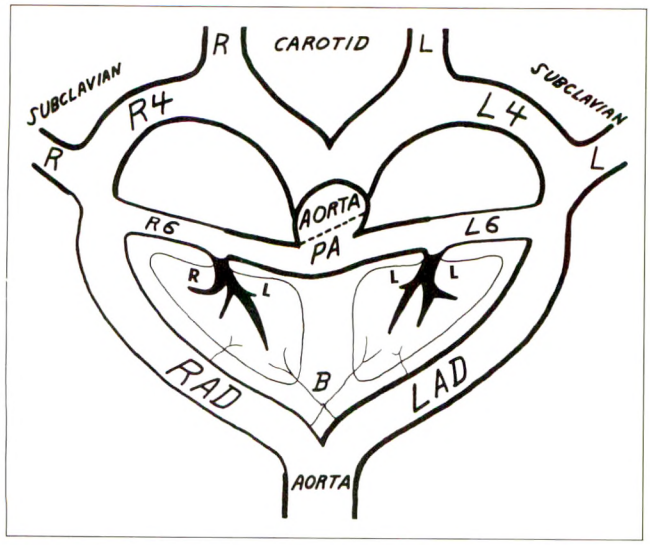



Fig. 1.—Diagram shows early development of great arteries. Normally, right dorsal aorta (RAD) and right ductus arteriosus (R6 = right sixth arch) regress early in gestation (eighth week), leaving a left aortic arch and a left ductus arteriosus (L6 = left sixth arch), which normally closes at birth. When a ductus arteriosus persists on the side opposite the aortic arch, it nearly always arises from the innominate or subclavian artery, which may be normal or aberrant. R4 and L4 = right and left fourth aortic arches, LAD = left dorsal aorta, RL and LL = right and left lungs and hilar region, B = bronchial arteries, PA = main pulmonary artery with its major right and left extensions to right and left hilar regions and lungs.

A patent ductus arteriosus may persist on one or both sides. Figure 1 shows the early paired development of the aortic arch system. The ductus arteriosus (L6 or R6) on the side of the persistent aortic arch will arise from that arch as it would normally. The arches are originally paired, so the arch on the side opposite the definitive persistent arch must have been interrupted. A persisting patent ductus arteriosus arising on that side (opposite the persisting aortic arch) has a variable origin depending on the site of arch interruption relative to the origin of the ductus arteriosus at the time. For example, if the right arch persisted and the left arch were interrupted, a left ductus arteriosus would arise from the region of the innominate artery if the left dorsal aorta were the site of interruption (as is most typical when congenital heart disease is present). On the other hand, if the left arch interruption were more proximal at the level of the left fourth arch, the ductal origin would be from an aberrant left subclavian artery. Exceptionally, resorption of the arch at two sites may leave an isolated left subclavian artery connected to the left pulmonary artery by a ductus arteriosus. Only rarely do both right and left patent ductus arteriosi persist through fetal life; usually they close as expected after birth [7, 8].

MAPCAs, which have many other names, are a striking form of alternative systemic blood supply to the lungs. These are relatively large arteries arising from the descending aorta and aortic branches. They generally are thought to represent abnormal persistence of primitive postbranchial arteries (Fig. 2) [9] supplying the lung bud before development of the main pulmonary arteries or sixth arches. At times they may be difficult to distinguish from a patent ductus arteriosus or enlarged bronchial arteries.

MAPCAs differ from the bronchial arteries [10]. They are present as large collateral arteries at birth. Anastomoses with the intrapulmonary arteries are typically at or near the lung hilum instead of in the periphery. They may accompany bronchi but do not form nutritive plexus around bronchi. Unlike bronchial arteries, MAPCAs virtually never are connected to intercostal arteries. Intimal stenoses in the MAPCAs are usually present adjacent to an anastomosis with pulmonary arteries and/or more proximally. Most MAPCAs have an elastic wall structure resembling the central pulmonary arteries rather than the bronchial arteries. MAPCAs do not usually connect with the bronchial arteries. MAPCAs tend to maintain the same relative caliber with aging instead of progressively enlarging, as is typical of bronchial arteries in congenital heart disease.

A direct origin of the right or left pulmonary artery from the ascending aorta implies an absence of origin of these arteries from the main pulmonary artery [6].

Other systemic arteries may reach the lungs. Nature is bountiful and a number of additional possible sources of pulmonary arterial supply exist, especially from the coronary arteries.

## Anomalous Systemic Arterial Supply to the Lungs in Congenital Heart Disease

In this condition, the main abnormal development is within the pericardium. Discussion of this subject is divided into four categories, but I will give special attention to two in which one or both lungs are completely dependent on systemic blood supplies: pulmonary atresia with ventricular septal defect and absent proximal right or left pulmonary artery. Truncus arteriosus and aorticopulmonary septal defect have been excluded because of both embryologic and space considerations.

### *Pulmonary Atresia with Ventricular Septal Defect*

This is a primitive, relatively common form of congenital heart disease that is a showcase for several alternatives in pulmonary blood supply [10–17]. Before and at birth, either a patent ductus arteriosus (Fig. 3) or MAPCAs provide pulmonary blood flow. The ductus may supply both lungs or part (Fig. 4) or all of one lung. Rarely, right and left patent ductus arteriosi both persist and supply separate lung regions. Virtually never, however, do MAPCAs supply a region of lung that is or was at birth directly supplied by a patent ductus arteriosus [15]. This observation suggests that MAPCAs persist for regions that otherwise would have no source of pulmonary blood supply in early fetal life (before the eighth fetal week).

Characteristically, the lungs supplied in utero by a patent ductus arteriosus will be normally developed at birth. After birth, however, the patent ductus arteriosus tends to narrow or close and leaves the bronchial arteries, which are generally small and not developed as collateral arteries at birth, as the

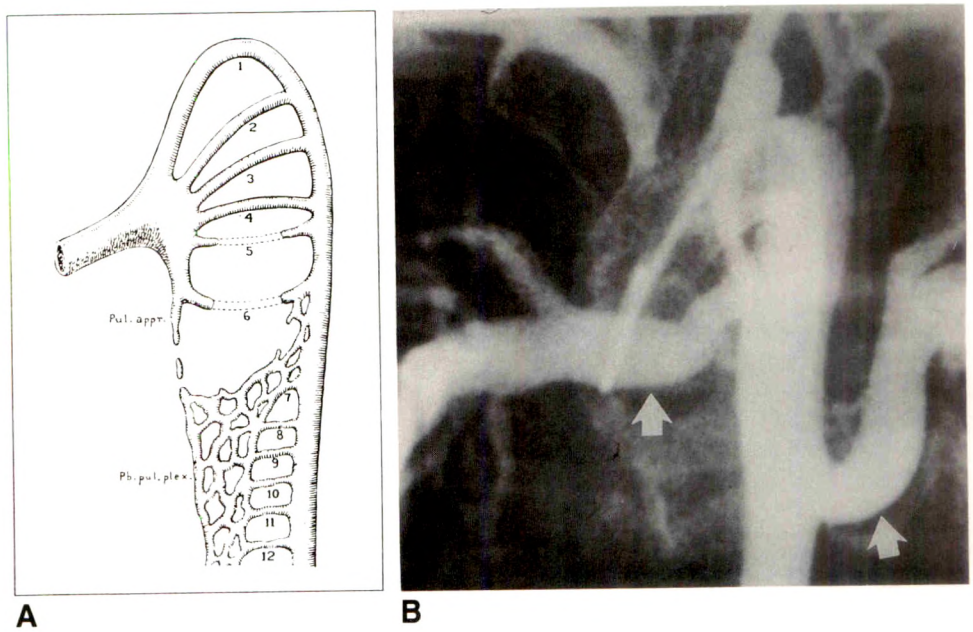



Fig. 2.—*A*, Drawing shows primitive aortic postbranchial branches (7–12) supplying pulmonary plexus (original lung-parenchyma arteries). Persistence of some of these primitive vessels apparently results in major aortopulmonary collateral arteries. Pb pul. plex. = postbranchial pulmonary plexus, Pul. appr. = pulmonary approach (of pulmonary artery) of sixth aortic arch, 1–6 = right or left set of the six aortic arches. (Reprinted with permission from Huntington [9].)

*B*, Aortogram shows patient with pulmonary atresia and ventricular septal defect with a major aortopulmonary collateral artery (*arrows*) supplying each lung from the descending aorta.

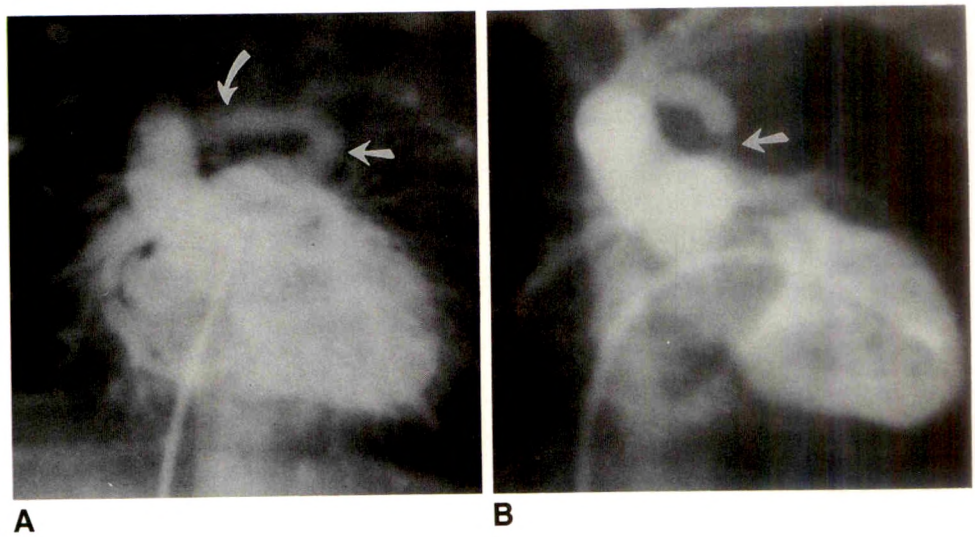



Fig. 3.—Pulmonary atresia and ventricular septal defect with pulmonary arterial blood supplied by patent ductus arteriosus.

*A*, Angiocardiogram of infant with pulmonary atresia and ventricular septal defect shows aortic arch on right and a large pulmonary artery flow supplied by a still-unobstructed left patent ductus (*straight arrow*) arising from left innominate artery (*curved arrow*).

*B*, Angiocardiogram of 6-day-old neonate with pulmonary atresia and ventricular septal defect and right aortic arch with pulmonary arterial blood supplied by patent ductus from left innominate artery. This left patent ductus, however, has closed almost completely (*arrow*). Emergent placement of a Blalock shunt (subclavian to pulmonary artery anastomosis) was lifesaving.

Both these patients are well more than 20 years later, after closure of septal defect and placement of valved conduit between right ventricle and central pulmonary artery.

only source of pulmonary blood flow. This causes severe hypoxia or death. If the infant survives, in subsequent months or years the bronchial collateral flow may greatly enlarge; some think that 5 or 6 years are required for substantial development of bronchial collaterals [17].

The MAPCAs are the main source of pulmonary blood supply in many cases (nearly half) of pulmonary atresia with VSD. These arteries are present and are large at birth. Thus, clinically the infant often has adequate (or in about 3%, excessive) pulmonary blood flow so that arterial oxygen saturation is relatively high and clinical cyanosis and symptoms are mild or not recognizable. The number of MAPCAs usually ranges from one to six arteries. They typically arise from the descending aorta but may arise from the arch or brachiocephalic branches (Fig. 5).

The pattern of these vessels is highly variable so that each patient must be evaluated individually [13, 14, 18–20]. Filling of a central continuity between native right and left pulmonary arteries can be shown in about 80% of cases, but these central arteries are often small (Fig. 6A); their size in large part is directly related to local blood flow and pressure, regardless of whether the source is a central pulmonary artery or a collateral artery. Angiographic demonstration of the central pulmonary artery continuity, the "seagull" [17], may require selective injection of multiple MAPCAs. Precise knowledge of the anatomy and physiologic function in these cases

UNIVERSITY COLLEGE LIBRARY

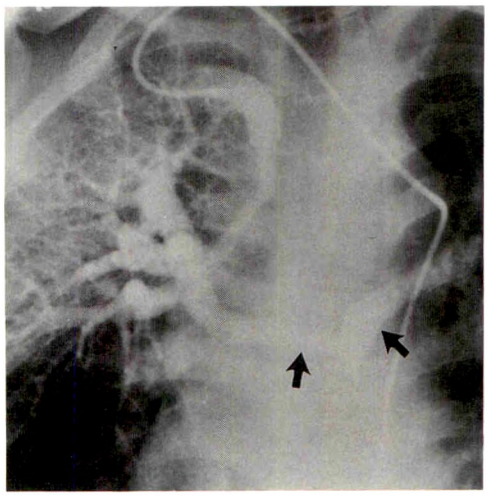


**Fig. 4.—Pulmonary atresia and ventricular septal defect with some lung segments supplied by apparent patent ductus arteriosus (PDA). Selective arteriogram shows apparent stenotic right-sided PDA supplying right upper lobe and confluence of right and left pulmonary arteries (*arrows*), a configuration resembling a seagull [17]. Not shown are three large branches of descending aorta that supplied other lung segments. Selective arteriography of these arterial branches also opacified central pulmonary artery confluence, implying interconnections within lungs.**

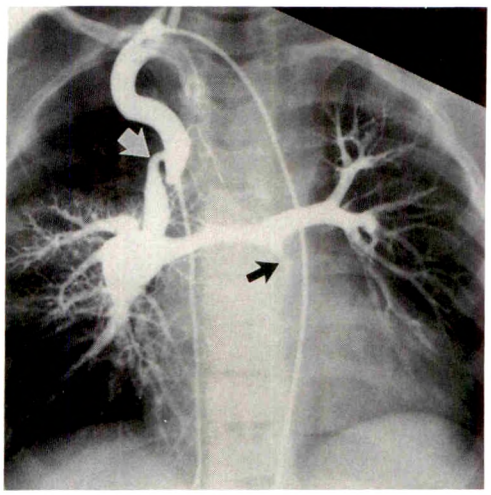


**Fig. 5.—Pulmonary atresia and ventricular septal defect with pulmonary arteries supplied by apparent major aortopulmonary collateral artery (MAPCA) arising from right internal mammary artery. Arteriogram shows filling of large internal mammary artery with stenotic branch, MAPCA (*white arrow*), which fills right hilar arteries and, retrograde, confluence of right and left pulmonary arteries, many of left segmental arteries, and hypoplastic stump of main pulmonary artery (*black arrow*). A majority of pulmonary segments were connected to central pulmonary arteries; subsequent repair was successful.**

has enabled increasingly innovative surgical repairs (Figs. 6B and 7).

*Pulmonary Stenosis and Ventricular Septal Defect (Tetralogy of Fallot) and Other Types of Complex Congenital Heart Disease, With or Without Pulmonary Obstruction*

Persistence of some patency of a ductus arteriosus [4] and development of acquired bronchial collateral circulation to the lung is common in this group. Persistence of MAPCAs is uncommon, with a prevalence of less than 1–3% in tetralogy of Fallot and about 5% in pulmonary atresia associated with more complex congenital heart disease [21].

*Absence (Atresia or Interruption) of Proximal Right or Left Pulmonary Artery*

Systemic supply to the distal pulmonary artery in this condition is provided by a patent ductus arteriosus or acquired bronchial collateral or the origin of right or left pulmonary artery directly from ascending aorta [22, 23].

MAPCAs are rare (or never occur) in this situation. Sotomora and Edwards [7], Presbitero et al. [24], and others showed that a major hilar pulmonary artery was present in nearly all cases (especially in the infant) in which the proximal right or left pulmonary artery was absent.

*Absent proximal right pulmonary artery with distal right pulmonary artery supplied by a patent ductus arteriosus or subsequently by acquired bronchial collateral circulation (Figs. 8 and 9).*—Several hundred cases have been reported in the literature with various degrees of proof of the anomaly. As the aortic arch has been on the left in nearly all cases, the right ductus supplying the right lung in utero must have arisen from the region of the right innominate artery or from an aberrant right subclavian artery in some cases. Typically, such a ductus closes spontaneously and asymptomatically after birth so that, not being suspected, its presence is seldom proved in life. Pathologically, however, a residual (typically extrapericardial), atretic cord or ductus diverticulum (e.g., from the innominate artery) may be identified (Fig. 9B) [27].

During childhood, a substantial bronchial collateral circulation is acquired. The transpleural collateral may be so marked as to cause radiologically visible pleural thickening, and rib notching may occur because of enlarged intercostal arteries. The right lung generally becomes smaller and slightly more dense than normal [25, 28]. The left-sided hilar vascular structures enlarge, whereas those on the right appear smaller than usual or are absent. Angiocardiography is the mainstay of radiologic diagnosis, but echocardiography, perfusion lung scans, CT, and MR have been used. Chronic thromboembolic occlusion of a pulmonary artery, however, can mimic congenital absence of a proximal pulmonary artery on angiography [29].

The anomaly was first recognized clinically in 1952 [25] (Fig. 8A). Patients with absent proximal right pulmonary arteries can be divided into four groups:

1. Isolated absent proximal right pulmonary artery without pulmonary hypertension. Such patients are typically asymptomatic, and the diagnosis usually is made on the basis of clinical and radiologic findings without surgical or pathologic confirmation. Pulmonary hypertension may develop eventually in some [28]. The outcome is too uncertain for a definite recommendation of surgical connection of the hilar pulmonary artery to the main pulmonary artery [28] unless pulmonary hypertension develops or cyanotic congenital heart disease is present.

2. Isolated absent proximal right pulmonary artery with

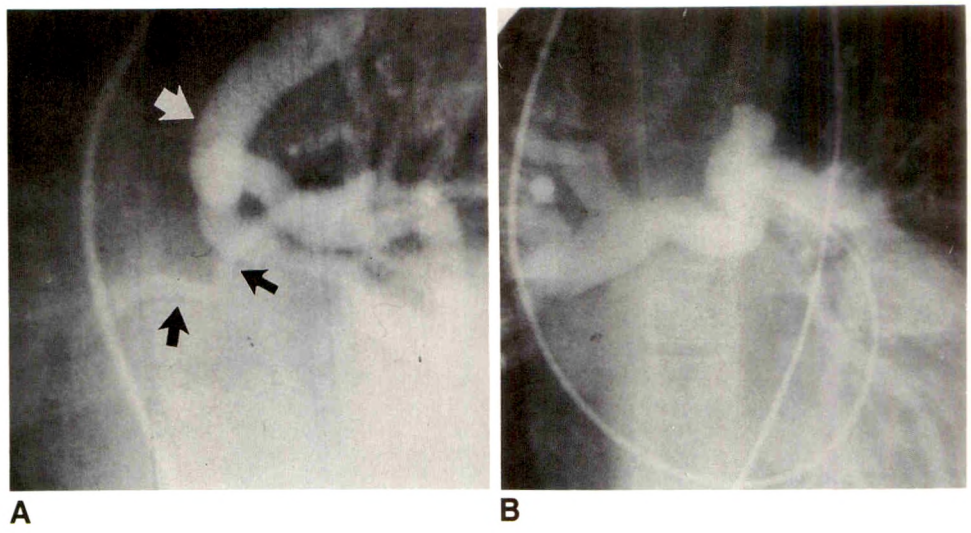


Fig. 6.—Pulmonary atresia and ventricular septal defect with markedly hypoplastic central pulmonary arteries.

*A*, Angiogram shows tiny seagull [17], or central confluence, of right and left pulmonary arteries (*black arrows*) supplied by a major aortopulmonary collateral artery (*white arrow*) in a young child.

*B*, Pulmonary arteriogram obtained several years later, after temporary placement of valveless conduit between right ventricle and central pulmonary arteries and subsequent surgical reconstruction, shows substantial enlargement of central pulmonary arteries and branches.

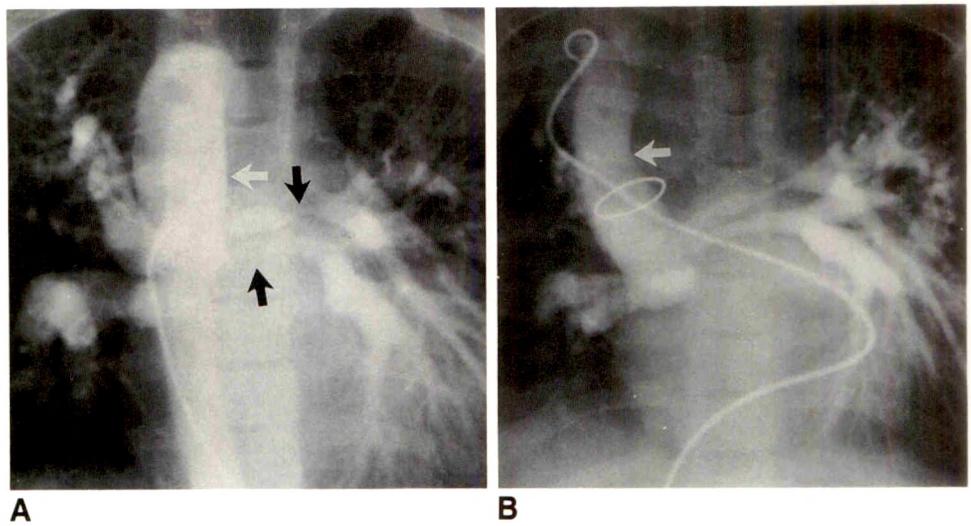


Fig. 7.—Pulmonary atresia and ventricular septal defect without central confluence of right and left pulmonary arteries.

*A*, Descending aortogram shows two major aortopulmonary collateral arteries (MAPCAs) to each lung from mid–descending aorta; those on left have stenotic segments (*black arrows*). *White arrow* labels descending aorta.

*B*, After surgical repair, selective injection shows distal portion (*arrow*) of long valved conduit from right ventricle to short segment of descending aorta from which MAPCA in *A* arose. Not shown is bypass graft from proximal to distal descending aorta and closed ventricular septal defect.

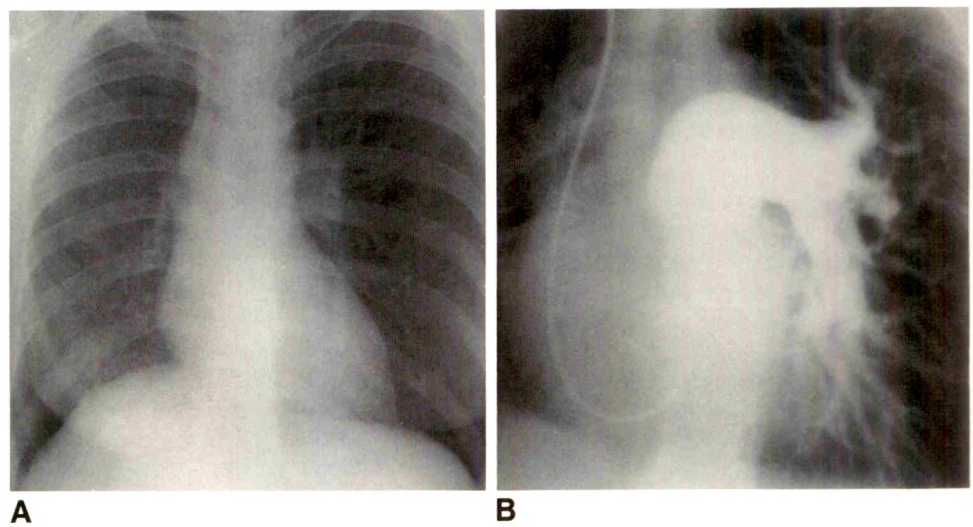
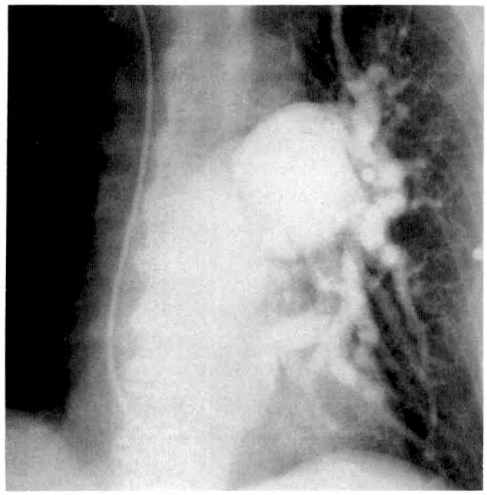


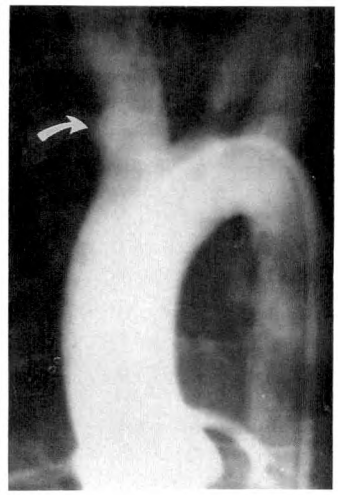
Fig. 8.—Congenital absence of proximal right pulmonary artery with pulmonary blood supplied by patent ductus arteriosus and/or acquired bronchial collateral.

*A*, Chest radiograph of a 31-year-old mother of six with mild pulmonary hypertension shows typical reduction of right lung and small hilar shadow. Seventeen years earlier she had had normal pulmonary artery pressures when reported as the first case diagnosed clinically [25]. (Courtesy of E. A. Gaensler, Boston.)

*B*, Pulmonary angiogram of 66-year-old woman with absent right pulmonary artery and moderate pulmonary hypertension.



A



B

Fig. 9.—Congenital absence of proximal right pulmonary artery with pulmonary blood supply by patent ductus arteriosus or acquired bronchial collateral or both.

*A*, Pulmonary angiogram of 80-year-old man shows absent proximal right pulmonary artery. Pulmonary artery pressure was 45/22 mm Hg (mean, 35 mm Hg). Forty years earlier, life-threatening pulmonary edema had developed while he was hunting at a high altitude. A remarkable sensitivity of these patients to high-altitude pulmonary edema has been recognized [26].

*B*, Aortogram in asymptomatic 17-year-old man with congenital absence of right pulmonary artery and normal main and left pulmonary artery pressures shows slight bulge (*arrow*) protruding from innominate artery, which is a typical remnant of right-sided ductus arteriosus that had supplied right pulmonary artery up to time of birth [7, 27, 28]. (Courtesy of E. A. Gaensler, Boston.)

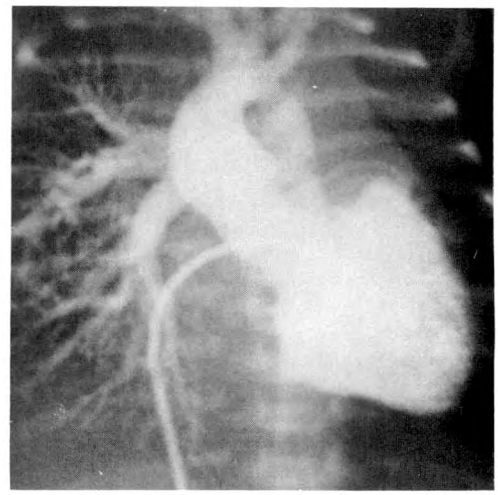


Fig. 10.—Origin of right pulmonary artery from ascending aorta (absence of normal origin of right pulmonary artery from main pulmonary artery). Selective left ventriculogram in 5-day-old neonate shows a large right pulmonary artery that arose from posterior aspect of proximal ascending aorta. A right ventriculogram had shown only left pulmonary artery arising from main pulmonary artery; normal origin of right pulmonary artery was absent. Surgical transfer of origin of this right pulmonary artery to main pulmonary artery was curative (pulmonary pressures were normal 10 years later).



A



B

Fig. 11.—Congenital absence of proximal left pulmonary artery (with left lung supplied by closing patent ductus arteriosus) in tetralogy of Fallot.

*A*, Right ventriculogram of 2-day-old neonate shows severe infundibular stenosis (*black arrow*). A large right-to-left shunt via a ventricular septal defect opacifies a large right aortic arch. No filling of left pulmonary artery is seen because of congenital absence of proximal left pulmonary artery. *White arrow* labels main pulmonary artery.

*B*, Left ventriculogram shows right aortic arch even better and shows a large branch of left innominate artery, which opacifies left pulmonary artery. This is a left-sided patent ductus arteriosus, arising as expected on side opposite aortic arch from left innominate artery. Distal patent ductus arteriosus (*arrow*) is almost completely closed; it was closed 1 day later.

pulmonary hypertension. Patients may be any age, but most are infants and young children. Surgical connection of the right hilar artery to the main pulmonary artery can be lifesaving and should be considered prophylactically [18, 23]. Pulmonary hypertension may be occult, and such patients appear to be remarkably vulnerable to development of high-altitude pulmonary hypertension and edema (Fig. 9A) [26].

3. Isolated absent proximal right pulmonary artery with intractable pulmonary infection or hemoptysis from the right lung. Resection or bronchial artery embolization may be required. Some of the lungs are susceptible to infection because of malformations of the lung parenchyma [18]. Hemoptysis usually is related to the bronchial collateral circulation.

4. Absent proximal right pulmonary artery with left patent ductus arteriosus or other congenital heart disease (about 15% of all patients with absent proximal right pulmonary arteries). All of the patients with left patent ductus arteriosus or other congenital heart disease with left-to-right shunts have pulmonary hypertension. They generally benefit greatly from closure of the shunt. Anastomosis of the right hilar artery to the main pulmonary artery may offer further benefit [18].

Fortunately, the majority apparently are in the first group.

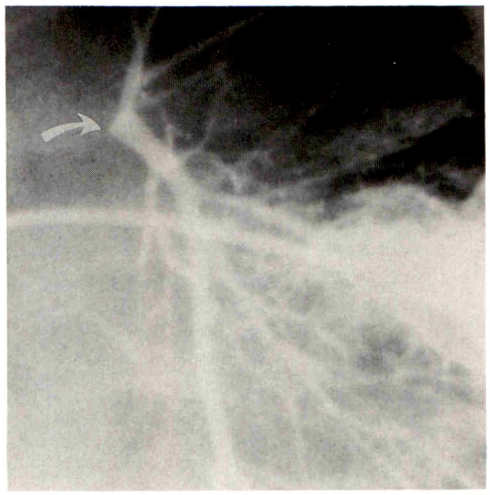


**Fig. 12.—Congenital absence of proximal left pulmonary artery without other congenital heart disease (except right aortic arch). Selective injection via catheter wedged into a left pulmonary vein results in excellent retrograde filling of atrophied peripheral portion of proximally occluded left pulmonary artery (*arrow*) in an asymptomatic 11-year-old girl. Until birth, this artery presumably was supplied by a left patent ductus arteriosus from left innominate artery. After closure of patent ductus arteriosus after birth, left pulmonary artery and lung have atrophied, with only an acquired bronchial collateral type of pulmonary blood supply.**

Exercise tolerance is usually good, and survival may be long despite pulmonary hypertension in some (Figs. 8 and 9A).

*Absent proximal right pulmonary artery with origin of distal right pulmonary artery from ascending aorta (Fig. 10).*—Anomalous origin of a pulmonary artery from the ascending aorta has been studied recently by Kutsche and Van Mierop [6]. They were able to collect and analyze 108 cases, 89 on the right and 19 on the left. No relationship was found to truncus arteriosus. All of the 89 cases with the right pulmonary artery from the ascending aorta had a left aortic arch, and more than two thirds had a patent ductus arteriosus on the left; many were infants. Fourteen also had aorticopulmonary septal defects; eight of these had coarctation or an interrupted aortic arch, but other congenital heart disease was uncommon. (Kutsche and Van Mierop [6] rejected a number of cases in which the right pulmonary artery arose from the region of the innominate artery; all of these were regarded as persistent right-sided patent ductus arteriosi).

Typically, pulmonary hypertension and high pulmonary blood flow result in congestive heart failure and death in early childhood, even if no other anomalies are present [30]. Plain chest films show cardiomegaly and increasing vascular engorgement. Surgery in early infancy with transfer of the origin of the right pulmonary artery from the ascending aorta to the main pulmonary artery is quite regularly a curative procedure. The operative risks, however, progressively increase as the pulmonary resistance rapidly rises in the first months after birth.

*Absent proximal left pulmonary artery with distal left pulmonary artery supplied by a patent ductus arteriosus or acquired bronchial collateral circulation.*—This anomaly is typically associated with congenital heart disease [22], usually tetralogy of Fallot (Fig. 11). The aortic arch can be either right- or left-sided but is nearly always right-sided when other congenital heart disease is absent (Fig. 12). In some infants, if congenital heart disease is symptomatic, angiocardiography may be performed early enough in infancy to show a patent ductus supplying the peripheral left pulmonary artery (Fig. 11). Presbitero et al. [24] performed surgical exploration in four infants with right aortic arch and absent origin of the left pulmonary artery. Each infant had an extrapericardial ligamentum connecting the left innominate artery to the left pulmonary artery. The authors suggested that early embryologic involution of the proximal left pulmonary artery had occurred, leaving the left ductus arteriosus to supply the left lung in utero.

The same authors also performed surgical exploration in five infants with left aortic arch and absent left pulmonary artery. Each infant had an intrapericardial left pulmonary artery in continuity with the (left) hilar vessels, even though the left pulmonary artery was occluded proximally. All of these cases also had severe pulmonary outflow tract obstruction and a left ductus that descended vertically from under the aortic arch, as is characteristic of anomalies dependent on reversed ductal flow in utero (i.e., flow from aorta to pulmonary artery), such as pulmonary atresia with ventricular septal defect [31]. The authors postulated that this type of absent left pulmonary artery may be acquired after birth as a result of narrowing or closure of the ductus.

In 1986, Elzenga and Gittenberger-deGroot [32], in a large pathologic study of the pulmonary arteries in pulmonary atresia, found left pulmonary artery stenosis (or atresia in one case) in 16 of 20 cases with left aortic arch and left ductus. The left pulmonary stenosis or atresia occurred exclusively in relation to the ductus and in the segment of the artery between the main pulmonary trunk and the ductus. The majority of cases also had a ridge on the interior wall of the pulmonary artery opposite the site of ductal entry [32, 33] (analogous to the aortic shelf found opposite the entry of the ductus in classic coarctation of the aorta). Thus, absence of the proximal left pulmonary artery with left aortic arch appears to develop with ductal closure after birth almost exclusively in patients with pulmonary atresia (or severe pulmonary stenosis) and ventricular septal defect.

On the other hand, absence of the proximal left pulmonary artery with right aortic arch appears to develop long before birth. The hilar left pulmonary artery is supplied in utero by a patent ductus arteriosus arising from the region of the innominate artery, and the intrapericardial left pulmonary artery may be absent (Fig. 11).

Particularly in the clinically cyanotic infant with an absent proximal left pulmonary artery, early consideration should be given to surgical exploration of the left hilum, with the goal of creating a systemic shunt or main pulmonary artery anastomosis to the hilar artery [24]. Successful operations not only provide additional pulmonary blood flow but also may keep the peripheral left pulmonary artery large and available for future procedures and permit more normal maturation of the left lung.

*Absent proximal left pulmonary artery with origin of the distal left pulmonary artery from the ascending aorta.*—This condition is much less common than right pulmonary artery

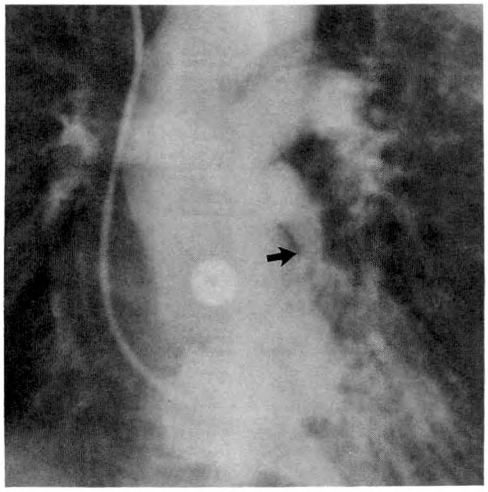


**Fig. 13.—Origin of left pulmonary artery from ascending aorta in tetralogy of Fallot (absence of normal origin of left pulmonary artery from main pulmonary artery). Right ventriculogram shows infundibular stenosis (*arrow*). Large right-to-left shunt opacifies left ventricle and aorta, including left aortic arch. Relatively large left pulmonary artery arises directly from ascending aorta and not from pulmonary artery.**

from the ascending aorta; only 19 cases were in the 1988 review by Kutsche and Van Mierop [6]. Fourteen (74%) of these had tetralogy of Fallot. All cases had either tetralogy of Fallot or a right aortic arch or both. Half of these patients had an anomalous origin of a subclavian artery and three had a right-sided patent ductus arteriosus, but none had an aorticopulmonary septal defect or coarctation.

The majority with tetralogy of Fallot survive infancy with the possible advantage of some extra pulmonary flow via the anomalous connection. In the case illustrated (Fig. 13), the tetralogy was corrected and the left pulmonary artery origin was transferred to the main pulmonary artery with a good clinical result. The left lung, however, had a low flow because of presumed acquired high peripheral pulmonary vascular resistance. The diagnosis usually is made on the basis of angiocardiography, although echocardiography, MR, and CT may be helpful.

I studied an infant with left pulmonary artery origin from the ascending aorta and right arch but no other congenital heart disease in whom severe congestive heart failure occurred in infancy. Immediate surgical correction appeared to be lifesaving. This infant clinically resembled those with right pulmonary artery from the ascending aorta.

### *Coronary Artery to Pulmonary Artery and Other Systemic Arterial Connections to the Lungs*

Tiny anastomoses between the coronary arteries and mediastinal branches of the bronchial arteries evidently are present at all ages. These connections may enlarge under conditions stimulating increased bronchial blood flow and have been shown on many occasions, especially by coronary arteriography [18, 34]. A few cases have been reported in which a proximal fistula between a major coronary artery and the main or proximal right or left pulmonary artery is the major supplier of pulmonary blood flow, nearly always in the context of pulmonary atresia with a ventricular septal defect [35].

Unique cases continue to be encountered [18]. Both pulmonary arteries may arise directly from the ascending aorta. A heart with three arterial trunks has been described, an extra one from the left ventricle supplying the left lung [36]. It is not possible to encompass all of the variations found in nature.

In this review the focus is on developmental abnormalities in the systemic arterial supply to the lung in situs solitus (normal visceroatrial situs). Analogous connections may be observed in situs inversus or situs ambiguous. Also, surgical intervention may be responsible for alterations in the pulmonary blood supply. Many surgical procedures are possible so that a precise accurate history is invaluable when prior surgery has been performed.

## Anomalous Systemic Arterial Supply to the Lungs in Congenital Lung Disease

No classification of congenital lung disease has been generally accepted. In recent years, experts in the field have tended to regard the major clinical pulmonary anomalies as a spectrum. For example, Panicek et al. [37] defined a continuum of pulmonary developmental anomalies including congenital lobar emphysema, bronchogenic cyst, congenital cystic adenomatoid malformation, bronchopulmonary sequestration, hypogenetic lung syndrome (scimitar syndrome), and pulmonary arteriovenous malformation. Only sequestration and the hypogenetic lung syndrome (scimitar syndrome) have been consistently associated with a high prevalence of systemic arterial supply by large anomalous aortic branches (MAPCAs). This review discusses bronchopulmonary sequestrations, acquired sequestrations, hypogenetic lung syndrome (scimitar syndrome), and other congenital lung disease with anomalous systemic arterial connections.

### *Bronchopulmonary Sequestration*

In the late 1940s, Pryce et al. [38, 39] described and named intralobar sequestration of the lung, clinically the most common of the major lung anomalies. They presented a total of eight cases and found only three others had been reported previously. The abnormality was twofold: (1) a large anomalous systemic artery arising from the aorta near the diaphragm, which supplied (2) a congenital bronchopulmonary dislocation (sequestration or ectopia).

The large artery (Fig. 14), not related to a cardiac malformation, typically enters the lung via the pulmonary ligament and generally has an elastic wall resembling a pulmonary artery rather than a bronchial artery. The arterial distribution may be just to the sequestered lung, or it may include adjacent normal lung. The anomalous artery was considered a persistent primitive aortic branch (MAPCA) that originally had supplied the developing lung bud. Atheromatous changes commonly are found in these arteries after infancy. Venous drainage is nearly always via the pulmonary veins.

A congenital intralobar sequestration is dissociated from

the normal bronchial tree and nearly always [40] is located in the posterior medial base of the lung. The parenchyma of such sequestrations characteristically is cystic, single or multiple. The sequestered, and therefore obstructed, bronchi may be distended by plugs of mucus. Inflammatory changes are common because infection tends to become chronic in these poorly draining regions. Rarely, sequestration is bilateral, and whole lobes or even the entire lungs may be involved.

Pryce [38] also recognized extralobar sequestrations (Fig. 15), lung tissue with its own visceral pleura separate from the normal lungs, usually a mass between the lung and the diaphragm or liver and often associated with diaphragmatic hernias. These anomalies were called lower accessory lungs. Extralobar sequestrations also are supplied by anomalous aortic branches but nearly always drain into the systemic veins (azygous system or inferior vena cava). Pryce [38] noted that 40 of 43 previously reported extralobar sequestrations were on the left. They generally contain no air and do not communicate with the bronchial tree or lungs.

Since 1947, many additional examples of sequestration anomalies have been reported, including some with fistulous connections to other foregut derivatives such as the esophagus and stomach [41]. By 1979, Savic et al. [42] were able to review 540 reported sequestrations, 400 of which were intrapulmonary sequestrations. The large systemic artery (MAPCA) averaged 6–7 mm in diameter and arose from the lower thoracic or upper abdominal aorta in both types of sequestration. In 15-20%, the arteries were multiple. Savic et

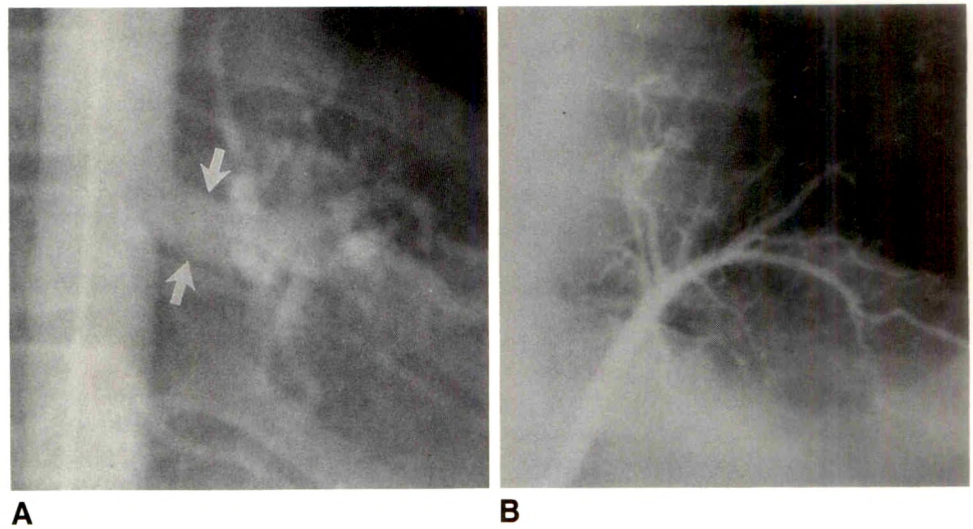



**Fig. 14.—Anomalous major aortopulmonary collateral arteries supplying intralobar sequestrations.**

***A*, Aortogram in 7-year-old boy shows aortic branch (*arrows*) supplying intralobar sequestration.**

***B*, Selective arteriogram in 22-year-old patient shows large aortic branch supplying intralobar sequestration.**

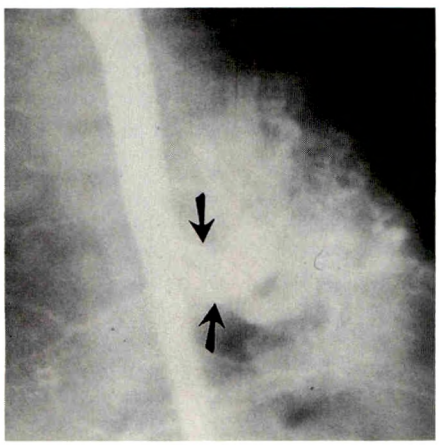


**Fig. 15.—Extralobar sequestration presenting with congestive heart failure in infancy. Descending thoracic aortogram in infant with clinical congestive heart failure shows two large arteries (*arrows*), considered major aortopulmonary collateral arteries, richly supplying extralobar sequestration at base of left hemithorax. Venous drainage was from a large hemiazygous vein to a left superior vena cava, coronary sinus, and right atrium.**

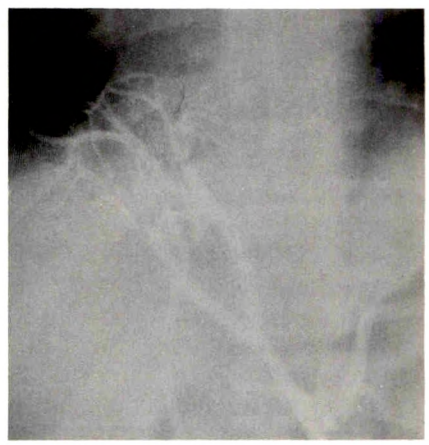


**Fig. 16.—Scimitar syndrome with large aortic branch to right lung. Selective arteriogram in a 20-year-old woman with scimitar syndrome shows large artery from aorta supplying right lung base.**



**Fig. 17.—Large systemic arteries considered major aortopulmonary collateral arteries (MAPCAs) supplying a systemic to pulmonary arteriovenous fistula in otherwise apparently normal lung. Aortogram in infant shows two large arteries (MAPCAs) supplying left lower lung. Severe congestive heart failure resolved after ligation of arteries, which were supplying an apparent arteriovenous fistula. No bronchial sequestration was found.**

al. [42] apparently showed in 1971 that sequestered lung is not supplied by bronchial arteries.

The first radiologic sign of a sequestration is usually a paraspinal opacity or an air/fluid–filled cavity or cyst in the lower lung field. Aortography is the most definitive technique for establishing the presence and position of the large anomalous systemic artery, although CT, Doppler sonography, and MR imaging all have been valuable at times. Intractable infection, hemoptysis, and, occasionally, congestive heart failure may require surgical intervention. It is most important that the diagnosis be considered preoperatively so that the surgeon will be alert to the presence of large anomalous systemic arteries.

### *Acquired Intrapulmonary Sequestrations*

Remarkably, large systemic collateral arteries to the lung can be acquired [43], mainly reaching the lungs by the pulmonary ligaments, which normally carry only tiny arteries from the aorta to the lung [44]. Such large aortic branches may evolve in relation to bronchiectasis, other chronic inflammation, or previous surgery for cyanotic congenital heart disease. Such observations, together with a low prevalence of intralobar (compared with extralobar) sequestration in the neonate at autopsy [45], have raised the question as to whether many intralobar sequestrations are truly congenital anomalies. Confusion is most likely when an acquired inflammatory process with abscess is located in the posterior medial lung base. Webb and Jacobs [46] noted that such an acquired systemic arterial collateral tends to derive from the inferior phrenic arteries and become a tangle of small vessels at the pleural surface. In many cases it may not be possible to prove whether a large systemic collateral artery is of congenital or acquired origin. These considerations led Felson [47] to concede that some cases of "sequestration" are acquired.

### *Hypogenetic Lung Syndrome (Scimitar Syndrome)*

The scimitar image [48], resembling a Turkish sword, is produced on the frontal chest radiograph by an anomalous pulmonary vein that usually drains all or part of the right lung into the inferior vena cava just above or below the diaphragm (Fig. 16). Often a large anomalous systemic artery (MAPCA) arising from the lower thoracic or upper abdominal aorta or inferior phrenic artery supplies at least the basal part of the maldeveloped right lung. The right lung is to a variable degree malformed and usually hypoplastic, most commonly with only two lobes and a hypoarterial bronchus, thus resembling an anatomic left lung. Dextrocardia associated with a smaller right lung may be marked. About one fourth of the patients have congenital heart disease, most often atrial septal defects [49]. Other anomalies are associated, such as bronchial cysts or diverticula, horseshoe lung, accessory diaphragm, or hernias. A spectrum of variations occurs with each feature of the scimitar syndrome. Several cases have had an associated bronchopulmonary sequestration [18].

### *Other Congenital Lung Disease with Anomalous Systemic Arterial Connections*

Large aortic branches (MAPCA) apparently have been encountered in at least three of more than 200 reported cases of congenital cystic adenomatoid malformation of the lung [10]. A number of reports have mentioned a combination of intralobar sequestration and cystic adenomatoid malformation. Virtually all of the other major congenital pulmonary anomalies have been described in at least one case as having an associated large systemic MAPCA.

Some other unusual systemic vascular connections to the pulmonary arteries have been encountered. These include rare congenital pulmonary arteriovenous fistulae with a large systemic arterial supply from the chest wall [50].

## Anomalous Systemic Arterial Supply to Apparently Normal Lung

Rounding out the spectrum of anomalous systemic arterial supply to the lung is the rare case in which an MAPCA supplies apparently normal lung [51–55] (i.e., overt congenital heart or lung disease is absent). The artery typically is large, drainage is by the pulmonary veins, and the lung bases are involved most often. The systemic arterial supply may be accessory [51] to the normal pulmonary artery supply, it may substitute [52] for the normal pulmonary artery, or it may supply extremely rapid flow to a region of such low vascular resistance that the connection can be regarded as an arteriovenous fistula [53, 54]. Although most patients have been asymptomatic, congestive heart failure can occur even in the neonate (Fig. 17) [55]. Continuous murmurs are common.

The cause for persistence of these remnants of the embryonic arterial circulation is not known. Few cases have been studied in great detail. As suggested by Pryce [38], these rare anomalies are perhaps best regarded as a mild form of the process that, when more severe, can cause both persistence of a primitive arterial connection (MAPCA) and sequestration of the bronchi of a portion of lung.

## Conclusions

This limited review of the various forms of normal and anomalous systemic arterial supply to the lungs has shown the following: (1) The bronchial arteries offer an acquired collateral systemic blood supply, typically developing after birth. (2) One or two patent ductus arteriosi may supply the central pulmonary arteries or exclusively part or all of the right or left pulmonary artery, especially when pulmonary stenosis or atresia is present. Such patent ductus arteriosi usually narrow or close as expected after birth, inducing an acquired bronchial collateral circulation. (3) Primitive MAPCAs develop in the early embryo and may persist if not supplanted by the normal pulmonary arteries. They are characteristic of pulmonary atresia with ventricular septal defect, of pulmonary sequestration, and perhaps of the scimitar syndrome. Rarely they persist in other anomalies or to supply otherwise normal lungs. (4) The origin of the right or left pulmonary artery rarely can be from the ascending aorta in the absence of normal origin from the main pulmonary artery. (5) Anomalous systemic blood supply is usually a response to congenital absence (or failure of development) of the normal pulmonary blood supply in the context of congenital heart or lung disease.

ACKNOWLEDGMENTS

I appreciate the support of many colleagues in radiology, pediatric and adult cardiology, cardiothoracic surgery, and the pediatric and

adult cardiovascular laboratories of the Columbia-Presbyterian Medical Center and the inspiration of Melvin M. Figley.

## REFERENCES


1. Liebow AA. Patterns of origin and distribution of the major bronchial arteries in man. *Am J Anat* **1965**;117:19–32
2. Deffebach ME, Charan NB, Lakshminarayan S, Butler J. The bronchial circulation. *Am Rev Respir Dis* **1987**;135:463–481
3. Boyden EA. Time lag in the development of bronchial arteries. *Anat Rec* **1970**;166:611–614
4. Cassels D, Bharati S, Lev M. The natural history of the ductus arteriosus in association with other congenital cardiac defects. *Perspect Biol Med* **1975**;18:541–572
5. Congdon ED. Transformation of the aortic-arch system during development of the human embryo. *Carnegie Inst Contrib Embryol* **1922**;14:47–110
6. Kutsche LM, Van Mierop LHS. Anomalous origin of a pulmonary artery from the ascending aorta: associated anomalies and pathogenesis. *Am J Cardiol* **1988**;61:850–856
7. Sotomora RF, Edwards JE. Anatomic identification of so-called absent pulmonary artery. *Circulation* **1978**;57:624–633
8. Freedom RM, Moes CAF, Pelech A, et al. Bilateral ductus arteriosus (or remnant): an analysis of 27 patients. *Am J Cardiol* **1984**;53:884–891
9. Huntington GS. The morphology of the pulmonary artery in the mammalia. *Anat Rec* **1919**;17:165–201
10. Macartney F, Haworth SG. Investigation of pulmonary atresia with ventricular septal defect. In: Anderson RH, Macartney FJ, Shinebourne EA, Tynan M. *Paediatric cardiology*, vol. 5. New York: Churchill-Livingstone, **1983**;111–125
11. Jefferson K, Rees S, Somerville J. Systemic arterial supply to the lungs in pulmonary atresia and its relation to pulmonary artery development. *Br Heart J* **1972**;34:418–427
12. Bharati S, Paul MH, Idriss FS, Potkin RT, Lev M. The surgical anatomy of pulmonary atresia with ventricular septal defect: pseudotruncus. *J Thorac Cardiovasc Surg* **1975**;69:713–721
13. Rees S. Arterial connections of the lung: the inaugural Keith Jefferson lecture. *Clin Radiol* **1981**;32:1–15
14. Davis GD, Fulton RE, Ritter DG, Mair DD, McGoon DW. Congenital pulmonary atresia with ventricular septal defect: angiographic and surgical correlates. *Radiology* **1978**;128:133–144
15. Frescura C, Talenti E, Pellegrino PA, Mazzuco A, Faggian G, Thiene G. Coexistence of ductal and systemic pulmonary arterial supply in pulmonary atresia with ventricular septal defect. *Am J Cardiol* **1984**;53:348–349
16. Liao P, Edwards WD, Julsrud PR, Puga FJ, Danielson GK, Feldt RH. Pulmonary blood supply in patients with pulmonary atresia and ventricular septal defect. *J Am Coll Cardiol* **1985**;6:1343–1350
17. Somerville J. Clinical identification of the pulmonary blood supply in pulmonary atresia. In: Anderson RH, Neches WH, Park SC, Zuberbuhler JR, eds. *Perspectives in pediatric cardiology*, vol. 1. Mount Kisco, NY: Futura, **1988**:155–168
18. Ellis K. The bronchial arteries and anomalous systemic arteries to the lungs in congenital heart and lung disease. In: Butler J, ed. *The bronchial circulation*. New York: Marcel Dekker (in press)
19. Levin DC, Baltaxe HA, Goldberg HP, et al. The importance of selective angiography of the systemic arterial to the lungs in planning surgical correction of pseudotruncus arteriosus. *AJR* **1974**;121:606–613
20. Hruda J, Julsrud PR. Diagnostic selective balloon occlusion technique in pulmonic valve atresia and ventricular septal defect. *Am J Cardiol* **1989**;63:1408–1409
21. Marino B, Calabro R, Gagliardi MG, Bevilacqua W, Ballerini L, Marcelletti C. Patterns of pulmonary arterial anatomy and blood supply in complex congenital heart disease with pulmonary atresia. *J Thorac Cardiovasc Sug* **1987**;94:518–520
22. Pool PE, Vogel JHK, Blount SG. Congenital unilateral absence of a pulmonary artery. *Am J Cardiol* **1962**;10:706–732
23. Shakibi JG, Rastan H, Nazarian I, Paydar M, Aryanpour I, Siassi B. Isolated unilateral absence of the pulmonary artery. *Jpn Heart J* **1978**;19:439–451
24. Presbitero P, Bull C, Haworth SG, deLeval MR. Absent or occult pulmonary artery. *Br Heart J* **1984**;52:178–185
25. Madoff IM, Gaensler EA, Strieder JW. Congenital absence of the right pulmonary artery. *N Engl J Med* **1952**;247:147–157
26. Hackett P, Creagh CE, Grover RF, et al. High altitude pulmonary edema in patients without the right pulmonary artery. *N Engl J Med* **1980**;302:1070–1073
27. Pfefferkorn JR, Loser H, Pech G, Toussaint R, Hilgenberg F. Absent pulmonary artery: a hint to its embryogenesis. *Pediatr Cardiol* **1982**;3:283–286
28. Ferguson A, Belleau R, Gaensler EA. Congenital absence of one pulmonary artery. *Respiration* **1969**;26:300–312
29. Moser KM, Olson LK, Schlusselberg M, Daly PO, Dembitsky WP. Chronic thromboembolic occlusion in adult can mimic pulmonary artery agenesis. *Chest* **1989**;95:503–508
30. Griffiths SP, Levine OR, Anderson DH. Aortic origin of the right pulmonary artery. *Circulation* **1962**;25:73–84
31. Santos MA, Moll JN, Drumond C, Araujo WB, Roma O, Reis NB. Development of the ductus arteriosus in right ventricular outflow tract obstruction. *Circulation* **1980**;62:818–822
32. Elzenga NJ, Gittenberger-de Groot AC. The ductus arteriosus and stenoses of the pulmonary arteries in pulmonary atresia. *Int J Cardiol* **1986**;11:195–208
33. Mommo K, Takao A, Ando M, et al. Juxtaductal pulmonary artery obstruction in pulmonary atresia. *Br Heart J* **1986**;55:39–44
34. Thompson JA, Lewis SA, Mauck HP. Absence of left pulmonary artery: anomalous collateral from coronary artery to affected lung. *Am Heart J* **1986**;111:418–420
35. Pahl E, Fong L, Anderson RA, Park SC, Zuberbuhler JR. Fistulous communications between a solitary coronary artery and the pulmonary arteries as a primary source of pulmonary blood supply in tetralogy of Fallot with pulmonary atresia. *Am J Cardiol* **1989**;63:140–143
36. Diaz-Gongora G, Quero-Jiminez M, Espino-Vela J, Arteaga M, Bargeron LM Jr. A heart with three arterial trunks (tritruncal heart): report of a case. *Pediatr Cardiol* **1982**;3:293–299
37. Panicek DM, Heitzman ER, Randall PA, et al. The continuum of pulmonary developmental anomalies. *RadioGraphics* **1987**;7:747–772
38. Pryce DM. Lower accessory pulmonary artery with intralobar sequestration of lung: report of seven cases. *J Pathol* **1946**;58:457–467
39. Pryce DM, Sellors TH, Blair LG. Intralobar sequestration of lung associated with an abnormal pulmonary artery. *Br J Surg* **1947**;35:18–29
40. Hoeffel J, Bernard C. Pulmonary sequestration of the upper lobe in children. *Radiology* **1986**;160:513–514
41. Gerle RD, Jaretzki A III, Ashley CA, Berne AS. Congenital bronchopulmonary-foregut malformation. *N Engl J Med* **1968**;278:1413–1419
42. Savic B, Birtel FJ, Tholen W, Funke HD, Knoche R. Lung sequestration: report of seven cases and review of 540 published cases. *Thorax* **1979**;34:96–101
43. Gebauer PW, Mason CB. Intralobar pulmonary sequestration associated with anomalous pulmonary vessels: a nonentity. *Chest* **1959**;35:282–288
44. Stocker JT, Malczak HT. A study of pulmonary ligament arteries: relationship to intralobar pulmonary sequestration. *Chest* **1984**;86:611–615
45. Stocker JT. Sequestration of the lung. *Semin Diagn Pathol* **1986**;3:106–121
46. Webb WR, Jacobs RP. Transpleural abdominal systemic artery: pulmonary artery anastomosis in patients with chronic pulmonary infection. *AJR* **1977**;129:233–236
47. Felson B. Pulmonary sequestration revisited. *Med Radiogr Photogr* **1988**;64:1–27
48. Neill CA, Ferenz C, Sabiston DC, Sheldon H. The familial occurrence of hypoplastic right lung with systemic arterial supply and venous drainage "scimitar syndrome." *Johns Hopkins Med J* **1960**;107:1–21
49. Kiely B, Filler J, Stone S, Doyle EF. Syndrome of anomalous venous drainage of the right lung to the inferior vena cava. *Am J Cardiol* **1967**;20:102–116
50. Burke CM, Safai C, Nelson DP, Raffin TA. Pulmonary arteriovenous malformations: critical update. *Am Rev Respir Dis* **1986**;134:334–339
51. Boyden EA. *Segmental anatomy of the lungs*. New York: McGraw-Hill, **1955**:227
52. Hessel EA II, Boyden EA, Stamm SJ, Sauvage LR. High systemic origin of the sole artery to the basal segments of the left lung: findings, surgical treatment, and embryologic interpretation. *Surgery* **1970**;67:624–632
53. Currarino G, Willis K, Miller W. Congenital fistula between aberrant systemic artery and a pulmonary vein without sequestration. *J Pediatr* **1975**;87:554–557
54. Kirks DR, Kane PE, Free EA, Taybi H. Systemic arterial supply to normal basilar segments of left lower lobe. *AJR* **1976**;126:817–821
55. Litwin SB, Plauth WH, Nadas AS. Anomalous systemic arterial supply to lung causing pulmonary hypertension. *N Engl J Med* **1970**;283:1098–1099

# Book Review

**Clinical Profiles of Diffuse Interstitial Pulmonary Disease.** By Richard A. DeRemee. Mt. Kisco, NY: Futura, 203 pp., 1990. $43

Richard DeRemee is an eminent pulmonologist. He is both an academician and a clinician, and he is respected equally for his contributions to the pulmonary literature and for his skill and dedication in caring for patients with pulmonary disease. He states in the introduction that his purpose in writing this book was to create a "compilation and synthesis of the kind of information needed by a clinician who is caring for patients." Clinicians, as he goes on to say, do not need to understand "sophisticated nuances of physiology and pathology to be first-rate," but they "must be highly sophisticated in ['clinicology']." Clinicology, according to DeRemee, is a discipline devoted to the cobbling together of relevant bits of knowledge from various other "ologies" (e.g., pathology, radiology, microbiology) to form a structured, clinically useful approach to the diagnosis and treatment of disease. To this end, he presents "a distillate of knowledge concerning a clinical approach to interstitial pulmonary disease" and voices his hope that the "use of this basic fundamental approach, avoiding the ultracurrent, almost sensational, newer data cascading from research, will provide a message that will be durable."

DeRemee largely has succeeded in realizing his objectives; his book details a pragmatic, down-to-earth approach to the diagnosis and treatment of interstitial lung disease. In many ways, this monograph is like a conversation with a favorite uncle; the tone is conversational, and the content is eclectic (including alveolar proteinosis in a book about interstitial lung disease) and, by turns, factual (lucid discussions of abnormalities in pulmonary function associated with interstitial lung disease and the correct way to diagnose digital clubbing), anecdotal (the tale of how Velcro got its name and the author's experience in using colchicine to treat idiopathic pulmonary fibrosis), and apocryphal (Kerley B lines are "dilated lymphatics," open lung biopsy specimens should be taken from the most radiologically abnormal areas of the lung, and eggshell calcifications of the hilar lymph nodes are "characteristic" of longstanding sarcoidosis), but always interesting.

The book is composed primarily of a number of algorithmic syntheses. Each synthesis deals with a specific disease (e.g., histiocytosis X, sarcoidosis, hypersensitivity pneumonitis) and includes pertinent demographic and pathophysiologic information and descriptions of the signs, symptoms, and laboratory abnormalities typically associated with that particular disease. An all-inclusive, integrated algorithm is presented then that underscores and emphasizes select clinical and laboratory findings that are particularly useful in distinguishing among the various diffuse pulmonary interstitial diseases discussed. In the final section, 10 clinical case studies are presented; each is an object lesson demonstrating the usefulness of the previously presented algorithmic syntheses in diagnosing interstitial lung disease.

This tidy, compact volume contains a great deal of clinical fact, along with an entertaining mixture of clinical folklore. Although it is not encyclopedic, it presents a practical approach to diffuse pulmonary disease that is certain to be useful to practicing pulmonologists. Radiologists, however, are not likely to find this book worthwhile. The radiologic evaluation of patients with interstitial lung disease scarcely is addressed, and, of greater importance, the quality of the radiographs reproduced in the text is truly abysmal; the images are grainy and grimy, and most are approximately the size of a postage stamp. This flaw greatly diminishes the overall value of the book and specifically limits its appeal for radiologists.

Stuart A. Groskin
*SUNY Health Science Center at Syracuse*
*Syracuse, NY 13210*

## Edward B. D. Neuhauser Memorial Lecture

# Bronchopulmonary Dysplasia and Research in Diagnostic Radiology

William H. Northway, Jr.[1]



It is a great honor to give the 1990 Edward B. D. Neuhauser Memorial Lecture. Dr. Neuhauser made many significant contributions to pediatric radiology during his distinguished career, including helping found this society and serving as its first president. He was recognized for elucidating the pathogenesis of Hirschsprung disease with Dr. Ovar Swenson, receiving the Mead Johnson Award of the American Academy of Pediatrics, and, for his work in the diagnosis and treatment of Wilms tumor, he shared the Jurgkowski Award in Medical Science. It is with great pleasure that I celebrate an outstanding pediatric radiologist whose personal contributions and trainees continue to enrich the practice of pediatric radiology.

I am going to review my investigations of bronchopulmonary dysplasia (BPD) as background for a discussion of research in diagnostic radiology, with particular emphasis on sponsored research. Before beginning the review of these investigations, I would like to acknowledge the research technicians, medical students, residents, and faculty members in and outside of diagnostic radiology at Stanford University Medical Center who have contributed to these studies.

The initial report on BPD was published in 1967 [1]. This article was a retrospective review of the history, chest radiographs, and autopsy pathology of all 32 infants treated for severe respiratory distress syndrome (RDS) from September 1962 to November 1965 who had not responded to conventional therapy and required 24 hr or more of positive-pressure ventilation and oxygen supplementation. The clinical and radiologic progression of RDS was significantly modified by the treatment. The usual course of RDS had been that infants who survived the first 4 days of life recovered completely, and by 7–10 days of life normal lungs were seen on radiographs [2]. Those infants who did not survive died by 3 days of age. The two major findings reported in this study were the prolongation of the healing phase of RDS and the appearance of a new chronic pulmonary syndrome, BPD, which was associated with the use of mechanical ventilation and 80–100% concentrations of supplemental oxygen for longer than 150 hr.

BPD was initially divided into four developmental stages based on radiologic and pathologic findings [1]. Stage I (2–3 days) was a period in which the acute disease was indistinguishable from any severe case of RDS. Stage II (4–10 days) represented a period of regeneration. Radiographs showed nearly complete opacification of both lungs in severe cases. Pathologically, there was necrosis and repair of alveolar epithelium, squamous metaplasia of the bronchial and bronchiolar mucosa, patchy bronchiolar necrosis, and thick exudate in the bronchiolar lumen. At the end of this stage, weaning of the infants from the highest concentrations of oxygen could

Received September 7, 1990; accepted after revision October 19, 1990.
Presented at the annual meeting of the Society for Pediatric Radiology, Cincinnati, April 1990.
[1] Department of Diagnostic Radiology and Nuclear Medicine, Stanford University Medical Center, Stanford, CA 94305.

*AJR* **156:681–687, April 1991** 0361–803X/91/1564–0681 © American Roentgen Ray Society

usually be started. Stage III (10–20 days) was a period of transition to chronic disease. Radiologic findings changed to a characteristic picture of small cystlike lucencies throughout hyperexpanded lungs. Pathologic findings at this stage consisted of circumscribed groups of emphysematous alveoli with atelectasis of adjacent alveoli, bronchiolar mucosal metaplasia and hyperplasia, copious mucous secretion, interstitial edema, and pulmonary fibrosis. Stage IV (beyond 1 month) was the stage of chronic disease. The period of 1 month was arbitrarily chosen to indicate chronicity of the disease. The chest radiograph showed enlargement of the cystlike lucent areas in the hyperexpanded lungs (Fig. 1). Congestive heart failure and cor pulmonale with right ventricular hypertrophy were recognized as complications of BPD. Pathologically, the chronic lung disease stage showed true emphysema, atelectasis, marked hypertrophy of peribronchiolar smooth muscle, widespread epithelial metaplasia, pulmonary fibrosis, and vascular lesions of the pulmonary hypertensive type.

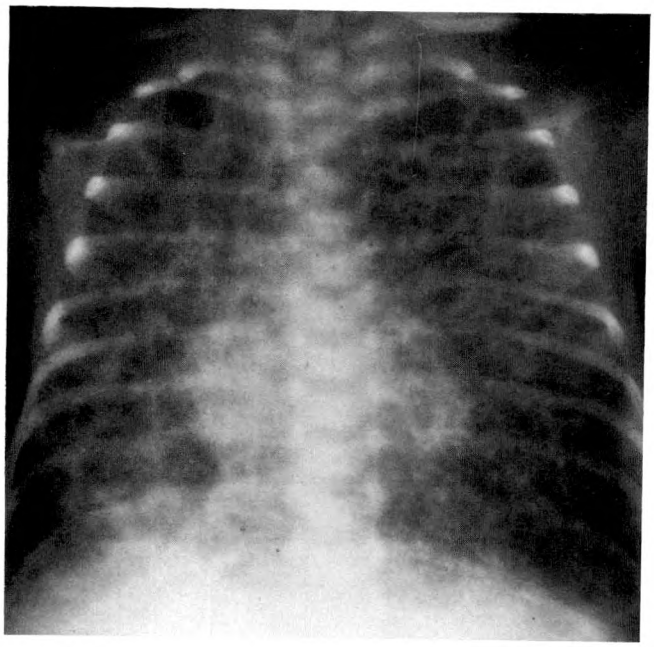


Fig. 1.—Characteristic anteroposterior chest radiograph of stage IV bronchopulmonary dysplasia with hyperexpansion, cystic areas of lucency, and alternating areas of radiopacity.

Pulmonary oxygen toxicity was originally recognized as a causative factor. Thirteen of the 32 infants were treated with high oxygen concentrations (80–100%) for more than 150 hr [1]. Nine lived beyond 2 weeks of age and all nine demonstrated BPD beyond 4 weeks of age. Nineteen infants were treated for less than 150 hr with high oxygen concentrations and nine survived. Eight of the survivors were normal clinically and radiologically. One of the survivors had persistent respiratory distress due to a subglottic stenosis.

Since the original description of BPD, our research has taken two directions: (1) investigation of the mechanism of the disease and (2) further investigation into the clinical course and prognosis of the disease. These efforts involved basic laboratory research and clinical research.

### Laboratory Research in Pulmonary Oxygen Toxicity

The initial hypothesis we tested in the laboratory was that high concentrations of oxygen might produce in the lungs of a newborn animal pathologic and radiologic changes that resembled BPD in human infants. This investigation used the newborn guinea pig [3]. Twenty-three newborn guinea pigs were maintained in a 96–100% oxygen environment at normal atmospheric pressure. Daily chest radiographs were obtained. The 19 newborn guinea pigs that lived longer than 4 days showed radiologic progression of lung disease until death (Fig. 2). All of the animals exposed to the 96–100% oxygen environment died by 6½ days, so no chronic lung disease was produced. Histologically, diseased lungs exhibited three progressive stages of injury: (1) pulmonary edema and intraalveolar hemorrhage; (2) mucosal metaplasia and hyperplasia, lymphatic dilatation, and increased alveolar macrophages; and (3) necrosis of bronchial and bronchiolar epithelium, hypertrophy of vascular and bronchial smooth muscle, and irregular alveolar aeration. The 17 control newborn guinea pigs maintained in room air showed no radiologic or pathologic

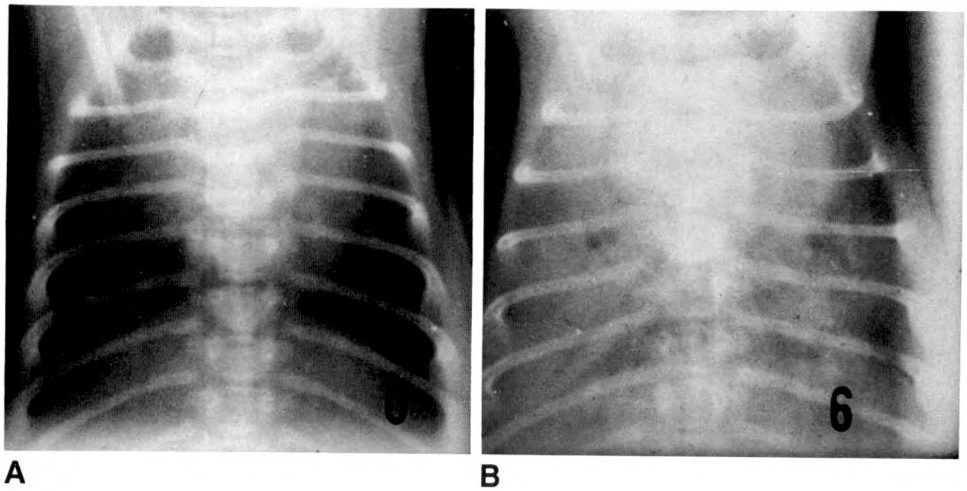



Fig. 2.—*A*, Chest radiograph of a normal guinea pig before it was placed in 96–100% oxygen.

*B*, Radiograph shows marked increase in patchy infiltrate with faint air bronchogram in the same animal after 6 days exposure to 96–100% oxygen.

(Reprinted with permission from Northway et al. [3].)

evidence of lung disease. We concluded from this study that oxygen-induced lung disease in the newborn guinea pig resembled the early stages of BPD in the human premature infant.

These results were presented at a departmental seminar, where Dr. Henry Kaplan, then department chairman, questioned the effect of pulmonary oxygen toxicity on DNA synthesis in the growing lung. That question was pivotal in directing our future laboratory research. Shortly thereafter we began a series of investigations, which did not involve radiologic imaging, on the effects of pulmonary oxygen toxicity on lung growth in the newborn mouse. The newborn mouse was chosen for these experiments because a colony of KaC57 black mice was available for research purposes in our radiobiology section. Our research on pulmonary oxygen toxicity in the newborn mouse extended over the next 20 years.

The hypothesis we first tested was that continuous exposure to 100% oxygen at normal atmospheric pressure might cause inhibition of lung growth in the newborn mouse in vivo [4]. Incorporation of tritiated thymidine into the newborn lung was inhibited by the initial 3-day exposure, indicating that exposure to 100% oxygen retarded lung growth in the newborn mouse by inhibiting DNA synthesis and cell replication (Fig. 3). This study confirmed the in vitro cell culture results of Reuckert and Mueller [5] and Brosemer and Rutter [6], which showed that increased oxygen concentration could inhibit cell growth. We subsequently showed that this inhibition of lung DNA synthesis underwent spontaneous reversal at 96–140 hr of continuous exposure to 100% oxygen [7]. After this reversal, DNA synthesis, total lung DNA, and body weight continued to increase, and mortality rate declined sharply, even with continued exposure to 100% oxygen.

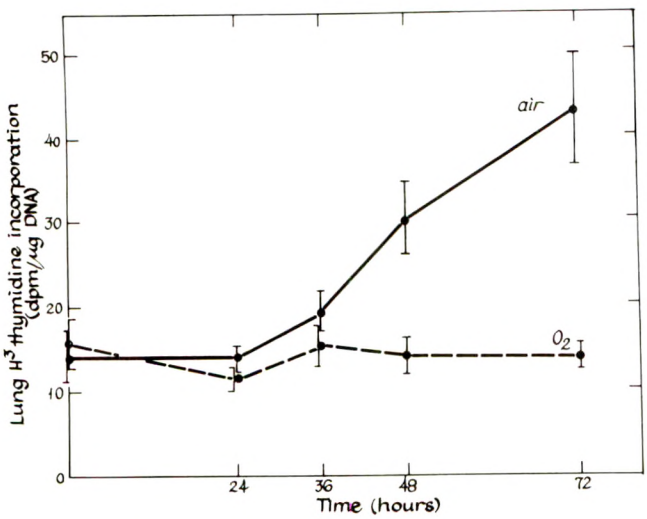



**Fig. 3.—Tritiated thymidine incorporation into pulmonary DNA in newborn mice exposed to air and 96–100% oxygen. The differences at 48 and 72 hr are significant ($p < .005$) by Student's t test of paired littermate differences. Points represent mean values for 12 animals, with the exception of 0 and 24 hr, where each point represents four and 16 animals, respectively. The range is 1 SEM about the mean. (Reprinted with permission from Northway et al. [4].)**

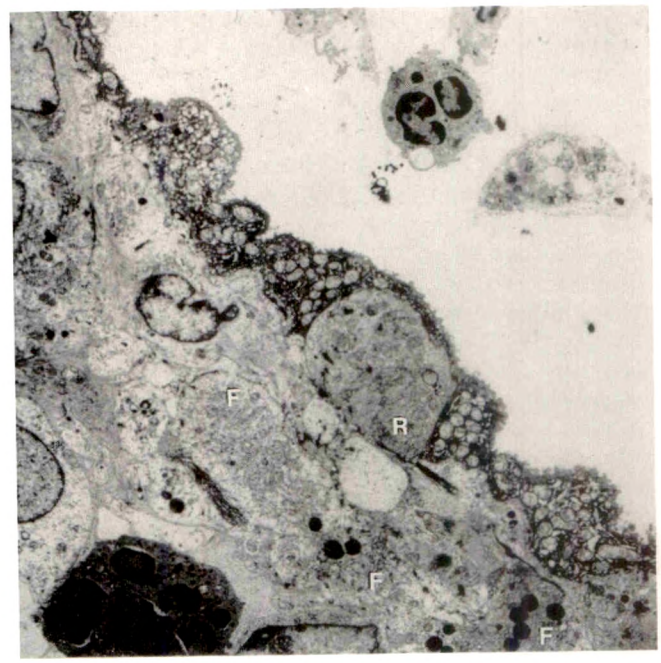



**Fig. 4.—This part of a bronchiole from a newborn mouse exposed to 96–100% oxygen for 7 days is lined by an attenuated layer of electron-opaque degenerating and dying cells, among which is a regenerating cell (R) with prominent ribosomes. There is accumulation of fibroblasts (F) in subbronchial tissue, among which bundles of collagen are identifiable. Acute inflammatory cells are present in the bronchial wall and lumen. (×4000) (Reprinted with permission from Ludwin et al. [8].)**

Our initial report on the pathologic findings caused by continuous exposure to 100% oxygen in newborn mice emphasized the changes seen in the bronchioles [8]. Before this report, some investigators had believed that bronchiolar cells were resistant to oxygen toxicity. We found that newborn mice exposed continuously to 100% oxygen for 3 days showed swelling of bronchiolar epithelium, increased protrusion of ciliated cells into the lumen, and loss of cilia and microvili. By 7 days of such exposure, a fully developed necrotizing bronchiolitis was seen (Fig. 4).

We also studied the effect of continuous exposure to 100% oxygen on the air-blood barrier in newborn mice [9]. Injury from the initial 7 days of exposure was divided into an acute toxic phase that lasted 3–4 days; a high mortality phase; and a third phase at the end of the exposure period, which was a chronic injury and repair phase characterized by the appearance of fibroblasts and an increase in the amount of collagen. Subsequently, we extended our investigation through 6 weeks of continuous exposure to 100% oxygen [10]. Fifty-nine percent of the exposed newborn mice survived 3 weeks and 18% survived 6 weeks of such exposure. These mice developed progressive diffuse pulmonary fibrosis, chronic bronchitis, bronchiolitis, and emphysema resembling the pathologic findings seen in stage IV BPD. We had at last developed a newborn animal model of lung injury that was similar to BPD.

We demonstrated later a difference in lethal susceptibility between young and adult mice exposed continuously to 100%

oxygen [11]. Mice younger than 15 days old at initiation of exposure to 100% oxygen could survive beyond 8 days of exposure. Mice 15 days old or older could not survive beyond 8 days during such exposure. Subsequent investigations by others have indicated that the ability to increase cellular antioxidant defenses is present in the newborn mouse but not in the adult mouse or newborn guinea pig [12]. This may explain our inability to develop a chronic pulmonary oxygen toxicity model with the newborn guinea pig.

We also tested the hypothesis that continuous exposure to lower concentrations of oxygen might produce significant pathologic changes in the newborn mouse lung. Lung injury does occur with continuous exposure to 80% oxygen. It is reflected primarily by an increase in the interstitial compartment of the lung and in pulmonary fibrosis as measured by electron microscopic morphometry at 2 and 6 weeks of exposure [13]. The newborn mice exposed to 80% oxygen for 6 weeks demonstrated a marked increase in survival (82%) compared with newborn mice exposed to 100% oxygen for 6 weeks (36%). Reduction of the oxygen exposure from 100% to 80% reduced the early exudative phase of pulmonary oxygen toxicity. A reduction in the early exudative phase of pulmonary oxygen toxicity could explain the reduction in stage II BPD seen with the therapeutic use of reduced oxygen concentrations in premature infants with RDS [14].

Our most recent laboratory investigation tested the hypothesis that dexamethasone treatment from day 14 to 18 in infant mice continually exposed from birth to either humidified air or 80% oxygen for 18 days might increase lung distensibility [15]. This study was designed to simulate the clinical situation in which infants with BPD are respirator dependent and an attempt is made to wean them from the respirator by use of steroid therapy. We found that dexamethasone significantly decreased lung water, lung growth, and thymus growth in both air- and oxygen-exposed animals but had no effect on lung distensibility. This study did not support the clinical impression that steroid therapy for the respiratory-dependent infant with BPD improved lung distensibility.

In summary, our laboratory research established that pulmonary oxygen toxicity could produce lung disease in newborn guinea pigs and mice that was similar to that seen in BPD in newborn infants. The in vivo inhibition of lung growth produced in newborn mice by oxygen toxicity was identified and measured, as was the reduction in lung injury seen when supplemental oxygen concentrations were decreased. We demonstrated that pulmonary oxygen toxicity could produce changes on chest radiographs, but were unable to confirm that steroid treatment improved lung distensibility in pulmonary oxygen toxicity in newborn mice.

### Clinical Research in Bronchopulmonary Dysplasia

Our clinical investigations of the course and prognosis of BPD included the initial demonstration of progressive tracheal aspirate cytologic changes in BPD [16], demonstration of the degree to which the radiologic and pathologic stages of BPD correlated [17], and more extensive description by light and electron microscopy of the pathologic changes seen in BPD [18]. This latter report emphasized that all infants with BPD studied showed damage of the bronchioles and bronchiolar ciliary apparatus and mucous membranes, severe necrotizing bronchiolitis, and marked bronchiolar and alveolar fibrosis.

We also have continued to follow both the course and changing epidemiology of BPD. In a retrospective study of 299 successive infants requiring respirator therapy for RDS between 1962 and 1973, we demonstrated that the degree of immaturity, initial severity of disease, pulmonary oxygen toxicity, and barotrauma all played a role in the development of BPD [19]. We found that 37% of the infants surviving with stage IV BPD became clinically normal by 3 years of age, but 29% had minor handicaps and 34% had a significant handicap, including cerebral palsy, mental retardation, deafness, or blindness. However, we also noted that this degree of handicap was not significantly different from that found in infants without BPD who previously had severe RDS and received more than 24 hr of respiratory therapy.

Children with BPD may have persistent pulmonary function abnormalities [20–23]. It has not been clear to what degree these abnormalities are present in adolescence or young adulthood. Our latest clinical investigation, begun in 1986 and sponsored by the National Institutes of Health (NIH), addressed the hypothesis that young adults who had had BPD might have abnormal pulmonary function. We have reported our studies of 22 young adults with prior BPD who were born between 1964 and 1973 and compared them with two control groups. One control group consisted of 20 age-matched young adults of similar birthweight and gestational age who did not develop BPD and a second control group of 48 age-matched normal volunteers. We found that most of the young adults who had had BPD, in contrast to the two control groups, had pulmonary dysfunction consisting of airway obstruction, airway hyperreactivity, and hyperexpansion [24]. Other studies to evaluate this pulmonary dysfunction are planned.

In summary, our clinical research established BPD as a clinical entity, defined the radiologic and pathologic development of the disease, contributed to its epidemiology, and documented persistent pulmonary dysfunction in young adults who had had BPD.

### Research in Diagnostic Radiology

I have been fortunate over the years to have had my research sponsored, first by the radiology department at Stanford, and subsequently by the Rosenberg Foundation; the James Picker Foundation (National Science Foundation); and the NIH Heart, Lung, and Blood Institute. During this 25-year period, significant interest has been expressed in increasing sponsored research in diagnostic radiology. The Conjoint Committee on Diagnostic Radiology was established to facilitate and promote the initiation of research grants supportive of diagnostic imaging at the NIH and other federal agencies [25]. Since 1982, funding for imaging research supported by NIH in departments of radiology has increased from $6 million to almost $30 million [26]. These efforts to increase support for research in diagnostic imaging have been successful and should continue.

There is, however, another way to increase the competitiveness of our research proposals for NIH support. This involves a fundamental change in the way that diagnostic radiology perceives radiologic research.

Clinical scientific research consists of an initial observation, followed by developing a hypothesis, testing the hypothesis by a controlled experiment, interpreting the results, and drawing a conclusion. Using these criteria, Effmann [27] looked at research in diagnostic radiology by reviewing all original articles (not case reports) appearing in 1985 in both *Pediatric Radiology* and the pediatric section of *Radiology* and then compared these publications with those appearing in the *New England Journal of Medicine* and the *Journal of Pediatrics*. His results are summarized in Table 1. Studies reported in the *New England Journal of Medicine* and *Journal of Pediatrics* were much more likely to have (1) a clearly stated hypothesis, (2) control groups, (3) statistics in the data analysis, (4) citations of the previous work of one or more of the coauthors, and (5) funding support. Effmann noted that a common justification for publication in either *Radiology* or *Pediatric Radiology* was, "We wish to report our experience." Effmann's review suggests that the best journals in pediatric radiology are publishing a great deal of medical reporting and not a lot of medical scientific research.

What should be the aim of medical research? Laennec [28] states, "The aim of medicine is the cure of disease" [28]. In 1924, Albert Cohn, the first editor of the *Journal of Clinical Investigation*, wrote in the first issue, "We believe it necessary as a base of therapeutics to understand the mechanisms, that is to say, the processes which underlie the manifestations of diseases. The methods to be employed are those which are appropriate to illuminating the specific problems in question" [29]. John Platt, a professor of biophysics and physics at the University of Chicago, asked the question, "Why should there be such rapid advances in some fields of science and not in others?" His conclusion is that the consistent use of what he calls strong inference is responsible [30]. His definition of strong inference consists of setting up alternative hypotheses, devising a crucial experiment that will exclude one or more of the hypotheses, carrying out the experiment to get a clean result, and then recycling the procedure to refine the possibilities. Platt also states, "Beware of the man of one method or one instrument, either experimental or theoretical. He tends to become method-oriented rather than problem-oriented. The method-oriented man is shackled, the problem-oriented man is at least reaching freely toward what is most important" [30].

It is my thesis that the NIH is interested in the cure of disease by understanding the basic mechanism of disease through research that involves hypothesis testing by experiment. To increase our success in obtaining NIH research support, our investigations should address this goal.

The guidelines for NIH study section grant proposal reviewers include evaluation of (1) the significance and originality of the project, (2) the validity of the hypothesis, (3) the logic of the aims, (4) the feasibility and adequacy of the procedures, and (5) the likelihood of new data and new concepts being developed [31]. If one wishes to compete successfully for research support at the NIH, one needs to understand not only the rules of the competition but also recognize who is judging the proposal. The respiratory and applied physiology study section of the National Heart, Lung, and Blood Institute, which approved and funded my last clinical research grant, included 12 professors of medicine, nine professors of physiology or cell biology, and one professor of pediatrics. This 22-person group consisted of 11 with MD degrees, nine with PhD degrees, and two with MD/PhD degrees. No diagnostic radiologist was a member of the study section. Only the National Cancer Institute at the NIH includes a diagnostic imaging research branch.

Differences in the research environment in diagnostic radiology have been suggested as part of the reason for the low level of NIH-sponsored research in radiology [32]. These differences include (1) lack of control of patient populations, (2) increasing demands to provide efficient clinical service, (3) the breadth of the discipline with a subsequent lack of research focus, and (4) the macroscopic technology–related nature of most radiologic research. With the exception of the lack of control of patient populations, these differences are primarily of degree and are related to prevailing attitudes about research within the discipline of diagnostic radiology.

Diagnostic radiologists do not control the course and therapy of the patients they may wish to study in a clinical research proposal. However, significant research proposals testing important hypotheses are likely to be attractive to investigators from all disciplines. If the diagnostic radiologist as a principal investigator takes the time to draft such a proposal, participation by physicians from other disciplines, as coinvestigators, is more likely. Radiologists, by drafting the proposal, document their interest and expertise and the

**TABLE 1: Comparison of Original Articles Published in Four Journals in 1985**

| Journal | No. of Articles[a] | % of Articles | | | | |
|---|---|---|---|---|---|---|
| | | Hypothesis | Controls | Statistics | Citation | Sponsored |
| *New England Journal of Medicine* | 20 | 80 | 45 | 65 | 90 | 85 |
| *Journal of Pediatrics* | 20 | 60 | 45 | 65 | 90 | 60 |
| *Radiology* | 52 | 12 | 13 | 2 | 40 | 8 |
| *Pediatric Radiology* | 59 | 22 | 17 | 25 | 36 | 5 |

Note.—Data reprinted with permission from Effmann [27].

[a] Includes all original articles appearing in *Radiology* and *Pediatric Radiology* in 1985 and the first 20 appearing in the *New England Journal of Medicine* and the *Journal of Pediatrics*, January–March 1985.

coinvestigators save time by reviewing and correcting the proposal rather than having to draft a proposal de novo.

The time that a diagnostic radiologist spends doing clinical work need be no more than an internist spends in clinical care. The key to having enough time for research in internal medicine or diagnostic radiology is having adequate physician staffing of the clinical service to allow for such time. The faculty members in the Department of Internal Medicine at Stanford spend an average of 30% of their time on patient care activities and argue that an increase in the clinical time would decrease time for research, which would impair the quality of the research as well as the competitiveness of proposals for research funds [33]. After a year-long evaluation of the sources of revenue for the internal medicine department and taking into account the direct research awards as well as indirect cost recovery, they found that the gross revenue per full-time–equivalent faculty member from research was 86% more than revenue generated by the faculty in cardiology (the highest revenue-generating clinical practice in the department) [33]. It is no wonder that the attitude of the Department of Internal Medicine is supportive of faculty time for research.

Because of the breadth of our field, research in diagnostic radiology frequently involves the application of a single technologic method to a broad spectrum of diseases. The diagnostic radiologist may consider this as focused research, since it uses only a single technology. The concept of focused research in internal medicine has meant studying the mechanism of a particular disease or group of related diseases. Investigators use whatever research technology is appropriate for testing their hypotheses. With the latter approach, the technology is seen as a research tool, not the research focus. Research that uses diagnostic technology and assessment of that technology generally will not fit within the framework for research proposals funded by the NIH unless it can be demonstrated that such research will directly address issues of basic mechanisms of disease. Limiting research in diagnostic radiology to those technologies used in our clinical practice restricts our ability to address questions of basic disease mechanism.

If one chooses to do medical scientific research, can one be both an effective clinician and a productive scientist? R. J. Mason, Chairman of the Department of Medicine and pulmonary specialist at the National Jewish Center, Denver, CO, answers this question in the affirmative [34]. He believes that to succeed you need (1) a focused research program, (2) sufficient protected time for research, and (3) appropriate research training. His definition of a scientist is one who uses the scientific method to increase knowledge. The effective clinician is carefully defined to be one who need not do everything nor be an expert in all facets of the clinical specialty. Mason states that there should be enough direct patient care done by the faculty to maintain clinical skills. He also advocates that for the junior faculty person, this should be approximately 25% of his or her time. He does note that in most departments, young faculty internists will have to spend more than 25% time in clinical care activities. In diagnostic radiology, Bruce Hillman found that, "Overwhelmingly, academic clinicians perceive finding time to do research and conflicting pressures to perform clinical work as the most severe obstacles to performing and publishing research" [35]. In his survey of diagnostic radiology researchers, "academic faculty members spent an average of 11% of their time performing research, and only 27% had time set aside during working hours for this purpose" [35]. I was fortunate to have had approximately 35% of my time available for research. The contrast in the attitude of the disciplines of internal medicine and diagnostic radiology toward the allocation of time for medical scientific research is dramatic. The lack of time for research undoubtedly contributes to the low level of NIH-sponsored research in departments of diagnostic radiology.

Mason [34] indicates that there is a price to pay for focusing on medical scientific research. He states that "by combining the two careers, one cannot expect to be as accomplished at either one as one would if only one career were undertaken." The decision to do medical scientific research and compete for research support involves significant personal choices. The individual must weigh how important it is to him or her to be a scientist and to discover something new against how important it is to be a doctor who diagnoses and treats the sick.

Mason [34] recommends that the appropriate training for doing research in internal medicine should include (1) an initial clinical year, (2) 2 years as a research fellow, and (3) 2 years as a protected junior faculty with no more than 25% time allocated for clinical care activities. Can junior faculty in departments of radiology compete effectively for research support at the NIH without similar research training? I suspect that they can not.

Choosing a subject for research requires considerable thought. The subject must be of great interest to the investigator since he or she may devote 20–25 years to it during an academic career. It is hoped the area chosen will lead to diagnosis, prevention, treatment, or cure of a disease. The investigator must have the skills to do the experiments necessary to test the hypotheses. Finally, the investigator should be aware of the competition in the area being considered for his or her research activity.

Mason [34] has made some predictions regarding the future of academic medical specialty research in internal medicine and, in particular, in pulmonary medicine, which I have summarized. (1) More basic biologic research will be done by PhDs. These PhDs will have an important role in research training in clinical departments. (2) Fellows interested in basic research careers will be trained in basic science laboratories. (3) Fellows who wish to become clinical investigators will follow a more organized scientific curriculum. (4) Physician researchers will focus their investigations on mechanisms of disease and clinical research. (5) Departments will have a heterogeneous clinical and research faculty by design to meet the increasing demands of clinical care and clinical and basic research. (6) Within departments and divisions, research programs will be very focused to answer specific questions and effectively use limited resources.

These predictions are made so that internal medicine can develop strategies to maintain its strong position with regard to doing significant medical scientific research and obtaining support for this research. They would seem to be predictions that should be heeded by departments of diagnostic radiology

and pediatric radiology if we wish to increase our competitiveness for NIH grant support.

Medicine is well over 2000 years old. Diagnostic radiology and pediatric radiology are not yet 100 years old. As a discipline, we have made remarkable progress in a relatively short time. Diagnostic radiology will assume an even more important role in academic medicine as it increases its commitment to medical scientific research. Success in this endeavor requires a supportive medical school dean, a supportive departmental environment, sufficient faculty time and departmental resources devoted to medical scientific research, increased faculty skills and training in research, increased attention to medically focused research, and careful selection of those persons who are best suited for careers in medical scientific investigation.

## REFERENCES


1. Northway WH Jr, Rosan RC, Porter DY. Pulmonary disease following respirator therapy of hyaline membrane disease. Bronchopulmonary dysplasia. *N Engl J Med* **1967**;276:357–367
2. Peterson HG Jr, Pendleton ME. Contrasting roentgenographic pulmonary patterns of hyaline membrane and fetal aspiration syndromes. *AJR* **1955**;74:800–817
3. Northway WH Jr, Rosan RC, Shahinian L, Castellino RA, Gyepes MT, Durbridge T. Radiologic and histologic investigation of pulmonary oxygen toxicity in the newborn guinea pig. *Invest Radiol* **1969**;4:148–155
4. Northway WH Jr, Petriceks R, Shahinian L. Quantitative aspects of oxygen toxicity in the newborn: inhibition of lung DNA synthesis in the mouse. *Pediatrics* **1972**;50:67–72
5. Reuckert RR, Mueller GC. Effect of oxygen tension on hela cell growth. *Cancer Res* **1960**;20:944–949
6. Brosemer RW, Rutter WJ. The effect of oxygen tension on the growth and metabolism of a mammalian cell. *Exp Cell Res* **1961**;25:101–113
7. Northway WH Jr, Petriceks R, Rezeau L, Bensch KG. Oxygen toxicity in the newborn: reversal of inhibition of DNA synthesis in the mouse. *Pediatrics* **1976**;57:41–46
8. Ludwin SK, Northway WH Jr, Bensch KG. Oxygen toxicity in the newborn: necrotizing bronchiolitis in mice exposed to 100 percent oxygen. *Lab Invest* **1974**;31:425–435
9. Bonikos DS, Bensch KG, Ludwin SK, Northway WH Jr. Oxygen toxicity in the newborn: the effect of prolonged 100% oxygen exposure on the lungs of newborn mice. *Lab Invest* **1975**;32:619–635
10. Bonikos DS, Bensch KG, Northway WH Jr. Oyxgen toxicity in the newborn: the effect of chronic continuous 100 percent oxygen exposure on the lungs of newborn nice. *Am J Pathol* **1976**;85:623–650
11. Northway WH Jr, Petriceks R, Canty E, Bensch KG. Maturation as a factor in pulmonary oxygen toxicity; a preliminary report. *J Pediatr* **1979**;95:859–864
12. Wispe R, Roberts JR. Development of antioxidant systems. In: Merritt TA, Northway WH Jr, Boynton BR, eds. *Bronchopulmonary dysplasia*. Boston: Blackwell Scientific, **1988**:103–116
13. Obara H, Pappas CT, Northway WH Jr, Bensch KG. Comparison of the effect of two and six week exposure to 80% and 100% oxygen on the lung of the newborn mouse: a quantitative SEM and TEM correlative study. *Int J Radiat Oncol Biol Phys* **1985**;11:285–298
14. Edwards DK III. The radiology of bronchopulmonary dysplasia and its complications. In: Merritt TA, Northway WH Jr, Boynton BR, eds. *Bronchopulmonary dysplasia*. Boston: Blackwell Scientific, **1988**:185–234
15. Ohtsu N, Ariagno RL, Sweeney TE, et al. The effect of dexamethasone on chronic pulmonary oxygen toxicity in infant mice. *Pediatr Res* **1989**;25:353–359
16. Northway WH Jr, Rosan RC. Oxygen therapy hazards in the neonate. *Hosp Pract* **1969**;4:59–67
17. Edwards DK, Colby TV, Northway WH Jr. Radiographic-pathologic correlation in bronchopulmonary dysplasia. *J Pediatr* **1979**;95:834–836
18. Bonikos DS, Bensch KG, Northway WH Jr, Edwards DK. Bronchopulmonary dysplasia: the pulmonary pathologic sequal of necrotizing bronchiolitis and pulmonary fibrosis. *Hum Pathol* **1976**;7:643–666
19. Edwards D, Dwyer W, Northway WH Jr. Twelve years' experience with bronchopulmonary dysplasia. *Pediatrics* **1977**;59:839–846
20. Smythe JA, Tabachnik E, Duncan WJ, Reilly BJ, Levison H. Pulmonary function and bronchial hyperreactivity in long term survivors of bronchopulmonary dysplasia. *Pediatrics* **1981**;68:336–340
21. Riedel F. Long term effects of artificial ventilation in neonates. *Acta Paediatr Scand* **1987**;76:24–29
22. Bader D, Ramos AD, Lew CD, Platzker ACG, Stabile MW, Keens TG. Childhood sequelae of infant lung disease: exercise and pulmonary function abnormalities after bronchopulmonary dysplasia. *J Pediatr* **1987**;110:693–699
23. Andreasson B, Lindroth M, Mortensson W, Svenningsen NW. Lung function eight years after neonatal ventilation. *Arch Dis Child* **1989**;64:108–113
24. Northway WH Jr, Moss RB, Carlisle KB, et al. Twenty-three year followup of bronchopulmonary dysplasia (BPD). *Pediatr Res* **1989**;25:370A
25. Putman CE. The activities of the Conjoint Committee on Diagnostic Radiology. *Invest Radiol* **1987**;22:925–926
26. Maynard CD, Witcofski RL, Putman CE, Al-Alish M. Research directions in diagnostic imaging. *Invest Radiol* **1990**;25:101–108
27. Effmann EL. Research by pediatric radiologists—past accomplishments and future opportunities. *Pediatr Radiol* **1987**;17:355–361
28. Laennec RTH. Presentation at the opening of the course in medicine at the Royal College of France. *Arch Gen Med* **1823**;1:5–20
29. Cohn AE. Purposes in medical research. *J Clin Invest* **1924**;1:1–11
30. Platt JP. Strong inference. *Science* **1964**;146:347–353
31. Cuca JM, McLaughlin WJ. Why clinical research grant applications fare poorly in review and how to recover. *Cancer Invest* **1987**;5:55–58
32. Rockoff SD. Diagnostic radiologic research: the disincentives to its propagation. *Invest Radiol* **1980**;15:353–355
33. Chin D, Hopkins D, Melmon K, Holman HR. The relation of faculty academic activity to financing sources in a department of medicine. *N Engl J Med* **1985**;312:1029–1034
34. Mason RJ. The academic pulmonary physician: can one be both a productive scientist and an effective clinician? *Am Rev Respir Dis* **1989**;139:1551–1552
35. Hillman BJ. Selection and training of radiology researchers. *Radiology* **1990**;174:887–888

# Book Review

**Radiation Protection.** A Guide for Scientists and Physicians, 3rd ed. By Jacob Shapiro. Cambridge, MA: Harvard University Press, 494 pp., 1990. $35

The contents and organization of this manual are based on experience gained in conducting courses and seminars on the principles and practice of radiation protection for workers in the research laboratories at Harvard University and its affiliated hospitals. Reviews of atomic and radiation physics are not necessary; mathematics has been confined to elementary arithmetic and algebraic operations.

Part I gives a concise overview of the roles and varieties of ionizing particles in nature. Part II contains the core material of the manual. The central role of energy imparted by ionizing radiation is introduced; this is followed by a description of the properties and main sources of such radiation. The difference between directly and indirectly ionizing radiation is described. Units for expressing radiation levels are defined. Limits for exposure to radiation from internal and external sources are compared with naturally occurring levels of exposure. Part II continues with some simple calculations for radiation protection and discussion of technical considerations in minimizing the dose to patients from diagnostic procedures. It concludes with a brief description of particle accelerators and their special problems.

Part III addresses the calculation of dose from distributed beta- and gamma-emitting radionuclides, both to the body as a whole and to specific organs. Evaluations of doses from important radionuclides, both ingested and inhaled in air, are followed by a discussion of organ doses imparted by nuclear medicine and external-beam X-ray diagnostic procedures.

Part IV covers detection instruments and their use in making the more common radiation measurements. A summary of the statistical considerations in event-counting procedures is followed by a discussion of making measurements at the limits of sensitivity of the radiation detectors.

Part V discusses the responsibilities and working procedures of persons who use radionuclides. Subjects addressed include authorization to use isotopes and to administer them to human beings; approval of new radioactive drugs; protection of the patient; training requirements; responsibilities of those who use radionuclides; personnel and area monitoring; area posting; isotope handling and shipping; and waste disposal. Part V is supplemented by three appendixes: "Emergency Instructions," "Regulatory Processes," and "Control of Airborne Releases."

Part VI is concerned with ionizing radiation and public health. This part opens with a discussion of the formulation of standards for radiation protection and the medical findings on which they are based. Under the rubric of current issues in radiation protection, quotations from recognized authorities are provided on reducing population radiation exposure from medical and dental X-ray procedures, environmental effects of nuclear power, and so forth. This part concludes with a personal statement of philosophy with regard to nuclear war. Part VI is followed by five appendixes: "Problems" (with answers), "Data on Selected Isotopes," "Anatomical and Physiological Data," "Constants and Conversion Factors," and "Calculations Using Powers of Ten."

The selected bibliography is grouped under headings of radiation protection and dosimetry, nuclear radiation physics, radiobiology, medical radiation physics, nuclear medicine, and handbooks. The last group includes addresses for purchasing specific reports.

The manual is organized so that readers can find material of immediate interest easily and expeditiously. The illustrations are good and to the point. The use of units is a little confused, but conversion factors between traditional and SI units are provided. The style is elegant, a pleasure to read. In a sense, the workmanship of the text has been its greatest liability; the author found appropriate references and quotations for the first edition in 1972, jewels he has added to but has been reluctant to replace. The half-lives for sodium-22 and potassium-40 as given in appendix II are in error, and the name of one reference is misspelled (differently) twice, a low error rate. The last half of part VI is not effective out of the classroom.

The manual addresses the principles and practices of radiation protection for those nonspecialists whose work in research or the field of medicine requires the use of radiation sources. I do not know of another text that fulfills that role so well.

Peter Wootton
*University of Washington*
*Seattle, WA 98195*

Review Article

# Radiation Injury of the Brain

Peter E. Valk[1,2] and William P. Dillon[2]

**The clinical, radiologic, and pathologic findings in radiation injury of the brain are reviewed. Late radiation injury is the major, dose-limiting complication of brain irradiation and occurs in two forms, focal and diffuse, which differ significantly in clinical and radiologic features. Focal and diffuse injuries both include a wide spectrum of abnormalities, from subclinical changes detectable only by MR imaging to overt brain necrosis. Asymptomatic focal edema is commonly seen on CT and MR following focal or large-volume irradiation. Focal necrosis has the CT and MR characteristics of a mass lesion, with clinical evidence of focal neurologic abnormality and raised intracranial pressure. Microscopically, the lesion shows characteristic vascular changes and white matter pathology ranging from demyelination to coagulative necrosis. Diffuse radiation injury is characterized by periventricular decrease in attenuation on CT and increased signal on proton-density and T2-weighted MR images. Most patients are asymptomatic. When clinical manifestations occur, impairment of mental function is the most prominent feature. Pathologic findings in focal and diffuse radiation necrosis are similar. Necrotizing leukoencephalopathy is the form of diffuse white matter injury that follows chemotherapy, with or without irradiation. Vascular disease is less prominent and the latent period is shorter than in diffuse radiation injury; radiologic findings and clinical manifestations are similar. Late radiation injury of large arteries is an occasional cause of postradiation cerebral injury, and cerebral atrophy and mineralizing microangiopathy are common radiologic findings of uncertain clinical significance. Functional imaging by positron emission tomography can differentiate recurrent tumor from focal radiation necrosis with positive and negative predictive values for tumor of 80–90%. Positron emission tomography of the blood-brain barrier, glucose metabolism, and blood flow, together with MR imaging, have demonstrated some of the pathophysiology of late radiation necrosis. Focal glucose hypometabolism on positron emission tomography in irradiated patients may have prognostic significance for subsequent development of clinically evident radiation necrosis.**

Recognition of injury to normal brain as a complication of cerebral radiation therapy has increased since the advent of noninvasive imaging and the use of more aggressive schemes of irradiation and chemotherapy. This probably reflects a true increase in the prevalence of cerebral radiation injury, as well as an increase in the rate of diagnosis. Delivery of higher radiation doses causes more injury to normal as well as to abnormal tissue, while improvement in long-term survival increases the time available for development of late radiation effects. CT and MR imaging have increased the recognition rate of radiation injury when it occurs.

Cerebral radiation injury has been classified according to time of appearance of symptoms after therapy. Acute injury appears during radiation therapy as a transient worsening of symptoms, and has little prognostic significance. Early delayed injury occurs a few weeks to 3 months after therapy and also is transient in most cases. By contrast, late radiation injury, which occurs a few months to 10 or more years after therapy, is irreversible, progressive, and sometimes fatal, and constitutes the major, dose-limiting complication of cerebral irradiation [1]. There are two main forms of late radiation injury, which may occur separately or together: focal injury

Received Jaunary 24, 1990; revision requested March 23, 1990; revision received August 30, 1990; accepted September 6, 1990.
This work was supported in part by the Director, Office of Energy Research, Office of Health and Environmental Research of the U.S. Department of Energy, under contract DE-AC03-76F00098, and in part by U.S. Public Health Service grant R01 HL38824.
[1] Research Medicine and Radiation Biophysics Division, Lawrence Berkeley Laboratory, Mail Stop 55-121, University of California, Berkeley, CA 94720. Address reprint requests to P. E. Valk.
[2] Department of Radiology, University of California School of Medicine, San Francisco, CA 94143.

*AJNR* 12:45–62, January/February 1991; *AJR* 156:689–706, April 1991 0361–803X/91/1564–0689 © American Roentgen Ray Society

and diffuse white matter injury. The basic pathology is probably the same in both instances, but the clinical manifestations and radiologic findings of the two syndromes differ sufficiently to warrant separate consideration.

### Prevalence of Symptomatic Late Radiation Injury

The prevalence of radiation injury is difficult to determine and few reliable figures have been reported. Marks et al. [2] followed a population of 139 patients who had received photon therapy for primary brain and pituitary tumors. Seven patients (5%) developed histologically documented radiation necrosis. Marsa et al. [3] found necrosis in 10 (15%) of 66 autopsied patients, out of a total population of 256 patients (4%) irradiated for tumor. These figures are bound to be underestimates, since patients who died without autopsy and patients who survived without a tissue diagnosis were not included. Hohweiler et al. [4] studied 76 patients with primary brain tumors and found 10 patients with clinical and CT evidence of necrosis, including eight who were alive and had no evidence of tumor. The overall prevalence was 14%, with a 50% prevalence in surviving patients. An even higher rate of neurologic complications has been reported after chemotherapy combined with prophylactic cranial irradiation for small cell carcinoma of the lung. Frytak et al. [5] found neurotoxicity in 37% of patients who survived 1½ years or longer, and Laukkanen et al. [6] reported neuropsychological impairment and CT abnormalities in seven of 12 patients who survived 2 years or more. Imaging abnormalities without clinical manifestations are more frequent still, but the clinical significance of such findings has not been determined and prospective studies of irradiated patient groups are needed.

The term "injury" is used here to describe all degrees of injury, from asymptomatic edema to necrosis. The most frequent clinical, pathologic, and radiologic features of symptomatic radiation- and drug-related cerebral injury are summarized in Table 1.

### Focal Injury

#### *Clinical Manifestations*

Focal radiation injury of the brain was recognized clinically by Fischer and Holfelder [7] in 1930. Focal necrosis presents as a mass lesion, with focal neurologic abnormalities and evidence of raised intracranial pressure. Unilateral motor or sensory loss, aphasia, disturbance of consciousness, and seizures are common. Although symptoms may develop from 3 months to more than 10 years after irradiation, approximately 70% of all cases occur during the first 2 years [1]. The clinical course is unpredictable. Changes are usually irreversible and frequently progressive, and extension of necrosis leads to death in many cases [1, 8]. However, resolution of a mass lesion is encountered occasionally [9], and some patients stabilize clinically with permanent neurologic deficits [10, 11]. Surgical removal of the necrotic mass is the treatment of choice and may be lifesaving [11–13].

#### *Radiologic Findings*

The angiographic [9, 12, 14] and CT [10, 11, 15–17] features of focal radiation necrosis are well known. On angiography, the injured area most commonly appears as an avascular mass, with no specific features, and in some cases the angiogram is normal. Unenhanced CT shows a low-density region, with surrounding vasogenic edema and variable mass effect. Following contrast administration, irregular enhancement is seen at the margins of the mass.

These radiologic features can be interpreted most readily when injury follows irradiation of an extracerebral or extracranial lesion (Fig. 1) [10, 11, 14] or when it occurs at a distance from an intracerebral tumor [2]. When injury occurs at the site of an intracerebral tumor, it is not possible to differentiate the effects of radiation from those of residual or recurrent tumor on the basis of angiographic or CT findings. MR imaging provides no additional differentiating information (Fig. 2). MR spectroscopy may become useful in the future, but limited volume resolution at present precludes its use in most patients. In both conditions, increase in tissue water content causes increase in mobile hydrogen density and prolongation of T1 and T2 relaxation times. These changes result in decreased signal on T1-weighted images and increased signal on T2-weighted and proton-density images (Fig. 3). The blood-brain barrier (BBB) defect results in enhancement following the administration of paramagnetic contrast material.

When necrosis follows irradiation for cerebral tumor, it

**TABLE 1: Clinical Syndromes of Treatment-Related Cerebral Injury**

| Characteristic | Focal Radiation Necrosis | Diffuse Radiation Injury | Necrotizing Leukoencephalopathy |
|---|---|---|---|
| Cause | Radiation | Radiation | Chemotherapy ± radiation |
| Latent period | Months to years | Months to years | Weeks to months |
| Clinical features | Focal deficits, raised intracranial pressure | Mental impairment ± focal deficits | Mental impairment ± focal deficits |
| CT findings | Focal hypodensity, contrast enhancement, mass effect | Diffuse white matter hypodensity | Diffuse white matter hypodensity |
| MR findings | Focal hyperintensity on T2-weighted images, contrast enhancement, mass effect | Diffuse white matter hyperintensity on T2-weighted images | Diffuse white matter hyperintensity on T2-weighted images |
| Pathology | Arteriolar hyalinization and fibrinoid necrosis, demyelination, coagulation necrosis | Same as for focal radiation necrosis[a] | Same as for focal radiation necrosis; vascular pathology less prominent[a] |

[a] Necrosis is the most common finding when biopsy or autopsy is performed in diffuse white matter injury with frank dementia. However, the pathologic findings are unknown in most patients.



Fig. 1.—Focal radiation necrosis following extracerebral irradiation. Lesion detected 6 months after irradiation of overlying plasmacytoma of the skull. Contrast-enhanced CT scan shows left frontal hypodensity with central area of enhancement. Diagnosis was confirmed by surgical biopsy.

occurs most frequently at or near the site of the tumor [18], even after whole-brain irradiation. Tissue adjacent to the tumor appears to be rendered more susceptible to injury, possibly by the vasogenic edema that usually surrounds the lesion [19]. However, focal injury also can occur at a distance from the primary lesion, and radiation necrosis contralateral to the lesion has been described after whole-brain irradiation [2].

Necrosis is the most common clinically recognized form of focal radiation injury, but recent studies after focal charged-particle therapy have revealed a higher prevalence of lesser, subclinical injury [20]. MR (Fig. 3) and CT changes are similar to those of radiation necrosis, with the exception of contrast enhancement, which is not seen in these asymptomatic patients. In our experience, an asymptomatic focal increase in signal on T2-weighted MR images has been a common incidental finding following focal or limited-field photon irradiation.

Hemorrhagic focal radiation injury has been reported by Woo et al. [21]. They found radiation-induced telangiectasia at the margin of a region of cerebral hemorrhage, in associa-

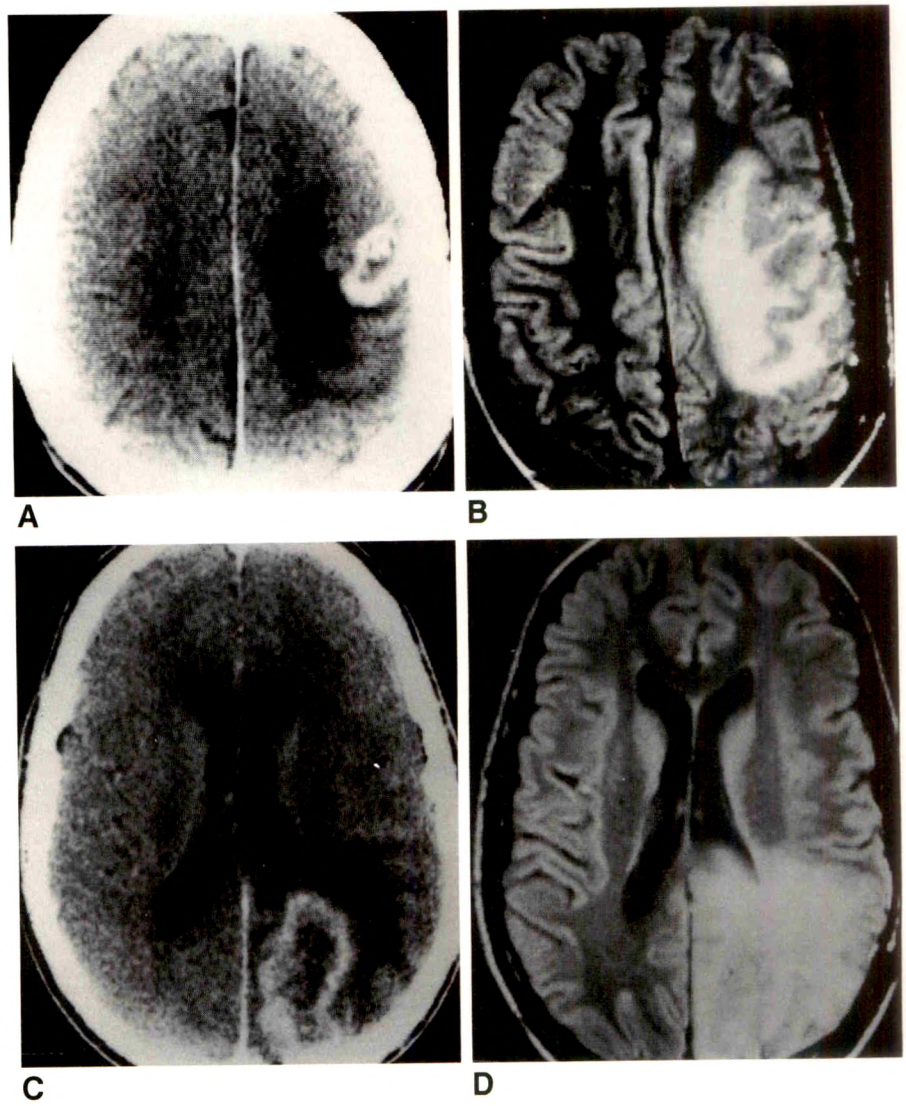



Fig. 2.—*A* and *B*, Focal radiation necrosis. Contrast-enhanced CT scan (*A*) and proton-density MR image, 2000/33 (*B*), 11 months after external irradiation and interstitial brachytherapy of glioblastoma multiforme. CT shows hypodensity in left frontoparietal region, with central area of ring enhancement. MR shows diffuse increase in signal in region of CT hypodensity, consistent with edema. On follow-up, there was no further deterioration and the patient was alive 9 months later without antitumor therapy. This excludes a diagnosis of tumor recurrence and establishes radiation necrosis as the most probable cause of CT change.

*C* and *D*, Recurrent malignant glioma. Contrast-enhanced CT scan (*C*) and proton-density MR image, 2000/33 (*D*), 8 months after external irradiation and interstitial brachytherapy of anaplastic astrocytoma. CT shows left occipital hypodensity and mass lesion with irregular contrast enhancement at margins. MR shows diffuse increase in signal in region of CT hypodensity, consistent with edema. The patient continued to deteriorate, clinically as well as radiologically, and antitumor chemotherapy was commenced 3 weeks later with positive response. Deterioration with response to chemotherapy established diagnosis of tumor recurrence.

The CT and MR findings in these two patients are nonspecific and do not help differentiate radiation necrosis from recurrent tumor.

tion with evidence of late radiation necrosis. We have now seen five cases of radiation-associated focal hemorrhage on MR, unaccompanied by other manifestations of radiation necrosis. These patients had been treated with conventional doses of photon radiation. MR revealed multiple foci of hemosiderin, mixed with subacute hemorrhagic change (Fig. 4). Some of the lesions appeared calcified and showed contrast enhancement, similar to cryptic vascular malformations. These lesions probably were radiation induced, as they occurred only within the irradiated volume of brain and in one case were not present before radiation therapy.

*Pathologic Findings*

Focal necrosis affects white matter more severely than gray [10, 19, 22]. Hyalinization and fibrinoid necrosis of small arteries and arterioles are the most characteristic findings, together with narrowing of the lumen and endothelial proliferation (Fig. 5). A perivascular mononuclear inflammatory response may be seen. White matter changes vary from rarefaction of myelin and reactive gliosis to coagulation necrosis and cavitation. The microscopic appearance of severely affected regions does not vary with lesion topography, and the same histologic changes may be seen in focal and diffuse forms of injury [8]. De Reuck and Eecken [8] have suggested that the topography of damage may be determined by the distribution of vascular lesions, with occlusion of deep perforating arteries producing focal lesions in the corresponding vascular territories, and more generalized disturbances of cerebral perfusion producing lesions in the periventricular arterial end and border zones. The relatively rich blood supply of the cortex and subcortical white matter could explain the relative sparing of those regions.

The pathology of subclinical focal radiation injury has not been determined, since patients with these lesions have no symptoms and no histologic diagnosis is obtained.

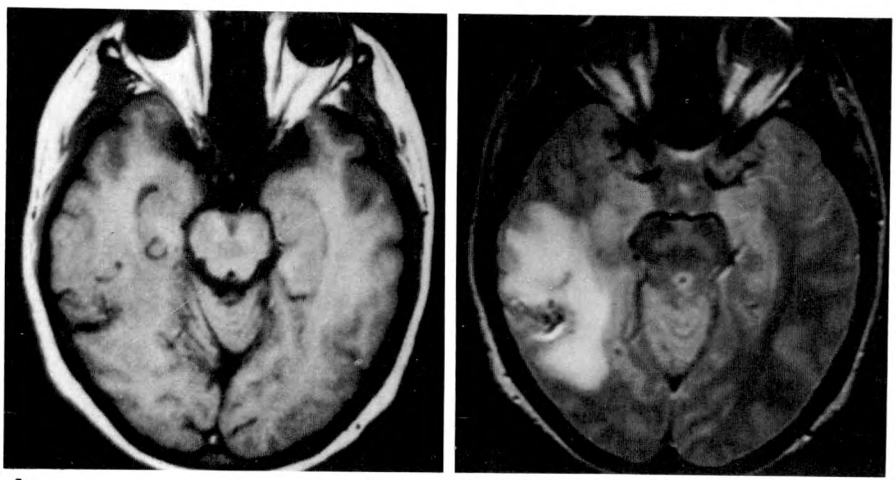



Fig. 3.—Focal radiation injury, asymptomatic.
*A* and *B*, T1-weighted, 600/30 (*A*), and proton-density, 2000/30 (*B*), MR images 2 years after focal helium ion irradiation of a right temporal arteriovenous malformation (AVM). AVM vasculature is seen as foci of flow void in right temporal lobe, surrounded by extensive zone of increased signal on proton-density image. Prolongation of T1 relaxation by edema has reduced white matter signal on T1-weighted image, thereby reducing gray-white differentiation. MR changes reflect degree of edema, rather than underlying tissue disease, and cannot be used to differentiate asymptomatic edema from radiation necrosis.

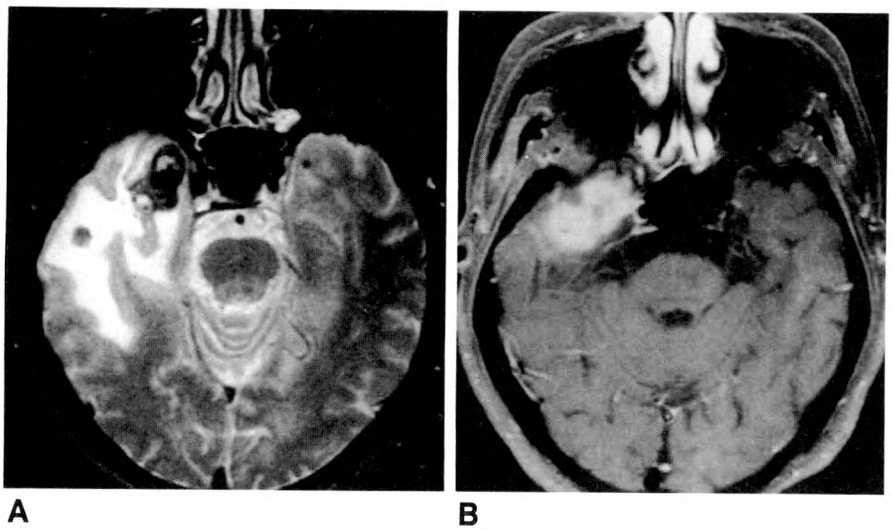



Fig. 4.—Hemorrhagic radiation injury, asymptomatic.
*A* and *B*, T2-weighted, 2800/80 (*A*), and enhanced T1-weighted, 600/20 (*B*), MR images through temporal lobes in patient who had received helium ion irradiation for nasopharyngeal carcinoma 3 years earlier. Increased signal in right temporal white matter is consistent with focal radiation injury or tumor spread. Three hypointense abnormalities, two in the right and one in the left temporal lobe, probably represent hemorrhagic radiation damage. The largest of these has a complex appearance and shows enhancement following administration of gadopentetate dimeglumine. This lesion may consist of focal necrosis or metastatic tumor, as well as hemorrhagic cerebral injury.

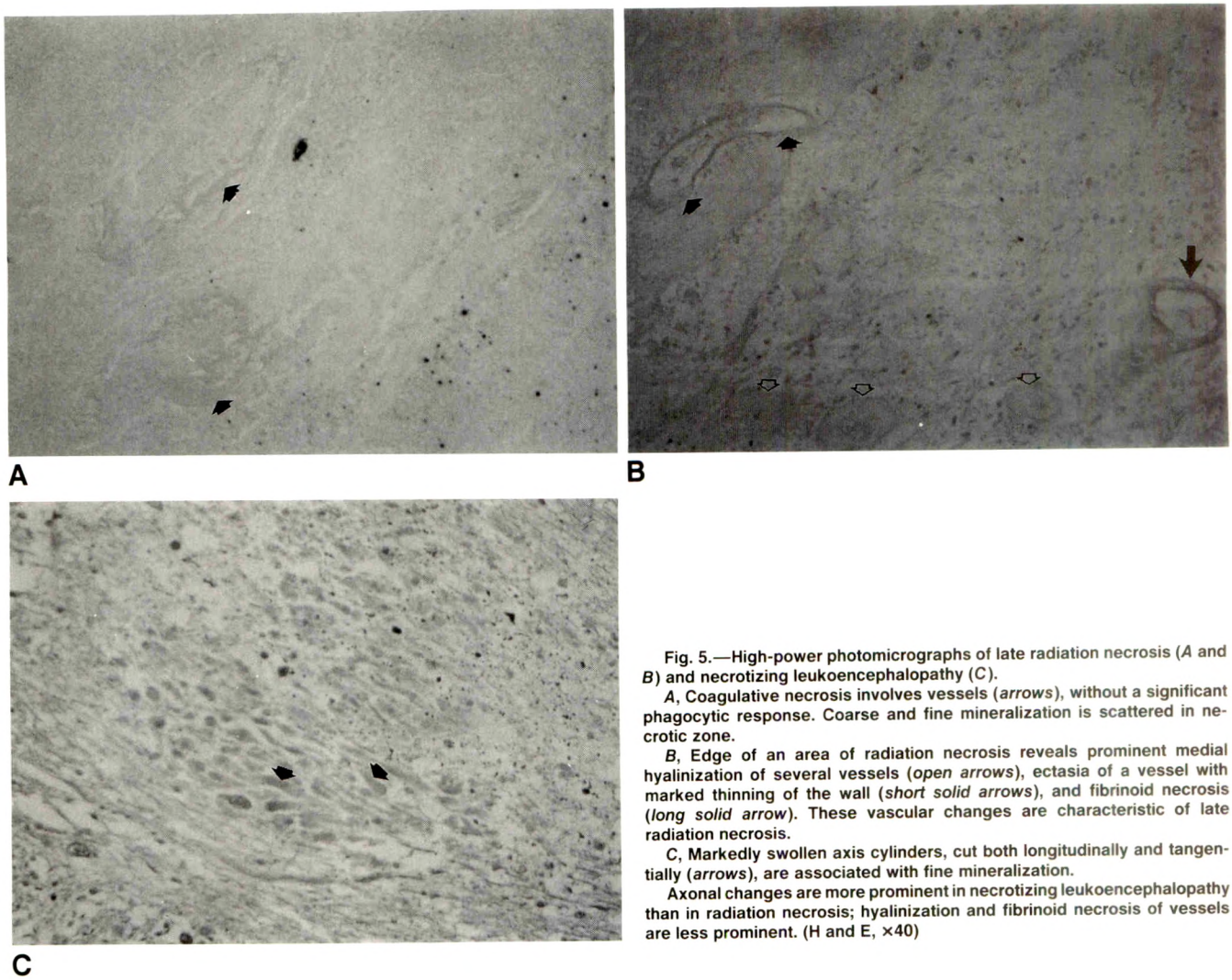



Fig. 5.—High-power photomicrographs of late radiation necrosis (*A* and *B*) and necrotizing leukoencephalopathy (*C*).

*A*, Coagulative necrosis involves vessels (*arrows*), without a significant phagocytic response. Coarse and fine mineralization is scattered in necrotic zone.

*B*, Edge of an area of radiation necrosis reveals prominent medial hyalinization of several vessels (*open arrows*), ectasia of a vessel with marked thinning of the wall (*short solid arrows*), and fibrinoid necrosis (*long solid arrow*). These vascular changes are characteristic of late radiation necrosis.

*C*, Markedly swollen axis cylinders, cut both longitudinally and tangentially (*arrows*), are associated with fine mineralization.

Axonal changes are more prominent in necrotizing leukoencephalopathy than in radiation necrosis; hyalinization and fibrinoid necrosis of vessels are less prominent. (H and E, ×40)

## Diffuse White Matter Injury

### *Clinical Manifestations*

The most prominent clinical features of severe diffuse white matter injury involve impairment of mental function: personality change, impairment of memory, confusion, learning difficulties (in children), and frank dementia, leading to death in the most severe cases [23–26]. Seizure disorders and motor abnormalities may occur also. These manifestations are usually irreversible. Neurologic symptoms commonly develop when the underlying tumor is cured or in remission, particularly after treatment for childhood leukemia [27–30]. While the fiber tracts of the deep, periventricular white matter include the short and long commissural networks; the ipsilateral association pathways; and the main motor, sensory, visual, and language tracts [31]; dysfunction related to these pathways is seen in only a fraction of the patients affected, even of those with the most severe lesions on imaging. Most patients with periventricular MR abnormalities are asymptomatic and have no clinical abnormality.

### *Radiologic Findings*

Prior to CT, there was no diagnostic method for premortem demonstration of diffuse white matter disease. The CT findings of diffuse white matter injury (Fig. 6) were first reported by Martins et al. [10], who described six patients with radiation injury, including one with diffusely reduced attenuation in both frontal lobes. Mikhael [16] subsequently reported eight patients with bilateral, diffuse, low-density lesions involving much of the hemispheric white matter, with no contrast enhancement and no localized mass. Awareness of diffuse white matter injury grew with the advent of MR imaging, which is extremely sensitive to increased water content within the white matter. The first description of postradiation MR findings [32] included five patients with diffusely increased signal in the deep periventricular white matter on T2-weighted images and no focal abnormalities. Since then, more extensive studies have confirmed this finding and have related the MR appearances to clinical manifestations [23, 33, 34].

Periventricular white matter lesions appear as high-signal areas on proton-density and T2-weighted images, varying in

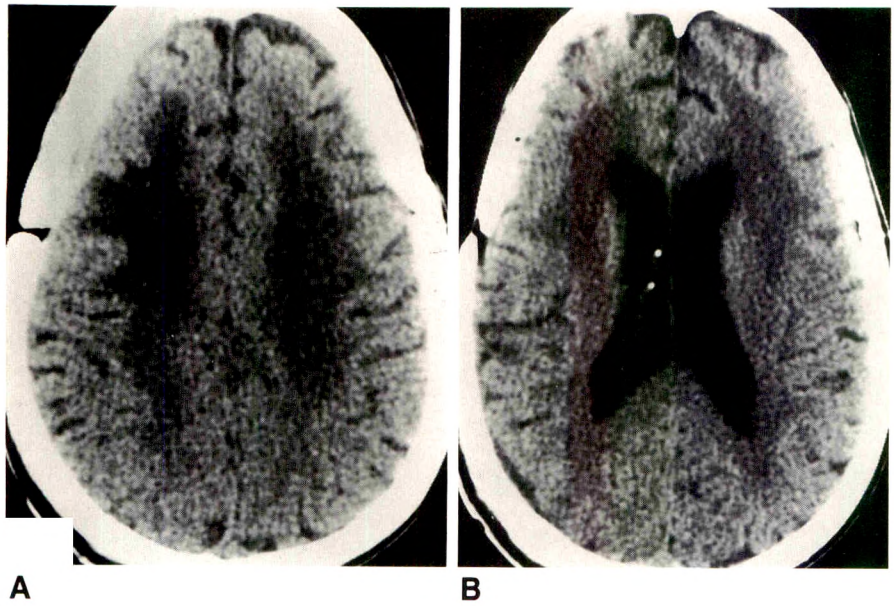



Fig. 6.—Diffuse white matter injury, asymptomatic.

*A* and *B*, CT examination shows bilateral white matter hypodensity without focal abnormality or contrast enhancement in a patient who had received whole-brain photon irradiation for anaplastic astrocytoma 3 years earlier. There is also enlargement of lateral ventricles.

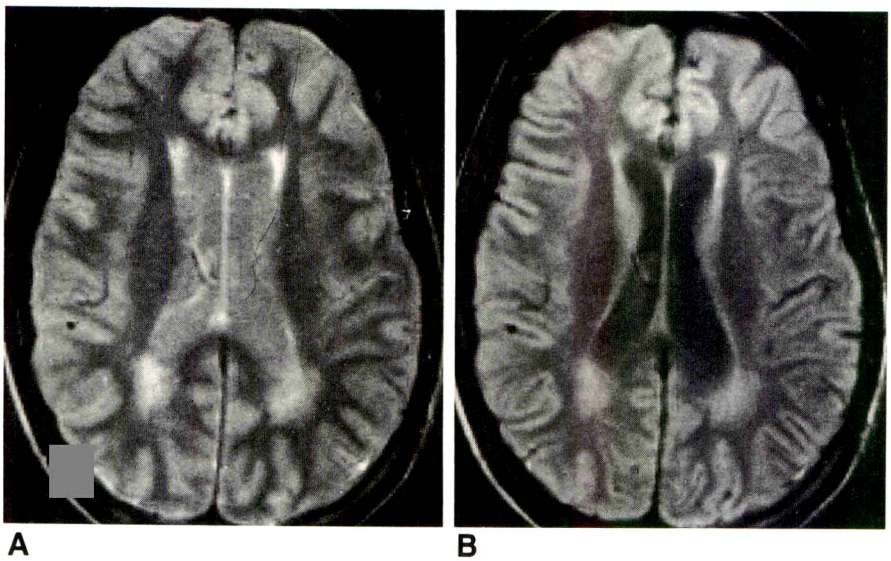



Fig. 7.—Mild diffuse white matter injury, asymptomatic.

*A* and *B*, Proton-density, 2000/30 (*A*), and T2-weighted, 2000/60 (*B*), MR images 17 months after limited-field posterior fossa photon irradiation for cerebellar medulloblastoma. Symmetric foci of increased signal are seen at occipital horns. The patient had no intellectual deficit or other neurologic abnormality and CT examination was normal.

extent from small foci at the angles of the frontal and occipital horns to a confluent band of hyperintensity extending from the ventricular lining to the corticomedullary junction (Figs. 7–10). As in the case of focal injury, there is increase in mobile hydrogen density and prolongation of T1 and T2 relaxation times. The lesions are best seen on proton-density, 2000/30 (TR/TE), or T2-weighted, 2000/80–100, images. The abnormalities are usually symmetric and are indistinguishable from the deep white matter changes seen in ostensibly normal older people and in patients with risk factors for cerebral vascular disease [35–37].

Constine et al. [23] reported periventricular white matter abnormalities on MR in all of 41 irradiated brain tumor patients, but only 32% (56% of adults and 20% of children) showed severe abnormalities. The prevalence of severe abnormalities increased with age, volume of brain irradiated, radiation dose, and interval between irradiation and imaging. Fifty percent of patients who had received whole brain irradiation showed severe abnormalities, compared with 14% of patients treated with local fields. Six patients were imaged before irradiation and five had no pretreatment abnormality. After treatment, all patients showed abnormalities that were mild to moderate in extent, indicating that these changes were caused by irradiation.

Other investigators have reported a lower prevalence of radiation-related white matter lesions on MR. Tsuruda et al. [34] found probable radiation-related lesions in 36 (38%) of 95 irradiated patients, while Curran et al. [33] found lesions in 24 (43%) of 56 patients. Tsuruda et al. also found an increase in the prevalence and severity of lesions with age, with no lesions seen before the age of 20. They attributed the absence of lesions in young patients to shorter follow-up

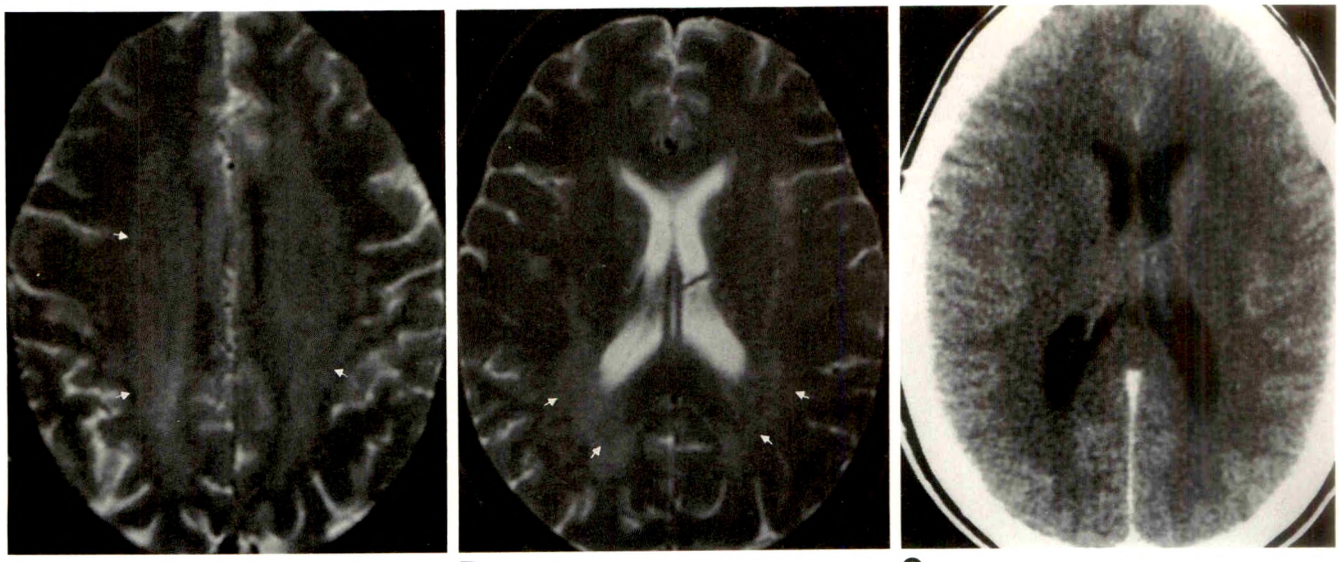



Fig. 8.—Moderate diffuse white matter change, asymptomatic.

*A–C*, T2-weighted, 2000/80, MR images (*A* and *B*) and CT image (*C*) 20 months after regional photon irradiation for brainstem glioma. On MR, there is slight increase in periventricular white matter signal bilaterally, most marked around posterior horns, but also extending anteriorly. Abnormality is mild in degree and moderate in extent. CT image shows no white matter hypodensity.

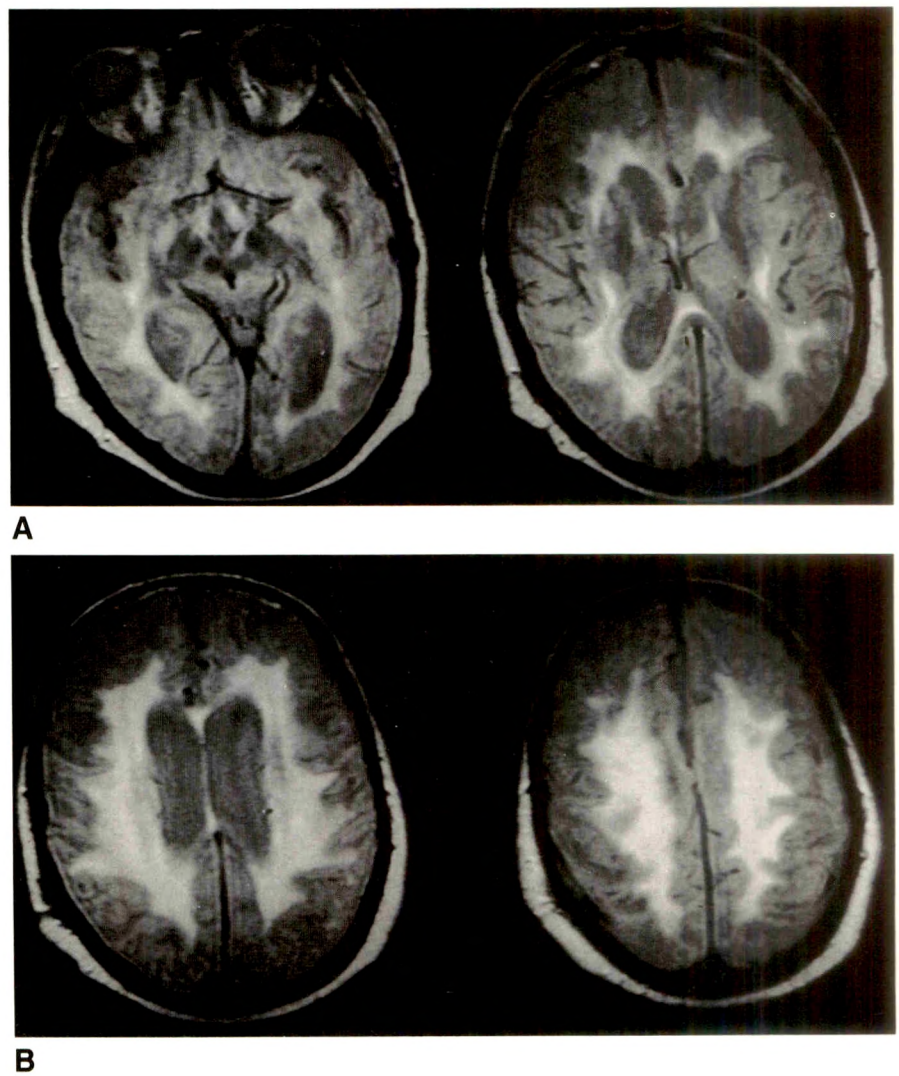



Fig. 9.—Severe diffuse white matter change, asymptomatic.

*A* and *B*, Proton-density axial MR images, 2000/30, 14 months after whole-brain photon irradiation for malignant glioma. There is diffuse increase in white matter signal bilaterally, extending from ventricular lining to corticomedullary junction. The patient had no intellectual or neurologic abnormality.

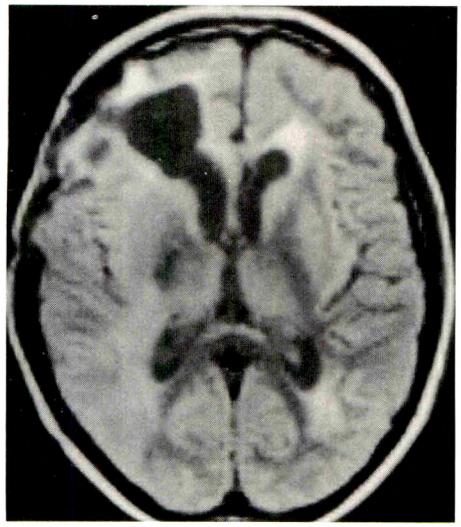


**Fig. 10.—Severe diffuse white matter change, symptomatic. Proton-density MR image, 2000/30, 2 years after whole-brain photon irradiation for right frontal anaplastic astrocytoma. Porencephaly is present at tumor site. Diffusely increased white matter signal is seen bilaterally, surrounding ventricles and extending as far as corticomedullary junction in some areas. Abnormality is more extensive on right, and involves posterior limb of internal capsul on that side. Clinically, there was no evidence of residual or recurrent tumor, but severe dementia had developed during the preceding year.**

(18 months average vs 42 months average in adults) and a high rate (45%) of limited-field irradiation for posterior fossa lesions. The reason for the higher prevalence of MR abnormalities in the patients reported by Constine et al. [23] was not apparent. In our experience, the majority of patients irradiated for posterior fossa tumors will develop focal white matter hyperintensities near the trigones of the lateral ventricles, best seen on T2-weighted images. The rate at which these changes develop is variable, but appears time and dose dependent.

Curran et al. [33] described the MR findings of 24 patients as mild (six patients), moderate (nine patients), or severe (nine patients), and found that seven of eight patients with symptomatic radiation injury had severe MR abnormalities. Three of these patients underwent craniotomy and were found to have coagulation necrosis and perivascular fibrosis, without evidence of tumor. No patients with mild abnormalities and only one patient with moderate abnormalities had symptoms of injury. Constine et al. [23] found a less clear-cut relationship between severity of MR abnormality and clinical injury. Mental dysfunction attributable to radiation was found in seven adults, and five of these had severe MR changes. However, four of 14 asymptomatic adults also had severe changes, while three patients with seizures and one patient with hemiparesis had only minor changes. It is significant that some of the patients with the most severe changes were asymptomatic.

It is clear that severe MR changes do represent clinically significant white matter disease in some cases, but the significance of early changes is more doubtful. No direct association between mild white matter changes and abnormal clinical findings has been reported. However, Constine et al. [23] performed follow-up MR imaging in 13 patients and reported progression of changes in six, over intervals of 8–20 months, suggesting that mild white matter lesions may progress to symptomatic lesions in some patients.

In a study of 31 survivors of malignant glioma, 13 younger and 18 older than age 40, Stylopoulos et al. [38] found an association between postirradiation CT abnormality, mental status, and age. By 2 years postirradiation, all of the older group and over half of the younger group had white matter hypodensities on CT, and all patients who survived 4 years or more developed this finding. CT evidence of white matter injury and cerebral atrophy was always more severe in the older patients. More importantly, the younger survivors maintained a nearly normal mental status despite white matter abnormalities, while those over 40 showed progressive decline.

All studies that compared MR and CT in irradiated patients found that the sensitivity of MR for detecting white matter lesions was two- to threefold higher [23–25, 33] and that CT abnormalities were more closely associated with clinical evidence of injury. CT white matter lesions and early MR lesions probably represent different stages of the same pathologic processes, the CT lesions being more advanced, with more clinical manifestations.

Diffuse white matter injury appears to be a complication of large-volume or whole-brain irradiation. The group studied by Tsuruda et al. [34] included 16 patients who had been irradiated for pituitary tumors, using limited treatment fields. These patients showed no significant increase in the prevalence of diffuse white matter lesions, compared with a nonirradiated control group with pituitary tumors. This observation is consistent with the findings of Rodriguez et al. [20] and Marks et al. [39], who found no diffuse white matter abnormalities following focal irradiation with charged particles.

The nonspecificity of MR imaging led Curran et al. [33], Tsuruda et al. [34], and Constine et al. [23] to exclude the actual tumor site from their studies, since the cause of an abnormality at this site could not be established. As this was frequently the site of highest radiation dose, the results were bound to underestimate focal white matter injury. Exclusion of the primary site also would exclude most cases of focal necrosis, which usually is centered on the primary lesion. However, none of the patients reported by Constine et al. or Tsuruda et al. had clinical findings suggesting focal necrosis.

Focal and diffuse white matter injury may occur together (Fig. 11). On CT examination, some patients have bilateral, diffuse white matter hypodensities, as well as a focal enhancing mass [4, 8, 10, 24]. The focal and diffuse lesions usually occur at the same time [8, 10, 24], but one may follow the other. Cases have been reported where resolution or resection of a mass lesion was followed by development of bilateral white matter hypodensities at a later time [4, 10, 40].

Deterioration of intellectual function with no associated MR abnormality has been reported in survivors of childhood acute lymphoblastic leukemia [41]. All patients had been treated with intrathecal methotrexate and whole-brain irradiation with doses of 18–24 Gy. No patients showed white matter abnormality on MR imaging, but seven of the 10 were below

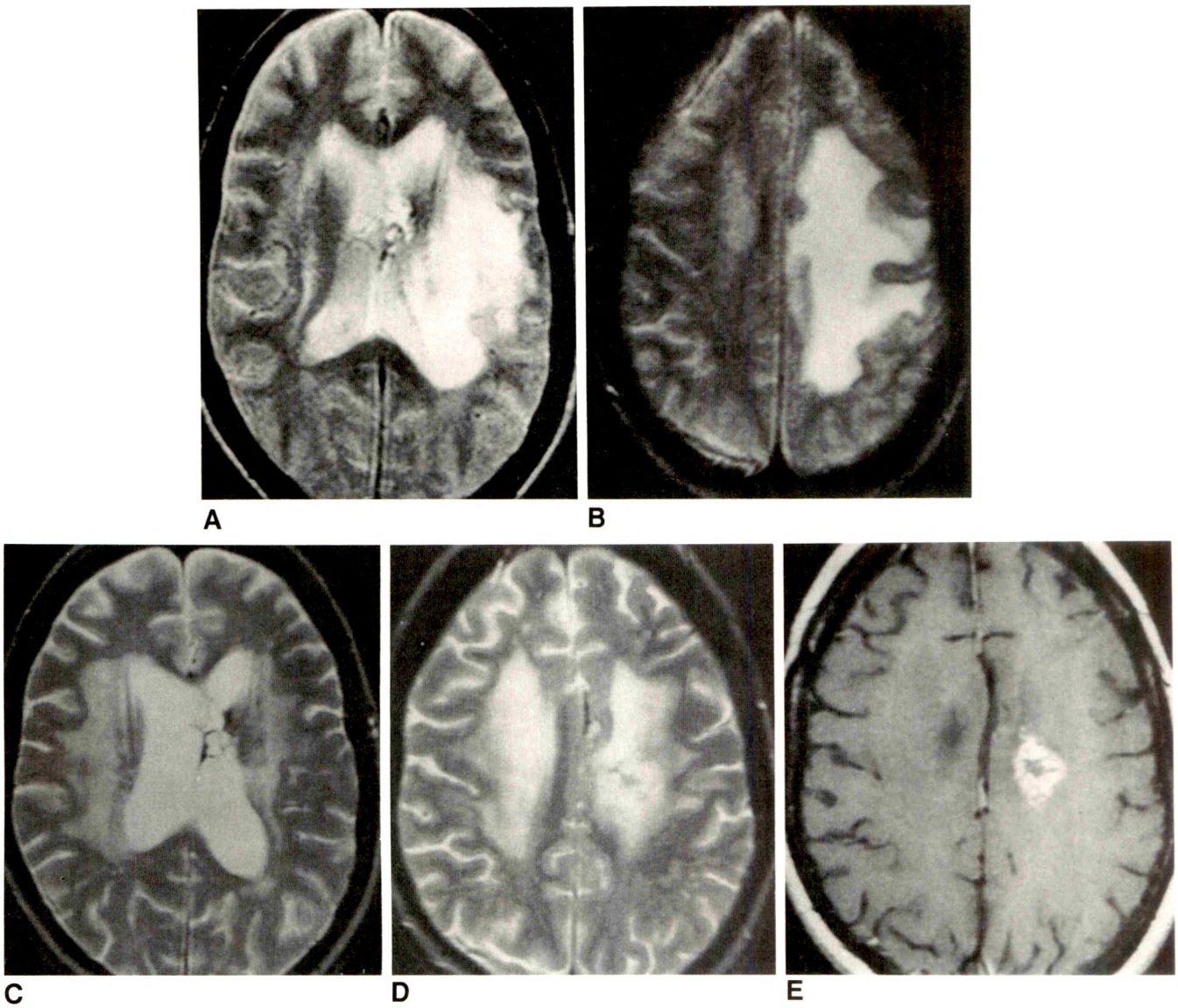



**Fig. 11.—Concurrent focal and diffuse white matter injury, symptomatic.**

***A–E*, T2-weighted MR images, 2000/80, 6 (*A* and *B*) and 11 (*C* and *D*) months after irradiation of left-sided intraventricular neurocytoma and T1-weighted enhanced image, 600/20 (*E*), at 11 months. The patient developed weakness of the right arm 6 months after irradiation, and MR imaging showed severe white matter changes in the left hemisphere, as well as mild changes on the right. During the next 5 months, the patient developed dementia and the motor lesion progressed to right hemiparesis. T2-weighted images at this time (*C* and *D*) showed severe white matter changes bilaterally and imaging with gadopentetate dimeglumine (*E*) demonstrated a focal blood-brain barrier (BBB) defect on the left. Positron emission tomography with $^{18}$F-FDG showed low activity at the site of the BBB defect, confirming the diagnosis of radiation necrosis, rather than tumor recurrence.**

average on neurocognitive testing, and most were experiencing learning difficulties and language deficits. Lack of correlation between CT or MR findings and neuropsychological measures in children has also been reported by other investigators [42, 43], suggesting that the mechanisms underlying intellectual deficits in children may not be related to deep white matter disease.

### *Pathologic Findings*

Diffuse white matter injury, as demonstrated by CT and MR, can reflect a wide spectrum of disease. All stages of radiation injury have in common an increase in free tissue water, which produces hypodensity on CT and increased signal intensity on T2-weighted MR images. This may result from endothelial cell damage, causing increased capillary permeability and vasogenic edema, or from demyelination, leading to replacement of hydrophobic myelin by water [44]. The tissue changes that accompany the increase in water content may vary from minimal change to coagulation necrosis. The MR abnormality is related to water content, rather than tissue damage, and the extent of edema produced by a given lesion may vary from patient to patient. This could explain the finding of severe MR changes in some patients

who have no clinical abnormality, and the occasional finding of only mild changes in symptomatic patients [23, 33]. When necrosis occurs, the pathologic findings are identical to those seen in focal injury: vascular lesions, demyelination, gliosis, and necrotic foci coalescing to form large necrotic areas. Necrosis is the usual autopsy or biopsy finding in patients with frank dementia and diffuse white matter hypodensity on CT [2, 8, 25]. Diffuse white matter necrosis also may be associated with contrast enhancement on CT [2, 25].

There are fewer reports of histologically documented diffuse white matter necrosis than focal necrosis, possibly owing to differences in clinical and radiologic presentations. Focal necrosis presents as a mass lesion, which often must be differentiated from recurrent tumor, and this leads to surgery and biopsy in many cases. On the other hand, diffuse white matter necrosis presents with dementia and bilateral imaging abnormalities, and biopsy usually is not undertaken.

The pathologic findings in patients with mild MR changes, with or without some intellectual deterioration, have not been determined, as such patients rarely come to biopsy or autopsy. The mild changes are identical to those seen in some ostensibly normal people over the age of 65. It has been proposed that these age-related lesions may represent zones of perivascular atrophic demyelination or small areas of infarction resulting from vascular insufficiency [45, 46]. Early lesions of radiation injury may represent similar effects, accelerated by radiation [34].

Caveness and Carsten [47] reported sequential histologic changes in monkeys that were subjected to whole-brain irradiation within the therapeutic range. They found minute foci of necrosis throughout the white matter, which underwent healing or multiplied and coalesced, depending on dose and individual susceptibility. Caveness and Carsten suggested that a large number of acute foci may produce sufficient breakdown in the BBB to cause vasogenic edema, while a large number of healed lesions may produce a loss of brain substance and cerebral atrophy.

### Necrotizing Leukoencephalopathy

Necrotizing leukoencephalopathy is the term used to describe diffuse white matter injury that follows treatment with chemotherapeutic agents, with or without associated radiation. This condition was first reported in survivors of childhood leukemia who had been treated with intrathecal methotrexate [48]. Subsequently this entity was also described after combined radiation and chemotherapy in adult leukemia [49–51], glioma [52, 53], bone or soft tissue sarcoma [26], and small cell carcinoma of the lung [6, 54]. Necrotizing leukoencephalopathy shows similar changes on CT and MR (Fig. 12) and clinical manifestations similar to those seen in postradiation diffuse white matter injury [26, 31, 55]. Initially, it may be manifested as excessive drowsiness [26]. Focal necrosis also may occur after chemotherapy, and we have seen this complication together with diffuse necrotizing leukoencephalopathy, as well as alone.

The prevalence of injury following either treatment method alone is low; when the two are used together, the rate of injury increases markedly [27]. Prophylactic whole-brain irradiation has caused clinical radiation injury with doses as low as 24 Gy, when used together with IV and intrathecal chemotherapy [56].

Most cases of drug-related white matter injury have been described in children, whereas diffuse white matter radiation injury alone is seen mainly in adults. Diffuse injury in adults is manifested primarily by personality change, impairment of memory, and confusion, progressing to frank dementia, whereas injury in children presents with learning and speech difficulties and often is associated with neuroendocrine abnormalities [28].

The latent period between treatment and onset of symptoms is shorter after chemotherapy than after radiation. A group of 39 adult cancer patients with treatment-related white matter hypodensities on CT was studied by Lee et al. [26]. Clinically evident white matter injury developed in seven pa-

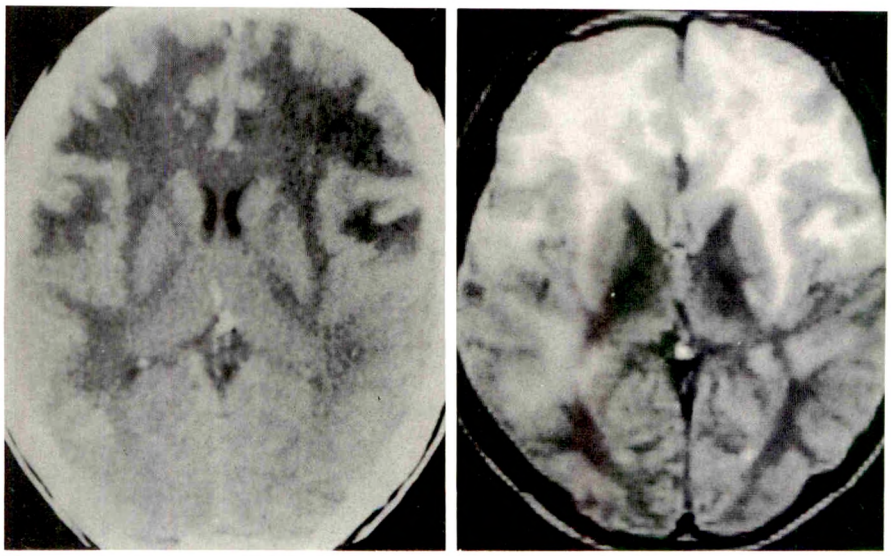



**Fig. 12.—Diffuse necrotizing leukoencephalopathy, symptomatic.**

***A* and *B*, CT scan (*A*) and T2-weighted MR image, 2000/60 (*B*), 10 months after treatment with doxorubicin (Adriamycin) and whole-brain irradiation for adenocarcinoma of the lung. Both studies show evidence of white matter edema, as hypodensity on CT and increased signal on MR, which is most marked anteriorly and extends posteriorly to parietal regions. Clinically, the patient had mild intellectual impairment. CT and MR findings in diffuse necrotizing leukoencephalopathy are similar to the diffuse white matter changes seen after radiation alone.**

tients: in one patient after radiation only, in two after chemotherapy only, and in four after radiation and chemotherapy. In the patients who had chemotherapy only, clinical onset was acute, occurring 1–3 weeks after treatment, and was accompanied by CT changes in two of the three cases. In those who were treated by radiation and chemotherapy, chemotherapy followed radiation by 1–4 years; onset of symptoms followed chemotherapy by 2–4 months. Less frequently, leukoencephalopathy may occur as an acute syndrome, within 12–24 hr of intrathecal or high-dose IV therapy with methotrexate or cytosine arabinoside [26]. Acute symptoms usually resolve within hours to days after cessation of therapy, but some neruologic deficit may persist.

The pathologic findings in necrotizing leukoencephalopathy resemble those of radiation-related white matter necrosis (Fig. 5). Axonal swelling, multifocal demyelination, coagulation necrosis, and gliosis are seen in the periventricular regions and centrum semiovale in both conditions [26, 27, 49, 50]. However, hyalinization and fibrinoid necrosis of arterioles are not seen consistently after chemotherapy, while axonal dysplasia is more common [26, 27, 49, 50].

### Mineralizing Microangiopathy

Mineralizing microangiopathy with dystrophic calcification is the most commonly seen neuroradiologic abnormality in children who have been treated for cancer [28, 57, 58]. Approximately 25–30% of patients who survive more than 9 months after intrathecal methotrexate and cranial irradiation have evidence of intracerebral calcification on CT examination [27]. This is usually seen after combined chemotherapy and radiation, but may occur after radiation alone [27]. Calcification occurs in the basal ganglia, particularly in the putamen, and in the border zone between basal ganglia and cortical perforating vessels [59]. Cortical calcification also may be seen. These findings are frequently associated with evidence of cortical atrophy, as well as white matter hypodensity on CT [29, 59, 60]. Pathologically, there is deposition of calcium in small blood vessels, which are surrounded by varying amounts of mineralized necrotic brain. It is uncertain whether these lesions produce any abnormal clinical manifestations. Price and Birdwell [57] found premortem evidence of abnormal neurologic function in only four of 28 patients who had mineralizing microangiopathy at autopsy, and even in these patients the relationship between the symptoms and the histologic lesions was unclear.

### Cerebral Atrophy

Cerebral atrophy is a frequent late finding after irradiation, almost certainly related to diffuse white matter injury. Constine et al. [23] found enlarged sulci and dilated ventricles in approximately one half (50% by CT and 60% by MR) of 41 irradiated brain tumor patients. Curnes et al. [25] reported MR and CT evidence of atrophy in six of nine patients with symptoms of radiation injury, and Packer et al. [24] found atrophy in all of 11 symptomatic children studied by MR imaging. Microscopically, the lesion of radiation injury involves mainly white matter, whereas CT and MR imaging studies have shown evidence of both white and gray matter atrophy. Injury to deep perforating arteries is one possible mechanism for causing cortical atrophy secondary to white matter disease. The clinical significance of cerebral atrophy, as demonstrated by MR or CT, is uncertain. Evidence of atrophy usually accompanies the clinical syndrome of diffuse white matter injury; however, atrophy also is seen commonly in patients who have no demonstrable intellectual compromise [23]. It must be remembered that corticosteroids and inanition also may lead to the appearance of atrophy on CT and MR studies in brain tumor patients.

### Radiation Injury of Large Arteries

Damage to small and medium-sized arteries of the brain is a prominent feature of late radiation injury, but damage to larger arteries also may be seen [61–65]. Pathologically, fibrinoid necrosis of vessels may occur, but more commonly the changes are those of atherosclerosis, with vascular narrowing and occlusion [66]. Since such changes are common in the general population and the prevalence increases with age, radiation can be implicated as the cause only when vascular disease occurs in childhood [63, 67, 68] or is seen in a radiation field that is away from the usual sites of atheroma. Following focal charged-particle therapy, vascular radiation injury has caused brain necrosis that was remote from the site of irradiation [39]. The diagnosis is made by angiography, which may show stenosis or occlusion of a major artery or narrowing of smaller cortical vessels [65].

In our own experience, we have noted several instances of a moyamoya-like syndrome [69] in young patients treated for craniopharyngioma with focal irradiation fo the sellar and suprasellar regions. This entity may be diagnosed by MR imaging, which demonstrates occlusion of the supraclinoid carotid artery and associated watershed infarctions.

### Early Delayed Radiation Injury

Early delayed radiation injury was first described clinically in 1963 by Rider [70]. He reported two patients who had received radiation therapy for extracranial lesions and 10 weeks later developed brainstem and cerebellar symptoms. Recovery took 10–12 weeks and was spontaneous and complete in both cases; both patients were alive and well 6 years later. Subsequent reports [71–73] have confirmed the usually transient nature of this reaction, which occurs most frequently in the second month after radiation and usually improves within 6 weeks [70]. However, the syndrome can be more severe and has been fatal in extreme cases [73, 74]. Pathologic examination in these cases showed disseminated demyelination.

The main significance of early delayed radiation injury lies in the need to differentiate this condition, which is transient and requires no therapy, from late radiation injury and tumor progression. CT shows nonspecific low-density changes involving the basal ganglia, cerebral peduncles, and deep white matter bilaterally; these resolve completely without treatment

[75]. The early delayed reaction should be suspected when symptoms develop within 3 months of treatment, but the diagnosis can be established only in retrospect, after spontaneous recovery has taken place.

Early CT changes, occurring within a few weeks to months of irradiation, may be due to tumor necrosis alone, without associated cerebral injury. Graeb et al. [76] described three cases in which irradiation was followed by CT changes suggesting tumor progression: increase in central necrosis, new or increased contrast enhancement, and adjacent low-density change. These changes appeared 3 weeks to 3 months after radiotherapy. However, there was no clinical deterioration, and repeat CT study 3–6 months later, without change in therapy, showed regression of the abnormal findings. These early, transient changes almost certainly were due to tumor necrosis, without injury to normal brain.

### Positron Emission Tomography (PET) in the Differentiation of Radiation Necrosis from Recurrent Tumor

Radiation necrosis following irradiation of cerebral tumor presents a problem in diagnosis as well as therapy. Clinical deterioration or change in CT appearance, occurring months to years after irradiation, may be due to tumor recurrence or to radiation necrosis, and it is generally not possible to differentiate the two on radiographic or clinical grounds. PET using the glucose metabolic tracer $^{18}$F-2-fluoro-2-D-deoxyglucose ($^{18}$F-FDG) provides a functional approach to the problem. The potential usefulness of this technique was demonstrated by Patronas et al. [77] and Doyle et al. [78] and was confirmed in later more extensive studies [79, 80].

We performed 38 PET studies in patients who had been treated for malignant glioma by interstitial brachytherapy [79, 81]. Following initial stabilization after irradiation, PET examination was carried out when the CT appearance changed or there was clinical deterioration. Imaging was performed with the Donner 280-crystal positron tomograph, which has in-plane resolution of 8 mm and axial resolution of 11 mm, full width at half maximum [82]. Rubidium-82 was used as a BBB tracer, to define the extent of the lesion in terms of BBB defect. The sensitivity of $^{82}$Rb to change in BBB permeability in our experience is comparable to that of X-ray contrast material used in CT studies. $^{18}$F-FDG was then injected IV and a comparison was made of $^{18}$F-FDG uptake in the lesion and in the immediately adjacent cortex. Active tumor was diagnosed when lesion activity was equal to or greater than adjacent activity; lower lesion activity was interpreted as radiation injury (Figs. 13 and 14). The tumor often was surrounded by a region of metabolic suppression involving the adjacent cortex, and tumor activity was frequently less than contralateral cortical activity but usually greater than adjacent activity. Low lesion activity cannot distinguish radiation injury from other nonfunctioning lesions, such as hematoma or metabolically inactive tumor. However, in this clinical context, exclusion of tumor recurrence does establish radiation injury as the likely cause of posttreatment deterioration.

To determine the prognostic value of the PET diagnosis, we compared the PET result with a clinical diagnosis of tumor recurrence or no tumor recurrence, which was established by following the patient's progress and response to therapy after the PET study [79]. Clinically, it was clear that in some patients tumor was proliferating, while in others it was not. The PET result agreed with the follow-up diagnosis in 15 of 17 cases of tumor recurrence and in 17 of 21 cases of radiation injury. On this basis, the overall accuracy of the PET examination was 84% and the positive and negative predictive values were 79% and 89%, respectively. PET examination frequently provided the only effective means of prospectively differentiating tumor recurrence from necrosis in this patient group. A histologic diagnosis was obtained at reoperation after 18 of the 38 PET studies and apparently viable tumor cells as well as necrotic tissue were seen in all cases, regardless of clinical outcome. This lack of correlation between histologic appearance and biological behavior has been observed also by other investigators [83] and may reflect difficulty in differentiating radiation-induced cytolytic changes and reactive gliosis from tumor.

Di Chiro et al. [80] studied 95 patients with a variety of primary and secondary cerebral tumors who had been referred for evaluation of posttreatment deterioration. They found PET evidence of necrosis in 10 irradiated patients, and these findings were confirmed at surgery or at autopsy. They also found necrosis in four patients who had received chemotherapy only; two of these patients had residual or recurrent tumor as well. In an earlier study of tumor metabolism, Di Chiro et al. [84] found that only high-grade gliomas showed $^{18}$F-FDG uptake equal to or greater than that of normal gray matter and that low-grade gliomas usually showed less, suggesting that the $^{18}$F-FDG technique may not be applicable to low-grade tumors. However, recurrence of low-grade glioma has been demonstrated by PET with $^{18}$F-FDG in a small number of cases [77], so that recurring tumor may show higher $^{18}$F-FDG uptake than a primary lesion does. At the present time there are insufficient data regarding the metabolic level of recurrent low-grade gliomas to use this technique for clinical diagnosis.

### PET and MR Imaging of Focal Radiation Injury

Most studies of radiation injury in humans have involved whole-brain or large-volume photon irradiation, usually given for treatment of intracerebral tumor. In many instances, it has not been possible to differentiate radiation effects near the site of the lesion from the effects of the lesion itself, and in several imaging studies the actual tumor site has been excluded from consideration for this reason [33, 34]. Patients with surgically inoperable cerebral arteriovenous malformations (AVMs) are now being treated with focal irradiation [85], and at the Lawrence Berkeley Laboratory a group of these patients is being followed long-term by MR imaging and PET. These patients present a unique opportunity to study the effects of radiation on normal brain tissue within and immediately around the target region. The AVM is localized, nongrowing, and produces no distant effects. The main local complication is hemorrhage, which usually can be identified

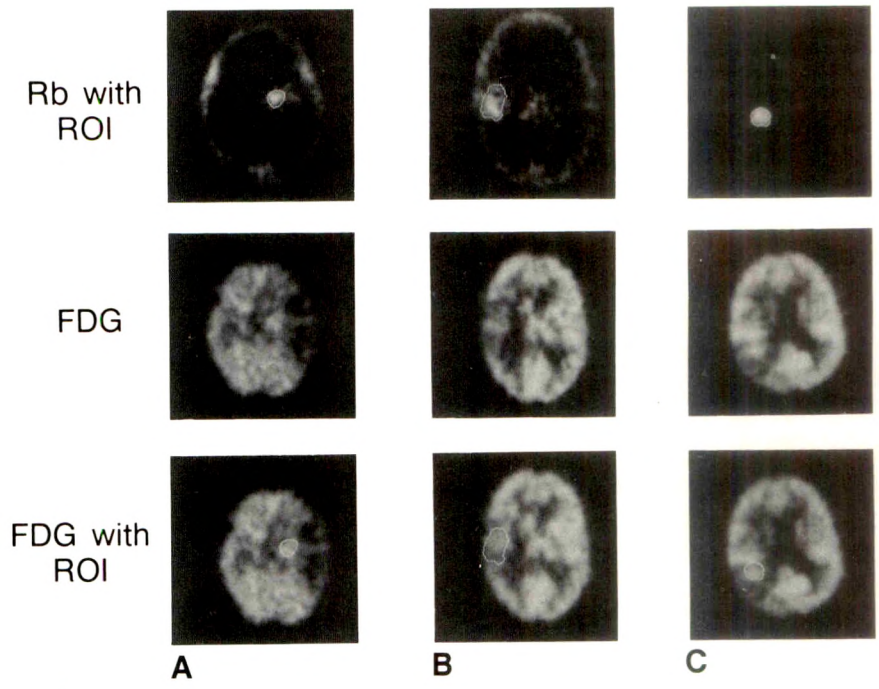



Fig. 13.—Recurrent malignant glioma.
*A–C*, Positron emission tomographic (PET) studies of three patients who had been treated for malignant glioma by interstitial brachytherapy. $^{82}$Rb and $^{18}$F-FDG were used as tracers of blood-brain barrier (BBB) and glucose metabolism. In each case, the patient had stabilized after brachytherapy and then showed deterioration on CT 7–15 months later. BBB defects on $^{82}$Rb images (top row) have been outlined by regions of interest (ROI) superimposed on $^{18}$F-FDG images (bottom row) in order to define extent of lesions. Maximum lesion activity on $^{18}$F-FDG images is greater than activity in immediately adjacent brain region, suggesting a diagnosis of tumor recurrence. In each case, there is peritumoral metabolic suppression. In *B*, maximum lesion activity is less than contralateral normal activity, while exceeding immediately adjacent activity. Clinical follow-up confirmed the PET diagnosis in all cases.

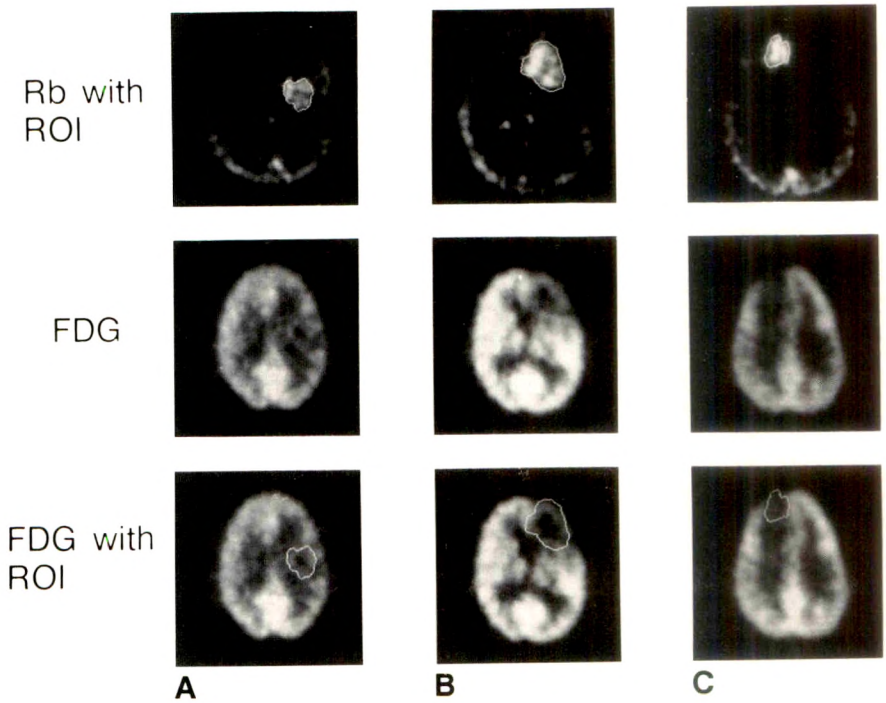



Fig. 14.—Focal radiation necrosis.
*A–C*, Positron emission tomographic (PET) studies in three patients who had been treated for malignant glioma by interstitial brachytherapy. $^{82}$Rb and $^{18}$F-FDG were used as tracers of blood-brain barrier (BBB) and glucose metabolism. Each patient had stabilized after brachytherapy and then showed clinical or CT deterioration 11–23 months later. BBB defects on $^{82}$Rb images (top row) have been outlined by regions of interest (ROI) and superimposed on $^{18}$F-FDG images (bottom row) to define extent of lesions. Maximum lesion activity on $^{18}$F-FDG images is less than activity in immediately adjacent cortex. In *A*, there is suppression of uptake in most of left hemisphere. Clinical follow-up confirmed PET diagnosis in all cases.

by characteristic clinical features and MR findings [86]. Any other changes detected after therapy are likely to be due to radiation, rather than to the AVM itself. Irradiation is performed with a stereotaxically directed helium ion beam, so that the dose is sharply localized, with the 10% isodose contour placed at the periphery of the lesion [85]. Fifteen to 25 Gy is given in a single day, or in two doses given on two consecutive days.

Neurologic deficits related to focal charged-particle therapy have developed in approximately 8% of cases so far [20]. Marks et al. [39] have reported CT and MR findings in seven AVM patients who developed new neurologic and imaging abnormalities 4–22 months after therapy. Five patients had findings consistent with late radiation injury, including low attenuation on CT, high signal on T2-weighted MR images, and mass effect. The abnormality was centered in the target region, but extended beyond the 10% isodose contour in all cases. The pattern of abnormality was consistent with edema, extending out from the injured region along white matter fiber tracts. Abnormal contrast enhancement was also seen, indi-

cating breakdown in BBB. This breakdown was localized to the irradiated region itself and was consistent with radiation necrosis within the target volume. Follow-up imaging showed partial or complete resolution of the CT or MR abnormality in four patients, but significant clinical improvement was seen in only one. This combination of permanent neurologic changes with focal BBB defect and transient edema, occurring several months or more after irradiation, is characteristic of late radiation injury. The remaining two patients had radiation injury of large arteries.

PET studies of BBB, metabolism, and blood flow in irradiated AVM patients have demonstrated some of the pathophysiology of radiation injury. The tracers used were $^{82}$Rb for BBB breakdown, $^{18}$F-FDG for glucose metabolism, and $^{122}$I-HIPDM for perfusion. MR and PET findings in a patient with late radiation necrosis are shown in Figure 15. Nine months after irradiation of a large right thalamic AVM, the patient experienced gradual onset of left hemiparesis and left homonymous hemianopia. MR examination 6 months after clinical onset showed edema and mass effect in the right hemisphere, and a repeat study 6 months later showed persisting edema involving areas of cortex as well as white matter. The AVM appeared obliterated. On PET examination 15 months after commencement of symptoms, $^{82}$Rb uptake showed a region of defective BBB, and $^{18}$F-FDG activity within this region was markedly reduced. There was also markedly reduced metabolism in most of the ipsilateral cortex, where the BBB was intact. The $^{122}$I-HIPDM blood flow study showed that reduced perfusion accompanied the cortical hypometabolism.

The clinical and imaging findings supported the diagnosis of late radiation necrosis. The BBB defect followed the outline of the target region, as shown by isodose contours, and $^{18}$F-FDG uptake here was markedly reduced. The extensive reduction in metabolism and perfusion of the right cerebral cortex probably was due to diaschisis (deafferentation) secondary to destruction of the right thalamus or white matter tracts [87, 88]. A second PET study, performed 1 year after the first, showed more complete metabolic suppression in the right cortex, together with crossed cerebellar diaschisis. There had been interval reduction in $^{18}$F-FDG and $^{82}$Rb accumulation in the irradiated region, probably due to progressive gliosis and loss of vascularity at this site. This sequence of PET and MR findings is consistent with primary radiation necrosis and gliosis in the target area, secondary vasogenic edema spreading through the adjacent white matter, and diaschisis affecting the ipsilateral cortex and contralateral cerebellum.

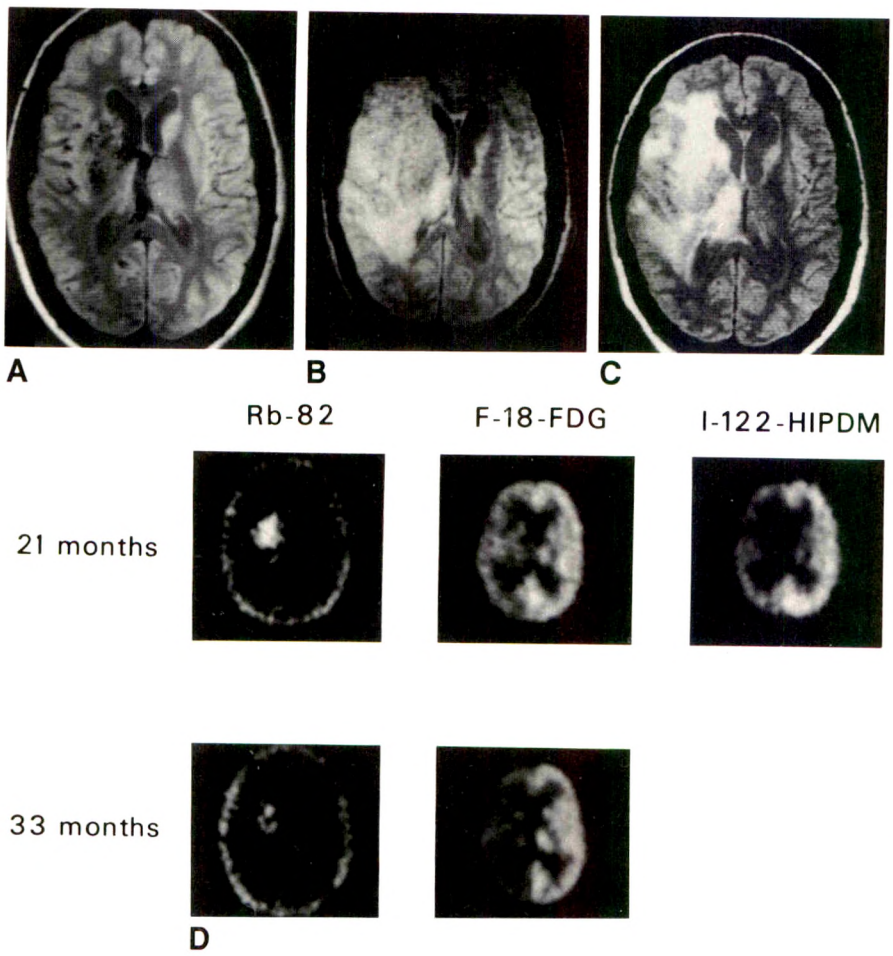



**Fig. 15.—Focal radiation necrosis. The patient was treated with focal helium ion irradiation for arteriovenous malformation (AVM) in right thalamic region and 9 months later experienced gradual onset of left-sided weakness. Neurologic examination 15 months after irradiation showed a severe left hemiparesis and left homonymous hemianopia.**

***A–C*, Proton-density MR images, 2000/33. Pretreatment MR image (*A*) shows numerous small AVM vessels in right thalamic region. Image 15 months later (*B*) shows increased signal throughout much of right-sided white matter, also involving gray matter, and mass effect. At 21 months (*C*), swelling has resolved, but extensive hyperintensity persists in white matter and cortex. AVM is no longer seen.**

***D*, Positron emission tomographic (PET) studies 21 months (top row) and 33 months (bottom row) after irradiation. At 21 months (12 months after onset of hemiparesis), $^{82}$Rb image shows blood-brain barrier (BBB) defect limited to treated area and $^{18}$F-FDG uptake in this region is markedly reduced. There is also markedly reduced $^{18}$F-FDG and $^{122}$I-HIPDM uptake throughout most of right cortex, indicating reduced glucose metabolism and perfusion, with no associated BBB defect. MR and PET findings probably represent radiation necrosis in irradiated region, white matter injury in right hemisphere, and diaschisis affecting right cortex. (Crossed cerebellar diaschisis was also present.) Twelve months later there is decrease in $^{82}$Rb and $^{18}$F-FDG accumulation at site of primary injury, as well as further decrease in $^{18}$F-FDG uptake in right cortex. This probably represents progressive gliosis and reduced vascularity of irradiated tissue. Deafferentation of cortex is more complete.**

Asymptomatic MR hyperintensity is seen more frequently than radiation necrosis. Over 200 AVM patients have been followed for 2 or more years after treatment and evidence of edema has been seen on routine follow-up MR imaging in approximately 40% of asymptomatic patients [20]. The edema is centered on the region of maximum dose and may be restricted to the treated volume or may extend further. Typically, edema becomes apparent during the second post-treatment year and regresses after persisting for a variable period of time. Total resolution has been seen in most cases. The extent of edema that may be seen without clinical manifestations has been surprising: the MR images in Figure 16 show increased signal throughout much of the white matter of the affected hemispheres in two asymptomatic patients.

When neurologic deficits develop in association with an MR abnormality, MR evidence of edema precedes clinically manifested injury in most patients (Fig. 17) [89]. At present, it is not possible to predict which patients with focal edema will develop a neurologic deficit, and we are evaluating the use of PET metabolic studies for this purpose. We found extensive suppression of $^{18}$F-FDG metabolism in the two asymptomatic patients shown in Figure 16. The BBB was intact; we have seen BBB breakdown only in association with clinical neurologic abnormality. Seventeen months later, one of these patients developed expressive dysphasia, difficulty with handwriting, and increased frequency of seizures. These symptoms gradually worsened over a 6-month period. Repeat PET study showed no significant change in the extent of hypometabolism. Rubidium-82 PET and gadopentetate dimeglumine–enhanced MR imaging now showed evidence of a BBB defect. The diagnosis of radiation necrosis was confirmed by histologic examination of tissue obtained at surgery. This case history suggests a possible predictive relationship between metabolic suppression and clinically evident radiation injury. We are performing prospective PET studies of irradi-

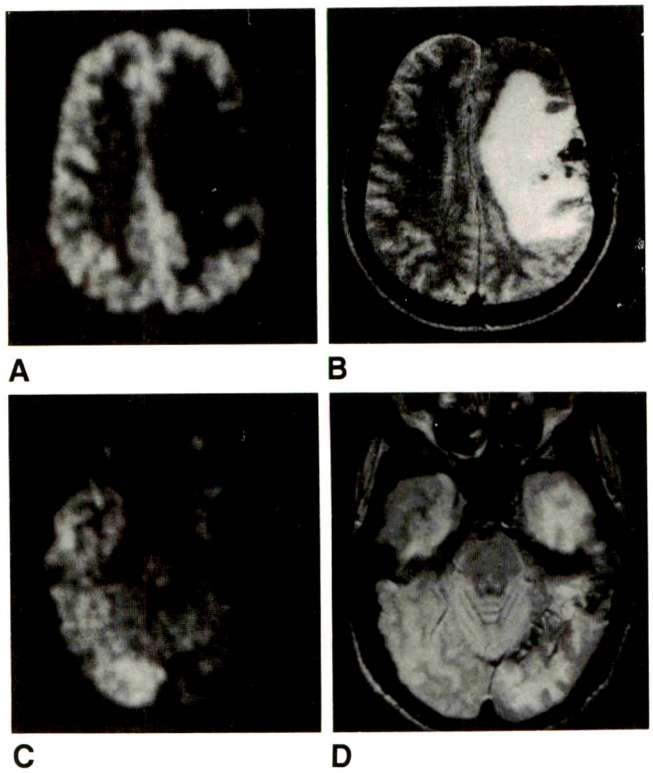



**Fig. 16.—Focal radiation injury, asymptomatic.**

***A–D*, High-resolution positron emission tomographic (PET) and MR images in two patients with arteriovenous malformations (AVMs) 25 (*A* and *B*) and 29 (*C* and *D*) months after helium ion irradiation. AVMs are still visible in left parietal and left temporal lobes, respectively. T2-weighted, 2000/100 (*B*), and proton-density, 2000/30 (*D*), MR images show large areas of hyperintensity around AVM, extending beyond irradiated region. In one patient (*A* and *B*) there was mass effect and abnormal signal involved gray matter as well as white. In both cases, there was marked suppression of cortical glucose metabolism on affected side, and this suppression was similar in extent to MR abnormality. The second patient (*C* and *D*) had no abnormal clinical findings, while the first had a minimal upper motor neuron weakness in the right leg that had been present before irradiation. This patient subsequently developed memory deficit, right hand clumsiness, and increased frequency of seizures. The diagnosis of radiation necrosis was established at surgery.**

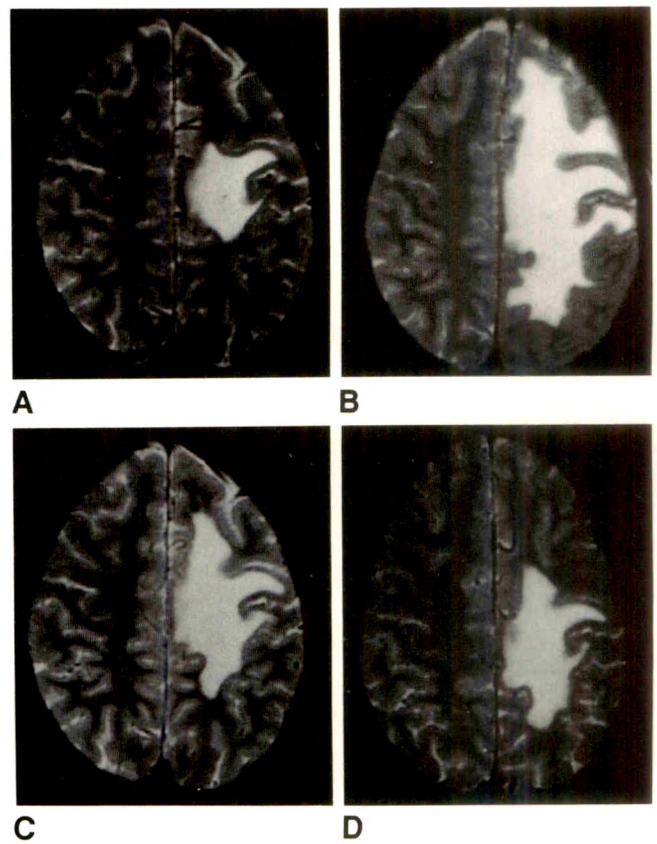



**Fig. 17.—Focal radiation injury, symptomatic. T2-weighted MR images (2000/80) were obtained in a 15-year-old girl who had received focal helium ion irradiation for a large left temporoparietal arteriovenous malformation (AVM).**

***A*, 13 months after treatment. Region of markedly increased signal is in left hemispheric white matter. No neurologic abnormality was present at this time.**

***B*, 20 months after treatment, following development of right hemiparesis. Edema is more extensive, involving gray matter as well as white; mass effect is present. Steroid therapy was commenced and the neurologic deficit gradually improved.**

***C*, MR image 30 months after treatment shows marked resolution of edema.**

***D*, Further resolution is seen at 34 months. At this time, only slight weakness of dorsiflexion of the right foot remained.**

ated patients to investigate this possibility. Steroid therapy has been effective in the treatment of late radiation injury in some cases [13, 20] and difluoromethylornithine has shown promise as an agent for reducing postradiation edema [90]. Prediction of neurologic abnormality would allow therapeutic trials with these or other drugs before irreversible effects develop.

## Conclusions

The radiographic findings of focal radiation necrosis are well recognized. Diagnosis presents a problem only when necrosis occurs at the site of an irradiated cerebral tumor. Tumor recurrence and focal cerebral necrosis cannot be differentiated by CT or MR, but functional imaging by PET now presents an effective means of differential diagnosis. Diffuse white matter injury has been generally recognized only since the advent of MR imaging, which is extremely sensitive to changes in white matter water content. A high rate of bilateral, periventricular MR abnormalities has been found in irradiated patients, but the clinical significance of such findings is still uncertain. Diffuse white matter abnormality on MR imaging may represent a spectrum of disease, ranging from white matter necrosis to minimal lesions that could be related to diffuse vascular disease. Prospective studies of irradiated patient populations are required to establish the relationship between these radiologic appearances and clinical manifestations of radiation injury. Punctate foci of hemorrhage in irradiated brain associated with telangiectasia of blood vessels may represent an unusual vascular response to radiation.

PET has been useful in demonstrating some of the pathophysiologic changes associated with radiation necrosis, and for determining the functional significance of abnormal anatomic images. Metabolic PET abnormalities, occurring in asymptomatic, radiation-treated patients, may have prognostic significance for development of clinically manifested late radiation injury. Confirmation of diagnosis after the onset of symptoms has limited value, as no effective therapy of established neurologic injury exists. Prediction of impending neurologic abnormality is needed to allow evaluation of early therapy with steroids and possibly other drugs, prior to the development of irreversible changes.

## REFERENCES


1. Sheline GE, Wara WM, Smith V. Therapeutic irradiation and brain injury. *Int J Radiat Oncol Biol Phys* **1980**;6:1215–1228
2. Marks JE, Baglan RJ, Prassad SC, Blank WF. Cerebral radionecrosis: incidence and risk in relation to dose, time, fractionation and volume. *Int J Radiat Oncol Biol Phys* **1981**;7:243–252
3. Marsa GW, Goffinet DR, Rubinstein LJ, Bagshaw MA. Megavoltage irradiation in the treatment of gliomas of the brain and spinal cord. *Cancer* **1975**;36:1681–1689
4. Hohwieler ML, Lo TCM, Silerman ML, Freidberg SR. Brain necrosis after radiotherapy for primary intracerebral tumor. *Neurosurgery* **1986**;18(1): 67–74
5. Frytak S, Shaw JN, O'Neill BP, et al. Leukoencephalopathy in small cell lung cancer patients receiving prophylactic cranial radiation. *Am J Clin Oncol* **1989**;12:27–33
6. Laukkanen E, Klonoff H, Allan B, Graeb D, Murray N. The role of prophylactic brain irradiation in limited stage small cell lung cancer: clinical, neuropsychologic and CT sequelae. *Int J Radiat Oncol Biol Phys* **1988**;14:1109–1117
7. Fischer AW, Holfelder H. Lokales Amyloid in Gehirn. *Dtsch Z Chir* **1930**;227:475–483
8. De Reuck J, Eecken V. The anatomy of the late radiation encephalopathy. *Eur Neurol* **1975**;13:481–494
9. Peck FC Jr, McGovern ER. Radiation necrosis of the brain in acromegaly. *J Neurosurg* **1966**;25:536–542
10. Martins AN, Johnston JS, Henry JM, Stoffel TJ, Di Chiro G. Delayed radiation necrosis of the brain. *J Neurosurg* **1977**;47:336–345
11. Glass PJ, Hwang TL, Leavens ME, Libshitz HI. Cerebral radiation necrosis following treatment of extracranial malignancies. *Cancer* **1984**;54:1966–1972
12. Eyster EF, Nielsen SL, Sheline GE, Wilson CB. Cerebral radiation necrosis simulating a brain tumor. *J Neurosurg* **1974**;40:267–271
13. Edwards MS, Wilson CB. Treatment of radiation necrosis. In: Gilbert HA, Kagan AR, eds. *Radiation damage to the nervous system: a delayed therapeutic hazard*. New York: Raven, **1980**:129–143
14. Rottenberg DA, Chernik NL, Deck MDF, Ellis F, Posner JB. Cerebral necrosis following radiotherapy of extracranial neoplasms. *Ann Neurol* **1977**;1:339–357
15. Brismar J, Roberson GH, Davis KR. Radiation necrosis of the brain. Neuroradiological considerations with computed tomography. *Neuroradiology* **1976**;12:109–113
16. Mikhael MA. Radiation necrosis of the brain: correlation between patterns on computed tomography and dose of radiation. *J Comput Assist Tomogr* **1979**;3(2):241–249
17. Kingsley DPE, Kendall BE. CT of the adverse effects of therapeutic radiation of the central nervous system. *AJNR* **1981**;2:453–460
18. Burger PC, Mahley MS, Dudka L, Vogel FS. The morphologic effects of radiation administered therapeutically for intracranial gliomas: a postmortem study of 25 cases. *Cancer* **1979**;44:1256–1272
19. Caveness WF. Experimental observations: delayed necrosis in normal monkey brain. In: Gilbert HA, Kagan AR, eds. *Radiation damage to the nervous system: a delayed therapeutic hazard*. New York: Raven, **1980**: 1–38
20. Rodriguez A, Levy RP, Fabrikant JI. Experimental central nervous system injury following charged particle irradiation. In: Gutin PH, Leibel SA, Sheline GE, eds. *Radiation injury to the nervous system*. New York: Raven, (in press)
21. Woo E, Chen YF, Lam K, Lok AS, Yu YL, Huang CY. Apoplectic intracerebral hemorrhage, an unusual complication of cerebral radiation necrosis. *Pathology* **1987**;19:95–98
22. Groothuis DR, Vick NA. Radionecrosis of the central nervous system: the perspective of the clinical neurologist and neuropathologist. In: Gilbert HA, Kagan AR, eds. *Radiation damage to the nervous system: a delayed therapeutic hazard*. New York: Raven, **1980**:93–106
23. Constine LS, Konski A, Ekholm S, McDonald S, Rubin P. Adverse effects of brain irradiation correlated with MR and CT imaging. *Int J Radiat Oncol Biol Phys* **1988**;15:319–330
24. Packer RJ, Zimmerman RA, Bilaniuk LT. Magnetic resonance imaging in the evaluation of treatment related central nervous system damage. *Cancer* **1986**;58:635–640
25. Curnes JT, Laster DW, Ball MR, Moody DM, Witcofski RL. MRI of radiation injury to the brain. *AJNR* **1986**;147:119–124
26. Lee YY, Nauert C, Glass JP. Treatment-related white matter changes in cancer patients. *Cancer* **1976**;57:1473–1482
27. Bleyer WA, Griffin TW. White matter necrosis, mineralizing microangiopathy, and intellectual abilities in survivors of childhood leukemia. In: Gilbert HA, Kagan AR, eds. *Radiation damage to the nervous system: a delayed therapeutic hazard*. New York: Raven, **1980**:155–174
28. Packer RJ, Meadows AT, Rorke LB, Goldwein JL, D'Angio G. Long-term sequelae of cancer treatment on the central nervous system in childhood. *Med Pediatr Oncol* **1987**;15:241–253
29. Crosley CJ, Rorke LB, Evans A, Nigro M. Central nervous system lesions in childhood leukemia. *Neurology* **1978**;28:678–685
30. DeAngelis ME, Delattre JY, Posner JB. Radiation-induced dementia in patients cured of brain metastasis. *Neurology* **1989**;39:789–796
31. Frytak S, Earnest F, O'Neill BP, Lee RE, Creagan ET, Trautmann JC. Magnetic resonance imaging for neurotoxicity in long-term survivors of carcinoma. *Mayo Clin Proc* **1985**;60:803–812

32. Dooms GC, Hecht S, Brant-Zawadski M, Berthiaume Y, Norman D, Newton TH. Brain radiation lesions: MR imaging. *Radiology* **1986**;158:149–155
33. Curran WJ, Hecht-Leavitt C, Schut L, Zimmerman RA, Nelson DF. Magnetic resonance imaging of cranial radiation lesions. *Int J Radiat Oncol Biol Phys* **1987**;13:1093–1098
34. Tsuruda JS, Kortman KE, Bradley WG, Wheeler DC, Dalsem WV, Bradley TP. Radiation effects on cerebral white matter; MR evaluation. *AJR* **1987**;149:165–171
35. Zimmerman RD, Fleming CA, Lee BCP, Saint-Louis LA, Deck MDF. Periventricular hyperintensity as seen by magnetic resonance: prevalence and significance. *AJNR* **1986**;7:13–20
36. Brant-Zawadski M, Fein F, Van Dyke C, Kierman R, Davenport L, de Groot J. Magnetic resonance imaging of the aging brain: patchy white matter lesions and dementia. *AJNR* **1985**;6:675–682
37. Bradley WG, Waluch V, Brant-Zawadzki M, Yadley RA, Wycoff RR. Patchy, periventricular white matter lesions in the elderly: a common observation during NMR imaging. *Noninvas Med Imaging* **1984**;1:35–41
38. Stylopoulos LA, George AE, de Leon MJ, et al. Longitudinal CT study of parenchymal brain changes in glioma survivors. *AJNR* **1988**;9:517–522
39. Marks MP, Delapaz RL, Fabrikant JI, et al. Intracranial vascular malformations: imaging of charged-particle radiosurgery. Part II. Complications. *Radiology* **1988**;168:457–462
40. Rottenberg DA, Horten B, Kim J, Posner JB. Progressive white matter destruction following irradiation of an extracranial neoplasm. *Ann Neurol* **1980**;8:76–78
41. Kramer JH, Norman D, Brant-Zawadzki M, Albin A, Moore IM. Absence of white matter changes on magnetic resonance imaging in children treated with CNS prophylaxis therapy for leukemia. *Cancer* **1988**;61:928–930
42. Moss HA, Nannis ED, Poplack DG. The effects of prophylactic treatment of the central nervous system on the intellectual functioning of children with acute lymphocytic leukemia. *Am J Med* **1981**;71:47–52
43. Pennock JM, Bydder GM, Dubowitz LMS, Johnson MA. Magnetic resonance imaging of the brain in children. *Magn Reson Imaging* **1986**;4:11–24
44. Holland BA. Diseases of white matter. In: Brant-Zawadzki M, Norman D, eds. *Magnetic resonance of the central nervous system*. New York: Raven, **1987**:259–278
45. Kirkpatrick JB, Hayman LA. White-matter lesions in MR imaging of clinically healthy brains of elderly subjects: possible pathologic basis. *Radiology* **1987**;162:509–511
46. Marshall VG, Bradley WG Jr, Marshall CE, Bhoopat T, Rhodes RH. Deep white matter infarction: correlation of MR imaging and histopathologic findings. *Radiology* **1988**;167:517–522
47. Caveness WF, Carsten AL. Late effects of whole brain irradiation within the therapeutic range. In: *Late biological effects of ionizing radiation*, vol. 2, Vienna: International Atomic Energy Agency, **1978**:221–239
48. Kay HEM, Knapton PJ, O'Sullivan JP, et al. Encephalopathy in acute leukemia associated with methotrexate therapy. *Arch Dis Child* **1972**;47:344–354
49. Rubinstein LJ, Herman MM, Long TF, Wilbur JR. Disseminated necrotizing leukoencephalopathy: a complication of treated central nervous system leukemia and lymphoma. *Cancer* **1975**;35:291–305
50. Price RA, Jamieson PA. The central nervous system in childhood leukemia. II. Subacute leukoencephalopathy. *Cancer* **1975**;35:306–318
51. Allen JC, Rosen G, Mehta BM, Horten B. Leukoencephalopathy following high-dose IV methotrexate chemotherapy with leucovorin rescue. *Cancer Treat Rep* **1980**;64:1261–1273
52. Bresnan MJ, Gilles FH, Lorenzo AV, Wahers GV, Barlow CF. Leukoencephalopathy following combined irradiation and intraventricular methotrexate therapy of brain tumors in childhood. *Trans Am Neuro Assoc* **1972**;97:204–206
53. Norrell H, Wilson CB, Slagel DE, Clark DB. Leukoencephalopathy following the administration of methotrexate therapy into the cerebrospinal fluid in the treatment of primary brain tumors. *Cancer* **1974**;33:923–932
54. Craig JB, Jackson DV, Moody D, et al. Prospective evaluation of changes in computed cranial tomography in patients with small cell lung carcinoma treated with chemotherapy and prophylactic cranial irradiation. *J Clin Oncol* **1984**;2:1151–1156
55. DiChiro G, Arimitsu T, Brooks RA, et al. Computed tomography profiles of periventricular hypodensity in hydrocephalus and leukoencephalopathy. *Radiology* **1979**;130:661–666
56. Leibel SA, Sheline GE. Radiation therapy for neoplasms of the brain. *J Neurosurg* **1987**;66:1–22
57. Price RA, Birdwell DA. The central nervous system in childhood leukemia. III. Mineralizing microangiopathy and dystrophic calcification. *Cancer* **1978**;42:717–728
58. Peylan-Ramu N, Poplak DG, Blei CL, Herdt JR, Vermess M, Di Chiro G. Computer assisted tomography in methotrexate encephalopathy. *J Comput Assist Tomogr* **1977**;1:216–221
59. Flament-Durand J, Ketelbant-Balasse P, Maurus R, Regnier R, Spehl M. Intracerebral calcifications appearing during the course of acute lymphocytic leukemia treated with methotrexate and x-rays. *Cancer* **1975**;35:319–325
60. Giralt M, Gil JL, Borderas F, et al. Intracerebral calcifications in childhood lymphoblastic leukemia. A new iatrogenic disease? *Acta Haematol* (Basel) **1978**;59:193–204
61. Kagan AR, Bruce DW, Di Chiro G. Fatal foam cell arteritis of the brain after irradiation for Hodgkin's disease: angiography and pathology. *Stroke* **1971**;2:232–238
62. Kramer S, Lee KF. Complications of radiation therapy: the central nervous system. *Semin Roentgenol* **1974**;9:75–83
63. Painter MJ, Chutorian AM, Hilal SK. Cerebrovasculopathy following irradiation in children. *Neurology* **1975**;25:189–194
64. Conomoy JP, Kellermeyer RW. Delayed cerebrovascular consequences of therapeutic radiation. *Cancer* **1975**;26:1702–1708
65. Brant-Zawadzki M, Anderson M, DeArmond SJ, Conley FK, Jahnke RW. Radiation-induced large intracranial vessel occlusive vasculopathy. *AJR* **1980**;134:51–55
66. Deck MDF. Imaging techniques in the diagnosis of radiation damage to the central nervous system. In: Gilbert HA, Kagan AR, eds. *Radiation damage to the nervous system: a delayed therapeutic hazard*. New York: Raven, **1980**:107–127
67. Hilal SK, Solomon GE, Gold AP, Carter S. Primary cerebral arterial occlusive disease in children. *Radiology* **1971**;99:87–93
68. Wright TL, Bresmar MJ. Radiation induced cerebrovascular disease in children. *Neurology* **1976**;26:540–543
69. Wilms G, Marchal G, Van Fraeyenhoven L, et al. Unilateral moya-moya disease: MRI findings. *Neuroradiology* **1989**;31(5):442
70. Rider WD. Radiation damage to the brain—a new syndrome. *Can Assoc Radiol J* **1963**;14:67–69
71. Boldrey E, Sheline G. Delayed transitory clinical manifestations after radiation treatment of intracranial tumors. *Acta Radiol* (Stockh) **1967**;5:5–10
72. Hoffman WF, Levin VA, Wilson CB. Evaluation of malignant glioma patients during the postirradiation period. *J Neurosurg* **1979**;50:624–628
73. Lampert P, Tom MI, Rider WD. Disseminated demyelination of the brain following $^{60}$Co (gamma) radiation. *Arch Pathol Lab Med* **1959**;68:322
74. Lampert PW, Davis RL. Delayed effects of radiation on the human central nervous system. "Early" and "late" delayed reactions. *Neurology* **1964**;14:912–917
75. Yamashita J, Handa H, Yumitori K, Mitsuyuki A. Reversible delayed radiation effects on the brain after radiotherapy of malignant astrocytoma. *Surg Neurol* **1980**;13:413–417
76. Graeb DA, Steinbok P, Robertson WD. Transient early computed tomographic changes mimicking tumor progression after brain tumor irradiation. *Radiology* **1982**;144:813–817
77. Patronas NJ, Di Chiro G, Brooks RA, et al. Work in progress: [$^{18}$F] Fluorodeoxyglucose and positron emission tomography in the evaluation of radiation necrosis of the brain. *Radiology* **1982**;144:885–889
78. Doyle WK, Budinger TF, Valk PE, Levin VA, Gutin PH. Differentiation of cerebral radiation necrosis from tumor recurrence by [$^{18}$F]FDG and $^{82}$Rb positron emission tomography. *J Comput Assist Tomogr* **1987**;11:563–570
79. Valk PE, Budinger TF, Levin VA, Silver P, Gutin PH, Doyle WK. PET of malignant cerebral tumors after interstitial brachytherapy. Demonstration of metabolic activity and correlation with clinical outcome. *J Neurosurg* **1988**;69:830–838
80. Di Chiro G, Oldfield E, Wright DC, et al. Cerebral necrosis after radiotherapy and/or intracranial chemotherapy for brain tumors: PET and neuropathologic studies. *AJR* **1988**;150:189–197
81. Gutin PH, Phillips TL, Wara WM, et al. Brachytherapy of recurrent malignant brain tumors with removable high-activity iodine-125 sources. *J Neurosurg* **1984**;60:61–68

82. Derenzo SE, Budinger TF, Huesman RH, Cahoon JL, Vuletich T. Imaging properties of a positron tomograph with 280 BGO crystals. *IEEE Trans Nucl Sci* **1981**;NS-28:81–89
83. Daumas-Duport C, Blond S, Vedrenne CL, et al. Radiolesion versus recurrence: bioptic data in 39 gliomas after interstitial, or combined interstitial and external radiation treatment. *Acta Neurochir Suppl* (Wien) **1984**;33:291–299
84. Di Chiro G, Delapaz RL, Brooks RA, et al. Glucose utilization of cerebral gliomas measured by [$^{18}$F]fluorodeoxyglucose and positron emission tomography. *Neurology* **1982**;32:1323–1329
85. Fabrikant JI, Lyman JT, Frankel KA. Heavy charged-particle Bragg-peak radiosurgery for intracranial vascular disorders. *Radiat Res* **1984**;104[suppl]:244–258
86. Gomori JM, Grossman RI, Goldberg HI, Zimmerman RA, Bilaniuk LT. Intracranial hematomas: imaging by high-field MR. *Radiology* **1985**;157:87–92
87. Feeney DM, Baron JC. Diaschisis. *Stroke* **1976**;17:817–830
88. Baron JC, D'Antona R, Pantano P, Serdaru M, Samson Y, Bousser MG. Effects of thalamic stroke on energy metabolism of the cerebral cortex: a positron tomography study in man. *Brain* **1986**;109:1243–1259
89. Levy RP, Fabrikant JI, Frankel KA, Phillips MH, Lyman JT. Stereotactic heavy-charged-particle Bragg peak radiosurgery for the treatment of intracranial arteriovenous malformations in childhood and adolescence. *Neurosurgery* **1989**;24:841–852
90. Friedman M, Strickland DL, Cheney EL, Kwok L. The role of polyamines in oxidant-induced endothelial cell injury. *Fed Proc* **1987**;46:1399

# Chest CT Combined with Artificial Pneumothorax: Value in Determining Origin and Extent of Tumor

Atsushi Watanabe[1]
Kaoru Shimokata[1]
Hideo Saka[1]
Fumio Nomura[1]
Shuzo Sakai[2]

**To determine the presence of chest wall and mediastinal invasion by lung cancer and to establish the origin of chest tumors, we studied 12 patients with intrathoracic tumors by using chest CT combined with artificial pneumothorax. Six patients had primary lung cancer, two had metastases, and one each had neurofibroma, pericardial cyst, chondroma of the rib, and malignant mesothelioma. All 12 tumors abutted the chest wall or mediastinum and could not be separated by conventional CT. Between 400 and 800 ml of air was injected into the pleural space before a second CT scan was obtained. No invasion was found at surgery in cancers that were separated from chest wall or mediastinum on CT scans. Surgery revealed chest wall invasion in three patients in whom the CT scans showed that the tumor was not separated from the chest wall. Only one patient with a tumor that was not separated from the mediastinum on CT did not have mediastinal invasion: in this case, only adhesions were found at surgery. Thus, in the eight patients with primary lung cancer and metastasis, sensitivity, specificity, and accuracy were 100%, 80%, and 88%, respectively. In four patients with mediastinal or pleural tumor, CT combined with pneumothorax was useful for establishing the origin of tumors. In all, 11 of the 12 patients were correctly evaluated by using this method. No complications occurred, except for mild chest discomfort in one patient.**

**This study suggests that chest CT combined with artificial pneumothorax is useful for the evaluation of the extension of lung cancer into the chest wall and mediastinum and for the diagnosis of the site of origin of intrathoracic tumors.**

*AJR* **156:707–710, April 1991**

CT is useful for the staging of lung cancer, but the information it provides may be limited when the lesion is contiguous to the normal structures. In fact, CT of the chest has relatively low accuracy for detecting chest wall invasion by lung cancer [1–3]. Also, intrathoracic diseases, such as mediastinal tumor, pleural disease, and chest wall lesions, are sometimes mistaken for intrapulmonary lesions [4].

To improve the accuracy of chest CT scans for the detection of chest wall and mediastinal invasion and to establish the origin of the intrathoracic tumors, we performed CT of the chest in combination with artificial pneumothorax. We describe the efficacy and feasibility of this method.

## Subjects and Methods

From July 1987 to September 1989, 12 patients (five men, seven women) with various intrathoracic tumors underwent chest CT in combination with artificial pneumothorax. All tumors abutted the chest wall or mediastinum and could not be separated on conventional CT scans. Patients' ages ranged from 35 to 80 years. Six patients had primary cancer of the lung, two patients had pulmonary metastasis of colonic cancer, and one each had neurofibroma, pericardial cyst, chondroma of the rib, and malignant mesothelioma.

We induced artificial pneumothorax just before CT was performed. The technique for creating the artificial pneumothorax is described by Brandt et al. [5]. We used a pneumothorax needle with a dull tip and a sidehole, which was originally used for pneumoperitoneum, and

Received August 21, 1990; accepted after revision November 16, 1990.

[1] First Department of Internal Medicine, Nagoya University School of Medicine, 65 Tsurumai-cho, Showa-ku, Nagoya 466, Japan. Address reprint requests to K. Shimokata.

[2]Department of Internal Medicine, The Japanese Red Cross Nagoya First Hospital, 3-35, Michishita-cho, Nakamura-ku, Nagoya 453, Japan.

0361–803X/91/1564–0707
© American Roentgen Ray Society

a pneumothorax instrument manufactured by Sugiyama-Gen Co. (Tokyo, Japan; Fig. 1). This instrument operates according to the principle of communicating tubes and uses a water manometer. A pneumothorax needle was inserted, with the patient under local anesthesia, at the fourth or fifth intercostal space of the anterior or middle axillary line or the second intercostal space at the midclavicular line, unless the tumor interfered. When the needle enters the intrapleural space, the water manometer attached to the needle moves in proportion to the intrathoracic pressure. Between 400 and 800 ml of air was injected, depending on the patient's physique and/or the size of the lesion. The degree of the pneumothorax was determined under fluoroscopy. It took from 10 to 15 min to induce the pneumothorax.

CT scanning was performed with CT/T 9200 (Yokogawa Medical Systems, Tokyo, Japan). Scanning time was usually 5 sec per slice, and the interslice gap was 1 cm. Scans were obtained with the patient positioned so that the area of interest was at the top of the body. To evaluate the pneumothorax, we used a wide setting (window width, 1000–1500 H; window level, −700 H). All scans were interpreted by two or more chest physicians and/or radiologists. After completion of this procedure, the patient was carefully observed. The air was not evacuated unless the patient complained of dyspnea. A follow-up chest radiograph was made on the next day. If the pneumothorax did not expand, no further radiographs were obtained.

Eleven of the 12 patients underwent surgical resection. Patients with tumors that were not separated from the chest wall on CT with artificial pneumothorax underwent lobectomy combined with chest wall resection. Resected specimens were examined macroscopically and histologically. One patient did not have surgery because multiple pulmonary nodules in contact with the mediastinal and visceral pleura were considered to be inoperable.

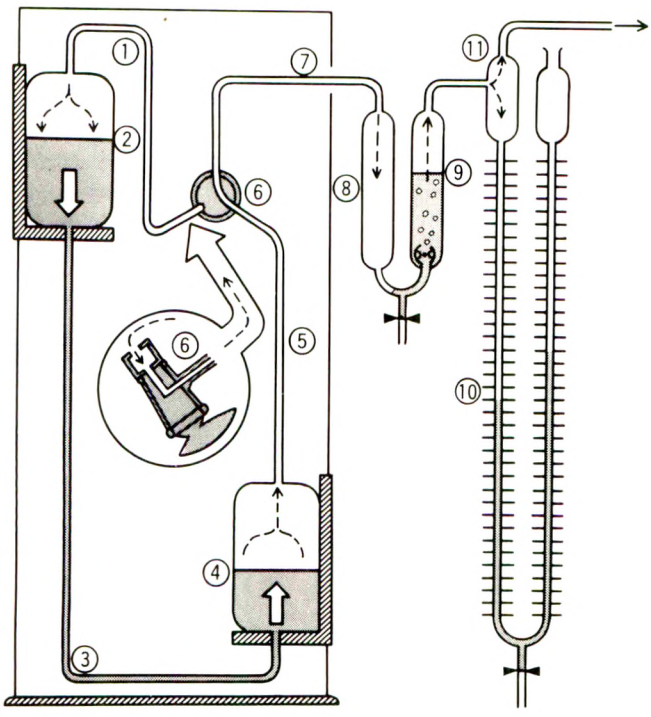



**Fig. 1.—Schematic drawing of pneumothorax instrument. At first, nozzle is placed at neutral position (6), and then a pneumothorax needle (connected to 11) is inserted while manometer (10) is observed. When needle enters intrapleural space, manometer moves in proportion to intrathoracic pressure. Then, nozzle is switched toward upper bottle. Water in upper bottle (2) moves into lower bottle (4), and air in lower side bottle (4) moves through tube (5–6–7–8–9–11) into intrapleural space. Additional air can be injected by changing position of bottle. Air is evacuated by switching stopcock at reversal side.**

## Results

Twelve patients with intrathoracic diseases were studied. Six patients with lung cancer had CT combined with pneumothorax to identify chest wall or aortic invasion. Tumor size ranged from 2.3 to 9.0 cm. The amount of contact between each tumor and the chest wall or mediastinum ranged from 1.6 to 4.0 cm, and in four cases it exceeded 3.0 cm. In three of these patients, the CT scan obtained with pneumothorax showed no separation between the tumor and the chest wall (Fig. 2). In all of these cases, chest wall invasion was identified at surgery. In the three patients in whom the tumors were separated from the chest wall or aorta (Figs. 3 and 4), no invasion was observed at surgery.

Two patients each had a single pulmonary metastasis from colonic cancer that was thought to invade the descending aorta or spine on the conventional CT scan. In one patient, the tumor that abutted the descending aorta on conventional CT was clearly separated from the aorta on the CT combined with pneumothorax; left lower lobectomy was performed uneventfully. The tumor of another patient with pulmonary metastasis was not separated from the spine on the CT with pneumothorax. During surgery, severe pleural adhesion was found. Indeed, the surgical specimen did not extend to the extrapulmonary space. Therefore CT combined with pneumothorax was not useful in this case (Fig. 5). Thus, in eight cases of lung cancer and pulmonary metastasis, sensitivity, specificity, and accuracy of this procedure for determining chest wall or mediastinal invasion were 100%, 80%, and 88%, respectively.

Mediastinal tumors and chondroma of the rib were well separated from the lung on CT scans obtained with pneumothorax. In a case of mesothelioma, the chest radiograph showed multiple nodules in contact with the mediastinum. On CT scans with pneumothorax, most nodules were seen to be attached to the mediastinum or the visceral pleura. These findings were useful for determining the origin of tumors. Thus, 11 of 12 patients were satisfactorily examined.

Complications were rare. One patient had chest discomfort, which was relieved by aspiration of the air. Chest tube drainage was not required.

## Discussion

Artificial pneumothorax has been used in conventional fluoroscopy [6, 7]. However, CT combined with artificial pneumothorax to diagnose various intrathoracic lesions has rarely been reported. Yokoi et al. [8] reported use of pneumothorax CT for the detection of aortic invasion by lung cancer. We used this method for the evaluation of the direct extension of lung cancer and for determining the origin of intrathoracic diseases. In the present study, of the eight patients with primary lung cancers and pulmonary metastases, seven were satisfactorily evaluated for chest wall and mediastinal involvement by using CT combined with pneumothorax. Thus, this procedure can prevent unnecessary thoracotomy and detect potentially curable problems.

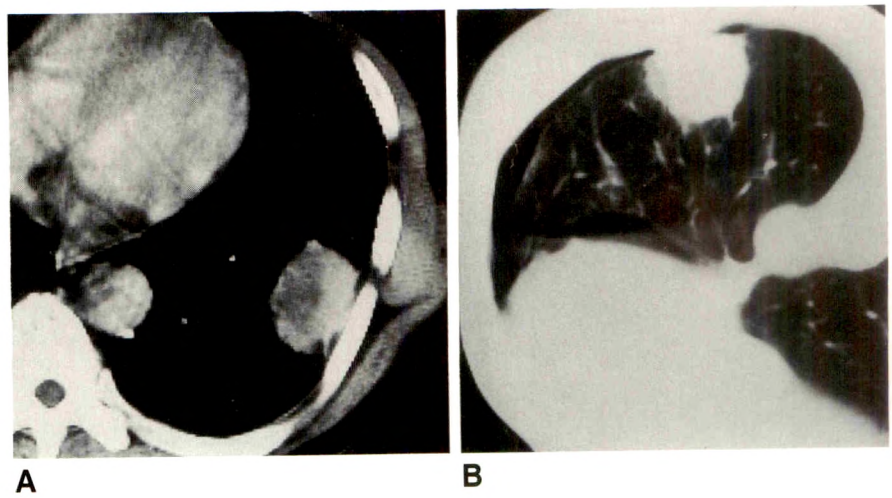



Fig. 2.—Lung cancer in left lower lobe of 64-year-old man.
*A*, Conventional CT scan shows tumor is in contact with chest wall.
*B*, CT scan made after artificial pneumothorax shows tumor is still in contact with chest wall. This finding was verified during surgery, and tumor was resected with chest wall. Histologic diagnosis was adenocarcinoma with invasion of chest wall.

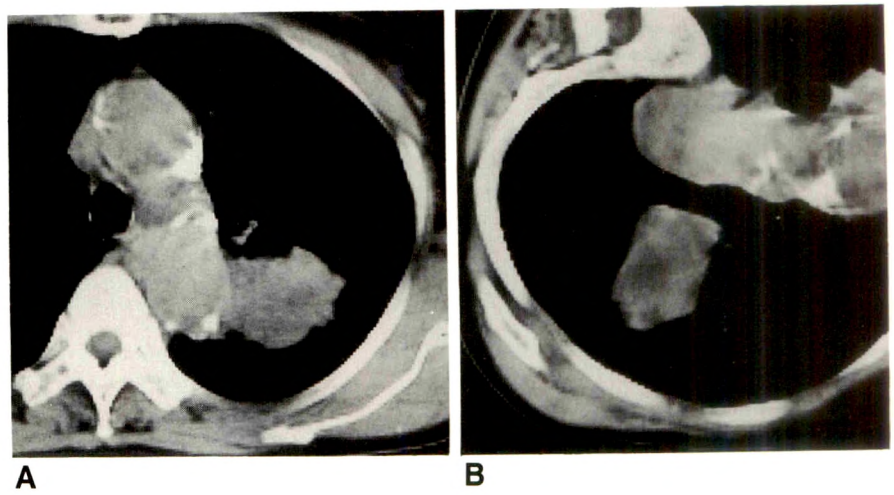


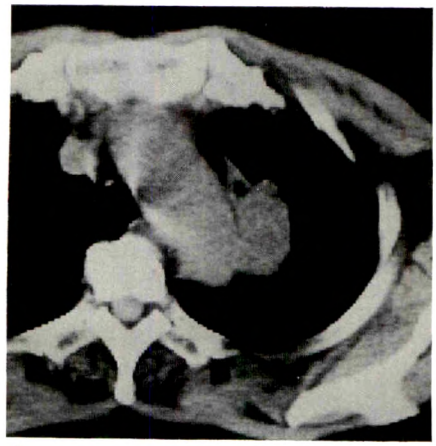

Fig. 3.—Tumor in left upper lobe of 71-year-old woman.
*A*, Conventional CT scan of chest shows a mass in contact with aortic arch.
*B*, CT scan made after induction of pneumothorax shows tumor is separate from aorta. Left upper lobectomy was performed with no evidence of invasion at surgery. Histologic diagnosis was adenocarcinoma.

In a recent report, Glazer et al. [2, 9] suggested CT criteria for chest wall or mediastinal invasion by lung cancer. Conventional CT criteria for chest wall invasion were an obtuse angle between the mass and the pleural surface, more than 3 cm of contiguity with a peripheral pleural margin, and focal pleural thickening. Criteria for mediastinal invasion that was still likely to be technically resectable were contact of 3 cm or less with the mediastinum, less than 90° of direct contact between the mass and the aorta with the total aortic circumference as 360°, and presence of mediastinal fat between mass and mediastinal structures. Applying these criteria to our eight cases of primary lung cancer and pulmonary metastasis, five cases were thought to be unresectable; namely, in four cases, the amount of contact exceeded 3 cm, and in one case, contact with the aorta exceeded 90°. Two of those five tumors appeared to be separated on CT scans obtained with pneumothorax. Thus, CT combined with pneumothorax is a useful technique for improving the accuracy of diagnosis.

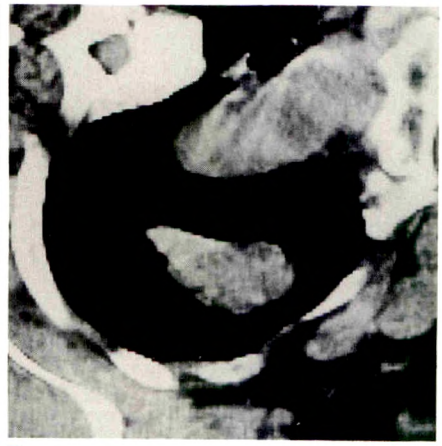
As for other thoracic diseases, the procedure could provide information on the origin of the lesions. In our study, mediastinal tumors, chest wall tumor, and pleural tumor were studied. In those cases, no significant extrapleural line was seen, and it was difficult to diagnose the original sites of the tumors by reviewing chest radiographs and conventional CT scans. These problems do not exist on CT scans obtained with pneumothorax. Therefore, this technique is useful for precise differentiation of intrapulmonary and extrapulmonary lesions and for making a decision on operative procedure.

Complications were minimal. Only one patient complained of mild chest discomfort. Using the pneumothorax instrument, we can monitor the intrathoracic pressure and easily confirm the position of the needle. Therefore, misinsertion into lung parenchyma and subcutaneous and intramuscular emphysema can be avoided [5]. The amount of air can be measured by volume change in the water bottle of the pneumothorax instrument, so we can avoid sending excessive air into the intrapleural space. In this study, we performed this procedure in the hospital, but we think it can be done on an outpatient basis for fully ambulatory patients.

The limitation of this procedure is its unavailability in cases of severe pleural adhesion and impaired pulmonary function. In patients with severe adhesion, careful examination of conventional CT and MR imaging is needed. In our study, we had one false-positive result. As McLoud [10] comments, identification of tumors with mediastinal invasion that are unlikely to be resectable is more difficult than identification of resectability. If tumor was not separated by pneumothorax, careful observation of CT scans obtained with pneumothorax is



A



B

Fig. 4.—Lung cancer in left upper lobe of 58-year-old woman.
*A*, Conventional CT scan shows tumor in contact with aortic arch.
*B*, CT scan obtained with artificial pneumothorax shows tumor is separated from aorta. Left upper lobectomy was done, and no evidence of invasion was seen. Histologic diagnosis was adenocarcinoma.

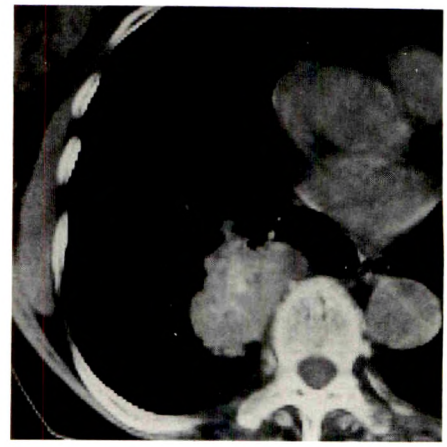


Fig. 5.—Conventional CT scan of pulmonary metastasis in an 80-year-old woman shows tumor with calcification in contact with spine. Even after induction of pneumothorax, most of pleural space, including space between tumor and spine, was not filled with air. During surgery, severe pleural adhesions were found to be cause of failure of separation of pleura by pneumothorax.

necessary. Severe pleural adhesion due to inflammatory diseases must be excluded, and further study including more patients should be done. In patients with impaired pulmonary function, the patient would not be considered a candidate for surgery, and inoperability itself is not an indication for this procedure.

In conclusion, chest CT combined with artificial pneumothorax is useful for the evaluation of the extent of lung cancer. It also clarifies the exact site of intrathoracic diseases, and it can be applied without any troublesome complications.

ACKNOWLEDGMENT

The authors thank Hidehiko Saito, First Department of Internal Medicine, Nagoya University School of Medicine, for his supervision.

REFERENCES

1. Pennes DR, Glazer GM, Wimbish KJ, Gross BH, Long RW, Orringer MB. Chest wall invasion by lung cancer: limitations of CT evaluation. *AJR* **1985**;144:507–511
2. Glazer HS, Duncan-Meyer J, Aronberg DJ, Moran JF, Levitt RG, Sagel SS. Pleural and chest wall invasion in bronchogenic carcinoma: CT evaluation. *Radiology* **1985**;157:191–194
3. Rendina EA, Bognolo DA, Mineo TC, et al. Computed tomography for the evaluation of intrathoracic invasion by lung cancer. *J Thorac Cardiovasc Surg* **1987**;94:57–63
4. Webb WR. Diseases of the mediastinum. In: Putnum CE, Ravin C, eds. *Textbook of diagnostic imaging*. Philadelphia: Saunders, **1988**:456
5. Brandt HJ, Loddenkemper R, Mai J. *Atlas of diagnostic thoracoscopy: indications-technique*, 1st ed. Stuttgart: Georg Thieme Verlag, **1985**:16–23
6. Felson B. The pleura. In: Felson B, ed. *Chest roentgenology*, 1st ed. Philadelphia: Saunders, **1973**:350–379
7. Sautter RD, Myers WO. The amazing case of the mobile chest tumor. *Chest* **1974**;65:341–342
8. Yokoi K, Mori K, Miyazawa N, Magota S, Honda K, Sasagawa M. The role of pneumothorax CT in the evaluation of aortic invasion by lung cancer. *Nippon Igaku Hoshasen Gakkai Zasshi* **1987**;47:1198–1200
9. Glazer HS, Kaiser LR, Anderson DJ, et al. Indeterminate mediastinal invasion in bronchogenic carcinoma: CT evaluation. *Radiology* **1989**;173:37–42
10. McLoud TC. CT of bronchogenic carcinoma: indeterminate mediastinal invasion. *Radiology* **1989**;173:15–16

# Lymphoma of the Lung: CT Findings in 31 Patients

Elaine R. Lewis[1]
Cynthia I. Caskey[1,2]
Elliot K. Fishman[1]

**Lymphomatous involvement of the lungs is often a difficult clinical and radiologic diagnosis to make, yet is often critical in determining treatment. To better define the CT appearance of pulmonary lymphoma, we undertook a retrospective review of 31 patients with recurrent or secondary non-Hodgkin lymphoma or Hodgkin disease and lung parenchymal involvement on CT scans. Diagnoses were confirmed either by lung biopsy or by disease regression or progression with appropriate therapy. The CT scans were evaluated for the following findings: (1) nodules less than 1 cm, (2) a mass or masslike consolidation greater than 1 cm with or without cavitations or bronchograms, (3) alveolar or interstitial infiltrates, (4) masses of pleural origin, (5) peribronchial or perivascular thickening with or without atelectasis, (6) pleural effusions, and (7) hilar or mediastinal lymphadenopathy. The most common CT finding was a mass or masslike consolidation larger than 1 cm, seen in 21 (68%) of the 31 patients. The second most common finding was nodules less than 1 cm (19 patients). Sixty-eight percent of patients had three or more of the CT abnormalities.**

**Lymphoma involving the lung parenchyma causes a variety of CT findings, the most common being a mass or masslike consolidation. Two-thirds of patients have more than one type of CT finding simultaneously.**

*AJR* **156:711–714, April 1991**

Lymphoma involves the lung more frequently in secondary or recurrent disease than as a primary manifestation, particularly in Hodgkin disease (HD) [1, 2]. The frequency of lung involvement also has changed owing to the improvement in prognosis resulting from aggressive therapy [3]. Lymphomatous involvement of the lung is often asymptomatic, and when symptoms do occur, they are often nonspecific, thus making the clinical diagnosis difficult.

CT is used routinely in patients with lymphoma to stage disease; assess response to therapy; evaluate recurrence; monitor patients before and after bone marrow transplantation; and diagnose complications such as pneumonia, radiation injury, and the occasional occurrence of secondary tumors [2, 4, 5]. The radiologic differentiation of pulmonary lymphoma from other diseases can be difficult. Our study was undertaken to characterize the CT findings of lymphomatous involvement of the lung parenchyma, and by doing so, to identify any characteristics that may be useful in this differentiation.

## Materials and Methods

We retrospectively reviewed the medical records of 31 consecutive patients with recurrent or secondary non-Hodgkin lymphoma (NHL) or HD and parenchymal abnormalities on chest CT examinations who were seen at our institution from January 1987 to June 1989. Patients were included in the study if parenchymal involvement and other manifestations of lymphoma were recognized at initial diagnosis or during initial therapy (secondary lymphoma) or if pulmonary findings developed after a disease-free interval after therapy (recurrent lymphoma).

Received August 6, 1990; accepted after revision October 12, 1990.

[1] The Russell H. Morgan Department of Radiology and Radiological Science, The Johns Hopkins Medical Institutions, 600 N. Wolfe St., Baltimore, MD 21205. Address reprint requests to E. K. Fishman.

[2] Department of Radiology, The Union Memorial Hospital, 201 E. University Parkway, Baltimore, MD 21218.

0361–803X/91/1564–0711
© American Roentgen Ray Society

Patients with known infections, additional malignant tumors, or a known immunocompromised state preceding the diagnosis of lymphoma were excluded from the study. The diagnosis was confirmed by lung biopsy or by disease regression or progression with appropriate therapy.

The final study group comprised 15 patients with HD, 12 men and three women 13–56 years old (mean, 27 years), and 16 patients with NHL, eight men and eight women 23–79 years old (mean, 48 years). Of the 15 patients with HD, six (40%) had secondary lymphoma and nine (60%) had recurrent lymphoma. Of the 16 patients with NHL, three (19%) had secondary lymphoma and 13 (81%) had recurrent lymphoma. Confirmation by biopsy was obtained in seven patients with HD and eight patients with NHL. Confirmation in the remaining eight patients with HD and eight patients with NHL was by course of the disease.

CT scans in all patients were obtained with either a Siemens DR3 or DRH scanner with scanning parameters of 3 sec, 230 mAs, and 125 kVp or 4 sec, 310 mAs, and 125 kVp. Contrast-enhanced scans during the infusion of 100 ml of meglumine diatrizoate (60%) were obtained with consecutive 8-mm sections at 1-cm intervals from the lung apex to the diaphragm. All images were viewed at lung (width, 1350; center, −400) and mediastinal (width, 420; center, 36) windows.

For study purposes, the CT findings were divided into seven categories. These categories were chosen on the basis of previous classifications from studies evaluating plain chest radiographs as well as an attempt to use a pattern approach to aid in the differentiation of lymphoma from other disease entities. Five categories included findings involving the lung parenchyma: (1) nodules less than 1 cm, (2) a mass or masslike consolidation greater than 1 cm with or without cavitations and air bronchograms, (3) alveolar or interstitial infiltrates, (4) masses of pleural origin, and (5) peribronchial or perivascular thickening with or without atelectasis. Note was also made of the presence of any pleural effusions and hilar or mediastinal lymphadenopathy, which were recorded as two additional extraparenchymal categories. All patients included in the study had at least one lung parenchymal abnormality in the first five categories. All cases were reviewed independently by two radiologists. Discrepancies in interpretation were evaluated by a third radiologist.

## Results

Mass or masslike consolidation greater than 1 cm with or without cavitations and air bronchograms was the most common finding in secondary or recurrent lymphoma involving the pulmonary parenchyma. This finding was present in 21 (68%) of the 31 patients (Table 1). The diameters of these masses ranged from just over 1 cm to 8 cm. Most had shaggy borders: 93% in NHL and 82% in HD. Forty-seven percent of the masses in NHL had air bronchograms and 32% of the masses in HD had air bronchograms. The air bronchograms were more common in larger masses. A nodule smaller than 1 cm was the second most common CT abnormality, seen in 19 (61%) of the 31 patients. The majority of these nodules had shaggy borders and none contained air bronchograms. The nodules were almost always multiple. Twenty-nine (94%) of the 31 patients had abnormalities in one or both of these two categories, 15 (100%) of the 15 HD patients and 14 (88%) of the 16 NHL patients. None of the patients had a cavitary lesion.

**TABLE 1: Frequency of Findings in Hodgkin Disease and Non-Hodgkin Lymphoma**

| Finding | No. of Patients (%) | | |
|---|---|---|---|
| | Hodgkin Disease ($n$ = 15) | Non-Hodgkin Lymphoma ($n$ = 16) | Total ($n$ = 31) |
| Nodules | 10 (67) | 9 (56) | 19 (61) |
| Masses | 12 (80) | 9 (56) | 21 (68) |
| Infiltrates | 6 (40) | 5 (31) | 11 (35) |
| Pleurally based masses | 5 (33) | 5 (31) | 10 (32) |
| Peribronchial thickening | 6 (40) | 11 (69) | 17 (55) |
| Pleural effusion | 6 (40) | 7 (44) | 13 (42) |
| Adenopathy | 8 (53) | 3 (19) | 11 (35) |

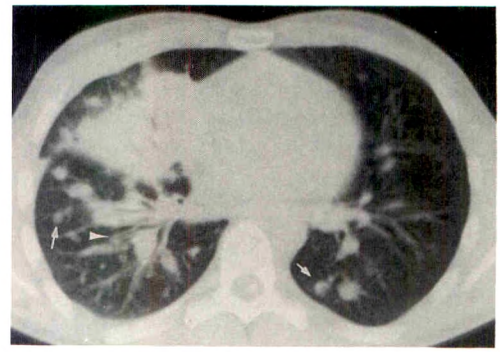


**Fig. 1.—23-year-old man with biopsy-proved nodular sclerosing Hodgkin disease involving lungs. CT scan of lungs shows multiple nodules less than 1 cm bilaterally (*arrows*), a shaggy 5-cm mass with air bronchograms in right middle lobe, and peribronchial thickening on right (*arrowhead*). Note small amount of fluid posteriorly and extending into fissure on right.**

The most common CT abnormality in HD was a mass or masslike consolidation, seen in 12 (80%) of 15 patients. This was not true for NHL, where the most common CT abnormality was peribronchial and/or perivascular thickening, seen in 11 (69%) of 16 patients.

Lymphadenopathy in the chest was more common in HD, seen in eight (53%) of 15 patients, than in NHL, seen in three (19%) of 16 patients. Nodules less than 1 cm, infiltrates (alveolar or interstitial), pleurally based masses, and effusions were seen with fairly equal frequency in both HD and NHL.

Of the 31 patients in the study, 21 (68%) had abnormalities in three or more of the seven categories (Figs. 1–3).

## Discussion

With advances in the treatment of lymphoma and the addition of bone marrow transplantation as a therapeutic option, patients are surviving longer [6]. Patients with a diagnosis of lymphoma are now evaluated with CT as an initial staging procedure, to determine the cause of pulmonary symptoms or fever, or as a routine follow-up for recurrence in an asymptomatic patient. CT is used in preference to plain chest radiography because CT often detects abnormalities in the pulmonary parenchyma that are not visualized on the chest radiograph. Not infrequently, the patients have pulmonary parenchymal findings, and the question is then raised as to whether the parenchymal abnormality is due to lymphomatous involvement or another process.

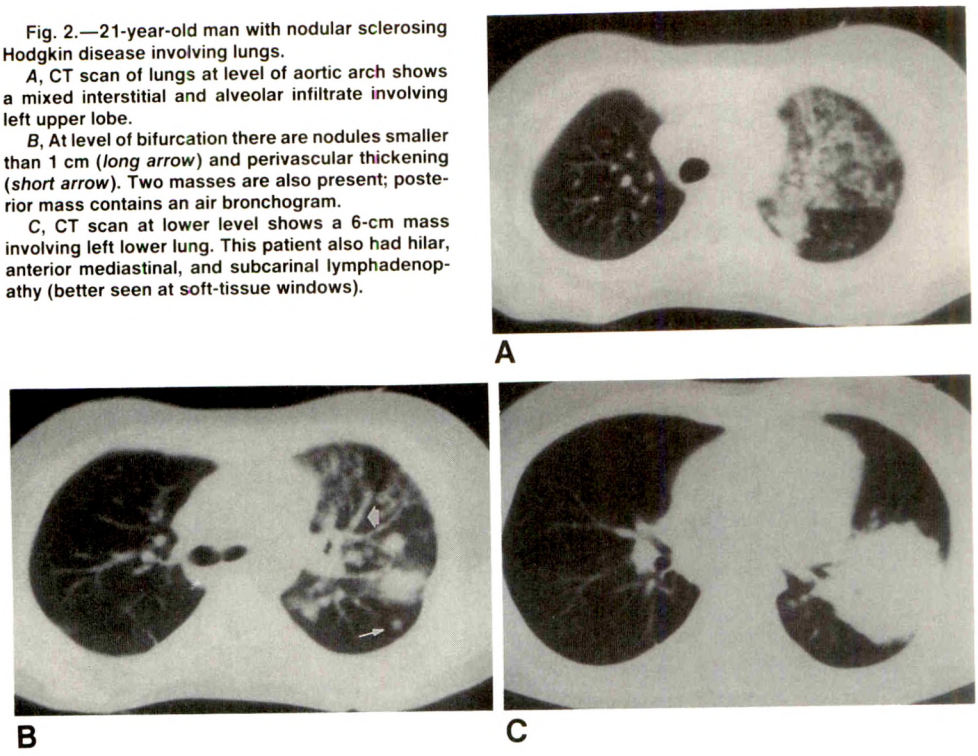



Fig. 2.—21-year-old man with nodular sclerosing Hodgkin disease involving lungs.

*A*, CT scan of lungs at level of aortic arch shows a mixed interstitial and alveolar infiltrate involving left upper lobe.

*B*, At level of bifurcation there are nodules smaller than 1 cm (*long arrow*) and perivascular thickening (*short arrow*). Two masses are also present; posterior mass contains an air bronchogram.

*C*, CT scan at lower level shows a 6-cm mass involving left lower lung. This patient also had hilar, anterior mediastinal, and subcarinal lymphadenopathy (better seen at soft-tissue windows).

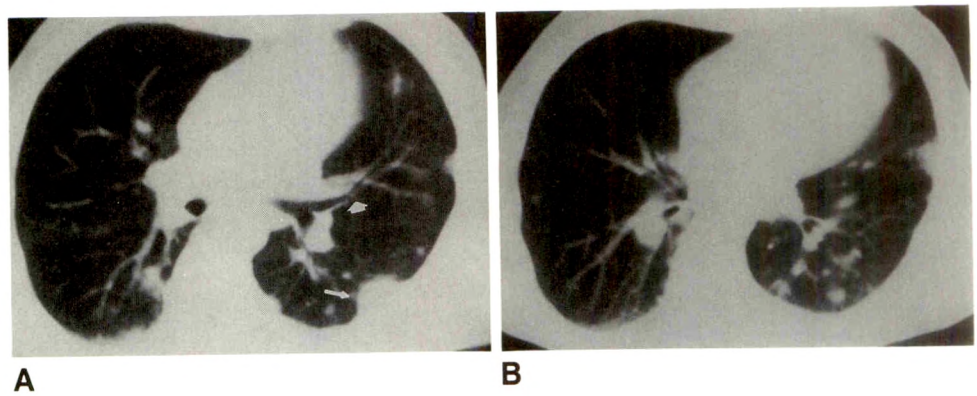



Fig. 3.—75-year-old man with non-Hodgkin lymphoma involving lungs.

*A*, CT scan shows pleurally based mass on left (*long arrow*) with peribronchial thickening (*short arrow*) and a few nodules.

*B*, CT scan at a lower level shows many shaggy nodules smaller than 1 cm in left lung. Lymphadenopathy was also present (better seen at soft-tissue windows).

The prevalence of pulmonary parenchymal disease in lymphoma has been estimated at 12% for HD and 4% for NHL, on the basis of chest radiographic findings at initial presentation [7]. An early study by Robbins [8] of 715 patients being treated for both HD and NHL found a 7% overall involvement of the pulmonary parenchyma on chest radiographs. In a later study, Costello and Mauch [9] detected parenchymal lung involvement in 48% of patients with intrathoracic recurrence of HD. Autopsy series demonstrate an even higher frequency of lung parenchymal involvement of up to 62% [10]; however, this presumably reflects cases of advanced disease. CT studies, which are more sensitive in the detection of parenchymal and pleural disease, demonstrated an 8% prevalence of parenchymal involvement in patients with newly diagnosed HD [11] and a 12% prevalence in patients with suspected relapse of HD [12].

In view of the greater frequency of lung parenchymal involvement in lymphoma after treatment, it is even more important to be able to separate parenchymal involvement due to lymphoma from that due to other disease processes. Currently, the differentiation is often made with biopsy; however, skinny-needle biopsy is often nondiagnostic, particularly at initial diagnosis when a specific subtype is needed to direct treatment. The general paucity of the Reed-Sternberg cells in tissue involved with HD often requires an incisional or excisional biopsy to make a diagnosis [1, 2]. Therefore, it would be particularly useful if a differentiation could be made on the basis of a noninvasive study such as CT.

Lymphoma involving the lung parenchyma has been shown to have a wide variety of radiologic appearances [8, 9, 13–15]. These findings often can be explained on the basis of the anatomy of the lymphatic system in the lungs. One of the

hallmarks of pulmonary lymphoma is spread along the route of the lymphatics [1, 16], most commonly in the form of retrograde spread of tumor directly from involved hilar or mediastinal nodes. It has also been suggested, however, that parenchymal involvement can result from antegrade spread from multiple foci [10, 17]. Hematogenous spread is believed to be rare [10].

Previously, the manifestations of parenchymal lymphoma have been classified on the basis of autopsy and chest radiographic findings. To our knowledge, no classification based on CT findings has yet been described. We divided the radiologic findings of lung involvement by lymphoma seen on CT scans into categories that were readily distinguished when the previous chest radiographic classifications were used as a guide [8, 10, 13]. As interstitial and alveolar infiltrates frequently overlapped, we grouped these findings together. By using this rationale, we devised five parenchymal categories of involvement with pleural effusions and lymphadenopathy as associated findings.

No single finding was found to be typical for lymphoma, although masses greater than 1 cm and nodules less than 1 cm were the most common findings. Nodules had both sharp and poorly defined borders. Peribronchial and/or perivascular thickening also was fairly common (55%). This multiplicity of findings might be expected on the basis of the concept of the spread of lymphoma in the lungs along the lymphatics.

Pleurally based masses were found in 32%, which corresponds to a study by Shuman and Libshitz [14] of 71 patients with HD and NHL in which 31% had solid pleural manifestations of pulmonary lymphoma.

As might be expected, lymphadenopathy was more common in HD patients, because this group included secondary as well as recurrent lymphoma. In untreated patients with HD, a parenchymal abnormality without lymphadenopathy is very rare and most likely represents another process [1, 7, 15]. This is not necessarily the case with NHL or in recurrent disease for either HD or NHL [9, 13].

The prevalence of pleural effusions in association with parenchymal disease (42%) matched a previous description by Balikian and Herman [13] of a 41% prevalence of pleural effusions associated with NHL involving the lung parenchyma. The prevalence of pleural effusions was somewhat lower (6–11%) in another study by Ellert and Kreel [3]. At autopsy, Stolberg et al. [10] found a 76% prevalence of pleural effusions.

Interestingly, Castellino et al. [11] found that 50% of cases of lung parenchymal involvement diagnosed by CT and chest radiography were due to direct invasion. We found no cases of extension of lymphadenopathy into the lung parenchyma; however, the category of peribronchial and/or perivascular disease could be attributed to direct extension.

Possibly the most significant finding of our study is that 68% of patients had more than one abnormal finding. Stolberg et al. [10] also noted simultaneous involvement of the lung parenchyma at different sites at autopsy. It should be acknowledged that this multiplicity of findings may partially be a result of a skewed population, because ours is a tertiary referral hospital with a greater percentage of patients with advanced disease. These various CT findings, particularly when seen in combination, may help differentiate lymphoma involving the lung parenchyma from other processes that may tend to have a predominantly singular pattern, such as vascular congestion, allergic reactions, pulmonary emboli, or opportunistic infections. The importance of knowing the clinical history, however, should be emphasized, because other diseases such as sarcoidosis, Kaposi sarcoma, or bronchoalveolar cell carcinoma also can have a multiplicity of CT findings and therefore a similar appearance. The patients included in this study had a known diagnosis of lymphoma at the time of CT scanning. Even with a known diagnosis of lymphoma, the possibility that some of the findings may be due to a concomitant process cannot be discounted. The usefulness of using this multiplicity of CT findings in an attempt to differentiate pulmonary parenchymal lymphoma from other pathologic processes requires further evaluation with a prospective study.

## REFERENCES


1. Castellino RA. Hodgkin disease: practical concepts for the diagnostic radiologist. *Radiology* **1986**;159:305–310
2. Hoppe RT. The contemporary management of Hodgkin disease. *Radiology* **1988**;169:297–304
3. Ellert J, Kreel L. The role of computed tomography in the initial staging and subsequent management of the lymphomas. *J Comput Assist Tomogr* **1980**;4:368–391
4. Khoury MB, Godwin JD, Halvorsen R, Hanun Y, Putman CE. Role of chest CT in non-Hodgkin lymphoma. *Radiology* **1986**;158:659–662
5. Hopper KD, Diehl LF, Lesar M, Barnes M, Granger E, Baumann J. Hodgkin disease: clinical utility of CT in initial staging and treatment. *Radiology* **1988**;169:17–22
6. Kaplan HD. Hodgkin's disease and other human malignant lymphomas: advances and prospects. Clowes Memorial Lecture. *Cancer Res* **1976**;36:3863–3878
7. Filly R, Blank N, Castellino RA. Radiographic distribution of intrathoracic disease in previously untreated patients with Hodgkin's disease and non-Hodgkin's lymphoma. *Radiology* **1976**;120:277–281
8. Robbins LI. The roentgenological appearance of parenchymal involvement of the lung by malignant lymphoma. *Cancer* **1953**;61:81–88
9. Costello P, Mauch P. Radiographic features of recurrent intrathoracic Hodgkin's disease following radiation therapy. *AJR* **1979**;133:201–206
10. Stolberg HO, Patt NL, MacEwen KF, Warwick OH, Brown TC. Hodgkin's disease of the lung. Roentgenologic-pathologic correlation. *AJR* **1964**; 92:96–115
11. Castellino RA, Blank N, Hoppe RT, Cho C. Hodgkin disease: contributions of chest CT in the initial staging evaluation. *Radiology* **1986**;160:603–605
12. Heron CW, Husband JE, Williams MP. Hodgkin disease: CT of the thymus. *Radiology* **1988**;167:647–651
13. Balikian JP, Herman PG. Non-Hodgkin lymphoma of the lungs. *Radiology* **1979**;132:569–576
14. Shuman LS, Libshitz HI. Solid pleural manifestations of lymphoma. *AJR* **1984**;142:269–273
15. Blank N, Castellino RA. The intrathoracic manifestations of the malignant lymphomas and the leukemias. *Semin Roentgenol* **1980**;15:227–245
16. Rosenberg SA, Kaplan HS. Evidence for an orderly progression in the spread of Hodgkin's disease. *Cancer Res* **1966**;26:1225–1231
17. Rose RM, Grigas D, Strattemeir E, Harris NL, Linggood RM. Endobronchial involvement with non-Hodgkin's lymphoma: a clinical-radiologic analysis. *Cancer* **1986**;57:1750–1755

Case Report

# Mediastinal Seroma After Esophagogastrectomy

Alan J. Kronthal,[1] Richard F. Heitmiller,[2] Elliot K. Fishman,[1] and Janet E. Kuhlman[1]

Mediastinal fluid collections appearing after esophageal surgery may result from anastomotic leakage, abscesses, lymphoceles, or esophageal mucoceles. We present two cases of mediastinal seromas with distinctive CT appearances that occurred after esophagogastrectomy. Because the risk of surgical reexploration is high, recognition of this entity and appropriate treatment is crucial. In the absence of symptoms, we think that these fluid collections can be followed up conservatively. If symptoms of dysphagia or sepsis occur, an initial attempt at percutaneous or transesophageal aspiration and drainage should be made.

## Case Reports

*Case 1*

A 72-year-old man with a history of achalasia and an infiltrating squamous cell carcinoma underwent an esophagogastrectomy and cervical esophagogastric anastomosis. The postoperative course was complicated by recurrent chylous effusions. A postoperative barium swallow revealed no leak. The patient was discharged in good condition, only to return several days later with sepsis. CT (Fig. 1A) revealed moderate pleural effusions and a mediastinal fluid collection. The fluid formed a discrete, well-defined tubular collection within the entire bed of the resected esophagus. No appreciable air or solid component was present. The intrathoracic stomach was compressed and displaced to the right by this collection. Barium swallow (Fig. 1B) again revealed compression and displacement of the intrathoracic stomach without evidence of leak. Because an abscess was suspected, mediastinoscopy was performed, yielding only clear, straw-colored fluid. No leak was identified. Analysis of the fluid suggested a simple seroma. The patient's sepsis was later found to be due to cytomegalovrius colitis, which responded well to antibiotics. He is now being followed up and has had no further difficulty.

*Case 2*

A 68-year-old man with a distal esophageal squamous cell carcinoma underwent a transhiatal esophagogastrectomy after irradiation and chemotherapy. The postoperative course was complicated by recurrent chylous effusions. A barium swallow revealed no leak or obstruction. The patient was eventually discharged in good condition. A routine follow-up CT examination (Fig. 2) showed a loculated mediastinal fluid collection. Again, the fluid collection extended from the thoracic islet to the level of the diaphragm. The intrathoracic stomach was compressed and displaced to the right. The collection lacked any appreciable surrounding wall or solid component. A second barium swallow still showed no leak or obstruction. Because the patient was asymptomatic, he was followed up conservatively. CT examinations in the following 9 months showed no change in the collection. The patient has remained without symptoms.

## Discussion

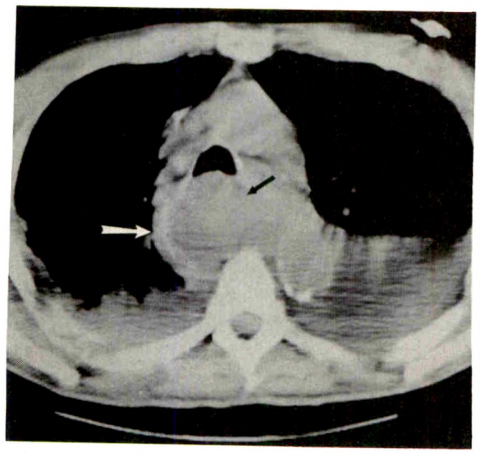
Transhiatal esophagogastrectomy without thoracotomy is used for attempted curative or palliative therapy for esophageal carcinoma and for a variety of benign intractable esophageal abnormalities. The thoracic esophagus is resected, and the stomach is moved into the mediastinum in the original esophageal bed, with reanastomosis to the cervical esophagus. CT is routinely used to examine patients after esophagogastrectomy. Early complications include anastomotic leak, abscess formation, gastric-outlet obstruction, and gastric necrosis. Late complications include recurrent malignant tumor, benign strictures, tracheal aspiration, reflux esophagitis, and bronchoesophageal fistula [1]. Reported causes of mediastinal fluid collections after esophagogastrectomy include esophageal leak, abscesses, lymphoceles, and esophageal mucoceles. We present two cases of an additional cause, mediastinal seroma.

Received October 3, 1990; accepted October 30, 1990.

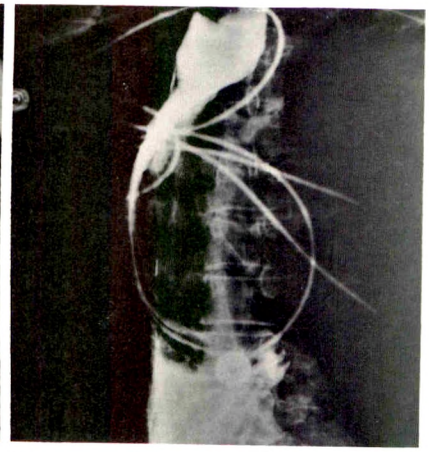
[1] The Russell H. Morgan Department of Radiology and Radiological Science, The Johns Hopkins Hospital, 600 N. Wolfe St., Baltimore, MD 21205. Address reprint requests to E. K. Fishman.

[2] Department of Surgery, The Johns Hopkins Medical Institutions, Baltimore, MD 21205.

*AJR* 156:715–716, April 1991 0361–803X/91/1564–0715 © American Roentgen Ray Society



A



B

Fig. 1.—*A*, CT scan at level of tracheal bifurcation shows mediastinal fluid collection (*black arrow*) compressing adjacent intrathoracic stomach (*white arrow*). Small amount of contrast material is present in lumen of stomach. Bilateral pleural effusions are present.

*B*, Barium swallow shows intrathoracic stomach markedly compressed and displaced to right by an extrinsic mass.

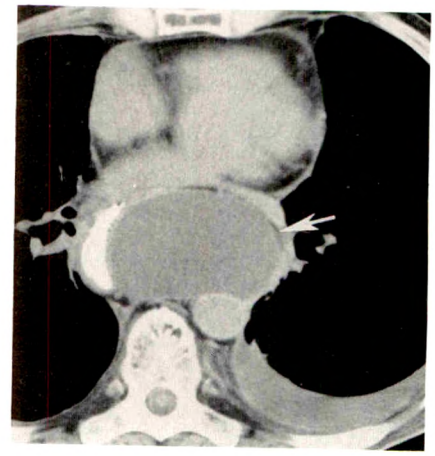


Fig. 2.—CT scan reveals 5.0 × 7.5 cm posterior mediastinal fluid collection (*arrow*). Stomach is compressed and displaced to right. Note small bilateral pleural effusions.

Esophageal anastomotic leaks are diagnosed by contrast extravasation on CT or barium swallow. The prevalence has ranged from 25% to 40% [2]. The patients are usually symptomatic with fever and pain. Many small leaks can be treated conservatively if there is minimal self-contained extravasation without pleural contamination or overt signs of sepsis. Although surgery has been the treatment for larger leaks, percutaneous catheter placement and drainage has had recent success [3]. Abscesses may have associated air collections or communication with an empyema or subphrenic abscess [4]. Virtually all patients have symptoms. As with leaks, percutaneous or transesophageal aspiration and drainage increasingly have replaced surgical treatment [5].

Lymphoceles result from damage to the thoracic duct or one of its tributaries. In such instances, chylous effusions are common postoperative complications. Mediastinal fluid collections that have negative CT attenuation, indicating fat content, are highly suggestive of lymphoceles. If symptoms are present, reexploration with ligation of the thoracic duct has been a successful treatment [6]. Limited success also has been obtained with long-term percutaneous catheter drainage [7]. Esophageal mucoceles result from surgical isolation of the thoracic esophagus, a procedure rarely performed when malignant disease is too extensive to allow definitive resection, or in benign disease for temporary bypass to allow reestablishment at a later date. The proximal and distal portions of the thoracic esophagus are divided, with ligation of the isolated thoracic segment. The stomach is then moved cephalad and anastomosed to the proximal esophagus, thereby reestablishing continuity. The isolated segment of the esophagus then becomes a mucocele, a closed, cystic structure filled with proteinaceous secretions. Clinical history obviously aids in differentiating this entity from other mediastinal fluid collections after surgery [8].

Two cases of mediastinal seromas occurring after esophagogastrectomy are presented. One was treated by mediastinoscopy and drainage, whereas the other has been followed up conservatively. The fluid, judging by its CT configuration, appears to accumulate in a space created by surgical dissection of fascial planes during esophagectomy. The importance lies in differentiating this entity from other postoperative mediastinal fluid collections such as abscess or anastomotic leak. The absence of contrast extravasation on barium swallow or CT, and the lack of an associated air collection or solid component, should suggest a mediastinal seroma. Without an associated soft-tissue mass, fluid collections are unlikely to represent recurrent malignant tumors.

In an asymptomatic patient, we believe that these seromas can be managed conservatively. If symptoms such as dysphagia or sepsis evolve, percutaneous or transesophageal drainage can be attempted. Because of the high risks of reexploration, surgical intervention should be used only as a last resort.

## REFERENCES


1. Owen JW, Balfe DM, Koehler RE, Roper CL, Weyman PJ. Radiologic evaluation of complications after esophagogastrectomy. *AJR* **1983**;140: 1163–1169
2. Agha FP, Orringer MB, Amendola MA. Gastric interposition following transhiatal esophagectomy: radiographic evaluation. *Gastrointest Radiol* **1985**;10:17–24
3. Maroney TP, Ring EJ, Gordon RL, Pellegrini CA. Role of interventional radiology in the management of major esophageal leaks. *Radiology* **1989**;170:1055–1057
4. Glazer HS, Siegel MJ, Sagel SS. Low-attenuation mediastinal masses on CT. *AJR* **1989**;152:1173–1177
5. Meranze SG, LeVeen RF, Burke DR, Cope C, McLean GK. Transesophageal drainage of mediastinal abscesses. *Radiology* **1987**;165:395–398
6. Ngan BH, Fok M, Wong J. The role of lymphography in chylothorax following thoracic surgery. *Br J Radiol* **1988**;61:1032–1036
7. van Sonnenberg E, Wittich GR, Casola G, et al. Lymphoceles: imaging characteristics and percutaneous management. *Radiology* **1986**;161: 593–596
8. Glickstein MF, Gefter WB, Low D, Stephenson LW. Esophageal mucocele after surgical isolation of the esophagus. *AJR* **1987**;149:729–730

Case Report

# Noncompaction of Ventricular Myocardium: CT Appearance

Dewey J. Conces, Jr.,[1] Thomas Ryan,[2] and Robert D. Tarver[1]

During early embryonic development, the heart consists of a trabecular network of spongelike myocardium [1]. The intertrabecular spaces communicate with the chambers of the heart. As the heart develops, the myocardium becomes compacted and the meshlike pattern disappears.

Failure of normal myocardial differentiation results in noncompaction of the myocardium, a rare disorder in which the trabecular myocardium persists. We report a case of myocardial noncompaction involving the left ventricle that was imaged with CT.

## Case Report

A 44-year-old woman had numbness and weakness in her left hand for 5 days before admission. CT examination of her head showed an infarct in the right parietal lobe. Echocardiography was performed and showed a left ventricle mass. Findings on Doppler sonography of the carotid artery were normal. The patient was transferred to our institution for evaluation of the cardiac mass.

By the time of transfer, the patient had experienced significant neurologic recovery. On cardiac examination, a short midsystolic murmur was present with multiple systolic clicks. An ECG showed left ventricular hypertrophy. A chest radiograph showed left ventricular prominence consistent with left ventricular hypertrophy.

Two-dimensional (2-D) echocardiography showed marked thickening and trabeculation of the apical, lateral, and inferior walls of the left ventricle (Fig. 1A). Cystlike areas were seen within the thickened myocardium. Doppler examination demonstrated flow within the cystic areas.

A contrast-enhanced thoracic CT scan showed marked thickening of the left ventricular wall (Fig. 1B). The thickening was seen to involve the apical, anterior, lateral, and inferior portions of the left ventricle. The distal portion of the intraventricular septum also was involved; the proximal portion was spared. The thickened wall was made up of two zones of differing density. The outer portion of the ventricular wall consisted of a band of uniform tissue with a density similar to that of muscle. This zone was approximately 0.7 cm thick. More centrally, the appearance of a wider inner zone suggested that it was composed of a mixture of contrast-enhanced blood and soft tissue with a density similar to that of muscle. This region measured in thickness from 2.4 cm in the basilar region to 3.0 cm in the apex.

The patient was given anticoagulants and discharged to continue physical therapy as an outpatient.

## Discussion

The persistence of trabeculated myocardium has been reported involving both the right and left ventricles [2, 3]. Reported cases are frequently associated with other cardiac anomalies, including pulmonary atresia and coronary artery abnormalities [3, 4]. No associated cardiac anomalies were identified in our patient, although the presence of coronary artery anomalies has not been excluded.

Previously reported patients with isolated left ventricular involvement ranged from 11 months to 22 years old [2, 5]. Our patient, at 44 years old, was significantly older than previously reported patients. Patients may be asymptomatic or exhibit signs and symptoms of heart failure, arrhythmias, or systemic emboli [2, 5]. The cause of the decreased left ventricular function is not clear, but may be related to faulty intramural perfusion due to the presence of the trabeculations

Received October 19, 1990; accepted after revision November 29, 1990.

[1] Department of Radiology, Indiana University Medical Center, 926 W. Michigan St., Indianapolis, IN 46202-5253. Address reprint requests to D. J. Conces, Jr. (X-64).

[2] Department of Internal Medicine, Indiana University Medical Center, Indianapolis, IN 46202.

*AJR* 156:717–718, April 1991 0361–803X/91/1564–0717 © American Roentgen Ray Society

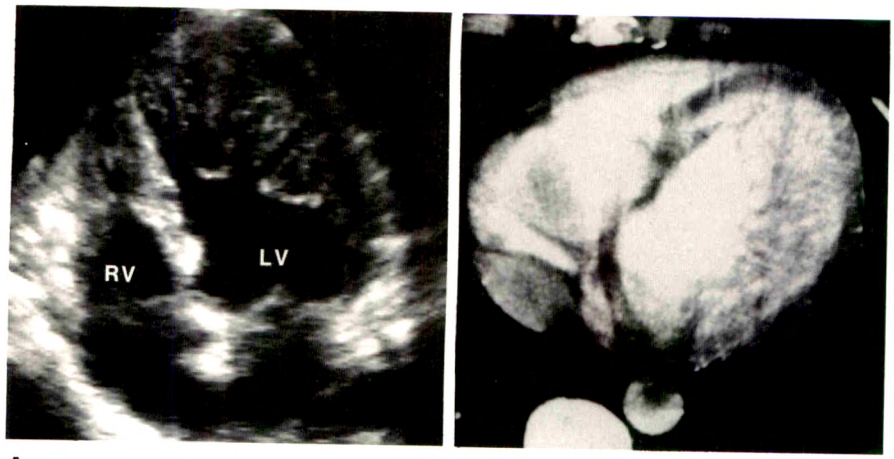



**Fig. 1.—*A*, Apical four-chamber echocardiogram shows thickening and trabeculation of left ventricular free wall and septum. LV = left ventricle, RV = right ventricle.**

***B*, Contrast-enhanced CT scan through level of left ventricle. A thin outer zone of compact myocardium is easily distinguished from inner zone of trabeculated noncompacted myocardium.**

or decreased diastolic function due to abnormal left ventricular compliance. The cause of the ventricular arrhythmias also is unclear, but these arrhythmias can be fatal. The trabecular recesses present in the noncompacted ventricle predispose to the development of mural thrombi. The thrombi may subsequently break free and form an embolus in the systemic circulation. Chin et al. [2] reported eight patients with left ventricular involvement, four of whom had dysmorphic facies. Our patient presented with a cerebral embolus but had no signs or symptoms of left ventricular dysfunction, arrhythmias, or abnormal facies.

Chest radiographs may appear normal or may show changes of congestive heart failure when left ventricular dysfunction is present [2, 5]. In our patient, the chest radiograph showed left ventricular prominence, reflecting the increased thickness of the left ventricular wall. Ventriculography, if performed, shows a honeycombed appearance of the inner contour of the involved ventricle [5].

Echocardiography, which is diagnostic of the disorder, reveals large prominent trabeculations and deep intertrabecular recesses [2]. The trabeculations are least numerous near the mitral valve, with the thickness of the wall and the depth of the intertrabecular recesses greatest at the apex. In this case, Doppler examination revealed flow within the blood-filled intertrabecular recesses, suggesting communication between these recesses and the ventricular chamber.

The CT findings of this disorder are diagnostic also and mirror the findings of echocardiography. The ventricular wall is composed of two layers. The outer layer consists of a thin layer of compacted myocardium that is of a uniform density similar to that of muscle. Within this is a much thicker layer that appears to represent a mixture of contrast-enhanced blood and soft tissue. This represents the trabeculated myocardium with ventricular blood filling the intertrabecular recesses.

## REFERENCES

1. Carlson BM. *Patten's foundations of embryology*, 5th ed. New York: McGraw Hill, **1988**:586–627
2. Chin TK, Perloff JK, Williams RG, Jue K, Mohrmann R. Isolated noncompaction of left ventricular myocardium: a study of eight cases. *Circulation* **1990**;82:507–513
3. Williams RR, Kent GB, Edwards JE. Anomalous cardiac blood vessel communicating with the right ventricle. *Arch Pathol* **1951**;52:480–487
4. Dusek J, Ostadal B, Duskova M. Postnatal persistence of spongy myocardium with embryonic blood supply. *Arch Pathol* **1975**;99:312–317
5. Jenni R, Goebel N, Tartini R, Schneider J, Arbenz U, Oelz O. Persisting myocardial sinusoids of both ventricles as an isolated anomaly: echocardiographic, angiographic, and pathologic anatomical findings. *Cardiovasc Intervent Radiol* **1986**;9:127–131

Perspective

# Medicolegal Aspects of Breast Imaging: Variable Standards of Care Relating to Different Types of Practice

R. James Brenner[1]

The increasing use of mammography and related breast imaging techniques in the past 10 years has caused both great optimism and consternation in the radiologic community. The efficacy of preclinical detection of breast cancer by mammography demonstrated during the Breast Cancer Detection Demonstration Project (BCDDP) [1] and the reduction in mortality due to periodic screening evidenced in the 1963 New York Health Insurance Plan Study [2] and ongoing Swedish trials [3] has served to focus the attention of the medical and lay community on this radiologic study. The United States Congress and nearly half the states in this country have proposed or passed legislation providing mandatory reimbursement for screening mammography [4]. A recent report from the National Cancer Institute indicated that over half the eligible women in this country have had at least one mammogram, with approximately half that number receiving more than one such examination [5]. Such results, although suboptimal, show significantly improved compliance from a decade ago.

The customary consultative approaches of diagnostic radiologists are being challenged by such emerging trends. Traditional notions of an on-site, full diagnostic workup for every patient entering an imaging facility may not lend themselves to the more public health–oriented objective of screening nearly 50 million women in this country with a low-cost, easily accessible imaging examination. Indeed, it has been suggested that nonradiologists and even nonphysician personnel might be employed to meet this challenge [6, 7].

The increased use of mammography has been attended by an increased number of lawsuits filed for negligence [8]. Perhaps this is a natural consequence of both increased use and focused public attention. Although there is no way to insulate a mammographic practice from legal redress, certain risk management measures applied to different kinds of practices can be established depending on the needs of the community and the goals of the imaging center. An understanding of the medicolegal consequences of different standards of care should lead to an appropriate allocation of resources and successful completion of designated objectives.

The basic principles of tort law, establishing the duty of the radiologist to perform a satisfactory mammographic study and offer a reasonable interpretation, have been reviewed in another publication [9]. The purpose of this essay is to define different parameters regarding standard-of-care issues that need to be addressed under various circumstances and delivery systems. No prescription for one system or another should be inferred from this discussion, and indeed different practices may use any or all approaches.

## Screening vs Diagnostic Mammography

The purpose of the screening mammogram is to identify that relatively small segment of patients with mammographic abnormalities from the overwhelming number of women with normal studies. As such, a number of cost-containing mechanisms have been proposed to meet both the medical and legal standards required [10, 11].

Received August 24, 1990; accepted after revision October 31, 1990.

[1] Department of Diagnostic Radiology, Section of Breast Imaging, Cedars-Sinai Medical Center and University of California, Los Angeles, School of Medicine, P. O. Box 48750, Los Angeles, CA 90048-0750. Address reprint requests to R. J. Brenner.

*AJR* **156:719–723, April 1991** 0361–803X/91/1564-0719 © American Roentgen Ray Society

Radiographs are usually admissible as objective evidence in a court of law. High-quality films and appropriate positioning techniques are essential for lesion detection in the screening setting. The American College of Radiology's mammography accreditation program attempts to ensure and monitor such film quality [12]. Although the program's accreditation does not ensure reasonable interpretation, it provides a national standard for reasonable images. Alternatively, images may be sent periodically for critical review to major university centers specializing in mammography.

Because the standard of care attendant to screening mammography is concerned with the detection of a focal mammographic abnormality, a precise diagnosis is not always possible or even advised. The appearance on a screening mammogram of a spiculated mass in a patient without a history of infection or trauma, may be sufficient evidence for surgical referral. Similarly, lesions such as intramammary lymph nodes and lipomas frequently are characterized sufficiently on screening mammography to be definitively diagnostic [13]. The screening interpretation is limited by the prescribed number of mammograms obtained for the study. Once an abnormality is identified, the fundamental standard of care of "detection" has been satisfied. Under many circumstances, however, the examination as such is incomplete and further diagnostic evaluation is required. The role of the mammographer in this context is to communicate the need for additional diagnostic studies [14]. Supplementary examinations, such as spot magnification mammography, problem-oriented special views, and sonography, will usually provide additional information to allow the radiologist to make an appropriate diagnosis and recommend a course of action [15].

When a mammographic facility undertakes diagnostic examinations, the standard of care changes. Whereas a reasonable screening mammogram interpretation will detect focal abnormalities, diagnostic interpretation should under most circumstances be more definitive. Indeed, reimbursement schedules are often predicated on the extra time and resources required for such diagnostic evaluation. An impression such as "indeterminate mass, further studies advised" may be sufficient in a medical and legal context for a screening mammogram, but a more definitive impression is the goal in the diagnostic setting. This higher standard of care is simply an application of the basic elements of duty established in a tort of negligence: "One who undertakes gratuitously or for consideration to render services to another which he should recognize as necessary for the protection of the other person or things, is subject to liability to the other for physical harm resulting from his failure to exercise reasonable care or perform his undertaking if his failure to exercise such care increases the risk of such harm" [16]. Because additional studies usually provide increased information, the standard of care with respect to interpretation is likely to be assessed accordingly [17, 18].

The representation of an imaging facility should clearly define its purpose as a screening institution, diagnostic institution, or both. Medical and possibly legal difficulties result if the practice is limited to screening when the expectations of the referring physician and patient are otherwise.

The ability to distinguish probably benign lesions from those suggestive of malignancy varies in individual practices. Periodic auditing of a practice is essential to establish levels of competence in both detection and diagnosis. This can be accomplished in a number of ways that have been discussed at length elsewhere [19]. The individual audit of a 1- to 5-year experience showing high sensitivity and relatively high specificity is a good preferred defense in a legal action concerning an equivocal mammographic interpretation [20].

Reporting systems should be tailored to the specific nature of the examination, be it screening or diagnostic. Rapid checklists or simple computerized printouts lend themselves well to a screening population wherein about 90% of the studies will most likely be normal [21]. Diagnostic examination, however, may require a more deliberate report specifically addressing either the mammographic abnormality or the mammographic findings corresponding to a clinically suspicious area. Dictated reports are more appropriate in such settings, although computerized programs with variable menus that permit problem-specific interpretation may satisfy the same requirement.

Beyond the legal considerations, the appropriate interplay between screening and diagnostic mammography will result in greater public confidence and realistic expectations. Meyer et al. [22] reported cancellation of nearly 9% of surgical cases referred to their institution for preoperative localization of lesions improperly considered suggestive of cancer by physicians at outside institutions. The added cost involved with surgery of lesions that ultimately are proved to be benign has caused some to reconsider the use of screening mammography, especially in women 40–50 years old [23, 24]. The ideal nonmalignant/malignant biopsy ratio is controversial, but the decision of how to evaluate a lesion based on experience and expertise should provide both a medically and legally sound approach [25].

### Physician-Referred vs Self-Referred Patients

Traditional radiologic consultation is predicated on the referral of patients from primary care physicians. In the field of breast screening, this limits the role of the radiologist to providing adequate mammographic images (screening and/or diagnostic) and reasonable interpretations. With the advent of public health–oriented mammographic screening centers, some imagers have placed themselves in the position of primary care physicians as they accept patients who are not referred by another clinician. Although this is a laudatory step in attempting to reach women outside of customary medical practice, additional medicolegal concerns must be addressed.

A physician who accepts such self-referred patients is probably required to perform a physical examination or ensure that one is done in tandem with the mammographic examination. The BCDDP project showed that approximately 10% of malignancies that are palpable on physical examination may be missed if only a mammographic examination is used [1]. Such mammographically occult lesions may be detected clinically and shown subsequently by sonography or may be

referred directly for surgical evaluation. Many of the cost-saving mechanisms suggested earlier [10, 11], such as the absence of an on-site radiologist during the screening mammographic examination, may not be possible under such circumstances. Whether or not a mammographic facility can legally impose on the patient the responsibility for obtaining a physical examination with another physician is beyond the scope of this discussion. Potential legal actions of abandonment and shifting responsibility need to be considered by facilities that use the latter approach.

Liability has been found when primary care physicians have failed to order a mammogram when a suspicious physical finding is present [26, 27]. The duty to order a screening mammogram is less decided, but at least one lower court decision has elected to impose such a duty (trial court nonappellate decisions have no significant precedent-setting value) [9, 28]. Although such a duty may at first appear appropriate, the lack of uniformity among medical specialty societies may be used to challenge the compelling basis for such a duty. For example, the American College of Physicians has not yet fully endorsed the American Cancer Society's recommendations for periodic screening mammograms. The future of such a duty at present is unclear, but any practice engaged in self-referred patients needs to pay strict attention to such developing trends. If a radiologist accepts a self-referred patient who does not maintain a relationship with another primary care physician and if the duty to order regular screening mammograms becomes recognized as a standard of care, then this duty may indeed be legally applied to the radiologist.

Errors committed by personnel under the supervision of and acting for an imaging facility are attributed to that facility under the general guidelines of agency law and are more specifically discussed under the doctrines of *respondeat superior* and *vicarious liability* [29]. Mistakes made in the traditional physician-referred practices regarding patient demographic data may frequently be corrected by checking with the primary care physician's patient file. Imaging centers accepting a self-referred patient for mammography must be especially careful to obtain correct information regarding that patient. Traditionally, the primary care physician/patient relationship is long-standing and often protects against erroneous information recorded by clerks and employees. Although many successful breast imaging center–patient associations are afforded the same relationship, other such practices with more intermittent contact may invite serious consequences based on such errors.

In this context, reporting of results becomes a crucial subject. Any primary care physician must be able to report the results of the mammographic examination directly to the patient, a duty that clearly arises when results suggestive of cancer are obtained. The inability of a physician to contact a self-referred patient may be disastrous both in medical and legal terms.

Considerable controversy exists as to the duty of physicians to tell the results of mammography to patients referred by their physician. It is the practice of many radiologists to report results both to the referring physician and to the patient. The issue is not decided, but two leading appellate decisions in California indicate that the duty of radiologists in a referral-based practice is to report results to the treating physician and not to the patient [30, 31]. Reporting such results directly to the patient may be commendable, especially if endorsed by the primary care physician, but has not been held to be a uniformly required standard. Indeed, the court in one such case commented that "to impose a duty on a consulting physician to communicate with the patient regarding his evaluations would create an undue burden on the [physician] and could also be disruptive of the primary physician's relation with his patients" [31]. Robertson and Kopans [32] have reviewed these problems, showing that a percentage of patients fail to undergo short-term follow-up examinations as recommended in the mammographic report. If indeed such problems are foreseeable, legal constraints may necessitate a record-keeping system that prompts some additional reminder to the referring physician and/or patient for such follow-up. Reminder systems play a strategic role in such record-keeping systems and probably should be used, although their status in the standard of care remains unproved. In this regard, however, it should be noted that any clearly suspicious mammographic finding should be reported directly by telephone to the referring physician and/or patient. The recognition of a potential malignant lesion increases the responsibility of communication on the part of the mammographer, as was succinctly stated by the Ohio court: "The communication of a diagnosis so that it may be beneficially utilized may be altogether as important as the diagnosis itself" [33].

### Collateral Issues in Mammography

Second opinions may be useful in the evaluation of a clinically occult mammographic abnormality, especially in equivocal cases [34]. Dictated second opinions often oblige the patient to a small service charge but provide an appropriate permanent record of the consulting radiologist's opinion. In an attempt to circumvent such fees, however, informal consultations are occasionally used.

When such an informal consultation is given, the radiologist is nonetheless held to a reasonable standard of care. Problems may arise when the primary care physician enters the results of such discussion in a formal medical record. The "business records" exception to standard hearsay rules of evidence permits such entries to be admitted during trial [35]. The danger of the recording physician's misinterpeting the substance of the second opinion places the radiologist in the precarious position of being named in a lawsuit for an opinion that in fact may never have been rendered. Some radiologists have declined to give undictated second opinions for this reason. A log kept of all informal second opinions might be useful as evidence (under the same business records exception rule) of the actual substance of the impression rendered, but such procedures are often difficult to use in a busy practice. Challenges to the primary physician's recording may be offered at trial, and specifically oriented jury instructions may be directed toward limiting the effect of such uncorroborated clinical notes regarding second opinions. Un-

fortunately, the law provides few restrictions of such potential misinterpretation abuses that may derive from the normal collegiate relationships in medical settings [36].

Comparison of a current mammogram with the previous one might be useful in arriving at an appropriate diagnosis. New densities are of greater mammographic and clinical concern and are recognized only when old studies are available and carefully compared [37]. Benign impressions also are corroborated by long-term unchanging mammographic appearances, although exceptions to this rule also have been documented [38]. The law is unclear as to the duty of the imaging facility to retrieve old films. Fundamental legal principles indicate that a documented best or reasonable effort be exerted to retrieve such films.

### Risk Management/Loss Prevention Approaches

Although relatively few lawsuits actually reach adjudication in a court of law [39], the frequency of malpractice claims, which peaked in 1985 [40], continues to haunt physicians and especially those involved in the diagnosis of breast cancer. The Physicians Insurers Association of America recently published a detailed analysis of the variables involved in delayed diagnosis of breast malignancy. This disease was the second most common cause for indemnity payments and the leading cause for dollar amounts awarded [8]. The reader is referred to the complete report, but examination of the reasons for delay (Table 1) is especially important to imaging facilities that accept self-referred patients.

**TABLE 1: Physician-Based Causes for Delays in the Diagnosis of Breast Cancer**

| Suspected Reason | No. (% of 269 Cases) |
|---|---|
| Physical findings failed to impress | 147 (55) |
| Negative mammographic report | 96 (36) |
| Failure to perform appropriate biopsy | 72 (27) |
| Repeat examinations did not arouse suspicion | 66 (25) |
| Delay in consultation, failure to confer | 49 (18) |
| Failure to react to patient history of mass | 44 (16) |
| Failure to order a mammogram | 44 (16) |
| Inadequate physician-to-physician communication | 37 (14) |
| Distracted by other health problems | 33 (12) |
| Mammogram misread | 24 (9) |
| Other | 20 (7) |
| Poor record keeping | 18 (7) |
| Failure to react to mammogram reading | 16 (6) |
| Poor examination by physician | 16 (6) |
| Mammogram suspicious but no palpable mass | 11 (4) |
| No true delay in diagnosis by physician, not treatment error | 8 (3) |
| Mammogram filed without physician's knowledge | 7 (3) |
| Not recorded | 5 (2) |
| Not known | 4 (2) |
| Inferior mammogram | 4 (2) |
| Treatment error, not delay in diagnosis | 2 (1) |
| Total | 723 |

Note.—This study was intended to investigate the nature and causes of malpractice claims for alleged delays in the diagnosis of breast cancer. Data reprinted with permission from the breast cancer study of the Physician Insurers of America [8].

In an analysis by Adamson et al. [41], the most effective risk management approach toward preventing the filing of nonmeritorious malpractice claims was improved communication between physicians and patients. Such loss-prevention approaches may be available to the breast imaging facility accepting self-referred patients who are in direct communication with the radiologist, but do not apply easily to most referral-based practices. Nonetheless, all personnel involved in breast imaging facilities should be alerted to such risk management benefits of careful communication. Such an approach extends to the communication, both written and oral, between the radiologist and primary care physician. The decision to follow up probably benign lesions involves an initial understanding between the radiologist and the primary care physician, but that discussion also must at some point involve the patient.

Simplified approaches under the disguise of "defensive medicine" may entail further medicolegal consequences. The indiscriminate surgical excision of all mammographic and clinical abnormalities may not only subject physicians in certain jurisdictions to the torts of intentional or negligent infliction of mental distress, but also increases the difficulty of subsequently detecting cancer on a mammogram complicated by extensive postsurgical scarring changes [20]. Newer procedures such as fine-needle aspiration may be introduced judiciously into breast care management with the active involvement of the patient, evidenced by means of appropriately obtained informed consent. Again, proper communication and deliberate management supported by expertise, experience, and self-auditing should provide a reasonable foundation for such an approach.

The reluctance to practice "legal medicine" is often a reluctance to practice good medicine. The perils of the legal system are unavoidable. Reasonable planning and attention to detail should provide for both a satisfying and legally sound breast imaging practice.

### REFERENCES


1. The Breast Cancer Detection Demonstration Project. End results. *Cancer* **1987**:37(5)
2. Strax P. Detection of breast cancer. *Cancer* **1990**;66[suppl]:1336–1340
3. Tabar L. Control of breast cancer through screening mammography. *Radiology* **1990**;174:6556
4. *ACR bulletin.* Chicago, IL: American College of Radiology, April **1990**
5. NCI Breast Cancer Screening Consortium. Screening mammography: a missed clinical opportunity. *JAMA* **1990**;264:54–58
6. Hall F. Screening mammography: potential problems on the horizon (sounding board). *N Engl J Med* **1986**;314:53–54
7. Gleicher N. Breast disease programs in obstetrics/gynecology: a plea for training in mammography. *Am J Obstet Gynecol* **1989**;161:267–270
8. Physicians Insurers Association of America. *Breast cancer study.* Lawrenceville, NJ: Physicians Insurers Association of America, **1990**
9. Brenner RJ. Medicolegal aspects of screening mammography. *AJR* **1989**;153:53–56
10. Sickles EA, Weber WN, Galpin HD, et al. Mammographic screening: how to operate successfully at low cost. *Radiology* **1986**;160:95–97
11. Bird RE, McLelland R. How to initiate and operate a low-cost screening mammography center. *Radiology* **1986**;161:43–47
12. Mclelland R, Hendrick RE, Zinninger MD, et al. The importance of the American College of Radiology mammography accreditation program. *AJR* (in press)

13. Homer MJ. Imaging features and management of characteristically benign and probably benign breast lesions. *Radiol Clin North Am* **1987**;25: 939–951
14. *Merriman v. Toothhaker*, 810, 515 P.2d 509 (Wash, App. **1973**)
15. Sickles EA. Practical solutions to common mammographic problems: tailoring the examination to the needs of the individual patient. In: Feig SA, ed. *ARRS categorical course syllabus on breast imaging*. Reston, VA: American Roentgen Ray Society, **1988**:59–68
16. Restatement (second) of Torts, §323(a)
17. Sickles EA. Further experience with microfocal spot magnification mammography in the assessment of clustered breast microcalcifications. *Radiology* **1980**;137:9–14
18. Tabar L. Microfocal spot magnification mammography. In: Brunner S, Cargfeldt B, Andersen PE, eds. *Early detection of breast cancer*. Berlin: Springer, **1984**:62–68
19. Sickles EA, Ominsky SH, Sollito RA, et al. Medical audit of a rapid throughput mammography screening practice: methodology and results of 27,114 examinations. *Radiology* **1990**;175:323–328
20. Brenner RJ. Screening mammography, medical legal considerations. *Cancer* **1990**;105[suppl]:187–198
21. Andersson I, Andren L, Hildell J, et al. Breast cancer screening with mammography: a population based, randomized trial with mammography as the only screening mode. *Radiology* **1979**;32:273–276
22. Meyer JE, Sonnenfeld MR, Greenes RA, et al. Cancellation of preoperative breast localization procedures: analysis of 53 cases. *Radiology* **1988**; 169:629–630
23. Cyrlak D. Induced costs of low-cost screening mammography. *Radiology* **1988**;168:661–663
24. Eddy DM. Screening for breast cancer. *Ann Intern Med* **1989**;111:389
25. Brenner RJ, Sickles SA. Acceptability of periodic follow-up as an alternative to biopsy for mammographically detected lesions interpreted as probably benign. *Radiology* **1989**;171:645–646
26. *Beckcom v. United States*, 584 F. Suppl. 1471 (Applying New York Law) (ND N.Y. **1984**)
27. *Barenbrugge v. Rich*, 141 Ill App. 3d 1046, 490 N.E. 2d 1368 (1st Dist, **1986**)
28. *Mary Ann Clayton v. George Sabeh, MD* (GD 88-02505, Jan 19, **1990**, Penn)
29. Reuter SR. Toward a more realistic and consistent age of respondent superiority in the hospital. *St. Louis University Law J* **1985**;29:601–664
30. *Townsend v. Turk*, 266 Cal Rptr 821 218 Cal App 3d 278 (**1990**)
31. *Mahannah v. Hirsch*, 191 Cal App. 3d 1520, 237 Cal Rptr 140 (**1987**)
32. Robertson CL, Kopans DB. Communicating problems after mammographic screening. *Radiology* **1989**;172:443–444
33. *Phillips v. Good Samaritan Hospital*, 416 NE 2d 646 (Ohio **1979**).
34. Hall FM. Mammography second opinions prior to biopsy of nonpalpable breast lesions. *Arch Surg* **1990**;125:298–299
35. Fed R. Evid 808(6)
36. J. Wigmore on Evidence 1517–1533 (3d Ed. **1940**)
37. Kopans DB. *Breast imaging*. Philadelphia: Lippincott, **1989**:144
38. Meyer JE, Kopans DB. Stability of a mammographic mass: false sense of security. *AJR* **1981**;137:595–598
39. Mills DH. Medical insurance feasibility study. *West J Med* **1978**;128: 360–368
40. Jacobson PD. Medical malpractice and the tort system. *JAMA* **1989**; 262:3320–3327
41. Adamson TE, Tschann JM, Gullion DS, et al. Claims, a complex relationship. *West J Med* **1989**;150:356–360

# Adrenal Myelolipoma

William E. Palmer,[1] Elizabeth L. Gerard-McFarland, and Felix S. Chew

A 36-year-old man had sudden onset of right flank pain but no hematuria. Sonograms showed a large hyperechoic mass containing curvilinear hypoechoic regions in the region of the right adrenal gland. CT scans showed a heterogeneous lesion, with fat and curvilinear soft-tissue attenuation (Fig. 1), that was sharply marginated anteriorly but contiguous posteriorly with soft-tissue thickening in the posterior pararenal space. MR images showed heterogeneous high and intermediate signal intensity in the mass on both T1- and T2-weighted images. The mass displaced the liver and right kidney without invading them; the right adrenal gland could not be identified. An 18.5 × 15.0 × 9.0 cm mass, consisting of adipose and myeloid tissue, was resected. Extensive infarction and acute and organizing hematoma were present. The final pathologic diagnosis was adrenal myelolipoma.

Adrenal myelolipoma is an uncommon, benign, endocrinologically inactive tumor of unknown pathogenesis composed of adipose and myeloid tissue. In most lesions, the fatty component is predominant and is recognizable on radiologic images [1, 2]. Such lesions are radiolucent on radiographs, hyperechoic on sonograms, have low attenuation on CT scans, and have bright signal intensity on T1-weighted MR images and intermediate signal intensity on T2-weighted MR images. Tumors composed primarily of myeloid tissue may be hypoechoic on sonograms and will have the imaging characteristics of red marrow on other kinds of images [1, 2]. In complicated cases in which infarction or hematoma is present, the margins of the lesions may be irregular and infiltrative, with blood dissecting through the retroperitoneum. The imaging findings of acute, subacute, or chronic hematoma will then be superimposed on the lesion. When lesions are fatty, well marginated, uncomplicated, and in the position of the adrenal gland, a specific radiologic diagnosis is possible. However, the mere presence of fat in an adrenal mass is insufficient for diagnosis, because a metastasis or other aggressive lesion may engulf fat as it spreads [3]. Nonspecific calcification is sometimes present.

Adrenal myelolipoma is usually an incidental diagnosis in adults being imaged for unrelated clinical indications. Virtually all adrenal myelolipomas originate in the adrenal cortex. In autopsy series, its prevalence is between 0.08% and 0.20%, with equal sex distribution [2, 4]. Nearly half of the resected lesions in one survey of the literature were 10 cm or larger [4]. Symptoms, when present, typically relate to simple mass effect, but spontaneous bleeding can cause acute flank pain or even hemodynamic shock. Bleeding is more likely in lesions primarily composed of myeloid tissue.

Surveillance has been suggested for incidentally discovered adrenal myelolipomas [4]. However, if metastases are suspected, if endocrinologic assays are abnormal, or if radiologic findings are inconsistent with uncomplicated myelolipoma, a histologic diagnosis becomes necessary. CT-guided or sonographically guided percutaneous needle biopsy can provide tissue. Surgical excision is reserved for myelolipomas with mass effect or bleeding.

## REFERENCES


1. Asch MR, Poon PY, McCallum RW, Bird BI. Myelolipoma: radiographic findings in seven patients. *Can Assoc Radiol J* **1989**;40:247–250
2. Musante F, Derchi LE, Zappasodi F, et al. Myelolipoma of the adrenal gland: sonographic and CT features. *AJR* **1988**;151:961–964
3. Greene KM, Brantly PN, Thompson WR. Adenocarcinoma metastatic to the adrenal gland simulating myelolipoma: CT evaluation. *J Comput Assist Tomogr* **1985**;9:820–821
4. Dieckmann KP, Hamm B, Pickartz H, Jonas D, Bauer HW. Adrenal myelolipoma: clinical, radiologic, and histologic features. *Urology* **1987**;29:1–8

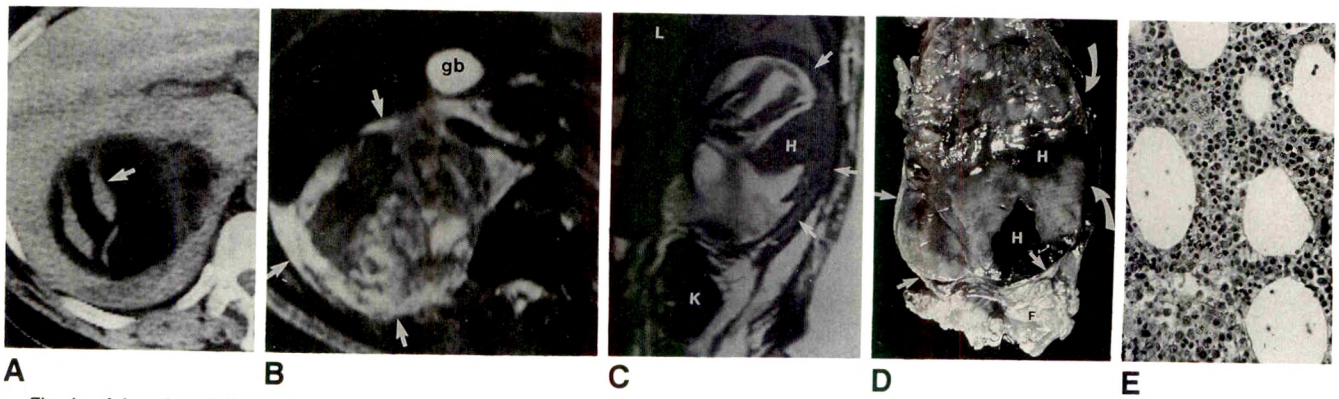




**Fig. 1.—Adrenal myelolipoma.**

***A*, CT scan shows fat-containing mass indenting underside of liver, with curvilinear regions of hematoma (*arrow*).**

***B*, T2-weighted axial MR image shows heterogeneous mass in position of right adrenal gland. Regions of high signal represent hematoma infiltrating surrounding tissues (*arrows*). gb = gallbladder**

***C*, T1-weighted sagittal MR image shows fatty mass displacing liver (L) and right kidney (K). Regions of lower signal represent hematoma (H) extending into and around (*arrows*) lesion.**

***D*, Cut gross specimen shows hematoma (H) within and surrounding (*curved arrows*) lesion. Cut surface was grossly hemorrhagic. Residual adrenal cortex surrounds lower portion (*straight arrows*). Retroperitoneal fat (F) is at bottom.**

***E*, Micrograph shows myeloid elements surrounding mature adipocytes (round, clear spaces). (H and E, ×79)**

From the weekly radiologic-pathologic correlation conferences conducted by Jack Wittenberg. Pathology editor: Andrew E. Rosenberg. Radiology editors: Felix S. Chew, Daniel P. Barboriak, Daniel I. Rosenthal.

[1]All authors: Department of Radiology, Massachusetts General Hospital and Harvard Medical School, 32 Fruit St., Boston, MA 02114. Address reprint requests to F. S. Chew.

# Detection of Active Intraabdominal Arterial Hemorrhage: Value of Dynamic Contrast-Enhanced CT

R. Brooke Jeffrey, Jr.[1]
Jimmy D. Cardoza[1]
Eric W. Olcott[2]

**Contrast-enhanced dynamic CT was used prospectively to diagnose and locate the site of active arterial intraabdominal hemorrhage in 18 patients. Active arterial extravasation was confirmed by angiography in five patients and by immediate surgery in nine. Two patients not undergoing surgery or angiography required multiple blood tranfusions to correct rapidly falling hematocrit due to a coagulopathy. One patient died of hypovolemic shock, and autopsy confirmed a large acute retroperitoneal hematoma. Another patient with a splenic laceration and massive hemoperitoneum on CT had no active bleeding at the time of surgery, which was delayed 1 hr from the time of the CT. All patients were clinically thought to be hemodynamically stable and had systolic blood pressures greater than 110 mm Hg at the time of CT. In seven patients, hypotension developed either during (two patients) or immediately after (five patients) CT scanning, necessitating either immediate surgery or angiographic embolization.**

**Contrast-enhanced dynamic CT is valuable in the diagnosis and localization of active arterial intraabdominal hemorrhage. Identification of the anatomic site of this potentially life-threatening hemorrhage is critical in determining whether immediate laparotomy or angiographic embolization is the preferred method of treatment.**

*AJR* 156:725–729, April 1991

In a recent case report, Sivit et al. [1] described the contrast-enhanced CT appearance of active intraabdominal arterial extravasation due to splenic rupture from blunt abdominal trauma. The patient was clinically thought to be hemodynamically stable when scanning was started. A focal high-density area (64–74 H) was noted adjacent to a ruptured spleen. During CT, the patient became hypotensive, and immediate laparotomy confirmed active arterial bleeding from the spleen. In this report, we analyze the clinical and CT features of 18 patients with active intraabdominal bleeding. The clinical importance of recognizing this potentially life-threatening form of hemorrhage is stressed, as is the value of angiographic embolization for surgically inaccessible sites of bleeding such as the lumbar artery.

## Subjects and Methods

The CT scans, medical records, and clinical outcome were reviewed in 18 adult patients with CT evidence of active intraabdominal arterial bleeding diagnosed from January 1987 to August 1990. There were 14 men and four women with ages ranging from 22 to 76 years (mean, 42 years). Abdominal arterial hemorrhage was due to trauma in 13 patients (blunt, 12; penetrating, one) and excessive anticoagulation therapy in three patients. One had spontaneous rupture of a splenic artery pseudoaneurysm, and one had a ruptured abdominal aortic aneurysm. All 18 patients underwent dynamic bolus contrast-enhanced CT with both oral and IV contrast agents. A total of 150 ml of 60% iodinated contrast material was administered IV (2–3 ml/sec for a total of 50 ml, 1.0–1.5 ml/sec for a total of 100 ml).

In all 18 patients, the anatomic site of suspected active arterial bleeding was noted on CT and compared with surgical reports and angiographic findings to correlate with sites of active bleeding. The CT attenuation values in the region of active arterial extravasation were

Received September 5, 1990; accepted after revision October 18, 1990.

[1] Department of Diagnostic Radiology and Nuclear Medicine, Stanford University School of Medicine, Stanford, CA 94305. Address reprint requests to R. B. Jeffrey, Jr. (Rm. H-1307).

[2] Department of Diagnostic Radiology, University of California, San Francisco, San Francisco General Hospital, San Francisco, CA 94101.

0361–803X/91/1564–0725
© American Roentgen Ray Society

compared with adjacent major arteries by using regions-of-interest cursors.

In five patients, transient hypotension (systolic blood pressure <90 mm Hg) was noted before CT. After either fluid resuscitation or blood transfusion (two patients), all five patients were thought clinically to be hemodynamically stable enough to undergo contrast-enhanced CT, and all had recorded systolic blood pressure greater than 110 mm Hg. All 13 patients with abdominal trauma were scanned within 4 hr of hospital admission.

Active arterial bleeding diagnosed by CT was confirmed by selective arteriography in five patients and by immediate surgery in nine others. The surgical report and direct consultation with the surgeon confirmed active arterial bleeding in all nine patients. Surgery revealed massive hemoperitoneum in another patient with a splenic fracture, but no active arterial hemorrhage was noted by the surgeon at the time of laparotomy. Surgery in this patient was not performed, however, until approximately 1 hr after CT. Two patients not undergoing surgery or angiography had abdominal wall hemorrhage from excessive anticoagulation therapy. Active arterial bleeding was inferred from the clinical evidence of ongoing blood loss with falling hematocrit requiring multiple transfusions (three units in one patient, four units in another). A final patient who died of hypovolemic shock had autopsy confirmation of a large, acute retroperitoneal hemorrhage within the posterior pararenal space due to traumatic transection of the lumbar artery.

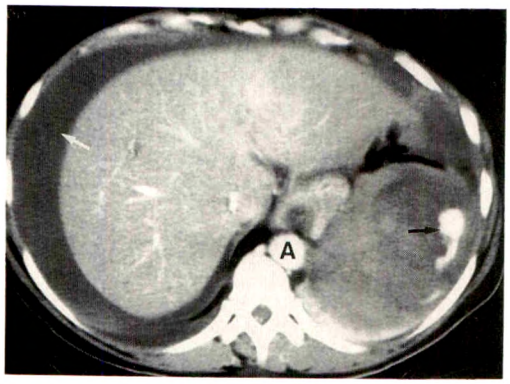



**Fig. 1.—CT scan of splenic laceration after blunt trauma with active arterial extravasation. Note focal high-density area (*black arrow*) adjacent to lacerated spleen, indicating site of arterial hemorrhage. Area of extravasation is isodense with aorta (A). Note lower attenuation of hemoperitoneum adjacent to liver (*white arrow*).**

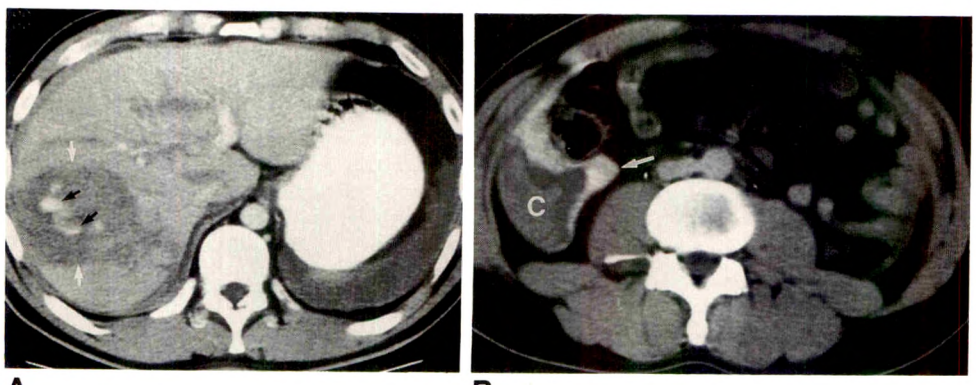
## Results

Of the 18 patients, 11 had intraperitoneal sites of active arterial bleeding that were identified prospectively with CT. Hemorrhage from the spleen was found in six patients, from the liver in three patients, and from the mesenteric arteries in two patients. Of the seven patients with extraperitoneal sites of active bleeding, three patients had bleeding confined to the abdominal wall or paraspinous musculature. The remaining four patients had active bleeding identified in the anterior pararenal space (two patients), posterior pararenal space (one patient), and psoas compartment (one patient).

### *CT Appearance of Active Arterial Extravasation*

In 14 patients, active arterial extravasation on CT appeared as a focal high-density area (attenuation values, 80–130 H) surrounded by a large hematoma (Figs. 1–3). In the four remaining patients, active arterial extravasation appeared as a diffuse area of high density (Figs. 4 and 5). In two of these patients with mesenteric arterial laceration, high-density contrast-enhanced blood was noted throughout the peritoneal cavity, mixed with hemoperitoneum and clot. No evidence of perforation of the gastrointestinal tract or urinary bladder was found at the time of laparotomy. In the two remaining patients, extraperitoneal hemorrhage was due to a ruptured abdominal aortic aneurysm in one patient and a traumatic laceration of a lumbar artery in the other. The diffuse form of arterial extravasation had somewhat higher attenuation values ranging from 120 to 170 H. The CT attenuation values measured for the areas of active arterial extravasation were within 15 H of the attenuation values for the abdominal aorta or major adjacent arterial structures on the same CT image in all 18 cases.

The clinical outcome was determined by review of all relevant medical records, radiologic examination, and direct interview with the operating surgeons. Seven patients, or 38% (including three of the patients with prior transient hypotension), experienced hypotension either during CT (two patients) or immediately after CT (five patients). This necessitated immediate surgical intervention in five of these patients and angiographic embolization in two patients.




A B

**Fig. 2.—*A* and *B*, CT scans of hepatic laceration after blunt trauma with active arterial extravasation. In *A*, note focal areas of high density (*black arrows*) within right hepatic lobe hematoma (*white arrows*). In *B*, clotted blood (C) in right paracolic gutter is noted medially, displacing higher density free-flowing active arterial hemorrhage (*arrow*).**

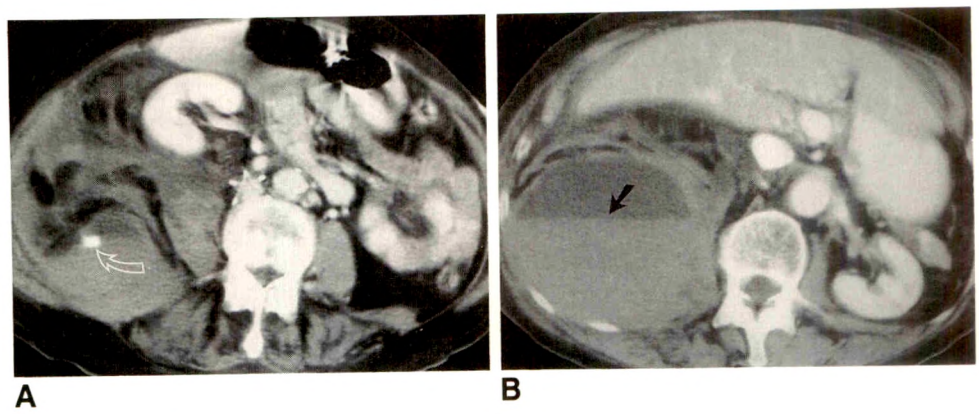



Fig. 3.—*A* and *B*, CT scans of lumbar artery arterial extravasation from blunt trauma. In *A*, note focal high-density area (*arrow*) within large posterior pararenal space hematoma. In *B*, note massive posterior pararenal space hematoma with hematocrit effect (*arrow*). This patient was successfully treated with selective lumbar artery embolization.

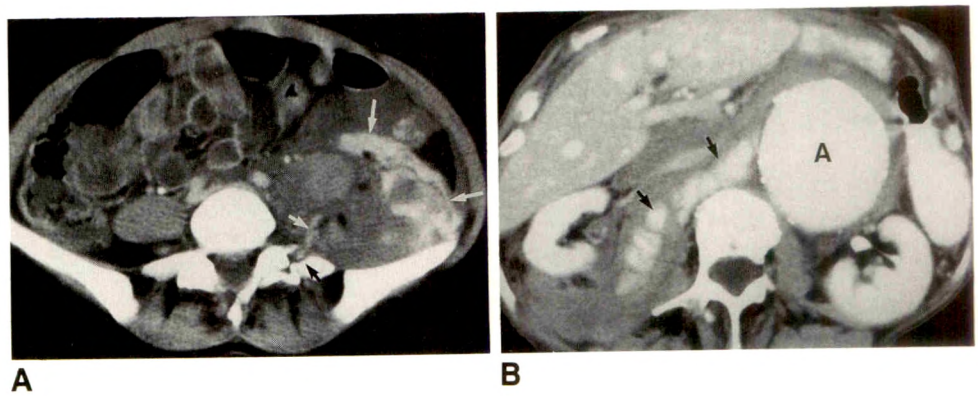



Fig. 4.—*A* and *B*, CT scans of diffuse extraperitoneal acute arterial extravasation in two patients. Patient in *A* had a traumatic lumbar artery laceration from blunt trauma resulting in hypovolemic shock and death. Note left L4 transverse fracture (*black arrow*) and active lumbar arterial extravasation extending from this site (*white arrows*). Diffuse high-density fluid is seen in iliac fossa and posterior pararenal space. In another patient (*B*), diffuse arterial extravasation (*arrows*) is identified within posterior pararenal space from rupture of an abdominal aortic aneurysm (A).

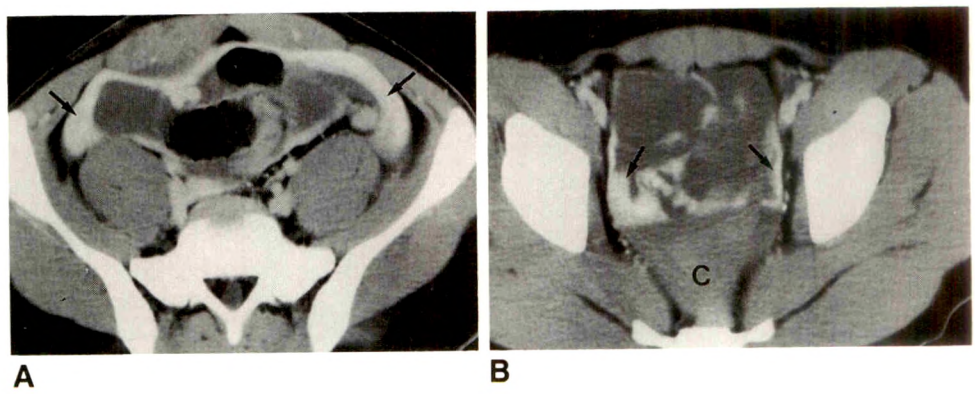



Fig. 5.—*A* and *B*, CT scans of superior mesenteric artery laceration with diffuse high-density intraperitoneal fluid representing extravasated IV contrast material. In *A*, high-density fluid (170 H) is noted throughout lower peritoneal cavity (*arrows*). In *B*, active arterial hemorrhage (*arrows*) layers anteriorly to clotted blood (C) in pelvis. At surgery, no evidence of bowel or urinary bladder perforation was found.

One patient died of hypovolemic shock after blunt trauma and acute posterior pararenal space hematoma due to transection of a lumbar artery. A second patient died of pulmonary and renal failure 3 days after successful angiographic embolization of bleeding hepatic metastases. The remaining 16 patients survived.

Of the surviving patients, two patients with extraperitoneal abdominal wall hematomas were successfully treated with multiple blood transfusions alone and did not require surgical or angiographic intervention. Eleven patients underwent immediate surgical intervention with successful control of hemorrhage in 10 cases. In one remaining patient with a stab wound to the left flank, preoperative CT showed a large posterior pararenal, perinephric, and paraspinous hematoma. An area of active extravasation was seen in the left paraspinous musculature (Fig. 6). No intrinsic laceration of the kidney was noted on CT. At surgery, a large, perinephric hematoma was noted, but no renal injury or active bleeding was found. In the operating room, however, the patient became hypotensive and was immediately transferred to the angiography suite, where an arterial extravasation from the lumbar artery was diagnosed and embolization with 3-mm steel coils was performed. Three remaining patients with lateral flank injuries and extraperitoneal bleeding identified in either the psoas

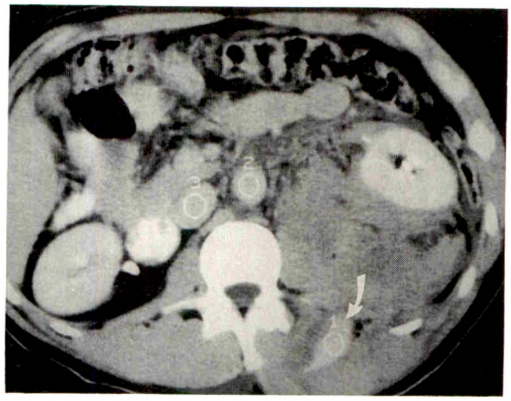


**Fig. 6.—Stab wound to left flank with lumbar artery extravasation not detected at surgery. Preoperative enhanced CT scan shows large posterior pararenal, perinephric, and paraspinous hematoma. Focal extravasation is noted in left paraspinous region in distribution of a lumbar artery (*arrow*). Findings on surgical exploration of left kidney were normal except for surrounding hematoma. Intraoperatively, patient became hypotensive and was transferred to angiography suite, where lumbar artery extravasation was found and embolization was performed with 3-mm steel coils.**

compartment or posterior pararenal space had lumbar arterial hemorrhage demonstrated by angiography. All three underwent successful angiographic embolization with either Gelfoam (Upjohn, Kalamazoo, MI) or stainless steel coils.

## Discussion

Patients with blunt abdominal trauma or other causes of acute intraabdominal hemorrhage are generally excluded from CT if hemodynamic instability or ongoing blood loss is clinically evident [2–7]. However, as this report indicates, a small number of patients may have clinically inapparent active arterial hemorrhage that is potentially life-threatening [1]. Active arterial bleeding can be diagnosed on contrast-enhanced CT on the basis of its characteristic high density, isodense with adjacent major arterial structures. Both focal and diffuse forms can be recognized. In our series, focal areas of extravasation on CT were often associated with large hematomas. Patients with diffuse forms of extravasation had high-density fluid conforming to the peritoneal cavity or involved extraperitoneal spaces.

The CT appearance of active bleeding from a mesenteric arterial laceration has not been reported before. In the absence of a visualized laceration to the liver or spleen, the presence of hemoperitoneum after blunt trauma should always raise the suspicion of an injury to the mesenteric vasculature. As Orwig and Federle [8] have noted, actual measurement of the attenuation values of hemoperitoneum may be helpful in determining the anatomic site of visceral injury. Attenuation values for clotted blood in their series were significantly higher than those for unclotted blood (60 H vs 35–45 H) [8]. In questionable cases, recognition of the "sentinel clot" sign may be of value, therefore, in identifying the source of intraperitoneal hemorrhage. In their series, clotted blood in an interloop location or adjacent to a segment of intestine was the only finding in six of 15 patients with proved mesenteric or gastrointestinal injuries [8]. As demonstrated by our two patients, active arterial extravasation from mesenteric arterial hemorrhage may result in attenuation values of hemoperitoneum even higher than those for clotted blood (120–170 H).

Seventeen of our 18 patients had active arterial bleeding correctly diagnosed prospectively. In one patient with a false-positive finding for active bleeding, CT showed a splenic fracture and active arterial bleeding adjacent to the spleen. More than a liter of blood was found in the peritoneum during surgery, but no active arterial extravasation was noted. There was, however, a 1-hr delay between the CT scanning and laparotomy, and it is very possible that the active arterial hemorrhage had stopped.

The CT demonstration of diffuse intraperitoneal high-density fluid from mesenteric arterial laceration may cause diagnostic difficulty. This finding may mimic gastrointestinal rupture with extravasation of high-density oral contrast material or possibly intraperitoneal rupture of the urinary bladder with leakage of excreted IV contrast material. Points that may serve to distinguish mesenteric arterial laceration from bowel perforation include the lack of pneumoperitoneum, focal bowel wall thickening, or discrete mesenteric hematoma. Intraperitoneal rupture of the bladder could resemble mesenteric arterial extravasation as well, but is generally associated with pelvic fractures, localized pelvic hematoma, bladder contusion, and hematuria [9, 10]. Unless the patient had previously received IV contrast material, the rapid scan acquisition with dynamic scanning precludes sufficient contrast material reaching the bladder to extravasate into the peritoneal cavity. As noted by Mee et al. [9] demonstration of intraperitoneal rupture of the bladder with cystography requires significant retrograde distention of the bladder with a minimum of 250–300 ml of contrast material. This degree of bladder distention is difficult to achieve with IV contrast injection alone.

Precise anatomic localization of extraperitoneal sites of active hemorrhage may have important implications for treatment of patients, particularly in hemorrhage from a lumbar artery distribution. Surgical access to the lumbar arteries may be difficult and imprecise in the assessment of acute vascular injury. In one of our patients with a stab wound to the back, surgical exploration did not show acute bleeding, but angiography identified a lumbar artery extravasation. The CT demonstration of a lateral extraperitoneal hematoma with involvement of the psoas component, posterior pararenal space, or paraspinous musculature is highly suggestive of extravasation from a lumbar artery. Angiographic embolization is often the treatment of choice in these patients [11, 12].

Hypotension developed in seven (38%) of 18 patients in this series either during or immediately after CT, underscoring the critical importance of careful hemodynamic monitoring of patients during scanning. Two of our patients died of complications of hypovolemic shock, thus emphasizing the potential life-threatening nature of the intraabdominal bleeding. Even if a patient is hemodynamically stable at the start of the CT examination, this does not ensure that with ongoing blood loss the patient will maintain a normal blood pressure.

REFERENCES

1. Sivit CJ, Peclet MH, Taylor GA. Life-threatening intraperitoneal bleeding: demonstration with CT. *Radiology* **1989**;171:430
2. Federle MP, Goldberg HI, Kaiser JA, et al. Evaluation of abdominal trauma by computed tomography. *Radiology* **1981**;136:637–644
3. Jeffrey RB, Laing FC, Federle MP, Goodman PC. Computed tomography of splenic trauma. *Radiology* **1981**;141:729–732
4. Berger PE, Kuhn JP. CT of blunt abdominal trauma in childhood. *AJR* **1981**;136:105–110
5. Druy EM, Rubin BE. Computed tomography in the evaluation of abdominal trauma. *J Comput Assist Tomogr* **1979**;3:40–44
6. Goldstein AS, Sclafani SJ, Kupferstein NH, et al. The diagnostic superiority of computerized tomography. *J Trauma* **1985**;25:938–941
7. Peitzman AB, Makaroun MS, Slasky BS, Ritter P. Prospective study of computed tomography in initial management of blunt abdominal trauma. *J Trauma* **1986**;26:585–592
8. Orwig D, Federle MP. Localized clotted blood as evidence of visceral trauma on CT: the sentinel clot sign. *AJR* **1989**;153:747–749
9. Mee SL, McAninch JW, Federle MP. Computerized tomography in bladder rupture: diagnostic limitations. *J Urol* **1987**;137:207–209
10. Lowe FC, Fishman EK, Oesterling JE. Computerized tomography in diagnosis of bladder rupture. *Urology* **1989**;33:341–343
11. Sclafani SJA, Lo F, Phillips TF, et al. Lumbar arterial injury: radiologic diagnosis and management. *Radiology* **1987**;165:709–714
12. Haydu P, Chang J, Knox G, Nealon TF Jr. Transcatheter arterial embolization of a traumatic lumbar artery false aneurysm. *Surgery* **1978**;84:288–291

Radiology Outreach Foundation

The Radiology Outreach Foundation (ROF) is a nonprofit corporation whose goal is to help disadvantaged countries improve their health care by providing radiology equipment, books, consultation, education, and training to their practitioners. This assistance is on an application basis that is independent of political, ethnic, or religious orientation of the grantee. It depends on the need of the people and the ability of the ROF to meet that need. The ROF is approved by the U.S. Internal Revenue Service as a tax-exempt organization. It is endorsed by the following radiologic societies: American Association of Women Radiologists, American College of Radiology, American Roentgen Ray Society, Association of University Radiologists, Radiological Society of North America, Society of Chairmen of Academic Radiology Departments, Society for Pediatric Radiology, European Society of Pediatric Radiology.

All donations to the ROF are tax deductible. Persons who would like to contribute financially to the ROF, would be interested in being a visiting professor, would like to send books or journals to any of the institutions supported by the ROF, or would like further information about the ROF should write to Charles A. Gooding, M.D., President, Radiology Outreach Foundation, 3415 Sacramento St., San Francisco, CA 94118 USA.

# Book Review

**The Abdominal Plain Film.** By Stephen R. Baker. Norwalk, CT: Appleton & Lange, 422 pp., 1990. $95

As the author states in the preface, the plain film of the abdomen is a neglected area of radiology. Although a tremendous proliferation of books covering the more modern imaging techniques has occurred, little has been published on conventional radiology of the abdomen. The author fills this void excellently.

The book starts with the uses, limitations, technical considerations, and basic principles of interpretation of abdominal plain films. These are followed by separate chapters on findings in the peritoneal and retroperitoneal spaces; stomach and duodenum; intestines and appendix; liver, bile ducts, and spleen; pancreas and adrenal glands; urinary tract; and genital tract. The last chapter covers the appearance of various opaque surgical clips and staples. Within each chapter, the material is divided into the causes and appearance of various calcifications and lucencies, with soft-tissue masses discussed wherever appropriate. The illustrations are of excellent quality. Numerous rare conditions are depicted. The book is organized primarily by the radiologic appearance rather than by diseases. The strong point of the text is a discussion of intraabdominal calcifications. These are covered in great detail. This text should serve as the current definitive work on this topic.

Numerous tables throughout the book list causes for the various calcifications, lucencies, and hollow-organ distensions. The tables are relatively detailed. For example, under adrenal gland calcifications, separate tables list calcifications in the normal-sized gland, calcifications in the enlarged gland, and adrenal cysts that calcify.

Any discussion of the technical aspects is bound to produce disagreement. In my opinion, the author places too much emphasis on the supine film. On page 8, he states, "The right side up lateral decubitus view should not be done routinely." I think that for most examinations of the acute abdomen, supine, right-side-up decubitus, and upright views of the abdomen and chest should be part of every examination. If the patient cannot stand, an additional underexposed lateral decubitus view can be used to detect a subtle pneumoperitoneum. That the referring physician can be interfering with the correct sequence or timing of films is not a reason to take short cuts. This applies both to plain films and to the more complex imaging techniques. Although it is important for a radiologist to become familiar with the signs of pneumoperitoneum on a supine film, it is just as important to realize that a subtle pneumoperitoneum in many patients will not be detected on the supine film.

I found only a few errors for a book this size. The legends for Figures 4-29A and 4-29B are reversed. I think that Figure 4-45 is upside-down. Table 5-9 lists various calcifications and other densities in the large intestine; although bismuth and conjugated Telepaque are included in the table, the most common such substance, barium sulfate, is not. On page 244, it is stated that the lobe of Riedel represents a focal enlargement of the liver (Riedel's name is misspelled). It is controversial whether such a lobe really represents focal hepatic enlargement. In his original publication, Riedel postulated that traction on the liver from the gallbladder or other inflammation was the cause of this finding, an opinion not shared by more recent investigators. This abnormality is found in children and may be developmental.

The book has detailed references that appear complete. Many of the signs and conditions discussed were first described decades ago. Therefore, of necessity, many of the references listed are old; yet, overall the references are up to date.

This book should be in every department of radiology library. It is probably best suited as a reference, to be used to look up the etiology and differential diagnosis of findings seen in day-to-day radiology rather than as a text to be read cover to cover. In addition, it should be available to radiology residents, for whom it could serve as a reference on any unusual lucency or calcification encountered in daily practice.

Jovitas Skucas
*University of Rochester, Medical Center*
*Rochester, NY 14642*

# Diagnosis of Pneumoperitoneum on Supine Abdominal Radiographs

Marc S. Levine[1]
Jac D. Scheiner
Stephen E. Rubesin
Igor Laufer
Hans Herlinger

**A blinded, retrospective study was performed to determine the value of supine abdominal radiographs in diagnosing pneumoperitoneum. Supine films from 44 cases of pneumoperitoneum were randomly interspersed among supine films from 87 control subjects without free air, and the films were reviewed for the presence or absence of various signs of pneumoperitoneum, including Rigler's sign (gas on both sides of the bowel wall), the falciform ligament sign (gas outlining the falciform ligament), the football sign (gas outlining the peritoneal cavity), the inverted-V sign (gas outlining the medial umbilical folds), and the right-upper-quadrant gas sign (localized gas in the right upper quadrant). One or more of these signs were present in 26 cases (59%) of pneumoperitoneum, including the right-upper-quadrant gas sign in 18 cases (41%), Rigler's sign in 14 cases (32%), and the falciform ligament and football signs in one case each (2%). Unfortunately, there were frequent errors in the interpretation of the right-upper-quadrant gas sign and Rigler's sign, with a total of 11 false-positive cases (13%). Further analysis of the true-positive right-upper-quadrant gas signs showed that these gas collections were always triangular or linear with an inferolateral to superomedial orientation and, if triangular, a concave superolateral border. In the true-positive Rigler's signs, the bowel wall thickness ranged from 1 to 8 mm, whereas the false positives all had a bowel wall thickness of 1 mm or less.**

**Proper interpretation of the various signs of pneumoperitoneum on supine films should lead to more accurate diagnosis of this condition.**

*AJR* **156:731–735, April 1991**

Since the early 1900s, upright or left lateral decubitus films of the abdomen have been recognized as a valuable aid for the diagnosis of pneumoperitoneum [1, 2]. In clinical practice, however, many patients with an acute abdomen are too sick or debilitated to stand or lie on their side, so that supine abdominal radiographs may be the only films obtained. Various signs of pneumoperitoneum that have been described on supine films include Rigler's sign (visualization of both sides of the bowel wall) [3], the falciform ligament sign (visualization of the falciform ligament as a thin, linear density in the right upper quadrant), the football sign (visualization of the peritoneal cavity as an oval gas shadow) [4], the inverted-V sign (visualization of the medial umbilical folds in the pelvis) [5, 6], and the right-upper-quadrant gas sign (visualization of localized extraluminal gas collections in the right upper quadrant) [7–9]. Nevertheless, many authors believe that supine abdominal radiographs have limited value in diagnosing pneumoperitoneum [10–12]. This study was undertaken to determine the value of supine films in these patients.

## Materials and Methods

Inpatient radiology log sheets at our hospital were used to identify 44 cases of pneumoperitoneum diagnosed on upright or left lateral decubitus films of the abdomen in which supine abdominal radiographs also had been obtained. No portable abdominal radiographs

Received September 10, 1990; accepted after revision October 23, 1990.

[1] All authors: Department of Radiology, Hospital of the University of Pennsylvania, 3400 Spruce St., Philadelphia, PA 19104. Address reprint requests to M. S. Levine.

0361–803X/91/1564–0731
© American Roentgen Ray Society

were included in this study. The 44 supine films were randomly interspersed among supine films from 87 other control cases in which there was no evidence of pneumoperitoneum on upright or decubitus films.

Each of those 131 supine films were then reviewed by an experienced gastrointestinal radiologist who had no knowledge of the findings on upright or decubitus films. The supine films were evaluated for the presence or absence of five previously described signs of pneumoperitoneum, including Rigler's sign, the falciform ligament sign, the football sign, the inverted-V sign, and the right-upper-quadrant gas sign. Subsequently, the films were analyzed to determine the location and thickness of the bowel wall in all patients with Rigler's sign and the size, shape, and location of the gas collections in all patients with the right-upper-quadrant gas sign.

The amount of free intraperitoneal air in the 44 cases of pneumoperitoneum was also quantified by measuring the vertical distance from the apex of the diaphragm to the liver on upright films or from the right lateral wall of the abdomen to the liver on decubitus films. The presence or absence of these various signs of pneumoperitoneum on supine films was then correlated with the amount of free air on upright or decubitus films.

## Results

The results are summarized in Table 1.

### *Right-Upper-Quadrant Gas Sign*

The right-upper-quadrant gas sign was present on supine films in 18 (41%) of 44 cases of pneumoperitoneum (Fig. 1). Thirteen (30%) had a triangular gas collection (Fig. 1A) and five (11%) had a linear gas collection (Fig. 1B) in the right upper quadrant. Whether triangular or linear, these 18 gas collections all had an inferolateral to superomedial orientation, and all were located in the medial half of the right upper quadrant. The 13 triangular collections all had a concave superolateral border, and their mean longest dimension was 3.2 cm (range, 2–7 cm). The five linear collections had a mean length of 4.0 cm (range, 2–5 cm).

At the same time, false-positive right-upper-quadrant gas signs (five triangular and one linear) were present in six (7%) of 87 patients who had no evidence of pneumoperitoneum on upright or left lateral decubitus films (Fig. 2). Of the five false-positive triangular collections, three had a convex superolateral border (Fig. 2A), one had an inferomedial to superolateral orientation (Fig. 2B), and one was located in the lateral half of the right upper quadrant. In retrospect, most of these collections probably represented gas in the duodenal bulb. The one false-positive linear gas collection in the right upper quadrant also extended into the lateral half of the right upper quadrant (Fig. 2C) and, in retrospect, probably represented fat in the subhepatic space.

**TABLE 1: Summary of Radiographic Findings in 44 Cases of Pneumoperitoneum and 87 Controls**

| Sign | No. of Cases | | % Sensitivity |
|---|---|---|---|
| | True Positive | False Positive | |
| Right-upper-quadrant gas | | | |
| Triangular | 13 | 5 | 30 |
| Linear | 5 | 1 | 11 |
| Total | 18 | 6 | 41 |
| Rigler's | 14 | 5 | 32 |
| Falciform ligament | 1 | 0 | 2 |
| Football | 1 | 0 | 2 |
| Inverted V | 0 | 0 | 0 |
| One or more | 26 | 10 | 59 |

### *Rigler's Sign*

Rigler's sign was present on supine films in 14 (32%) of 44 cases of pneumoperitoneum (Fig. 3). Of these 14 cases in which gas was seen on both sides of the bowel wall, the stomach was involved in three, the small bowel in two, the colon in five, the small bowel and colon in three, and the stomach and colon in one. The mean wall thickness in those 14 cases was 5.8 mm (range, 4–8 mm) for the stomach, 1.8 mm (range, 1–2 mm) for the small bowel, and 1.1 mm (range, 1–2 mm) for the colon. In all 14 patients with a true-positive Rigler's sign, the wall thickness therefore was 1 mm or greater. Of the five false-positive cases (6%) of Rigler's sign, the small bowel was involved in two and the colon in three (Fig. 4). The mean wall thickness in those five cases was 0.6 mm (range, 0.5–1.0 mm). In all five patients with a false-positive Rigler's sign, the apparent wall thickness therefore was 1 mm or less.

One patient had a variant of Rigler's sign in which gas was seen only outside the wall of several fluid-filled loops of dilated small bowel, producing a distinctive radiologic appearance (Fig. 5).

### *Other Signs*

The falciform ligament sign (Fig. 6) and football sign (Fig. 3A) were each present on supine films in only one of 44 cases (2%) of pneumoperitoneum. These cases had a positive right-upper-quadrant gas sign (Fig. 6) or Rigler's sign (Fig. 3A), so that pneumoperitoneum would have been diagnosed even in the absence of these findings. Finally, the inverted-V sign was not present on supine films in any cases of pneumoperitoneum.

### *Amount of Free Intraperitoneal Air*

The mean distance between the diaphragm and liver or the right lateral abdominal wall and liver on upright or left lateral decubitus films was 1.9 cm (range, 0.1–5.0 cm) in the 26 cases of pneumoperitoneum that were diagnosed on supine films but only 0.6 cm (range, 0.1–1.2 cm) in the 18 cases of pneumoperitoneum that were not diagnosed on these films. Thus, a greater amount of free intraperitoneal air was present in patients who had one or more signs of pneumoperitoneum on supine abdominal radiographs.

## Discussion

Unless a considerable amount of free air is present in the abdomen, supine abdominal radiographs are generally

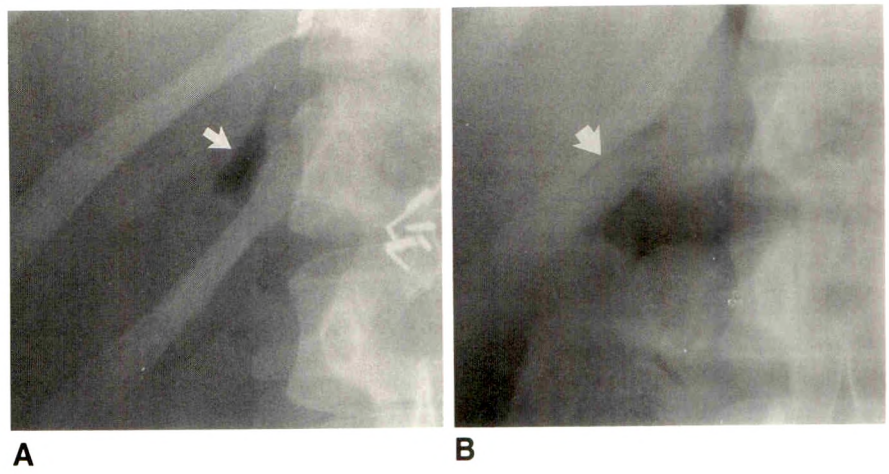



Fig. 1.—Right-upper-quadrant gas sign on radiographs in two patients with pneumoperitoneum.

*A*, Triangular lucency (*arrow*) with inferolateral to superomedial orientation and concave superolateral border. Also note medial location of gas adjacent to lower thoracic spine.

*B*, Linear lucency (*arrow*) in subhepatic region. Again note inferolateral to superomedial orientation of gas.

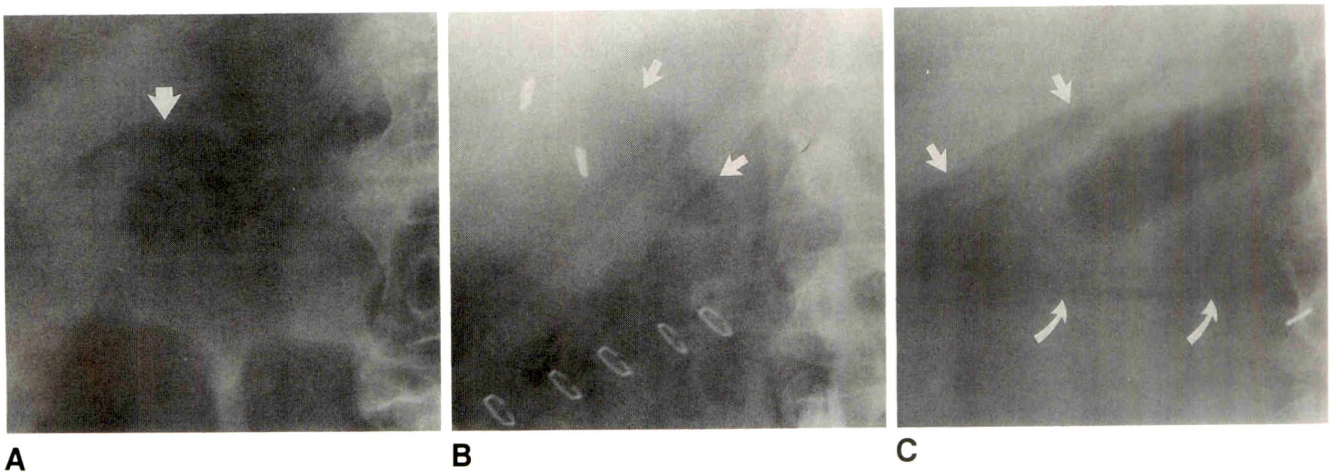



Fig. 2.—False-positive right-upper-quadrant gas sign on radiographs in three patients without pneumoperitoneum.

*A*, Triangular lucency (*arrow*) with convex superolateral border. In retrospect, this probably represents gas in duodenal bulb.

*B*, Triangular lucency (*arrows*) with inferomedial to superolateral orientation. In retrospect, this also may be gas in duodenal bulb.

*C*, Linear lucency (*straight arrows*) extending into lateral half of right upper quadrant. In retrospect, this probably represents fat in subhepatic space. Note skin fold (*curved arrows*) more inferiorly.

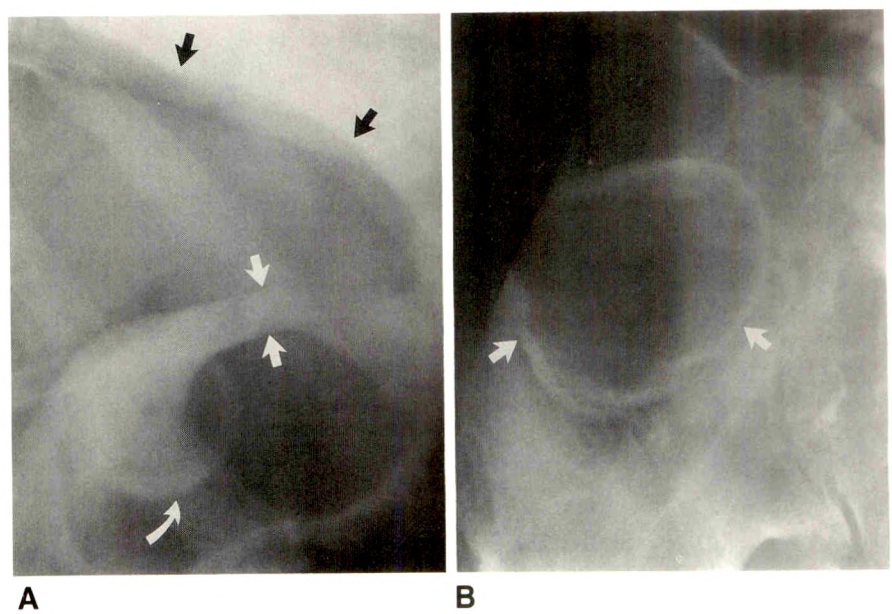



Fig. 3.—Rigler's sign on radiographs in patient with pneumoperitoneum.

*A*, Close-up view of left upper quadrant shows gas outlining both sides of gastric wall (*straight white arrows*), which appears quite thick. This patient also has football sign (*straight black arrows*) of pneumoperitoneum. Gastrostomy tube (*curved arrow*) is present in stomach.

*B*, Close-up view of right lower quadrant shows gas outlining both sides of cecal wall (*arrows*), which is several millimeters thick.

thought to have limited value in diagnosing pneumoperitoneum [10–12]. Our study confirmed that patients with smaller amounts of free air are less likely to have radiologic evidence of pneumoperitoneum on supine films. Nevertheless, one or more signs of pneumoperitoneum were present on these films in 59% of cases. Because pneumoperitoneum may indicate a life-threatening situation, radiologists need to be aware of these various signs and of their relative value in diagnosing this condition.

In our study, the most frequent sign of pneumoperitoneum on supine abdominal radiographs was the right-upper-quadrant gas sign, which was present in 41% of cases (Fig. 1). Surprisingly, this important sign of pneumoperitoneum has received little attention in the radiologic literature [7–9]. In a retrospective study by Menuck and Siemers [8], localized right-upper-quadrant gas collections were present on supine films in 49% of patients with pneumoperitoneum, whereas the more well-known signs of pneumoperitoneum (i.e., Rigler's sign and the falciform ligament sign) were present in only 17% of patients. In our study and that by Menuck and Siemers, these gas collections appeared as obliquely oriented, triangular or linear lucencies in the right upper quadrant. It has been postulated that the linear collections represent gas in the right subhepatic space, whereas the triangular collections represent gas in the posterior recess of the right subhepatic space, also known as the hepatorenal fossa or Morison pouch [7–9].

Further analysis of our patients revealed that all of the true-positive right-upper-quadrant gas collections were located in the medial half of the right upper quadrant with an inferolateral to superomedial orientation, and, if triangular, with a concave superolateral border (Fig. 1). In contrast, all of the false-positive right-upper-quadrant collections had a convex superolateral border or an inferomedial to superolateral orientation or were located in the lateral half of the right upper quadrant (Fig. 2). Thus, if properly interpreted, the right-upper-quadrant gas sign is probably the single best sign of pneumoperitoneum on supine films.

The second most frequent sign of pneumoperitoneum on supine abdominal radiographs was Rigler's sign, which was present in 32% of cases (Fig. 3). However, a false-positive Rigler's sign was present in five cases (6%) in which there was no evidence of pneumoperitoneum on upright or left lateral decubitus films (Fig. 4). These false-positive findings may have resulted from Mach bands, a phenomenon in which there is the perception of a line at the interface of two regions of differing densities [13]. This problem is more likely to occur when two bowel loops are overlapping, so that the edge of one bowel wall is superimposed on the gas-filled lumen of another loop. However, all of the false-positive cases had an apparent wall thickness of 1 mm or less (Fig. 4), whereas all of the true positives had a wall thickness of 1 mm or greater (Fig. 3). Thus, evaluation of wall thickness is a useful criterion for differentiating Mach bands from true-positive Rigler's signs in patients with pneumoperitoneum. Furthermore, there were no false-positive cases with gas on both sides of the wall of the stomach, so that the latter finding should be considered a particularly reliable sign of pneumoperitoneum (Fig. 3A). Interestingly, one patient had a variant of Rigler's sign in which air was only seen outside the wall of several fluid-filled loops of dilated small bowel (Fig. 5).

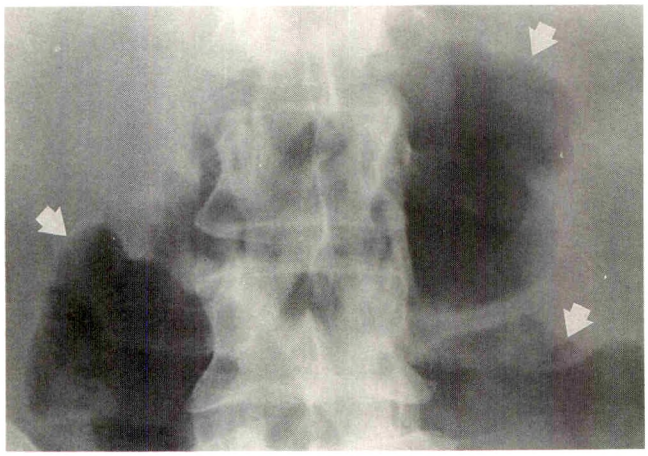
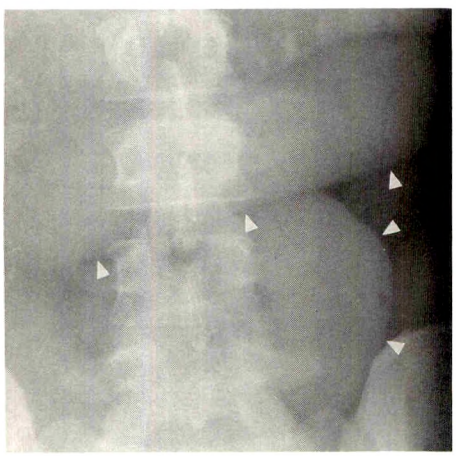
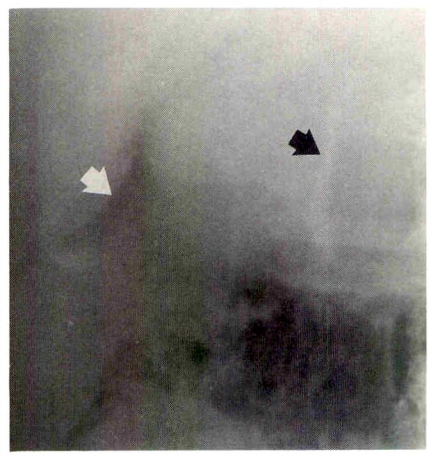


**Fig. 4.—False-positive Rigler's sign on radiograph in patient without pneumoperitoneum. Note how line (*arrows*) along margin of bowel has no discernible thickness in this case.**



**5**

**Fig. 5.—Variant of Rigler's sign in patient with pneumoperitoneum. Radiograph shows unusually sharp, well-defined outer border (*arrowheads*) of several fluid-filled loops of dilated small bowel caused by gas in peritoneal cavity.**



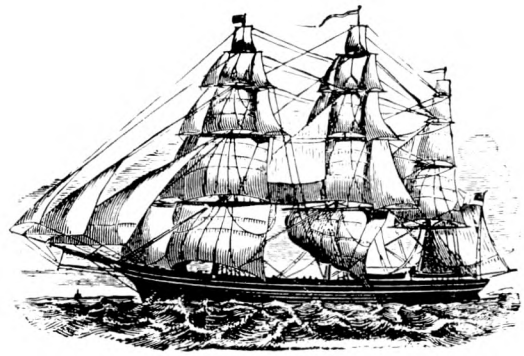
**6**

**Fig. 6.—Falciform ligament sign and right-upper-quadrant gas sign in patient with pneumoperitoneum. Thin, linear, soft-tissue density (*black arrow*) in right upper quadrant is due to gas outlining falciform ligament. More lateral triangular lucency (*white arrow*) is due to gas in subhepatic region.**

Other well-known signs of pneumoperitoneum on supine films, such as the falciform ligament sign, football sign, and inverted-V sign, were each present in less than 3% of cases and were always seen in patients who had a positive Rigler's sign (Fig. 3A) or right-upper-quadrant gas sign (Fig. 6). Thus, for all practical purposes, pneumoperitoneum is primarily diagnosed on supine films by the presence of gas on both sides of the bowel wall or by triangular or linear gas collections in the right upper quadrant. Proper interpretation of these signs should lead to more accurate diagnosis of this condition.

## REFERENCES


1. Vaughn RT, Brams WA. Early recognition of acute perforation of gastric and duodenal ulcer by x-ray examination of spontaneous pneumoperitoneum. *Surg Gynecol Obstet* **1924**;39:610–617
2. Miller RE, Nelson SW. The roentgenologic demonstration of tiny amounts of free intraperitoneal gas: experimental and clinical studies. *AJR* **1971**;112:574–585
3. Rigler LG. Spontaneous pneumoperitoneum: a roentgenologic sign found in the supine position. *Radiology* **1941**;37:604–607
4. Miller RE. Perforated viscus in infants: a new roentgen sign. *Radiology* **1960**;74:65–67
5. Weiner CI, Diaconis JN, Dennis JM. The "inverted V": a new sign of pneumoperitoneum. *Radiology* **1973**;107:47–48
6. Bray JF. The "inverted V" sign of pneumoperitoneum. *Radiology* **1984**;151:45–46
7. Hajdu N, de Lacey G. The Rutherford Morison pouch: a characteristic appearance on abdominal radiographs. *Br J Radiol* **1970**;43:706–709
8. Menuck L, Siemers PT. Pneumoperitoneum: importance of right upper quadrant features. *AJR* **1976**;127:753–756
9. Brill PW, Olson SR, Winchester P. Neonatal necrotizing enterocolitis: air in Morison pouch. *Radiology* **1990**;174:469–471
10. Berdon WE, Baker DH, Leonidas J. Advantages of prone positioning in gastrointestinal and gastrourological roentgenologic studies in infants and children. *AJR* **1968**;103:444–445.
11. Harned RK. Diagnosis of pneumoperitoneum in the adult. *Nebr Med J* **1974**;59:185–191
12. Markowitz SK, Ziter FM. The lateral chest film and pneumoperitoneum. *Ann Emerg Med* **1986**;15:425–427
13. Edholm P. Boundaries in the radiographic image. I. General principles for perception of boundaries and their application to the image. *Acta Radiol* **1981**;22:457–473



# Come to the American Roentgen Ray Society 91st ANNUAL MEETING

## Boston, MA

Sheraton Boston Hotel
May 5-10, 1991

Scientific Program (200 papers)
Instructional Courses (60 hours)
Categorical Course on Body MR Imaging
The Caldwell Lecture
Award Papers
Scientific Exhibits
Social, Golf, and Tennis Programs
Guest Programs



Pictorial Essay

# Imaging the Gallbladder: A Historical Perspective

Rick Feld,[1] Alfred B. Kurtz,[1] and Robert K. Zeman[2]

**After Wilhelm Conrad Roentgen's discovery of the X-ray in 1895, it was initially thought that gallstones could not be visualized. Surgeons relied solely on the clinical examination to detect biliary disease. Today, no evaluation of the gallbladder would be complete without the performance of an imaging study. Radiology has gone through several eras in the imaging of gallstones. The plain film era, 1895–1924, was characterized by techniques that improved soft-tissue detail, allowing better detection of radiopaque stones. The contrast media era, 1924–1960, was initiated by the invention of IV cholecystography. In 1925, oral cholecystography was developed. During the era of expanding technology, 1960–1979, percutaneous transhepatic cholangiography, scintigraphy, and sonography came into use. The therapeutic era began in the 1980s.**

## The Plain Film Era, 1895–1924

In 1897, William Osler [1] asked skeptically, "Can you see gallstones with the X-ray?" No one could give him an answer. Carl Beck [2] published the first report of radiologic detection of gallstones in a living patient in 1900. He presented two cases at the New York County Medical Society, but the audience was reluctant to accept his interpretation as correct. Others made a slightly more convincing plain film diagnosis of gallstones (Fig. 1).

In 1910, the first radiographs of gallstones in which the diagnosis was undisputed were obtained by three independent physicians, George E. Pfahler, Lewis Gregory Cole, and James T. Case [3–5]. The introduction of intensifying screens and the Potter-Bucky diaphragm with a movable grid in 1918 significantly improved soft-tissue detail (Figs. 2 and 3).

In 1921, Burckhardt and Muller [7] of Marburg, Germany, showed the gallbladder by using percutaneous transhepatic puncture with a 0.8-mm needle. They used a silver-containing contrast agent and air.

## The Contrast Media Era, 1924–1960

Experimental work established that phenolphthalein compounds were excreted by the liver into the bile (1909) [8] and that bile was concentrated in the gallbladder (1921) [9]. On the basis of this information, Warren H. Cole and Evarts Graham devised IV cholecystography. Cole, a surgical resident, failed to visualized the gallbladder in dogs by the injection of IV tetrabromophenolphthalein. After 200 attempts, one dog's gallbladder was visualized. Cole recalled "as I was standing near the viewbox studying the film, out of the corner of my eye I saw Dr. Mills (a radiologist) come through the door. I heard him walking rapidly and then suddenly skid to a stop." Mills' sharp eye had noted something on the film that he had never seen before, and he said, "Young fellow, where did you get that film?" Cole explained and added that he was afraid the shadow might be something the dog had swallowed. Mills replied, "Don't be silly, young man, this is a shadow of the gallbladder." [10]

Received August 2, 1990; accepted after revision October 17, 1990.

[1] Department of Radiology, Division of Diagnostic Ultrasound, Thomas Jefferson University Hospital, 132 S. 10th St., Philadelphia, PA 19107-5244. Address reprint requests to R. Feld.

[2] Department of Radiology, Georgetown University Hospital, 3800 Reservoir Rd., N.W., Washington, DC 20007-2197.

*AJR* **156:737–740, April 1991** 0361–803X/91/1564–0737 © American Roentgen Ray Society



Fig. 1.—Plain radiograph made by an electrical engineer of the era with accompanying handwritten interpretation. Diagnosis of biliary calculi seems apocryphal. (Fuchs WC, Chicago, circa 1900.)

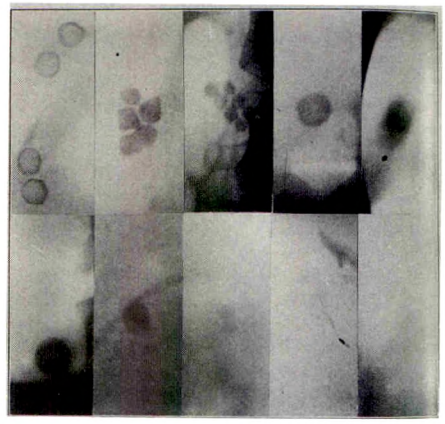


Fig. 2.—Plain radiographs from 1914 show the first undisputed gallstones in 10 different patients. (Reprinted from Cole [3].)

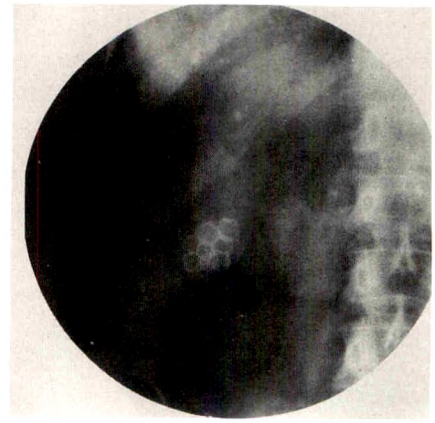
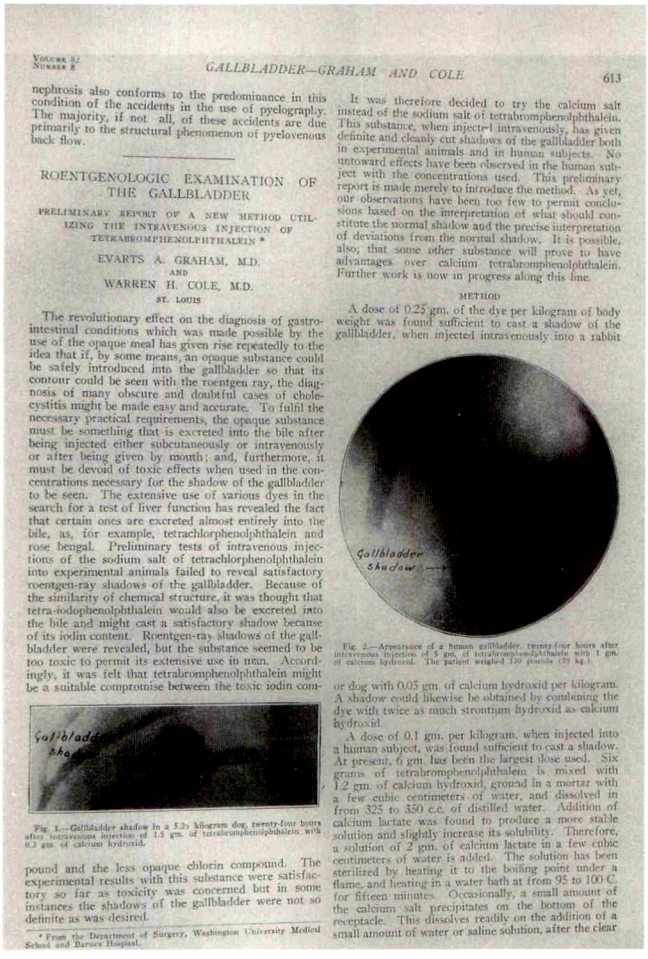


Fig. 3.—Plain film made in 1922 shows gallstones clearly. (Reprinted with permission from George and Leonard [6].)



VOLUME 8 / NUMBER 8 GALLBLADDER—GRAHAM AND COLE 613

nephrosis also conforms to the predominance in this condition of the accidents in the use of pyelography. The majority, if not all, of these accidents are due primarily to the structural phenomenon of pyelovenous back flow.

ROENTGENOLOGIC EXAMINATION OF THE GALLBLADDER

PRELIMINARY REPORT OF A NEW METHOD UTILIZING THE INTRAVENOUS INJECTION OF TETRABROMPHENOLPHTHALEIN *

EVARTS A. GRAHAM, M.D.
AND
WARREN H. COLE, M.D.
ST. LOUIS

The revolutionary effect on the diagnosis of gastrointestinal conditions which was made possible by the use of the opaque meal has given rise repeatedly to the idea that if, by some means, an opaque substance could be safely introduced into the gallbladder so that its contour could be seen with the roentgen ray, the diagnosis of many obscure and doubtful cases of cholecystitis might be made easy and accurate. To fulfil the necessary practical requirements, the opaque substance must be something that is excreted into the bile after being injected either subcutaneously or intravenously or after being given by mouth; and, furthermore, it must be devoid of toxic effects when used in the concentrations necessary for the shadow of the gallbladder to be seen. The extensive use of various dyes in the search for a test of liver function has revealed the fact that certain ones are excreted almost entirely into the bile, as, for example, tetrachlorphenolphthalein and rose bengal. Preliminary tests of intravenous injections of the sodium salt of tetrachlorphenolphthalein into experimental animals failed to reveal satisfactory roentgen-ray shadows of the gallbladder. Because of the similarity of chemical structure, it was thought that tetra-iodophenolphthalein would also be excreted into the bile and might cast a satisfactory shadow because of its iodin content. Roentgen-ray shadows of the gallbladder were revealed, but the substance seemed to be too toxic to permit its extensive use in man. Accordingly, it was felt that tetrabromphenolphthalein might be a suitable compromise between the toxic iodin compound and the less opaque chlorin compound. The experimental results with this substance were satisfactory so far as toxicity was concerned but in some instances the shadows of the gallbladder were not so definite as was desired.

* From the Department of Surgery, Washington University Medical School and Barnes Hospital.

It was therefore decided to try the calcium salt instead of the sodium salt of tetrabromphenolphthalein. This substance, when injected intravenously, has given definite and cleanly cut shadows of the gallbladder both in experimental animals and in human subjects. No untoward effects have been observed in the human subject with the concentrations used. This preliminary report is made merely to introduce the method. As yet, our observations have been too few to permit conclusions based on the interpretation of what should constitute the normal shadow and the precise interpretation of deviations from the normal shadow. It is possible, also, that some other substance will prove to have advantages over calcium tetrabromphenolphthalein. Further work is now in progress along this line.

METHOD

A dose of 0.25 gm. of the dye per kilogram of body weight was found sufficient to cast a shadow of the gallbladder, when injected intravenously into a rabbit or dog with 0.05 gm. of calcium hydroxid per kilogram. A shadow could likewise be obtained by combining the dye with twice as much strontium hydroxid as calcium hydroxid.

A dose of 0.1 gm. per kilogram, when injected into a human subject, was found sufficient to cast a shadow. At present, 6 gm. has been the largest dose used. Six grams of tetrabromphenolphthalein is mixed with 1.2 gm. of calcium hydroxid, ground in a mortar with a few cubic centimeters of water, and dissolved in from 325 to 350 c.c. of distilled water. Addition of calcium lactate was found to produce a more stable solution and slightly increase its solubility. Therefore, a solution of 2 gm. of calcium lactate in a few cubic centimeters of water is added. The solution has been sterilized by heating it to the boiling point under a flame, and heating in a water bath at from 95 to 100 C. for fifteen minutes. Occasionally, a small amount of the calcium salt precipitates on the bottom of the receptacle. This dissolves readily on the addition of a small amount of water or saline solution, after the clear

Fig. 1.—Gallbladder shadow in a 5.2-kilogram dog, twenty-four hours after intravenous injection of 1.5 gm. of tetrabromphenolphthalein with 0.3 gm. of calcium hydroxid.

Fig. 2.—Appearance of a human gallbladder, twenty-four hours after intravenous injection of 6 gm. of tetrabromphenolphthalein with 1 gm. of calcium hydroxid. The patient weighed 130 pounds (59 kg.).

Fig. 4.—Graham and Cole's report of gallbladder opacification in dogs and humans. (Reprinted from Graham and Cole [12].)

Despite the single success, further experiments continued to fail. In desperation, Cole asked the animal caretaker what had been different about that one dog. Hesitating and fearing reprimand, the animal caretaker muttered, "I forgot to feed that dog the morning you injected him." Cole seized the importance of this statement [11]. Further experiments in unfed dogs established the importance of an overnight fast (Fig. 4).

Graham and Cole [12] were successful in opacifying the gallbladder in a human; however, the patient developed nausea, back pain, and vomiting. Improvements occurred rapidly [13–15]. Whitaker, Milliken, and Vogt [16] showed that a smaller dose of the iodinated compound (tetraiodophenolphthalein), instead of the bromine derivative, achieved a similar result and with less systemic toxicity. Sodium salts also were found to be more soluble than calcium salts, allowing easier preparation for IV administration (Fig. 5).

Oral cholecystography, with the same sodium salt of tetraiodophenolphthalein, was introduced in 1925, and the procedure quickly became a routine office practice.

The ensuing years saw the development of compounds that differed in their degree of lipid and aqueous solubility (Fig. 6). Finally, in 1951, oral cholecystography achieved the standards that are known today, with the introduction of iopanoic acid, a highly lipid-soluble oral agent.

## The Era of Expanding Technology, 1961–1979

Advances in gallbladder imaging with other procedures began in the 1960s. John Evans et al. [17] performed percutaneous transhepatic cholangiography with a rigid 18- to 20-gauge sheathed needle (Fig. 7). Because of the large caliber

Fig. 5.—*A* and *B*, IV cholecystograms obtained by Graham and Cole in 1925. (Reprinted from Graham et al. [15].)

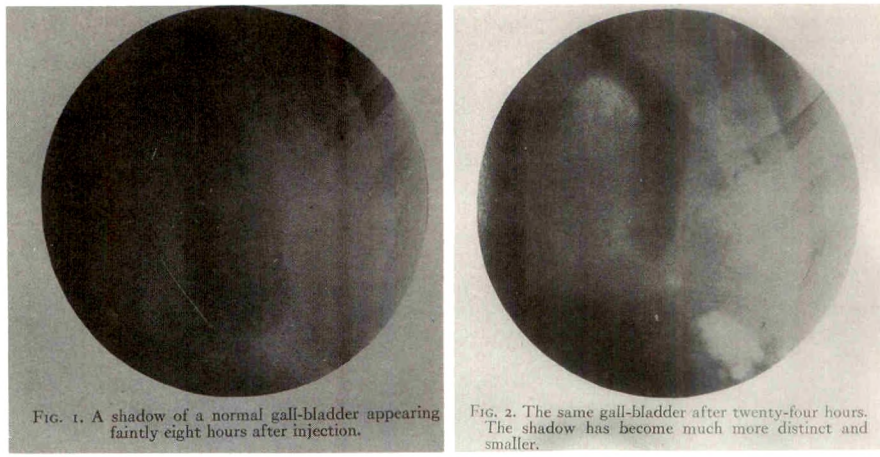


FIG. 1. A shadow of a normal gall-bladder appearing faintly eight hours after injection.

FIG. 2. The same gall-bladder after twenty-four hours. The shadow has become much more distinct and smaller.

A B

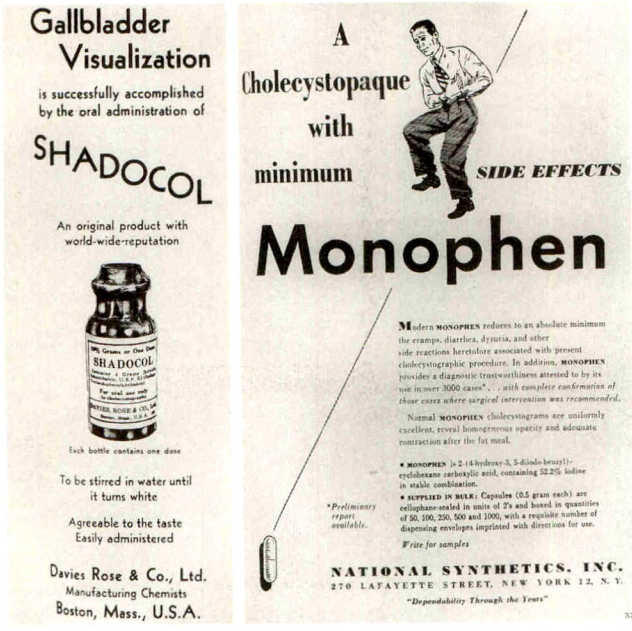



Fig. 6.—*A* and *B*, Advertisements for cholecystographic agents published in *AJR* in 1941 (*A*) and 1951 (*B*). (Reprinted from *AJR* 1941;46:v and *AJR* 1951;65:xxix.)

of the needle, bleeding and bile leaks were not uncommon. In 1974, a flexible 22-gauge skinny Chiba needle, developed by Okuda et al. [18] made the procedure safer and much more successful.

Rose bengal labeled with iodine-131 was introduced in 1970. Although the rose bengal moiety had many physical properties that permitted high concentration and excretion in the bile, the iodine-131 had poor imaging properties (Fig. 8). In 1975 Harvey, Loberg, and Cooper [20] introduced HIDA (*N*-substituted 2,6-dimethylphenylcarbamoylethyl iminodiacetic acid). Newer IDA derivatives that varied in the location and side-chain substitution on the phenyl ring allowed visualization of the gallbladder even in the presence of significant jaundice (Fig. 9).

Early sonographic machines produced A-mode and bistable B-mode images (Figs. 10 and 11). In 1970, Weill and coworkers [21], of France, were among the first to visualize gallstones as small as 2 mm by using gray-scale sonography. Goldberg et al. and Leopold et al. confirmed the value of gray-scale sonography in the mid-1970s [22–24]. However, even with real-time scanning, the resolution of sonography with awkward linear-array probes was limited. With improvements in sector probes, including better beam forming and focusing, high-resolution real-time sonography became the technique of choice in the detection of gallstones [25].

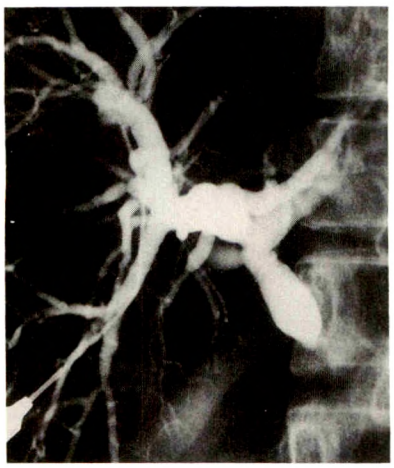


Fig. 7.—The last large-needle-sheath cholangiogram obtained with an 18-gauge needle at Yale–New Haven Hospital shows a transected common bile duct due to trauma. (Courtesy of M. Burrell, circa 1973.)

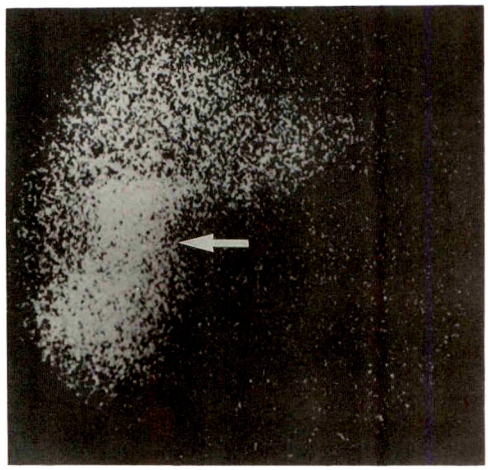


Fig. 8.—Rose bengal scan in a patient with biliary obstruction. It is difficult to distinguish gallbladder (*arrow*) from liver. (Reprinted with permission from Gottschalk [19]. Courtesy of B. Oppenheim and P. Hoffer, circa 1975.)

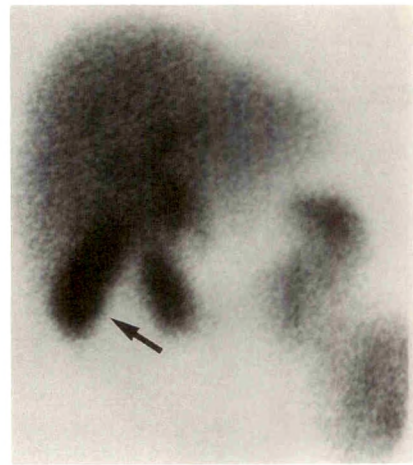
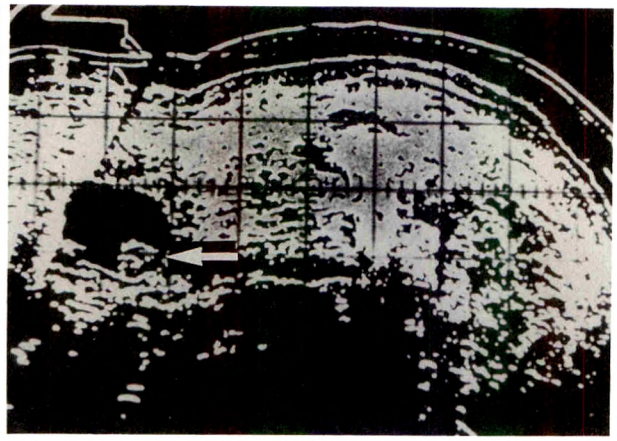


Fig. 9.—Normal technetium-99m DISIDA (diisopropyl iminodiacetic acid) scan at 30 min shows gallbladder (*arrow*).



10

Fig. 10.—Early bistable B-mode sonogram (longitudinal) with patient erect shows a gallstone (*arrow*). (Courtesy of B. B. Goldberg, circa 1968.)



11

Fig. 11.—Bistable B-mode sonogram (transverse) with patient supine shows a gallstone (*arrow*). (Courtesy of B. B. Goldberg, circa 1972.)

### The Therapeutic Era, 1980–Present

Burhenne [26] reported the first use of intracorporeal electrohydrolytic fragmentation of retained common duct stones in 1975. In 1986 Sauerbruch, Paumgartner, and associates [27] used extracorporeal shock-wave therapy for the treatment of gallstones. Sonography plays a vital role in targeting the stones during lithotripsy. A stone-free rate 2 months after treatment as high as 45% can be achieved in patients with noncalcified solitary stones, less than 20 mm in size [28].

Numerous nonsurgical treatments are now evolving. These involve percutaneous catheter drainage of the gallbladder allowing contact dissolution (methyl *tert*-butyl ether and monooctanoin), laser fragmentation, and intracorporeal electrohydraulic lithotripsy [29]. As we enter the 1990s, the efficacy of these techniques vs conventional and laparoscopic cholecystectomy will be the focus of intense investigation.

REFERENCES


1. Cushing H. In: *The life of Sir William Oster*. Oxford: Oxford University Press, **1940**:434–435
2. Beck C. On the detection of calculi in the liver and gallbladder. *NY Med J* **1900**;71:73–77
3. Cole LG. The detection of pure cholesterine gallstones by the roentgen rays. *AJR* **1914**;2:640–651
4. Pfahler GE. An improvement in the technique of gallbladder diagnosis. *AJR* **1915**;2:774–775
5. McCoy CC. Development of roentgenologic examination of the biliary tract. *Radiology* **1928**;11:13–26
6. George AW, Leonard RD. *The pathologic gallbladder*. Philadelphia: Lippincott (Paul B. Hoeber), **1922**:38
7. Burckhardt H, Muller W. Versuche über die Punktion der Gallenblase und ihre Roentgendarstellung. *Dtsch Z Chir* **1921**;162:163
8. Abel JJ, Rowntree LG. On the pharmacological action of some phthaleins and their derivatives, with special reference to their behavior and purgatives. *J Pharmacol Exp Ther* **1909**;1:231–264
9. Rous P, McMaster PD. The concentrating activity of the gallbladder. *J Exp Med* **1921**;34:47–73
10. Cole WH. Historical features of cholecystography. *Radiology* **1961**;76:354–375
11. Brecher E, Brecher R. In: *The rays. A history of radiology in the United States and Canada*. Baltimore, MD: Williams & Wilkins, **1969**:233–242
12. Graham EA, Cole WH. Roentgenologic examination of the gallbladder: new method utilizing intravenous injection of tetrabromphenolpthalein. *JAMA* **1924**;82:613–614
13. Graham EA, Cole WH, Copher GH. Cholecystography: an experimental and clinical study. *JAMA* **1925**;84:14–16
14. Graham EA, Cole WH, Copher GH. Cholecystography: the use of sodium tetraiodophenolphthalein. *JAMA* **1925**;84:1175–1177
15. Graham EA, Cole WH, Copher G. Cholecystography: its development and application. *AJR* **1925**;14:490–491
16. Whitaker LR, Milliken G, Vogt EC. The oral administration of sodium tetraiodophenolphthalein for cholecystography. *Surg Gynecol Obstet* **1925**;41:847–851
17. Evans JA, Glenn F, Thorbjarnarson B, Mujahed Z. Percutaneous transhepatic cholangiography. *Radiology* **1962**;78:362–370
18. Okuda K, Tanikawa K, Emura T, et al. Nonsurgical percutaneous transhepatic cholangiography: diagnostic significance in medical problems of the liver. *Dig Dis Sci* **1974**;19:21–36
19. Oppenheim BE, Gottschalk A, Hoffer PB. In: Gottschalk A, Potchen EJ, eds. *Diagnostic nuclear medicine*. Baltimore, MD: Williams & Wilkins, **1976**:448
20. Harvey E, Loberg M, Cooper M. Tc-99m-HIDA: a new radiopharmaceutical for hepatobiliary imaging. *J Nucl Med* **1975**;16:533
21. Weill F, Becker JC, Kraehenbuhl JR, Heriot G, Walter JP. *Atlas clinique de radiographic ultrasonore*. Paris: Masson & Cie, 1973
22. Goldberg BB, Harris K, Broocker W. Ultrasonic and radiographic cholecystography. *Radiology* **1974**;111:405–409
23. Goldberg BB. Ultrasonic cholangiography. *Radiology* **1976**;118:401–404
24. Leopold GR, Amberg J, Gosink B, Mittelstaedt C. Gray scale ultrasonic cholecystography. *Radiology* **1976**;121:445–448
25. Cooperberg PL, Burhenne HJ. Real-time ultrasonography diagnostic technique of choice in calculous gallbladder disease. *N Engl J Med* **1980**;320:1277–1279
26. Burhenne JH. Electrohydrolytic fragmentation of retained common duct stones. *Radiology* **1975**;117:721–722
27. Sauerbruch T, Delius M, Paumgartner G, et al. Fragmentation of gallstones by extracorporeal shockwaves. *N Engl J Med* **1986**;314:818–822
28. Sackmann M, Delius M, Sauerbruch T, et al. Shock-wave lithotripsy of gallbladder stones: the first 175 patients. *N Engl J Med* **1988**;318:393–397
29. Ferrucci JT. Biliary lithotripsy: 1989. *AJR* **1989**;153:15–22

# Amyloidosis of the Small Intestine: Findings on Double-Contrast Radiographs

Shuji Tada[1]
Mitsuo Iida[1]
Toshiyuki Matsui[1]
Tadahiko Fuchigami[2]
Akinori Iwashita[3]
Tsuneyoshi Yao[4]
Masatoshi Fujishima[1]

**The appearance of the small intestinal mucosa on double-contrast barium examinations was studied in 26 patients with proved intestinal amyloidosis. Findings included innumerable fine granular densities 1–3 mm in diameter (16 patients), multiple nodular densities 3–4 mm in diameter (four patients), multiple polypoid protrusions 4–10 mm in diameter (three patients), irregularities of Kerckring folds (12 patients), and multiple erosions (eight patients). The multiple nodular densities and erosions disappeared after the patients were treated with total parenteral nutrition. The other abnormalities remained unchanged on follow-up examinations.**

**Our results indicate that double-contrast radiographic findings of the small intestine in patients with amyloidosis include mucosal abnormalities that vary according to the pathologic type of amyloid deposition.**

***AJR* 156:741–744, April 1991**

Amyloidosis commonly involves the gastrointestinal tract, resulting in a wide variety of clinical and radiologic manifestations [1–3]. The small intestine is the most frequent site [4, 5]. Radiographs of the small intestine reflect the morphologic changes in this disease [6–8].

Numerous reports have described the radiologic findings of small intestinal amyloidosis; emphasis has been given to thickening of the valvulae conniventes and decreased intestinal motility [6–9]. However, these radiologic findings are not specific and are not useful in the differentiation of amyloidosis from other diseases. In the present study, we analyzed the findings of amyloidosis on double-contrast barium examinations of the small intestine and compared them with clinical symptoms, endoscopy, and biopsy findings.

## Materials and Methods

Between 1978 and 1990, amyloidosis was diagnosed in 46 patients. Of these, 26 had both double-contrast barium studies of the small intestine and jejunal endoscopy with a long duodenofiberscope [10]. In all patients, endoscopic biopsies of the jejunum revealed amyloid deposition. Five patients had primary amyloidosis, three had myeloma-associated amyloidosis, one had familial amyloidosis, and 17 had secondary amyloidosis (rheumatoid arthritis in 10, Crohn disease in two, unclassified intestinal ulcers in one, multiple myositis in one, Chédiak-Higashi syndrome in one, ankylosing spondylitis in one, and pulmonary tuberculosis in one). Principal amyloid proteins consisted of amyloid light chain protein in six patients and amyloid A protein in 19 patients. In two patients without an antecedent or coexisting disease, affinity for Congo red was reduced after treatment with potassium permanganate [11]. Amyloid F protein was demonstrated in one patient with type I familial amyloid polyneuropathy.

The average age of the patients was 45 years (range, 20–71 years). The male-to-female ratio was 1:1. At the time of examination, gastrointestinal symptoms, such as abdominal pain, diarrhea, hemorrhage, obstruction, and malnutrition, were present in 24 of the 26 patients.

The patients were divided into four groups according to the degree of digestive symptoms: (1) severe (four patients), comprising patients with severe abdominal pain, frequent diarrhea

Received July 5, 1990; accepted after revision October 16, 1990.

[1] Department of Internal Medicine II, Kyushu University, Maidashi 3-1-1, Higashi-ku, Fukuoka 812, Japan. Address reprint requests to S. Tada.

[2] Department of Gastroenterology, Matsuyama Red Cross Hospital, Matsuyama 790, Japan.

[3] Department of Pathology, Chikushi Hospital of Fukuoka University, Fukuoka 812, Japan.

[4] Department of Gastroenterology, Chikushi Hospital of Fukuoka University, Fukuoka 812, Japan.

0361–803X/91/1564–0741
© American Roentgen Ray Society

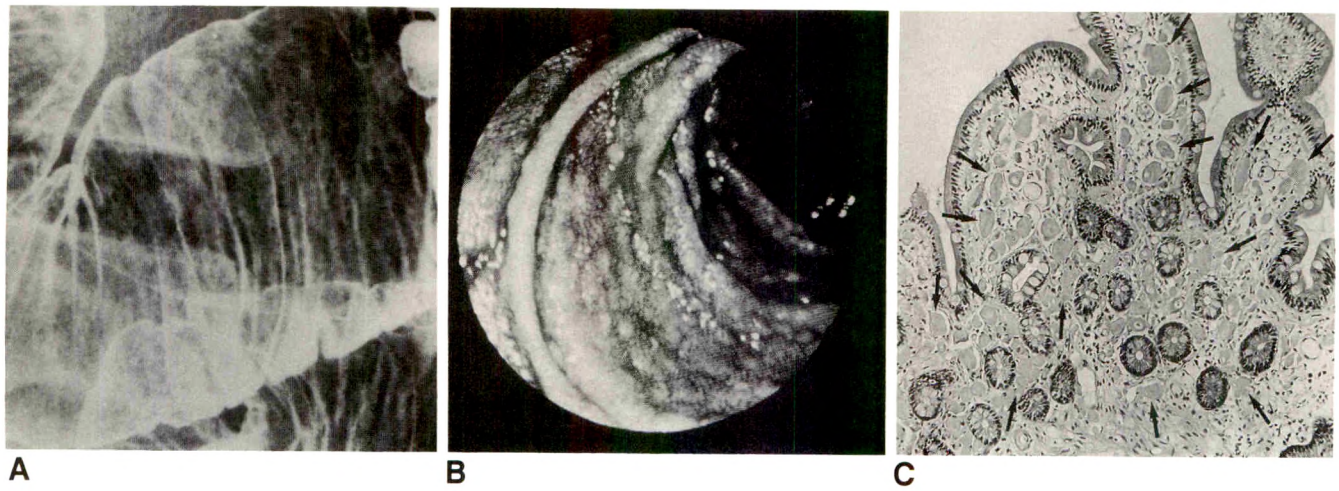



Fig. 1.—*A*, Double-contrast study of upper jejunum shows multiple fine granular densities and irregularities of Kerckring folds caused by amyloidosis. *B*, Jejunal endoscopy performed with a sprayed dye technique reveals innumerable fine granular elevations. Minute elevations are seen on Kerckring folds.
*C*, Jejunal specimen shows obvious amyloid (amyloid A protein) deposition in lamina propria mucosae (*arrows*) and wide, blunted villi. (H and E, original magnification ×146)

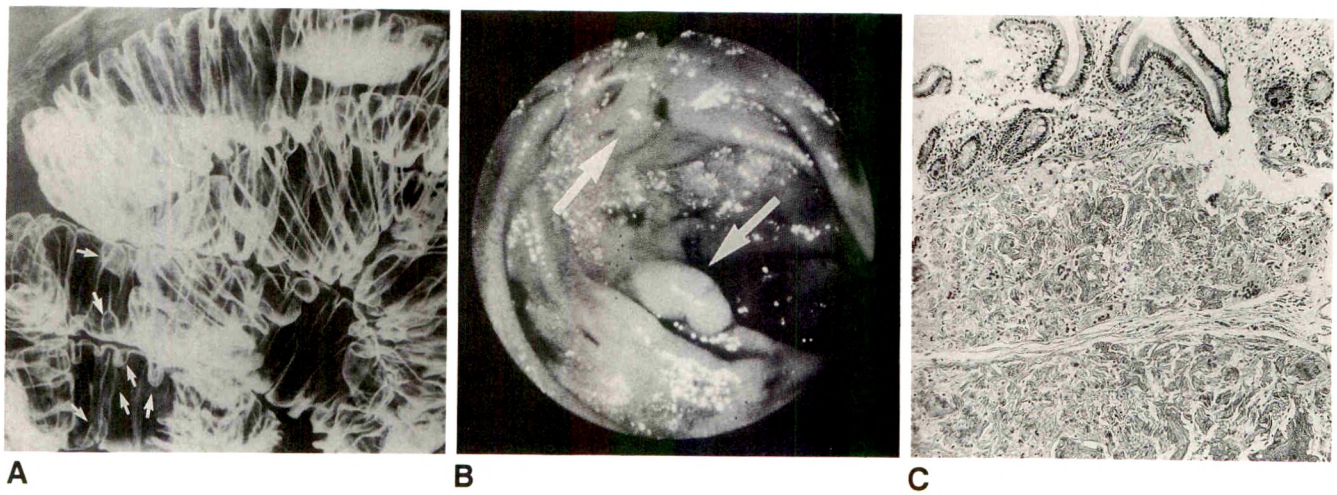



Fig. 2.—*A*, Double-contrast study of jejunum reveals markedly thickened folds and multiple polypoid protrusions (*arrows*) caused by amyloidosis. *B*, Endoscopy of upper jejunum shows multiple yellow white polypoid protrusions (*arrows*).
*C*, Biopsy specimen from upper jejunum reveals massive amyloid (amyloid light chain protein) deposition in submucosa. (Congo red, original magnification ×110)

(six or more movements per day) or obstruction, malnutrition, and dehydration; (2) mild (13 patients), comprising patients with occasional diarrhea (three or fewer movements per day) and mild abdominal pain; (3) moderate (seven patients), in which the severity of symptoms was between that of the severe and mild groups; and (4) no digestive symptoms (two patients).

Double-contrast barium study of the small intestine was performed as follows, modifying the methods reported by Nakamura et al. [12] and Kobayashi et al. [13]: (1) a duodenal tube with a balloon on the tip was inserted as far as the third portion of the duodenum; (2) the balloon was filled with 15–20 ml of air; (3) 250–350 ml of 60% (w/v) barium sulfate was slowly injected via the tube until the terminal ileum was filled and radiographs were obtained; (4) 700–800 ml of air was injected; (5) an anticholinergic agent (scopolamine butylbromide) was administered IV; and (6) double-contrast radiographs of the small intestine were obtained.

The upper jejunum was examined in all patients with a long duodenofiberscope [10]. Three to five biopsy specimens were taken from the upper jejunum. Endoscopic examinations were performed at almost the same time as the radiologic examinations in all 26 patients. In all cases, formalin-fixed, paraffin-embedded sections were stained with hematoxylin and eosin or Congo red and examined under polarized light for the presence of green birefringence.

## Results

Double-contrast examinations revealed innumerable fine granular densities 1–3 mm in diameter in 16 patients (Fig. 1A). The findings were accompanied by irregularities of Kerckring folds in 12 patients (Fig. 1A). Multiple erosions were observed in eight patients. In addition, multiple polypoid protrusions 4–10 mm in diameter (Fig. 2A) were present in three

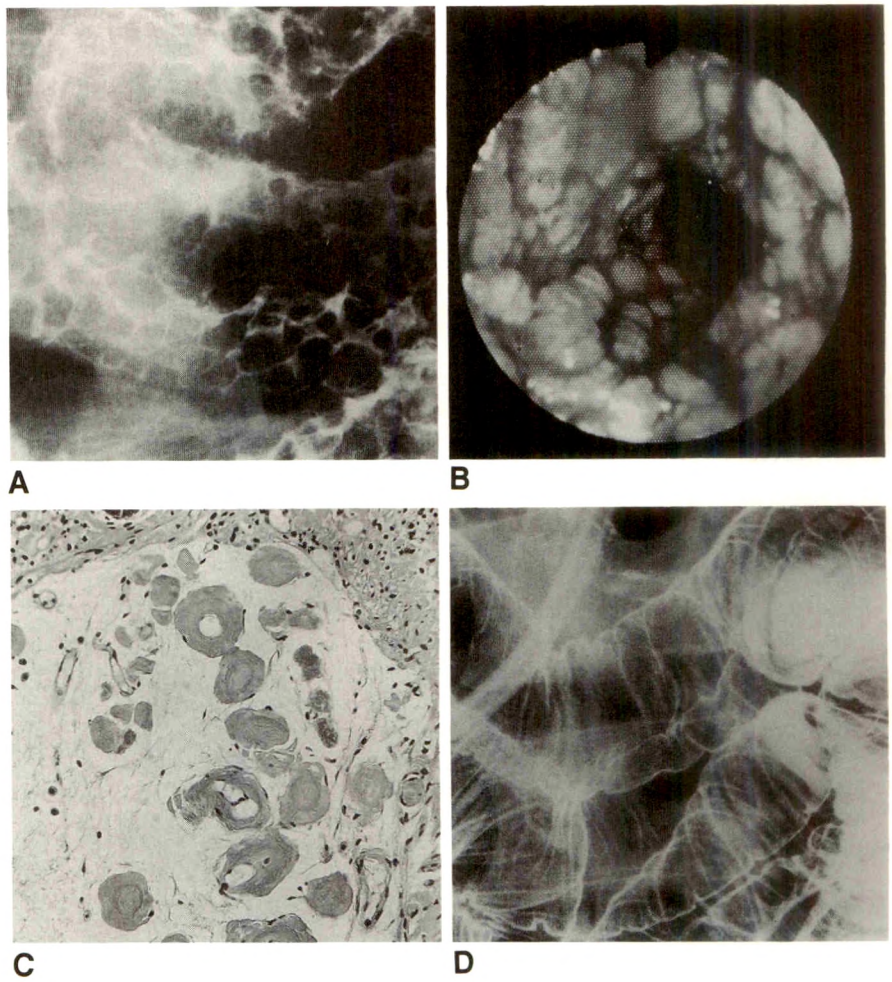



Fig. 3.—*A*, Double-contrast radiograph of jejunum shows multiple nodular densities caused by amyloidosis.

*B*, Endoscopy of upper jejunum shows multiple nodular elevations and shallow ulcers.

*C*, Jejunal specimen shows obvious amyloid (amyloid A protein) deposition in wall of submucosal vessels. (H and E, original magnification ×230)

*D*, Follow-up radiograph after total parenteral nutrition therapy shows that nodular changes have disappeared. Multiple fine granular radiolucencies and irregularities of Kerckring folds are faint.

patients and multiple nodular densities 3–4 mm in diameter (Fig. 3A) in four. These findings were observed throughout the small intestine, but were found most often in the jejunum. No abnormalities were seen in three patients.

On endoscopy, the fine granular appearance reflected innumerable, somewhat whitish granules of varying size (Fig. 1B). On biopsy, mucosal granularity represented marked amyloid deposition in the lamina propria mucosae and wide, blunted villi (Fig. 1C). Irregularities of Kerckring folds on radiographs corresponded to multiple fine granules located on Kerckring folds (Fig. 1B). Multiple polypoid protrusions appeared sessile and yellow white compared with surrounding mucosa (Fig. 2B). On biopsy, polypoid protrusions represented massive amyloid deposits in the mucosa and submucosa (Fig. 2C). Multiple nodular elevations were white, bled easily when touched, and often were associated with multiple erosions or shallow ulcers (Fig. 3B). On biopsy, the mucosa and submucosa showed the presence of marked edema with inflammatory cells. Marked amyloid deposition in the wall of the submucosal vessels also was evident (Fig. 3C).

According to the biochemical categorization of amyloid disease [14], the major amyloid fibril proteins are known to be amyloid A protein in secondary amyloidosis and amyloid light chain protein in primary and myeloma-associated amyloidosis. Our study revealed some differences in the preferential sites of amyloid deposition between the amyloid A protein and amyloid light chain protein types: diffuse parenchymal deposition in the lamina propria mucosae was observed mainly in the former type (Fig. 1C), whereas nodular parenchymal deposition in the muscularis mucosa and submucosa was often revealed in the latter type (Fig. 2C).

Radiographs of all patients with severe digestive symptoms showed multiple nodular densities and erosions. Radiographs of all patients with moderate digestive symptoms and of 12 patients with mild symptoms demonstrated fine granular densities and irregularity of Kerckring folds, or multiple polypoid protrusions. In two patients with no digestive symptoms and one patient with mild symptoms, no abnormalities were seen on radiographs. The more severe the clinical symptoms, the more remarkable the radiologic changes tended to be.

Four patients with severe digestive symptoms received total parenteral nutrition, which led to improvement of subjective symptoms and laboratory data. Double-contrast study of the small intestine 1.5–7.0 months after the start of therapy revealed that multiple nodular densities and erosions disappeared, but innumerable fine granular densities and irregularities of Kerckring folds were seen more clearly than before (Fig. 3D).

Eight patients with moderate or mild digestive symptoms were followed for an average of 2.7 years (range, 13–61

months). During the follow-up period, gastrointestinal symptoms and radiographs of the small intestine remained unchanged.

## Discussion

Gastrointestinal symptoms are common in patients with amyloidosis, and the digestive tract is often a site of amyloid deposition [1, 2, 15]. Gilat et al. [4] reported that gastrointestinal amyloid deposition was found in 68 of 70 autopsied cases of systemic amyloidosis, and amyloid was found to be deposited more frequently in the mucosa of the small intestine than in the stomach or colon. Clinically, patients with amyloid deposits in the small intestine may present with diarrhea, obstruction [16, 17], malabsorption [5, 18], hemorrhage [18–20], infarction [21, 22], and perforation [23, 24].

Seliger et al. [3] compared radiologic features with pathologic findings in small- and large-bowel amyloidosis, and concluded that vascular amyloid deposition affected the radiologic changes most strongly. In patients with intestinal amyloidosis, the vessel walls are thickened and the lumen is gradually reduced and eventually occluded, leading to ischemia, ulceration, infarction, and even perforation [21, 23]. In our patients with severe symptoms, marked amyloid deposition was found in the submucosal vessels (Fig. 3C). This finding supports the view that multiple nodular densities and erosions may be caused by ischemic changes in the submucosa.

In our patients with severe symptoms, follow-up radiographs of the small intestine after total parenteral nutrition revealed the disappearance of multiple nodular densities and erosions. However, there was no difference in the amount of amyloid deposits in the biopsy specimens before and after the therapy, thereby suggesting that these findings were secondary and probably resulted from ischemic change associated with amyloid deposition in the vascular walls [3, 5, 21]. In contrast, multiple polypoid protrusions, fine granular densities, and irregularities of Kerckring folds remained unchanged during the follow-up period. As elevated lesions on radiographs became more prominent, histologic studies of the biopsy specimens tended to show more remarkable amyloid deposits in the mucosa and submucosa of the jejunum. Therefore, these three radiologic findings may directly reflect amyloid deposition in the mucosa and submucosa.

Diffuse mucosal granularity in the small intestine was reported by Glick and Teplick [25] in 39 patients with small-bowel Crohn disease. They described a granular pattern consisting of a diffuse reticular network of round or occasionally angular radiolucent filling defects 0.5–1.0 mm in diameter. Recently, Jones et al. [26] reported that small-bowel granularity was also demonstrated in four patients with conditions other than Crohn disease, namely, radiation ileitis, pancreatic glucagonoma, protein-losing enteropathy, and small-bowel ischemia. Most recently, Matsumoto et al. [27] have reported a granular mucosal pattern in patients with immunoproliferative small intestinal disease. We found the fine granules demonstrated in patients with small-bowel amyloidosis to be slightly larger and more variable in size than those reported by these authors.

Finally, our histologic study showed villous abnormalities such as widening or blunting together with amyloid deposition in the lamina propria mucosae and massive amyloid deposition in the submucosa. These findings seem to affect the radiologic abnormalities, but biopsy specimens were not large enough to lead to a proper understanding of the overall structure.

ACKNOWLEDGMENT

We thank Peter Flaherty for critical readings of the manuscript.

REFERENCES

1. Cohen AS. Amyloidosis (concluded). *N Engl J Med* **1967**;277:628–638
2. Kyle RA, Bayrd ED. Amyloidosis: review of 236 cases. *Medicine* (Baltimore) **1975**;54:271–299
3. Seliger G, Krassner RL, Beranbaum ER, Miller F. The spectrum of roentgen appearance in amyloidosis of the small and large bowel: radiologic-pathologic correlation. *Radiology* **1971**;100:63–70
4. Gilat T, Revach M, Sohar E. Deposition of amyloid in the gastrointestinal tract. *Gut* **1969**;10:98–104
5. Pettersson T, Wegelius O. Biopsy diagnosis of amyloidosis in rheumatoid arthritis: malabsorption caused by intestinal amyloid deposits. *Gastroenterology* **1972**;62:22–27
6. Golden R. Amyloidosis of the small intestine. *AJR* **1954**;72:401–408
7. Pear BL. Radiographic studies of amyloidosis. *Crit Rev Diagn Imaging* **1972**;3:425–452
8. Legge DA, Carlson HC, Wollaeger EE. Roentgenologic appearance of systemic amyloidosis involving gastrointestinal tract. *AJR* **1970**;110:406–412
9. Marshak RH, Lindner AE. *Radiology of the small intestine*, 2nd ed. Philadelphia: Saunders, **1976**:62–68
10. Iida M, Yamamoto T, Yao T, Fuchigami T, Fujishima M. Jejunal endoscopy using a long duodenofiberscope. *Gastrointest Endosc* **1986**;32:233–236
11. Wright JR, Calkins E, Humphrey RL. Potassium permanganate reaction in amyloidosis: a histologic method to assist in differentiating forms of this disease. *Lab Invest* **1977**;36:274–281
12. Nakamura U, Tani K, Nakamura T, Yao T, Fuyuno S, Koga S. X-ray examination of the small intestine by means of duodenal intubation. *Stomach Intestine* **1974**;9:1461–1469
13. Kobayashi S, Nishizawa M, Mizuno K, et al. Roentgenographic examinations of the small intestine. *Rinsho Hoshasen* **1974**;19:619–625
14. Glenner GG. Amyloid deposits and amyloidosis. The β-fibrilloses. *N Engl J Med* **1980**;302:1283–1292, 1333–1343
15. Tada S, Iida M, Iwashita A, et al. Endoscopic and biopsy findings of the upper digestive tract in patients with amyloidosis. *Gastrointest Endosc* **1990**;36:10–14
16. Yoshida T, Kanbe H, Haraguchi Y, Sakamoto A, Iwashita T, Tanaka K. Significance of abnormal gastrointestinal gas in systemic amyloidosis. *Am J Gastroenterol* **1982**;77:917–921
17. Wald A, Kickler J, Mendelow H. Amyloidosis and chronic intestinal pseudoobstruction. *Dig Dis Sci* **1981**;26:462–465
18. Jarnum S. Gastrointestinal haemorrhage and protein loss in primary amyloidosis. *Gut* **1965**;6:14–18
19. Long L, Mahony TD, Jewell WR. Selective amyloidosis of the jejunum: case report of a rare cause for gastrointestinal bleeding. *Am J Surg* **1965**;109:217–220
20. Levy DJ, Franklin GO, Rosenthal WS. Gastrointestinal bleeding and amyloidosis. *Am J Gastroenterol* **1982**;77:422–426
21. Mallory A, Struthers JE Jr, Kern F Jr. Persistent hypotension and intestinal infarction in a patient with primary amyloidosis. *Gastroenterology* **1975**;68:1587–1592
22. Choi HH, Heller D, Picken MM, Sidhu GS, Kahn T. Infarction of intestine with massive amyloid deposition in two patients on long-term hemodialysis. *Gastroenterology* **1989**;96:230–234
23. Gilat T, Spiro H. Amyloidosis and the gut. *Dig Dis Sci* **1968**;13:619–633
24. Griffel B, Man B, Kraus L. Selective massive amyloidosis of small intestine. *Arch Surg* **1978**;110:215–217
25. Glick SN, Teplick SK. Crohn disease of the small intestine: diffuse mucosal granularity. *Radiology* **1985**;154:313–317
26. Jones B, Hamilton SR, Rubesin SE, Bayless TM, Ravich WJ, Hendrix TR. Granular small bowel mucosa: a reflection of villous abnormality. *Gastrointest Radiol* **1987**;12:219–225
27. Matsumoto T, Iida M, Matsui T, Tanaka H, Fujishima M. The value of double-contrast study of the small intestine in immunoproliferative small intestinal disease. *Gastrointest Radiol* **1990**;15:159–163

Case Report

# Visceral Calcification in Patients with AIDS May Not Always Be Due to *Pneumocystis carinii*

Mark J. Towers,[1] Cynthia E. Withers,[1] Paul A. Hamilton,[1] Arnost Kolin,[2] and Sharon Walmsley [3]

Recent reports of widespread visceral calcifications in patients with AIDS have implicated disseminated *Pneumocystis carinii* as the sole causal agent [1–3]. It has been suggested that in a patient with *Pneumocystis* infection, nodal or visceral calcification should be considered as part of the infection and treatment should proceed without an extensive workup for superimposed disease [2].

Calcification occurring in areas of necrosis is a common result of many infectious and inflammatory processes in the body. We suggest that other opportunistic infections may result in visceral calcification and describe two cases illustrating this possibility.

## Case Report

A 28-year-old bisexual man was admitted for investigation of anemia, night sweats, weight loss, and fever. Human immunodeficiency virus (HIV) seropositivity was diagnosed in 1986 after a blood donation. Two episodes of pulmonary *Pneumocystis carinii* infection had been successfully treated with IV pentamidine in January 1988 and September 1989. Aerosol prophylaxis with pentamidine had been instituted after the first episode and continued up to the present admission. A sonographic examination revealed multiple echogenic foci in both kidneys (Fig. 1A) and the spleen. These measured 1–2 mm in diameter. Percutaneous renal (Fig. 1B) and liver biopsies were positive for cytomegalovirus infection. Special stains for *Pneumocystis carinii* and *Mycobacterium avium-intracellulare* (MAI) were negative.

The patient developed multiple pulmonary infiltrates and died of respiratory failure 2 weeks after admission. Autopsy confirmed systemic cytomegalovirus infection, including the kidneys and spleen. Radiographs of organ specimens and histology (Fig. 1C) showed calcifications in these organs. No evidence of *Pneumocystis* or MAI was identified at autopsy.

## Discussion

Dense hepatic and splenic calcifications are often recognized on sonography or CT and usually are ascribed to histoplasmosis or other granulomatous infection. Recent descriptions [1–3] of multiple discrete visceral calcifications in patients with AIDS have implicated *Pneumocystis carinii* as the causal agent, although Feuerstein et al. [2] suggest that this is not likely to be a pathognomonic finding. The same authors, however, propose that visceral calcification in patients known to have *Pneumocystis* be considered as part of the infection and that treatment proceed without investigation for other diseases.

Our patient had an episode of *Pneumocystis carinii* pneumonia 4 months before presentation. This was treated with IV pentamidine, and aerosol maintenance with pentamidine was continued. Biopsy of liver and kidneys showed only changes due to cytomegalovirus, and this was confirmed at autopsy. Radiographs of renal tissue specimens and dissection of the calcifications showed that they were amorphous clumps not associated with granulomas. Widespread cyto-

Received September 25, 1990; accepted after revision November 8,1990.

[1]Department of Radiology, Sunnybrook Health Science Centre, University of Toronto, 2075 Bayview Ave., Toronto, Ontario, Canada M4N 3M5. Address reprint requests to C. E. Withers.

[2]Department of Pathology, Sunnybrook Health Science Centre, University of Toronto, 2075 Bayview Ave., Toronto, Ontario, Canada M4N 3M5.

[3]Department of Medicine, Sunnybrook Health Science Centre, University of Toronto, 2075 Bayview Ave., Toronto, Ontario, Canada M4N 3M5.

*AJR* 156:745–747, April 1991 0361–803X/91/1564–0745 © American Roentgen Ray Society

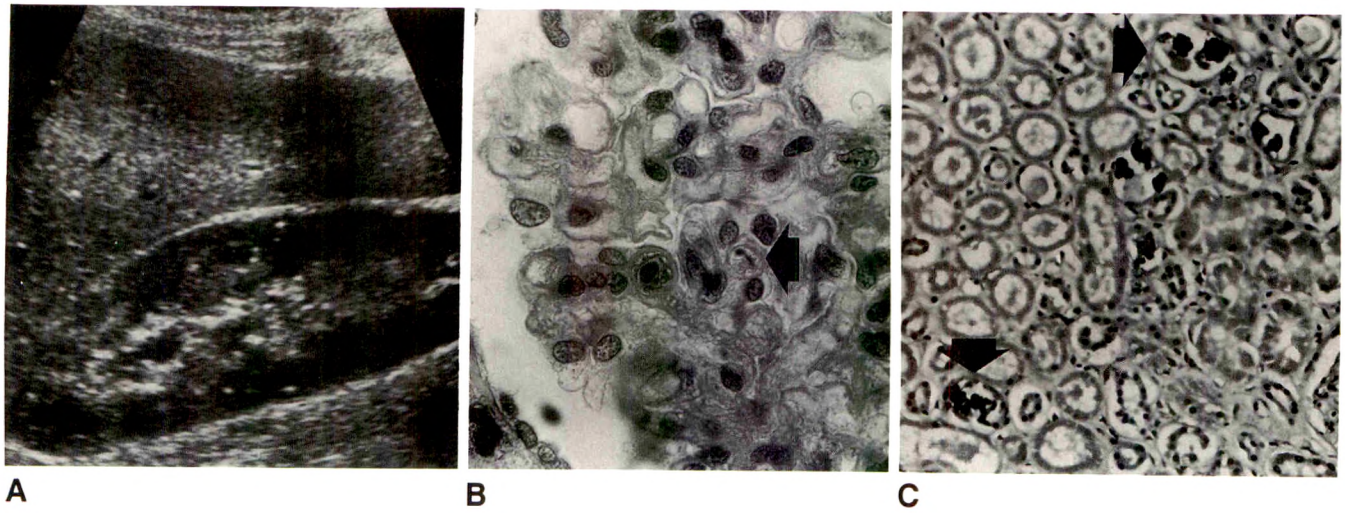



Fig. 1.—Renal cytomegalovirus.
*A*, Sagittal sonogram of right kidney shows scattered echogenic foci throughout cortex.
*B*, Photomicrograph of renal biopsy specimen shows cytomegalic inclusion body (*arrow*) in endothelial cell of glomerulus. (H and E, ×800)
*C*, Photomicrograph of biopsy specimen shows microscopic calcifications (*arrows*) in renal tubules. (H and E, ×200)

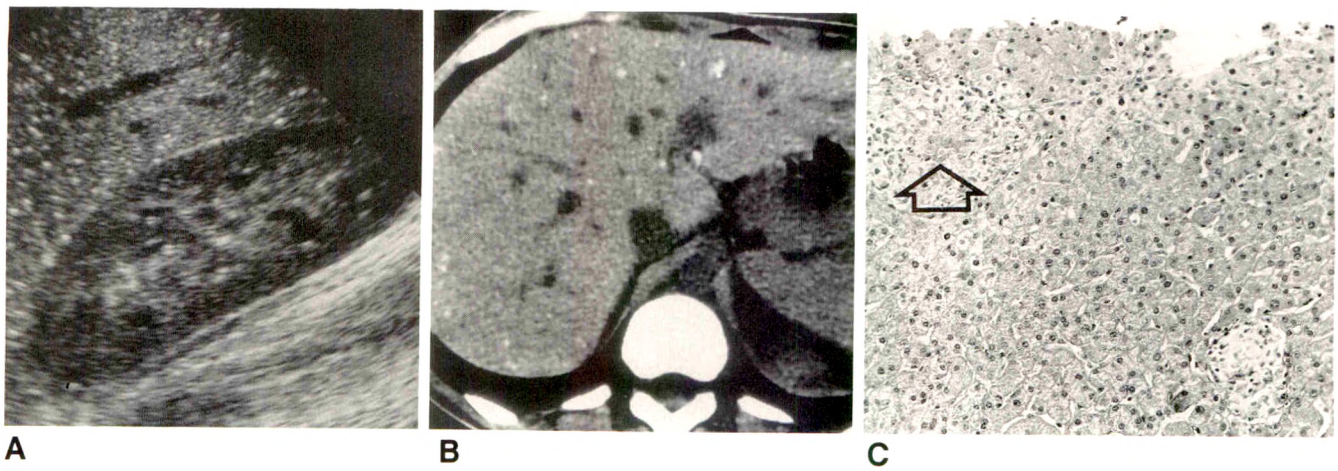



Fig. 2.—Hepatic *Mycobacterium avium-intracellulare* (MAI).
*A*, Sagittal sonogram of right lobe of liver shows widespread punctate echogenic foci.
*B*, Unenhanced CT scan of liver confirms calcific nature of foci.
*C*, Photomicrograph of liver biopsy specimen shows two granulomas, one with central necrosis (*arrow*) due to MAI. (Masson's trichrome, ×200)

megalovirus was found in the liver, spleen, both kidneys, lungs, and small intestine. We think that cytomegalovirus may have caused the calcifications. Cytomegalovirus hepatitis associated with focal fatty infiltration has been described [4], but calcification has not. Necrotizing viral infections causing hemorrhage, however, may predispose the patient to calcium deposition. Granuloma formation is known to be deficient in AIDS owing to defects in cell-mediated immunity. An alternative hypothesis is that the calcifications were due to the earlier *Pneumocystis* infection and that the organism was completely eradicated by therapy. The natural history of visceral calcifications after *Pneumocystis* infection is unknown. When they are present, active infection is often assumed. We believe that biopsy confirmation is necessary.

We have seen a second AIDS patient with similar calcifications in the liver and no evidence of *Pneumocystis carinii*. A 30-year-old woman had a single episode of *Pneumocystis carinii* pneumonia successfully treated in April 1988. Maintenance aerosol pentamidine was continued, and no further clinical infections occurred. Sonographic examination of the abdomen 18 months later showed no abnormality. The patient presented recently with widespread small echogenic foci in the liver consistent with calcification (Fig. 2A) and confirmed with unenhanced CT (Fig. 2B). Liver biopsy showed multiple small granulomas, some with necrosis, associated with MAI (Fig. 2C). No evidence of other opportunistic organisms could be shown with a range of specific histologic techniques. The patient had been unwell for 3 months before a diagnosis of

hilar, hepatic, and splenic MAI infection was proved by biopsy of these sites. Calcification may develop in necrotic tissue, and the duration of the patient's illness was long enough for calcium to be deposited. We consider MAI to have caused the calcifications because no *Pneumocystis* was evident on biopsy, and no abnormality had been identified on the sonographic examination after her previous *Pneumocystis carinii* pneumonia. These calcifications may represent inactive *Pneumocystis carinii* infection, rendered sterile by a 4-day course of oral trimethoprim-sulfamethoxazole the patient received immediately before admission. We consider this unlikely. Calcification in the renal cortex and medulla has been described in AIDS-associated MAI infection [5], but to our knowledge, hepatic calcification due to MAI has not been reported.

Extrapulmonary *Pneumocystis carinii* is being recognized more frequently. It has been suggested that aerosol prophylaxis allows dissemination of the infection [6]. As visceral infection may be clinically silent, sonographic examination of these patients is recommended. IV pentamidine causes significant morbidity in almost 50% of patients, including renal dysfunction, neutropenia and anemia, nausea, vomiting, hypotension, and hypoglycemia. The alternative, trimethoprim-sulfamethoxazole, has a similar frequency of side effects in patients with AIDS. These include rash, fever, neutropenia, thrombocytopenia, and hepatitis.

We suggest that opportunistic organisms other than *Pneumocystis carinii*, specifically cytomegalovirus and *M. avium-intracellulare*, may cause discrete visceral calcifications in patients with AIDS. Although the sonographic and CT appearances of discrete foci of calcification were similar to those previously described associated with extrapulmonary *Pneumocystis carinii* [1–3], no evidence of active *Pneumocystis* infection was seen in our cases. As treatment carries risks in these patients, we recommend that proof of the infectious agent(s) be obtained by biopsy.

## REFERENCES

1. Radin DR, Baker EL, Klatt EC, et al. Visceral and nodal calcification in patients with AIDS-related *Pneumocystis carinii* infection. *AJR* **1990**;154:27–31
2. Feuerstein IM, Francis P, Raffeld M, Pluda J. Widespread visceral calcifications in disseminated *Pneumocystis carinii* infection: CT characteristics. *J Comput Assist Tomogr* **1990**;141:149–151
3. Spouge AR, Wilson S, Gopinath N, Sherman M, Blendis LM. Extrapulmonary *Pneumocystis carinii* in a patient with AIDS: sonographic findings. *AJR* **1990**;155:76–78
4. Vieco PT, Rochon L, Lisbona A. Multifocal cytomegalovirus-associated hepatic lesions simulating metastases in AIDS. *Radiology* **1990**;176:123–124
5. Falkoff GE, Rigsby CM, Rosenfield AT. Partial, combined cortical and medullary nephrocalcinosis: US and CT patterns in AIDS-associated MAI infection. *Radiology* **1987**;162:343–344
6. Telzak EE, Cote RJ, Gold JWM, Campbell SW, Armstrong D. Extrapulmonary *Pneumocystis carinii* infections. *Rev Infect Dis* **1990**;12:380–386

# Book Review

**The Radiologic Clinics of North America.** Imaging the Lymphomas. Guest editor: Herman I. Libshitz. Philadelphia: Saunders, July 1990;28(4):669–903. $25; by subscription, 6 issues annually for $93

Thirty-three contributing authors have reviewed the clinical, pathologic, and radiologic manifestations of lymphoma in the various organ systems. The emphasis is on the use of various imaging studies for diagnosing and staging lymphomas, thus helping clinicians in therapeutic decision making. A pathologist introduces the subject by explaining the classifications of Hodgkin and non-Hodgkin lymphoma, with an introduction to the newer diagnostic techniques such as flow cytometry and immunophenotyping. The second chapter was written by a radiation and a medical oncologist who describe the impact of the development of the various imaging techniques on the ability of the clinician to diagnosis, stage, and manage cases of lymphoma. The following chapters cover lymphoma of the CNS, head and neck, chest, abdomen, breast, bone, and the genitourinary tract. The final two chapters discuss fine-needle aspiration biopsy and lymphoma in the immunocompromised patient.

The chapter on CNS lymphoma covers both primary and secondary involvement with Hodgkin and non-Hodgkin lymphoma. The author uses the old terminology, such as reticulum cell sarcoma and lymphosarcoma, which is somewhat surprising in view of the emphasis on classification in the introductory chapters. Both CT scans and MR images are used to illustrate the protean manifestations of lymphomatous involvement of the brain and spinal cord. The implications for the use of noninvasive studies for the diagnosis of intracranial involvement and cord compression in an acute setting are stressed.

The chapter on lymphoma of the head and neck discusses the differential diagnosis of cervical lymph node involvement as well as orbital, paranasal sinus, tonsillar, salivary, and thyroid gland diseases and their differential diagnosis. It is illustrated primarily with examples of advanced disease on CT scans, although a couple of MR images are included.

The chapter on thoracic lymphoma covers mediastinal, pulmonary, and chest wall involvement and emphasizes the well-known fact that although chest radiographs show the presence of moderate to extensive involvement, CT is much more sensitive in showing subtle disease and is essential for accurate staging. MR imaging has not been found useful in contributing additional information except in selected cases. A short chapter discusses follow-up chest examinations during and after treatment, with emphasis on potential complications.

Lymphomatous involvement of the abdomen is subdivided into chapters covering the hollow abdominal viscera (including the esophagus), the solid abdominal viscera, and, finally, a chapter on imaging of the abdominal and pelvic lymph nodes. For obvious reasons, the first chapter emphasizes barium studies, with some CT correlation. The last two cover the use of CT, sonography, radionuclide imaging, and lymphangiography. The accuracy of these techniques and their relative roles in the evaluation of the various abdominal and retroperitoneal structures are described.

The chapter on lymphomatous involvement of the skeleton is illustrated primarily with plain radiographs, but the role of nuclear medicine, CT, and MR is addressed. Lymphomatous involvement of the genitourinary tract is illustrated by examples of primary extranodal disease involving the kidney, adrenal glands, testes, bladder, prostate, and female genital organs. The effect of nodal disease on this system is referred to.

A short chapter on fine-needle aspiration biopsy in lymphoma discusses the contributions and limitations of this technique to the diagnosis and management of lymphoma and reviews the technique as it applies to various anatomic locations.

The final chapter addresses the timely subject of lymphoma in the immunocompromised patient. Most of the chapter reviews non-Hodgkin lymphoma in the AIDS population, with a paragraph on Hodgkin disease and a brief discussion of transplant-related lymphoma. The characteristics that distinguish lymphoma in this population from lymphoma in the general population are emphasized and illustrated with various radiologic images.

In conclusion, this text provides an excellent overview of the multiorgan involvement by lymphoma. As in any text written by several contributors, redundancy is unavoidable. Obviously, in a volume of this size, none of the systems can be covered in depth, but the extensive and current bibliographies provided at the end of each chapter provide an opportunity for reference and further study. The illustrations throughout are of high quality, and the legends are clear, with liberal use of arrows to point out the salient features. This latest volume of this quarterly publication meets its objective to provide an update on current imaging for the general radiologist. It also can be recommended to medical and radiation oncologists who want a comprehensive review of the role of imaging in the diagnosis and management of lymphoma.

Herbert F. Gramm
*New England Deaconess Hospital*
*Harvard Medical School*
*Boston, MA 02215*

Case Report

# Pancreatic Microcystic Adenoma Presenting with Acute Hemoperitoneum: CT Diagnosis

Geoffrey D. Rubin,[1] R. Brooke Jeffrey, Jr.,[1] and Joseph F. Walter[2]

Microcystic adenomas of the pancreas are uncommon causes of abdominal masses. Clinical symptoms are often vague, nonspecific complaints related to mass effect or pain. To our knowledge, acute intraperitoneal hemorrhage has not been imaged in association with these neoplasms. In this report, we analyze the CT and angiographic findings in a patient with hypotension and pain resulting from massive hemoperitoneum after a microcystic adenoma ruptured into the lesser peritoneal sac.

## Case Report

A previously healthy, 78-year-old woman experienced the sudden onset of severe diffuse abdominal pain followed immediately by several episodes of loss of consciousness of 2–3 min duration.

On clinical presentation, the patient had a supine systolic blood pressure of 90 mm Hg and pulse rate of 90/min. Diffuse abdominal guarding with rebound tenderness was present in all four quadrants. A bruit could be auscultated within a palpable mass in the left upper quadrant. The initial hematocrit was 39%, but it rapidly dropped to 30% after saline hydration.

Dynamic abdominal CT with IV contrast administration revealed a 10 × 7 × 7 cm multiseptated cystic mass with intensely enhancing septa and capsule in the left upper quadrant, contiguous with the tail of the pancreas. Large vascular structures could be identified at the periphery of the mass with a saccular dilatation of one of these peripheral vessels present posteriorly. Extensive hemoperitoneum was present in the lesser sac (H = 46) and throughout the peritoneal cavity (Figs. 1A and 1B).

Selective splenic angiography revealed a large hypervascular mass in the left upper quadrant with tumor staining and contrast pooling. The mass was supplied by enlarged pancreatica magna and short pancreatic branches. A 2-cm venous aneurysm was present in the midportion of the mass, associated with very large venous channels draining into the splenic vein (Fig. 1C). On the basis of these imaging studies, a diagnosis of nonfunctioning islet cell tumor was entertained primarily, with pancreatic microcystic adenoma considered less likely because of the presence of hemoperitoneum.

The patient underwent emergent laparotomy, and approximately 1 l of hemoperitoneum was noted. A mobile mass was identified emanating from the tail of the pancreas, and a very large vein on the surface of the mass was noted to be actively bleeding. A distal pancreatectomy was performed. On histologic examination, the mass was a typical microcystic adenoma with innumerable small cystic spaces lined by a single layer of flat cuboid cells. No evidence of malignancy was found.

## Discussion

Microcystic adenomas represent 10% of cystic pancreatic lesions and typically occur in women in their fourth to ninth decades [1, 2]. The most frequent symptoms are mostly related to local mass effect and include abdominal pain, weight loss, eructation, nausea, and vomiting. Pain after meals has been attributed to mesenteric ischemia due to vascular compression [2]. Obstructive jaundice, associated with lesions in the pancreatic head, has been reported in up

Received September 17, 1990; accepted after revision October 19, 1990.

[1] Department of Diagnostic Radiology and Nuclear Medicine, Stanford University School of Medicine, Stanford, CA 94305. Address reprint requests to G. D. Rubin (H-1350).

[2] Palo Alto Medical Clinic, 300 Homer, Palo Alto, CA 94301.

*AJR* 156:749–750, April 1991 0361–803X/91/1564/0749 © American Roentgen Ray Society

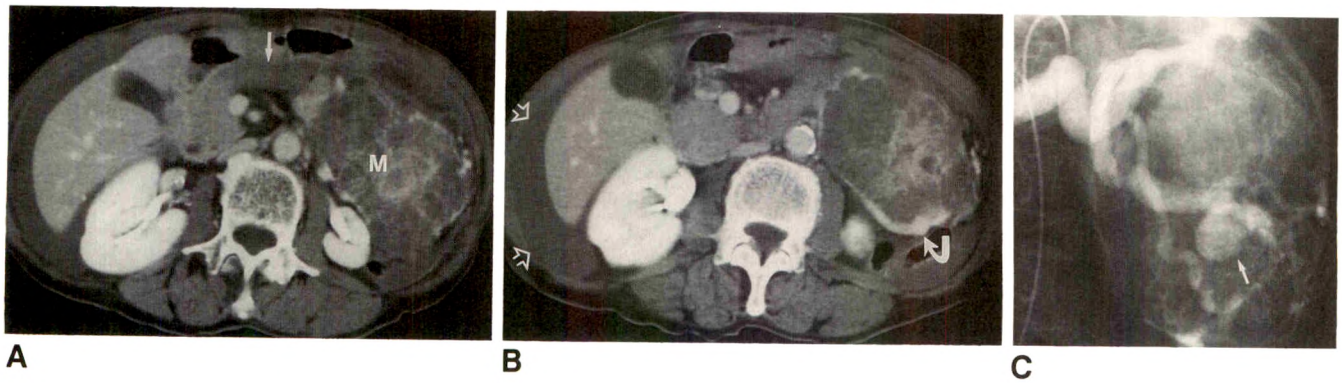



**Fig. 1.—*A*, CT scan shows multiseptated enhancing mass (M) adjacent to pancreas (*arrow*).**
***B*, Hemoperitoneum (*open arrows*) is noted on CT scan, as well as posterior venous aneurysm (*curved arrow*) with associated draining vein.**
***C*, Venous phase of a selective splenic arteriogram. *Arrow* indicates venous aneurysm.**

to 12% of cases [2]. Gastrointestinal hemorrhage, due to the development of gastric or duodenal ulcers adjacent to the mass [1, 3] or gastroesophageal varices caused by portal or splenic vein occlusion [2, 4], has been described rarely as a presenting symptom. A single case of intraperitoneal hemorrhage caused by microcystic adenoma has been reported in the pathologic literature, but the imaging features specifically have not been reported [1].

On CT, microcystic adenomas may appear as a multilocular cystic mass with contrast-enhancing septa [5, 6]. In some patients with exceedingly small cysts, the lesions may simulate a solid mass on CT [5, 6]. Calcification has been described in 30–38% of cases [5, 6], and a central scar has variably been reported [1, 6]. In spite of the architectural detail afforded by CT, differentiation of microcystic adenomas from other neoplasms of the pancreas can be difficult. The differential diagnosis includes macrocystic adenoma, nonfunctioning islet cell tumors, papillary or solid epithelial neoplasms, pancreatic lymphangiomas, pseudocysts, and some ductal adenocarcinomas [5, 6]. A method of distinguishing benign microcystic adenoma and premalignant mucinous cystadenoma, based on CT analysis of the number and size of the cysts, has been proposed [6]. Johnson et al. [6] noted that of patients with more than six cysts that were less than or equal to 2 cm in diameter, 93% had microcystic adenoma. In 95% of patients with fewer than 6 cysts with a majority larger than 2-cm diameter, the diagnosis was mucinous cystadenoma [6].

The classic angiographic description of pancreatic microcystic adenoma includes (1) displacement of major vessels, (2) the presence of large feeding arteries, and (3) a tumor blush occasionally associated with pooling of contrast material [4, 7]. Although the majority of lesions appear to conform to this description, many reports of hypovascular microcystic adenomas have been documented [4, 7]. Although arterial dilatation, neovascularity, and venous obstruction or encasement have been reported, venous aneurysm, as was present in this case, has never been described in association with microcystic adenoma or other pancreatic neoplasms.

Venous aneurysms are uncommon entities, especially when compared with arterial aneurysms. Of the 495 venous aneurysms reported in the world literature before 1983, the majority were either in the leg or neck, with only 17 reported in the portal venous system [8]. Of these, 13 involved the portal vein, two the splenic vein, one the cystic vein, and one the superior mesenteric vein. Although portal hypertension has been suggested as a cause for venous aneurysm formation, it has been proposed that the altered hemodynamics created by regions of ectasia from traumatic, pancreatitic, or congenital causes result in the development of associated venous hypertension. In this case, the creation of the aneurysm probably related to the markedly venous flow created by the tumor. It is of interest that the unique development of the venous aneurysm appears to have been directly responsible for the patient's presentation. Dissection of blood into the lesser sac resulted in generalized hemoperitoneum.

## REFERENCES

1. Compagno J, Oertel JE. Microcystic adenomas of the pancreas (glycogen-rich cystadenomas). *Am J Clin Pathol* **1978**;69:289–298
2. Hodgkinson DJ, ReMine WH, Weiland LH. Pancreatic cystadenoma. *Arch Surg* **1978**;113:512–519
3. Rosenbaum H, Connolly PJ, Climie ARW, Reveno WS. Pancreatic cystadenoma with intestinal hemorrhage. *AJR* **1963**;90:735–739
4. Pressman BD, Asch T, Casarella WJ. Cystadenoma of the pancreas: a reappraisal of angiographic findings. *AJR* **1973**;119:115–120
5. Itai Y, Ohhashi K, Furui S, et al. Microcystic adenoma of the pancreas: spectrum of computed tomographic findings. *J Comput Assist Tomogr* **1988**;12:797–803
6. Johnson CD, Stephens DH, Charboneau JH, et al. Cystic pancreatic tumors: CT and sonographic assessment. *AJR* **1988**;151:1133–1138
7. Feeny PC, Weinstein CJ, Taft DA, Allen FH. Cystic neoplasms of the pancreas: new angiographic and ultrasonographic findings. *AJR* **1978**; 131:795–802
8. Cholankeril JV. Superior mesenteric venous aneurysm. *Am J Gastroenterol* **1985**;80:624–626

Case Report

# Hydatid Cyst of the Liver: Identification of Detached Cyst Lining on CT Scans Obtained After Cyst Puncture

Bülent Acunaş,[1] İzzet Rozanes,[1] Gülden Acunaş,[1] Levent Çelik,[2] Aydin Alper,[3] and Erdem Gökmen[1]

We describe a patient with proved hydatid cyst of the liver in whom a membrane in the lumen of the cyst became visible on CT scans obtained after cyst puncture. This apparently represents the lining of the cyst and may be a unique CT finding for hydatid cysts. The patient was treated with percutaneous injection of hypertonic saline into the cavity.

## Case Report

A 40-year-old woman with a 3-month history of vague pain in the right upper quadrant was seen. Her medical history was unremarkable and routine laboratory values were normal. CT examination revealed a round, purely cystic mass in the liver that measured 55 mm in diameter and had well-defined borders (Fig. 1A). Results of the complement fixation test for hydatid disease were negative.

Considering hydatid disease or a simple serous cyst in the differential diagnosis, percutaneus aspiration was performed for diagnosis and therapy. A 20-gauge needle was inserted into the cyst cavity under CT guidance. The cyst cavity was approached via the transhepatic route rather than transperitoneally in order to prevent spillage of hydatid material. The cyst had a high intraluminal pressure; clear fluid spurted out as soon as the stylet of the needle was withdrawn.

A CT scan obtained immediately after aspiration while the needle was still in place revealed a membrane detached and floating in the remaining cystic fluid (Fig. 1B). It was postulated that this membrane represented the detached endocyst of a hydatid cyst. Microscopic examination revealed fragments of membranes and scoleces and clarified the diagnosis. Hypertonic saline (20% sodium chloride solution) was injected into the cavity as a scolecidal agent. The amount injected was a little less than the amount aspirated. After 5 min, the fluid was reaspirated and the needle was withdrawn. The hypertonic saline acted as a contrast agent owing to its high density (about 180 H), enabling assessment of the cavity (Fig. 1C). No biliary tract communications were detected. No complications occurred during or after the procedure.

A CT scan 1 month later showed enlargement of the cyst, probably because of the osmotic effect of the remaining hypertonic saline, and fragments of detached membranes were still detectable. A hypodense halo was seen around the lesion, probably owing to edema. In the follow-up period of 6 months, the patient was asymptomatic and a significant reduction in the size of the cyst, with a persistent small cavity, was observed.

## Discussion

Hydatid disease is endemic to many parts of the world, including the Mediterranean and Baltic areas, South America, Australia, the Middle East, and Northern Canada. Increasing immigration is said to have led to a rise in the prevalence of this disease in North America, primarily in adults who have harbored the parasite since childhood [1]. The appearance of hydatid disease on sonographic or CT examinations is characteristic only when daughter cysts or a floating membrane is detected [2]. In the absence of these features, the diagnosis cannot be established with certainty. It was postulated that MR imaging, with its ability to differentiate subtle differences in tissue characteristics, might provide a definite diagnosis in

Received August 17, 1990; accepted after revision October 18, 1990.
[1] Department of Radiology, İstanbul Medical Faculty, Çapa 34390 İstanbul, Turkey. Address reprint requests to B. Acunaş.
[2] Department of Radiology, Haydarpaşa Numune Hospital, 81324 İstanbul, Turkey.
[3] Hepatobiliary Surgery Unit, Department of General Surgery, İstanbul Medical Faculty, Çapa 34390 İstanbul, Turkey.

*AJR* 156:751–752, April 1991 0361–803X/91/1564–0751 © American Roentgen Ray Society

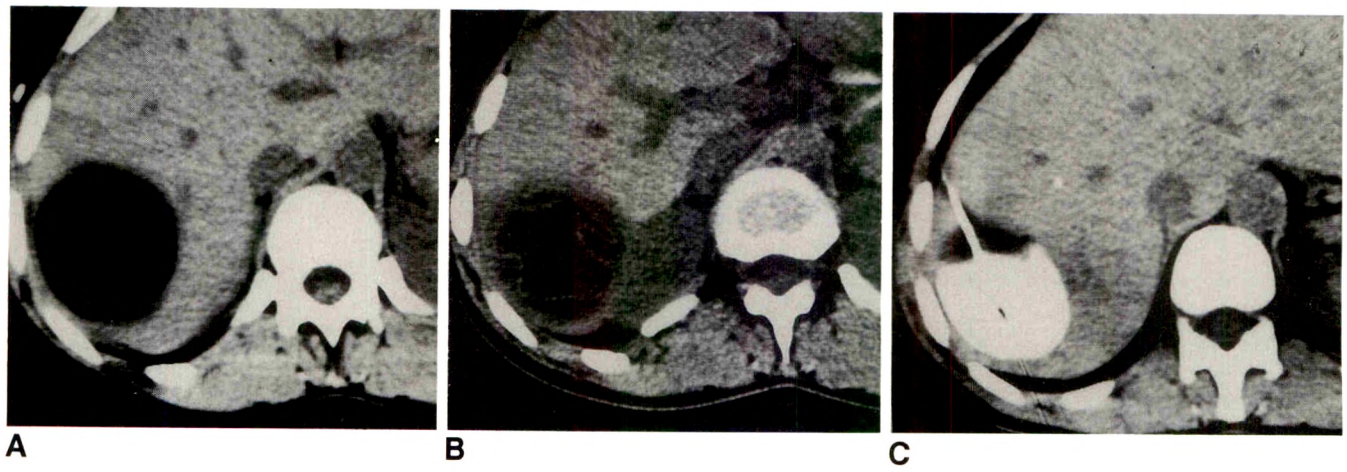



**Fig. 1.—*A*, CT scan shows purely cystic mass 55 mm in diameter in posterior segment of right lobe of liver. *B*, After aspiration, detached lining of cyst is visible on CT scan. *C*, CT scan shows hypertonic saline in cavity.**

unclear cases by unequivocally demonstrating daughter cysts and other debris [3]. Unfortunately no imaging technique, including MR imaging [4], has yet been able to differentiate purely cystic hydatid lesions, which comprise the majority of hydatid manifestations [5], from simple cysts. Until recently, the Casoni skin test was the only way of testing for exposure to hydatid disease, but it has high false-positive and false-negative rates and has been abandoned in many centers. Many new, more sensitive and specific serologic tests are now available.

Even after percutaneous aspiration of the cystic fluid, the results of microscopic analysis of the specimens might be negative [2]. Because of the limitations in imaging techniques and serologic tests, aspiration of a hydatid cyst cannot always be avoided. In some cases, the differentiation of a serous liver cyst from a purely cystic hydatid lesion is possible only with percutaneous aspiration of the cyst. Although percutaneous aspiration of hydatid cysts of the liver is still considered contraindicated by some physicians, several cases of aspiration have been reported with minor complications [2]. With the use of fine needles and the transhepatic route, the chance of spillage is extremely low and may be less than might occur with surgical manipulation.

Echinococcal cysts are composed of both host and parasite tissue. The pericyst is a layer derived from compressed host tissues and chronic inflammatory cells. The true cyst wall is derived from the parasite and is composed of two layers: the acellular outer layer (the ectocyst) and the one-cell-thick germinal membrane (the endocyst). These two layers are usually referred to as the endocyst. The intracystic fluid pressure rises as high as 80 cm $H_2O$, and this pressure keeps the endocyst tightly adhered to the pericyst. Layers of the cyst wall cannot be differentiated by imaging techniques.

In the present study, percutaneous cyst aspiration was performed in a patient with a purely cystic liver lesion. The fall of the intracystic pressure caused by the aspiration detached the membrane (endocyst) from the wall (pericyst). This phenomenon is called the membrane detachment sign and it is analogous to the water lily sign, which is a well-established radiologic sign of hydatid cyst rupture into an airway in the lung, in which the membrane is seen in profile floating at an air-fluid level and is reminiscent of a floating water lily. A sonographic water lily sign has also been described for the appearance of the detached and collapsed germinal membrane after leak of fluid from a hydatid cyst [6]. The membrane detachment sign is unique for hydatid disease, as no other cystic mass has been described with an inner lining that would detach when the pressure inside the cavity falls.

In addition to the case reported here, we have subsequently performed percutaneus aspiration in four more patients with presumed purely cystic hydatid disease of the liver without serious complications. One of these patients had a history of hydatid disease and two patients had positive complement fixation tests. The membrane detachment sign was positive after aspiration in each case. Microscopic examination verified the diagnosis in three patients. In the remaining patient the fluid was acellular but antigenic. Serologic examination of the aspirated fluid verified the diagnosis.

Scolecidal agents commonly used during surgery include 80% alcohol, a 0.5% silver nitrate solution, and hypertonic saline solutions. We used hypertonic saline as a scolecidal agent. One advantage of hypertonic saline is that, because of its high density, it acts as a contrast agent; this enables one to assess the cavity better and to detect biliary tract communications if any are present, without using iodinated contrast media.

We believe that percutaneous hydatid cyst aspiration without injection of a scolecidal agent will not be effective therapy and recurrences must be expected.

## REFERENCES

1. Langer JC, Rose DB, Keystone JS, Taylor BR, Langer B. Diagnosis and management of hydatid disease of the liver. *Ann Surg* **1984**;199:412–417
2. Bret PM, Fond A, Bretagnolle M, et al. Percutaneous aspiration and drainage of hydatid cysts in the liver. *Radiology* **1988**;168:617–620
3. Wojtasek DA, Teixidor HS. Echinococcal hepatic disease: magnetic resonance appearance. *Gastrointest Radiol* **1989**;14:158–160
4. Morris DL, Buckley J, Gregson R, Worthington BS. Magnetic resonance imaging in hydatid disease. *Clin Radiol* **1987**;38:141–144
5. Gharbi HA, Hassine W, Brauner MW, Dupuch K. Ultrasound examination of the hydatid liver. *Radiology* **1981**;139:459–463
6. Niron EA, Özer H. Ultrasound appearances of liver hydatid disease. *Br J Radiol* **1981**;54:335–338

# Carcinoma of the Cervix: Value of MR Imaging in Detecting Parametrial Involvement

Sandro Sironi[1]
Carlo Belloni[2]
Gian Luca Taccagni[3]
Alessandro DelMaschio[1]

**In patients with cervical carcinoma, precise knowledge of parametrial tumor extension affects the therapeutic decision between surgery and radiation therapy. The purpose of this prospective study was to determine the efficacy of MR imaging in detecting the presence or absence of parametrial invasion in patients with cervical cancer thought clinically to be confined to the cervix. Twenty-five consecutive patients were included in the study. All patients underwent radical hysterectomy or total abdominal hysterectomy and had detailed histologic evaluation of the parametrium. Ten had pathologic evidence of parametrial invasion; in the remaining 15, no parametrial invasion was identified pathologically. MR findings were compared with pathologic findings in all cases. For determining parametrial involvement, MR imaging had an accuracy of 88%, a sensitivity of 100%, and a specificity of 80%.**

**Our results suggest that MR imaging is a reliable means of assessing parametrial invasion by cervical cancer.**

*AJR* 156:753–756, April 1991

Uterine cervical carcinoma is one of the most common gynecologic malignant neoplasms. Surgery is usually reserved for patients with tumor confined to the cervix, whereas patients with parametrial involvement or more advanced disease are referred for radiation therapy [1]. Thus, an important question in staging carcinoma of the cervix is whether the tumor extends into the parametrium. The degree of parametrial tumor extension has been assessed mainly by clinical examination. Clinical staging, however, is often inaccurate [2].

Previous studies suggest that sonography and CT are limited in providing accurate assessment of tumor extent [3–6]. Recently, several studies have emphasized the value of MR imaging in the evaluation of regional extension of the disease [7–13].

The purpose of the present study was to determine the efficacy of MR imaging in detecting parametrial invasion in patients considered on the basis of clinical examination to have cervical carcinoma confined to the cervix.

## Subjects and Methods

Twenty-five consecutive patients 33–69 years old with primary untreated carcinoma of the cervix were included in a prospective study. All patients were referred for MR imaging after histologic diagnosis of the disease by means of colposcopic biopsy. All 25 patients included in the study were clinically considered to have invasive tumor (<3 cm in diameter) confined to the cervix. Patients with preinvasive (in situ) cervical tumor or with microinvasive carcinoma were excluded. Patients with advanced stages of disease on the basis of clinical examination also were excluded because radiation therapy is the treatment of choice in these patients and they do not undergo surgery. No patients were excluded because of either incompleteness of the MR examination or refusal of surgery.

Clinical staging was based on the staging classification of the International Federation of Gynecology and Obstetrics. Before MR imaging, all patients underwent barium enema,

Received August 7, 1990; accepted after revision October 18, 1990.

[1] Department of Radiology, Scientific Institute S. Raffaele, University Hospital, Olgettina 60, 20132 Milan, Italy. Address reprint requests to S. Sironi.

[2] Department of Gynecology and Obstetrics, Scientific Institute S. Raffaele, University Hospital, 20132 Milan, Italy.

[3] Department of Pathology, Scientific Institute S. Raffaele, University Hospital, 20132 Milan, Italy.

0361–803X/91/1564–0753
© American Roentgen Ray Society

excretory urography, and chest radiography. In all cases, MR imaging was performed before any operative procedure.

Pathologic proof was obtained by means of radical hysterectomy (21 patients) and total abdominal hysterectomy (four patients) within 2 weeks of the MR examination. Two parameters were measured by the pathologist: tumor size and parametrial tumor extension, or the mean thickness of the intact cervical stroma when no parametrial invasion was identified at histologic analysis.

MR imaging was performed with a 0.5-T superconducting magnet (MRT 50-A, Toshiba Medical Systems, Tokyo, Japan). Data were collected with use of a 256 × 256 matrix and were displayed in a 512 × 512 matrix. The section thickness was 7.5 mm with an intersection gap of 1 mm. The spin-echo (SE) technique was used and T1-weighted, 500/20 (TR/TE), and T2-weighted, 2000/40,90, images were obtained. Imaging times were 8.3 min for T1-weighted images and 17.4 min for T2-weighted images; four excitations were obtained in all cases. MR images were acquired in both sagittal and axial planes in all patients.

MR images were interpreted prospectively by two radiologists. No clinical information, other than the diagnosis of primary cervical carcinoma, was available at the time of analysis. In 22 of 25 cases the two radiologists agreed in determining the presence or absence of parametrial invasion; in three cases they disagreed. In these three cases, only the opinion of the more experienced radiologist was considered.

Cervical carcinomas were defined as areas of enlargement of the cervix that had higher signal intensity on T2-weighted images than the normal low-signal-intensity cervical stroma. The preservation of the low-intensity ring of the cervical stroma was considered a reliable indication that the parametrium was not involved by tumor. We defined as "preserved" the cervical stromal rings that did not appear completely interrupted by high-intensity tumor. The segmental disruption of the full thickness of the cervical stromal ring was considered an indication of tumor invasion. Both parametria were evaluated in each patient and the apparent depth of penetration of tumor into the parametrium was recorded.

## Results

In 25 patients in whom tumor was clinically confined to the cervix, MR imaging had an accuracy of 88%, a sensitivity of 100%, and a specificity of 80% in demonstrating parametrial status. The maximum diameter of the primary tumor as measured by the pathologist ranged from 1.7 to 3.9 cm.

On axial T2-weighted MR images, 12 of 25 cases had preserved cervical stromal rings (normal MR findings). In all these patients, no parametrial invasion by tumor was found on pathologic examination (no false-negative results) (Fig. 1). In these 12 true-negative cases, the mean thickness of the intact stromal rings established by histologic analysis was 1.2 cm.

On axial T2-weighted images in 13 of 25 cases, the full thickness of the stromal ring appeared disrupted by high-intensity tumor that extended into the parametrium (abnormal MR findings). In 10 of these 13 cases, parametrial involvement was confirmed on the basis of histologic analysis (true-positive cases) (Fig. 2). In these 10 true-positive cases, the apparent depth of parametrial spread measured on MR images ranged from 0.7 to 2.5 cm; in the same cases, the depth of parametrial invasion that was histologically demonstrated ranged from 0.4 to 2.1 cm. In all 10 true-positive cases, parametrial spread was slightly overestimated by MR imaging relative to the true pathologic results (mean error, 3.7 mm).

In the remaining three cases, pathologic study revealed carcinoma of the cervix without evidence of tumor extension into the parametrium (false-positive cases). In these three false-positive cases, pathologic analysis demonstrated the presence of an intact outer stripe of cervical stroma (mean thickness, 2.3 mm) still surrounding the tumor. In one false-positive case, invasion of the right portion of the vaginal fornix was also suspected on the basis of MR examination; at histologic analysis, tumor-free outer cervical margins were found and there was no infiltration of the parametrium or vaginal fornix (Fig. 3).

## Discussion

Decisions about treatment of uterine cervical cancer depend mainly on the stage of the disease at the time of

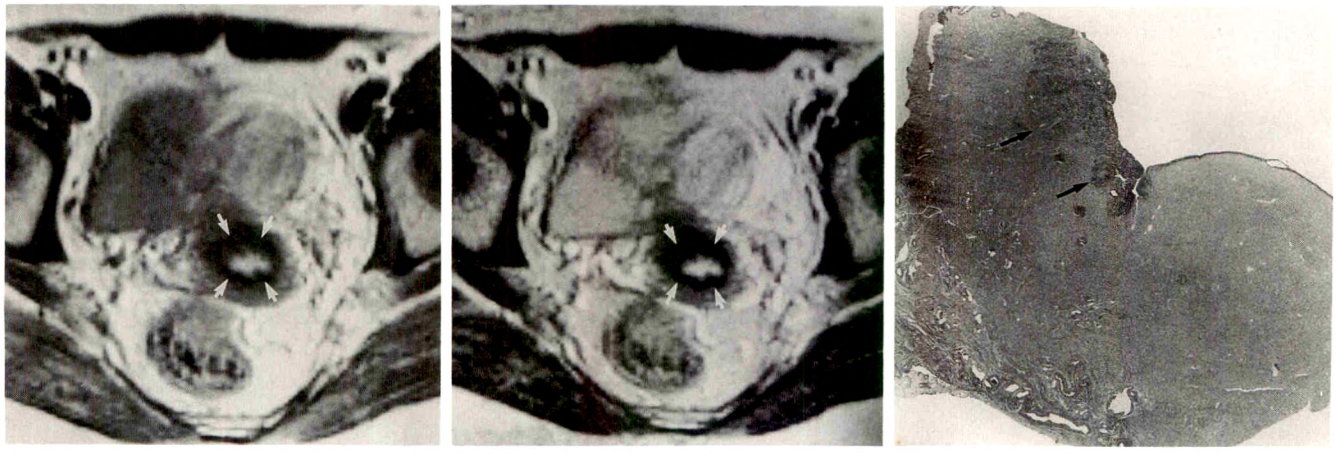



**Fig. 1.—Carcinoma of cervix in a 56-year-old woman.**

***A* and *B*, SE 2000/40 (*A*) and SE 2000/90 (*B*) axial MR images at same level show high-signal-intensity tumor completely surrounded by low-signal-intensity ring of cervical stroma (*arrows*). No parametrial invasion is present.**

***C*, Transmural section of cervix reveals tumor partially invading inner portion of cervical stroma (*arrows*). Major part of cervical wall is not involved by tumor.**

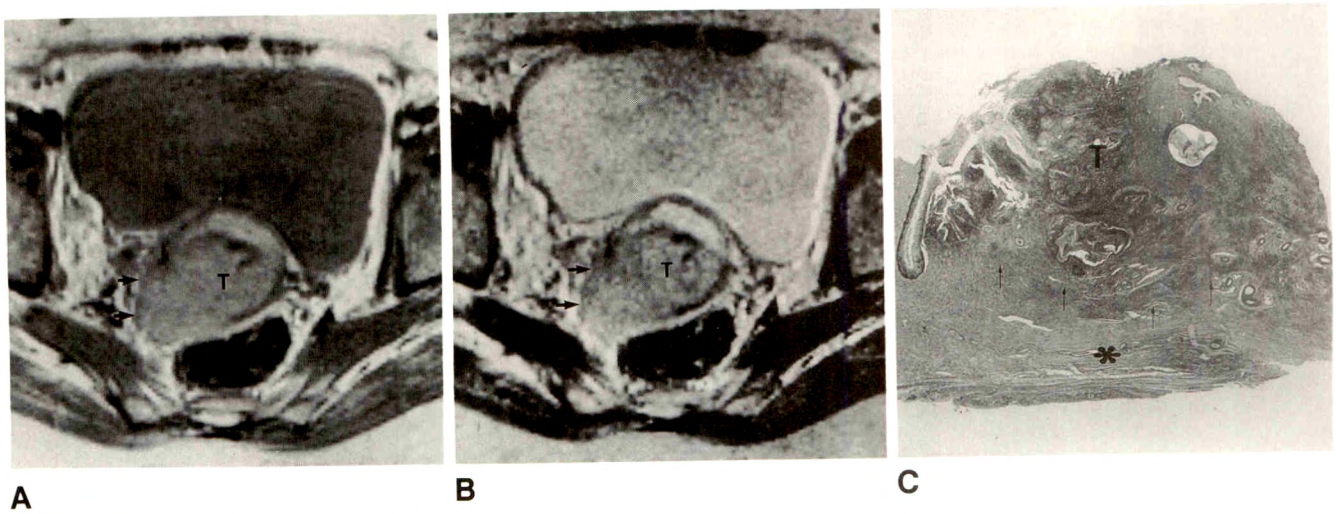



Fig. 2.—Carcinoma of cervix in a 61-year-old woman.
*A* and *B*, SE 2000/40 (*A*) and SE 2000/90 (*B*) axial MR images at same level show large cervical tumor (T) invading right side of parametrium (*arrows*). Low-signal-intensity stromal ring is not visible owing to extensive stromal invasion.
*C*, Corresponding specimen shows tumor (T) invading full thickness of cervical stroma with parametrial involvement (*arrows*). Parametrium (*asterisk*).

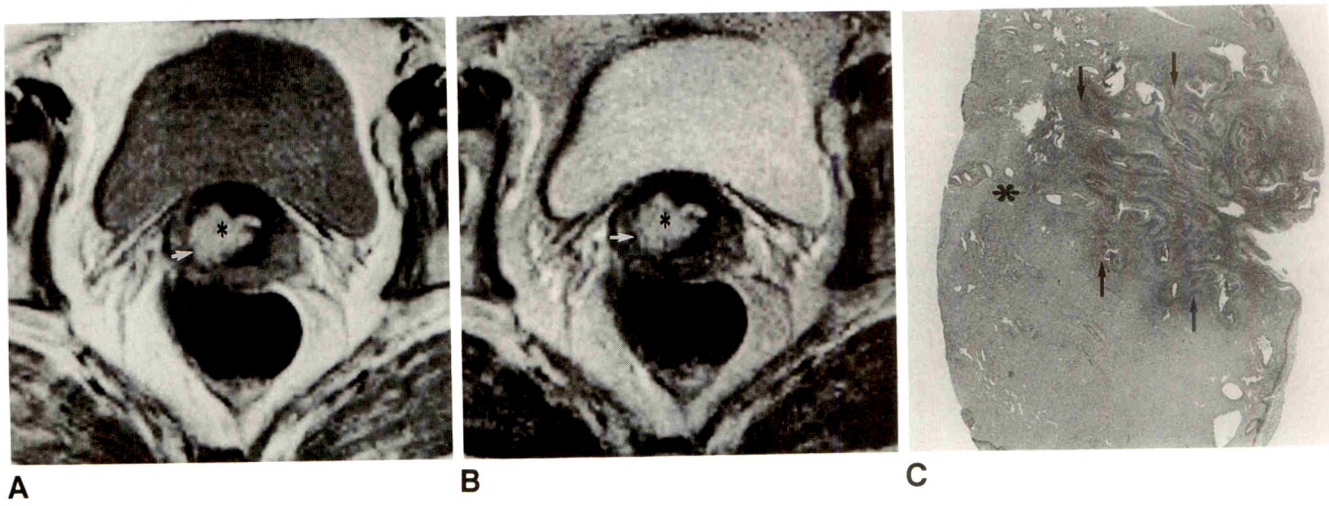



Fig. 3.—Carcinoma of cervix in a 65-year-old woman.
*A* and *B*, SE 2000/40 (*A*) and SE 2000/90 (*B*) axial MR images at same level show right half of low-signal-intensity stromal ring locally disrupted by tumor (*asterisks*), which apparently invades right side of parametrium and right lateral portion of vaginal fornix (*arrows*).
*C*, Corresponding resected specimen reveals deep tumor invasion of cervical stroma (*arrows*) without transmural extension of lesion; a thin outer stripe of normal cervix (*asterisk*) is still present. No invasion of parametrium or of vaginal fornix was proved pathologically.

diagnosis. Precise knowledge of tumor size and location affects the therapeutic decision between surgery and radiation therapy [1]. Surgery is usually reserved for patients in whom tumor is confined to the cervix. In patients in whom tumor has spread to the parametrium or beyond, radiation therapy is the treatment of choice [1]. Therefore, accurate assessment of parametrial tumor extension is one of the most crucial points in preoperative staging of cervical cancer. Clinical staging has limited accuracy: a discrepancy of 34–39% has been reported between clinical and surgical staging [2].

MR imaging, because of its contrast sensitivity and its direct multiplanar imaging ability, has been shown to be an excellent noninvasive means of evaluating the pelvis [6]. Recently, several studies have emphasized the role of MR imaging for preoperative staging in patients with uterine cervical cancer [7–13].

According to previous reports, the transverse plane is essential for detection of tumor extension to the parametrium, and the optimal pulse sequence for imaging the cervix and surrounding structures is SE with a long TR and intermediate to long TEs (T2-weighted images) [8–10]. In our experience also, T2-weighted images proved most efficacious for the evaluation of tumor extension.

On axial T2-weighted images, cervical carcinoma appears as a high-intensity mass that deforms or replaces the low-intensity stromal ring of the cervix. In several previous reports, the presence of an undisrupted low-intensity stromal ring on T2-weighted images has been used as important evidence

that the parametrium is not invaded by tumor [8–13]. Our results indicate that this is true. When the cervical stromal ring was intact, parametrial invasion could not be proved pathologically.

In our series, there were 10 true-positive and three false-positive results. In all true-positive cases, comparison between MR imaging and pathologic estimate of penetration of tumor into the parametrium indicates that MR imaging slightly overestimated parametrial spread. In all false-positive cases, pathologic study revealed the presence of a thin peripheral stripe of normal cervix still surrounding the lesion. In these cases, the thickness of the intact outer stripe of cervical stroma was very small (mean, 2.3 mm); therefore, in our series, false-positive MR evaluations of parametrial involvement seem to be related mainly to the inadequate spatial resolution of MR imaging.

The explanation given for false-positive CT studies of the parametria [14] could also explain false-positive MR studies of the parametria [15]. These include misinterpretation of parametrial vascular structures for tumor or of inflamed parametrial tissue resulting from infection of the primary tumor [14].

In the present study, all MR imaging errors in the evaluation of parametrial status represented false-positive cases. These results confirm those reported recently by Kim et al. [11]. In our study, the accuracy of MR imaging for parametrial evaluation was 88%; this is equal to that reported by Hricak et al. [10] and a littler lower than the 89% reported by Togashi et al. [9] and the 92% reported by Kim et al. [11]. When a comparison is made between our data and those of others, it should be noted that in the present study only patients with tumor clinically confined to the cervix were included, whereas in the other studies [9–11] patients with higher clinical stages of disease were considered also.

Several reports have recently indicated that MR imaging is a reliable imaging method for evaluating the parametrium in patients with cervical cancer [9–11]. In our study also, MR imaging had a high rate of accuracy in directly demonstrating parametrial status.

## REFERENCES


1. Stafl A, Mattingly RF. Cervical intraepithelial neoplasia: invasive carcinoma of the cervix. In: Mattingly RF, Thompson JD, eds. *Te Linde's operative gynecology*, 6th ed. Philadelphia: Lippincott, **1985**:759–844
2. Van Nagell JR Jr, Roddick JW Jr, Lowin DM. The staging of cervical cancer: inevitable discrepancies between clinical and pathologic findings. *Am J Obstet Gynecol* **1971**;110:973–978
3. Villasanta U, Whitley NO, Haney PJ, Brenner D. Computed tomography in invasive carcinoma of the cervix: an appraisal. *Obstet Gynecol* **1983**;62:218–224
4. Walsh JW, Goplerud DR. Prospective comparison between clinical and CT staging in primary cervical carcinoma. *AJR* **1981**;137:997–1003
5. Whitley NO, Brewer DE, Francis A, et al. Computed tomographic evaluation of carcinoma of cervix. *Radiology* **1982**;142:439–446
6. Hricak H. MRI of the female pelvis: a review. *AJR* **1986**;146:1115–1122
7. Worthington JL, Balfe DM. Lee JKT, et al. Uterine neoplasms: MR imaging. *Radiology* **1986**;159:725–730
8. Togashi K, Nishimura K, Itoh K, et al. Uterine cervical cancer: assessment with high-field MR imaging. *Radiology* **1986**;160:431–435
9. Togashi K, Nishimura K, Sagoh T, et al. Carcinoma of the cervix: staging with MR imaging. *Radiology* **1989**;171:245–251
10. Hricak H, Lacey CG, Sandles LG, Chang YCF, Winkler ML, Stern JL. Invasive cervical carcinoma: comparison of MR imaging and surgical findings. *Radiology* **1988**;166:623–631
11. Kim SH, Choi BI, Lee HP, et al. Uterine cervical carcinoma: comparison of CT and MR findings. *Radiology* **1990**;175:45–51
12. Lee JKT. The role of MR imaging in staging of cervical carcinoma. *Radiology* **1988**;166:895–896
13. Rubens D, Thornbury JR, Angel C, et al. Stage IB cervical carcinoma: comparison of clinical, MR, and pathologic staging. *AJR* **1988**;150:135–138
14. Vick CW, Walsh JW, Wheelock JB, Brewer WH. CT of the normal and abnormal parametria in cervical cancer. *AJR* **1984**;143:597–603
15. Waggenspack GA, Amparo EG, Hannigan EV. MR imaging of uterine cervical carcinoma. *J Comput Assist Tomogr* **1988**;12:409–414

# Prostatic Urethra Dilatation with the Gianturco Self-expanding Metallic Stent: A Feasibility Study in Cadaver Specimens and Dogs

Richard L. Dobben[1,2]
Kenneth C. Wright[1]
Kimble Dolenz[1]
Sidney Wallace[1]
Cesare Gianturco[1]

**In an effort to develop a transcatheter technique for dilatation of the prostatic urethra without the use of balloons, the feasibility of using Gianturco self-expanding stents was evaluated. Initially, eight human cadaveric prostatic urethras were stented to evaluate the ability of the stent to dilate the lumen. In all cases, the device attained its unconstrained diameter immediately on placement. Subsequently, stents were placed in the prostatic urethra of 12 dogs and followed up for 1 month (four dogs), 3 months (one dog), and 6 months (seven dogs). Five bare straight-end prostheses, one nylon-covered straight-end device, and six flared-end stents were used. Three of the bare straight-end stents migrated during the follow-up, whereas the nylon-covered and flared-end stents did not. Stent diameters greater than 1.3 times the urethral diameter caused moderate to marked edema and inflammation. After 6 months, white deposits were found on the solder points, presumably from electrolysis.**

**Our experience suggests that placement of Gianturco self-expanding stents may be a useful method of dilating and maintaining the luminal diameter of the prostatic urethra, although care must be taken to select the proper stent size.**

*AJR* **156:757–761, April 1991**

Transurethral resection of the prostate and total prostatectomy are the standard treatments for benign prostatic hypertrophy. In 1910, Hollingsworth [1] described his suprapubic cystotomy approach to digitally dilate the bladder neck and prostatic urethra. Twenty-eight years later, Franch [2] described his technique of transvesical digital splitting of the commissures. In 1956, Deisting [3] constructed his prostatic urethral dilator and described its use in transurethral splitting of the commissures. In 1965, Aalkjaer [4] compared transurethral resection/prostatectomy with dilatation of the prostatic urethra and found transurethral resection/prostatectomy to be superior. After the mid 1960s, little progress was made in devising new techniques. In 1984, however, advances in balloon angioplasty technology led Burhenne to perform a study on 10 human cadavers and then on himself [5]. Shortly thereafter, Quinn et al. [6], and later Castaneda et al. [7], performed balloon dilatation of the prostatic urethra in dogs and humans.

Reddy et al. [8] found that, after balloon dilatation, urine flow was not as good as after transurethral resection. They also found that redilatation was not beneficial and that neither patients with large prostates (more than 40 g) nor those with an enlarged median lobe benefited from dilatation.

In an effort to determine the feasibility of dilating the prostatic urethra without using balloons, this study was conducted to evaluate the use of the Gianturco self-expanding metallic stent. The study was divided into two parts. The first part involved the stenting of eight human cadaveric prostatic urethras. The second part involved the stenting of the prostatic urethra in 12 old mongrel dogs.

Received September 17, 1990; accepted after revision October 30, 1990.

This work was supported in part by a grant from the John S. Dunn Research Foundation and by the George A. Cook Memorial Fund.

[1] Department of Diagnostic Radiology, Box 57, The University of Texas M. D. Anderson Cancer Center, 1515 Holcombe Blvd., Houston, TX 77030. Address reprint requests to K. C. Wright.

[2] Present address: Department of Radiology, University of Illinois Hospital, Chicago, IL 60602.

0361–803X/91/1564–0757
© American Roentgen Ray Society

## Materials and Methods

### *Human Cadaver Prostatic Stents*

Eight fresh human cadaver prostates, with the urinary bladder removed, were obtained. The patients had been 25–75 years old at the time of death. In every case, the cause of death was not genitourinary disease.

The length of the prostatic urethra was measured by using a graduated probe, and stent length was selected accordingly. Each prostate specimen was radiographed in the anteroposterior and lateral projections before and after stent placement.

The stents were made of stainless steel wire (0.035 cm in diameter), which was bent into a zigzag pattern and then formed into a cylinder. The stents had six bends at each end; five of the stents were straight and three were flared at each end. The stents were 2.0–2.5 cm long and 1.5 cm in diameter when fully expanded. The stents were placed by using a 12-French Teflon catheter system and stent pusher (Cook Inc., Bloomington, IN).

One stent was placed in each of five specimens (four straight-end stents and one flared-end stent) and immediately measured (length and diameter) on radiographs. The specimens were then placed in normal saline and refrigerated. Radiographs were obtained again 48 hr later, and stent measurements were compared with those obtained immediately after stenting.

Two additional specimens were stented, one with a straight-end stent and one with a flared-end stent. These specimens were placed in normal saline and refrigerated for 1 week. After this time, radiographs were obtained again, and the length and diameter of each stent were measured and compared with the dimensions obtained immediately after stenting.

One flared-end stent was placed into the final prostate specimen, and the same procedure described above was followed, except that the specimen was kept refrigerated for 1 month. Immediate and 1-month measurements were compared.

### *Animal Study*

Twelve adult mongrel dogs weighing 20–30 kg were used. Each was judged to be old on the basis of gray muzzle hair and dental characteristics. One animal exhibited dribbling and frequency of urination, which was later resolved by stenting of the prostatic urethra. Each animal received either a straight-end or flared-end stent made from stainless steel wire (0.035 cm in diameter) with six bends at each end.

Five dogs received straight-end stents, which were 1.5 cm long and 0.8 cm in diameter when fully expanded. A similar stent constructed of 0.030-cm wire and covered with rip-stop nylon material was placed in one additional dog.

Six dogs received flared-end stents; the dog in whom dribbling and frequency of urination resolved after stenting was in this group. The stents were 1.5 cm long and had a fully expanded diameter that measured 0.8 cm at each end and 0.6 cm in the center.

Anesthesia was induced in each dog with IV thiopental sodium (18 mg/kg) and maintained with halothane (1.5%), nitrous oxide (0.3 l/min), and oxygen (0.8 l/min) by endotracheal intubation. A plain film of the pelvis was obtained. The urethra was lubricated with a 50:50 mixture of 2% lidocaine hydrochloride (viscous, Rugby Laboratories Inc., Rockville Centre, NY) and Surgilube (E. Fougera & Co, Melville, NY). This mixture was placed into a 3-ml syringe and injected directly into the urethral meatus in a retrograde fashion. The 2% lidocaine hydrochloride (viscous) was used to prevent spasm of the urethra during manipulation. Next, a single-film retrograde urethrogram (Fig. 1A) was obtained through an 8-French pediatric Foley catheter (C. R. Bard Inc., Murray Hill, NJ) that had the tip removed. This catheter was placed into the meatus at a distance of 2.0 cm, and the balloon was inflated with 2.0 ml of contrast material (diatrizoate meglumine, Berlex Laboratories, Wayne, NJ). The retrograde urethrogram was obtained by hand-injecting 20 ml of contrast material after a similar volume of contrast material was instilled into the bladder through the Foley catheter. This technique delineated the trigone region of the bladder better than urethrography without contrast material in the bladder.

The Foley balloon was deflated, and the catheter was advanced into the membranous urethra to a point just beyond where the urethra dips into the urethral bulb of the penis. A 0.095-cm straight guidewire was inserted through the Foley catheter into the bladder and the catheter was removed.

A 10-French coaxial Teflon introducer system (Cook Inc.) was passed into the bladder over the guidewire, which was then removed along with the inner catheter. The bladder was drained through the catheter. The stent was then placed into the 10-French Teflon catheter and pushed to the end of the catheter. The internal and external sphincters were identified on the retrograde urethrogram, and the catheter tip was positioned just distal to the internal sphincter. The catheter was then slowly withdrawn while the pusher was held immobile. This deployed the stent in the prostatic urethra between the internal and external sphincters. Care was taken to avoid the external sphincter. The catheter and stent pusher were removed, and a plain film of the pelvis was obtained. The Foley catheter was again inserted 2.0 cm into the urethral meatus and the balloon inflated. A retrograde urethrogram was obtained as before (Fig. 1B).

Repeat plain films and retrograde urethrograms were obtained 2, 4, 8, 12, and 24 weeks after stent placement (Fig. 1C). The stent diameter was measured on the plain radiographs of the pelvis and compared with the diameter immediately after placement. The diameter of the contrast column through the stent was measured and compared with the immediate poststenting retrograde urethrogram. The contrast column also was examined for irregularities.

Four dogs (two with straight-end stents and two with flared-end stents) were sacrificed 1 month after stent placement, and one dog with a flared-end stent was killed 3 months after placement. The other seven dogs were sacrificed after 6 months. All dogs were administered an overdose of IV pentobarbital sodium (70 mg/kg). The urethra, prostate, and urinary bladder were excised en bloc and examined grossly and microscopically.

## Results

### *Human Cadaver Prostatic Stents*

Straight-end and flared-end stents were evaluated in cadaveric specimens to ensure that both configurations would dilate the prostatic urethra. In all cases, immediate urethral dilatation was achieved. Upon placement, the stents opened to their fully expanded diameter, which was maintained for the subsequent period of observation. No stent movement was noted during follow-up.

### *Animal Study*

The stents reached 85–88% of their fully expanded diameter immediately on placement. By 2 weeks after placement, 100% expansion was achieved in all cases and maintained for the duration of the study. Three bare straight-end stents migrated between 1.5 and 3.0 mm into the proximal membra-

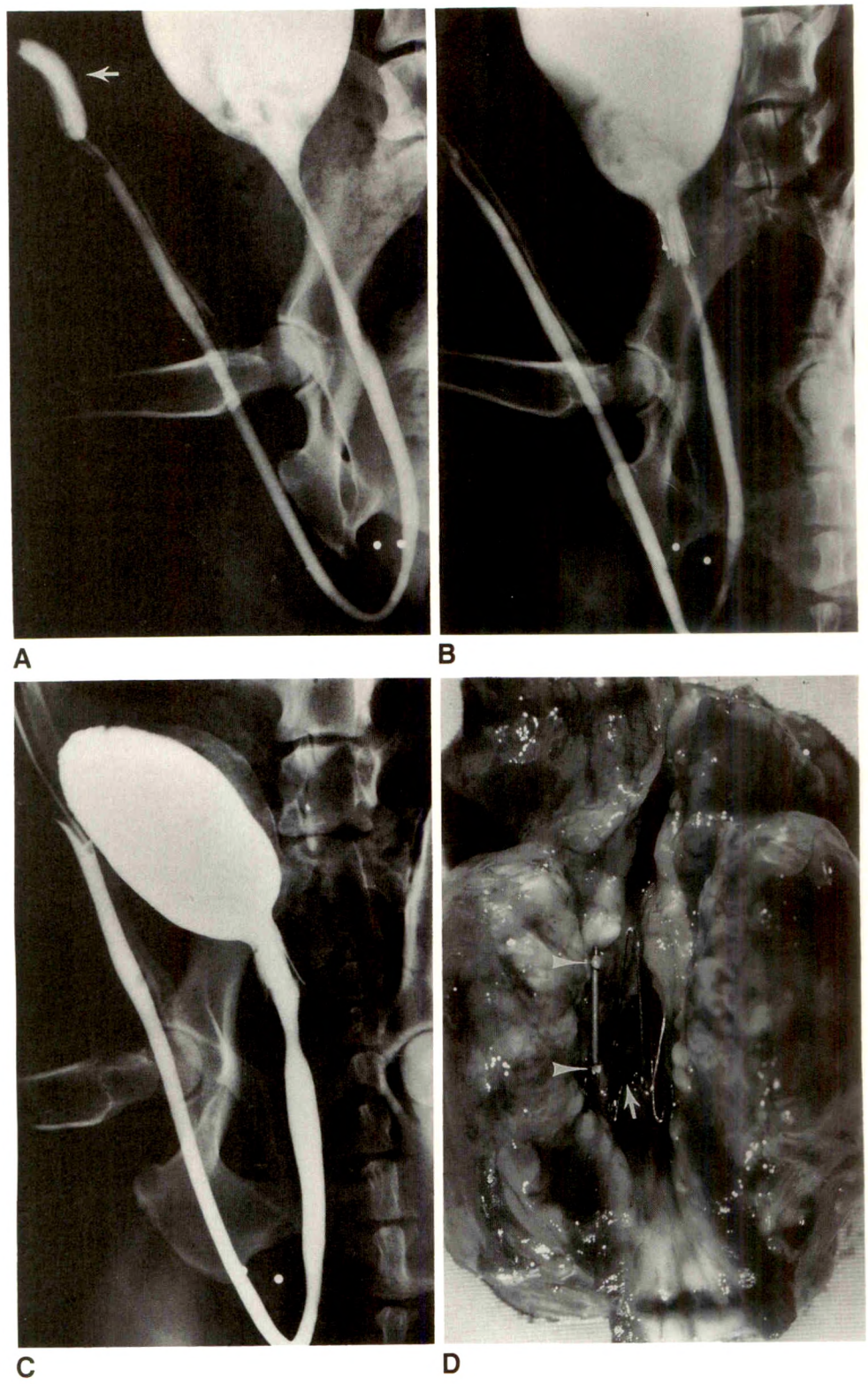



Fig. 1.—Urethrograms of the same dog before and various times after stent placement.

*A*, Before stent placement in prostatic portion of urethra. Balloon of Foley catheter is seen in penile urethra (*arrow*).

*B*, Immediately after placement of a flared-end stent in prostatic urethra. Fully expanded diameter of stent was 1.3 times diameter of prostatic urethra when fully distended.

*C*, 6 months after stent placement. Stent has expanded somewhat since deployment, and portions of stent wire appear outside urethra because of partial covering by longitudinal mucosal folds.

*D*, Gross specimen photograph 6 months after stenting. Dorsal surface of prostate was cut longitudinally to expose stent within urethra. Neck of urinary bladder is seen at top. Portions of stent wire are covered by longitudinal mucosal folds (*arrow*), and white deposits are visible on solder points (*arrowheads*).

nous urethra by 4 weeks after placement, at which time one of the dogs was sacrificed. Of the other two stents, one showed no further movement during the follow-up, while one stent migrated back into the prostatic urethra by 8 weeks after placement and remained there until the end of the study. None of the other stents (six flared-end, two straight-end, and one straight-end covered with nylon) moved after placement.

Radiologically, every stent dilated the recipient prostatic

urethra. On each 2-week urethrogram, there was a 0.5- to 1.0-mm increase in the diameter of the contrast column within the stent, but no changes were seen thereafter. No flow defects were noted in any of the prostatic urethras after stent placement. Two stents (one bare straight-end that never moved after placement and one flared-end) appeared to be outside the urethral lumen on the 6-month follow-up urethrogram. The unconstrained diameter of both of these stents was greater than 1.3 times the diameter of the normal prostatic urethra when fully distended.

Clinically, all dogs tolerated stent placement well. No change in the frequency of urination was noticed, and no incontinence, hematuria, or urinary infection occurred.

At autopsy the prostates ranged in weight from 28.0 to 33.9 g. The largest prostate was from the dog that exhibited dribbling and frequency of urination before stent placement. The wall of the urethra folded to various degrees around the stent wire, but even after 6 months, no overgrowth of urothelium occurred. Longitudinal urethral folds completely covered the wire of both stents that radiologically appeared to be outside the urethra. No localized reaction to the stents was noted grossly. The stents that were in place for 6 months developed small white incrustations on the solder, while the wire itself remained clean (Fig. 1D).

Microscopically, no epithelial overgrowth of the stent wire was noted. All bare stents were found to be at least partially covered by longitudinal folds in the mucosa of the urethral wall. In the two cases in which the fully expanded diameter of the prosthesis was greater than 1.3 times that of the fully distended prostatic urethra, the entire stent was covered (Fig. 2). In addition, the lamina propria in both of these dogs exhibited extensive and prominent alterations. The connective tissue core of some of the longer mucosal folds was markedly edematous and occasionally contained multifocal hemorrhage. There were numerous dilated capillaries and a moderate to marked diffuse infiltration of lymphoid cells. Inflammation and edema extended into the prostate immediately adjacent to the stent wire. Only a mild inflammatory infiltrate was observed in the lamina propria of the animals that received a stent with a diameter equal to or less than 1.3 times the normal urethral lumen.

In the presence of the nylon-covered stent, the prostatic urethra was dilated and the mucosa did not form villouslike folds. A mild diffuse infiltration of the lamina propria by lymphocytes was observed, and some of the capillaries were mildly congested.

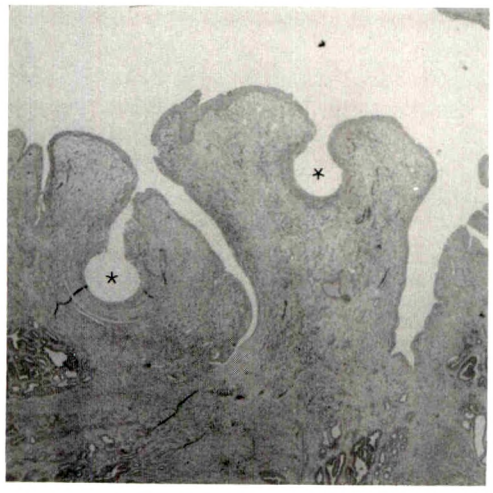


**Fig. 2.—Photomicrograph of dog's prostatic urethra 6 months after stent placement. Open circular spaces are where stent wire was located (*asterisks*). Unconstrained diameter of prosthesis was 1.6 times larger than prostatic urethra when fully distended. Note that wire was completely covered by folds in mucosa, and no epithelial overgrowth occurred. Epithelium below stent wire is ulcerated, and lamina propria contains edema and multifocal hemorrhage. (H and E, original magnification ×25)**

## Discussion

As investigators have proved the efficacy of balloon dilatation of the prostatic urethra [5–10], some limitations of the procedure have become apparent. Two of these limitations are the need to repeat the balloon dilatation or to do a transurethral resection if symptoms recur and that median lobe enlargement cannot be treated by balloon dilatation because of a particular ball-valve effect [8, 9]. These problems may be solved by placing stents in the prostatic urethra. Self-expanding metallic stents have the ability to provide continuous circumferential force, which should obviate retreatment. This is supported by the work of Milroy et al. [11], in which Wallstents were placed in the urethra of eight patients. Placing the proximal end of the stent about 0.1 cm into the bladder should prevent the ball-valve effect of an enlarged median lobe.

In this study, the prostatic urethra was not dilated with balloons prior to stent placement even in the dog that exhibited dribbling and frequency of urination. The reason for this was that Castaneda et al. [7] showed that balloon dilatation of the canine prostatic urethra resulted in long-lasting (up to 1 year) luminal enlargement. Because of this, the ability of the stent to dilate and maintain the urethral lumen could not have been determined had balloon dilatation preceded stent placement.

Although three of the bare straight-end stents moved after placement, this problem was avoided by either covering the device with nylon or flaring the ends. Covering the stent increased the surface area in contact with the urethral wall; thus, the coefficient of friction was increased, which in turn prevented movement. The nylon material also prevented the longitudinal mucosal folds in the urethral wall from passing between the stent "legs" and compromising the luminal diameter. However, the nylon also covered the orifices of the uterus masculinus, deferent ducts, and numerous prostatic ducts. Therefore, depending on degree of porosity, the material covering the stent may prevent ejaculate and prostatic secretions from entering the urethra. It may also conceivably lead to abscess formation, especially in the presence of genitourinary infections.

Milroy et al. [11] reported that after 6 months in the canine urethra, the Wallstent device was partially covered by epithelial overgrowth. This was not seen in the present study. The wire of the Gianturco self-expanding stents became covered

by longitudinal folds in the urethral mucosa, but no cellular overgrowth was noted. This may be due to stent location, because the Wallstents were placed just proximal to the os penis in the penile urethra, not in the prostatic urethra. It may also be the result of the Wallstent being constructed from wire of smaller diameter or the prosthesis exerting less expansive force on the urethral wall than the Gianturco stent. If the stent wire does not become covered by urothelial proliferation, the stent could possibly be repositioned or removed after placement. A repositionable self-expanding stent, now being developed, may be useful if stent position is not adequate. This may also make it possible to remove the stent after the prostatic urethra has been dilated for some time.

As is the case in the vasculature [12], it is important to choose a stent diameter on the basis of the diameter of the normal urethral lumen. Although no major complications were encountered in any of the dogs, only the two stents larger than 1.3 times the diameter of the fully distended urethra produced extensive and prominent histopathologic changes in the tissues surrounding the stent wire. This suggests that when selecting a self-expanding metallic stent for placement in the prostatic urethra, the diameter of both the fully distended urethra and stent must be considered. Specifically, the unconstrained stent diameter should not exceed 1.3 times that of the normal prostatic urethra.

A white incrustation of the solder occurred on all stents left in place for 6 months. The deposits possibly were due to electrolysis resulting from a galvanic current created by silver solder being placed in direct contact with stainless steel wire. If so, these electrodeposits probably could be avoided by spot welding or crimping the ends of the stent wire to form the cylinder. The wire itself remained clean.

In conclusion, placement of Gianturco self-expanding stents appears to be a viable means of dilating and maintaining the luminal diameter of the prostatic urethra. However, care must be taken in selecting the appropriate stent diameter.

## ACKNOWLEDGMENTS

We thank Raquel Collins and Irene Szwarc for technical assistance, Peggy Bergmanson for secretarial help, and Bob Czimny for photographic expertise.

## REFERENCES

1. Hollingsworth E. Dilatation of the prostatic urethra for the relief of the symptoms of prostatic enlargement. *Ann Surg* **1910**;57:597–599
2. Franch O. Die sprengung des Prostataringes. *Munch Med Wochenschr* **1938**;21:77–82
3. Deisting W. Transurethral dilatation of the prostate. A new method in the treatment of prostatic hypertrophy. *Urol Int* **1956**;2:158–171
4. Aalkjaer V. Transurethral resection/prostatectomy versus dilatation treatment in hypertrophy of the prostateae. *Urol Int* **1965**;20:17–22
5. Burhenne HJ, Chisholm RJ, Quenville NF. Prostatic hyperplasia: radiologic intervention. Work in progress. *Radiology* **1984**;152:655–657
6. Quinn SF, Dyer R, Smathers R, et al. Balloon dilatation of the prostatic urethra. *Radiology* **1985**;157:57–58
7. Castañeda F, Lund G, Laarson BW, et al. Prostatic urethra: experimental dilatation in dogs. *Radiology* **1987**;163:645–648
8. Reddy PK, Wasserman N, Castañeda F, Castañeda-Zúñiga WR. Balloon dilatation of the prostate for treatment of benign hyperplasia. *Urol Clin North Am* **1988**;15:529–535
9. Castañeda F, Reddy P, Wasserman N, et al. Benign prostatic hypertrophy: retrograde transurethral dilatation of the prostatic urethra in humans. *Radiology* **1987**;163:649–653
10. Scales LE, Katzen BT, Van Breda A, et al. Impassable urethral strictures: percutaneous transvesical catheterization and balloon dilatation. *Radiology* **1985**;157:59–61
11. Milroy EJG, Cooper JE, Wallsten H, et al. A new treatment for urethral strictures. *Lancet* **1988**;1:1424–1427
12. Duprat G Jr, Wright KC, Charnsangavej C, Wallace S, Gianturco C. Self-expanding metallic stents for small vessels: an experimental evaluation. *Radiology* **1987**;162:469–472

# Book Review

**Quantitative Imaging.** Neuroreceptors, Neurotransmitters, and Enzymes. Edited by J. James Frost and Henry N. Wagner, Jr. New York: Raven, 199 pp., 1990. $98

This book is a compilation of 12 chapters, written by 16 authors, each of which contains a relatively independent review of the subject matter. A concise historical review and overview of the understanding of receptor binding and localization is presented in the first chapter. The possible role of abnormalities in receptor binding in disease is reviewed briefly in the second chapter.

The book has an excellent chapter on methodological approach that can be used in the development of new radiotracers to study various processes that involve the receptors for neurotransmitters. Inclusion of $^{123}$I-labeled compounds in the discussion is welcome and demonstrates the potential for performing the types of regional justification studies by using single-photon emission CT. The chapter on physics and instrumentation is valuable, particularly because of the discussion of the various potentially error-producing factors that must be considered in order to attempt to do in vivo quantitative imaging. After a chapter that presents a detailed look into compartmental modeling, a series of seven chapters deals with the different neuroreceptors, neurotransmitters, and enzymes: opiate receptors, dopamine receptors, benzodiazepine receptors, muscarinic acetylcholine receptors, serotonin receptors, dopa metabolism, and monoamine oxidase utilization. Each of these chapters contains a discussion of the methods of evaluation and a brief description of potential clinical use. The topics of discussion include spatial ateration of opiate receptors in patients who have epilepsy and quantification of receptor occupancy as means of optimizing drug therapy, particularly as related to dopamine receptors.

I think the book is an excellent compilation of the scientific methodology currently being used to evaluate neurotransmitters, neuroreceptors, and neuroenzymes in vivo. It is not a basic textbook from which to acquire a detailed understanding of the scanner/cyclotron for positron emission tomography (PET) or the current status of clinical PET as it relates to the brain. However, it should serve as a valuable reference text for those in the clinical or basic neurosciences and those imagers who wish a single-source reference of present in vivo quantitative methods of imaging the distribution and interactions of neurotransmitters, neuroreceptors, and enzymes.

Michael E. Siegel
*University of Southern California, School of Medicine*
*Los Angeles, CA 90033*

Technical Note

# A Simplified Method for Antegrade Ureteral Stent Placement

Richard Krauthamer[1]

Percutaneous placement of antegrade ureteral stents has become a common interventional uroradiologic procedure. Advances in stent materials and design have led to longer patency rates and improved patient tolerance [1–3]. The most recent delivery systems use either peel-away sheaths [1, 4] or coaxial stent-pusher combinations [3]. We recently adopted a simplified technique that eliminates the need for a radiologic ureteral stent set and positioning of suture loops. We describe our approach, which uses retrograde ureteral stents that are readily available in multiple lengths from any hospital urology department.

## Technique

A percutaneous nephrostomy is performed first by using a favorable caliceal approach to allow easy access to the ureter. If the urine is grossly bloody or infected, in order to prevent occlusion of the ureteral stent, antegrade stenting is deferred until drainage from the nephrostomy tube is clear. Antibiotics are administered to patients who have signs of infection. Once a rigid guidewire such as a 0.038-in. (0.97-mm) Teflon-coated Lunderquist-Ring torque guidewire or a 0.038-in. Amplatz superstiff guidewire (Cook, Bloomington, IN) is manipulated into the bladder, an 11-French peel-away sheath 45 cm long with coaxial introducer (Medi-tech, Watertown, MA) is advanced over the guidewire into the bladder, and the introducer and guidewire are removed.

An 8.5-French urologic retrograde ureteral soft silicone or stiffer Silitek Uropass stent (Surgitek, Racine, WI) of appropriate length is selected by bending an extra guidewire or marking a catheter at appropriate distal and proximal sites fluoroscopically within the sheath. The stent is placed over the 0.038-in. guidewire (Fig. 1) as follows: The tips of the soft silicone stent, if used, are cut off with a scalpel blade because the soft silicone stent ends are closed. The stiff end of the 0.038-in. guidewire is used to pierce the side holes of the proximal stent by first passing the guidewire through the distal (bladder) pigtail end hole. For the silicone stent, the wire carefully is stitched out and then back in on one side of two contiguous proximal side holes and then is passed back out through the most proximal side hole at the beginning curve of the proximal (renal) pigtail on the side opposite to the stitch. The stiffer Uropass stent has less friction with larger side holes and requires an additional stitch through more distal side holes opposite the more proximal side stitch. Care must be taken to use a large loop of wire to stitch the side holes and avoid kinking the wire. After the stent is lubricated with mineral oil, the stent-wire combination is advanced by hand into the peel-away sheath, and the stiff wire is pushed by hand until the distal pigtail with its slightly protruding wire exits the sheath within the bladder. The pusher supplied with the urologic stent kit is placed within the sheath over the guidewire to the internal straightened proximal tip of the stent.

The peel-away sheath then is partially withdrawn while the pusher is held against the internal stent. If additional stent is needed within the bladder, the pusher is advanced while the guidewire is held. Once the distal end of the stent is coiled properly within the bladder, the pusher is held against the

Received October 9, 1990; accepted after revision November 20, 1990.
[1] Department of Radiology, Torrance Memorial Medical Center, 3330 Lomita Blvd., Torrance, CA 90505. Address reprint requests to R. Krauthamer.

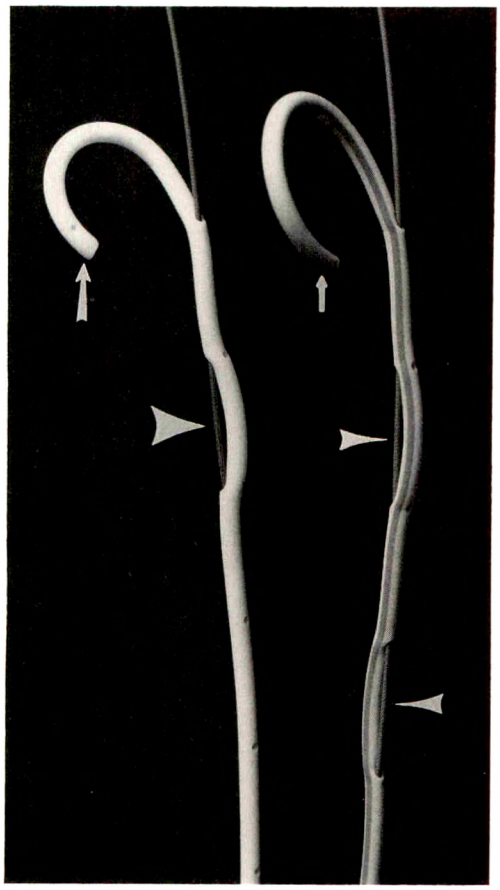


**Fig. 1.—Photograph shows soft 8.5-French silicone stent (*large arrow*) and stiffer, larger-lumen Uropass stent (*small arrow*) proximal pigtail coils with single side stitch (*large arrowhead*) for soft silicone stent and double side stitch (*small arrowheads*) for Uropass stent. Note guidewire exiting side hole at beginning of pigtail.**

stent to ensure that the stent does not retract; the peel-away sheath is removed further and left just within the collecting system to allow easy subsequent placement of a nephrostomy tube. This maneuver usually requires the use of an assistant. During retraction of the sheath, the proximal stent coil reforms because the guidewire exits the proximal side hole (Fig. 1). Also, enough friction exists between the smaller side holes of the stent and the guidewire that retraction or advancement of the stent for final positioning is possible if necessary. Dilute contrast material can be injected into the renal pelvis at this time via the peel-away sheath by using a 5-French vessel dilator after temporarily removing the pusher.

Once the final position is obtained, the pusher is held against the stent side hole, and the guidewire is retracted slowly into the pusher, freeing the proximal stent coil. The wire must be retracted slowly and steadily to avoid kinking the stent. The guidewire then can be readvanced within the peel-away sheath into the collecting system, allowing placement of a temporary nephrostomy tube until the urine clears. The nephrostomy tube is removed after an antegrade pyelogram shows the stent is patent. With this method, we have placed eight ureteral stents successfully and without difficulty in a variety of benign and malignant conditions.

## Discussion

Previous reports have described the use of peel-away sheaths and coaxial stent-pusher combinations for placement of ureteral stents, but both methods require the use of a suture loop, which can be difficult to remove and can tear the stent wall, become entangled in the proximal coil, or wedge the proximal stent in the ureter [1, 3]. The Amplatz ureteral stent set (Cook) does not require a suture loop, but it does require a readily available supply of stents in different lengths, and the final coiled position is not seen before the guidewire is removed. Our method of placing a 0.038-in. guidewire through the proximal side holes, instead of an end hole, eliminates the need for a suture loop and relies on urologic ureteral stents. These are more readily available in our institution and come in various lengths. The use of a peel-away sheath eliminates buckling and friction of the softer silicone stents. The coiling of the proximal stent with the guidewire still in position and the ability to retract the stent by pulling the guidewire makes final positioning of the stent technically simple. In addition, the possibility of retracting the stent into the renal parenchyma is eliminated. In summary, we think that our simplified method for placing an antegrade ureteral stent is easily learned and eliminates the need for a suture loop and reliance on an available supply of prefabricated radiologic stent sets.

## REFERENCES

1. Rozenblit G, Tarasov E, Srur MF, Neithamer CD, Sumers EH, Sos TA. Druy ureteral stent set: clinical experience in 25 patients. *Radiology* **1986**;160:737–740
2. Mitty HA, Dan SJ, Train JS. Antegrade ureteral stents: technical and catheter related problems with polyethylene and polyurethane. *Radiology* **1987**;165:439–443
3. Mitty HA, Rackson ME, Dan SJ, Train JS. Experience with a new ureteral stent made of a biocompatible polymer. *Radiology* **1988**;168:557–559
4. Lee WJ, Rich M. Universal introducer: a simplified approach to antegrade ureteral stent insertion. *AJR* **1986**;147:830–831

# Acute Effects of Exercise on MR Imaging of Skeletal Muscle:
## Concentric vs Eccentric Actions

Frank G. Shellock[1]
Tetsuo Fukunaga[2,3]
Jerrold H. Mink[1]
V. R. Edgerton[2]

**Eccentric (lengthening) muscle actions involve the forced lengthening of active muscles. Compared with concentric (shortening) muscle actions subjected to the same relative work load, eccentric actions have lower oxygen consumption requirements, fewer activated motor units, and less lactate production. This study was conducted to determine if T2-weighted MR could show any difference in muscles performing these specific types of actions and, therefore, be useful for physiologic investigations of eccentric and concentric actions. Five subjects performed exhaustive exercise by doing isolated concentric actions (raising a dumbbell, flexing at the elbow) and eccentric muscle actions (lowering a dumbbell, extending the contralateral arm). T2-weighted MR images of the arms were obtained immediately before and after exercise. Muscles that performed concentric actions had increases in signal intensity, whereas muscles that performed eccentric actions showed little or no change. T2 relaxation times increased significantly ($p < .01$) in all volunteers, but T2 relaxation times for the muscles that performed concentric actions were significantly higher than those for muscles that performed eccentric actions ($p < .01$). Therefore, T2 times increased with both concentric and eccentric actions, but the images failed to show the changes in the muscles that performed the eccentric actions.**

**These data demonstrate that assessment of T2 values can be used to distinguish between muscles that perform concentric actions and those that perform eccentric actions, and this phenomenon may be useful for further physiologic investigations of these specific types of muscle actions.**

***AJR* 156:765–768, April 1991**

Eccentric (lengthening) muscle actions involve the forced lengthening of active muscles and the transfer of external power from the environment to the subject [1, 2]. Examples include the use of resistance equipment, such as weight-lifting devices, or deceleration processes during activity, such as running downhill. Therefore, eccentric muscle actions produce active tension while the muscle is being lengthened. Various investigations have shown that, compared with concentric (shortening) muscle actions, eccentric actions are associated with reduced oxygen consumption, fewer activated motor units, and less lactate production for the same power output [3–7]. Therefore, concentric actions apparently require more energy than eccentric actions do when subjected to the same relative work load [3–7].

Fleckenstein et al. [8] first reported that T2-weighted spin-echo images of active skeletal muscle showed increased signal intensity immediately after exercise. Other studies have also investigated this phenomenon [9–11]. This contrast enhancement of exercised muscle was suggested to be caused by increased vascular and extracellular volumes [8], as well as by changes in intracellular water [11]. Research has additionally shown that T2 relaxation times of active skeletal muscles depend on exercise intensity [8, 11].

In consideration of these facts, the present study was conducted to determine if

Received September 24, 1990; accepted after revision October 23, 1990.

[1] Tower Musculoskeletal Imaging Center, Cedars-Sinai Medical Center, Los Angeles, CA 90048 and Department of Radiological Sciences, UCLA School of Medicine, Los Angeles, CA 90024. Address reprint requests to F. G. Shellock, Cedars-Sinai Medical Center, MRI, 8700 Beverly Blvd., Los Angeles, CA 90048.

[2] Department of Kinesiology, University of California, Los Angeles, Los Angeles, CA 90024.

[3] Present address: Department of Sports Sciences, University of Tokyo, Tokyo, Japan.

0361–803X/91/1564–0765
© American Roentgen Ray Society

T2-weighted MR images could show any difference in the acute exercise response of muscles that perform concentric vs eccentric actions at the same relative work load. This information is important because, currently, no sufficiently accurate technique is available for obtaining biopsy samples of muscles performing concentric vs eccentric actions [1], and MR could be used to precisely direct sampling of the involved muscles.

## Subjects and Methods

### *Study Subjects*

Five normal volunteer subjects (three men and two women; average age, 36 years; range, 21–48 years) were involved in this investigation. These individuals were untrained and had not performed any arm resistance training for at least 6 months before involvement in the study.

### *Exercise Protocol*

A single dumbbell weighted to a normalized percentage (i.e., 15% for women and 20% for men) of the subject's body weight was used for the resistance exercise. The weights ranged from 12 to 15 lb. for the women and from 25 to 30 lb. for the men. The subjects performed a "biceps curl" movement for the exercise while in a standing position. One arm was selected randomly to perform concentric (i.e., shortening) actions. This was accomplished with strict form, by bending the arm at the elbow and raising the dumbbell with the palm up, moving from extension to full flexion. The weight was then passed to the contralateral arm by an assistant to perform the eccentric (i.e., lengthening) actions. This was accomplished by lowering the dumbbell with strict form, beginning with the arm at full flexion and lowering it to extension. The extremities were in supinated positions throughout the range of motion of each movement. The rate at which the concentric and eccentric actions took place was monitored, so that each movement took approximately 2 sec. Using this protocol, the subjects performed isolated concentric and eccentric actions in an alternating manner.

Exercise was performed by each of the subjects to the point of perceived exhaustion and "failure" (i.e., the subject no longer could raise the dumbbell) and the same number of repetitions were achieved with each extremity. Therefore, the concentric and eccentric actions were performed to the same relative work level. This exercise protocol was similar to those used by others to study concentric vs eccentric actions [12] and was also designed to simulate resistive training techniques frequently used by body builders and strength trainers [13].

The estimated total work performed by each arm was calculated by measuring power, as follows:

$$\frac{\text{mass (kg)} \times \text{distance (m)}}{\text{time (sec)}}.$$

This calculation yielded the following results for the subjects in this study: 100 kg m/sec (woman), 109 kg m/sec (woman), 155 kg m/sec (man), 142 kg m/sec (man), and 155 kg m/sec (man).

### *MR Protocol*

MR was performed with a 1.5-T, 64-MHz MR imager and quadrature-driven, transmit/receive body coil (General Electric Company, Milwaukee, WI). Inasmuch as Fleckenstein et al. [8] showed that active muscles are most conspicuous on MR when pulse sequences with a long TE and long TR are used, T2-weighted and proton-density, spin-echo images were obtained immediately before and after exercise with the following parameters: axial imaging plane; 2000/80, 20 (TR/TE); 128 × 256 matrix; two excitations; 44-cm field of view; 10-mm slice thickness; and 2-mm interslice gap. These parameters were selected to minimize data acquisition time while still obtaining the necessary image information from both exercising limbs for analysis.

The subjects were placed supine in the MR imager, and images were obtained from the mid-forearms to the deltoids, with the subjects' arms placed together over their head and held in place with loosely applied cloth tape to inhibit motion.

### *Data Analysis*

The images were filmed with standardized window settings, and the relative signal intensities of the active muscles in the arms involved in concentric and eccentric actions were compared visually with those of the nonexercising muscles (i.e., the triceps).

Regions of interest were selected in the center of the biceps (i.e., the active muscles) and triceps (i.e., inactive muscles) of each subject's mid-upper arms that performed the concentric and eccentric actions, with special care to avoid inclusion of subcutaneous fat, fascia, blood vessels, or bony anatomy. T2 relaxation times were determined for these regions of interest by using the software provided by General Electric.

T2 relaxation times measured before and after exercise for each muscle group (e.g., biceps before exercise concentric action vs biceps after exercise concentric action, triceps before exercise concentric action extremity vs triceps after exercise concentric action extremity) were compared by using a paired t-test. A comparison between the postexercise concentric action biceps data and the postexercise eccentric action biceps data also was made by using a paired t-test.

## Results

Visual inspection of the images (Fig. 1) showed no apparent differences in the signal intensities of any of the muscle groups before exercise (i.e., the biceps and triceps). Immediately after exercise, increases were apparent in the signal intensity of the biceps and brachialis muscles that performed concentric actions, whereas little or no change occurred in the signal intensity of the biceps and brachialis muscles that performed eccentric actions (Fig. 1). The signal intensity of the triceps muscles (i.e., inactive muscles) of the extremities that performed concentric and eccentric actions appeared to be unchanged from that on the preexercise images.

The data on T2 relaxation times are summarized in Figure 2. The T2 relaxation times were not significantly different for the triceps muscles of the extremities performing concentric and eccentric actions (note: all reported values are mean ± SD, triceps preexercise concentric action extremity, 29.5 ± 0.4 msec, triceps postexercise concentric action extremity, 29.8 ± 0.5 msec, $p$ = N.S.; triceps preexercise eccentric action extremity, 29.6 ± 0.3 msec, triceps postexercise eccentric action extremity, 29.6 ± 0.5 msec, $p$ = N.S.).

Statistically significant increases in T2 relaxation times were seen for the biceps muscles performing concentric actions (biceps preexercise concentric action, 29.1 ± 0.6 msec, biceps postexercise concentric action, 38.5 ± 0.9 msec, $p$ = .0001) and the biceps performing eccentric actions (biceps

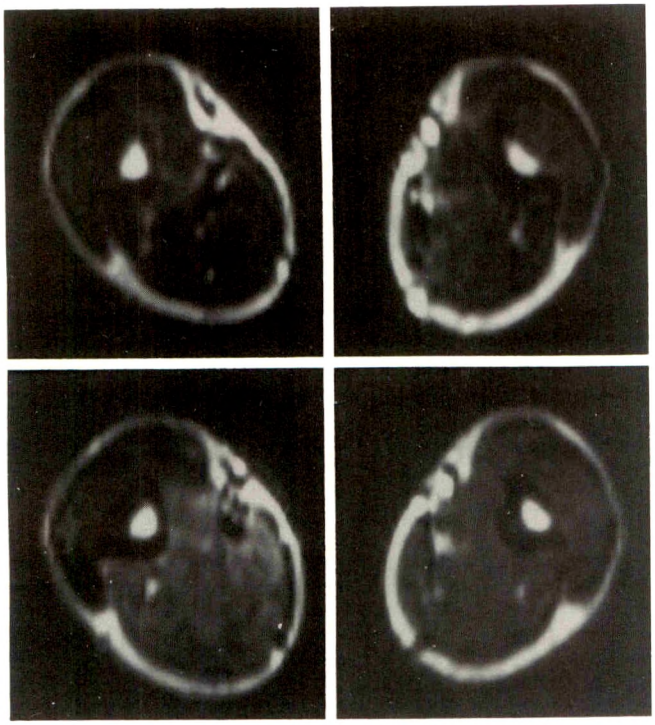


**Fig. 1.—Axial plane, T2-weighted (2000/80) spin-echo images of mid-upper arms of a subject obtained immediately before (top row) and after (bottom row) the subject performed concentric (left column) and eccentric (right column) actions. Note that active muscles (biceps and brachialis) that performed concentric actions are differentiated easily on postexercise image by an increase in signal intensity. By comparison, little or no change occurs in signal intensity of active muscles that performed eccentric actions, and they are not differentiated as easily.**

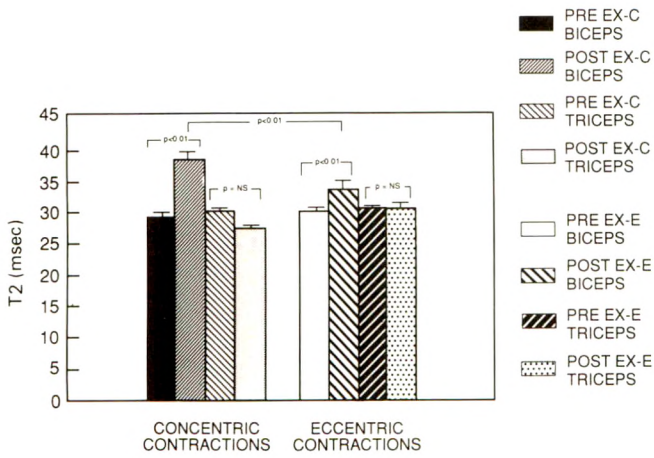



**Fig. 2.—Graph shows T2 values of biceps and triceps measured before and after extremities performed concentric and eccentric actions. Values are means ± SD. EX-C = concentric actions; EX-E = eccentric actions.**

preexercise eccentric action, 29.5 ± 0.5 msec, biceps postexercise eccentric action, 33.1 ± 1.1 msec, $p = .004$). In addition, the T2 relaxation times for the biceps performing concentric action were significantly higher than those for the biceps performing eccentric actions (biceps postexercise concentric action, 38.5 ± 0.9 msec, biceps postexercise eccentric action, 33.1 ± 1.1 msec, $p = .0006$).

## Discussion

MR imaging has developed into the foremost noninvasive imaging technique for examining normal and diseased conditions of the musculoskeletal system [14]. When MR imaging is used, biological tissues and fluids with excess amounts of free water have long T2 values and, therefore, tend to be the most conspicuous on T2-weighted images [14, 15].

Exercise-induced changes in extracellular and intracellular water content produce changes in proton relaxation times [8–11] and correlate with the level of exertion [8, 11]. Fleckenstein et al. [8] first showed that exercise is associated with statistically significant changes in T1, T2, and spin-density relaxation times observed on MR. The greatest effect was seen on images obtained with T2-weighted pulse sequences and, to a lesser degree, on those obtained with gradient-reversal techniques in which the flip angle was reduced to decrease the effect of T1 differences on the images [8]. In consideration of the results of previous studies [8, 11], we decided to use T2-weighted MR selectively for our investigation to maximize the suspected differences between muscles performing concentric actions and those performing eccentric actions.

The preexercise T2 values for the muscles evaluated in this study were comparable to those reported by Fleckenstein et al. [8] and others [13, 16, 17]. The immediate postexercise T2 values for the muscles performing concentric and eccentric actions also were within the ranges reported by previous investigators for active muscles [8, 11].

Additionally, we observed that muscles performing eccentric actions had a statistically significant lower T2 value than did muscles performing concentric actions. Research studies have shown that muscle actions that involve eccentric actions require less oxygen, produce less lactate, and use fewer muscle fibers than do concentric actions subjected to the same relative work load [1–7]. Of further note, Fisher et al. [11] reported a strong correlation between the increase in T2 values and the mean force during exercise. Therefore, considering that T2 values are related to exercise intensity and eccentric action requires less of an energy expenditure than does concentric action, it is not surprising that we found statistically significant differences between T2 values for each of these specific types of muscle action.

Exercise produces rapid alterations in the content of water found in skeletal muscle [18, 19]. Several mechanisms appear to be involved in this process. The water content in the exercising muscles increases as a result of the movement of water across the capillary wall, which is mediated by the hydrostatic pressure in the capillary and the osmotic forces in both the capillary blood and interstitial fluid [18, 19]. The increase in muscle lactate during exercise causes an increased tissue osmolality that also contributes to the increased water content of skeletal muscle observed with exercise [18, 19]. Additionally, the vascular bed of active muscles has an enlarged functional capillary surface area and

an increased mean capillary pressure that produces an increased filtration of water from the capillary bed into the interstitial space [18, 19].

Mild to moderate levels of exercise appear to be associated with a large (i.e., up to 100%) increase in extracellular water and a slight increase (i.e., about 10%) in intracellular water [18]. However, with maximal work loads, the greatest increase in muscle water content occurs in the intracellular space [19]. Fleckenstein et al. [8] indicated that the increased signal intensity seen in muscles that performed fatiguing exercise were caused mainly by an increase in extracellular water, but other processes also may be involved. The preliminary work by Fisher et al. [11] suggested that the increased signal intensity seen on T2-weighted images of active muscles was largely due to increases in intracellular free water related to maximal exercise. In consideration of this, we presume that the signal intensity changes observed on T2-weighted images in our present study depended primarily on an increase in intracellular water of the active muscles that performed the concentric action, with a minor contribution from an increase in extracellular water, as our subjects performed a maximal exercise protocol. However, the relative contribution of extracellular and intracellular water changes related to maximal concentric or eccentric muscle actions has not been studied before and could not be determined from our data.

Fleckenstein et al. [9] proposed that exercise-enhanced MR is a useful localization technique for guiding MR spectroscopic studies of active muscles because variations in muscle anatomy and individual differences in muscle recruitment patterns exist, and palpation techniques used to identify the sample volume are relatively inaccurate. Therefore, the use of exercise-induced contrast enhancement is particularly important for avoiding admixtures of spectroscopic signals from active and inactive muscles [9]. However, because signal intensity changes are not visually apparent on T2-weighted images of muscles that perform isolated eccentric actions, it may not be possible to rely simply on visual inspection of images to identify transient increases in signal intensity. Accordingly, it may be necessary to measure T2 relaxation times or to quantify the signal intensity changes to identify the sensitive volume for MR spectroscopy studies involving only eccentric actions.

There is currently no sufficiently accurate technique available for obtaining biopsy samples of muscles performing concentric vs eccentric actions [1] and, therefore, MR could be used to precisely direct the sampling of the involved active muscles. MR also may be helpful in further elucidation of physiologic differences between these specific types of muscle actions.

ACKNOWLEDGMENTS

We gratefully thank Yoshio Ohira, John Hodgson, Tracey Meeks, Gina Slimp, and Kathy Day for their involvement in this study.

REFERENCES

1. Armstrong RB. Mechanisms of exercise-induced delayed onset muscular soreness: a brief review. *Med Sci Sports Exer* **1984**;16:529–538
2. Stauber WT. Eccentric action of muscles: physiology, injury, and adaption. In: *Exercise and sports sciences reviews*. Philadelphia: The Franklin Institute, **1988**:157–185
3. Armstrong RB, Laughlin MH, Rome L, Taylor CR. Metabolism of rats running up and down an incline. *J Appl Physiol* **1983**;55:518–521
4. Asmussen E. Positive and negative muscular work. *Acta Physiol Scand* **1952**;28:364–382
5. Bigland-Ritchie B, Woods M. Integrated electromyogram and oxygen uptake during positive and negative work. *J Physiol* **1976**;260:267–277
6. Davies CTM, Barnes C. Negative (eccentric) work. II. Physiological responses to walking uphill and downhill on a motor-driven treadmill. *Ergonomics* **1972**;15:121–131
7. Schwane JA, Watrous BG, Johnson SR, Armstrong RB. Is lactic acid related to delayed-onset muscle soreness? *Physician Sportsmed* **1983**;11:124–131
8. Fleckenstein JL, Canby RC, Parkey RW, Peshock RM. Acute effects of exercise on MR imaging of skeletal muscle in normal volunteers. *AJR* **1988**;151:231–237
9. Fleckenstein JL, Bertocci LA, Nunnally RL, Parkey RW, Peshock RM. Exercise-enhanced MR imaging of variations in forearm muscle anatomy and use: importance in MR spectroscopy. *AJR* **1989**;153:693–698
10. Peshock R, Fleckenstein J, Payne J, Lewis S, Mitchell J, Haller R. Muscle usage patterns during cycling: MRI evaluation (abstr.). *Magn Reson Imaging* **1990**;7:23
11. Fisher MJ, Meyer RA, Adams GR, Foley JM, Potchen EJ. Direct relationship between proton T2 and exercise intensity in skeletal muscle MR images. *Invest Radiol* **1990**;25:480
12. Clarkson PM, Tremblay I. Exercise-induced muscle damage, repair, and adaption in humans. *J Appl Physiol* **1988**;65:1–6
13. Fleck SJ, Kraemer WJ. *Designing resistance training programs*. Champaign, IL: Human Kinetics Books, **1987**
14. Mink JH, Deutsch A. *MRI of the musculoskeletal system: a teaching file*. New York: Raven, **1990**
15. Fisher MR, Dooms GC, Hricak H, Reinhold C, Higgins CB. Magnetic resonance imaging of the normal and pathologic muscular system. *Magn Reson Imaging* **1986**;4:491–496
16. Hazelwood CF, Chang DC, Nichols BL, Woessner DE. Nuclear magnetic resonance transverse relaxation times of water protons in skeletal muscle. *Biophys J* **1974**;14:583
17. Pettersson H, Fitzsimmons J, Krop D, Hamlin D. Magnetic resonance imaging of the extremities. II. T1 and T2 relaxation times of muscle and fat: normal values, reproducibility and dependence on physiologic variations. *Acta Radiol Diagn* **1985**;26:413–416
18. Sjogaard G, Saltin B. Extra- and intracellular water spaces in muscles of man at rest and with dynamic exercise. *Am J Physiol* **1982**;243:R271–R280
19. Sjogaard G, Adams RP, Saltin B. Water and ion shifts in skeletal muscle of humans with intense dynamic knee extension. *Am J Physiol* **1985**;248:R190–R196

# Repair of Achilles Tendon Ruptures with a Polylactic Acid Implant: Assessment with MR Imaging

Marina D. Liem[1]
Harry G. Zegel[1]
Frederick C. Balduini[2]
Melvin L. Turner[1]
Joseph M. Becker[1]
Annette Caballero-Saez[3]

**An investigational tendon repair device composed of a polymer of lactic acid (PLA) is currently undergoing multicenter clinical trials for use in repairing rupture of the Achilles tendon. The advantages of the PLA device include high tensile strength and the induction of a rapid proliferative tissue response resulting in a shorter rehabilitation period than with conventional surgical repair. We reviewed 16 MR examinations performed in 10 patients 3–35 months after repair to characterize the MR appearance. All 16 T1-weighted sagittal images revealed a thickened fusiform tendon with streaks of moderate signal within the tendon corresponding to the PLA device and its surrounding collagenogenic response. The double-echo T2-weighted axial images at the mid tendon level demonstrated progressive changes in the signal pattern of the central portion of the tendon that reflected the maturation of the healing tendon. All tendons repaired with PLA implants were uniformly hypertrophied relative to the contralateral normal side because of the induced proliferative collagenogenic ingrowth. Two follow-up MR examinations were performed in six patients and showed mean reductions in tendon caliber of 24% and 30% at the mid and inferior levels.**

**MR imaging of the Achilles tendon repaired with PLA implants shows a diffusely thickened tendon with streaks of signal within the tendon that distinguish it from tendons repaired by conventional techniques.**

*AJR* 156:769–773, April 1991

An investigational synthetic device has been developed for the surgical repair of tendons and ligaments and is currently undergoing multicenter clinical trials for the repair of Achilles tendon ruptures. This device is composed of multiple filaments of a polymer of lactic acid (PLA) that are twisted together and have suture needles placed at both ends (Fig. 1). The physical properties that make it attractive for tendon repairs include high tensile strength, the inducement of rapid tissue healing, and potential absorbability (Clemow AJ and Chen EH, presented at the annual meeting of the Orthopedic Research Society, February 1986).

We prospectively reviewed 16 MR examinations of 10 patients who underwent surgical repair of ruptured Achilles tendons with the PLA device. The purpose of this study was to assess MR appearance of this type of repair.

## Materials and Methods

Sixteen patients participated in a clinical trial using the PLA device (Johnson & Johnson Orthopaedics, Inc., Raynham, MA) for the repair of Achilles tendon ruptures. We performed MR imaging in 10 of these 16 patients. All of the patients were initially assessed by an experienced orthopedic surgeon. All repairs were performed with a modified Kessler stitch in which the PLA device is sewn through the closely approximated ends of the torn tendon in a rectangular stitch with stabilizing loops at each corner (Fig. 2). Two Kessler stitches were used for each repair, resulting in a total of four strands bridging the ruptured tendon ends. A standard postoperative protocol was followed that included immobilization in a short leg cast

Received September 6, 1990; accepted after revision October 29, 1990.

Presented at the annual meetings of the American Roentgen Ray Society, Washington, DC, May 1990, and the Pennsylvania Radiological Society, Hershey, PA, May 1990.

This work was supported by a grant from Johnson & Johnson Orthopaedics, Inc., Raynham, MA.

[1] Department of Medical Imaging, Presbyterian Medical Center, 51 N. 39th St., Philadelphia, PA 19104. Address reprint requests to H. G. Zegel.

[2] South Jersey Sports Medicine Center, 53 Haddonfield Rd., Cherry Hill, NJ 08003.

[3] MRI Diagnostics, 3820 Powelton Ave., Philadelphia, PA 19104.

0361–803X/91/1564–0769
© American Roentgen Ray Society

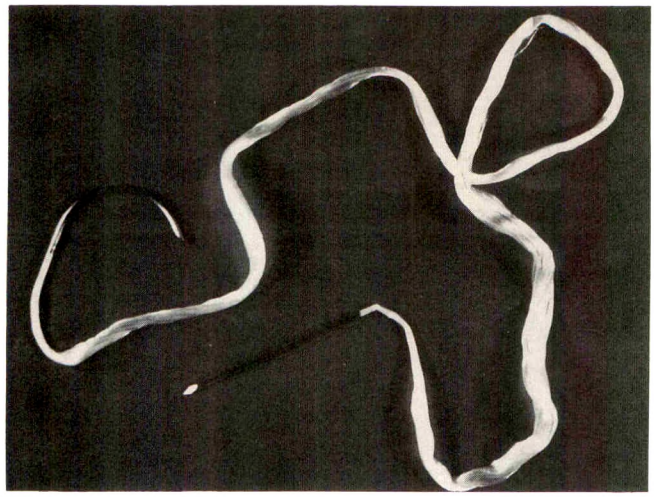


**Fig. 1.—Tendon repair device consists of several intertwined strands of a polymer of lactic acid secured by suture needles at both ends.**

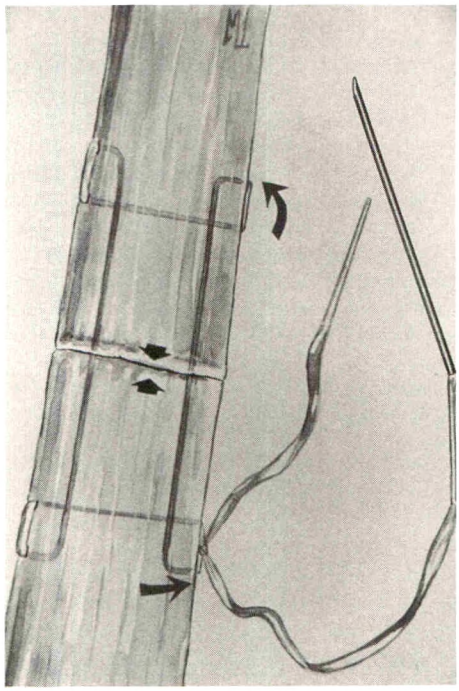


**Fig. 2.—Modified Kessler stitch used to repair Achilles tendon ruptures (*short arrows*) is a rectangular stitch with stabilizing corner loops (*long arrows*) oriented along longitudinal axis of tendon.**

an additional period of isokinetic exercises for up to 3 months, patients were gradually allowed to resume their normal activities. Cybex II isokinetic strength and power testing (Cybex, Ronkonkoma, NY) at 3 and 6 months after the repair provided an objective measure of functional recovery.

We imaged 10 patients between December 1987 and February 1990 during a postoperative period of 3–35 months. Six of these patients underwent two MR examinations, for a total of 16 MR studies. The intervals between surgery and imaging were grouped as follows: 3 months (three patients), 6–9 months (three patients), 12–16 months (seven patients), and 20–35 months (three patients). In the six sets of double studies, the interval between studies ranged between 9 and 22 months. Our study population consisted of nine men and one woman 28–54 years old. The 10 Achilles tendon ruptures were equally divided between the right and left sides; all ruptures occurred during recreational sports or step-up injuries. We also imaged one patient after a conventional Achilles tendon repair with heavy nonabsorbable suture 15 months after surgery.

All images were obtained on a 0.5-T superconductive magnet (Picker International, Highland Heights, OH) with both ankles placed in a standard head coil. All studies included sagittal T1-weighted spin-echo (SE) images, 420–650/20/4 (TR/TE/excitations), of the repaired side and axial double-echo T2-weighted images (SE 2000/20–100/2) of both sides. In seven of 16 studies, axial T1-weighted images (420–650/20/4) also were obtained before and after administration of gadopentetate dimeglumine (Magnevist, Berlex Laboratories, Wayne, NJ). All sagittal images were obtained with a 5-mm slice thickness and a 1-mm interspace gap, and the axial images had a 10-mm slice thickness with a 2-mm gap. The field of view ranged from 23 to 26 cm for the axial and 25 to 40 cm for the sagittal images. A 192 × 256 matrix was used for all studies except for seven T2-weighted sequences, in which a 145 × 145 matrix was used.

In each MR examination, the midsagittal image through the repaired tendon was used as a localizer. Three levels in the axial sequences representing the superior, mid, and inferior levels of the device within the tendon were chosen for analysis. The inferior level was generally 2–4 cm above the calcaneal insertion, and 2–3 cm separated sequential levels.

Four radiologists independently reviewed each case without knowing the postrepair interval. The parameters evaluated at each axial level follow.

*Central signal pattern.*—The intratendinous signal was of moderate intensity on all T1-weighted, spin-density, and T2-weighted images. The pattern, signal intensity, and location within the tendon were recorded.

*Tendon caliber.*—As the Achilles tendon has an elliptical configuration in the axial projection, the cross-sectional areas of the repaired and normal sides were calculated as an ellipse by using the formula, area = $\pi ab$, where a and b are the measured long and short axes of the tendon in centimeters. We compared the relative caliber of both sides by taking the cross-sectional ratios of the repaired to normal sides. In the six sets of double studies, the chronologic change in tendon caliber was quantified by comparing the tendon areas at the same level in both studies and expressing the difference as a percent change.

*Contrast enhancement.*—The seven MR examinations with IV gadopentetate dimeglumine were evenly distributed throughout the 3–35 postrepair months. The degree of peri- and intratendinous signal enhancement was recorded as 0 = none (no change from unenhanced MR), 1 = minimal, 2 = moderate, and 3 = marked (similar to subcutaneous fat). Any disagreements were resolved by consensus opinion established on review of the study.

## Results

### *MR Imaging*

The T1-weighted sagittal MR images of all 16 Achilles tendons repaired with PLA implants showed a hypointense, thickened, fusiform tendon. Several well-defined streaks of moderate intratendinous signal along the entire length of the tendon were constant and recognizable features (Fig. 3). MR imaging of the conventionally repaired tendon revealed a low repair that was locally thickened in the area of the repair and had a compact central zone of moderate intratendinous signal (Fig. 4A). A similar low repair with the PLA device showed more diffuse tendon thickening with thin, well-defined streaks spread throughout most of the tendon (Fig. 4B).

The central signal pattern at the mid level on the spin-density and T2-weighted axial scans differed with the postrepair interval. All three MR studies performed 3 months after

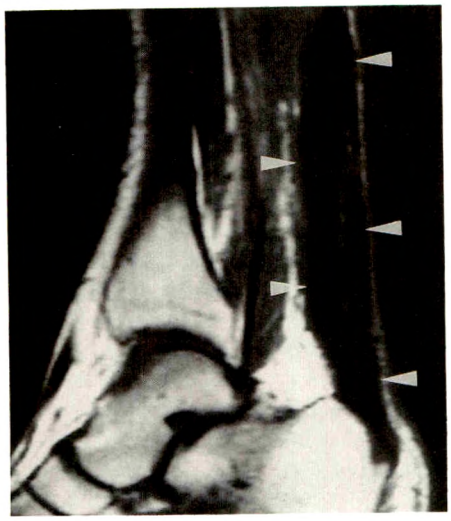


Fig. 3.—Midline T1-weighted sagittal MR image (SE 500/20) after repair shows a fusiform, thickened Achilles tendon (*arrowheads*) with vertically oriented streaks of intermediate intratendinous signal.

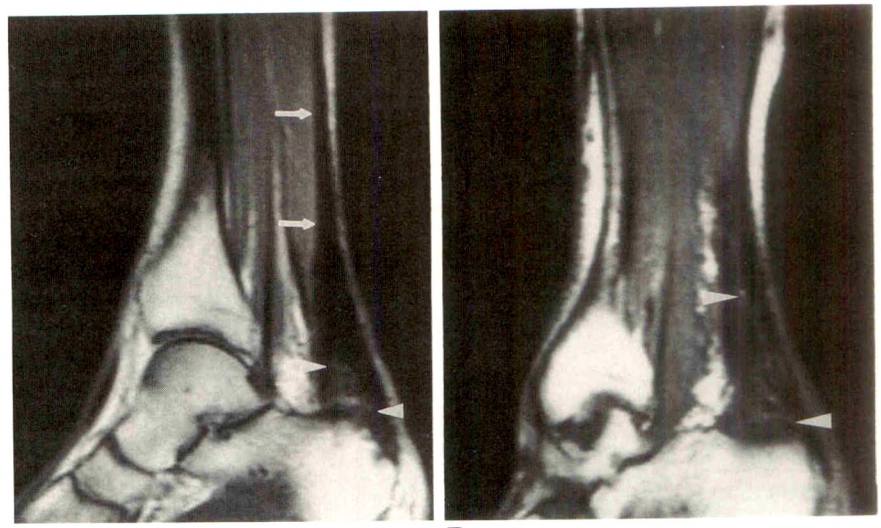



Fig. 4.—*A*, T1-weighted sagittal MR image (SE 500/20) 15 months after low conventional repair shows tendon thickening in region of repair that tapers to normal caliber proximally (*arrows*). Note circumscribed zone of intermediate intensity localized to repair site near calcaneal insertion (*arrowheads*).

*B*, T1-weighted sagittal MR image (SE 500/20) 18 months after low repair with polylactic acid implant shows generalized thickening of Achilles tendon and well-defined streaks of intratendinous signal throughout tendon (*arrowheads*).

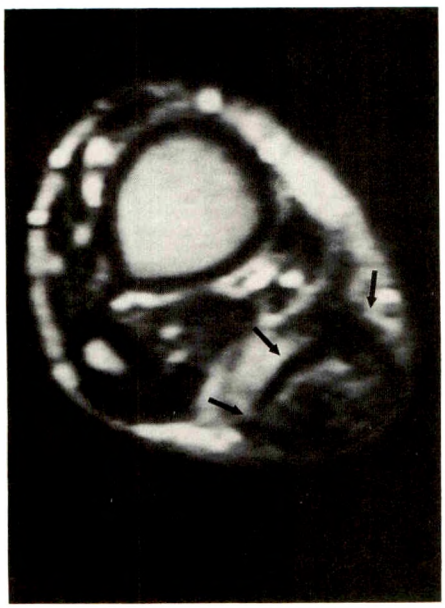


Fig. 5.—T2-weighted axial MR image (SE 2000/100) 3 months after repair shows amorphous clump of mixed signal (*arrows*) at mid level reflecting generalized collagenogenic and hydrophilic response.



Fig. 6.—Mid-level spin-density axial MR image (SE 2000/20) 12 months after repair shows a group of sharply defined punctate foci (*arrowheads*) corresponding to strands of polylactic acid against low-signal background of fully healed tendon.



Fig. 7.—Mid-level spin-density axial MR image (SE 2000/26) 6 months after repair shows two clusters of partially separated foci (*arrowheads*) corresponding to strands of polylactic acid covered with maturing collagenogenic activity.

repair revealed an amorphous clump of mixed signal (Fig. 5). Four of the seven MR studies in the 12- to 16-month postrepair period showed a group of punctate foci ("dots") arranged in a row or cluster (Fig. 6). The three remaining examinations in this period and the three examinations from the 6- to 9-month interval showed a central signal pattern that was intermediate between the clump and punctate dot patterns (Fig. 7). This pattern had discrete areas of increased signal with margins that tended to blend together and therefore were not as sharply defined as the punctate dot pattern ("fuzzy dots"). Two of the three late postrepair MR examinations showed a central area of uniformly moderate signal, and the third study had the fuzzy dot pattern.

The chronologic change in signal pattern at the mid level was evident in two of the six sets of double studies. The initial MR images of both patients were obtained at 3 months postrepair and revealed the clump pattern. The same level at 14 and 16 months, respectively, showed progression into the

dot pattern (Fig. 8). The remaining four double studies did not show significant change at the mid level. In these double studies, the initial MR study was performed 6–13 months after repair and the follow-up study was performed at 12–35 months.

A delicate reticular pattern was found only at the superior and inferior axial levels. Eleven of the 16 superior levels and five of the 16 inferior levels had this type of central signal pattern. A few of these cases demonstrated a slightly curved, well-defined line (Fig. 9) corresponding closely to the horizontal portion of the Kessler stitch.

In the seven MR examinations performed with IV gadopentetate dimeglumine, there was no appreciable peritendinous or intratendinous enhancement.

*Tendon Caliber*

All of the tendons repaired with PLA devices were hypertrophied relative to the contralateral side at the same level regardless of the postrepair interval. The mean cross-sectional area for all levels was 14.2 $cm^2$ for the repaired side and 3.2 $cm^2$ for the contralateral normal side. When the ratios of the repaired side to normal side were calculated, the repaired tendon averaged 4.4, 6.4, and 5.0 times larger than the normal side at the superior, mid, and inferior levels, respectively.

In assessing the chronologic change in tendon caliber in the six sets of double studies, there were reductions in the cross-sectional areas at the mid and inferior levels averaging 24% (range, 0–40%) and 30% (range, 14–55%), respectively. At the superior level, there were no consistent differences in tendon caliber, and therefore the average percent reduction was only 5% (range, 36% increase to 14% reduction).

*Clinical Outcome*

The average total casting period for all patients was 4 weeks. The mean recovery in strength compared with the uninjured side was 91 ± 13% (SD), indicating nearly full recovery of functional strength. All patients were able to resume their normal activities and their participation in sports.

The only major complication encountered was one tendon rerupture occurring 2 weeks after the repair when a patient fell while not wearing the removable cast. Surgical repair of the rerupture revealed that it occurred around an intact PLA device. MR examination 14 months after the rerupture repair showed no differences from the other MR examinations in our series. No mechanical failures of the PLA device were encountered.

## Discussion

Current surgical techniques in the repair of Achilles tendon ruptures use either suture alone or suture reinforced with tendinous or fascial grafts [1–3]. Because the suture becomes a permanent support for the injured tendon, the ultimate integrity of the repair is limited by the mechanical strength of the suture over a prolonged period and by shear forces caused by the stress imbalance between the suture and surrounding healing tendon [4]. These limitations have prompted the investigation of several synthetic materials for ligamentous and tendinous repair that improve the overall functional strength of the repair.

An investigational synthetic device composed of a PLA has been introduced in the past decade and is currently undergoing multicenter clinical trials for the repair of Achilles tendon ruptures. Animal model research using the PLA device to

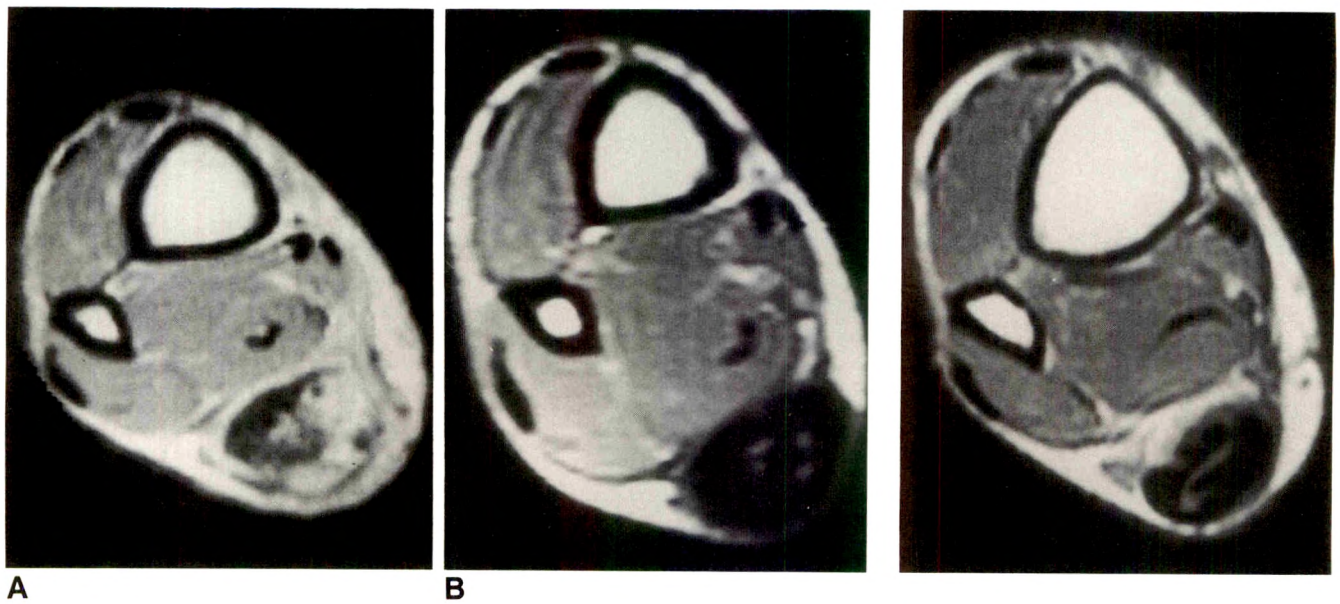



Fig. 8.—*A*, Spin-density axial MR image (SE 2000/20) at mid level 3 months after repair shows an amorphous clump pattern of mixed signal.
*B*, Axial image at same level 16 months after repair shows a cluster of punctate foci.

Fig. 9.—Spin-density axial MR image (SE 2000/20) at superior level shows a well-defined curvilinear intratendinous pattern corresponding to horizontal portion of Kessler stitch.

repair induced Achilles tendon ruptures in rabbits shows that the PLA device acts as a scaffold for soft-tissue ingrowth (Clemow AJ and Chen EH, ORS meeting, February 1986). The firm bond between the device and surrounding tissue reduces failure by shear forces by distributing tissue growth over a larger surface area [5]. Histologically, the PLA device induces a proliferative collagenogenic response that matures with time (Clemow AJ and Chen EH, ORS meeting, February 1986). PLA is biodegraded into lactic acid, which is eliminated primarily through the respiratory cycle [6]. Slow, complete resorption of PLA in rod and powder forms has been demonstrated in animal models [6, 7], but the in vivo resorption rate of the PLA device has not been established.

Repair with the PLA device results in a shorter immobilization time and faster ambulation when compared with conventional surgical methods. All of the patients in our protocol had an average casting time of 4 weeks with rehabilitation beginning 2 weeks after repair. Conventional surgical techniques require an average casting time of 5–9 weeks before beginning rehabilitation [4]. The shorter casting time allowed by the PLA device and other synthetic implants permits an early, aggressive rehabilitation program, which is believed to be important for the recovery of full functional strength and range of motion [8, 9].

Although there have been several previous reports correlating MR imaging with the diagnosis and preoperative planning of Achilles tendon ruptures [10–15], the role of MR imaging in the postoperative phase has not yet been explored. To our knowledge, three reports have been published on the MR appearance of healing Achilles tendon ruptures. In one patient treated nonsurgically with equinus casting, MR imaging 4 months after the injury revealed a discontinuous tendon with interposed intermediate-intensity tissue compatible with a fibrous rather than direct union [13]. The second patient had a generally thickened, partially continuous tendon with areas of mixed signal within and between the tendon ends consistent with clinical evidence of incomplete healing [14]. MR imaging of an uncomplicated repair in the third patient 4 months after surgery showed an intact, slightly thickened tendon that was uniformly hypointense [15]. The conventionally repaired tendon in our series was thickened locally at the site of the repair and had a central localized zone of intermediate signal within it.

The variable appearance of healing Achilles tendons as illustrated by the limited number of reported cases and our own example precludes generalizations of the typical MR appearance of a conventionally repaired Achilles tendon. However, two consistent features of the tendon repaired with PLA distinguish it from a conventional repair. First, the thin streaks of intermediate signal seen diffusely throughout the tendon repaired with PLA contrast with the thicker, localized zone of intratendinous signal found in some conventionally repaired tendons. Second, the tendon repaired with PLA is markedly thickened in a diffuse, fusiform manner, whereas tendon thickening in a conventional repair is less pronounced and usually localized to the site of repair. The diffuse hypertrophy of the tendon repaired with PLA, which persists as late as 35 months after repair, is most likely a reflection of the induced collagenous ingrowth surrounding the length of the PLA device and may be a significant factor in the continued strength and integrity of this type of repair. The lack of peritendinous intermediate-signal tissue supports the presence of a direct rather than fibrous union.

The thin streaks of moderate intratendinous signal on the sagittal images correspond to the PLA strands in the Kessler stitch with its surrounding collagenogenic response. The axial central signal pattern observed at the mid level varied depending on the postrepair interval. There was a chronologic progression from a clump pattern at 3 months to a fuzzy dot pattern at 6–9 months to either a fuzzy dot or punctate dot pattern at 12–16 months. This chronologic progression from clump to dots can best be explained by the induced collagenogenic response in the early postoperative period, which is a property of the PLA device. The clump pattern with its amorphous areas of mixed signal corresponds to the early generalized hydrophilic and collagenogenic response. When this response begins to organize into mature tendon matrix, the normal low signal of the tendon is recovered. The PLA strands covered by the residual collagenous ingrowth then become more apparent as partially separated foci of moderate signal. With further maturation, the PLA strands become well-defined dots against the low-signal background of the fully healed tendon.

ACKNOWLEDGMENTS

We thank Patty Fry and Frieda Liem for assistance in manuscript preparation.

REFERENCES

1. Beskin JL, Sanders RA, Hunter SC, Hughston JC. Surgical repair of Achilles tendon ruptures. *Am J Sports Med* **1987**;15:1–8
2. Inglis AE, Sculco TP. Surgical repair of ruptures of the tendo Achilles. *Clin Orthop* **1981**;156:160–169
3. Kellam JF, Hunter GA, McElwain JP. Review of the operative treatment of Achilles tendon rupture. *Clin Orthop* **1985**;201:80–83
4. Wills CA, Washburn S, Caiozzo V, Prietto CA. Achilles tendon rupture: a review of the literature comparing surgical versus nonsurgical treatment. *Clin Orthop* **1986**;207:156–163
5. Aragona J, Parsons JP, Alexander H, Weiss AB. Soft tissue attachment of a filamentous carbon-absorbable polymer tendon and ligament replacement. *Clin Orthop* **1981**;160:268–278
6. Kulkarni RK, Pani KC, Neuman C, Leonard F. Polylactic acid for surgical implants. *Arch Surg* **1966**;93:839–843
7. Kulkarni RK, Moore EG, Hegyeli AF, Leonard F. Biodegradable poly(lactic acid) polymers. *J Biomed Mater Res* **1971**;5:169–181
8. Parsons JR, Weiss AB, Schenk RS, Alexander H, Pavlisko F. Long-term follow-up of Achilles tendon repair with an absorbable polymer carbon fiber composite. *Foot Ankle* **1989**;9:179–184
9. Lieberman JR, Lozman J, Czajka J, Dougherty J. Repair of Achilles tendon ruptures with Dacron vascular graft. *Clin Orthop* **1988**;234:204–208
10. Beltran J, Noto AM, Herman LJ, Lubbers LM. Tendons: high-field-strength surface coil MR imaging. *Radiology* **1987**;162:735–740
11. Daffner RH, Riemer BL, Lupetin AR, Dash N. Magnetic resonance imaging in acute tendon ruptures. *Skeletal Radiol* **1986**;15:619–621
12. Keene JS, Lash EG, Fisher DR, DeSmet AA. Magnetic resonance imaging of Achilles tendon ruptures. *Am J Sports Med* **1989**;17:333–337
13. Marcus DS, Reicher MA, Kellerhouse LE. Achilles tendon injuries: the role of MR imaging. *J Comput Assist Tomogr* **1989**;13:480–486
14. Quinn SF, Murray WT, Clark RA, Cochran CF. Achilles tendon: MR imaging at 1.5 T. *Radiology* **1987**;164:767–770
15. Reinig JW, Dorwart RH, Roden WC. MR imaging of a ruptured Achilles tendon. *J Comput Assist Tomogr* **1985**;9:1131–1134

# Book Review

**Trauma Radiology.** Edited by James J. McCort. New York: Churchill Livingstone, 483 pp., 1990. $110

*Trauma Radiology* attempts to combine all aspects of radiology involving trauma into one textbook. The book is primarily for any physician who works within an emergency department or who evaluates trauma patients. It is also for those radiologists who evaluate trauma patients. This would include residents in both radiology and surgery.

The text is divided into nine chapters that cover aspects of craniocerebral, spinal, thoracic, abdominal, genitourinary, facial, pelvic, and upper- and lower-extremity trauma. In each chapter, the appropriate radiologic examination for different traumatic conditions and the appropriate radiologic technical factors are presented. In addition, the advantages and disadvantages of different radiologic techniques are presented, whether conventional radiography, CT, MR imaging, or sonography.

The radiographs throughout the text are quite good in illustrating the abnormalities presented. In addition, many chapters have a line drawing corresponding to the radiologic images that more clearly defines the abnormalities. One interesting aspect is the attempt to explain the mechanism of injury by means of the radiographs and by illustrations within the text. Illustrations and drawings throughout the text are excellent.

The editor has accomplished the goal of making available a book for precise and rapid determination of patients' conditions for imaging examination, definition of technical factors, and description of pertinent radiologic changes. The text is, again, primarily for those physicians who care for acutely injured patients or interpret radiographs of such patients. The same information probably is available in many separate texts, but this one text manages to bring a varied amount of material together.

Stanley B. Novy
*St. Joseph Hospital*
*Houston, TX 77002*

# Extension of Growth-Plate Cartilage into the Metaphysis: A Sign of Healing Fracture in Abused Infants

Paul K. Kleinman[1]
Sandy C. Marks, Jr.[2]
Melissa R. Spevak[1]
Patricia L. Belanger[1]
Joann M. Richmond[3]

**The present study was carried out to determine if healing metaphyseal injury in abused infants is accompanied by an increase in the thickness of the growth-plate zone of hypertrophic cartilage and if a radiolucent extension from the growth plate into the metaphysis correlates with this histologic indicator of healing fracture. The radiologic studies of 13 infants who died with evidence of inflicted injury were reviewed. Thirteen distal metaphyseal fractures were identified. Histologically, nine of these fractures were noted to be healing and four showed no evidence of healing. The nine healing injuries were accompanied by statistically significant thickening of the zone of hypertrophic cartilage. Seven of these demonstrated localized areas of hypertrophic cartilage extension; in six of these, corresponding radiolucent extensions of the growth plate into the metaphysis were seen. The extensions tended to be single and focal with minimal osseous injury and broad and multiple with extensive injury. No similar extension was visible in the four acute injuries.**

**Because metaphyseal injuries are notoriously difficult to date, the presence of a reliable radiologic indicator of healing metaphyseal fracture can be important in the evaluation of infant abuse. Because the radiologic findings reflect the histologic alterations, extension of the growth-plate cartilage into the metaphysis may have implications for estimating fracture age.**

*AJR* 156:775–779, April 1991

Metaphyseal lesions as described by Caffey are highly specific for infant abuse [1–9]. Unfortunately, these lesions are difficult to date. Periosteal reaction is usually lacking, and other radiologic indicators of healing are not easily applied to these subtle anatomic alterations [10]. Discrete areas of radiolucency extending from the growth plate to the metaphysis have been described and have been attributed to fracture repair, but proof has not been provided that these radiolucent extensions are reliable indicators of healing [5].

In 1960, Trueta and Amato [11] noted an increase in the thickness of the hypertrophic cell zone of the cartilage growth plate in rabbits with experimental disruption of metaphyseal vasculature. Since vascular injury occurs with metaphyseal fracture, a similar pattern of hypertrophic cartilage can be expected. The current study was carried out to determine if healing metaphyseal injury in abused infants is accompanied by an increase in the thickness of the zone of hypertrophic cartilage and if a radiolucent extension from the growth plate into the metaphysis correlates with this histologic indicator of healing fracture.

## Materials and Methods

The radiologic and pathologic studies of 13 infants who died with evidence of inflicted skeletal injury were reviewed. Their average age was 14 weeks (range, 5–22 weeks). High-detail skeletal surveys, specimen radiology, and histologic studies were performed according to methods previously described [10].

Received August 14, 1990; accepted after revision October 30, 1990.

Presented at the annual meeting of the Society for Pediatric Radiology, Cincinnati, OH, April 1990.

[1] Department of Radiology, University of Massachusetts Medical Center, 55 Lake Ave. N., Worcester, MA 01655. Address reprint requests to P. K. Kleinman.

[2] Department of Cell Biology, University of Massachusetts Medical Center, Worcester, MA 01655.

[3] Chief Medical Examiner's Officer, University of Massachusetts Medical Center, Worcester, MA 01655.

0361–803X/91/1564–0775
© American Roentgen Ray Society

A total of 33 metaphyseal injuries were identified radiologically. Because this total population of fractures represented a wide variety of fracture sites and patterns, for purposes of uniformity it was elected to study lesions occurring in one anatomic region. The distal tibia was involved most often, and the 13 lesions identified at this site form the basis of this study. Frontal and lateral radiographs of the distal tibiae were studied, with particular attention to the growth plate. Any extension of the radiolucent growth plate into the metaphysis was noted and subsequently correlated with histologic material sectioned in similar anatomic planes.

The histologic material was reviewed and the presence or absence of osseous repair was noted. Histomorphometric analyses were performed on all distal tibial specimens as follows. Sections of epiphyseal plates of distal tibiae were examined at 65× magnification, and the proliferative and hypertrophic zones of individual cartilage columns were measured with a calibrated ocular micrometer. The limits of each zone were defined by using criteria previously employed by Farnum and Wilsman [12]. Longitudinal measurements of each zone were expressed in arbitrary units, which at the magnification used corresponded to 0.019 mm/U. Data were expressed as a ratio of the length of the hypertrophic to that of the proliferative zone—the cartilage hypertrophy index (CHI).

The distal tibial fractures were examined and the maximal CHI was recorded for each site of osseous injury. In addition to the CHI, the absolute number of hypertrophic chondrocytes at these sites was noted.

Histomorphometric control data were obtained from three sites. A randomly selected CHI was calculated from normal areas adjacent to a healing fracture, the normal opposite tibia in cases of unilateral injury, and the distal tibia of a 3-month-old infant who died of accidental injury.

Last, a comparison of histologic and radiologic material from injured tibiae was carried out to identify if a radiologic correlate to the histologic pattern of injury was present.

## Results

Of 13 radiologically documented distal tibial metaphyseal injuries, nine showed healing and four showed no evidence of healing. The healing injuries were bilateral in three infants and unilateral in three. The acute injuries were bilateral in one and unilateral in two cases. The nine healing injuries were accompanied by varying degrees of thickening of the hypertrophic zone of growth-plate cartilage. Seven of the nine healing injuries demonstrated localized areas of hypertrophic cartilage extension. In six of these seven lesions, a corresponding radiolucent extension of the growth plate into the metaphysis was seen. In general, when the osseous injury was focal, the corresponding radiolucent extension was focal (Fig. 1). With more extensive injury, the areas of radiolucent extension tended to be broader and multiple (Fig. 2).

In the two instances of diffuse thickening of the hypertrophic zone, a bucket-handle pattern was evident radiologically, but no localized extension of the growth plate into the metaphysis was present to indicate healing. The four lesions without histologic evidence of healing showed no focal metaphyseal radiolucency comparable to that seen in the healing group.

Histomorphometric measurements from the area of healing were compared with the measurements from the adjacent normal area in eight instances. In one healing injury no adjacent normal measurements were possible; thus, only eight healing injuries were analyzed. Statistical analysis with paired t tests showed a significant difference ($p < .001$) between the absolute measurement of the hypertrophic zone in the area of healing compared with the adjacent normal area. A

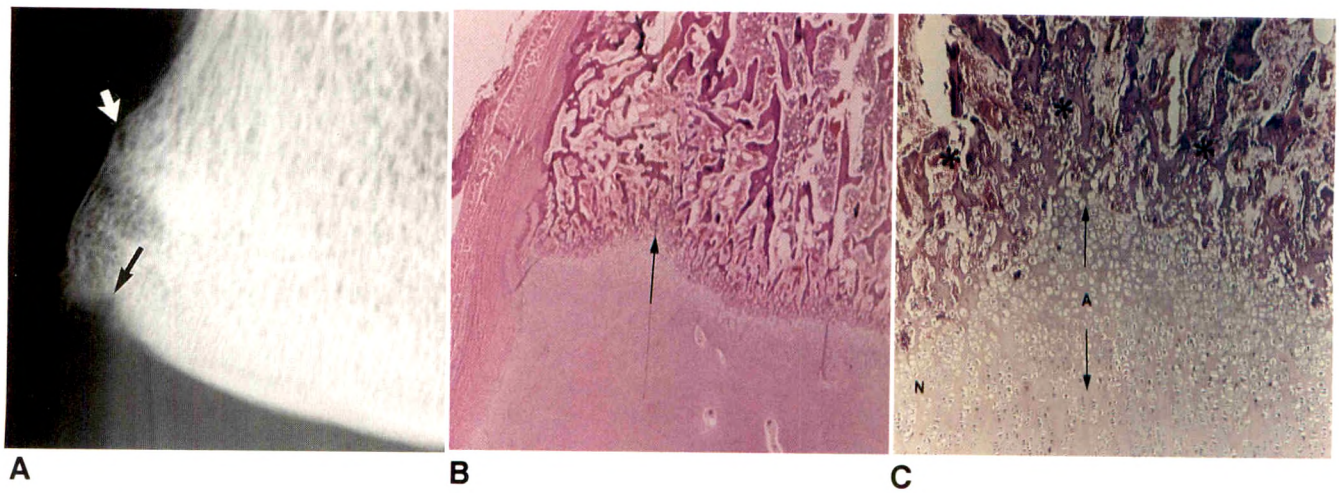



Fig. 1.—Focal osseous injury.

*A*, Postmortem industrial radiograph of medial aspect of distal tibia in a 3-month-old infant shows a corner-fracture type of injury (*white arrow*) and radiolucent extension of growth plate into primary spongiosa (*black arrow*).

*B*, Corresponding low-power histologic section shows extension of growth-plate cartilage into primary spongiosa (*arrow*), which corresponds closely to lucent extension evident radiologically in *A*.

*C*, Medium-power view of same region. A healing osseous injury is noted through primary spongiosa (*asterisks*). A focal increase in thickness of hypertrophic zone at site of extension of growth-plate cartilage into primary spongiosa (A) is visible. Compare thickness of hypertrophic zone in abnormal area with that in adjacent normal margin (N).

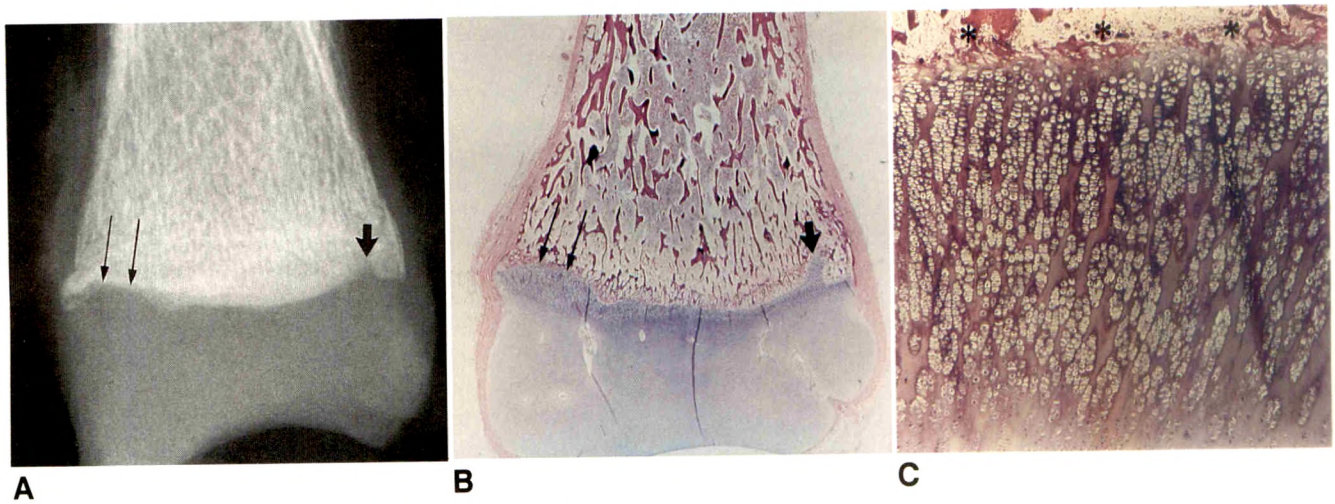



Fig. 2.—Diffuse osseous injury. Distal tibia of 3½-month-old infant.
*A*, Postmortem specimen radiograph shows extensive metaphyseal injury with broad extension of radiolucent growth plate into medial tibial margin (*long arrows*). Bucket-handle pattern is evident at this site. Laterally, a more focal invagination is present with a corner-fracture type of pattern (*short arrow*).
*B*, Low-power histologic section shows extensive injury involving primary spongiosa across metaphysis. Diffuse cartilage extension is noted medially (*long arrows*) and a focal extension is noted laterally (*short arrow*), corresponding to findings on radiograph.
*C*, Medium-power photomicrograph through diffuse injury shows a marked increase in thickness of hypertrophic zone. Note trabecular disruption and resorption at site of osseous injury (*asterisks*).

significant difference also occurred between the CHIs (ratios of the hypertrophic zone to the proliferative zone) in each area ($p < .001$). No significant difference was noted between the absolute measurement of the proliferative zones at sites of healing and the adjacent normal areas. The analysis provided a mean value for the thickness of the normal hypertrophic zone of 0.29 ± 0.05 mm. The abnormal hypertrophic zone had a mean thickness of 1.27 ± 0.43 mm.

Histomorphometric measurements in the normal opposite tibia and in the distal tibia of an infant who died of accidental injury were significantly different from those in infants with healing injuries ($p < .01$). Because of the small number of acute injuries and the difficulty in obtaining measurements of the adjacent normal area, data from the four infants with nonhealing fractures were not formally analyzed; however, there appeared to be no significant difference between the injured and normal areas.

## Discussion

The current study confirms the hypothesis that an increase in the thickness of the hypertrophic cell zone of the growth-plate cartilage occurs with healing of a metaphyseal fracture. When localized, this extension of cartilage into the primary spongiosa has a lucent counterpart radiologically. This radiologic appearance does not seem to occur in lesions without healing, and is therefore of potential value as an indicator of healing fracture.

Diffuse increase in the thickness of the hypertrophic zone is known to occur with a variety of pathologic processes. It has been described in cartilaginous injuries extending through the proliferative zone in experimental animals [13]. It occurs in rickets [14]. It has recently been noted in mucolipidosis II [15]. Radiographs in these entities reveal apparent widening of the growth plate. The experiments of Trueta and Amato [11], in which metaphyseal vascularity was disrupted, revealed a similar increase in the number of hypertrophic chondrocytes with penetration into the metaphysis. Caffey [16] suggested that vascular injury played a role in the premature fusion of the growth plate observed in some cases of inflicted injury.

The current concepts regarding the role of metaphyseal vasculature in the biology of the chondroosseous junction provide support for the view that the thickening of the hypertrophic zone in the metaphyses of abused infants also is caused by a vascular injury [12, 17, 18].

Each lacuna contains a normal-appearing hypertrophied chondrocyte (Fig. 3). The last chondrocyte in an individual column, the terminal chondrocyte, can be seen to undergo a morphologic change preceding cell death and subsequent vascular penetration of the lacunae. Current evidence suggests that a signal is provided by the metaphyseal vasculature that initiates the changes leading to cellular death [19]. Vascular invasion of the chondrocyte lacunae takes place, and mineralization of osteoid deposits around the cartilage cores derived from the growth plate occurs. Thus, the anatomic site of the most distal portion of hypertrophic cartilage is transformed to the most proximal portion of primary spongiosa. This results in an incremental shift of the chondroosseous junction away from the diaphysis and provides longitudinal growth of the bone.

This concept can be applied to the metaphyseal injury currently under study, and a hypothesis regarding the devel-

opment of cartilage hypertrophy caused by a vascular injury can be developed (Fig. 4). As has been pointed out, metaphyseal injury generally occurs in a planar fashion [10]. This injury extends across the primary spongiosa and may involve all or only a portion of the metaphysis. The injury results in varying degrees of vascular disruption. Those regions supplied by this vasculature lose the signal that normally leads to death of the terminal chondrocyte. A focal osseous growth arrest occurs with persistence of the terminal chondrocyte. The continued proliferation of cells proximally, and survival of cells distally, results in a net increase in the number of cells present within the affected cartilage columns. When the injury is localized, the endochondral bone growth normally occurring adjacent to the site of metaphyseal vascular injury gradually surrounds a projection of cartilage persisting within primary spongiosa. With increasing growth, these surviving chondrocytes are found deeper and deeper within the primary spongiosa. When vascular injury is diffuse, a broad region of thickening of the hypertrophic zone will be encountered.

This histologic indicator of healing injury appears to have a clear radiologic correlate, as shown in this study. Radiologically, these extensions of hypertrophied chondrocytes into the metaphysis are seen as zones of lucency that are continuous with the growth plate. They may be single and focal with minimal osseous injury or broad and multiple with extensive injury. They can provide the only indication that a fracture is in a healing phase.

This study shows that the depth of penetration of the radiolucent growth plate into the metaphysis corresponds to the length of the adjacent bone that has formed since the injury occurred. As relative rates of growth of various long bone metaphyses in infancy are known [19, 20], it may be possible to estimate the minimum age of a focal metaphyseal injury on the basis of its radiologic appearance. These concepts are being evaluated further with a larger group of more varied pathologic material. At this time, however, there is sufficient evidence to conclude that focal radiolucent extension of the growth-plate cartilage into the metaphysis is an indication of healing fracture.

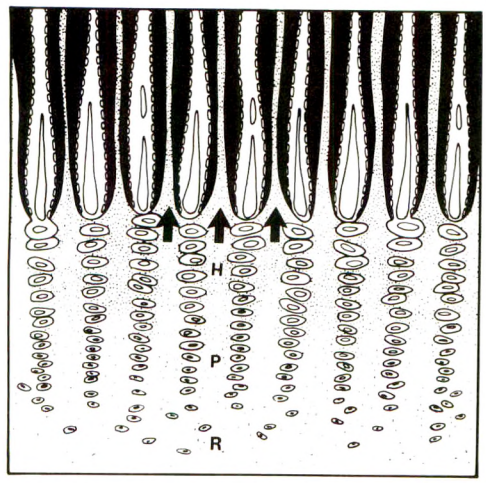



**Fig. 3.—Normal growth plate. Schematic representation of normal growth plate and primary spongiosa shows cartilage columns within physis. An orderly pattern of maturation of chondrocytes is present. At chondroosseous junction, bone is laid down around cartilage cores (*arrows*). H = hypertrophic chondrocyte zone, P = proliferative chondrocyte zone, R = resting chondrocyte zone.**

ACKNOWLEDGMENTS

We thank Kathy Delongchamp for preparing the manuscript, Stephen Baker for statistical analysis, Joan Zeveska for editorial assistance, and William Koenigsberg of G.T.E. Corporation for assistance with high-detail radiography.

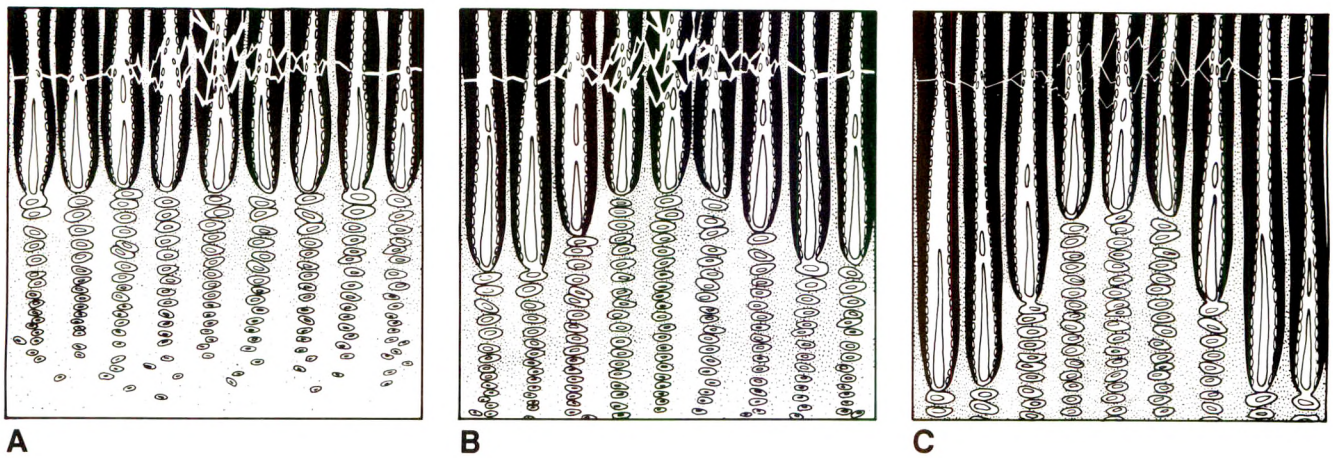



**Fig. 4.—Schematic representation of development of cartilage extension into metaphysis.**
***A*, A fracture is noted through primary spongiosa with maximal disruption and vascular injury centrally.**
***B*, With healing, osseous growth is arrested centrally with persistence of hypertrophic chondrocytes. Growth continues peripherally.**
***C*, With further healing, this focal extension into primary spongiosa is increased, and continued osseous growth is evident at margins. Note that original level of chrondroosseous junction centrally is maintained owing to growth arrest. A normal increment of longitudinal growth has occurred peripherally. A quantification of this incremental growth may provide an estimate of minimum time that has elapsed since original injury.**

## REFERENCES


1. Caffey J. Some traumatic lesions in growing bones other than fractures and dislocations: clinical and radiologic features. *Br J Radiol* **1957**;30: 225–238
2. Silverman FN. Unrecognized trauma in infants, the battered child syndrome, and the syndrome of Ambroise Tardieu: Rigler lecture. *Radiology* **1972**;104:337–353
3. Kempe CH, Silverman FN, Steele BF, Droegemueller W, Silver HK. The battered-child syndrome. *JAMA* **1962**;181:105–112
4. Barrett IR, Kozlowski K. The battered child syndrome. *Australas Radiol* **1979**;23:72–82
5. Kleinman PK. *Diagnostic imaging of child abuse*. Baltimore: Williams & Wilkins, **1987**:5–102
6. Haller JO, Kassner EG. The "battered child" syndrome and its imitators; a critical evaluation of specific radiological signs. *Appl Radiol* **1977**;6: 88–111
7. Kogutt MS, Swischuk LE, Fagan CJ. Patterns of injury and significance of uncommon fractures in the battered child syndrome. *AJR* **1974**;121: 143–149
8. Merten DF, Radkowski MA, Leonidas JC. The abused child: a radiological reappraisal. *Radiology* **1983**;146:337–381
9. Leonidas JC. Skeletal trauma in the child abuse syndrome. *Pediatr Ann* **1983**;12:875–881
10. Kleinman PK, Marks SC, Blackbourne BD. The metaphyseal lesion in abused infants: a radiologic-histopathologic study. *AJR* **1986**;146: 895–905
11. Trueta J, Amato VP. The vascular contribution to osteogenesis. III. Changes in the growth cartilage caused by experimentally induced ischaemia. *J Bone Joint Surg [Br]* **1960**;42-B:571–587
12. Farnum CE, Wilsman NJ. Morphologic stages of the terminal hypertropic chondrocyte of growth plate cartilage. *Anat Rec* **1987**;219:221–232
13. Salter RB, Harris WR. Injuries involving the epiphyseal plate. *J Bone Joint Surg [Am]* **1963**;45-A:587–622
14. Aegerter E, Kirkpatrick JA Jr, eds. Metabolic diseases of bone. In: *Orthopedic diseases: physiology, pathology, radiology*, 4th ed. Philadelphia: Saunders, **1975**:341–348
15. Pazzaglia UE, Beluffi G, Campbell JB, Bianchi E, Colavita N, Diard F, et al. Mucolipidosis II: correlation between radiological features and histopathology of bones. *Pediatr Radiol* **1989**;19:406–413
16. Caffey J. Traumatic cupping of the metaphyses of growing bones. *AJR* **1970**;108:451–460
17. Farnum CE, Wilsman NJ. Condensation of hypertrophic chondrocytes at the chondro-osseous junction of growth plate cartilage in Yucatan swine: relationship to long bone growth. *Am J Anat* **1989**;186:346–358
18. Farnum CE, Wilsman NJ. Cellular turnover at the chondroosseous junction of growth plate cartilage: analysis by serial sections at the light microscopical level. *J Orthop Res* **1989**;7:654–666
19. Maresh MM. Linear growth of long bones of extremities from infancy through adolescence. *Am J Dis Child* **1955**;89:725–742
20. Pavlov S, Petrov I. Caracteristique morphometrique des os des membres chez les nouveau-nes. *Gegenbaurs Morphol Jahrb* **1971**;117:145–161

# Book Review

**Nuclear Medicine Annual 1990.** Edited by Leonard M. Freeman. New York: Raven, 256 pp., 1990. $98

This annual book, as it begins its second decade, is a compilation of nine thorough state-of-the-art reviews on currently existing procedures in nuclear medicine and also the major areas of "cutting-edge" research in this field. These articles were written by a renowned international group with expertise in each field. The result is an excellent review book with exceptionally readable materials, illustrations, and narratives that are of excellent quality. The references and subject index are comprehensive. Throughout, this book is enriched with the authors' extensive experiences, as well as those of others in each field.

The articles are entitled "Bone Scanning in Osteoporosis: The Role of the Radionuclide Bone Scan and Photon Absorptiometry," "Nuclear Medicine in the Management of the AIDS Patient," "Functional Brain Imaging with Single-Photon Emission Computed Tomography Using $^{99m}$Tc-Labeled HMPAO," "Assessing Coronary Angioplasty with Myocardial Perfusion Imaging," "Radioimmunoscintigraphy of Cancer: Problems, Pitfalls and Prospects," "Design and Use of Radiation Detector Probes for Intraoperative Tumor Detection Using Tumor-Seeking Radiotracers," "Role of Radiopharmaceuticals in Detection of Osteomyelitis," "The Use of Radiopharmaceuticals in the Measurement of Glomerular Filtration Rate," and "Radionuclide Cystography."

In "Bone Scanning in Osteoporosis," the quantification of skeletal uptake of $^{99m}$Tc-diphosphonate and the measurement of bone mass and their clinical and research applications are discussed extensively. In the chapter on functional brain imaging, the pharmacology of $^{99m}$Tc-HMPAO and the clinical usefulness of HMPAO brain single-photon emission CT are thoroughly presented. In "Radioimmunoscintigraphy of Cancer," many problems and pitfalls related to the antigen, antibody, radionuclide, radiolabeling, and imaging techniques are reviewed, and future prospects and ongoing progress in overcoming the difficulties are mentioned briefly. In the chapter on radiation detector probes, clinical experience with various intraoperative probes for tumor detection is discussed fully, and future directions for tumor-detecting probes are stated. The chapter on nuclear medicine and AIDS adequately reviews complications of AIDS and discusses the clinical role of nuclear medicine techniques with various radiopharmaceuticals.

The chapter on myocardial perfusion scintigraphy reviews the current status of myocardial scintigraphy as a noninvasive means of assessing and monitoring patients who need percutaneous transluminal coronary angioplasty.

The chapter on radiopharmaceuticals and osteomyelitis reviews various imaging techniques used to detect osteomyelitis in patients with diabetes and sickle cell disease. The chapter on radiopharmaceuticals and measurement of glomerular filtration rate (GFR) examines the concept of GFR and reviews various methods of GFR measurement with relative diagnostic accuracy. "Radionuclide Cystography" reviews imaging techniques and their clinical role to evaluate vesicoureteral reflux.

The cost of this book is somewhat prohibitive compared with that of other recent texts; however, for those interested in reviewing updated information on functional nuclear brain imaging, radioimmunoscintigraphy, radiation detector probes for tumor detection, osteoporosis, and glomerular filtration rate, this book provides useful information in a readable and succinct style. I recommend this book to nuclear medicine specialists. It also should be available in imaging or hospital libraries. It is unlikely that it would be useful to general radiologists, residents, fellows, or students.

E. Edmund Kim
*M. D. Anderson Cancer Center*
*University of Texas*
*Houston, TX 77030*

Pictorial Essay

# Normal Metaphyseal Radiologic Variants Not to Be Confused with Findings of Infant Abuse

Paul K. Kleinman,[1] Patricia L. Belanger, Andrew Karellas, and Melissa R. Spevak

**Postmortem high-detail skeletal radiography of 78 infants who died of the sudden infant death syndrome was performed during a 3-year period. Review of the studies reveals a variety of distinct radiologic variants that should not be confused with the metaphyseal injuries caused by infant abuse.**

The development of clinical high-detail radiographic systems has led to refinements in the detection and delineation of metaphyseal injuries in infant abuse. A wide variety of patterns of metaphyseal injury have been described, and visualization depends on both the morphology of the injury and technical factors [1–4]. Expectedly, these high-resolution radiographic systems also result in definition of anatomic variations that were difficult to appreciate with earlier techniques.

During the past 3 years, postmortem radiography has been performed in 78 cases of the sudden infant death syndrome studied at the chief medical examiner's office in Worcester. Surveys were performed according to a standard protocol [3] with a high-detail single-emulsion film, single high-detail screen, and cassettes with either a standard or a carbon-fiber front plate. A variety of configurations of the long-bone metaphyses have been encountered that may be confused with the metaphyseal lesions associated with abuse. The purpose of this pictorial essay is to familiarize the reader with these variable appearances of the normal metaphyses to allow differentiation from bona fide metaphyseal injury in abused infants.

### Step-off

This is an acute angulation in the extreme portion of the metaphysis adjacent to the physis (Fig. 1). This results in a near 90° angulation in the cortex. The adjacent cortical margins are often indistinct, a finding that correlates with the histologic findings. The trabecular pattern is maintained throughout this area. It is seen in the distal femur (3% of our patients), proximal tibia (4%), proximal fibula (1%), distal radius (15%), and distal ulna (5%). It is bilateral in 41% of cases.

### Beak

This is a medial projection (Fig. 2) seen off the proximal humerus (16%) and proximal tibia (1%). In the humerus, the beak tends to be well defined and is often quite dense. In the tibia, the lesion is somewhat less distinct. It is bilateral in 77% of cases.

### Proximal Tibial Cortical Irregularity

This curious finding (Fig. 3) is seen only in the tibia (4%). It consists of an area of focal cortical irregularity in the medial aspect of the proximal tibial metaphysis. The appearance suggests focal periosteal new-bone formation. It may be seen in association with physiologic periosteal reaction. It is bilateral in 25% of cases.

Received August 31, 1990; accepted after revision October 18, 1990.

[1] All authors: Department of Radiology, University of Massachusetts Medical Center, 55 Lake Ave., N., Worcester, MA 01655. Address reprint requests to P. K. Kleinman.

 0361–803X/91/1564–0781 © American Roentgen Ray Society

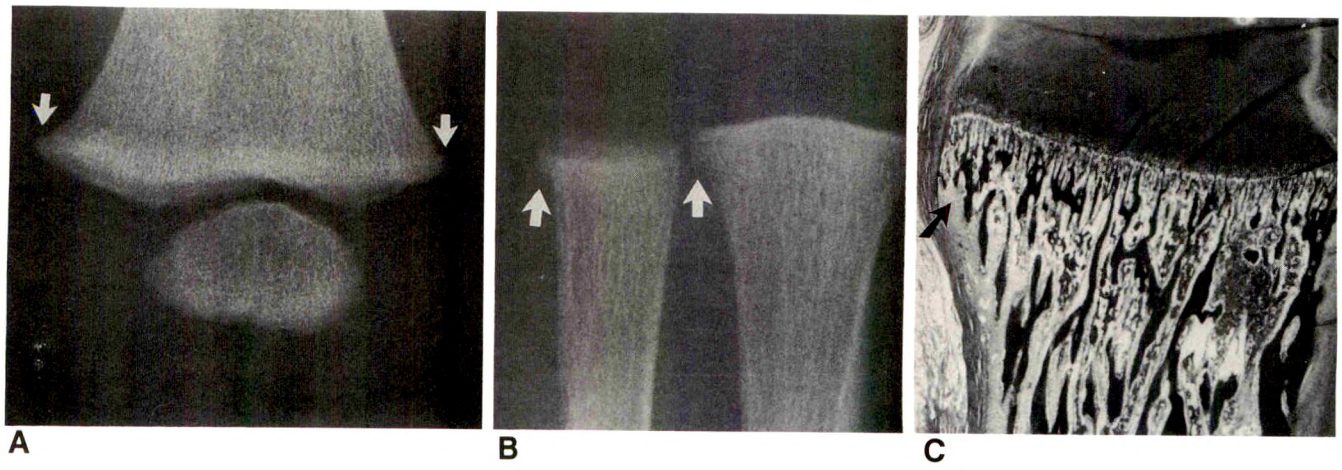



Fig. 1.—Step-off.
*A* and *B*, Note acute angulation (*arrows*) of distal femur of a 5-month-old infant (*A*) and distal radius and ulna of a 2-month-old infant (*B*).
*C*, A corresponding histologic section of distal ulna of another infant shows a focal paucity of cortical bone corresponding to radiologic step-off pattern (*arrow*).

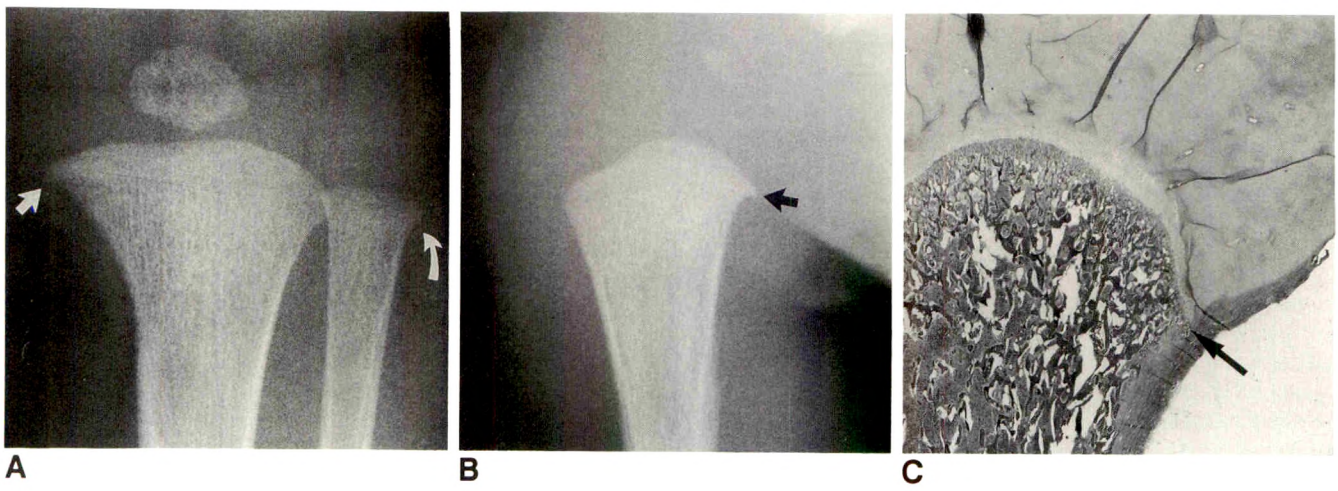



Fig. 2.—Beak.
*A*, A poorly defined medial projection is noted arising from proximal tibial metaphysis (*straight arrow*) in this 3-month-old infant. Also note step-off pattern of proximal fibula (*curved arrow*).
*B*, A dense medial projection (*arrow*) is noted arising from proximal humerus in this 2-month-old infant.
*C*, A histologic section of proximal humerus from another infant shows a medial extension of metaphysis corresponding to this beak (*arrow*).



Fig. 3.—Proximal tibial cortical irregularity. A slightly raised area with indistinct cortical margins (*open arrow*) is noted along medial aspect of proximal tibia of this 1-month-old infant. A proximal tibial step-off is noted (*solid arrow*). Note fine physiologic periosteal reaction along medial aspect of diaphysis.

### Spur

This is a discrete longitudinal projection of bone that is continuous with the cortex and extends beyond the metaphyseal margin (Fig. 4). It appears to represent an extension of cortex beneath the perichondrial ring of the physis. It is noted in the lateral aspect of the distal femur (1%), the lateral aspect of the distal radius (3%), the medial aspect of the distal ulna (3%), and also can be seen in the metacarpals (1%) and metatarsals (1%) laterally. It is bilateral in 25% of cases.

These normal variations may initially raise concerns of abuse. However, careful analysis shows them to be quite

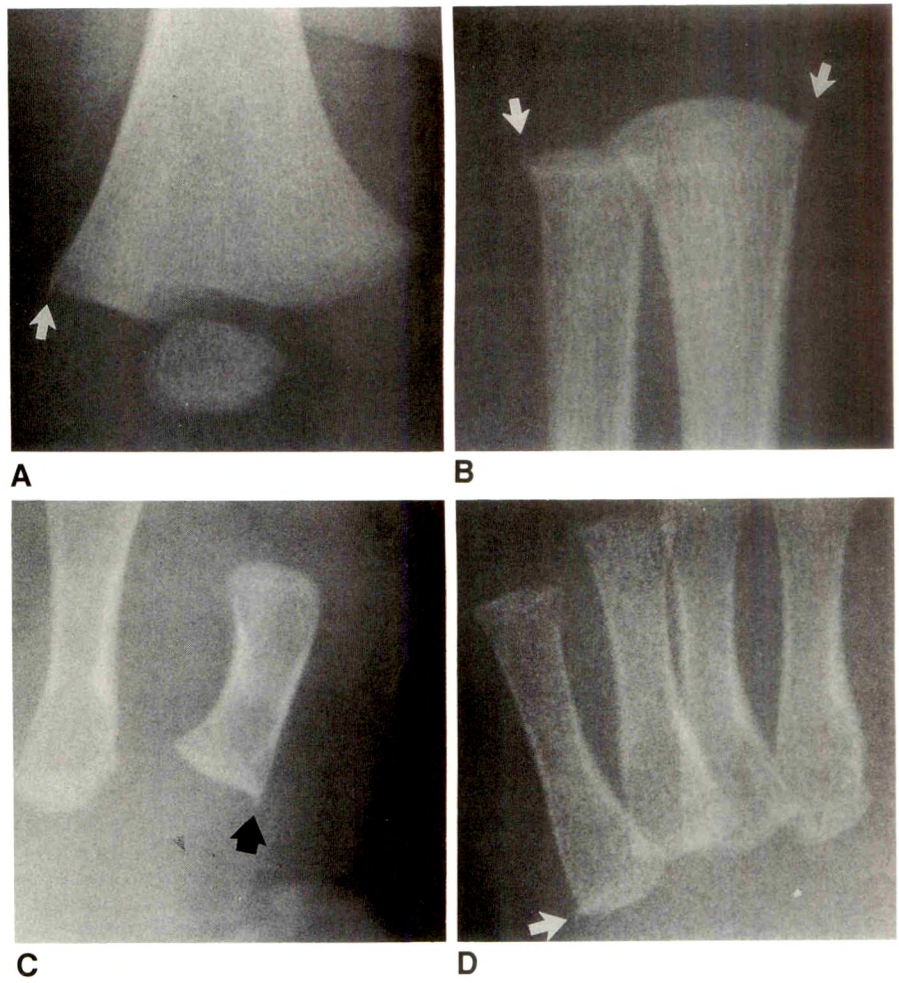



**Fig. 4.—*A–D*, Spurs (*arrows*) arise from lateral aspect of femur of a 6-week-old infant (*A*), from distal radius and ulna of a 2-month-old infant (*B*), from base of first metacarpal in a 3-month-old infant (*C*), and from base of fifth metatarsal of a 6-week-old infant (*D*).**

distinct from the metaphyseal injuries found in infant abuse. High-detail radiographs in several projections will reveal metaphyseal lesions to be discrete fracture fragments separated by a radiolucency from the remainder of the metaphysis. In contrast, these normal variants are simply contour changes in the absence of a separate osseous fragment. Familiarity with these variants and the application of high-detail radiographic techniques in skeletal surveys performed for abuse should minimize any diagnostic difficulties.

REFERENCES

1. Caffey J. Some traumatic lesions in growing bones other than fractures and dislocations: clinical and radiological features. *Br J Radiol* **1957**;30:225–238
2. Kleinman PK, Marks SC Jr, Blackbourne B. The metaphyseal lesion in abused infants: a radiologic-histopathologic study. *AJR* **1986**;146:895–905
3. Kleinman PK. Diagnostic imaging of infant abuse (review article). *AJR* **1990**;155:703–712
4. Kleinman PK. Skeletal trauma: general considerations. In: *Diagnostic imaging of child abuse.* Baltimore: Williams & Wilkins, **1987**:5–28

# Book Review

**MRI.** Musculoskeletal System. By Javier Beltran. New York: Gower Medical (distributed by Lippincott, Philadelphia), 250 pp., 1990. $79.50

Javier Beltran, a well-known authority, has drawn on his extensive experience to produce a state-of-the-art text on the use and limitations of MR imaging in the study and treatment of musculoskeletal disorders. *MRI: Musculoskeletal System* depicts detailed multiplanar anatomy through high-quality MR images obtained with a high-field-strength magnet. Images included provide the best possible examples of common and infrequent pathologic conditions. Concise text and detailed line drawings accompany and facilitate interpretation of the images.

Each chapter opens with a description of the pertinent imaging techniques. Following each introductory section is a discussion of the normal anatomy of the specific articulation, with extensive illustrations. The third section of each chapter is devoted to the pathologic processes that affect the particular site in question. Special chapters are devoted to tumors and infections, and the first chapter provides a clear and concise explanation of the basic physical principles of MR imaging, including image formation, pulse sequences, and artifacts related specifically to musculoskeletal imaging.

The book includes 400 high-quality, striking MR images from one of the most prolific MR imaging centers in the United States, which greatly helps the reader identify normal and pathologic conditions. Schematic diagrams trace the chain of decision making, indicating situations in which MR is the diagnostic technique of choice. Technical considerations for each joint are included at the beginning of each chapter. Specific chapters on the temporomandibular joint, the shoulder, the elbow, the hand and wrist, the pelvis and hip, the knee, the ankle and foot, the spine, musculoskeletal tumors, and musculoskeletal infections are included. A detailed discussion of bone marrow diseases is found in chapter 6, "The Pelvis and Hip," as most diffuse marrow abnormalities can be seen in the pelvis. Avascular necrosis is covered as a separate entity in the chapters dedicated to the joints.

The intent of this book is to acquaint the reader with the common MR manifestations of musculoskeletal disorders. Most of the images presented were obtained with 1.5-T superconducting magnets (Signa, General Electric). The technical considerations discussed in each chapter, therefore, are based primarily on the technical parameters used at this field strength. Readers interested in more detailed discussion of the physics and imaging techniques of MR are referred to widely available texts on the subject.

Beltran painstakingly has matched images of striking clarity with diagrams documenting their anatomic correlation and pathologic findings that allow readers of all levels of expertise access to his diagnostic acumen. The book provides significant insight into the theory, technology, interpretation, and usefulness of MR imaging and would be a valuable acquisition for any physician who deals with afflictions of the musculoskeletal system. The book is well worth its moderate cost and compares favorably with other available texts on the subject, including those by Mink and Stoller.

David J. Sartoris
*University of California, San Diego*
*La Jolla, CA 92093*

# Osteomyelitis of the Talus: An Unusual Cause of Limping in Childhood

J. Damien Grattan-Smith[1]
Milton L. Wagner[1]
Douglas A. Barnes[2]

**Hematogenous osteomyelitis of the talus is a rare and infrequently considered cause of limping in children. We describe five children younger than 2 years of age with osteomyelitis of the talus who had a limp and a paucity of constitutional symptoms. Conventional radiography and scintigraphy were the imaging techniques used. The usual radiologic features include soft-tissue swelling and an osteolytic defect in the talus without sequestrum formation or periosteal reaction. Bone scans were positive in all cases and led to the localization of the lesion in two patients. Definitive diagnosis was made in all cases only after needle aspiration or open biopsy and curettage.**

**Increased awareness of this unusual lesion and its subtle early radiologic manifestations will allow prompt diagnosis and treatment.**

***AJR* 156:785–789, April 1991**

Considerable literature exists that describes the diagnosis and therapy of limping in children [1–3]. An awareness of the numerous causes is essential in early detection of the abnormality. One such lesion that has received little attention is osteomyelitis of the talus. This disease is often subacute, and as such its diagnosis and definitive treatment are often delayed. The diagnostic difficulty is accentuated by the inability of the young child to provide a detailed history.

Five infants with proved osteomyelitis of the talus are described. Symptoms consisted mainly of a limp, failure to bear weight, and ankle swelling. The usually prominent systemic features that accompany osteomyelitis were generally lacking. The delay in diagnosis from the onset of limping to the institution of therapy ranged from 5 days to 4 weeks. The final diagnosis was made only after needle aspiration or open biopsy in all five cases.

The use of conventional radiographs of the foot and ankle, as well as scintigraphy, provided adequate imaging information in these patients before surgical intervention.

## Subjects and Methods

From October 1986 through September 1989, osteomyelitis of the talus was diagnosed in five infants referred to the Texas Children's Hospital for evaluation of a limp. Four were apparently healthy children without a history of trauma or of an underlying disorder. One child had previously been admitted for a thalamic arteriovenous malformation and had undergone angiography. Their clinical presentation, time of delay in diagnosis, and laboratory findings are summarized in Table 1. All patients had radiographs of their foot and ankle as well as technetium-99m methylene diphosphonate ($^{99m}$Tc-MDP) bone scans. Two patients also had gallium-67 citrate ($^{67}$Ga) scans. After surgical intervention or needle aspiration, all patients were treated with IV antibiotics for 2 weeks, followed by oral antibiotics until the erythrocyte sedimentation rate fell below 20 mm/hr. The patients were immobilized with a posterior splint until the surgical incision healed and the limb could comfortably bear weight. All routine

Received August 20, 1990; accepted after revision October 25, 1990.

[1] Department of Radiology, Texas Children's Hospital and Baylor College of Medicine, 6621 Fannin, Houston, TX 77030. Address reprint requests to M. L. Wagner.

[2] Department of Orthopedic Surgery, Texas Children's Hospital and Baylor College of Medicine, 6621 Fannin, Houston, TX 77030.

0361–803X/91/1564–0785
© American Roentgen Ray Society

**TABLE 1: Clinical and Laboratory Features**

| Case | Age (months) | Sex | Symptoms Before Admission | Physical Examination | ESR[a] | WBC[b] |
|---|---|---|---|---|---|---|
| 1 | 21 | M | 5 days—limp | Afebrile, no erythema, minimal left ankle tenderness | 25 | 10.8 |
| 2 | 21 | M | 7 days—limp | Febrile but not in toxic state, no erythema or swelling | 24 | 11.1 |
| 3 | 12 | F | 10 days—ataxia, failure to bear weight | Afebrile, normal physical examination | 20 | 11.6 |
| 4 | 16 | F | 4 weeks—limp | Afebrile, mild swelling with minimal tenderness over ankle | 45 | 5.3 |
| 5 | 19 | F | 3 weeks—refusal to walk, previous angiogram | Afebrile, swelling of left knee and ankle | 9.0 | 9.5 |

[a] ESR = erythrocyte sedimentation rate in mm/hr (normal, 0–10).
[b] WBC = white blood count in cells/$mm^3$.

cultures of the aspirates, as well as anaerobic, tuberculous, and fungal cultures, were negative except for those from cases 4 and 5, which grew *Bacteroides melaninogenicus* and *Staphylococcus aureus*, respectively. Blood cultures were negative in all cases.

*Case 1*

A 21-month-old boy had been limping for 5 days. Physical examination elicited mild tenderness over his left foot. Radiographs showed a lytic, wedge-shaped defect of the head of his left talus (Figs. 1A and 1B). The lesion extended to the subchondral surface and was associated with mild soft-tissue swelling. The medial oblique view (Fig. 1B) showed the defect to best advantage. A bone scan revealed diffuse increase in activity in the region of the tarsal bones. Under fluoroscopic guidance, needle aspiration of the talus was performed, yielding serosanguineous fluid. No organisms grew on culture of the aspirate. Follow-up radiographs in 6 weeks showed nearly complete healing of the lesion.

*Case 2*

A 21-month-old boy had been limping and favoring his left leg for 1 week. On examination, his temperature was 101°F, but he did not appear to be in a toxic condition. He had mild swelling and erythema of his left foot, but no restriction of movement. A lateral radiograph showed considerable fluid within the ankle joint and a poorly defined area of radiolucency at the posterior aspect of the body of the talus (Fig. 2A). A medial oblique view revealed a more obvious lytic lesion with destruction of the posterior cortex (Fig. 2B). No sequestrum or periosteal new bone formation was seen. The triple-phase bone scan displayed increased activity on both the blood pool and delayed images (Figs. 2C and 2D). Because clinical findings suggested a noninfectious cause, a $^{67}$Ga scan was obtained which also showed abnormally increased activity within the talus.

During surgical exploration, watery fluid was noted in both the ankle and subtalar joints. Minimal pus was encountered within the talus itself. The pathologic specimen consisted of necrotic bone and granulation tissue containing a polymorphonuclear infiltrate. No organisms were seen, and all cultures were negative.

*Case 3*

A 1-year-old girl who had previously walked unassisted had suddenly stopped bearing weight on her right foot and had begun to drag it along the ground. She was admitted to the hospital 2 days later for neurologic investigation of ataxia. Multiple studies were performed, including CT of the brain, and all results were normal. She was subsequently discharged with a diagnosis of viral labyrinthitis. Three days later she was readmitted with a continued limp. Findings on physical examination remained normal, and the provisional diagnosis on readmission was diskitis. $^{67}$Ga studies and $^{99m}$Tc-MDP bone scans revealed only mild, diffusely increased activity in the right tarsal bones. Radiographs of this region showed a destructive lesion of the posterior body of the talus accompanied by fluid within the ankle joint (Fig. 3A). Conventional tomography was used to define the nature of the lesion more precisely (Fig. 3B).

During surgery, a large amount of pus was noted in the ankle joint with marked softening of cartilage. A large defect that contained pus was found within the talus. Histologically acute and chronic synovitis were found together with acute and chronic inflammation and granulation tissue within the talus. No organisms were cultured.

*Case 4*

A 16-month-old girl who had been limping for 1 month was examined. She was afebrile and had no localizing signs. She had been extensively examined at an outside institution before a bone scan showed increased activity in her right talus. Conventional radiographs showed a lytic, subchondral defect adjacent to the right ankle joint with a slightly sclerotic margin in some areas. Only minimal soft-tissue swelling was present (Fig. 4).

Surgical exploration revealed a cavity within the posterior lateral aspect of the talus. No purulent material was encountered, but some fibrous tissue with new bone formation was identified. Cultures were positive for *B. melaninogenicus*.

*Case 5*

A 19-month-old girl was admitted to the hospital in May 1989 with seizures. During angiography and subsequent intracranial surgery she was found to have a thrombosed thalamic arteriovenous malformation. A postoperative angiogram was complicated by local infection at the puncture site in her left groin. This soon resolved, and she was discharged. Six weeks later she was readmitted with swelling of her left knee and ankle and refusal to walk. Bone scans and radiographs were consistent with talar osteomyelitis. Cortical destruction of the body of the left talus posteriorly was seen with some accompanying soft-tissue swelling (Fig. 5A). The medial oblique view showed better

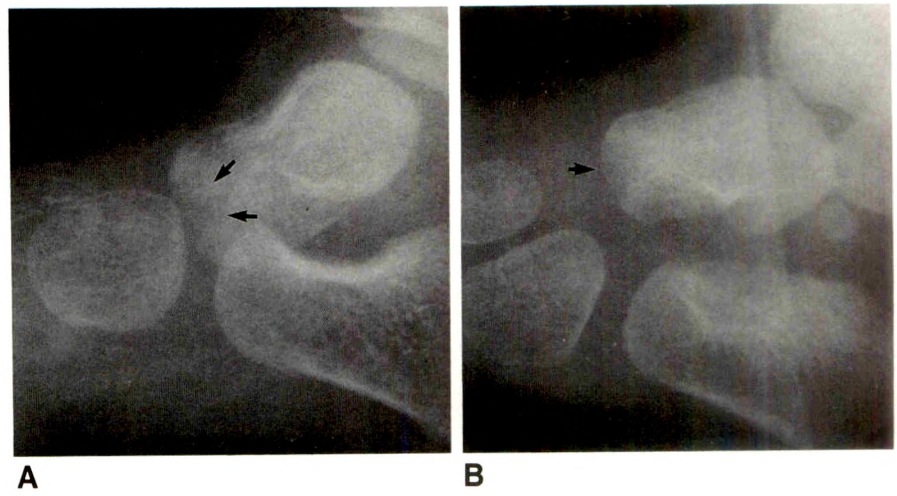



Fig. 1.—Case 1.
*A*, Lateral radiograph of ankle shows a lytic defect of head of talus (*arrows*).
*B*, Medial oblique radiograph shows defect to better advantage (*arrow*).

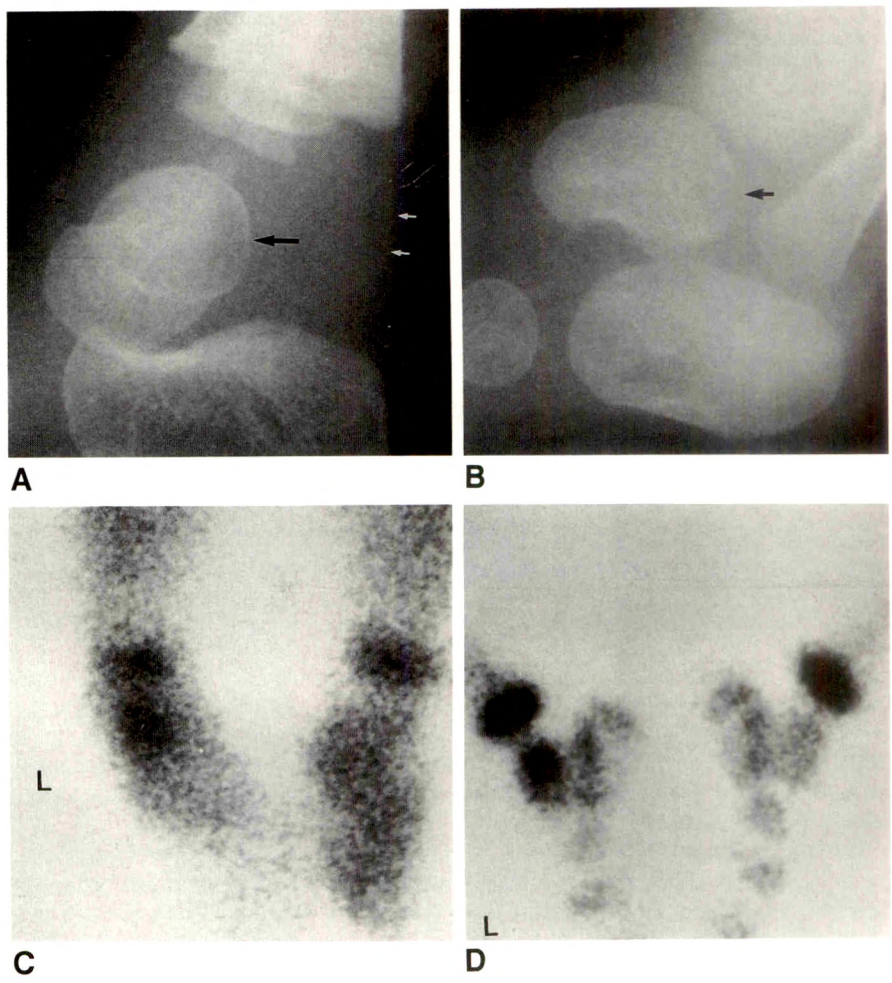


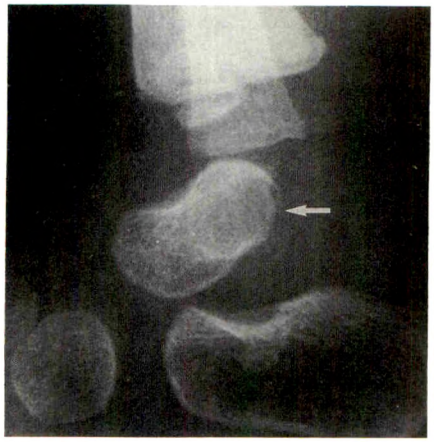

Fig. 2.—Case 2.
*A*, Lateral radiograph of ankle shows poorly defined lucent area of posterior body of talus (*large arrow*). Fluid in ankle joint displaces pretalar fat pad anteriorly, producing teardrop sign (*small black arrows*). Posterior juxtaarticular fat pad is displaced posteriorly (*small white arrows*). Pre-Achilles fat pad is compressed.
*B*, Medial oblique radiograph better delineates defect (*arrow*).
*C*, Triple phase, $^{99m}$Tc-methylene diphosphonate blood pool bone scan.
*D*, Delayed bone scans show increased activity in region of left talus.

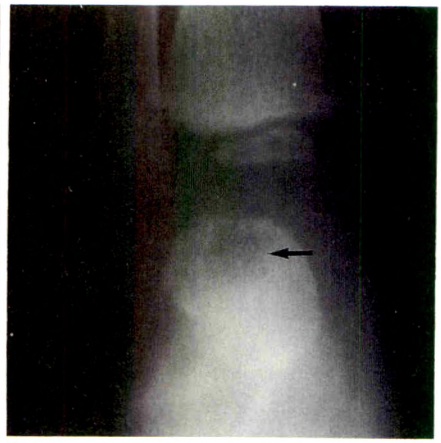
definition of the defect (Fig. 5B). No osseous abnormalities of the knee were found.

At surgery, the cartilage overlying the defect was intact. Chronic infection was noted, and considerable granulation tissue was recovered from the talus. Histologic studies showed chronic active osteomyelitis due to Gram-positive cocci. Cultures grew *S. aureus*.

## Discussion

Hematogenous osteomyelitis usually presents clinically with a rapid onset of fever, toxicity, and other systemic symptoms followed by local signs of inflammation [4–6]. It occurs more





A B

Fig. 3.—Case 3.
*A*, Lateral radiograph of ankle shows destructive lesion of posterior body of talus (*arrow*). Considerable ankle joint fluid is present with capsular bulging. Pre-Achilles fat pad is compressed, and talus appears to be distracted from calcaneus.
*B*, Frontal tomogram further defines defect (*arrow*).

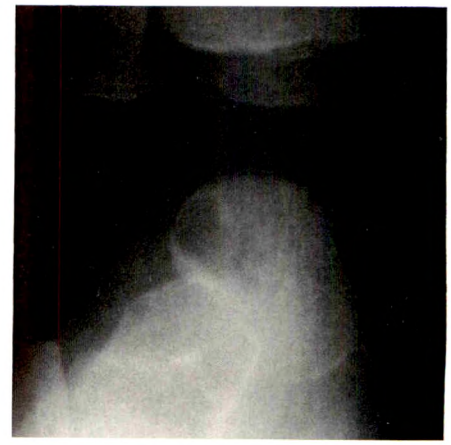
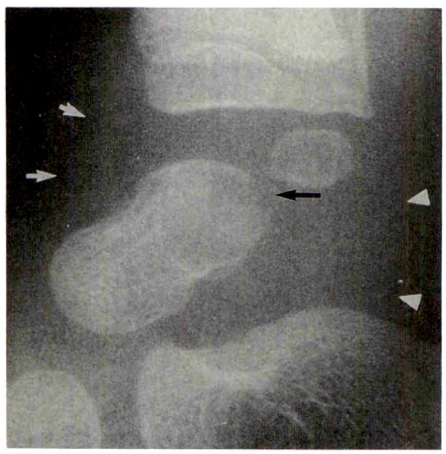
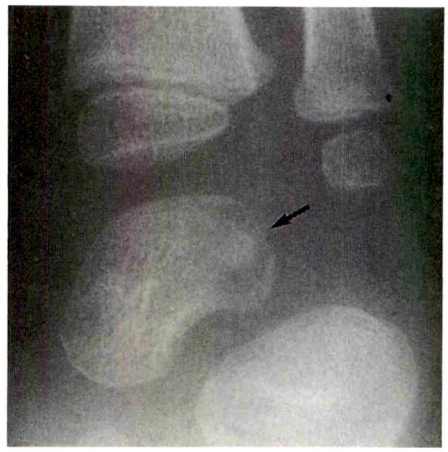


Fig. 4.—Case 4. Frontal view of ankle shows a radiolucent defect in body of talus. Minimal sclerosis is visible at inferior and lateral aspects.





A B

Fig. 5.—Case 5.
*A*, Lateral radiograph of ankle shows an irregular lucent lesion of body of talus (*black arrow*). Note teardrop sign (*white arrows*). Posterior juxtaarticular fat pad (*arrowheads*) is displaced, and pre-Achilles fat pad is compressed. Talus is separated from calcaneus.
*B*, Medial oblique radiograph again delineates area of destruction more clearly (*arrow*).

commonly in males and in children [4]. Tubular bones are most frequently involved; however, the prevalence in flat or irregularly shaped bones is 18–30% [4, 7]. Whereas osseous structures usually manifest the inflammatory reaction rather acutely, short or flat bones often present in a subacute or chronic fashion [8, 9].

Although childhood osteomyelitis is not an uncommon disease, isolated involvement of the talus is rare [10–12], and only two recent publications deal specifically with this entity [8, 9]. Nixon [7] describes flat and irregular bones, including the talus, as having anatomic subdivisions comparable to those of long bones. He has termed these subdivisions metaphyseal-equivalent locations because they have a vascular anatomy similar to that of metaphyses. These areas lie adjacent to cartilage and border apophyseal growth plates, articular cartilage, or fibrocartilage. Just as the metaphyses are commonly involved in hematogenous osteomyelitis, so are these metaphyseal-equivalent locations in flat and irregular bones affected. In his series of 49 cases with hematogenous osteomyelitis at metaphyseal-equivalent sites, only two cases involve the talus [7]. Our five cases further substantiate this principle, as all foci of destruction were located in subchondral areas.

The typical radiologic features of acute hematogenous osteomyelitis have been well described [4, 5]. When long bones in children are involved, the metaphysis is usually the primary site affected. The initial finding on radiographs is deep soft-tissue swelling, which occurs within the first 3 days after the onset of symptoms [5]. The swelling progresses with enlargement of surrounding muscles and obliteration of intermuscular fat planes. This is soon followed by subcutaneous edema. Bone destruction and periosteal new bone formation become apparent on radiographs 10–12 days after the onset of symptoms [5].

Acute inflammatory disease of the talus is frequently more subtle, both clinically and radiologically [8, 9]. Bone destruction around the head of the talus may be accompanied by some soft-tissue swelling or joint effusion. When the lesion involves the posterior and especially the superior aspect, ankle joint effusion may be prominent. When fluid distends the anterior recess of the ankle joint, the pretalar fat pad is displaced anteriorly, allowing visualization of the bulging capsule. This is known as the teardrop sign of ankle-joint effusion [13] (Figs. 2A and 5A). Posterior capsular distention distorts the posterior juxtaarticular fat pad in a similar fashion but is an inconstant radiologic finding (Figs. 2A and 5A). With large ankle effusions, the pre-Achilles fat pad may be compressed [13] (Figs. 2A, 3A, and 5A). If a subtalar effusion is present, it may spread the talus and calcaneus (Figs. 3A and 5A). A well-positioned lateral view is necessary, and comparison films of the opposite side may be needed before the effusion in this area can be verified [14]. Arthrographic examinations have shown the subtalar joint to communicate with the ankle joint in 20% of cases [15]. Early osseous destruction may be so subtle that it goes undetected initially. Multiple radiographic projections may be required to show the lesion to better advantage (Figs. 1B, 2B, and 5B), and conventional tomography confirms the suspected defect (Fig. 3B). The lack of periosteal reaction and sequestrum formation is noteworthy. In addition, the destructive lesion is usually purely lytic.

Skeletal scintigraphy usually becomes abnormal very early in the course of osteomyelitis and is highly sensitive from 24 to 72 hr after the onset of symptoms [6, 16]. The sensitivity of $^{99m}$Tc-MDP scintigrams for the diagnosis of osteomyelitis ranges from less than 60% to more than 90% [6]. $^{67}$Ga also may be helpful in suspected cases in which the $^{99m}$Tc-MDP results are equivocal.

ACKNOWLEDGMENT

We thank Warren M. Granberry for his contribution of case 5 to this manuscript.

REFERENCES

1. Phillips WA. The child with a limp. *Orthop Clin North Am* **1987**;18:489–501
2. Hensinger RN. Limp. *Pediatr Clin North Am* **1986**;33:1355–1364
3. Alexander JE, FitzRandolph RL, McConnell JR. The limping child. *Curr Probl Diagn Radiol* **1987**;16:235–270
4. Resnick D, Niwayama G. Osteomyelitis, septic arthritis, and soft tissue infection: the mechanisms and situations. In: Resnick D, Niwayama G. *Diagnosis of bone and joint disorders*, 2nd ed. Philadelphia: Saunders, **1988**:2525–2546
5. Capitanio MA, Kirkpatrick JA. Early roentgen observations in acute osteomyelitis. *AJR* **1970**;108:488–496
6. Young LW. Neonatal and infantile osteomyelitis and septic arthritis. In: Taveras JM, Ferrucci JT. *Radiology: diagnosis—imaging—intervention*, vol. 5, chapter 20. Philadelphia: Lippincott, **1989**:1–15
7. Nixon GW. Hematogenous osteomyelitis of metaphyseal-equivalent locations. *AJR* **1978**;130:123–129
8. Skevis XA. Primary subacute osteomyelitis of the talus. *J Bone Joint Surg [Br]* **1984**;66-B:101–103
9. Antoniou D, Conner AN. Osteomyelitis of the calcaneus and talus. *J Bone Joint Surg [Am]* **1974**;56-A:338–345
10. King DM, Mayo KM. Subacute haematogenous osteomyelitis. *J Bone Joint Surg [Br]* **1969**;51-B:458–463
11. Mollan RAB, Piggot J. Acute osteomyelitis in children. *J Bone Joint Surg [Br]* **1977**;59-B:2–7
12. Trueta J, Morgan JD. Late results in the treatment of 100 cases of acute haematogenous osteomyelitis. *Br J Surg* **1954**;41:449–457
13. Towbin R, Dunbar JS, Towbin J, Clark R. Teardrop sign: plain film recognition of ankle effusion. *AJR* **1980**;134:985–990
14. Eggli KD. Radiographic observations of subtalar joint effusion in two children. *Skeletal Radiol* **1989**;18:207–209
15. Resnick D. Radiology of the talocalcaneal articulations: anatomic considerations and arthrography. *Radiology* **1974**;111:581–586
16. Howie DW, Savage JP, Wilson TG, Patterson D. The technetium phosphate bone scan in the diagnosis of osteomyelitis in childhood. *J Bone Joint Surg [Am]* **1983**;65-A:431–437

# Book Review

**MRI.** Central Nervous System. Edited by Walter Kucharczyk. New York: Gower Medical (distributed by Lippincott, Philadelphia), 288 pp., 1990. $79.50

Some jobs just cannot be done with a book. In a rapidly changing field such as MR, a few sets of words seem mutually exclusive. One such set is "compact" and "comprehensive." Another is "up-to-date" and "book." This text tries to reconcile these words, but it succeeds only partially. The price is sufficiently low ($79.50), and the book is certainly worth it. However, a little more than twice this price can bring you far more than twice this book.

The work is arranged in five chapters. The unifying theme is an attempt at presenting each anatomic portion by first reviewing normal anatomy, then talking about imaging technique, and finishing with imaging pathologic changes. The first two chapters, on the brain and skull base, are the best. They provide a nice teaching file for the casual reader. It almost seems as if the book were laid out specifically for this type of reader: The cases are presented with the pathologic diagnosis in bold type followed by a brief description outlined in color. A pictorial chart illustrating myelin maturation from 1 week to 2 years of age is provided; however, only T2-weighted images are shown. In normal term infants, T2-weighted imaging is useful only after the infant is about 6 months old. T1-weighted imaging is essential before this time in normal infants and in any case of suspected abnormal maturation of myelin. The case of venous sinus thrombosis was a poor choice. Flow-weighted gradient-echo and gadolinium-enhanced images are essential in this evaluation. Evaluation of venous infarcts and dural venous sinus flow can be confusing without these sequences. Brain metastases, a common entity, are discussed in a single paragraph and illustrated with two T2-weighted brain images, when contrast-enhanced T1-weighted images are essential.

The discussion of multiple sclerosis (MS) is disappointing. Even in a brief work, the admittedly nonspecific, but still relatively distinctive, MR characteristics of the disease could have been discussed in only one paragraph. Leaving the reader with the idea that "differential diagnosis may be impossible" is accurate, but it grossly undersells the power of MR in the diagnosis of MS.

Central pontine myelinosis is discussed as if the signal characteristics are specific for the clinical syndrome. Identical signal alteration in the pons can appear with no focal pontine signs or symptoms. Such pontine signal aberrations can be seen in all types of severe liver disease as well as in many other chronic systemic diseases. In the discussion of NPH (normal pressure hydrocephalus)-type communicating hydrocephalus, ataxia is given as one of the components of the classical clinical triad. These patients have a gait disorder, but ataxia is a poor term to describe it. The word ataxia generally is assumed to mean cerebellar ataxia. NPH patients have gait apraxia, a cerebral disorder.

The second chapter, on the skull base, suffers mainly from the near absence of contrast-enhanced images. Contrast enhancement is critical in many diseases that are manifested in and about the skull base. This chapter is otherwise so well written and illustrated that it leaves the impression that it was composed before gadolinium became widely used. This limits its usefulness. The third chapter, on the head and neck, again suffers from almost no discussion of contrast material. A beautiful diagram, one of the clearest illustrations I have seen yet of the drainage of the frontal sinus along the infindibulum and into the hiatus semilunaris, is provided. . This would have been an ideal point at which to discuss the important ostiomeatal complex, but it is never mentioned. The fourth chapter, on the orbit, lacks contrast-enhanced and fat-suppressed images. These two types of MR images are important in extending the usefulness of orbital MR. The last paragraphs in the techniques section mention these sequences as if the sequences were esoteric. Such sequences are now used daily in clinical practice. This dates the book.

The last chapter, on the spine, dwells heavily on T1-weighted images for its atlas portion. T1-weighted axial images are generally not valuable in radiculopathy, the most common spinal disorder studied with MR. The authors discuss gradient-echo and T2-weighted imaging, but they do not illustrate this imaging adequately. The chart on MR technique for examination of the cervical and thoracic spine seems to lump together freely myelopathic and radiculopathic imaging. The authors list six separate sequences for evaluating these parts of the spine, which could be taken to mean that they recommend all six sequences. Reading the technique section of the text near this chart clarifies this misconception somewhat. However, as this book seems to have been designed as a pictorial essay, charts are more important than text. Again, the lack of contrast-enhanced images and the statement that "the recent introduction of paramagnetic contrast agents will change many imaging strategies" dates the chapter.

This book is delightful to thumb through or kill time with. However, because of the simplification apparently forced by the brevity of the work and the near absence of contrast-enhanced images, I cannot recommend it as a reference work. *Clinical Magnetic Resonance Imaging* by Edelman and Hesselink is far more than twice the book. I would not purchase the Kucharczyk work for my own use, but I would recommend that any radiology library purchase a copy, as it provides a limited but useful bound teaching file at a small price.

Stephen S. Gebarski
*University of Michigan Hospital*
*Ann Arbor, MI 48109-0030*

# MR Evaluation of Spinal Dermal Sinus Tracts in Children

A. James Barkovich[1,2]
Michael S. B. Edwards[2]
Philip H. Cogen[2]

**The MR studies of seven pediatric patients with surgically proved spinal dorsal dermal sinuses were reviewed retrospectively. Five of the seven had associated congenital tumors (three epidermoids, two dermoids). The subcutaneous portions of the spinal tracts and intramedullary portions of tumor were easily identified with the use of standard spin-echo techniques. However, except for limited areas where they were lined by fat, the intraspinal portions of the dermal sinuses were poorly seen. Moreover, diffuse subarachnoid tumor was missed in two patients. Three-dimensional Fourier transform gradient-echo acquisition using a volumetric radiofrequency pulse as a "spoiler" proved to be helpful in evaluating these abnormalities.**

**Optimal radiologic workup of patients with dorsal dermal sinuses awaits the development of new MR imaging sequences. For now, heavily T1-weighted MR sequences should be obtained and supplemented with sonography in infants and with CT myelography in older children.**

*AJNR* 12:123–129, January/February 1991; *AJR* 156:791–797, April 1991

The advent of MR imaging has greatly facilitated the diagnosis of developmental anomalies of the CNS, which are now easily and noninvasively diagnosed [1–3]. The improvement in imaging techniques has been especially valuable in the spine, where the shape and location of the spinal cord and the presence of associated fatty tumors are readily demonstrated [1, 4, 5].

We have recently had the opportunity to review the imaging studies of seven patients with surgically proved spinal dermal sinus tracts, five of whom had associated dermoid or epidermoid tumors. All were examined with standard spin-echo MR techniques. We found that, in contradistinction to most spinal anomalies, spinal dorsal dermal sinuses were difficult to assess adequately by using conventional spin-echo imaging techniques. The purpose of this article is to report the pathologic anatomy of these patients as detected by MR, to compare the MR findings with the surgical findings, to point out the potential pitfalls of MR in the workup of this anomaly, and to make suggestions for the most efficacious radiologic workup.

## Materials and Methods

MR scans of seven patients with surgically proved dorsal dermal sinuses of the spine were reviewed retrospectively (Table 1). The average age of the five girls and two boys was 4 years old (range, 4 months to 11 years). Three patients were asymptomatic; the abnormalities were detected by the presence of a midline skin dimple at the lumbosacral level (one) or a focal skin dysplasia, cutis aplasia (two). Two patients presented with urinary bladder dysfunction and lower extremity spasticity; one of these patients had a dimple at the L5 level, the other at S1. Patient 6 presented because of persistent low back pain that worsened with flexion and extension. Patient 4 presented with an acute myelopathy and a C5 sensory level.

Six patients were studied at 1.5 T; the seventh was studied at 0.6 T. Sagittal 3-mm spin-

Received June 26, 1990; revision requested September 6, 1990; revision received September 27, 1990; accepted September 28, 1990.

[1] Department of Radiology, Box 0628, Neuroradiology Section, L371, University of California, San Francisco, CA 94143. Address reprint requests to A. J. Barkovich.

[2] Department of Neurological Surgery, University of California, San Francisco, CA 94143.

0361–803X/91/1564–0791
© American Roentgen Ray Society

echo (SE) 600–1000/20/2 (TR/TE/excitations) images were obtained in patients 1, 3, 4, 5, and 6, using a 256 × 192 matrix. Sagittal 5-mm SE 1800/30, 80/2 images were obtained in patient 6, and sagittal 5-mm SE 533/28/2 images were obtained in patient 2. Axial 5-mm SE 600–1000/20/2 images were obtained in patients 1, 3, 4, 5, 6, and 7. No axial images were available for patient 2.

The MR studies were assessed for the presence and level of the cutaneous lesion, the presence of any bony spinal deformities, the

**TABLE 1: Data for Seven Patients with Spinal Dermal Sinus**

| Patient No. | Age | Sex | Presenting Signs/Symptoms | Conus Level | Skin Defect Level | Character of Tract | Character of Tumor | |
|---|---|---|---|---|---|---|---|---|
| | | | | | | | Surgical | Radiologic |
| 1 | 4 mo | M | Lumbar cutis aplasia | L3–L4 | L4 | Short T1, curvilinear L2–L5 adherent to right dorsal roots | N/A | N/A |
| 2 | 6 mo | F | Thoracic cutis aplasia | T12–L1 | T10 | Intraspinal part not seen | Intra- and extramedullary dermoid at T8–T9 | Intra- and extramedullary mass at T8–T9, isointense with CSF |
| 3 | 18 mo | F | Sacral dimple | L4–L5 | L5/S1 | Lined by fat (short T1), tract itself not seen, curvilinear L3 to L4–L5 | N/A | N/A |
| 4 | 20 mo | F | Acute myelopathy, C5 sensory level | L1 | T7 | Intraspinal part not seen | Intramedullary dermoid at T3 to T5–T6 | Intramedullary mass at T3 to T5–T6, isointense with CSF |
| 5 | 3 yr | M | Lower extremity weakness and spasticity, neurogenic bladder | L3 | L5 | Intraspinal part not seen | Midlumbar extramedullary epidermoid | Midlumbar extramedullary epidermoid, circle of nerve roots surrounded mass, isointense with CSF |
| 6 | 6 yr | F | Back pain, meningismus | T12–L1 | L4–L5 | Intraspinal part not seen | Ruptured intra- and extramedullary epidermoid from T12 to sacrum | Indistinct mass, slightly short T1 |
| 7 | 11 yr | F | Back pain | Mid L3 | S1 | Intraspinal part not seen | Ruptured extramedullary dermoid, conus to sacrum | Areas of short T1 and T2, most areas isointense with CSF |

Note. — N/A = not applicable.

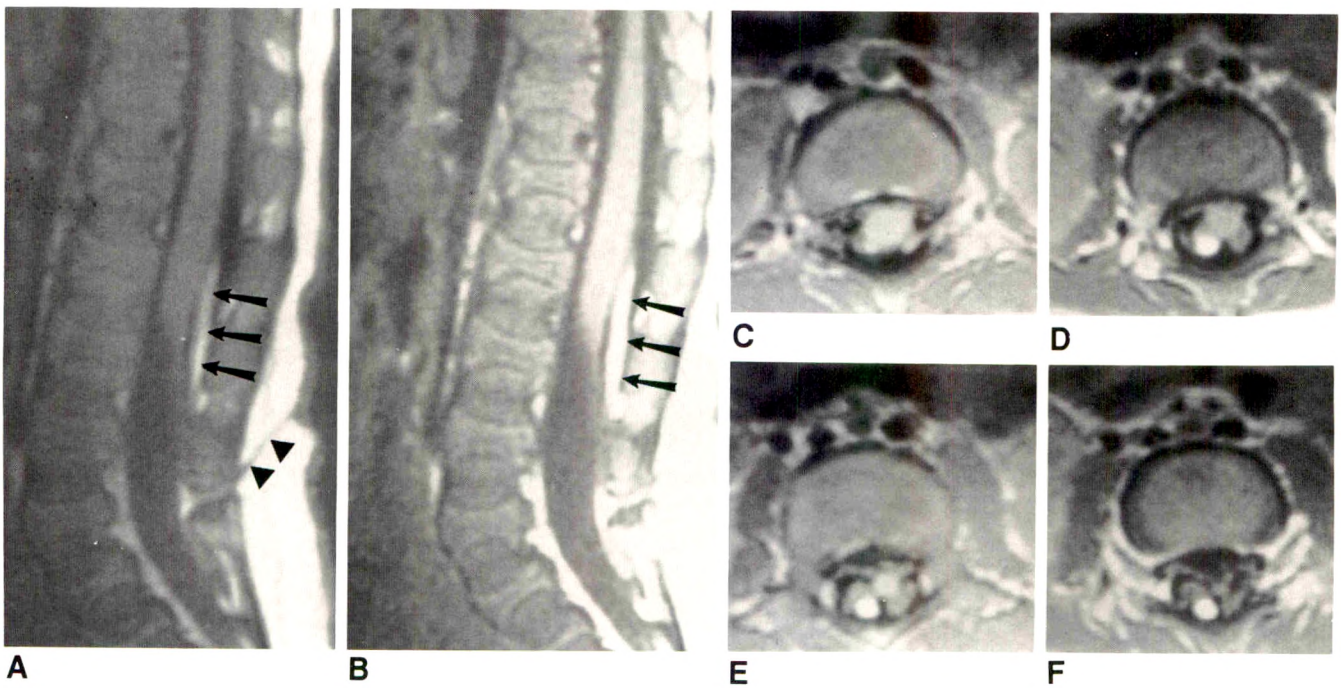



**Fig. 1.—Patient 1.**

***A* and *B*, Sagittal SE 600/20 images with wide windowing (*A*) and narrow windowing (*B*). Both images show tethering of cord, with conus at L3–L4 level and fat-filled intradural portion of dermal sinus (*arrows*) lying posterior to conus. However, subcutaneous portion of dermal sinus (*arrowheads*) is not seen on the image with narrow windowing.**

***C–F*, Axial SE 600/20 images through conus medullaris and proximal cauda equina show fat-lined dermal sinus ascending adjacent to right posterolateral nerve roots before ending in right posterolateral aspect of conus.**

level of the conus medullaris, the location and signal characteristics of the sinus tract, and the size, location, and signal characteristics of any associated dermoid or epidermoid tumors. The MR findings were then compared with surgical findings.

Follow-up examination of patient 7 included a 3D Fourier transform gradient-echo acquisition using a volumetric RF pulse as a "spoiler" (SPGR, General Electric, Milwaukee). Sagittal 2-mm 40/5/2 images were obtained using theta = 40°.

## Results

Cutaneous abnormalities were seen on the MR images in six of the seven patients. On short TR sagittal and axial images the sinus tracts and ostia were seen as linear, curvilinear, or conelike dorsal midline areas of hypointensity within the continuous layer of high-intensity subcutaneous fat (Figs. 1 and 2). The tract could sometimes be followed through the subcutaneous tissue and posterior elements of the spinal column to the dura, which was "tented" posteriorly at the site of penetration of the sac in two patients (Fig. 3). The tract coursed slightly caudally from the skin to the spine in three patients, slightly rostrally in one, and coursed straight (horizontally) in two. Proper window settings were critical in the detection of subcutaneous tracts. In patient 1, the subcutaneous tract was not seen when standard window settings were used (Fig. 1). The lack of visualization of the subcutaneous tract in patient 7 probably relates to improper windowing.

The dermal sinus tracts themselves were not visible in their intraspinal portion. Portions of the tract were detected in patient 3, in whom it was lined by fat, and in patients 1 and 7, in whom fatty material was present within a portion of the tract (Fig. 1). Aside from these three locations, the intraspinal portions of the tracts could not be detected, presumably because of their small size and their isointensity with CSF on the short TR/TE images obtained. In the patients in whom portions of the tract were visible, they ascended in the dorsal aspect of the thecal sac from their point of dural penetration to the distal spinal cord. In patient 3, the tract ascended in the midline and ended in the dorsum of the conus medullaris, whereas in patient 1, the tract ascended adjacent to the right posterior nerve roots of the cauda equina (Fig. 1) before terminating adjacent to the right posterolateral aspect of the conus. Only a small portion of the tract was seen in patient 7 (Fig. 4).

Intradural tumors were present in five patients. In three of these five the tumor was both intra- and extramedullary. Patients 2 and 4 had large (1 cm × 2½ cm) masses within the cord substance at the T8–T9 and T3–T5 levels, respectively. The masses were isointense with CSF and expanded the cord at the affected levels (Fig. 2). Extramedullary tumor components were found at surgery in both of these patients but were not detected on the images that were obtained. Patient 6 had a mass that filled the entire thecal sac from the sacrum to T12 and then extended rostrally within the cord substance from the conus (at T12–L1) to T10. The extramedullary tumor was difficult to categorize on the short TR/TE sagittal and axial images, appearing as a poorly defined iso- to slightly hyperintense mass intermingling with the roots of

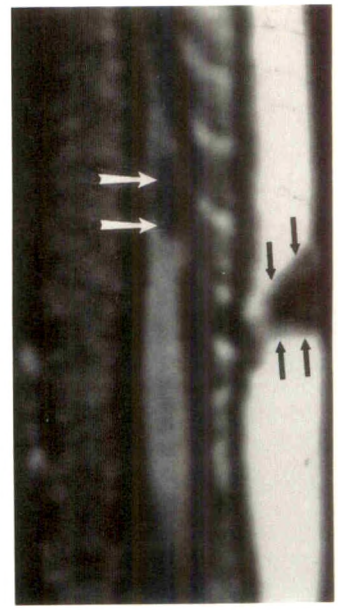


**Fig. 2.—Patient 2. Sagittal SE 600/20 image shows a large cone-shaped area of hypointensity (*black arrows*) in subcutaneous fat. This is subcutaneous portion of dermal sinus. Intraspinal portion of dermal sinus is not seen. An intramedullary dermoid is seen as an oval-shaped area of hypointensity (*white arrows*) within spinal cord at T8–T9 level.**

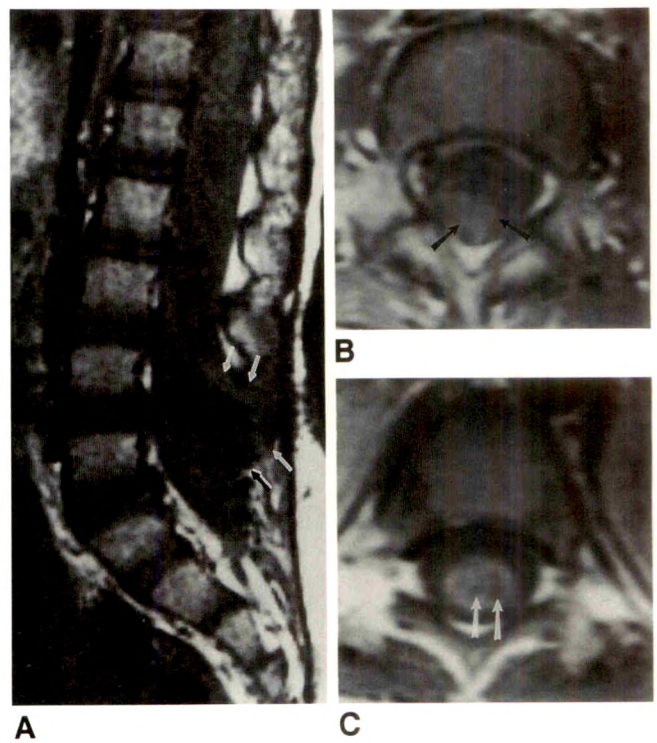



**Fig. 3.—Patient 6.**

***A*, Sagittal SE 1000/20 image shows spina bifida at L4 and L5 levels. Dorsal "tenting" of thecal sac (*arrows*) is present. Some streaky increased signal is present in thecal sac; this was interpreted as being misregistration artifact from abdominal motion.**

***B*, Axial SE 600/20 image at L2–L3 level shows hyperintense mass (*arrows*) filling a portion of subarachnoid space. At surgery, epidermoid tumor was seen filling entire lumbar thecal sac.**

***C*, Axial SE 1000/20 image at level of conus medullaris. Several foci of hypointensity are seen within cord substance (*arrows*). At surgery, hypointense area was found to be intramedullary epidermoid tumor.**

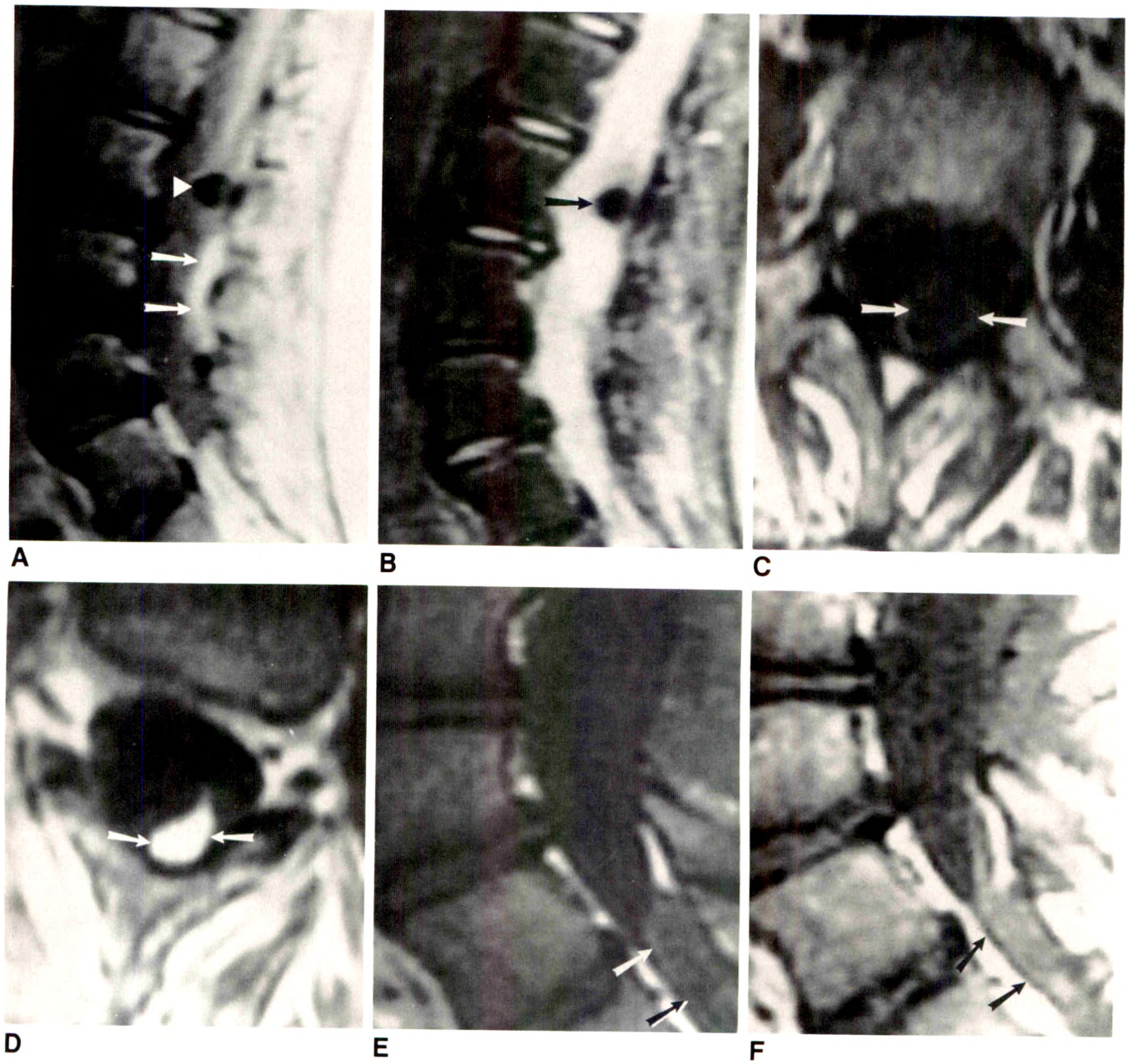



Fig. 4.—Patient 7.

*A*, Sagittal SE 1800/30 image shows conus medullaris ending at bottom of L2. A round area of hypointensity (*arrowhead*) is seen immediately caudal to conus. No focal lesion corresponding to this hypointensity was found at surgery. A curvilinear area of hyperintensity (*arrows*) is seen dorsally within canal at L4 level, corresponding to fat within dermal sinus tract. The remaining lumbar subarachnoid space looks normal. At surgery, the entire lumbar subarachnoid space was filled with ruptured dermoid tumor.

*B*, SE 1800/80 image also shows the mass at L2 (*arrow*) and a homogeneous appearance of the lumbar subarachnoid spaces.

*C*, Axial SE 500/20 at L3 level shows a circular positioning of nerve roots (*arrows*) within thecal sac, indicating that they are wrapped around a central mass.

*D*, SE 500/20 image at L4 level shows fat (*arrows*) within sinus tract in dorsal lumbar subarachnoid space.

*E*, SE 600/20 image 4 months after surgery. The residual dermoid tumor (*arrows*) lying in the most caudal subarachnoid space is difficult to see.

*F*, 3D Fourier transform gradient-echo acquisition 40/5 (theta = 40°) image provides better lesion conspicuity (*arrows*) because of the increased T1 weighting.

the cauda equina (Fig. 3). The intramedullary portion appeared as several fingerlike cords of hypointensity within the substance of the expanded spinal cord (Fig. 3). Patient 5 had an entirely extramedullary epidermoid that was found at surgery to extend from L3 to L4. The mass was invisible on sagittal spin-echo images and could only be detected on axial images by the ringlike configuration of the nerve roots of the cauda equina as they surrounded the isointense mass. Patient 7 had

a ruptured dermoid that filled the thecal sac from the sacrum to T12. Compared with extensive tumor found at surgery, the MR was minimally abnormal. Axial short TR/TE images (Fig. 4C) showed a circular arrangement of nerve roots immediately caudal to the conus, similar to what was seen in patient 4. This region was hypointense relative to neural tissue on long TR images and was initially suspected to be a focus of hemorrhage or a hemorrhagic mass. Further caudally, at the L4 and L5 levels, a curvilinear stripe of tissue with a short T1 relaxation time (described earlier) coursed through the dorsal aspect of the thecal sac (Fig. 4). The remainder of the lumbar subarachnoid space was interpreted as being normal. A follow-up scan 3 months after surgery was obtained on patient 7 using both standard spin-echo techniques and a T1-weighted 3DFT gradient-echo technique with volumetric RF spoiler (SPGR). The SPGR technique resulted in greater conspicuity of the remaining dermoid (Fig. 4F).

The conus medullaris was low-lying (and therefore presumably tethered) in four of the seven patients (Table 1). None of these had a thickened filum terminale. Although fat lined the dermal sinuses in patients 1, 3, and 7, the cord itself was not dysraphic and the lipomas did not extend all the way to the spinal cord. Therefore, the lipomas were thought to be associated lesions, not the cause of the tethering. The level of the conus in the patients with tethering ranged from L2–L3 to L4–L5.

Bone anomalies were detected by MR in three patients. Patient 3 had a spina bifida at L5 and S1, patient 5 had spina bifida of S1, and patient 6 had spina bifida of L4 and L5. Patient 7 had multilevel sacral spina bifida that was not detected by MR because the sacrum was not imaged.

## Discussion

Dorsal dermal sinuses are developmental anomalies of the spine in which epithelium-lined tracts extend inward from the skin surface for a variable distance. They may terminate within the subcutaneous tissues or dura, or they may pass through the dura to terminate in the spinal cord, conus medullaris, filum terminale, a nerve root, or a fibrous nodule in the dorsal spinal cord [6]. A hyperpigmented patch, hairy nevus, or capillary angioma is usually present at the skin surface [7]. Approximately half of all dermal sinuses have associated dermoid or epidermoid cysts [8], usually at the termination of the tract. Approximately 25% of spinal dermoids are associated with dermal sinuses [6, 9, 10]. Patients typically present with infection (cutaneous abscess, intraspinal abscess, or meningitis) as a result of seeding of bacteria through the dermal sinus, or with symptoms of cord or nerve root compression by the associated dermoid or epidermoid tumor [6].

Dorsal dermal sinuses are thought to result from faulty neurulation. As has been well described [6, 11], the spinal cord forms as the result of separation of midline neural ectoderm from more lateral cutaneous ectoderm in the dorsal surface of the embryo and a nearly simultaneous closure of the neural tube. Mount [12] postulated that dorsal dermal sinuses result from focal incomplete separation of cutaneous ectoderm from neural ectoderm during the process of neurulation. When the spinal cord later becomes surrounded by mesenchyme and undergoes its relative ascent with respect to the spinal column, this adherence remains and forms a long, epithelium-lined tract (Fig. 5). Infections result from seeding of bacteria into the subcutaneous or intraspinal regions through the tract. Dermoids or epidermoids may develop as the result of desquamation of the tract lining.

Mount's proposed mechanism of formation [12] explains the phenomenon that the dermatomal level of the cutaneous defect corresponds to the neural ectodermal level of the CNS structure with which it connects via the tract (i.e., a tract with an L5 dermatomal cutaneous orifice extends to the L5 neural ectodermal level of the spinal cord). It may also explain the high rate of occurrence of tethered spinal cords in this series

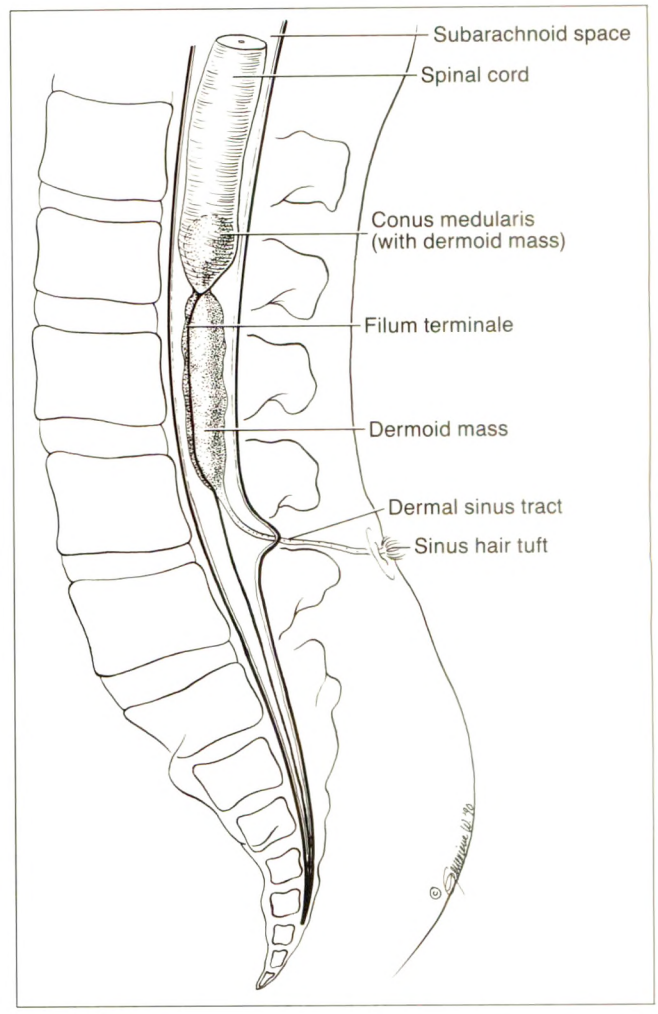



**Fig. 5.—Schematic showing a typical appearance of a dorsal dermal sinus with an associated intra- and extramedullary dermoid. Epithelium-lined tract extends inward from skin surface to connect with CNS. The tract may terminate in the dura, spinal cord, conus medullaris, filum terminale, a nerve root, or a fibrous nodule in the dorsal spinal cord. A pigmented patch, hairy nevus, or capillary angioma is usually present at skin surface. Approximately half of all dermal sinuses have associated dermoid or epidermoid tumors, which are usually at the termination of the tract but may occur anywhere along the tract.**

(four of seven). All of the patients with tethered cords (diagnosis made by identification of the level of the conus below the bottom of L2) had a cutaneous tract opening at L4 or below, and two of the three patients without evidence of tethering had thoracic dermal sinuses. One might, therefore, postulate that the sinus tract tethers the spinal cord in some patients. Obviously, as illustrated by patient 6, some patients with low lumbar cutaneous sinus openings have a conus positioned at the normal level.

Many of the features of dorsal dermal sinuses were seen well by standard spin-echo imaging techniques. The cutaneous and subcutaneous portions of the tracts were seen on short TR/TE images as linear, curvilinear, or conelike areas of low signal intensity coursing through the high-intensity fat (Figs. 1 and 2). Some care must be taken in the photography of these lesions, because the narrow window setting typically used for images of the spinal cord can obscure the sinus tract (Fig. 1). It is, therefore, imperative that the radiologist look at the images with variable window settings for optimal demonstration of both the intra- and extraspinal pathology. Although the cutaneous defects, cord tethering, and intramedullary tumors were demonstrated well by spin-echo MR, several critical features of the pathologic process were more difficult to identify. The intraspinal segments of the dermal sinus tracts were poorly visualized and, more importantly, diffuse subarachnoid tumor was difficult to diagnose on the basis of the MR scans in patients 6 and 7.

Adequate determination of the entire extent of the dermal sinus tract is important in preoperative planning and counseling of patients. If the tract ends external to the dura, resection is a relatively minor procedure because opening of the dura is unnecessary. If the tract extends into the thecal sac, however, the dura must be opened and the laminectomy extended rostrally, often for several levels, in order to adequately treat the patient. The tracts are composed largely of epithelial tissue (epidermis) and are, therefore, of low signal intensity on MR studies. The low signal intensity of the tract is difficult to distinguish from the low intensity of the CSF on the short TR/TE images. Moreover, the tracts are usually small in diameter and CSF pulsations almost certainly result in motion of the sinus tract within the subarachnoid space, factors that further compound the problem.

More disturbing than the lack of sensitivity in the detection of the sinus tracts is the lack of sensitivity in the detection of the extramedullary dermoid and epidermoid tumors. The appearance of CNS dermoid and epidermoid tumors on MR has been described [13–15]. Most epidermoids are nearly isointense with CSF (long T1, long T2) whereas dermoids mimic fat (short T1, short T2) on spin-echo images. However, both epidermoids with short T1 and short T2 relaxation times [16] and dermoids with long T1 and long T2 relaxation times [14, 15] have been described. In our study, all of the dermoids and epidermoids were nearly isointense with CSF on both long TR and short TR spin-echo images. Intramedullary tumors, therefore, contrasted with the adjacent spinal cord and were easily identified. However, the identification of extramedullary tumors was difficult. Although abnormalities on the MR scans of patient 6 (Fig. 3) were identified easily, determining whether the heterogeneity in the lumbar subarachnoid space represented epidermoid tumor or clumped nerve roots resulting from prior infections was not possible. Identification of the tumor in patient 7 (Fig. 4) was even more difficult. The low-lying conus medullaris and the adjacent focus of low signal intensity on long TR/short TE and long TR/long TE spin-echo images suggested tethering of the cord by a hemorrhagic mass. The surrounding subarachnoid spaces were interpreted as being normal. In retrospect, the circular pattern of the cauda equina on axial images (Fig. 4C), similar to the pattern in patient 5, and the curvilinear area of fat in the dorsal thecal sac (Figs. 4A and 4D) suggested the correct diagnosis. Nonetheless, the treating surgeon was quite surprised when, upon opening the meninges, he encountered thick, white dermoid material filling every portion of the lumbar subarachnoid space. No focal lesion was found to explain the area of short T2 relaxation time adjacent to the conus.

The lack of sensitivity of the standard spin-echo MR sequences in the detection of the intraspinal portion of the sinus tract and extramedullary tumors raises the question of the optimal way to image patients with dorsal dermal sinuses. CT myelography is excellent in the detection of the intradural portion of the sinus tract and intradural, extramedullary tumors [6] but is relatively insensitive to intramedullary processes. Sonography [17, 18] can be used in infants in the first year of life, at which time the small size of the bony posterior elements of the spinal column are small and incompletely ossified. The interlaminar spaces function as sonographic windows, allowing visualization of the sinus tract and both intra- and extramedullary tumor [17]. Unfortunately, sonography is ineffective in older children. We have noticed that SPGR images give better conspicuity of intracranial epidermoid tumors than do short TR/TE spin-echo sequences, which are considerably less T1-weighted [19]. Trying this technique in patient 7, who was known to have some residual tumor, we subjectively judged the tumor to be more easily identifiable on SPGR images. This single observation warrants further investigation of the technique in the workup of patients with dorsal dermal sinuses. It is also possible that diffusion imaging, which is helpful in the identification of intracranial epidermoids [20] may be useful in the spine. Another possibility is that T2-weighted images with motion compensation techniques (gradient moment nulling, peripheral gating) may allow more confident identification of the intraspinal portion of the sinus tract. For now, we recommend sonography or MR using heavily T1-weighted images (inversion recovery or SPGR) in infants and inversion recovery or SPGR in children more than 1 year old as the initial screening process. Plain film or CT myelography may be helpful to supplement the information obtained by the less invasive methods, although in patients 6 and 7 lumbar puncture would have been unsuccessful and myelography would certainly have shown a myelographic block at approximately T12 after subsequent cervical puncture. The surgeon, therefore, would nevertheless have been unaware of what he was going to find at laminectomy.

To summarize, a review of the MR and surgical findings in seven patients with dorsal dermal sinuses revealed that stand-

ard spin-echo imaging techniques are excellent for the detection of the subcutaneous portion of the sinus tract, intermedullary dermoid or epidermoid tumor, and associated cord tethering. However, the intraspinal segment of the sinus tract and extramedullary tumor were very difficult to identify. Optimal radiologic workup of patients with dorsal dermal sinuses awaits the development of new MR imaging sequences. For now, heavily T1-weighted MR sequences should be obtained and supplemented with sonography in infants and with CT myelography in children more than 1 year old.

## REFERENCES


1. Barkovich AJ. *Pediatric neuroimaging*. New York: Raven Press, **1990**
2. Barkovich AJ, Chuang SH, Norman D. Anomalies of neuronal migration: MRI. *AJNR* **1987**;8:1009–1017
3. Smith AS, Weinstein MA, Quencer RM, et al. Association of heterotopic gray matter with seizures: MR imaging. *Radiology* **1988**;168:195–198
4. Davis PC, Hoffman JC Jr, Ball TI, et al. Spinal abnormalities in pediatric patients: MR imaging findings compared with clinical, myelographic, and surgical findings. *Radiology* **1988**;166:679–685
5. Raghavan N, Barkovich AJ, Edwards MSB, Norman D. MR imaging in the tethered cord syndrome. *AJNR* **1989**;10:27–36
6. Naidich TP, McLone DG, Harwood-Nash DC. Spinal dysraphism. In: Newton TH, Potts DG, eds. *Modern neuroradiology*, vol. 1. *Computed tomography of the spine and spinal cord*. San Anselmo, CA: Clavadel Press, **1982**: 299–353
7. Haworth JC, Zachary RB. Congenital dermal sinuses in children: their relation to pilonidal sinuses. *Lancet* **1955**;2:10–14
8. Cardell BS, Laurance B. Congenital dermal sinuses associated with meningitis: report of a fatal case. *Br Med J* **1951**;2:1558–1561
9. Harwood-Nash DC, Fitz CR. *Neuroradiology in infants and children*, Vol. 3. St. Louis: Mosby, **1976**: 1054–1227
10. Guidetti B, Gagliardi FM. Epidermoid and dermoid cysts: clinical evaluation and late surgical results. *J Neurosurg* **1977**;47:12–18
11. Naidich TP, McLone D. Growth and development. In: Kricun ME, ed. *Imaging modalities in spinal disorders*. Philadelphia: Saunders, **1988**: 1–19
12. Mount LA. Congenital dermal sinuses as a cause of meningitis, intraspinal abscess, and intracranial abscess. *JAMA* **1949**;139:1263–1268
13. Vion-Dury J, Vincentelli F, Jiddane M, et al. MR imaging of epidermoid cysts. *Neuroradiology* **1987**;29:333–338
14. Newton DR, Larson TC, Dillon WP, Newton TH. Magnetic resonance characteristics of cranial epidermoid and teratomatous tumors. *AJNR* **1987**;8:945
15. Awwad EE, Backer R, Archer CR. The imaging of an intraspinal cervical dermoid tumor by MR, CT, and sonography. *Comput Radiol* **1987**;11: 169–173
16. Horowitz BL, Chari MV, James R, Bryan RN. MR of intracranial epidermoid tumors: correlation of in vivo imaging with in vitro C-13 spectroscopy. *AJNR* **1990**;11:299–302
17. Kangarloo H, Gold RH, Diament MJ, Boechat MI, Barrett C. High-resolution spinal sonography in infants. *AJNR* **1984**;5:191–195
18. Naidich TP, Gorey M, Raybaud C, McLone DG, Byrd SE. Malformations congenitales de la moelle. In: Manelfe C, ed. *Imagerie du rachis et de la moelle*. Paris: Vigot, **1988**:571–620
19. Crawley AP, Wood ML, Henkelman RM. Elimination of transverse coherences in FLASH MRI. *Magn Reson Med* **1988**;8:248–260
20. Tsuruda JS, Chew WM, Moseley ME, Norman D. Diffusion-weighted MR imaging of the brain: value of differentiating between extraaxial cysts and epidermoid tumors. *AJNR* **1990**;11:925–931

# Book Review

**Cancer Imaging with Radiolabeled Antibodies.** (Vol. 46 in the series Cancer Treatment and Research.) Edited by David M. Goldenberg. Boston: Kluwer, 467 pp., 1990. $160

This is volume 46 in the series Cancer Treatment and Research, which was started in 1981. The manuscript probably was submitted to the publisher in 1988, as most references are to 1987 and earlier literature, a few are from 1988, and at least one refers to a 1989 publication as being "in press." The book has five sections, consisting of 22 chapters. The volume is claimed "to present a current perspective of the use of one set of molecules, antibodies, to target diagnostic isotopes to tumors." An overall impression is that the approach is successful, although a key development of the past 2 years is not mentioned in any detail (see the following).

Of the 60 contributors listed, 12 are associated with David M. Goldenberg's Center for Molecular Medicine and Immunology in New Jersey and its affiliates (and Dr. Hildegard Goldenberg is listed twice). The first chapter is an overview of the field of radioimmunoimaging and covers 1948 to about 1988. It is must reading for those entering the field and contains four tables that summarize the history of radiolabeled antitumor antibodies. The second chapter is principally a discussion of S. D. Rockoff's 1980 paper on the theoretical limitations of immunoimaging, and it brings relevant factors into clearer perspective. The second section of the book (four chapters) discusses model systems, such as the intraperitoneal delivery of monoclonal antibodies. However, the related chapter on antibody lymphoscintigraphy is separated from this by about 240 pages. A four-page table (starting on page 56) provides a comprehensive summary of subcutaneous tumor models used to study the use of monoclonal antibodies in tumor detection. Included are the tumor (principally human), animal host, class of the antibody, form of the antibody (intact or fragment), radionuclide used, and reference.

The third section, on radiochemistry, shows how far researchers have come in devising bifunctional chelates (those that bind to a protein at one end of the chelate molecule and to a radiolabel at the other end). Radioindium and several metals appear as leading candidates to be used in selected situations, in lieu of radioiodine. However, the inability to readily, and stably, bind 99m-technetium to most antibody molecules has been a source of major frustration. Section 4 (six chapters) is concerned with clinical studies. This includes a discussion of the requirements for radioimmunodetection of tumors, including the use of subtraction techniques (and its limitations). A table lists a variety of factors that may affect antibody targeting. The final chapter of the section discusses the human immune response to murine monoclonal antibodies. The last section of the book is devoted to new approaches. It consists of four chapters, which cover antibody lymphoscintigraphy, radioimmunoguided surgery, augmentation of tumor antigen expression by human interferons, and the use of anti-antibodies to enhance tumor imaging.

The book is printed on nonglossy paper, which somewhat detracts from the radionuclide images. The major missing element is a detailed discussion of single-chain antibodies (the "artificial" molecules developed within the last few years). (For a review, see *J Natl Cancer Inst* 1990;82:1173.) The other important concepts are mentioned, such as chimeric antibodies, anti-antibodies, and (in other contexts) biological response modifiers. I could quibble with certain statements, such as the one that the maximal amount of antibody to be used is 100 $\mu$g. I also wonder what happened to the arrows for the figure on page 253.

Overall this is a useful, and nearly timely, collection of papers. Although the price is a bit high, the book is a large gathering of information on radioimmunodetection and radioimmunoimaging of tumors. Books with a slightly wider subject area are also available, for example, the 1990 volume published by Karger, *Symposium on Monoclonal Antibodies for Therapy, Prevention and in Vivo Diagnosis of Disease*, edited by Vandedonk and Hennessen. By contrast, the Goldenberg book has but few references to therapy—perhaps justifiably, as the topic is urgently in need of further development.

Richard P. Spencer
*University of Connecticut Health Center*
*Farmington, CT 06030*

Case Report

# Polysplenia Syndrome with Congenital Short Pancreas

Thomas E. Herman[1] and Marilyn J. Siegel

A syndrome of polysplenia with bilobed lungs, congenital heart disease, intestinal malrotation, and short pancreas has been described recently in the pathologic literature [1], but to our knowledge no reports of this malformation complex have been published in radiology journals. We have recently seen a patient with polysplenia and short pancreas whom we wish to describe in order to report this association in the radiologic literature.

## Case Report

An 8-year-old boy was admitted to St. Louis Children's Hospital with pneumococcal meningitis. He had a previous diagnosis of congenital heart disease, absence of the left kidney, and possible asplenia syndrome. The patient was treated with appropriate antibiotics for pneumococcal meningitis and responded well. Because of increasing liver size, an abdominal CT scan was performed to exclude an abscess. The scan showed a short, round pancreas adjacent to the duodenum (Figs. 1A and 1B). A preduodenal portal vein also was present. No duodenal obstruction was present. Two small splenules were seen in the left upper quadrant. The left kidney was absent. MR imaging was performed for further evaluation of the cardiac anomalies. The MR image showed azygous continuation of the inferior vena cava, marked right ventricular hypertrophy, and an anomalous right lower lobe pulmonary vein to the right atrium. A high sinus venosus atrial septal defect also was present. MR imaging of the upper abdomen (Fig. 1C) showed a short globular pancreas without pancreatic body or tail. Two small spleens were seen in the left upper quadrant. The left kidney was absent.

## Discussion

The association of polysplenia with short pancreas has been reported [1] in an autopsy series of five patients who ranged in age from 2 days to 12 years. All of those patients had bilobed lungs and severe congenital heart disease. One of the patients had an absent left kidney. The only other patient we are aware of with polysplenia syndrome and a short pancreas was a 53-year-old woman [2] with no known heart disease. She was found to have multiple spleens, a left-sided gallbladder, a preduodenal portal vein and absence of the pancreatic tail. A carcinoma of the pancreas was present within the short pancreas. Although anular pancreas has been described in large series of patients with polysplenia in the radiologic literature [3], no mention is made of short pancreas associated with polysplenia.

The cause of the short pancreas in our patients is presumed to be agenesis of the dorsal pancreas. Embryologically, the pancreas arises from ventral and dorsal buds. The ventral bud gives rise to a portion of the pancreatic head and to the uncinate process. The dorsal pancreas gives rise to the remainder of the pancreatic head, body, and tail. Because both the spleen and the dorsal pancreas develop in the dorsal mesogastrum, concomitant anomalies of both organs would not be surprising. Alternatively, the gland may be short because of dysgenesis of pancreatic buds.

Several reports of short pancreas in patients with normal situs have been published [4]. Short pancreas in these patients has been attributed to agenesis of the dorsal pancreas. The CT appearance of congenital short pancreas in these patients is similar to that seen in our patient. Most patients

Received September 25, 1990; accepted after revision October 17, 1990.

[1] Both authors: Mallinckrodt Institute of Radiology, Washington University School of Medicine, 510 S. Kingshighway Blvd., St. Louis, MO 63110. Address reprint requests to T. E. Herman.

*AJR* **156:799–800, April 1991** 0361–803X/91/1564–0799 © American Roentgen Ray Society

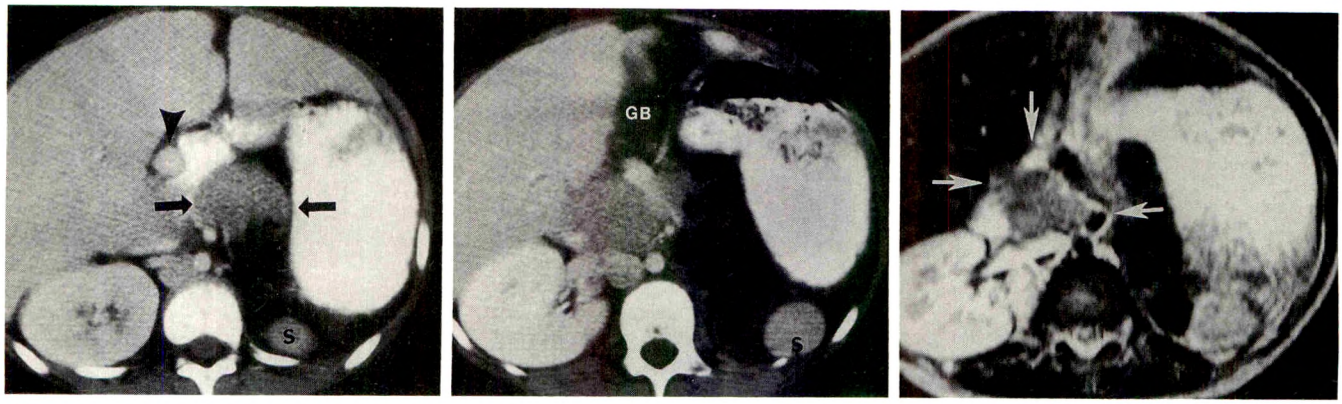



**Fig. 1.—*A*, CT scan of abdomen shows soft-tissue nodule consistent with a small spleen (S) in left upper quadrant. A rounded superior portion of pancreas (*arrows*) lies to left of contrast-containing duodenum. Portal vein (*arrowhead*) is anterior to duodenum. Azygos vein is adjacent to aorta. No intrahepatic inferior vena cava is present.**

***B*, CT scan 2 cm caudad shows a second spleen (S) posterolaterally on left side. Round, short pancreas is seen posterior to gallbladder (GB), which is a midline structure.**

**C, T2-weighted MR image shows round pancreas (*arrows*) and absence of left kidney and inferior vena cava.**

with congenital short pancreas with normal situs have had diabetes mellitus, occasionally associated with pancreatitis. In contrast, patients with polysplenia and short pancreas are not diabetic and have normal amylase levels. It is also important to recognize the congenital short pancreas in order to avoid mistaking the pancreas for a mass.

REFERENCES

1. Hatayama C, Wells TR. Syndrome of externally bilobed lungs with normal bronchial pattern, congenital heart disease, multiple spleens, intestinal malrotation and short pancreas, an apparently hither to undefined malrotation complex. *Pediatr Pathol* **1984**;2:127–133
2. Matsusue S, Kashihara S, Koizumi S. Pancreatectomy for carcinoma of the head of the pancreas associated with multiple anomalies including preduodenal portal vein. *Jpn J Surg* **1984**;14:394–398
3. Peoples WM, Moller, JH, Edwards JE. Polysplenia: a review of 146 cases. *Pediatr Cardiol* **1983**;4:129–137
4. Rosenstock E, Achkar E. A "short pancreas." *Gastrointest Endosc* **1986**; 32:296–297

# Evaluation of CSF Shunt Function: Value of Functional Examination with Contrast Material

Edward C. Benzel[1]
Mansour Mirfakhraee[2]
Theresa A. Hadden[1]

**Functional positive-contrast shuntography includes a patency check of both limbs of the shunt and the shunt valve by fluoroscopy following the injection of an iodinated contrast agent (anatomic shuntogram) and an assessment of the adequacy of ventricular fluid drainage under physiologic conditions by using serial CT scans to assess the rate of iodine dissipation from the ventricular system (physiologic shuntogram). To demonstrate its efficacy and utility, 82 functional shuntograms were obtained in 55 patients. Fifty-one of the 82 studies were abnormal. Of these, 22 demonstrated patency of both the proximal and distal limbs with an accompanying slow dissipation of contrast material after injection (21 of 22 patients were adults). Eighteen of these 22 patients improved following the reduction of shunt drainage pressure. In the case of frank shunt obstruction, the site of obstruction was delineated clearly in all 29 cases. Correlation of clinical outcome with test results confirmed the utility of this technique, especially when applied to the shunted adult hydrocephalic patient whose response to the shunt had been inadequate.**

**The technique described here allows the clinician to differentiate between physiologic and anatomic shunt failure and between shunt failure and normal shunt function. It also allows for precise localization of the shunt obstruction in anatomic shunt failure and for demonstration of physiologic shunt failure when shunt patency is demonstrated in the presence of the slow dissipation of intraventricular contrast medium.**

*AJNR* 12:143–147, January/February 1991; *AJR* 156:801–805, April 1991

The evaluation of postoperative shunt function is a challenging problem. The pathophysiology of CSF dynamics and its alteration by CSF shunting procedures are poorly understood. Complicating this is the fact that shunt failure may manifest itself in two ways: frank shunt obstruction and physiologic malfunction. A straightforward positive-contrast shuntogram should suffice for the evaluation of a frankly obstructed shunt. However, if a shunt is anatomically patent but not lowering the intraventricular pressure enough to ensure physiologic homeostasis (physiologic undershunting), a more comprehensive mechanism is needed for evaluating the shunt.

In order to evaluate both types of shunt failure, we have employed functional positive-contrast shuntography. This procedure includes a patency check of both limbs of the shunt (anatomic shuntogram) and an assessment of the adequacy of ventricular fluid drainage under physiologic conditions (physiologic shuntogram).

The technique of functional shuntography has been outlined previously, specifically with respect to the Pudenz shunting system [1]. The linear relationship between iodine concentration and CT number (in Hounsfield units) has also been demonstrated [2]. The utility of this information when applied to the physiologic aspect of functional shuntography (i.e., the ability to quantitatively observe the rate of decline in iodine concentration following intraventricular injection) has been demonstrated [2]. However, clinical follow-up of a large number of patients was not included in the two previous reports [1, 2]. Therefore, in order to evaluate the

Received March 12, 1990; revision requested May 9, 1990; revision received August 16, 1990; accepted August 17, 1990.

[1] Division of Neurosurgery, University of New Mexico School of Medicine, Albuquerque, NM 87131. Address reprint requests to E. C. Benzel.

[2] Department of Radiology, Louisiana State University Medical Center, Shreveport, LA 71130-3932.

0361–803X/91/1564–0801
© American Roentgen Ray Society

anatomic component and to evaluate and emphasize the dynamic (physiologic) component of functional positive-contrast shuntography for the assessment of shunt malfunction, we reviewed 82 shuntograms obtained in 55 patients over a 6-year period. The technique as applied to non-Pudenz systems is described also.

## Materials and Methods

The study population comprised 55 patients who had previously undergone ventricular shunting procedures (either ventriculoperitoneal [40 patients] or ventriculopleural [15 patients]) and who were evaluated with functional positive-contrast shuntography at Louisiana State University Medical Center and the Veterans Administration Medical Center in Shreveport, LA, during a 6-year period ending December 31, 1987. All patients had been evaluated for suspected shunt failure. The suspicion of shunt failure was based on clinical criteria in all cases. Either the patient's clinical condition deteriorated or did not improve following shunting. CT confirmation of the clinical suspicion was obviously necessary prior to shuntography. A total of 82 procedures were performed. Twenty patients underwent two or more studies. All but three of these 20 patients were children.

### *Description of the Procedure*

Prior to the procedure, the patient is kept in the supine position for at least 1 hr. The patient is then placed on a fluoroscopy table in a supine position with a shoulder (ipsilateral to the shunt) elevated with a log roll. The region surrounding the reservoir is then shaved, cleansed, and draped. If a Pudenz-like shunting system has been inserted, the protocol described by Mirfakhraee et al. [1] is used.

If another type of shunting system has been placed (four patients in this series), the reservoir is punctured by a 25-gauge butterfly needle. If CSF does not return spontaneously following placement of the 25-gauge needle in the reservoir or after gentle aspiration with a syringe, the needle should be repositioned. If this is unsuccessful, less than 1 ml of water-soluble iodinated contrast medium (170–200 mg I/ml) may be injected. This is performed under fluoroscopic control. This allows for needle localization (necessary in only two patients). Care must be taken to avoid the injection of air into the system.

Metrizamide and iopamidol were the contrast agents used exclusively in this series. The last 12 patients injected in this series were injected with iopamidol; the remainder were injected with metrizamide.

Distal flow of the shunt is obstructed by applying pressure to the tubing distal to the reservoir (or by applying pressure to the distal reservoir in a multiple-reservoir system). Then, 1–1½ ml of the iodinated contrast agent is injected into the reservoir, allowing flow through the proximal limb of the shunt and into the ventricle. If this limb is patent, a jet of contrast material may be observed fluoroscopically [1]. If no flow is observed, a proximal limb obstruction exists.

In order to test distal limb function, the proximal limb of the shunt is obstructed by applying pressure to the shunt tubing proximal to the reservoir (or by applying pressure to the proximal reservoir in a two-reservoir system). Then, 2–3 ml of contrast agent is injected. This should opacify the distal tubing and spill into the absorptive cavity (i.e., peritoneal cavity) if the distal limb is patent. If no flow is observed, a distal obstruction is present.

The evaluation of other types of shunting systems requires an alteration of the shuntogram technique as indicated. The anatomy of the shunting system may be such that both the proximal and distal limbs cannot be checked for frank obstruction. This might occur, for example, when a valveless reservoir or no reservoir at all has been placed in the shunting system.

When frank patency of the shunt is observed by the above procedure, the ability of the shunt to drain adequately under physiologic conditions may be assessed. A cranial CT scan is obtained 0–4, 24, and possibly 48 hr following injection (a 48-hr CT scan was obtained in 18 of the 22 patients undergoing the dynamic aspect of the shuntogram). In this series, midventricular cuts only were obtained in patients who were believed to be especially sensitive to excessive radiation exposure owing to their young age or to the accumulative nature of previous radiographic procedures (five procedures in three patients were performed with midventricular cuts only). This limitation of the study did not interfere with the test accuracy in any of these patients.

In order to avoid pooling of contrast material in the ventricular system, the head must be gently shaken in both the supine position and especially the prone position. This should ensure adequate mixing of the contrast agent with the ventricular fluid for the initial scan (on subsequent scans, mixing is almost always complete). If two regions of interest are evaluated on the same scan, an average is obtained (the difference was not significant on the 24- and 48-hr scans in any study in this series).

The point of obstruction of a nonpatent shunt can be visualized by using the first part of the protocol and observing the location of the blockage of flow (anatomic shuntogram). Physiologic failure of the shunt in an undershunted patient may be evaluated by the dynamic aspect of the study with serial CT scans (physiologic shuntogram). If the CT number of the ventricular fluid at 24 hr is less than or equal to 18 H, the shunt is most likely functioning properly and/or the normal CSF pathways are draining adequately. If it is greater than 18 H, but less than or equal to 25 H, a repeat CT scan at 48 hr is indicated. If the CT number is greater than 25 H at 24 hr, neither the normal CSF pathways nor the shunting system is draining the ventricular fluid rapidly enough. These criteria were derived from previous clinical experience [1] and from midventricular CT numbers observed in 48 control patients [2].

## Results

Thirty-one of the 82 studies did not demonstrate an abnormality of function. Fifty-one studies were abnormal. Of these 51 studies, 22 demonstrated patency of both the proximal and distal limbs of the shunt, while also demonstrating the slow dissipation of contrast material from the ventricular system (undershunting). Most cases of undershunting were observed in adults (21 of 22 studies). Of the 22 undershunted patients (22 studies, one study in each patient), 18 were diagnosed by demonstrating a CT number of greater than 18 H at 48 hr while only four patients were diagnosed with a 24-hr scan demonstrating a CT number greater than 25 H. In 25 studies, the CT number was between 18 and 25 H at 24 hr and a 48-hr scan was required. Seven 48-hr scans demonstrated a CT number less than or equal to 18 H. These studies did not result in a shunt revision. Of the 18 patients who had a CT number greater than 18 H at 48 hr, 14 improved. All four patients whose 24-hr CT scan demonstrated a CT number greater than 25 H improved following shunting.

Overall, a lowering of the shunt drainage pressure was performed in all 22 cases with an abnormal physiologic shuntogram. Eighteen patients improved following this procedure,

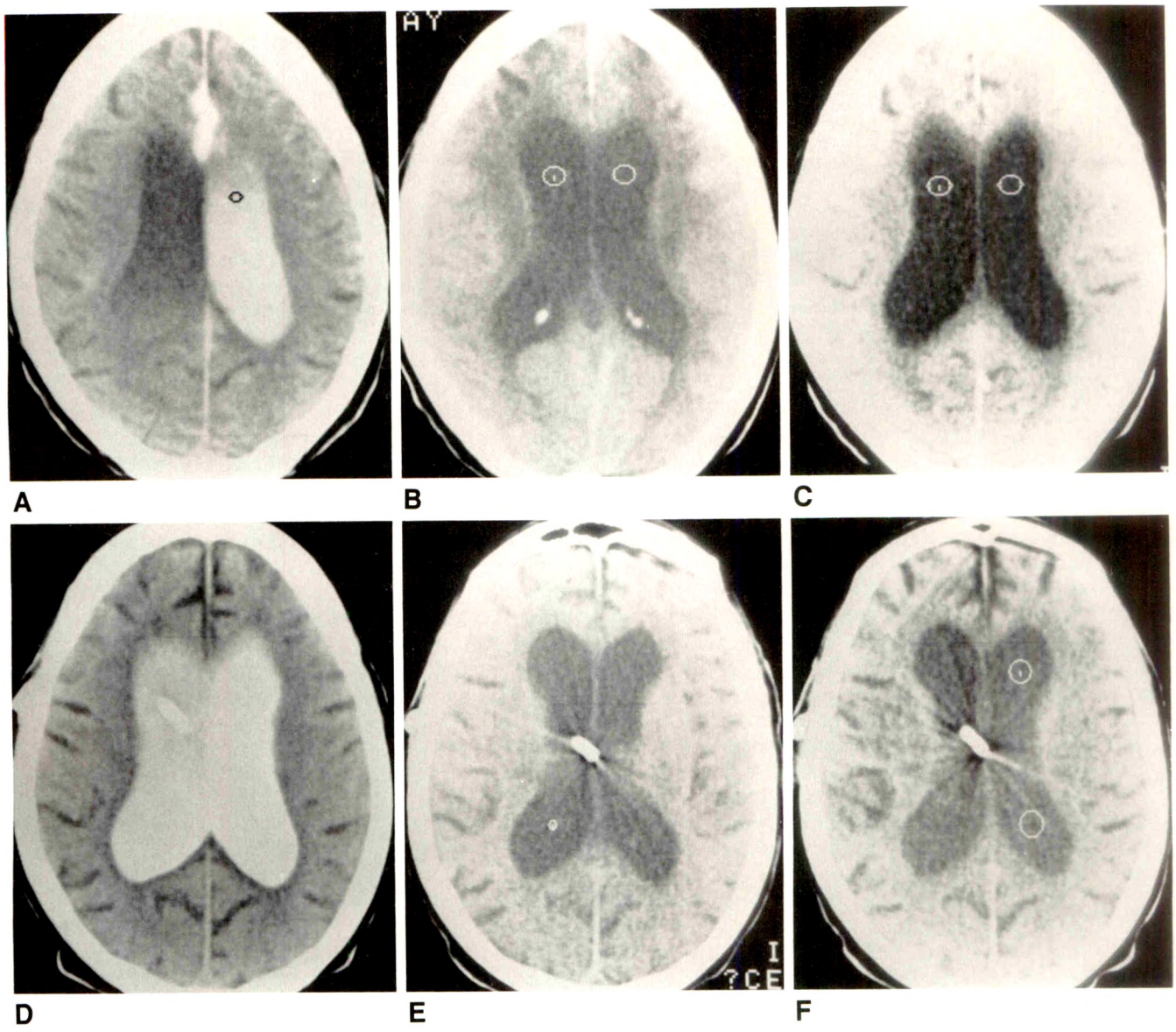



**Fig. 1.—A patient with the syndrome of dementia, ataxia, and urinary incontinence underwent a routine CT study and positive-contrast CT cisternography with 5 ml of iopamidol (200 mg I/ml) injected into the lumbar subarachnoid space.**

***A*, 6-hr scan reflects a high concentration of ventricular contrast material.**

***B* and *C*, 24- and 48-hr scans show midventricular CT numbers to be 26 and 21 H, respectively.**

**Since the contrast material did not dissipate from the lateral ventricles rapidly (≤18 H by 48 hr), a ventriculoperitoneal shunt (high-pressure Pudenz system) was placed. The patient did not respond well clinically. Therefore, functional positive-contrast shuntogram was obtained. Patency was noted fluoroscopically in both the proximal and distal limbs of the shunt.**

***D*, CT scan 1 hr after intraventricular injection of 3 ml of iopamidol (200 mg I/ml).**

***E* and *F*, Although the midventricular CT number at 24 hr was 23 H (*E*), the CT number at 48 hr was 15 H (*F*).**

**Despite lack of desired clinical response, the shunt was judged to be effectively draining the ventricular fluid and a second operation was not performed.**

while three were unchanged (Fig. 1) and one worsened. The latter patient developed a subdural hematoma 2 weeks after surgery. He did not recover his baseline neurologic status following evacuation of the hematoma.

When frank obstruction was present (29 studies), its site was clearly delineated by the procedure. Most cases of frank shunt obstruction were located in the distal limb (17 of 29 studies) and most were noted in children (24 of 29 studies). No difference in outcome was noted regarding the type of shunt placed.

Twenty-nine normal shuntograms were obtained (in 27 patients). Seven of these required a 48-hr scan (CT number less than or equal to 18 H at 48 hr). Two procedures were unsuccessful in demonstrating abnormality secondary to an inability to successfully cannulate the ventricular reservoir. No complications (including contrast toxicity, cortical injury, shunt infection, and disruption of or injury to the shunt system) were associated with functional shuntography. No difference with respect to complications or efficacy was noted between the use of ionic (metrizamide) or nonionic (iopamidol) injection.

Functional positive-contrast shuntography was most useful in determining the absence of physiologic shunt patency in adults (21 of 22 patients with physiologic shunt failure were adults) and the location of a frank shunt obstruction in children (24 of 29 patients with frank shunt obstruction were children).

## Discussion

The clinical problem of shunt malfunction has plagued neurosurgeons for decades. Both the diagnosis of obstruction, as well as the location of the obstruction, are of importance [3–6]. There are many cases in which the shunt may function properly under high pressures (such as under the pressure of the injected contrast agent during a shuntogram), but does not drain under physiologic conditions. This is an undershunting phenomenon and should be considered as a specific type of shunt failure (physiologic failure). This type of shunt malfunction, which perhaps has previously been underdiagnosed, was found to be relatively common in the adult population reported here. French and Swanson [7] likewise have documented the common occurrence of physiologic shunt malfunction, but it is rare in the pediatric population. A low-pressure shunt is usually placed in the pediatric hydrocephalic patient in order to compensate for high brain parenchymal compliance. These patients are much more likely to have complications associated with overshunting (such as the slit ventricle syndrome or subdural effusions) than those associated with undershunting (physiologic shunt failure). On the other hand, a higher-pressure shunting system is usually placed in adults in order to avoid the complications of overshunting (such as formation of subdural hematomas). Adult patients, therefore, susceptible to the complication of inadequate ventricular fluid drainage (an undershunting problem). This in turn may result in a less than optimal response to a shunting procedure, for which French and Swanson [7] coined the term "deceptive patency," implying a nonobstructive physiologic failure of a shunt. They observed this problem in 40% of their patients who were evaluated by radionuclide shuntography.

The problem of undershunting is complicated further by the requirement of large hydrocephalic ventricles for a lower drainage pressure than that required by smaller ventricles. This is according to the law of La Place [8]. A fine line, therefore, exists between overshunting (with associated complications such as subdural hematoma, subdural hygroma, and the slit ventricle syndrome) and undershunting (inadequate drainage resulting in the failure of effective ventricular pressure reduction). In some patients this fine line may present a situation that is impossible to respond to effectively and safely.

The pressure within the shunt system during injection of the contrast agent at the time of shuntography is higher than that during normal ventricular drainage. Patency of a shunt system, as demonstrated by such an injection, might not reflect a true evaluation of ventricular fluid flow under normal conditions. However, the observation of appropriate dissipation of the contrast agent on serial CT scans, combined with routine shuntography, offers a complete evaluation of a shunt system. This is illustrated here with respect to positive-contrast cisternography and shuntography (Fig. 1). Others have used 3- and 9-min radiographs of the reservoir after the injection of the positive contrast agent [1, 9]. The dye should be radiographically imperceptible 9 min after injection into a shunt system that flows properly. If contrast material within the reservoir is observed on the 9-min film, the shunt may not be draining properly. This implies the presence of an undershunting phenomenon. However, it might also indicate that the ventricular system is draining by another pathway (i.e., normal CSF pathways) and that contrast stasis in the reservoir is a manifestation of a shunting system that was placed in a ventricular system that was adequately draining through existing pathways. This might be the case, for example, in a patient with Alzheimer disease who harbors large ventricles. This test, therefore, may lead to erroneous conclusions.

Positive-contrast CT cisternography, ventriculography, and shuntography are proven useful tools [1, 2, 10]. The utility of these tools can be increased by quantifying the test. The CT number (in Hounsfield units) can be used to assess the intraventricular iodine concentration following injection of the contrast agent (Fig. 1) [2]. The CT density of the normal ventricular system is 18 H or less [2]. Dissipation of intraventricular contrast material to an insignificant level (a midventricular CT number less than or equal to 18 H) within the first 24–48 hr following injection, therefore, is indicative of a physiologically normal system. Any excess intraventricular contrast material indicates a situation of apparent undershunting.

French and Swanson [7] believed that patients undergoing functional shuntography should be left in the horizontal position for a short period prior to the injection of a contrast agent. It was conjectured that the intraventricular pressure should be allowed to equilibrate before a study of CSF dynamics could be performed accurately. The delayed examination of the shunt by the protocol presented herein should minimize this potential inaccuracy. This precaution was undertaken despite the fact that there is a substantial delay from the time of injection to the time of the first CT scan in order to ensure maximum test reproducibility and accuracy.

Various other techniques have been used to evaluate shunt patency. These include subarachnoid infusion tests [11], sonography [12], temperature change evaluations [13], and radionuclide imaging [7, 14–16]. Each of these techniques has drawbacks and none is able to completely evaluate a shunt for both physiologic and frank anatomic patency. Specific advantages of functional positive-contrast shuntography over other dynamic techniques, such as radionuclide cisternography, are related to its ability to quantify the extent of intraventricular contrast retention and to the clear definition of the point of shunt dysfunction in the case of frank shunt obstruction. The extent of intraventricular contrast retention is an indicator of the degree of obstruction of flow of ventricular fluid, either through conventional anatomic pathways or through the existing shunt system.

It is not known whether or not the CT number changes described here are affected by the type of contrast material used (ionic or nonionic). The type of contrast agent used, however, appears to not affect the efficacy or risks of the procedure.

In summary, anatomic localization of the point of shunt obstruction allows one to tailor the procedure of shunt revision. This aspect of the procedure is most helpful in children and occasionally in adults. The physiologic evaluation of shunt function allows one to differentiate between the undershunted patient (who may improve clinically following shunt pressure reduction) and true nonresponders. This aspect of the shuntogram procedure is used almost exclusively in shunted hydrocephalic adult patients. It allows for a true physiologic evaluation of a shunt and may accurately predict the phenomenon of physiologic undershunting in patients who otherwise would have been inadequately treated.

## REFERENCES


1. Mirfakhraee M, Benzel EC, Crofford MJ, et al. Metrizamide shuntography for evaluation of shunt malfunction in hydrocephalus. *AJNR* **1985**;6:815–822
2. Benzel EC, Chesson AL. Computed tomography number correlations for metrizamide computed tomographic ventriculography. *Surg Neurol* **1987**;27:126–130
3. Evans RC, Williams T, Williams LA. Shunt blockage in hydrocephalic children: the use of the valvogram. *Clin Radiol* **1976**;27:489–495
4. Faria MA, O'Brien MS, Tindall GT. A technique for evaluation of ventricular shunts using amipaque and computerized tomography. *J Neurosurg* **1980**;53:92–96
5. Murtagh FR, Quencer RM, Poole CA. Cerebrospinal fluid shunt function and hydrocephalus in the pediatric age group. *Radiology* **1979**;132:385–388
6. Savoiardo M, Solero CL, Passerini A, Migliavacca F. Determination of cerebrospinal fluid shunt function with water-soluble contrast medium. *J Neurosurg* **1978**;49:398–407
7. French BN, Swanson M. Radionuclide-imaging shuntography for the evaluation of shunt patency. *Surg Neurol* **1981**;16:173–182
8. Early CB, Fink LH. Some fundamental applications of the law of La Place in neurosurgery. *Surg Neurol* **1976**;6:185–189
9. Dewey RC, Kosnik EJ, Sayers MP. A simple test of shunt function: the shuntogram. *J Neurosurg* **1976**;44:121–126
10. Drayer BP, Rosenbaum AE. Studies of the third circulation. *J Neurosurg* **1978**;48:946–956
11. Brisman R, Schneider S, Carter S. Subarachnoid infusion and shunt function. *J Neurosurg* **1973**;38:379–381
12. Flitter MA, Buchheit WA, Murtagh F, Lapayowker MS. Ultrasound determination of cerebrospinal fluid shunt patency. *J Neurosurg* **1975**;42:728–730
13. Go KG, Lakke JPWF, Beks JWF. A harmless method for the assessment of patency of ventriculoatrial shunts in hydrocephalus. *Dev Med Child Neurol* **1968**;16:100–106
14. Graham P, Giles-Howman R, Johnston I, Besser M. Evaluation of CSF shunt patency by means of technetium-DTPA. *J Neurosurg* **1982**;57:262–266
15. Hayden PW, Rudd TG, Shurtleff DB. Combined pressure-radionuclide evaluation of suspected cerebrospinal fluid shunt malfunction: a seven year clinical experience. *Pediatrics* **1980**;66(5):679–684
16. Rudd TG, Shurtleff DB, Loeser JD, Nelp WB. Radionuclide assessment of cerebrospinal fluid shunt function in children. *J Nucl Med* **1973**;14:683–686

# Book Review

**The Year Book of Diagnostic Radiology, 1990.** Edited by David G. Bragg. Chicago: Year Book Medical, 569 pp., 1990. $54.95

The 1990 *Year Book of Diagnostic Radiology* continues the fine tradition. The editors have included abstracts of more than 300 articles on a wide range of subjects. Although the dominance of the major radiologic journals is evident, the book also has articles from important nonradiologic clinical journals and from sometimes obscure overseas publications. The text has seven chapters: neuroradiology, cardiovascular and interventional radiology, thorax, abdomen, musculoskeletal system, pediatrics, and technical developments and quality assurance. The abstracts are prepared with great care. They do not just summarize the articles but include radiographs, tables, and graphs. Each abstract is accompanied by a brief editorial that highlights important points, sometimes indicating areas of disagreement and often including a brief bibliography that the interested reader can use to pursue a topic further. These editorial comments are written in an informal, engaging, and often witty style. The selected articles reflect a satisfactory blend of topics of great current interest, more traditional topics, and, occasionally, those that reflect the special interests of the editors.

The section on neuroradiology by Anne Osborn is particularly well written. In addition to brain, spine, and head and neck, miscellaneous topics related to psychiatry and to legal issues are included. Franklin Miller's section on cardiovascular and interventional radiology includes a great deal of statistical data, with detailed tables and graphs. David Bragg's section on the thorax includes a variety of topics especially related to mammography and the mediastinum, and the topics in mammography are particularly well chosen. William Thompson had the difficult task of covering the gastrointestinal tract, the genitourinary system, and obstetrics and gynecology. He has chosen well but probably deserves even more space for these important topics. Theodore Keats has selected many interesting cases, especially from journals not widely read by general radiologists. John Kirkpatrick's selections in the section on pediatric radiology will be interesting even to those radiologists who seldom see radiographs of children. The section edited by William Hendee includes important technical topics such as instrumentation, contrast agents, and quality assurance. The index is detailed, complete, and easy to use. The radiographs are well reproduced.

*The Year Book of Diagnostic Radiology, 1990* will be of great value to a wide audience. By selecting articles from an extremely wide spectrum of publications, the editors have brought to the busy general radiologist valuable articles that otherwise would be missed. The abstracts are of extremely high quality, coherently condensing a large amount of information in a readable fashion. The editorial comments and suggestions for further reading are, in my opinion, especially helpful. I recommend this book enthusiastically to all members of the radiologic community.

J. Eric Blum
*Akron City Hospital*
*Akron, OH 44309*

# Diagnosis of Ruptured Intracranial Dermoid Cyst: Value of MR over CT

Alison S. Smith[1,2]
Jane E. Benson[2,3]
Susan I. Blaser[4]
Akira Mizushima[1,5]
Robert W. Tarr[1]
Errol M. Bellon[2]

**The CT and MR findings of seven patients with pathologically proved ruptured dermoid cysts were reviewed to analyze the MR characteristics and to see if MR evaluation had significant advantages over CT. In six cases, both CT and MR identified fatty material in the CSF spaces. Hemorrhage complicated preoperative diagnosis in one case. Patterns of extraaxial fat distribution were as follows: intraventricular fat/CSF levels (three patients), generalized subarachnoid spread (six patients), and localized subarachnoid spread with sulcal widening (one patient). There was no correlation between fat distribution and clinical symptoms. MR showed the vascular involvement better than CT did in five of seven cases, and showed extension of the cysts into the skull base in two cases. Signal intensity of the solid mass was low on T1-weighted MR images and inhomogeneously high on T2-weighted images, which correlated pathologically with the presence of crystal cholesterol, hair, sebaceous glands, and epithelial cells in all cases. On MR, brain parenchyma showed little edema or other reaction to the masses, which were typically large.**

**The value of MR over CT in the examination of ruptured dermoid cysts is the conspicuity of the extent of subarachnoid spread, involvement of the extraaxial structures, and evidence of vascular compromise, which can obviate angiography. MR had no advantage over CT in making the initial diagnosis of ruptured dermoid, but it would be the preferred preoperative study.**

***AJNR* 12:175–180, January/February 1991; *AJR* 156:807–812, April 1991**

In the past, it was thought that intracranial dermoid cyst rupture was uniformly fatal [1]. With CT, however, rupture of intracranial dermoid cysts has been well documented and shows a spectrum of brain involvement and symptomatology [2–7]. We retrospectively reviewed seven cases of ruptured dermoid cysts studied by MR and CT to determine the degree to which the two studies agreed or were complementary. These cases also add to the number of patients who have survived cyst rupture and surgery.

## Materials and Methods

Seven cases of ruptured intracranial and dermoid cysts studied by MR were collected from four hospitals between September 1985 and February 1989. Patient data appear in Table 1. MR and CT examinations were reviewed retrospectively. MR evaluations were performed on a variety of scanners owing to referral patterns. Two were performed at 0.5 T, one at 1.0 T, three at 1.5 T, and one patient was scanned on a 0.15 T prototype unit. Intraarterial digital subtraction angiography was performed in five cases, three of which were available for review. All patients had pathologic confirmation of the dermoid cyst by craniotomy. Follow-up varied from 6 months to 3 years.

## Results

In all cases, pathologic study showed the presence of an epithelial cyst wall and a mass containing epithelial cells, cholesterol crystals, hair, and sebaceous glands.

Received September 7, 1989; revision requested November 13, 1989; revision received July 16, 1990; accepted July 30, 1990.

[1] Department of Radiology, University Hospitals of Cleveland, 2074 Abington Rd., Cleveland, OH 44106. Address reprint requests to A. S. Smith.

[2] Department of Radiology, MetroHealth Medical Center, Cleveland, OH 44109.

[3] Department of Radiology, Johns Hopkins Hospital, Baltimore, MD 21205.

[4] Department of Special Studies and Neuroradiology, Hospital for Sick Children, Toronto, Ontario, Canada.

[5] Present address: Kyushu University, Kukuoka, Japan.

0361–803X/91/1564–0807
© American Roentgen Ray Society

Sweat glands were not specifically reported. No comments were made on the ratio of cholesterol or keratin. In five cases, the cysts were found in a very similar location; that is, in the parasellar region (cases 1–5). The masses in the other two cases were in the left frontal lobe extending into the lateral ventricle and in the sylvian fissure (cases 6 and 7, respectively).

The bright intensity of the fat on the short TR/short TE MR images subjectively made the fat more conspicuous in cases 1 through 6. Three patterns of fat distribution were apparent. In cases 1 through 3, material of high signal intensity relative to brain on short TR/short TE images resulted in a fluid/fluid level with CSF within the ventricles (Fig. 1). This finding correlated with the fat density seen on CT examination.

The fat was seen in extraventricular subarachnoid spaces in cases 1 through 6. The distribution was non–gravity dependent. Foci of fat above and below a narrowed aqueduct of Sylvius and fourth ventricle involvement were additional findings in case 2 (Fig. 2). The third pattern of fat distribution followed and widened the sulci in case 3 (Fig. 3). On long TR/long TE images, this material was iso- to hypointense relative to brain.

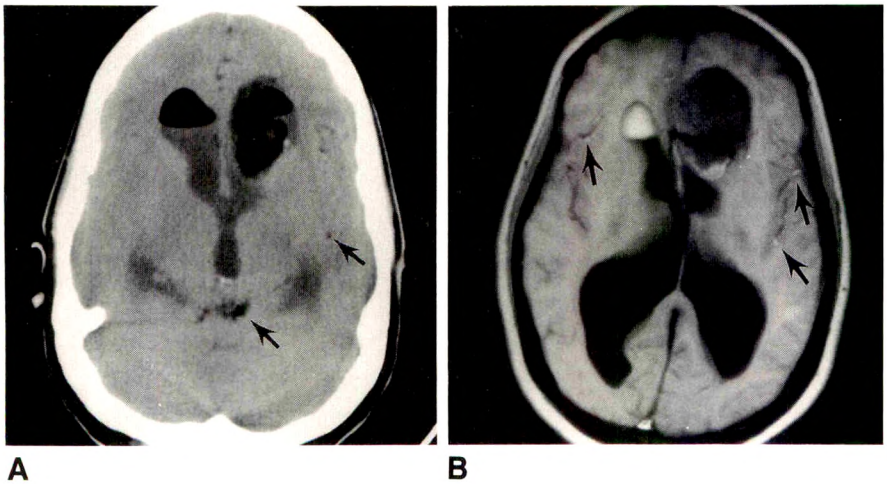
On short TR/short TE images, the solid component of the parasellar or intraparenchymal masses was low in intensity relative to brain with areas of isointense soft tissue and less prominent areas of hyperintensity. Long TR/long TE images showed the core or solid component of the mass to be inhomogeneously bright (Fig. 4). The latter correlated with surgical reports of the solid masses found to contain cholesterol crystals, epithelial lining, and hair and/or sebaceous glands. Case 7 was complicated by subacute and remote hemorrhage. The core mass in the sylvian fissure was of low intensity relative to the large bloody cyst on short TR/short TE images (Fig. 5). At surgery, the mass was green, solid, and contained dense cholesterol crystals, blood, and a focus of ossification. On the surgical report, the lesion was considered ruptured due to the presence of satellite lesions extending from the intraparenchymal mass into and widening the sylvian fissure.

Involvement of the orbital apex was clearly evident by MR,

**TABLE 1: Clinical Symptoms and Imaging Studies in Seven Patients with Ruptured Intracranial Dermoid Cysts**

| Case No. | Age (years) | Sex | Presentation | CT | MR | Angiography | Surgery | Follow-up |
|---|---|---|---|---|---|---|---|---|
| 1 | 23 | F | 5 yr history of headache, new visual symptoms | 01/30/88 | 02/02/88 | 02/24/88 | 03/03/88 | Required shunting at 3 weeks |
| 2 | 24 | F | Dermoid diagnosed at age 9, new visual symptoms | 1983, 1986<br>04/21/87 | 1983<br>11/09/87 | 1983 | 1973 | Another recurrence in 1989 |
| 3 | 43 | M | New seizure, headache for 2 days, 1 month of blurred vision | 06/07/88 | 06/09/88 | 06/10/88 | 06/14/88 | Doing well at 1 yr |
| 4 | 35 | M | Acute hemiparesis, 8 yr history of anisocoria | 10/22/87 | 11/11/87 | 11/30/87 | 12/01/87 | Doing well at 6 months |
| 5 | 49 | M | New seizures, benign brain tumor removed 10 yr earlier | 04/16/88 | 05/03/88 | N.A. | 04/16/88 | Post-op confusion, slight improvement at 6 months |
| 6 | 45 | F | Progressive seizures and aphasia, over 2 yr | 09/27/85 | 05/22/85 | (01/20/86) | 01/21/86 | Doing well at 1 yr |
| 7 | 80 | F | Acute confusion and right hemiparesis | 02/08/89 | 02/08/89 | (06/88) | 02/13/89 | Did well until died of pulmonary embolism 2/27/89 |

Note.—Parentheses indicate study unavailable for review.



A B

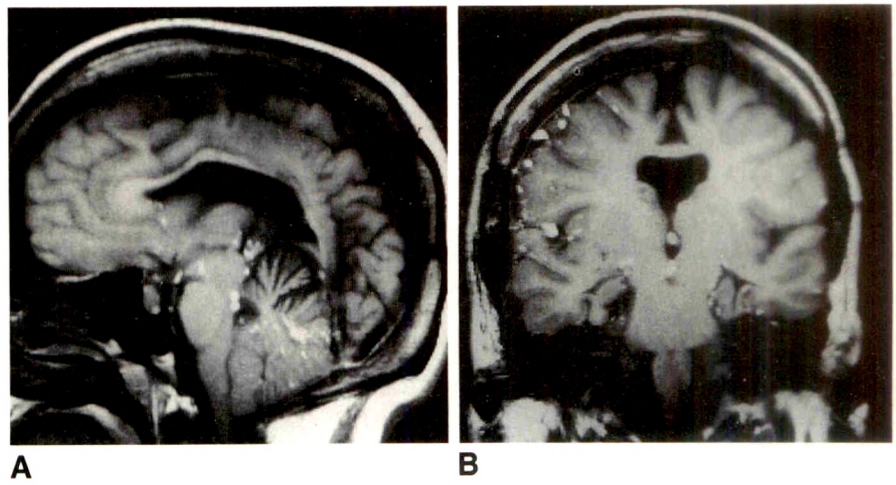
**Fig. 1.—Case 1: 23-year-old woman with 5-year history of intermittent headaches associated with leg weakness. A mass of heterogeneous soft tissue and fat, which extended from the parasagittal region, intrudes into frontal horn of left lateral ventricle. Fat/CSF level is seen within right lateral ventricle. Fat globules can also be seen scattered within other subarachnoid spaces (*arrows*).**

***A*, Unenhanced CT scan.**

***B*, T1-weighted (400/14) MR image shows better delineation of fat from extraventricular CSF compared with CT scan.**

Fig. 2.—Case 2: 24-year-old woman who had a ventriculostomy shunt placed at 7 weeks of age for aqueductal stenosis, and debulking of a left middle fossa dermoid at ages 9 and 19. The patient also had multiple congenital defects including an absence of the septum pellucidum and aqueductal stenosis.

*A* and *B*, Sagittal (*A*) and coronal (*B*) T1-weighted (500/20) MR images show fat signal within third and fourth ventricles and extensive subarachnoid seeding.



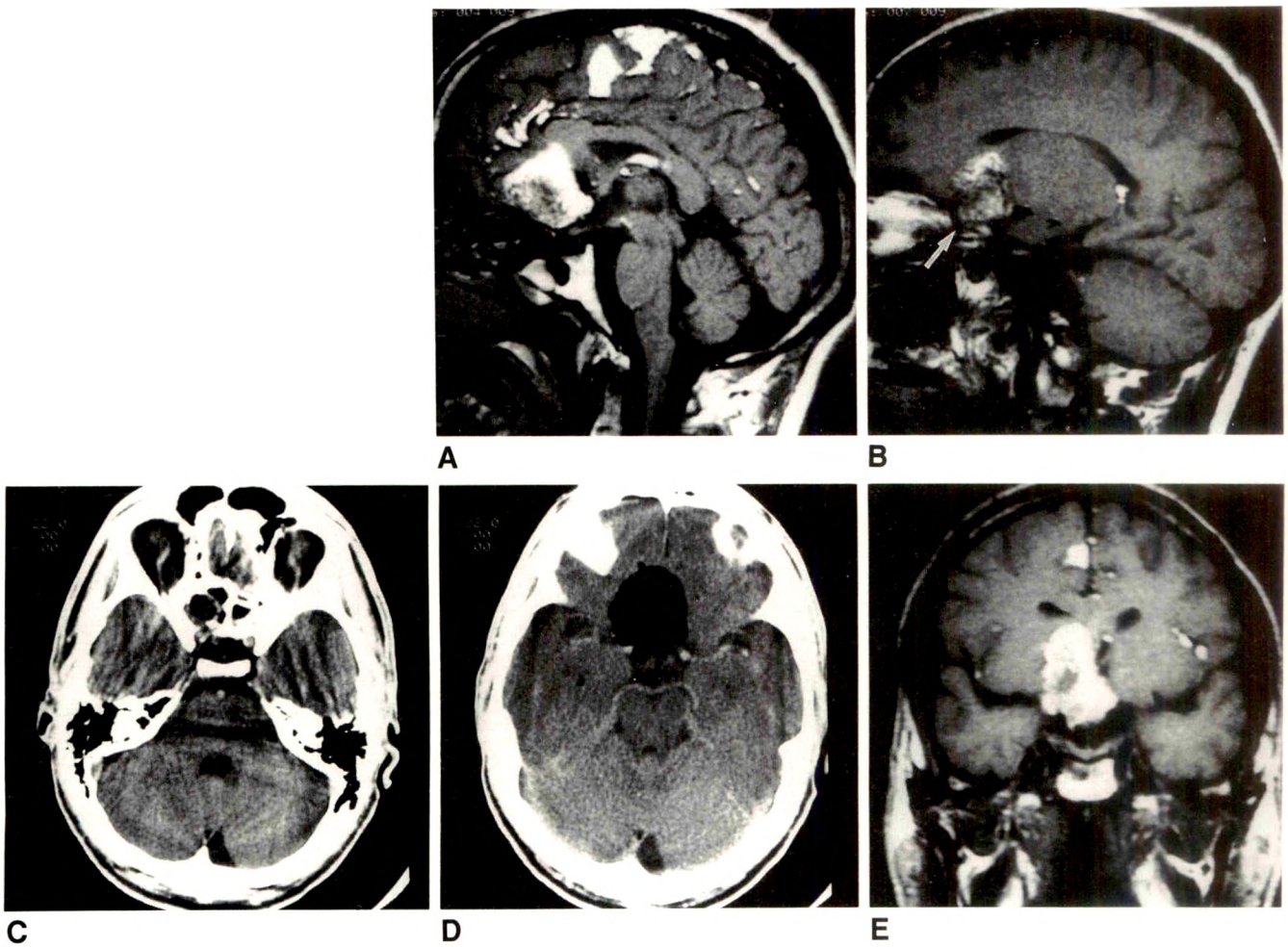




Fig. 3.—Case 3: 43-year-old man who presented with headache and 1 month of blurred vision.

*A*, T1-weighted (500/20) MR image shows suprasellar mass of heterogeneous signal intensity. Material of increased signal intensity widens the sulci at the interhemispheric fissure.

*B*, T1-weighted (500/20) MR image shows impingement on orbital apex by mass (*arrow*).

*C*, CT scan shows mass at orbital apex but impingement on orbit must be surmised.

*D*, CT scan at region of chiasm indicates some encroachment.

*E*, Coronal T1-weighted (600/20) MR image shows chiasm nearly engulfed by the mass.

while only suspected by CT in cases 2 and 3. Involvement of the optic chiasm in case 3 was also dramatically demonstrated. Both of these patients had visual symptoms. Angiographic correlation was available in three cases. Displacement and encasement of the right internal carotid artery and displacement of the basilar and right posterior cerebral arteries were predicted by MR in case 4 and confirmed by angiography (Fig. 4).

MR accurately predicted displacement without encasement of the anterior cerebral arteries in cases 1 and 3. Cases 2 and 7 clearly showed flow void within the displaced middle cerebral arteries, but angiographic correlation was not available. Case 5 did not have angiographic or CT/MR suggestion of major vessel displacement. Patient 6 was imaged on a 0.15-T prototype unit and the study was inadequate for evaluation of vessels. There was no evidence of edema in parenchyma surrounding the dermoid cysts by CT or MR examination. Ventricular enlargement was present in four patients (cases 1, 4, 5, 7), three with interstitial edema (cases 4, 5, 7). Small-rim calcifications seen by CT in cases 3, 4, and

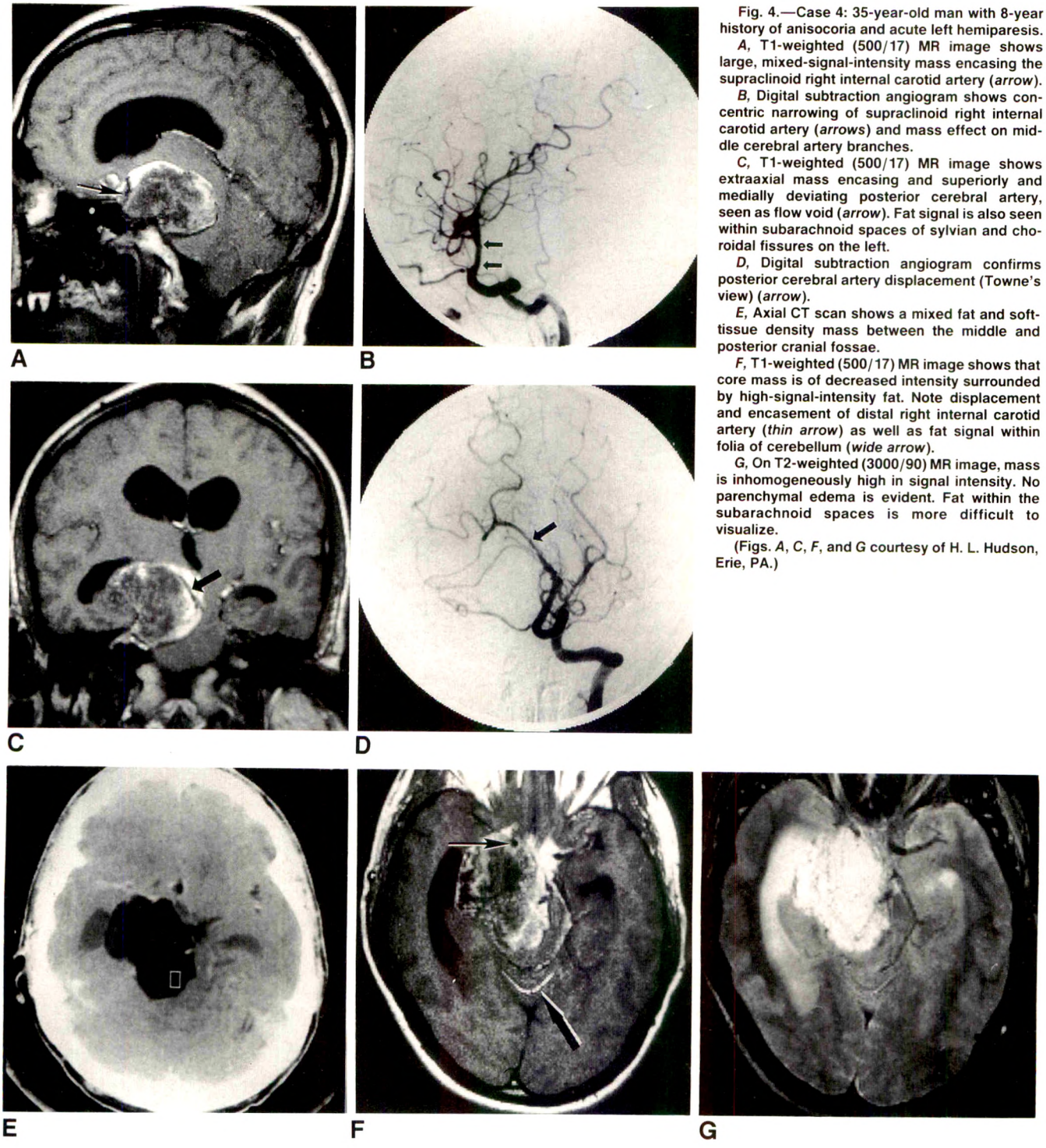



Fig. 4.—Case 4: 35-year-old man with 8-year history of anisocoria and acute left hemiparesis.

*A*, T1-weighted (500/17) MR image shows large, mixed-signal-intensity mass encasing the supraclinoid right internal carotid artery (*arrow*).

*B*, Digital subtraction angiogram shows concentric narrowing of supraclinoid right internal carotid artery (*arrows*) and mass effect on middle cerebral artery branches.

*C*, T1-weighted (500/17) MR image shows extraaxial mass encasing and superiorly and medially deviating posterior cerebral artery, seen as flow void (*arrow*). Fat signal is also seen within subarachnoid spaces of sylvian and choroidal fissures on the left.

*D*, Digital subtraction angiogram confirms posterior cerebral artery displacement (Towne's view) (*arrow*).

*E*, Axial CT scan shows a mixed fat and soft-tissue density mass between the middle and posterior cranial fossae.

*F*, T1-weighted (500/17) MR image shows that core mass is of decreased intensity surrounded by high-signal-intensity fat. Note displacement and encasement of distal right internal carotid artery (*thin arrow*) as well as fat signal within folia of cerebellum (*wide arrow*).

*G*, On T2-weighted (3000/90) MR image, mass is inhomogeneously high in signal intensity. No parenchymal edema is evident. Fat within the subarachnoid spaces is more difficult to visualize.

(Figs. *A*, *C*, *F*, and *G* courtesy of H. L. Hudson, Erie, PA.)

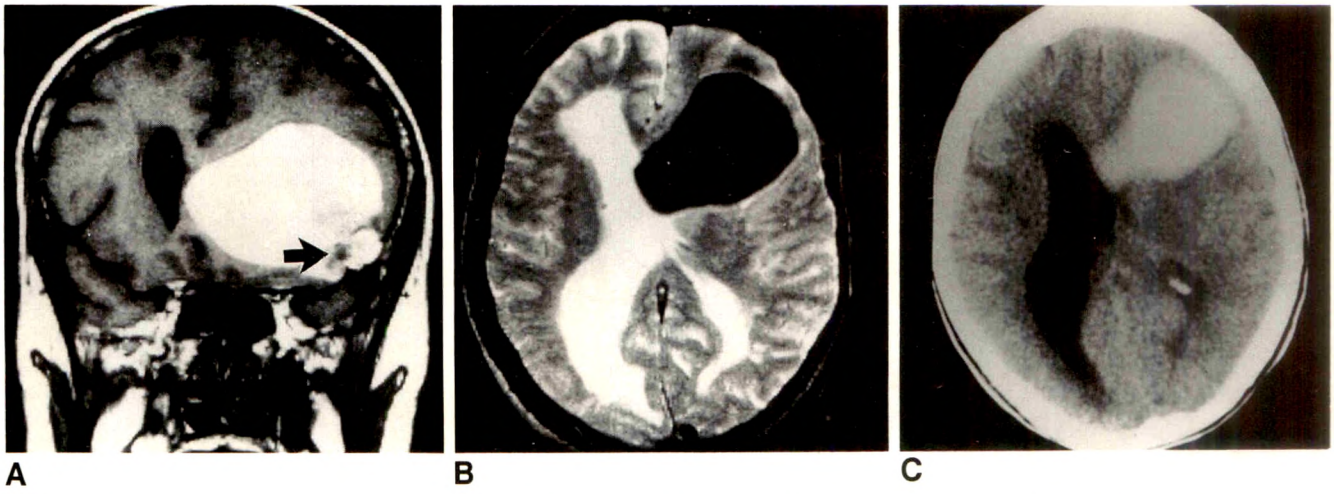



**Fig. 5.—Case 7: 80-year-old woman with acute confusion, right hemiparesis, and frontal headaches of several months duration.**
***A*, T1-weighted (500/20) MR image shows large hyperintense mass within left frontal parenchyma ruptured into sylvian fissure. The hypointense focus (*arrow*) was a solid mass of cholesterol crystals.**
***B*, T2-weighted (2400/120) MR image shows that marked hypointensity of cyst correlates with the presence of acute blood.**
***C*, CT scan confirms the presence of blood and paucity of edema.**

5 were not definable by MR. On follow-up two of seven patients required ventricular shunts for enlarging ventricular size [1, 5].

## Discussion

Dermoid cysts are within the category of epithelial cysts. Their location in the midline or posterior fossa and their presentation in the first two to three decades of life helps to differentiate dermoids from epidermoids. Epidermoids tend to present in the fifth decade and are less often in the midline, frequently at the cerebellopontine angle [8, 9]. Like epidermoid cysts, intracranial dermoid cysts are thought to originate from ectodermal inclusions from defects of closure at approximately 3 to 5 weeks gestation [10]. Histologically, the dermoid cyst has a lining of stratified squamous epithelial cells, a feature shared with epidermoid cysts. Unlike epidermoid cysts, however, dermoid cysts can contain additional elements of hair or sebaceous or sweat glands [8, 11]. These additional dermal elements are of ectodermal origin [12]. The presence of all epidermal layers in dermoid cysts leads to the theory that they originated from the inclusion of a slightly more primitive, pluripotential cell than that which gives rise to epidermoid cysts [10]. The elements of the dermoid cyst can vary in relative proportions. In general, there is a thick, viscous, greenish-brown fluid composed of lipid metabolites and liquid cholesterol from decomposed epithelial cells. Cholesterol crystals result in more lumpy masses. Hair can be present as a few strands or a matted clump [11]. Calcifications of dental enamel, another ectodermal derivative, are present less often [13].

The liquid products of lipid metabolism and cell breakdown and resulting increased hydrogen density could explain the increased signal intensity seen on short TR/short TE images within the subarachnoid and intraventricular spaces. The liquid nature of the fatty acids and liquid portion of the cholesterol may affect the protons available for use in MR signal. Protons bound to cholesterol crystals, hair, and intact cells of the solid tumor mass are less available to yield an MR signal; thus, this part of the mass is hypo-to isointense relative to brain. The inhomogeneous signal on long TR/long TE images from the more solid core of the mass reflects the mixture of intact and partially degenerated materials of the hair, glandular elements, and more solid cholesterol.

The CT characteristics of ruptured dermoid cysts were first described by Fawcitt and Isherwood in 1976 [2] and are typified by fat/CSF levels within the ventricles and/or fat densities in subarachnoid spaces [4, 5]. An extraaxial or combined extra- and intraaxial soft-tissue mass is present. Although, this is not the first report of MR findings of ruptured dermoid cyst, to the best of our knowledge, the cases presented here are the first MR demonstration of the imaging characteristics and utility of MR in diagnosing this disease.

This series demonstrates three patterns of distribution for the spilled contents of intracranial dermoid cysts. The classic CT appearance of fat/fluid levels in the ventricles was present in less than half the cases (three of seven). The first six cases also displayed extraventricular subarachnoid spread, six of which were diffuse. The images show that the non–gravity-dependent fat is not merely trapped between sulci, implying that it is adherent. The first MR report of ruptured intracranial dermoid by Hahn et al. [14] displayed the curious finding of sulci widened by fat deposits on short TR/short TE images. This third pattern of localized spread in sulci, as seen in case 3 in our series, may represent ruptured contents contained by pia or inflammatory tissue. Indeed, this may have been the appearance of case 7 (Fig. 5) prior to hemorrhage, since thick inflammatory reaction encasing the extension of the mass into the sylvian fissure was present at surgery. The possibility that the pattern of fat distribution may relate to the chronicity of the rupture and the patient's symptoms was considered. It was tempting to surmise that fat/fluid levels may correlate with more recent cyst rupture and the localized fat with sulcal widening due to a more chronic, indolent leak. This hypothesis was not borne out by the clinical data in this series of patients.

Aside from the ease of multiplanar imaging, MR has additional advantages over CT in imaging dermoid cysts as demonstrated by these cases. The extent of the mass and the relation to the skull base was more easily evaluated by MR because of the lack of bone artifacts. Five of these large

dermoid cysts extended from the parasellar region of the skull base, invaginating deeply into brain parenchyma. No evidence of connection to the skull could be seen on MR or CT to suggest a definable dermal sinus, which is often associated with posterior fossa dermoids [10, 15]. Possible connections to the skull (i.e., at the areas of otic and optic closure) may be small, but Currarino and Rutledge [16] suggest they may be more common than previously thought. Indeed, the patient in case 4 was known to have an intraorbital dermoid on the side opposite the intracranial lesion as well as a midline parietal skull defect, indicating faults in closure.

Generally, epidermoids have been reported as areas of hypo- to isointensity on short TR/short TE images [17]. Six of seven of our cases of dermoids displayed high signal on short TR/short TE images. However, in a minority of cases the T1 signal is not a reliable criterion for the MR differentiation of dermoids from epidermoids. Epidermoids have been reported to have areas of high signal on short TR/short TE sequences [18, 19]. The opposite situation has been reported in which two proved dermoids and two lipomas have yielded low signal on T1- and T2-weighted images at 0.15 T [20]. We have seen two cases of recurrent dermoid having only an isointense mass. Since the complications of dermoids and epidermoids are similar, the lack of specificity in these occasional cases with varying MR characteristics is probably of less clinical significance than the size and location of the mass. The lack of MR visualization of calcification seen by CT is of no clinical significance.

We were impressed by the large size of the lesions relative to the lack of edema in these patients at the time of presentation. The slow rate of growth and their tendency to extend through subarachnoid spaces along the base of the brain is reflected in the relative paucity of symptoms in relation to tumor size [9]. The most frequent symptoms are headache, seizure, dementia, meningitis, and transient ischemic attacks associated with arterial spasm. The latter has been associated temporally with rupture of the cysts [2] and was probably implicated as the cause of hemiparesis in cases 2 and 5 of this series. In general, however, symptoms may not be related to the time of rupture [5] and may be a response to the cholesterol rather than lipid content [4]. Five of our cases showed compression or displacement of intracranial vessels. In this retrospective review, four of the cases had correlative angiography. However, the MR, especially if paired with MR angiography, should obviate conventional angiography for evaluation of arterial anatomy on a prospective basis.

Earlier studies reported that the rupture of an intracranial dermoid with consequent ventriculitis and meningitis was fatal [1]. The cases in this series add to the body of patients surviving rupture and subsequent removal of intracranial dermoid cysts [4, 6, 7]. However, chronic arachnoiditis does appear to be a frequent sequela. The rate of occurrence of bleeding into a dermoid cyst or association with rupture is unknown.

In summary, MR had no advantage over CT for the initial diagnosis of ruptured intracranial dermoid cyst. The MR characteristics were that of a relatively large mass, which was usually parasellar. This mass contained a solid portion that was of decreased signal on short TR/short TE images and of mixed intensity on long TR/long TE images, corresponding to pathologic findings of cholesterol crystals, epithelial lining, and glandular structures. The spread of the liquid contents of the dermoid cyst was more conspicuous on MR than CT owing to bright signal intensity on short TR/short TE images. The patterns of the fat signal were reflected in fat/fluid levels in the ventricles, generalized spread through the subarachnoid spaces, and a pattern of more limited spread within widened sulci. The duration of patient symptoms could not be correlated with the appearance of the fat distribution and cyst rupture. The capability of MR to evaluate the associated vessel displacement, either by flow void or MR angiography, paired with better visualization of the lesions relative to the base of the skull owing to lack of bone interference and multiplanar imaging capability, make MR the preferred preoperative imaging method. The cases in this series also add to the number of patients who have survived rupture of intracranial epithelial cysts.

## REFERENCES


1. Manlapaz JS. Ruptured intracranial dermoid: report of a case and survey of previously reported cases. *Am J Surg* **1960**;100:723–730
2. Fawcitt RA, Isherwood I. Radiodiagnosis of intracranial pearly tumors with particular reference to the value of computed tomography. *Neuroradiology* **1976**;11:235–242
3. Ford K, Drayer B, Osborne D, Dubois P. Case report: Transient cerebral ischemia as a manifestation of ruptured intracranial dermoid cyst. *J Comput Assist Tomogr* **1981**;5:895–897
4. Amendola MA, Garfinkle WB, Ostrum BJ, Katz MR, Katz RI. Preoperative diagnosis of a ruptured intracranial dermoid cyst by computerized tomography. Case report. *J Neurosurg* **1978**;48:1035–1037
5. Laster DW, Moody DM, Ball MR. Epidermoid tumors with intraventricular and subarachnoid fat: report of 2 cases. *AJR* **1977**;128:504–507
6. Hamer J. Diagnosis by computerized tomography of intradural dermoid with spontaneous rupture of the cyst. *Acta Neurochir* (Wien) **1980**;51:219–226
7. Healy JF, Brahme FJ, Rosenkrantz H. Dermoid cysts and their complications as manifested by computed cranial tomography. *Comput Tomogr* **1980**;4:111–115
8. Rubinstein LJ. *Atlas of tumor pathology*, second series, fasicle 6. Bethesda, MD: Armed Forces Institute of Pathology, **1972**:228–292
9. Fleming R, Botterell EH. Cranial dermoid and epidermoid tumors. *Surg Gynecol Obstet* **1959**;109:403–411
10. Schijman E, Monges J, Cragnaz R. Congenital dermal sinuses, dermoid and epidermoid cysts of the posterior fossa. *Childs Nerv Syst* **1986**;2:83–89
11. Martin J, Davis L. Intracranial dermoid and epidermoid tumors. *Arch Neurol Psychol* **1943**;49:56–70
12. Smith AS. Myth of the mesoderm: ectodermal origin of dermoids. *AJNR* **1989**;8:449
13. Arey LB. *Developmental anatomy*. Philadelphia: Saunders, **1982**:89, 230–235
14. Hahn FJ, Ong E, McComb RD, et. al. MR imaging of ruptured intracranial dermoid. *J Comput Assist Tomogr* **1986**;10:888–892
15. Tytus JS, Pennybacker J. Pearly tumors in relation to the central nervous system. *J Neurol Neurosurg Psychiatry* **1959**;19:241–259
16. Currarino G, Rutledge JC. Temporoparietal dermoid cysts with intracranial extension. *AJNR* **1988**;9:385–387
17. Tampieri D, Melanson D, Ethier R. MR imaging of epidermoid cysts. *AJNR* **1989**;10:351–356
18. Mackay IM, Bydder GN, Young IR. MR imaging of central nervous system tumors that do not display increase in T1 or T2. *J Comput Assist Tomogr* **1985**;9:1055–1061
19. Lee BCP, Kneeland JB, Deck MDF, Cahill PT. Posterior fossa lesions: magnetic resonance imaging. *Radiology* **1984**;153:137–143
20. Latack JT, Kartush JM, Kenink JL, et. al. Epidermoidomas of the cerebellopontine angle and temporal bone: CT and MR aspects. *Radiology* **1985**;157:361–366

Review Article

# Inferior Vena Caval Filters: Analysis of Five Currently Available Devices

Clement J. Grassi[1]

The use of an effective, safe, and easily introducible percutaneous vena caval filter is crucial in the treatment of certain patients with pulmonary embolism or deep venous thrombosis. Until recently, the choice of a vena caval filter was limited to one device, the 24-French Greenfield filter, the sole filter accepted by the Food and Drug Administration (FDA) for use in the United States. Now, several devices are FDA-approved and available in the United States, and other newer filters are currently in use in Europe. These filters feature easier insertion, improved filtering, antitilt abilities, memory-wire properties, and potential retrievability.

The purpose of this article is to review such newer filters in terms of their ease of use, efficacy, and associated morbidity, focusing on the five devices available for use in the United States; to review the current indications for use of transvenous filters; and to put into perspective the trends that are likely to occur in the future use of inferior vena caval (IVC) filters.

## The "Ideal" IVC Filter

The characteristics of the ideal IVC filter are listed in Table 1. No caval filter, to date, has successfully achieved all of these objectives. Several factors must be considered when selecting an IVC filter. The most important factors are a high filtering efficiency (large and small emboli) without impedance of blood flow, stability of positioning, and a low rate of associated morbidity.

Some of these criteria for optimal filter design may be incompatible within a single filter type. For instance, a filter design that has excellent fixation within the IVC and is secure may be extremely difficult to retrieve. The duration of time after insertion also has an effect. Retrievability of the Amplatz filter is initially satisfactory; however, in dogs, Amplatz filter retrieval at 3 weeks was more difficult and may have caused slight vena caval damage [1]. Given the constraints of thromboembolic protection in most patients, and the known continued endothelialization that occurs at the vena caval wall, the practical usefulness of retrievability may be limited.

Although much emphasis has been placed by manufacturers on the small size (Fig. 1) of current introduction systems, the size advantage alone should not overshadow the three major factors mentioned before. Especially in patients with filter placement for prophylaxis, and those with full-life expectancies, the funtional performance of the device should be the primary consideration.

A crucial factor in selecting an IVC filter is how efficiently the filter can trap thrombus in vivo. However, a balance must be created between highly effective clot trapping with the concomitant risk of IVC occlusion and maintenance of high IVC patency with the possible failure to trap thrombus. A case in point is the Mobin-Uddin filter, used between 1969 and 1977. Although its rate of recurrent pulmonary embolism was very low (0.5%), the prevalence of vena caval occlusion was high, 60–70% [2, 3]. Its use declined when the Greenfield filter became available, primarily because of this morbidity, which resulted in venous stasis and leg edema.

Received July 31, 1990; accepted after revision November 1, 1990.

[1] Department of Radiology, Harvard Medical School and Brigham and Women's Hospital, 75 Francis St., Boston, MA 02115. Address reprint requests to C. J. Grassi.

*AJR* 156:813–821, April 1991 0361–803X/91/1564–0813 © American Roentgen Ray Society

**TABLE 1: Characteristics of an "Ideal" Vena Caval Filter**

| |
|---|
| Nonthrombogenic, biocompatible, long-life material |
| High filtering efficiency (large and small emboli) without impedance of flow |
| Secure fixation within the vena cava |
| Rapid percutaneous insertion |
| Small caliber |
| Release mechanism simple and controlled |
| Amenable to repositioning |
| MR imaging compatibility (e.g., nonferromagnetic) |
| Low cost |
| Retrievability |

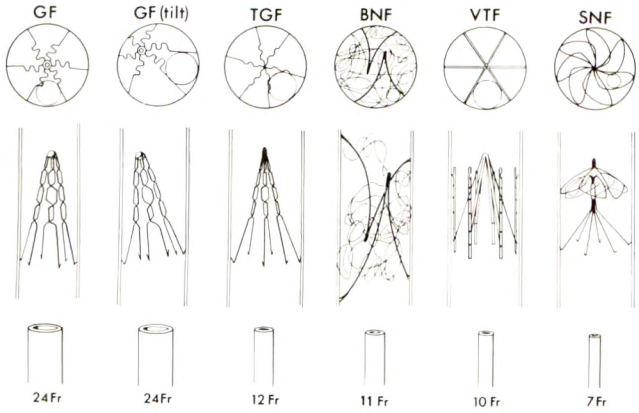



**Fig. 1.—Diagram of implanted filters shows cross sections (*top*), frontal views (*middle*), and carrier sizes (*bottom*). GF = Greenfield filter, GF (tilt) = tilted Greenfield filter, TGF = titanium Greenfield filter, BNF = bird's nest filter, VTF = Vena-Tech filter, SNF = Simon nitinol filter. Tilted Greenfield stainless steel filter, which theoretically leaves larger unprotected spaces for thromboembolism passage, is compared with a centered GF and with other filters. (Modified from a diagram provided by courtesy of Morris Simon.)**

Exact comparison of filter device function can be problematic. Although in vitro models may be helpful initially, they do not consistently reflect clinical reality and may be misleading. For example, Katsamouris et al. [3] demonstrated in vitro that the bird's nest, Simon nitinol, Amplatz, and Gunther filters show superior clot trapping for both large and small emboli, and that the stainless steel Greenfield filter trapped clots sufficiently when centered, but allowed emboli to pass when tilted [3] (Fig. 1). However, another in vitro study in sheep showed that the Greenfield filter is capable of stopping both large and smaller emboli [4]. This underscores the importance of having in vivo studies in addition to in vitro testing. In order to evaluate the clinical efficacy of percutaneous IVC filters, there is no substitute for randomized, prospective clinical studies [5]. However, even in the currently published clinical evaluations on filter efficacy, the quality of the comparative data is quite variable. For instance, some series have high numbers of filters placed for prophylaxis [6], other series have conducted follow-up on such important factors as recurrent pulmonary embolism by clinical means, telephone contact, or mail [7], and still other series do not specify how recurrent emboli were verified [8]. Given these limitations, this review has used the major series published for each filter approved by the FDA, supplemented with updates of these devices.

## Older Filters

### *Mobin-Uddin Umbrella Filter*

This filter is mentioned for historical reasons only, because the Mobin-Uddin filter (MUF) is no longer available in the United States. It is constructed as an inverted umbrella with six flat stainless steel spokes, and covered with a thin Silastic membrane. A 23-mm-diameter size was originally used, but episodes of filter migration led to the development of a larger 28-mm filter [9].

The low rate of recurrent pulmonary embolism (0.5%) was overshadowed by the high prevalence of vena caval occlusion, 60–70%, and lower extremity venous stasis. With this major disadvantage, it is not surprising that the MUF was supplanted by the Greenfield filter when it became available.

### *Greenfield Stainless Steel Filter*

With its longer period of availability, the Greenfield stainless steel filter (GF; Medi-tech, Watertown, MA; Fig. 2) has had the most numerous clinical evaluations. It first was described in 1973, and the first clinical series were published in 1977 [6, 10–16]. The GF design permits filling of 70% of the filter cone by thrombus with a reduction in the filter's effective cross-sectional area of only 50% [17]. Its construction consists of six stainless steel wires in a conical shape extending from a central hub, and the tips form a circular base with a maximal diameter of 30 mm (recommended for IVC sizes of 28 mm) [18]. Percutaneous insertion is performed via a 24-French system from femoral or jugular routes, with specific carrier-introduction systems.

Misplacement or malposition of the filter into the renal veins, hepatic veins, or right atrium has been reported [19]. Asymptomatic penetration of the filter foot prongs through the vena caval wall occurs with some frequency although therate of clinically symptomatic vena caval perforation is low. Penetration has been described at multiple sites including the ureter, intestine, aorta, and vertebral body [15, 20].

The GF has a reported recurrent embolism rate of 5% [16, 21] and a vena caval occlusion rate of approximately 3–5% [6, 11, 14–16]. Optimal filtration of caval blood flow results with angles less than 15° tilt from the vertical; this was a potential long-term problem of the filter.

Reduced filtration efficiency with tilting has been a much-publicized disadvantage of the GF [3]. Subsequently published experiments in sheep, whose vena caval diameters approximate that of humans, have shown that the tendency toward deteriorating clot-trapping performance when the Greenfield filter is tilted within the vena cava is not as dramatic as once believed [4]. A possible explanation for this apparent discrepancy between clinical and experimental data may be that not all pulmonary emboli are symptomatic and that the Greenfield filter protects against massive, potentially lethal pulmonary emboli, whereas small emboli pass through the

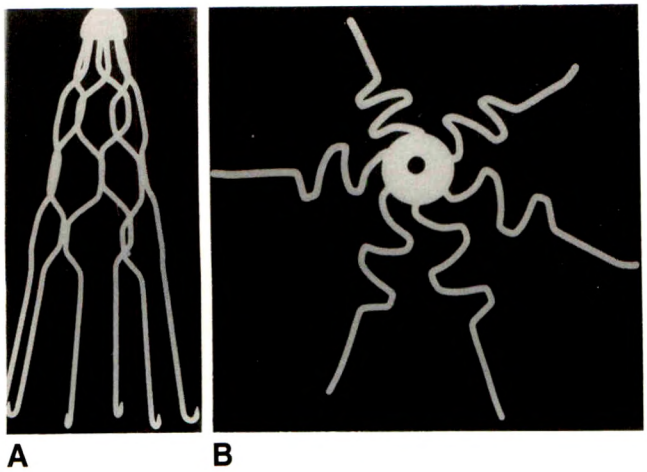



Fig. 2.—*A* and *B*, Lateral (*A*) and axial (*B*) radiographs of Greenfield filter.

filter and remain asymptomatic. Significant thrombus has been observed on both sides of the filter on follow-up venacavography [21], yet may not be apparent on subsequent examinations. Possibly, these thrombi are lysed in situ by the flow of blood, or fragment further into sufficiently small sizes that they may pass through the GF and cause no clinical symptoms on reaching the lungs. Other thrombi are symptomatic, and for any patient with clinical or radiologic evidence of pulmonary emboli despite the presence of a Greenfield IVC filter, there should be a high suspicion for recurrent thrombus on the filter itself (Fig. 3).

The GF's established rate of high vena caval patency (95–98%) is an advantage in those uncommon situations in which a suprarenal vein placement is necessary. These indications, which are derived from limited numbers of patients, include caval thrombosis extending above the renal veins, renal vein thrombosis, thromboemboli despite prior IVC interruption, or recurrent thromboemboli with a large, patent left ovarian vein (with or without thrombus itself) [22].

The large 24-French size of the stainless steel Greenfield filter system is its principal disadvantage. A 10–24% prevalence of sonographically identified femoral vein thrombosis [23], most likely related to venous dilatation and endothelial injury locally, is another important consideration.

## Newer Filters

### *Bird's Nest and Modified Filter*

The bird's nest filter (BNF; Cook, Bloomington, IN; Fig. 4) was first tested clinically in 1982 and has the advantage of a small sheath size, 12-French internal diameter in the modified version. Its mesh configuration consists of a series of preshaped wires that are formed by the operator in a series of maneuvers with a special applicator, and the wires assume an original shape that resembles a bird's nest [24]. Initially, the mesh was affixed by a series of V-struts 0.25 mm in diameter, intended to hold the BNF securely within the IVC. However, in the original BNF model, five of 422 filters migrated

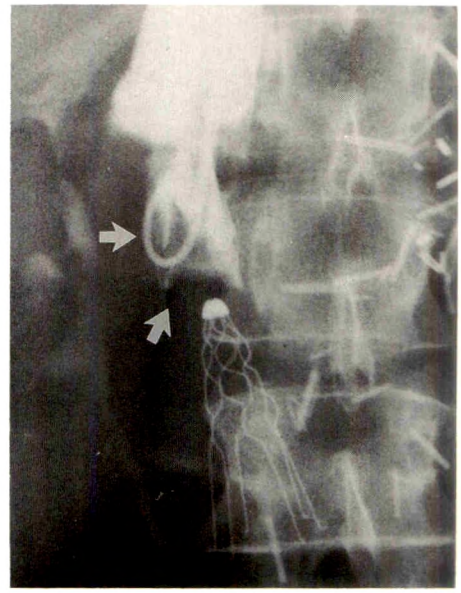


Fig. 3.—Venacavogram obtained with right internal jugular vein approach shows thrombus (*arrows*) superior to Greenfield filter, which is tilted within vena cava.

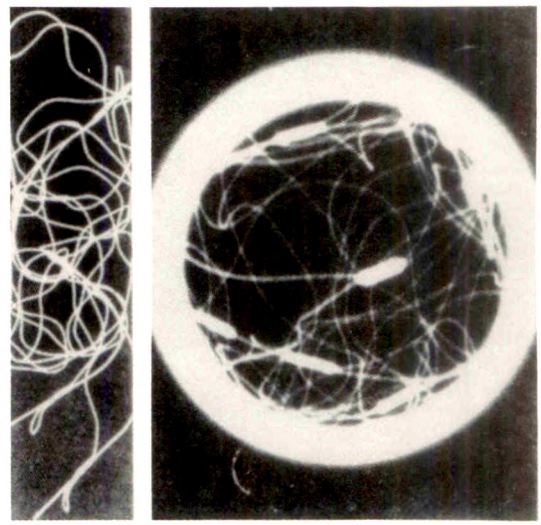



Fig. 4.—*A* and *B*, Lateral (*A*) and axial (*B*) venacavograms of mesh configuration of bird's nest filter.

(four to the right atrium without fatality, and one to the pulmonary artery with death 10 days later due to pulmonary embolism) [7]. The design of the BNF was modified, and a second-generation device with stiffer securing struts, 0.46 mm in diameter, has had no reported episodes of migration [7].

The rate of recurrent pulmonary embolism reported is 2.7%, and the rate of caval occlusion is 2.9% [7]. However, this follow-up was largely clinical and consisted of telephone or questionnaire contact in 400 of the 440 patients after 6 months; sonography, venacavography, or pulmonary angiog-

raphy was infrequently performed. Vena caval occlusion was documented in 19% of a subset of 40 patients who underwent radiologic follow-up [25]. Additionally, vena caval occlusion with phlegmasia cerulean dolens has been reported in one case that led to the patient's death [26], and a significant perforation of the caval wall has also been identified [25].

An advantage of the bird's nest filter is its free-form configuration within the IVC, because it is not subject to the need for centering as are several other filters. It can be inserted in vena cavas up to 40 mm in diameter. In very large vena cavas, it can eliminate the need to use bilateral iliac vein filters (Figs. 5A and 5B), because a single bird's nest filter will suffice (Figs. 5C and 5D). The free-form nature allows positioning of the filter mesh to include unexpected collateral veins or anomalous veins (Fig. 6).

*Titanium Greenfield Filter*

The titanium Greenfield filter (TGF; Medi-tech; Fig. 7), actually a significantly modified design of the stainless steel GF, was created to provide a smaller introduction size for percutaneous insertion. Its design lacks a central apical hole for guidewire insertion, and once the sheath and dilator are placed, the TGF carrier is passed directly under fluoroscopic control. Its elastic properties permit the TGF to be compressed into a 12-French carrier. The TGF has several differences from the stainless Greenfield filter: it is broader at the base (38 mm vs 30 mm), lighter (0.25 g vs 0.56 g), and it exerts a force of fixation on the wall of the vena cava that is greater than the stainless steel Greenfield filter's force at diameters over 22 mm, but less at diameters under 22 mm

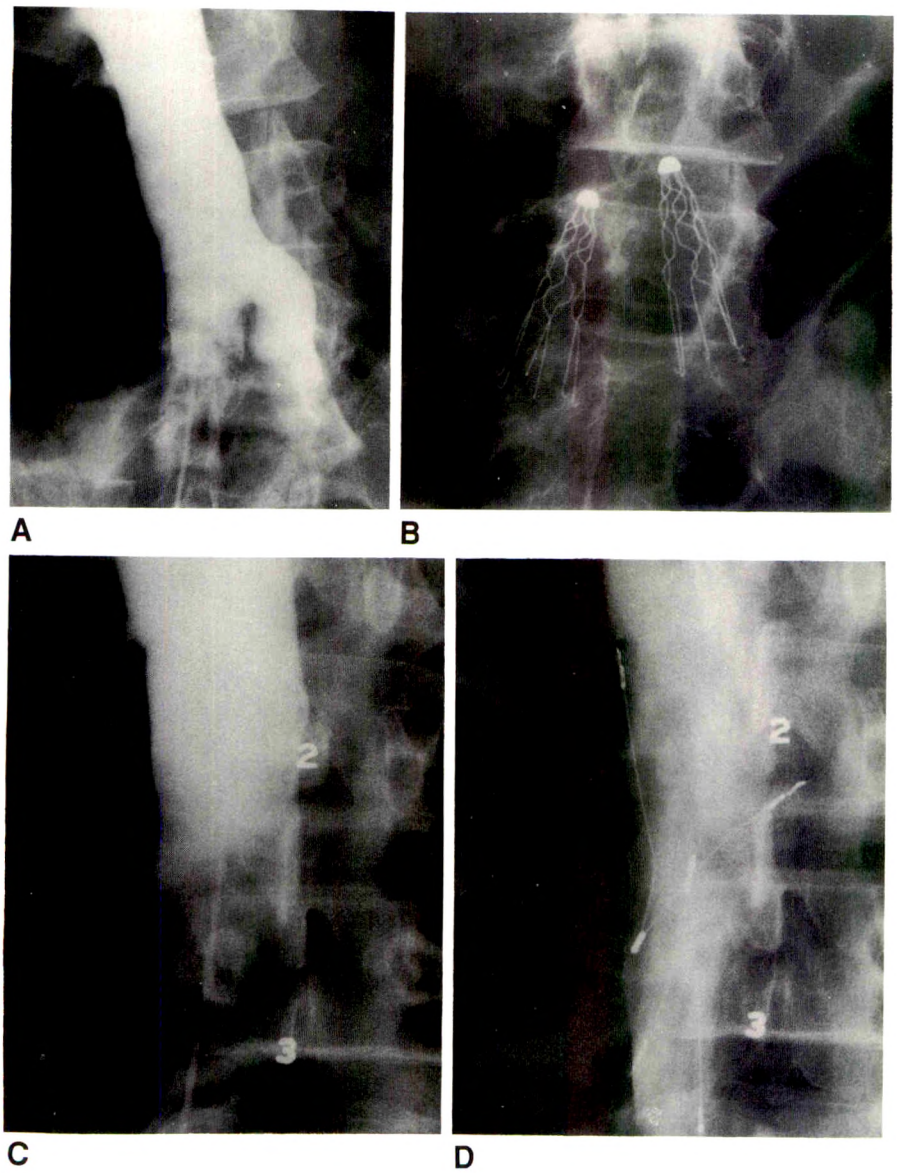



Fig. 5.—*A–D*, Venacavograms of large vena cava (*A*) that necessitated bilateral iliac vein filters when Greenfield filter was sole device available (*B*). A more recent case with a large vena cava (*C*) of 39 mm diameter was more easily managed with bird's nest filter alone (*D*).

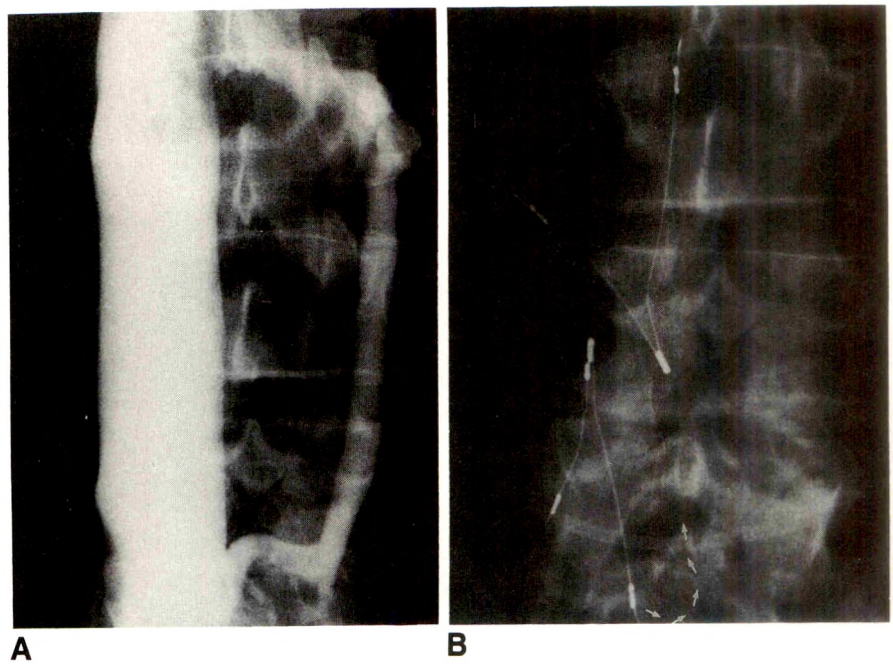



Fig. 6.—*A* and *B*, Venacavograms show large left-sided anomalous vein (*A*) or collateral vein contiguous with left renal vein (*B*). By positioning a portion of the bird's nest mesh well caudad (faintly seen on radiograph, *small arrows* in *B*), filtration of this extra vein was included.

[27]. TGF placement, as for the stainless-steel Greenfield filter, is recommended for caval diameters up to but not exceeding 28 mm.

This filter was available at selected centers for clinical trials, but these were terminated because of a high frequency of vena caval perforation by the filter legs [27] (Belmont M, personal communication). One in vitro study published at a participating center in the clinical trials attributed this higher rate of caval wall perforation to the possibility of filter splaying associated with the physical design of the TGF, clot retraction, and the possibility of changes in intracaval pressures [28]. The design of the filter hooks has been changed to avoid caval wall perforation, and the TGF is now available for clinical use.

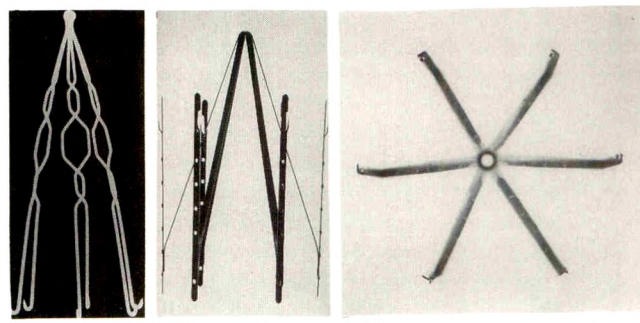



Fig. 7.—Lateral radiograph of titanium alloy version of Greenfield filter.

Fig. 8.—*A* and *B*, Lateral (*A*) and axial (*B*) photographs of Vena-Tech filter.

*Vena-Tech Filter*

The Vena-Tech filter (VTF; Fig. 8) is the American-marketed and FDA-approved version of the LGM filter (L. G. Medical, Chasseneuil, France). It has been accepted for use under a 510(K) application, that is, as a modification of a previously accepted device, the stainless steel Greenfield filter. Constructed of a cone with six flat, metallic diagonal struts and side rails that run parallel to the walls of the IVC, additional small barbs hold the filter in place. The VTF comes prepackaged in a 10-French carrier and requires a 12-French outer diameter sheath. Filter orientation within the carrier syringe is inverted when transjugular placement is used as compared with the transfemoral approach.

The Vena-Tech filter has been evaluated in a series of 100 patients abroad reported in two different journals [29, 30], and clinical usage in the United States is under way. Of the 100 attempts at insertion, the internal jugular route had an initial failure rate of 2% (two cases) and a 16% rate of malpositioning (eight filters tilted 15° or more, five filters incompletely opened and correctly aligned, and three filters incompletely opened and tilted) [30]. Follow-up at 1 year, including an abdominal radiograph, showed migration of the filter in 13% (nine cases inferiorly not exceeding the height of one vertebral body, and four superiorly toward the renal veins). Clinical follow-up shows a rate of recurrent pulmonary embolism of 2%, and vena caval occlusions in 7% during 1-year follow-up.

An advertised advantage of the VTF design is the feature of "positive positioning" by means of the barbed side rails. However, as these data indicate, the prevalence of initial malpositioning is significant, and the rate of later migration is lower. It is likely that several of these malpositionings were operator-related, occurring early in the VTF experience. Sev-

eral other malpositionings have been associated with jugular insertion. For best insertion, a technique of rapid deployment from the introducer should be used, with a quick motion of release into the IVC.

In the United States, F.C. Taylor et al. (unpublished data) have reported 65 successful placements with low morbidity. Recently, investigators have cautioned against placement above the renal veins and have avoided using the VTF from the left femoral vein because of malpositioning (Vogelzang RL, unpublished data). Several thousand LGM filters have been placed in Europe, and although United States experience is growing, further data will be necessary.

### *Simon Nitinol Filter*

The Simon nitinol filter (SNF; Nitinol Medical Technologies, Woburn, MA; Fig. 9) is made of a thermal memory alloy composed of nickel and titanium, which gives the filter unique properties. The filter wires are in straightened form at cooled temperatures (4–10°C) and these re-form into a predetermined filter shape at body temperature [31]. The filter shape is that of an umbrella dome with seven petal loops, which provide the major filtering, and six legs for fixation to the caval wall. Insertion is performed with a cold saline infusion through the plastic filter holder [32], and the device is easily inserted through a 7-French carrier with a 9-French outer diameter sheath. Both transfemoral and jugular insertion sets are available.

The Simon nitinol filter has been accepted by the FDA (April 1990) for clinical use. The multicenter clinical trials show a symptomatic recurrent pulmonary embolism rate of 1.1%, and asymptomatic pulmonary embolism of 0.7%, detected by ventilation/perfusion lung scan, or pulmonary arteriogram, added in select cases. The vena caval occlusion rate reported is 7.8% (symptomatic) and 1.9% (asymptomatic), with the latter detected by additional sonography, CT, or MR imaging (Simon M, Grassi CJ, Kim D, unpublished data).

The SNF has a unique design and very appealing small introduction size. Its memory-wire properties enable it to achieve the smallest introduction size of all the filters. The "SNF 7/6" (seven dome loops and six legs) rate of vena caval occlusion appears to be slightly higher; however, it will be necessary to see how its long-term caval patency compares with those of the bird's nest and Vena-Tech filters with more clinical usage, before a final comparison can be made.

## Current Indications

With the increase in percutaneous filter placement by using small French systems, and greater experience with the natural outcome of venous thrombosis, the indications for vena caval filters have been expanded. There are now three major categories for filter placement in venous thromboembolism: contraindication to anticoagulation, failure of adequate anticoagulation therapy, and prophylactic placement in high-risk patients.

Of these, the first two categories are well established [10, 17, 33] and apply to the older and newer filters. However, the

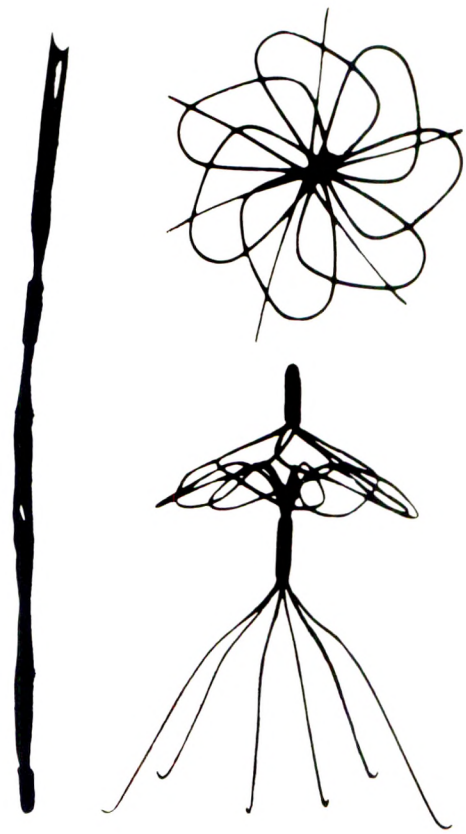


**Fig. 9.—Photographs of Simon nitinol filter in straight form within carrier (*left*), lateral view (*lower right*), and axial view (*upper right*).**

role of vena cava filter placement in patients with deep venous thrombosis that develops despite adequate anticoagulation is less clear. Most agree that the presence of iliofemoral thrombosis is a high-risk factor for pulmonary embolus, and they will place a filter when anticoagulation is contraindicated [10, 33]. This risk is significant particularly in patients with free-floating femoral or iliac vein thrombus greater than 5 cm in length [34].

The third category, prophylaxis for high-risk patients (e.g., before neurologic, spine, or hip surgery, and patients with paraplegia or pelvic fractures), has evolved largely because the percutaneous IVC filter is such an attractive therapy that its placement in patients without established pulmonary embolism or deep venous thrombosis has been advocated [10, 35]. It is my belief that the ease of insertion should not lead to an uncontrolled situation in which technology becomes the motivating force for IVC filter placement. Rather, firm medical indications should be the prime determinant of which patients receive vena caval filters [36, 37].

One indication for prophylactic filter use is in the setting of cor pulmonale in patients with severe pulmonary hypertension. These patients may not tolerate a subsequent pulmonary embolus [38], and filter placement has a valuable role. Additionally, when a previous IVC filter has been misplaced, has migrated, or has functionally failed to prevent pulmonary embolus, a second vena caval filter can be added (Fig. 10).

### Contraindications

Contraindications to percutaneous filter placement of all types include the relatively uncommon situations in which surgical venotomy and closure may be preferred. Patients with severe blood coagulopathy predisposing them to bleeding from the puncture site, patients who cannot or will not comply with postprocedure rest orders (especially with older 24-French system), and those with obstructing thrombus along all available routes of transvenous insertion are included.

Traditionally, placement of a permanent IVC filter has been discouraged in the young, and in patients with a long life expectancy. There are no strict guidelines, because the longevity of these filters in the human body can only be estimated.

### Technique

Before filter placement, a venacavogram should be obtained, which is another reason why percutaneous filter placement should be performed by interventional radiologists who are prepared to perform venacavography by means of cut film, digital subtraction angiography, or cineangiography. Venacavography is necessary [36] for obtaining information (1) to check IVC patency and the extent of thrombus, if any, within the vena cava or along the route of intended filter delivery; (2) to determine the caval diameter and the suitability of the intended filter device; and (3) to delineate the IVC anatomy, including location of the renal veins, possible IVC anomalies, and any significant collateral vessels.

The newer IVC filters require careful percutaneous technique, as do all filter devices. For punctures of the femoral or jugular vein, a single-wall puncture technique, preferably with a percutaneous entry needle, is recommended. During the insertion of this open-ended needle, continuous suction is applied with an attached syringe, and a visual check is made for any arterial blood. If arterial blood is obtained, the needle is removed, and the puncture is performed again. I prefer a single-wall technique in order to avoid the complication of arteriovenous fistula [39].

Puncture of the right internal jugular vein is performed with a similar technique [11], by using a venous puncture midway between the mastoid tip and the sternal notch, after visualization of the venous pulsation. The use of mild Trendelenberg positioning of the patient at the start of the procedure aids in a jugular venous distention, and having the patient sitting when the venous introducer is withdrawn facilitates hemostasis at the puncture site on the right side of the neck.

For the choice of access route, just as percutaneous transvenous access has become favored over surgical venotomy, so has the transfemoral vein route become popular with the newer filters because it is well tolerated by the patient and straightforward for the physician operator. The right femoral vein is most commonly used. The left femoral vein route can be used; however, greater resistance in filter passage due to the angle of the common iliac vein into the inferior vena cava can be encountered [13], especially with the 24-French introduction system. Some have avoided the left femoral vein approach in 97% of patients [25], yet others have experienced no more difficulty from the left side than from the right [11].

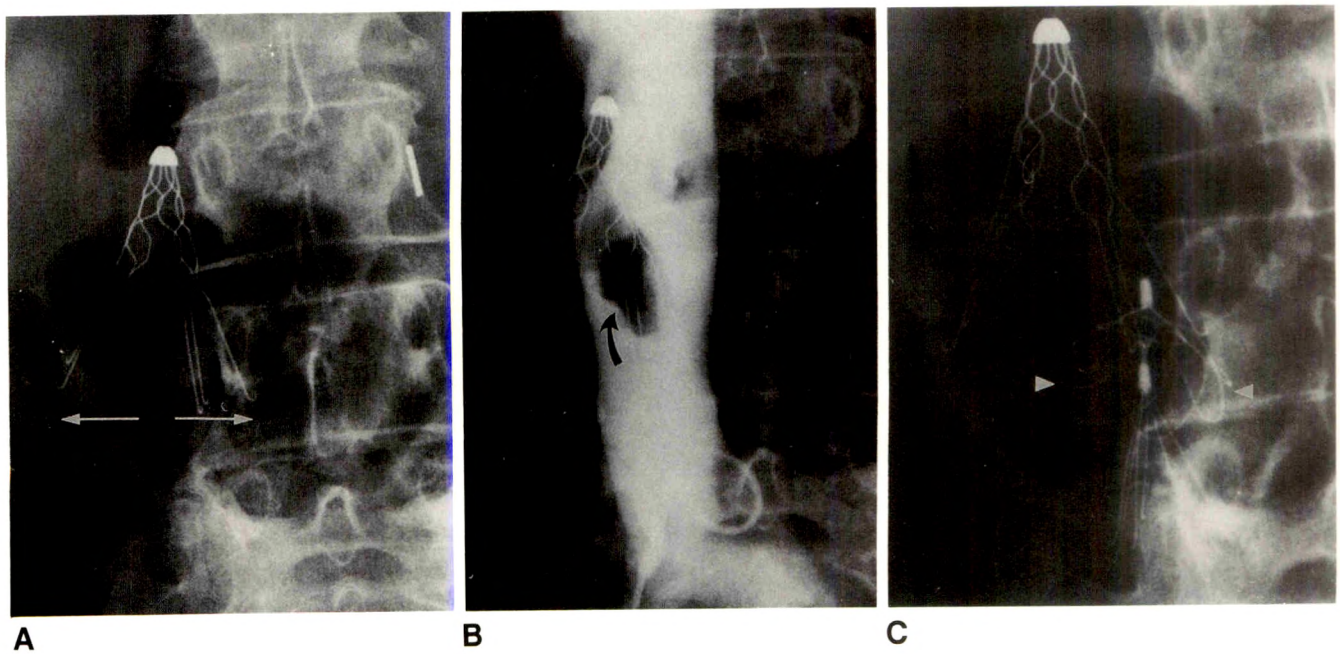



Fig. 10.—68-year-old woman with a Greenfield filter in place who had recurrent shortness of breath.
*A*, Abdominal radiograph shows abnormal widening of filter base (*arrows*) to 38 mm (normal, 28 mm); this is virtually diagnostic of perforation of infrarenal cava by foot process of filter.
*B*, Venacavogram confirms perforation of caval wall and shows filling defect of thrombus within filter (*arrow*).
*C*, Radiograph shows Simon nitinol filter that was added within true vena caval lumen inferiorly (*arrowheads*) for treatment.

**TABLE 2: Comparison of Five Inferior Vena Caval (IVC) Filters**

| Filter Type | Introducer Size (OD) in French | Carrier Size in French | Maximum IVC Diameter Recommended (mm) | Tilting Significant? |
|---|---|---|---|---|
| Greenfield stainless steel | 29 | 24 | 28 | Yes |
| Greenfield titanium | 14 | 12 | 28 | Yes |
| Bird's nest | 14 | 11 | 40 | No |
| Vena-Tech | 12 | 10 | 28 | Yes |
| Simon nitinol | 9 | 7 | 28 (24[a]) | No |

Note.—OD = outer diameter.

[a] Manufacturer's recommendation before surgical procedures requiring general anesthesia.

At our institution, the left femoral vein approach has been useful in the past, even with the 24-French Greenfield system (six [9%] of 68 patients in 1 year). With the new, smaller introduction systems (outer diameter 14-, 12-, 9-French), the past sequence of access choice (first, right femoral vein; second, internal jugular vein; third, left femoral vein) is changing, with a trend toward more transfemoral placements from either the right or left side. The advantages of femoral, compared with jugular vein, puncture do include avoidance of the risks of air embolism, pneumothorax, and inadvertent puncture of the carotid artery, as well as the fact that radiologists generally are more familiar with puncture of the femoral vein. External jugular [40], subclavian, and even brachial vein insertions (Brown R, personal communication) have been performed.

### Filter Advantages and Disadvantages

As shown in Table 2, the smaller introduction size is a significant advantage for the newer generation filters available for clinical use. The versatility of accommodating larger vena caval sizes up to 40 mm is an added advantage of the bird's nest filter since the titanium Greenfield, Vena-Tech, and Simon nitinol types are limited to caval sizes up to 28 mm. Because of this size versatility, a radiology department that can afford to keep only one filter on inventory for all patients should logically choose the bird's nest filter.

However, the bird's nest filter's stainless steel construction poses a relative disadvantage, because the increased use of MR imaging has introduced a new consideration for filter construction. Those devices fabricated from stainless steel are ferromagnetic, whereas those devices composed of eligloy, nitinol, or beta-III titanium alloy are less ferromagnetic [41, 42]. Although the heat or torque effects on the filter or adjacent structures do not appear to be detrimental to patient's safety during routine clinical imaging [41], filters fabricated from stainless steel are highly ferromagnetic and create marked magnetic susceptibility artifact on MR. This artifact degrades abdominal imaging. As MR imaging provides a noninvasive method of assessing vena caval patency and the presence of intracaval thrombus, the potential advantage of a nonferromagnetic filter is clear. Gradient-echo imaging of intracaval filters and trapped thromboemboli can be performed rapidly and effectively (Grassi CJ et al., unpublished data) [43]. In the future, it is likely that all IVC filters will be constructed of high-strength, nonferromagnetic materials.

The 24-French Greenfield filter has one relative advantage, that is, its well-documented rate of high vena caval patency. It is indicated for use in the uncommon situation of suprarenal vein placement [22] with the attendant risk of thrombosis and renal compromise, at least until more experience can be accumulated with suprarenal placement of the newer IVC filters to confirm their patency in this position.

At our institution, the bird's nest and Simon nitinol devices are used. The Simon nitinol filter is valuable when the smaller 9-French percutaneous puncture is advantageous, or where the longitudinal distance between the renal veins and iliac bifurcation is reduced, favoring the shorter 3-cm length of the Simon nitinol over the bird's nest. The bird's nest filter is used routinely. Specifically, it is the only filter device suitable at this time for vena caval sizes between 29 and 40 mm diameter.

### Conclusions

A group of new, smaller percutaneous filter devices are now available, each with its advantages and disadvantages, as described. The ideal vena caval filter is not yet available.

Further clinical trials of these devices with randomized, prospective study are necessary, in order to further refine the existing filters and to assist in the development of a filter that will be superior for the prevention of pulmonary embolism. Until that time, the choice of an IVC filter from those available should be based not only on the interventional radiologist's preference, but also on the specific clinical situation and the filter's performance.

REFERENCES

1. Hunter DW, Lund G, Rysavy JA, et al. Retrieving the Amplatz retrievable vena cava filter. *Cardiovasc Intervent Radiol* **1987**;10:32–36
2. McIntyre AB, McCready RA, Hyde GL, Mattingly W. A ten year followup study of the Mobin-Uddin filter for vena cava interruption. *Surg Gynecol Obstet* **1984**;158:513–516
3. Katsamouris AA, Waltman AC, Delichatsios MA, Athanasoulis CA. Inferior vena cava filters: in vitro comparison of clot trapping and flow dynamics. *Radiology* **1988**;166:361–366
4. Thompson BH, Cragg AH, Smith TP, Barenieweski H, Barnhart WH, De

Jong SC. Thrombus-trapping efficiency of the Greenfield filter in vivo. *Radiology* **1989**;172:979–981
5. Yune HY. Inferior vena cava filter: search for an ideal device. *Radiology* **1989**;172:15–16
6. Pais S, Tobin K, Austin C, Queral L. Percutaneous insertion of Greenfield inferior vena cava filter: experience with ninety-six patients. *J Vasc Surg* **1988**;8:460–464
7. Roehm JOF, Johnsrude IS, Barth MH, Gianturco C. The bird's nest inferior vena cava filter: progress report. *Radiology* **1988**;168:745–749
8. Ricco J, Crochet D, Sebilotte P, et al. Percutaneous transvenous caval interruption with the "LGM" filter: early results of a multicenter trial. *Ann Vasc Surg* **1988**;3:242–247
9. Mensoian JO, LoGerfo FW, Weitzman AF, Ezpleta M, Sequeira JC. Clinical experience with the Mobin-Uddin vena cava umbrella filter. *Arch Surg* **1980**;115:1179–1181
10. Jones T, Barnes R, Greenfield L. Greenfield vena caval filter: rationale and current indications. *Ann Thorac Surg* **1986**;42:S48–S55
11. Pais SO, Tobin KD. Percutaneous insertion of the Greenfield filter. *AJR* **1989**;152:933–938
12. Denny DF, Cronan JJ, Dorfman GS, Esplin C. Percutaneous Kimray-Greenfield filter placement by femoral vein puncture. *AJR* **1985**;145:827–829
13. Rose BS, Simon DC, Hess ML, Van Aman ME. Percutaneous transfemoral placement of the Kimray Greenfield filter. *Radiology* **1987**;165:373–376
14. Greenfield LJ, Zocco J, Wilk J, Schroeder TM, Elkins RC. Clinical experience with the Kimray-Greenfield vena caval filter. *Ann Surg* **1977**;185:692–698
15. Wingerd M, Bernhard VM, Maddison F, Towne JB. Comparison of caval filters in the management of venous thromboembolism. *Arch Surg* **1978**;113:1264–1270
16. Greenfield LJ, Michna BA. Twelve-year clinical experience with the Greenfield vena caval filter. *Surgery* **1988**;104:706–712
17. Simon M, Palestrant AM. Transvenous devices for the management of pulmonary embolism. *Cardiovasc Intervent Radiol* **1980**;3:308–318
18. Messmer JM, Greenfield LJ. Greenfield filters: long-term radiographic follow-up study. *Radiology* **1985**;156:613–618
19. Yakes W. Percutaneous retrieval of a Kimray Greenfield filter from right atrium and placement in the inferior vena cava. *Radiology* **1988**;169:849–851
20. Kim D, Porter DH, Siegel JB, Simon M. Perforation of the inferior vena cava with aortic and vertebral penetration by a suprarenal Greenfield filter. *Radiology* **1989**;172:721–723
21. Geisinger MA, Zelch MG, Risius B. Recurrent pulmonary emboli after Greenfield filter placement. *Radiology* **1987**;165:383–384
22. Orsini RA, Jarrell BE. Superarenal placement of vena caval filters: indications, techniques, and results. *J Vasc Surg* **1984**;1:124–135
23. Mewissen MW, Erickson SJ, Foley WD, et al. Thrombosis at venous insertion sites after inferior vena caval filter placement. *Radiology* **1989**;173:155–157
24. Roehm JOF. The Bird's nest filter: a new percutaneous transcatheter inferior vena cava filter. *J Vasc Surg* **1984**;1:498–501
25. Dorfman GS. Percutaneous inferior vena cava filters. *Radiology* **1990**;174:987–992
26. Aruny JE, Kandarpa K. Phlegmasia cerulea dolens, a complication after placement of a bird's nest vena cava filter. *AJR* **1990**;154:1105–1106
27. Greenfield LJ, Cho KJ, Pais SO, Van Aman M. Preliminary clinical experience with the titanium Greenfield filter. *Arch Surg* **1989**;124:657–659
28. Teitelbaum GP, Jones DL, van Breda A, et al. Vena caval filter splaying: potential complication of use of the titanium Greenfield filter. *Radiology* **1989**;173:809–814
29. Crochet D, Petitier H, Ricco JB, et al. Le nouveau fitre cave LEM preventif de l'ebolie pulmonaire. *J Radiol* **1988**;69:431–436
30. Ricco JB, Crochet D, Seibilotte P, et al. Percutaneous transvenous caval interruption with the "LGM" filter: early results of a multicenter trial. *Ann Vasc Surg* **1988**;3:242–247
31. Simon M, Kaplow R, Salzman E, Friedman D. A vena cava filter using thermal shape memory alloy: experimental aspects. *Radiology* **1977**;125:89–94
32. Simon M, Athanasoulis CA, Kim D, et al. Simon nitinol inferior vena cava filter: initial clinical experience. *Radiology* **1989**;172:99–103
33. Alexander J, Gewerk B, Lu C, Zarins C. New criteria for placement of a prophylactic vena cava filter. *Surg Gynecol Obstet* **1986**;163:405–409
34. Norris C, Greenfield L, Hermanson J. Free-floating iliofemoral thrombus: a risk of pulmonary embolism. *Arch Surg* **1985**;120:806–808
35. Goluek PJ, Garrett WV, Thompson JE, Smith BL, Talkington CM. Interruption of the vena cava by means of the Greenfield filter: expanding the indications. *Surgery* **1988**;103:111–117
36. Grassi CJ, Goldhaber SZ. Interruption of the inferior vena cava for prevention of pulmonary embolism. *Herz* **1989**;14:182–191
37. Goldhaber SZ, Grassi CJ. Management of pulmonary embolism. In: Sabiston DC Jr, ed. *Textbook of surgery*, Update 8. Orlando, FL: Saunders, **1990**:115–127
38. Stewart JR, Greenfield LJ. Transvenous vena caval filtration and pulmonary embolectomy. *Surg Clin North Am* **1982**;62:411–430
39. Grassi CJ, Bettmann MA, Rogoff P, Reagan K, Harrington DP. Femoral arteriovenous fistula after placement of a Kimray-Greenfield filter. *AJR* **1988**;151:681–682
40. McCowan TC, Ferris EJ, Carver DK, Harshfield DL. Use of external jugular vein as a route for percutaneous inferior vena cava filter placement. *Radiology* **1990**;176:527–530
41. Teitelbaum GP, Bradley WG, Klein BD. MR imaging artifacts, ferromagnetism, and magnetic torque of intravascular filters, stents and coils. *Radiology* **1988**;166:657–664
42. Teitelbaum GP, Ortega HV, Vinitski S, et al. Low-artifact intravascular devices: MR imaging evaluation. *Radiology* **1988**;168:713–719
43. Teitelbaum GP, Ortega HV, Vinitski S, et al. Optimization of gradient-echo imaging parameters for intracaval filters and trapped thromboemboli. *Radiology* **1990**;174:1013–1019

# Memorial

## Andrew H. Geiger, 1956–1990

Andrew H. Geiger of Boston died at home with his family on September 3, 1990, after a battle of nearly 3 years with the AIDS virus. He was 33 years old. His death is an inestimable personal loss to me and to his colleagues, family, and friends.

Andrew was born on November 6, 1956, in Boston, and grew up in Wayland, MA, where his parents still reside. He received his bachelor of science degree in biology from the Massachusetts Institute of Technology and attended the University of Massachusetts Medical School, graduating in May of 1982. After a 1-year internship at Berkshire Medical Center, he entered a radiology residency at Saint Vincent Hospital in Worcester, MA. He was the most distinguished member of his residency group and was appointed chief resident in 1987. In June 1988, he was made a diplomate of the American Board of Radiology.

It was after his residency, and the onset of his illness, that Andrew came to work with my group in private practice. He quickly became a valued consultant to the medical staff, beloved new member of the department to the technicians, and final arbiter of many diagnostically difficult cases. Andrew was a remarkably talented radiologist with what often seemed to be a boundless fund of knowledge in every subspecialty. In addition, he was uniquely capable of devising innovative solutions to problem cases. These skills and his charm and fresh outlook earned him the respect of all of his colleagues.

Beyond radiology, Andrew enjoyed music and was an avid traveler to many exotic destinations. Most important, however, was his family and large circle of devoted friends, who were spread throughout the United States. It was these relationships that allowed Andrew to battle vigorously against his disease and to overcome several daunting setbacks over the years.

During the short time that I knew him, Andrew always faced the future with courage. Work was a form of recovery for him, and he continued his daily schedule until just 2 months before his death. His loss is ours, and it leaves an emotional void that can never be filled. Andrew was an easily approachable, unselfconscious, and competent individual who was never without warmth and a sense of humor. He always seemed able to identify some element of the human comedy in the grim realities of his struggle.

He leaves behind his mother, Betty Ann, and his father, Karl, who provided constant and reliable emotional and physical support throughout his illness. Andrew often spoke of his good fortune to have parents strong enough to fight with him. In addition, he leaves four brothers; one sister; many nieces and nephews; his good friend, Mary Beth Annarella; and Concord Radiologists.

Susan A. Stafford
*Concord, MA 01742*

Technical Note

# Kissing-Balloon Technique for Angioplasty of the Popliteal Artery Trifurcation

Mark W. Mewissen,[1] Robert A. Beres, Jeffrey C. Bessette, Elliot O. Lipchik

The kissing-balloon technique, also termed the two-balloon technique, is a procedure designed for percutaneous transluminal angioplasty of arterial bifurcations. It was initially described for percutaneous transluminal angioplasty of the aortic bifurcation, which used simultaneous inflation of two balloons, one introduced through each common femoral artery, to avoid occlusion or embolization of the opposite common iliac artery [1]. Percutaneous transluminal angioplasty of such bifurcation lesions with a single angioplasty catheter is contraindicated because inflation of the balloon may displace the plaque laterally and occlude the contralateral iliac artery or result in distal embolization. We describe use of the technique for angioplasty of the popliteal artery trifurcation after single antegrade puncture of the ipsilateral common femoral artery.

## Materials and Methods

A 51-year-old, insulin-dependent, diabetic man was admitted for treatment of a 2 × 2 cm nonhealing ischemic ulcer of the left foot. The patient had a below-the-knee femoral-popliteal in-situ bypass graft placed 2 years before this admission. After diagnostic angiography, which showed a patent graft and high-grade stenoses at the tibioperoneal bifurcation (Fig. 1A), the left common femoral artery was punctured in an antegrade fashion, and a 6-French sheath (Cordis, Miami, FL) was passed through the proximal portion of the in situ bypass graft. A Tegtmeyer guidewire angioplasty balloon catheter (TEGwire, Medi-tech, Watertown, MA) with a 20 × 3 mm balloon was advanced through the sheath and positioned across the anterior tibial artery stenosis. A 3.5-French Medtronic angioplasty catheter (Medtronic, Minneapolis, MN) with a 20 × 2.5 mm balloon was then advanced through the same sheath over an 0.018-in. steerable guidewire (Peripheral System Group, Mountain View, CA) and was placed across the stenotic origin of the tibioperoneal trunk. Both balloons were simultaneously inflated (Fig. 1B). Subsequent arteriography showed a good angioplasty result at the bifurcation point, with good flow into the runoff vessels (Fig. 1C).

## Discussion

Infrapopliteal atherosclerotic lesions are not always amenable to percutaneous transluminal angioplasty, particularly when the disease involves the popliteal artery trifurcation. In such cases, dilatation of one branch vessel with a single balloon may cause occlusion or embolization of the other branch vessel. This occurs because no support is present opposite the expanding balloon to contain the plaque and prevent it from fragmenting and causing distal embolization of the opposite vessel. With the double-guidewire technique [2, 3], a safety guidewire maintains access within the vessel opposite the angioplasty site. After dilatation of the first branch vessel, the angioplasty catheter can be removed and advanced over the safety wire to dilate the second branch vessel. However, the technique may not guarantee safe passage of the balloon catheter over the protecting guidewire should an occlusion of the second branch vessel occur during angioplasty of the first. In addition, a wire may not necessarily prevent embolization down the second vessel.

Received September 17, 1990; accepted after revision October 23, 1990.

[1] All authors: Department of Radiology, Veterans Affairs Medical Center and the Medical College of Wisconsin, Milwaukee, WI 53295. Address reprint requests to M. W. Mewissen.

*AJR* 156:823–824, April 1991 0361–803X/91/1564–0823 © American Roentgen Ray Society

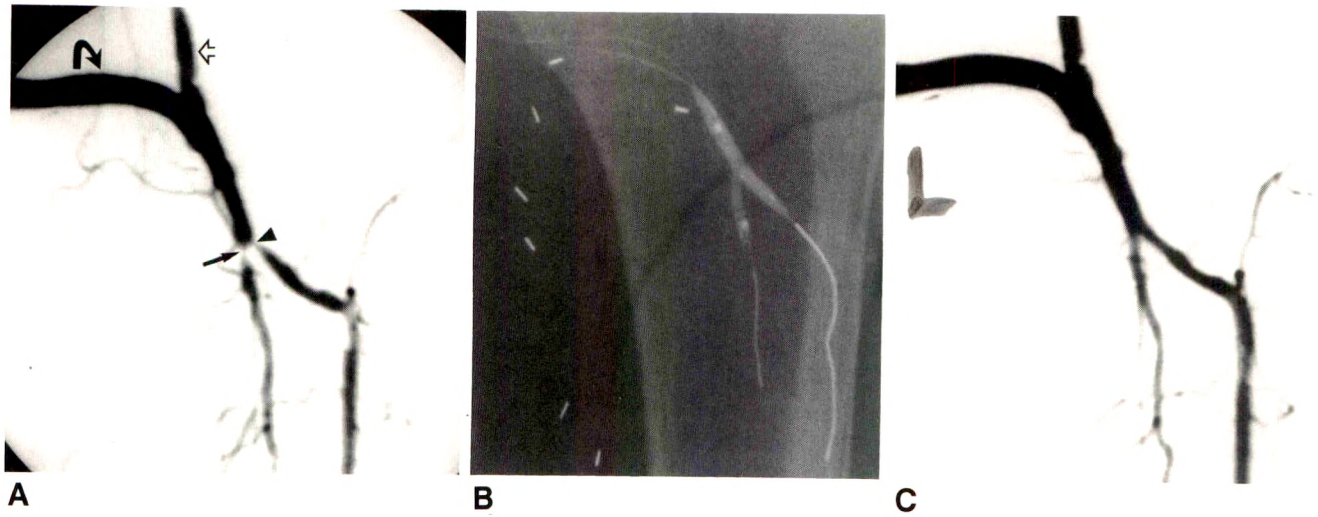



**Fig. 1.—*A*, Digital subtraction angiogram of left leg reveals high-grade stenoses at origins of tibioperoneal trunk (*straight solid arrow*) and anterior tibial artery (*arrowhead*), accounting for decreased velocities in leg with below-the-knee femoral-popliteal in situ bypass graft (*curved arrow*) (above-knee: 35 cm/sec; below-knee: 40 cm/sec). Ankle-brachial index, 0.54 on admission, had dropped from 1.0, 6 months before. Distal popliteal artery is patent (*open arrow*).**

***B*, Radiograph shows kissing balloons. Note TEGwire angioplasty balloon guidewire (3 mm in diameter) across anterior tibial artery and 3.5-French angioplasty balloon catheter (2.5 mm in diameter) across tibioperoneal trunk.**

***C*, Digital angiogram after angioplasty shows good flow into both vessels. Studies 1 week after angioplasty revealed left-graft velocities of 65 cm/sec above knee and 70 cm/sec below knee. Ankle-brachial index improved to 1.0 on a 1-month follow-up study.**

With the kissing-balloon technique, the atherosclerotic plaque is trapped and compressed between the two balloons, which are inflated simultaneously. Because the plaque is not displaced, distal embolization to the contralateral branch vessel should not occur. When both angioplasty balloon devices are introduced through the same 6-French sheath, the morbidity and patient's discomfort inherent to a second arterial puncture are eliminated.

In our experience, the largest catheter shaft that easily fits side by side through a 6-French sheath in combination with a 0.035-in. guidewire is 3.5-French. Therefore, a 3.5-French angioplasty catheter is used in conjunction with a 0.035-in. TEGwire for percutaneous transluminal angioplasty of the infrapopliteal bifurcation. Angioplasty of popliteal and tibial vessels with the TEGwire has been previously reported [4]. The combination we describe may not fit all 6-French sheaths because inner-sheath diameter may vary among manufacturers. Combinations should be tested before catheterization.

The kissing-balloon technique is technically feasible for use in the diseased infrapopliteal bifurcating vessels. Recent refinements in balloon catheter technology should broaden the indications for infrapopliteal percutaneous transluminal angioplasty.

## REFERENCES

1. Tegtmeyer CJ, Kellum CD, Kron IL, Mentzer RM. Percutaneous transluminal angioplasty in the region of the aortic bifurcation. *Radiology* **1985**;157:661–665
2. Oesterle SN, Mcavley BJ, Buchbinder M, Simpson JB. Angioplasty at coronary bifurcations: single-guide, two wire technique. *Cathet Cardiovasc Diagn* **1986**;12:57–63
3. Teitelbaum GP, Joseph GJ, Matsumoto AH, Barth KH. Double-guide-wire access through a single 6 F vascular sheath. *Radiology* **1989**;173: 871–873
4. Tegtmeyer CJ. Guide wire angioplasty balloon catheter: preliminary report. *Radiology* **1988**;169:253–254

# The Risks of Death and of Severe Nonfatal Reactions with High- vs Low-Osmolality Contrast Media: A Meta-analysis

J. Jaime Caro[1,2]
Evelinda Trindade[2]
Maurice McGregor[1,2]

**Estimates of the risks associated with the use of radiologic contrast agents frequently are based on a subjective review of some of the numerous articles that have been published on the subject. We have chosen instead to synthesize the existing evidence in an objective, quantitative way by statistically combining the data from individual studies through meta-analysis. Although meta-analysis is subject to whatever biases may exist in the underlying data, and may inappropriately pool data from studies with significant differences, the estimates draw proportionately from each original study and, in addition, gain considerable precision owing to the increased amounts of data considered. Using this technique, we analyzed the data from all available original reports appearing since 1980. Crude rates derived from all reports were used to estimate risks with high-osmolality media. Weighted rate differences based on comparative studies only were used in the estimation of the reductions in risk obtainable with low-osmolality media. The risk of death with high-osmolality media was 0.9 per 100,000 uses (95% confidence interval, 0.3–2.6 per 100,000). The difference in risk produced by using low-osmolality media was 0 (95% confidence interval, −1.1 to 1.1 per 100,000). The risk of severe reactions associated with high-osmolality media was 157 per 100,000 uses (95% confidence interval, 144–172 per 100,000). The reduction in risk that can be obtained by the use of low-osmolality media was estimated to be 126 per 100,000 (95% confidence interval, 110–142 per 100,000).**

**This meta-analysis shows that the risk of death is very low with either type of contrast material and that there is no difference between them. Severe nonfatal reactions with high-osmolality media, although more frequent, are still rare; approximately 80% of them can be prevented by using low-osmolality media.**

*AJR* 156:825–832, April 1991

A new generation of contrast media, thought to be safer because of lower osmolality, was introduced at the beginning of the last decade. The new media would rapidly have displaced the old if the difference in price had been small. That difference, however, is still substantial, and the vexing question remains as to how much of society's resources should be committed to reduce the frequency of adverse reactions when they are either infrequent or mild.

Few today would take the position that all risk and discomfort, no matter how minor, must be kept to an absolute minimum, whatever the cost. There is a point at which the risk of severe complications becomes so small, and the discomfort becomes so mild, that the cost of preventing them becomes unreasonable. Thus, in forming policy regarding the use of contrast media, it is necessary to know what the risk is when using the older media and how much this risk can be reduced by using the newer media. Finally, one must know the cost of achieving this reduction in risk.

Unfortunately, individual studies, particularly randomized trials, addressing these risks tend to be far too small to provide reliable quantitative estimates of the risks in question. Therefore, to estimate the risks of death and of severe nonfatal

Received June 25, 1990; accepted after revision October 30, 1990.

This work was supported by the Conseil d'évaluation des technologies de la santé du Québec.

[1] Department of Medicine, McGill University, Royal Victoria Hospital, A4–24, 687 Pine Ave. W., Montreal, Quebec, Canada H3A 1A1. Address reprint requests to J. J. Caro.

[2] Conseil d'évaluation des technologies de la santé du Québec, P.O. Box 215, Montreal, Quebec, Canada H4Z 1E3.

0361–803X/91/1564–0825
© American Roentgen Ray Society

reactions incurred by parenteral administration of high-osmolality contrast agents, we statistically combined (meta-analysis) the data from all reports appearing after 1980 concerning the frequency of these adverse reactions. To estimate the reduction in these risks that may be obtained by conversion to the newer media, we carried out a meta-analysis of the data from those reports that compare the two types of contrast media. We believe that the estimates obtained in this way are more informative than those that can be obtained from any one of the individual sets of data. The limitations of this method of synthesizing data have been extensively discussed elsewhere [1–4].

## Materials and Methods

For the purpose of this report, "parenteral" administration of contrast material refers to IV or intraarterial injection. Intracardiac uses, which are associated with much higher risks, were excluded from this analysis. "High-osmolality media" (HOM) refers to the conventional agents such as diatrizoate (Angiografin, Angiovist, Diatrizoate, DTZ, Hypaque, Renografin, Reno-M-DIP, Renovist, Urografin, Urovision), iothalamate (Angio-conray, Conray, Vascoray), ioglicinate (Rayvist), ioglicate, iodamide (Uromiro), amidotrizoate, ioxithalamate (Telebrix), and metrizoate (Isopaque), which are ionic and highly osmolal (up to eight times) in relation to plasma. "Low-osmolality media" (LOM) refers to the new agents, either dimers such as sodium meglumine ioxaglate (Hexabrix) or completely nonionic substances such as iohexol (Ominpaque), iopromide (Ultravist), metrizamide (Amipaque), ioversol (Optiray), and iopamidol (Iopromiro, Isovue, Jopamiron, Niopam, Solutrast), which are of lower osmolality (about one third that of HOM), although still double the osmolality of plasma.

To estimate the risks of death and of severe nonfatal reactions associated with the use of HOM and the reductions in such risks attainable by substitution with LOM, a quantitative meta-analysis was carried out of all relevant data reported between January 1, 1980, and December 31, 1989. These cutoff dates were chosen to minimize the effects of changes in medical practice over time while providing sufficient data to make reasonably precise estimates of the risks at issue.

### *Sources of Data*

DIALOG software (from Lockheed Corporation) was used to search seven data bases (Medline, International Pharmaceutical Abstracts, Drug Information Fulltext, Clinical Abstracts, Health Planning and Administration, Pascal, and Embase) for all articles that included any of the key words: high-, low-, or nonionic contrast media (dyes, material, agent, or substance); clinical trials and adverse events or reactions; or toxicity. The *Index Medicus* since 1980; the index of the journal *Radiology*; the table of contents of all major radiology and cardiology periodicals and the bibliography of the reviews, studies, and editorials also were reviewed. Investigators known to be working, or to have worked, on adverse reactions to contrast media were contacted to inquire about any unpublished data of their own or known to them.

All of the reports uncovered by this search were examined. Those that provided original data in sufficient detail regarding the occurrence of the adverse events of interest were selected for further study if there were at least 60 observations in noncomparative series, or at least 30 observations in each group in comparative studies [5–96] (Caro JJ et al., unpublished data; Corbett R et al., unpublished data). All sources of data were carefully verified to avoid duplication of data.

Three articles published after January 1, 1980 [7, 55, 86], reported data entirely collected before 1980 and for this reason are not included in the main estimates. One article [25] reported data collected from 1964 to 1982 and provided results by year. The data collected from 1980 onward are included in the main estimates. Some reports published after 1980 included patients studied before 1980, but, because results were not identified by year, all of these data were used indiscriminately in deriving estimates.

Reports were classified according to study design: randomized trials, crossover trials, nonrandomized studies with concurrent controls, nonrandomized studies with historical controls, and uncontrolled series. All studies with a crossover design, in which each patient received both contrast agents sequentially, were excluded because, in the event of serious reactions after the procedure, attribution would be impossible. No other data were excluded on the basis of quality of study design. A detailed listing of the studies selected, their characteristics, and the data abstracted can be obtained from the authors [97].

### *Data Abstraction*

From each of the studies accepted for review, the number of deaths and of severe nonfatal reactions and the number of uses of each type of contrast material were abstracted. This was done initially by one person and was subsequently repeated by a different person. Where discrepancies arose, a third verification was carried out by the two abstractors jointly.

Only severe reactions, including fatal ones, that closely followed the administration of contrast material were included. Although authors did not always specify the timing of reactions, it is reasonable to presume from the descriptions provided that no event included in this analysis occurred beyond 3 hr after administration of contrast material.

Reactions labeled severe were those considered life-threatening and requiring urgent intervention: anaphylaxis, hypotension or hypertension of sufficient severity to require urgent intervention, prolonged chest pain unresponsive to nitrates within 10 min, arrhythmia requiring urgent electroconversion or pacing, pulmonary edema, laryngeal edema, and laryngeal or bronchospasm sufficient to cause respiratory obstruction.

Authors' definitions of what constituted renal dysfunction varied considerably and most of them did not reflect severe renal dysfunction. For these reasons no meta-analysis was done of the risk of renal dysfunction.

Although there are reports that HOM have a greater antiplatelet and anticoagulant effect (e.g., Bashore et al. [98]), strokes were not included because data on this are scanty, and it is probable that through use of heparin and more frequent catheter flushing the risk of catheter-related thrombosis with LOM can be eliminated. Venous thrombosis, although a potential hazard, also was not included because it was not considered a severe reaction as defined in this study.

It was sometimes impossible to be sure from the descriptions provided in the reports if the reactions labeled as "severe" corresponded to life-threatening events requiring urgent intervention. Whenever possible, the sources were contacted to request clarification. In the few situations in which the details of the reactions reported as severe remained unclear, the authors' classifications were accepted.

Uncomfortable reactions not affecting safety as defined here were not included in this meta-analysis.

The authors' attribution of events was accepted because very few reports provided unattributed data. When attribution was uncertain,

we considered reactions to be the consequence of contrast administration.

*Stratification*

Most nonrandomized studies were based on series of patients presenting routinely for contrast-enhanced radiographs. Although these series were not explicitly restricted by investigators according to determinants of risk, it is likely that the clinicians responsible for the procedure did restrict the type of patients studied according to whatever criteria were perceived to represent unacceptable risk. Most randomized trials excluded patients with some characteristics thought to indicate higher risk, although there was little consistency among studies regarding the set of exclusion criteria. Thus, it is difficult, from published information, to analyze the data according to determinants of risk or even to stratify them into groups of patients with more or less homogeneous risks. In a few studies the data for patients considered to be at high-risk were provided separately, and in a small number of studies only patients perceived to be at higher risk were included. The data pertaining to these high-risk groups were analyzed separately. The remaining data were analyzed without distinction according to risk.

Data were insufficient to allow for stratification according to other factors such as specific contrast agents or volumes of material used. A subgroup of LOM, excluding the low-osmolar dimer Hexabrix, was analyzed. No distinction was made between intraarterial and IV use of contrast material in most of the large studies, and, thus, these types of use could not be analyzed separately.

Subsets of data were analyzed according to study design, although no exclusions, other than crossover studies, were made on this basis.

*Estimation of Risk Incurred with the Use of HOM*

The risks of death and of severe reactions associated with the use of HOM were estimated by deriving crude overall rates from the data from all studies that reported the use of HOM. These rates were calculated as the total number of adverse events occurring soon after the use of HOM, divided by the number of uses of that type of contrast agent. The time of occurrence of adverse events was not taken into account because only those events occurring within 3 hr of contrast use were considered. Confidence intervals for the overall rates were calculated by using the chi-square function described below. Also, estimates were calculated for the subset of studies comparing HOM with LOM, for studies with randomized allocation, for the subset of studies excluding Hexabrix use, and for subsets with selected outlier studies removed.

*Estimation of the Reduction in Risk Obtainable with the Use of LOM*

The reduction in risk that can be obtained by using LOM instead of HOM is equal to the difference in the respective rates of occurrence of the particular adverse reaction at issue.

For each type of adverse reaction, estimates of the overall rate difference were derived by taking a weighted average of the rate differences obtained in each comparative study.

An alternative would have been to estimate the risk of adverse events with LOM in the same way the risk for HOM was estimated and then subtract this from the corresponding HOM risk. The reduction in risk was not estimated in this way because it was believed that this would yield a less valid result given the large differences in design and implementation among studies and the consequent potential for confounding by study. With the weighted average, each comparative study is treated as a stratum, thus controlling for study-specific confounding.

The weight for each study was the ratio of the inverse of the variance of the rate difference in that study to the sum of the inverse of variance from each of the comparative studies. The variance of the rate difference in each study was estimated as the square of one quarter the width of the 95% confidence interval around the rate difference [97]. A formulation of chi-square with the theoretical variance in place of the empirical variance was used to calculate a 95% confidence interval for the estimate of rate difference in each study. This formulation was used because many studies reported few or no events, and in this situation confidence intervals based on the common approximation for chi-square do not function well (e.g., yielding limits of 0 and 0 if there are no events) [99]. The limits were calculated by using a computer program that derives the chi-square function by iteration. The theoretical basis for this calculation and details of its implementation can be found elsewhere [99 (pp. 155–164), 100].

For the overall rate differences, confidence intervals were calculated by using the inverse of the sum of the inverses of variance from all of the studies as an estimate of variance [97].

Weighted overall rate differences were calculated also by using the data in the subset of studies with randomized allocation, in the subset of studies excluding Hexabrix use, and in subsets with selected outlier studies removed.

*The Risk of Adverse Events with LOM*

Although estimation of this risk was not an object of this study, an estimate of this risk can be derived by subtracting the estimated reduction in risk with LOM use from the estimated risk with HOM use.

## Results

Table 1 shows the estimates of the risk of death, and of severe reactions, in patients receiving HOM parenterally, together with the estimates of reductions in these risks obtainable by complete conversion to LOM. Also shown is the 95% confidence interval for each estimate. The risks associated with LOM use are not shown, but, as already noted, these can be derived by subtracting the estimated risk reduction from the estimated risk with HOM.

*Death*

Among the 333,692 parenteral administrations of HOM in the 41 reports concerning such use after 1980, three deaths attributable to contrast material were noted, a mortality of 0.9

**TABLE 1: Risk and Risk Reduction per 100,000 Parenteral Uses of Contrast Media**

| Variable | Best Estimate (95% Confidence Interval) | |
|---|---|---|
| | Death | Severe Reactions |
| Risk with high-osmolarity media | 0.9 ( 0.3 to 2.6) | 157 (144 to 172) |
| Risk reduction with low-osmolarity media | 0.0 (−1.1 to 1.1) | 126 (110 to 142) |

per 100,000 uses of HOM (95% confidence interval [CI], 0.3–2.6 per 100,000). No details of these deaths are available; concerning one of them, the authors note that the contrast material was not proved to be the cause [32].

The estimate of mortality with the use of HOM was fairly insensitive to changes in the subset of studies used to derive it. If the largest study [32] was taken out, thus removing over 50% of the patients, the estimate was 1.2 deaths per 100,000. The identical value was obtained if only comparative studies were used. No deaths occurred among the 3820 patients receiving HOM in randomized trials.

On the basis of the data in the 37 comparative reports only, the difference in mortality between use of LOM and of HOM was found to be 0 (95% CI, −1.1 to 1.1 per 100,000).

The estimate of mortality reduction increased slightly if the largest study was removed, but the confidence interval still included 0 (95% CI, −12 to 17 per 100,000). Restriction of the data to randomized studies only led to an estimate slightly lower than the best estimate, but again the confidence interval was very wide and included 0. Removal of the studies in which the LOM agent was Hexabrix did not change any of the estimates.

Thus, the risk of death with the use of LOM is estimated to be identical to that with HOM use, 0.9 per 100,000. Among the 251,572 parenteral uses of LOM reported on in all studies (both comparative and series of LOM only), there were three deaths, yielding a crude rate of 1.2 per 100,000, quite comparable to the estimate derived by subtraction. Of the deaths that occurred with LOM, in one the contrast material was considered definitely to be at fault [6]; in another the causal relationship was considered unproved [32]; and one was of a patient at high risk owing to advanced age (80 years), chronic obstructive pulmonary disease, hypertension, arteriosclerotic heart disease, and cachexia [41].

Taking the data from the high-risk subset of patients in the three reports that provided separate data [36, 37, 47], together with the data from the two studies that focused on high-risk patients alone [74, 75], provides information on 6649 high-risk patients receiving HOM. In this subset, one death was recorded, a mortality of 15 per 100,000 (95% CI, 2.7–85.1 per 100,000). No deaths occurred in the smaller subset of comparative studies concerning high-risk patients, nor in studies of use of LOM alone in high-risk patients.

### *Severe Reactions*

Among the 320,706 parenteral uses of HOM in the 40 studies of such use, there were 505 severe reactions, a rate of 157 per 100,000 (95% CI, 144–172 per 100,000).

When the largest study [32] was removed, the estimate of risk with HOM use dropped to 91 per 100,000. If only comparative studies were used, the estimate increased slightly to 179 per 100,000. Use of the data from randomized trials only yielded an estimate of risk with HOM of 62 per 100,000, but the 95% confidence interval was wide (17–225 per 100,000).

Drawing only from the data in the 37 comparative studies, the reduction in risk of severe reactions obtainable by using LOM instead of HOM was estimated to be 126 per 100,000 (95% CI, 110–142 per 100,000).

Exclusion of the largest study [32] yields a lower estimate of the reduction in risk, 90 per 100,000 (95% CI, 68–111 per 100,000). Use of the data from randomized studies only results in a much lower estimate of reduction, but the confidence interval not only includes 0, but the estimate obtained in the main analysis as well (23 per 100,000; 95% CI, −357 to 403 per 100,000). Removal of the studies in which the LOM agent was Hexabrix did not change the estimates.

Taking 126 per 100,000 to be the best estimate of the reduction in risk obtainable through use of LOM and subtracting this from the estimated risk with use of HOM yields an estimated risk of severe reactions with use of LOM of 31 per 100,000. If, instead, a crude rate of severe reactions with use of LOM is derived from the data in all studies concerning such use, the estimate is 36 per 100,000.

Taking the data from the high-risk subset of patients in the reports that provided separate data [37, 47], together with the data from the studies that focused on high-risk patients alone [36, 74, 75], yielded 25 severe reactions among 6649 uses of HOM, a rate of 376 per 100,000 (95% CI, 255–554 per 100,000). With use of the comparative studies dealing with high-risk patients only [47, 74], the reduction in risk with conversion to LOM was estimated to be 342 per 100,000 (95% CI, −1 to 686 per 100,000).

### *Renal Dysfunction*

Investigators concerned with renal dysfunction after the use of contrast material have focused on the occurrence of a transient elevation of serum creatinine level. In 21 reports [12, 77–95] (Caro et al., unpublished data), such elevations occurred in 3.5% of 2854 patients receiving HOM (excluding patients at particularly high risk). On the basis of the data in the nine comparative studies among these [77–85], LOM use is estimated to reduce this risk by 0.44 per 100 uses (95% CI, −1.04 to 1.92 per 100).

These overall estimates are difficult to interpret because the rates vary greatly among studies. In patients receiving HOM, for example, the reported rate of renal dysfunction ranged from 0 to 23%. This degree of variation is due, among other things, to differences in the criteria used to define a rise in creatinine level that denotes significant renal dysfunction. Although a more clinically significant estimate could be obtained by focusing on serious renal dysfunction only, these data are not available from most studies. Nevertheless, these reports include seven episodes of renal dysfunction requiring temporary dialysis, three leading to permanent dialysis, and one death from renal failure 3 months after administration of HOM. In none of them was dialysis reported after LOM use.

## Discussion

### *Choice of Measures*

To estimate the risk of a given adverse event with the use of HOM, we have chosen the crude overall rate, calculated by using the data from all relevant studies, regardless of

whether they were comparative or not, because it maximizes the use of available data without unduly compromising validity. This rate makes use of data from large studies that examined only patients receiving HOM and appropriately weighs the information regarding HOM risk in each study by the size of the HOM series in each study.

To estimate the reduction in risk that can be expected with substitution of HOM by LOM we chose the rate difference. Not only is this the measure of direct relevance for decisions regarding the choice of contrast media, but it is the only one that can be derived, given the numerous studies with no events, a situation in which the rate ratio is uninformative.

The overall rate difference was derived by weighting the individual rate differences according to the amount of comparative information in each study. Crude overall rate differences were not used because studies differed greatly in their design, suggesting that confounding by study would be a problem. A weighted average derived in the manner described is tantamount to the result of a stratified analysis, with each study constituting a stratum.

### *Validity*

Validity of the overall estimates, regardless of the method used to produce them, rests on validity of the individual estimates from which they are derived. Limiting the review only to studies meeting strict design criteria would have reduced the data to a point at which no useful estimates could be made; their confidence intervals are so broad that almost any conclusion could be supported by them. Rather than limiting the data to those resulting from the studies with the best designs, an attempt could be made to assess the direction and magnitude of biases in each study and correct the estimates accordingly. Unfortunately, this was not possible given the paucity of information in most of the reports in which the possibility of bias existed. We chose not to grade studies according to a set of criteria presumed to measure their "quality" and then weight them according to this score before computing an overall effect [101], because this technique does not remove any of the bias that may exist and introduces an additional arbitrary factor with little methodologic justification. Thus, the estimates made here reflect any biases that may exist in the sources of data.

One of the main sources of bias is incomparability between the HOM and LOM populations in the distributions of risk-relevant characteristics, a situation likely to result when the choice of agent is guided by perceived contraindications to the use of HOM. If present, this sort of selective allocation according to determinants of the outcome would weigh the results against LOM. It also would reduce the estimates of risk with HOM in noncomparative series if patients were selectively excluded from receiving contrast medium or even from appearing in the series. The estimates of risk and of risk reductions based on data restricted to randomized trials only are consistently lower than the main estimates that include nonrandomized studies, a fact that does not favor the presence of a selection bias.

Other sources of bias, such as lack of blinding and differences in patient management, are less likely to be seriously affecting the estimates. In the setting of parenteral use of contrast material (as opposed to intracardiac), it is very unlikely that attribution of events is a problem because the procedures themselves very rarely, if ever, contribute to the occurrence of adverse events. Underreporting of events would affect the estimates of risk with HOM but would not affect the estimates of risk reduction unless it differed according to the type of contrast material used. There is no evidence to support or refute this possibility.

Thus, despite the problems inherent in a quantitative review of this sort, we believe that the estimated rates and rate differences, together with their confidence intervals, provide a reasonable basis on which to make decisions regarding the use of these agents.

### *Comparison with Previous Estimates*

The extremely low estimate of the risk of death incurred with parenteral use of HOM obtained in this report (0.9 per 100,000) is lower than previous estimates [7, 102, 103]. In the four studies reviewed here on the use of HOM before 1980 [7, 25, 55, 86], the average mortality rate was 3.2 per 100,000. This change probably reflects improved emergent management of potentially fatal reactions in recent years, but it is possible that it reflects to some extent selection of higher-risk patients to receive LOM among the more recent studies.

By contrast, the estimate of the frequency of severe reactions after parenteral administration of HOM arrived at in this report (157 per 100,000) is somewhat higher than most previous estimates, which include 100 per 100,000 [104], 90 per 100,000 [102], 30 per 100,000 [7, 103], and 10 per 100,000 [105]. The frequency of 157 severe reactions per 100,000 uses estimated in this analysis has a narrow confidence interval and is a reflection of more recent studies.

Although in this analysis, parenteral use of LOM instead of HOM did not lead to a reduction in mortality, it did produce approximately an 80% reduction in the risk of severe reactions. Though these adverse reactions are nonfatal and short lived, each might prove fatal if not properly managed, and in this sense the use of LOM can be said to increase safety.

### *Indicators of Increased Risk*

Many indicators of increased risk have been postulated [106–111]. That it is possible to predict, to some extent, which patients are at high risk is demonstrated by those studies that focus on patients believed to be at increased risk of reactions [37, 47, 74, 75]. In these, the frequency of severe reactions (376 per 100,000) was more than double the rate of 157 per 100,000 estimated in the main analysis, and in a study of patients thought to be at particularly high risk [55], the rate was more than 10 times higher at 3.7%. Furthermore, it is estimated here that this increased risk can be almost eliminated with the use of LOM. This finding is consistent with a strategy of using LOM in all patients at increased risk of reactions [106–112]. Unfortunately, there are insufficient data on which to base precise recommendations regarding selection of patients and from which accurate predictions of

the risk of particular persons can be derived. For this reason, analysis of risk indicators has not been carried out here.

### *Renal Dysfunction*

The risk of severe renal dysfunction could not be estimated on the basis of the data reviewed here. In a meta-analysis of 100 randomized controlled trials published between 1980 and 1987 [113], no difference in the frequency of nephrotoxicity was found. In a recent comparison of nephrotoxicity in high-risk patients suffering from cyclosporine-induced renal insufficiency, no difference was found between an LOM agent (iopamidol) and an HOM agent (diatrizoate) [114]. All of these studies, however, were too small to be able to detect significant differences between very low event rates.

### *Applicability*

Limitations on the applicability of these estimates must be noted. These estimates may not apply to special populations, to particular types of examinations, or to special conditions, such as examinations carried out where resuscitation is of a lower standard. Even if studies address different domains, overall estimates still provide an "average" over whatever mix of domains prevail in the studies. This mix, however, may not correspond to any identifiable mix encountered in practice. Furthermore, these estimates should be used with great caution to deduce the risks to individuals.

## Conclusions

Available evidence suggests that the risk of death associated with parenteral use of HOM, excluding intracardiac uses, is extremely low, 0.9 per 100,000 uses, and cannot be reduced further through the use of LOM. Thus, the risk of death does not appear to be an adequate reason to substitute LOM for all parenteral uses.

The risk of severe reactions with HOM is also low, 157 per 100,000 uses, but almost 80% of this risk can be eliminated through use of LOM. Although the reactions in question are transient and, by definition, nonfatal, the use of LOM can be said to yield an increase in safety in the sense that it would lead to a reduction in the occurrence of extremely unpleasant reactions, each of which has the potential to become fatal in the absence of appropriate management.

The decision to convert to LOM for these reasons will, in the final analysis, also be influenced by the costs involved and the resources available.

## REFERENCES


1. DerSimonian R, Laird N. Meta-analysis in clinical trials. *Controlled Clin Trials* **1986**;7:177–188
2. Jenicek M. Meta-analysis in medicine: where we are and where we want to go. *J Clin Epidemiol* **1989**;42:35–44
3. L'Abbé KA, Detsky AS, O'Rourke K. Meta-analysis in clinical research *Ann Intern Med* **1987**;107:224–233
4. Laird NM, Mosteller F. Some statistical methods for combining experimental results. *Int J Technol Assess Health Care* **1990**;6:5–30
5. Adam A, Hemingway AP, Allison DJ. Iohexol and diatrizoate: comparison in visceral arteriography. *Radiology* **1985**;155:529
6. Akamine JS, Albertson GR, Dang T, Smith DC. Severe idiosyncratic reactions to low-osmolality contrast agents. *Radiology* **1989**;169:366
7. Ansell G, Tweedie MC, West CR, Evans P, Couch L. The current status of reactions to intravenous contrast media. *Invest Radiol* **1980**;15:S32–S39
8. Bagg MNJ, Horwitz TA, Bester L. Comparison of patient responses to high- and low-osmolality contrast agents injected intravenously. *AJR* **1986**;147:185–187
9. Barth KH, Mertens MA. A double-blind comparative study of Hexabrix and Renografin-76 in aortography and visceral arteriography. *Invest Radiol* **1984**;19[suppl 6]:S323–S325
10. Bettmann MA, Robbins A, Braun SD, Wetzner S, Dunnick NR, Finkelstein J. Contrast venography of the leg: diagnostic efficacy, tolerance, and complication rates with ionic and nonionic contrast media. *Radiology* **1987**;165:113–116
11. Bettmann MA. Clinical experience with Ioversol for angiography. *Invest Radiol* **1989**;24[suppl 1]:S61–S66
12. Billström A, Heitala S-O, Lithner F, Merikanto J, Wirell M, Wirell S. Nephrotoxicity of contrast media in patients with diabetes mellitus. *Acta Radiol* **1989**;30:509–515
13. Bryan RN, Miller SL, Roehm JOF Jr, Weatherall PT. Neuroangiography with iohexol. *AJNR* **1983**;4:344–346
14. Burbank FH, Bradley BR, Yegnashankaran S, Enzmann DR. Contrast media tonicity: part II. Isotonic ioxaglate vs. standard Renografin for IV-DSA evaluation of the carotid bifurcation, a double-blind prospective clinical trial. *Invest Radiol* **1986**;21:340–347
15. Davies P, Panto PN, Buckley J, Richardson RE. The old and the new: a study of five contrast media for urography. *Br J Radiol* **1985**;58:593–597
16. Davies P, Glaves J, Panto P, Richardson RE. Comparison of two strengths of iohexol and iothalamate in urography. *Urol Radiol* **1987**;9:30–35
17. Drayer BP, Velaj R, Bird R, et al. Comparative safety of intracarotid iopamidol, iothalamate meglumine, and diatrizoate meglumine for cerebral angiography. *Invest Radiol* **1984**;19[suppl 6]:S212–S218
18. Edgren J, Kivisaari A, Laasonen L, Standertskiöld-Nordenstam C-G. Urography with iohexol: comparison with metrizoate and iodamide. *Acta Radiol Suppl* (Stockh) **1983**;366:46–49
19. Egsgaard H, Horup A, Praestholm J. A controlled clinical trial of iohexol and diatrizoate in aortofemoral angiography. *Eur J Radiol* **1983**;3:14–17
20. Eyes BE, Goldman M, Nixon TE, Scally J, Brown A. Low dose low osmolar intravenous urography. *Clin Radiol* **1987**;38:403–405
21. Gordon IJ, Sköblar RS, Chicatelli PD, Leon J. A comparison of iohexol and Conray-60 in peripheral angiography. *AJR* **1984**;142:563–565
22. Grainger RG. Patient reactions during Hexabrix, iopamidol and Conray angiography. In: *European workshop*. Lyon, France: Springer-Verlag, **1982**:265–268
23. Grainger RG. The optimal concentration of contrast medium for aortography and femoral arteriography: a comparison of Hexabrix 320 and Hexabrix 250. *Clin Radiol* **1986**;37:281–284
24. Hagen B. Iopamidol, ein neues, nichtionisches röntgenkontrastmittel. *Radiologe* **1982**;22:581–585
25. Hartman GW, Hattery RR, Witten DM, Williamson B Jr. Mortality during excretory urography: Mayo Clinic experience. *AJR* **1982**;139:919–922
26. Herd CM, Robertson AR, Frewin DB, Taylor WB. Adverse reactions during intravenous urography: are these due to histamine release? *Br J Radiol* **1988**;61:5–11
27. Heron CW, Underwood SR, Dawson P. Electrocardiographic changes during intravenous urography: a study with sodium iothalamate and iohexol. *Clin Radiol* **1984**;35:137–141
28. Hindmarsh T, Bergstand G, Ericson K, Olivecrona H. Comparative double-blind investigation of meglumine metrizoate, metrizamide, and iohexol in carotid angiography. *AJNR* **1983**;4:347–349
29. Holtas S, Cronqvist S, Renaa T. Contrast enhanced brain CT: comparison between iohexol and metrizoate. *Neuroradiology* **1983**;24:213–215
30. Jacobson BF, Jorulf H, Kalantar MS, Narasimham DL. Nonionic versus ionic contrast media in intravenous urography: clinical trial in 1,000 consecutive patients. *Radiology* **1988**;167:601–605
31. Kallehauge HE, Praestholm J. Iopamidol, a new nonionic contrast medium in peripheral angiography. *Cardiovasc Intervent Radiol* **1982**;5:325–328

32. Katayama H, Yamaguchi K, Kozuka T, Takashima T, Seez P, Matsuura K. Adverse reactions to ionic and nonionic contrast media. Report of the Japanese committee on the safety of contrast media. *Radiology* **1990**;175:621–628
33. Kido DK, Potts GP, Bryan RN, et al. Iohexol cerebral angiography: multicenter clinical trial. *Invest Radiol* **1985**;20[suppl 1]:S55–S57
34. Laerum F, Holm HA. Postphlebographic thrombosis: A double-blind study with methylglucamine metrizoate and metrizamide. *Radiology* **1981**; 140:651–654
35. Lalli AF, Williams B, Maynard E. Iohexol in urography. *Urol Radiol* **1983**;5:95–97
36. Langer M, Behrinds B, Langer R, Eichstädt H, Jänicke U-A. Tolerance of iopromide in angiography, a multicenter study. *ROFO* **1989**;128:61–66
37. Lasser EC, Berry CC, Talner LB, et al. Pretreatment with corticosteroids to alleviate reactions to intravenous contrast material. *N Engl J Med* **1987**;317:845–849
38. Longstaff AJ, Henson JHL. Bronchospasm following intravenous injection of ionic and non-ionic low-osmolality contrast media. *Clin Radiol* **1985**;36:651–653
39. Loughran CF. Clinical intravenous urography: comparative trial of ioxaglate and iopamidol. *Radiology* **1986**;161:455–458
40. McCullough M, Davies P, Richardson R. A large trial of intravenous Conray 325 and Niopam 300 to assess immediate and delayed reactions. *Br J Radiol* **1989**;62:260–265
41. McClennan BL, Ling D, Rholl KS, James M. Urography with a low osmolality contrast agent: comparison of Hexabrix with Conray 325. *Invest Radiol* **1986**;21:144–150
42. McClennan B, Lee JKT, Disantis DJ, James M. A double-blind clinical study comparing the safety and efficacy of Hexabrix and Renografin-76 in contrast enhanced computed body tomography. *Invest Radiol* **1984**;19:S378–S384
43. Murphy G, Campbell DR, Fraser DB. Pain in peripheral arteriography: an assessment of conventional versus ionic and non-ionic low-osmolality contrast agents. *Can Assoc Radiol J* **1988**;39:103–106
44. Nakstad P. Digital subtraction angiography of the carotid arteries: a comparison of iohexol and metrizoate. *Acta Radiol [Suppl]* (Stockh) **1983**;366:89–94
45. Norman D, Brant-Zawadzki M, Sobel D. Neuroradiology. Neuroangiography: tolerability and efficacy of Hexabrix in cerebral angiography. *Invest Radiol* **1984**;19:S306–S307
46. Nyman U, Nilsson P, Westergren A. Pain and hemodynamic effects in aortofemoral angiography: clinical comparison of iohexol, ioxaglate and metrizamide. *Acta Radiol Suppl* (Stockh) **1983**;366:171–172
47. Palmer FJ. The RACR survey of intravenous contrast media reactions: final report. *Australas Radiol* **1988**;32:426–428
48. Pathria M, Sommers S, Gill G. Pain during angiography: a randomized double-blind trial comparing ioxaglate and diatrizoate. *Can Assoc Radiol J* **1987**;38:32–34
49. Pelz D, Fox AJ, Viñuela F. Clinical trial of iohexol vs Conray 60 for cerebral angiography. *AJNR* **1984**;5:565–568
50. Rankin RN, Hong Tai Eng FW. Iohexol vs diatrizoate: a comparative study in intravenous urography. *Invest Radiol* **1985**;20[suppl 1]:S112–S114
51. Robbins AH, Thurm RH, Yeh T. Computed body tomography with iopamidol. *Invest Radiol* **1984**;19[suppl 6]:S234–S238
52. Sackett JF, Bergsjordet B, Seeger JF, Kieffer SA. Digital subtraction angiography: comparison of meglumine-na diatrizoate with iohexol. *Acta Radiol Suppl* (Stockh) **1983**;366:S81–S84
53. Schrott KM, Behrends B, Clauss W, Kaufmann J, Lehnert J. Iohexol in excretory urography. *Fortsch Med* **1986**;104:153–156
54. Seyferth W, Dilbat G, Zeitler E. Efficacy and safety of digital subtraction angiography with special reference to contrast agents. *Cardiovasc Intervent Radiol* **1983**;6:265–270
55. Shehadi WH, Toniolo G. Adverse reactions to contrast media: a report from the Committee on Safety of Contrast Media of the International Society of Radiology. *Radiology* **1980**;137:299–302
56. Shehadi WH. Contrast media adverse reactions: occurrence, recurrence, and distribution patterns. *Radiology* **1982**;143:11–17
57. Skalpe IO, Anke IM. Complications in cerebral angiography: a comparison between the non-ionic contrast medium iohexol and meglumine metrizoate (Isopaque Cerebral). *Neuradiology* **1983**;25:157–160
58. Skalpe IO, Hordvik M. Comparison of side effects during cerebral computed tomography with a nonionic (iohexol) and an ionic (metrizoate) contrast medium. *AJNR* **1983**;4:326–328
59. Skjennald A, Heldaas J, Hoiseth A. Comparison of iohexol and meglumine-na-ca metrizoate in visceral angiography. *Acta Radiol Suppl* (Stockh) **1983**;366:158–163
60. Smith DC, Yahiku PY, Maloney MD, Hart KL. Three new low-osmolality contrast agents: a comparative study of patient discomfort. *AJNR* **1988**;9:137–139
61. Spataro RF, Katzberg RW, Fischer HW, McMannis MJ. High-dose clinical urography with the low-osmolality contrast agent Hexabrix: comparison with a conventional contrast agent. *Radiology* **1987**;162:9–14
62. Stiris MG, Laerum F. Iohexol and ioxaglate in peripheral angiography. *Acta Radiol* **1987**;28:767–770
63. Thomas ML, Briggs GM, Kuan BB. Contrast agent-induced thrombophlebitis following leg phlebography: meglumine ioxaglate versus meglumine iothalamate. *Radiology* **1983**;147:399–400
64. Thomas ML, Briggs GM, Keeling FP. Iohexol and meglumine iothalamate in phlebography of the leg: comparison of the tolerance. *Acta Radiol Suppl* (Stockh) **1983**;366:S54–S57
65. Thomas ML, Briggs GM. Comparison of tri-iodoisophthaldiamide with meglumine iothalamate in phlebography of the leg. *AJR* **1982**;138: 725–727
66. Thron A, Ratzka M, Voigt K, Nadjmi M. Iohexol and ioxaglate in cerebral angiography. *Acta Radio Suppl* (Stockh) **1983**;366:S151–S152
67. Trigaux JP, de Fays R, de Fays F. Comparative study of two iodinated contrast media containing 20% iodine in lower-limb phlebography: ioxaglate versus a conventional product. *Br J Radiol* **1985**;58:203–205
68. Tschakert H. Contrast medium tolerance in computed tomography. *ROFO* **1983**;118:156–161
69. Van de Velde E, Van Rattinghe R, Holager T, Van Meerbeeck E. Iohexol (Omnipaque®) in cerebral angiography. *Belg Tijdschr Radiol* **1983**; 66:423–428
70. Van Sonnenberg E, Courtney CN, Pfister RC. Life-threatening hypotensive reactions to contrast media administration: comparison of pharmacologic and fluid therapy. *Radiology* **1987**;162:15–19
71. Whitehouse GH, Snowdon SL. A comparison between iohexol and metrizamide, two non-ionic contrast media, in aorto-femoral angiography. *Br J Radiol* **1984**;57:39–42

71a. Whitehouse GH, Snowdon SL. An assessment of iopamidol, a non-ionic contrast medium, in aortofemoral angiography. *Clin Radiol* **1982**;33:231–234

72. Wolf GL, Arenson RL, Cross AP. A prospective trial of ionic vs nonionic contrast agents in routine clinical practice: comparison of adverse effects. *AJR* **1989**;152:939–944
73. Gomes AS, Lois JF, Baker JD, McGlade CT, Bunnell DH, Hartzman S. Acute renal dysfunction in high-risk patients after angiography: comparison of ionic and nonionic contrast media. *Radiology* **1989**;170:65–68
74. Parfrey PS, Griffiths SM, Barret BJ, et al. Contrast material–induced renal failure in patients with diabetes mellitus, renal insufficiency, or both. *N Engl J Med* **1989**;320:143–149
75. Powe NR, Steinberg EP, Erickson JE, et al. Contrast medium–induced adverse reactions: economic outcome. *Radiology* **1988**;169:163–168
76. Taliercio CP, Vlietstra RE, Fisher LD, Burnett JC. Risks for renal dysfunction with cardiac angiography. *Ann Intern Med* **1986**;104:501–504
77. Zachrisson BE, Jagenburg R. Comparison of iohexol with metrizoate in urography. *Acta Radiol Suppl* (Stockh) **1983**;366:S30–S37
78. Berland LL. Double-blind comparison of Hexabrix and Renografin-76 in computed tomography. *Invest Radiol* **1984**;19[suppl 6]:S376–S377
79. Wolf GL. Adult peripheral angiography: results from North American randomized clinical trials of ionic media versus iohexol. *Acta Radiol Suppl* (Stockh) **1983**;366:166–170
80. Bettmann MA, Higgins C. Comparison of an ionic with a nonionic contrast agent for cardiac angiography: results of a multicenter trial. *Invest Radiol* **1985**;20[suppl 1]:S70–S74
81. Gertz EW, Wineski JA, Chiu D, Akin JR, Hu C. Clinical superiority of a new nonionic contrast agent (iopamidol) for cardiac angiography. *J Am Coll Cardiol* **1985**;5:250–258
82. Levorstad K, Simonsen S, Gervell J. Tolerability and usefulness of iohexol in cardioangiography. *Acta Radiol Suppl* (Stockh) **1983**;366:S101–S110
83. Miller DL, Chang R, Wells WT, Dowjat BA, Malinoshy RM, Doppman JL.

Intravascular contrast media: effect of dose on renal function. *Radiology* **1988**;167:607–611
84. Newman TJ. Evaluation of iopamidol in peripheral arteriography and coronary arteriography with left ventriculography. *Invest Radiol* **1984**; 19[suppl 6]:S181–S186
85. Schwab SJ, Hlatky MA, Pieper KS, et al. Contrast nephrotoxicity: a randomized controlled trial of a nonionic and an ionic radiographic contrast agent. *N Engl J Med* **1989**;320:149–153
86. Eisenberg RL, Bank WO, Hedgock MW. Renal failure after major angiography can be avoided with hydration. *AJR* **1981**;136:859–861
87. Cochran ST, Wong WS, Roe DJ. Predicting angiography-induced acute renal function impairment: clinical risk model. *AJR* **1983**;141:1027–1033
88. Corcos T, David PR, Bonan R, Paquet E, Lesperance J, Bourassa M. Clinical experience with ioxaglate (Hexabrix) in selective coronary arteriography. *Can Assoc Radiol J* **1984**;35:354–359
89. Cramer BC, Parfrey PS, Hutchinson TA, et al. Renal function following infusion of radiologic contrast material: a prospective controlled study. *Arch Intern Med* **1985**;145:87–89
90. Cruz C, Hricak H, Samhouri F, Smith RF, Eyler WR, Levin NW. Contrast media for angiography: effect on renal function. *Radiology* **1986**; 158:109–112
91. D'Elia JA, Gleason RE, Alday M, et al. Nephrotoxicity from angiographic contrast material: a prospective study. *Am J Med* **1982**;72:719–725
92. Davidson CJ, Hlatky M, Morris KG, et al. Cardiovascular and renal toxicity of a nonionic radiographic contrast agent after cardiac catheterization. *Ann Intern Med* **1989**;110:119–124
93. Kennedy C, Rickards D, Lee S, Buckley Sharp M, Dawson P. A double-blind study comparing the efficiency, tolerance and renal effects of iopromide and iopamidol. *Br J Radiol* **1988**;61:288–293
94. Kumar S, Hull JD, Lathi S, Cohen AJ, Pletka PG. Low incidence of renal failure after angiography. *Arch Intern Med* **1981**;141:1268–1270
95. Teruel JL, Marcén R, Onaindía JM, Serrano A, Quereda C, Ortuño J. Renal function impairment caused by intravenous urography. *Arch Intern Med* **1981**;141:1271–1274
96. Zeitler E, Georgi-Tönnesen M, Hinski HG, Mader H, Richter E-I. Angiography in lower extremities with new contrast media: review of double-blind studies. In: *European workshop*. Lyon, France: Springer-Verlag, **1982**:257–264
97. Conseil d'évaluation des technologies de la santé du Québec. Evaluation of low vs high osmolar contrast media. 2. Technical document. Quebec: Gouvernement du Quebec, **1989**
98. Bashore TM, Davidson CJ, Mark DB, Kisslo K, Hlatky MA, Skelton TN. Iopamidol use in the cardiac catheterization laboratory. A retrospective analysis of 3,313 patients. *Cardiology* **1988**;5:306–310
99. Miettinen OS. *Theoretical epidemiology: principles of occurrence research in medicine*. New York: Wiley, **1985**
100. Miettinen OS, Nurminen M. Comparative analysis of two rates. *Stat Med* **1985**;4:213–226
101. Chalmers TC, Smith H Jr, Blackburn B, et al. A method for assessing the quality of a randomized trial. *Controlled Clin Trials* **1981**;2:31–49
102. Witten DM, Hirsch FD, Hartman GW. Acute reactions to urographic contrast medium. *AJR* **1973**;119:832–840
103. Shehadi WH. Adverse reactions to intravascularly administered contrast media. A comprehensive study based on a prospective survey. *AJR* **1975**;124:145–152
104. Gertz EW. Contrast media—safety aspects of ionic versus low osmolar. *Can J Cardiol* **1990**;6[suppl A]:3A–4A
105. Goel V, Deber RB, Detsky AS. Nonionic contrast media: economic analysis and health policy development. *Can Med Assoc J* **1989**;140: 389–395
106. Corporation professionnelle des médecins du Québec. *Guide to the use of low-osmolality media as contrast agents*. Quebec: Corporation professionnelle des medécins du Québec, **1988**:1–16
107. Bettmann MA. Guidelines for use of low-osmolality contrast agents. *Radiology* **1989**;172:901–903
108. Grainger 1987. Annotation: radiological contrast media. *Clin Radiol* **1987**;38:3–5
109. Mishkin MM, Edeiken J, The Committee on Drugs and Contrast Media. The current efficacious use of water soluble contrast agents for intravascular injections. *ACR Bull* **1988**;44:9–10
110. Swanson DP. Drug review: Evaluation of intravascular low-osmolality contrast agents. *Clin Pharm* **1986**;5:877–891
111. Wolf GL. Safer, more expensive iodinated contrast agents: how do we decide? *Radiology* **1986**;159:557–558
112. McClennan BL. State of art. Low-osmolality contrast media. Premises and promises. *Radiology* **1987**;162:1–8
113. Kinnison ML, Powe NR, Steinberg EP. Results of randomized controlled trials of low versus high-osmolality contrast media. *Radiology* **1989**;170:381–389
114. Denys BG. Nephrotoxicity of a non-ionic vs an ionic (Diatrizoate) contrast agent in the patient after cardiac transplant with moderate cyclosporin-induced renal insufficiency. *Am J Cardiol* **1989**;64:405–406

Case Report

# Atypical Contrast Reactions Associated with Systemic Interleukin-2 Therapy

Joel E. Fishman,[1] Denise R. Aberle,[1] Nancy P. Moldawer,[2] Arie Belldegrun,[3] and Robert A. Figlin[2]

Adoptive immunotherapy with recombinant interleukin-2 (IL-2) can mediate significant regression of metastatic cancer in selected patients, especially renal cell carcinoma and metastatic melanoma [1]. Unfortunately, IL-2 therapy is associated with adverse side effects in a large percentage of patients. An IL-2–induced capillary leak syndrome, causing pulmonary edema and pleural and pericardial effusions, has been described [2]. More immediate side effects of IL-2 administration include fever, chills, nausea, vomiting, diarrhea, pruritis, rash, and lethargy, among others [3]. Changes in neutrophil count and a rise in serum creatinine level are also occasionally observed [4]. The occurrence of at least some of these reactions is nearly universal among patients receiving IL-2 and often depends on dosage and schedule.

We wish to report a form of adverse reaction in these patients, which occurs after the IV administration of iodinated contrast material and which resembles the more immediate side effects of IL-2 described above. Five patients on low-dose IL-2 protocols at our institution have variably experienced diarrhea, fever, chills, nausea, vomiting, and pruritis after IV contrast administration. One particularly severe case is described below. All patients had received a nonionic contrast agent.

## Case Report

A 51-year-old man with metastatic renal cell cancer had received a 1-month-long cycle of therapy with IL-2, alpha-interferon, and tumor-infiltrating lymphocytes. Symptoms after IL-2 administration had included fever, chills, nausea, diarrhea, mild leukocytosis, and a transient rise in serum creatinine level to more than 3 mg/dl. Two weeks after completion of the treatment cycle, the patient underwent thoracic and abdominal CT scanning. Contrast material was ingested, and 150 ml of iohexol was administered IV through an appropriately prepared central venous catheter. Approximately 3 hr after contrast administration, fever, chills, pruritis, nausea, vomiting, and severe diarrhea developed. Symptoms worsened, with temperature elevated to 102°F and profound lethargy. Eight hours after contrast administration, he was admitted to the hospital through the emergency department. His blood pressure was 80/60 mm Hg. The blood creatinine value had risen to 2.4 mg/dl, whereas its baseline value from the previous day had been 1.3 mg/dl. The WBC count rose to 14,000 per $\mu$l. Cultures of blood, urine, and stool were obtained, and the patient was treated with IV fluids and broad-spectrum antibiotics for possible sepsis. All cultures were negative, and the patient slowly improved during the next 3 days. Antibiotics were discontinued and the patient remained afebrile, and the creatinine level and the WBC count returned to normal. The patient was discharged on the fourth hospital day.

## Discussion

Our institution has enrolled 33 patients with metastatic renal cell cancer on protocols involving the outpatient administration of continuous IV infusion, low-dose recombinant IL-2 (Hoffmann-La Roche, Nutley, NJ) and recombinant alpha-interferon (Roferon-A; Hoffmann-La Roche, Nutley, NJ). Three

Received September 7, 1990; accepted after revision October 19, 1990.
This work was supported by the Jonsson Comprehensive Cancer Center, UCLA School of Medicine, and Hoffman-La Roche, Nutley, NJ.
[1] Department of Radiological Sciences, UCLA School of Medicine, UCLA Medical Center, 10833 Le Conte Ave., Los Angeles, CA 90024-1721. Address reprint requests to D. R. Aberle.
[2] Department of Internal Medicine, Division of Hematology-Oncology, UCLA School of Medicine, 10833 Le Conte Ave., Los Angeles, CA 90024.
[3] Department of Surgery, Division of Surgical Urology, UCLA School of Medicine, 10833 Le Conte Ave., Los Angeles, CA 90024.

 0361–803X/91/1564–0833 © American Roentgen Ray Society

of these patients received tumor-infiltrating lymphocytes also. Therapy is given in month-long cycles; from 10 to 14 days after the last IL-2 dose of each cycle, each patient undergoes body CT scanning to monitor progress. Oral contrast material is usually administered, consisting of a 5% solution of Gastroview (diatrizoate meglumine and diatrizoate sodium; Mallinckrodt, St. Louis, MO), followed by a 2% barium sulfate suspension. When IV contrast material is necessary, 80–150 ml of iohexol (Omnipaque; Winthrop Pharmaceuticals, New York) is used.

Five (15%) of the 33 patients on low-dose IL-2 protocols have experienced adverse effects after IV contrast administration for CT scanning. Symptoms have included diarrhea ($n$ = 5), fevers and chills ($n$ = 3), nausea and/or vomiting ($n$ = 3), itching ($n$ = 2), lethargy with hypotension ($n$ = 1), and acute renal insufficiency ($n$ = 1). The adverse effects occurred between 30 min and 4 hr after contrast injection. These symptoms more closely resemble those occurring after systemic IL-2 therapy than those occurring in typical contrast reactions. In all cases, a nonionic IV contrast agent was used. According to a recent large study [5], the most common side effects of nonionic contrast administration are nausea and heat sensation, each occurring in approximately 1% of cases. Vomiting, itching, and rigors occur in less than 0.5% of cases [5]. Diarrhea and fever, our most commonly observed symptoms, were not described in that report; the manufacturer's product information predicts a frequency of these symptoms of less than 1% [6].

Prior therapy with IL-2 appears to be a necessary link in the pathogenesis of the reaction. None of these patients had a history of allergy to iodinated contrast material. Furthermore, before beginning IL-2 therapy, all five patients had had body CT scans with oral and IV contrast material without ill effects. Oral contrast material alone does not precipitate this reaction, because two of the patients had undergone multiple prior CT scans with only oral contrast material without significant adverse reactions.

Adverse reactions to radiologic contrast material in patients who have received IL-2 have been reported in the oncologic literature [7, 8]. It has been proposed that patients receiving IV contrast material after IL-2 therapy may experience a "recall" of the symptoms of IL-2 administration [7]. In one report, 22 of approximately 200 patients on IL-2 protocols developed adverse effects after contrast administration [7]; our experience is in agreement with their estimate that at least 10% of patients receiving IL-2 will have a recall reaction after receiving IV contrast material. Whereas the findings of Oldham et al. [7] suggested a significantly lowered frequency of recall reactions after nonionic contrast administration than after ionic [7], all of the reactions at our institution occurred after nonionic contrast administration. Furthermore, our results differ from those of another report in which eight patients who had previously received intraarterial IL-2 developed contrast reactions, whereas patients who received IV IL-2 did not suffer from an increase in contrast reactions [8].

Significant nonionic contrast–induced recall reactions can occur after low-dose IV IL-2 therapy. It has been suggested that these reactions can be prevented by pretreatment with corticosteroids and antihistamines [8]. As more widespread use of IL-2 is likely to occur in the near future, radiologists must be familiar with this unusual contrast-related reaction.

## REFERENCES


1. Figlin RA, Citron M, Whitehead R, et al. Low dose continuous infusion recombinant interleukin-2 (rhIL-2) and Roferon-A: an active outpatient regimen for metastatic renal cell carcinoma. *Am Soc Clin Oncol* **1990**;9:142
2. Conant EF, Fox KR, Miller WT. Pulmonary edema as a complication of interleukin-2 therapy. *AJR* **1989**;152:749–752
3. Sondel PM, Kohler PC, Hank JA, et al. Clinical and immunological effects of recombinant interleukin 2 given by repetitive weekly cycles to patients with cancer. *Cancer Res* **1988**;48:2561–2567
4. Belldegrun A, Webb DE, Austin HA III, et al. Effects of interleukin-2 on renal function in patients receiving immunotherapy for advanced cancer. *Ann Intern Med* **1987**;106:817–822
5. Katayama H, Yamaguchi K, Kozuka T, Takashima T, Seez P, Matsuura K. Adverse reactions to ionic and nonionic contrast media. *Radiology* **1990**;175:621–628
6. Omnipaque (iohexol) product information insert. New York: Winthrop Pharmaceuticals, **1989**
7. Oldham RK, Brogley J. Contrast medium "recalls" interleukin-2 toxicity. *J Clin Oncol* **1990**;8:942
8. Zukiwski AA, David CL, Coan J, Wallace S, Gutterman JU, Mavligit GM. Increased incidence of hypersensitivity to iodine-containing radiographic contrast media after interleukin-2 administration. *Cancer* **1990**;65:1521–1524

# An Ultrafast Network for Communication of Radiologic Images

Brent K. Stewart[1]
S. L. Lou
W. K. Wong
H. K. Huang

**The three most difficult problems in making picture archiving and communication systems (PACS) a clinical reality in radiology are image archiving, very high-resolution display stations, and high-speed networking. This article considers high-speed image transmission through a high-capacity network. Our laboratory has tested several commercially available high-speed networks over the past year. Only one of these networks (UltraNet) has adequate throughput and capacity potential necessary for our PACS. The focus of this experiment is to determine the throughput and capacity characteristics of this star topology networking scheme as they relate to the operation of a PACS in the clinical environment. A large-scale test was done to gauge network performance for three networking configurations modeling those in a PACS: duplex, parallel, and relay. Ten computers used in our PACS (Sun 3 and 4 computers) were connected with UltraNet. For point-to-point throughput (half-duplex model), the network delivers up to 3.1 megabytes/sec for Sun 3 computers and 6.8 megabytes/sec for the Sun Sparcserver 490. As regards capacity considerations (parallel model), five parallel image transfer processes generated a maximum of 13.9 megabytes/sec through the network. Only a slight degradation in individual process throughput was observed (1.4%). With regard to shared access to high-contention resources on the PACS network (e.g., archive servers), this network demonstrated equal sharing of server networking capacity between the various client computers.**

**With the encouraging results of this experiment, we believe that the UltraNet network will be sufficient for the image communication requirements of our PACS. We are proceeding with the implementation of UltraNet as the high-speed backbone of our extended PACS network.**

*AJR* 156:835–839, April 1991

Digital medical images contain an enormous amount of data. For example, a computed radiography (CR) image (2048 × 2048 × 10 bits) is composed of 8 megabytes of digital data. A CT examination consisting of 64 0.5-megabyte images (512 × 512 × 12 bits) is composed of 32 megabytes. The timely communication of these images requires a high-speed, high-capacity network. A network consists of the transmission media, hardware, signaling protocols, and software necessary for one computer to communicate with another. The capacity of a network refers to its ability to manage many simultaneous communication processes between a number of computers. For picture archiving and communication systems (PACS) to be useful to the radiologist, we estimate that a CR image should be transferred within a network in less than 2 sec. This places a network throughput requirement at 4 megabytes/sec and a signaling rate requirement at several times this rate. This is because the effective network performance for an application can be much less than the theoretical performance based on the signaling rate. The network also should support many high-speed image transmission processes simultaneously without significant degradation in the performance of any individual process.

Received August 27, 1990; accepted after revision October 16, 1990.

This work was supported in part by Public Health Service grants R01 CA 39063 and R01 CA 51198, awarded by the National Cancer Institute, Department of Health and Human Services, and the University of California, Los Angeles, Department of Radiological Sciences Research Fund.

[1] All authors: Department of Radiological Sciences, Medical Imaging Division, University of California, Los Angeles, School of Medicine, 10833 Le Conte Ave., Los Angeles, CA 90024-1721. Address reprint requests to B. K. Stewart.

0361–803X/91/1564–0835
© American Roentgen Ray Society

## Materials and Methods

Two high-speed networks were tested in our laboratory and compared with Ethernet (Sun Microsystems, Inc., Mountain View, CA) [1, 2]: one with a tree topology (Canstar Super 100 network, Toronto, CA) [3] and one with a token-ring topology (the Fiber Distributed Data Interface [FDDI], Sun Microsystems, Inc.) [4]. Ethernet has a signaling rate of 1.25 megabytes/sec. The Canstar network has a concentrator signaling rate of 12.5 megabytes/sec, each node on the hub having a signaling rate of 1.25 megabytes/sec. The FDDI has a signaling rate of 12.5 megabytes/sec. The point-to-point throughput performance of Ethernet, Canstar, and FDDI were previously found to be 0.372, 0.518, and 0.833 megabytes/sec, respectively, for Sun 3 class computers [1]. The time required for transmission of a 64-slice CT examination at these transmission rates is 88.1, 63.3, and 39.3 sec, respectively.

As none of these networks even remotely approaches the 4-megabyte/sec requirements of our clinical PACS environment, we investigated another emerging network technology: UltraNet (UltraNetwork Technologies, San Jose, CA). The intent of this experiment was to confirm the hypothesis that UltraNet would satisfy the 4 megabytes/sec required of our clinical environment and would not suffer significant degradation with multiple communication processes.

The UltraNet network consists of two major components, a hub with a 125-megabytes/sec signaling rate and a host adapter with a signaling rate of up to 31.3 megabytes/sec. The host adapter inserts into the backplane of the host computer and connects to the hub with fiberoptic transceivers at each end and fiberoptic cable. The UltraNet network has a meshed star topology (i.e., several hubs can be interconnected by any configuration). The hub contains the UltraBus and link adapters. Link adapters are composed of a protocol processor and one or more link multiplexers. It also comes with network management through StarLan (IEEE 802.3) and a personal computer.

Two outstanding features of the UltraNet network account for its high speed and high capacity: the host adapter and the link adapter/UltraBus. The UltraNet host adapter hardware off-loads data transfer, protocol processing, and signaling chores from the host computer. The data are sent to the hub from the host adapter over serial fiberoptic links with signaling rates of 7.8, 15.6, or 31.3 megabytes/sec. A fiberoptic transceiver and link adapter at the hub convert these serial data and place them on the UltraBus, a massively parallel data link (64 data lines). The protocol processor within the link adapter routes the data to the receiving link adapter and out to the receiving host adapter over another fiberoptic serial line.

Although our test results of the FDDI and Canstar networks were reported elsewhere [1, 2], we had an opportunity to perform a large-scale study of the UltraNet network using 10 Sun workstations. Figure 1 shows the equipment and workstations used in the experiment. Six Sun 3 workstations and four Sun 4 workstations were used with an UltraNet Hub model 250C. Two transmission media were used. Three of the connections with the Hub 250C used 150-ft (50-m), 62.5-$\mu$m multimode fiberoptic cable; the other seven used RG-59 coaxial cable of various lengths. Two of the workstations (G and H) were in clinical use and required extremely long runs of coaxial cable. Eight of the workstations used Sun operating system version 4.0.3; two of them (G and H) used the 4.0.1 version.

Memory-to-memory data transfers were issued between computers as disk access times typically impede network throughput. To measure effective performance, TSOCK, a program using the UltraNet socket emulation library to perform many network exercises, was used. During memory transfers, this program creates a buffer of data in memory of the size requested by the user. The TSOCK software then transfers these data over the UltraNet network to the remote computer system memory. This was done repeatedly in the following tests to obtain an average throughput. Buffer sizes of 64, 128, 256, and 1024 kilobytes were used, although any size is possible. Each execution of TSOCK transferred 32 megabytes of data, simulating a 64-slice CT examination.

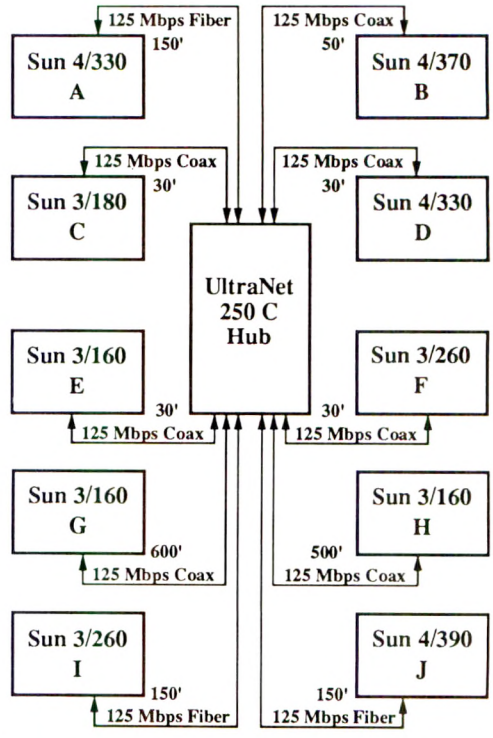



**Fig. 1.—Diagram shows computers and equipment used in this experiment. Six Sun 3 workstations (C, E, F, G, H, and I) and four Sun 4 workstations (A, B, D, and J) were used with an UltraNet Hub 250C. Both 62.5-$\mu$m multimode fiberoptic cable and RG-59 coaxial (coax) cable (lengths indicated) were used to connect computers with hub. Mbps = megabits per second.**

Three test models, designed to simulate network traffic in a PACS environment (duplex, parallel, and relay—described in greater detail later), were used to measure the performance of the UltraNet network. The duplex model tests half- and full-duplex communication between two computers, termed a client-server pair. The client computer is the initiator of the communication process, whereas the server computer completes the communication process, receiving data from the client.

The duplex model simulates transmission for the simplest PACS network environment possible: two nodes. It provides a point-to-point performance baseline from which to compare the performance of the same client-server pairs in the parallel and relay models. These baselines can also be used for point-to-point comparison with other networks (i.e., Ethernet and FDDI).

In the parallel model, the 10 workstations were arranged into five client-server pairs. One by one, different client-server pairs were added to the network, so that eventually all five client-server pairs were communicating simultaneously over the network. The parallel model tests overall network throughput characteristics under loading. The transmission rate integrity of the first client-server communication process is monitored as others are added to the network. The parallel model simulates the random image transfer between various client-server pairs on the same PACS network (e.g., between very high-resolution display stations in the various radiology sections).

With the relay model, successive communication processes are initiated between the Sun Sparcserver 390 (J in Fig. 1) and the nine

other workstations (A–I in Fig. 1). In five of the nine communication processes established, the Sparcserver 390 acted as a server; in the other four it participated as a client. The input/output (I/O) data rate of the Sparcserver was measured as each of the nine workstations was added to the network, one by one. The purpose of this model is to simulate the typical network traffic conditions indicative of a PACS centralized image management host that manages all incoming (e.g., from MR or CT acquisition computers) and outgoing (e.g., to very high-resolution display stations) image data. This model measures how well the network allocates the limited I/O capacity of the Sparcserver 390 between all contending communication processes with the other workstations.

## Results

Figure 2 shows the result of the duplex model for two Sun 3 class computers (E and F). The observed trends in the data were much the same between two Sun 4 class computers (B and J) and between a Sun 3 and Sun 4 computer (F and J). The mean transmission rate depends on the memory data buffer size used in the application program. Buffer sizes of 64, 128, 256, and 1024 kilobytes were used. The rate of transmission varies as this buffer size is changed. The mean transmission rate increases up to the 128-kilobyte buffer size for the half-duplex processes, where a plateau of 3.15 megabytes/sec is reached. This transmission rate corresponds to transferring a 64-slice CT examination in 10.2 sec. By using full-duplex transmission, an average of 4.15 megabytes/sec was realized between the Sun 3 computers for a 256-kilobyte buffer size.

Results from the parallel model are shown in Figure 3. With all 10 Sun workstations (five client-server communication processes), a total of 13.9 megabytes/sec was measured when routed through the Hub 250C for a 256-kilobyte buffer size. The plot is nearly linear, suggesting that each individual communication process proceeds independent of the others. At most, a 1.4% degradation was observed for the initial communication process (A to B) as the other four client-server pairs' communication processes (C to D, E to F, G to H, and I to J) were added to the network. This characteristic is quite different from that observed for Ethernet. Parallel-model Ethernet data from Wong et al. [2] are also plotted in Figure 3 for comparison. The cumulative throughput of Ethernet quickly saturates, and the initial client-server pair transmission rate decreases rapidly after the third client-server pair is added.

The relay model does not test the capacity of the network so much as it tests the capability of the network to allocate resources among the communication processes on the central server. Figure 4 shows the relay model network I/O of

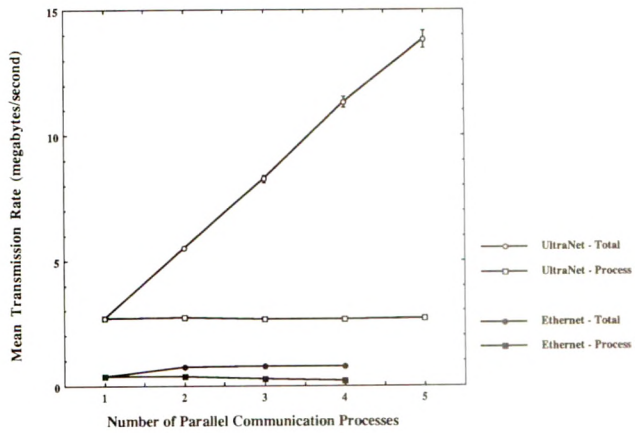



**Fig. 3.—Graph shows parallel model data for UltraNet and Ethernet networks. Mean transmission rate for UltraNet was measured both through hub (total) and for initial client-server pair (A to B, process 1) as other, independent client-server pairs were added to the network. UltraNet data were measured for transfer of 32 megabytes by using TSOCK software and a 256-kilobyte buffer size. Ethernet data are adapted from Wong et al. [2] for similar computers and same test model.**

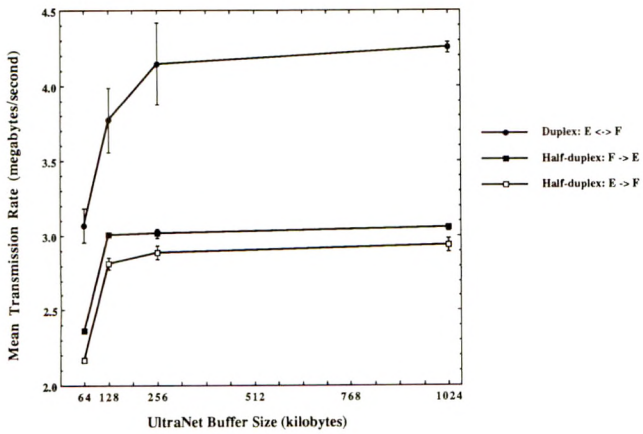



**Fig. 2.—Graph shows resulting data for the duplex and half-duplex models for two Sun 3 computers (E and F) (see Fig. 1). Transmission rate in megabytes/sec was measured for several transfers of 32 megabytes by using the TSOCK program and yields plotted mean transmission rate. UltraNet buffer sizes 64, 128, 256, and 1024 kilobytes were used. Error bars represent ±1 SD. Duplex transmission sustains a higher cumulative data rate than half-duplex because UltraNet link adapter spends less idle time.**

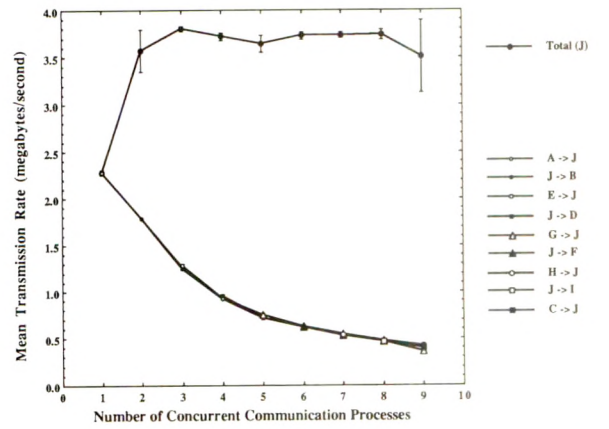



**Fig. 4.—Graph shows relay model results of measuring mean transmission rate into and out of Sparcserver 390 (J) as a function of number of concurrent communication processes with other nine workstations. Again, TSOCK software was used to transfer 32 megabytes of data, but buffer size used for each client-server communication process was 64 kilobytes. The upper line (total) is total of transmission rate for number of individual client-server connections with Sparcserver 390, which are plotted without error bars for greater clarity.**

the Sparcserver 390 for a 64-kilobyte buffer size. As the number of concurrent processes increases from one to nine, the cumulative I/O capacity increases up to 3.8 megabytes/sec, levels out, and then oscillates slightly, finally dropping appreciably for nine concurrent processes. The other nine curves show the falling transmission rate of the active communication processes as new ones are added. In general, these curves follow a c/x function ($r^2 > .962$), where c is a constant and x is the number of active communication processes.

The cumulative I/O transmission rate of the Sparcserver 390 for the relay model does not increase appreciatively after the number of concurrent processes reaches three. As the number of concurrent processes increases from four to eight, minor fluctuations in network throughput are observed until a falloff occurs at nine concurrent processes. These observations are related to the direct virtual memory access (DVMA) architecture of the Sun computer.

Though the transmission rate is greater for UltraNet as compared with Ethernet, the central processing unit (CPU) usage required for transmission is much less. The transfer of 32 megabytes by using TSOCK software on a Sun 4/370 (B) required an average of 49.8 sec for Ethernet and 11.5 sec for UltraNet (Table 1). The mean CPU usage for this transfer was 56.3% for Ethernet, as compared with 8.9% with UltraNet. This implies that transmission at 1 megabyte/sec requires 87.7% of the CPU for Ethernet, but only 3.2% of the CPU for UltraNet.

## Discussion

For the half-duplex and duplex model data, the transmission rate is strongly dependent on the memory data buffer size. This effect has been noted elsewhere [5]. Large data transfer buffer sizes reduce system overhead. The amount of memory actually used by the UltraNet driver for each communication process is 128 kilobytes. Data buffers larger than this are divided into 128-kilobyte pieces. This is why the half-duplex model curve flattens at a 128-kilobyte memory data buffer size and 256 kilobytes for the duplex data. Duplex transmission sustains a higher cumulative data rate than half-duplex does because the UltraNet link adapter spends less idle time.

**TABLE 1: CPU Time Usage of the UltraNet vs Ethernet Networks**

| Network | Average Transmission | | % CPU Time | |
|---|---|---|---|---|
| | Time (sec) | Rate (megabytes/sec) | Average Usage | Usage per megabyte/sec |
| UltraNet | 11.5 ± 0.3 | 2.76 ± 0.07 | 8.9 ± 0.3 | 3.2 ± 0.1 |
| Ethernet | 49.8 ± 2.5 | 0.64 ± 0.032 | 56.3 ± 3.4 | 87.7 ± 5.3 |

Note.—The average transmission rate observed and the average percent CPU time required for transmission of 32 megabytes from computer B to J were determined when TSOCK software was used. The standard buffer sizes for UltraNet (128 kilobytes) and Ethernet (1.5 kilobytes) were used. The average transmission rate and average percent CPU time usage can be used to extrapolate the percent CPU time usage required to transmit 1 megabyte/sec across the respective networks. This normalization of the two results indicates that UltraNet uses 27 times less CPU usage for the memory-to-memory transfer of 32 megabytes. This reduced host networking overhead frees CPU time for other computational or multiuser tasks. CPU = central processing unit.

The linearity of the parallel-model UltraNet data and the slight degradation observed for the initial communication process as four other client-server pairs were added to the network suggest that each individual communication process proceeds independent of the others. With all 10 Sun workstations transferring image data, a total of 13.9 megabytes/sec was routed through the UltraNet hub. This is in excess of the signaling rate of FDDI (12.5 megabytes/sec), indicating that with the large number of Sun computers in our PACS network, FDDI might not provide the necessary performance at peak usage times. The parallel-model results suggest that the computers on our PACS network (image acquisition, archiving, and display) can communicate simultaneously with negligible network throughput degradation by using UltraNet.

For the relay model, the I/O capacity of the Sparcserver 390 was equally shared between all the other Sun workstations communicating with it. This indicates that for our PACS network, high-contention resources, like the archive computers, will be shared equally on the network. As the DVMA space for the Sun computers used is only 1 megabyte and the default buffer size for UltraNet is 128 kilobytes, contention for DVMA space is witnessed as a decrease in network performance for nine concurrent processes. However, the I/O capacity is still shared very much equally between the nine processes, even though at least one process is not actively communicating at any instant. The UltraNet protocol processor services each of the nine processes in round-robin fashion, so that each process gets its share of the limited I/O capacity of the Sparcserver 390.

The transmission of data over UltraNet requires less CPU time usage than Ethernet because the UltraNet host adapter off-loads data transfer, protocol processing, and signaling chores from the host computer. In addition, the standard size of a datagram packet is 1.5 kilobytes for Ethernet, 4 kilobytes for FDDI, and 32 kilobytes for UltraNet. Thus, most of the overhead associated with constructing a frame of imaging data to transmit over the network and the overhead associated with decoding a frame and for error checking is eliminated. Freeing up CPU time allows the host computer to provide local user activity such as image display and manipulation, without incurring delays to the user due to network overhead by the workstation CPU.

UltraNet has measured a 96.5-megabyte/sec dedicated network rate between the UltraNet frame buffer and a Cray-2 supercomputer. The host adapters for Sun computers are rated up to 31.3 megabytes/sec. However, the maximum half-duplex data rate measured was 3.15 megabytes/sec for the Sun computers used in this test. Extremely rapid image transmission on the UltraNet is limited at this point by the host computer I/O architecture and not the host adapter. The computer backplane and system memory transfer schemes are bottlenecks to higher transfer rates.

The Sun computers used for this test use the VMEbus backplane. The VMEbus has a maximum signaling rate of 48 megabytes/sec; however, 10–20 megabytes/sec is more typical. This range places an upper limit on the maximum hardware transfer rate possible for the UltraNet host adapter if it

could use 100% of the VMEbus capacity. However, all of the devices connected to the VMEbus (memory, disks, video, and tape controllers) compete for access to the same bus. This can lead to a bus contention bottleneck.

The Sun computers used for this test also have a memory management unit that uses DVMA for all memory-host adapter I/O. With Sun DVMA, all data transferred over UltraNet has to pass through the CPU cache, which has a limited throughput rate (5.5 megabytes/sec). This places an upper limit on the maximum transfer rate possible for the UltraNet host adapter and represents the rate-limiting bottleneck observed in this test. The Sun Sparcserver 470 and 490 units have a new I/O architecture with a separate physical I/O cache that is supposed to raise the memory-I/O throughput rate to 22 megabytes/sec.

We are currently testing several means of improving the present UltraNet performance by using memory boards attached directly to the VMEbus of the Sun workstation, bypassing the DVMA bottleneck. In addition, we have upgraded our Sun Sparcserver 390 machines to the 490 configuration. High-performance UltraNet adapter boards manufactured specifically for the Sparcserver 490 have boosted the UltraNet transmission rate for this machine to 6.8 megabytes/sec, corresponding to the transfer of a 64-slice CT examination in 4.7 sec.

Our department is expanding radiologic services to a new outpatient-ambulatory care center. The optical fiber distance between this building and the current medical center is 1 km. A major effort is under way to connect these two buildings and the present and future PACS modules within them with a high-speed digital network [6]. With the encouraging results of this experiment, we believe that the UltraNet network will be sufficient for the image communication requirements of our department. We are proceeding with using UltraNet as the high-speed backbone of our extended PACS network. Fiberoptic cable has been laid within and between the two buildings, two hubs have been installed, and we are in the process of completing the network for clinical use in November 1990.

## ACKNOWLEDGMENTS

We thank UltraNetwork Technologies, Inc., for the use of the UltraNet 250C hub and 10 VMEbus host adapter boards and William Rissberger and Brian Connelly of UltraNetwork Technologies for help in setting up the equipment for this experiment.

## REFERENCES

1. Huang HK, Lou SL, Cho PS, et al. Radiologic image communication methods. *AJR* **1990**;155:183–186
2. Wong A, Lou SL, Stewart BK, Chan KK, Valentino DJ, Huang HK. Performance comparisons of image communication networks. *Proc SPIE* **1990**; 1234:461–470
3. Stallings W. *Handbook of computer-communications standards*, vol. 2. *Local area network standards*, 2nd ed. Carmel, IN: Howard W. Sams, **1990**:3–6
4. Templeton AW, Cox GG, Dywer SJ. Digital image management networks: current status. *Radiology* **1988**;169:193–199
5. Gonsalves TA. Measured performance of the Ethernet. In: Kümmerle K, Tobagi FA, Limb JO, eds. *Advances in local area networks*. New York: IEEE Press, **1987**:383–410
6. Huang HK, Kangarloo H, Cho PS, Taira RK, Ho BK, Chan KK. Planning a totally digital radiology department. *AJR* **1990**;154:635–639

## Books Received

Receipt of books is acknowledged as a courtesy to the sender. Books considered of sufficient interest are reviewed as space permits. If the book has been reviewed in the *AJR*, the date of its review is given in parentheses.

**Skeletal Radiology.** The Bare Bones. By Felix S. Chew. Rockville, MD: Aspen, 262 pp., 1989. $65 (1/91)

**Nuclear Cardiovascular Imaging.** Current Clinical Practice. Edited by Milton J. Guiberteau. New York: Churchill Livingstone, 247 pp., 1990. $65 (1/91)

**Two-dimensional Echocardiography and Cardiac Doppler,** 2nd ed. Edited by Jay N. Schapira and John G. Harold. Baltimore: Williams & Wilkins, 670 pp., 1990. $99.50 (1/91)

**Edeiken's Roentgen Diagnosis of Diseases of Bone,** 4th ed., vols. 1 and 2. By Jack Edeiken, Murray Dalinka, and David Karasick. Baltimore: Williams & Wilkins, 1832 pp., 1990. $195 (1/91)

**Osteoporosis.** Physiological Basis, Assessment, and Treatment. Edited by Hector F. DeLuca and Richard Mazess. New York: Elsevier, 346 pp., 1990. $95 (1/91)

**Review of Radiology.** By the faculty of Duke University Medical Center, Department of Radiology. Edited by Carl E. Ravin and Cirrelda Cooper. Philadelphia: Saunders, 360 pp., 1990. $35 (1/91)

**Optimization of Image Quality and Patient Exposure in Diagnostic Radiology** (BIR Report 20). Edited by B. M. Moores, B. F. Wall, H. Eriskat, and H. Schibilla. London: British Institute of Radiology, 288 pp., 1989. $60 (Available from Butterworths, Stoneham, MA) (1/91)

**RSNA Today,** Vol. 4, No. 2. Oak Brook, IL: The Radiological Society of North America, 1990. $55; by subscription, 6 issues annually at $185 for RSNA members and $225 for nonmembers (videotape) (1/91)

**Radiology of Renal Failure,** 2nd ed. By Harry J. Griffiths. Philadelphia: Saunders, 272 pp., 1990. $50 (1/91)

**Practical Nuclear Medicine.** Edited by P. F. Sharp, H. G. Gemmell, and F. W. Smith. New York: IRL Press, 349 pp., 1989. $75, hardcover; $40, softcover (2/91)

**The Radiologic Clinics of North America.** Lung Cancer. Guest editor: John H. Woodring. Philadelphia: Saunders, May 1990; 28(3):489–667. $25; by subscription, 6 issues annually for $93 (2/91)

**Christensen's Physics of Diagnostic Radiology,** 4th ed. By Thomas S. Curry III, James E. Dowdey, and Robert C. Murry, Jr. Philadelphia: Lea & Febiger, 504 pp., 1990. $39.50 (2/91)

**Pocket Atlas of Pediatric Ultrasound.** By Carol M. Rumack, J. Gerard Horgan, Thomas C. Hay, and Deborah Kindsfater. New York: Raven, 118 pp., 1990. $14.95 (2/91)

**Aids to Radiological Differential Diagnosis,** 2nd ed. By Stephen Chapman and Richard Nakielny. Philadelphia: Baillière Tindall, 576 pp., 1990. $24.95 (2/91)

**Dr. Susan Love's Breast Book.** By Susan M. Love. Reading, MA: Addison-Wesley, 385 pp., 1990. $18.95 (2/91)

**Computed Tomography of the Trunk.** Normal and Pathological Anatomy. By Jacques Hureau and Janine Pradel. (Translated by Gary Horn.) Padua, Italy: Piccin Nuova Libraria, 487 pp., 1988. (2/91)

**Disorders of the Patellofemoral Joint,** 2nd ed. By John P. Fulkerson and David S. Hungerford. Baltimore: Williams & Wilkins, 294 pp., 1990. $65 (2/91)

**CT Review.** Edited by Janet E. S. Husband. New York: Churchill Livingstone, 266 pp., 1989. $50 (3/91)

**CT and MRI of the Liver and Biliary System.** (Vol. 12 in the series Contemporary Issues in Computed Tomography.) Edited by Paul M. Silverman and Robert K. Zeman. New York: Churchill Livingstone, 328 pp., 1990. $75 (3/91)

**Primer of Sectional Anatomy with MRI and CT Correlation.** By Charles P. Barrett, Steven J. Poliakoff, and Lawrence E. Holder. Baltimore: Williams & Wilkins, 108 pp., 1990. $19.95 (3/91)

**MRI of the Musculoskeletal System.** A Teaching File. Edited by Jerrold H. Mink and Andrew L. Deutsch. New York: Raven, 640 pp., 1990. $120 (3/91)

**Imaging Anatomy of the Head and Spine.** A Photographic Color Atlas of MRI, CT, Gross, and Microscopic Anatomy in Axial, Coronal, and Sagittal Planes, 2nd ed. By H. N. Schnitzlein and F. Reed Murtagh. Baltimore: Urban & Schwarzenberg, 450 pp., 1990. $195 (3/91)

**Radionuclides in Nephro-Urology.** Edited by M. Donald Blaufox, Norman K. Hollenberg, and Claude Raynaud. (Vol. 79 in Contributions to Nephrology. Series editors: G. M. Berlyne and S. Giovannetti.) New York: Karger, 232 pp., 1990. $128.75 (3/91)

**The Basic Physics of Radiation Therapy,** 3rd ed. By Joseph Selman. Springfield, IL: Thomas, 749 pp., 1990. $120

**Radiolabelled Cellular Blood Elements.** (Vol. 355 in Progress in Clinical and Biological Research.) Edited by Helmut Sinzinger and Mathew L. Thakur. New York: Wiley-Liss, 379 pp., 1990. $98

**Radiation Oncology.** Radiobiological and Physiological Perspectives. By Hassan K. Awwad. Boston: Kluwer, 682 pp., 1990. $175

**Fully Hydrogenated Chlorofluorocarbons.** Environmental Health Criteria, No. 113. By World Health Organization. Albany, NY: World Health Organization, 164 pp., 1990. $16

**International Classification of Diseases for Oncology,** 2nd ed. Edited by Constance Percy, Valerie Van Holten, and Calum Muir. Albany, NY: World Health Organization, 144 pp., 1990. $24

**Atlante di Risonanza Magnetica dei tumori del sistema nervoso.** By Lucia Cecconi, Alfredo Pompili, Fabrizio Caroli, and Ettore Squillaci. Rome: Istituto Regina Elena, 248 pp., 1990.

**Diet, Nutrition, and the Prevention of Chronic Diseases.** By WHO Study Group. Geneva: World Health Organization, 203 pp., 1990. $20

# Meeting News

# Radiology Summit Meeting—1990: Action Strategies for the New Decade

Bruce L. McClennan[1]

The annual Radiology Summit Meeting was held in August 1990 at the Grove Park Inn in Asheville, NC, under the auspices of the Intersociety Commission of the American College of Radiology (ACR). Ninety-two representatives and 17 staff members from 35 different radiologic societies (Table 1) convened for 3 days to discuss some vital challenges facing our specialty. The theme for this year's gathering was "Action Strategies for the New Decade," and the roundtable discussion groups developed white papers on the following three specific topics: "Radiology's New Image" (moderated by Christopher R. B. Merritt, Ochsner Clinic, New Orleans, LA); "Generalists vs Specialists—Time to Decide" (moderated by James H. Thrall, Massachusetts General Hospital, Boston, MA); "Appropriateness of Care—Priorities for the Patient" (moderated by Theodore J. Brickner, Jr., St. Francis Hospital, Tulsa, OK).

At this year's summit, many issues and items seemingly well worn in the past decade still engendered vigorous debate. Credentials and privileges, subspecialization and certification, marketing and our image, and, of course, standards became recurring topics of conversation within each work group.

### ACR Leadership Reports

The general session was privileged to be addressed by the leadership of the ACR. Dr. Lee F. Rogers, chairman of the Board of Chancellors, spoke about the many hurdles our specialty had overcome since the last summit in 1989. As the first chairman (1980–1986) of the Intersociety Commission, Dr. Rogers has been part of the summit process for more than 10 years. He reminded those in attendance of the purpose of the Intersociety Commission, which is to promote collegiality within our specialty and to act as a forum (the summit) for the expression of concerns from all member societies, then to bring those concerns to the ACR and its Board of Chancellors through the chairman of the Intersociety Commission.

Dr. James M. Moorefield, Jr., then incoming and now current chairman of the Board of Chancellors of the ACR, spoke about the relative value scale now in place and radiology's future expectations. Cuts in the radiology fee schedules—those already in place and those proposed—were discussed, and the much maligned geographic variation factors were noted to be an unfortunate reality of modern-day practice. Recent budget reconciliation and deficit reduction efforts by Congress clearly will have an impact on radiology's reimbursement. Dr. Moorefield's astute predictions presaged this past fall's congressional budget turmoils.

Dr. Bruce J. Hillman carried a message to the summit attendees that might be called an old theme in a new wrapper, as he detailed his research on self-referral. He discussed data indicating overuse of imaging studies when physicians with ownership interest in an imaging facility ordered the testing. He showed examples to document that this was the case and indicated that, in addition to overuse, the imaging studies also cost more. By using validated methodology and existing records from third-party payers, he gave evidence that self-referral was a real phenomenon and that radiologist-per-

[1] Chairman, Intersociety Commission of the American College of Radiology, Mallinckrodt Institute of Radiology, Washington University School of Medicine, 510 S. Kingshighway, St. Louis, MO 63110. Address reprint requests to B. L. McClennan.

*AJR* 156:841–844, April 1991 0361–803X/91/1564–0841 © American Roentgen Ray Society

**TABLE 1: Radiologic Societies Represented at the Radiology Summit Meeting**

| Organization |
|---|
| American Medical Association Section Council on Radiology |
| American Association of Academic Chief Residents in Radiology |
| American Association of Physicists in Medicine |
| American Association of Women Radiologists |
| American Board of Radiology |
| American College of Medical Physics |
| American College of Radiology |
| American Institute of Ultrasound in Medicine |
| American Osteopathic College of Radiology |
| American Roentgen Ray Society |
| American Society for Therapeutic Radiology and Oncology |
| American Society of Head and Neck Radiology |
| American Society of Neuroradiology |
| Association of Residents in Radiation Oncology |
| Association of University Radiologists |
| Canadian Association of Radiologists |
| Council on Cardiovascular Radiology of the American Heart Association |
| Interamerican College of Radiology |
| National Medical Association, Inc., Section on Radiology |
| North American Society for Cardiac Radiology |
| Radiological Society of North America |
| Residency Review Committee |
| Society of Breast Imaging |
| Society of Magnetic Resonance Imaging |
| Society of Magnetic Resonance in Medicine, Inc. |
| Society for Pediatric Radiology |
| Society of Cardiovascular and Interventional Radiology |
| Society of Chairmen of Academic Radiation Oncology Programs |
| Society of Chairmen of Academic Radiology Departments |
| Society of Computed Body Tomography |
| Society of Nuclear Medicine |
| Society of Radiologists in Ultrasound |
| Society of Thoracic Radiology |
| Society of Uroradiology |
| Veterans Administration Chiefs of Radiology |

formed studies were more cost-effective and done less often. The results of Dr. Hillman's study, funded by the ACR, are being published [1].

### Radiology's New Image

Dr. Christopher Merritt chaired a work-group session with his laptop Macintosh computer in hand on the subject of radiology's new image or, more specifically, on what our collective image is and why it is important. Quoting from the poet Robert Burns, "O wad some Pow'r the giftie gie us, To see oursels as others see us!," the topic of a 1990's image of and for radiology was confronted with enthusiasm. All agreed that the perception held by others (referring physicians, the public, insurers, and students) is vital to our livelihood. In general, a consensus view was expressed that radiologists had attained a very positive image in the eyes of the public, insurers, and even government during the past decade. Our principal goals for the new decade should include maintenance and enhancement of that image, especially with government and third-party payers, but most particularly with the public. Marketing strategies should stress that we provide services of the highest quality that are cost-effective as well as radiation efficient, that is, the most information for the least amount of ionizing radiation. Objective documentation of quality and cost-effectiveness will be needed, and the kinds of studies being done by Dr. Hillman and the ACR research department will provide such data. The provision and maintenance of quality radiologic services cannot be done without the development of practice parameters and standards and optimal accreditation programs. Considerable discussion revolved around both the potential targets for projection of our image, for example, to government, industry, and the public, and the medium for doing so, for example, television, videotape, or publications. With the help of subspecialty societies and the ACR, the consciousness of the individual radiologist must be raised as regards his or her own unique responsibility to influence the attitudes of clinicians and students as well as the public. Attitudes can be influenced both by example and by involvement in hospital and community affairs, or even by seeking positions on advisory boards or panels within government or with major corporate health care providers.

### Generalists vs Specialists—Time to Decide

The moderator for the work group on the subject of the generalist vs specialist, Dr. James H. Thrall, challenged his session with the concept that subspecialization was already a reality as a consequence of the increasing complexity and sophistication of our field. Rather than choose to strictly define a subspecialist or a generalist, the task at hand was to decide how best to move forward through the morass of terms and potential traps such as accreditation, subcertification, and granting credentials. With the focus on the patient, the group moved through this difficult subject with the understanding that specific expertise may protect or defend turf, but it does not guarantee it. In the real world, subspecialists are occasionally generalists and vice versa. Patients benefit most when the most expert radiologists care for them, whether that care is cognitive, through the interpretation of a complex cross-sectional imaging test, or interventional, such as when a small angioplasty catheter is placed into the distal branches of the popliteal artery. In academic centers and large private groups, subspecialization is already well developed, and pressure is mounting on smaller practices for subspecialty expertise in pediatrics, neuroradiology, nuclear medicine, angiointervention, and mammography. Shortages in personnel have aggravated this situation. The ACR Committee on Manpower projects a current shortage of radiologists and a worsening shortage by the year 2000. Nonmetropolitan areas will be hardest hit, and a potential loss of turf exists if radiologists are not available to perform imaging and interventional services. Subspecialization in other fields is another driving force toward subspecialization in radiology. The expectations of our clinical colleagues and our patients have been raised by our increased expertise. This trend has not escaped the attention of third-party payers, who are reviewing reimbursement procedures and amounts for more complex (costly) examinations. Vocal proponents of subspecialization have

heightened a historic concern, that increased specialization will weaken the positive image or stature of the generalist with far-reaching implications, for example, medicolegal, coverage, and call problems. Emphasis on certification or granting credentials for subspecialists could affect resident training programs and diminish the significance of general radiologic training and, in turn, the overall significance of the American Board of Radiology certificate in diagnostic or general radiology.

Flexibility was believed to be a key factor in maintaining the integrity of the subspecialist and in dealing with the cross-coverage necessities of practice and the timely delivery of services, access to care, and growing staff shortages. This flexibility was considered to be fundamental to maintain the important role of the general radiologist. The group recommended that training curricula be organ system–based whenever feasible because of the importance of clinical knowledge when dealing with referring physicians, but they recognized the equal importance of technical skills and their maintenance. The group believed that residency and fellowship training requirements must be better defined. They encouraged both the ACR and the American Board of Radiology to develop clearer guidelines for residency program directors for structuring their residencies and fellowships. Flexibility was the watchword here also so as to ensure that programs could be tailored to particular circumstances or opportunities. Since strategies for granting credentials and privileges would be developed through the use of training and experience, both the subspecialists' and generalists' viewpoints must have room for expression. Some areas in interventional radiology may require newer standards linking training and experience, which inevitably will involve placing numbers or limits on some procedures.

All in all, specialization has strengthened our field and is a natural evolution of modern-day radiologic practice. Retaining flexibility will sustain subspecialization in both academic and private practice arenas. Practice models might be developed to accommodate both general and subspecialty interests, ever mindful of the needs of our patients. Specialization does promote better patient care, and perhaps cross-coverage or cross-affiliations between groups would be more desirable than intraspecialty turf wars over provision of subspecialty imaging or interventional services.

### Appropriateness of Care—Priorities for the Patient

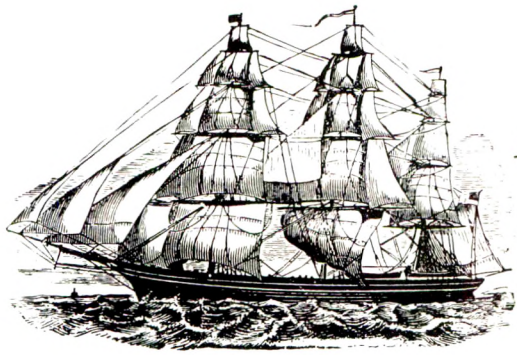
The patient continued to be the focus as the third workgroup session at this year's summit discussed their agenda. The moderator of this group, Dr. Ted Brickner, Jr., sought to focus opinion on the development of standards as guidelines for radiologic practice. Dr. Brickner has had considerable experience developing the "Patterns of Care" program for radiation oncology. His leadership and experience in this regard were very useful to his work group as they faced the fact that several nonradiologic medical groups and federal agencies (e.g., the Agency for Health Care and Policy Research [AHCPR]) have begun the process of developing patient care standards. The ACR has a long tradition of developing standards for patient care, with primary emphasis on optimal care and patient safety. The summit participants were expressly concerned that only radiologists have the depth of knowledge and expertise necessary to develop standards for imaging or intervention that most benefit the patient. The method for developing standards was reviewed and found to be incomplete but evolving. Input from Dr. Jerome Shapiro, who heads the Task Force on Standards for the ACR, was invaluable in directing the discussion and informing those in attendance of the many achievements already made by the ACR in this regard. Consensus wisdom or the "wise old men" approach was deemed appropriate for beginning any process of developing standards that affect a large number of practitioners and patients. All parties must be heard and all risks and benefits assessed prior to development of any standard or guideline. Although the new "buzz" phrase may be "outcome analysis"—and this is currently an in-vogue term—the method for developing practice guidelines that include outcome analysis is not yet established. Radiologists need to be involved in defining the outcome or endpoint of any standard and judging its significance or patient benefit. A "do it ourselves" and "do it first" attitude was very pervasive in Dr. Brickner's discussion group and the subsequent white paper that was submitted to the Board of Chancellors of the ACR. In fact, a resolution dealing with this subject was proposed and submitted to the Board of Chancellors at its September 1990 meeting in Nashville, TN. This resolution called for the ACR, through Dr. Shapiro's Task Force on Standards and through the organizatons that make up the Intersociety Commission, to establish a permanent and ongoing program for standards setting. The further intent of this proposed resolution was to develop a time schedule or set of priorities for standards development and, in addition, to promote the activities of the Task Force on Standards to others, specifically governmental and third-party payers. Broad input was encouraged by Dr. Shapiro, who assured the summit attendees that as many standards as societies could develop would be welcomed and acted on by his task force. He further noted that 12 standards had already been developed and were ready for passage or had been passed through the ACR council. Subspecialty societies were further charged by Dr. Brickner to get involved at all levels—local, state, and national—where standards were being developed and to become more aware of the players in this guidelines game, for example, the AHCPR and American Medical Association (AMA) practice parameter program. Although the method for developing standards is in flux despite continued direction from Dr. David Eddy and others, our approach should be to do it and be first, to cooperate and inform all interested parties, and to be sure our standards are broad based and flexible, with our patients as the focus. When they are put into place, a careful quality assurance program will be required to monitor both compliance and outcome. To add a pragmatic touch to these discussions, a standard on outpatient angiography that had been developed by the Society of Cardiovascular and Interventional Radiology was discussed by the work group. This process brought out the difficulties of both developing a standard and codifying it so that it suits all interested parties.

The group quickly came to realize that standards will be used by others to measure individual performances of both physicians and facilities, so issues such as continuing competence and/or privileging will continue to relate to the standards that we develop. Concern existed about the legal ramifications of standards development, despite the reassuring report by the legal counsel of the ACR, Thomas Greeson, who recently indicated to the members of the College that the AMA publication entitled "Legal Implications of Practice Parameters" was available. He further noted that this document implies that the risk of liability for claims resulting from standards development or compliance with standards is minimal.

True to the theme of this year's summit, there were calls for new action strategies on many fronts. With constant concern for the patient's welfare and with "the radiologist knows best" approach, issues related to our image, human resources shortages, subspecialization, turf, self-referral, and standards were discussed extensively. Three white papers that summarized the various summit discussions were submitted to the Board of Chancellors and the ACR Council in September 1990. Continued input from all societies and individual radiologists was encouraged by the summit leaders who met in Asheville. Increased awareness of our more pressing problems and their potential solutions has always been a goal of the annual Radiology Summit Meeting, and this year was certainly no different.

REFERENCE

1. Hillman BJ, Joseph CA, Mabry MR, et al. Frequency and cost of diagnostic imaging in office practice—a comparison of self-referring and radiologist-referring physicians. *N Engl J Med* **1990**;323:1604–1608



Scientific Program (200 papers)
Instructional Courses (60 hours)
Categorical Course on
Body MR Imaging
The Caldwell Lecture
Award Papers
Scientific Exhibits
Social, Golf, and Tennis Programs
Guest Programs



Come to the
American Roentgen
Ray Society
91st
ANNUAL MEETING
Boston, MA
Sheraton Boston Hotel
May 5-10, 1991

# Case of the Day

The Case of the Day series is among the most popular scientific exhibits at the annual meeting of the American Roentgen Ray Society. When Dr. Kirkpatrick asked me to supervise the preparation of these cases for the May meeting, I accepted with some reluctance, especially in view of the outstanding presentations that were prepared last year by Dr. Margaret A. Stull and colleagues of the Department of Radiology at Georgetown University School of Medicine.

With encouragement from the faculty and staff at the Boston University Medical Center, I accepted the challenge and, with Dr. Kirkpatrick's permission, have asked the residents at the Boston University Medical Center to help me with this formidable task. They have selected cases in five categories: general diagnosis, chest, abdominal, neuroradiology, and pediatrics. Each category includes four cases, one for each day of the ARRS meeting. The answers and brief descriptions of the entities will appear in the June issue of the *AJR*. If you plan to attend the meeting in Boston this year, please visit the exhibit and submit your diagnoses at the meeting. Participants who diagnose the cases correctly will be acknowledged at the meeting. I should like to emphasize that my role has been as a facilitator, and I am indebted to the Chief Resident, Dr. David Eschelman, and the resident staff at the Boston University Medical Center for their help in preparing the cases.

J. F. O'Connor
*Department of Radiology*
*Boston University School of Medicine*
*Boston, MA 02118*

# General Diagnosis Case of the Day

David J. Eschelman,[1] Ellen Panageas, Max P. Rosen, Laura V. Romo, and John F. O'Connor

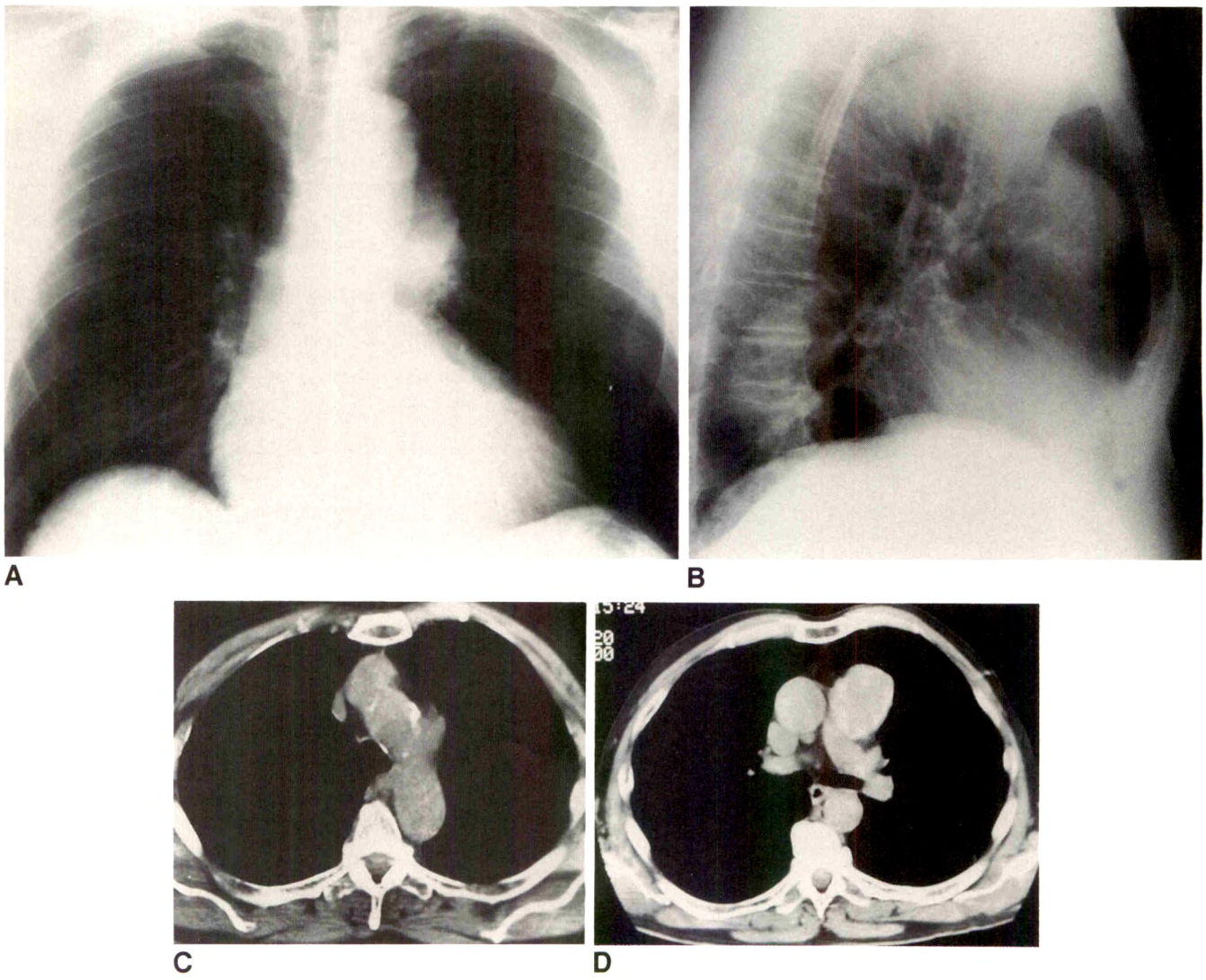


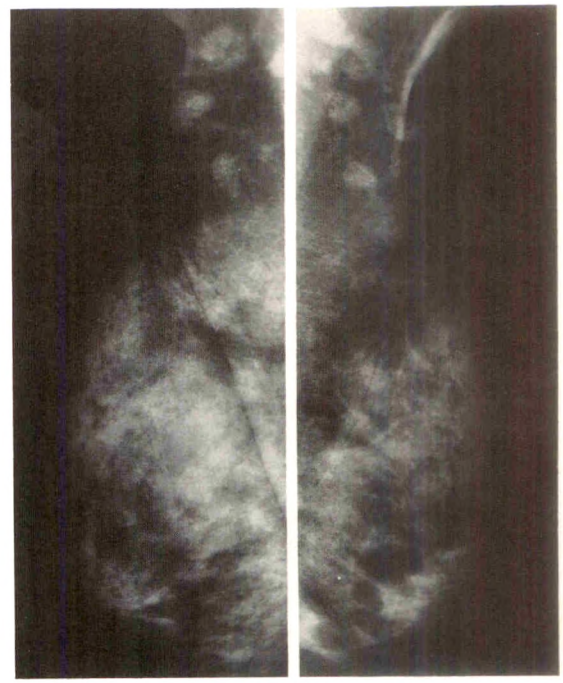

**Fig. 1.—Case 1: Asymptomatic 73-year-old man with chest radiograph followed by chest CT.**
***A* and *B*, Posteroanterior (*A*) and lateral (*B*) chest radiographs.**
***C*, Transaxial unenhanced CT scan of chest at level of aortic arch.**
***D*, Transaxial contrast-enhanced CT scan at level of carina.**

[1]All authors: Department of Radiology, Boston University Medical Center, 88 E. Newton St., Boston, MA 02118. Address reprint requests to J. F. O'Connor.

Case 1 was prepared by L. V. Romo and D. J. Eschelman. Case 2 was prepared by D. J. Eschelman. Case 3 was prepared by M. P. Rosen. Case 4 was prepared by E. Panageas. J. F. O'Connor is coordinator of the Case of the Day series.

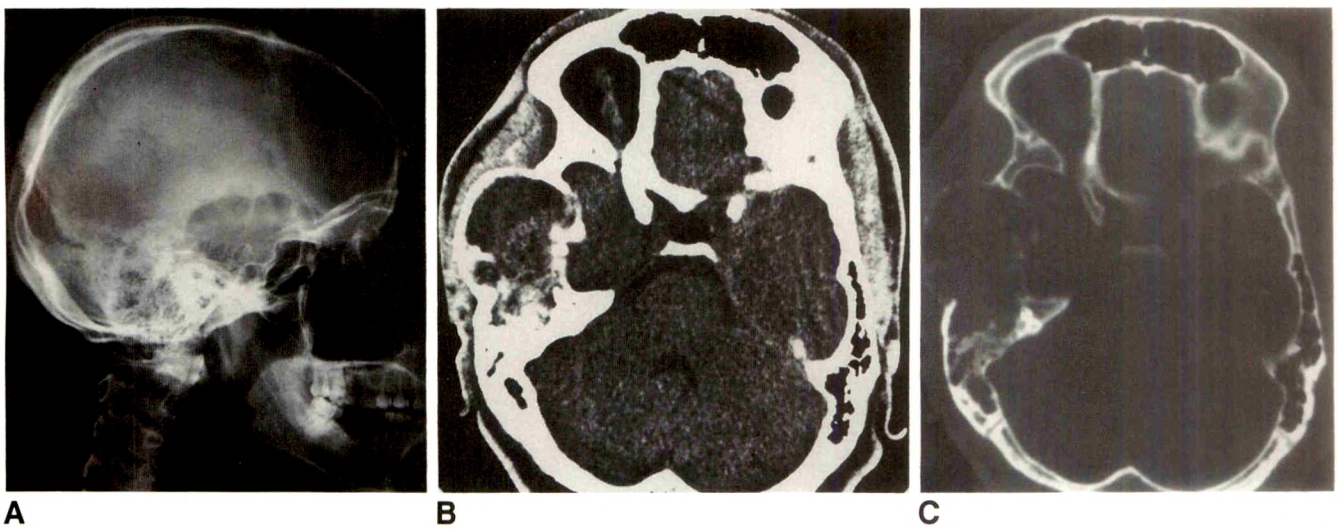
*AJR* **156:846–848, April 1991** 0361–803X/91/1564-0846 © American Roentgen Ray Society

►Fig. 2.—Case 2: 45-year-old woman who presented for screening mammography.
*A*, Right medial-lateral oblique mammogram.
*B*, Left medial-lateral oblique mammogram.

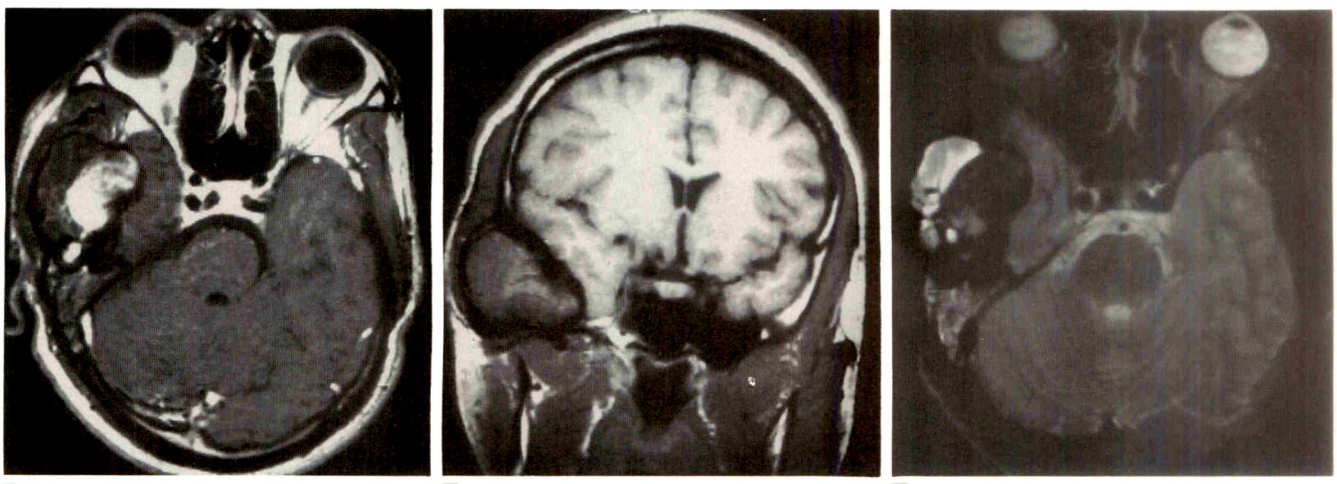


A B

▼Fig. 3.—Case 3: 25-year-old man with progressive swelling on right side of face.
*A*, Lateral skull radiograph.
*B*, Axial unenhanced CT scan of head at soft-tissue window settings.
*C*, Axial CT scan of head at bony window settings.
*D*, Axial T1-weighted (500/15) gadolinium-enhanced MR image of head.
*E*, Coronal T1-weighted (560/15) MR image of head.
*F*, Axial T2-weighted (3000/90) MR image of head.



A B C



D E F

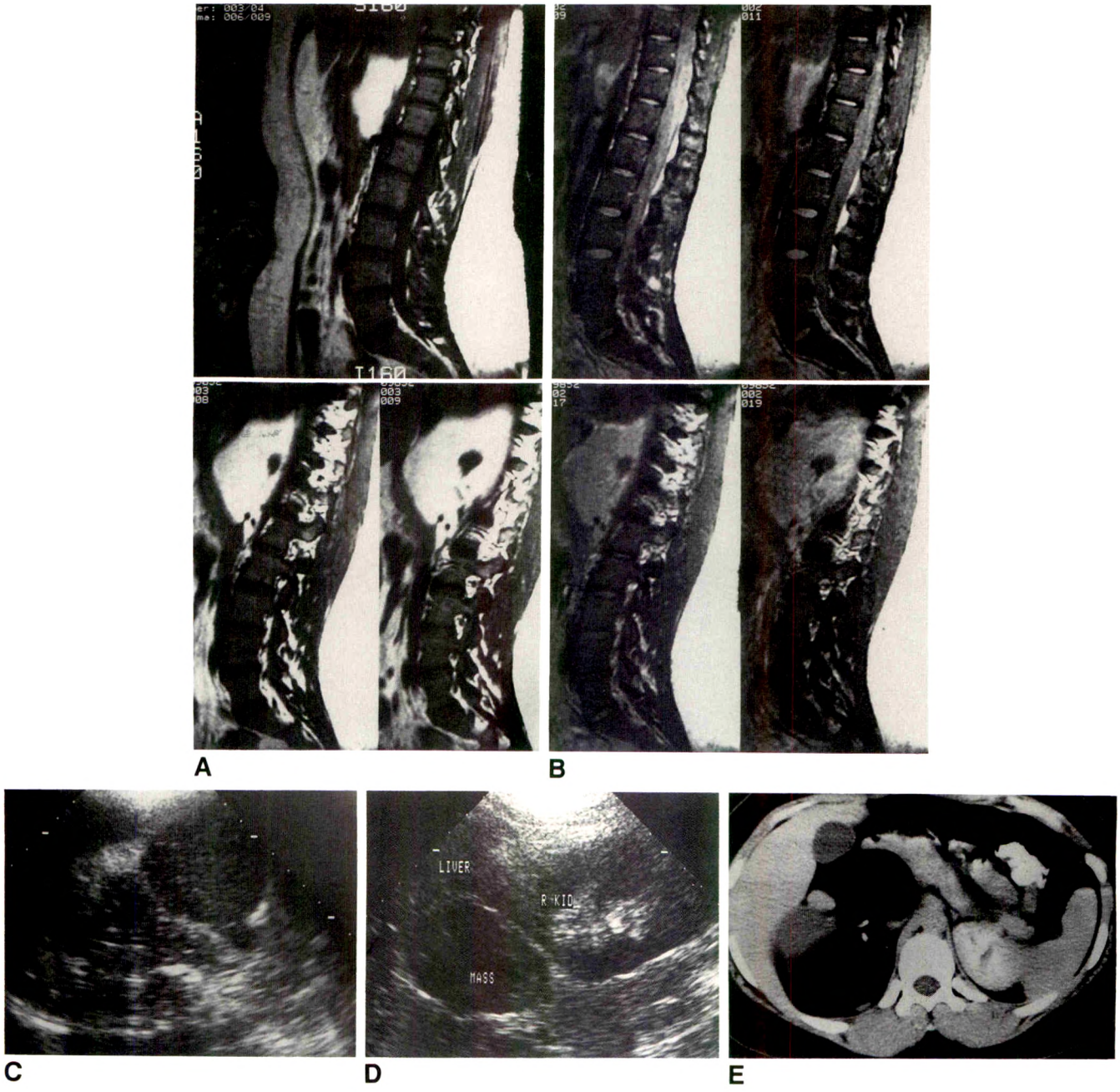



Fig. 4.—Case 4: 24-year-old woman with persistent pain in lower back 2 months after a motor vehicle accident. An MR examination of lumbosacral spine was performed initially.

*A*, Sagittal T1-weighted (500/20) MR images of lumbosacral spine.

*B*, Sagittal T2-weighted (2000/40) MR images of lumbosacral spine.

*C*, Longitudinal sonogram of right suprarenal region.

*D*, Longitudinal sonogram of right upper quadrant.

*E*, Transaxial contrast-enhanced CT scan of midabdomen.

# Chest Case of the Day

David J. Eschelman,[1] Douglas T. Gibbens, Julia R. Fielding, Laura V. Romo, Daryl R. Parker, Nicolas Argy, and John F. O'Connor

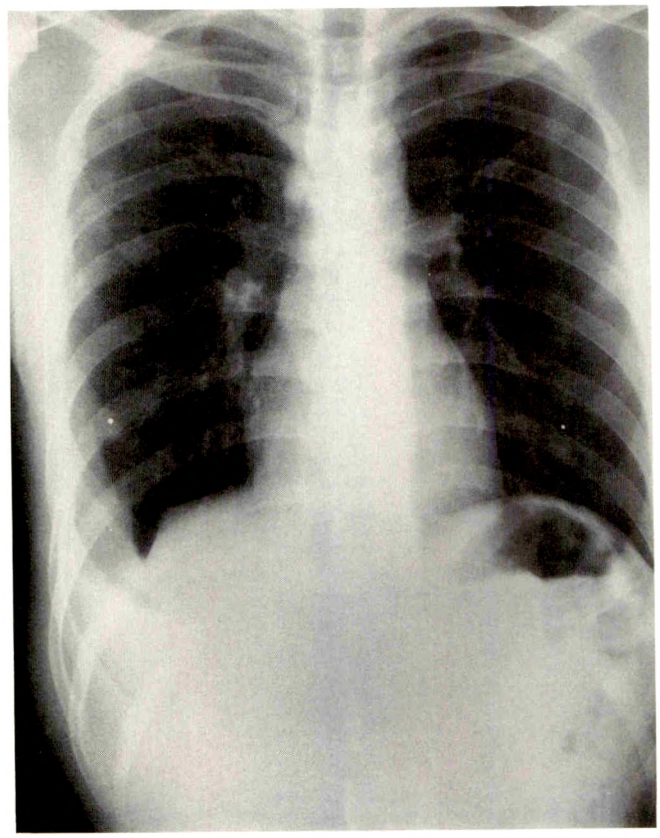


**Fig. 1.—Case 1: Posteroanterior chest radiograph of 24-year-old man who has had right pleuritic chest pain for several weeks.**

[1]All authors: Department of Radiology, Boston University Medical Center, 88 E. Newton St., Boston, MA 02118. Address reprint requests to J. F. O'Connor.

Case 1 was prepared by D. T. Gibbens and N. Argy. Case 2 was prepared by J. R. Fielding. Case 3 was prepared by L. V. Romo and D. R. Parker. Case 4 was prepared by D. T. Gibbens and N. Argy. J. F. O'Connor is coordinator of the Case of the Day series.

*AJR* **156:849–851, April 1991** 0361–803X/91/1564–0849 © American Roentgen Ray Society

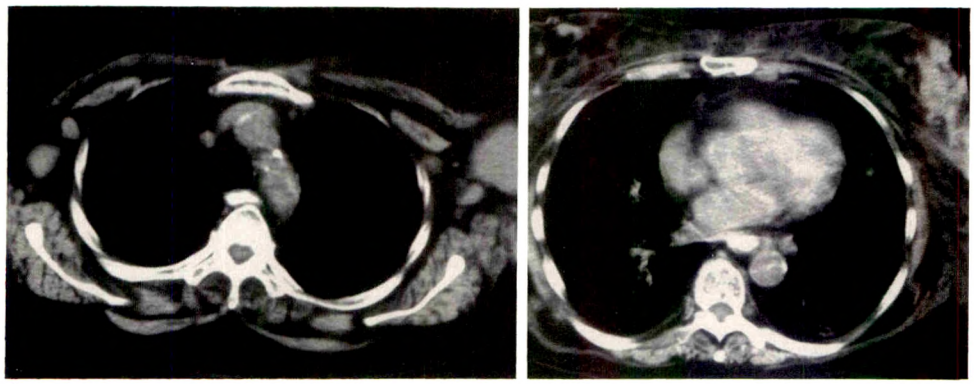



Fig. 2.—Case 2: 61-year-old woman with progressive facial and truncal skin lesions for past 8 years.
*A*, Transaxial unenhanced CT scan of chest at level of aortic arch.
*B*, Transaxial unenhanced CT scan of chest, 5 cm below carina.

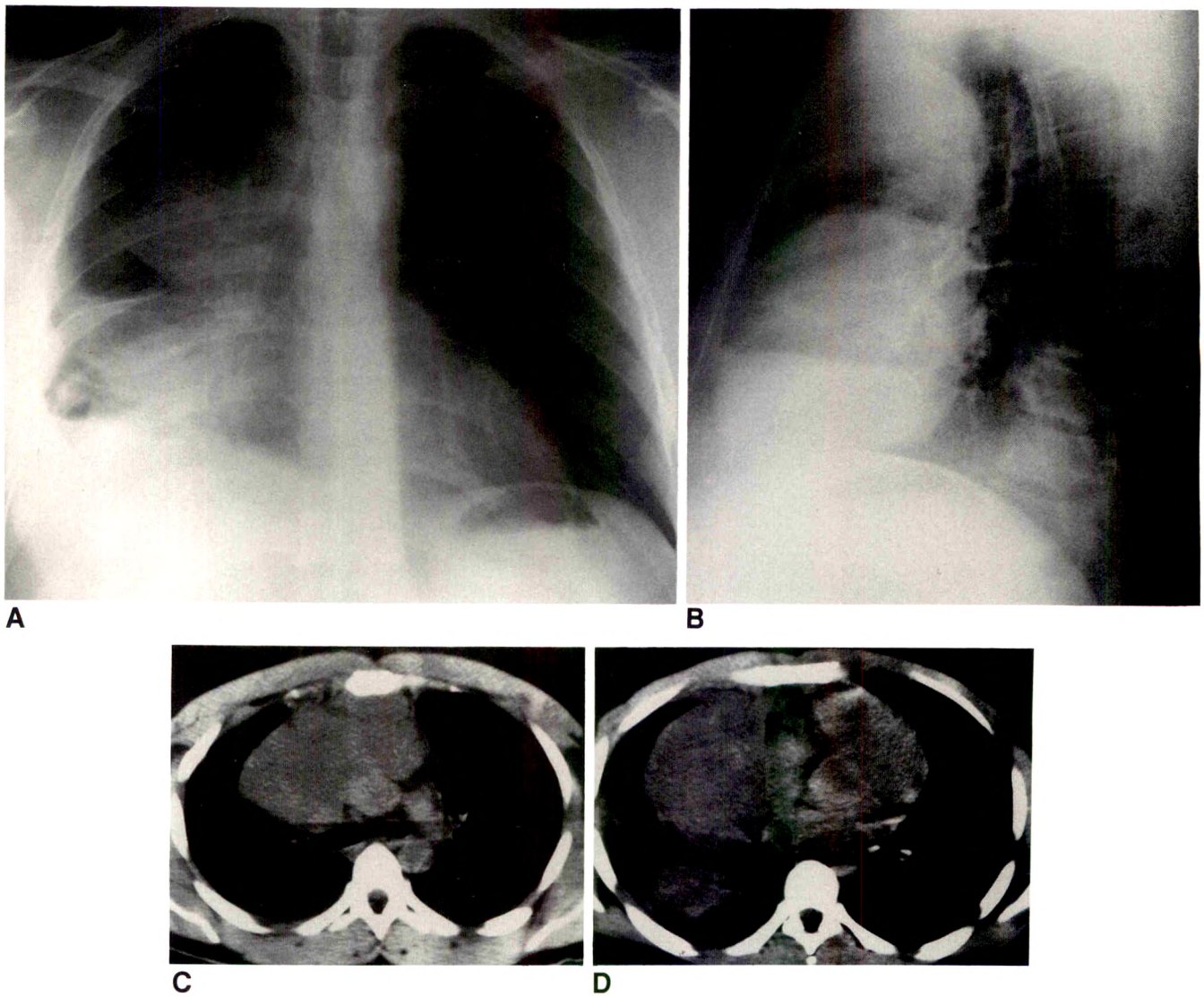
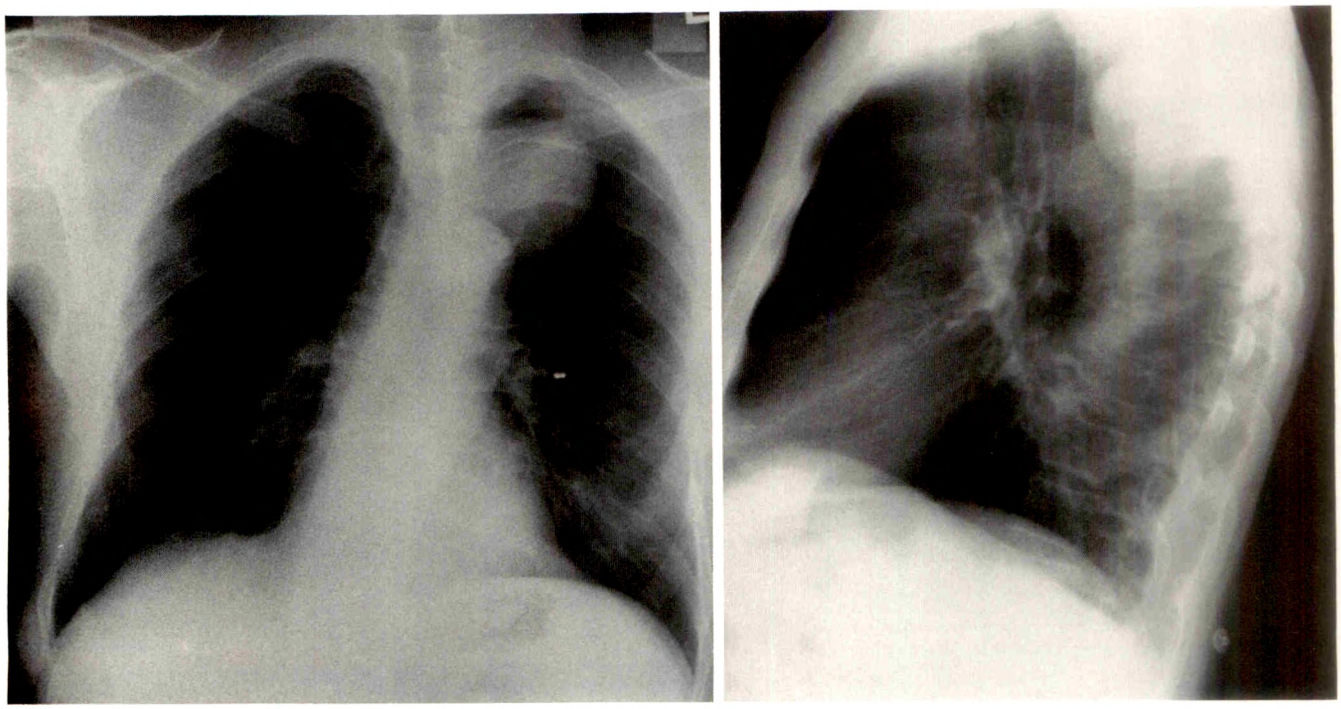



Fig. 3.—Case 3: 25-year-old man with a 3-month history of right shoulder pain and 1 month of hemoptysis, dysphagia, and night sweats.
*A* and *B*, Posteroanterior (*A*) and lateral (*B*) chest radiographs.
*C*, Transaxial unenhanced CT scan of chest at level of carina.
*D*, Transaxial unenhanced CT scan of chest, just above level of diaphragm.



A B

Fig. 4.—Case 4: *A* and *B*, Posteroanterior (*A*) and lateral (*B*) chest radiographs of 52-year-old man who presented to emergency department with shortness of breath and wheezing.

# Abdominal Case of the Day

David J. Eschelman,[1] Audrey D. Duva-Frissora, Lisa C. Martin, Daryl R. Parker, Margo M. Moskos, Douglas T. Gibbens, and John F. O'Connor

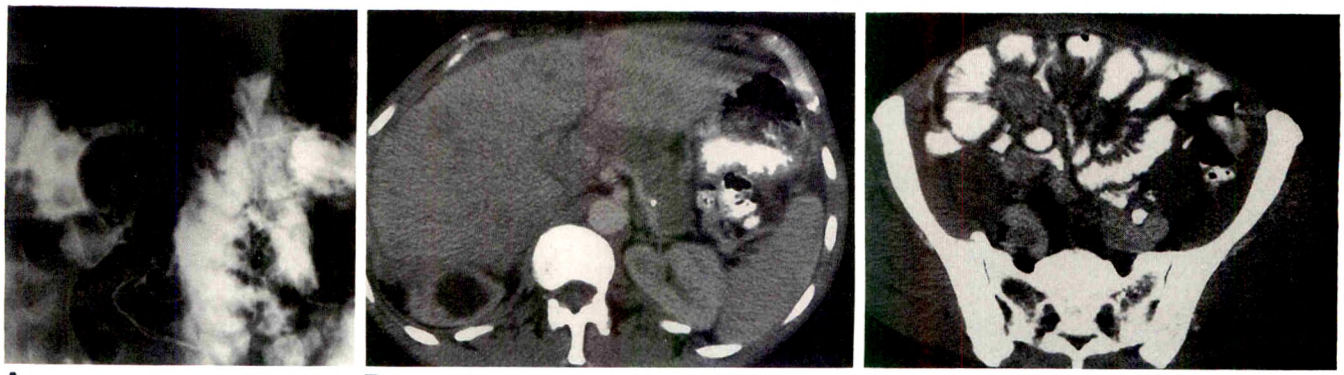



Fig. 1.—Case 1: 48-year-old man presented with 6 months of anorexia, 20-lb (9.1 kg) weight loss, abdominal pain, and episodic shortness of breath. Physical examination revealed periumbilical adenopathy and upper abdominal tenderness.
*A*, Spot radiograph of duodenal bulb from an upper gastrointestinal series.
*B*, Transaxial CT scan of upper abdomen.
*C*, Transaxial CT scan of midpelvis.

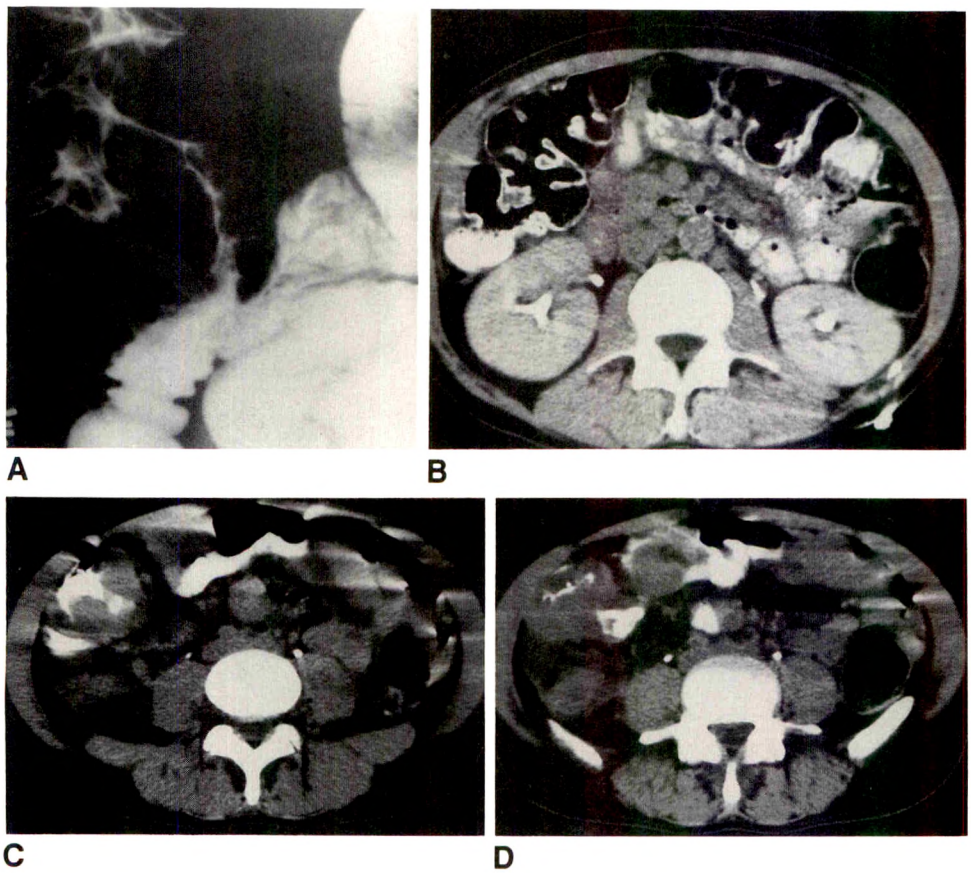



Fig. 2.—Case 2: 36-year-old man with AIDS and several weeks of watery diarrhea and episodic fever.
*A*, Spot radiograph of terminal ileum from upper gastrointestinal series.
*B*, Transaxial CT scan of midabdomen.
*C*, Transaxial CT scan of abdomen 2 cm above iliac crests.
*D*, Transaxial CT scan of abdomen at level of iliac crests.

[1]All authors: Department of Radiology, Boston University Medical Center, 88 E. Newton St., Boston, MA 02118. Address reprint requests to J. F. O'Connor.
Case 1 was prepared by D. T. Gibbens and D. R. Parker. Case 2 was prepared by A. D. Duva-Frissora. Case 3 was prepared by M. M. Moskos and D. J. Eschelman. Case 4 was prepared by L. C. Martin. J. F. O'Connor is coordinator of the Case of the Day series.

*AJR* **156:852–853, April 1991** 0361–803X/91/1564–0852 © American Roentgen Ray Society

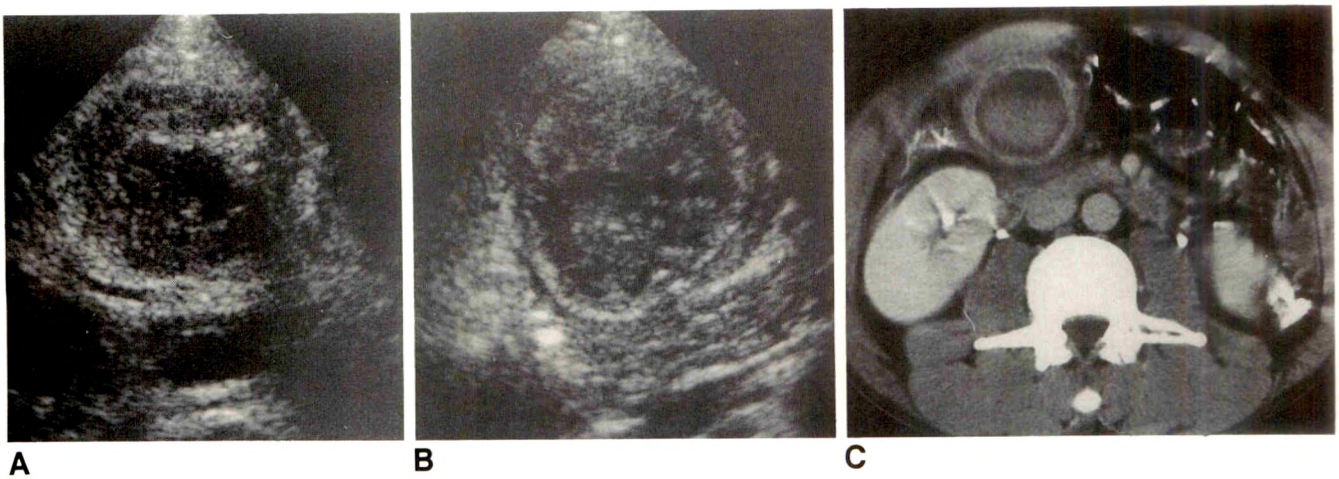



Fig. 3.—Case 3: 37-year-old male alcoholic with 4-day history of fever and sharp, constant, midepigastric pain.
*A* and *B*, Transverse sonograms of gallbladder.
*C*, Transaxial CT scan of midabdomen.

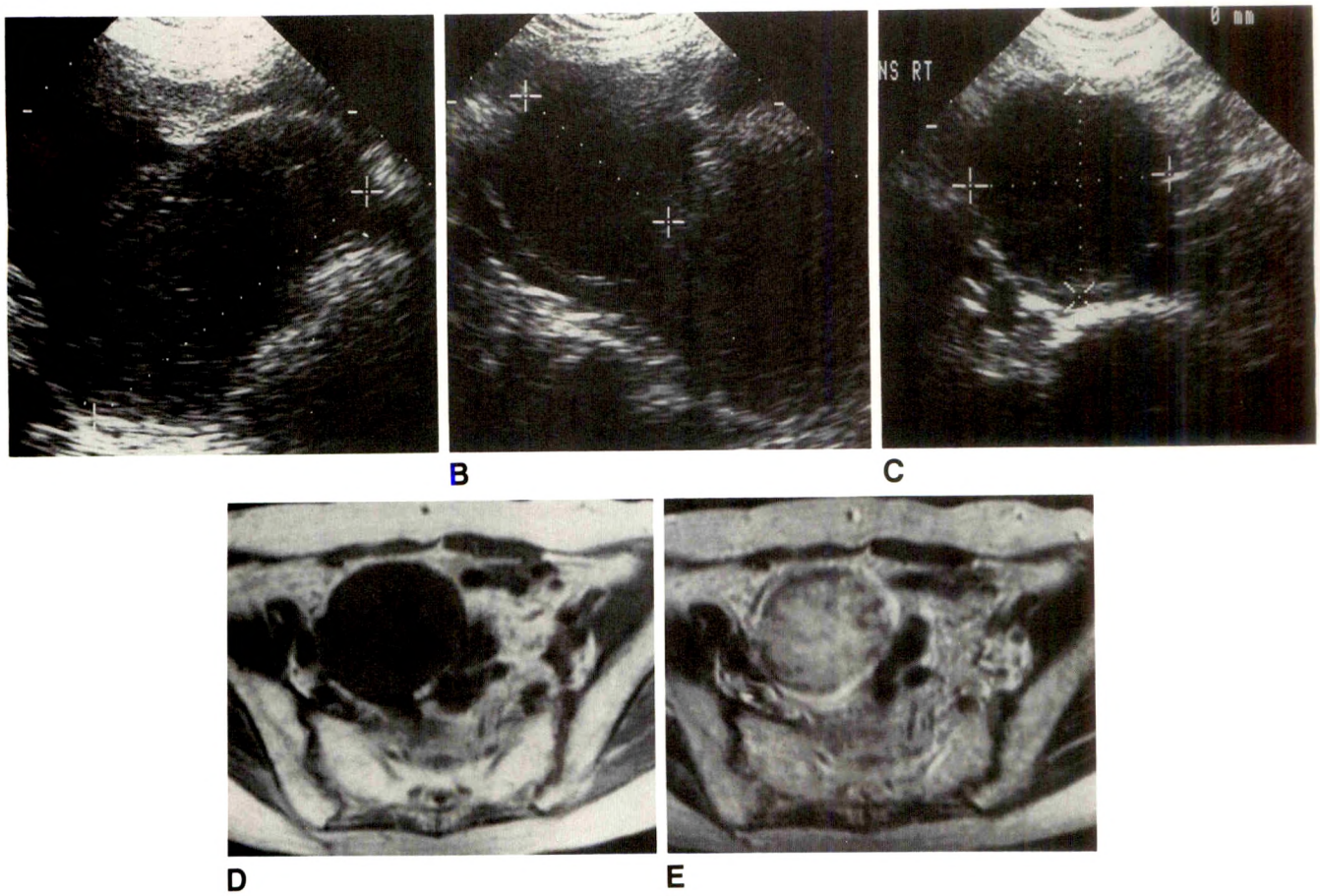



Fig. 4.—Case 4: 73-year-old woman with 2-week history of spotty vaginal discharge and lower abdominal discomfort.
*A*, Longitudinal sonogram of midpelvis.
*B*, Longitudinal sonogram of right adnexal region.
*C*, Transverse sonogram of right adnexal region.
*D*, Transaxial T1-weighted (571/16) MR image of midpelvis.
*E*, Transaxial T2-weighted (2000/60) MR image of midpelvis.

# Neuroradiology Case of the Day

Daryl R. Parker,[1] David J. Eschelman, Douglas T. Gibbens, James D. Rabinov, and John F. O'Connor

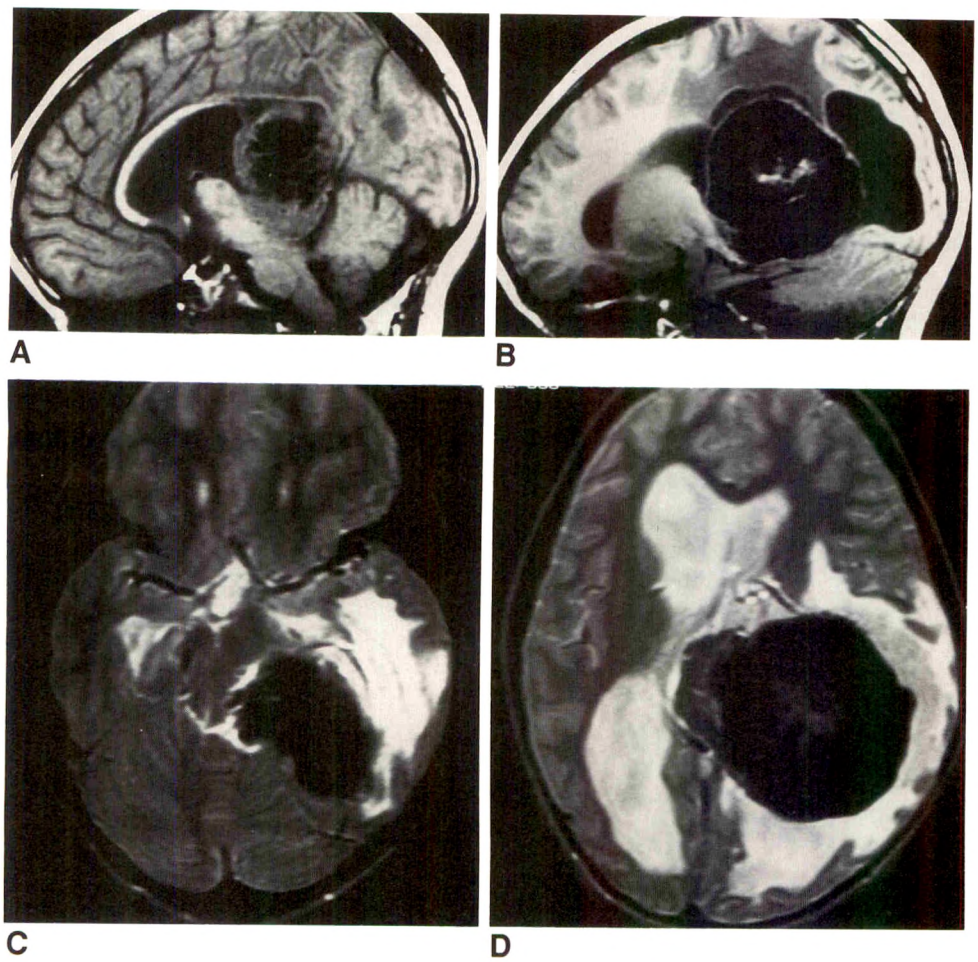



Fig. 1.—Case 1: 6-year-old girl with headache and increasing lethargy for 1 week.

*A* and *B*, Sagittal T1-weighted (600/15) MR images.

*C* and *D*, Axial T2-weighted (2000/80) MR images.

[1]All authors: Department of Radiology, Boston University Medical Center, 88 E. Newton St., Boston, MA 02118. Address reprint requests to J. F. O'Connor.

Case 1 was prepared by D. T. Gibbens and D. J. Eschelman. Case 2 was prepared by D. R. Parker and J. D. Rabinov. Case 3 was prepared by D. J. Eschelman. Case 4 was prepared by D. R. Parker. J. F. O'Connor is coordinator of the Case of the Day series.

*AJR* 156:854–857, April 1991 0361–803X/91/1564–0854 © American Roentgen Ray Society

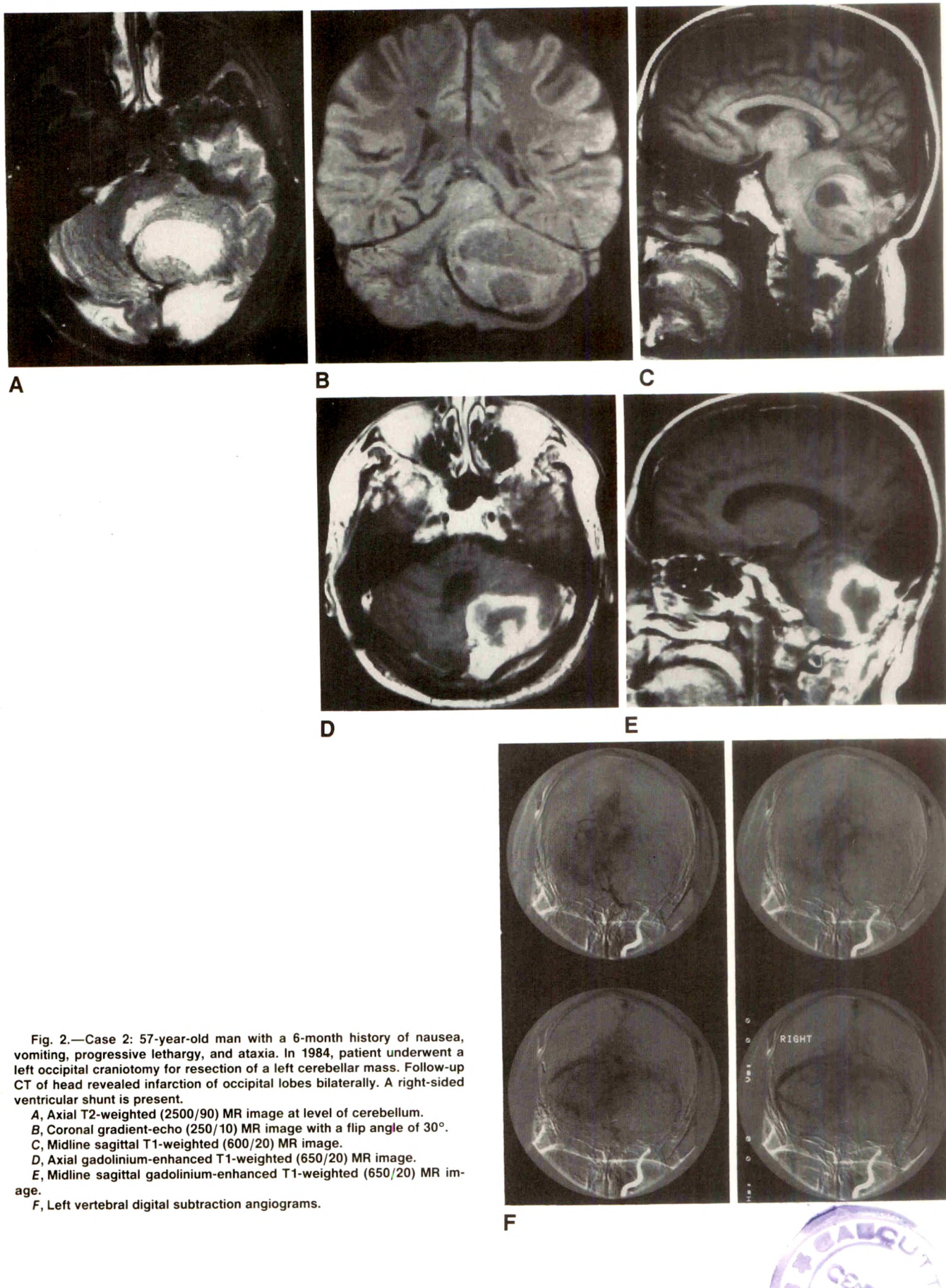



Fig. 2.—Case 2: 57-year-old man with a 6-month history of nausea, vomiting, progressive lethargy, and ataxia. In 1984, patient underwent a left occipital craniotomy for resection of a left cerebellar mass. Follow-up CT of head revealed infarction of occipital lobes bilaterally. A right-sided ventricular shunt is present.

*A*, Axial T2-weighted (2500/90) MR image at level of cerebellum.

*B*, Coronal gradient-echo (250/10) MR image with a flip angle of 30°.

*C*, Midline sagittal T1-weighted (600/20) MR image.

*D*, Axial gadolinium-enhanced T1-weighted (650/20) MR image.

*E*, Midline sagittal gadolinium-enhanced T1-weighted (650/20) MR image.

*F*, Left vertebral digital subtraction angiograms.

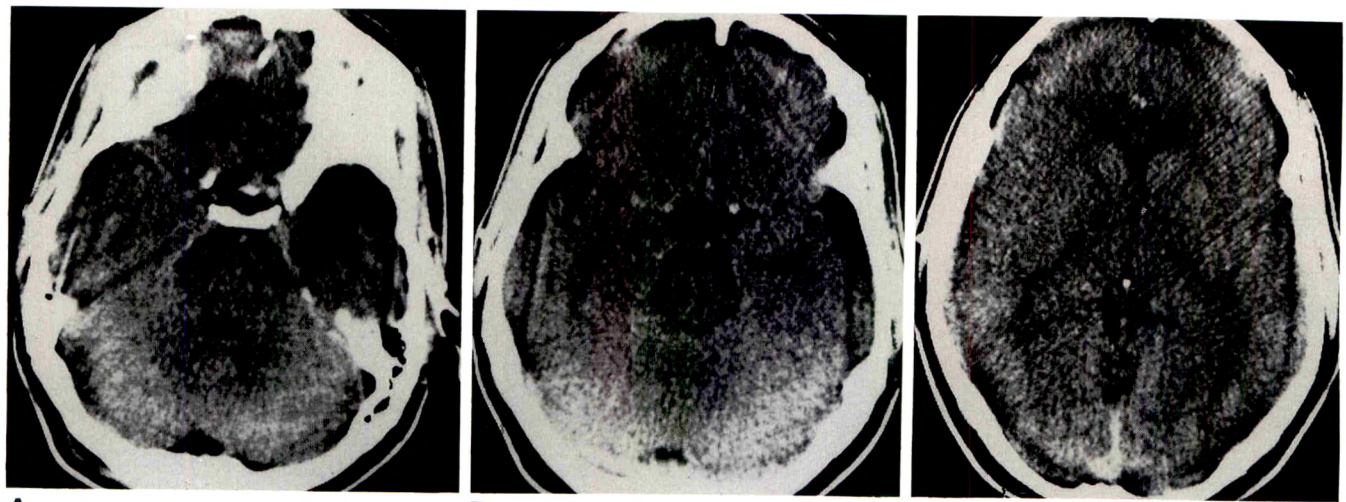



Fig. 3.—Case 3: 24-year-old woman with history of depression presented to emergency department in coma. *A–C*, Axial unenhanced CT scans of head.

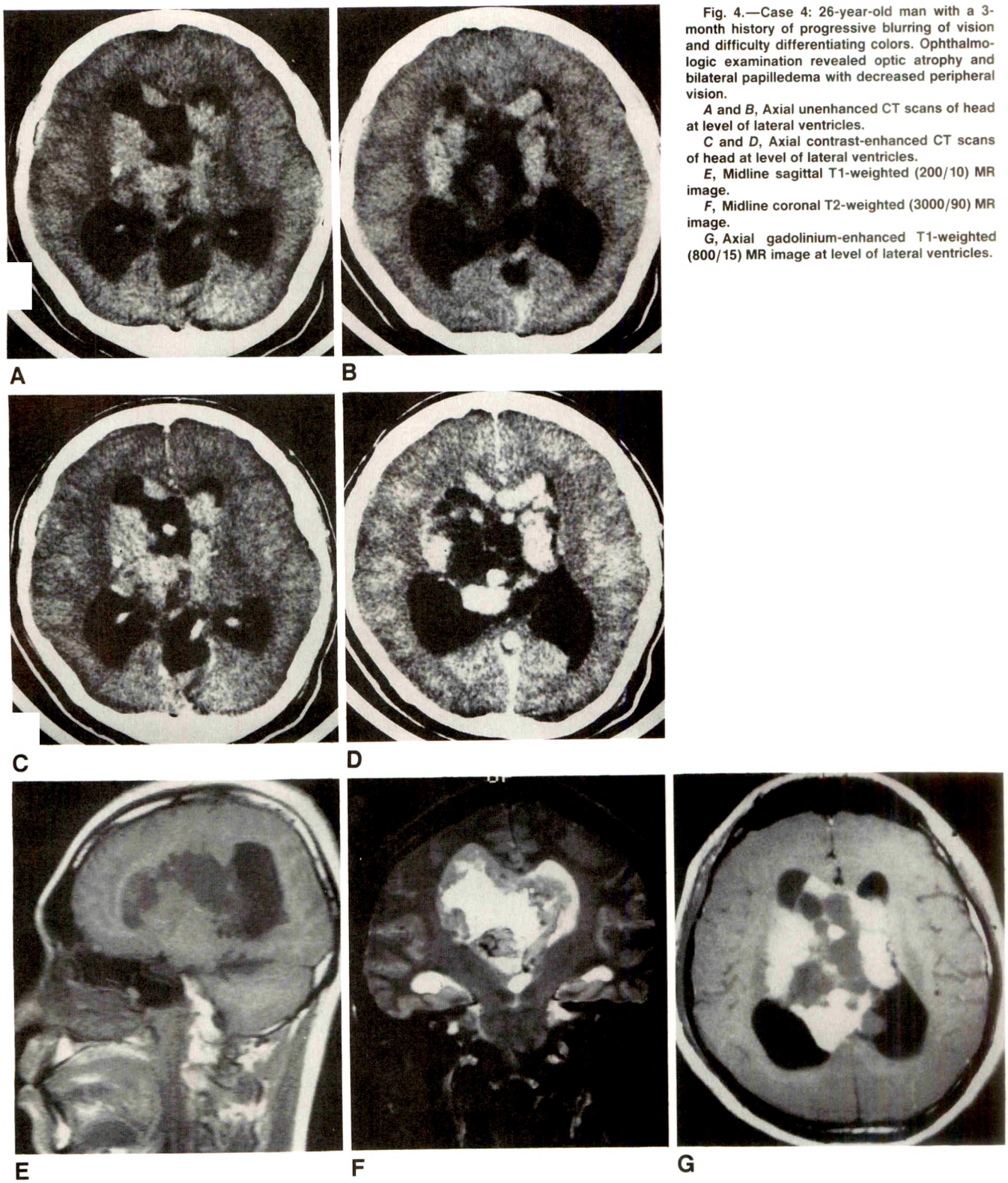



Fig. 4.—Case 4: 26-year-old man with a 3-month history of progressive blurring of vision and difficulty differentiating colors. Ophthalmologic examination revealed optic atrophy and bilateral papilledema with decreased peripheral vision.

*A* and *B*, Axial unenhanced CT scans of head at level of lateral ventricles.

*C* and *D*, Axial contrast-enhanced CT scans of head at level of lateral ventricles.

*E*, Midline sagittal T1-weighted (200/10) MR image.

*F*, Midline coronal T2-weighted (3000/90) MR image.

*G*, Axial gadolinium-enhanced T1-weighted (800/15) MR image at level of lateral ventricles.

# Pediatric Case of the Day

John F. O'Connor,[1] Lisa C. Martin, Henry H. Chen, Bonnie L. Dobkin, Eric J. Sax, Oliver H. Pomeroy, and David J. Eschelman

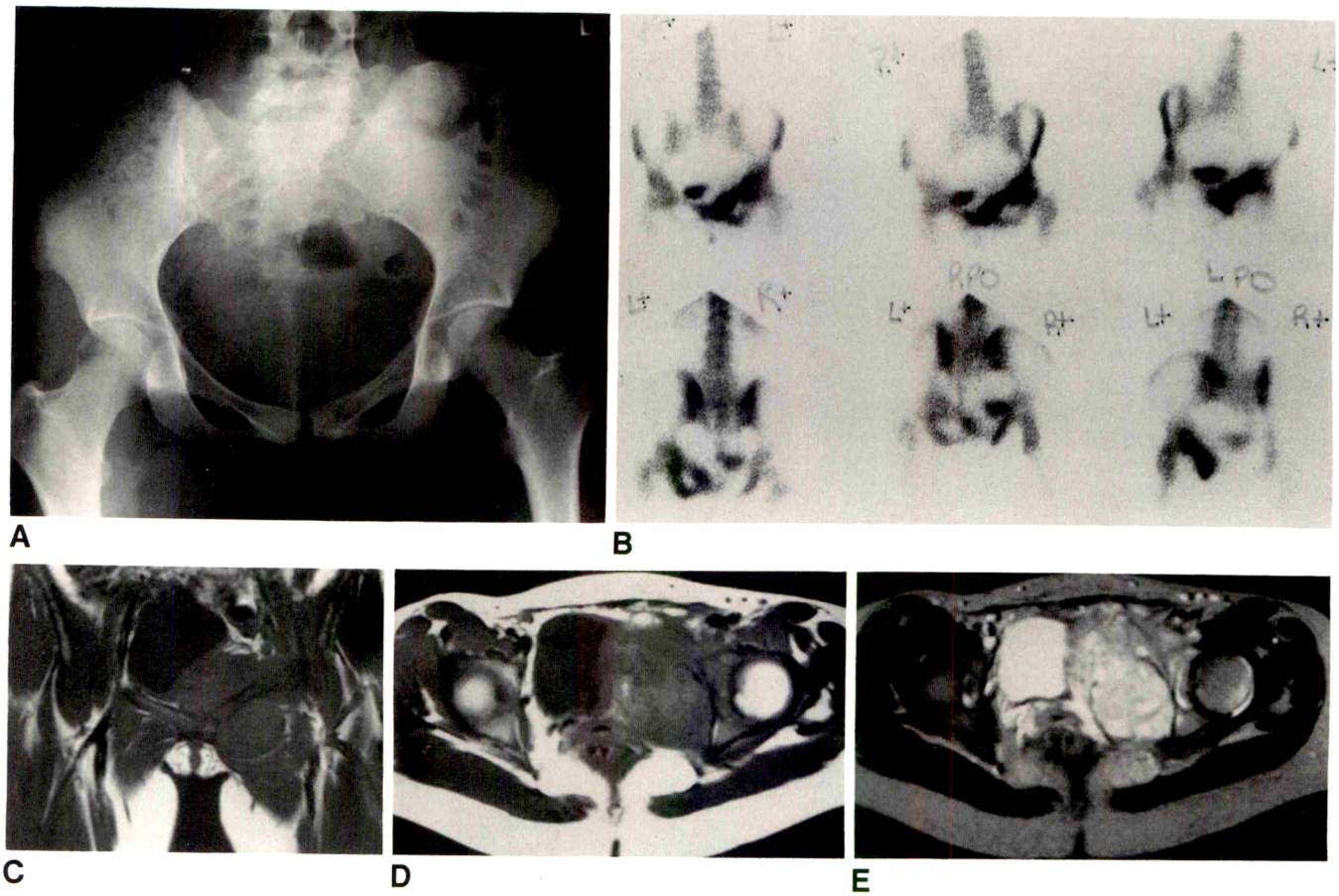



**Fig. 1.—Case 1: 15-year-old girl with 2-year history of intermittent right-sided groin pain.**
***A*, Pelvic radiograph.**
***B*, Multiple pelvic images from $^{99m}$Tc-methylene diphosphonate bone scan.**
***C*, Coronal T1-weighted (450/20) MR image of anterior pelvis.**
***D*, Axial T1-weighted (700/20) MR image at level of acetabulae.**
***E*, Axial T2-weighted (3000/80) MR image at level of acetabulae.**

[1]All authors: Department of Radiology, Boston University Medical Center, 88 E. Newton St., Boston, MA 02118. Address requests to J. F. O'Connor.

Case 1 was prepared by L. C. Martin. Case 2 was prepared by E. J. Sax. Case 3 was prepared by H. H. Chen. Case 4 was prepared by B. L. Dobkin and O. H. Pomeroy. J. F. O'Connor is coordinator of the Case of the Day series.

*AJR* **156:858–861, April 1991** 0361–803X/91/1564-0858 © American Roentgen Ray Society

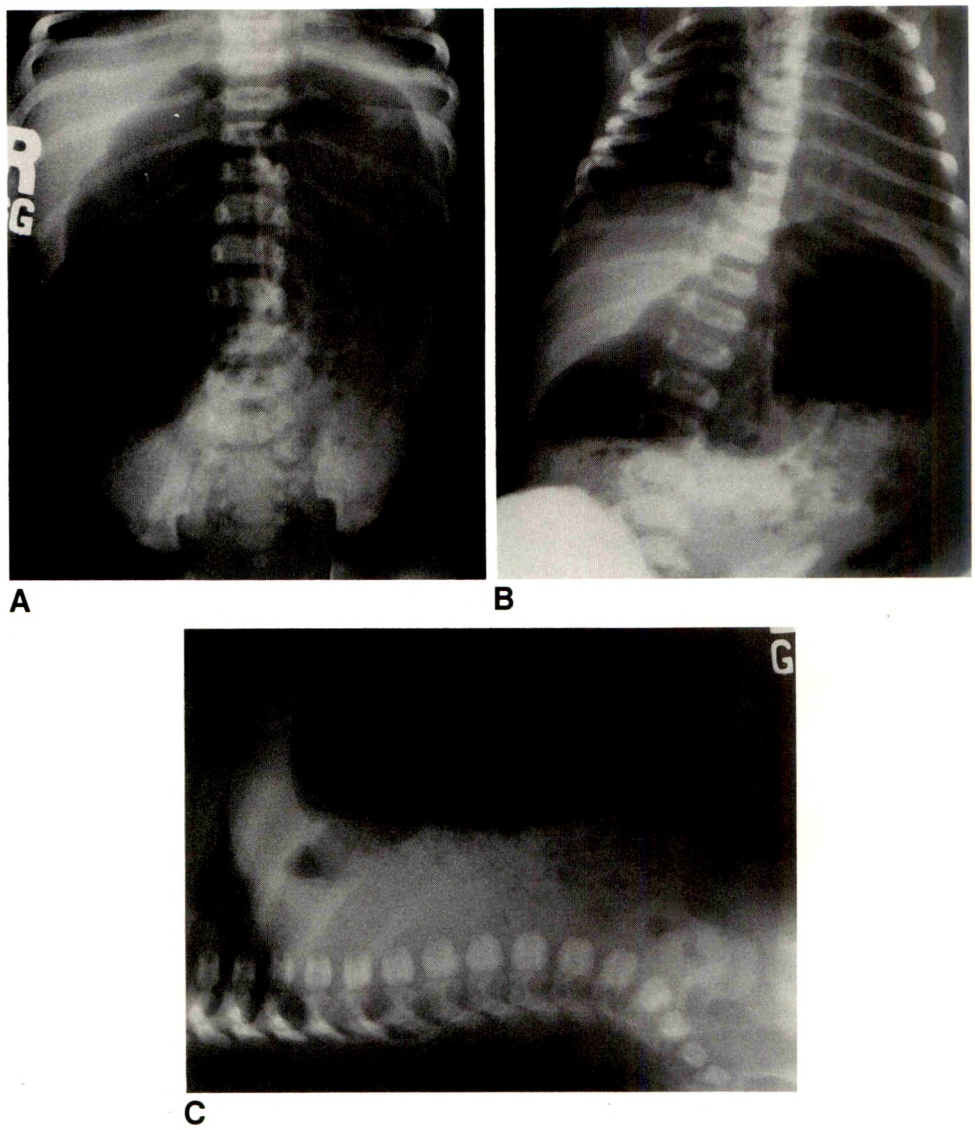



Fig. 2.—Case 2: 2-day-old neonate who passed meconium 2 hr after birth, was feeding well, and was discharged from nursery 24 hr after birth. Sudden onset of bilious vomiting occurred.
*A*, Anteroposterior abdominal radiograph of supine neonate.
*B*, Anteroposterior abdominal radiograph of upright neonate.
*C*, Cross-table lateral abdominal radiograph.

Fig. 3.—Case 3: 15-month-old Nigerian girl presented with fever and refusal to walk.

*A*, Anteroposterior radiograph of chest and abdomen.

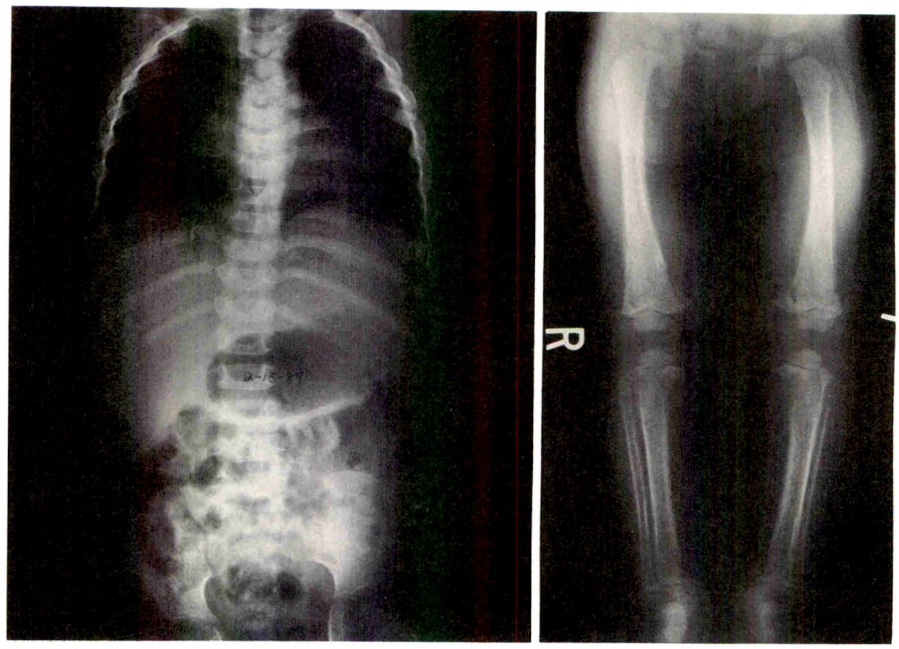
*B*, Anteroposterior radiograph of lower extremities.

*C*, Radiograph of left arm.

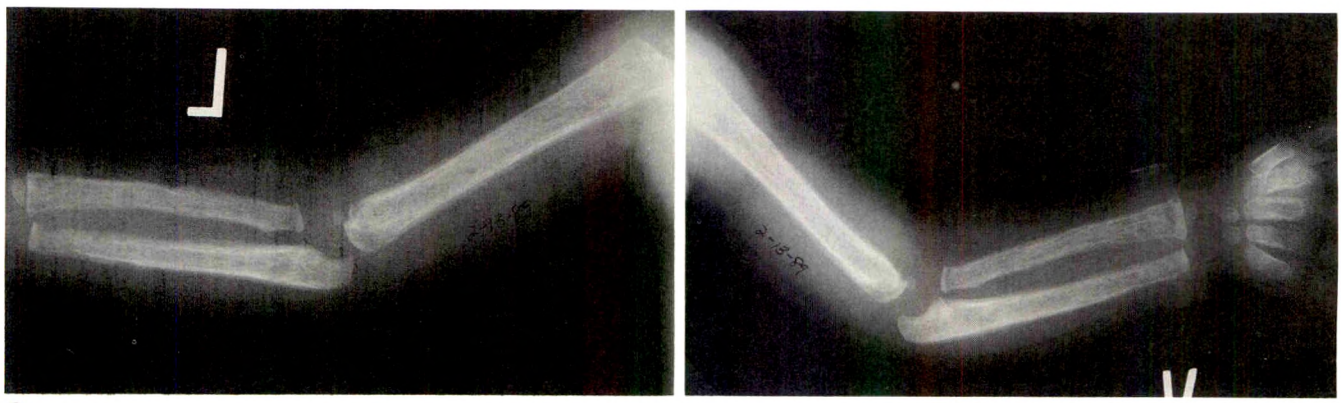
*D*, Radiograph of right arm.

*E*, Multiple images from $^{99m}$Tc-methylene diphosphonate bone scan. Left lower image is a posterior view; others are anterior views.

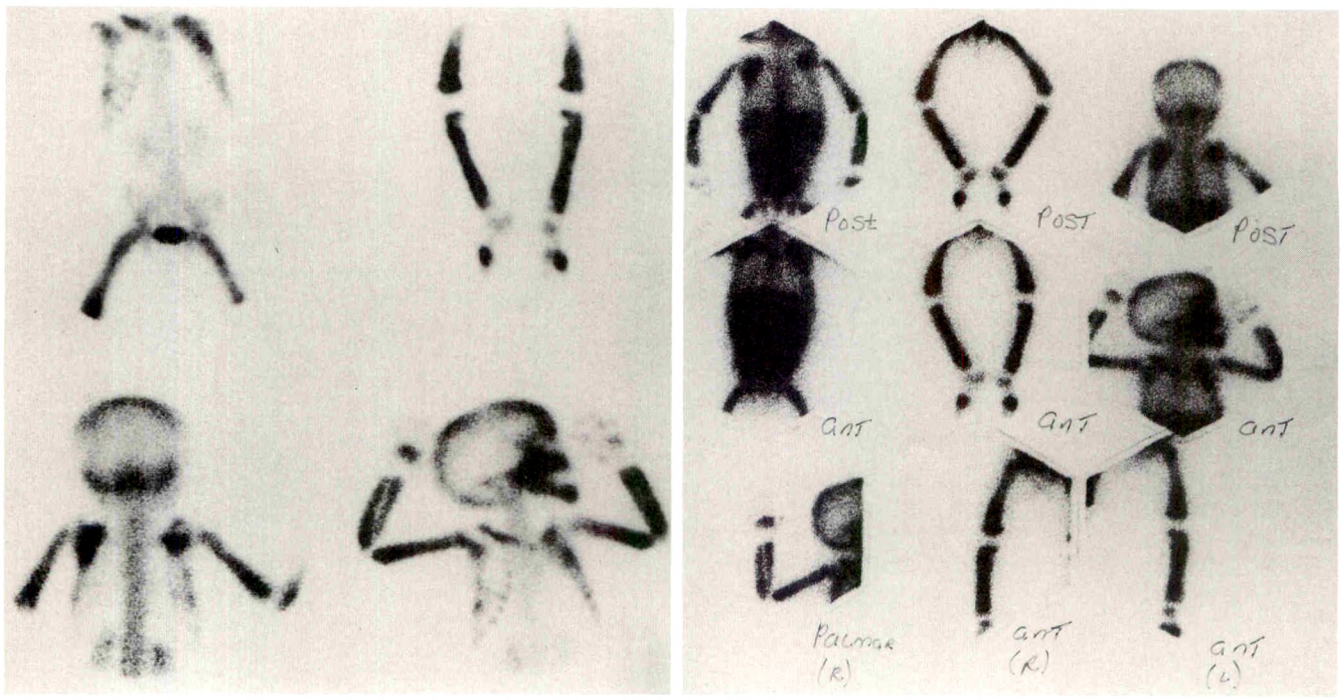
*F*, Multiple images from a gallium scan, 48 hr after injection.




A B



C D




E F

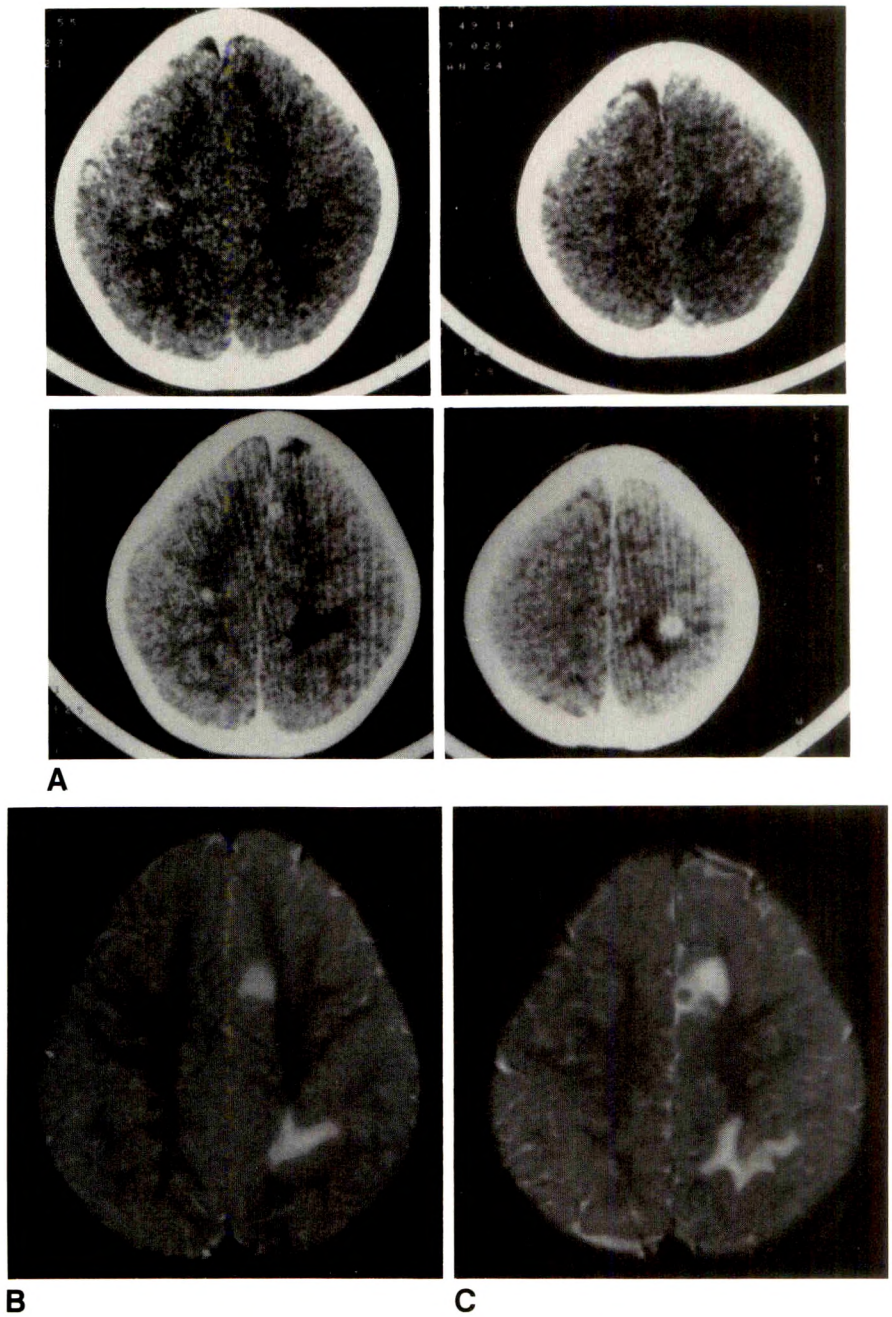



Fig. 4.—Case 4: 15-month-old girl presented to emergency department after a seizure.
*A*, Axial unenhanced (*top row*) and enhanced (*bottom row*) CT scans of head.
*B*, Axial T2-weighted (3000/90) MR image of head.
*C*, Axial T2-weighted (3000/90) MR image of head.

# Forthcoming Articles

## SPECIAL ARTICLE

**Anaphylaxis during barium enema examinations.** *Ownby DR, Tomlanovic M, Sammons N, McCullough J*

## REVIEW ARTICLES

**Imaging the pleura: sonography, CT, and MR imaging.** *McLoud TC, Flower CDR*

**Colorectal cancer: cross-sectional imaging for staging of primary tumor and detection of local recurrence.** *Thoeni RF*

## PULMONARY RADIOLOGY

**Factors affecting the development of pneumothorax associated with thoracentesis.** *Raptopoulos V, Davis LM, Lee G, Umali C, Lew R, Irwin RS*

**Incidence of air bronchogram in small peripheral adenocarcinomas of the lung on thin-section CT: comparison with benign tumors.** *Kuriyama K, Tateishi R, Doi O, et al.*

**CT evaluation of solitary pulmonary nodules: value of 185 H reference phantom.** *Swensen SJ, Harms GF, Morin RL, Myers JL*

**Pictorial essay. Imaging of the azygos lobe: normal anatomy and variations.** *Mata J, Cáceres J, Alegret X, Coscojuela P, De Marcos JA*

## GASTROINTESTINAL RADIOLOGY

**Perspective. The economic implications of radiologic screening for colonic cancer.** *Gelfand DW, Ott DJ*

**Sonography of the gallbladder: significance of striated (layered) thickening of the gallbladder wall.** *Teefey SA, Baron RL, Bigler SA*

**Case report. Giant esophageal ulcer due to Clinoril.** *Levine MS, Rothstein RD, Laufer I*

**Case report. CT appearance of retrograde jejunoduodenogastric intussusception: a rare complication of gastrostomy tubes.** *Weber A, Nadel S*

**Inverted colonic diverticulum: air contrast barium enema findings in six cases.** *Glick SN*

***Yersinia* terminal ileitis: sonographic findings in eight patients.** *Matsumoto T, Iida M, Sakai T, Kimura Y, Fujishima M*

**Pictorial essay. CT of AIDS-related lymphoma.** *Townsend RR*

**Pictorial essay. Anatomic variants and artifacts in ERCP interpretation.** *Gulliver DJ, Cotton PB, Baillie J*

**Subcapsular hepatic necrosis in liver transplantation: CT appearance.** *Abécassis J-P, Parienté D, Hazebroucq V, Houssin D, Chapuis Y, Bonnin A*

## GENITOURINARY RADIOLOGY

**Lucanae: a urographic finding in chronic obstructive uropathy.** *Talner LB, Webb JAW, Dail DH*

**Pictorial essay. MR imaging of the seminal vesicles.** *Secaf E, Nuruddin RN, Hricak H, McClure RD, Demas B*

**Stones and infection in renal caliceal diverticula: treatment with percutaneous procedures.** *Ellis JH, Patterson SK, Sonda LP, Platt JF, Sheffner SE, Woolsey EJ*

**Vaginal reconstruction with rectus abdominis myocutaneous flap: CT findings.** *Willing SJ, Pursell SH, Koch SR, Tobin GR*

**Case report. Pancreatitis causing focal caliectasis.** *Fishman M, Talner LB*

**Technical note. Retrograde replacement of internal "double-J" ureteral stents.** *Yedlicka JW Jr, Aizpuru R, Hunter DW, Castañeda-Zúñiga WR, Amplatz K*

## SKELETAL RADIOLOGY

**Condensing osteitis of the clavicle: a rare but frequently misdiagnosed condition.** *Greenspan A, Gerscovich E, Szabo RM, Matthews JG II*

**Fibrous dysplasia vs adamantinoma of the tibia: differentiation based on discriminant analysis of clinical and plain film findings.** *Bloem JL, van der Heul RO, Schuttevaer HM, Kuipers D*

**Pictorial essay. MR appearance of the distended iliopsoas bursa.** *Varma DGK, Richli WR, Charnsangavej C, Samuels BI, Kim EE, Wallace S*

## PEDIATRIC RADIOLOGY

**Sonographic inter- and intraobserver variations in renal length in children.** *Schlesinger AE, Hernandez RJ, Zerin JM, Marks TI, Kelsch RC*

**Anomaly of the descending aorta: a case of persistent double dorsal aorta.** *Formanek AG, Weisner KM, Lantz PE*

**Case report. Primary lymphoma of the CNS in an infant with AIDS: imaging findings.** *Douek P, Bertrand Y, Tran-Minh VA, Patet JD, Souillet G, Philippe N*

## NEURORADIOLOGY

**Diagnosis of cerebral metastases: double-dose delayed CT vs contrast-enhanced MR imaging.** *Davis PC, Hudgins PA, Peterman SB, Hoffman JC Jr*

**Hamartomas of the tuber cinereum: CT, MR, and pathologic findings.** *Boyko OB, Curnes JT, Oakes WJ, Burger PC*

**Intra- and paraorbital lesions: values of fat-suppression MR imaging with paramagnetic contrast enhancement.** *Tien RD, Chu PK, Hesselink JR, Szumowski J*

**Effects of magnetic susceptibility artifacts and motion in evaluating the cervical neural foramina on 3DFT gradient-echo MR imaging.** *Tsuruda JS, Remley K*

**Pictorial essay. Conventional MR neuroangiography.** *El Gammal T, Brooks BS*

**Pictorial essay. Imaging characteristics of tuberous sclerosis.** *Bell DG, King BF, Hattery RR, Charboneau JW, Hoffman AD, Houser OW*

## VASCULAR RADIOLOGY

**Intravascular sonography for the detection of arteriosclerosis and the evaluation of vascular interventional procedures.** *Engeler CE, Yedlicka JW Jr, Letourneau JG, Castañeda-Zúñiga WR, Hunter DW, Amplatz K*

**Conventional screen/film vs reduced exposure photostimulable phosphor plate imaging in lower extremity venography: an ROC analysis.** *Siegel EL, Cook LT, Parsa MB*

**Ligamentous compression of the celiac axis: CT findings in five patients.** *Patten RM, Coldwell DM, Ben-Menachem Y*

**Technical note. Retrieval of a 4-French diagnostic catheter fragment from the common carotid artery by using a stone basket.** *Travelli R, Cogbill TH*

## COMMENTARY

**Visual acuity testing of radiologists: is it time?** *Straub WH, Gur D, Good BC*

# Letters

## Radiology and the Environment

Radiologists have a unique opportunity to protect our environment and, at the same time, aid our school children. At my institution, we have been saving the cardboard inserts from each box of X-ray film. These are distributed to various schools throughout the community, where they are used for teaching aids, displays, and arts and crafts. This practice not only helps decrease the problem of solid-waste disposal but also benefits the schools, as many simply do not have the funds to provide creative material of this type. If only a fraction of the cardboard inserts discarded nationwide each year could be salvaged in this manner, it would make a significant impact.

David L. Magaram
*St. Vincent Medical Center*
*Los Angeles, CA 90057-0992*

## Recommended Textbooks for Radiology Residents

Radiology residents frequently ask faculty members and peers to recommend textbooks. These recommendations may be biased within an institution, with both residents and faculty members recommending the same books that were recommended to them. To compile an objective list of generally used textbooks, we solicited the recommendations of residents and faculty members throughout the United States.

We asked a random sampling of 100 radiology residents and 194 radiologists to list books they had found useful or would recommend to residents as either an introductory or a reference text in 14 different categories. We also asked if they thought a better introductory textbook was needed in any of the listed categories.

Fifty surveys (17%) were returned, some only partially completed. Thirty-four percent were from first- or second-year residents; 28% were from third- or fourth-year residents or fellows; 20% percent were from academic radiologists; and 18% were from radiologists in private practice. The recommendations from residents and radiologists were tabulated separately; no significant differences between their recommendations were found. The combined results are shown in Table 1. Books recommended by three or fewer respondents were included under "other." In several cases, two books are listed because only the author's name was given, and the specific book could not be discerned.

When asked which sections needed better introductory texts, respondents answered: sonography, 30%; gastrointestinal/genitourinary, 24%; MR, 20%; orthopedics, 16%; chest and angiography/

**TABLE 1: Textbooks Recommended by Radiologists and Radiology Residents**

| Recommended as | | Textbooks |
|---|---|---|
| Introductory Text | Reference | |
| **General Radiology** | | |
| 44 | 2 | *Paul and Juhl: Essentials of Radiologic Imaging* by Juhl and Crummy |
| 4 | 24 | *Radiology: Diagnosis, Imaging, Intervention* by Taveras and Ferrucci |
| 8 | 2 | *A Textbook of Radiology and Imaging* by Sutton |
| 2 | 6 | *Textbook of Diagnostic Imaging* by Puttman and Ravin |
| 10 | 0 | Four other books |
| **Chest Radiology** | | |
| 28 | 48 | *Diagnosis of Diseases of the Chest* by Fraser et al., 4 vols., or *Synopsis* by Fraser and Pare |
| 38 | 2 | *Chest Roentgenology* by Felson |
| 30 | 0 | *Chest Radiology: Plain Film Patterns and Differential Diagnosis* by Reed |
| 2 | 2 | Two other books |
| **Cardiology** | | |
| 16 | 4 | *Cardiovascular Radiology* by Gedgaudas and Moller |
| 10 | 4 | *Imaging of the Newborn, Infant and Young Child* by Swischuk |
| 10 | 0 | *Essentials of Cardiac Roentgenology* by Chen |
| 6 | 4 | Five other books |
| **Mammography** | | |
| 24 | 4 | *Teaching Atlas of Mammography* by Tabar and Dean |
| 18 | 4 | *Breast Imaging* by Kopans |
| 12 | 2 | Five other books |
| **Pediatrics** | | |
| 28 | 14 | *Practical Pediatric Imaging* by Kirks |
| 18 | 12 | *Essentials of Caffey's Pediatric X-Ray Diagnosis* by Silverman and Kuhn or *Caffey's Pediatric X-Ray Diagnosis* by Silverman, 2 vols. |
| 22 | 2 | *Imaging of the Newborn, Infant and Young Child* or *Differential Diagnosis in Pediatric Radiology* by Swischuk |
| 10 | 4 | Six other books |

*continued*

**TABLE 1: *Continued***

| Recommended as: Introductory Text | Recommended as: Reference | Textbooks |
|---|---|---|
| **Gastrointestinal and Genitourinary** | | |
| 42 | 10 | *Gastrointestinal Radiology: A Pattern Approach* by Eisenberg |
| 34 | 8 | *Radiology of the Kidney* by Davidson |
| 8 | 14 | *Alimentary Track Radiology* by Margulis and Burhenne, 2 vols. |
| 6 | 6 | *Emmett's Clinical Urography* by Witten, Myers, and Utz, 3 vols. |
| 30 | 10 | 11 other books |
| **Orthopedics** | | |
| 2 | 32 | *Bone and Joint Imaging* by Resnik or *Diagnosis of Bone and Joint Disorders* by Resnik and Niwayama, 6 vols. |
| 16 | 4 | *Radiology of Bone Diseases* by Greenfield |
| 10 | 0 | *Fundamentals of Skeletal Radiology* by Helms |
| 8 | 2 | *Orthopedic Radiology* by Weissman and Sledge |
| 10 | 0 | *Orthopedic Radiology: A Practical Approach* by Greenspan |
| 6 | 2 | *Edeikens Roentgen Diagnosis of Diseases of the Bone* |
| 4 | 4 | *Radiology of Skeletal Trauma* by Rogers |
| 10 | 0 | Three other books |
| **CT and MR** | | |
| 38 | 16 | *Computed Body CT with MRI Correlation* by Lee, Sagel, and Stanley |
| 10 | 20 | *Magnetic Resonance Imaging* by Stark and Bradley |
| 14 | 2 | *Cranial Computed Tomography and MRI* by Lee and Rao |
| 36 | 2 | 10 other books |
| **Sonography** | | |
| 26 | 6 | *Ultrasonography in Obstetrics and Gynecology* by Callen |
| 14 | 8 | *Diagnostic Ultrasound: Text and Cases* by Sarti |
| 4 | 14 | *Abdominal Ultrasound* by Mittelstaedt |
| 10 | 0 | *Diagnostic Sonography: Principles and Clinical Applications* by Fleischer and James |
| 6 | 4 | Five other books |
| **Nuclear Medicine** | | |
| 58 | 8 | *Essentials of Nuclear Medicine Imaging* by Mettler and Guiberteau |
| 14 | 10 | 11 other books |
| **Angiography and Interventional Radiology** | | |
| 32 | 6 | *Diagnostic Angiography* by Kadir |
| 8 | 8 | *Abrams Angiography: Vascular and Interventional Radiology* by Abrams |
| 8 | 4 | *Introduction to Cerebral Angiography* by Osborn |
| 28 | 8 | 10 other books |

Note.—The numbers in columns 1 and 2 are the percentages of respondents who recommended the indicated book as an introductory text and as a reference text.

interventional radiology, 14%; and pediatrics, nuclear medicine, general radiology, CT, cardiology, and mammography, 8% or less.

Richard M. Slone
Roger P. Tart
Barbara S. Martineau
*University of Florida, College of Medicine*
*Gainesville, FL 32610-0374*

## Modification of Standard Arterial Puncture Technique to Reduce Risk of Accidental Contact with Blood

In order to reduce the risk to the angiographer from uncontrolled spurting of blood during arterial catheterization, a number of closed systems for arterial puncture have been developed [1, 2]. We have developed a modified technique of arterial puncture with a standard Potts-Cournand needle (Becton-Dickinson, Rutherford, NJ) and a guidewire that reduces this risk.

Double-wall punctures are performed. Transversal of the arterial lumen is confirmed when a small amount of blood wells up through the tiny lumen in the central core of the stylet. The stylet is removed then, and a 0.035-in. (0.089 cm) or 0.038-in. (0.097 cm) guidewire is advanced into the midportion of the needle barrel. The needle is withdrawn until the arterial lumen is entered. When the lumen is entered, a snap or change in resistance is felt easily by the experienced angiographer. Blood also wells up around the coil of the guidewire at the point where the guidewire enters the metal core of the needle (Fig. 1). The guidewire then is advanced out of the needle into the arterial lumen, and the catheterization proceeds in the usual fashion.

We have used this technique on 70 patients. It was unsuccessful in three instances when the wire met resistance at the needle tip. In all three instances, the wire was removed, and the needle was withdrawn into the true arterial lumen, indicating that the cause for failure was not withdrawing the needle far enough. The technique was used in patients from 2 to 83 years old, in both common femoral and axillary arteries, and in retrograde and antegrade arterial catheterizations. The advantage of this technique is that it is a simple modification of a standard technique and requires no equipment other than an angiographic needle and guidewire and, therefore, may be universally applicable. The main disadvantage is that the reassuring, brisk, pulsatile flow of arterial blood is not observed when the arterial lumen is entered. If resistance to passage of the guidewire is encountered, fluoroscopic examination will show where the problem is. If it is within the arterial lumen at a distance from the needle tip, it can be dealt with in the usual manner. If the resistance is at the needle tip, two options are available. The first is to remove the guidewire and needle and repeat the puncture. The second is to remove the guidewire and then withdraw the needle until the true lumen is entered, as we did in our three cases in which this problem



**Fig. 1.—Arterial puncture technique to reduce risk of accidental contact with blood. Blood is seen welling up around guidewire at point where guidewire enters needle (*arrow*). Blood appeared after needle, with guidewire in midportion of needle core, was withdrawn into arterial lumen during a retrograde double-wall puncture of common femoral artery.**

was encountered. We have found that the consistent use of this technical modification is an important adjunct to other barrier and procedural adaptations for preventing accidental contact between the skin or mucous membranes of the angiographer and blood that potentially is infected with the AIDS or hepatitis virus.

Myron Marx
Jon P. Wack
Robert M. Bernstein
*Pacific Presbyterian Medical Center*
*San Francisco, CA 94120*

REFERENCES

1. Olsen WL, Jeffrey RB Jr, Tolentino CS. Closed system for arterial puncture in patients at risk for AIDS. *Radiology* **1988**;166:551–552
2. Cope C, Machan L. Method to control spraying of high-velocity infected blood droplets during arterial catheterization. *Radiology* **1990**;174:1055

## The Surgical Glove and Endorectal Sonography

Endorectal sonography is helpful in making the early diagnosis of prostatic disease, particularly in the early evaluation of prostatic carcinoma. Standard techniques are used to prepare the transducer before it is introduced into the rectum [1]. A condom is placed over the transducer and secured in place with several O-rings or rubber bands. These ensure that the condom will stay on the probe and allow fluid to be placed within the condom without leakage. The fluid, which is usually water, helps ensure better acoustic contact and provides a sharper focal zone.

At times, we have found ourselves in short supply of both condoms and rubber bands, and we have used a simple technique to help prepare the probe. This technique makes use of a surgical glove, which generally is available to all clinicians performing examinations. The sterile surgical glove has three purposes: (1) It covers the probe before the probe is introduced into the rectum. (2) A pair of scissors can be used to cut the finger of the glove into several thin slices that will act as rubber bands to hold the condom in place. (3) The person who is performing the examination uses the glove to maintain proper hygiene and prevent contamination of equipment and person.

We generally have used a sterile surgical glove because such gloves tend to be made of a thicker latex material and therefore provide better durability. This is important because when the glove is placed over the probe, it must be able to withstand the pressure of 20–50 ml of water being injected against the resistance of soft-tissue structures. In only a few episodes, the balloon formed at the end of the glove by the injection of water developed a leak. In addition, the gloves are readily available in virtually all departments, and they are generally cost-effective. After the examination, the glove can be discarded, and after the probe is cleaned, a new glove can be used for subsequent examinations. We are not suggesting that the surgical glove replace the condom, but that it can serve as a substitute when a condom is not available.

The glove also can be used to make bands to keep the glove or condom in position over the probe when O-rings or rubber bands are not available. One of the fingers of the glove is cut at the base and placed on the table. Subsequently, the finger is cut into several slices small enough to fit the grooves on the endorectal probe. It is possible to make at least five to 10 bands per finger. The bands then can be placed in position on the probe, but as they tend to be larger than the diameter of the probe, they must be tied several times to create a tight seal. We have found that the seal is quite effective; it prevents leakage of water, and this maintains good acoustic contact between the prostate and the transducer. The bands can be prepared quickly before the examination, which eliminates delays.

We think that the best method for performing endorectal sonographic examinations involves the well-planned use of condoms and O-rings or rubber bands. These should be readily available within all departments that perform this procedure. Our technique is best for emergencies, when these basic items may not be available, but the procedure must be performed.

Perry S. Gerard
Simindokt Zafaranloo
Ronald Frank
*Maimonides Medical Center*
*Brooklyn, NY 11219*

REFERENCE

1. Rifkin MD. Scanning techniques, equipment, and patient preparation. In: *Ultrasound of the prostate*. New York: Raven, 1988:31–49

## Guidelines for Use of Nonionic Contrast Media

In his recent article [1] on evolution and strategies for use of ionic and nonionic iodinated contrast material, McClennan eloquently summarizes the status quo of the implementation of nonionic contrast material in radiologic practice. Currently, development of guidelines for patients in whom and circumstances in which to use nonionic contrast material is taking place in most clinical institutions and some outpatient clinics. These guidelines are based on known risk factors outlined in current publications by Pfister [2], Cohan et al. [3], and the article by McClennan [1]. Typical guidelines for use of nonionic contrast material have also been approved in the University of Maryland Medical System. Risk factors included in these guidelines are cerebral angiography, pulmonary arteriography in patients with elevated pulmonary artery pressure, previous serious reaction to contrast material, elevated serum creatinine, asthma, sickle cell disease, multiple myeloma, significant cardiac dysfunction, patients less than 1 year old or more than 60 years old, and severely debilitated patients. Some of these points are included in "Guidelines for the Usage of Low-Osmolar Contrast Agents," which are currently before the Council of the American College of Radiology (Reference Committee III, Resolution 27) [4]. However, the term "debilitated" is vague and broad, and we prefer the category used by McClennan, "unstable patients of any age," especially if the grouping includes unconscious patients.

Institutions like ours that have a large shock trauma unit have a specific group of patients who are brought to the radiology department unconscious and with their history of risk factors unknown. Unconscious patients never were discussed or mentioned explicitly in recommendations for uniform application of nonionic iodinated contrast media. A significant difficulty is created in including this group of patients in local guidelines. Prolonged and delicate negotiations are required with the hospital administration at institutions in which such patients represent a significant number of clients. We would like to see this class of patients—"unconscious" as separate from "debilitated" and "unstable patients of any age"—included in further written recommendations.

Eduard Kotlyarov
Gerald S. Johnston
Stuart Mirvis
*University of Maryland Medical System*
*Baltimore, MD 21201*

REFERENCES

1. McClennan BL. Ionic and nonionic iodinated contrast media: evolution and strategies for use. *AJR* **1990**;155:225–233
2. Pfister RC. Contrast media toxicity and treatment of severe cardiorespiratory reactions. In: Uroradiology, ARRS categorical course syllabus. Res-

ton, VA: American Roentgen Ray Society, **1989**:7–12
3. Cohan RH, Dunnick NR, Bashore TM. Treatment of reactions to radiographic contrast material. *AJR* **1988**;151:263–270
4. *ACR Bulletin.* **1990**;46(August):6

*Reply*

I sincerely appreciate the comments of Kotlyarov et al. on my recent article [1]. I share their concern about the struggle that the development of appropriate guidelines for use of the new contrast agents has become. This is an expensive new technology, and its integration into current medical practice poses many dilemmas. The guidelines of the University of Maryland Medical System are similar to those in existence at many other institutions. Theirs include invasive angiographic studies, such as cerebral and pulmonary arteriography, and young and old patients. Although age, per se, is only one variable in the equation for determining the risk of using a particular contrast medium, nonetheless, it is an important one. However, often one of the other risk factors mentioned by Kotlyarov et al. also enters the decision-making process.

A resolution titled "Current Criteria for the Use of Water Soluble Contrast Agents for Intravenous Injections" recently passed by the American College of Radiology (ACR) Council at its Nashville meeting in September 1990 accepts the report of the ACR Committee on Drugs and Contrast Material and provides useful guidelines for the introduction of low-osmolar contrast media. Passage of this resolution was the culmination of several years of work on the part of that committee and intense debate on the council floor of the ACR over the past several years.

I wholeheartedly agree with Kotlyarov et al. that "debilitated" is a vague and broad term; thus, "unstable patients of any age" is indeed a more optimal category. I also think that radiologists recognize a sick patient when they see one, and I agree with Kotlyarov et al. that the unconscious patient is in a special risk category. That is why this category was dealt with in section IV, 5d of the ACR resolution: "Any other circumstances where, after due consideration, the radiologist believes there is a specific indication for the use of LOCA [low-osmolar contrast agents]. Examples of this include but are not restricted to ... patients with whom communication cannot be established in order to determine the presence or absence of risk factors." Unconscious patients or patients otherwise unable to give an adequate history are a significant portion of patients at the University of Maryland and elsewhere. I think that the best approach to developing guidelines for this specific class of patient is as outlined in the ACR resolution. I appreciate the opportunity to emphasize the importance of patient communication in the decisions about choice of contrast media.

Bruce L. McClennan
*Mallinckrodt Institute of Radiology*
*Washington University School of Medicine*
*St. Louis, MO 63110*

REFERENCE

1. McClennan BL. Ionic and nonionic iodinated contrast media: evolution and strategies for use. *AJR* **1990**;155:225–233

## Localization of Transected Wire

Needle localization of nonpalpable breast lesions has become an accepted preoperative technique to aid in the identification and excision of suspicious breast lesions [1–4]. Techniques for performing the localization have been reported, as have the complications, including hematoma, breakage of the wire during placement, and infection. An unusual complication that may occur is transection of the localization wire during breast biopsy. A previous report by Homer [5] described three occurrences of transection of the wire during 100 breast localizations. In our series of 650 needle localization procedures performed over 4 years, we encountered transection of the localization wire twice. In each instance, we were able to locate the transected wire by using the hookwire localizer.

Because the most popular wires used, the Kopans and the Homer, have thin guidewires, an inadvertently transected wire may be difficult to palpate. Rather than an attempt at wider surgical excision to obtain the transected tip, a second localization procedure can be performed to prevent what may be a disfiguring biopsy procedure. Homer has suggested the routine use of a postlocalization stiffening wire to avoid transection, but this has not received wide acceptance. The development of newer needles with transection-resistant or stiffer wires may further reduce this unusual complication of wire localization procedures.

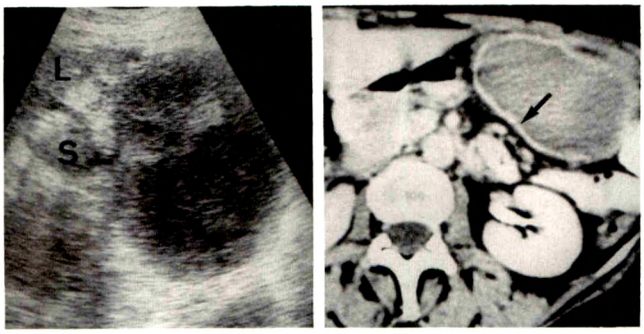
Julie S. Mitnick
Madeline F. Vazquez
Matthew N. Harris
*New York University Medical Center*
*The Tisch Hospital*
*New York, NY 10016*
Shalom S. Buchbinder
*The Albert Einstein College of Medicine*
*Bronx, NY 10461*

REFERENCES

1. Griffen MM, Welling RE. Needle-localized biopsy of the breast. *Surg Gynecol Obstet* **1990**;170:145–148
2. Hoehn JL, Hardacre JM, Swanson MK, Williams GH. Localization of occult breast lesions. *Cancer* **1982**;49:1142–1144
3. Meyer JE, Kopans DB, Stomper PC, Lindfors KK. Occult breast abnormalities: percutaneous preoperative needle localization. *Radiology* **1984**;150:335–337
4. Landercasper J, Gundersen SB, Gunderson AL, et al. Needle localization and biopsy of nonpalpable lesions of the breast. *Surg Gynecol Obstet* **1987**;164:399–403
5. Homer MJ. Transection of the localization hooked wire during breast biopsy. *AJR* **1983**;141:929–930

## Volvulus of a Pedunculated Hemangioma of the Liver

We report a case of pedunculated hemangioma of the left lobe of the liver that was complicated by subacute torsion and infarction. A 47-year-old woman had had left-sided abdominal pain for 2 months. Physical examination showed a mass in the left upper quadrant of the abdomen. Sonography (Fig. 1A) showed a large round hypoechoic mass containing disseminated echoes anterior to the left kidney, medial to the spleen, and lateral to the stomach. The mass appeared to be separated from the left lobe of the liver, the tail of the pancreas, and the left adrenal gland. Sonography also showed a small hyperechoic nodule in the left lobe of the liver. Sonographically guided percutaneous puncture of the large mass produced a mixture of fresh and clotted blood. No tumor cells were identified. Unenhanced CT showed an 8.5-cm homogeneous mass. CT after injection of contrast material showed that the wall of the mass enhanced up to 75 H and was irregularly thick (Fig. 1B). At surgery, a hepatic tumor was found attached by a thin pedicle to the inferior aspect of the left part of the falciform ligament. The lesion twisted around its pedicle. Left hepatic segmentectomy and resection of the mass were carried out. The small hepatic nodule was enucleated. The pathologic diagnosis was




A B

**Fig. 1.—Volvulus of a pedunculated hepatic hemangioma.**
***A*, Sonogram shows hypoechoic mass (M) displacing stomach (S) medially. L = left lobe of liver.**
***B*, Contrast-enhanced CT scan shows a cystic mass with enhancement of wall (*arrow*).**

pedunculated cavernous hemangioma of the liver with central hemorrhagic necrosis and a small hemangioma of the liver.

Most pedunculated hepatic tumors are hepatomas that develop in patients with cirrhosis [1, 2]. Rare causes of benign pedunculated tumors include mesenchymal hamartoma, focal nodular hyperplasia, and adenoma [2]. Only one report of pedunculated hemangioma has been published [3]. Rare cases of volvulus of hepatoma have been reported [4], but volvulus of pedunculated hemangioma of the liver has not been described. In our case, the pedicle of the mass was displaced by the stomach and was not shown by sonography or CT.

Van A. Tran-Minh
Thérèse Gindre
Jean-Pierre Pracros
Charles-Henri Morin de Finfe
Marie Kattan
*Hôpital Debrousse*
*Université Claude-Bernard Lyon I*
*F. 69322 Lyon cedex 05, France*
Jean-Louis Peix
*Hôpital de l'Antiquaille*
*Université Claude-Bernard Lyon I*
*F. 69321 Lyon cedex 05, France*

REFERENCES

1. Nobusawa S, Saito S, Sunakawa T, et al. Pedunculated hepatoma: report of two cases and review of the literature. *Gastroenterol Jpn* **1984**;19:464–471
2. Cunningham PL, Nava H, Lopez C, Douglass HO. Pedunculated primary hepatocellular carcinoma. *J Surg Oncol* **1984**;27:260–267
3. Ellis JV, Salazar JE, Gavant ML. Pedunculated hepatic hemangioma: an unusual cause for anteriorly displaced retroperitoneal fat. *J Ultrasound Med* **1985**;4:623–624
4. Molea N, Toni MG, Gori G, et al. Scintigraphic and angiographic findings in a peduncular trabecular adenocarcinoma of the liver. *J Nucl Med Allied Sci* **1979**;23:153–157

## Sonography in the Detection of Liver Tumors

Having long been an admirer of Dr. Ferrucci's practical approach to the problems of interventional and gastrointestinal radiology, I was puzzled by his recent article, "Liver Tumor Imaging: Current Concepts" [1], which appeared in the September 1990 issue of *AJR*. In addressing the issue of sonography in the detection of liver tumors, he makes an unreferenced statement that sonography's overall false-negative rate for liver metastases exceeds 50%. I would like to know the source of this information. As Dr. Ferrucci well knows, such data are impossible to derive. We need specifics about who is looking and with what equipment. The situation is further complicated by the time that often elapses between imaging studies and pathologic proof (often autopsy series). The pertinent paragraph then concludes with a statement that sonography is of limited value because it fails to differentiate between benign and malignant nodules. This is undeniably true, but it is just as true for all other imaging methods discussed in his paper. Until such time as convincing scientific proof is available, I, for one, find it hard to dismiss out of hand the role of sonography in the detection of liver metastases.

George R. Leopold
*University of California, San Diego, Medical Center*
*San Diego, CA 92103-1990*

REFERENCE

1. Ferrucci J. Liver tumor imaging: current concepts. *AJR* **1990**;155:473–484

## CT vs MR in Imaging Liver Tumors

I commend Ferrucci [1] for his lucid summary of the CT vs MR issue in the assessment of hepatic involvement by metastases or hepatocellular carcinoma. The growing literature on this subject is a quagmire of conflicting data, but the prevalence of these tumors and the fact that "as many as one fourth of all primary and secondary liver cancers are potentially resectable for cure" [1] emphasize the importance of the discussion. Ferrucci clearly leans toward MR but admits that "the debate as to which is best for liver tumor imaging will no doubt continue for years."

I think that the continuing arguments over the relative merits of CT and MR in the primary assessment of liver cancer are overemphasized. Until one of these examinations virtually can replace the other, including its use in the assessment of nonhepatic metastases, both will be needed in the preoperative assessment of candidates for possible curative partial hepatectomy. The medical and monetary implications of such major surgery would appear to justify the use of both examinations.

I would do dynamic CT scanning first because it is cheaper and more available and, if curative surgery is not contemplated, as in most cases, it could be used as a baseline for subsequent CT scans to assess the effectiveness of chemotherapy. If the initial examination, be it CT or MR, reveals no liver metastases, is equivocal for metastases, or shows potentially resectable lesions, and if the patient is otherwise a candidate for curative surgery, then the second examination could be performed.

Ferris M. Hall
*Beth Israel Hospital*
*Boston, MA 02215*

REFERENCE

1. Ferrucci JT. Liver tumor imaging: current concepts. *AJR* **1990**;155:473–484

*Reply to Drs. Leopold and Hall*

I am pleased that Dr. Leopold rises to the defense of sonography, because he is right that its role in the diagnosis of liver tumors has been given short shrift in the radiologic literature. Early prospective comparative studies such as that by Alderson et al. [1] in 1983 established a hierarchy of imaging tests for the detection of liver metastases, with CT as the gold standard. Receiver-operating-characteristic curves showed superior performance for CT over sonog-

raphy at a level that reached statistical significance. The commonly cited drawbacks of sonography vis a vis CT have been poor spatial resolution, especially for peripheral subcapsular lesions, and limited ability to provide a tissue-specific differential diagnosis. Dr. Leopold is again correct that data on accuracy have been difficult to derive for sonography. In studies done after those of Alderson et al., investigators have had little interest in immediate surgical pathologic proof of the results of sonography, whereas a number of such carefully documented studies [2, 3] have appeared for CT, including its various permutations, and for MR. My figure of less than 50% for the accuracy of sonography [4] therefore is derived from extrapolations of lesion-by-lesion detection data from several sources (and therefore unreferenced). For example, detection of subcentimeter nodules has become the standard for modern CT and MR [2, 3, 5]. On the contrary, the best reported results for sonography are found in a study by Matsui et al. [5], who identified only 2/20 (10%) proved liver metastases less than 2.0 cm in size by using a 3.5-MHz probe. In this context, it should be conceded that European and Japanese investigators are more confident of the usefulness of sonography than the American radiologic community seems to be, but their involvement in performing real-time scans is much more hands-on than is generally the custom in the United States, where technologists usually perform the scans. Moreover, poor reproducibility of image plane greatly limits the usefulness of sonography for the clear spatial mapping required preoperatively by the surgeon or for measuring tumor volume during oncologic follow-up.

With regard to the comment about the failure of other techniques to differentiate benign from metastatic liver nodules, I do not think that this would go unchallenged by most CT or, especially, MR experts. With MR, the accuracy in distinguishing hemangiomas from metastases reaches 90% even when the size of the lesion is 2–3 cm. Thus, while I applaud the reminder not to dismiss sonography, in practice, when a clear and definitive depiction and differential diagnosis of suspected liver tumors is required, CT and, more recently, MR have become the norm.

Dr. Hall suggests using both CT and MR, opting for CT as the first choice because it is cheaper and more available. The problem is that if CT is approximately 10% less sensitive in detecting a lesion and approximately 10% less accurate in differentiating benign from malignant lesions and carries the added risk of requiring use of iodinated contrast material, does its lower cost and better availability still justify its use? Using a technique because it is more available may fill local needs but does not address the more objective issue of superior performance. In my view, the principal remaining argument for CT is its acknowledged superiority in showing important extrahepatic disease. However, this advantage still must be balanced against the apparently superior sensitivity, accuracy in distinguishing benign from malignant lesions, and safety of MR for assessing the volume of the liver itself. Moreover, the use of both MR and CT is unlikely to be a widely defensible strategy fiscally, although sometimes this is often the outcome in daily practice. As I indicated in my article [4], for suspected tumors, either MR or CT would preferably be performed first, and if surgery is contemplated, more precise preoperative staging would then be carried out by the addition of CT after arterial portography or intraoperative sonography.

Finally, my comment that "the debate as to which is best [MR vs CT] for liver tumor imaging will no doubt continue for years" was couched in the context of innumerable technological developments, especially in terms of fast imaging and contrast agents for both CT and MR, not to mention the improved resolution and color flow capabilities that undoubtedly will enhance the performance of sonography as well.

Joseph T. Ferrucci
*Massachusetts General Hospital*
*Boston, MA 02114*

REFERENCES

1. Alderson PO, Adams DF, McNeil BJ, et al. Computed tomography, ultrasound, and scintigraphy of the liver in patients with colon or breast carcinoma: a prospective comparison. *Radiology* **1983**;149:225–230
2. Ward BA, Miller DL, Frank JA, et al. Prospective evaluation of hepatic imaging studies in the detection of colorectal metastases: correlation with surgical findings. *Surgery* **1989**;105:
3. Heiken JP, Weyman PJ, Lee JKT, et al. Detection of focal hepatic masses: prospective evaluation with CT, delayed CT, CT during arterial portography, and MR imaging. *Radiology* **1989**;171:47–51
4. Ferrucci JT. Liver tumor imaging: current concepts. *AJR* **1990**;155:473–484
5. Matsui O, Takashima T, Kadoya M, et al. Liver metastases from colorectal cancers: detection with CT during arterial portography. *Radiology* **1987**;165:65–69

## Regression of Hepatocellular Carcinoma

We present a case of primary hepatocellular carcinoma that regressed after radiotherapy for skeletal metastases. A 61-year-old man who had had liver cirrhosis for 8 years was seen because of severe pain in the back and face. The serum level of alpha-fetoprotein was 221,000 IU/ml. CT showed cirrhosis of the liver with portal hypertension and a large encapsulated mass in the liver (Fig. 1A). Scintigraphy showed uptake of radionuclide in the base of the skull, humerus, and femur. The diagnosis was hepatocellular carcinoma with multiple skeletal metastases, and the bone lesions were irradiated. Phantom dosimetry showed that the primary hepatic tumor received approximately 180 cGy of scattered radiation, an amount equivalent to 3% of the total dose given to the lumbar spine. This dose, however, usually is not effective for hepatocellular carcinoma. The patient's pain was relieved, and the serum level of alpha-fetoprotein decreased to 10 IU/ml. CT performed 9 months later showed remarkable regression of the hepatic lesion (Fig. 1B). The patient died of colonic hemorrhage and dyspnea 18 months after the radiation therapy. Autopsy showed metastatic hepatocellular carcinoma in the lung and ilium. Macroscopically, no tumor was seen in the liver, but a small amount was identified microscopically.

We think this case illustrates abscopal effect of radiation, regression of a tumor outside the irradiated field [1]. Unknown factors, some perhaps immunologic, may play a role in this uncommon phenomenon. Although several case reports of an abscopal effect on

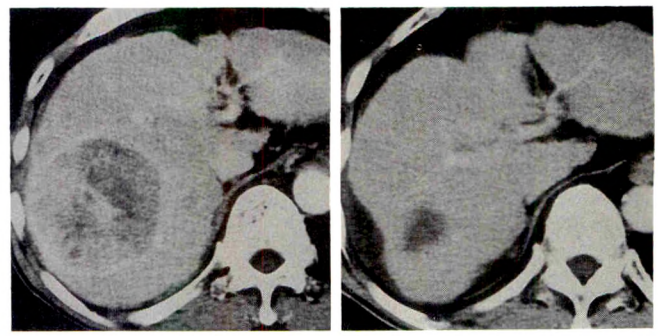



**Fig. 1.—Abscopal regression of hepatocellular carcinoma.**
***A*, Enhanced CT scan shows encapsulated tumor in liver.**
***B*, Enhanced CT scan made 9 months after radiotherapy for bone metastases shows marked reduction in size of hepatic tumor. Lesion no longer enhances with administration of contrast material.**

various tumors have been published [1–3], none has involved hepatocellular carcinoma.

Takao Mochizuki
Yasuo Takehara
*Seirei Mikatabara General Hospital*
*Mikatabara, Hamamatsu, 433 Japan*
Tetsuo Nishimura
Motoichirou Takahashi
Masao Kaneko
*Hamamatsu University School of Medicine*
*Hamamatsu 431-31, Japan*

REFERENCES

1. Ehlers G, Friedman M. Abscopal effect of radiation of papillary adenocarcinoma. *Br J Radiol* **1973**;46:220–222
2. Rees GJG. Abscopal regression in lymphoma: a mechanism in common with total body irradiation? *Clin Radiol* **1981**;32:475–480
3. Rees GJG, Ross CMD. Abscopal regression following radiotherapy for adenocarcinoma. *Br J Radiol* **1983**;56:63–66

## Screening Methods for Hepatocellular Carcinoma

Hepatocellular carcinoma, a frequently occurring cancer throughout the world, is accompanied by liver cirrhosis in 65–90% of patients. The Liver Cancer Study Group of Japan suggests that patients with chronic liver disease, particularly cirrhosis, should be examined at regular intervals by using sonography and that levels of alpha-fetoprotein also should be determined. The results of following these recommendations have been good [1]. In particular, screening with sonography has made possible early diagnosis of small hepatocellular carcinomas [2], which are now being diagnosed and treated in western countries and probably will be reported more, as their detection is increasing [3]. However, Ferrucci [4] reported that CT and MR imaging are better screening methods for detecting liver tumors. Sonography is not mentioned in the paragraph on hepatocellular carcinoma in his article, and he does not offer any evidence that CT or MR is more useful than sonography for detecting primary liver cancer. This may be because alcoholic cirrhosis with fatty liver is common or because many patients in western countries are obese. Hepatocellular carcinoma remains a largely untreated disease worldwide. The question is whether a unique diagnostic procedure should be used according to regional differences when patients are examined for the possible presence of this tumor.

Takahiro Ezaki
*National Kyushu Cancer Center*
*Fukuoka 815, Japan*

REFERENCES

1. The Liver Cancer Study Group of Japan. Primary liver cancer in Japan. *Ann Surg* **1990**;211(3):277–287
2. Okuda K. Early recognition of liver cell tumors. In: Bannasch P, Keppler D, Weber G, eds. *Falk Symposium 51: liver cell cancer*. Boston: Kluwer, **1988**:439–453
3. Kameny F, Vadrot J, Wu A, Smadja C, Meakins JL, Franco D. Morphological and histological features of resected hepatocellular carcinoma in cirrhotic patients in the West. *Hepatology* **1989**;9(2):253–257
4. Ferrucci JT. Liver tumor imaging: current concepts. *AJR* **1990**;155:473–484

*Reply*

I appreciate Dr. Ezaki's letter and fully agree with its thrust in emphasizing the validity of sonographic screening for liver cancer. My review [1] does not slight sonography intentionally; rather it focuses on the emerging role of MR, especially vis a vis CT, and some of the newer imaging procedures used for staging liver tumors before surgical resection.

Apart from the obesity of Americans vs Japanese (as well as Europeans), the major difference in the applicability and results of liver sonography in the United States is that in this country, the examination generally is performed by technicians. In Europe and the Far East, it is performed almost exclusively by physicians. In the United States, sonographic documentation of liver anatomy never has been standardized or routinized with regard to imaging plane, number of sections, field of view, and so forth. Consequently, with a more or less random collection of hard-copy images of the liver, it is difficult for the radiologist to interpret the images for completeness of coverage or quantitative measurement of the size of individual nodules. This has limited the reproducibility, sensitivity, and overall accuracy of sonography, especially vis a vis CT and MR, and clinicians do not often linger with sonographic data alone. Thus, in the United States, the role of sonography in the imaging of liver cancer unfortunately has evolved almost to one of serendipity. I firmly agree that the problem of hepatocellular carcinoma, and, indeed, liver cancer in general, is an area in which significant further strides in diagnosis and therapy are possible and required.

Joseph T. Ferrucci
*Massachusetts General Hospital*
*Boston, MA 02114*

REFERENCE

1. Ferrucci JT. Liver tumor imaging: current concepts. *AJR* **1990**;155:473–484

## Recall of E-Z-EM Balloon-Retaining Barium Enema Tips

The recent voluntary recall (letter to health care professionals, October 5, 1990) of balloon-retaining barium enema tips by E-Z-EM, Inc. (Westbury, NY) in cooperation with a recommendation of the U. S. Food and Drug Administration is a bit disconcerting. The latex balloons have been implicated in anaphylactic-type reactions.

We have found that noncuffed tips, even when they are taped to the patient's buttocks as recommended, are not an adequate solution to the problem, particularly for patients with poor rectal sphincter tone. We have developed a simple, temporary, inexpensive solution to the problem. A standard latex examining glove can be used as a protective cover. The tip of the middle finger of the glove is cut, and the glove is slipped over the enema tip so that the enema tip extends through the clipped finger of the glove. The rest of the finger covers the enema balloon. It is important to make the hole cut in the finger of the glove as small as possible so that the enema tip does not extend all the way through the finger. Only the openings in the enema tip should be exposed to allow free flow of barium for the procedure. It is easy to inflate the balloon inside the finger of the glove, which is easily expandible. The remainder of the glove extends well outside the rectum so no chance exists of losing the glove in the patient's rectum.

We have used this method since receiving the letter from E-Z-EM and find that it works quite well. Latex examining gloves have a proved track record as a large number of rectal examinations have been performed without known anaphylactic reactions.

Michael M. Tersegno
*Auburn Memorial Hospital*
*Auburn, NY 13021*

## CT Findings of a Rectal Intussusception

CT plays an important role in the workup of patients who have abdominal pain and palpable abdominal masses [1]. We present a case of rectal intussusception with classic CT findings.

A 47-year-old woman had lower back pain, which had worsened over the previous 10 days, and a watery, bloody rectal discharge of 1 week duration. Physical examination showed an enlarged uterus of about 20–22 weeks gestational size and a palpable mass of 4 to 5 cm in the rectal vault. CT showed a leiomyoma of the uterus and a circumferential telescoping of the rectum consistent with intussusception (Fig. 1A). The presence of small air bubbles between layers of the colonic wall was interpreted as indicating bowel ischemia, if not possible perforation (Fig. 1B).

The patient had surgery, and a large uterine leiomyoma was removed. Intussusception of a 12-cm segment of the rectum also was identified. The resected colon was partly necrotic, with evidence of perforations attendant to ulcerations. A villous adenoma was found, which was thought to be responsible for the intussusception.

Intussusception in adults is uncommon. The most common causes are polyps and cancer. Most often, the terminal ileum or cecum is affected. Transient rectorectal intussusception may be a normal occurrence during evacuation [2, 3]. CT is useful in establishing the diagnosis of intussusception because mesenteric fat, bowel wall, and intraluminal fluid can be distinguished [1]. Vascular perfusion is compromised in the intussuscepted mesentery, resulting in edema, which causes the fascial planes to become indistinct [1]. As the edema and vascular compromise progress, the bowel wall becomes gangrenous. This is reflected by air in the bowel wall. The underlying cause of the intussusception usually is not identified on CT scans, unless tumors, such as lipoma, are responsible [4].

Anselm Pottmeyer
Joseph McDowell
Erich K. Lang
*Louisiana State University Medical Center*
*New Orleans, LA 70112*

REFERENCES

1. Iko BO, Teal JS, Siram SM, Chinwuba CE, Roux VJ, Scott VF. Computed tomography of adult colonic intussusception: clinical experimental studies. *AJR* **1984**;143:769–772
2. Margulis AR, Burhenne HJ, eds. *Alimentary tract radiology*, 4th ed. St. Louis: Mosby, **1989**
3. Hoffman EJ, Kodna IJ, Fry RD. Internal intussusception of the rectum: diagnosis and surgical management. *Dis Colon Rectum* **1984**;27(7):435–441
4. Hodgman CG, Lantz EJ, Maus TR, Conley CR. Computed tomography of intussusception due to colon lipoma. *J Comput Assist Tomogr* **1987**;11(4):740–741

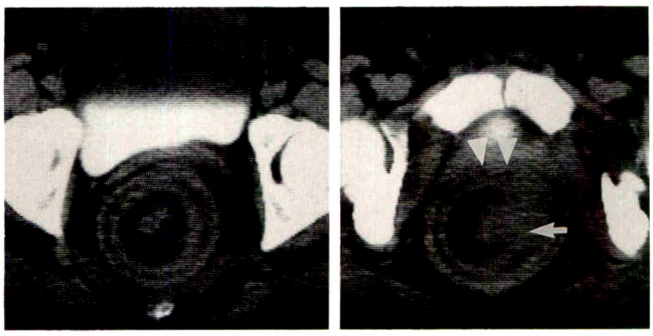



**Fig. 1.—Rectal intussusception.**
***A*, CT scan shows telescopic appearance of rectum, indicating a rectorectal intussusception.**
***B*, CT scan at slightly lower level than *A* shows small air bubbles between layers of colonic wall, indicating bowel ischemia (*arrowheads*). Mass projecting into lumen is lead point of intussusception. This proved to be a villous adenoma (*arrow*).**

## CT Findings in Anorectal Tuberculosis

Anorectal tuberculosis is a rare disorder. We encountered a case that on the basis of both clinical and CT findings initially was diagnosed as inflammatory bowel disease. A 53-year-old man had a 1-year history of painful draining perianal sinus tracts and a weight loss of 20 lb. (9.1 kg). Stool cultures, assay for *Clostridium difficile* toxin, barium studies, and tests for serum antibody to human immunodeficiency virus were negative or normal. Colonoscopy revealed no abnormalities, and multiple biopsies showed mild chronic inflammation. Treatment was with metronidazole for suspected perianal Crohn disease. Sinus drainage was persistent, and CT examination of the pelvis 7 months after treatment began showed findings consistent with an inflammatory process and a fistulous tract (Fig. 1). Subsequent biopsy and culture of the persistent perianal sinus drainage showed *Mycobacterium tuberculosis*. The patient had no clinical history of tuberculosis or exposure to *Mycobacterium* although chest radiographs showed apical scarring. Skin testing with intermediate-strength purified protein derivative was positive. After 1 year of antituberculosis therapy, complete resolution of the perianal sinus tracts had occurred. Follow-up CT showed resolution of the edematous process and a residual scar.

Anorectal tuberculosis has received little attention in the radiologic literature. In endemic areas, tuberculosis accounts for less than 10% of all cases of fistula in ano [1]. Inflammatory bowel disease, carcinoma, and other venereal infections can mimic this disorder [1–4]. Although the terminal ileum and cecum are the most common sites of gastrointestinal tuberculosis, any part of the gastrointestinal tract can be involved [4]. Tuberculosis should be considered in the differential diagnosis of perianal disease, especially in patients who have not responded to therapy for inflammatory bowel disease.

James M. Lieberman
Richard J. Blinkhorn
Bipin Sharma
*MetroHealth Medical Center*
*Cleveland, OH 44109*

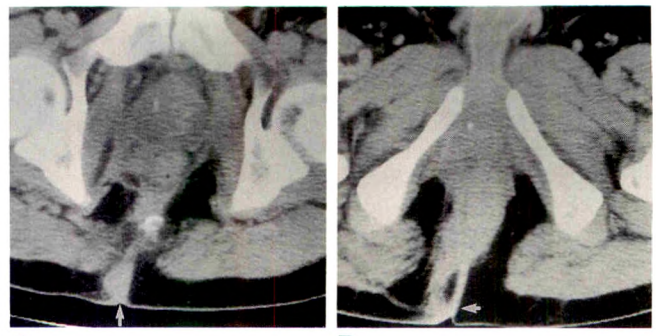



**Fig. 1.—Anorectal tuberculosis.**
***A*, CT scan of rectum shows abnormal soft-tissue density (*arrow*) in perirectal fat adjacent to coccyx and extending to skin.**
***B*, CT scan of anal region shows soft-tissue density (*arrow*) in fat and thickening of perianal skin.**

REFERENCES

1. Logan VS. Anorectal tuberculosis. *Proc R Soc Med* **1969**;62:1227–1230
2. Lax JD, Haroutiounian G, Attia A, Rodriguez R, Thayaparan R, Bashist B. Tuberculosis of the rectum in a patient with acquired immune deficiency syndrome: report of a case. *Dis Colon Rectum* **1988**;31:394–397
3. Paustian FF, Marshall JB. Intestinal tuberculosis. In: Berk JE, ed. *Bockus gastroenterology*. Philadelphia: Saunders, **1985**:2032–2035
4. Balthazar EJ, Bryk D. Segmental tuberculosis of the distal colon: radiographic features in seven cases. *Gastrointest Radiol* **1980**;5:75–80

## Intratumoral Fat in a Renal Cell Carcinoma

In a recent communication, Curry et al. [1] described the CT findings of a case of renal oncocytoma that mimicked angiomyolipoma because of the presence of discrete areas of fat density within the lesion. The authors also emphasized that in a review of 48 large renal cell carcinomas, they did not find any case in which the carcinoma engulfted renal sinus fat or perirenal fat. We describe a case of renal cell carcinoma that contained focal areas of intratumoral perirenal fat, thus simulating a benign renal mass.

A 62-year-old woman had pain in the right upper quadrant. Contrast-enhanced CT scans showed a large, mostly perirenal mass containing areas of fat density within and at the periphery of the lesion (Fig. 1). No clear cleavage plane was evident between the mass and the upper pole of the right kidney, which had an irregular contour.

Elevation of the right hemidiaphragm and pleural effusion also were detected. The right renal vein and the inferior vena cava were normal. The preoperative diagnosis was either exophytic renal angiomyolipoma or a malignant renal lipomatous tumor. At surgery, a large exophytic right-sided renal mass invading the hemidiaphragm was found. Pathologic examination revealed a 13-cm renal cell carcinoma (granular cells) invading the perirenal fat, with areas of necrosis and hemorrhage. Small amounts of mature adipose tissue were detected within and at the periphery of the lesion. The adipose tissue was considered to be perirenal fat engulfed by the renal mass. No evidence of nodal metastases was found.

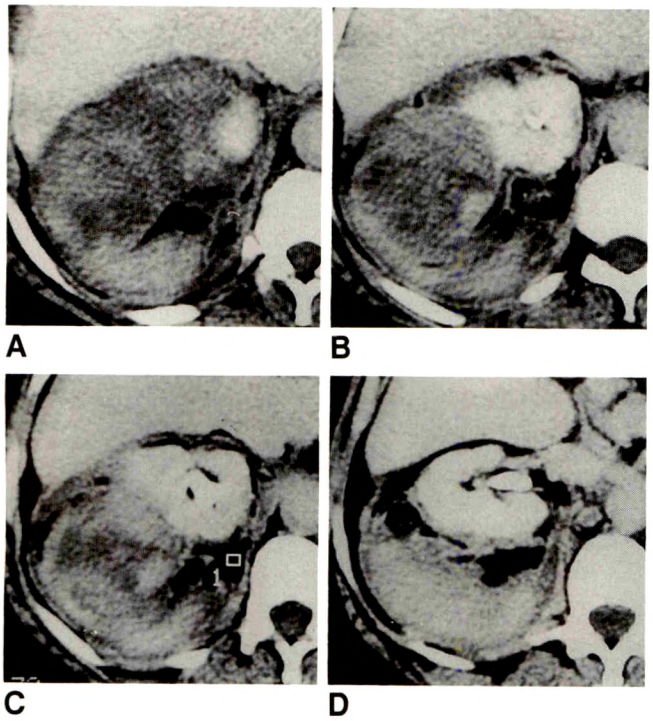



**Fig. 1.—Intratumoral fat in renal cell carcinoma.**
***A–D*, CT scans show large inhomogeneous tumor contiguous to superior and posterior aspects of right kidney. Scattered fat (−76 H) can be seen within and at periphery of mass. Irregular contour of renal upper pole (*A* and *B*) and signs of invasion of right diaphragmatic crus and posterior abdominal wall (*C and D*) are also present.**

This unusual case, similar to the one of Curry et al. illustrates that the presence of fat within a tumor does not necessarily mean that the tumor is a benign angiomyolipoma [2]. Our case is an example of the process predicted by Bosniak et al. [3]: that a large renal cell carcinoma can invade the perirenal fat and cause its entrapment, thus mimicking a benign lesion. Renal cell carcinoma should be considered in the differential diagnosis of lipomatous renal tumors [4].

Adilson Prando
*Radiologic Center of Campinas*
*13.020 Campinas, São Paulo, Brazil*

REFERENCES

1. Curry NS, Schabel SI, Garvin AJ, Fish G. Intratumoral fat in a renal oncocytoma mimicking angiomyolipoma. *AJR* **1990**;154:307–308
2. Bosniak MA. Angiomyolipoma (hamartoma) of the kidney: a preoperative diagnosis is possible in virtually every case. *Urol Radiol* **1981**;3:135–142
3. Bosniak MA, Megibow AJ, Hulnick DH, Horii S, Raghavendra BN. CT diagnosis of renal angiomyolipoma: the importance of detecting small amounts of fat. *AJR* **1988**;151:497–501
4. Parvey LS, Warner RM, Callihan TR, Magill HL. CT demonstration of fat tissue in malignant renal neoplasms: atypical Wilms' tumors. *J Comput Assist Tomogr* **1981**;5:851–854

*Reply*

Dr. Prando's case nicely illustrates our contention that the appearance of fat within a neoplasm should not be considered absolutely diagnostic of benign angiomyolipoma. Considerable attention should be paid to the distribution of the fat and its relationship to surrounding structures. Dr. Prando's case differs in appearance from the case we reported because it shows perirenal fat rather than renal sinus fat entrapped within a large tumor. This renal cell carcinoma has invaded the perirenal space, sparing only irregular islands of fat, which appear to be incorporated into the tumor itself.

Although most fat-containing tumors of the kidney probably are angiomyolipomas, these sporadic cases of entrapment of perirenal and renal sinus fat by large tumors suggest that some caution be observed. Surgical intervention may be necessary in these cases.

Nancy S. Curry
*Medical University of South Carolina*
*Charleston, SC 29425*

## Pregnancy Complicated by Ovarian Torsion

A 17-year-old pregnant woman with gestational age of 31 weeks was admitted with severe pains in the left flank. The pain was sudden in onset, radiated to the back and left leg, and was associated with nausea and vomiting. No fever was present. Physical examination showed a gravid uterus, localized tenderness, and guarding in the left flank. Sonography revealed a normal fetus of 31 weeks gestation and a 2.0 × 4.5 cm homogeneous echogenic mass at the area of tenderness. Color flow Doppler imaging showed blood flow to the hilum of the mass but no flow into the mass (Fig. 1). The mass was removed surgically, and pathologic examination showed a hemorrhagic infarct in a twisted ovary.

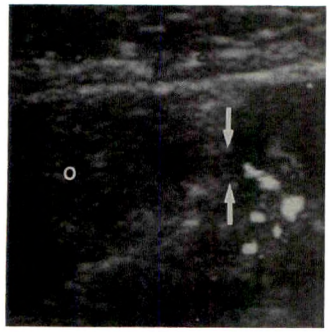



**Fig. 1.—Longitudinal color Doppler sonogram (printed here in black and white) shows base of ovary, narrow area of torsion (*arrows*) and, just to right, evidence of blood flow, which stopped at narrow segment and did not enter ovary (O).**

Pains during pregnancy may indicate torsion of a pelvic mass that is uterine or ovarian in origin or torsion of the ovary itself. Appendicitis and acute cholecystitis are other causes of acute abdominal pain in a pregnant patient. Torsion of the ovary is a surgical emergency. Preoperative diagnosis can be made on the basis of careful examination of the area of localized tenderness and demonstration of an echogenic or mixed echogenic mass with absence of blood flow on color Doppler imaging and by inducing pain over the mass by using transducer pressure.

Harry C. Press, Jr.
Hasan A. Nabhani
William E. Brown
Nathaniel G. Hagler
*Howard University Hospital*
*Washington, DC 20060*

REFERENCES

1. Graif M, Shalev J, Strauss S, Engelberg S, Mashiach S, Itzchak Y. Torsion of the ovary: sonographic features. *AJR* **1984**;143:1331–1334
2. Warner MA, Fleischer AC, Edell SL, et al. Uterine adnexal torsion: sonographic findings. *Radiology* **1985**;154:773–775
3. Helvie MA, Silver TM. Ovarian torsion sonographic evaluation. *JCU* **1989**;17:327–332
4. Hess WL, Peaceman A, O'Brien W, et al. Adnexal mass occurring with intrauterine pregnancy: report of fifty four patients requiring laboratory for definitive management. *Am J Obstet Gynecol* **1988**;158:1029–1034

## Medullary Sponge Kidney and Benign Tubular Ectasia

I commend Ginalski and his coauthors [1] on their recent article reporting a 12% frequency of medullary sponge kidney in patients with nephrolithiasis vs 1% in patients without urinary calculi. This confirms the results of earlier studies that found medullary sponge kidneys in 13% [2] and 21% [3] of patients with urolithiasis. The prevalence and importance of this entity was underestimated in earlier reports [4].

As pointed out by Ginalski et al. [1], the criteria for the diagnosis or exclusion of medullary sponge kidney are controversial. Yendt [3] thinks that this diagnosis cannot be excluded unless most caliceal fornices are outlined clearly and no ureteral obstruction is present. In a review of 53 excretory urograms of patients with nephrolithiasis, Yendt found only three that were acceptable in this regard. Yendt also thinks that ureteral compression can cause "pyelotubular backflow" and result in the false-positive diagnosis of medullary sponge kidney. Additional issues are whether the quantity of contrast media affects papillary blush and how many papillae must show tubular dilatation before the diagnosis can be made. These two criteria differed in each of the series mentioned [1–4].

The major difficulty in diagnosing medullary sponge kidney is the continuous spectrum of abnormality, ranging from the relatively common homogeneous papillary blush to the discretely dilated tubules that are pathognomonic for the diagnosis. Virtually every author who has written about this subject has commented on this problem. Most agree that the blush is "a possible minor form of medullary sponge kidney" [1] or that it may be "the mildest form of the disorder" [3]. However, almost all authors have omitted these cases of papillary blush from their series. This seems arbitrary inasmuch as Palubinskas [5] reported marked ectasia of the collecting tubules and the histologic diagnosis of medullary sponge kidney in a patient who had only a corresponding pyramidal blush on excretory urography.

In 1963 Paubinskas [5] suggested the term *benign tubular ectasia* for the radiologic finding of a homogeneous pyramidal blush. In the succeeding decade, this diagnosis was made frequently by radiologists. More recently, this terminology has fallen into disuse, and many of my younger urologic and radiologic colleagues are unfamiliar with it. Benign tubular ectasia is not even mentioned in recent articles on the subject [1–3]. The use of the term benign is supported by the findings of many authors, including Ginalski et al. [1], who found that "the frequency of blush on renal papillae was not significantly higher in the group of patients with nephrolithiasis (4%) than in the group without nephrolithiasis (3%)."

Because of the overlap between medullary sponge kidney and the more commonly seen papillary blush, and because the former diagnosis has adverse medical and insurance implications, I think the term benign tubular ectasia should be reinstated into the radiologist's lexicon. This advice can be ignored by older radiologists who never gave up use of the term.

Ferris M. Hall
*Beth Israel Hospital*
*Harvard Medical School*
*Boston, MA 02215*

REFERENCES

1. Ginalski JM, Portmann L, Jaeger Ph. Does medullary sponge kidney cause nephrolithiasis? *AJR* **1990**;155:299–302
2. Parks JH, Coe FL, Strauss AL. Calcium nephrolithiasis and medullary sponge kidney in women. *N Engl J Med* **1982**;306:1088–1091
3. Yendt ER. Medullary sponge kidney and nephrolithiasis. *N Engl J Med* **1981**;306:1106–1107
4. Palubinakas AJ. Medullary sponge kidney. *Radiology* **1961**;76:911–918
5. Palubinakas AJ. Renal pyramidal structure opacification in excretory urography and its relation to medullary sponge kidney. *Radiology* **1963**;81:963–970

*Reply*

We share Dr. Hall's opinion that the presence of papillary blush on excretory urography should not always be considered evidence for medullary sponge kidney. Indeed, our study [1] shows that the frequency of papillary blush on excretory urograms is almost identical in patients with (4%) and without (3%) nephrolithiasis, and preliminary results from another study of ours on 148 consecutive patients in which only low-osmolality contrast medium has been used seem to confirm this finding.

The proposal that the term *benign tubular ectasia* be reinstated is certainly relevant. However, we question it for the following reasons: (1) "Benign" is usually used as the opposite of "malignant," and both terms apply to pathologic conditions; however, papillary blush does not necessarily imply the presence of a pathologic process. (2) Our studies and others show only that a papillary blush is seen with equal prevalence in patients with and without nephrolithiasis. However, patients who have a blush might be particularly prone to urinary tract

infection, hematuria, or flank pain (i.e., the other signs and symptoms of medullary sponge kidney), a question that has not been answered so far. Therefore, as long as such questions remain open, "*possible* minor form of medullary sponge kidney" seems to be the most appropriate expression to qualify pyramidal blush on excretory urography.

J. M. Ginalski
*University Hospital*
*CH-1011 Lausanne, Switzerland*
Ph. Jaeger
*University Hospital-Inselspital*
*CH-3010 Berne, Switzerland*

REFERENCE

1. Ginalski JM, Portmann L, Jaeger Ph. Does medullary sponge kidney cause nephrolithiasis? *AJR* **1990**;155:299–302

## Conventional vs Color Carotid Doppler Imaging

I think that the conclusions of Steinke et al. [1] in their article on color Doppler flow imaging (CDFI) of the carotid arteries are not supported by the data presented. They used CDFI, conventional duplex Doppler imaging combined with continuous-wave Doppler, and carotid angiography to examine 60 carotid bifurcations. Interpretation of stenosis in the CDFI studies was based solely on color criteria, without using velocity spectral analysis. Among the conclusions were that CDFI is more sensitive, specific, and accurate than conventional duplex Doppler imaging for the detection of carotid stenoses and that the detection of ulcers is improved by using CDFI. I think that these conclusions are invalid for the following reasons:

First, the Subjects and Methods section contains inadequate information: (1) It is not stated if the stenosis was reduction in diameter or in cross-sectional area. I assume that diameter was used, although measurements of area more accurately reflect luminal reduction caused by eccentric plaque. (2) The gold standard is ambiguous. Selective arteriography is referred to as a "special angiographic technique," and it is unclear if nonselective studies were used to assess accuracy of the Doppler examinations. (3) The color Doppler image is described as representing peak frequency. It represents average frequency. (4) The category of disease called subtotal stenosis is not defined, but presumably represents exceedingly slow flow or impending occlusion because of a pinpoint stenosis (>90% reduction in diameter). (5) The criteria for diagnosis of a high-grade stenosis (81–90% stenosis) based on CDFI findings include marked color fading (Table 1). Figure 1 shows a study with "marked color fading" but only a minor stenosis (40%) on the arteriogram. This discrepancy is not explained, and Table 3 does not reveal a patient with a minor angiographic stenosis that was called severe on the basis of CDFI findings.

Second, the presentation of the results is misleading. (1) Categories of disease of 40–60% stenosis (10 patients), 60–80% stenosis (seven patients), 80–90% stenosis (eight patients), subtotal stenosis (four patients), and occlusion (10 patients) are described. Although in the first three categories, CDFI findings matched the angiographic findings in one additional patient compared with those of conventional Doppler imaging, the extremely small number of patients makes this difference insignificant. However, all four cases of subtotal stenosis were missed when CDFI was used but were detected with conventional Doppler imaging. This last category is not included in the calculation of sensitivity, specificity, and accuracy in Table 4. If surgical disease were considered to be stenosis greater than 80%, then 7/12 were detected with CDFI (sensitivity = 58%) and 10/12 with conventional Doppler imaging (sensitivity = 83%). It could be concluded from this that CDFI is an inferior technique for screening patients with surgical disease of the carotid artery, and particularly for screening those patients at highest risk of stroke, those with impending occlusion. Furthermore, published series [2, 3] with much larger numbers of patients have shown sensitivities and specificities of greater than 90% for the detection of surgical carotid disease when conventional Doppler imaging was used. (2) The conclusion that CDFI provides improved identification of ulcers is unsupported. The article does not compare the diagnosis of ulcer by CDFI vs gray-scale imaging, and no data are presented that compare the sonographic diagnosis with a gold standard such as the arteriogram or, more importantly, the pathologic diagnosis of ulcer [4].

For these reasons, the article by Steinke et al. does not substantiate the claim that CDFI is advantageous compared with conventional Doppler sonography.

David Sacks
*Reading Hospital*
*West Reading, PA 19603*

REFERENCES

1. Steinke W, Kloetzsch C, Hennerici M. Carotid artery disease assessed by color Doppler flow imaging: correlation with standard Doppler sonography and angiography. *AJNR* **1990**;11:259–266, *AJR* **1990**;154:1061–1068
2. Robinson ML, Sacks D, Perlmutter GS, Marinelli DL. Diagnostic criteria for carotid duplex sonography. *AJR* **1988**;151:1045–1049
3. Bluth EI, Stavros AT, Marich KW, Wetzner SM, Aufrichtig D, Baker JD. Carotid duplex sonography: a multicenter recommendation for standardized imaging and Doppler criteria. *RadioGraphics* **1988**;8:487–506
4. Eikelboom BC, Riles TR, Mintzer R, et al. Inaccuracy of angiography in the diagnosis of carotid ulceration. *Stroke* **1983**;14:882–885

*Reply*

We appreciate Dr. Sacks's careful reading of our article [1] but we were disappointed that his criticism focuses on only one sixth of the material presented, the findings of 60 angiographically examined carotid arteries. Because we and others such as Dr. Eikelboom think that angiography is not the gold standard but merely one among several imaging techniques, we did not limit our comparison of color Doppler flow imaging (CDFI) to angiography but expanded it to include standard sonographic techniques [2, 3] in our series of 360 arteries. We are puzzled by Dr. Sacks's claim that we thought that CDFI is "advantageous." We merely stated that it "preserves the advantages of conventional Doppler sonography and duplex sonography, but also provides important additional diagnostic information."

The local degree of stenosis in our study was determined from longitudinal and transverse luminal narrowing due to the plaque (stated in the Subjects and Methods section). The extent of the lesion and the tissue characteristics as revealed by CDFI were confirmed by the pathologic findings in 13 patients who had carotid endarterectomy [4]; these included suspected thrombosis, plaque hemorrhage, and four ulcerative plaques.

We were intrigued to find that four examples of "pseudoocclusions" were misdiagnosed with CDFI. We took special effort to define, extensively reference (references 28–32 in [1]), and deal separately with subtotal stenosis rather than mix it with high-grade (81–90%) stenosis. Dr. Sacks's reference to a "special angiographic technique" is unclear to us as we described in detail and referenced in the discussion the study by Countee and Vijayanathan (reference 29 in [1]). Further, we stated in the Subjects and Methods section that only selective intraarterial angiograms were used for comparison (Figs. 1–4 and Figs. 6–8).

Although Dr. Sacks read that velocity spectral analysis was used in the study, we actually used peak flow velocity from the separate

Doppler spectrum analyses rather than "average frequency" (Subjects and Methods, Table 1) for classification of the degree of stenosis, which relied on five criteria rather than on one single parameter. As stated in Table 1 and Figure 1, a particular feature of a low-grade stenosis was the long-segment color fading only during systole without associated turbulence and a peak systolic flow velocity between 4 and 8 kHz.

We recognized that statistical analysis of the four subtotal stenoses would have been inadequate and regret to have to point out that Dr. Sacks's recalculation is incorrect, as each of the angiographically diagnosed stenoses of 81–91% was detected with CDFI (rather, n = 8 than n = 7). Despite Dr. Sacks's claim, patients with high-grade stenosis are not at "highest risk of stroke," as has been shown in several prospective follow-up studies of asymptomatic patients with extracranial arterial disease (for review, see [5]). Today, only those asymptomatic patients with progression of stenosis can be accepted as having a poor prognosis [6].

W. Steinke
*Columbia University, Neurological Institute*
*New York, NY 10032*
M. Hennerici
*University of Heidelberg, Klinikum Mannheim*
*D-6800 Mannheim 1, Germany*

REFERENCES

1. Steinke W, Kloetzsch C, Hennerici M. Carotid artery disease assessed by color Doppler flow imaging: correlation with standard Doppler sonography and angiography. *AJR* **1990**;154:1061–1068
2. Hennerici M, Reifschneider G, Trockel U, Aulich A. Detection of early atherosclerotic lesions by duplex scanning. *JCU* **1984**;12:455–464
3. Hennerici M, Neuerburg-Heusler D. *Gefaessdiagnostik mit Ultraschall*. New York: Thieme Verlag, **1988**
4. Glagov S, Zarins CK. Quantitating atherosclerosis: problems of definition. In: Bond MG, Insull W, Glagov S, Chandler AB, Cornhill JF, eds. *Clinical diagnosis of atherosclerosis*. Stuttgart: Springer-Verlag, **1983**
5. Hennerici M, Aulich A, Freund H-J. Carotid system syndromes. In: Vinken PJ, Bruyn GW, Klawans HL, Toole JF, eds. *Handbook of clinical neurology*, revised series 54. New York: Elsevier, **1989**:291–337
6. Hennerici M, Hülsbömer H-B, Hefter H, Lammerts D, Rautenberg W. Natural history of asymptomatic extracranial arterial disease: results of a long-term prospective study. *Brain* **1987**;110:777–791

## Doppler Nomenclature, A New Frontier

With the advent of spectral and color abdominal Doppler technology, sonographers are entering a new area of investigation: hemodynamics. As we proceed, new terminology is coined, and old terminology is adapted to new applications.

Ralls's article [1], "Color Doppler Sonography of the Hepatic Artery and Portal Venous System," is a beautifully illustrated compilation of vascular pathologic changes. Ralls refers to increased arterial flow relative to portal venous flow in a diseased liver. He calls this "arterialization" of hepatic perfusion. An arterial flow pattern is characterized by systolic peaks and slower diastolic flow. When considering a flow pattern to be arterialized, I prefer to reserve this term for those vessels that normally do not manifest a systolic/diastolic waveform. Specifically, when an arteriovenous fistula occurs, and systolic peaks are identified in the venous circulation, this flow pattern should be described as arterialized. I propose that this is a more appropriate use of the term. When referring to severe liver disease and its hemodynamic alterations, I prefer the term "arterial dominant perfusion." Admittedlly, this is an issue of nomenclature. I think, however, that now is the time to standardize the basic terminology.

Myron A. Pozniak
*University of Wisconsin, Clinical Science Center*
*Madison, WI 53792*

REFERENCE

1. Ralls PW. Color Doppler sonography of the hepatic artery and portal venous system. *AJR* **1990**;155:517–525

*Reply*

I appreciate Dr. Pozniak's interest in and kind remarks on "Color Doppler Sonography of the Hepatic Artery and Portal Venous System" [1]. As new techniques and new observations occur in imaging, new terminology is required. The primary rule for the usage of such terminology should be clarity. The term "arterialization" of hepatic perfusion is defined clearly in my article. I used arterialization because I thought it best described the color Doppler appearance encountered in clinical situations. The arterialization pattern may occur in other clinical conditions, including certain types of hepatitis and vascular lesions such as hereditary hemorrhagic telangiectasia. Dr. Pozniak's suggested term, "arterial dominant perfusion," is more mechanistic than descriptive. When a finding on an image may have many causes, I prefer descriptive nomenclature. I am willing to support or participate in any effort to standardize the basic terminology of Doppler sonography. Until such standardization occurs, however, usage will remain the ultimate arbiter of appropriate nomenclature.

Philip W. Ralls
*University of Southern California, School of Medicine*
*Los Angeles, CA 90033*

REFERENCE

1. Ralls PW. Color Doppler sonography of the hepatic artery and portal venous system. *AJR* **1990**;155:517–525

## High-Velocity Jets from 5-French Catheters

Daniel et al. [1] and Hansen et al. [2] deserve much credit for addressing the timely topic of high-velocity jets from miniature angiographic catheters. Recent trends toward performing procedures on an outpatient basis have resulted in a proliferation of "high-flow" 5-French and smaller catheters, with a wide variety of hole sizes and numbers. The catheters are promoted for their alleged safety at the puncture site and their ability to deliver a large volume of contrast material, but due attention is not given to the problem of the high-velocity jets created.

As the authors [1, 2] have pointed out, the delivery of contrast material from small catheters can be quite uneven, with as much as eight times the volume of material emanating from the end hole as from a proximal side hole. Their solution to this problem is to reduce the sizes of the end and side holes. This does result in a more even flow profile. However, the problem with this solution is that the velocity of the jet is inversely proportional to the square of the diameter of the hole, and the pressure necessary to stagnate the jet is proportional to the square of the velocity. Therefore, as the diameter of the hole is decreased, the velocity of the jet and the pressure generated both increase.

By extracting data from Figures 4 and 7 in the paper by Daniel et al., we were able to estimate the effect of changing the end hole and 10 side holes from 0.035 in. (0.089 cm) each to 0.018 in. (0.046 cm) for the end hole and 0.015 in. (0.038 cm) for the side holes. At 25 ml/sec, the flow velocity from the end hole increases from 1240 to 1400 cm/sec. The flow velocity from a distal side hole increases from 560 cm/sec to 2400 cm/sec.

What are the dynamic pressures experienced by the vessel wall with jets of these velocities? The answer depends partly on the proximity of the catheter to the wall, as the blood also will stagnate the jet. For velocities in this range, the jet can be considered to have a constant peak velocity within a distance equal to five times the diameter of the hole or 2–4 mm in this case. It is not unreasonable

to assume that the catheter could be this close to the vessel wall at some point during the injection. The pressure dissipated by the wall is equal to one half the density of the contrast material times the velocity squared.

The pressure that must be dissipated in the example given here increases from 750 mm Hg to 960 mm Hg at the end hole and from 160 mm Hg to 2800 mm Hg at the distal side hole, as the diameters of the holes are reduced. For comparison, we measured the flow rates and calculated dynamic pressures for a 7.1-French pigtail catheter with 12 0.040-in. (0.102 cm) side holes and a 0.038-in. (0.097 cm) end hole. At 25 ml/sec, the dynamic pressure near the end hole is only 46 mm Hg, and the pressure near the side hole is 30 mm Hg.

This large difference in pressures is more than just an interesting physics problem. Two years ago we experienced four aortic subintimal injections with a particular brand of 5-French pigtail catheter that had small side holes. The injection rates were between 15 and 20 ml/sec. We assumed that the problem was related to the velocity of the jet from the end hole. After testing various 5-French catheters, we chose a brand with more and larger side holes, and we have had no further problems.

We hope that the article by Daniel et al. and this letter will stimulate catheter manufacturers to consider this problem, and lead to the design of safer catheters.

David L. Marinelli
*Baystate Medical Center*
*Springfield, MA 01199*
Robert Kirchhoff
*University of Massachusetts*
*Amherst, MA 01003*

REFERENCES

1. Daniel TB, Akins EW, Hawkins IF Jr. A solution to the problem of high-flow jets from miniature angiographic catheters. *AJR* **1990**;154:1091–1095
2. Hansen EC, Hawkins MC, Hawkins IF Jr, Akins EW, Miles SG, Collela JP. New high-flow "cloud" catheter for safer delivery of contrast material. *Radiology* **1989**;173:461–464

*Reply*

We thank Drs. Marinelli and Kirchhoff for their comments on our paper [1]. They point out the physical parameters related to the sizes of the end and side holes in angiographic catheters and the theoretical velocities of the jets of contrast material delivered by such catheters. Although we have not experienced any extravasation related to the small side holes we engineered for our test catheter, this certainly could be a problem, and we are working on it.

With the "cloud" catheter, during low-pressure test injections, most of the contrast material emanates from the first large side holes, although distribution from each side hole is equal during the high-pressure injection [2]. The purpose of the study by Daniel et al. [1] was to prove again experimentally that flow from the last several side holes was excessive. During the study, however, it was found that a catheter with multiple small side holes produced a flow profile closest to that produced by the cloud catheter. No question exists that extensive flow from the last hole not only increases the danger of extravasation but also results in a relatively poor aortogram. Also, if end-hole flow from a catheter with a large end hole is compared with equal flow from a catheter with a small end hole, the velocity and momentum of the flow, which translate to force, definitely are increased in the catheter with a small end hole. The cloud catheter was designed to reduce the 34% flow from the end hole to approximately 5–10%. This, by our calculations, reduces the force by approximately 2.5.

We have tested catheter-induced damage in a gelatin model. If a cloud catheter is embedded in gelatin and high-pressure injections are made with methylene blue–colored contrast medium, the penetration of the medium into the gelatin is about 2 cm for each of the side holes. At a flow rate of 17 ml/sec, disruption of the gelatin occurs with all catheters. The disruption occurs equally with both large and small side holes. For this reason, we currently are developing a new catheter that we hope will prevent this potential problem. Disruption is probably important only in the case of extremely soft plaque, which can be dislodged easily.

The main point of our paper [1] was that most extravasations are due to excessive flow out of the end hole of the catheter, which inadvertently can be touching a small vessel or be lodged in the wall of the artery. Thus, if flow from the end hole is reduced, and the side holes fill uniformly, it is more likely that the catheter will rest within the center of the vessel. Further work in this area clearly is needed.

Timothy B. Daniel
E. William Akins
Irvin F. Hawkins, Jr.
*University of Florida, College of Medicine*
*Gainesville, FL 32610-0374*

REFERENCES

1. Daniel TB, Akins EW, Hawkins IF Jr. A solution to the problem of miniature high-flow angiographic catheters. *AJR* **1990**;154:1091–1095
2. Hansen EC, Hawkins MC, Hawkins IF Jr, Akins EW, Miles SG, Collela JP. New high-flow "cloud" catheter for safer delivery of contrast material. *Radiology* **1989**;173:461–468

## Isolated Thrombosis of Left-Sided Vena Cava

Knowledge of vascular anomalies can prevent their confusion with pathologic masses. Bilateral vena cava is an incidental finding on CT scans in approximately 0.3% of cases [1]. We recently saw a patient in whom an isolated thrombus in the left side of a duplicated system was mistaken at first for adenopathy.

A 62-year-old woman had atypical pain in the right upper quadrant. The results of physical examination, laboratory tests, sonography of the gallbladder, and upper and lower gastrointestinal series were normal. CT of the abdomen showed a left paraaortic mass that extended from the renal hilus to the aortic bifurcation (Fig. 1A). Smaller retroperitoneal nodes were also evident. Biopsy of the mass revealed clot and atypical lymphocytes. The patient became less symptomatic with time and without specific treatment. Subsequent CT scans

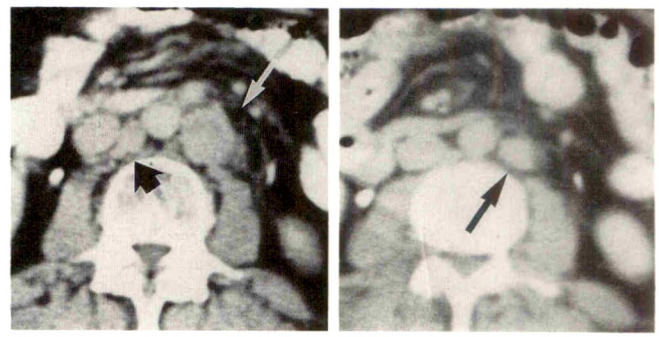



**Fig. 1.—Isolated thrombosis of left-sided vena cava.**
***A*, Initial CT scan shows 1-cm aortocaval node (*black arrow*) and 2.5-cm left-sided paraaortic structure (*white arrow*).**
***B*, CT scan obtained 6 months after *A* shows aortocaval node is smaller and left-sided paraaortic structure (*arrow*) is tubular and enhances homogeneously.**

showed that the mass was decreasing in size. A CT scan of the abdomen obtained 6 months after the initial presentation showed a smooth, enhancing, tubular structure extending from the left renal vein to the bifurcation, consistent with a vascular structure, that is, left-sided vena cava (Fig. 1B).

CT criteria for venous thrombosis have been described: enlargement of the thrombosed vein, a low-density central lumen, and a sharply defined enhancing wall [2]. In our case, the central hypodensity was confused with necrosis. Associated retroperitoneal adenopathy also delayed recognition of this thrombosed vascular anomaly, which has not been reported previously.

Jeffrey C. Allard
H. Scott Harris
*University of Miami School of Medicine*
*Miami, FL 33101*

REFERENCES

1. Mayo J, Gray R, St Louis E, Grossman H, McLoughlin M, Wise D. Anomalies of the inferior vena cava. *AJR* **1983**;140:339–345
2. Zerhouni EA, Barth KA, Siegelman SS. Demonstration of venous thrombosis by computed tomography. *AJR* **1980**;134:753–758

Letters are published at the discretion of the Editor and are subject to editing.

Letters to the Editor must not be more than two *double-spaced*, typewritten pages. One or two figures may be included. Abbreviations should not be used. See Author Guidelines, page A5.

Material being submitted or published elsewhere should not be duplicated in letters, and authors of letters must disclose financial associations or other possible conflicts of interest.

Letters concerning a paper published in the *AJR* will be sent to the authors of the paper for a reply to be published in the same issue. Opinions expressed in the Letters to the Editor do not necessarily reflect the opinions of the Editor.

# News

## Stereotactic Breast Biopsy

Stereotactic Breast Biopsy will be presented April 1–3 at the Inn at Aspen, Aspen CO. Topics will include percutaneous breast biopsy, covering core and cytologic sampling, mammography, and breast cancer. Course director: David G. Bragg. Category 1 credit: 8 hr. Information: Office of Continuing Medical Education, School of Medicine, Health Sciences Center, University of Utah, Salt Lake City, UT 84132; telephone: (801) 581-8664; fax: (801) 581-3647.

## Oncologic Imaging of Endocrine Gland Tumors

The Dept. of Diagnostic Imaging, Regina Elena Institute for Cancer Research, Rome, Italy, will present G.RA.D.O.4, an international meeting on oncologic imaging of endocrine gland tumors, May 9–10, at the Aula delle Conferenze C.N.R., National Research Center, Rome. The meeting will provide a clinically oriented review and analysis of current and future applications of diagnostic imaging of endocrine gland tumors. Specific topics will include tumors of the pituitary, thyroid, parathyroid, and adrenal glands and of the pancreas. Congress director: Saverio Squillaci. Congress secretary: Luigi Tipaldi. Faculty: D. J. Allison, P. Andreani, F. Todua, C. B. Higgins, J. Doppmann, H. Newton, U. Salvolini, and L. Bozzao. Fee: $100. Information: Luigi Tipaldi, M.D., Instituto Regina Elena, Radiologia e diagnostica per immagini, Viale Regine Elena, 291, 00161 Roma, Italia; telephone: 06/4985207 or 06/4985256; fax: 06/4452337.

## Yale Clinical MRI

The Dept. of Radiology, Yale University School of Medicine, will offer Yale Clinical MRI, May 20–22, at the Yale–New Haven Hospital MRI Center. Topics will include neurologic, musculoskeletal, and abdominal application of MR imaging. Enrollment will be limited to 20 persons. Course director: Ruben Kier. Category 1 credit: 21.5 hr. Fee: physicians, $550; residents, fellows, and technologists, $400. Information: Office of Post-Graduate & Continuing Medical Education, Yale University School of Medicine, 333 Cedar St., P. O. Box 3333, New Haven, CT 06510; (203) 785-4578.

## Yale Symposium on Duplex and Color Doppler Ultrasound

Yale Symposium on Duplex and Color Doppler Ultrasound will be held May 23–24 at Yale University, New Haven, CT. Course directors: Kenneth J. W. Taylor and Lynwood W. Hammers. Guest speakers: Brian L. Thiele and John Cronen. Category 1 credit: 15 hr. Fee: physicians, $350; sonographers and residents, $250. Information: call Lucille Marturano at (203) 785-4734.

## Mammography and the Search for Breast Cancer

Wende Logan-Young and the Rochester Roentgen Ray Society are sponsoring Mammography and the Search for Breast Cancer, July 12–13, in Rochester, NY. The course will address all aspects of screen-film mammography and other investigative procedures essential to early accurate diagnosis of breast cancer. Fee: physicians, $350; residents, $250. Information: Wende Logan-Young, M.D., 1351 Mt. Hope Ave., Rochester, NY 14620; (716) 442-8432.

## Alaska 91—Cruise the Inland Passage—Magnetic Resonance Imaging at Sea

J. Bruce Kneeland, an authority on musculoskeletal imaging, will present Alaska 91—Cruise the Inland Passage—Magnetic Resonance Imaging at Sea, July 14–21. The course will include lectures, discussions, and case analysis. Category 1 accreditation is pending. Fee (through April 12/after April 12): physicians, $450/$495; residents, interns, nurses, and technologists, $350/$395 (letter required). Information: ALASKA 91–MRI at Sea, Medical Seminars International, Inc., 18981 Ventura Blvd., Ste. 303, Tarzana, CA 91356; telephone: (818) 774-9077; fax: (818) 774-0244.

## Contemporary Diagnostic Imaging

The Dept. of Radiology, Stanford University Medical Center, Stanford, CA, will present Contemporary Diagnostic Imaging Featuring MRI, CT, US and Interventional Radiology, July 29–Aug. 2, at the Ritz-Carlton Hotel, Aspen, CO. The meeting will be held during the Aspen Music Festival. Program director: Brooke Jeffrey. Program chairman: Gary Glazer. Category 1 credit: 20 hr. Fee: physicians, $515; residents, fellows, and technologists, $325. Information: Dawne Ryals, Ryals & Associates, P. O. Box 1925, Roswell, GA 30077-1925; telephone: (404) 641-9773; fax: (404) 552-9859.

## Body Imaging

Lovelace Medical Center, Santa Fe, NM, will present Body Imaging: Ultrasound, CT, MR, Nuclear Medicine, Aug. 5–9, at the El Dorado Hotel, Santa Fe. Program director: Robert W. Jahnke. Guest faculty:

George R. Leopold, R. Brooke Jeffrey, Robert J. Herfkens, David J. Sartoris, N. Reed Dunnick, Joel Lipman, and Michael F. Hartshorne. Information: Dawne Ryals, Ryals & Associates, P. O. Box 1925, Roswell, GA 30077-1925; telephone: (404) 641-9773; fax: (404) 552-9859.

## Imaging of the Head, Spine, and Musculoskeletal System

The Medical College of Wisconsin will present Imaging the Head, Spine, and Musculoskeletal System: A Discussion of Protocols and Applications, Aug. 12–16, at the Chateau Whistler Resort, Whistler, B.C. Topics will include imaging of the brain, spine, knee, shoulder, and temporomandibular joint; brain cutting; and spinal anatomy. Program chairmen: Victor Haughton, Robert Quencer, Thomas Naidich, and Joachim Seeger. Category 1 credit: 25 hr. Fee: through June 30, $445; after June 30, $495. Information: Marti Carter, CME, Inc., 11011 W. North Ave., Milwaukee, WI 53226; (414) 771-9520.

## Radiology for Clinicians

The Dept. of Radiology, University of California, San Diego School of Medicine, will present Radiology for Clinicians, Aug. 12–16, at the Hotel Del Coronado, Coronado (San Diego), CA. The course, which is intended for nonradiologists, will provide state-of-the-art information on the role of diagnostic imaging and interventional procedures in the evaluation and treatment of patients. A faculty of expert subspecialists will outline the status of the most important services provided by diagnostic radiologists in both hospital and outpatient settings. The goal is to provide clinicians with the information needed to request and evaluate imaging and interventional procedures. Program director: David S. Feigin. Category 1 credit: pending. Fee: physicians, $400; residents, fellows, and technologists, $250. Information: Dawne Ryals, Ryals & Associates, P. O. Box 1925, Roswell, GA 30077-1925; telephone: (404) 641-9773; fax: (404) 552-9859.

## Society of Computed Body Tomography Summer Practicum

The Summer Practicum of the Society of Computed Body Tomography will be held at the Keystone Resort, Keystone, CO, Aug. 18–22. Lectures, case presentations, and workshops will provide updated, useful information on CT and MR imaging of the body, including anatomy, techniques, and interventional procedures. Category 1 credit: 25 hr. Fee (through July 19/after July 19: physicians, $500/$550; residents and fellows, $400/$450. Information: Society of Computed Body Tomography, c/o Matrix Meetings, Inc., Barbara McLeod, Meeting Manager, P. O. 1103, Rochester, MN 55903; (507) 288-5620.

## Diagnostic Imaging Update

The Stanford Medical Center, Stanford, CA, will present Diagnostic Imaging Update: MRI, CT, US, and Interventional, Aug. 26–30, at the Hotel Vancouver, Vancouver, B.C. The course will address areas in neuroradiology, abdominal and musculoskeletal imaging, obstetric and gynecologic sonography, and interventional radiology. Specific topics will include diagnostic advances in cerebral and spinal MR imaging, new techniques in body MR imaging, pediatric musculoskeletal imaging, imaging of the acute abdomen, and abdominal and thoracic interventions. Program chairman: Gary M. Glazer. Program director: R. Brooke Jeffrey. Category 1 credit: 19.5 hr. Fee: physicians, $540; residents, fellows, and technologists, $350. Information: Dawne Ryals, Ryals & Associates, P. O. Box 1925, Roswell, GA 30077-1925; telephone: (404) 641-9773; fax: (404) 552-9859.

## Picture Archiving and Communication System in Medicine

The North Atlantic Treaty Organization (NATO) Advanced Study Institutes sponsored a 2-week workshop, Picture Archiving and Communication System [PACS] in Medicine, in Evian, France, Oct. 14–26, 1990. Ninety-two participants, including 20 lecturers, from 15 countries (Austria, Belgium, Canada, France, Germany, Greece, Italy, Luxemburg, Netherlands, Portugal, Sweden, Switzerland, Turkey, the United Kingdom, and the United States) attended the workshop. Participants from the United States included representatives from the American College of Radiology; the National Institutes of Health; and the Army, Navy, and Air Force Surgeon Generals' Offices.

The scientific program was organized into four categories. The first category was PACS components and system integration. Topics included image acquisition; workstations; data storage; networking; interfacing between hospital information systems, radiology information systems, and PACS; clinical reports; American College of Radiology/National Electronics Manufacturers' Association standards; databases; and system integration and reliability. The second category was PACS and related research in various countries and by various manufacturers. Invited lecturers who are responsible for major PACS research and development summarized the current status, including technical, administrative, and financial aspects. The third category was clinical experience and research support. Representatives from the University of Pennsylvania, Hokkaido University (Japan), Georgetown University, and University of California, Los Angeles, presented their clinical experience. Two major PACS funding sources in the United States are the National Institutes of Health and the U. S. Armed Forces. The program directors of these two governmental agencies presented the current PACS funding situations. The last category was the participants' short scientific communications. In addition, three workshops on data security, image quality and perception, and cost analysis and two demonstrations on radiologic literature search and receiver-operating-characteristics software packages were presented.

## RSNA 1991 Officers and Board of Directors

The Radiological Society of North America installed the following officers during its annual meeting in Chicago, Nov. 25–30, 1990: Carl J. Zylak, president; Robert G. Parker, president-elect; Lee F. Rogers, first vice-president; James D. Cox, second vice-president; Gary T. Barnes, third vice-president; and William R. Eyler, historian. Thomas S. Harle was installed as chairman of the board of directors, and David B. Fraser was elected to a position on the board. Other members of the current board are O. Wayne Houser, Helen C. Redman, Ernest J. Ferris, Michael A. Sullivan, Carl J. Zylak, and Robert G. Parker.

## The American Board of Radiology Examinations

Written examinations for the American Board of Radiology (ABR) are scheduled for Oct. 3–4. Oral examinations will be held at the Executive West Hotel in Louisville, KY, June 3–7. The ABR will accept applications for admission to the examinations after July 1, but not later than Sept. 30, in the year *preceding* the year in which

the examination is to be taken. For application forms and further information: Office of the Secretary, The American Board of Radiology, 300 Park, Ste. 440, Birmingham, MI 48009.

## Meeting and Course Review

For the reader's convenience, a summary of upcoming meetings and courses is provided. Detailed listings are given in the *AJR* issue given in parentheses.

**Cyanoacrylate Embolization Course,** times arranged, Baltimore (July 1990)
**Visiting Fellowships in Ultrasound,** times arranged, Baltimore (Aug 1990)
**Visiting Fellowships in Interventional Radiology,** times arranged, Baltimore (Oct 1990)
**Swallowing Center Preceptorship,** times arranged, Baltimore (Jan)
**Imaging Fellowship,** times arranged, Miami Beach, FL (Jan)
**MR Imaging Fellowships at LAC/USC Imaging Science Center,** April 1–5, May 6–10, June 3–7, Aug. 5–9, Sept. 16–20, Oct. 7–11, and Nov. 4–8, Los Angeles (Feb)
**Ultrasound 1991,** April 2–5, Boston (Nov 1990)
**National Council on Radiation Protection and Measurements Annual Meeting,** April 3–4, Washington, DC (Nov 1990)
**Neonatal Neurosonography,** April 4–5, Philadelphia (March)
**CT Symposium,** April 5–6, Madison, WI (Jan)
**Differential Diagnosis in Radiology,** April 6–8, Ann Arbor, MI (Jan)
**Joint American-European Course in Davos,** April 7–12, Davos, Switzerland (March)
**General Radiology Review Course,** April 7–12, Santa Monica, CA (March)
**MRI Fellowships at Johns Hopkins,** April 8–12 and June 17–21, Baltimore (Oct 1990)
**Fetal Assessment Practicum,** April 8–12, Baltimore (Feb)
**Ultrasound in Obstetrics and Gynecology,** April 10–12, Ann Arbor, MI (Feb)
**Society for Magnetic Resonance Imaging Annual Meeting,** April 13–17 (Nov 1990)
**Skeletal Radiology Course,** April 13–18, Scottsdale, AZ (Feb)
**Society of Computed Body Tomography Annual Course,** April 15–19, Washington, DC (Feb)
**Fundamentals of Medical Ultrasonics,** April 17–19, London (March)
**San Diego Residents' Radiology Review Course,** April 21–26, La Jolla, CA (Dec 1990)
**Clinical Nuclear Medicine 1991,** April 22–25, Boston (Nov 1990)
**Practicum in Diagnostic Ultrasound,** April 22–26, Baltimore (Oct 1990)
**Obstetrics and Gynecology,** April 22–26, Philadelphia (Dec 1990)
**Radiation Oncology Clinical Research Seminar,** April 25–27, Gainesville, FL (March)
**New Orleans Radiology Society Spring Roentgen Conference,** April 25–28, New Orleans (March)
**Symposium on Diagnostic Ultrasound,** April 26–28, New York City (March)
**Introduction to Interventional Radiology,** April 27, La Jolla, CA (Dec 1990)
**Radiology Review Course,** April 28–May 3, Miami Beach, FL (Feb)
**Abdominal Ultrasound,** April 29–May 2, Philadelphia (March)
**Prostate Ultrasound,** May 3, Philadelphia (March)
**International Radiopharmaceutical Dosimetry Symposium,** May 7–10, Oak Ridge, TN (Jan)
**Thoracic Imaging 1991,** May 13–17, Toronto (Jan)
**Leading Edge in Diagnostic Ultrasound,** May 16–17, Atlantic City, NJ (March)
**Mammographic Interpretation: A Practical Approach,** May 20–23, Sept. 23–26, and Oct. 28–31, Boston (March)
**Sonography Symposium,** May 24–25, Nashville, TN (Feb)
**International Pediatric Radiology '91,** May 27–31, Stockholm (March)
**American College of Cryosurgery Annual Meeting,** June 6–10, La Jolla, CA (March)
**Contemporary Medical Imaging VIII,** June 19–23, Destin, FL (Feb)
**Advanced Techniques in MRI,** June 22–28, Kiawah Island, SC (March)
**Leeds Gastroenterology Course for Radiologists,** July 1–5, Leeds, England (Dec 1990)
**International Congress of Radiation Research,** July 7–12, Toronto (May 1990)
**Neuroradiology in the Rockies,** July 7–12, Snowmass at Aspen, CO (Feb)
**Advances in Gastroenterology,** July 15–19, Coronado (San Diego), CA (March)
**Radiology for the Non-Radiologist,** July 18–21, Coronado (San Diego), CA (March)
**Issues in Musculoskeletal Imaging and Magnetic Resonance Imaging,** July 22–27, Laguna Niguel, CA (March)
**World Congress in Ultrasound,** Sept. 1–6, Copenhagen (Sept 1990)
**International Workshop on Hypertrophic Osteoarthropathy,** Sept. 8–11, Dubrovnik, Yugoslavia (Jan)
**European Society of Gastrointestinal Radiologists Annual Meeting,** Sept. 8–11, Oxford, England (March)
**European Congress of Radiology 1991,** Sept. 15–20, Vienna, Austria (Oct 1990)

*AJR* carries announcements of courses, symposia, and meetings of interest to its readers if received a minimum of 5 months before the event. There is no charge; receipt of items by the *AJR* Editorial Office is not acknowledged. Submit items for publication typed double-spaced. Provide title, date, location, brief description, sponsor, course directors, fees, category I credit, and address and telephone number for additional information. Faculty from the host institution will not be listed. Guest faculty names will appear **only** if initials are provided. Mail news items to *AJR* Editorial Office, 2223 Avenida de la Playa, Suite 103, La Jolla, CA 92037-3218.

# Review of Current Literature

Initials and addresses of corresponding authors are provided in parentheses for each article so that the reader can obtain reprints directly. Abstracts are printed verbatim from each journal.

## The New England Journal of Medicine

**Prevalence of the human immunodeficiency virus among university students.** Gayle HD, Keeling RP, Garcia-Tunon M, et al. (HDG, Division of HIV/AIDS (MS E50), Centers for Disease Control, Atlanta, GA 30333). *N Engl J Med* 323(22):1538–1541, Nov. 1990

*Background and Methods.* To estimate the magnitude of the human immunodeficiency virus (HIV) epidemic among university students, we conducted a blinded HIV-seroprevalence survey at 19 universities throughout the United States. HIV-antibody testing was performed on blood collected for routine medical purposes at the student health centers of the participating institutions. At each campus, from 250 to 1000 blood specimens were collected consecutively and tested for HIV antibodies by enzyme-linked immunosorbent assay and Western blot analysis. Nonidentifying demographic data were linked with the test results.

*Results.* Of 16,863 specimens in the sample, 30 (0.2 percent) were positive for antibodies to HIV. Positive specimens were found at 9 of the 19 schools. All were from students over 18 years old; 19 (63 percent) were from students over 24. All but 2 of the 30 infected students were men. The seroprevalence rate for men was 0.5 percent (95 percent confidence interval, 0.3 to 0.7), and for women it was 0.02 percent (95 percent confidence interval, 0.002 to 0.066). Seroprevalence increased with age—from 0.08 percent (95 percent confidence interval, 0.04 to 0.15) for students 18 to 24 years old to 1.0 percent (95 percent confidence interval, 0.2 to 2.9) for those 40 or older.

*Conclusions.* HIV infection is present on U.S. university campuses, although the rate appears to be far lower than that of populations known to be at high risk. The potential clearly exists, however, for the further spread of HIV infection in this population, and preventive measures are needed.

## Chest

**Atypical presentations of *Pneumocystis carinii* pneumonia in patients receiving inhaled pentamidine prophylaxis.** Edelstein H, McCabe RE (HE, Veterans Administration Medical Center, Martinez, CA). *Chest* 98:1366–1369, Dec. 1990

Inhaled pentamidine is used commonly to prevent *Pneumocystis carinii* pneumonia (PCP) in patients with advanced human immunodeficiency virus infection. Case reports indicate that PCP can recur in patients who receive inhaled pentamidine and that clinical features may be atypical. To determine the magnitude of this problem, we reviewed retrospectively the medical records of patients with proven PCP during a 30-month period at two hospitals. Four (31 percent) of 13 patients with previous PCP who received inhaled pentamidine prophylaxis had recurrent *P carinii* infection, including one patient with widely metastatic extrapulmonary disease. Chest roentgenographic findings included cavities, pneumothoraces, bilateral and upper lobe interstitial infiltrates, and pleural effusion. False-negative bronchoaveolar lavage and induced sputum examinations were frequent. We conclude that recurrent PCP in patients maintained on a regimen of inhaled pentamidine prophylaxis occurs frequently, causes chest roentgenographic abnormalities other than interstitial infiltrates, and may be difficult to diagnose. Clinicians who choose to use this effective and convenient mode of prophylaxis should be aware of the problems attendent to its use.

## Gastroenterology

**Antroduodenal motility studied by real-time ultrasonography: effect of enprostil.** Hausken T, Ødegaard S, Berstad A (TH, Dept. of Medicine, Section of Gastroenterology, Haukeland Hospital, Bergen, Norway). *Gastroenterology* 100:59–63, 1991

Transabdominal real-time ultrasonography was used to investigate antroduodenal motility effects of the prostaglandin $E_2$ analogue enprostil. Ten healthy subjects were studied on two separate days, once after oral administration of one capsule of enprostil 35 $\mu$g 1 hour before the ingestion of 500 mL of meat soup and once without drug administration before the meal. The ultrasound probe was positioned at the level of the transpyloric plane to visualize the antrum, pylorus, and proximal duodenum simultaneously and thereafter vertically to visualize the antrum, superior mesenteric vein, and aorta simultaneously. The motility was videotaped for 15 minutes. The antroduodenal coordination, frequency and amplitude of antral contractions, and size of antral area were reduced, whereas the time during which the pylorus was wide open (>5 mm) was increased after enprostil. It is concluded that antroduodenal motility can easily be visualized by ultrasonography. Therapeutic doses of enprostil impair antroduodenal peristalsis and coordination and open the pylorus in healthy subjects.

Reprinted with permission by the American Gastroenterological Association.

**Screening colonoscopy in asymptomatic average-risk persons with negative fecal occult blood tests.** Rex DK, Lehman GA, Hawes RH, Ulbright TM, Smith JJ (DKR, Dept. of Medicine, Division of Gastroenterology, Indiana University Medical Center, Indianapolis, IN). *Gastroenterology* 100:64–67, 1991

Colonoscopy was performed on 210 asymptomatic average-risk persons, aged 50–75 years, who had negative fecal occult blood test results. Colonoscopy was complete to the cecum in 209 subjects. Fifty-three subjects (25%) had adenomas and two had cancer. All of the adenomas ≥1 cm in size and both cancers occurred in subjects aged ≥60 years. Fifty-once percent of subjects with adenomas and one with cancer had no neoplasms distal to the sigmoid-descending colon junction. One subject had a major postpolypectomy hemorrhage that stopped spontaneously. Screening colonoscopy, therefore, has a high yield for detection of neoplasms in asymptomatic average-risk persons aged ≥60 years with negative fecal occult blood test results. The yield is low in persons aged 50–54 years and intermediate in persons aged 55–59 years.

Reprinted with permission by the American Gastroenterological Association.

**Physicochemical determinants of in vitro shock-wave biliary lithotripsy.** Barkun AN, Valette PJ, Montet JC, et al. (ANB, Dept. of Hepatogastroenterology, Hôpital Edouard Herriot, INSERM U 281, Lyon, France). *Gastroenterology* 100:222–227, 1991

Human gallstones were studied by visual inspection, computerized tomographic imaging, and chemical analysis to assess physicochemical characteristics that may determine the outcome of in vitro shock-wave fragmentation. Eighty-five stones (mean diameter: 13.2 ± 5 mm) were each collected from different patients. Fifty-five (65%) calculi were angular and 30 (35%) round or oval-shaped. Three easily obtained measures were derived from each stone's optimal computerized tomographic image including the mean stone density, a measure corresponding to the standard deviation of the mean stone density value which we termed the stone density distribution index and which may reflect the physicochemical heterogeneity of a given gallstone, as well as the density range. After the administration of 2500 shock waves using an electrohydraulic generator, fragmentation was noted in 68 calculi (80%) and was satisfactory in 27 (32%) (where the largest resulting fragment diameters were all ≤5 mm). Strong determinants of satisfactory fragmentation on multivariate analysis included a stone diameter of ≤15 mm, the presence of an angular stone shape, and a stone density distribution index of ≥60 Hounsfield units. The other parameters did not independently determine satisfactory fragmentation. Prospective clinical trials are needed to assess whether these findings result in a better prediction of the success of extracorporeal biliary lithotripsy and a broadening of its indications.

Reprinted with permission by the American Gastroenterological Association.

## Digestive Diseases and Sciences

**Pyloric deformation from peptic disease: radiographic evidence for incompetence rather than obstruction.** Lu CC, Schulze-Delrieu K (KSD, University of Iowa Hospitals and Clinics, Iowa City, IA 52242). *Dig Dis Sci* 35(12):1459–1467, Dec. 1990

We have used double-contrast radiographic techniques to clarify what changes in the configuration and movements of the gastroduodenal junction result when peptic lesions involve the distal gastric segment between the proximal (PPL) and the distal pyloric muscle loop (DPL). Among 50 cases of pyloric ulceration diagnosed during a four-year study period, 18 cases fulfilled all study criteria. Ulcers maintained a consistent location with regard to the muscular structures of the pylorus, and by affecting these structures, led to many strange deformations of the gastric outlet including permanent pseudodiverticula and reversal of pyloric angulation. The most common site for peptic lesions in the pyloric segment was the protuberance of the lesser curvature called the pyloric torus; many torus lesions extended into and destroyed the DPL. This led to widening of the gastric outlet and radiographic evidence of increased duodenogastric reflux. Pyloric closure was further impaired in this setting because the mucosa no longer prolapsed into the gastric outlet and did not occlude the pyloric lumen as it normally does. Less common lesions involved the greater curvature and the PPL. In one patient, scarring of the PPL led to an antral web and gastric hyperperistalsis. This was the only patient who required operation for chronic gastric outlet obstruction. One-third of the 18 patients had reflux esophagitis in addition to peptic pyloric disease. In most patients without additional ulcerogenic risk factors, treatment with antisecretory agents led to the healing of ulcer craters. We conclude that the morphologic and functional changes of the gastric outlet caused by peptic lesions depend, in part, on the effect the ulcer has on the ulderlying pyloric musculature. We also propose that pyloric incompetence (and hence possibly dumping and bile reflux gastritis) may be a more common complication of pyloric ulceration than hitherto appreciated.

## Gastrointestinal Endoscopy

**Endoscopic ultrasonography in diagnosis of the extent of gallbladder carcinoma.** Mitake M, Nakazawa S, Naitoh Y, et al. (MM, Second Dept. of Internal Medicine, Nagoya University School of Medicine, 65 Tsurumai-cho, Showa-ku, Nagoya 466, Japan). *Gastrointest Endosc* 36(6):562–566, 1990

Endoscopic ultrasonography (EUS) was performed preoperatively in 39 patients with gallbladder carcinoma. Diagnosis of the anatomical extent of gallbladder carcinoma was compared with histologic analysis, and staging accuracy was evaluated according to the TNM classification. Carcinoma considered to be at an early stage with no lymph node metastasis was correctly diagnosed in 87.5%. Differential diagnosis between early and advanced staged tumors was possible in 79.5%. Overall accuracy for depth of tumor invasion (T) was 76.9%. Limitations were due to many stones in the gallbladder and microinfiltration of carcinoma. Assessment of regional lymph node metastasis (N) was at a sensitivity of 81.8% and specificity of 92.9%, for an overall accuracy of 89.7%. We believe endoscopic ultrasonography is useful in the clinical staging of gallbladder carcinoma.

**Endoscopic findings in *Yersinia enterocolitica* enterocolitis.** Matsumoto T, Iida M, Matsui T, et al. (TM, Second Dept. of Internal Medicine, Faculty of Medicine, Kyushu University, Maidaishi 3-1-1, Higashi-ku, Fukuoka 812, Japan). *Gastrointest Endosc* 36(6):583–587, 1990

The endoscopic findings in the colon and terminal ileum in eight cases of *Yersinia enterocolitica* enterocolitis infection were studied. The diagnosis was based on the isolation of *Y. enterocolitica* in the feces and/or elevated serum antibody titers to the organism. Total colonoscopy was performed between 7 and 38 days (mean, 24 days) after the onset of symptoms. In all patients, the terminal ileum was affected, followed by frequent involvement of the ileocecal valve and the cecum, and less frequently, the ascending colon. In the terminal ileum, round or oval elevations with or without ulcers were detected. Small ulcers were detected on the ileocecal valve and in the cecum. These findings were observed even 4 to 5 weeks after the onset of symptoms, suggesting a relatively long course for this disease.

## Clinical Orthopaedics and Related Research

**Giant-cell reparative granuloma of the hand and foot bones.** Ratner V, Dorfman HD (HDD, Head, Section of Orthopaedic Pathology, Dept. of Orthopaedic Surgery, Montefiore Medical Center, 111 E. 210th St., Bronx, NY 10467-2490). *Clin Orthop* 260:251–258, Nov. 1990

Giant-cell reparative granuloma (GCRG) is an uncommon benign reactive intraosseous lesion. It occurs in the skull, jaw, hand, foot, and facial bones and rarely in other skeletal sites. It is a solitary, lytic, expanded lesion and infrequently may extend into the surrounding soft tissue. Histologically, it is composed of fibrous stroma with spindle-shaped fibroblasts, multinucleated giant cells, and inflammatory mononuclear cells. Areas of hemorrhage are uniformly present. It may be difficult to distinguish this entity from an aneurysmal bone

cyst, giant-cell tumor, or brown tumor of hyperparathyroidism because of roentgenographic and histologic similarities. Accurate diagnosis is essential for appropriate treatment; serum calcium, phosphorus, and parathyroid hormone levels should be measured. Curettage and bone graft are effective treatments for both primary lesions and recurrences. Second recurrences are rare.

## The Journal of Urology

**Magnetic resonance imaging for assessment of vena caval tumor thrombi: a comparative study with venacavography and computerized tomography scanning.** Goldfarb DA, Novick AC, Lorig R, et al. (ACN, Dept. of Urology, Cleveland Clinic Foundation, 9500 Euclid Ave., Cleveland, OH 44106). *J Urol* 144:1100–1104, Nov. 1990

We assessed the accuracy of magnetic resonance imaging in demonstrating the presence and extent of vena caval tumor thrombi. The study group included 20 patients with vena caval thrombi from renal cell carcinoma (18), renal pelvic transitional cell carcinoma (1) and adrenal pheochromocytoma (1). Preoperative diagnostic studies included magnetic resonance imaging in all patients, inferior venacavography in 16 and computerized tomography scanning in 15. All patients underwent an operation in which the presence and extent of the vena caval thrombus were confirmed. Magnetic resonance imaging accurately delineated the presence and extent of the thrombus in all 20 patients (100%). Venacavography was accurate in 15 patients (94%) but 8 (50%) required a retrograde and antegrade study. Computerized tomography scanning demonstrated the presence of a tumor thrombus in all 15 patients but accurately delineated the cephalad extent of the thrombus in only 5 (33%). In patients with vena caval tumor thrombi magnetic resonance imaging can provide accurate information regarding the extent of vena caval involvement while avoiding the need for an invasive contrast imaging study.

## Pediatrics

**Arthropathy of Down syndrome.** Olson JC, Bender JC, Levinson JE, Oestreich A, Lovell DJ (JCO, Pediatric Rheumatology, Medical College of Wisconsin, 8701 Watertown Plank Rd., Milwaukee, WI 53226). *Pediatrics* 86(6):931–936, Dec. 1990

A juvenile rheumatoid arthritis-like arthropathy has previously been documented in 12 patients with Down syndrome. An additional 9 patients are described and the literature is reviewed. It is unknown whether these patients have juvenile rheumatoid arthritis or a unique arthropathy in light of the genetic and immunologic abnormalities associated with Down syndrome. Most of the patients had a progressive course with polyarticular disease complicated by subluxations and a long lag time to diagnose. The purpose of reporting these children is to increase awareness of this association and facilitate more appropriate and timely diagnosis of arthritis in Down syndrome patients.

Reprinted by permission of PEDIATRICS © 1990.

## The Journal of Pediatrics

**Liver disease in alpha-1-antitrypsin deficiency: prognostic indicators.** Ibarguen SE, Gross CR, Savik SK, Sharp HL (HLS, Dept. of Pediatrics, Box 279 UMHC, University of Minnesota, 516 Delaware St. S.E., Minneapolis, MN 55455). *J Pediatr* 117:864–870, Dec. 1990

We reviewed the clinical presentation, subsequent course, and outcome of 98 patients with $\alpha_1$-antitrypsin deficiency seen at our institution during the past 20 years to obtain answers to the following questions: (1) What prognostic factors aid in determining the course of liver disease in affected patients? (2) When is the appropriate time for referral to a liver transplant center? (3) Does breast-feeding prevent chronic liver disease? (4) What is the incidence of severe liver disease in family members? Our analysis revealed that the initial values of alanine aminotransferase, prothrombin time, and trypsin inhibitory capacity may have prognostic value. During clinical follow-up the recurrence or persistence of hyperbilirubinemia along with deteriorating results of coagulation studies indicated the need for liver transplantation because of imminent poor outcome. Girls had a worse prognosis than boys. Initial breast-feeding versus feeding of commercial formulas did not influence overall outcome. The incidence of significant liver disease among "at risk" siblings was 21% (3/14); if one assumes mendelian inheritance from heterozygous parents, the overall risk for siblings in our families was 5%.

## The Journal of Nuclear Medicine

**Significance of fill-in after thallium-201 reinjection following delayed imaging: comparison with regional wall motion and angiographic findings.** Tamaki N, Ohtani H, Yonekura Y, et al. (NT, Dept. of Radiology and Nuclear Medicine, Kyoto University Hospital, Shogoin, Sakyo-ku, Kyoto, 606 Japan). *J Nucl Med* 31:1617–1623, Oct. 1990

To identify reversible defects, reinjection of a small amount of thallium-201 ($^{201}$Tl) following 3-hr delayed imaging was performed in 60 patients with coronary artery disease who had perfusion abnormalities on their post-exercise $^{201}$Tl images. Thallium-201 uptake was visually scored and judged as normal (Group I), reversible defect (Group II), new fill-in after reinjection (Group IIIa) and no fill-in even after reinjection (Group IIIb). New fill-in after reinjection was observed in 27 segments of the 85 segments (32%), showing persistent defect on the stress and delayed images. The wall motion in Group IIIa was worse than Group II but better than Group IIIb. Group IIIa showed Q-wave on ECG more often (69%) than Group II (27%) ($p < 0.01$), but less often than Group IIIb (85%) ($p < 0.05$). These data indicate that the reinjection $^{201}$Tl imaging often identifies new fill-in in the areas of no redistribution on the delayed images and it may hold promise for assessing tissue viability which the conventional imaging may underestimate.

## Gastrointestinal Radiology

**Evaluation of the esophagus with a marshmallow bolus: clarifying the cause of dysphagia.** Ott DJ, Kelley TF, Chen MYM, Gelfand DW (DJO, Dept. of Radiology, Bowman Gray School of Medicine, 300 S. Hawthorne Rd., Winston-Salem, NC 27103). *Gastrointest Radiol* 16:1–4, Jan. 1991

We reviewed the radiographic examinations of the esophagus and medical records in 117 patients (55 women and 62 men; mean age, 52 years) in which a marshmallow bolus was also given. A one-third to one-half piece of a standard marshmallow was used with a mean size of 23 mm (±4.5 mm SD) measured in vivo. In 62 patients with no intrinsic structural narrowing of the esophagus, impaction occurred in only seven (11%). Four of these patients had an esophageal motility disorder, and three had a previous Nissen fundoplication. The remaining 55 patients had lower esophageal mucosal rings (47) or peptic strictures (8). Marshmallow impaction was seen in 27 of 47 rings (57%) and was inversely related to ring size, and in six of eight strictures (75%). Also, impaction was related to the ratio of bolus size to ring caliber, and invariably occurred when this ratio was greater than 1.5. Dysphagia was the presenting complaint in 76 (65%) patients, but was found equally in those without intrinsic narrowing and in those with ring or stricture. However, dysphagia was reproduced by the marshmallow bolus only in patients with esophageal narrowing or abnormal motility.

**Diverticulitis of the jejunum: clinical and radiological features.** Benya EC, Ghahremani GG, Brosnan JJ (GGG, Dept. of Diagnostic Radiology, Evanston Hospital, 2650 Ridge Ave., Evanston, IL 60201). *Gastrointest Radiol* 16:24–28, Jan. 1991

This article describes three cases of jejunal diverticulitis in elderly women, who had presented with pain and tenderness in the periumbilical region or the left side of the abdomen, low-grade fever, anemia, and weight loss. The findings were initially attributed to possible inflammatory or neoplastic lesions of the colon. However, gastrointestinal barium studies and computed tomography (CT) of the abdomen proved crucial in establishing the preoperative diagnosis of jejunal diverticulitis and its associated abscess in the adjacent mesentery or abdominal wall. The clinical and radiological manifestations of this uncommon entity are herein presented along with a brief review of the pertinent literature.

**CT appearance of the Roux limb following choledochojejunostomy in liver transplantation.** Greenler DP, Sumkin JH, Campbell WL (WLC, Dept. of Radiology, Presbyterian-University Hospital, Pittsburgh, PA 15213). *Gastrointest Radiol* 16:41–44, Jan. 1991

Choledochojejunostomy in Roux-en-Y is a frequent form of biliary reconstruction in liver transplants. On computed tomography (CT), fluid in the Roux limb may simulate a fluid collection. We studied the CT appearance of the Roux jejunal limb in 25 normal and complicated liver transplant patients. The Roux limb was identified in 21 (84%) of 25 cases. Most frequently useful features were characteristic location, continuous tubular appearance, biliary stent, "bull's eye" appearance, and gas in the loop. Two of 18 normal Roux loops were initially suspected of being abscesses and one gas-containing abscess was initially mistaken for the Roux limb. In five of seven patients with complications (four abscesses, two bile leaks, one anastomotic hemorrhage), identification of the Roux limb was possible and was useful in interpreting CT scans. Knowledge of the appearance of the normal and abnormal Roux limb is essential for proper interpretation of CT scans in liver transplant patients.

**Variations of common bile duct diameter after endoscopic sphincterotomy.** Persson B, Olsson J (BP, Dept. of Diagnostic Radiology ADR, Karolinska Hospital, S 104 01, Stockholm, Sweden). *Gastrointest Radiol* 16:45–48, Jan. 1991

Diameters of the common bile duct (CBD) and common hepatic duct (CHD) were measured before and after endoscopic sphincterotomy (EPT) in 100 patients. There was a significant reduction of the lumen diameter in both the CBD and CHD ($p < 0.01$) after EPT. A comparison between 32 patients without symptoms (such as pain, residual stones, and elevated levels of liver enzymes) and 19 patients with remaining symptoms after EPT, showed a statistically significant reduction in both CBD and CHD diameters ($p < 0.001$) in the former group, and no statistically proven changes in the diameters in the latter group, since a change of <1.5 mm was not considered significant. Therefore, the absence of a reduction or a dilatation of the diameter of the CBD after EPT may suggest that these patients may have persisting complaints after EPT.

Measurements on models (phantoms) show that body position of the patient during endoscopic retrograde cholangiopancreatography (ERCP) has little and negligible influence on the measured diameters of the CBD and CHD.

**Cystic tumors of the pancreas: evaluation by ultrasonography and computed tomography.** Fugazzola C, Procacci C, Andreis IAB, et al. (CF, Dept. of Radiology, University Hospital, 37134 Verona, Italy). *Gastrointest Radiol* 16:53–61, Jan. 1991

The personal series of 30 cystic tumors of the pancreas [12 serous cystic tumors (SCT) and 18 mucinous cystic tumors (MCT)] is presented. All neoplasms were evaluated with ultrasonography (US) 28 of 30 with computed tomography (CT); the tumoral histotype could be correctly defined in 73% of cases (seven of 12 SCT and 15 of 18 MCT). Percutaneous fine-needle aspiration (FNA) with diagnostic aims (preparation of cytological smears and/or biochemical assays) was performed in only 10 of 30 cases, yielding a 100% sensitivity; on the whole, the combined use of imaging modalities and FNA allowed correct characterization of the cystic tumors in 27 of 30 cases (90%). The usefulness of a precise diagnostic workup of these neoplasms is emphasized, due to their prognostic and therapeutic outcome.

## Journal of Ultrasound in Medicine

**Translabial ultrasound of the third-trimester uterine cervix: correlation with digital examination.** Mahony BS, Nyberg DA, Luthy DA, Hirsch JH, Hickok DE, Petty CN (BSM, 1229 Madison St., Ste. 1150, Seattle, WA 98104). *J Ultrasound Med* 9:717–724, Dec. 1990

This prospective blinded study compared translabial ultrasound (TLU) and digital palpation of the cervix among women whose cervix could not be visualized adequately or at all with transabdominal ultrasound during the third trimester of pregnancy. The cervical canal and internal cervical os were adequately visualized during 109 of 113 TLUs (96%). The TLU was well tolerated by the patients; only two patients refused the TLU pending discussion of the technique with their obstetrician. Among 43 examinations of patients without clinical cervical effacement, TLU showed a cervical length of 2.5 to 4.2 cm (mean, 2.9 cm). An excellent correlation ($R = 0.90$) was noted between cervical length on TLU and percentage of cervical effacement on digital examination. The correlation between amount of cervical dilatation on TLU and on digital examination was not high ($R = 0.58$). We conclude that the measurements of cervical length on TLU correlate well with the amount of cervical effacement on digital examination and that TLU provides a rapid and well-tolerated alternative technique to visualize the third-trimester uterine cervix.

Reprinted with permission by the American Institute of Ultrasound in Medicine.

# 1991 ARRS Meeting Summary, May 5–10, 1991 Boston, MA

A comprehensive description of the meeting, including the instructional courses, categorical course, the Friday symposium, and the scientific program appears in this issue of the *AJR*. Meeting and registration forms also can be found in the February and March issues. These may be photocopied.

## Accreditation

All courses and scientific sessions carry AMA Category 1 credit on an hour-for-hour basis.

## Meeting Format

*Scientific Program.* Sessions will be grouped in parallel sessions so that registrants may choose topics related to their interests. A total of 189 scientific papers will be presented, Monday–Thursday, May 6–9. In addition, on Wednesday, May 8, the afternoon session will feature award papers and the Caldwell Lecture, which will be delivered by N. Thorne Griscom, M.D. On Friday, May 10, there will be a special 4-hr symposium on breast imaging.

*Categorical Course on Spine and Body MR.* This 15.5-hr course will be held Sunday–Thursday.

*Luncheon Sessions.* Registrants may enroll in special luncheon sessions, Monday–Thursday. A box lunch will be provided.

## Exhibits

*Scientific and Technical Exhibits and Case of the Day* will be set up in the Hynes Convention Center, Hall A, adjacent to the Sheraton Boston Hotel, Monday–Thursday, May 5–9. The Case of the Day will be presented by John F. O'Connor of Boston University School of Medicine.

## Local Activities

*General Reception.* Sunday evening, May 5, for all registrants.

*Golf Tournament.* Monday, May 6 at a local country club.

*Men's and Women's Tennis Tournaments.* Monday, May 6, at the Winchester Tennis Club.

*Local Tours.* See February issue of the *AJR* for a description of the activities.

## Meeting Registration

Preregistration will be accepted until April 20. There will be on-site registration. Official badges and program books will be available at the registration desk, Sheraton Boston Hotel. No confirmations will be mailed.

## Course Registration

Register early—enrollment is limited. List first, second, and third choices for each period. Also, indicate whether you wish to take the categorical course. Deadline for registration by mail is April 20. All ticket orders will be filled according to postmarked date. Course tickets *will not* be mailed. Tickets will be available beginning at 1:00 p.m. on Saturday, May 4, at the ARRS registration desk in the Sheraton Boston Hotel. There will be on-site registration for courses not already filled.

## Hotel Registration

Reservations are handled by the ARRS Housing Bureau, Sheraton Boston Hotel, Attn: Reservations Office, 39 Dalton St., Boston, MA 02199. These must be received by April 13. Make check payable to Sheraton Boston Hotel. See reservation form in this issue for prices and complete instructions.

## Fees

| | |
|---|---|
| Meeting: | |
| ARRS members and resident members | No fee |
| Nonmembers | $250 |
| Nonmember physicians in training (with verification) | 25 |
| Categorical course | 75 |
| Luncheon sessions/each | 12 |
| Local tours | 20–75 |

## Cancellations and Fee Refunds (Excluding Hotel Fees)

Fees will be refunded only if cancellation is received by April 20, 1991. Send to American Roentgen Ray Society, 1891 Preston White Drive, Reston, VA 22091.

## Transportation Discounts

United Airlines is offering discounts of up to 40% on airfares. Call (800) 521-4041 and reference ARRS account number 429JW.

Hertz Rent-A-Car is offering special rates on car rentals. Reserve a Hertz car at these special rates through United Airlines when you make your plane reservations, or call Hertz directly at (800) 772-3773.

# 1991 American Roentgen Ray Society Instructional Courses and Symposium

Robert J. Stanley, Director, and Bruce L. McClennan, Associate Director

Sixty Instructional Courses will be presented during the 91st annual meeting of the American Roentgen Ray Society (ARRS) beginning Monday, May 6, and continuing through Thursday, May 9. Each of the Instructional Courses listed on the next page will be 90 min long. In addition, there will be a week-long Categorical Course in Spine and Body MR Imaging and a half-day Symposium, Current Topics in Breast Imaging.

The Categorical Course in Spine and Body MR Imaging will have 15.0 hr of instruction and will begin on Sunday, May 5, and conclude on Thursday, May 9. The Symposium, Current Topics in Breast Imaging, will be on Friday, May 10, from 8 a.m. to 12 noon. All courses carry Category 1 credit on an hour-to-hour basis.

### Registration Information

To register for courses, complete the meeting registration form in this section and mail promptly. Tickets also will be available at the Instruction Course Registration Desk, Sheraton Boston Hotel for courses that have not been sold out. All courses will take place in the headquarters' hotel.

After reviewing the course list, select three for each morning and afternoon session. Write the course number and name of the first instructor on the registration form. Please note that the -01 residents'-masters' tutorials are intended primarily for residents and that attendance will be limited.

All who register for the Categorical Course in Spine and Body MR Imaging (including ARRS members) must pay a fee of $75 and must take the entire series of classes. The Categorical Course totals 15.0 hr of instruction and includes a syllabus.

## Course Schedule

### Sunday, May 5, through Thursday, May 9

The Categorical Course in Spine and Body MR Imaging will have 15.0 hr of instruction over 5 days. Topics and instructors are listed on p. 658.

### Monday, May 6, through Friday, May 10

A total of 60 courses will be offered (see next page) plus a symposium, Current Issues in Breast Imaging.

## ACR Luncheon Presentations on Socioeconomics of Radiology

A series of luncheon presentations on the socioeconomics of radiology will be arranged by the American College of Radiology (ACR). A box lunch will be provided. The presentations will be from 12:30 to 1:30 p.m. and do not conflict with other elements of the program. Advance registration is required. Cost per session is $12.

**Date, Topic, Speaker**

**Monday, May 6:** Governmental Issues for Radiology, Gary Price, ACR Director of Government Relations

**Tuesday, May 7:** Economic Issues of Radiology Practice, Emmett O. Templeton, M.D., Chairman, ACR Commission on Economics

**Wednesday, May 8:** Current Legal Issues in Radiology, Thomas W. Greeson, J.D., ACR Legal Counsel

**Thursday, May 9:** Update on ACR Activities, James M. Moorefield, M.D., Chairman, ACR Board of Chancellors

**Symposium: Current Issues in Breast Imaging**
**Friday, May 10, 1991, 8:00 a.m. to 12:00 noon**

| Time | Topic (*Presenter*) |
|---|---|
| 8:00 a.m. | Introduction and ACR accreditation (*Kopans DB*) |
| 8:30 a.m. | Are the screening guidelines wrong? (*Moskowitz M*) |
| 9:00 a.m. | Proper positioning—not just basic, but required (*Eklund GW*) |
| 9:30 a.m. | Now that I've found it, what should I do about it? (*Kopans DB*) |
| 10:00 a.m. | Questions and break |
| 10:30 a.m. | The therapeutic implications of diagnostic findings—extensive intraductal component and the pre- and postirradiated breast (*Sadowsky NL*) |
| 11:00 a.m. | How can you tell that you are screening at appropriate thresholds? (*Sickles EA*) |
| 11:30 a.m. | Questions and panel discussion |

Note.—There is no fee for this symposium. However, to facilitate planning, please register on the meeting registration form.

**American Roentgen Ray Society Instructional Courses: May 6–May 9, 1991**

| Topic | Monday | Tuesday | Wednesday | Thursday |
|---|---|---|---|---|
| | | Morning (all sessions begin at 8:00 a.m.) | | |
| Residents'-masters' tutorial | 101. Some basic signs of chest X-ray diagnosis including plain film/CT correlation. *Fraser RG, Heitzman ER* | 201. Advances in imaging the brain and spine: impact on diagnosis and treatment of CNS abnormalities. *Quencer RM.* | 301. The role of ultrasound in pediatric gastrointestinal tract disease. *McAlister WH* | 401. Angioplasty—past and present. *Tegtmeyer CJ* |
| Pediatrics | 102. Evaluation of pneumonia in the pediatric patient. *Singleton EB* | 202. A practical approach to pediatric abdominal diagnosis. *Wood BP, Senac MO* | 302. Diagnostic imaging of child abuse. *Kleinman PK* | 402. Musculoskeletal and cranial pediatric ultrasonography. *Teele RL, Share J* |
| Technique and technology | 103. Ultrafast CT scanning—an update. *Sheedy PF* | 203. CT and US guided biopsies: practical approaches, pitfalls and new techniques. *Charboneau JW, Reading CC* | 303. Advances in abdominal CT examination techniques. *Berland LL, Megibow AJ* | 403. Computer assisted 3-D imaging: state of the art. *Fishman EK, Ney D* |
| Chest | 104. CT of the lung parenchyma. *Pugatch RD* | 204. Pulmonary manifestations of the immunocompromised patient. *Vydareny KH, Gross BH* | 304. Plain chest radiograph manifestations of esophageal and diaphragmatic diseases. *Stark P, Tarver RD* | 404. Thoracic infections and their complications. *Choplin RH, Reed JC* |
| Gastrointestinal | 105. Biliary diagnosis: a problem oriented approach. *Koehler RE, Balfe DM* | 205. Inflammatory bowel disease from beginning to end. *Gore RM, Laufer I* | 305. Radiologic screening for colorectal cancer. *Gelfand DW, Ott D* | 405. Radiologic evaluation of the pharynx and esophagus. *Rubesin SE, Levine MS* |
| Genitourinary/retroperitoneum | 106. CT/MRI of the retroperitoneum. *Lee JKT, Heiken JP* | 206. The radiologic evaluation of the adrenal. *Kenney PJ* | 306. Imaging of acute renal inflammatory disease. *McClennan BL* | 406. CT and MRI of the kidney. *Newhouse JH, Amis ES* |
| Body imaging/CT, MR imaging, sonography | 107. Staging of lymphoma. *Gedgaudas-McClees RK, Torres WE* | 207. The peritoneum and mesentery: anatomy, pathology, and technique. *Halvorsen RA, Silverman PM* | 307. Computed tomographic evaluation of the liver. *Moulton JS* | 407. Sonographic evaluation of the adult acute abdomen. *Wilson SR* |
| Neuroradiology | 108. Supratentorial neoplasms—MRI. *Leeds NE* | 208. MRI and CT in the evaluation of head trauma. *Davis KR* | 308. MRI of the sella and parasellar region. *El Gammal T, Brooks BS* | 408. Imaging CNS vascular disease: radiologic-pathologic correlation. *Osborn AG* |
| Radiologic practice | 109. The battle over turf: who has it and how to get it. *Hillman BJ* | 209. Cost containment in radiology departments. *Janower ML* | 309. Pointers on scientific manuscript preparation. *Berk RN, Levene M, Hilton S, Spiller KL* | 409. The future of digital radiology: technical and clinical considerations. *Ovitt TW, Hunter TB* |
| Radiologic-pathologic correlation | 110. Radiographic pathology of the GI mucosa. *Ghahremani GG* | 210. Radiologic-pathologic correlation of GI tract tumors. *Lichtenstein JE, Olmsted WW* | 310. Arthropathies: radiologic-pathologic correlations. *Madewell J* | 410. Imaging and pathologic correlation of bone and soft-tissue neoplasms. *Hudson TM* |
| | | Afternoon (all sessions begin at 4:00 p.m.) | | |
| Musculoskeletal | 111. The analytic approach to the film (an imaging discipline). *Jacobson HG, Edeiken J* | 211. Current practice in musculoskeletal ultrasonography. *Adler RS, Fornage BD* | 311. The pelvis and hip: anatomic-clinical correlations. *Pitt MJ* | 411. Evaluation of bone and marrow in osteoporosis and other metabolic conditions. *Rosenthal DI* |
| Body imaging/sonography | 112. Imaging and biopsy of the prostate. *Papanicolaou N, Tung GA* | 212. Transvaginal sonography in obstetrics and gynecology. *Fleischer AC, Rao BK* | 312. Update on ultrasound in hepatobiliary imaging. *Kane RA* | 412. Peripheral vascular ultrasound imaging. *Carroll BA* |
| Head and neck/nuclear medicine | 113. Imaging of the sinonasal cavities. *Som PM* | 213. Imaging of head and neck cancers. *Curtin HD* | 313. SPECT brain imaging. *Mountz JM* | 413. Nuclear cardiology in clinical practice. *Thrall JH* |
| Body imaging/CT, MR imaging, sonography | 114. Use of diagnostic imaging for the follow-up of treated cancer patients. *Kagan AR, Steckel RJ* | 214. Pitfalls in plain film and CT analysis of the mediastinum. *Glazer HS, Molina P* | 314. Radiologic evaluation of the transplant kidney. *Baumgartner BR, Pozniak MA* | 414. MRI of the thorax with CT correlation. *McLoud TC* |
| Angiography/interventional | 115. New devices in peripheral vascular intervention: diagnosis and therapy. *Becker G, Katzen BT* | 215. Biliary calculus disease: interventional management. *Mueller PR, vanSonnenberg E, Teplick SK* | 315. Update on embolotherapy. *Keller FS, Waltman AC* | 415. Plugging vessels and opening ureters: treating kids with catheters. *Fellows KE, Hoffer FA* |

## Categorical Course in Spine and Body MR Imaging

## American Roentgen Ray Society 91st Annual Meeting

***May 5–9, 1991, Sheraton Boston Hotel, Boston, MA***

*Course Director, Anton N. Hasso, M.D.*
*Course Codirector, David D. Stark, M.D.*

| | |
|---|---|
| **Sunday, May 5** | **Fundamentals/New Developments** |
| 9:50–10:00 | Welcome/Introduction (*Hasso/Stark*) |
| 10:00–10:30 | Fundamental MRI (*Matwiyoff*) |
| 10:30–11:00 | Fast Scanning (*Hendrick*) |
| 11:00–11:40 | Sedation/Anesthesia/Patient Monitoring (*Hinshaw/Shellock*) |
| 11:40–12:20 | MR Angiography |
| | Body (*Edelman*) |
| | Head and Neck (*Hasso*) |
| 12:20–2:00 | Lunch Break |
| | **Spine/Neck** |
| 2:00–2:30 | Flow/Spine CSF Flow (*Bradley*) |
| 2:30–3:00 | Congenital/Developmental Lesions (*Naidich*) |
| 3:00–3:30 | Mass Lesions/Myelopathy (*Sze*) |
| 3:30–4:00 | Coffee Break |
| 4:00–4:30 | Infective Spondylitis (*Sharif*) |
| 4:30–5:00 | 3D Spine/Degenerative/Postoperative (*Ross*) |
| 5:00–5:30 | Neck Soft Tissues (*Vogl*) |
| **Monday, May 6** | **Contrast Agents/Motion Artifact Suppression** |
| 1:30–2:00 | MR Contrast Agents, Introduction (*Wolf*) |
| 2:00–2:30 | Contrast Agents for Body MR (*Stark*) |
| 2:30–3:00 | Motion Artifact Suppression (*Ehman*) |
| 3:00–3:30 | Coffee Break |
| | **Pediatric** |
| 3:30–4:15 | Pediatric Abdomen/Pelvis (*Dietrich*) |
| 4:15–5:00 | Pediatric Musculoskeletal/Marrow (*Moore*) |
| 5:00–5:45 | Pediatric Cardiovascular (*Higgins*) |
| **Tuesday, May 7** | **Abdomen/Pelvis** |
| 3:45–4:15 | Liver (*Mitchell*) |
| 4:15–5:00 | Male Pelvis |
| | Prostate/Bladder (*Rifkin*) |
| | Testes/Scrotum (*Fritzsche*) |
| 5:00–5:45 | Female Pelvis |
| | Neoplasms (*Hricak*) |
| | Non-neoplastic Disorders (*McCarthy*) |
| **Wednesday, May 8** | **Neck/Musculoskeletal** |
| 3:45–4:25 | Infection and Avascular Necrosis (*Beltran*) |
| 4:25–5:05 | Soft Tissue/Bone Neoplasms (*Seeger*) |
| 5:05–5:45 | Knee (*Reiser*) |
| **Thursday, May 9** | **Musculoskeletal** |
| 3:45–4:15 | Temporomandibular Joints (*Fulmer*) |
| 4:15–4:45 | Wrist (*Kneeland*) |
| 4:45–5:15 | Shoulder (*Crues*) |
| 5:15–5:45 | Foot and Ankle (*Solomon*) |

# American Roentgen Ray Society 1991 Scientific Program

The scientific program is divided into parallel sessions so that registrants may choose topics related to their interests. A total of 188 papers will be presented Monday–Thursday, May 6–9, 1991. In addition, on Monday morning, after the opening ceremonies, a special session will be devoted to award-winning papers.

## Monday, May 6, 1:30 p.m.–3:30 p.m.

### I. Bone—Articular

**1:30 1. Notts disease: an atypical erosive arthritis.** Cobby MJ, Cushnahan J, Dieppe PA, Watt I

**1:42 2. Paraspinal calcification: An unrecognized cervical manifestation of collagen vascular disease.** Schweitzer ME, Cervilla V, Resnick D, Gerharter J, Nemcek A, Kricun M, Manaster BJ

**1:54 3. Angiographic changes in the neuropathic foot.** Menanteau BP, Marcus C, Ladam V, Gausserand F

**2:06 4. MR imaging in dialysis-related amyloid arthropathy.** Cobby MJ, Adler RS, Swartz R, Martel W

**2:18 5. Hip fracture–dislocation: evaluation by MRI.** Spritzer CE, Poggi J, Callahan J

**2:30 6. CT measurement of acetabular deficiency in congenital and paralytic hip instability.** Magid D, Buckley SL, Sponseller PD, Fishman EK

**2:42 7. MRI evaluation of congenital dislocation of the hip.** Berman CG, Arrington JA, Murtagh FR, Silbiger ML, Guidera KJ, Clark RA

**2:54 8. MR imaging of proximal femoral focal deficiency (PFFD).** Li DBK, Pirani S, Beauchamp RD, Sawatzky B

**3:06 9. MR imaging of the rotator cuff: evaluation of criteria for diagnosis of full thickness tear.** Farley TE, Neumann CH, Steinbach LS, Morgan FW, Holt RG, Jahnke AH, Petersen SS

**3:18 10. Fluoroscopic and computed arthrotomographic assessment of shoulder instability.** Mitchell MJ, McMillan CL

### II. Breast

**1:30 11. Galactography: a 10-year experience with pathologic correlation.** Baker KS, Davey DD, Stelling CB

**1:42 12. Mobile mammographic screening of self-referred women in New York City.** Dershaw DD, Liberman L, O'Moore P, Smolek B

**1:54 13. Data management in a population-based breast cancer detection program: cost analysis of participant tracking and surveillance.** Kessler HB, Gatenby RA, Rimer BK, Engstrom PF

**2:06 14. The indeterminate breast mass: increasing specificity with ultrasound guided fine-needle aspiration cytology.** Harris KM, Hogg JP, Kanbour A, Skolnick ML, Ilkhanipour ZS, Ganott MD, Staiger MJ

**2:18 15. Stereotactic fine-needle aspiration cytology for evaluation of nonpalpable breast lesions: prospective comparison with surgical biopsy.** Fajardo LL

**2:30 16. Stereotactic aspiration cytology of breast lesions: results and indications for use.** Schmidt RA, Morrow M, Bibbo M, Dowlatshahi K

**2:42 17. Complications of breast implants.** Ganott MA, Harris KM, Ilkhanipour ZS, Costa-Greco MA

**2:54 18. Immediate complications of breast imaging procedures.** Helvie MA, Ikeda DM, Adler DD

**3:06 19. Mobile mammography: is subsidization necessary?** Wolk RB

**3:18 20. Cost analysis of screening mammography: a more realistic accounting.** Tocino I

## Tuesday, May 7, 10:00 a.m.–12:30 p.m.

### III. Gastrointestinal

**10:00 21. The incidence and significance of small (<15 mm) hypodense hepatic lesions in abdominal CT.** Jones EC, Bernardino ME, Chezmar JL, Nelson RC

**10:12 22. Appropriate volume of nonionic contrast agent for dynamic, abdominal CT.** Baker ME, Stewart R, Beam C, Cohan R, Leder R, Nadel S, Dunnick NR

**10:24 23. MR imaging features of small HCC treated by percutaneous ethanol injection.** Sironi S, Livraghi T, Vanzulli A,

DelMaschio A

**10:36 24. Enteral feeding tube placement: fluoroscopic and endoscopic success.** Ott DJ, Mattox HE III, Gelfand DW, Chen MYM, Wu WC

**10:48 25. Radiographic evaluation of achalasia immediately following pneumatic dilatation using the rigiflex dilator.** Ott DJ, Donati D, Chen MYM, Wu WC, Gelfand DW

**11:00 26. CT evaluation of esophageal carcinoma recurrence following transhiatal esophagectomy.** Carlisle JG, Quint LE, Francis IR, Smick JF, Orringer MB, Gross BH

**11:12 27. Abdominal paracentesis and gastropexy as an aid to percutaneous gastrostomy in patients with extensive ascites.** Lee MJ, Mueller PR, Saini S, Brink JA, Hahn PF

**11:24 28. CT imaging of the gastroepiploic vein in pancreatic disease.** Moody A, Poon PY

**11:36 29. Contribution of enteroclysis in malabsorption syndrome.** Schmutz GR, Bui TB, Gangi A, Vetter D

**11:48 30. Superparamagnetic particles as oral gastrointestinal contrast agent in MRI of abdomen.** Boudghene F, Lambrechts M, Gansmo TB, Nantois C, Frey I, Bigot JM

**12:00 31. Gastrointestinal MR contrast: delineation of abdominal masses with superparamagnetic iron oxide.** Hahn PF, Saini S, Stark DD

**12:12 32. Comparison of abdominal CT studies using different iodine concentrations in nonionic contrast agents.** Thoeni RF, Gorczyca DP, Goldberg HI

**12:24 33. CT differentiation of benign and malignant adrenal masses: a comparison of CT attenuation value, size and observer interpretation.** Lee MJ, Hahn PF, Simeone JF, Papanicolaou N, Egglin T, Mueller PR

## IV. Interventional Radiology—Vascular

**10:00 34. MR imaging of coronary artery fistulas in correlation with cineangiography.** Wu D-K, Jaw T-S, Liu G-C

**10:12 35. MR imaging for pulmonary arterial abnormalities in correlation with angiography.** Liu G-C, Wu D-K

**10:24 36. Rapid-phase contrast MR angiography of the head and neck.** Applegate GR, Talagala L, Jacobs B, Irilli LB, Augustine L

**10:36 37. MR angiography and color Doppler sonography for the diagnosis of internal carotid stenosis.** Polak JF, Bajakian RL, O'Leary DH, Anderson MC, Jolesz FA

**10:48 38. The brachial venous approach for chronic central venous access.** Andrews JC, Marx MV, Williams DM, Walker-Andrews SC

**11:00 39. Infrapopliteal small vessel angioplasty.** Brown KT, Moore ED

**11:12 40. PTA of celiac and superior mesenteric arteries for mesenteric ischemia.** Johnson CM, Welch TJ, Sheedy PF, Stanson AW, Glovickzi P, Hammond C.

**11:24 41. Results of excimer laser femoral angioplasty.** Vogelzang RL, Joseph A, Nemcek AA, McCarthy WJ, Pearce WH, Flynn WR, Yao JST

**11:36 42. Three-year experience with the Simpson Atherocath in the treatment of arterial stenoses and occlusion.** Kim D, Gianturco LE, Porter DH, Siegel JB, Orron DE, Kent KC, Skillman JJ

**11:48 43. Result of the Simon nitinol filter clinical trial.** Kim D, Grassi CJ, Porter DH, Siegel JB, Kleshinski S, Simon M

**12:00 44. Urokinase enhancement of PAD.** Lahorra J, Haaga J, Stellato T, Flanagan T, Graham R

**12:12 45. Inhibition of blood-clot formation in nonionic contrast material.** Dean LM, Kerr HH, Gagliardi RA

**12:24 46. The use of activated clotting time (ACT) in vascular interventional procedures.** Vogelzang RL, Parikh S, Nemcek AA

## V. Genitourinary Radiology

**10:00 47. The role of diagnostic imaging in puerperal febrile morbidity.** Lev-Toaff AS, Baka JJ, Friedman AC, Radecki PD, Caroline DF

**10:12 48. Assessment of myometrial invasion in stage I endometrial carcinoma: MRI-pathologic correlation.** Sironi S, Vanzulli A, Taccagni G, DelMaschio A

**10:24 49. Advanced cervical carcinoma treated with preoperative chemotherapy: MR imaging findings.** Sironi S, Vanzulli A, Taccagni G, DelMaschio A

**10:36 50. Postoperative hysterosalpingography (HSG): radiographic appearance following tubal surgery.** Young GP, Ott DJ, Chen MYM, Fayez JA, Gelfand DW

**10:48 51. Quality of urography and renal clearance of contrast media.** Thomsen H, Vestergaard A

**11:00 52. Quantitative assessment of renal function using dynamic Gd-DTPA–enhanced MR imaging.** Furukawa A, Murata K, Kawaguchi N, Takahashi M, Mori M, Pak K, Nakane Y, Kikkawa R, Haneda M, Moriya H, Morita R

**11:12 53. Dynamic Gd-DTPA–enhanced MR evaluation of indeterminate renal masses.** Borrello JA, Lee JKT, Brown JJ

**11:24 54. Renal MR angiography: "time of flight" vs. "phase contrast."** Spritzer CE, Debatin JF, Grist T, Svetky L, Weinerth J, Sostman D

**11:36 55. Renal artery imaging with phase-contrast MR angiography.** Debatin JF, Spritzer CE, Grist T, Svetky L

**11:48 56. CT peritoneography in the evaluation of chronic ambulatory peritoneal dialysis complications.** Hollett MD, Marn CS, Francis IR, Swartz RD, Ellis JH

**12:00 57. Color Doppler sonography of the penis: patterns of arterial variation.** Fitzgerald SW, Erickson SJ, Foley WD, Lawson TL

**12:12 58. Vasculogenic impotence: duplex and color doppler penile ultrasound.** Roth JC, King BF, Hattery RR, James EM, McKusick MA, Lewis RW

**12:24 59. MR and sonographic appearance of intratesticular tubular ectasia.** Tartar VM, Trambert MA, Mattrey RF

# Tuesday, May 7, 1:30 p.m.–3:30 p.m.

## VI. Bone—Knee

**1:30 60. Optimal fast scan parameters for MR imaging of normal joints.** Yao L, Sinha S, Seeger L

**1:42 61. Radial MPGR images of the knee for the evaluation of meniscal tears: comparison with spin-echo technique.** Quinn SF, Brown T

**1:54 62. MR appearance of normal and abnormal depressions in the tibial plateau.** Fritz RC, Helms CA, Genant HK

**2:06 63. Differential MR features of acute and chronic anterior cruciate ligament tears.** Vahey TN, Broome DR, Kayes KJ, Shelbourne KD

**2:18 64. Acute and chronic ACL-deficient knees: progression of the associated hyaline cartilage abnormalities.** Bula V, Isler R, Pope CF, Brown D, Anson P, Avery FL, Heinz B

**2:30 65. Changes in the MRI appearance of the ACL graft during the initial postoperative 12 months.** Smith A, Pope CF, Jokl P, Lynch K

**2:42 66. The MRI appearance of the healing patella tendon: 12-month follow-up.** Smith A, Pope CF, Jokl P, Lynch K

**2:54 67. Stress radiography of the patellar ligament following patellar tendon-bone reconstruction of anterior cruciate ligament.** Rijke AM, Goitz HT, McCue FC, Delp J

**3:06 68. Evaluation of patellar cartilage with axial MR.** Swan JS, Norris MA, Keene JS, De Smet AA

**3:18 69. MR imaging of postoperative stiff knee.** Li DKB, Jessurun LA, McConkey JP

## VII. Nuclear Medicine

**1:30 70. Correlation of radionuclide bone scans and radiographs in the evaluation of metastatic bladder carcinoma.** Kim EE, Chung SK, Cho BJ, Podoloff DA, Haynie TP

**1:42 71. Ventilation/perfusion lung scanning with angiographic correlation in a community hospital.** Lowe V, Elliot G, Tocino I

**1:54 72. Comparison of MRI and radionuclide bone scan detection of vertebral metastasis.** Butler MG, Hall LC

**2:06 73. Soft-tissue masses: comparison of Gd-DTPA–enhanced MR with angiography and dynamic scintigraphy.** Kransdorf MJ, Jelinek JS, Benedict RA, Davidson M, Moser RP, Berrey BH

**2:18 74. Reverse mismatch from pleural effusion on aerosol inhalation/MAA perfusion lung scintigrams: CT correlation.** Miron SD, Crass JR, Feiglin DH, Cohen AM, Bellon EM

**2:30 75. Extrapulmonary tuberculosis: detection with Ga-67 scan and correlation with CT.** Yang SO, Lee MC, Koh C-S, Choi BI, Park JH, Han MC, Kim C-W

**2:42 76. Assessment of cerebrovascular reserve capacity by transcranial Doppler and $^{99m}$Tc-HMPAO-SPECT.** Rosenkranz K, Langer R, Kierholzer J, Hepp W, Palenker J, Mauz M, Felix R

**2:54 77. Diagnosing cardiac allograft rejection with MR imaging/spectroscopy and positron emission tomography.** Spritzer CE, D'Amico T, Charles C, Negro-Vilar R, Buchanan S, Berry J, Van Tright P

**3:06 78. Assessing brain tumors by FDG and amino acid (ACBC) dynamic PET scanning.** Tucker R, Hubner KF, Buonocore E, Chan A, Smith GT, Kliefoth AB, Keller B.

**3:18 79. $^{99m}$Tc nanocolloid intraperitoneal injection to demonstrate peritoneal to mediastinal lymph node communication: a rat study.** Shih W-J, Coupal JJ, Chia HL, Coulston C

## VIII. Pediatrics

**1:30 80. Prognostic implications of sonographically detected fetal intraabdominal calcifications.** Chaffey MH, Goldstein RB, Russell S, Golbus MS

**1:42 81. Prenatal sonographic observations: the correlation of omphalocele contents with karyotype abnormalities.** Getachew MM, Goldstein RB, Edge V, Filly RA, Goldberg JD

**1:54 82. Prenatal recognition of CNS complications of alloimmune thrombocytopenia.** Kuhn MJ, Couch SM, Binstadt DH, Rightmire D, Morales A, Khanna NN

**2:06 83. Pericardial effusion and its relationship to cardiac disease in children with AIDS.** Mast HL, Haller JO, Schiller MS

**2:18 84. Hepatic venocclusive disease in pediatric BMT recipients: clinical and duplex sonographic findings.** Day DL, Parker SL

**2:30 85. Symptomatic pulmonary complications of bone marrow transplantation in children.** Kao SCS, Wagener JS, Smith WL, Sato Y, Franken EA Jr, Trigg ME

**2:42 86. Tracheal compression in childhood lymphoma.** Zobel MS, Glazer HS, Siegel MJ

**2:54 87. Urinary tract calculi that form on surgical staples: a characteristic roentgen appearance.** Dangman BC, Lebowitz RL

**3:06 88. Perforation of the augmented bladder.** Braverman RM, Lebowitz RL

**3:18 89. MR imaging of Duchenne muscular dystrophy.** Chan WP, Miller RG, Lang P, Majumdar S, Genant HK

# Wednesday, May 8, 1:30 p.m.–3:30 p.m.

## IX. Bone—Nonarticular

**1:30 90. Fractal analysis of trabecular bone.** Richardson ML, Gillespy T III, Hunt KA

**1:42 91. Precision of bone densitometry using the Hologic-1000 ODR system.** Crim JR, Sayre J, Seeger LL

**1:54 92. Pitfalls in dual-energy radiographic absorptiometry using the Hologic-1000 system.** Crim JR, Seeger LL

**2:06 93. 3D reconstruction of skeletal muscle.** Theriault G, Bowers J, Fleckenstein J, Faber T, McColl R, Opperman R, Peshock R

**2:18 94. Comparison of CT to plain films in acute pelvic trauma.** Resnik CS, Young JWR

**2:30 95. Bone-SPECT and 3D-reconstruction in patients with hip-head necrosis before and after implantation of a pedicled pelvic bone graft.** Hierholzer J, Keske U, Cordes M, Henkes H, Langer R, Schwetlick G, Weber U, Felix R

**2:42 96. Traumatic osteolysis of the clavicle.** Moore TE, Flood MJ, Robinson RA, Kathol MH, Yuh WT, El-Khoury GY

**2:54 97. Radial fracture analysis using neural networks.** Gross GW, Boone JM

**3:06 98. Digital radiography: musculoskeletal applications.** Harcke HT, Mandell GA, Grissom LE, Finkelstein MS, James CM

**3:18 99. Phosphor plate computed radiography system in musculoskeletal imaging.** Murphey MD, Quale JL, Martin NL, Cook LT, Dwyer SJ III

## X. Interventional Neuroradiology

**1:30 100. A new interventional neuroradiology technique: percutaneous catheter placement for cyst drainage in the subarachnoid space.** Kuhn MJ, Pencek T, Pearson DH, Russell BK, Long S

**1:42 101. Automated percutaneous diskectomy in the treatment of foraminal and extraforaminal lumbar disk herniation: report of 17 cases.** Vanneroy F, Courtheoux F, Huet H, Theron J

**1:54 102. Combined high-flow lumbar epidural injection of saline and dilatation in the treatment of postsurgical epidural symptomatic scarring: work in progress.** Vanneroy F, Courtheoux F, Cornille X, Houtteville JP, Theron J

**2:06 103. Contrast extravasation during embolization of intracranial AVM without associated intracranial hematoma.** Azar-Kia B, Horowitz SW, Fine M, Budris D

**2:18 104. CT and MR of Surgicel and Gelfoam in vitro.** Bronstein AD, Maravilla KR

**2:30 105. Treatment of carotid and cerebral vascular occlusion with tissue plasminogen activator: a radiologic analysis.** Wolpert SM

**2:42 106. Parathyroid lesion localization: MRI and surgical correlation.** Norconk JJ, Leight GS, Spritzer CE

**2:54 107. Floor-of-mouth cancers: role of CT, US, and MRI.** Potter JL, Patel JR, Otto PM, Floyd MK, Otto RA

**3:06 108. Screening Sinus and MR appearance of antrochoanal polyps.** Pollei SR, Harnsberger HR, Schellhas KP

**3:18 109. Economic and utilization analysis of MR imaging units in the United States in 1990.** Evens R, Evens R Jr

## XI. Gastrointestinal Radiology

**1:30 110. Altered gallbladder contractility following biliary extracorporeal shock-wave Cholecystolithotripsy (BESWL).** Rawat B, Fache JS, Burhenne HJ

**1:42 111. Hemoglobinuria and hematuria following biliary extracorporeal shock-wave cholecystolithotripsy (BESWL).** Rawat B, Riddler C, Fache JS, Burhenne HJ

**1:54 112. Clinical results in pulsed-dye laser lithotripsy of retained common duct stones.** Dawson SL, Mueller PR, Saini S, Lee MJ, Brink JA, Kelsey P, Nishioka N, Schapiro R, Ferrucci JT

**2:06 113. Prediction of gallstone composition: synthesis of growth patterns and radiographic features.** Brink JA, Kammer B, Mueller PR, Simeone JF, Saini S, Ferrucci JT

**2:18 114. In vitro dissolution kinetics of calcified gallstones in MTBE: correlation with pattern of calcification by CT.** Kammer B, Brink JA, Mueller PR, Simeone JF, Saini S, Ferrucci JT

**2:30 115. Periportal contrast enhancement on CT scans of the liver.** Hammerman AM, Kotner LM, Doyle TB

**2:42 116. MRI assessment of hepatic dysfunction with manganese dipyridoxal diphosphate (Mn-DPDP).** Coley BD, Mattrey RF, Trambert MA, Baker KG, Heiberg E

**2:54 117. MRI of the liver: technical development and clinical implementation.** Stark DD, Tanimoto A, Baba Y, Zhao L, Chen J

**3:06 118. Assessment of hepatitis by NMR: performance of cell-specific contrast agents.** Tanimoto A, Baba Y, Zhao L, Chen J, Pouliquen D, Stark DD.

**3:18 119. Gadolinium-enhanced fast MR of the liver at 1.5 Tesla.** Gazelle GS, Wielopolski PA, Haaga JR, Haacke EN

# Thursday, May 9, 10:00 a.m.–12:30 p.m.

## XII. Chest

**10:00 120. CT of laryngotracheal trauma.** Lupetin AR, Daffner RH

**10:12 121. Emphysema in IV talc granulomatosis.** Rahman M, Weisbrod GL, Herman SJ

**10:24 122. Broncholithiasis: CT evaluation.** Conces DJ, Tarver RD, Vix VA

**10:36 123. Bedside radiographic and clinical evaluation of aspiration following prolonged mechanical ventilation.** Isler RJ, LaPrad PJ, Altman FM, Hillman KA

**10:48 124. Single-exposure dual-energy imaging of chest nodules.** Kelcz F, Zink F, Peppler WW, Mistretta CA, Ergun DL, Sze WK

**11:00 125. Features of MRI in the detection of tumor invasion of pleura and chest wall.** Bittner RCh, Schorner W, Schonfeld N, Loddenkemper R, Felix R

**11:12 126. The value of gadolinium (Gd)-DTPA in MR imgaing of the chest.** Bittner RCh, Gurok J, Schorner W, Hieckel HG, Felix R

**11:24 127. Imaging of acute aortic dissection: a national survey.** Bisceglia M, Kubicka RA, Smith C, Najafi H

**11:36 128. Ciné MRI of arrhythmogenic right ventricular dysplasia: new insights into regional morphology and diastolic dysfunction.** Aufferman W, Wichter T, Skutta W, Peters PE

**11:48 129. Evaluation of pulmonary blood flow by CT in chronic thromboembolic pulmonary hypertension.** Falaschi F, Palla A, Fratini L, Formichi B, Marini C, Perri G, Giuntini C

**12:00 130. CT vs chest radiography in monitoring thoracic metastatic disease in patients on interleukin-2/alpha-interferon therapy.** Fishman JE, Aberle DR, Moldawer N, Belledegrun A, Figlin RA

**12:12 131. Invasive pulmonary aspergillosis after bone marrow transplantation: sensitivity of chest radiograph vs high resolution.** Aufferman W, Zwicker C, Beyer J, Felix R

**12:24 132. Atypical multicystic radiologic appearance of bronchiolalveolar cell carcinoma.** Towers MJ, Weisbrod GL, Herman SJ, Chamberlain DW

## XIII. Interventional Radiology—Nonvascular

**10:00 133. Abdominal abscesses associated with enteric fistula percutaneous management.** Schuster MR, Crummy AB, McDermott JC, Wojtowycz MM

**10:12 134. Characteristics of fluid aspirates as an indicator of the need for subsequent drainage.** Marn CS, Ludka MR, Korobkin MT, Ellis JH

**10:24 135. Percutaneous drainage in liver abscesses with and without biliary communication: a comparison.** Do HM, Deyoe LA, Lambiase RE, Cronan JJ, Dorfman GS

**10:36 136. Radiologic intervention in complicated pancreatitis: catheters, clinical care, caveats and cost-effectiveness.** Lee MJ, Saini S, Brink JA, Hahn PF, Simeone JS, Rattner D, Warshaw AL, Mueller PR

**10:48 137. Percutaneous drainage associated with somatostatin analog (Octreotide) for pancreatic pseudocysts: early experience.** D'Agostino H, vanSonnenberg E, Casola G, May S, Taggart S, Sanchez R, Goodacre B

**11:00 138. The cystic duct: in vitro analysis as a preliminary to percutaneous manipulations.** Majidian M, vanSonnenberg E, D'Agostino H, Sanchez R, Goodacre B, Esch O

**11:12 139. Embolotherapy of uterine arteriovenous malformations.** Vogelzang R, Nemcek AA

**11:24 140. Percutaneous access for ureteroscopic management of ureteral calculi.** Krebs TL, Papanicolaou N, Lee M, Dretler SP, Tung GA, Yoder IC

**11:36 141. Retrograde replacement of internal double-J ureteral stents.** Yedlicka JW, Aizpuru RN, Hunter DW, Castañeda-Zúñiga WR, Amplatz K

**11:48 142. Use of the Wallstent endoprosthesis for palliation of malignant biliary obstruction.** Selby JB, Tegtmeyer CJ, Eaton B

**12:00 143. MR imaging in experimental lymphatic filariasis using an interstitially injected iron oxide compound.** Tanoura TT, Darkazankli A, Elam E, Unger EC, Bernas MJ, Witte M, Green A

**12:12 144. Transcatheter embolization of acute lower gastrointestinal tract hemorrhage.** Guy GE, Shetty PC, Sharma RP, Burke MW, Burke TH

**12:24 145. CT-assisted gastrostomy placement.** Sanchez R, vanSonnenberg E, D'Agostino H, Casola G, Moyers JP, Goodacre B

## XIV. Diagnostic Neuroradiology

**10:00 146. Cocaine-related cerebrovascular injury in adults: a neuroradiologic update.** Gean-Marton A, Rowley HA, Ciricillo SF, Olsen WL

**10:12 147. Utilization of head CT by emergency department.** Erickson KK, Reinus WR, Wippold FJ

**10:24 148. Traumatic atlantooccipital dislocation: diagnosis and treatment.** Ahuja A, Alker G, Flasauer FE, Hopkins LN, Bedi D

**10:36 149. Improving signal-to-noise in MRI by averaging of multiecho images.** Halpern E, Newhouse J, McLachlan S, Simon H, Kelley D

**10:48 150. Estimation of blood-brain barrier breakdown and lesion size: quantitative comparison of contrast-enhanced cranial CT and MR.** Harris RD, Hoopes PJ, Roberts DW, Douple EB, Ryan TP

**11:00 151. Quantitative measurements of the spinal cord and canal by MR imaging and myelography.** Bidgood WD, Ros LH

**11:12 152. Preliminary experience with new nonionic (zero net charge) gadolinium preparation in patients with intracranial tumors.** Pollei SR, Atlas S, Drayer B, Rosa L, Runge V, Sze G, Yuh WTC

**11:24 153. Contrast-enhanced gradient echo imaging.** Mihara F, Joslyn JN, Gupta KL

**11:36 154. The role of Gd-DTPA–enhanced 2-D FLASH MR imaging in evaluation of the patients with pulsatile tinnitus.** Wang AM, Bojrab DI, Wesolowski DP

**11:48 155. The role of gadopentetate dimeglumine in the routine evaluation of the lumbar spine.** West JW, Lee C, Dean BL, Kirsch JE, Runge VM

**12:00 156. Double dosing of Gd-DTPA in MRI of intracranial tumors.** Haustein J, Bauer W, Hilbertz T, Louton T, Niendorf HP, Planitzer J, Schorner W, Schubeus P

**12:12 157. Value of 3D- and 2D-reconstructions in HR-CT of the petrous bone.** Keske U, Langer M, Astinet F, Zwicker C, Hippel K, Jahnke V, Felix R

**12:24 158. Subfrontal recurrence of medulloblastoma.** Donnal JF, Friedman HS, Boyko OB, Oakes WJ, Halperin EC

# Thursday, May 9, 1:30 p.m.–3:30 p.m.

## XV. Bone—Fracture

1:30 **159. Value of bone scintigraphy in the initial management of gunshot wounds to the extremities.** Davis LP, Guyot D, Muz J, Fitzgerald R, Kling GA

1:42 **160. MR imaging of stress fractures of the sacrum.** Fedyshin PJ, Daffner R

1:54 **161. Unstable Jefferson variant atlas fractures: an unrecognized cervical injury.** Lee C, Woodring JH

2:06 **162. Interactive 3-D display for the assessment of tibial plateau fractures**. Murphy WD, Diaz PJ, Crass JR, Bellon EM, Kondow A, Behrens AF

2:18 **163. Adamantinoma with associated cortical fibrous dysplasia.** Hudson TM, Sweet DE, Aoki J, Moser RP

2:30 **164. Postradiation sarcomas of bone: radiologic findings.** Engle MR, McLeod RA, Unni KK

2:42 **165. Gd-DTPA–enhanced MR imaging in cartilage tumors: correlation with histology.** Geirnaerdt MJA, Bloem JL, Eulderink F, Taminiau AH

2:54 **166. The use of IV Gd-DTPA in MR imaging of synovial lesions.** Moore TE, Whitten CG, Yuh WTC, Kathol MH, Renfrew DL, Walker CW

3:06 **167. Differentiation of posttreatment changes from recurrent musculoskeletal sarcomas using Gd-DTPA–enhanced MRI and ultrasonography.** Kim EE, Choi H, Varma DGK, Fornage BD, Cho BJ, Wallace S, Benjamin R

3:18 **168. Isointense metastatic bone tumors on T1-weighted MR images.** Fujimoto H, Murakami K, Yuasuda S, Ichikawa T, Kashimada A, Matsubara T, Tsumurai Y, Masuda S, Arimizu N

## XVI. Ultrasonography

1:30 **169. Transabdominal graded-compression US of the stomach.** Op den Orth JO

1:42 **170. Ultrasound screening for renal artery stenosis in hypertensive patients.** Kriegshauser JS, Kliewer M, Carroll BA, Svetkey LP, Bowie JD

1:54 **171. Color Doppler ultrasonographic findings in scrotal inflammatory conditions.** Horstman WH, Middleton WD, Melson GL

2:06 **172. Large amniotic sac predicts nonviability.** Horrow MM

2:18 **173. Color and pulsed Doppler evaluation of the normal menstrual cycle.** Gutstein LL, Wang KY, Mack LA, Cyr D, Soules MR, Anderson D

2:30 **174. The utility of ultrasound as outcome prediction in first-trimester threatened abortion.** Harris RD, Moore LL, Beaurivage N, Sargent SK, Crow HC

2:42 **175. Duplex evaluation following in-situ saphenous vein bypass grafts.** Althaus SJ, King NJ III, Letourneau JG, Hunter DW

2:54 **176. Comparison of duplex sonography and arteriography for lower extremity stenoses in a dog model.** Althaus SJ, Yedlicka JW, Longley DG, Hunter DW, Letourneau JG

3:06 **177. Outcome of patients evaluated with ultrasound for lower extremity deep venous thrombosis.** Grantham JR

3:18 **178. Color flow Doppler ultrasound comparison with peripheral arteriography.** Whelan JF, Barry MH, Moir JD, Lund GE

## XVII. Gastrointestinal Radiology

1:30 **179. Manganese-DPDP-enhanced MRI of liver metastases.** Aicher KP, Kopp AF, Gronewaller E, Rummeny E, Laniado M

1:42 **180. T1 and T2-weighted pulse sequences provide similar contrast discrimination at high-field MR imaging of liver metastases.** Saini S, Li W, Wallner B, Edelman RE

1:54 **181. Turbo-FLASH MR imaging: perfusion patterns of hepatic tumors.** Rummeny E, Stober U, Adolph J, Bongartz G, Vestring T, Fervers J, Peters PE

2:06 **182. Pre- and post-barium MRI: normal abdominal/pelvic anatomy.** Ros PR, Torres GM, Burton SS, Steinman R, Panaccione JL, Rappaport D

2:18 **183. Documentation of the importance of radiologic ward rounds in interventional procedures of the abdomen and chest: the value of the daily visit.** Goldberg MA, Lee MJ, Saini S, Hahn PF, Brink JA, Girard MJ, Morrison M, Hallisey M, Cortell E, Hahn PF, Mueller PR

2:30 **184. Percutaneous laser ablation of the cystic duct and chemical sclerosis of the gallbladder: in vivo animal experiments.** Girard MJ, Saini S, Flotte T, Lee MJ, Goldberg MA, Brink JA, Ribeiro R, Ferrucci JT, Nishioka N, Mueller PR

2:42 **185. Hepatic in vivo video microscopic abnormalities following administration of a perfluorocarbon emulsion.** Kruskal JB, Lunderquist A, Clouse ME

2:54 **186, Hepatic in vivo video microscopy for evaluating MR imaging agents.** Kruskal JB, Lunderquist A, Clouse ME

3:06 **187. Complications of pancreatic biopsies in patients with biliary tract dilatation.** Watson LJ, Kane NM, Ellis JH, Korobkin M

3:18 **188. CT features of metastatic carcinoid tumors.** Francis IR, Quint LE, Ellis JH, Korobkin MT

# American Roentgen Ray Society:
## Officers, Committees, and Membership Information

### Officers

**President:** M. Paul Capp
**President-elect:** John A. Kirkpatrick, Jr.
**1st Vice-president:** A. Everette James, Jr.
**2nd Vice-president:** Andrew K. Poznanski
**Secretary:** Joseph T. Ferrucci, Jr.
**Treasurer:** Beverly P. Wood

**Executive Council:** R. J. Alfidi, R. N. Berk, M. P. Capp, W. J. Casarella, N. R. Dunnick, R. G. Evens, J. T. Ferrucci, Jr., A. E. James, Jr., J. A. Kirkpatrick, Jr., A. M. Landry, Jr., J. E. Madewell, A. A. Moss, A. K. Poznanski, L. F. Rogers, R. J. Stanley, J. H. Thrall, K. H. Vydareny, N. O. Whitley, B. P. Wood, G. R. Leopold, chairman

### Committees

**Editorial Policy:** R. N. Berk, E. Buonocore, Melvin M. Figley, S. v. W. Hilton, M. S. Huckman, C. A. Rohrmann, Jr., R. J. Stanley, R. I. White, W. J. Casarella, chairman

**Education and Research:** C. B. Higgins, B. J. Hillman, R. A. McLeod, R. J. Stanley, W. M. Thompson, N. O. Whitley, chairman

**Finance and Budget:** R. J. Alfidi, R. K. Gedgaudas-McClees, J. R. Thornbury, K. H. Vydareny, J. H. Thrall, chairman

**Nominating:** G. A. W. Gooding, L. F. Rogers, K. H. Vydareny, chairman

**Publications:** E. Buonocore, C. A. Rohrmann, Jr., R. J. Stanley, R. I. White, W. J. Casarella, chairman

**Membership:** J. E. Madewell, A. A. Moss, K. H. Vydareny, R. J. Alfidi, chairman

### Representatives to Other Organizations

**American Board of Radiology:** J. A. Kirkpatrick, Jr., E. C. Klatte, L. F. Rogers

**American College of Radiology:** J. M. Dennis, R. A. Gagliardi, J. E. Madewell, B. L. McClennan, R. J. Stanley

**American Medical Association:** S. F. Ochsner, delegate; K. L. Krabbenhoft, alternate; K. L. Kidd, CPT Advisory Committee

**American National Standards Institute:** M. E. Haskin

**National Council on Radiation Protection and Measurements:** F. Miraldi, E. L. Saenger

**Armed Forces Institute of Pathology:** J. E. Madewell

### Meeting Arrangements

**Annual Meetings:** May 5–10, 1991, Sheraton Boston, Boston; May 10–15, 1992, Marriott's World Center, Orlando, FL

**Annual Meeting Committee:** H. C. Carlson, J. K. Crowe, N. R. Dunnick, R. R. Lukin, R. J. Stanley, R. D. Steele, Jr., A. M. Landry, Jr., chairman

**Instructional Courses:** Bruce L. McClennan, associate chairman; R. J. Stanley, chairman

**Scientific Program:** P. Arger, E. Buonocore, D. O. Davis, K. B. Hunter, D. Kushner, T. C. McLoud, W. A. Murphy, Jr., L. B. Talner, J. H. Thrall, J. A. Kirkpatrick, chairman

**Scientific Exhibits:** J. R. Haaga, R. G. Ramsey, N. R. Dunnick, chairman

### ARRS Membership

An application form is printed in the February issue of the Journal. For consideration at the 1992 ARRS meeting, send completed forms before February 1, 1992, to American Roentgen Ray Society, 1891 Preston White Dr., Reston, VA 22091. Active members are graduates of an approved medical or osteopathic school or hold an advanced degree in an allied science. They must practice radiology or work in an associated science in the United States or Canada and be certified by the American Board of Radiology, American Osteopathic Board of Radiology, or Royal College of Physicians of Canada or otherwise adequately document training and credentials. Corresponding members are foreign radiologists or scientists who are active in radiology or an allied science. Members-in-training are residents or fellows in radiology or postgraduate students in an allied science. Additional application forms can be obtained from the ARRS offices in Reston, VA.

### Business Office

Paul Fullagar, Executive Director, American Roentgen Ray Society, 1891 Preston White Dr., Reston, VA 22091; (703) 648-8992.

# Classified Advertisements

## Positions Available

**THE UNIVERSITY OF MICHIGAN, DEPT. OF RADIOLOGY**—The University of Michigan Medical School is seeking an academic leader to chair its Dept. of Radiology. Qualifications include an M.D. degree and board-certification in diagnostic radiology; a record of scholarly accomplishment sufficient to justify a tenured faculty appointment; ability to provide leadership to the teaching, research, and clinical programs of an academic dept. in a large and complex medical center; administrative skills; and substantial management experience. The position includes an instructional (tenure) track faculty appointment. To respond, please send a CV by May 1, 1991, to Radiology Search Committee, c/o Ms. Jeanne Kin, Staff Associate, Medical Administration, M7330 Med Sci I, University of Michigan Medical School, Ann Arbor, MI 48109-0624. The University of Michigan is a nondiscriminatory/affirmative action employer. Women and minority candidates are encouraged to apply. 4a

**RADIOLOGIST**—Large, private-practice group in upstate New York seeks board-certified radiologist with general interests and preferably with fellowship training. Practice includes mix of private and teaching hospitals, offices, urban and rural settings. All modalities including 3 MRI units. This is an extremely high-quality practice offering excellent benefits and an opportunity for long-term security through shareholder status. Send CV to Box K50, *AJR* (see address this section). 4–6a

**NEURORADIOLOGIST** for established, free-standing, MRI/CT facility in Brooklyn Heights, NY. Excellent salary, profit-sharing first yr, plus very early full partnership. Senior member ASNR or eligibility desired. Call Dr. Ramanathan; (718) 624-2222 (a.m.) or (718) 802-0406 (p.m.). 4ap

**RADIOLOGIST, CAPITOL DISTRICT, NEW YORK STATE**—Well-established, hospital-based group practice in upstate New York seeks board-certified, general diagnostic radiologist with special competence and interest in nuclear medicine and MRI. Angiography and interventional experience will be helpful. This will be an additional opening to a 5-person group currently performing all aspects of radiology. Salary first yr leading to full partnership. Please send CV to John J. Gorman, M.D., Dept. of Medical Imaging, St. Clare's Hospital, 600 McClellan St., Schenectady, NY 12304; (518) 382-2310. 4–7ap

**CHIEF OF DIAGNOSTIC RADIOLOGY**—The Louis A. Weiss Memorial Hospital is a 275-bed, expanding affiliate of The University of Chicago that performs approximately 65,000 radiologic exams/yr. Applicants should have broad experience in general diagnostic radiology and administrative skills. An interest in teaching or research would be advantageous. The successful applicant will be appointed to the faculty at The University of Chicago. Academic rank and compensation commensurate with experience. Candidate should be board-certified and licensed to practice in Illinois. Interested parties should send their CVs to Heber MacMahon, M.D., Chairman, Weiss Search Committee, Dept. of Radiology, The University of Chicago, 5841 S. Maryland, Box 429, Chicago, IL 60637; (312) 702-1604, fax (312) 702-1161. Affirmative action/equal opportunity employer. 4–6ap

**LARGE, PROGRESSIVE RADIOLOGY PRACTICE**, located in Central New Jersey/Bucks County, PA region, seeks a radiologist with angio/interventional expertise. Immediate availability. Send letter and CV to S. Meshkov, M.D., 838 W. State St., Trenton, NJ 08618. 4a

**DIAGNOSTIC RADIOLOGIST**—Due to the recent merger of residency programs with St. Luke's Hospital and Truman Medical Center, UMKC, School of Medicine, we are expanding the number of staff positions at the academic rank of assistant or associate professor level. The dept. currently performs 87,000 exams/yr. Strong teaching background required. Compensation commensurate with qualifications and experience. Send letter of interest and CV to Fong Tsai, M.D., Professor and Chairman, University of Missouri-Kansas City, Radiology Dept., 2301 Holmes, Kansas City, MO 64108. 4–6ap

**DIAGNOSTIC RADIOLOGIST, IMMEDIATE OPENING**—Ten-person radiology group seeks a diagnostic radiologist with fellowship training, including body MRI/body imaging, to join a busy, hospital-based practice located in rapidly growing north Dallas. GE 1.5-T magnet, Toshiba midfield magnet, 2 GE 9800 scanners, Acuson 128 with color flow Doppler, and new special procedures suite with DSA. Please send CV to Box K54, *AJR* (see address this section). 4xa

**RADIOLOGIST**—Faculty position for ABR- or FRCP-qualified radiologist at assistant- or associate-member level in the Diagnostic Imaging Dept., St. Jude Children's Hospital, Memphis, TN. Growing, well-equipped dept. includes ultrasound, CT, nuclear radiology, MR imaging, and spectroscopy. Position provides excellent opportunities for clinical research in oncologic imaging. Candidate may also receive faculty appointment at University of Tennessee. Interested parties should contact Barry D. Fletcher, M.D., Chairman, Dept. of Diagnostic Imaging, St. Jude Children's Research Hospital, Memphis, TN 38101. Affirmative action/equal opportunity employer. 4–5ap

**UTMB, GALVESTON, TX**—The Dept. of Radiology of the University of Texas Medical Branch in Galveston has openings for persons trained and experienced in ultrasonography and mammography. The opportunity for academic advancement is great and benefits are generous. Salaries are competitive and living conditions are desirable. Interested persons should contact Melvyn H. Schreiber, M.D., Chairman, Dept. of Radiology, UTMB, Galveston, TX 77550; (409) 761-1823. UTMB is an equal opportunity M/F/H/V affirmative action employer. UTMB hires only individuals authorized to work in the United States. 4–9a

**RADIOLOGIST**—The Elko Regional Medical Center seeks a board-certified/eligible diagnostic radiologist to work at the medical center as well as the local community hospital. CT, mammography, ultrasound, nuclear medicine, and some interventional training or experience required. Guaranteed salary for 6 mo leading to full partnership. Excellent benefit package including malpractice insurance. Elko is a thriving community surrounded by mountains and wilderness areas. Recreation yr round. Please send CV to Cherie Atwood, Administrator, Elko Regional Medical Center, 762 14th St., Elko, NV 89801; (702) 738-3111. 4–6ap

**COUNTRY HOSPITALS**—$150,000. Central Kentucky. CV to 114 Kensington, Campbellsville, KY 42718. 4ap

**DALLAS, TX**—A 12-member, subspecialty group seeks a board-certified, general radiologist for an immediate opening. Fellowship training preferred, but will consider qualified individual with special expertise. CT/ultrasound, MRI, nuclear medicine, or angiography background particularly helpful. All imaging modalities available (state-of-the-art CT, angio, ultrasound, R & F, SPECT nuclear medicine, and MRI center). Salary and bonuses are excellent. Health and malpractice paid. No buy-in to partnership. Send CV to H. Stuart Peake, M.D., P.O. Box 814129, Dallas, TX 75381; (214) 888-7055. 4–9ap

**DIAGNOSTIC IMAGING GROUP, UNIVERSITY CITY, MIDWEST**—Join a 6-person group in a hospital- and office-based practice. BC/BE diagnostic radiologist. Practice includes diagnostic radiology, CT, ultrasound, and nuclear medicine. MRI experience available through medical school radiology dept. affiliation. Salary and terms negotiable based on experience. Send CV to Box K56, *AJR* (see address this section). 4ap

**IMMEDIATE OPENING FOR BC/BE GENERAL RADIOLOGIST** with experience in interventional and vascular radiology. Join a group of 4 radiologists in a 160-bed hospital located in Allentown, PA, about 60 mi. northwest of Philadelphia. The daily practice includes all aspects of general radiology, CT, ultrasound, and nuclear medicine. Please call or send CV to Asad Shohadai, M.D., Allentown Osteopathic Medical Center, 1736 Hamilton St., Allentown, PA 18104; (215) 770-8700. 4xap

**SENIOR FACULTY POSITION IN GI/GU RADIOLOGY**—Dartmouth-Hitchcock Medical Center is seeking a senior faculty member at the associate or full professor level with experience and interest in GI/GU radiology. Clinical responsibility will be in an entirely new, 400-bed, clinical facility opening Sept. 1991, with state-of-the-art instrumentation. Position will involve responsibility for residency training in GI/GU area. Proven record of academic performance including research and teaching with an interest in providing academic guidance for energetic staff of younger radiologists necessary. Interested candidates write with CV to P. K. Spiegel, M.D., Chairman, Dept. of Diagnostic Radiology, Dartmouth-Hitchcock Medical Center, Hanover, NH 03756. AA/EOE. 4xa

**CHEST RADIOLOGIST, THOMAS JEFFERSON UNIVERSITY HOSPITAL**—The Dept. of Radiology at Jefferson has an opening for a thoracic radiologist at either the junior or senior level. The position encompasses plain film radiography, CT, and percutaneous thoracic interventions. Involvement in mammography, other general diagnostic areas, and ultrasound can also be incorporated, depending on the interests of the candidate. Dedicated, nonclinical research time is provided, and the dept. has excellent research facilities and support. Our chest radiology practice is expanding rapidly and close working relationships are maintained with pulmonary medicine and thoracic surgery. Teaching is also emphasized, with a large residency program and a thoracic radiology fellowship. Excellent faculty income and benefits. This is a fine opportunity for a radiologist with academic interests to join a dynamic and rapidly growing dept. Interested candidates should contact David C. Levin, M.D., Chairman, Dept. of Radiology, Thomas Jefferson University Hospital, Philadelphia, PA 19107; (215) 955-7264. Jefferson is an equal opportunity/affirmative action employer. 4–6a

**NEBRASKA**—Diagnostic radiologist with proficiency in general diagnostic radiology, nuclear medicine, CT scanning, MRI, mammography, and special procedures needed for hospital-based practice. Generous salary and benefits. If you are looking for quality of life, look no further than this "all-American city" and please call Barbara Lakoski (800) 243-4353 or send your CV to Strelcheck & Associates, Inc., 10624 N. Port Washington Rd., Mequon, WI 53092. 4ap

**COLORADO MOUNTAINS**—Opportunity for BC/BE radiologist in part-time, solo practice available July 1991. Gunnison has abundant outdoor activities including water sports and excellent downhill skiing. Four yr college in town. Hospital-based or private practice available. Contact Robert Austin, Gunnison Valley Hospital, 214 E. Denver, Gunnison, CO 81230; (303) 641-1456. 4–5a

**RADIOLOGISTS**—A 4-member, rapidly growing practice in McAllen, TX needs 2 general, BC/BE radiologists. Hospital-based practice plus imaging center with 1.5-T GE MRI, 9800 GE CT, Sophy SPECT camera, color Doppler ultrasound, mammography, and fluoroscopy. Early partnership, excellent salary/opportunity. Contact William Martin, M.D.; (512) 682-0888. 4–6ap

**VASCULAR/INTERVENTIONAL RADIOLOGIST** The University of Miami, School of Medicine, is currently recruiting a full-time vascular and interventional radiologist. The Interventional Section provides radiologic services at Jackson Memorial Medical Center and Veterans Administration Medical Center. About 3000 exams per yr are performed by this section, including all diagnostic and interventional vascular procedures except for cardiac and neuroradiologic studies. We also have an active nonvascular interventional service involving thoracic and abdominal intervention. The section currently consists of 5 staff members and 3 fellows. Residents rotate through the service on a monthly basis. Candidates must be board-certified or eligible, with fellowship training or equivalent experience. Rank and salary commensurate with qualifications. Please send CV to Jose M. Yrizarry, M.D., Chief, Vascular/Interventional Radiology Section, University of Miami School of Medicine, Dept. of Radiology (R-109), P.O. Box 016960, Miami, FL 33101; (305) 549-6894. The University is an affirmative action/equal opportunity employer. 4–5ap

**ANGIOGRAPHER/INTERVENTIONAL RADIOLOGIST, TOLEDO, OH**—Quality-oriented, 22-radiologist group is seeking a board-certified, university-trained radiologist with angiography/interventional fellowship experience. Group covers 850-bed tertiary hospital, 350-bed suburban hospital, 3 outpatient offices, and performs 240,000 exams/yr. Position leads to equal partnership and combines excellent salary with very generous vacation time. All practice locations within 15 min of each other and are situated in an area of superb, family-oriented living with excellent schools. Send CV to Drs. David Parker or Keith Wilson, Roemer Bldg., 3912 Sunforest Ct., Toledo, OH 43623; (419) 471-4438 days. 4–6ap

**MARYLAND**—The Dept. of Radiology, University of Maryland Medical System/Hospital in Baltimore is seeking additional faculty members for the sections of pediatric radiology, ultrasound, nuclear medicine, GI radiology, mammography, neuroradiology, and skeletal radiology. Also, a chief of abdominal imaging, a Ph.D. MRI consultant, and a research assistant for MRI are needed. Fellowship training or equivalent experience desired. ABR certification required where appropriate. The medical center is an 800-bed, acute-care hospital and tertiary referral center with an active and varied practice. A new, affiliated VA hospital with 324 beds is now under construction and will be adjacent to and connected with the university in the spring of 1992. The duties of new faculty members will include research and teaching. Academic rank and salary commensurate with experience. The radiologists are organized as a professional corporation offering excellent fringe benefits. Baltimore is a superb place in which to live and work. It has all the amenities of a large metropolitan center, yet is small enough to avoid most of the problems (traffic, inflated property values, etc.) of our largest cities. Washington, Philadelphia, and New York are readily accessible, only 3 hr from Ocean City, MD. Submit CV to Gerald S. Johnston, M.D., Dept. of Diagnostic Radiology, 22 S. Greene St., Baltimore, MD 21201; (800) 866-8667, ext. 3477. Affirmative action/equal opportunity employer and applications from members of minority groups are encouraged. 4ap

**NO-CALL RADIOLOGIST FOR SOUTHERN CALIFORNIA BEACHES**—Position is now available with premier, 21-member group to help staff a growing number of outpatient facilities. Fellowship training in mammography/ultrasound is required. The group operates 5 Acuson imagers and 8 dedicated mammography units. Please send CV to Robert Hurwitz, M.D., 355 Placentia Ave., Ste. 207, Newport Beach, CA 92663. For faster reply, please call our dept. secretary, Denise, at (714) 645-9500. 4–6ap

**DIAGNOSTIC RADIOLOGIST**—Yale University School of Medicine seeks a board-certified radiologist, with additional experience or training in ultrasound/CT, for a full-time faculty position. Academic rank is at the level of assistant or associate professor, depending on qualifications. Candidates must be competent in all aspects of ultrasound, including vascular, and must be able to do cross-sectional interventional procedures. Must have credentials to work at the local VA hospital as well as a strong adademic background with research goals. Candidates must be U.S. citizens or must qualify as permanent residents in the United States. Please send CV and bibliography to Lynwood Hammers, D.O., or Kenneth J. W. Taylor, M.D., Diagnostic Radiology, Yale University School of Medicine, 333 Cedar St., New Haven, CT 06510. Yale University is an equal opportunity employer; applications from women and minority group members are encouraged. Application deadline is May 1, 1991. 3–4a

**MUSCULOSKELETAL RADIOLOGIST, MALLINCKRODT INSTITUTE OF RADIOLOGY/WASHINGTON UNIVERSITY**—The musculoskeletal section is enlarging and has need for an additional person at the instructor, assistant professor, or associate professor level. The section performs all aspects of musculoskeletal imaging including CT, MRI, bone biopsy, and arthrography of all joints. The section also performs all diagnostic and screening mammography and breast procedures and directs emergency dept. radiology. The volume of clinical material is large. Teaching, academic, and working conditions are well-supported. Send CV to Louis A. Gilula, M.D., or William A. Murphy, M.D., Mallinckrodt Institute of Radiology, Barnes Hospital, 510 S. Kingshighway Blvd., St. Louis, MO 63110. 3–6a

**MICHIGAN**—Opportunity for a BE/BC radiologist to join 1 other in a hospital-based, rural practice. Experience in CT, ultrasound, nuclear medicine, mammography, and general radiology. Competitive salary. Send CV to David L. Carter, M.D., 6796 Garfield St., Cass City, MI 48726. 3–4ap

**DIAGNOSTIC RADIOLOGIST, PART-TIME, TUCSON, AZ**—Radiologist to join 24-person group on approximately 1/2-time basis with 1-yr renewable contract. No night or weekend call, work every other Saturday a.m. Includes health, life, disability, and malpractice insurance. General diagnosis, mammography, CT, and ultrasound. Contact R. O. Broome, M.D., Radiology, Ltd., 6516 E. Carondelet Dr., Bldg. C, Tucson, AZ 85710. 3–5ap

**CROSS-SECTIONAL IMAGING/MRI, CT, ULTRASOUND**—The Dept. of Radiology, Strong Memorial Hospital, University of Rochester, Rochester, NY, is seeking a board-eligible/certified radiologist for its body imaging section. An appointment as assistant professor or higher is available at a level appropriate to experience. One yr fellowship training or equivalent experience is required. Research and teaching opportunities are afforded in a strong academic dept. with state-of-the-art radiologic equipment. Send letter of inquiry to Robert E. O'Mara, M.D., Chair, Dept. of Radiology, Box 648, University of Rochester Medical Center, Rochester, NY 14642; (716) 275-2733. EO/AA/M-F employer. 3–6ap

**THE DEPT. OF RADIOLOGY, VIRGINIA COMMONWEALTH UNIVERSITY/ MEDICAL COLLEGE OF VIRGINIA AND THE MCGUIRE VA MEDICAL CENTER, RICHMOND, VA**, seek faculty for positions in diagnostic radiology (chest, GI, mammography, CT/ultrasound/MRI, musculoskeletal, pediatrics, ER, angio/interventional, and neuroradiology), nuclear medicine, and radiological physics. MCV is a 1,058-bed facility (205 for pediatric patients) and a Level I Trauma Center. The McGuire VAMC is an 800-bed facility (pediatrics excluded). ABR certification of eligibility required. Individual should have experience working in a culturally diverse environment. Academic rank and salary commensurate with experience. For position description or to submit CV, write or phone A. V. Proto, M.D., Dept. of Radiology, MCV Box 470, Richmond, VA 23298-0470; (804) 786-7212. VCU/MCV is an equal opportunity/affirmative action employer. Women and minorities are encouraged to apply. 3–4a

**HEAD, CROSS-SECTIONAL IMAGING SECTION** The Dept. of Radiology, University of Rochester Medical Center, Strong Memorial Hospital, Rochester, NY, is seeking a board-certified radiologist with subspecialty experience in body imaging for a faculty position as Head of Cross-Sectional Imaging Section, including ultrasound, CT, MRI, and body interventional. Strong Memorial Hospital is a 750-bed, tertiary-care hospital. State-of-the-art MRI, CT, and ultrasound equipment is available. Teaching of medical students, radiology residents, and fellows and the opportunity for developing research projects are afforded. Rank and salary are commensurate with experience. Interested candidates should forward CV to Robert E. O'Mara, M.D., Chair, Dept. of Radiology, Box 648, University of Rochester Medical Center, Rochester, NY 14642; (716) 275-2733. EO/AA/M-F employer. 3–6ap

**RADIOLOGIST, CT/ABDOMINAL IMAGING**—An opening exists for a board-certified/eligible radiologist with fellowship training or equivalent experience in CT to serve on the CT service in abdominal imaging with participation in other aspects of the division. Extensive clinical research opportunities exist at the Yale Medical School and the Yale–New Haven Hospital. Academic rank commensurate with experience. Numerous benefits including paid sabbatical. Candidates must be U.S. citizens or must qualify as a permanent resident in the United States. Please send CV and bibliography to Arthur T. Rosenfield, M.D., Yale University School of Medicine, Dept. of Diagnostic Radiology, 333 Cedar St., New Haven, CT 06510. Yale is an equal opportunity/affirmative action employer. Applications from women and members of minority groups are encouraged. Applications should be submitted no later than May 1, 1991. 3–4a

**BC/BE RADIOLOGIST**—Full-time staff radiologist needed at active tertiary-care medical center for interpreting general diagnostic films (excluding mammography) and performing radiologic procedures and fluoroscopy. Supervision and training of residents with affiliated medical center required. Additional subspecialty skills, training in ultrasound, CT, and/or angiographic and interventional procedures are beneficial. Candidate should be qualified to hold a faculty position with Yale University School of Medicine and must be a U.S. citizen or must qualify as a permanent resident of the United States. Send CV and letters of reference to Caroline Taylor, M.D., Chief, Radiology, Dept. of Veterans Affairs Medical Center, West Haven, CT 06516. The DVA Medical Center and Yale University are equal opportunity/affirmative action employers. Applications from women and minority group members are encouraged. Application deadline is May 1, 1991. 3–4a

**INTERVENTIONAL RADIOLOGIST**—Board-certified radiologist with fellowship training in vascular/interventional radiology needed for a position starting July 1, 1991. Academic rank is at the assistant or associate professor level depending on qualifications. This active clinical service performs the entire range of diagnostic and interventional procedures including embolization, angioplasty, infusion therapy, IVC filter placement, and atherectomy. The interventional inpatient service admits 100 patients per yr, primarily for embolization and angioplasty. The interventional clinic evaluates referred patients with peripheral and renal vascular disease and vascular malformations. Clinical and fundamental research interests are ongoing in atherectomy, embolization devices, and endourology. Please send applications with CV to Robert I. White, Jr., M.D., Professor and Chairman, Diagnostic Radiology, Yale University School of Medicine, P.O. Box 3333, New Haven, CT 06510. Yale University is an equal opportunity/affirmative action employer. Applications from women and minority group members are encouraged. Application deadline is May 1, 1991. 3–4a

**MAMMOGRAPHY**—Immediate opening for a board-certified or eligible radiologist in the mammography section. Large screening and diagnostic program performs approximately 13,000 exams/yr including needle localization, cyst aspiration, and ultrasound through a mobile unit and an outpatient screening program. Program is very interactive with patients and referring physicians. Academic rank commensurate with experience. Yale University is an equal opportunity/affirmative action employer. Applications from women and minority group members are encouraged. Send current CV or phone Carol Lee, M.D., Yale University School of Medicine, Dept. of Diagnostic Radiology, 333 Cedar St., New Haven, CT 06510; (203) 785-2425. Application deadline is May 1, 1991. 3–4a

**UCLA SCHOOL OF MEDICINE, CARDIOVASCULAR RADIOLOGIST**—The UCLA Dept. of Radiological Sciences is recruiting for a full-time position in academic cardiovascular radiology. Title will be determined by level of training and experience. American Board of Radiology certification and eligibility for California licensure is required. Send detailed resume, including references, to Hooshang Kangarloo, M.D., Chair, Dept. of Radiological Sciences, UCLA School of Medicine, Los Angeles, CA 90024-1721. An equal opportunity/AA employer. 3–5a

**SEATTLE COLLEAGUE WANTED**—Growing radiology group seeks new member. Full-service radiology dept. (50,000 procedures/yr) offers diagnostic, nuclear medicine, ultrasound (including vascular-Doppler), interventional, CT, and MRI. Outpatient imaging dept. (building permits pending) scheduled to open late 1991 that will include high-field GE Signa MR with MRA. Extremely favorable track for partnership. For further information regarding this opening, please contact Mr. Richard G. Wedig, Highline Community Hospital, 16251 Sylvester Rd., S.W., Seattle, WA 98166; (206) 248-4561. 3–4ap

**DIAGNOSTIC RADIOLOGIST**—Dept. of Veterans Affairs Medical Center, Dayton, OH, offers a full-time position for a diagnostic radiologist. The Dayton VA consists of a 495-bed general and medical hospital, 284-bed nursing home, and 625-bed domiciliary. A new, state-of-the-art, acute-care hospital will be ready for occupancy by the end of 1991. Excellent cultural activities include theater, museums, symphony, and ballet. Send CV to Berta H. Baumann, M.D., Chief, Radiology Service, VA Medical Center, 4100 W. Third St., Dayton, OH 45428; (513) 268-6511, ext. 2151. An equal opportunity employer. 4a

**IMMEDIATE OPENINGS, CHARLOTTE, NC**—Service-oriented, 7-member group seeks 2 new associates in CT/ultrasound/MR and nuclear medicine. Fellowship training and/or staff level experience required. Must be willing to participate in all phases of general diagnostic radiology practice. Interventional experience helpful but not required. We serve 2 hospitals with a total of 260 beds. Equipment includes 3 GE 9800 CT, GE Signa 1.5-T MRI, Acuson and Toshiba ultrasound with color Doppler, 3 Toshiba SPECT, and Siemens 750 ZLC. Competitive salary leading to partnership after 2 yr. Send CV to Carl J. Eisenberg, M.D., Mercy Hospital, 2001 Vail Ave., Charlotte, NC 28105; (704) 379-5860. 3–5ap

**COME TO CALIFORNIA WITH A LICENSE FROM ANY STATE**—Loma Linda VA Hospital has a vacancy for a board-certified radiologist. A current license from any state is acceptable. Loma Linda is located 70 mi. east of Los Angeles near beaches, mountain ski resorts, and southland theme parks. This is a 500-bed, full-service hospital with a comprehensive diagnostic facility including ultrasound, CT, and MRI integrated with the Loma Linda University Medical Center residency training program. Opportunities exist to pursue clinical or academic interests. For additional information, contact Peter Dure-Smith, M.D., Chief, Radiology (114), Jerry L. Pettis Memorial Veterans Hospital, 11201 Benton St., Loma Linda, CA 92357; (714) 422-3069, fax (714) 422-4106. Equal opportunity employer. 3–8ap

**SAN ANTONIO, TX**—Group covering multiple hospitals and clinics seeks radiologists with imaging and angiography skills. Send CV to Search Committee, M & S X-Ray Associates, P.O. Box 15920, San Antonio, TX 78212-9510. 3–8ap

**DIAGNOSTIC RADIOLOGIST**—Two young, progressive radiologists seek a third, recently trained, BC/BE, general radiologist to join in a rapidly growing practice in a 100-bed hospital. 31,000 exams/yr, including ultrasound, nuclear medicine, mammography, and CT. No angiography. An MR rotation is available at a free-standing center. Call will be shared equally. 9-wk vacation. The Oneida City Hospital is located in the scenic eastern Finger Lakes, with a 4-season climate, near a medical school. Excellent starting salary, with full partnership following 2 yr; no buy-in. Please send CV with letter to Ralph Stevens, M.D., Dept. of Radiology, Oneida City Hospital, 321 Genesee St., Oneida, NY 13421. 2–4ap

**NEURORADIOLOGIST, BIG SKY COUNTRY**—Group of 5 radiologists seek a BC, fellowship-trained colleague. Hospital and busy clinical practice. Must be a capable, general diagnostic radiologist. One yr to partnership. Send letter/CV to Bruce Pinkerton, M.D., Dept. of Diagnostic Radiology, Deaconess Medical Center, P.O. Box 2547, Billings, MT 59103. 2–7ap

**DUKE UNIVERSITY MEDICAL CENTER/STAFF RADIOLOGISTS**—Duke University Medical Center is seeking qualified candidates for staff positions in the Dept. of Diagnostic Radiology. A limited number of staff positions currently are available in the following sections: general diagnostic, pediatric, chest, vascular/interventional, and musculoskeletal radiology. We offer an excellent salary and benefits package. The radiology dept. is state-of-the-art in diagnostic imaging with diverse resources available for clinical, teaching, and academic pursuits. Staff members have guaranteed academic time and research support. Interested board-certified radiologists with appropriate experience should phone Robert Vandemark, M.D. at (919) 681-2711 ext. 5233, for additional information. Letters of inquiry should be sent to Carl E. Ravin, M.D., Dept. of Radiology, Box 3808, Duke University Medical Center, Erwin Rd., Durham, NC 27710. AA/EOE. 2–7a

**PEDIATRIC RADIOLOGIST**—Yale–New Haven Medical Center and Yale University School of Medicine seek a pediatric radiologist for a full-time faculty appointment. Academic rank is at the level of assistant or associate professor, depending on qualifications. A strong interest in patient care, research, and teaching is required. Please send inquiries, along with CV, to Marc Keller, M.D., Diagnostic Radiology, Yale University School of Medicine, 333 Cedar St., New Haven, CT 06510. Yale University is an equal opportunity/affirmative action employer. Applications from women and minority group members are encouraged. Application deadline is May 1, 1991. 3–4a

**TWO DIAGNOSTIC RADIOLOGISTS** with recent training are sought for growing hospital practice of 3 BC radiologists in Elizabethtown, KY. Fellowship training in body imaging and intervention welcome. Modern, well-equipped radiology dept. at 300-bed regional hospital that includes 2 GE 9800 CT, GE 1.5-T MR, GE LU dedicated angiographic suite with DSA, ultrasound, nuclear medicine, and ACR-certified, dedicated mammography. Position available immediately. Send letters of inquiry with CV to Elizabethtown Radiology, P.S.C., P.O. Box 2489, Elizabethtown, KY 42701; (502) 765-4144. 2–4ap

**MAMMOGRAPHY FACULTY POSITION**—The Dept. of Radiology at Johns Hopkins University Hospital has a faculty position available in mammography. The mammography section is part of the thoracic imaging division. The section offers a strong potential for academic growth with emphasis on original research and teaching. Protected academic time is available for candidates interested in developing a strong academic career. Support, resources, and opportunities are available for creative research. The candidate can also participate in all other aspects of diagnostic imaging as desired. Academic rank and salary will be determined by previous experience. Candidate must be board-certified. Contact Elias A. Zerhouni, M.D., Director, Thoracic Imaging and MRI Divisions, Dept. of Radiology, Johns Hopkins Hospital, Baltimore, MD 21205; (301) 955-4062. 1–6a

**MUSCULOSKELETAL / MRI RADIOLOGIST, THOMAS JEFFERSON UNIVERSITY HOSPITAL** We are recruiting a faculty musculoskeletal radiologist (either junior or senior level) for an important and challenging position in our dept. The position encompasses MRI of the musculoskeletal system and other body applications, plain film musculoskeletal radiology, tomography, and arthrography. Jefferson currently operates 4 GE 1.5-T Signa MRI units and 3 CT scanners. Close relationships are maintained with busy orthopedic, rheumatology, trauma, and spinal cord injury services. A thriving clinical practice, active teaching program, and well-equipped research facilities all combine to make this an outstanding career opportunity. Excellent faculty incomes and many other benefits are provided. Interested applicants should contact David C. Levin, M.D., Chairman, Dept. of Radiology, Thomas Jefferson University Hospital, 11th and Walnut Sts., Philadelphia, PA 19107; (215) 955-7265. Jefferson is an equal opportunity/affirmative action employer. 1–4a

**BC RADIOLOGIST, KANSAS CITY, MO**—Seven radiologists currently covering a 600-bed, tertiary medical center seek a radiologist with a special competency or fellowship in nuclear medicine. The position, open immediately, includes competitive salary and fringe benefits, and leads to full partnership. Send CV and letter of inquiry to J. M. Speckman, M.D., 6400 Prospect, Ste. 310, Kansas City, MO 64132. 1–4ap

**DIRECTOR, DIAGNOSTIC RADIOLOGY**—Applications accepted for Director, Diagnostic Radiology, OHSU, Portland, OR. Faculty position opens on or about July 1, 1991. Associate or full professor based on experience. Musculoskeletal radiology fellowship, minimum of 5 yr as Vice-Chairman or Director of Diagnostic Radiology required. Send CV to William Weidner, M.D., Diagnostic Radiology, UHN-72, Oregon Health Sciences University, Portland, OR 97201-3098; (503) 494-4498. Equal opportunity, affirmative action employer. 3–6a

**PEDIATRIC RADIOLOGIST**—Division of Pediatric Radiology, OHSU, Portland, OR, invites applications for a faculty position available on or about July 1, 1991. Completion of approved fellowship in pediatric radiology and ABR certification required. Send CV to William Weidner, M.D., Diagnostic Radiology, UHN-72, Oregon Health Sciences University, Portland, OR 97201-3098; (503) 494-4498. Equal opportunity, affirmative action employer. 3–6a

**DIAGNOSTIC RADIOLOGIST**—University of Florida Health Science Center/Jacksonville is seeking a staff radiologist for a full-time faculty position. Special interest, expertise, or fellowship training in CT, ultrasound, MR, interventional, or nuclear radiology is preferable. Salary and fringe benefits are excellent. An academic appointment will be at the instructor, assistant professor, associate professor, or professor academic rank based on training, background, and experience. Application recruiting deadline is May 1, 1991. Send CV and references to Chairman, Search Committee, Dept. of Radiology, University Medical Center, 655 W. Eighth St., Jacksonville, FL 32209. AA/EOE. 3–4a

**DIAGNOSTIC RADIOLOGIST**—BC/BE radiologist wanted to join expanding practice of 12 radiologists in northeastern Pennsylvania. Practice includes 3 hospitals (720 beds) and free-standing MRI. Candidate must have experience in angiography and interventional radiology, and be willing to cover other areas of diagnostic imaging. Contact Paul M. Leiman, M.D., Dept. of Radiology, Moses Taylor Hospital, 700 Quincy Ave., Scranton, PA 18501; (717) 963-2601. 3–4ap

**CHIEF OF RADIOLOGY, VAMC, DENVER, CO** The Dept. of Radiology at the University of Colorado Health Sciences Center, in conjunction with the Denver Veterans Administration Medical Center, invites applications for the Chief of the Imaging Service at the Denver VAMC. Position requires interest in general diagnostic radiology, but those with special experience in nuclear medicine, interventional radiology, or neuroradiology are encouraged to apply. The 401-bed Denver VAMC has a recently renovated 20,000 sq. ft. imaging service and is closely affiliated with the UC Health Sciences Center. All diagnostic modalities are represented. Interested candidates should contact Michael L. Manco-Johnson, M.D., Professor and Chairman, Dept. of Radiology, University of Colorado Health Sciences Center, Campus Box C-277, 4200 E. 9th Ave., Denver, CO 80262; (303) 270-7719. The University of Colorado Health Sciences Center and Veterans Administration are committed to equal opportunity and affirmative action. 3–4a

**RADIOLOGIST NEEDED** with experience in CT, ultrasound, nuclear medicine, mammography, and general radiology to provide vacation coverage for 2 practices in rural western Montana. One practice requires some traveling. Position would be excellent for person who wishes to semiretire in a pleasant scenic area. Great opportunity for recreational activities. Send inquiries to Tyler H. Gill, M.D., 1200 Westwood Dr., Hamilton, MT 59840; (406) 363-2211. 2–6a

**RADIOLOGIST, BRIGHAM AND WOMEN'S HOSPITAL** — The Dept. of Radiology at the Brigham and Women's Hospital/Harvard Medical School wishes to recruit a staff person in ultrasound. This position offers diverse clinical work and extensive opportunities for research in abdominal, obstetric, vascular, and other areas of ultrasound. Rank and salary commensurate with experience. Evidence of interest in academic radiology and certification by the American Board of Radiology are preferred. Please send CV to B. Leonard Holman, M.D., Chairman, Dept. of Radiology, Brigham and Women's Hospital, 75 Francis St., Boston, MA 02115. Brigham and Women's Hospital/Harvard Medical School is an affirmative action/equal opportunity educator and employer. 2–4a

**MINNEAPOLIS, MINNESOTA**—Private practice opportunity for a neuroradiologist with procedural orientation to join an expanding group of 5 radiologists; 2 are ASNR members. Practice is primarily based at growing, free-standing, outpatient imaging centers and includes two 1.5-T Signa MR units, 3 GE 9800 CT scanners, and accompanying fluoroscopic-radiography equipment. A third MR unit is being installed in the Twin Cities and should be operational in early spring 1991. We are heavily oriented toward spine and musculoskeletal imaging and related procedures. Candidates must be interested in spine imaging and related procedures, such as myelography, nerve blocks, facet arthrograms/therapeutic procedures, and diskography. We are also affiliated with a 750-bed, tertiary hospital in Minneapolis. The practice is academically oriented and encourages clinical research and publication, although this is not required. No calls please. Send letters of inquiry and complete CV to Kurt P. Schellhas, M.D., Center for Diagnostic Imaging, 5775 Wayzata Blvd., Ste. 190, St. Louis Park, MN 55416. 2–4ap

**OREGON**—Group of 13 radiologists in Salem, OR, seeks BC/BE radiologist with general radiology skills. Practice includes 454-bed community hospital, large out-patient office, and multispecialty clinic. Near ideal family community and recreational amenities. Send CV to John Eyre, M.D., Salem Radiology, 919 Oak St., S.E., Salem, OR 97301. 2–5ap

**FLORIDA, STAFF RADIOLOGIST**—Opportunity for board-certified/eligible diagnostic radiologist with experience in reading plain films, fluoroscopy, ultrasound, CT, nuclear medicine, and some angiography in the radiology service at this GM&S, Dept. of Veterans Affairs (VA) Medical Center. Affiliation in surgery with the University of Florida. Excellent employment benefits including 30 days paid vacation and 15 days sick leave per yr; liberal life and health insurance benefits; malpractice insurance; and retirement program. Moving expenses paid. "Florida's new gateway city" is located in northern Florida with a mild climate yr round. Extensive outdoor recreational activities, reasonable cost of living, no state income tax, and fine schools and nearby universities provide opportunity for continuing education and cultural diversion. Florida license not required. Contact or send CV to Richard Parker, M.D., Chief of Radiology, VA Medical Center, Lake City, FL 32055-5898; (904) 755-3016, ext. 2543. An equal opportunity employer. 2–4a

**FAIRBANKS, AK**—Four diagnostic radiologists seek fifth partner for diversified practice including general radiology, ultrasound, nuclear medicine, MRI (GE 1.5-T), and CT (GE 9800). Hospital and office practice. Desirable life-style advantages in a university town. Unlimited access to the outdoors. Excellent salary, benefits, retirement, and vacation. One yr to full partnership. Contact Douglas Hutchinson, M.D., 1919 Lathrop #5, Fairbanks, AK 99701; (907) 452-5092. 2–4ap

**THE PENN STATE UNIVERSITY, MILTON S. HERSHEY MEDICAL CENTER, CHIEF OF MRI** The Pennsylvania State University Dept. of Radiology is seeking a full-time faculty chief of the section of Magnetic Resonance Imaging (MRI). The MRI section performs over 3000 MRI scans/yr on our 1-T Siemens system. We have just purchased a second magnet (1.5-T Toshiba MRI-150A). Both our in-house and outpatient magnet systems have significant research capacity for clinical and applications projects. A Nuclear Magnetic Resonance (NMR) Imaging/Spectroscopy center, directed by Michael B. Smith, Ph.D., with over 6500 sq. ft., is completed. It is connected to our outpatient MRI system. In this NMR center, we have 3 magnets: a 9.4-T Bruker AM-400 widebore spectrometer with micro imaging; a 1.9-T Oxford 26-cm-bore horizontal magnet interfaced to a Nicolet 1280 computer; and a 3.0-T Bruker 90-cm-bore spectrometer/imager which will be the first of its kind and 100% dedicated to research. The NMR center will also be completely equipped with surgical and animal preparation area, biochemistry laboratory, radiofrequency and electronics laboratory, full machine shop, computer resources, and office space for faculty, staff, postdoctorates, and students. The successful candidate must be experienced in both clinical and research MR, and have publications that confirm his/her experience. The chief of MRI will be responsible for developing further our clinical MRI service and integrating it with our new NMR research center. Clinical responsibility will be in MRI, either in neuroradiology, body imaging, or both, depending on the successful candidate's experience and certification. Independent original research is expected and is amply funded both in time and money. The academic rank will depend upon the candidate's achievement. The salary is dependent on the achieved rank and experience. The position is open to individuals who have completed an accredited residency program in radiology; can obtain a Pennsylvania medical license; can obtain medical staff privileges at University Hospital; and are board certified by the American Board of Radiology or its equivalent. Applicants should respond as soon as possible with a letter of interest and current CV. Please direct inquiries to John E. Madewell, M.D., Professor and Chairman, Dept. of Radiology, The Penn State University, Milton S. Hershey Medical Center, P.O. Box 850, Hershey, PA 17033. Penn State University is an affirmative action, equal opportunity employer. Women and minorities are encouraged to apply. 2–4a

**FACULTY OPENING IN THORACIC IMAGING** The Johns Hopkins University Hospital has an opening at the junior faculty level in the Division of Thoracic Imaging. The division is fully integrated across all modalities including MRI, CT, and interventional procedures. Research opportunities are exceptional with protected research time available to rapidly establish an academic career. Academic rank and salaries will be determined by previous experience. The candidate must be board-certified. Contact Elias A. Zerhouni, M.D., Director, Thoracic Imaging & MRI Divisions, Dept. of Radiology, Johns Hopkins Hospital, Baltimore, MD 21205; (301) 955-4062. 1–6a

**IMMEDIATE OPENING, DIAGNOSTIC RADIOLOGIST**—Excellent opportunity for a young, dynamic, preferably board-certified radiologist to join an active, 9-member group. Growing practice includes a 700-bed hospital system with state-of-the-art equipment and excellent working facilities. Skills in all phases of diagnostic radiology desired. Attractive and competitive benefits package leading to full partnership. Contact Sanford E. Rabushka, M.D., 11133 Dunn Rd., Ste. 1017, St. Louis, MO 63136; (314) 653-4300. 11–4ap

**RADIOLOGIST, WESTERN MASSACHUSETTS** Large radiology group in western MA is seeking a general diagnostic radiologist with experience and interest in body imaging, and expertise in nonvascular interventional procedures. Primary assignment at 868-bed, tertiary-care hospital with radiology residency program. Practice also includes 3 community hospitals and 6 private offices. Full partnership after 1 yr. Available on or before July 1, 1991. Send CV to Director of Recruiting, Radiology & Imaging, Inc., 130 Maple St., Springfield, MA 01103. 2–4ap

**PENN STATE UNIVERSITY, THE MILTON S. HERSHEY MEDICAL CENTER, FACULTY POSITION IN NUCLEAR MEDICINE**—The Division of Nuclear Medicine of the Dept. of Radiology at the Penn State University's Milton S. Hershey Medical Center is recruiting a physician with board certification in nuclear medicine (ABNM) for a full-time academic position. Board certification in diagnostic radiology (ABR) is desirable but not essential. Penn State University Hospital is a 350-bed, tertiary-care facility (currently expanding to 500 beds) in Hershey, PA, near Harrisburg, the state capitol. Nuclear Medicine is a division of the Dept. of Radiology, which has an academic faculty of 20 physicians and 6 Ph.D.'s. The Nuclear Medicine Division currently performs 5000 exams/yr and is expected to increase as renovations and expansion are completed in subsequent years. There are currently 5 gamma cameras and a Hologic QDR 1000W bone-density unit in place, with 1 additional camera being added in 1991 or 1992. Four or 5 of the 6 will be tomographic. Areas of emphasis currently include cardiac and pediatric nuclear medicine. An interest in neuronuclear medicine and brain tomography is desirable but not essential. An interest in clinical and/or basic research is desirable. Applicants should respond as soon as possible with a letter of interest and current CV. Please direct inquiries to Douglas F. Eggli, M.D., Chief, Division of Nuclear Medicine, Dept. of Radiology, Penn State University/Hershey Medical Center, P.O. Box 850, Hershey, PA 17033. Penn State University is an affirmative action, equal opportunity employer. Women and minorities are encouraged to apply. 2–4a

**CONNECTICUT**—Expanding group of 8 radiologists has a position available for an additional angio/interventional, BC/BE radiologist with expertise in general radiology also. Practice includes a 435-bed, fully equipped, university-affiliated, community hospital and a 47-physician, multispecialty clinic. Excellent salary and benefits leading to full partnership after second yr. For information, send CV to Paul C. Lakin, M.D., Dept. of Radiology, New Britain General Hospital, 100 Grand St., New Britain, CT 06050. 1–4ap

**DIAGNOSTIC RADIOLOGIST, TEXAS**—Progressive, well-diversified group (15 radiologists) has immediate opening for a BC/BE diagnostic radiologist with competence in a broad range of modalities. Additional consideration for fellowship. Excellent opportunity with excellent salary and benefits. Send CV with letter of inquiry to Will Gray, M.D., 1101 N. 19th St., Abilene, TX 79601. 3–5ap

**DIAGNOSTIC RADIOLOGIST** needed in Conway Hospital, a community hospital located 10 mi. west of the resort/seaside community of Myrtle Beach, SC. The dept. performs 44,000 exams/yr including CT, MRI, nuclear medicine, ultrasound, mammography, and special procedures. All exams are done on state-of-the-art equipment. Our 3-person group offers a very strong financial package with all benefits including 17-wk vacation. Lovely, rapidly growing resort area includes 60 mi. of sandy beaches, 70 golf courses, and beautiful seaside homes. Contact Gary Rike, M.D., P.O. Box 917, Conway, SC 29526; (803) 347-7277. 12–5ap

**THE DEPT. OF RADIOLOGY AT TRIPLER ARMY MEDICAL CENTER, HONOLULU, HI**, is recruiting academic radiologists for several divisions of the dept. including ultrasound, chest, skeletal, neuro, and general diagnostic radiology. Our dept. offers a fully accredited residency program with 20 residents and 16 attending full-time staff. Numerous consultants from across the country lecture on a continuing and regular basis. The hospital is a modern, tertiary-care center serving Hawaii and the entire Pacific Basin. A strong residency program, diverse and interesting patient population, excellent equipment, and a tropical lifestyle are positive aspects of the practice. Academic credentials and/or experience are necessary. Recently graduated fellows are encouraged to apply. Board certification is mandatory. Candidates should be particularly interested in patient care, teaching, and research. Salary and benefits are competitive and generous. Tripler is an EO/EEO employer. Please contact Mark F. Hansen, M.D., Col., MC, Chief, Dept. of Radiology, TAMC, HI 96859-5000; (808) 433-6393. 8–7a

**TEN-PERSON RADIOLOGY GROUP** located in Corpus Christi is seeking a new associate to start July 1990 or as late as July 1991. Must be board-certified or eligible. Will perform all diagnostic studies, including interventional, CT, MRI, nuclear medicine, and ultrasound. Please send CV to Search Committee, P.O. Box 5608, Corpus Christi, TX 78465-5608. 4xa

**RADIOLOGIST** — Full-time; nice, small, well-located North Carolina town. Join active, hospital-based, service-oriented practice. General diagnostic, nuclear medicine, ultrasound, CT, and mobile MRI. No arteriography. Reply with CV to Box I95, *AJR* (see address this section). 2–4ap

**NORTHERN CALIFORNIA/SAN FRANCISCO BAY AREA** — The Permanente Medical Group is seeking a BC radiologist with multimodality interests and fellowship training in MR or interventional radiology to join a 10-person group serving a 337-bed acute-care hospital and 2 outpatient clinics. Teaching opportunities are available with residents of subspecialty services on rotation from Stanford University Hospital and our own medical residents. We are currently siting a GE 1.5-T MRI system and installing a new LU arm. Competitive salary and excellent benefits. Please send inquiries and CV to Bruce Baker, M.D., Chief, Dept. of Radiology, Kaiser-Permanente Medical Center, 900 Kiely Blvd., Santa Clara, CA 95051; (408) 236-4444. EOE. 2–4a

**DENVER, CO**—Group of 8 diagnostic radiologists engaged in a predominantly hospital-based practice is seeking a new member on or about 10-1-90. The group provides diagnostic imaging services for a 565-bed, tertiary-care teaching hospital. The new member should be trained in diagnostic radiology and have fellowship training, and/or additional experience beyond residency level, in nuclear medicine. The new member will be primarily responsible for nuclear medicine but must be willing to participate in other modalities of diagnostic imaging. Salary, benefits, vacation time, and time to partnership are all competitive for the Rocky Mountain region. Interested parties should send their CV to Steve A. Holt, M.D., Western Radiologists, P.C., 3665 Cherry Creek Dr., N., Ste. 350, Denver, CO 80209. 2–4ap

**BROAD SPECTRUM RADIOLOGIST/UPSTATE NEW YORK** — Radiologist wanted for hospital-based practice 90 mi. northwest of New York City. Excellent recreational activities and easy access to metropolis. All modalities available. Excellent salary and benefits leading to early partnership. Immediate availability, but can wait for right applicant. Call G. Bilick; (914) 794-3300, ext. 2216 or send CV to P.O. Box 144, Harris, NY 12742. 3–6ap

**SALT LAKE CITY, UT** — Opportunity for board-certified diagnostic radiologist, with recent MRI fellowship training, to join group of 7 board-certified radiologists. Experience in all aspects of general radiology required. Practice includes 2 hospitals, 2 private offices, and a freestanding MRI center. Send letter and CV to Neel E. Bennett, M.D., Medical Director and Chairman, Dept. of Radiology, Holy Cross Hospital, 1050 E. S. Temple, Salt Lake City, UT 84102; (801) 350-4636. 4xa

**ULTRASOUND/CT/MRI** — Opportunity for a board-certified radiologist specializing in ultrasound, body CT, and body MRI to pursue an academic career at the New York Hospital-Cornell Medical Center. Dept. provides state-of-the-art equipment, including Acuson ultrasound, GE 9800 CT, and GE Signa 1.5-T MR. Wide variety of ultrasound exams include abdominal, OB-GYN, color Doppler, small parts, neonatal head, transvaginal, and transrectal. Prefer candidate with prior fellowship in sectional imaging or ultrasound. Responsibilities include clinical practice, teaching, and research. Position available 7/1/91 or earlier. Please send CV to Elias Kazam, M.D., Dept. of Radiology, The New York Hospital-Cornell Medical Center, 525 E. 68th St., New York, NY 10021. 1–4ap

**UCSD SCHOOL OF MEDICINE**—The Dept. of Radiology seeks a diagnostic radiologist to participate in clinical service, medical student and resident teaching, and research projects in the subspecialty of osteoradiology. Qualifications required are board-eligibility/certification, California medical license, and 1-yr fellowship in osteoradiology. One yr experience in osteoradiology, including MRI, in an academic program is preferred. Title series is assistant professor (in-resident or clinical series, not currently a tenure-track position); level based on years experience; salary commensurate with rank, and step of appointment based on the established salary schedule of the UCSD School of Medicine Faculty Compensation Plan. The University of California, San Diego, is an equal opportunity/affirmative action employer. All CVs received by April 30, 1991, or thereafter, will be considered until the position is filled. Send to Donald Resnick, M.D., Chief of Radiology, VA Medical Center, 3350 La Jolla Village Dr., San Diego, CA 92161. 4a

**UCSD SCHOOL OF MEDICINE** — The Dept. of Radiology is seeking an ultrasonologist to assist in clinical service, medical student and resident teaching, and research projects. Participation in other diagnostic subspecialties is available. Qualifications required are board-eligibility/certification, California medical license, and 1 yr fellowship training in ultrasound. Title series is assistant or associate professor (in residence or clinical series, not currently a tenure-track position); level based on years experience; salary commensurate with rank, and step of appointment based on the established salary schedule of the UCSD School of Medicine Faculty Compensation Plan. The University of California, San Diego, is an equal opportunity/affirmative action employer. All CVs received by April 30, 1991, or thereafter will be given full consideration until the position is filled. Send to Dolores Pretorius, M.D., Chief of Ultrasound (H-759), UCSD Medical Center, 225 Dickinson St., San Diego, CA 92103. 4a

**FULL/PART-TIME BC/BE RADIOLOGIST** wanted for 187-bed GM&S VA Medical Center. Excellent GE equipment, duplex Doppler ultrasound, diagnostic, and fluoroscopic. CT interpretation desirable. 18,000 procedures/yr. State university city amid hills and lakes in northwest Arkansas with cultural and recreational attractions. Competitive salary and excellent benefits/retirement. Call chief of staff; (501) 444-5050. 4xa

**PEDIATRIC RADIOLOGIST, PORTLAND, OR**—Immediate opening for a pediatric radiologist at Emanuel Hospital in Portland, OR. Either a pediatric fellowship or significant work experience is required. Opportunity to do general radiology as well. The hospital is a Level I trauma center, as well as a major pediatric referral center. The position leads to full partnership after second year. Please send CV to Blaine E. Kozak, M.D., Chairman, Dept. of Radiology, Emanuel Hospital, 2801 N. Gantenbein, Portland, OR 97227; (503) 280-4032. 4ap

## Positions Desired

**ASSISTANT PROFESSOR, DIRECTOR MRI CENTER**—Significant experience in musculoskeletal and neuro MR (MR fellowship), interventional bone, and MR and bone teaching. Responsible for MR fellowship. Looking for academic position with clinical research, musculoskeletal MR and/or neuro MR, and/or interventional. Please reply to Box K52, *AJR* (see address this section). 4–5bp

**JULY 1991 RADIOLOGY RESIDENCY POSITION SOUGHT**—Second yr radiology resident, with training in all modalities and strong qualifications, seeks position at third yr level in a university radiology program. Reply Box H93, *AJR* (see address this section). 4bp

**PGY-2 RADIOLOGY RESIDENCY POSITION SOUGHT**—Radiology resident in first yr of training seeks second yr position (to start 7/91) in university-based program. Hardworking. Strong credentials. Reply Box J7, *AJR* (see address this section). 4bp

## Fellowships and Residencies

**IMAGING FELLOWSHIP (CT, ULTRASOUND, MRI)**—William Beaumont Hospital, a 970-bed, modern, tertiary-care teaching and academic institution in southeast Michigan, offers a 1-yr fellowship in sectional body imaging. The fellowship will provide extensive clinical experience in body CT, ultrasound, and MRI including CT and ultrasound-guided procedures, conventional and color-flow Doppler exams, prostatic and endovaginal sonography. Ample elective time is also provided for other rotations of individual interest. Candidates must be board-certified or eligible in diagnostic radiology and have a valid Michigan medical license. Four positions are available for July 1992. Salary and fringe benefits are highly competitive. For further information, write to Ali Shirkhoda, M.D., Chief, Imaging Division, William Beaumont Hospital, 3601 W. 13 Mile Rd., Royal Oak, MI 48073; (313) 551-1001. 4–6c

**NEURORADIOLOGY FELLOWSHIP**—One yr beginning July 1, 1991. Exposure to all aspects of clinical/academic neuroradiology. Participation in research/teaching. Send cover letter/CV to Te-Hua Liu, M.D., Director, Neuroradiology Section, Dept. of Diagnostic Imaging, Temple University Health Sciences Center, 3401 N. Broad St., Philadelphia, PA 19140. Temple University Health Sciences Center is an affirmative action/equal opportunity employer. 4c

**WOMEN'S IMAGING FELLOWSHIP**—A 1-yr fellowship is available at Oregon Health Sciences University, Portland, OR. Training includes hysterosalpingography, fallopian tube recanalization, mammography and breast procedures, obstetrical ultrasound, pelvic ultrasound including vaginal ultrasound, and pelvic and breast MRI. Please contact Amy Thurmond, M.D., Director of Women's Imaging, Oregon Health Sciences University, L340, 3181 S.W. Sam Jackson Park Rd., Portland, OR 97201; (503) 494-7576. 4–6c

**VASCULAR AND INTERVENTIONAL FELLOWSHIP, TUFTS NEW ENGLAND MEDICAL CENTER HOSPITALS, BOSTON, MA**—One yr starting July 1. Angiography includes PA grams, selection carotids, and pediatric angio. Interventions include angioplasty, laser, atherectomy, lytic RX, and biliary and endourology. Candidate must have MA license and be board-eligible. Two positions available each yr. Victor G. Millan, M.D., Tufts New England Medical Center Hospitals, Box 253, 750 Washington St., Boston, MA 02111; (617) 956-5961 (Barbara). 4cp

**FELLOWSHIPS AT ALBANY MEDICAL CENTER** The Dept. of Radiology at the Albany Medical Center offers the following fellowship programs each yr with openings available July 1992: ultrasound and body CT/MR — Wide variety of exams with state-of-the-art equipment including Acuson ultrasound, 3 GE CT scanners, and GE Signa 1.5-T MR. Contact James Peters, M.D.; neuroradiology — regional referral center for neurosciences with extensive exposure to MR, CT, and angiography. Abundant research opportunities. Contact William Wagle, M.D.; angiography/interventional — busy, clinical service with in-depth experience in arteriography, lymphangiography, angioplasty, and interventional procedures. Contact Mohammad Sarrafizadeh, M.D. All program directors can be reached at the Dept. of Radiology, A-113, Albany Medical Center, 43 New Scotland Ave., Albany, NY 12208; (518) 445-3277. AMC is an equal opportunity, affirmative action employer. 4–6cp

**FELLOWSHIP IN CARDIOVASCULAR/INTERVENTIONAL RADIOLOGY**—A 1-yr fellowship is available July 1991 at Beth Israel Medical Center in New York involving all aspects of vascular and interventional radiology. Opportunities for clinical research available. For more information, call or write Marlene E. Rackson, M.D., Beth Israel Medical Center, First Ave. at 16th St., New York, NY 10003; (212) 420-2529. EEO/AA employer. 4c

**RADIOLOGY RESIDENCY**—Unexpected position available for third or fourth yr resident in radiology. For further information, please contact Arthur R. Clemett, M.D., St. Vincent's Hospital and Medical Center, 153 W. 11th St., New York, NY 10011; (212) 790-8717. 4cp

**FELLOWSHIP IN CARDIOVASCULAR/INTERVENTIONAL RADIOLOGY**—A 1-yr fellowship in cardiovascular/interventional radiology is available at the Dartmouth-Hitchcock Medical Center in Hanover, NH, beginning July 1992. DHMC is the major teaching component of Dartmouth Medical School and is situated in a classic northern New England town. Training includes all aspects of diagnostic angiography (including neuro and pulmonary), vascular and nonvascular interventional techniques. This includes IVC filter placement, atherectomy, thrombolysis, biliary and urologic interventions, as well as biopsy and drainage procedures using multiple imaging modalities. We have a close working relationship with the depts. of vascular and general surgery. Approximately 2000 diagnostic and interventional procedures are performed/yr. The dept. will be moving to a new, tertiary-care, 429-bed hospital, in fall 1991, equipped with 2 new, state-of-the-art digital interventional suites and a 4-bed recovery room. Candidates must have completed an accredited diagnostic radiology residency program, must be certified or eligible by the ABR, and must be eligible for medical licensure in the state of New Hampshire. For further information, please contact Louis I. Juravsky, M.D., FRCPC, Dept. of Diagnostic Radiology, Dartmouth-Hitchcock Medical Center, 2 Maynard St., Hanover, NH 03756. Dartmouth College is an equal opportunity/affirmative action educator and employer. 4cp

**FELLOWSHIP IN ANGIOGRAPHY AND INTERVENTIONAL RADIOLOGY, HOSPITAL OF THE UNIVERSITY OF PENNSYLVANIA**—The Dept. of Radiology at the Hospital of the University of Pennsylvania has an unexpected vacancy in 1 of its 4 1-yr angio/interventional fellowships beginning July 1, 1991. This fellowship is primarily clinical, with approximately 25% of the time being available for research and clinical investigation. The section performs approximately 4300 angio/interventional procedures per yr and the section is staffed by 4 full-time, interventional radiologists. Training includes all interventional procedures, including vascular, urologic, and biliary. Three state-of-the-art angiographic suites are available. For further information, contact Constantin Cope, M.D., Professor of Radiology, Dept. of Radiology; (215) 662-4034, or Stanley Baum, M.D., Professor and Chairman, Dept. of Radiology; (215) 662-3030. 4cp

**FELLOWSHIP IN MRI** at Central Massachusetts Magnetic Imaging Center, July 1992 through June 1993. CMMIC is a consortium of 3 area teaching hospitals (The Medical Center of Central Massachusetts, St. Vincent Hospital, and the University of Massachusetts Medical Center) with clinical, research, and teaching responsibilities. CMMIC currently uses 2 clinical 1.5-T GE Signa systems and a 2.0-T GE Fremont CSI research system. The fellowship will include thorough training in MRI physics, imaging principles, clinical applications, and image interpretation. Duties will include image interpretation of neuro, musculoskeletal, abdominal, pediatric, and cardiac studies; daily supervision of scanning; teaching file maintenance; and participation in CMMIC's teaching and research activities. Requirements include satisfactory completion of a 4-yr, accredited radiology training program and board-eligibility/certification. Please send inquiries to James Lingley, M.D., Medical Director, CMMIC, Inc., 367 Plantation St., Worcester, MA 01605. 4–5cp

**FELLOWSHIP IN CARDIOVASCULAR/INTERVENTIONAL RADIOLOGY**—A 1-yr fellowship in cardiovascular/interventional radiology is available at the Dartmouth-Hitchcock Medical Center in Hanover, NH, beginning July 1991. DHMC is the major teaching component of Dartmouth Medical School and is situated in a classic northern New England town. Training includes all aspects of diagnostic angiography (including neuro and pulmonary), vascular and nonvascular interventional techniques. This includes IVC filter placement, atherectomy, thrombolysis, biliary and urologic interventions, as well as biopsy and drainage procedures using multiple imaging modalities. We have a close working relationship with the depts. of vascular and general surgery. Approximately 2000 diagnostic and interventional procedures are performed/yr. The dept. will be moving to a new, tertiary-care, 429-bed hospital, in fall 1991, equipped with 2 new, state-of-the-art digital interventional suites and a 4-bed recovery room. Candidates must have completed an accredited diagnostic radiology residency program, must be certified or eligible by the ABR, and must be eligible for medical licensure in the state of New Hampshire. For further information, please contact Louis I. Juravsky, M.D., FRCPC, Dept. of Diagnostic Radiology, Dartmouth-Hitchcock Medical Center, 2 Maynard St., Hanover, NH 03756. Dartmouth College is an equal opportunity/affirmative action educator and employer. 4xcp

**SECOND YR RADIOLOGY RESIDENT**—Unexpected opening on July 1, 1991, for a radiology resident at the second yr training level. Candidate must have completed 1 yr of radiology residency in an approved training program. Send CV to David Bryk, M.D., Director of Radiology, Maimonides Medical Center, 4802 10th Ave., Brooklyn, NY 11219. 3–4cp

**FELLOWSHIP IN NEURORADIOLOGY**—A fellowship position in neuroradiology is available July 1, 1991, in the Dept. of Radiology at New England Medical Center Hospitals, Boston, MA. The hospital is the teaching unit of Tufts University School of Medicine. The program is for 1 or 2 yr and includes both adult and pediatric case material. The fellow will be trained in the technique and interpretation of carotid and vertebral angiography as well as myelography. CT and MRI of the head and spine form major components of the Neuroradiology Service, as does interventional neuroradiology. Neuroradiologic services at the New England Medical Center Hospitals are carried out in liaison with the Depts. of Neurology, Neurosurgery, and Pediatric Neurology. Joint radiologic and clinical conferences are held frequently and, within a short time, the applicants will have considerable exposure to an array of neuroradiologic material. The Dept. of Neuropathology also runs conferences, allowing correlation to be made between radiologic interpretation and pathology. Interested applicants should call Samuel M. Wolpert, M.D., Professor of Radiology and Neurology, Director of Fellowship Program, (617) 956-6333. 3–4cp

**IMAGING FELLOW IN CARDIOVASCULAR IMAGING**—Yale is offering a unique environment for training in echocardiography, cardiovascular MRI, cineangiogram interpretation, as well as extensive research opportunities. Candidates must be U.S. citizens or must qualify as a permanent resident in the United States. Please send CV and bibliography to Gregory Weltin, M.D., Yale University School of Medicine, Dept. of Diagnostic Radiology, 333 Cedar St., New Haven, CT 06510. Yale is an equal opportunity/affirmative action employer. Applications from women and members of minority groups are encouraged. Applications should be submitted no later than May 1, 1991. 3–4c

**VASCULAR / INTERVENTIONAL RADIOLOGY FELLOWSHIP, ST. LOUIS VASCULAR INSTITUTE AT THE CHRISTIAN HOSPITAL, ST. LOUIS, MO**—A 1- to 2-yr fellowship in vascular and interventional radiology is offered beginning July 1, 1991. Training includes all aspects of diagnostic angiography and vascular and nonvascular interventional techniques. Candidates must have completed a diagnostic radiology residency in an accredited training program, must be certified by or eligible for certification by the ABR, and must be able to obtain a Missouri license. Direct inquiries to Saadoon Kadir, M.D., Dept. of Radiology, Christian Hospital Northeast, 11133 Dunn Rd., Ste. 1017, St. Louis, MO 63136. 11–4cp

**DUKE UNIVERSITY MEDICAL CENTER FELLOWSHIP POSITIONS** — Duke University Medical Center is seeking qualified candidates for fellowship positions in the Dept. of Diagnostic Radiology. Currently there are positions available in the following areas: chest, musculoskeletal, and vascular/interventional radiology, ultrasound, advanced diagnostic imaging, MRI, neuroradiology, abdominal imaging, mammography, and research fellowships. The radiology dept. is state-of-the-art in diagnostic imaging with diverse resources available for clinical, teaching, and academic pursuits. Fellowship training is generally organized by organ systems, although experience can be individualized to accommodate special interests. Salary and benefits are competitive and academic time is guaranteed. For additional information, please phone Richard Leder, M.D. at (919) 681-2711 ext. 5310. Applications are due Feb. 1 of the preceding yr and can be obtained by writing to N. Reed Dunnick, M.D., Dept. of Radiology, Duke University Medical Center, Erwin Rd., Box 3808, Durham, NC 27710. AA/EOE. 2–7c

**CARDIOVASCULAR AND INTERVENTIONAL RADIOLOGY**—The Harvard Medical School and Brigham and Women's Hospital, Dept. of Radiology, is offering a 2-yr fellowship starting July 1, 1992, in cardiovascular and interventional radiology including peripheral and coronary angiography, cardiac catheterization, digital vascular imaging, all types of interventional procedures, noninvasive vascular techniques, and cardiovascular MRI. Research time available for participation in original or ongoing clinical and/or laboratory projects. Please send CV to B. Leonard Holman, M.D., Chairman, Dept. of Radiology, Brigham and Women's Hospital, 75 Francis St., Boston, MA 02115. Brigham and Women's Hospital/Harvard Medical School is an affirmative action/equal opportunity educator and employer. 3–8c

**UNEXPECTED OPENING FOR VASCULAR AND INTERVENTIONAL FELLOWSHIP BEGINNING JULY 1991** is offered at the University of Maryland. The fellow will participate in all aspects of diagnostic vascular radiology, as well as nonvascular interventional procedures, including percutaneous and laser angioplasty, embolization, biliary and GU intervention, and insertion of IVC filters. Contact Gerald S. Johnston, M.D., 22 S. Greene St., Baltimore, MD 21201; (301) 328-3477. The University of Maryland is an affirmative action/equal opportunity employer and encourages applications from members of minority groups. 3–5cp

**FELLOWSHIP IN ULTRASOUND / CT / ANGIO / INTERVENTIONAL**—A 1-yr fellowship program available beginning July 1992 at Lehigh Valley Hospital Center in Allentown, PA. LVHC is a 492-bed, acute-care, university-affiliated hospital. The fellowship program offers training in CT (head and body), ultrasound, angiography (neuro and visceral), and interventional radiography. MRI experience is also available. For further information, contact Robert Kricun, M.D., Dept. of Radiology, Lehigh Valley Hospital Center, P.O. Box 689, Allentown, PA 18105. 2–7c

**FELLOWSHIPS AT THOMAS JEFFERSON UNIVERSITY HOSPITAL**—The Dept. of Radiology at Thomas Jefferson University Hospital in Philadelphia offers the following fellowship programs each yr. Ultrasound/CT/MRI — Jefferson's ultrasound division is 1 of the largest in the world and performs all currently available exams including obstetric, vascular, lithotripsy, invasive, and endoluminal. We also operate 4 GE 1.5-T MRI units and 3 CT scanners. Contact Barry Goldberg, M.D., regarding this program. Cardiovascular/interventional — this division is housed in a new suite containing Philips angio units with DSA and performs the full range of vascular and nonvascular interventional procedures. Contact Geoffrey Gardiner, Jr., M.D. Neuro/ENT radiology — very active clinical services supply a wealth of material to this division, which is housed in a neurosciences imaging center containing all imaging modalities. Contact Carlos Gonzalez, M.D. Breast Imaging — Jefferson's new breast imaging center performs approximately 85 studies/day including ultrasound and needle localizations. Contact Stephen Feig, M.D. Chest — includes biopsies and CT. Contact Robert Steiner, M.D. MRI — a dedicated body MRI program including excellent research opportunities in addition to a large clinical case load. Contact Matthew Rifkin, M.D. Ultrasound — a dedicated ultrasound program. Contact Barry Goldberg, M.D. Musculoskeletal — includes MRI of the musculoskeletal system. Contact David Karasick, M.D. All program directors listed above can be contacted at the Dept. of Radiology, Thomas Jefferson University Hospital, Philadelphia, PA 19107. Jefferson is an equal opportunity / affirmative action employer. 4xc

**FELLOWSHIP IN ULTRASOUND AND BODY CT-MRI**—Unexpected position available July 1, 1991. A 1-yr body imaging fellowship at the Dept. of Radiology, University of Rochester Medical Center, a 750-bed, tertiary-care hospital. State-of-the-art equipment is available, including a free-standing MR center. Applicants must have completed an approved residency in diagnostic radiology and must be board-eligible or certified. For inquiries, please contact Deborah J. Rubens, M.D., Dept. of Radiology, Box 648, University of Rochester Medical Center, Rochester, NY 14642; (716) 275-8365. EO/AA/M-F employer. 2–4c

**FELLOWSHIP IN ULTRASOUND AND BODY CT/MRI** — July 1, 1992, to June 30, 1993, at the New York Hospital-Cornell Medical Center. Dept. provides state-of-the-art equipment including Acuson ultrasound, GE 9800 CT, and GE Signa 1.5-T MR. Wide variety of ultrasound exams include abdominal, OB-GYN, color Doppler, small parts, neonatal head, transvaginal, and transrectal. Applicant should be ABR eligible or certified. Send CV to Elias Kazam, M.D., Dept. of Radiology, The New York Hospital-Cornell Medical Center, 525 E. 68th St., New York, NY 10021. 1–4cp

**FELLOWSHIP POSITIONS**—The University of Texas, M. D. Anderson Cancer Center, Dept. of Diagnostic Radiology, is currently accepting applications for fellowships in different subspecialties in diagnostic imaging, including oncologic radiology, body imaging, and vascular/interventional radiology for the academic yr 1992. The dept. is equipped with state-of-the-art ultrasonography, CT, MRI, PET, angiography, routine fluoroscopy, radiography, and mammography. Candidates interested in these positions should write to Chusilp Charnsangavej, M.D., Professor and Deputy Chairman for Academic Affairs, Dept. of Diagnostic Radiology, Box 57, University of Texas M. D. Anderson Cancer Center, 1515 Holcombe Blvd., Houston, TX 77030. An employer equal opportunity affirmation action. 2–4c

**ABDOMINAL IMAGING FELLOWSHIP** — The Dept. of Radiology at the University of Florida is offering 1-yr fellowships in abdominal imaging beginning July 1, 1991, and July 1, 1992. Minimum requirements include successful completion of an accredited radiology residency. The fellowship includes training in all aspects of abdominal imaging (gastrointestinal and genitourinary radiology, CT, ultrasound, and MRI) by a 3-person subspecialty faculty. The program offers full clinical experience and research opportunities. Applicants must be eligible to obtain a license in the state of Florida. For additional information, contact Pablo R. Ros, M.D., Professor, Dept. of Radiology, Box J-374, Gainesville, FL 32610-0374; (904) 395-0288. The University of Florida is an equal opportunity / affirmative action employer and encourages applications from women and minorities. 10–6c

**INTEGRATED CHEST RADIOLOGY FELLOWSHIP AT JOHNS HOPKINS UNIVERSITY HOSPITAL**—The Dept. of Radiology, Division of Thoracic Imaging, Johns Hopkins University is offering a 1- to 2-yr academically oriented fellowship in chest radiology. The fellowship offers an integrated experience in cross-sectional imaging, including over 4000 chest CT and 1000 thoracic MRI exams/yr. Strong research interests in high-resolution CT, MRI, digital imaging methods, and interventional thoracic radiology offer the candidate an exciting environment to work in. The fellowship is available starting July 1, 1991. Contact Elias A. Zerhouni, M.D., Director of Thoracic Imaging and MRI, Dept. of Radiology, Johns Hopkins Hospital, Baltimore, MD 21205; (301) 955-4062. 1–6c

**NEURORADIOLOGY FELLOWSHIP**—The Dept. of Radiology, Strong Memorial Hospital, University of Rochester School of Medicine and Dentistry offers a 1- or 2-yr neuroradiology fellowship to begin July 1, 1991. Training is offered in MRI, CT, and special procedures, with the opportunity to perform both pediatric and carotid ultrasound. Assistance in teaching of medical students and residents is expected. Additional training in maxillofacial, dental, and ENT radiology also is available, as is the opportunity to perform both clinical and laboratory research. A very strong neuroscience community exists. The dept. consists of 25 radiologist faculty, 16 residents, and 3–5 fellows. State-of-the-art equipment is available in all modalities including new single and biplane angiographic systems, 3 third-generation CT, a 1.5-T MRI, and a midfield MR. Strong Memorial Hospital is a 750-bed, tertiary-care hospital with 100 beds dedicated to pediatric diseases. Candidates must have completed an accredited diagnostic radiology residency program, be board-certified or eligible, and have a New York state medical license by July 1, 1991. Send inquiries to Robert E. O'Mara, M.D., Box 648, University of Rochester Medical Center, Rochester, NY 14642; (716) 275-2733. EO/AA/M-F employer. 1–6c

## Tutorials/Courses

**ALASKA 1991-CRUISE THE INLAND PASSAGE, BREAST IMAGING AT SEA, JULY 7–14, 1991, AND MRI AT SEA, JULY 14–21, 1991**—Medical Seminars International, Inc., 18981 Ventura Blvd., Ste. 303, Tarzana, CA 91356; (818) 774-9077, fax (818) 774-0244. 3–6d

## Other

**VISITING PROFESSORSHIPS, THOMAS JEFFERSON UNIVERSITY HOSPITAL**—The Dept. of Radiology at Thomas Jefferson University Hospital in Philadelphia is offering visiting professorships over the next several yr, while some of our faculty members are on sabbatical leave. These positions can have either a 6-mo or 1-yr term. In particular, we are seeking candidates with expertise in either ultrasound or general diagnostic radiology, but emphasis in other areas may be acceptable as well. Funding for these positions is appropriate for a senior faculty member from another institution on sabbatical with partial funding of his/her own, or for a junior faculty member. These positions are also open to highly qualified foreign radiologists with current academic appointments at prestigious foreign medical schools. Visiting faculty members will do some clinical work in our dept. and also have access, for research or educational purposes, to state-of-the-art imaging modalities of all types, as well as well-equipped physics and physiology research laboratories. Interested persons should contact David C. Levin, M.D., Chairman, Dept. of Radiology, Thomas Jefferson University Hospital, Philadelphia, PA 19107. Jefferson is an equal opportunity/affirmative action employer. 4xe

# AJR Classified Advertisements Information

## Box Responses and Address for Ad Placement

Write Box _____, *AJR*, 2223 Avenida de la Playa, Suite 103, La Jolla, CA 92037-3218; Telephone: (619) 459-2229; FAX: (619) 459-8814.

## How to Place an Ad

*AJR* accepts classified advertising for Positions Available, Positions Desired, Fellowships and Residencies, and Tutorials/Courses. Ads are accepted by mail or FAX.

**Rates:** $6.00/line with a $30 minimum charge. Box service is $10 additional for each month the ad appears. There are discounts for multiple insertions: 10% for 2–3 insertions; 20% for 4 or more. To estimate lines, count all words and divide by 7.

**Billing:** Ads *must* be prepaid, or advertisers will be billed after the ad appears *providing* a purchase order number is submitted with the advertising copy. Terms are net 30 days.

**Deadlines:** 6 weeks prior to issue date. For specific deadlines, telephone the *AJR* editorial office.

## Estimating Ad Charges

| | |
|---|---|
| Line charge: divide total words by 7 and multiply by $6.00 | $ |
| Multiple insertions? If so, multiply by number | × |
| Subtotal | $ |
| Discount applies to two or more insertions. Subtract 10% if ad appears 2–3 months; 20% if 4 months or more | − |
| Subtotal | $ |
| Box response requested? If so, multiply number of months by $10.00 | + |
| Approximate advertising charge | $ |

# New look.
# New shape.

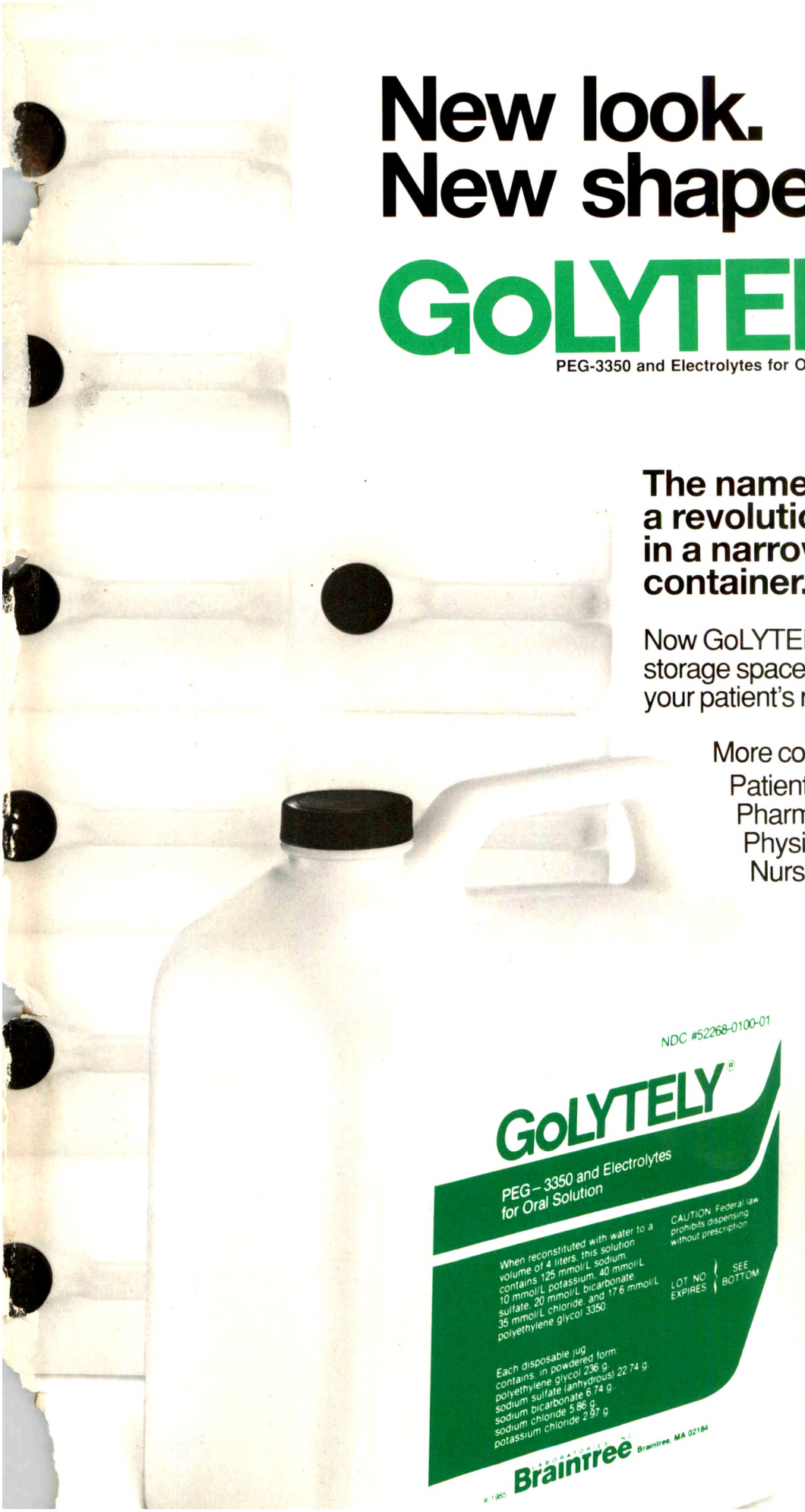
# GoLYTELY®

PEG-3350 and Electrolytes for Oral Solution

## The name that started a revolution now comes in a narrow, stackable container.

Now GoLYTELY takes up less storage space and less space in your patient's refrigerator.

More convenient for
Patients
Pharmacists
Physicians
Nurses




## New look.
## New shape.
## GoLYTELY.

Made by Lyne Laboratories, Stoughton, MA 02072, for BRAINTREE LABORATORIES, INC., P.O. Box 361, Braintree, MA 02184.

LABORATORIES, INC
**Braintree**

© 1989 BRAINTREE LABORATORIES, INC.
TRE-1039

Volume 156 American Journal of Roentgenology April 1991


SPECIAL ARTICLES

669 **Fleischner Lecture. Developmental abnormalities in the systemic blood supply to the lungs.** *Ellis K*

681 **Neuhauser Lecture. Bronchopulmonary dysplasia and research in diagnostic radiology.** *Northway WH Jr*

REVIEW ARTICLE

689 **Radiation injury of the brain.** *Valk PE, Dillon WP*

CARDIOPULMONARY RADIOLOGY

707 **Chest CT combined with artificial pneumothorax: value in determining origin and extent of tumor.** *Watanabe A, Shimokata K, Saka H, Nomura F, Sakai S*

711 **Lymphoma of the lung: CT findings in 31 patients.** *Lewis ER, Caskey CI, Fishman EK*

715 **Mediastinal seroma after esophagogastrectomy.** *Kronthal AJ, Heitmiller RF, Fishman EK, Kuhlman JE*

717 **Case report. Noncompaction of ventricular myocardium: CT appearance.** *Conces DJ Jr, Ryan T, Tarver RD*

BREAST RADIOLOGY

719 **Perspective. Medicolegal aspects of breast imaging: variable standards of care relating to different types of practice.** *Brenner RJ*

GASTROINTESTINAL RADIOLOGY

725 **Detection of active intraabdominal arterial hemorrhage: value of dynamic contrast-enhanced CT.** *Jeffrey RB Jr, Cardoza JD, Olcott EW*

731 **Diagnosis of pneumoperitoneum on supine abdominal radiographs.** *Levine MS, Scheiner JD, Rubesin SE, Laufer I, Herlinger H*

737 **Pictorial essay. Imaging the gallbladder: a historical perspective.** *Feld R, Kurtz AB, Zeman RK*

741 **Amyloidosis of the small intestine: findings on double-contrast radiographs.** *Tada S, Iida M, Matsui T, et al.*

745 **Case report. Visceral calcification in patients with AIDS may not always be due to *Pneumocystis carinii*.** *Towers MJ, Withers CE, Hamilton PA, Kolin A, Walmsley S*

749 **Case report. Pancreatic microcystic adenoma presenting with acute hemoperitoneum: CT diagnosis.** *Rubin GD, Jeffrey RB Jr, Walter JF*

751 **Case report. Hydatid cyst of the liver: identification of detached cyst lining on CT scans obtained after cyst puncture.** *Acunaş B, Rozanes İ, Acunaş G, Çelik L, Alper A, Gökmen E*

GENITOURINARY RADIOLOGY

753 **Carcinoma of the cervix: value of MR imaging in detecting parametrial involvement.** *Sironi S, Belloni C, Taccagni GL, DelMaschio A*

757 **Prostatic urethra dilatation with the Gianturco self-expanding metallic stent: a feasibility study in cadaver specimens and dogs.** *Dobben RL, Wright KC, Dolenz K, Wallace S, Gianturco C*

763 **Technical note. A simplified method for antegrade ureteral stent placement.** *Krauthamer R*

MUSCULOSKELETAL RADIOLOGY

765 **Acute effects of exercise on MR imaging of skeletal muscle: concentric vs eccentric actions.** *Shellock FG, Fukunaga T, Mink JH, Edgerton VR*

769 **Repair of Achilles tendon ruptures with a polylactic acid implant: assessment with MR imaging.** *Liem MD, Zegel HG, Balduini FC, Turner ML, Becker JM, Caballero-Saez A*

PEDIATRIC RADIOLOGY

775 **Extension of growth-plate cartilage into the metaphysis: a sign of healing fracture in abused infants.** *Kleinman PK, Marks SC Jr, Spevak MR, Belanger PL, Richmond JM*

781 **Pictorial essay. Normal metaphyseal radiologic variants not to be confused with findings of infant abuse.** *Kleinman PK, Belanger PL, Karellas A, Spevak MR*

785 **Osteomyelitis of the talus: an unusual cause of limping in childhood.** *Grattan-Smith JD, Wagner ML, Barnes DA*

791 **MR evaluation of spinal dermal sinus tracts in children.** *Barkovich AJ, Edwards MSB, Cogen PH*

799 **Case report. Polysplenia syndrome with congenital short pancreas.** *Herman TE, Siegel MJ*

NEURORADIOLOGY

801 **Evaluation of CSF shunt function: value of functional examination with contrast material.** *Benzel EC, Mirfakhraee M, Hadden TA*

807 **Diagnosis of ruptured intracranial dermoid cyst: value of MR over CT.** *Smith AS, Benson JE, Blaser SI, Mizushima A, Tarr RW, Bellon EM*

VASCULAR RADIOLOGY

813 **Review. Inferior vena caval filters: analysis of five currently available devices.** *Grassi CJ*

823 **Technical note. Kissing-balloon technique for angioplasty of the popliteal artery trifurcation.** *Mewissen MW, Beres RA, Bessette JC, Lipchik EO*

CONTRAST MATERIAL

825 **The risks of death and of severe nonfatal reactions with high- vs low-osmolality contrast media: a meta-analysis.** *Caro JJ, Trindade E, McGregor M*

833 **Case report. Atypical contrast reactions associated with systemic interleukin-2 therapy.** *Fishman JE, Aberle DR, Moldawer NP, Belldegrun A, Figlin RA*

COMPUTER PAGE

835 **An ultrafast network for communication of radiologic images.** *Stewart BK, Lou SL, Wong WK, Huang HK*

MEETING NEWS

841 **Radiology Summit Meeting—1990: Action strategies for the new decade.** *McClennan BL*

ARRS 1991 MEETING CASE OF THE DAY QUESTIONS

845 **Introduction.** *O'Connor JF*

846 **General diagnosis case of the day.** *Eschelman DJ, Panageas E, Rosen MP, Romo LV, O'Connor JF*

849 **Chest case of the day.** *Eschelman DJ, Gibbens DT, Fielding JR, et al.*

852 **Abdominal case of the day.** *Eschelman DJ, Duva-Frissora AD, Martin LC, et al.*

854 **Neuroradiology case of the day.** *Parker DR, Eschelman DJ, Gibbens DT, Rabinov JD, O'Connor JF*

858 **Pediatric case of the day.** *O'Connor JF, Martin LC, Chen HH, et al.*

OTHER CONTENT

**Book reviews** 680, 688, 730, 748, 762, 774, 780, 784, 790, 806

724 **Radiologic-Pathologic Conference**

822 **Memorial, Andrew H. Geiger**

840 **Books received**

862 **Forthcoming articles**

863 **Letters**

877 **News**

880 **Review of current literature**

884 **1991 ARRS meeting summary**

885 **1991 ARRS meeting courses and symposium**

888 **1991 ARRS scientific program**

894 **American Roentgen Ray Society information**

895 **Classified advertisements**

A8 ***AJR* business and subscriber information**

A14 **Guidelines for authors**